PROGRESS IN THEORETICAL CHEMISTRY AND PHYSICS

Frontiers in Quantum Systems in Chemistry and Physics

S. Wilson, P. J. Grout,
G. Delgado-Barrio, J. Maruani,
and P. Piecuch (Eds.)

Springer

FRONTIERS IN QUANTUM SYSTEMS IN CHEMISTRY AND PHYSICS

Progress in Theoretical Chemistry and Physics

VOLUME 18

For other titles published in this series, go to
www.springer.com/series/6464

Frontiers in Quantum Systems in Chemistry and Physics

Edited by

STEPHEN WILSON
University of Oxford, UK

PETER J. GROUT
University of Oxford, UK

JEAN MARUANI
Laboratoire de Chimie Physique, UPMC, Paris, France

GERARDO DELGADO-BARRIO
Instituto de Matemáticas y Física Fundamental, CSIC, Madrid, Spain

and

PIOTR PIECUCH
Michigan State University, East Lansing, USA

Springer

Editors
Stephen Wilson
Department of Chemistry
Physical & Theoretical
Chemistry Laboratory
University of Oxford
South Parks Road
Oxford
OX1 3QZ, United Kingdom
quantumsystems@gmail.com

Peter J. Grout
Department of Chemistry
Physical & Theoretical
Chemistry Laboratory
University of Oxford
South Parks Road
Oxford
OX1 3QZ, United Kingdom
peter.grout@chem.ox.ac.uk

Jean Maruani
UPMC
Laboratoire de Chimie Physique
Matière et Rayonnement
11 rue Pierre et Marie Curie
75005 Paris
France
jean.maruani@upmc.fr

Gerardo Delgado-Barrio
Instituto de Matemáticas y
Física Fundamental
CSIC
Serrano 123
28006 Madrid
Spain
gerardo@imaff.cfmac.csic.es

Piotr Piecuch
Department of Chemistry
Michigan State University
East Lansing, MI 48824
USA
piecuch@chemistry.msu.edu

ISBN 978-1-4020-8706-6 e-ISBN 978-1-4020-8707-3

Library of Congress Control Number: 2008931063

Printed on acid-free paper.

9 8 7 6 5 4 3 2 1

springer.com

Progress in Theoretical Chemistry and Physics

A series reporting advances in theoretical molecular and material sciences, including theoretical, mathematical and computational chemistry, physical chemistry, and chemical physics

Aim and Scope

Science progresses by a symbiotic interaction between theory and experiment: theory is used to interpret experimental results and may suggest new experiments; experiment helps to test theoretical predictions and may lead to improved theories. Theoretical Chemistry (including Physical Chemistry and Chemical Physics) provides the conceptual and technical background and apparatus for the rationalisation of phenomena in the chemical sciences. It is, therefore, a wide ranging subject, reflecting the diversity of molecular and related species and processes arising in chemical systems. The book series *Progress in Theoretical Chemistry and Physics* aims to report advances in methods and applications in this extended domain. It will comprise monographs as well as collections of papers on particular themes, which may arise from proceedings of symposia or invited papers on specific topics as well as from initiatives from authors or translations.

The basic theories of physics – classical mechanics and electromagnetism, relativity theory, quantum mechanics, statistical mechanics, quantum electrodynamics – support the theoretical apparatus which is used in molecular sciences. Quantum mechanics plays a particular role in theoretical chemistry, providing the basis for the spectroscopic models employed in the determination of structural information from spectral patterns. Indeed, Quantum Chemistry often appears synonymous with Theoretical Chemistry: it will, therefore, constitute a major part of this book series. However, the scope of the series will also include other areas of theoretical chemistry, such as mathematical chemistry (which involves the use of algebra and topology in the analysis of molecular structures and reactions); molecular mechanics, molecular dynamics and chemical thermodynamics, which play an important role in rationalizing the geometric and electronic structures of molecular assemblies and polymers, clusters and crystals; surface, interface, solvent and solid-state effects; excited-state dynamics, reactive collisions, and chemical reactions.

Recent decades have seen the emergence of a novel approach to scientific research, based on the exploitation of fast electronic digital computers. Computation provides a method of investigation which transcends the traditional division between theory and experiment. Computer-assisted simulation and design may afford a solution to complex problems which would otherwise be intractable to theoretical analysis, and may also provide a viable alternative to difficult or costly

laboratory experiments. Though stemming from Theoretical Chemistry, Computational Chemistry is a field of research in its own right, which can help to test theoretical predictions and may also suggest improved theories.

The field of theoretical molecular sciences ranges from fundamental physical questions relevant to the molecular concept, through the statics and dynamics of isolated molecules, aggregates and materials, molecular properties and interactions, and the role of molecules in the biological sciences. Therefore, it involves the physical basis for geometric and electronic structure, states of aggregation, physical and chemical transformation, thermodynamic and kinetic properties, as well as unusual properties such as extreme flexibility or strong relativistic or quantum-field effects, extreme conditions such as intense radiation fields or interaction with the continuum, and the specificity of biochemical reactions.

Theoretical chemistry has an applied branch – a part of molecular engineering, which involves the investigation of structure–property relationships aiming at the design, synthesis and application of molecules and materials endowed with specific functions, now in demand in such areas as molecular electronics, drug design or genetic engineering. Relevant properties include conductivity (normal, semi- and supra-), magnetism (ferro- or ferri-), optoelectronic effects (involving nonlinear response), photochromism and photoreactivity, radiation and thermal resistance, molecular recognition and information processing, and biological and pharmaceutical activities; as well as properties favouring self-assembling mechanisms, and combination properties needed in multifunctional systems.

Progress in Theoretical Chemistry and Physics is made at different rates in these various fields of research. The aim of this book series is to provide timely and in-depth coverage of selected topics and broad-ranging yet detailed analysis of contemporary theories and their applications. The series will be of primary interest to those whose research is directly concerned with the development and application of theoretical approaches in the chemical sciences. It will provide up-to-date reports on theoretical methods for the chemist, thermodynamician or spectroscopist, the atomic, molecular or cluster physicist, and the biochemist or molecular biologist who wishes to employ techniques developed in theoretical, mathematical or computational chemistry in his research programme. It is also intended to provide the graduate student with a readily accessible documentation on various branches of theoretical chemistry, physical chemistry and chemical physics.

Preface

In this volume we have collected some of the contributions made to the *Twelfth European Workshop on Quantum Systems in Chemistry and Physics* (QSCP-XII) in 2007. The workshop was held at Royal Holloway College, the most westerly campus of the University of London, and situated just a stone's throw from Windsor Great Park.

The workshop, which ran from 30 August to 5 September, continued the series that was established by Roy McWeeny in April 1996 with a meeting held at San Miniato, near Pisa. The purpose of the QSCP workshops is to bring together, in an informal atmosphere and with the aim of fostering collaboration, those chemists and physicists who share a common field of interest in the theory of the quantum many-body problem. Quantum mechanics provides a theoretical foundation for our understanding of the structure, properties and dynamics of atoms, molecules and the solid state, in terms of their component particles: electrons and nuclei. The study of 'Quantum Systems in Chemistry and Physics' therefore underpins many of the emerging fields in twenty-first century science and technology: nanostructure, smart materials, drug design – to name but a few.

Members of the workshop were keen to discuss their research and engage in collaboration centred upon the development of fundamental and innovative theory which would lead to the exploration of new concepts. The proceedings of all of the workshops, which have been held annually since 1996, have been published both to disseminate the latest developments within the wider community and to stimulate further collaboration.

We welcomed participants not only from most of the member states of the European Union, the United States of America and Canada, but also from China, Japan, Mexico and Russia. We were also honoured to be joined by Professor Walter Kohn, Nobel Laureate in Chemistry (1998), who gave a leading-edge lecture on density functional theory.

The 'Windsor' workshop was divided into 18 plenary sessions, during which a total of 39 lectures were delivered following the usual QSCP 'democratic' allocation of 30 minutes for each lecture. These lectures were complemented by a total of 21 poster presentations. Details of the QSCP-XII, including the abstracts for all lectures and posters, remain available on the workshop webpages at

quantumsystems.googlepages.com/2007qscpworkshop

The present volume is divided into two parts. The first and shorter part attempts to capture the essential spirit and dynamism of the workshop. It begins with the

introduction to the workshop and continues with a 'workshop report' which outlines the central themes of the meeting. In this report, particular attention is focussed on those lectures for which corresponding contributions are not included in these proceedings. Part 2 of this volume contains 25 contributions from those who gave lectures or poster presentations during the workshop. It is hoped that together these two parts give some insight into the stimulating experience that made the workshop such a success.

We are grateful to the members of the 2007 workshop not only for the high standard of the lectures and posters presented during the meeting, which is reflected in this volume, but also for the friendly and constructive spirit of both the formal and informal sessions. The QSCP workshops continue to provide a unique forum for the presentation and appraisal of new ideas and concepts.

We are grateful to other members of the International Scientific Committee for their continued and invaluable support. Specifically, we thank (in alphabetical order): Professor V. Aquilanti of the University of Perugia, Italy, Professor E. Brändas of Uppsala University, Sweden, Professor L. Cederbaum of Heidelberg University, Germany, Professor A. Mavridis of the National University of Athens, Greece, and Professor O. Vasyutinskii of the Ioffe Institute in St. Petersburg, Russia, for their advice and collective wisdom. Undoubtedly, their advice and council ensured the ultimate success of the workshop.

Finally, we are grateful to the officers of Royal Holloway College for their help in ensuring the smooth running of the workshop and for allowing access to their pleasant campus.

It is the editors' hope that this volume will not only convey some of the dynamism of the QSCP-XII workshop, but will also seed some innovative ideas in the wider research community.

April 2008

Stephen Wilson
Peter J. Grout
Gerardo Delgado-Barrio
Jean Maruani
Piotr Piecuch

Contents

Part I
Workshop

Introduction to the Workshop

Stephen Wilson

Abstract Introduction to the twelfth Quantum Systems in Chemistry and Physics workshop.

Keywords: Workshop introduction

WELCOME TO THE 2007 Quantum Systems in Chemistry and Physics workshop. Ten years ago the workshop was held in the ancient university city of Oxford. We met in Jesus College in April, 1997, to hear about the latest developments of the day[1]. This year the conference returns to England. The 2007 workshop is being held at Royal Holloway College (Fig. 1), the most westerly campus of the University of London, some 19 miles from the capital.

Royal Holloway College lies in an area steeped in English history. The water meadows of Runnymede beside the River Thames just a mile or so away witnessed the signing of the Magna Carta. Here, in 1215, King John signed one of the most important legal documents in the history of democracy. Nearby Windsor Castle, residence of the English monarchs since the time of the Norman Conquest, is situated in the Great Park a few miles to the north.

The study of quantum systems now has a distinguished history of its own. Eighty years ago, Heitler and London [1] applied the newly developed quantum mechanics

[1] Past venues of the Quantum Systems in Chemistry and Physics workshops are given in Appendix 1. The published proceedings of previous workshops are listed in Appendix 2.

S. Wilson
Physical & Theoretical Chemistry Laboratory, University of Oxford, South Parks Road, Oxford OX1 3QZ, England; Faculty of Mathematics, Physics and Informatics, Comenius University, 84215 Bratislava, Slovakia, e-mail: quantumsystems@gmail.com

S. Wilson et al. (eds.) *Frontiers in Quantum Systems in Chemistry and Physics*.

Fig. 1 Royal Holloway, University of London, venue of the twelfth Quantum Systems in Chemistry and Physics workshop

to the ground state of the hydrogen molecule and chemistry joined physics and the mathematical sciences. But by 1929, Dirac [2] had recognized that

> the difficulty lies only in the fact that application of these laws leads to equations that are too complex to be solved.

In the hands of Pauling, the nature of the chemical bond was revealed. The understanding of molecular structure provided the foundation for the spectacular growth in molecular biology in the second half of the twentieth century. At the same time, the advent of the digital computer promised a tool capable of handling the complexity of the equations governing quantum systems.

Today, we are in the early stages of a revolution in science which has been described[2]

> as profound as the one that occurred early in the last century with the birth of quantum mechanics.

The development of new instruments, such as electron microscopy, synchrotron X-ray sources, neutron scattering, lasers, scanning microscopy and nuclear magnetic resonance devices, are already providing complementary probes of matter and unprecedented understanding. Coupled with the availability of increasingly powerful computing and information technology these developments have

> brought science finally within reach of a new frontier, the frontier of complexity.

Studies of quantum systems will be central to progress. Our workshop[3] will provide a perspective on these new horizons.

Appendix 1 – Past Venues of Quantum Systems in Chemistry and Physics Workshops

The Quantum Systems in Chemistry and Physics workshops have been held at various venues[4] around Europe since 1996 – from Paris to St. Petersburg, from Uppsala

[2] J.H. Marburger, US President's Science Advisor, February, 2002.

[3] Members of the workshop are listed in Table 1.

[4] Past venues of the workshop are listed in Table 2.

Table 1 Members of the Quantum Systems in Chemistry and Physics workshop held at Royal Holloway, University of London, 2007

Vincenzo Aquilanti, *Università degli Studi di Perugia*,
Ioan Baldea, *Universität Heidelberg*,
Massimiliano Bartolomei, *Consejo Superior de Investigaciones Cientificas*,
David Bishop, *University of Ottawa*,
Raymond Bishop, *University of Manchester*,
Ana Carla Bitencourt, *Università degli Studi di Perugia*,
Erkki Brändas, *Uppsala University*,
Kieron J Burke, *University of California Irvine*,
Jose Campos-Martinez, *Consejo Superior de Investigaciones Cientificas*,
Garnet Chan, *Cornell University*,
Ove Christiansen, *University of rhus*,
Fernando Colmenares, *Universidad Nacional Autnoma de México*,
Daniel Crawford, *Virginia Tech*,
Qiang Cui, *University of Wisconsin-Madison*,
Hubert Cybulski, *University of Warsaw*,
Gerardo Delgado-Barrio, *Consejo Superior de Investigaciones Cientificas*,
Francois J. Fillaux, *Université Pierre et Marie Curie*,
Tamas Gal, *University of Debrecen*,
Nikitas Gidopoulos, *Rutherford Appleton Laboratory*,
Vitaly N. Glushkov, *National University of Dnepropetrovsk*,
Alexander Glushkov, *Odessa University*,
Peter J. Grout, *University of Oxford*,
Christopher M. Handley, *University of Manchester*,
Robert J. Harrison, *Oak Ridge National Laboratory*,
Trygve Helgaker, *University of Oslo*,
Katharine L. C. Hunt, *Michigan State University*,
Ilya G. Kaplan, *Universidad Nacional Autnoma de México*,
Jacek Karwowski, *Nicolaus Copernicus University*,
Walter Kohn, *University of California, Santa Barbara*,
Alexander Kuleff, *Universität Heidelberg*,
Luis Lain, *Universidad del Pas Vasco*,
Shuhua Li, *Nanjing University*,
Glauciete Maciel, *Università degli Studi di Perugia*,
Svetlana Malinovskaya, *Odessa University*,
Jean Maruani, *Université Pierre et Marie Curie*,
Aristides Mavridis, *National and Kapodistrian University of Athens*,
Salvador Miret-Artes, *Consejo Superior de Investigaciones Cientificas*,
Robert Moszynski, *University of Warsaw*,
Hiromi Nakai, *Waseda University*,
Hiroshi Nakatsuji, *Kyoto University*,
Jeppe Olsen, *University of rhus*,
Aristotle Papakondylis, *National and Kapodistrian University of Athens*,
E. Pérez-Romero, *Universidad de Salamanca*,
Piotr Piecuch, *Michigan State University*,
Boris N. Plakhutin, *Russian Academy of Sciences*,
Kenneth Ruud, *University of Tromsø*,
Gustavo E. Scuseria, *Rice University*,
Luis M. Tel, *Universidad de Salamanca*,
Francis Temme, *Queens University*,
Alicia Torre, *Universidad del Pas Vasco*,
Demeter Tzeli, *National and Kapodistrian University of Athens*,
Carmela Valdemoro, *Consejo Superior de Investigaciones Cientificas*,
Ad van der Avoird, *Radboud University*,
Antonio Varandas, *Universidade de Coimbra*,
Stephen Wilson, *University of Oxford*

Table 2 Past Venues of the Quantum Systems in Chemistry and Physics workshops[a]

Year		Venues	Country	Organizer
1996		San Miniato, Pisa	Italy	Roy McWeeny
1997	II	Jesus College, Oxford	England	Stephen Wilson
1998	III	Granada	Spain	Alfonso Hernandez-Laguna
1999	IV	Marly-le-Roi	France	Jean Maruani
2000	V	Uppsala	Sweden	Erkki Brändas
2001	VI	Boyana Palace, Sofia	Bulgaria	Yavor Delchev, Alia Tadjer
2002	VII	Casta Paprinicka, Bratislava	Slovakia	Ivan Hubač
2003	VIII	Spetses Island	Greece	Aristides Mavridis
2004	IX	Les Houches	France	Jean-Pierre Julien
2005	X	Tunisian Academy Carthage	Tunisia	Souad Lahmar
2006	XI	Kochubey Palace St. Petersburg	Russia	Oleg S. Vasyutinskii
2007	XII	Royal Holloway, University of London	England	Stephen Wilson

[a] For further details consult the Quantum Systems in Chemistry & Physics website at Quantum Systems.googlepages.com

to Granada, from the Greek Island of Spetses to the mountain retreat of Les Houches in the French Alps. The workshop has even traveled to the ancient Phoenician port of Carthage of the North African coast of Tunisia. The 2007 workshop is the twelfth in a series which began in April, 1996, with a workshop organized by Professor Roy McWeeny at San Miniato, near Pisa.

Appendix 2 – Published Proceedings of Past Quantum Systems in Chemistry and Physics Workshops

Each year selected scientific contributions to the workshops have been published.

□ 1996

Quantum Systems in Chemistry and Physics Trends in Methods and Applications, ed. R. McWeeny, J. Maruani, Y.G. Smeyers & S. Wilson, Kluwer Academic Publishers, 1997

□ 1997

Advances in Quantum Chemistry 31, Quantum Systems in Chemistry and Physics. I, eds. P.-O. Löwdin, J.R. Sabin, M.C. Zerner & E. Brändas, Guest editors: S. Wilson, J. Maruani, Y.G. Smeyers, P.J. Grout & R. McWeeny, Academic Press, 1998

Advances in Quantum Chemistry 32, Quantum Systems in Chemistry and Physics. II, eds. P.-O. Löwdin, J.R. Sabin, M.C. Zerner & E. Brändas, Guest editors: S. Wilson, J. Maruani, Y.G. Smeyers, P.J. Grout & R. McWeeny, Academic Press, 1998

□ 1998

Quantum Systems in Chemistry and Physics, 1, Progress in Theoretical Chemistry and Physics 2, ed. A. Hernandez-Laguna, J. Maruani, R. McWeeny & S. Wilson, Kluwer Academic Publishers, 2000

Quantum Systems in Chemistry and Physics, 2, Progress in Theoretical Chemistry and Physics 3, ed. A. Hernandez-Laguna, J. Maruani, R. McWeeny and S. Wilson, Kluwer Academic Publishers, 2000

□ 1999

New Trends in Quantum Systems in Chemistry and Physics, 1, Progress in Theoretical Chemistry and Physics 6, ed. J. Maruani, C. Minot, R. McWeeny Y.G. Smeyers & S. Wilson, Kluwer Academic Publishers, 2000

New Trends in Quantum Systems in Chemistry and Physics, 2, Progress in Theoretical Chemistry and Physics 7, ed. J. Maruani, C. Minot, R. McWeeny Y.G. Smeyers & S. Wilson, Kluwer Academic Publishers, 2000

□ 2000

Advances in Quantum Chemistry 39, New Perspectives in Quantum Systems in Chemistry and Physics, Part 1, eds. J.R. Sabin and E. Brändas, Guest editors: E. Brändas, J. Maruani, R. McWeeny, Y.G. Smeyers & S. Wilson, Academic Press, 2001

Advances in Quantum Chemistry 40, New Perspectives in Quantum Systems in Chemistry and Physics, Part 2, eds. J.R. Sabin and E. Brändas, Guest editors: E. Brändas, J. Maruani, R. McWeeny, Y.G. Smeyers & S. Wilson, Academic Press, 2001

□ 2001

International Journal of Quantum Chemistry 89, Issue 4 (2002) Proceedings of the Sixth European Workshop on Quantum Systems In Chemistry and Physics, Issue Edited by Yavor Delchev, Jean Maruani, Roy McWeeny, Yves Smeyers & Stephen Wilson

□ 2002

International Journal of Quantum Chemistry 99, Issue 6 (2004) Proceedings from the Seventh European Workshop on Quantum Systems in Chemistry and Physics, Issue Edited by Ivan Hubač, Jean Maruani & Stephen Wilson

□ 2003

International Journal of Quantum Chemistry 104, Issue 4 (2005) Proceedings from the Eighth European Workshop on Quantum Systems in Chemistry and Physics, Issue Edited by Aristides Mavridis

□ 2004

Advances in the Theory of Chemical and Physical Systems, Progress in Theoretical Chemistry and Physics 15, ed. J.-P. Julien, J. Maruani, D. Mayou, S. Wilson & G. Delgado-Barrio, Springer, 2006

□ 2005

Topics in the Theory of Chemical and Physical Systems, Progress in Theoretical Chemistry and Physics 16, ed. S. Lahmar, J. Maruani, S. Wilson & G. Delgado-Barrio, Springer, 2007

□ 2006

International Journal of Quantum Chemistry 107 Issue 14 (2007) Proceedings from the Eleventh European Workshop on Quantum Systems in Chemistry and Physics, Issue Edited by Oleg Vasyutinskii, Jean Maruani, Piotr Piecuch, Gerardo Delgado-Barrio & Stephen Wilson

For further details consult the Quantum Systems in Chemistry & Physics website at QuantumSystems.googlepages.com

References

1. Heitler, W., and London, F.: Zeitschrift für Physik **44**, 455 (1927)
2. Dirac, P.A.M.: Proc. Roy. Soc. A **123**, 714 (1929)

Quantum Systems in Chemistry and Physics XIIth Workshop Report

Stephen Wilson

Abstract A brief report on the Quantum Systems in Chemistry and Physics XII workshop is given.

Keywords: Workshop report

The twelfth European workshop on *Quantum Systems in Chemistry and Physics* opened with a reception in the Victorian baroque splendor of the Founders Building at Royal Holloway, University of London, on 30 August, 2007.

Lectures began the following day in the main Lecture Theatre of the Queen's Building. The workshop programme, together with a full set of abstracts, is available at the Quantum Systems website: quantumsystems.googlepages.com/2007qscpworkshop. In this report, we provide a brief overview of the lectures delivered at the workshop, along with a selection of the posters presented.

The programme of lectures delivered on the first full day of the workshop, 31 August, 2007, are listed in Table 1. Two sessions were held in the morning and two in the afternoon.

Session 1: 09:00, 31 August, 2007

The opening lecture was given by Professor Raymond Bishop of the School of Physics and Astronomy at the University of Manchester. He addressed the application of coupled cluster theory [Bishop 1] to quantum systems defined on an extended

S. Wilson
Physical & Theoretical Chemistry Laboratory, University of Oxford, South Parks Road, Oxford OX1 3QZ, England; Faculty of Mathematics, Physics and Informatics, Comenius University, 84215 Bratislava, Slovakia, e-mail: quantumsystems@gmail.com

S. Wilson et al. (eds.) *Frontiers in Quantum Systems in Chemistry and Physics*.

Table 1 Lectures delivered on the second day of the workshop, Friday, 31 August, 2007

- Session 1 (Chair: D.M. Bishop)

  Coupled Cluster Theory of Quantum Spin- Lattice Models of Magnetic Systems and their Quantum Phase Transitions

  R.F. Bishop (University of Manchester)

  Study of the electronic structure of the unconventional superconductor Sr_2RuO_4 by the embedded cluster method

  I.G. Kaplan (Universidad Nacional Autónoma de México)

- Session 2 (Chair: P. Piecuch)

  Some Recent Advances in Solving the Schrödinger Equation and in *SAC/SAC-CI* Methodology

  H. Nakatsuji (Kyoto University)

  Ab-initio DMRG and Canonical Transformation Theories of Electronic Structure

  G.K.-L. Chan (Cornell University)

- Session 3 (Chair: J. Karwowski)

  The calculation of energies and properties of large molecules

  T. Helgaker (University of Oslo)

  Renormalized Coupled-Cluster Methods: Theoretical Foundations and Applications to Radicals, Biradicals, and Bond Breaking

  P. Piecuch (Michigan State University)

- Session 4 (Chair: J. Maruani)

  Four new forms of the contracted Schrödinger equation: Crucial role played by the 4th order correlation energy terms

  C. Valdemoro (Consejo Superior de Investigaciones Cientificas, Madrid)

  The contracted Schrödinger equation: imposing S-representability constraints upon the correlation matrices

  L. Tel (Universidad de Salamanca)

  Correlated calculations in localized basis sets

  J. Olsen (Åarhus Universitet)

regular spatial lattice. Such systems, he explained, may have "novel ground states which display quantum order in some region of the Hamiltonian parameter space, delimited by critical values which mark the corresponding quantum phase transitions". Furthermore, "the subtle correlations present usually cannot easily be treated by standard many-body techniques". Bishop described recent work [Bishop 2] on the systematic inclusion of multispin correlations for a wide variety of quantum spin-lattice problems [Bishop 3]. Since the method is not restricted to bipartite lattices or to nonfrustrated systems, it can deal with problems for which alternative

techniques give rise to difficulties [Bishop 2, Bishop 3, Bishop 4, Bishop 5, Bishop 6, Bishop 7]. It can be easily extended to models of strongly interacting electrons on regular lattices, such as the Hubbard model [Bishop 8]. Further details of the work of Bishop and his co-workers can be found in the cited references.

In the second lecture of the Session, Professor Ilya Kaplan described a study of the electronic structure of the unconventional superconductor Sr_2RuO_4, which possesses an unconventional spin-triplet symmetry of Coopers pairs, using the embedded cluster method. A paper by Kaplan and his co-author is included in this volume.

The Chair for Session 1 was Professor David M. Bishop of the University of Ottawa.

Session 2: 11:00, 31 August, 2007

Professor Hiroshi Nakatsuji from Kyoto spoke about *Some Recent Advances in Solving Schrödinger Equation and in SAC/SAC-CI Methodology*. The symmetry-adapted cluster approach provides a general method for solving the Schrödinger equation for atomic and molecular systems [Nakatsuji 1, Nakatsuji 2, Nakatsuji 3]. The method can also be used to solve the Dirac-Coulomb equation [Nakatsuji 4]. The iterative complement interaction (ICI) method is a rapidly converging method leading to the exact solution of the Schrödinger equation and Dirac-Coulomb equation.

The SAC/SAC-CI method can be used to investigate electron correlation effects in ground and excited states, and also ionized and electron attached states of molecules. Code for performing calculations is distributed in GAUSSIAN03 and further details can be found on the website www.sbchem.kyoto-u.ac.jp/nakatsuji-lab/sacci.html. Recent achievements include:

(i) direct SAC-CI algorithm [Nakatsuji 5]
(ii) applications to photo-biology such as retinal proteins in vision and proton-pump [Nakatsuji 6], the mechanism of luminescence in the firefly [Nakatsuji 7]
(iii) formulation and applications of Giant SAC-CI methodology for giant molecular systems [Nakatsuji 8]

Professor Garnet Chan from Cornell University lectured on *ab initio* Density Matrix Renormalization Group (DMRG) [Chan 1] and canonical transformation theories of electronic structure [Chan 2]. A paper by Chan is included in this volume.

The Chair for Session 2 was Professor Piotr Piecuch.

Session 3: 14:00, 31 August, 2007

Professor Trygve Helgaker of the University of Oslo described the application of Hartree-Fock and Kohn-Sham self-consistent field methods to large molecular systems at a cost that scales linearly with system size. In his lecture, which was co-authored by S. Coriania, S. Høst, B. Jansik, P. Jørgensen, J. Olsen, S. Reine and P. Salek, he described methods based on an exponential parameterization of

the one-electron density matrix, which is described in a published paper entitled *Direct optimization of the AO density matrix in Hartree-Fock and Kohn-Sham theories* [Helgaker 1]. He discussed the choice of one-electron basis set using Lowdin orthogonalization of a basis of atomic Gaussian orbitals as presented in a paper entitled *Linear-scaling symmetric square-root decomposition of the overlap matrix* [Helgaker 2]. A linear scaling direct minimization of the density matrix can be used to avoid matrix diagonalization as described in a paper entitled *Linear-scaling implementation of molecular electronic self-consistent field theory* [Helgaker 3]. The calculation of time-dependent molecular properties for large systems, including excitation energies and polarizabilities, provides an example of the application of the approach of Helgaker and his co-workers. Details can be found in a paper entitled *Linear-scaling implementation of molecular response theory in self-consistent field electronic-structure theory* [Helgaker 4].

The second lecture in this session was given by P. Piecuch from Michigan State University. Piecuch described progress with renormalized coupled cluster methods, such as CR-CCSD(T), CR-CCSD(TQ), and the size extensive formulation of CR-CCSD(T), termed CR-CC(2,3). According to Piecuch, these methods "represent a new generation of single-reference approaches that eliminate the failures of conventional coupled-cluster approximations, such as CCSD(T), whenever non-dynamical correlation effects become more significant". A paper by Piecuch and his co-authors is included in this volume.

The Chair for Session 3 was Professor Jacek Karwowski of the Nicholas Copernicus University, Toruń.

Session 4: 16:00, 31 August, 2007

Session 4 opened with a lecture by Professor Carmela Valdemoro from Consejo Superior de Investigaciones Cientificas, Madrid, entitled *Four new forms of the contracted Schrödinger equation: Crucial role played by the 4th order correlation energy terms*. This was followed by a related talk by Professor Luis Tel from the University de Salamanca on *The contracted Schrödinger equation: imposing S-representability constraints upon the correlation matrices*. Valdemoro, Tel and their co-authors, D.R. Alcoba and E. Pérez-Romero, have contributed a substantial review to this volume entitled *Guidelines on the Contracted Schrödinger Equation Methodology*.

Session 4 closed with a lecture by Professor Jeppe Olsen from Åarhus University. Olsen spoke about *Correlated calculations in localized basis sets*.

The Chair for Session 4 was Professor Jean Maruani.

After dinner, the first poster session was held. A selection of the papers presented is included in this volume.

The programme of lectures delivered on the third day of the workshop, 1 September, 2007, is given in Table 2. Again there were two sessions in the morning and two in the afternoon.

Table 2 Lectures delivered on the third day of the workshop, Saturday, 1 September, 2007

- Session 5 (Chair: R.F. Bishop)

  Hybrid functionals for solid-state systems
  G. Scuseria (Rice University)

  The real reason DFT works: the semi-classical origin of modern functions
  K.J. Burke (University of California Irvine)

- Session 6 (Chair: T.D. Crawford)

  Dirac Coulomb equation: Playing with artifacts
  J. Karwowski (Nicolaus Copernicus University)

  Relativity and quantum mechanics
  E.J. Brändas (Uppsala University)

- Session 7 (Chair: T. Helgaker)

  Ab initio intermolecular force fields tested by spectroscopy: State of the art
  A. van der Avoird (Radboud University)

  Dielectric and optical properties of dilute atomic gases
  R. Moszynski (University of Warsaw)

- Session 8 (Chair: H. Nakatsuji)

  Computational chemistry at the petascale
  R.J. Harrison (Oak Ridge National Laboratory)

  Koopmans theorem in the ROHF method: General formulation
  B.N. Plakhutin (Russian Academy of Sciences)

  Electron Cross Relaxation as a function of Single Relaxation Contributions in 1*s*-2*p*-Double Core Ionization Energies and Spin-orbit Splitting of Atoms from Al to Ba
  J. Maruani (Université Pierre et Marie Curie)

Session 5: 09:00, 1 September, 2007

Professor Gustavo E. Scuseria from Rice University, Houston, opened this Session with a lecture entitled *Hybrid functionals for solid-state systems*. He described "current efforts to develop more accurate exchange-correlation functionals for density functional theory." One of the functionals that he discussed was "a screened hybrid known as HSE [Scuseria 1], which is particularly well suited for calculations of solids because it is much faster than regular hybrids and can also be used in metals. HSE yields an important improvement in band gap predictions [Scuseria 2] compared to LDA, GGAs, and meta-GGAs." Scuseria also presented "applications to transition metal oxides, silicon phase transitions and defects [Scuseria 3] and

other problems where electron localization seems to play a crucial role [Scuseria 4]. Preliminary results regarding the development of a promising new [Scuseria 5] local hybrid functional [Scuseria 6] [were] also discussed."

Professor Kieron Burke from the University of California Irvine spoke on the *Semi-classical Origins of Success of Modern Density Functionals*. He explained "how the successes of modern density functionals can be understood in terms of semiclassical approximations to the electronic structure problem." He used this understanding "to derive the one fit parameter in the Becke-88 exchange functional," and showed "how to improve the derivation of the PBE functional to produce a more appropriate functional for solids: PBEsol." He concluded by discussing "how semiclassical methods might yield a usefully-accurate kinetic energy functional, bypassing all of Kohn-Sham density functional theory." Papers entitled *Relevance of the slowly-varying electron gas to atoms, molecules, and solids* [Burke 1] and *Generalized gradient approximation for solids and their surfaces* [Burke 2] can be consulted for further details. Professor Burke's co-authors were P. Elliot, D. Lee and A. Cangi.

The Chair for Session 5 was Professor Raymond F. Bishop of the University of Manchester.

Session 6: 11:00, 1 September, 2007

Session 6 was chaired by Professor T. Daniel Crawford of Virginia Tech.

In the first lecture entitled *Dirac-Coulomb equation: Playing with artifacts*, Professor Jacek Karwowski from Toruń observed that "the [Dirac-Coulomb] equation constitutes the most important starting point to the development of numerous variational approaches, which are commonly, and very successfully, used in theoretical modelling of atoms and molecules [Karwowski 1]". He then described "[t]wo classes of variational approaches to the eigenvalue problem of the DC Hamiltonian". A paper by Karwowski and his co-authors is included in this volume. Further details can be found in two papers by G. Pestka, M. Bylicki and J. Karwowski published in *Journal of Physics B* [Karwowski 2].

The second lecture of this session was given by Professor Erkki Brändas of Uppsala University who spoke on *The Theory of Relativity and Quantum Mechanics*. A paper describing this work is included in the present volume.

Session 7: 14:00, 1 September, 2007

Professors A. van der Avoird, from Radboud University, and Robert Moszynski, from the University of Warsaw, gave the two lectures in Session 7.

In a paper co-authored by G.C. Groenenboom, van der Avoird spoke on *Ab initio intermolecular force fields tested by spectroscopy: state of the art*. His abstract,

which can be found on the Quantum Systems website (quantumsystems.googlepages.com), is as follows:

> In this talk I will review the state of the art in obtaining intermolecular potential surfaces from ab initio electronic structure calculations, by different methods. A critical test of the reliability of the resulting potentials is to use them in computations of the bound levels and spectra of Van der Waals complexes and compare with experimental high-resolution spectra. Such complexes are very oppy, they exhibit large amplitude vibration, internal rotation, and tunneling motions, and the spectra are extremely sensitive to the shape of the anharmonic wells in the potential and to the barriers between these wells.
>
> I will illustrate this by showing the latest knowledge of the pair and many-body potential of water, the application of some new potentials to the vibration-rotation- tunneling (VRT) spectra of the normal and perdeuterated water dimer and trimer, and the importance of this knowledge to establish the role of many-body forces in determining the intriguing properties of liquid water [Avoird 1].

The lecture by Moszynski was entitled *Dielectric and optical properties of dilute atomic gases*. His abstract, which again can be found on the Quantum Systems website (quantumsystems.googlepages.com), is as follows:

> Symmetry-adapted perturbation theory of intermolecular forces can be applied to compute the components of the interaction-induced polarizability tensor for atomic and molecular dimers. In my talk I will show on the example of the helium diatom how modern quantum chemical methods coupled with the quantum-statistical treatment can be applied with trust to describe the binary collision-induced Raman spectra, second dielectric virial coefficients, and second Kerr virial coefficients. Special attention will be paid to the state-of-the-art ab initio techniques for the calculation of the interaction-induced polarizability tensor invariants and to methods needed on the route from the polarizability tensor invariants to various macroscopic (optical and dielectric) properties of dilute atomic gases. General relations between the dielectric and Kerr virial coefficients and the thermodynamic (pressure) virial coefficients will be given, and the exact expressions within the quantum-statistical mechanics will be introduced. Nearly exact calculations of the binary collision-induced Raman spectra, second dielectric virial coefficients, and second Kerr virial coefficients will be reported, and compared with the available experimental data.

This paper was co-authored by W. Skomorowski.

The Chair for Session 7 was Professor Trygve Helgaker of the University of Oslo.

Session 8: 16:00, 1 September, 2007

Robert Harrison from Oak Ridge National Laboratory discussed *Computational chemistry at the petascale* in the first lecture of this Session. His co-authors were E. Apra, B.G. Sumpter, W.A. Shelton, V. Meunier, A. Beste and S. Sugiki from the Computational Chemical Sciences Group at Oak Ridge National Laboratory. Harrison described work to enable computational science at the petascale. He motivated this work by reference to ongoing scientific applications in chemistry and nanoscience. His abstract, which can be found on the Quantum Systems website (quantumsystems.googlepages.com), is as follows:

> By mid-2009, one or more institutions around the world will have available for open-science-use computers with a theoretical peak speed of over 1015 floatingpoint operations

per second (1 PFLOP). By 2011-2, machines with a sustained speed of 1 PFLOP and peak speeds in excess of 10 PFLOP are anticipated. These machines represent government investment in theoretical and computational science that for the first time starts to approach that made in large experimental photon and neutron sources. The potential for scientific discovery is truly profound. To appreciate the true scale of these machines consider a typical department cluster of 120 processors which provides about 1M cpu-hours per year a PFLOP computer can deliver that in about 8 hours which represents a dramatic compression of the time scale required for quantitative and predictive simulation. PFLOP computers are anticipated to have circa 2-500 terabytes of physical memory that will enable truly huge data-intensive simulations. However, we chemists are in danger of not being able to benefit from these exciting capabilties. Once at the forefront of scientific simulation, computational chemistry codes in general do not function efficiently on present TFLOP computers and have no credible path forward to machines 1000× larger. Even for those researchers without immediate access to such machines this is not an academic issue since todays supercomputer is tomorrows departmental resource, and the issues of multi-core technology and memory hierarchy are present in all modern computers.

In the second lecture of this session, Professor Boris N. Plakhutin, from the Russian Academy of Sciences in Novosibirsk, spoke on *Koopmans theorem in the ROHF method: General formulation*. The paper was co-authored by E.R. Davidson.

The Session closed with a lecture by Professor J. Maruani on *Electron Cross Relaxation as a function of Single Relaxation Contributions in 1s- 2p- Double Core Ionization Energies and Spin-orbit Splitting of Atoms from Al to Ba*. This paper was co-authored by C. Bonnelle. Maruani has contributed to this volume on a related topic.

Session 8 was chaired by Professor Hiroshi Nakatsuij from Kyoto University.

After dinner, the second poster session was held. Again, a selection of the papers presented is included in this volume.

On Sunday, 2 September, members of the workshop enjoyed a trip to Windsor Castle see (Fig. 1), which lies at the heart of Windsor Great Park. “Windsor Castle is an official residence of The Queen and the largest occupied castle in the world.

Fig. 1 Windsor Castle, official residence of The Queen and the largest occupied castle in the world, was the venue for the workshop outing on Sunday, 2 September, 2007. The visit provided an opportunity for informal discussions

A Royal home and fortress for over 900 years, the Castle remains a working palace today".[1] The visit provided an opportunity for informal discussions whilst enjoying the many unique attractions in the castle complex.

Session 9: 09:00, 3 September, 2007

Session 9 was the first of the four Sessions held on Monday, 3 September, 2007. The structure of the day is shown in Table 3. Again there were two sessions in the morning and two in the afternoon.

Professor Antonio Varandas from the University of Coimbra gave the first lecture which he entitled *Highly accurate potential energy surfaces via conventional ab initio methods: calculation and use in dynamics*. The abstract for this paper is as follows:

> This talk consists of two parts. First, we discuss a method to predict the potential energy surface (PES) of a molecule at a high level of ab initio theory by performing calculations with smaller basis sets and then scaling the electron correlation (in part or in all) at one [Varandas 1] or more [Varandas 2] geometries (pivots) calculated with the larger target basis set. The ability of this correlation scaling (CS) scheme to predict a PES corresponding to a larger basis set from smaller basis set calculations is then combined [Varandas 2] with the extrapolation to the complete basis set limit by using the uniform singlet and triplet-pair extrapolation [Varandas 3] (USTE) method. The full scheme allows a highly accurate PES to be obtained at a reasonable cost without resorting to any empiricism. Although applied thus far mostly to ground-state electronic PESs, the method is in principle valid for the complete manifold of electronic states. Since the whole procedure can be analytic, it may open a way for accurate on-the-fly dynamics studies. In the second part of the talk, we survey ongoing work on electronic manifolds that been calculated by ab initio methods and modeled using DMBE (double many-body expansion) theory, as well as on the corresponding nuclear dynamics. The focus will then be on H^{+}_{3} (in its lowest singlet and triplet electronic states [Varandas 4]) and ground-state HN_2 [Varandas 5], and the implications of the geometrical phase.

The second lecture in this Session was delivered by Professor Ioan Bâldea from the University of Heidelberg. His paper, which is co-authored with L. Cederbaum, is included in this volume. It is entitled *Unusual features in optical absorption and photo-ionization of quantum dot nanorings*.

The Chair for Session 9 was Professor Vincenzo Aquilanti of the University of Perugia.

Session 10: 11:00, 3 September, 2007

Session 10, which was chaired by Stephen Wilson, consisted of two lectures. The first by Hiromi Nakai of Waseda University was entitled *Novel Linear Scaling Techniques based on Divide-and-Conquer Method*.

[1] www.royal.gov.uk/OutPut/Page557.asp.

Table 3 Lectures delivered on the fifth day of the workshop, Monday, 3 September, 2007

- Session 9 (Chair: V. Aquilanti)

  Highly accurate potential energy surfaces via conventional ab initio methods: calculation and use in dynamics

  A.J.C. Varandas (Universidade de Coimbra)

  Unusual features in optical absorption and photo-ionization of quantum dot nanorings

  I. Bâldea (Universität Heidelberg)

- Session 10 (Chair: S. Wilson)

  Novel Linear Scaling Techniques based on Divide-and-Conquer Method

  H. Nakai (Waseda University)

  New methods for calculating vibrational wave functions, energies and molecular properties

  O. Christiansenn (University of øArhus)

- Session 11 (Chair: G. Delgado-Barrio)

  Approximate methods for ab initio calculations of very large molecules

  S. Li (Nanjing University)

  Combined QM/MM methods: Developments and applications

  Q. Cui (University of Wisconsin-Madison)

- Session 12 (Chair: E. Brändas)

  The Current State of Ab Initio Calculations of Optical Rotation and Electronic Circular Dichroism Spectra

  T.D. Crawford (Virginia Tech)

  A General Scheme for Higher Order SCF Responses

  K. Ruud (University of Tromsø)

  G-Invariant, QP-Carrier Space Map-theoretic Quantal Completeness of $\{T^k_{\tilde{v}}(11.1)\}$ Tensorial Sets: Role of S-duality in NMR Spin Dynamics

  F.P. Temme (Queens University)

The divide-and-conquer (DC) method proposed by Yang et al. [Nakai 1, Nakai 2] is one of the linear-scaling techniques, which avoids explicit diagonalization of the Fock matrix and reduces the Fock elements. So far, the DC method has been applied mainly to pure density functional theory (DFT) or semi-empirical molecular orbital (MO) calculations. We have applies the DC method to such calculations including the HartreeFock (HF) exchange terms as the HF and hybrid HF/DFT [Nakai 3]. Reliability of the DC-HF and DC-hybrid HF/DFT has been confirmed when adopting an adequate cut-off radius, which defines the localization region in the DC formalism. This dependence on the cut-off radius has been assessed from various points of view: that is, total energy, energy components, local energies, and density of states. Next, we have proposed a novel linear-scaling scheme for obtaining the second-order Mller-Plesset perturbation (MP2) energies based on the DC technique. This method, which we call DC-MP2 [Nakai 4], evaluates the correlation energy of the total system

by summing up DC subsystem contributions. The correlation energy corresponding to a subsystem is calculated from subsystem orbitals based on a scheme for partitioning the correlation energy, which is derived by analogy with the energy density analysis (EDA) [Nakai 5]. Numerical assessments have revealed that the present scheme provides reliable correlation energies with considerably less computational costs than the conventional canonical MP2 calculations.

Nakai's co-authors were M. Kobayashi and T. Akama.

The second lecture in Session 10 was given by Professor Ove Christiansenn, from the University of Åarhus, gave the second lecture of this Session. He subject was *New methods for calculating vibrational wave functions, energies and molecular properties*.

Recently a new formulation for the description of the dynamics of molecular systems has been developed [Christiansen 1]. The formalism is similar in spirit to the second quantization formulation of electronic structure theory. On the basis of this formalism a new program package and a number of new quantum mchanical based computational have been developed [Christiansen 1, Christiansen 3, Christiansen 4] and are currently being further developed for applications in many different contexts. The primary focus here is on methods for calculating bound states, in particular vibrational wave functions. In this talk we shall consider the theory and use of vibrations self consistent field (VSCF) [Christiansen 8], vibrational Møller Plesseth perturbation theory (VMP) [Christiansen 3, Christiansen 9], vibrational configuration interaction (VCI) [Christiansen 2, Christiansen 10] and vibrational coupled cluster (VCC) [Christiansen 1, Christiansen 2], as well as vibrational response theory. I shall describe benchmark calculation relating to various convergence issues [Christiansen 2, Christiansen 3, Christiansen 4, Christiansen 5, Christiansen 6, Christiansen 7]. I will describe certain aspects of the implementation in the MidasCpp program aiming at VSCF, VMP2, VCI, and VCC calculations on large molecular systems. New initiatives towards using the developed methods in calculating vibrational contributions to molecular properties shall be discussed [Christiansen 4] as well as new steps towards efficient application to larger molecules.

Session 11: 14:00, 3 September, 2007

Professor Shuhua Li of the School of Chemistry and Chemical Engineering, Key Laboratory of Mesoscopic Chemistry of Ministry of Education, Institute of Theoretical and Computational Chemistry, Nanjing University opened Session 11 with his lecture entitled *Approximate methods for ab initio calculations of large molecules*. He described "several molecular fragmentation approaches, which enable approximate Hartree-Fock (HF) and post-HF calculations of very large molecules to become routinely feasible [Li 1, Li 2, Li 3, Li 4]. The essence of these fragmentation methods is to divide a large molecule into a series of capped fragments (or subsystems), and then obtain the approximate energy or various properties of this molecule from constructed subsystems in some way. These methods are based on the high transferability of the localized molecular orbitals, or the fragment energies between subsystems and the parent molecule, respectively. Our test calculations demonstrated that these linear scaling techniques are able to reproduce the conventional HF or post-HF energies quite accurately for a wide variety of macromolecules

and molecular clusters. Especially, the energy-based fragmentation approach, combined with the existing quantum chemistry programs, can be directly employed to obtain optimized geometries, vibrational frequencies, and some molecular properties for very large molecules at the ab initio level. Illustrative calculations showed that this approach provides encouraging results for ground-state energies, structures, and dipole moments (or static polarizabilities) for various neutral or charged large molecules." Li has contributed to this volume.

Development and application of effective QM/MM methods for complex biological systems was the subject of the second lecture in Session 11 which was delivered by Professor Qiang Cui of the University of Wisconsin-Madison. His abstract, which can be found on the Quantum Systems website (quantumsystems.googlepages.com), is as follows:

> Motivated by the long-term goal of understanding vectorial biological processes such as proton transport in biomolecular ion pumps and energy transduction in biomolecular motors, a number of developments have been made in our group to establish combined quantum mechanical/molecular mechanical (QM/MM) methods suitable for studying complex chemical reactions in the condensed phase. These developments will be briefly summarized and discussed with representative applications. Specifically, free energy perturbation and boundary potential methods for treating long-range electrostatics have been implemented to test the robustness of QM/MM results for protein systems. It is shown that consistent models with sufficient sampling are able to produce quantitatively satisfactory results, such as pKa for titritable groups in the interior of proteins while an inconsistent treatment of electrostatics or lack of sufficient sampling may produce incorrect results. Modifications have been made to an approximate density functional theory (SCC-DFTB) to improve the description of proton affinity, hydrogen-bonding and phosphate chemistry, which are crucial for studying the systems of interest. Applications of the SCC-DFTB/MM methods generated novel insights into several biological problems, which include the role of proton hole in long-range proton transfers in the enzyme carbonic anhydrase and mechanochemical coupling in the molecular motor myosin.

Session 11 was chaired by Gerardo Delgado-Barrio.

Session 12: 16:00, 3 September, 2007

Session 12 began with a lecture entitled *The Current State of Ab Initio Calculations of Optical Rotation and Electronic Circular Dichroism Spectra* by Professor T. Daniel Crawford of Virginia Tech. His abstract, which can be found on the Quantum Systems website (quantumsystems.googlepages.com), is as follows:

> The current ability of ab initio models to yield accurate and reliable chiroptical properties such as optical rotatory dispersion and electronic circular dichroism spectra is reviewed. Comparison between coupled cluster linear response theory and experimental data (both gas- and liquid-phase) yield encouraging results for small to medium-sized chiral molecules including rigid species such as (S)-2-chloropropionitrile and (P)-[4]triangulane, as well as conformationally flexible molecules such as (R)-epichlorohydrin. More problematic comparisons are offered by (S)-methyloxirane, (S)-methylthiirane, and (1S,4S)-norbornenone, for which the comparison between theory and experiment is much poorer. The impact of basis-set incompleteness, electron correlation, zero-point vibration, and temperature are

discussed. In addition, future prospects and obstacles for the development of efficient and reliable quantum chemical models of optical activity are discussed.

Professor Kenneth Ruud of the University of Tromsø lectured on *A general scheme for higher-order SCF responses*. His abstract is as follows:

In the talk, a general formalism for the calculation of higher-order molecular properties will be presented. The formalism combines the quasi-energy [Ruud 1] and Lagrangian formalisms [Ruud 2] to derive expressions for response functions as derivatives of an SCF quasi-energy Lagrangian with respect to any external perturbation. The formalism can handle both time-dependent and static perturbations, as well take into account any dependence in the atomic basis set on the externally applied perturbations (such as perturbations due to the distortion of the nuclear framework or explicit magnetic-field dependent basis sets such as London atomic orbitals [Ruud 3] used to obtain magnetic gauge-origin independent results). The formalism uses the AO density matrix as the basic parameter, allowing us to utilize recent advances made in the field of linear-scaling methodology for the calculation of molecular properties [Ruud 4, Ruud 5]. Care is taken to reduce computational cost, allowing for maximum efficiency if the formalism is used in a linear-scaling approach. The implementation is focused on defining generic building blocks, making it straightforward to implement molecular properties of arbitrary order given that the required one- and two-electron integrals (and potentially DFT exchange-correlation kernels) are available. The code can, if computationally most efficient, utilize the 2n+1 rule for higher-order energy corrections, or instead calculate higher-order perturbed density matrices in cases where one perturbation has many components, thus avoiding the solution of response equations for these components (e.g. first-order geometry derivatives of the polarizability of large molecules). In addition to giving an introduction to the formalism and illustrating how the elementary building blocks of the formalism allows for the easy implementation of higher-order molecular properties, a few numerical examples will also be given.

Ruud's lecture was co-authored by A.J. Thorvaldsen.

The final lecture scheduled for delivery in Session 12 was cancelled. However, the author, Professor Francis Temme of Queen's University, has contributed to this volume.

Professor Erkki Brändas of Uppsala University chaired Session 12.

The four Sessions held on Tuesday, 4 September, 2007, are summarized in Table 4. Again there were two sessions in the morning and two in the afternoon.

Session 13: 09:00, 4 September, 2007

This session opened with a lecture on *Collision-induced absorption and light scattering by hydrogen molecule pairs* by Professor Katharine Hunt from Michigan State University. Her abstract reads as follows:

During collisions between molecules, interactions may break the symmetry of the isolated molecules, producing transient induced dipoles, and thus allowing the absorption of radiation in spectroscopic processes that are single-molecule forbidden. Similarly, transient changes in molecular polarizabilities give rise to collision-induced light scattering, impulsive stimulated scattering, and subpicosecond induced birefringence; the collision-induced changes in polarizabilities also affect refractive indices and dielectric functions of compressed gases and liquids. We have determined the dipoles and polarizabilities of pairs of

Table 4 Lectures delivered on the sixth day of the workshop, Tuesday, 4 September, 2007

- Session 13 (Chair: R.J. Harrison)

  Collision-induced absorption and light scattering by hydrogen molecule pairs

  K.L.C. Hunt (Michigan State University)

  Evidences of Macroscopic Quantum Entanglement of Protons in The Crystal of $KHCO_3$: Neutron Scattering Studies

  F. Fillaux (Universit Pierre et Marie Curie)

- Session 14 (Chair: I.G. Kaplan)

  Can quantum mechanics really handle systems consisting of VERY many atoms? Can Density Functional Theory and Nearsightedness help?

  W. Kohn (University of California, Santa Barbara)

  Theoretical investigation of the first row transition metal Borides, MB, M = Sc, Ti, V, Cr, Mn, Fe, Co, Ni and Cu

  D. Tzeli (National and Kapodistrian University of Athens)

- Session 15 (Chair: A.J.C. Varandas)

  Ab initio Intermolecular Potentials and Dynamics of Rg_2-Dihalogen Clusters

  G. Delgado-Barrio (Consejo Superior de Investigaciones Cientificas, Madrid)

  A simple stochastic theory of line-shape broadening in quasielastic He atom scattering with interacting adsorbates

  S. Miret-Arts (Consejo Superior de Investigaciones Cientificas, Madrid)

- Session 16 (Chair: H. Nakai)

  Quantum theory of chemical reactions: potential energy surfaces, resonances, cross sections, rate constants

  V. Aquilanti (Universit degli Studi di Perugia)

  The $O_2 + O_2$ systems. Some theoretical insights and experiments

  J. Campos-Martinez (Consejo Superior de Investigaciones Cientificas, Madrid)

  Stability of equilibrium under constraints

  T. Gal (University of Debrecen)

hydrogen molecules at the CCSD(T) level, with an aug-cc-pV5Z (spdf) basis set, for 18 different relative orientations of the two molecules, and intermolecular separations ranging from 2 a.u. to 10 a.u. [Hunt 1] For the two relative orientations of the hydrogen pair (linear and T-shaped) previously studied by Maroulis [Hunt 2] using a 6s4p1d basis and a fixed intermolecular separation of 6.5 a.u., we find good agreement of the $\Delta\alpha$ values. Our results for the collision-induced anisotropic polarizability also agree well with those obtained by Bounds [Hunt 3] using a much smaller basis for six relative orientations of the pair, but the values of the trace of $\Delta\alpha$ differ by factors of 2 or more from Bounds results. For use in spectroscopic line shape analyses, we have determined the coefficients for the expansions of the spherical tensor components of the pair dipole and polarizabilities as series in the

> spherical harmonics of the orientation angles of the two molecular axes and the intermolecular vector. As the intermolecular distance increases, the ab initio results for the spherical tensor components of $\Delta\mu$ and $\Delta\alpha$ converge to the results from long-range models that include dipole-induced-dipole interactions, quadrupole-induced dipoles, higher multipole induction, nonuniformity of the local field acting on each molecule, hyperpolarization, and van der Waals dispersion. [Hunt 4,Hunt 5] In the collision-induced polarizability, deviations from the first-order dipoleinduced- dipole model are still evident for molecular separations between 8 and 10 a.u., in most orientations of the pair. At short range, overlap damping, exchange, and orbital distortion reduce the trace and anisotropy of the collisioninduced polarizability below the long-range limiting forms.

Hunt and her co-author, X. Li, are from Michigan State University.

The second lecture of this Session was given by Professor Francois Fillaux of the Université Pierre et Marie Curie. His paper entitled *Evidences of Macroscopic Quantum Entanglement of Protons in The Crystal Of $KHCO_3$: Neutron Scattering Studies* is contained in this volume.

Session 13 was chaired by Professor Robert Harrison of Oak Ridge National Laboratory.

Session 14: 11:00, 4 September, 2007

In his lecture, Professor Walter Kohn, Nobel Laureate in Chemistry (1998), asked the question:

> *Can quantum mechanics really handle systems consisting of VERY many atoms? Can Density Functional Theory and 'Nearsightedness' help?*

He began by reminding us that "80 years ago, Schrödinger published his momentous equation which, in due course, revolutionized all of chemistry and much of physics. Properties of atoms, molecules, etc. could, for the first time, be 'accurately' calculated." He continued: "However, there was one important limitation: except for cases of high symmetry, only systems with less than $\sim$20 or 30 atoms were manageable." Beginning about 40 years ago, Density Functional Theory (DFT) extended this upper limit to $\sim$200 up to $\sim 1,000$ atoms with fairly good accuracy. Kohn reported some current work on further extensions and discussed possible "ultimate limits, taking advantage of a recently recognized fundamental property of fermions, called 'nearsightedness"'. (Professor Kohn is shown in Fig. 2 before the Workshop banquet which was held in the evening.)

The second lecture in this Session was given by Dr. Demeter Tzeli of the National and Kapodistrian University of Athens. Her paper entitled *Theoretical investigation of the first row transition Metal Borides, MB, M = Sc, Ti, V, Cr, Mn, Fe, Co, Ni and Cu* was co-authored by Professor Aristides Mavridis. Tzeli has contributed to this volume.

Session 14 was chaired by Professor Ilya Kaplan of Universidad Nacional Autónoma de México.

Fig. 2 Professor Walter Kohn *(right)*, Nobel Laureate in Chemistry 1998, is pictured here talking to Stephen Wilson *(Chair, QSCP-XII)* before the Workshop banquet. (Photograph by Boris N. Plakhutin)

Session 15: 14:00, 4 September, 2007

Session 15 began with a lecture entitled *Ab initio Intermolecular Potentials and Dynamics of Rg2-Dihalogen Clusters* by Professor Gerardo Delgado-Barrio from Consejo Superior de Investigaciones Cientificas, Madrid. His co-authors were R. Prosmiti, A. Valdés, C. Diez-Pardos and P. Villarreal. Delgado-Barrio has contributed to this volume.

The second lecture of this Session, which was chaired by Professor Antonio Varandas of the University of Coimbra, was entitled *A simple stochastic theory of line shape broadening in quasielastic He atom scattering with interacting adsorbates*. It was given by Professor Salvador Miret-Artés His co-authors were R. Martnez-Casadoa,b, J.L. Vega and A.S. Sanz. A paper is also contributed to this volume.

Session 15 was chaired by Professor Antonio Varandas of the University of Coimbra.

Session 16: 16:00, 4 September, 2007

The Chair for Session 16 was Professor Hiromi Nakai of Waseda University. Nakai introduced a lecture on *Quantum theory of chemical reactions: potential energy surfaces, resonances, cross sections, rate constants* given by Professor Vincenzo Aquilanti.

> In our laboratory, experimental and theoretical approaches are used for studying elementary chemical reactions. This presentation will focus on a prototypical example, that of fluorine atoms with hydrogen molecule or its deuterated isotopomer. Another example is the He + H_2 + reaction giving HeH^+ + H: for this reaction, the full route from the potential energy

surface to the cross section has also been studied. The fluorine reaction presents a variety of features, which are basic to chemical dynamics and kinetics.

Important aspects of this reaction are the open-shell and spin-orbit interactions in the atomic fluorine. These effects have been analyzed in detail and the entrance channel characteristics have been calibrated with respect to molecular beam scattering experiments carried out in our laboratory, where the atomic fluorine fine structure states have been monitored by Stern-Gerlach magnetic analysis. This has led to improved potential energy surfaces for this reaction, and to estimates of the role of non-adiabatic effects.

The exact quantum dynamics on the ground adiabatic potential energy surface has been carried out using hyperspherical coordinates and the hyperquantization algorithm. This algorithm has been developed by us to solve the very demanding problem of coupling among an extremely dense set of channels and yields very accurate scattering matrix elements.

For the scattering matrix as a function of energy and angular momentum, observable quantities such as cross sections and rate constants are generated: these quantities are compared with an ample set of experimental data which are available for this reaction. In particular, the branching ratio for the HD reaction, leading to HF or HD, has been determined as a prime example of the isotopic effects in chemical kinetics.

The hyperquantization algorithm program generates the full scattering matrix, that can be transformed in the stereodirected representation, introduced by us to exhibit orientation effects in quantum dynamics and therefore to provide a tool for the characterization of the steric effect. An important feature of this reaction is the role of resonances, that have been studied in detail regarding their energy ad angular momentum dependence, by the analysis of both the life time matrix in the energy domain and of poles in the complex angular momentum plane.

Aquilanti and his co-authors, S. Cavalli and D. De Fazio, cited a number of recent literature references [Aquilanti 1, Aquilanti 2, Aquilanti 3, Aquilanti 4, Aquilanti 5].

Professor José Campos-Martínez gave the second lecture of this Session. His paper, which is co-authored by E. Carmona-Novillo, M.I. Hernández, F. Dayou and R. Hernández-Lamoneda, is entitled *The O_2-O_2 system: Some theoretical insight into experimental data* and is included in the present volume.

There were two Sessions on the final day of the workshop, Wednesday 5 September, 2007, as summarized in Table 5.

Table 5 Lectures delivered on the seventh and final day of the workshop, Wednesday, 5 September, 2007

- Session 17 (Chair: A. Mavridis)

  Tracing Ultrafast Electronic Decay Processes in Real Time and Space
  A. Kuleff (Universität Heidelberg)

  A fresh viewpoint for the Kohn-Sham potential
  N.I. Gidopoulos (Rutherford Appleton Laboratory)

- Session 18 (Chair: P.J. Grout)

  Quantum Systems Forum

  Closing Remarks

Session 17: 09:00, 5 September, 2007

The first lecture of Session 17 was given by Professor Alexander Kuleff from the University of Heidelberg. In a paper co-author by L. Cederbaum, Kuleff spoke about *Tracing Ultrafast Electronic Decay Processes in Real Time and Space*. His abstract, which can be found on the Quantum Systems website (quantumsystems.googlepages.com), is as follows:

> An ab initio method for multielectron wave-packet propagation is presented [Kuleff 1]. It gives the possibility to describe fully ab initio the dynamics of various deexcitation processes taking into account all electrons of the system and their correlation. The approach is equally suitable for tracing in real time and space the electron dynamics of both decaying and non-decaying electronic states. As an example, the evolution of the electronic cloud throughout the interatomic Coulombic decay [Kuleff 2] (ICD) process in the rare gas cluster NeAr following Ne2s ionization is computed and analyzed [Kuleff 3].

The final lecture of this Session was given by Dr. Nikitas Gidopoulos of the Rutherford Appleton Laboratory. This talk replaced the scheduled lecture. Gidopoulos spoke on *A fresh viewpoint for the Kohn-Sham potential*.

The Chair for Session 17 was Professor Aristides Mavridis of the University of Athens.

Session 18: 11:00, 5 September, 2007 – Quantum Systems Forum

The Chair for the final session was Peter Grout of the University of Oxford. Grout led a wide ranging but informal discussion.

Many members of the workshop felt that QSCP offered a unique perspective on the study of the quantum many-body problem. Too often meetings concentrate on the computational aspects of the problem or on specific applications or application areas at the expense of the underlying theory. It was felt that the QSCP-XII workshop succeeded in its aims of bringing together chemists and physicists with a common interest in the study of many-body systems in an informal atmosphere so as to encourage discussion and foster collaboration on fundamental and innovative theory. A number of participants had expressed their appreciation of the specifically allocated discussion time of 10 or 15 minutes after each talk, which had been a new feature for the twelfth workshop. It was suggested that, if possible, this feature should be repeated at future workshops.

Some members suggested that in choosing venues for future workshops consideration should be given to the travel involved given the growing concern about air transport and its contribution to climate change. It was agreed that in planning future QSCP workshops their impact on climate change should be taken into account.

The meeting was closed by Stephen Wilson who thanked all who had contributed to the success of the workshop.

References

[Bishop 1] R.F. Bishop, in Microscopic Quantum Many-Body Theories and Their Applications, (eds. J. Navarro and A. Polls), Lecture Notes in Physics Vol. 510, Springer, Berlin (1998), 1.

[Bishop 2] C. Zeng, D.J.J. Farnell and R.F. Bishop, J. Stat. Phys. 90 (1998), 327; D.J.J. Farnell, R.F. Bishop and K.A. Gernoth, J. Stat. Phys. 108 (2002), 401.

[Bishop 3] D.J.J. Farnell and R.F. Bishop, in Quantum Magnetism, (eds. U. Schollwöck, J. Richter, D.J.J. Farnell and R.F. Bishop), Lecture Notes in Physics Vol. 645, Springer, Berlin (2004), 307.

[Bishop 4] R.F. Bishop, D.J.J. Farnell and J.B. Parkinson, Phys. Rev. B 58 (1998), 6394.

[Bishop 5] R.F. Bishop, D.J.J. Farnell and C. Zeng, Phys. Rev. B 59 (1999), 1000.

[Bishop 6] S.E. Krueger, J. Richter and J. Schulenburg, D.J.J. Farnell and R.F. Bishop, Phys. Rev. B 61 (2000), 14607.

[Bishop 7] D.J.J. Farnell, R.F. Bishop and K.A. Gernoth, Phys. Rev. B 63 (2001), 220402(R).

[Bishop 8] R.F. Bishop, Y.Xian and C. Zeng, Int. J. Quantum Chem. 55 (1995), 181.

[Helgaker 1] T. Helgaker, H. Larsen, J. Olsen and P. Jørgensen, Direct optimization of the AO density matrix in HartreeFock and KohnSham theories, Chem. Phys. Lett. 327, 397403 (2000).

[Helgaker 2] B. Jansk, S. Høst, P. Jørgensen, J. Olsen and T. Helgaker, Linear-scaling symmetric square-root decomposition of the overlap matrix, J. Chem. Phys. 126, 124104 (2007).

[Helgaker 3] P. Salek, S. Høst, L. Thøgersen, P. Jørgensen, P. Manninen, J. Olsen, B. Jansk, S. Reine, F. Pawlowski, E. Tellgren, T. Helgaker and S. Coriani, Linear-scaling implementation of molecular electronic self-consistent field theory, J. Chem. Phys. 126, 114110 (2007).

[Helgaker 4] S. Coriani, S. Høst, B. Jansk, L. Thøgersen, J. Olsen, P. Jørgensen, S. Reine, F. Pawlowski, T. Helgaker and P. Salek, Linear-scaling implementation of molecular response theory in self-consistent field electronic-structure theory, J. Chem. Phys. 126, 154108 (2007).

[Nakatsuji 1] H. Nakatsuji, J. Chem. Phys. 113, 2949 (2000); H. Nakatsuji and E. R. Davidson, J. Chem. Phys. 115, 2000 (2001); H. Nakatsuji and M. Ehara, J. Chem. Phys. 117, 9 (2002); 122, 194108 (2005).

[Nakatsuji 2] H. Nakatsuji, Phys. Rev. Lett. 93, 030403 (2004); Phys. Rev. A, 72, 062110 (2005).

[Nakatsuji 3] Y. Kurokawa, H. Nakashima and H. Nakatsuji, Phys. Rev. A, 72, 062502 (2005).

[Nakatsuji 4] H. Nakatsuji and H. Nakashima, Phys. Rev. Lett. 95, 050407 (2005).

[Nakatsuji 5] R. Fukuda and H. Nakatsuji, submitted.

[Nakatsuji 6] K. Fujimoto, J. Hasegawa, S. Hayashi, S. Kato and H. Nakatsuji, Chem. Phys. Lett., 414, 239 (2005); K. Fujimoto, J. Hasegawa, S. Hayashi and H. Nakatsuji, Chem. Phys. Lett. 432, 252 (2006); K. Fujimoto, S. Hayashi, J. Hasegawa and H. Nakatsuji, J. Chem. Theo. Comp. 3, 605–618 (2007).

[Nakatsuji 7] N. Nakatani, J. Hasegawa and H. Nakatsuji, J. Am. Chem. Soc., 129, 8756 (2007).

[Nakatsuji 8] H. Nakatsuji, T. Miyahara and R. Fukuda, J. Chem. Phys. 126, 084104 (2007).

[Chan 1] J. Hachmann, W. Cardoen, and G.K.-L. Chan, J. Chem. Phys. 125, 144101 (2006).

[Chan 2] T. Yanai and G.K.-L. Chan J. Chem. Phys. 124, 194106 (2006).

[Scuseria 1] J. Heyd, G.E. Scuseria, and M. Ernzerhof, J. Chem. Phys. 118, 8207 (2003); J. Heyd and G. E. Scuseria, J. Chem. Phys. 120, 7274 (2004); J. Heyd and G. E. Scuseria, J. Chem. Phys. 121, 1187 (2005).

[Scuseria 2] J. Heyd, J.E. Peralta, G.E. Scuseria and R.L. Martin, J. Chem. Phys. 128, 174101 (2005); J. E. Peralta, J. Heyd, G. E. Scuseria and R. L. Martin, Phys. Rev. B 74, 073101 (2006).
[Scuseria 3] E.R. Batista, J. Heyd, R.G. Hennig, B.P. Uberuaga, R.L. Martin, G.E. Scuseria, C.J. Umrigar and J.W. Wilkins, Phys. Rev. B 74, 121102(R) (2006).
[Scuseria 4] I.D. Prodan, G.E. Scuseria, and R.L. Martin, Phys. Rev. B 73, 045104 (2006).
[Scuseria 5] B.G. Janesko and G.E. Scuseria, J. Chem. Phys. 127, 164322 (2007).
[Scuseria 6] J. Jaramillo, M. Ernzerhof and G. E. Scuseria, J. Chem. Phys. 118, 1068 (2003).
[Burke 1] J.P. Perdew, L.A. Constantin, E. Sagvolden and K. Burke, Phys. Rev. Lett. 97, 223002 (2006).
[Burke 2] J. Perdew, A. Ruzsinszky, G.I. Csonka, O.A. Vydrov, G.E. Scuseria, L.A. Constantin, X. Zhou and K. Burke, arXiv:0707.2088.
[Karwowski 1] I.P. Grant, Relativistic Quantum Theory of Atoms and Molecules, Springer Series on Atomic, Optical, and Plasma Physics, vol. 40, Heidelberg 2006.
[Karwowski 2] G. Pestka, M. Bylicki and J. Karwowski, J. Phys. B: At. Mol. Opt. Phys. 39 (2006) 2979; ibid. 40 (2007) 2249–2259.
[Avoird 1] R. Bukowski, K. Szalewicz, G. C. Groenenboom and A. van der Avoird, Science 315, 1249 (2007).
[Varandas 1] A.J.C. Varandas and P. Piecuch, Chem. Phys. Lett. 430, 448 (2006).
[Varandas 2] A.J.C. Varandas, Chem. Phys. Lett. 443, 398 (2007). J. Chem. Phys. 126, 244105 (2007).
[Varandas 3] A.J.C. Varandas, J. Chem. Phys. 126, 244105 (2007); Phys. Scr. (Comm. Atom. Opt. & Mol. Phys.) 76, C28 (2007).
[Varandas 4] L.P. Viegas, A. Alijah and A.J.C. Varandas, J. Chem. Phys. 126, 074309 (2007); and references therein.
[Varandas 5] V.C. Mota and A.J.C. Varandas, J. Phys. Chem. A 111, 10191 (2007).
[Nakai 1] W. Yang, Phys. Rev. Lett., 66, 1438 (1991).
[Nakai 2] W. Yang and T.-S. Lee, J. Chem. Phys., 103, 5674 (1995).
[Nakai 3] T. Akama, M. Kobayashi and H. Nakai, J. Comput. Chem. 28, 2003 (2007).
[Nakai 4] M. Kobayashi, Y. Imamura and H. Nakai, J. Chem. Phys. 127, 074103 (2007).
[Nakai 5] H. Nakai, Chem. Phys. Lett., 363, 73 (2002).
[Christiansen 1] O. Christiansenn, J. Chem. Phys, 120, 2140 (2004).
[Christiansen 2] O. Christiansenn, J. Chem. Phys, 120, 2149 (2004).
[Christiansen 3] O. Christiansenn, J. Chem. Phys, 119, 5773 (2003).
[Christiansen 4] O. Christiansenn, J. Chem. Phys. 122, 194105 (2005).
[Christiansen 5] J. Kongsted and O. Christiansenn, J. Chem. Phys. 125, 124108 (2006).
[Christiansen 6] P. Seidler and O. Christiansenn, J. Chem. Phys. 126, 204101 (2007).
[Christiansen 7] O. Christiansenn, J. Kongsted, M. J. Paterson and J. M. Luis, J. Chem. Phys. 125, 214309 (2006).
[Christiansen 8] O. Christiansenn and J. M. Luis, Int. J. Quantum. Chem. 104, 667 (2005), Spec. Issue.
[Christiansen 9] J.M. Bowman, J. Chem. Phys, 68, 608 (1978).
[Christiansen 10] L.S. Norris, M.A. Ratner, A.E. Roitberg and R.B. Gerber, J. Chem. Phys, 105, 11261 (1996).
[Christiansen 11] S. Carter, J.M. Bowman and N.C. Handy, Theor. Chim. Acta. 100, 191 (1998).
[Li 1] S. Li, W. Li and T. Fang, J. Am. Chem. Soc. 127, 7215 (2005).
[Li 2] W. Li and S. Li, J. Chem. Phys. 122, 194109 (2005).
[Li 3] W. Li, T. Fang and S. Li J. Chem. Phys. 124, 154102 (2006).
[Li 4] W. Li, S. Li and Y. Jiang J. Phys. Chem. A 111, 2193 (2007).
[Ruud 1] O. Christiansenn, P. Jørgensen and C. Hättig. Int. J. Quantum Chem. 68, 1 (1998).
[Ruud 2] T. Helgaker, P. Jrgensen and N.C. Handy. Theor. Chim. Acta 76, 227 (1989).
[Ruud 3] F. London, J. Phys. Radium 8, 397 (1937).
[Ruud 4] M. A. Watson, P. Sa lek, P. Macak and T. Helgaker. J. Chem. Phys. 121, 2915 (2004).

[Ruud 5] C. Ochsenfeld, J. Kussmann and F. Koziol. Angew. Chemie, Int. Ed. 43, 4485 (2004).
[Hunt 1] X. Li, C. Ahuja, J. F. Harrison and K. L. C. Hunt, J. Chem. Phys. 126, 214302 (2007).
[Hunt 2] G. Maroulis, J. Phys. Chem. A 104, 4772 (2000).
[Hunt 3] D. G. Bounds, Molec. Phys. 38, 2099 (1979).
[Hunt 4] X. Li and K.L.C. Hunt, J. Chem. Phys. 100, 7875 (1994).
[Hunt 5] X. Li and K.L.C. Hunt, J. Chem. Phys. 100, 9276 (1994).
[Aquilanti 1] D. Sokolovski, S.K. Sen, V. Aquilanti, S. Cavalli and D.De Fazio, J. Chem. Phys. 126, 084305 (2007).
[Aquilanti 2] D. De Fazio, V. Aquilanti, S. Cavalli, A. Aguilar and J. M. Lucas, J. Chem. Phys. 125, 133109 (2006).
[Aquilanti 3] T.A. Grinev, T.V. Tscherbul, A.A. Buchachenko, S. Cavalli and V. Aquilanti, J. Phys. Chem A 110, 5458 (2006).
[Aquilanti 4] V. Aquilanti, S. Cavalli, D. De Fazio, A. Simoni and T.V. Tscherbul, J. Chem. Phys. 123, 054314 (2005).
[Aquilanti 5] V. Aquilanti, S. Cavalli, D. De Fazio, A. Volpi, A. Aguilar, J.M. Lucas, Chem. Phys. 308, 237 (2005).
[Kuleff 1] A.I. Kuleff, J. Breidbach and L.S. Cederbaum, J. Chem. Phys. 123, 044111 (2005).
[Kuleff 2] L.S. Cederbaum, J. Zobeley and F. Tarantelli, Phys. Rev. Lett. 79, 4778 (1997).
[Kuleff 3] A.I. Kuleff and L.S. Cederbaum, Phys. Rev. Lett. 98, 083201 (2007).

Part II
Proceedings

Study of the Electronic Structure of the Unconventional Superconductor Sr_2RuO_4 by the Embedded Cluster Method

Ilya G. Kaplan(✉) and Jacques Soullard

Abstract After a short account of the present state in the superconductivity (SC), the non-copper perovskite ruthenate, Sr_2RuO_4, superconductor is discussed. This superconductor possesses unconventional spin-triplet symmetry of Cooper's pairs and has been a subject of intense researches. It was revealed that the substitution of Ru atoms by small amount of non-magnetic Ti atoms leads to creation of magnetic order and destruction of superconductivity. Comparative study of the electronic structure of pure and Ti-doped Sr_2RuO_4 was performed by the developed by our group embedded cluster method at the Hartree-Fock and MP2 electron correlation level. The representative cluster was embedded into the *Madelung* potential that mimic a real crystal. Accounting of interatomic interaction in our calculations leads, in contrast with the tight-binding model usually applied for study Sr_2RuO_4, to the large electron transfer from O to Ru. Already at the HF level the ionic model failed. At the MP2 level, the electron correlation considerably increases the electron transfer making the values of charges on atoms far enough from the charges in the formal ionic model. Calculation at the DFT level gives the similar results.

The Ti substitution induces the essential charge redistribution between d-orbitals of Ru. A drastic effect of the Ti impurity on the spin density distribution was revealed. In the Ti-substituted crystals, the local spin density near impurity disappears on Sr and localizes on Ru and four O atoms surrounding it. The NBO analysis shows that the spin density in doped crystals is localized on orbitals directed along z axis. These results are in complete agreement with experiments.

Keywords: Unconventional superconductivity, Impurity effect, Ruthenate, Electronic correction

I.G. Kaplan
Instituto de Investigaciones en Materiales, Universidad Nacional Autónoma de, México, A.P. 70-360, 04510 México, D.F., México, e-mail: kaplan@iim.unam.mx

J. Soullard
Instituto de Física, Universidad Nacional Autónoma de México, A.P.20-364, 01000, México, D.F., México

S. Wilson et al. (eds.) *Frontiers in Quantum Systems in Chemistry and Physics*.

1 Introduction and Background

Superconductivity (SC) was discovered in 1911 in liquid Hg by Kamerlingh-Onnes and during subsequent 75 years the progress with increasing of the critical temperature, T_c, was very slow.

Date	1911	1913	1930	1954	1971	1973
T_c, K	4.1	7.2	9.2	18.1	20.3	23.2
Substance	Hg	Pb	Nb	Nb_3Sn	Nb_3Ga	Nb_3Ge

Till 1986 $T_c = 23.2\,K$ for the alloy Nb_3Ge was the maximum critical temperature. The discovery of high-Tc SC with T_c = appr. 30 K in $La_{2-x}Ba_xCuO_4$ by George Bednorz and Alex Müller (IBM Zurich Research Lab.) was not expected. Their paper initially was rejected by Physical Review Letters and published later, in September 1986, in other journal [1].

Boom or "golden rush", started only after S. Tanaka (Tokyo University) in November 1986 confirmed the Bednorz-Müller results. Immediately they were reproduced in many physical laboratories. Paul Chu (University of Houston) in February 1987 using Y-ceramics obtained in $YBa_2Cu_3O_{7-x}$ $T_c = 93\,K$ that was above liquid nitrogen temperature. These results were reported on 1987 March APS meeting in New York at an historical marathon session that is often named "Woodstock of physics", as a reference to the legendary 1969 Woodstock Music and Art Festival. In the same 1987 year Bednorz and Müller won the Nobel Prize.

At present, it is more than 150 HTSC-compounds with $T_c > 23\,K$ are synthesized. The maximum $T_c = 134\,K$ was achieved in 1993 for the Hg-ceramics, $HgBa_2CaCu_2O_{6+x}$, at normal conditions and it is 164 K under pressure, see reviews [2, 3].

There are many factors that produce an effect on T_c. In high T_c cuprates, one of the crucial is the oxygen concentration

(a) YBa_2CuO_x

x	6.9	6.7	6.3
T_c, K	90	60	0

(b) $TlBa_2CuO_x$

x	5.90	5.95	6.0
T_c, K	80	60	15

At present, the explanation of such drastic effect does not exist.

HTSC with $T_c > 30\,K$ was also observed in non-Cu and non-O materials, e.g. MgB_2 ($T_c = 39\,K$), and even in organic molecular compounds. In alkali-metal doped fullerene structures A_3C_{60} $T_c = 52\,K$ [4]. In 2001 was revealed that T_c rises when

the single crystal C_{60} is intercalated by some organic molecules, it "expands" C_{60}-crystal. For the intercalated crystal $C_{60} \cdot CHBr_3$, a very high transition temperature was achieved, $T_c = 117\,K$ [5].

In spite of such progress in the creation of new superconducting materials, the search has been performed empirically by the *trial-and-error* method. The predictive theory that connects T_c with peculiarities of the electronic and crystal structure of superconductor still does not exist. The study of the electronic structure of superconducting materials must help to understand the mechanism of high-T_c SC.

In this aspect it is instructive to study unconventional superconductors. Among them Sr_2RuO_4 discovered by Maeno et al. [6] in 1994 attracts a strong interest [7]. It has a layered perovskite structure as La_2CuO_4. But if the latter with a small Ba substitution belongs to high-Tc SC, Sr_2RuO_4 is a low-Tc SC with $T_c = 1.5\,K$. However, the main characteristic of Sr_2RuO_4, which make it *unconventional*, is the triplet spin state of its Cooper's pairs.

The wave function of Cooper's pair must obey the Pauli principle, that is, be antisymmetric. In nonrelativistic approach, it can be presented as a product of orbital and spin wave functions

$$\Psi_a(1,2) = \Phi_{orb}^{[\lambda]} \Omega_{spin}^{[\tilde{\lambda}]}. \tag{1}$$

Young diagram $[\lambda]$ is dual to $[\tilde{\lambda}]$.They determine the permutation symmetry. For two electrons there are only two possibilities

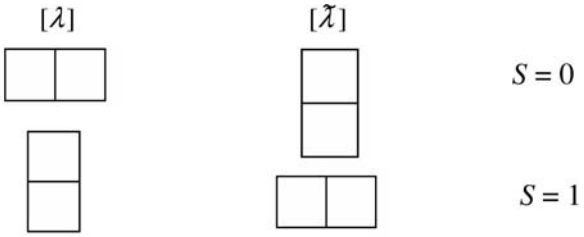

$$\Psi_a(S=0) = \Phi_{orb}^{[2]} \Omega_{spin}^{[1^2]} = \frac{1}{\sqrt{2}} \left[\varphi_1(1)\varphi_2(2) + \varphi_1(2)\varphi_2(1)\right] \Omega_{spin}^{[1^2]} \quad (S=0) \tag{2}$$

$$\Psi_a(S=1) = \Phi_{orb}^{[1^2]} \Omega_{spin}^{[2]} = \frac{1}{\sqrt{2}} \left[\varphi_1(1)\varphi_2(2) - \varphi_1(2)\varphi_2(1)\right] \Omega_{spin}^{[2]} \quad (S=1) \tag{3}$$

$\Phi_{orb}^{[2]}$ is symmetric with respect to permutation, that is, it has even parity.
$\Phi_{orb}^{[1^2]}$ is antisymmetric, it has odd parity.

We obtain

Even parity $\leftrightarrow$ spin-singlet state.
Odd parity $\leftrightarrow$ spin-triplet state.

The permutation of pair electrons produces a factor

$$(-1)^L.$$

L is the total orbital moment of Cooper's pair. Thus,

$$\text{The symmetric } \Phi_{orb}^{[2]} \text{ corresponds to even L.}$$

$$\text{The antisymmetric } \Phi_{orb}^{[1^2]} \text{ corresponds to odd L.}$$

Hence, the Pauli principle permits only ${}^1S, {}^1D, \ldots$ and ${}^3P, {}^3F, \ldots$ states of Cooper's pairs. In all known superconductors, except Sr_2RuO_4, Cooper's pairs are in the singlet states: *s*-wave in the low-Tc and *d*-wave in high-Tc superconductors.

On the other hand, because of absence of the central field symmetry, *s*-, *p*-, *d*-wave description is an approximation. In crystal field L is not a good quantum number and instead of L-waves, the crystal group symmetry waves, which are consistent with the odd parity, must be considered.

The theoretical arguments in favor of the spin-triplet *p*-wave Cooper pairing in Sr_2RuO_4 were formulated by Rice and Sigrist [8] and independently by Bascaran [9]. Their arguments were based on the similarity of the ruthenate Fermi-liquid properties to those of liquid ^{3}He and on the fact that closely related oxides, such as $SrRuO_3$, are ferromagnetic. The consequent detailed analysis of experimental data and the possible symmetry properties of this unusual pairing state has confirmed that it has the odd-parity [10, 11]. The first experimental confirmation of the spin-triplet pairing in Sr_2RuO_4 came from the NMR Knight shift measurements [12]. However, it was realized that the interpretation of the Knight shift results is not unique. The direct evidence of the spin-triplet nature of Cooper's pairing in ruthenate was obtained in phase-sensitive experiments with superconducting quantum interference devices (SQUID) by Nelson et al. [13].

If the odd-parity and spin-triplet nature of the Cooper pairing state (or the order parameter) in Sr_2RuO_4 have been established, the precise orbital symmetry of the order parameter is still unclear. The *p*-wave symmetry contradicts some experimental findings and, as was suggested in Refs. [14–16], the *f*-wave nature of the order parameter looks more preferable. However, as was stressed by Zhitomirsky and Rice [18], *f*-wave state is also in contradiction with experimental data. It should not surprise, as we discussed above, because in crystal field the angular momentum L is not a good quantum number, therefore both *p*- and *f*-wave descriptions are approximations. In the crystal field, the order parameter must possess the symmetry of one of the irreducible odd parity representations of the crystal group. It must possess the odd parity, because the latter provides the antisymmetry of the total wave function of Cooper's pair in the spin-triplet state. The analysis of possible irreducible representations of the point group D_{4h} showed that the order parameter should belong to the two-dimensional representation E_u [10]. Nevertheless, the problem with the symmetry of the order parameter still remains complicated. The theoretical models allowing the agreement with experimental data are presented in Refs. [17–19].

A large number of theoretical calculations of the electronic structure of the Sr_2RuO_4 crystal have been performed [20–30]. The first theoretical study of the electronic band structure of Sr_2RuO_4 was carried out by Oguchi [20] and Singh [21]. Their calculations were based on the local density approximation (LDA) of the

density functional theory (DFT). It was revealed that there are three bands crossing the Fermi energy level and they all have the antibonding Ru (4d) – O (2p) coupling: $4d_{xy} - 2p\pi$, $4d_{xz} - 2p\pi$, and $4d_{yz} - 2p\pi$. The calculated Fermi surface was associated with these orbitals. It consists of three cylindrical sheets: two electronlike sheets and one holelike sheet. This electronic band structure can be characterized as a quasi-two-dimensional Fermi liquid for Sr_2RuO_4, its properties are reviewed in Ref. [31].

Almost all subsequent calculations [22–27] were performed by the same rather crude LDA method, and in some of the studies even a more approximate tight-binding approach was applied. These calculations confirmed the results of the first two studies [20, 21]. It is worth-while to mention that although in all theoretical studies the large hybridization between Ru (4d) and O (2p) was claimed, the charge distribution was corresponded to the ionic or approximately ionic model; the three bands, crossing the Fermi energy level, were occupied by 4 electrons (or 2 holes), the Ru $d(x^2 - y^2)$ and $d(z^2)$ orbitals were empty, so they did not participate in the occupied bands and in the Fermi surface as well. In the last published calculation [30], LDA was refined by adding dynamical mean-field theory with quantum Monte-Carlo approach (LDA + DMFT (QMC)) [32]. However, the influence of this refinement on the orbital population was not considered. As in the previous LDA studies, the authors [30] assumed that only the t_{2g} level is occupied.

Theoretically predicted at the LDA level the three-sheet structure of the Fermi surface was confirmed in the de Haas – van Alphen experiments [33, 34]. On the other hand, from the angle-resolved photoemission spectroscopy experiments [35–37], a significantly different Fermi-surface topology was predicted. Such discrepancy could be due to a rather approximate level of LDA predictions, however, it was revealed that it is the surface reconstruction, which is responsible for conflicting interpretations [38, 39], see also the theoretical study [40].

Recently, the crystal Hartree-Fock (HF) calculations of the electronic structure of Sr_2RuO_4 were performed [28, 29]. Remarkable that in Ref. [29], the $d_{x^2-y^2}$ and d_{z^2} orbitals were found partly populated and the total number of holes transferred to oxygens due to the strong Ru (4d) – O (2p) hybridization turned out to be about 2. We will discuss these results in Sect. 3 in connection with ours.

At present, the impurity-ion substitution became a powerful tool to study the nature of superconductivity. The effects of Ru or Sr substitution by different atomic dopants are discussed in the review [7]. As was revealed by Minakata and Maeno [41], the substitution of the Ru atoms by the nonmagnetic Ti atoms induces local magnetic moments on Ru and/or O surrounding the impurity and destroys the superconductivity at very small Ti concentrations. The ordered magnetic moment points along the c-direction. These results were confirmed in subsequent studies [42]. It was established that the Ti-doped samples exhibit incommensurate magnetic ordering corresponding to the Fermi-surface nesting instability.

In this paper, we present the results of comparative calculations of the electronic structure of the pure and Ti-doped Sr_2RuO_4 performed by the electron-correlated embedded clusters method developed by our group [43, 44]. The embedded cluster method is the most appropriate method to study the changes in the local electronic

structure induced by impurities. This method was recently successfully applied to study the mechanism of T_c suppression by Zn and Ni impurities in high-T_c cuprates [45].

Our calculations of the spin distribution confirmed the experimental data on the magnetic ordering in Ti-doped samples [41, 42]. The charge distribution obtained at the HF and the electron correlated second-order Møller-Plesset perturbation theory (MP2) level revealed the large electron transfer from O to Ru. The latter leads to Ru ($4d^6$) population instead of Ru ($4d^4$) accepted in the ionic model. The consequences of this electron transfer are discussed. Preliminary results of our study were published in Refs. [46, 47].

2 Methodology

Clusters representing the crystal were calculated in an external potential simulating the Madelung potential of the real crystal. The cluster $[Sr_2Ru_4O_{20}]^{-20}$, Fig. 1, was selected to study the local electronic structure of the pure crystal; the cluster $[Sr_2Ti_2Ru_2O_{20}]^{-20}$, Fig. 2, was used to study the local electronic structure near the

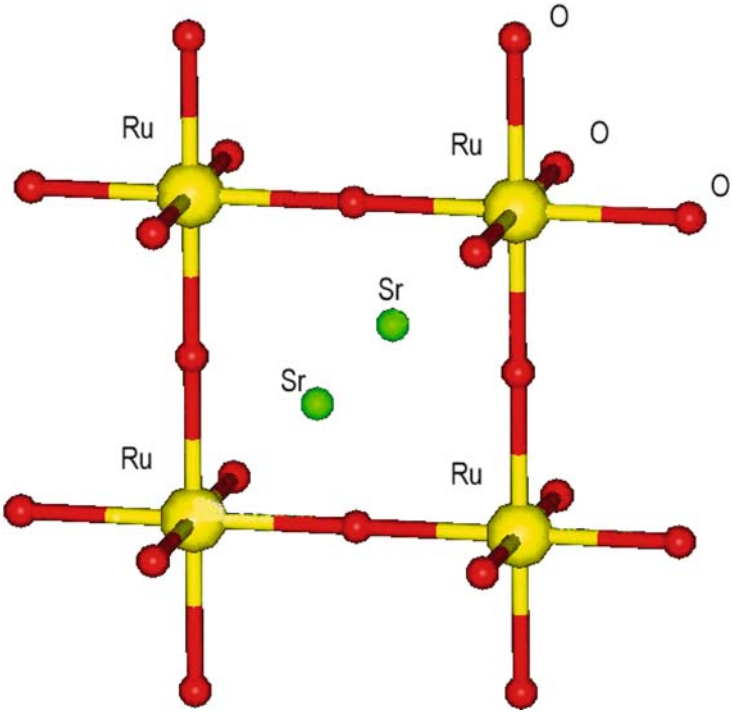

Fig. 1 Cluster $Sr_2Ru_4O_{20}$ used in the ECM calculations of the pure crystal Sr_2RuO_4

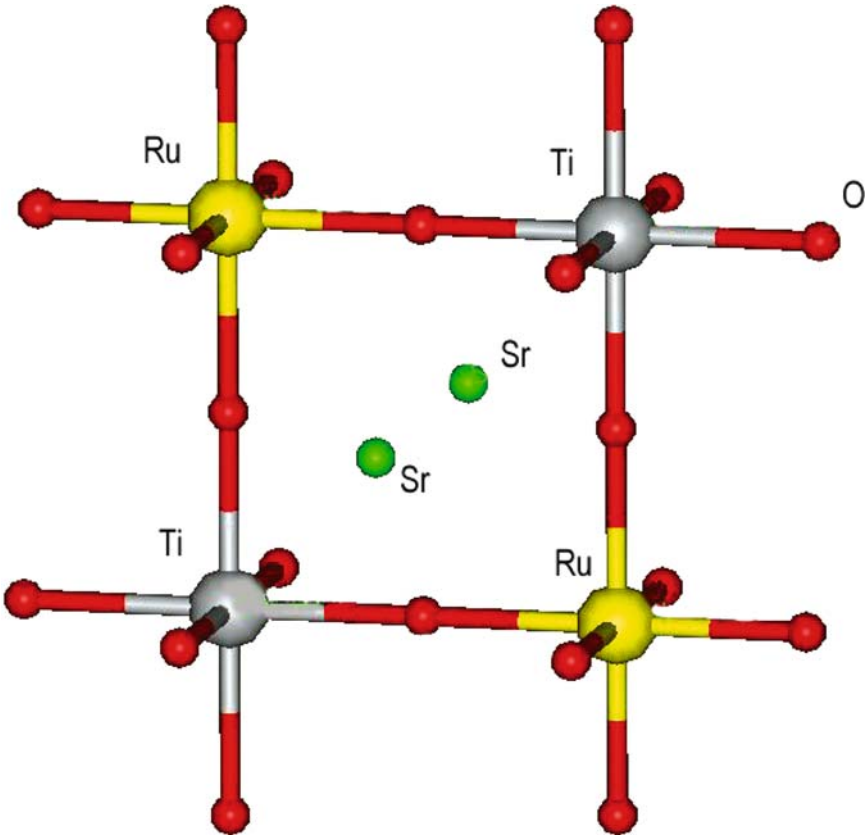

Fig. 2 Cluster $Sr_2Ti_2Ru_2O_{20}$ used in the ECM calculation of the Ti-doped crystal Sr_2RuO_4

Ti impurity. The cluster charge, -20, is determined by the charges of atomic ions defined by the formal valence rules (ionic model): Sr^{2+} Ru^{4+}, Ti^{4+}, and O^{2-}.

Selected cluster was embedded into a finite array of background charges located on each lattice site. This set of charges is divided into core charges corresponding to the ion-model charges and several shells of external charges associated with charge scaling factors which are adjusted in order to provide the correct value of the Madelung potential on each cluster site and the electrical neutrality as well [43,44].

In the present case, the scaling factors are solution of a set of 27 linear algebraic equations. For each cluster a combination of 27 shells could be found so that the matrix corresponding to the set of equations is non-singular. The set of equations is solved exactly by means of the standard subroutine package LAPACK; the difference between the Madelung potential given by our background charges and that given by the infinite crystal is less than 10^{-10}.

The electronic structure of the embedded finite cluster was calculated by the restricted (or unrestricted) Hartree-Fock self-consistent field method. Based on these calculations the second-order Møller-Plesset perturbation theory (MP2) allows

taking into account the electron correlation. In the present work, we use these methods as implemented in the Gaussian-03 program [48], they form all together the ECM-MP2 approach [49]. The core electrons of Ru, Sr, and Ti atoms are described by the Los Alamos National Laboratory pseudopotential (LANL2) with its proper DZ basis set. On oxygen atoms all electrons are taken into account, a doubly split valence basis set 6-31G supplemented by a shell of *d* functions is used. The orbital populations are obtained from the natural bond orbital (NBO) analysis.

Generally, the cluster ion charges obtained at the MP2 level are different from those of the background charges and a self-consistent charge calculation is performed in order to get consistency between background and cluster charges [43,44]. However, in the present work this procedure was not applied. Usually the difference between the first iteration and the final one is small [43, 44].

3 Results and Discussion

3.1 Pure Sr_2RuO_4

Charge distribution (without the population in the Rydberg states) obtained at the HF and MP2 levels in the pure and Ti-doped Sr_2RuO_4 crystal is represented in Tables 1–4. In both the total spin cases: S = 0 (Tables 1 and 2) and S = 1 (Tables 3 and 4), the obtained atomic charges are considerably lower than the formal valence charges following from the one-electron tight-binding model and accepted in DFT studies (see discussion in Introduction). The reason for these great deviations from the ionic-model charges has a simple explanation. The Ru – O bond does not have a pure ionic character and to a considerable degree possesses also a covalent nature

Table 1 Charge distribution at the HF level (NBO analysis) in the pure and Ti-substituted Sr_2RuO_4 crystal (S = 0) calculated by embedded cluster method

	Atomic charge density	Valence orbital population	Detailed charge population on *d*(Ru) and *p*(O) orbitals
(a) *Pure crystal*			
Ru	1.74	$5s^{0.25}4d^{6.01}$	$d_{xy}^{1.71}+d_{xz}^{1.47}+d_{yz}^{1.47}+d_{x^2-y^2}^{0.63}+d_{z^2}^{0.73}$
Sr	1.84	$5s^{0.16}$	
O1	−1.07	$2s^{1.78}2p^{5.29}$	$p_x^{1.66}+p_y^{1.78}+p_z^{1.85}$
O2	−1.43	$2s^{1.88}2p^{5.55}$	$p_x^{1.90}+p_y^{1.90}+p_z^{1.75}$
(b) *Impure crystal*			
Ti	1.74	$4s^{0.27}3d^{1.99}$	$d_{xy}^{0.41}+d_{xz}^{0.40}+d_{yz}^{0.38}+d_{x^2-y^2}^{0.38}+d_{z^2}^{0.42}$
Ru	1.91	$5s^{0.26}4d^{5.83}$	$d_{xy}^{0.65}+d_{xz}^{1.97}+d_{yz}^{0.51}+d_{x^2-y^2}^{1.94}+d_{z^2}^{0.76}$
Sr	1.84	$5s^{0.16}$	
O1	−1.20	$2s^{1.76}2p^{5.44}$	$p_x^{1.80}+p_y^{1.79}+p_z^{1.85}$
O2	−1.45	$2s^{1.88}2p^{5.57}$	$p_x^{1.84}+p_y^{1.87}+p_z^{1.86}$

Table 2 Charge distribution at the MP2 electron correlation level (NBO analysis) in the pure and Ti-substituted Sr_2RuO_4 crystal (S = 0) calculated by the embedded cluster method

	Atomic charge density	Valence orbital population	Detailed charge population on d(Ru) and p(O) orbitals
(a) *Pure crystal*			
Ru	1.57	$5s^{0.32}4d^{6.11}$	$d_{xy}^{1.40} + d_{xz}^{1.47} + d_{yz}^{1.47} + d_{x^2-y^2}^{0.86} + d_{z^2}^{0.91}$
Sr	1.75	$5s^{0.25}$	
O1	−0.94	$2s^{1.76}2p^{5.18}$	$p_x^{1.71} + p_y^{1.71} + p_z^{1.76}$
O2	−1.13	$2s^{1.87}2p^{5.26}$	$p_x^{1.82} + p_y^{1.82} + p_z^{1.62}$
(b) *Impure crystal*			
Ti	1.11	$4s^{0.31}3d^{2.58}$	$d_{xy}^{0.47} + d_{xz}^{0.55} + d_{yz}^{0.53} + d_{x^2-y^2}^{0.54} + d_{z^2}^{0.49}$
Ru	1.41	$5s^{0.31}4d^{6.28}$	$d_{xy}^{0.75} + d_{xz}^{1.94} + d_{yz}^{0.80} + d_{x^2-y^2}^{1.93} + d_{z^2}^{0.86}$
Sr	1.76	$5s^{0.24}$	
O1	−0.95	$2s^{1.75}2p^{5.20}$	$p_x^{1.41} + p_y^{2.00} + p_z^{1.79}$
O2	−1.13	$2s^{1.83}2p^{5.30}$	$p_x^{1.74} + p_y^{1.78} + p_z^{1.78}$

Table 3 Charge distribution at the HF level (NBO analysis) in the pure and Ti-substituted Sr_2RuO_4 crystal (S = 1) calculated by the embedded cluster method

	Atomic charge density	Valence orbital population	Detailed charge population on d(Ru) and p(O) orbitals
(a) *Pure crystal*			
Ru	1.90	$5s^{0.27}4d^{5.83}$	$d_{xy}^{1.84} + d_{xz}^{1.27} + d_{yz}^{1.27} + d_{x^2-y^2}^{0.66} + d_{z^2}^{0.79}$
Sr	1.59	$5s^{0.41}$	
O1	−1.16	$2s^{1.78}2p^{5.38}$	$p_x^{1.64} + p_y^{1.85} + p_z^{1.89}$
O2	−1.36	$2s^{1.87}2p^{5.49}$	$p_x^{1.87} + p_y^{1.87} + p_z^{1.75}$
(b) *Impure crystal*			
Ti	1.71	$4s^{0.27}3d^{2.02}$	$d_{xy}^{0.42} + d_{xz}^{0.41} + d_{yz}^{0.39} + d_{x^2-y^2}^{0.38} + d_{z^2}^{0.42}$
Ru	1.82	$5s^{0.25}4d^{5.93}$	$d_{xy}^{0.63} + d_{xz}^{0.96} + d_{yz}^{1.65} + d_{x^2-y^2}^{1.96} + d_{z^2}^{0.73}$
Sr	1.84	$5s^{0.16}$	
O1	−1.18	$2s^{1.76}2p^{5.42}$	$p_x^{1.80} + p_y^{1.81} + p_z^{1.81}$
O2	−1.40	$2s^{1.85}2p^{5.55}$	$p_x^{1.83} + p_y^{1.86} + p_z^{1.86}$

due to the hybridization of 4d(Ru) and 2p(O) orbitals. The interatomic interaction leads to an effective electron transfer from O to Ru (and partly to Sr) at both the HF and MP2 levels.

According to the definition by Löwdin [50] accepted in molecular and cluster studies, the electron correlation effects correspond to the calculations beyond the HF approach. The MP2 calculations give the correlation effects in the second order of the perturbation theory, since the first order of the Møller-Plesset perturbation theory corresponds to the HF approximation, see Ref. [51], Appendix 3. Allowing for the electron correlation at the MP2 level considerably increases the electron transfer from the O atoms surrounding Ru and Sr making the values of charges on atoms very far from the ionic-model charges. For the ground state (S = 0) we obtained +1.57 on Ru (instead of +4), +1.75 on Sr (instead of +2), and −0.94 on

Table 4 Charge distribution at the MP2 electron correlation level (NBO analysis) in the pure and Ti-substituted Sr_2RuO_4 crystal (S = 1) calculated by embedded cluster method

	Atomic charge density	Valence orbital population	Detailed charge population on d(Ru) and p(O) orbitals
(a) *Pure crystal*			
Ru	1.31	$5s^{0.39}4d^{6.30}$	$d_{xy}^{1.75} + d_{xz}^{1.43} + d_{yz}^{1.43} + d_{x^2-y^2}^{0.80} + d_{z^2}^{0.89}$
Sr	1.62	$5s^{0.38}$	
O1	−0.95	$2s^{1.77}2p^{5.18}$	$p_x^{1.50} + p_y^{1.91} + p_z^{1.77}$
O2	−1.07	$2s^{1.87}2p^{5.20}$	$p_x^{1.77} + p_y^{1.77} + p_z^{1.66}$
(b) *Impure crystal*			
Ti	1.12	$4s^{0.31}3d^{2.57}$	$d_{xy}^{0.48} + d_{xz}^{0.53} + d_{yz}^{0.52} + d_{x^2-y^2}^{0.55} + d_{z^2}^{0.49}$
Ru	1.61	$5s^{0.32}4d^{6.07}$	$d_{xy}^{0.84} + d_{xz}^{0.75} + d_{yz}^{1.60} + d_{x^2-y^2}^{1.93} + d_{z^2}^{0.95}$
Sr	1.76	$5s^{0.24}$	
O1	−0.98	$2s^{1.74}2p^{5.24}$	$p_x^{1.67} + p_y^{1.68} + p_z^{1.89}$
O2	−1.14	$2s^{1.83}2p^{5.31}$	$p_x^{1.77} + p_y^{1.77} + p_z^{1.77}$

O1 and −1.13 on O2 (instead of −2). We must not consider the obtained absolute values of the atomic charges as real ionic charges in the crystal; these values depend on the cluster chosen and a calculation method. However, they reflect the real trends in the crystal.

In contrast with the accepted Ru ($4d^4$) population, the 4d Ru population is, according to Tables 1 and 2, $4d^{6.11}$ at the MP2 level and $4d^{6.01}$ at the HF level. Thus, there is a two-electron increase in the 4d-orbital population. In this connection, it is interesting to compare it with the crystal HF calculation in Ref. [29]. As follows from their results, the total number of holes transferred to oxygens is about 2. If all holes are transferred from Ru, then it corresponds to two additional electrons in its 4d shell. Such precise agreement between our cluster HF charge distribution and the crystal HF charge distribution is very important, since it is a strong evidence that the results obtained by our embedded cluster method reflect properly the real charge distribution in the crystal.

In Ref. [29] the e_g ($d_{x^2-y^2}$, d_{z^2}) level, which was assumed empty in previous studies, was found partly populated (appr. 0.5 e). The population of e_g level obtained in our calculation is considerably larger, at the MP2 correlation level it is more than three times larger, see Fig. 3a. The charge transfer from O provides the covalent bonding between O and Ru and populates the e_g level.

The comparison of the results obtained at the HF and MP2 levels for the pure crystal (Fig. 3a) shows that the t_{2g} population at the MP2 level is decreased by 0.31 e with respect to the HF level whereas the e_g population is increased by a slightly greater amount (0.41 e). According to Tables 1 and 2, the decrease of the d_{xy} population alone accounts for the decrease of the t_{2g} population. Therefore, the electron correlation contributes to the e_g population.

As was discussed in Introduction, in numerous calculations of Sr_2RuO_4 by DFT approach, including the more refine LDA + DMFT (QMC) calculation, the charge population has not been analyzed. Authors postulated that the Ru ion has charge +4

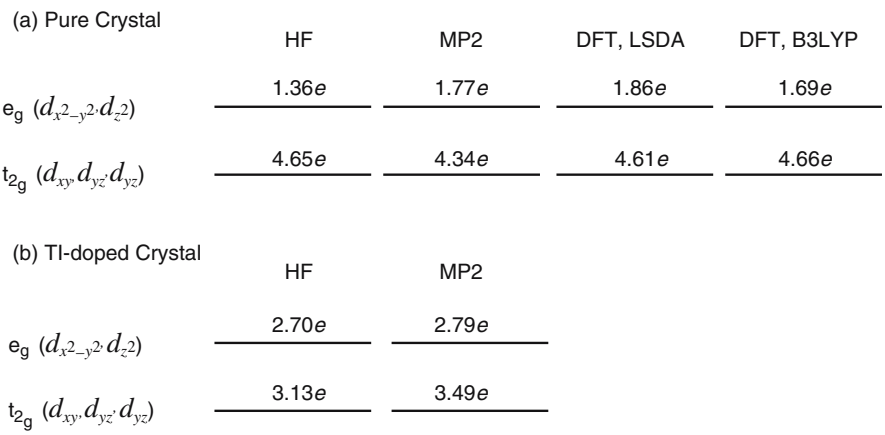

Fig. 3 The population of the e_g and t_{2g} levels obtained at HF, MP2, and DFT approximations in the pure and Ti-doped Sr_2RuO_4 crystal in the singlet state

Table 5 Comparative calculation of charge distribution in the ground state (S = 0) of Sr_2RuO_4 performed by different methods

	HF		MP2		DFT, LSDA		DFT, B3LYP	
	Atomic charge	Valence population	Atomic charge	Valence population	Atomic charge	Valence population	Atomic charge	Valence population
Ru	1.74	$5s^{0.25}4d^{6.01}$	1.57	$5s^{0.32}4d^{6.11}$	0.92	$5s^{0.61}4d^{6.47}$	1.29	$5s^{0.36}4d^{6.35}$
Sr	1.84	$5s^{0.16}$	1.75	$5s^{0.25}$	1.59	$5s^{0.41}$	1.68	$5s^{0.32}$
O1	−1.07	$2s^{1.78}2p^{5.29}$	−0.94	$2s^{1.68}2p^{5.18}$	−0.82	$2s^{1.79}2p^{5.03}$	−0.94	$2s^{1.78}2p^{5.16}$
O2	−1.43	$2s^{1.88}2p^{5.55}$	−1.13	$2s^{1.87}2p^{5.26}$	−1.1	$2s^{1.88}2p^{5.23}$	−1.18	$2s^{1.88}2p^{5.30}$

and the e_g level is empty. For verification of these conclusions we calculated our cluster by DFT method using two exchange-correlation functionals: the local-spin-density approximation (LSDA) and the hybrid functional B3LYP. The results are presented in Table 5.

As follow from Table 5, the effective charge transfer $O \xrightarrow{e} Ru$ takes place at both DFT approaches. The e_g level is also occupied, as it has to be when the calculation includes the interaction between atoms, see Fig. 3a.

In crystal the atomic and molecular levels are transformed into appropriate bands. Thus, in contrast with the accepted concepts, from the obtained essential e_g population it follows that the $d_{x^2-y^2}$ and d_{z^2} orbitals give also a contribution to the Fermi surface of the Sr_2RuO_4 crystal.

3.2 Ti-Doped Sr_2RuO_4

In Ti-doped crystals in the ground state (S = 0), the Ti substitution does not change at the MP2 level the charges on Sr and O and leads to a small decrease of positive

charge on Ru (0.16 e), see Table 2. However, it induces the essential charge redistribution among the 4d orbitals of Ru. The charge on the t_{2g} (d_{xy}, d_{xz}, d_{yz}) level is decreased on 0.85 e, while the population of the e_g level is increased on 1.02 e and achieved 2.79 e, Fig. 3b. Comparing the e_g and t_{2g} populations at the HF and MP2 levels for the Ti-substituted crystal reveals that the electron correlation increases the orbital population.

On the whole, the charge population on the e_g level of the Ru atoms surrounding the Ti impurity is considerably increased and the $d_{x^2-y^2}$ orbital is almost filled. The charge transfers mostly from the t_{2g} level, the population of d_{xy} and d_{yz} is decreased by about two times and the orbital d_{xz} is filled. If the electrons of the d_{xy} band are responsible for the spin triplet superconductivity in Sr_2RuO_4 [52], a decrease of the d_{xy} population obtained in our calculations and a consequent increase of the e_g population can be one of the reasons of the destruction of superconductivity induced by small Ti concentrations. Another reason is connected with the spin redistribution, which we discuss below.

The study of the triplet state allows finding the spin distribution (see Tables 6 and 7). The spin distribution found at the MP2 level considerably differs from that found at the HF level. This reflects the great influence of the electron correlation on the spin distribution. Taking into account the electron correlation leads to qualitative changes in the spin density, which is located only on Ru and Sr at the MP2 level, in contrast with the HF spin distribution (compare Tables 6a and 7a). In the undoped crystal, the MP2 spin density on Ru is twice as much as that on Sr. It is important to stress that the spin density in the pure crystal is located on Ru_2O plane, on the $4d_{xy}$(Ru) orbital and partly on the 5s (Sr) orbital.

The Ti-substitution leads to drastic changes in the local spin distribution. The spin density disappears on Sr and is localized on the neighboring to Ti-impurity Ru atoms and four O1 atoms surrounding Ru. What is also important is that the spin density in doped crystals is localized on the orbitals directed along the z-axis; $2p_z$ (O1) and

Table 6 Spin distribution at the HF level (NBO analysis) in the pure and Ti-substituted Sr_2RuO_4 crystal (S = 1) calculated by embedded cluster method

	Atomic spin density	Valence orbital spin population	Detailed spin population on d(Ru) and p(O) orbitals ($\alpha - \beta$)
(a) *Pure crystal*			
Ru	0.14	$5s^{0.01}4d^{0.13}$	$d_{xy}^{0.10} + d_{xz}^{0.01} + d_{yz}^{0.01} + d_{x^2-y^2}^{0.0} + d_{z^2}^{0.01}$
Sr	0.25	$5s^{0.25}$	
O1	0.15	$2s^{0.01}2p^{0.14}$	$p_x^{0.0} + p_y^{0.13} + p_z^{0.01}$
O2	−0.03	$2s^{0.0}2p^{-0.03}$	$p_x^{-0.01} + p_y^{-0.01} + p_z^{-0.01}$
(b) *Impure crystal*			
Ti	0.02	$4s^{0.0}3d^{0.02}$	$d_{xy}^{0.0} + d_{xz}^{0.01} + d_{yz}^{0.01} + d_{x^2-y^2}^{0.0} + d_{z^2}^{0.0}$
Ru	0.96	$5s^{0.01}4d^{0.95}$	$d_{xy}^{0.03} + d_{xz}^{0.56} + d_{yz}^{0.33} + d_{x^2-y^2}^{0.0} + d_{z^2}^{0.03}$
Sr	0.0	$5s^{0.0}$	
O1	−0.02	$2s^{0.0}2p^{-0.02}$	$p_x^{0.0} + p_y^{-0.01} + p_z^{-0.01}$
O2	−0.01	$2s^{0.0}2p^{-0.01}$	$p_x^{-0.01} + p_y^{0.0} + p_z^{0.0}$

Table 7 Spin distribution at the MP2 electron correlation level (NBO analysis) in the pure and Ti-substituted Sr_2RuO_4 crystal (S = 1) calculated by embedded cluster method

	Atomic spin density	Valence orbital spin population	Detailed spin population on d(Ru) and p(O) orbitals ($\alpha - \beta$)
(a) *Pure crystal*			
Ru	0.28	$5s^{0.05}4d^{0.23}$	$d_{xy}^{0.19} + d_{xz}^{0.01} + d_{yz}^{0.01} + d_{x^2-y^2}^{0.01} + d_{z^2}^{0.01}$
Sr	0.15	$5s^{0.15}$	
O1	−0.02	$2s^{0.01}2p^{-0.03}$	$p_x^{-0.02} + p_y^{-0.01} + p_z^{0.0}$
O2	−0.01	$2s^{0.01}2p^{-0.02}$	$p_x^{-0.01} + p_y^{-0.01} + p_z^{0.0}$
(b) *Impure crystal*			
Ti	−0.12	$4s^{-0.01}3d^{-0.11}$	$d_{xy}^{-0.01} + d_{xz}^{-0.05} + d_{yz}^{-0.03} + d_{x^2-y^2}^{-0.01} + d_{z^2}^{-0.01}$
Ru	0.30	$5s^{0.01}4d^{0.31}$	$d_{xy}^{0.02} + d_{xz}^{-0.07} + d_{yz}^{0.36} + d_{x^2-y^2}^{0.0} + d_{z^2}^{0.0}$
Sr	−0.02	$5s^{-0.02}$	
O1	0.23	$2s^{0.01}2p^{0.22}$	$p_x^{-0.01} + p_y^{0.0} + p_z^{0.23}$
O2	0.06	$2s^{0.01}2p^{0.05}$	$p_x^{0.05} + p_y^{0.0} + p_z^{0.0}$

$4d_{yz}$ (Ru). These results are in the complete agreement with the experiment [41, 42] and support their conclusions, since in Ref. [41] the authors were not sure about location of the spin on oxygen.

The two parallel spins in the cluster triplet state can be associated with the ferromagnetic fluctuations in the crystal [53]. As was revealed in Ref. [54], the Ti impurities induce a magnetic ordering, which corresponds to the spin density wave (SDW). Our local calculations do not allow us to study a long-range magnetic order. On the other hand, the obtained magnetic moments in both the pure and Ti-doped crystals do not contradict SDW.

4 Conclusions

1. The calculations performed by the embedded cluster method revealed at the HF, MP2, and DFT levels the large electron transfer from O to Ru. At the MP2 correlation level, the NBO population analysis gives $Ru^{1.57+}(5s^{0.32}\ 4d^{6.11})$ instead of Ru^{4+} $(5s^0\ 4d^4)$ in the formal ionic model accepted in all DFT studies. This electron transfer provides the effective hybridization between Ru(4d) and O(2p) and makes the Ru – O bond partly covalent. It is also responsible for the population of the e_g level, which is assumed to be empty in most of the previous studies.

   The results of the crystal HF calculations performed in Ref. [30] support our conclusions about a large electron transfer to Ru from neighboring O; they also obtained a partly populated e_g level.
2. From the obtained essential e_g population (at all applied calculation levels) follows that the $d_{x^2-y^2}$ and d_{z^2} orbitals contribute to the Fermi surface of the Sr_2RuO_4 crystal.

3. The Ti substitution induces a large charge redistribution among the 4d orbitals of Ru. The population of e_g level formed by the Ru atoms surrounding the Ti impurity is considerably increased, by 1.02 e, at the expense of the $4d_{xy}$ population on Ru, and the $d_{x^2-y^2}$ orbital becomes almost filled. These changes can be one of the reasons of the destruction of the superconductivity induced by small Ti doping.
4. The Ti substitution induces drastic changes in the local spin distribution. The spin density is localized on the neighboring to Ti-impurity Ru atoms and four O1 atoms surrounding Ru. While in the pure crystal the spin density is localized predominantly in the basal plane (on the d_{xy} orbitals), in the Ti-doped crystal it is localized on the orbitals directed toward the z axis. These results are agreed with the experiment [41, 42] and can also be a reason of the superconductivity destruction in the Ti-doped crystal, in particular if the pairing mechanism is based on a magnetic interaction in the basal plane.

Acknowledgements The authors acknowledge Manfred Sigrist for numerous helpful discussions and comments. The study was partly supported by grants CONACyT (Mexico) No. 46770 and UNAM No. IN107305.

References

1. J.G. Bednorz and K.A. Müller, Z. Phys. B – Condens. Mat. **64**, 189 (1986).
2. C.W. Chu, Physica C **341–348**, 25 (2000).
3. C.W. Chu, Physica B (in press).
4. O. Gunnarsson, Rev. Mod. Phys. **69**, 575 (1997).
5. J.H. Schön, Ch. Kloc, and B Batlogg, Science, **293**, 2432 (2001).
6. Y. Maeno, H. Hashimoto, K. Yoshida, S. Nishizaki, T. Fujita, J.G. Bednorz, and F. Lichtenberg, Nature **372**, 532 (1994).
7. A.P. Mackenzie and Y. Maeno, Rev. Mod. Phys.**75**, 657 (2003).
8. T.M. Rice and M. Sigrist, J. Phys.: Condens. Mat. **7**, L643 (1995).
9. G. Bascaran, Physica B **223–224**, 490 (1996).
10. M. Sigrist, D. Agterberg, A. Furusaki, C. Honerkamp, K.K. Ng, T.M. Rice, and M.E. Zhitomirsky, Physica C **317–318**, 134 (1999).
11. M. Sigrist, A Furusaki, C. Honerkamp, M. Matsumoto, K.K. Ng, and Y. Okuno, J. Phys. Soc. Jpn. **69**, Suppl. B, 127 (2000).
12. K. Ishida, H. Mukuda, Y. Kitaoka, K. Asayama, Z.Q. Mao, Y. Mori, and Y. Maeno, Nature (London) **396**, 658 (1998).
13. K.D. Nelson, Z.Q. Mao, Y. Maeno, and Y. Liu, Science **306**, 1151 (2004).
14. Y. Hasegawa, K. Machida, and M. Osaki, J. Phys. Soc. Jpn. **69**, 336 (2000).
15. M.J. Graf and A.V. Balatsky, Phys. Rev. B **62**, 9697 (2000).
16. H. Won and K. Maki, Europhys. Lett. **52**, 427 (2000).
17. M.E. Zhitomirsky and T.M. Rice, Phys. Rev. Lett. **87**, 057001 (2001).
18. J.F. Annett, B.L. Györffy, G. Litak, and R. I. Wysokinski, Eur. Phys. J. B **36**, 301 (2003).
19. J.F. Annett, G. Litak, B.L. Györffy, and R. I. Wysokinski, Phys. Rev. B **73**, 134501 (2006).
20. T. Oguchi, Phys. Rev. B **51**, 1385 (1995).
21. D.J. Singh, Phys. Rev. B **52**, 1358 (1995).
22. G.J. McMullan, M.P. Ray, and R.J. Needs, Physica B **222–224**, 529 (1996).
23. I. Hase and Y. Nishinara, J. Phys. Soc. Jpn. **65**, 3957 (1996).

24. C. Noce and M. Cuoco, Phys. Rev. B **59**, 2659 (1999).
25. T. Mishonov and E. Penev, J. Phys.: Condens. Mat. **12**, 143 (2000).
26. I.I. Mazin, D.A. Papaconstantopoulos, and D.J. Singh, Phys. Rev. B **61**, 5223 (2000).
27. A. Pérez-Navarro, J. Costa-Quintana, and E. López-Aguilar, Phys. Rev. B **61**, 10125 (2000).
28. T.T. Tran, T. Mizokawa, S. Nakatsiji, H. Fukazawa, and Y. Maeno, Phys. Rev. B **70**, 153106 (2004).
29. Han-Jin Noh, S.-J. Oh, B.-G. Park, J.-H. Park, J.-Y. Kim, H.D. Kim, T. Mizokawa, L.H. Tjeng, H.-J. Lin, C.T. Chen, S. Schuppler, S. Nakatsuji, H. Fukazawa, and Y. Maeno, Phys. Rev. B **72**, 052411 (2005).
30. Z.V. Pchelkina, I.A. Nekrasov, Th. Pruschke, A. Sekiyama, S.Suga, V.I. Anisimov, and D. Vollhardt, Phys. Rev. B **75**, 035122 (2007).
31. C. Bergemann, A.P. Mackenzie, S.R. Julian, D. Forsythe, and E. Ohmichi, Adv. Phys. **52**, 639 (2003).
32. V.I. Anisimov, D.E. Kondakov, A.V. Kozhevnikov, I.A, Nekrasov, Z.V. Pchelkina, J.W. Allen, S.-K. Mo, H.-D. Kim, P. Metcalf, S. Suga, A. Sekiyama, G. Keller, I. Leonov, X. Ren, and D. Vollhardt, Phys. Rev. B **71**, 125119 (2005).
33. A.P. Mackenzie, S.R. Julian, A.J. Diver, G.J. McMullan, M.P. Ray, G.G. Lonzarich, Y. Maeno, S. Nishizaki, and T. Fujita, Phys. Rev. Lett. **76**, 3786 (1996).
34. A.P. Mackenzie, S.R. Julian, G.G. Lonzarich, Y. Maeno, and T. Fujita, Phys. Rev. Lett. **78**, 2271 (1997).
35. D. H. Lu, M. Schmidt, T.R. Cummins, S. Schuppler, F. Lichtenberg, and J.G. Bednorz, Phys. Rev. Lett. **76**, 4845 (1996).
36. T. Yokoya, A. Chainani, T. Takahashi, H. Katayama-Yoshida, M. Kasai, and Y. Tokura, Phys. Rev. Lett. **76**, 3009 (1996).
37. T. Yokoya, A. Chainani, T. Takahashi, H. Ding, J.C. Campuzano, H. Katayama-Yoshida, M. Kasai, and Y. Tokura, Phys. Rev. B **54**, 13311 (1996).
38. R. Matzdorf, Z. Fang, Ismail, Jiandi Zhang, T. Kimura, Y. Tokura, K. Terakura, and E.W. Plummer, Science **289**, 746 (2000).
39. Damascelli, D.H. Lu, K.M. Shen, N.P. Armitage, F. Ronning, D.L. Feng, C. Kim, Z.X. Shen, T. Kimura, Y. Tokura, Z.Q. Mao, and Y. Maeno, Phys. Rev. Lett. **85**, 5194 (2000).
40. A. Liebsch and A. Lichtenstein, Phys. Rev. Lett. **84**, 1591 (2000).
41. M. Minakata and Y. Maeno, Phys. Rev. B **63**, 180504 (2001).
42. M. Braden, O. Friedt, Y. Sidis, P. Bourges, M. Minakata, and Y. Maeno, Phys. Rev. Lett. **88**, 197002 (2002).
43. I.G. Kaplan, J. Soullard, J. Hernández-Cobos, and R. Pandey, J. Phys.: Condens. Mat. **11**, 1049 (1999).
44. I.G. Kaplan, J. Hernández-Cobos and J. Soullard, Quantum Systems in Chemistry and Physics, Kluwer, Dordrecht, vol. 1, 143–158, 2000.
45. I.G. Kaplan, J. Soullard, and J. Hernández-Cobos, Phys. Rev. B **65**, 214509 (2002).
46. J. Soullard and I.G. Kaplan, Physica C **460–462**, 1008 (2007).
47. I.G. Kaplan and J. Soullard, Physica B (in Press).
48. Gaussian 03, Revision B.05, M.J. Frisch, G.W. Trucks, H.B. Schlegel, G.E. Scuseria, M.A. Robb, J.R. Cheeseman, J.A. Montgomery, Jr., T. Vreven, K.N. Kudin, J.C. Burant, J.M. Millam, S.S. Iyengar, J. Tomasi, V. Barone, B. Mennucci, M. Cossi, G. Scalmani, N. Rega, G.A. Petersson, H. Nakatsuji, M. Hada, M. Ehara, K. Toyota, R. Fukuda, J. Hasegawa, M. Ishida, T. Nakajima, Y. Honda, O. Kitao, H. Nakai, M. Klene, X. Li, J.E. Knox, H.P. Hratchian, J.B. Cross, C. Adamo, J. Jaramillo, R. Gomperts, R.E. Stratmann, O. Yazyev, A.J. Austin, R. Cammi, C. Pomelli, J.W. Ochterski, P.Y. Ayala, K. Morokuma, G.A. Voth, P. Salvador, J.J. Dannenberg, V.G. Zakrzewski, S. Dapprich, A.D. Daniels, M.C. Strain, O. Farkas, D.K. Malick, A.D. Rabuck, K. Raghavachari, J.B. Foresman, J.V. Ortiz, Q. Cui, A.G. Baboul, S. Clifford, J. Cioslowski, B.B. Stefanov, G. Liu, A. Liashenko, P. Piskorz, I. Komaromi, R.L. Martin, D.J. Fox, T. Keith, M. A. Al-Laham, C.Y. Peng, A. Nanayakkara, M. Challacombe, P.M.W. Gill, B. Johnson, W. Chen, M.W. Wong, C. Gonzalez, and J.A. Pople, Gaussian, Inc., Pittsburgh, PA, 2003.

49. I.G. Kaplan and J. Soullard, Int. J. Quantum Chem. **80**, 320 (2000).
50. P.O. Löwdin, Adv. Chem. Phys. **2**, 207 (1959).
51. I.G. Kaplan, Intermolecular Interactions: Physical Picture, Computational Methods and Model Potentials, Wiley, Chichester, 2006.
52. O. Friedt, P. Steffens, M. Braden, Y. Sidis, S. Nakatsuji, and Y. Maeno, Phys. Rev. Lett. **93**, 147404 (2004).
53. I.I. Mazin and D.J. Singh, Phys. Rev. Lett. **82**, 4324 (1999).
54. M. Braden, O. Friedt , Y. Sidis, P. Bourges, P. Pfeuty, S. Nakatsuji, Z. Mao, N. Kikugawa, M. Minakata, Y. Maeno, Physica C **388**, 489 (2003).

An Introduction to the Density Matrix Renormalization Group Ansatz in Quantum Chemistry

Garnet Kin-Lic Chan(✉), Jonathan J. Dorando, Debashree Ghosh, Johannes Hachmann, Eric Neuscamman, Haitao Wang, and Takeshi Yanai

Abstract The Density Matrix Renormalisation Group (DMRG) is an electronic structure method that has recently been applied to *ab-initio* quantum chemistry. Even at this early stage, it has enabled the solution of many problems that would previously have been intractable with any other method, in particular, multireference problems with very large active spaces. Historically, the DMRG was not originally formulated from a wavefunction perspective, but rather in a Renormalisation Group (RG) language. However, it is now realised that a wavefunction view of the DMRG provides a more convenient, and in some cases more powerful, paradigm. Here we provide an expository introduction to the DMRG ansatz in the context of quantum chemistry.

Keywords: Density Matrix Renormalization Group, multireference, nondynamic correlation, active space, matrix product state

1 Introduction

The Density Matrix Renormalization Group (DMRG) is an electronic structure method that has recently been applied to *ab-initio* quantum chemistry. The method originated in the condensed matter community with the pioneering work of White [1, 2]. Although the earliest quantum chemistry implementations are only a few years old, the DMRG has already been used to solve many problems that would

G.K.-L. Chan, Jonathan J. Dorando, Debashree Ghosh, Johannes Hachmann, Eric Neuscamman, and Haitao Wang
Department of Chemistry and Chemical Biology, Cornell University, Ithaca, New York 14853-1301, USA, e-mail: gkc1000@gmail.com

Takeshi Yanai
Department of Theoretical and Computational Molecular Science, Institute for Molecular Science, Okazaki, Aichi 444-8585, Japan.

S. Wilson et al. (eds.) *Frontiers in Quantum Systems in Chemistry and Physics*.

have been intractable with any other method, and especially, multireference problems with very large active spaces. For example, we have used the DMRG to study systems ranging from molecular potential energy curves [3, 4], to excited states of large conjugated polymers [5, 6], to metal-insulator type transitions in hydrogen chains [7]. In each case, we have obtained accuracies close to the (estimated) exact Complete Active Space Configuration Interaction (CASCI) or Complete Active Space Self-Consistent-Field (CASSCF) result, for active spaces well outside the range of traditional algorithms e.g. 100 active electrons in 100 active orbitals [7]. Unlike a traditional CAS (where the active space wavefunction is obtained in a brute-force Full Configuration Interaction expansion) the DMRG utilises a compact wavefunction ansatz. However, this ansatz is very flexible, is well-suited to nondynamic correlation, and in the cases of long molecules, provides a near optimal, local description of multireference correlations.

Historically, the DMRG was not originally formulated from a wavefunction ansatz perspective, but rather in the Renormalisation Group (RG) language of Wilson's Numerical RG [1, 2, 8, 9], from which it is descended. The original quantum chemical implementations of the DMRG were also described from an RG point of view (e.g. [10–14]). Although the mathematical form of the DMRG ansatz has been known for some time [15–18], only in recent years has it been realised that the wavefunction view of the DMRG provides a more convenient and in many cases more powerful paradigm, and this has led to fundamental advances in the DMRG method itself [7, 19–32].

The current article provides an expository introduction to the DMRG in quantum chemistry from the wavefunction point of view. This is complementary to earlier articles that use the RG based formulation and the first-time reader will benefit from reading such articles alongside the current one. It is not our intention to provide a comprehensive review of the DMRG method even within the restricted domain of quantum chemistry. Thus we do not pretend to survey the literature except to say at the start that the field of quantum chemical DMRG has developed through the work of White et al. [10, 33, 34], Mitrushenkov et al. [11, 35, 36], our contributions [3–7, 12, 37, 38], the work of Legeza, Hess et al. [13, 39–41], the work of Reiher et al. [14, 42–44], and most recently the work of Zgid and Nooijen [45]. Also related, but too numerous to cite in full here, are the developments with semi-empirical Hamiltonians; some representative early works are those in [46–52]. In addition, we mention again that the DMRG has its origins in the condensed matter community and thus excellent sources of information which provide this perspective are the recent reviews of Schollwöck [32] and Hallberg [30, 31].

The structure of our article is as follows. We begin by introducing the underlying DMRG ansatz and examining some of its special properties in Sects. 2 and 3. In Sects. 4 and 5 we explain the connection between the wavefunction ansatz, and the original Renormalisation Group language within which the DMRG is usually described. In Sect. 6 we describe how the structure of the DMRG wavefunction allows the efficient evaluation of Hamiltonian matrix elements. Finally, we finish with some brief thoughts and conclusions in Sect. 7.

2 Motivation for the DMRG Ansatz

The primary challenge in quantum chemistry is to find a good approximation to the electronic wavefunction of a quantum state. We can express any N-electron wavefunction in a complete basis of Slater determinants, through the Full Configuration Interaction (FCI) expansion,

$$|\Psi\rangle = \sum_{n_1 n_2 n_3 \ldots n_k} \Psi^{n_1 n_2 n_3 \ldots n_k} |n_1 n_2 n_3 \ldots n_k\rangle, \tag{1}$$

$$\{n_i\} = \{|0\rangle, |1^\alpha\rangle, |1^\beta\rangle, |2^{\alpha\beta}\rangle\}, \tag{2}$$

$$\sum_i n_i = N. \tag{3}$$

Here $|n_1 \ldots n_k\rangle$ is the occupation number representation of the Slater determinant where n_i is the occupation of site (i.e. orbital) i. The total number of orbitals is k and N is the total number of electrons.

The dimension of the coefficient tensor Ψ in the above expansion is 4^k, which is intractable for values of k much larger than 10. Therefore, we would like to find an ansatz where Ψ is expressed more compactly. In particular, we would want such an ansatz to require only a *polynomial* amount of information as a function of the number of orbitals in the system, k.

A very simple ansatz would be to approximate the high-dimensional coefficient tensor Ψ by a tensor product of vectors $\psi^1 \ldots \psi^k$, which we shall call site functions,

$$\Psi \approx \psi^1 \otimes \psi^2 \otimes \psi^3 \ldots \otimes \psi^k. \tag{4}$$

Using the notation ψ^{n_1} to denote the nth element of ψ^1, i.e. $\psi^{n_1} = \psi^1_n$, we can also write

$$\Psi^{n_1 n_2 n_3 \ldots n_k} \approx \psi^{n_1} \psi^{n_2} \psi^{n_3} \ldots \psi^{n_k}. \tag{5}$$

Note that each site function ψ is *not* an orbital but rather a vector of length 4, and ψ^{n_1}, ψ^{n_2} represent elements of the different vectors ψ^1, ψ^2. This ansatz contains only $4k$ parameters and is certainly tractable. However, it is also not, in general, very accurate. So, let us try to improve the ansatz by increasing the flexibility of the site functions ψ. We can introduce additional *auxiliary* indices, i.e.

$$\psi^{n_p} \rightarrow \psi^{n_p}_{ii'}. \tag{6}$$

The new indices i, i' are auxiliary in the sense that they do not appear in the final coefficient tensor Ψ and must be contracted over in some fashion. The simplest arrangement is to contract the indices sequentially from one ψ site function to the next, i.e.

$$\Psi^{n_1 n_2 n_3 \ldots n_k} \approx \sum_{i_1 i_2 i_3 \ldots i_{k-1}} \psi^{n_1}_{i_1} \psi^{n_2}_{i_1 i_2} \psi^{n_3}_{i_2 i_3} \ldots \psi^{n_k}_{i_{k-1}}. \tag{7}$$

For simplicity, we will assume that the dimensions of all auxiliary indices are chosen to be the same, and we shall call this dimension M. Then each site function ψ is a 3-tensor of dimension $4 \times M \times M$, and the total number of parameters in the wavefunction ansatz is $4M^2k$.

This is, in essence, the DMRG ansatz for M states. (More precisely, it is the ansatz used in the one-site DMRG algorithm, as explained later.) Note that by increasing the dimension M, we can make the approximation arbitrarily exact. Because (for given $n_1 \dots n_k$) the contraction in Eq. (7) is a series of matrix products, this ansatz is referred to in the literature as the Matrix Product State [15–19,25,53–55]. Combining the site functions explicitly with the Slater determinants we have

$$|\Psi_{\mathrm{DMRG}}\rangle = \sum_{\substack{n_1 n_2 n_3 \dots n_k \\ i_1 i_2 i_3 \dots i_{k-1}}} \psi^{n_1}_{i_1} \psi^{n_2}_{i_1 i_2} \psi^{n_3}_{i_2 i_3} \dots \psi^{n_k}_{i_{k-1}} |n_1 n_2 n_3 \dots n_k\rangle. \tag{8}$$

Before continuing, let us first establish some notation. The site functions ψ in Eq. (8) are 3-tensors. However, the notation of linear algebra is designed primarily for vectors (1-tensors) and matrices (2-tensors). Naturally, any 3-tensor can be considered as an array of matrices, so long as we specify which two indices are the matrix indices and which is the 3rd (array) index. When viewing the site function as an array of matrices, we will write the 3rd (array) index on the top. Thus in this notation, we have

$$\begin{aligned} \text{Matrix} &: [\psi^{n_p}] \ (\text{dimension } M \times M) \\ \text{Elements} &: \psi^{n_p}_{i_{p-1} i_p} \end{aligned} \tag{9}$$

and the DMRG wavefunction (8) is written as

$$|\Psi_{\mathrm{DMRG}}\rangle = \sum_{n_1 n_2 n_3 \dots n_k} [\psi^{n_1}][\psi^{n_2}][\psi^{n_3}] \dots [\psi^{n_k}] |n_1 n_2 n_3 \dots n_k\rangle \tag{10}$$

(Note that the first and last site functions $[\psi^{n_1}], [\psi^{n_k}]$ have dimensions $1 \times M$ and $M \times 1$ respectively).

Alternatively, we can view a 3-tensor as a single matrix if we group two indices together to make a compound index. This view will be useful when discussing the renormalised basis and canonical representations of the DMRG wavefunction in sections 4 and 5. Depending on the context, we will either group the n index with the left or the right auxiliary indices, giving

$$\begin{aligned} \text{Matrix} &: [\psi^{p}] \ (\text{dimension } 4M \times M) \\ \text{Elements} &: \psi^{p}_{ni,i'} \\ \textit{or} \quad \text{Matrix} &: [\psi^{p}] \ (\text{dimension } M \times 4M) \\ \text{Elements} &: \psi^{p}_{i,ni'} \end{aligned} \tag{11}$$

Note that the superscript p here denotes the pth site function in the DMRG ansatz (8), not any particular element of the site function.

3 Properties of the DMRG Ansatz

Let us now examine some properties of the DMRG ansatz.

1. *Variational*: Since we have an explicit wavefunction, the expectation value of the energy provides a variational upper bound to the true energy and in practice DMRG energies are evaluated in this way. As M is increased, the DMRG energy converges from above to the exact energy.
2. *Multireference*: There is no division into occupied and virtual orbitals, all orbitals appear on an equal footing in the ansatz (8). In particular, the Hartree-Fock reference has no special significance here. For this reason, we expect (and observe) the ansatz to be very well-balanced for describing nondynamic correlation in multireference problems (see e.g. [4, 7, 37]). Conversely, the ansatz is inefficient for describing *dynamic* correlation, since this benefits from knowledge of the occupied and virtual spaces.
3. *Size-consistency*: The DMRG ansatz is size-consistent within a localised basis. Consider a system AB composed of two spatially separated, non-interacting subsystems A and B. Associate localised orbitals $1 \dots a$ with subsystem A and $a+1 \dots a+b$ with subsystem B. Then, the DMRG wavefunction for AB factorises into a product of DMRG wavefunctions for A and B. First expand the DMRG wavefunction

$$\begin{aligned}
|\Psi^{\mathrm{AB}}_{\mathrm{DMRG}}\rangle &= \sum_{\substack{n_1 \dots n_{a+b} \\ i_1 \dots i_{a+b-1}}} \psi^{n_1}_{i_1} \dots \psi^{n_a}_{i_{a-1} i_a} \psi^{n_{a+1}}_{i_a i_{a+1}} \dots \psi^{n_{a+b}}_{i_{a+b-1}} |n_1 \dots n_a n_{a+1} n_{a+b}\rangle \\
&= \sum_{i_a} \Big(\sum_{\substack{n_1 \dots n_a \\ i_1 \dots i_{a-1}}} \psi^{n_1}_{i_1} \dots \psi^{n_a}_{i_{a-1} i_a} |n_1 \dots n_a\rangle \\
&\quad \times \sum_{\substack{n_{a+1} \dots n_{a+b} \\ i_{a+1} \dots i_{a+b-1}}} \psi^{n_{a+1}}_{i_a i_{a+1}} \psi^{n_{a+b}}_{i_{a+b-1}} |n_{a+1} \dots n_{a+b}\rangle \Big). \qquad (12)
\end{aligned}$$

   Then note that we can write a separable wavefunction $|\Psi^{\mathrm{AB}}\rangle = |\Psi^{\mathrm{A}}\rangle |\Psi^{\mathrm{B}}\rangle$ formally as $|\Psi^{\mathrm{AB}}\rangle = \sum_{i=1}^{1} |\Psi^{\mathrm{A}}_i\rangle |\Psi^{\mathrm{B}}_i\rangle$ and thus we can take the dimension of index i_a which couples systems A and B above to be 1, giving

$$\begin{aligned}
|\Psi^{\mathrm{AB}}_{\mathrm{DMRG}}\rangle &= \sum_{\substack{n_1 \dots n_a \\ i_1 \dots i_{a-1}}} \psi^{n_1}_{i_1} \dots \psi^{n_a}_{i_{a-1}} |n_1 \dots n_a\rangle \sum_{\substack{n_{a+1} \dots n_{a+b} \\ i_{a+1} \dots i_{a+b}}} \psi^{n_{a+1}}_{i_{a+1}} \psi^{n_{a+b}}_{i_{a+b-1}} |n_{a+1} \dots n_{a+b}\rangle \\
&= |\Psi^{\mathrm{A}}_{\mathrm{DMRG}}\rangle |\Psi^{\mathrm{B}}_{\mathrm{DMRG}}\rangle. \qquad (13)
\end{aligned}$$

4. *Compactness and efficiency of the ansatz*: The number of variational parameters in the DMRG ansatz is $O(M^2 k)$. How large do we need M to be to achieve a good accuracy? If we choose, for a given index i_p, $M = 1$, then the wavefunction factorises into a simple product of contributions from the spaces $\{n_1 \dots n_p\}$ and $\{n_{p+1} \dots n_k\}$. Increasing M then introduces additional correlations or entanglement between the wavefunction components in the two

spaces. The M required for a given accuracy thus depends on the correlations in the specific state of the molecule. However, we have seen in our applications that for appropriate problems, even modest $M = O(100-1{,}000)$ can allow us to obtain very good accuracy and to solve problems that are insoluble with other techniques. Of course, having a small number of variational parameters does not guarantee that an ansatz can be manipulated efficiently. (Witness the difficulty in evaluating the variational energy corresponding to a Coupled Cluster wavefunction!) As we shall see in Sect. 6, the product structure of the DMRG ansatz enables matrix elements to be evaluated without ever reconstructing the DMRG coefficients in the full Slater determinant expansion, thus bypassing the exponential complexity. (Although one can do so if one wishes, e.g. for the purposes of analysing the DMRG wavefunction, as in [14]). Finally, we note that the DMRG incorporates correlations between orbital spaces in a sequential manner, i.e. the first set of auxiliary indices i_1 entangles spaces $\{n_1\}$ and $\{n_2 \ldots n_k\}$, i_2 entangles spaces $\{n_1 n_2\}$ and $\{n_3 \ldots n_k\}$ and so on. For this reason, the DMRG ansatz performs best if strongly-correlated orbitals are placed next to each other in the ansatz [12, 34, 39, 42].

5. *A local multireference ansatz for long molecules*: The DMRG wavefunction is particularly well-suited to long molecules where it can be viewed as a naturally local multireference ansatz. In long molecules (i.e. those where one of the dimensions is much larger than the other two) with a finite electronic correlation length, we can divide the molecule at any point along the backbone and expect the degree of entanglement between the two resulting subsystems to be independent of the point of division and the length of the chain. Thus, for such problems, the M required for a given accuracy is *independent* of the length of the system and the number of variational parameters in the DMRG wavefunction is simply const $\times O(k)$, as should be in a local ansatz. However, unlike in other local correlation approaches the DMRG provides a local *multireference* ansatz. It is this local nature even in the presence of strong nondynamic correlations which has allowed us to solve very large active space multireference correlation problems in long molecules [5–7].

   In problems which are large in two or three dimensions, the degree of entanglement between two subsystems grows exponentially with the length of the border, and thus the preceding considerations no longer apply. We might then ask, can we modify the DMRG ansatz to obtain a naturally local multireference description for large systems with arbitrary dimensionality? Recently, this has been shown to be possible. Consider, for example, two rows of atoms (each with one localised orbital) arranged as in Fig. 1. The first sub-figure illustrates the sequential coupling between orbital spaces that is contained in the DMRG wavefunction, which is inefficient at describing correlations between atoms in different rows. In the second sub-figure, however, we have added additional auxiliary indices to couple the site functions both along the rows as well as along the columns in a non-sequential manner. This is the basis for the so-called Projected Entangled Pair State wavefunctions which present one of the most promising new developments in this area [21–23].

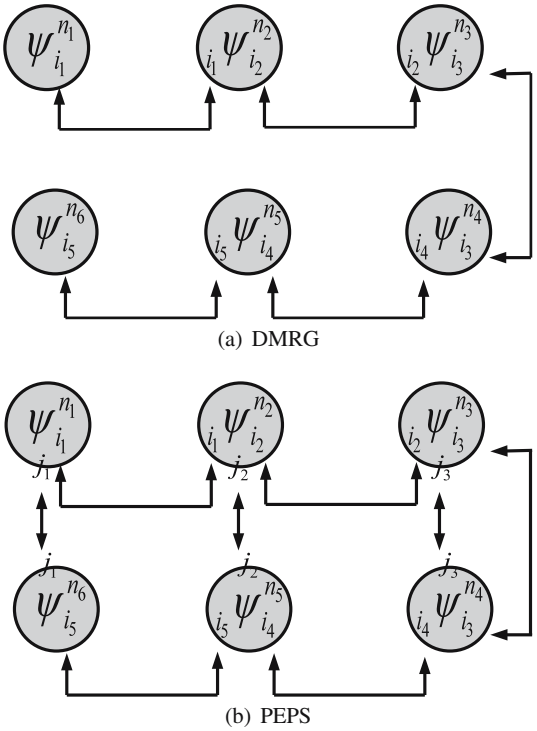

Fig. 1 Density Matrix Renormalisation Group and Projected Entangled Pair State wavefunctions for two rows of atoms. Note in the DMRG ansatz, the site functions are coupled sequentially, which prevents the efficient description of correlations between the rows. However, in the PEPS ansatz, addition indices are added to the site functions (e.g. $\psi^{n_2}_{i_1 i_2} \rightarrow \psi^{n_2}_{i_1 i_2 j_2}$) whose coupling directly captures the inter-row correlations

4 The Renormalized Basis

As we have discussed above, the auxiliary indices of the site functions introduce couplings between the orbital spaces in the DMRG ansatz. In addition, they can also be provided with a direct physical interpretation. Just as the index n_i is associated with the Fock space of orbital i, so can we also associate a set of *renormalised many-body spaces* with the auxiliary indices of each site function ψ. This provides the Renormalisation Group (RG) interpretation of the DMRG wavefunction. Consider, for example, the first set of auxiliary indices i_1. We first perform the summation in the DMRG wavefunction expression over n_1, which couples $\psi^{n_1}_{i_1}$ with the set of states $\{|n_1\rangle\} = \{|0\rangle, |1^\alpha\rangle, |1^\beta\rangle, |2^{\alpha\beta}\rangle\}$. This formally defines a space $\{i_1\}$ with basis functions $|i_1\rangle$

$$|i_1\rangle = \sum_{n_1} \psi^{n_1}_{i_1} |n_1\rangle \tag{14}$$

or more succinctly

$$\{i_1\} = \hat{\psi}^1 \cdot \{n_1\}. \tag{15}$$

Of course, the transformation of the $\{n_1\}$ orbital Fock space by the ψ^1 site function is trivial. (Indeed, if, as is usual, we do not allow ψ to mix states with different particle numbers or spin, we would simply have $|i_1\rangle = |n_1\rangle$ for all 4 states). However, things are more interesting, when we consider the spaces associated with later sets of auxiliary indices. For example, repeating the above exercise for i_2

$$|i_2\rangle = \sum_{\substack{n_1 n_2 \\ i_1}} \psi^{n_1}_{i_1} \psi^{n_2}_{i_1 i_2} |n_1 n_2\rangle \tag{16}$$

$$= \sum_{\substack{n_2 \\ i_1}} \psi^{n_2}_{i_1 i_2} |i_1 n_2\rangle, \tag{17}$$

$$\{i_2\} = \hat{\psi}^2 \cdot \{i_1 n_2\} = \hat{\psi}^2 \cdot \hat{\psi}^1 \cdot \{n_1 n_2\}. \tag{18}$$

In general for the space $\{i_p\}$ and the associated basis $|i_p\rangle$, we write

$$\begin{aligned} \{i_p\} &= \hat{\psi}^p \cdot \{i_{p-1} n_p\} \\ &= \hat{\psi}^p \cdot \hat{\psi}^{p-1} \cdots \hat{\psi}^1 \cdot \{n_1 n_2 \ldots n_p\}, \end{aligned} \tag{19}$$

$$\begin{aligned} |i_p\rangle &= \sum_{\substack{n_p \\ i_{p-1}}} \psi^{n_p}_{i_{p-1} i_p} |i_{p-1} n_p\rangle \\ &= \sum_{\substack{n_1 \ldots n_p \\ i_1 \ldots i_{p-1}}} \psi^{n_1}_{i_1} \psi^{n_2}_{i_1 i_2} \ldots \psi^{n_{p-1}}_{i_{p-2} i_{p-1}} \psi^{n_p}_{i_{p-1} i_p} |n_1 n_2 \ldots n_p\rangle. \end{aligned} \tag{20}$$

Note that the matrix representation of $\hat{\psi}^p$ is simply the matrix form of the site function $[\psi^p]$ described in Eq. (11), i.e.

$$\langle i_p | \hat{\psi}^p | i_{p-1} n_p \rangle = \psi^p_{i_p, i_{p-1} n_1} \tag{21}$$

and thus we can also write Eq. (20) as

$$|i_p\rangle = \sum_{n_1 \ldots n_p} \left([\psi^{n_1}][\psi^{n_2}] \ldots [\psi^{n_{p-1}}][\psi^{n_p}] \right)_{i_p} |n_1 n_2 \ldots n_p\rangle. \tag{22}$$

Now the dimension of the i_p index and $\{i_p\}$ space is fixed to be at most M in the original ansatz (8). Thus, the action of $\hat{\psi}^p \cdots \hat{\psi}^1$ is a projective transformation from the full many-body space down into a *renormalised* many-body space of M basis states, where each basis state $|i_p\rangle$ is expressed as a linear combination of many product functions $|n_1 \ldots n_p\rangle$ with coefficients given by Eq. (20). The renormalised spaces have a recursive structure: $\{i_p\}$ is obtained from $\{i_{p-1}\}$ which is obtained from $\{i_{p-2}\}$ and so on.

The construction of one renormalised space from the previous one may be considered to proceed in two stages. To construct the space $\{i_p\}$, first we form the

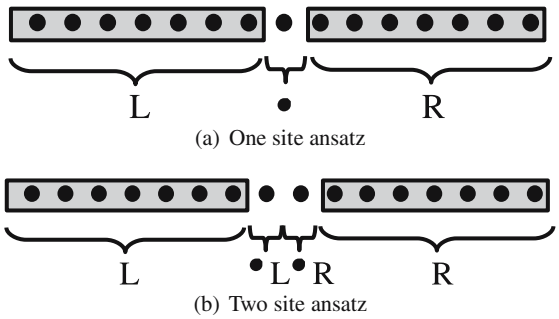

(a) One site ansatz

(b) Two site ansatz

Fig. 2 Block diagrams for the one and two site DMRG ansaetze

product space

$$\{i_{p-1}\} \otimes \{n_p\} \rightarrow \{i_{p-1} n_p\} \tag{23}$$

and then we apply the projective transformation

$$\hat{\psi}^p \cdot \{i_{p-1} n_p\} \rightarrow \{i_p\}. \tag{24}$$

The first step is called "blocking" and the second step "decimation" in the traditional language of the Renormalisation Group, and therein lies the basic connection between the DMRG ansatz and its RG interpretation. It is common to represent these blocking and decimation steps in the pictorial fashion shown in Fig. 2.

5 The Canonical Representation and Sweep Algorithm

The DMRG wavefunction is invariant to a class of transformations of the site functions ψ, since the associated nested many-body spaces $\{i_p\}$ are themselves invariant with respect to transformations within each space. The original DMRG algorithm, which was formulated in the language of orthogonal projective transformations following Wilson's Numerical Renormalisation Group, in fact corresponds to particular choices of representation of the site functions within the above invariant class. We shall call such representations "canonical representations". All existing DMRG implementations in quantum chemistry work with canonical representations of the DMRG wavefunction. In addition, the use of canonical representations is closely linked with the density matrix interpretation of the DMRG and also with the DMRG sweep algorithm, which provides a natural algorithm to optimise the DMRG wavefunction.

Associated with each DMRG wavefunction Ψ there are k canonical representations, one for each site. At site p, the canonical representation is written as

$$|\Psi\rangle = \sum_{n_1 \ldots n_p \ldots n_k} [L^{n_1}] \ldots [L^{n_{p-1}}][C^{n_p}][R^{n_{p+1}}] \ldots [R^{n_k}] |n_1 \ldots n_p \ldots n_k\rangle \tag{25}$$

$$= \sum_{\substack{n_1 \ldots n_p \ldots n_k \\ l_1 \ldots l_{p-1}, r_p \ldots r_{k-1}}} L^{n_1}_{l_1} \ldots L^{n_{p-1}}_{l_{p-2} l_{p-1}} C^{n_p}_{l_{p-1} r_p} R^{n_{p+1}}_{r_p r_{p+1}} \ldots R^{n_k}_{r_{k-1}} |n_1 \ldots n_p \ldots n_k\rangle. \tag{26}$$

Here, the site functions to the left of p have been given the symbol L, while those to the right have been given the symbol R. The L and R site functions, which are in this context usually called transformation matrices, are each orthogonal matrices when written in the matrix representation of Eq. (11). We interpret the L site functions as matrices by grouping the n index with the first auxiliary index,

$$(q < p : L^q_{ln,l'} := L^{n_q}_{ll'}) \tag{27}$$

and in this form we have

$$[L^q]^T [L^q] = [1], \tag{28}$$

$$\sum_{ln} L^q_{ln,l'} L^q_{ln,l''} = \delta_{l'l''}. \tag{29}$$

For the R site functions, we group the n index with the second auxiliary index

$$(q > p : R^q_{r',rn} := R^{n_q}_{r'r}) \tag{30}$$

and in this form we have

$$[R^q][R^q]^T = [1], \tag{31}$$

$$\sum_{rn} R^q_{r',rn} R^q_{r'',rn} = \delta_{r'r''}. \tag{32}$$

The L and R matrices each define a set of orthogonal projective transformations, which give rise, respectively, to two sets of renormalised spaces $\{l\}$ and $\{r\}$ associated with the site p representation of the DMRG wavefunction. The $\{l\}$ spaces, $\{l_1\}, \{l_2\} \ldots$ are built up by incorporating the orbitals in the order $1, 2 \ldots p$,

$$\begin{aligned}(q < p) : \{l_q\} &= \hat{L}^q \cdot \{l_{q-1} n_q\} \\ &= \hat{L}^q \cdot \hat{L}^{q-1} \cdot \{l_{q-2} n_{q-1} n_q\} \\ &= \hat{L}^q \cdot \hat{L}^{q-1} \cdots \hat{L}^1 \cdot \{n_1 \ldots n_q\}\end{aligned} \tag{33}$$

and the $|l\rangle$ functions form an orthogonal renormalised basis (from the orthogonal nature of the $[L]$ transformation matrices) for each $\{l\}$ space

$$|l_q\rangle = \sum_{n_1 \ldots n_p} [L^{n_1}][L^{n_2}] \ldots [L^{n_{q-1}}][L^{n_q}] |n_1 n_2 \ldots n_1\rangle, \tag{34}$$

$$\langle l_q | l'_q \rangle = \delta_{ll'}. \tag{35}$$

The $\{r\}$ spaces and $|r\rangle$ basis functions are defined similarly, but now the orbitals are incorporated "backwards" in the order $k, k-1 \ldots p+1$

$$\begin{aligned}(q > p) : \{r_q\} &= \hat{R}^q \cdot \{n_q r_{q+1}\} \\ &= \hat{R}^q \cdot \hat{R}^{q+1} \cdot \{n_q n_{q+1} r_{q+2}\} \\ &= \hat{R}^q \cdot \hat{R}^{q+1} \cdots \hat{R}^k \cdot \{n_q \ldots n_k\}, \qquad (36)\end{aligned}$$

$$|r_q\rangle = \sum_{n_q \ldots n_k} [R^{n_q}][R^{n_{q+1}}] \ldots [R^{n_{k-1}}][R^{n_k}] |n_q n_{q+1} \ldots n_k\rangle, \qquad (37)$$

$$\langle r_q | r'_q \rangle = \delta_{rr'}. \qquad (38)$$

Having defined the renormalised spaces, we now see that the C^p site function gives the wavefunction coefficients in the product space formed from the renormalised left basis $\{l_{p-1}\}$, the orbital space $\{n_p\}$, and the renormalised right basis $\{r_p\}$

$$|\Psi\rangle = \sum_{lnr} C^p_{lnr} |l_{p-1} n_p r_p\rangle \qquad (39)$$

where we have used the notation $C^p_{lnr} := C^{n_p}_{l_{p-1} r_p}$.

We now consider the DMRG wavefunction expressed in the canonical representations of sites other than p. Since the same wavefunction is simply being expressed in a different representation, this implies a relationship between the wavefunction coefficients C and transformation matrices L, R at different sites. Comparing representations at sites p, $p+1$ we see

$$\begin{aligned}|\Psi\rangle &= \sum_{n_1 \ldots n_p \ldots n_k} [L^{n_1}] \ldots [L^{n_{p-1}}][C^{n_p}][R^{n_{p+1}}][R^{n_{p+2}}] \ldots [R^{n_k}] |n_1 \ldots n_p \ldots n_k\rangle \qquad (40) \\ &= \sum_{n_1 \ldots n_p \ldots n_k} [L^{n_1}] \ldots [L^{n_{p-1}}][L^{n_p}][C^{n_{p+1}}][R^{n_{p+2}}] \ldots [R^{n_k}] |n_1 \ldots n_p \ldots n_k\rangle. \qquad (41)\end{aligned}$$

This implies

$$[C^{n_p}][R^{n_{p+1}}] = [L^{n_p}][C^{n_{p+1}}] \qquad (42)$$

or, switching to the alternative matrix interpretation of Eq. (11) for C^p, C^{p+1} and likewise for L^p, R^{p+1}

$$\sum_r C^p_{ln,r} R^{p+1}_{r,r'n} = \sum_{l'} L^p_{ln,l'} C^{p+1}_{l',n'r'}. \qquad (43)$$

From C^p, we can determine the quantities in the site $p+1$ canonical form that do not explicitly appear in the site p canonical form, namely C^{p+1}, L^p, by the singular value decomposition (SVD) of C^p,

$$C^p_{ln,r} = \sum_{l'} L^p_{ln,l'} \sigma_{l'} V_{l'r}, \qquad (44)$$

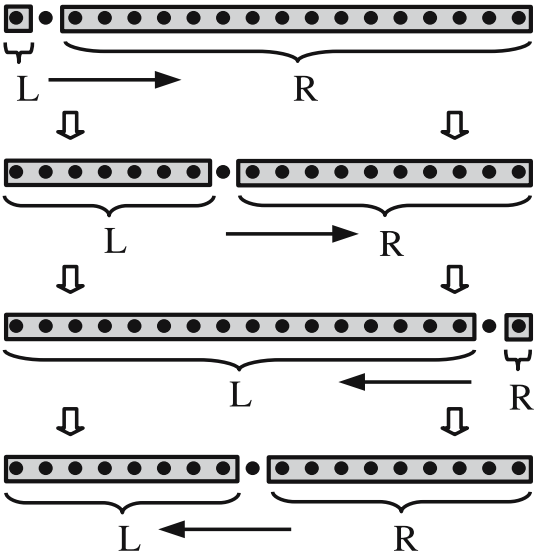

Fig. 3 The DMRG sweep algorithm with the one site ansatz. After all L blocks are constructed going from $L \rightarrow R$, the sweep direction is reversed

$$C^{p+1}_{l,nr} = \sum_{r'} \sigma_l V_{lr'} R^{p+1}_{r',rn}. \tag{45}$$

The connection through the SVD between the representations at different sites leads to the density matrix formulation of the DMRG. Recall that the singular vectors of a matrix M may be related to the eigenvectors of $M^T M$ and MM^T. Thus from C^p, we can define a symmetric object $[\Gamma^p] = [C^p]^T [C^p]$, i.e.

$$\Gamma^p_{ln,l'n'} = \sum_r C^p_{lnr} C^p_{l'n'r}. \tag{46}$$

Γ^p is none other than the *density matrix* associated with the left subsystem, or "block" of orbitals $1 \ldots p$, and the left transformation matrix L^p is obtained as the matrix of M eigenvectors

$$\sum_{l'n'} \Gamma^p_{ln,l'n'} L^p_{l'n',l''} = L^p_{ln,l''} \sigma^2_{l''}. \tag{47}$$

This corresponds to the traditional density matrix interpretation of the DMRG: to obtain the canonical representation at a new site requires a basis change into the eigenvectors of the subsystem density matrix.

The sequential set of transformations from representation to representation along the sites also yields a natural optimisation procedure for the DMRG wavefunction known as the *sweep algorithm*. At each site p, we solve the Schrödinger equation in the basis $\{l_{p-1} n_p r_p\}$ to obtain the coefficient matrix C^p, thus (dropping the

subscripts on the basis functions for simplicity)

$$\langle l'n'r'|\hat{H}-E|\Psi\rangle = 0, \tag{48}$$

$$\sum_{lnr}\langle l'n'r'|\hat{H}-E|lnr\rangle C^{p}_{lnr} = 0. \tag{49}$$

From this coefficient matrix, we obtain the new transformation matrix at site $p \pm 1$ from the SVD in Eq. (44) (or equivalently, in the density matrix formulation, from the eigenvectors of the density matrix in Eq. (47)). If we move through the sites from left to right ($p \rightarrow p+1$) in a sweep, we successively determine new L^p matrices, while moving from right to left ($p \rightarrow p-1$) determines new R^p matrices. After the sites are traversed in one direction, we traverse in the opposite direction thus allowing improvement of all the L^p and R^p matrices. (Of course, to initialise the procedure, requires some starting guess for the L^p and R^p matrices). This is the basic method that is employed to optimise the DMRG energy.

We usually depict the canonical representation at site p in a block-configuration diagram as shown in Fig. 2 consisting of a left block of orbitals $1 \ldots p-1$, the site p and a right block of orbitals $p+1 \ldots k$. Then, moving from one site to another corresponds to moving from block-configuration to block-configuration, sweeping from left-to-right and then right-to-left as shown in Fig. 3.

So far we have always been working within what is known as the *one-site* DMRG algorithm, since, as can be seen from the block diagram in Fig. 2, there is only one site between the left and right blocks. However, in earlier formulations of the DMRG algorithm it was common to use the so-called two-site algorithm, corresponding to the second block configuration in Fig. 2. Here the wavefunction at site p is written in the renormalised product space as

$$|\Psi\rangle = \sum_{lnn'r} C^{p}_{lnn'r}|l_{p-1}n_p n'_{p+1}r_{p+1}\rangle \tag{50}$$

where we see that two complete orbital Fock spaces $\{n_p\},\{n_{p+1}\}$ appear in the wavefunction expansion. Unlike in the one-site configuration, we can only approximately relate the canonical representations of the two-site wavefunctions at different sites, and thus there is no single consistent DMRG wavefunction across a two-site DMRG sweep, but rather a whole family of DMRG wavefunctions, one at each site. Originally, the two-site algorithm was introduced to eliminate some numerical problems associated with local minima when optimising the DMRG wavefunction in the sweep algorithm [2,12,37], but with the introduction of newer methods which avoid such minima [56], the one-site formulation should now be viewed as preferred.

6 Evaluation of Matrix Elements

For completeness, we now outline briefly how the DMRG wavefunction allows the efficient evaluation of the matrix elements necessary to solve the Schrodinger equation in the renormalised product basis (49). We first note that any operator in the

complete Fock space $\{n_1\} \otimes \{n_2\} \otimes \{n_3\} \otimes \ldots \otimes \{n_k\}$ can be expressed as a sum of products of "local" operators that each act individually in the Fock space of a single site. For example, the unit operator $\hat{I}$ in the full Fock space may be considered as a single tensor product of local unit operators

$$\hat{I} = \hat{I}^1 \otimes \hat{I}^2 \otimes \hat{I}^3 \otimes \ldots \otimes \hat{I}^k \tag{51}$$

where e.g. $\langle n_1 | \hat{I}^1 | n_1 \rangle = \delta_{n_1 n_1'}$. To see how the quantum chemistry Hamiltonian

$$H = \sum_{ij} t_{ij} a_i^\dagger a_j + \sum_{ijkl} v_{ijkl} a_i^\dagger a_j^\dagger a_k a_l \tag{52}$$

can be written as a sum of products of local operators, it is sufficient to show that the creation and annihilation operators can be expressed in this form. Note that a single creation or annihilation operator does not simply act in the Fock space of a single orbital, because of the anticommutation relations between operators. Instead, we write for $a_i^\dagger, a_i$

$$a_i^\dagger = \prod_{j<i} (-)^{n_j} \otimes P_i a_i^\dagger P_i, \tag{53}$$

$$a_i = \prod_{j<i} (-)^{n_j} \otimes P_i a_i P_i. \tag{54}$$

Here the operator $\prod_{j<i}(-)^{n_j}$ formally keeps tracks of the anticommutation, since if we consider e.g. a_i acting on a determinant, it counts the number of sign changes involved in moving orbital i to the front of the orbital string. P_i denotes the projection of operator onto the $\{n_i\}$ space alone.

Given that all operators can be written as a sum of products of local operators, we now examine how the matrix elements of a single product of local operators are obtained. Consider the product

$$\hat{O} = \hat{O}^1 \otimes \hat{O}^2 \otimes \ldots \hat{O}^k. \tag{55}$$

In terms of the product basis $\{|l_{p_1} n_p r_p\rangle\}$ of site p, we can write (dropping the subscripts on the basis functions for simplicity)

$$\langle l' n' r' | \hat{O} | l n r \rangle = \langle l' | \hat{O}^1 \otimes \ldots \otimes \hat{O}^{p-1} | l \rangle \langle n' | \hat{O}^p | n \rangle \langle r' | \hat{O}^p \otimes \ldots \otimes \hat{O}^k | r \rangle \tag{56}$$

$$= \langle l' | \hat{O}_L | l \rangle \langle n' | \hat{O}^p | n \rangle \langle r' | \hat{O}_R | r \rangle. \tag{57}$$

It is sufficient to demonstrate how the matrix elements $\langle l | \hat{O}_L | l' \rangle$ are calculated as those for O_R are obtained in a similar manner. From the recursive definitions of the renormalised basis functions $|l\rangle, |l'\rangle$ in Eqs. (34), (37) we have

$$\langle l' | \hat{O}_L | l \rangle = \sum_{\substack{n_1 \ldots n_p \\ n_1' \ldots n_p'}} [L^{n_1}][L^{n_2}] \ldots [L^{n_{p-1}}] \big(O^1_{n_1 n_1'} O^2_{n_2 n_2'} \ldots O^{p-1}_{n_{p-1} n_{p-1}'} \big) [L^{n_1'}][L^{n_2'}] \ldots [L^{n_{p-1}'}]. \tag{58}$$

These multiple transformations may be efficiently organised into groups of two step procedures (corresponding to the familiar blocking and decimation steps of the RG). Writing

$$O^1_{l_1 l'_1} = \langle l_1 | \hat{O}_1 | l'_1 \rangle = L^{n_1}_{l_1} O^1_{n_1 n'_1} L^{n_1}_{l_1} \tag{59}$$

the blocking step corresponds to

$$O^1_{l_1 l'_1} \otimes O^2_{n_2 n'_2} \rightarrow \left(O^1 O^2\right)_{l_1 n_1 l'_1 n'_1} \tag{60}$$

while the decimation corresponds to the transformation into the renormalised basis ($\{l_1 n_2\} \rightarrow \{l_2\}$)

$$\sum_{l_1 n_2 l'_1 n'_2} L^{n_2}_{l_1 l_2} \left(O^1 O^2\right)_{l_1 n_2 l'_1 n'_2} L^{n'_2}_{l'_1 l'_2} \rightarrow \left(O^1 O^2\right)_{l_2 l'_2}. \tag{61}$$

Each such transformation has the cost of a matrix multiplication i.e $O(M^3)$, and because of the recursive structure of the transformations, the complete matrix element $\langle l' | O_L | l \rangle$ may be efficiently evaluated as a sequence of matrix products with a total cost $O(M^3 k)$.

For complicated operators such as the quantum chemical Hamiltonian which consist of sums over many products of operators, it is clear that there are intermediates which can be reused and saved. For example, the matrix elements of $a^\dagger_1 a^\dagger_2 a_9 a_{10}$ and $a^\dagger_1 a^\dagger_2 a_4 a_5$ both involve as an intermediate the renormalised representation of $a^\dagger_1 a^\dagger_2$, which may be stored and reused. In practice, therefore, the optimal implementation of the DMRG algorithm in quantum chemistry requires an efficient organisation of intermediates and this is primarily where most of the complexity may be be found. The interested reader is referred to the literature for further details e.g. [10–14, 37].

7 Conclusions

In this article we have attempted to introduce the Density Matrix Renormalisation Group (DMRG) primarily from the view that it provides quantum chemistry with a new kind of wavefunction ansatz. Consequently, we can analyse and manipulate the ansatz in the way to which we are accustomed in quantum chemistry. By examining its structure we arrive at an intuitive understanding of the strengths of the DMRG method e.g. in multireference problems, or in long molecules, where it is a naturally local multireference approach. A striking feature of the DMRG ansatz as compared to other quantum chemical wavefunctions is the recursive structure. This is the connection between the DMRG wavefunction and the traditional language of the Renormalisation Group, and provides the central mechanism behind the efficient evaluation of matrix elements in the method.

Traditionally quantum chemistry has understood electronic structure in terms of the many-electron wavefunction. We hope that by thinking about the DMRG in this language, it will not only become more accessible, but new possibilities will arise for cross-fertilisation between quantum chemical techniques and the Density Matrix Renormalisation Group.

Acknowledgements Garnet Kin-Lic Chan would like to acknowledge support from Cornell University, the Cornell Center for Materials Research (CCMR), the David and Lucile Packard Foundation, the National Science Foundation CAREER program CHE-0645380, the Alfred P. Sloan Foundation, and the Department of Energy, Office of Science through award DE-FG02-07ER46432. Johannes Hachmann would like to acknowledge support provided by a Kekulé Fellowship of the Fond der Chemischen Industrie. Eric Neuscamman would like to acknowledge support provided by a National Science Foundation Graduate Research Fellowship.

References

1. S.R. White, Phys. Rev. Lett. **69**(19), 2863 (1992)
2. S.R. White, Phys. Rev. B **48**(14), 10345 (1993)
3. G.K.L. Chan, M. Head-Gordon, J. Chem. Phys. **118**(19), 8551 (2003)
4. G.K.L. Chan, M. Kállay, J. Gauss, J. Chem. Phys. **121**(13), 6110 (2004)
5. J. Hachmann, J.J. Dorando, M. Avilés, G.K.L. Chan, J. Chem. Phys. **127**(13), 134309 (2007)
6. J.J. Dorando, J. Hachmann, G.K.L. Chan, J. Chem. Phys. **127**(8), 084109 (2007)
7. J. Hachmann, W. Cardoen, G.K.L. Chan, J. Chem. Phys. **125**(14), 144101 (2006)
8. K.G. Wilson, Rev. Mod. Phys. **47**(4), 773 (1975)
9. K.G. Wilson, Rev. Mod. Phys. **55**(3), 583 (1983)
10. S.R. White, R.L. Martin, J. Chem. Phys. **110**(9), 4127 (1999)
11. A.O. Mitrushenkov, G. Fano, F. Ortolani, R. Linguerri, P. Palmieri, J. Chem. Phys. **115**(15), 6815 (2001)
12. G.K.L. Chan, M. Head-Gordon, J. Chem. Phys. **116**(11), 4462 (2002)
13. Ö. Legeza, J. Röder, B.A. Hess, Phys. Rev. B **67**(12), 125114 (2003)
14. G. Moritz, M. Reiher, J. Chem. Phys. **126**(24), 244109 (2007)
15. M. Fannes, B. Nachtergaele, R.F. Werner, Comm. Math. Phys. **144**(3), 443 (1992)
16. M. Fannes, B. Nachtergaele, R.F. Werner, J. Funct. Anal. **120**(2), 511 (1994)
17. S. Östlund, S. Rommer, Phys. Rev. Lett. **75**(19), 3537 (1995)
18. S. Rommer, S. Östlund, Phys. Rev. B **55**(4), 2164 (1997)
19. F. Verstraete, J.J. García-Ripoll, J.I. Cirac, Phys. Rev. Lett. **93**(20), 207204 (2004)
20. F. Verstraete, D. Porras, J.I. Cirac, Phys. Rev. Lett. **93**(22), 227205 (2004)
21. F. Verstraete, J.I. Cirac, arXiv:cond-mat **0407066v1** (2004)
22. D. Pérez-Garciá, F. Verstraete, J.I. Cirac, M.M. Wolf, arXiv:quant-ph **0707.2260v1** (2007)
23. N. Schuch, M.M. Wolf, F. Verstraete, J.I. Cirac, Phys. Rev. Lett. **98**(14), 140506 (2007)
24. V. Murg, F. Verstraete, J.I. Cirac, Phys. Rev. A **75**(3), 033605 (2007)
25. F. Verstraete, A. Weichselbaum, U. Schollwöck, J.I. Cirac, J. von Delft, arXiv:cond-mat **0504305v1** (2005)
26. S.R. White, A.E. Feiguin, Phys. Rev. Lett. **93**(7), 076401 (2004)
27. A.J. Daley, C. Kollath, U. Schollwöck, G. Vidal, J. Stat. Mech.: Theor. Exp. (04), P04005 (2004)
28. G. Vidal, Phys. Rev. Lett. **93**(4), 040502 (2004)
29. G. Vidal, arXiv:quant-ph **0610099v1** (2006)
30. K. Hallberg, in *Theoretical Methods for Strongly Correlated Electrons*, ed. by D. Sénéchal, A.M. Tremblay, C. Bourbonnais, CRM Series in Mathematical Physics (Springer, New York, 2003)

31. K.A. Hallberg, Adv. Phys. **55**(5), 477 (2006)
32. U. Schollwöck, Rev. Mod. Phys. **77**(1), 259 (2005)
33. S. Daul, I. Ciofini, C. Daul, S.R. White, Int. J. Quantum Chem. **79**(6), 331 (2000)
34. J. Rissler, R.M. Noack, S.R. White, Chem. Phys. **323**(2–3), 519 (2006)
35. A.O. Mitrushenkov, R. Linguerri, P. Palmieri, G. Fano, J. Chem. Phys. **119**(8), 4148 (2003)
36. A.O. Mitrushenkov, G. Fano, R. Linguerri, P. Palmieri, arXiv:cond-mat **0306058v1** (2003)
37. G.K.L. Chan, J. Chem. Phys. **120**(7), 3172 (2004)
38. G.K.L. Chan, T. Van Voorhis, J. Chem. Phys. **122**(20), 204101 (2005)
39. Ö. Legeza, J. Sólyom, Phys. Rev. B **68**(19), 195116 (2003)
40. Ö. Legeza, J. Röder, B.A. Hess, Mol. Phys. **101**(13), 2019 (2003)
41. Ö. Legeza, J. Sólyom, Phys. Rev. B **70**(20), 205118 (2004)
42. G. Moritz, B.A. Hess, M. Reiher, J. Chem. Phys. **122**(2), 024107 (2005)
43. G. Moritz, A. Wolf, M. Reiher, J. Chem. Phys. **123**(18), 184105 (2005)
44. G. Moritz, M. Reiher, J. Chem. Phys. **124**(3), 034103 (2006)
45. D. Zgid, M. Nooijen, J. Chem. Phys. **128**, 014107 (2008)
46. S. Ramasesha, S.K. Pati, H.R. Krishnamurthy, Z. Shuai, J.L. Brédas, Synth. Met. **85**(1–3), 1019 (1997)
47. D. Yaron, E.E. Moore, Z. Shuai, J.L. Brédas, J. Chem. Phys. **108**(17), 7451 (1998)
48. Z. Shuai, J.L. Brédas, A. Saxena, A.R. Bishop, J. Chem. Phys. **109**(6), 2549 (1998)
49. G. Fano, F. Ortolani, L. Ziosi, J. Chem. Phys. **108**(22), 9246 (1998)
50. G.L. Bendazzoli, S. Evangelisti, G. Fano, F. Ortolani, L. Ziosi, J. Chem. Phys. **110**(2), 1277 (1999)
51. C. Raghu, Y. Anusooya Pati, S. Ramasesha, Phys. Rev. B **65**(15), 155204 (2002)
52. C. Raghu, Y. Anusooya Pati, S. Ramasesha, Phys. Rev. B **66**(3), 035116 (2002)
53. J. Dukelsky, M.A. Martín-Delgado, T. Nishino, G. Sierra, Europhys. Lett. **43**(4), 457 (1998)
54. F. Verstraete, J.I. Cirac, Phys. Rev. B **73**(9), 094423 (2006)
55. D. Pérez-Garciá, F. Verstraete, M.M. Wolf, J.I. Cirac, Quant. Inf. Comp. **7**(5&6), 401 (2007)
56. S.R. White, Phys. Rev. B **72**(18), 180403 (2005)

Method of Moments of Coupled Cluster Equations Employing Multi-Reference Perturbation Theory Wavefunctions: General Formalism, Diagrammatic Formulation, Implementation, and Benchmark Studies

Maricris D. Lodriguito and Piotr Piecuch

Abstract A new class of non-iterative single-reference coupled-cluster (CC) and equation-of-motion CC (EOMCC) methods that combines the idea of energy corrections due to higher-order excitations defining the method of moments of CC equations (MMCC) with the multi-reference many-body perturbation theory, which is used to provide information about the most essential correlation effects relevant to electronic quasi-degeneracies, is described. The key elements of the resulting theory, termed MMCC/PT, are formulated using diagrammatic methods. The performance of the basic MMCC/PT approximations, in which inexpensive corrections due to triple (MMCC(2,3)/PT) or triple and quadruple (MMCC(2,4)/PT) excitations are added to ground- and excited-state energies obtained with the CC/EOMCC singles and doubles (CCSD/EOMCCSD) approach, is illustrated by the results of benchmark calculations including bond breaking in HF, H_2O, and F_2, and excited states of CH^+. The efficient, highly vectorized implementations of the triply and quadruply excited moments of the CCSD/EOMCCSD equations that enter the MMCC(2,3)/PT and MMCC(2,4)/PT energy formulas and other approaches based on the MMCC formalism, including other externally corrected MMCC theories and renormalized CC/EOMCC approaches, are discussed, and the most essential details of the MMCC/PT algorithm are presented.

Keywords: Coupled-cluster theory, Single-reference methods, Multi-reference methods, Method of moments of coupled-cluster equations, Many-body perturbation theory, Renormalized coupled-cluster methods, Diagrammatic methods, Potential energy surfaces, Excited states, Externally corrected coupled-cluster methods

M.D. Lodriguito
Michigan State University, East Lansing Michigan 48824, e-mail: lodrigui@msu.edu

P. Piecuch
Michigan State University, East Lansing Michigan 48824, e-mail: piecuch@chemistry.msu.edu

S. Wilson et al. (eds.) *Frontiers in Quantum Systems in Chemistry and Physics*.

1 Introduction

Not long after the discovery of Schrödinger's equation [1] in 1926, one of the pioneers of quantum mechanics, Dirac, made a widely publicized statement that "the underlying physical laws necessary for the mathematical treatment of a large part of physics and the whole of chemistry are thus completely known, and the difficulty is only that the exact application of these laws leads to equations much too complicated to be soluble" [2]. Because of this statement, chemists at that time were skeptical about the prospects of quantum theory as a way to study molecular properties. However, what has not been publicized as broadly, in the same paper Dirac also wrote that "it therefore becomes desirable that the approximate practical methods should be developed, which can lead to an explanation of the main features of complex atomic system without too much computation" [2]. Inspired by this less known remark and despite the early reluctance of the chemical community, the field of quantum chemistry has undergone revolutionary advances brought about in part by the advent of computers and in part by much improved understanding of many-electron systems, particularly in recent four decades. The tremendous improvements in accuracy and predictive power of electronic structure methods and significant advances in the fundamental understanding of many-electron wavefunctions, which continues to improve every year, have paved the way to widespread applicability of quantum-chemical methods in solving increasingly complex chemical problems, surpassing what was originally expected in the late 1920s by a wide margin. Furthermore, because of its rigorous and predictive nature, quantum chemistry has become a powerful, important tool not only for theorists but also for experimentalists, while inspiring similar developments in computational nuclear physics, biochemistry, molecular biology, and materials science, among others.

Nowadays, highly accurate *ab initio* (meaning from "first principles") quantum mechanical calculations for small and medium size molecular systems, with up to 20–30 light atoms, a few transition metal atoms and about 100 explicitly correlated electrons, are routine. Theoretical calculations of the energetics and other molecular properties of smaller molecules can often rival those obtained experimentally.

The above successes of quantum chemistry do not mean that there are no open or challenging problems in modern electronic structure theory. Indeed, the key to a successful description of chemical systems is an accurate assessment of many-electron correlation effects. Electrons in molecules move in a complicated, highly correlated fashion and one cannot describe molecular properties by using a simple mean-field description, which ignores electron correlation effects, as is done in the Hartree-Fock (H–F) calculations, particularly in cases involving bond breaking, open-shell systems, and excited electronic states. The least expensive ways of accurately accounting for electron correlation effects have computational steps that typically scale as $\mathcal{N}^6 - \mathcal{N}^7$ with the system size $\mathcal{N}$ and this limits the applicability of correlated *ab initio* methods to systems with about 100 correlated electrons (defined as electrons outside the frozen core). Thus, one of the challenges of modern quantum chemistry is to go to systems with hundreds or thousands of correlated electrons and basis functions. Another challenge is an accurate treatment of bond stretching

or breaking, chemical reaction pathways, and excited states, particularly those dominated by many-electron transitions, i.e., problems where a traditional description in which one starts from a single Slater determinant and builds the electronic wavefunctions on top of a single determinant through particle-hole excitations, and which works for non-degenerate states of closed-shell molecules, is no longer adequate. The present work focuses on the latter challenge.

Generally, there are two types of electron correlation effects: dynamical and non-dynamical (static). Dynamical correlations can be regarded as short-range correlations due to electrons instantaneously avoiding each other, particularly when they come close to each other. On the other hand, non-dynamical correlations can be treated as long-range correlations which arise from the multi-configurational character of systems having quasi(near)-degenerate states, as in the case of the electrons constituting an electron pair undergoing the bond breaking process, biradicals, and the majority of excited states. A well-balanced account of both dynamical and non-dynamical electron correlation is important to obtain a uniformly accurate description of reactants, products, reaction intermediates, and transition states as well as the precise description of electronic excitations in molecules.

Over the years, there has been tremendous progress in the development of electron correlation methods. In this chapter, we primarily focus on the wavefunction-based approaches which can be divided into three main categories: (1) configuration interaction (CI) approaches [3–5]; (2) many-body perturbation theory (MBPT) [6–10]; and (3) coupled-cluster (CC) methods [11–15]. The electron correlation methods can also be classified as single-reference and multi-reference methods. Single-reference electron-correlation methods, from the name itself, are defined by building a correlated wavefunction through electronic excitations out of a single Slater determinant (e.g. a H–F determinant). Multi-reference (MR) methods, on the other hand, utilize a multi-determinantal reference wavefunction to build the desired correlated electronic state or states. In this chapter, we focus on combining the single-reference CC ideas with low-order methods based on the multi-reference MBPT (MRMBPT) treatment.

Let us recall that all CC methods are based on the exponential ansatz for the wavefunction, allowing CC approaches to describe higher-order correlation effects at the low level approximation by generating higher-order excitations in the wavefunction as products of low-order excitations. Of all single-reference methods, the single-reference CC approaches [11–15], in which the H–F wavefunction is usually chosen as a reference state, are generally considered as the best compromise between high accuracy and relatively low computer cost. Another notable characteristic of CC theory is its ability to preserve size extensivity at any level of truncation. These and other attractive features of the CC theory have inspired and continue to inspire significant research work toward the development of high-accuracy methods which can be used as general-purpose tools by experts and non-experts (see [16–23] for selected reviews). In particular, there has been a great deal of interest in extending the single-reference CC methods to quasi-degenerate situations, such as molecular bond dissociation and excited states dominated by two- and other many-electron transitions, which are very challenging because of the large

non-dynamical electron correlation effects that traditional single-reference theories cannot capture.

The basic ground state CC approach with singles and doubles (CCSD) [24–26] is reasonably accurate in describing closed-shell systems and dynamical correlation effects with relatively low computer costs that scale as $n_o^2 n_u^4$ (n_o and n_u are, respectively, the numbers of occupied and unoccupied orbitals used in the correlated calculations), but fails in describing bond breaking because it neglects higher-than-pair (e.g. triply and quadruply excited or T_3 and T_4) clusters. The CCSDT [27, 28] and CCSDTQ [29–32] methods, which incorporate T_3 or T_3 and T_4 clusters, respectively, are capable of giving an accurate description for certain classes of systems with electronic quasi-degeneracies, in spite of their single-reference character, since they describe correlation effects to very high orders, often compensating for the inadequacies of a single-reference description, but the computer costs of the CCSDT and CCSDTQ calculations are extremely high, limiting their applicability to small molecular problems with a few light atoms. In particular, the CCSDT and CCSDTQ methods require iterative steps that scale as $n_o^3 n_u^5$ and $n_o^4 n_u^6$, respectively, which make them applicable to systems with up to $\sim$10 correlated electrons.

To considerably reduce the computational costs of the CCSDT, CCSDTQ, and other high-order CC schemes, several CC approaches, in which the effects of higher-than-doubly excited clusters are included in approximate manner, have been developed. One of the most popular CC methods in this category is the CCSD(T) [33] approach, in which the connected triply excited (T_3) clusters are incorporated in a computationally efficient fashion through the suitably designed non-iterative correction to the CCSD energy derived using arguments that originate from MBPT. The CCSD(T) method and its CCSD[T] analog [34, 35] are currently available in the majority of popular quantum chemistry software packages, enabling highly accurate *ab initio* calculations of useful molecular properties by experts as well as non-experts. However, while the CCSD[T] and CCSD(T) methods improve the description of molecular properties in the region of equilibrium geometry, they completely fail when chemical bonds are stretched or broken [21, 36–67]. The inclusion of non-iterative quadruples (T_4 clusters) using arguments originating from MBPT, which leads to schemes, such as CCSD(TQ$_f$) and CCSDT(Q$_f$) [68], and their various modifications, further improves the results in the equilibrium region but cannot help when the configurational quasi-degeneracy sets in [40–44, 47, 49–52, 59–66].

Similar remarks about the performance and failures of single-reference CC methods can be made when extending the discussion to excited states calculations. The most natural extensions of the single-reference CC formalism to excited states are the linear-response CC theory [69–75] and the closely related equation-of-motion (EOM) CC [76–80] and symmetry-adapted cluster configuration interaction (SAC-CI) approaches [81–85]. The basic linear response CCSD [74, 75] and EOMCCSD [77–79] approximations, which are characterized by the manageable computational steps that scale as $n_o^2 n_u^4$ or $\mathcal{N}^6$ with the system size, and the analogous SAC-CISD method provide reliable information about excited states dominated by one-electron transitions. Unfortunately, the linear response CCSD and EOMCCSD methods cannot describe excited states having significant double excitation components and

excited-state potential energy surfaces along bond breaking coordinates [52, 55, 56, 60–62, 64, 86–100].

High-order EOMCC methods including higher-than-double excitations, such as full EOMCCSDT (EOMCC singles, doubles, and triples) [94, 95, 101] and EOMCCSDTQ (EOMCC singles, doubles, triples, and quadruples) [100, 102], provide an excellent description of excited states dominated by doubles [94, 95, 100] as well as excited-state potential energy surfaces [95], but large costs of the EOMCCSDT and EOMCCSDTQ calculations, which are defined by the iterative steps that scale as $\mathcal{N}^8$ and $\mathcal{N}^{10}$ with the system size, respectively, limit their applicability to small molecules with a few light atoms and relatively small basis sets in the same way the ground-state CCSDT and CCSDTQ methods are limited to small many-electron problems. For this reason, a number of approximate and less expensive ways of incorporating triple or triple and quadruple excitations in the EOMCC and linear response CC formalisms have been developed in order to make these methods applicable to a wider range of molecular sizes. Among those are the iterative EOMCCSDT-*n* approaches and their non-iterative EOMCCSD(T), EOMCCSD($\tilde{\text{T}}$), and EOMCCSD(T$'$) counterparts [87,88], and the analogous linear-response CC methods, such as CC3 [86, 90–92] and CCSDR(3) [86, 92], which use elements of MBPT to estimate triples effects. All of these methods are characterized by the relatively inexpensive $\mathcal{N}^7$ steps of the $n_o^3 n_u^4$ type and all of them improve the EOMCCSD/linear response CCSD results for excited states dominated by two-electron transitions, but there are many cases where the results of EOMCCSDT-*n*, EOMCCSD(T), CC3, and similar calculations are far from satisfactory or become even poor. This can be illustrated by the large 0.4–0.5 and 0.9 eV errors in the description of the lowest $^1\Pi_g$ and $^1\Delta_g$ states of the C_2 molecule, respectively, by the EOMCCSDT-1 and CC3 approaches [86] or the failure of the CC3 and CCSDR(3) methods to provide accurate information about excited-state potential energy surfaces along bond breaking coordinates [103] (see also [98] for an additional analysis).

The above problems encountered in the single-reference CC/EOMCC calculations for various cases of electronic quasi-degeneracies clearly indicate that a traditional single-reference description is not sufficient and that more flexible quantum-chemical models are needed. The conventional wisdom is to turn to multi-reference approaches, in which instead of using a single-determinantal reference state, one selects a certain number of reference determinants to construct the appropriate zeroth-order wavefunction(s) adjusted to the type of bond breaking or excited states of interest. The less intuitive and yet potentially very useful is an idea of improved single-reference methods, which completely or largely rely on a single-determinantal reference state, while being capable of describing at least some of the most frequent cases of electronic quasi-degeneracies. We first overview the traditional multi-reference methods, which are classified as multi-reference CI (MRCI), multi-reference MBPT (MRMBPT), and multi-reference CC (MRCC) approaches.

In CI, the multi-reference formulation is typically accomplished by adopting a more sophisticated zeroth-order reference in the form of a multi-configuration self-consistent field (MCSCF) wavefunction instead of using a single H–F determinant.

The basic MRCISD approach (abbreviated here as MRCI) involves single and double excitations out of all reference determinants. The most popular MRCI schemes using complete active space self-consistent field (CASSCF) reference wavefunctions (CASSCF is a variant of MCSCF obtained by a distribution of a number of active electrons among a number of active orbitals in all possible ways) provide potential energy surfaces which are closely parallel to full CI surfaces, at least for small molecules. Because of this, the MRCI methods are among the most useful benchmark techniques of quantum chemistry [104–106], particularly in cases where full CI results are not available, and among the most popular approaches to calculations of potential energy surfaces of smaller molecular systems. One of the biggest advantages of the MRCI techniques, in addition to high accuracy in calculations of potential energy surfaces, is their ability to describe ground and excited states, near-degeneracy effects, and all kinds of open-shell systems. The fundamental drawback of the MRCI methods, their lack of size extensivity, can be addressed through either the *a posteriori* Davidson-type energy corrections [107–112] or the *a priori* refinements through suitable Hamiltonian dressing techniques, such as, for example, the multi-reference average coupled pair functional (MR-ACPF) [113] and multi-reference average quadratic coupled-cluster (MR-AQCC) [114, 115] approaches. Neither of these propositions is ideal, but benchmark calculations show that at least the main problems related to inextensivity of MRCI can be addressed in this manner (see, e.g. [116]). Several other approximately extensive modifications of MRCI have been developed [117–119].

In addition to inextensivity, the main challenge for the MRCI methods is the fact that the lengths of the corresponding CI wavefunction expansions and the related computational effort rapidly increase with the system and basis set sizes. Although several clever ideas, such as the use of the configuration selection thresholds combined with the appropriate extrapolation techniques [112], and the internal contractions of configuration state functions [120, 121], have been developed to reduce the costs of MRCI calculations, all MRCI methods are generally very costly in all aspects of computing resources [122]. Even with the substantial progress in terms of algorithms, efficient implementation, and parallelization (cf., e.g. [120–128]), practically all applications of MRCI remain limited to relatively small molecular systems. In addition, the existing MRCI approaches remain quite complex for the average end user due to several choices the user has to make to run the MRCI calculations in a proper manner. This makes MRCI approaches popular among experts, but much less popular among non-experts.

A cost effective alternative to MRCI is represented by methods based on the multi-reference extension of MBPT. Historically, the general MRMBPT formalisms for quasi-degenerate and open-shell states have been formulated in the late 1960s [129] and early 1970s [130], but much of the development work geared toward practical computational schemes has been done in the last two decades. Two general categories of MRMBPT methods are distinguished in the literature: the "perturb then diagonalize" and the "diagonalize then perturb" approaches [131–133]. The "perturb then diagonalize" approaches involve deriving the effective Hamiltonian in a multi-configurational reference space, which in the case of the most

popular second-order MRMBPT schemes is truncated at the first-order terms, and then obtaining the final energies as eigenvalues of the resulting operator [129, 132–137]. The most popular second-order "diagonalize then perturb" methods use the first-order contributions to the Schrödinger equation to define the perturbed wavefunctions, and then use the second-order equation to get the energy. Various methods, particularly in the latter family, differ from one another in the choice of the zeroth-order Hamiltonian, and other details of the algorithms used in the computer implementation [138–161]. Among the most popular and widely used variants of MRMBPT are the complete active space second-order perturbation theory (CASPT2) [138, 139], the multi-reference Moller-Plesset perturbation theory (MRMP) [140], and the multi-configurational quasi-degenerate perturbation theory (MC-QDPT) [149].

A general difficulty of MRMBPT is the choice of the zeroth-order Hamiltonian, which is less straightforward than in the single-reference case. Another difficulty concerns the choice of reference determinants in some, more demanding, applications. For example, the underlying CASSCF calculations may generate too many configurations, and the size of the active space may, in some cases, outgrow the capacity of the present computer technology, causing difficulty in obtaining converged results, which then strongly vary with the numbers of active electrons and orbitals, and the number of roots included in the calculations [162–164]. In addition, at least some MRMBPT methods suffer from lack of size extensivity [165] and intruder state problems leading to divergent behavior [166–168]. Among the most promising approaches to eliminate intruders, while retaining size extensivity, are state-specific MRMBPT methods that start with a multi-determinantal reference space but target one state of interest at a time. The state-specific MRMBPT method advocated by Mukherjee et al. [152] seems particularly promising, showing smooth performance in and around the region of intruders and reasonable accuracy.

Overall, in spite of the aforementioned problems, the MRMBPT methods have been successfully applied to many chemical and spectroscopic problems and have established themselves as efficient techniques for treating non-dynamical and leading dynamical correlations. Compared to MRCI and genuine MRCC methods discussed below, the second-order MRMBPT approaches are much more practical. The low-order MRMBPT approaches have a drawback in that they are not as accurate as MRCI or CC methods in describing dynamical correlations, but this can be taken care of by combining the low-order MRMBPT theory with the CC theory, as demonstrated in the present work through the MRMBPT-inspired corrections to CC energies.

The last type of multi-reference methods are the multi-reference coupled-cluster (MRCC) approaches. The existing MRCC approaches can be classified into the following three basic categories: the Fock-space (FS) or the valence-universal approaches [169–172], the Hilbert-space (HS) or the state-universal methods [173–182], and the state-specific or state-selective (SS) approaches, such as, for example, those described in [183] and [184], the Brillouin-Wigner MRCC approaches [185–190], and the SSMRCC methods based on the wavefunction ansätze introduced in [31, 32], and [191] for the ground-state problem, [93–95] for excited

states, and [192–194] for the electron attached and ionized states, which are nowadays referred to as the active-space CC/EOMCC methods [66, 67, 93–95, 192–194]. The FSMRCC theories employ a single valence universal exponential wave operator to generate ground and excited states of a given system and its ions obtained by removing active electrons, one by one, until one is left with core electrons only. Thus, the FSMRCC approaches are particularly useful for valence systems around closed-shells and various differential properties, such as ionization energies and electron affinities. The HSMRCC theories based on the Jeziorski-Monkhorst ansatz [173], which employs different particle-conserving cluster operators for different reference determinants, are particularly well suited for severe electronic quasi-degeneracies due to several interacting states. Both the FSMRCC and HSMRCC approaches are genuine multi-root procedures. This should be contrasted by the SSMRCC theories, which treat one electronic state at a time. We will return to the SSMRCC methods when we discuss the active-space CC/EOMCC approaches some more below. With an exception of, perhaps, the active-space CC/EOMCC and Brillouin-Wigner MRCC methods, the existing MRCC approaches are greatly limited in the range of chemical applications they can address. Part of the problem is the fact that no efficient, general purpose MRCC codes have been developed owing to several recurring issues, such as computational complexity, intruder solution problem [195], difficulties with retaining size extensivity in incomplete model space considerations, difficulties in going beyond the basic MRCCSD approximation, and difficulties in developing robust algorithms for larger reference spaces due to, for example, excessive numbers of cluster amplitudes in the HSMRCC considerations. Although significant progress has been made in recent few years in all of these areas (see, e.g. [196–204]), it may be more worthwhile to focus on simpler methods that rely, at least in part, on a single-reference formalism. In general, the single-reference CC methods are much easier to implement and use than the genuine MRCC approaches of the FS or HS type. Thus, it is useful to develop new classes of single-reference CC methods that eliminate failures of standard CC/EOMCC approximations in the bond breaking region and for excited states having a manifestly multi-configurational character, without involving the intrinsic complexities of the FSMRCC and HSMRCC considerations.

As summarized in Table 1, the MRCI and MRCC approaches are the only existing wavefunction methods that may offer an excellent treatment of both dynamical and non-dynamical correlation effects. As described earlier, these methods are computationally very expensive and very difficult to use, which greatly limits their applicability. Thus, we need alternative approaches, which are more practical than MRCI and MRCC and which are capable of balancing dynamical and non-dynamical correlations, particularly in studies of bond breaking and excited states having a significant configuration mixing.

One can think of two general ways of developing such approaches, at least within the CC formalism. The first way is to improve the existing single-reference CC methods such that they can describe at least the selected classes of bond breaking and excited states in a purely "black-box" fashion, i.e., without using any elements of a multi-reference calculation. A few ideas of this type have been

Table 1 The quality of the overall description of the dynamical and non-dynamical electron correlation effects by selected wavefunction methods of quantum chemistry

Method	Type of electron correlations	
	Dynamical	Non-dynamical
MBPT(2), MP2, ...	Low-order	Poor
CCSD(T), CCSD(TQ), ...	Excellent	Poor
MRMBPT(2)	Low-order	Excellent
MRCI	Excellent[a]	Excellent[a]
MRCC	Excellent	Excellent

[a] MRCI is not size extensive, so there is a loss of accuracy as the system becomes larger

proposed in recent years, including the non-iterative single-reference CC methods based on the partitioning of the similarity-transformed Hamiltonian [49, 205–209], the spin-flip CC approaches [210–212], and the renormalized CC/EOMCC methods [39–41, 51, 53–55, 57, 60–65, 98, 99]. The latter approaches are particularly promising. They are based on the idea of correcting the CC (e.g. CCSD) or EOMCC (e.g. EOMCCSD) energies for the effects of higher-order (e.g. triply excited) clusters using expressions for the leading terms toward full CI obtained using the formalism of the method of moments of CC equations (MMCC) [39–41, 51, 53–55, 60–65, 96, 97,201–203]. Renormalized CC/EOMCC methods are particularly useful in calculations of single bond breaking, reaction pathways involving biradicals, singlet-triplet gaps in magnetic systems, and excited states dominated by two-electron transitions [39–65, 98, 99, 133, 162, 163, 213–226].

Renormalized CC/EOMCC methods can be very successful, enabling accurate, inexpensive, "black-box" CC calculations for some of the most frequent multi-reference situations, but there are quasi-degeneracy problems that cannot be handled in this manner. An example is provided by the excited states of a highly degenerate Be_3 system, where the accuracy of the renormalized EOMCC calculations is comparable to the small energy spacings between excited states [227, 228]. In such situations and in other severe cases of electronic quasi-degeneracies, where pure "black-box" single-reference solutions are no longer effective, it may be useful to look for alternative approaches that mix single- and multi-reference concepts within a single mathematical theory. One of the best and most successful examples of such theory is provided by the aforementioned active-space CC and EOMCC methods [42, 66, 67, 93–95, 192–194, 227, 228], which can be viewed as the SSM-RCC approaches exploiting a single-reference CC formalism [31, 32, 36, 37, 191, 229–234]. These methods use active orbitals, which are normally exploited to define reference determinants in a multi-reference calculation, to select the dominant three-body and other higher-than-two-body clusters and excitation amplitudes within an otherwise conventional single-reference CC or EOMCC formalism. As a result, they offer a tremendous amount of flexibility, since one can always improve the results by enlarging the active space. At the same time, they have a well-defined relationship with higher-order single-reference CC or EOMCC methods.

For example, the active-space CC/EOMCC approach with up to triple excitations (CCSDt/EOMCCSDt) becomes equivalent to the full CCSDT/EOMCCSDT theory when all orbitals are active. On the other hand, as demonstrated in numerous calculations by the original inventors of these methods (Piecuch, Adamowicz, and co-workers) [31, 32, 36, 37, 42, 66, 67, 93–95, 191–194, 227–234], and others who adopted active space approaches in recent years (cf., e.g. [235–241]), it is sufficient to use small numbers of active orbitals in the active space CC/EOMCC calculations to obtain extremely accurate results for bond breaking and multi-determinantal excited states. In particular, the active space EOMCC methods lead to the virtually perfect description of the excited states of the aforementioned Be_3 system, where many other methods, including the renormalized EOMCC approaches, have significant problems [227, 228].

Active space CC/EOMCC methods mix single- and multi-reference CC concepts, but one can go even one step further and mix CC and non-CC concepts, so that the advantages of different kinds of electronic structure theories are utilized to the utmost. One of the most successful methods in this broad category is the idea of the externally corrected single-reference CC methods [242–250] in which the T_3 and T_4 cluster components, instead of being calculated by solving the CCSDT, CCSDTQ, or other higher-order and expensive CC equations, are obtained by a cluster analysis of the wavefunctions provided by some external non-CC source, such as the projected unrestricted Hartree-Fock [242, 247], valence bond [243, 244], MCSCF or CASSCF [245, 246, 249], and MRCI [250] wavefunctions.

The MRCI-corrected CC methods, which define the so-called reduced MRCC approaches [250], are particularly impressive, since the MRCI method itself is already quite accurate in applications involving potential energy surfaces along bond breaking coordinates, so that by reading the T_3 and T_4 clusters extracted from MRCI calculations and solving the resulting T_3- and T_4-corrected CCSD equations, one obtains the virtually perfect description of both dynamical and non-dynamical correlations. The only problem of the reduced MRCC methods is the fact that they are currently limited to the lowest-energy electronic state of a given symmetry. Moreover, the MRCI calculations needed to estimate the T_3 and T_4 clusters for the subsequent CCSD calculations can be quite expensive if the dimension of the corresponding multi-determinantal reference space becomes large.

There is, however, a major lesson resulting from the remarkable success of the reduced MRCC approach in that it is very useful to mix a multi-reference theory, which can be used to provide information about the non-dynamical and leading dynamical correlation effects, with a single-reference CC theory, which gives the information about the remaining many-electron correlation effects. The success of the reduced MRCC method has inspired the development of the CI (MRCI)-corrected approaches exploiting the aforementioned formalism of the method of moments of CC equations (MMCC) [39, 60–62, 96, 97, 251–254]. The MMCC formalism enables one to determine the mathematical structure of terms which, when added to CC or EOMCC (e.g. CCSD or EOMCCD) energies, give, in the exact limit, the exact full CI energies. One can use the MMCC theory to design the "black-box" renormalized CC approximation, which we mentioned earlier, or to

develop the externally corrected MMCC methods, such as the (MR)CI-corrected MMCC schemes, in which one uses selected components of the (MR)CI wavefunctions to design the MMCC energy corrections due to higher-order correlation effects on top of CCSD or EOMCCSD. The major advantages of the (MR)CI-corrected MMCC schemes are their applicability to ground and excited states, not just to the lowest-energy states of a given symmetry [39,60–62,96,97], and very high accuracy that can compete with the results of reduced MRCC calculations [252–254]. The (MR)CI-corrected MMCC methods work extremely well for single, double, or even triple bond breaking and all kinds of excited states [39, 60–62, 96, 97, 251–254], but they still require additional CI calculations to generate trial wavefunctions that enter the MMCC corrections to CCSD or EOMCCSD energies. Although the main idea of the CI-corrected MMCC methods is straightforward, the CI-corrected MMCC calculations can be quite expensive if the CI calculations used in designing the MMCC corrections use larger active orbital spaces. Undoubtedly, it would be desirable to examine if one could use another, less expensive, multi-reference method to generate the wavefunctions that enter the MMCC energy corrections, while retaining the high accuracy of the CI-corrected MMCC calculations.

In this chapter, we examine, in detail, the possibility of replacing the relatively expensive (MR)CI-like wavefunctions in the CI-corrected MMCC (MMCC/CI) schemes by the wavefunctions obtained in the low-order MRMBPT calculations, introduced, for the first time, at the level of triples corrections to CCSD/EOMCCSD energies in [55, 56], and extended to corrections due to quadruples in this work. As described earlier, the low-order MRMBPT methods are known to provide a reasonable description of non-dynamical and leading dynamical correlation effects in the presence of electronic quasi-degeneracies (cf., e.g. [133,134,137–140,142,146,148, 149,152,158–160,255–259]). At the same time, the computer costs of the low-order (e.g. second-order) MRMBPT calculations are very small compared to the analogous MRCI calculations. By combining the wavefunctions obtained in the low-order MRMBPT calculations, which provide a reasonable description of electronic quasi-degeneracies, with the MMCC formalism, in which these MRMBPT wavefunctions are used to design the MMCC corrections to single-reference CC or EOMCC energies, we obtain a new class of the MRMBPT-corrected MMCC methods, referred to here and elsewhere in this chapter as the MMCC/PT approaches [55, 56]. Just like the MMCC/CI methods, which combine the CC and CI concepts, the MMCC/PT approaches described and benchmarked in this work can be viewed as the externally corrected MMCC methods. All externally corrected MMCC methods are similar, in the overall philosophy, to the externally corrected CC methods pioneered by Paldus and collaborators, in which the CC and non-CC concepts are combined together to improve the CC results in the presence of electronic quasi-degeneracies. We demonstrate in this work that by combining the single-reference CC and EOMCC methods with the low-order MRMBPT-like wavefunctions via non-iterative MMCC/PT corrections to CC or EOMCC energies, we can considerably improve the results of the standard CC and EOMCC calculations in the bond breaking region and for excited states dominated by two-electron transitions, while keeping the computer costs at the low level. Thus, the MRMBPT-corrected MMCC methods may provide

a potentially useful and relatively inexpensive alternative to other CC/EOMCC and MMCC schemes, and the reduced MRCC approach of Li and Paldus, which in the long-term may facilitate accurate calculations of reaction pathways and electronic excitations in larger molecular systems.

The rest of this chapter is organized as follows: In Sect. 2, we summarize the main objectives of this work. In Sect. 3, we provide a formal background needed to formulate the MMCC/PT methods. In particular, we outline the single-reference CC theory for ground states and its extension to excited states via the EOMCC formalism. We also introduce the basic elements of the MMCC theory, on which the MMCC/PT work is based. The existing MMCC approaches, such as the CI-corrected MMCC methods and the selected renormalized CC/EOMCC schemes, and the key concepts of the MRMBPT methodology are reviewed in Sect. 3 as well. In Sect. 4, we describe the details of the MRMBPT-corrected MMCC (MMCC/PT) methods. One of the most essential parts of that section is the diagrammatic formulation and factorization of the central components of the MMCC/PT equations, called the generalized moments of CC/EOMCC equations, which leads to a highly efficient computer implementation of the MMCC/PT and other MMCC methods, and which has not been described in the earlier papers on the MMCC methodology. In Sect. 5, we present selected benchmark calculations to illustrate the performance of the MMCC/PT approximations developed in this work. In the last Sect. 6, we present a summary and future perspectives of this work. An overview of the diagrammatic methods exploited in this work and the relevant diagrams representing the key components of the CC, EOMCC, and MMCC equations that are used to formulate the MMCC/PT and other MMCC methods are provided in Appendices 1–3.

2 The Main Objectives of the Present Work

The main goal of this chapter is to describe how to combine the low-order multi-reference many-body perturbation theory (MRMBPT) with the coupled-cluster (CC) and equation-of-motion CC (EOMCC) methodologies via the method of moments of CC (MMCC) equations. In addition to the relevant review material on the CC, EOMCC, MMCC, and MRMBPT methodologies, the specific objectives addressed of this work are:

A. Development of the MRMBPT-corrected MMCC (MMCC/PT) theory and the underlying low-order MRMBPT formalism used in the present implementation of the MMCC/PT methods.
B. Derivation of the key elements of the MMCC/PT theory and other MMCC approaches, which are the generalized moments of the CC/EOMCC equations, using diagrammatic methods.
C. Efficient formulation and computer implementation of the leading MMCC/PT approximations, termed MMCC(2,3)/PT and MMCC(2,4)/PT, which enable one to correct the CCSD and EOMCCSD energies for the effects of triples

(MMCC(2,3)/PT) or triples and quadruples (MMCC(2,4)/PT), using the idea of diagram factorization and recursively generated intermediates.

D. Benchmarking the basic MMCC/PT approaches in calculations of ground and excited states of selected molecular systems, for which the exact, full CI data can be generated.

In addition to the above objectives, we provide an overview of the diagrammatic and diagram factorization techniques used in our considerations.

3 Theory

In this section, we review the single-reference coupled-cluster (CC) theory and its extension to excited states via the equation-of-motion (EOM) CC formalism. We also introduce the method of moments of CC equations (the MMCC theory) and discuss the selected existing MMCC approximations, namely, the CI-corrected MMCC methods and a few examples of the completely renormalized CC/EOMCC approaches.

3.1 An Overview of Single-Reference Coupled-Cluster (CC) Theory

3.1.1 Ground-State Formalism

The single-reference CC theory is based on the exponential ansatz for the ground-state wavefunction,

$$|\Psi_0\rangle = |\Psi_0^{(\mathrm{CC})}\rangle \equiv e^T|\Phi\rangle, \tag{1}$$

where T is a particle-hole excitation operator referred to as the cluster operator and $|\Phi\rangle$ is the reference determinant (usually, the Hartree-Fock determinant). In the exact CC theory, T is a sum of all many-body cluster components that one can write for a given N-electron system,

$$T = \sum_{n=1}^{N} T_n\,, \tag{2}$$

where the n-body cluster component T_n is defined in a usual way as

$$T_n = \left(\frac{1}{n!}\right)^2 t_{a_1\ldots a_n}^{i_1\ldots i_n} a^{a_1}\ldots a^{a_n} a_{i_n}\ldots a_{i_1}\,, \tag{3}$$

with $t_{a_1\ldots a_n}^{i_1\ldots i_n}$ representing the corresponding antisymmetrized cluster amplitudes, $i_1\ldots i_n$ $(a_1\ldots a_n)$ referring to the single-particle states (spin-orbitals) occupied (unoccupied) in the reference determinant $|\Phi\rangle$, and a^p (a_p) designating the standard creation (annihilation) operators associated with the orthonormal spin-orbitals $|p\rangle$.

Here and elsewhere in this paper, the Einstein summation convention over repeated upper and lower indices is employed, so that the summation symbols corresponding to the unrestricted summations over occupied and/or unoccupied spin-orbitals are omitted.

In all standard CC approximations, the many-body expansion for the cluster operator T is truncated at a given excitation level $m_A < N$ (usually, $m_A << N$). The general form of the truncated cluster operator defining a standard CC approximation A, characterized by the excitation level m_A, is

$$T^{(A)} = \sum_{n=1}^{m_A} T_n. \tag{4}$$

An example of the standard CC approximation is the CCSD method. In this case, $m_A = 2$ and the cluster operator T is approximated by

$$T^{(\mathrm{CCSD})} = T_1 + T_2, \tag{5}$$

where

$$T_1 = t_a^i a^a a_i \tag{6}$$

and

$$T_2 = \tfrac{1}{4} t_{ab}^{ij} a^a a^b a_j a_i \tag{7}$$

are the singly and doubly excited cluster components and t_a^i and t_{ab}^{ij} are the corresponding singly and doubly excited cluster amplitudes. In accordance with our general notation, $i, j \ldots (a, b \ldots)$ are the occupied (unoccupied) spin-orbitals in the reference determinant $|\Phi\rangle$.

In all conventional CC approximations, the cluster amplitudes $t_{a_1 \ldots a_n}^{i_1 \ldots i_n}$ are determined by solving a coupled system of energy-independent non-linear algebraic equations of the form:

$$\langle \Phi_{i_1 \ldots i_n}^{a_1 \ldots a_n} | \bar{H}^{(A)} | \Phi \rangle = 0, \quad i_1 < \cdots < i_n, \ a_1 < \cdots < a_n, \tag{8}$$

where $n = 1, \ldots, m_A$,

$$\bar{H}^{(A)} = e^{-T^{(A)}} H e^{T^{(A)}} = (H e^{T^{(A)}})_C \tag{9}$$

is the similarity-transformed Hamiltonian of the CC/EOMCC theory, subscript C designates the connected part of the corresponding operator expression, and $|\Phi_{i_1 \ldots i_n}^{a_1 \ldots a_n}\rangle \equiv a^{a_1} \cdots a^{a_n} a_{i_n} \cdots a_{i_1} |\Phi\rangle$ are the n-tuply excited determinants relative to reference $|\Phi\rangle$. In particular, the standard CCSD equations for the singly and doubly excited cluster amplitudes t_a^i and t_{ab}^{ij}, defining T_1 and T_2, respectively, can be written as

$$\langle \Phi_i^a | \bar{H}^{(\mathrm{CCSD})} | \Phi \rangle = 0, \tag{10}$$

$$\langle \Phi_{ij}^{ab} | \bar{H}^{(\mathrm{CCSD})} | \Phi \rangle = 0, \quad i < j, \ a < b, \tag{11}$$

where

$$\bar{H}^{(\mathrm{CCSD})} = e^{-T^{(\mathrm{CCSD})}} H e^{T^{(\mathrm{CCSD})}} = (H e^{T^{(\mathrm{CCSD})}})_C \tag{12}$$

is the similarity-transformed Hamiltonian of the CCSD/EOMCCSD approach. The explicit and computationally efficient form of $\bar{H}^{(\mathrm{CCSD})}$ and other equations used in the CC calculations, in terms of one- and two-body matrix elements of the Hamiltonian in the normal-ordered form, $f_p^q \equiv \langle p|f|q\rangle$ and $v_{pq}^{rs} \equiv \langle pq|v|rs\rangle - \langle pq|v|sr\rangle$, respectively, where f is the Fock operator and v is the operator representing the electron-electron interaction energy, and cluster amplitudes $t_{a_1\ldots a_n}^{i_1\ldots i_n}$ or, in the CCSD (m_A = 2) case, t_a^i and t_{ab}^{ij}, can be derived by applying the powerful diagrammatic techniques of many-body theory [260, 261] combined with technique of diagram factorization, which yields highly vectorized computer codes [29, 30]. The algebraic and diagrammatic structure of $\bar{H}^{(\mathrm{CCSD})}$ is presented in detail in Appendix 2 and the factorized form of $\bar{H}^{(\mathrm{CCSD})}$ is shown in Appendix 3. The introduction to diagrammatic methods used in this work is given in Appendix 1.

Unlike in the CI approaches, which use the expectation value of the Hamiltonian to define the energy, the CC energy is obtained by projecting the connected cluster form of the Schrödinger equation on the reference configuration $|\Phi\rangle$. In other words, once the system of equations, Eq. (8), is solved for $T^{(A)}$ or $t_{a_1\ldots a_n}^{i_1\ldots i_n}$ (or, in the CCSD case, Eqs. (10) and (11) are solved for T_1 and T_2 or t_a^i and t_{ab}^{ij}), the CC energy corresponding to approximation A, characterized by the excitation level m_A, is calculated using the equation

$$E_0^{(A)} = \langle \Phi|\bar{H}^{(A)}|\Phi\rangle \equiv \langle \Phi|\bar{H}^{(A)}_{\mathrm{closed}}|\Phi\rangle, \tag{13}$$

where $\bar{H}^{(A)}_{\mathrm{closed}}$ is a "closed" part of $\bar{H}^{(A)}$, which is represented by those diagrams contributing to $\bar{H}^{(A)}$ that have no external (uncontracted) Fermion lines (as opposed to the "open" part of $\bar{H}^{(A)}$ which is represented by the diagrams having external or uncontracted Fermion lines).

3.1.2 Extension to Excited States via the Equation-of-Motion Formalism (EOMCC)

The ground-state CC theory has a natural extension to excited electronic states $|\Psi_\mu\rangle$ via the EOMCC formalism, in which we write

$$|\Psi_\mu\rangle = |\Psi_\mu^{(\mathrm{CC})}\rangle \equiv R_\mu e^T |\Phi\rangle, \tag{14}$$

where T is obtained in the ground-state CC calculations and R_μ is a linear particle-hole excitation operator, similar to T, obtained by diagonalizing the similarity-transformed Hamiltonian $\bar{H} = e^{-T} H e^T$ in the space of excited determinants $|\Phi_{a_1\ldots a_n}^{i_1\ldots i_n}\rangle$ that typically correspond to excitations included in T.

In the following, we use a notation where $\mu = 0$ refers to the ground state, while $\mu > 0$ designates excited states. Thus, the excitation operator R_μ is defined as a

unit operator for $\mu = 0$, that is, $r_0(\mu = 0) = 1$ and $r^{i_1 \ldots i_n}_{a_1 \ldots a_n}(\mu = 0) = 0$ for $n \geq 1$, where $r_0(\mu)$ is a coefficient defining the zero-body component of R_μ and $r^{i_1 \ldots i_n}_{a_1 \ldots a_n}(\mu)$ are the excitation amplitudes defining the n-body components of R_μ when $n > 1$ (see the explicit definitions below). In this way, the EOMCC ansatz, Eq. (14), reduces to the ground-state CC ansatz, Eq. (1), when $\mu = 0$.

In the exact EOMCC theory, the cluster operator T and the excitation operators R_μ are sums of all relevant many-body components that can be written for a given N-electron systems. As in the ground-state case, the standard EOMCC approximations are obtained by truncating the many-body expansion for the operator R_μ at a given excitation level $m_A < N$, which typically is the same as the excitation level used to define the truncated form of T. In the majority of applications of EOMCC, when T is approximated by $T^{(A)}$, Eq. (27), the corresponding excitation operator R_μ defining the EOMCC method A is approximated by

$$R^{(A)}_\mu = R^{(A)}_{\mu,0} + R^{(A)}_{\mu,\mathrm{open}}, \tag{15}$$

where

$$R_{\mu,0} = r_0(\mu)\,\mathbf{1}, \tag{16}$$

and the "open" part of $R^{(A)}_\mu$ is defined as

$$R^{(A)}_{\mu,\mathrm{open}} = \sum_{n=1}^{m_A} R_{\mu,n}, \tag{17}$$

with

$$R_{\mu,n} = \left(\frac{1}{n!}\right)^2 r^{i_1 \ldots i_n}_{a_1 \ldots a_n}(\mu)\, a^{a_1} \cdots a^{a_n} a_{i_n} \cdots a_{i_1} \tag{18}$$

representing the n-body component of $R^{(A)}_\mu$. For instance, in the EOMCCSD theory, which is a basic EOMCC approximation where m_A is set at 2, the excitation operator $R^{(\mathrm{CCSD})}_\mu$ is approximated by

$$R^{(\mathrm{CCSD})}_\mu = R_{\mu,0} + R_{\mu,1} + R_{\mu,2}, \tag{19}$$

where $R_{\mu,0}$ is given by Eq. (16) and

$$R_{\mu,1} = r^i_a(\mu)\, a^a a_i \tag{20}$$

and

$$R_{\mu,2} = \tfrac{1}{4}\, r^{ij}_{ab}(\mu)\, a^a a^b a_j a_i \tag{21}$$

are the one- and two-body components of $R^{(\mathrm{CCSD})}_\mu$, with $r^i_a(\mu)$ and $r^{ij}_{ab}(\mu)$ representing the corresponding excitation amplitudes ($\mathbf{1}$ in Eq. (16) is a unit operator).

The excitation amplitudes $r^{i_1 \ldots i_n}_{a_1 \ldots a_n}(\mu)$ defining the excitation operator $R^{(A)}_{\mu,\mathrm{open}}$, Eq. (17), are obtained by solving the eigenvalue problem involving the

similarity-transformed Hamiltonian $\bar{H}^{(A)}$ in the space spanned by the excited determinants $|\Phi^{a_1\ldots a_n}_{i_1\ldots i_n}\rangle$ with $n = 1,\ldots,m_A$, i.e.,

$$\langle \Phi^{a_1\ldots a_n}_{i_1\ldots i_n}|(\bar{H}^{(A)}_{\rm open} R^{(A)}_{\mu,{\rm open}})_C|\Phi\rangle = \omega^{(A)}_\mu r^{i_1\ldots i_n}_{a_1\ldots a_n}(\mu), \quad i_1 < \cdots < i_n,\ a_1 < \cdots < a_n, \tag{22}$$

where

$$\bar{H}^{(A)}_{\rm open} = \bar{H}^{(A)} - \bar{H}^{(A)}_{\rm closed} = \bar{H}^{(A)} - E^{(A)}_0 \mathbf{1} \tag{23}$$

is the "open" part of $\bar{H}^{(A)}$, represented by the diagrams of $\bar{H}^{(\rm A)}$ that have external Fermion lines, and

$$\omega^{(A)}_\mu = E^{(A)}_\mu - E^{(A)}_0 \tag{24}$$

is the vertical excitation energy obtained with the EOMCC method A. In particular, the $r^i_a(\mu)$, and $r^{ij}_{ab}(\mu)$ amplitudes of the EOMCCSD theory and the corresponding excitation energies $\omega^{(\rm CCSD)}_\mu$ are obtained by diagonalizing the similarity-transformed Hamiltonian $\bar{H}^{(\rm CCSD)}$, Eq. (12), in the space of singly and doubly excited determinants, $|\Phi^a_i\rangle$ and $|\Phi^{ab}_{ij}\rangle$, respectively. Equation (22) alone does not provide information about the coefficient $r_0(\mu)$ at the reference determinant $|\Phi\rangle$ in the corresponding EOMCC excited-state wavefunction $R^{(A)}_\mu e^{T^{(A)}}|\Phi\rangle$. This coefficient is determined *a posteriori* using the equation

$$r_0(\mu) = \frac{\langle\Phi|(\bar{H}^{(A)}_{\rm open} R^{(A)}_{\mu,{\rm open}})_C|\Phi\rangle}{\omega^{(A)}_\mu}, \tag{25}$$

once the excitation amplitudes $r^{i_1\ldots i_n}_{a_1\ldots a_n}(\mu)$ defining $R^{(A)}_{\mu,{\rm open}}$ are determined (Eq. (25) is valid for $\mu > 0$, meaning excited states only; for $\mu = 0$, $r_0(\mu = 0) = 1$, as explained above). As mentioned earlier, diagrams representing the many-body components of $\bar{H}^{(A)}$ for the EOMCCSD case (i.e., $\bar{H}^{(\rm CCSD)}$) are given in Appendices 2 and 3. The EOMCCSD equations (Eq. (22) for $m_A = 2$) use one- and two-body, and selected three-body components of $\bar{H}^{(\rm CCSD)}$ [79, 80].

3.2 Method of Moments of CC Equations (MMCC)

3.2.1 An Overview of the Exact MMCC Formalism

We are now equipped with the basic elements of the CC/EOMCC theory which are necessary to explain the non-iterative MMCC approaches to ground and excited electronic states. We now describe the exact MMCC formalism. In this work, we focus on the original form of the MMCC theory introduced in 2000 for the ground-state problem [39–41] and extended to excited states in 2001 [96]. The alternative formulations of the MMCC theory, including the generalized MMCC formalism which applies to non-standard CC methods [50, 62], the numerator-denominator-connected MMCC expansions [51], the multi-reference extensions of

MMCC [201–203], and the most recent biorthogonal MMCC formalism which leads to rigorously size extensive renormalized CC methods [53–55, 57], are of no use for the MRMBPT-corrected MMCC methods and are not discussed here.

As described in Sect. 3.1, the standard CC and EOMCC equations are obtained by projecting $\bar{H}^{(A)}|\Phi\rangle$ and $\bar{H}^{(A)}R_\mu^{(A)}|\Phi\rangle$ on the excited determinants $|\Phi_{i_1\ldots i_n}^{a_1\ldots a_n}\rangle$ with $n=1,\ldots,m_A$ that correspond to the particle-hole excitations included in the cluster operator $T^{(A)}$ and linear excitation operator $R_\mu^{(A)}$. The corresponding ground-state CC energy is obtained by projecting $\bar{H}^{(A)}|\Phi\rangle$ on the reference determinant $|\Phi\rangle$. It is, therefore, quite natural to expect that in order to correct the results of the standard CC/EOMCC calculations employing the cluster and excitation operators truncated at m_A-body terms, the projections of $\bar{H}^{(A)}|\Phi\rangle$ and $\bar{H}^{(A)}R_\mu^{(A)}|\Phi\rangle$ on the excited determinants $|\Phi_{i_1\ldots i_n}^{a_1\ldots a_n}\rangle$ with $n>m_A$, which span the orthogonal complement of the subspace of the N-electron Hilbert space spanned by the reference determinant $|\Phi\rangle$ and the excited determinants $|\Phi_{i_1\ldots i_n}^{a_1\ldots a_n}\rangle$ with $n=1,\ldots,m_A$, have to be considered. These projections, which are the essence of the MMCC formalism, designated by $\mathfrak{M}_{\mu,a_1\ldots a_n}^{i_1\ldots i_n}(m_A)$, define the generalized moments of the CC/EOMCC equations corresponding to method A.

The original single-reference MMCC theory [39–41,96,97], which is particularly useful in this work, is based on a simple idea that the exact, full CI, energies of the electronic states μ, E_μ, can be recovered by adding the state-selective, non-iterative energy corrections

$$\begin{aligned}\delta_\mu^{(A)} &\equiv E_\mu - E_\mu^{(A)} \\ &= \frac{\sum_{n=m_A+1}^{N}\sum_{k=m_A+1}^{n}\langle\Psi_\mu|C_{n-k}(m_A)M_{\mu,k}(m_A)|\Phi\rangle}{\langle\Psi_\mu|R_\mu^{(A)}e^{T^{(A)}}|\Phi\rangle}\end{aligned} \tag{26}$$

to the ground ($\mu=0$) and excited ($\mu>0$) states energies $E_\mu^{(A)}$ obtained in the standard CC/EOMCC calculations, such as CCSD/EOMCCSD, etc. The $T^{(A)}$ and $R_\mu^{(A)}$ operators entering Eq. (26) are the truncated cluster and linear excitation operators used in the underlying CC and EOMCC calculations defining approximation A, and in the exact theory $|\Psi_\mu\rangle$ are the full CI states. The

$$C_{n-k}(m_A) = (e^{T^{(A)}})_{n-k} \tag{27}$$

quantity is the $(n-k)$-body component of the wave operator $e^{T^{(A)}}$, defining the CC method A, which is trivial to determine. The zero-body term, $C_0(m_A)$, equals 1; the one-body term, $C_1(m_A)$, equals T_1; the two-body term, $C_2(m_A)$, equals $T_2+\frac{1}{2}T_1^2$ if $m_A\geq 2$; the three-body term $C_3(m_A)$ equals $T_1T_2+\frac{1}{6}T_1^3$ if $m_A=2$ and $T_3+T_1T_2+\frac{1}{6}T_1^3$ if $m_A\geq 3$, etc. The

$$M_{\mu,k}(m_A) = \left(\frac{1}{k!}\right)^2 \mathfrak{M}_{\mu,a_1\ldots a_k}^{i_1\ldots i_k}(m_A)\, a^{a_1}\ldots a^{a_k}a_{i_k}\ldots a_{i_1} \tag{28}$$

operator in Eq. (26) is the particle-hole excitation operator defined through the aforementioned generalized moments of the CC/EOMCC equations of method A,

$$\mathfrak{M}^{i_1\ldots i_k}_{\mu,a_1\ldots a_k}(m_A) = \langle \Phi^{a_1\ldots a_k}_{i_1\ldots i_k} | (\bar{H}^{(A)} R^{(A)}_{\mu}) | \Phi \rangle, \tag{29}$$

which represent the projections of the CC/EOMCC equations of method A on the excited determinants $|\Phi^{a_1\ldots a_k}_{i_1\ldots i_k}\rangle$ with $k > m_A$ that are normally disregarded in the standard CC/EOMCC calculations. Consistent with our notation in which $R^{(A)}_{\mu=0} = \mathbf{1}$, Eq. (29) includes the ground-state ($\mu = 0$) case as well. In this case, moments $\mathfrak{M}^{i_1\ldots i_k}_{\mu,a_1\ldots a_k}(m_A)$ reduce to the generalized moments of the ground-state CC equations, $\mathfrak{M}^{i_1\ldots i_k}_{0,a_1\ldots a_k}(m_A)$, defining approximation A, i.e.,

$$\mathfrak{M}^{i_1\ldots i_k}_{0,a_1\ldots a_k}(m_A) = \langle \Phi^{a_1\ldots a_k}_{i_1\ldots i_k} | \bar{H}^{(A)} | \Phi \rangle. \tag{30}$$

As demonstrated, for example, in [61,62,96–98], the generalized moments of the CC/EOMCC equations can be calculated using the following expression:

$$\begin{aligned}\mathfrak{M}^{i_1\ldots i_k}_{\mu,a_1\ldots a_k}(m_A) = {} & \langle \Phi^{a_1\ldots a_k}_{i_1\ldots i_k} | (\bar{H}^{(A)}_{\text{open}} R^{(A)}_{\mu,\text{open}})_C | \Phi \rangle \\ & + \sum_{p=m_A+1}^{k-1} \langle \Phi^{a_1\ldots a_k}_{i_1\ldots i_k} | (\bar{H}^{(A)}_{p} R^{(A)}_{\mu,k-p})_{DC} | \Phi \rangle \\ & + r_0(\mu)\, \mathfrak{M}^{i_1\ldots i_k}_{0,a_1\ldots a_k}(m_A),\end{aligned} \tag{31}$$

where $r_0(\mu)$ is the coefficient at the reference determinant $|\Phi\rangle$ in the many-body expansion of $R^{(A)}_{\mu}|\Phi\rangle$, defined by Eq. (25), subscripts "open," C, and DC refer to open (i.e., having external lines), connected, and disconnected parts of a given operator expression, O_j represents the j-body component of operator O, and $\mathfrak{M}^{i_1\ldots i_k}_{0,a_1\ldots a_k}(m_A)$ are the generalized moments of the ground-state CC equations defined by Eq. (30).

In particular, if the goal is to recover the full CI energies E_μ by correcting the CCSD/EOMCCSD energies $E^{(\text{CCSD})}_\mu$ (the $m_A = 2$ case), then the following *a posteriori* corrections $\delta^{(\text{CCSD})}_\mu$,

$$\delta^{(\text{CCSD})}_\mu = \frac{\sum_{n=3}^{N}\sum_{k=3}^{n} \langle \Psi_\mu | C_{n-k}(2)\, M_{\mu,k}(2) | \Phi \rangle}{\langle \Psi_\mu | R^{(\text{CCSD})}_\mu e^{T^{(\text{CCSD})}} | \Phi \rangle}, \tag{32}$$

have to be added to the $E^{(\text{CCSD})}_\mu$ energies. Here, the generalized moments $\mathfrak{M}^{i_1\ldots i_n}_{\mu,a_1\ldots a_n}(2)$ of the CCSD/EOMCCSD equations corresponding to projections of these equations on triply, quadruply, etc., excited determinants, i.e.,

$$\mathfrak{M}^{ijk}_{\mu,abc}(2) = \langle \Phi^{abc}_{ijk} | (\bar{H}^{(\text{CCSD})} R^{(\text{CCSD})}_{\mu}) | \Phi \rangle, \tag{33}$$

$$\mathfrak{M}^{ijkl}_{\mu,abcd}(2) = \langle \Phi^{abcd}_{ijkl} | (\bar{H}^{(\text{CCSD})} R^{(\text{CCSD})}_{\mu}) | \Phi \rangle, \tag{34}$$

etc., should be evaluated. Again, $\bar{H}^{(\mathrm{CCSD})}$ is the similarity-transformed Hamiltonian of the CCSD method defined by Eq. (12) and $R_\mu^{(\mathrm{CCSD})}$ is the EOMCCSD excitation operator described in Eq. (19).

Equation (26) defines the exact MMCC formalism for ground and excited states. This equation can formally be derived by considering the asymmetric energy expression,

$$\Lambda[\Psi] = \frac{\langle\Psi|(H - E_\mu^{(A)})R_\mu^{(A)}e^{T^{(A)}}|\Phi\rangle}{\langle\Psi|R_\mu^{(A)}e^{T^{(A)}}|\Phi\rangle}, \tag{35}$$

referred to as the MMCC functional, which was introduced for the first time in the original MMCC papers by Kowalski and Piecuch in [40] for the ground-state case and [96] for the excited-state generalization. This expression satisfies the property

$$\Lambda[\Psi_\mu] = E_\mu - E_\mu^{(A)}, \tag{36}$$

where E_μ is the exact, full CI, energy, if $|\Psi_\mu\rangle$ is a full CI state. The details of the derivation of Eq. (26) using functional $\Lambda[\Psi]$, Eq. (35), can be found in [40] and [96] (see, also, the appendices in [61]).

To this point we have focused the discussion on the exact forms of the MMCC energy expansions, Eqs. (26) and (32). However, in order to develop practical MMCC methods based on these equations, the following two issues must be addressed. First, the exact MMCC corrections $\delta_\mu^{(A)}$, Eq. (26), or $\delta_\mu^{(\mathrm{CCSD})}$, Eq. (32), are represented by complete many-body expansions including the N-body contributions, where N is the number of electrons in a system, corresponding to all many-body components of the wavefunctions $|\Psi_\mu\rangle$ that enter Eqs. (26) and (32) (cf. the summations over n in Eqs. (26) and (32)). In order to use Eqs. (26) or (32) in practical calculations, the many-body expansions for $\delta_\mu^{(A)}$ or $\delta_\mu^{(\mathrm{CCSD})}$ must be truncated at some, preferably low, excitation level $m_B > m_A$. This leads to the MMCC(m_A,m_B) schemes [39–41, 60–65, 96–98]. The second issue that has to be addressed is the fact that the wavefunctions $|\Psi_\mu\rangle$ entering the exact Eqs. (26) and (32) are the full CI states, which are normally not available. To resolve this dilemma, wavefunctions $|\Psi_\mu\rangle$ must be approximated in some way. Depending on the form of $|\Psi_\mu\rangle$, we can distinguish between externally corrected MMCC methods where $|\Psi_\mu\rangle$ is obtained in the non-CC (e.g. CI) calculations, and renormalized CC approaches, in which the form of $|\Psi_\mu\rangle$ is determined using CC arguments. The CI-corrected MMCC(2,3) and MMCC(2,4) approaches, which are the basic CI-corrected MMCC approximations, and the CR-CCSD(T)/CR-EOMCCSD(T) methods, which are examples of renormalized CC/EOMCC approaches, are reviewed in Sect. 3.3. The theoretical details of the new variant of the MMCC theory, the MRMBPT-corrected MMCC method, abbreviated as MMCC/PT, which is based on the idea of approximating $|\Psi_\mu\rangle$ by the relatively inexpensive, low-order, MRMBPT-like expansions, and which is explored in this work, is presented in Sect. 4 and its performance is tested in Sect. 5. First, however, we discuss the formal considerations that lead to all MMCC(m_A,m_B) truncations.

3.2.2 An Overview of the Approximate MMCC Approaches: The MMCC(m_A,m_B) Truncation Schemes

The main goal of all approximate MMCC calculations, including the CI-corrected MMCC approaches and the renormalized CC/EOMCC methods overviewed in this section, as well as the MRMBPT-corrected MMCC schemes discussed in detail in Sects. 4 and 5, is to approximate the exact corrections $\delta_\mu^{(A)}$, Eq. (26), such that the resulting energies, defined as

$$E_\mu^{(\mathrm{MMCC})} = E_\mu^{(A)} + \delta_\mu^{(A)}, \tag{37}$$

are close to the corresponding full CI energies E_μ. A systematic hierarchy of approximations called the MMCC(m_A,m_B) schemes that allows us to achieve this goal is described below.

All MMCC(m_A,m_B) schemes are obtained by assuming that the CI expansions of the ground- and excited-state wavefunctions $|\Psi_\mu\rangle$ entering Eq. (26) do not contain higher–than–m_B-tuply excited components relative to the reference $|\Phi\rangle$, where $m_A < m_B < N$. This requirement reduces the summation over n in Eq. (26) to $\sum_{n=m_A+1}^{m_B}$. The resulting MMCC(m_A,m_B) energies, $E_\mu^{(\mathrm{MMCC})}(m_A,m_B)$, can be given the following form:

$$E_\mu^{(\mathrm{MMCC})}(m_A,m_B) = E_\mu^{(A)} + \delta_\mu(m_A,m_B), \tag{38}$$

where $E_\mu^{(A)}$ is the energy of the μ-th electronic state, obtained with some standard CC/EOMCC method A, and

$$\delta_\mu(m_A,m_B) = \frac{\sum_{n=m_A+1}^{m_B}\sum_{k=m_A+1}^{n}\langle\Psi_\mu|C_{n-k}(m_A)M_{\mu,k}(m_A)|\Phi\rangle}{\langle\Psi_\mu|R_\mu^{(A)}e^{T^{(A)}}|\Phi\rangle} \tag{39}$$

is the relevant MMCC correction to $E_\mu^{(A)}$.

We restrict our discussion to the MMCC(m_A,m_B) schemes with $m_A = 2$, which enable us to correct the results of the CCSD or EOMCCSD calculations. In this category, two MMCC(m_A,m_B) schemes are particularly useful, namely, MMCC(2,3) and MMCC(2,4). These schemes can be used to correct the results of the CCSD/EOMCCSD calculations for the effects of triple (the MMCC(2,3) case) or triple and quadruple (the MMCC(2,4) case) excitations. The MMCC(2,3) and MMCC(2,4) energy expressions are as follows:

$$E_\mu^{(\mathrm{MMCC})}(2,3) = E_\mu^{(\mathrm{CCSD})} + \frac{\langle\Psi_\mu|M_{\mu,3}(2)|\Phi\rangle}{\langle\Psi_\mu|R_\mu^{(\mathrm{CCSD})}e^{T^{(\mathrm{CCSD})}}|\Phi\rangle}, \tag{40}$$

$$E_\mu^{(\mathrm{MMCC})}(2,4) = E_\mu^{(\mathrm{CCSD})} + \frac{\langle \Psi_\mu | M_{\mu,3}(2) + [M_{\mu,4}(2) + T_1 M_{\mu,3}(2)] | \Phi \rangle}{\langle \Psi_\mu | R_\mu^{(\mathrm{CCSD})} e^{T^{(\mathrm{CCSD})}} | \Phi \rangle}, \quad (41)$$

where $E_\mu^{(\mathrm{CCSD})}$ is the CCSD ($\mu = 0$) or EOMCCSD ($\mu > 0$) energy, $T^{(\mathrm{CCSD})}$ is the cluster operator obtained in the CCSD calculations (cf. Eq. (5)), $R_\mu^{(\mathrm{CCSD})}$ is the corresponding EOMCCSD excitation operator (cf. Eq. (19); when $\mu = 0$, $R_\mu^{(\mathrm{CCSD})} = \mathbf{1}$), and $M_{\mu,3}(2)$ and $M_{\mu,4}(2)$ are defined as

$$M_{\mu,3}(2) = \tfrac{1}{36}\, \mathfrak{M}_{\mu,abc}^{ijk}(2)\, a^a a^b a^c a_k a_j a_i, \quad (42)$$

and

$$M_{\mu,4}(2) = \tfrac{1}{576}\, \mathfrak{M}_{\mu,abcd}^{ijkl}(2)\, a^a a^b a^c a^d a_l a_k a_j a_i, \quad (43)$$

with $\mathfrak{M}_{\mu,abc}^{ijk}(2)$ and $\mathfrak{M}_{\mu,abcd}^{ijkl}(2)$ representing the triply and quadruply excited moments of the CCSD/EOMCCSD equations, respectively.

The explicit expression for the triply excited moment $\mathfrak{M}_{\mu,abc}^{ijk}(2)$, entering the MMCC(2,3) and MMCC(2,4) approximations and corresponding to the projections of the CCSD/EOMCCSD equations on the triply excited determinants $|\Phi_{ijk}^{abc}\rangle$, in terms of the many-body components of the CCSD/EOMCCSD similarity-transformed Hamiltonian $\bar{H}^{(\mathrm{CCSD})}$, Eq. (12), and operator $R_\mu^{(\mathrm{CCSD})}$, Eq. (19), is

$$\begin{aligned} \mathfrak{M}_{\mu,abc}^{ijk}(2) = {} & \langle \Phi_{ijk}^{abc} | (\bar{H}_2^{(\mathrm{CCSD})} R_{\mu,2})_C | \Phi \rangle + \langle \Phi_{ijk}^{abc} | [\bar{H}_3^{(\mathrm{CCSD})} (R_{\mu,1} + R_{\mu,2})]_C | \Phi \rangle \\ & + \langle \Phi_{ijk}^{abc} | (\bar{H}_4^{(\mathrm{CCSD})} R_{\mu,1})_C | \Phi \rangle + r_0(\mu)\, \mathfrak{M}_{0,abc}^{ijk}(2), \end{aligned} \quad (44)$$

where the ground-state moment $\mathfrak{M}_{0,abc}^{ijk}(2)$, obtained by projecting the CCSD equations on the triply excited determinants, is given by

$$\mathfrak{M}_{0,abc}^{ijk}(2) = \langle \Phi_{ijk}^{abc} | [H_N (T_2 + T_1 T_2 + \tfrac{1}{2} T_2^2 + \tfrac{1}{2} T_1^2 T_2 + \tfrac{1}{2} T_1 T_2^2 + \tfrac{1}{6} T_1^3 T_2)]_C | \Phi \rangle. \quad (45)$$

The analogous expression for the quadruply excited moments $\mathfrak{M}_{\mu,abcd}^{ijkl}(2)$, entering the MMCC(2,4) approximation, has the form

$$\begin{aligned} \mathfrak{M}_{\mu,abcd}^{ijkl}(2) = {} & \langle \Phi_{ijkl}^{abcd} | (\bar{H}_3^{(\mathrm{CCSD})} R_{\mu,2})_C | \Phi \rangle + \langle \Phi_{ijkl}^{abcd} | [\bar{H}_4^{(\mathrm{CCSD})} (R_{\mu,1} + R_{\mu,2})]_C | \Phi \rangle \\ & + \langle \Phi_{ijkl}^{abcd} | (\bar{H}_3^{(\mathrm{CCSD})} R_{\mu,1})_{DC} | \Phi \rangle + r_0(\mu)\, \mathfrak{M}_{0,abcd}^{ijkl}(2), \end{aligned} \quad (46)$$

where the ground-state moment $\mathfrak{M}_{0,abcd}^{ijkl}(2)$, obtained by projecting the CCSD equations on the quadruply excited determinants, is expressed as

$$\mathfrak{M}_{0,abcd}^{ijkl}(2) = \langle \Phi_{ijkl}^{abcd} | [H_N (\tfrac{1}{2} T_2^2 + \tfrac{1}{2} T_1 T_2^2 + \tfrac{1}{6} T_2^3 + \tfrac{1}{4} T_1^2 T_2^2)]_C | \Phi \rangle. \quad (47)$$

The operators $\bar{H}_p^{(\mathrm{CCSD})}$ in Eqs. (44) and (46) represent the p-body components of $\bar{H}^{(\mathrm{CCSD})}$ and $H_N = H - \langle \Phi | H | \Phi \rangle$ is the Hamiltonian in the normal-ordered form.

The diagrammatic techniques of many-body theory greatly facilitate the derivation of the explicit expressions for $\mathfrak{M}^{ijk}_{\mu,abc}(2)$ and $\mathfrak{M}^{ijkl}_{\mu,abcd}(2)$. The diagrams and algebraic expressions representing the triply and quadruply excited moments of the CCSD/EOMCCSD equations, in terms of molecular intergrals f^q_p and v^{rs}_{pq} and cluster and excitation amplitudes t^i_a, t^{ij}_{ab}, r^a_i, and r^{ab}_{ij}, are shown in Sect. 4.3 and Appendix 2. The fully factorized expressions for $\mathfrak{M}^{ijk}_{\mu,abc}(2)$ and $\mathfrak{M}^{ijkl}_{\mu,abcd}(2)$, which can be used in the efficient implementations of all MMCC(2,3) and MMCC(2,4) approximations, including the CI-corrected MMCC methods and the renormalized CC/EOMCC approaches overviewed in Sect. 3.3 as well as the MRMBPT-corrected MMCC methods discussed in Sects. 4 and 5, are described in Sect. 4.4.

3.3 The CI-Corrected MMCC(m_A,m_B) Approximations and the Renormalized CC and EOMCC Methods

Depending on the form of $|\Psi_\mu\rangle$ in the MMCC energy equations, the MMCC(m_A,m_B) methods fall into one of the following three categories: (i) the CI-corrected MMCC(m_A,m_B) schemes, (ii) the renormalized CC methods for the ground-state problem, and their excited-state extensions based on EOMCC, and (iii) the MRMBPT-corrected MMCC(m_A,m_B) approaches. In this section, we overview a few basic CI-corrected MMCC(m_A,m_B) schemes and renormalized CC/EOMCC methods.

3.3.1 The CI-Corrected MMCC(2,3) and MMCC(2,4) Methods

In the CI-corrected MMCC(2,3) and MMCC(2,4) calculations, the wavefunctions $|\Psi_\mu\rangle$ in Eqs. (40) and (41) are replaced by the wavefunctions obtained in the active-space CISDt [39, 60, 96, 97, 251] and CISDtq [97, 251] calculations, respectively, as shown below:

$$E^{(\mathrm{MMCC/CI})}_\mu(2,3) = E^{(\mathrm{CCSD})}_\mu + \frac{\langle \Psi^{(\mathrm{CISDt})}_\mu | M_{\mu,3}(2) | \Phi\rangle}{\langle \Psi^{(\mathrm{CISDt})}_\mu | R^{(\mathrm{CCSD})}_\mu e^{T^{(\mathrm{CCSD})}} | \Phi\rangle}, \tag{48}$$

$$E^{(\mathrm{MMCC/CI})}_\mu(2,4) = E^{(\mathrm{CCSD})}_\mu + \frac{\langle \Psi^{(\mathrm{CISDtq})}_\mu | M_{\mu,3}(2) + [M_{\mu,4}(2) + T_1 M_{\mu,3}(2)] | \Phi\rangle}{\langle \Psi^{(\mathrm{CISDtq})}_\mu | R^{(\mathrm{CCSD})}_\mu e^{T^{(\mathrm{CCSD})}} | \Phi\rangle}. \tag{49}$$

In order to define the relevant CISDt and CISDtq wavefunctions, $|\Psi^{(\mathrm{CISDt})}_\mu\rangle$ and $|\Psi^{(\mathrm{CISDtq})}_\mu\rangle$, respectively, we follow the philosophy of multi-reference calculations, i.e., we first divide the available spin-orbitals into four groups (see Fig. 1) of core

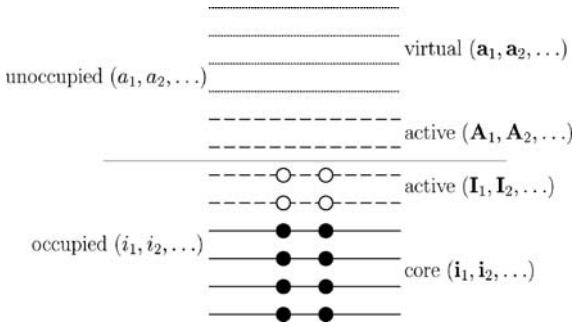

Fig. 1 The orbital classification used in the active-space CI, MRMBPT, and the CI- and MRMBPT-corrected MMCC methods, such as MMCC(2,3)/CI, MMCC(2,4)/CI, MMCC(2,3)/PT, and MMCC(2,4)/PT. Core, active, and virtual orbitals are represented by solid, dashed, and dotted lines, respectively. Full and open circles represent core and active electrons of the reference determinant $|\Phi\rangle$ used in the CC/EOMCC and MMCC calculations (the closed-shell reference determinant $|\Phi\rangle$ is assumed)

spin-orbitals ($\mathbf{i}_1$, $\mathbf{i}_2$, … or $\mathbf{i}$, $\mathbf{j}$, …), active spin-orbitals occupied in reference $|\Phi\rangle$ ($\mathbf{I}_1$, $\mathbf{I}_2$, … or $\mathbf{I}$, $\mathbf{J}$, …), active spin-orbitals unoccupied in reference $|\Phi\rangle$ ($\mathbf{A}_1$, $\mathbf{A}_2$, … or $\mathbf{A}$, $\mathbf{B}$, …), and virtual spin-orbitals ($\mathbf{a}_1$, $\mathbf{a}_2$, … or $\mathbf{a}$, $\mathbf{b}$, …). The choice of active spin-orbitals (typically, a few highest-energy occupied spin-orbitals and a few lowest-energy unoccupied spin-orbitals) is dictated by the dominant orbital excitations in the ground and excited states that we would like to calculate. A few examples of reasonable choices of active orbitals in calculations involving bond breaking and excited states are discussed in Sect. 5. Once the active orbitals are selected, the CISDt and CISDtq wavefunctions are defined as follows:

$$|\Psi_\mu^{(\mathrm{CISDt})}\rangle = (C_{\mu,0} + C_{\mu,1} + C_{\mu,2} + c_{\mu,3})|\Phi\rangle, \tag{50}$$

$$|\Psi_\mu^{(\mathrm{CISDtq})}\rangle = (C_{\mu,0} + C_{\mu,1} + C_{\mu,2} + c_{\mu,3} + c_{\mu,4})|\Phi\rangle, \tag{51}$$

where

$$C_{\mu,0} = c_0(\mu)\,\mathbf{1}, \tag{52}$$

$$C_{\mu,1} = c_a^i(\mu)\,a^a a_i = \sum_{i,a} c_a^i(\mu)\,a^a a_i, \tag{53}$$

and

$$C_{\mu,2} = \tfrac{1}{4}\,c_{ab}^{ij}(\mu)\,a^a a^b a_j a_i = \sum_{i<j,a<b} c_{ab}^{ij}(\mu)\,a^a a^b a_j a_i \tag{54}$$

are the operators defining the usual reference, singly, and doubly excited contributions, respectively, to $|\Psi_\mu^{(\mathrm{CISDt})}\rangle$ and $|\Psi_\mu^{(\mathrm{CISDtq})}\rangle$, and

$$c_{\mu,3} = \sum_{i<j<\mathbf{K},\mathbf{A}<b<c} c_{\mathbf{A}bc}^{ij\mathbf{K}}(\mu)\,a^{\mathbf{A}} a^b a^c a_{\mathbf{K}} a_j a_i \tag{55}$$

and

$$c_{\mu,4} = \sum_{i<j<\mathbf{K}<\mathbf{L},\mathbf{A}<\mathbf{B}<c<d} c^{ij\mathbf{KL}}_{\mathbf{AB}cd}(\mu)\, a^{\mathbf{A}}a^{\mathbf{B}}a^{c}a^{d}a_{\mathbf{L}}a_{\mathbf{K}}a_{j}a_{i} \tag{56}$$

define the corresponding triply and quadruply excited components. Thus, in the CISDt approach, used in the CI-corrected MMCC(2,3) calculations (cf. Eq. (48)), the wavefunctions $|\Psi_\mu\rangle$ are constructed by including all singles and doubles from $|\Phi\rangle$, and a relatively small set of internal and semi-internal triples containing at least one active occupied and one active unoccupied spin-orbital indices defined by Eq. (55). For the CISDtq approach, used for the CI-corrected MMCC(2,4) calculations, an additional relatively small set of quadruples containing at least two active occupied and at least two active unoccupied spin-orbital indices is also required. The CI coefficients defining the CISDt and CISDtq wavefunctions are determined variationally, as in all CI calculations.

One of the main advantages of the CI-corrected MMCC schemes, including the MMCC(2,3)/CI and MMCC(2,4)/CI methods, is a very good control of the quality of wavefunctions $|\Psi_\mu\rangle$ used to construct the non-iterative corrections $\delta_\mu(m_A, m_B)$, which is accomplished through the judicious choice of active orbitals that can always be adjusted to the type of bond breaking or excited excited states of interest. Another advantage of the CI-corrected MMCC methods is their relatively low computer cost, which is a consequence of the fact that it is often sufficient to use small active orbital spaces to obtain accurate results [39, 60–62, 96, 97, 251]. If N_o (N_u) is the number of active orbitals occupied (unoccupied) in $|\Phi\rangle$, the most expensive steps of the CISDt and CISDtq methods scale as $N_oN_un_o^2n_u^4$ and $N_o^2N_u^2n_o^2n_u^4$, respectively, which are considerable savings in the computer effort compared to the $n_o^3n_u^5$ and $n_o^4n_u^6$ scalings of the parent CISDT (CI singles, doubles, and triples) and CISDTQ (CI singles, doubles, triples, and quadruples) approaches, respectively. Furthermore, the numbers of triples and quadruples considered in the CISDt and CISDtq calculations are $\sim N_oN_un_o^2n_u^2$ and $\sim N_o^2N_u^2n_o^2n_u^2$, respectively, which is significantly less than the numbers of all triples and quadruples if the number of active orbitals is small. For instance, the number of triples used in the CISDt-corrected MMCC(2,3) calculations is usually very small (no more than $\sim$30% of all triples, in many cases even less than that). Additionally, the CPU times required to construct the relevant $\delta_\mu(2,3)$ corrections are often on the order of the CPU time of a single CCSD/EOMCCSD iteration. Similar remarks apply to the CISDtq-corrected MMCC(2,4) calculations.

Thus, the CI-corrected MMCC methods can be regarded as useful approaches to accurate calculations of ground- and excited-state potential energy surfaces. One may contemplate, however, an idea of reducing the costs of the CISDt-corrected MMCC(2,3) and CISDtq-corrected MMCC(2,4) calculations even further by replacing the CISDt or CISDtq wavefunctions in the MMCC(2,3) and MMCC(2,4) expressions by the wavefunctions obtained with low-order MRMBPT approaches, as in the MMCC/PT schemes discussed in Sects. 4 and 5.

In the next subsection, we describe an alternative to the externally corrected MMCC schemes using nothing else but the cluster and excitation operators obtained

in the CC/EOMCC calculations instead of non-CC wavefunctions to define the relevant wavefunction $|\Psi_\mu\rangle$.

3.3.2 The Renormalized CC and EOMCC Methods Based on the Original MMCC Theory

An interesting alternative to the CI-corrected MMCC methods, discussed in Sect. 3.3.1, is offered by the completely renormalized (CR) CC/EOMCC approaches which can be considered as purely single-reference, "black-box" methods based on the MMCC(m_A,m_B) truncation schemes.

Let us begin with the ground-state CR-CC methods. The basic CR-CCSD(T) method is an example of the MMCC(2,3) scheme, whereas the higher-level CR-CCSD(TQ) approach is an example of the MMCC(2,4) approximation. The energy formula defining CR-CCSD(T) method is [39–41]

$$E_0^{(\text{CR-CCSD(T)})} = E_0^{(\text{CCSD})} + \frac{\langle \Psi_0^{(\text{CCSD(T)})} | M_{0,3}(2) | \Phi \rangle}{\langle \Psi_0^{(\text{CCSD(T)})} | e^{T^{(\text{CCSD})}} | \Phi \rangle}. \tag{57}$$

Here, again, $T^{(\text{CCSD})}$ refers to the cluster operators obtained in the CCSD calculations and $M_{0,3}(2)$ is given by Eq. (42) using the generalized moments $\mathfrak{M}^{ijk}_{0,abc}(2)$ defined by Eq. (44). The $|\Psi_0^{(\text{CCSD(T)})}\rangle$ wavefunction, entering Eq. (57), is a simple MBPT-like expression

$$|\Psi_0^{(\text{CCSD(T)})}\rangle = [1 + T_1 + T_2 + R_0^{(3)}(V_N T_2)_C + R_0^{(3)} V_N T_1] |\Phi\rangle, \tag{58}$$

with $R_0^{(3)}$ representing the three-body component of the MBPT reduced resolvent and V_N designating the two-body part of the Hamiltonian in the normal-ordered form. The CR-CCSD(T) approach reduces to standard CCSD(T) method when the $\langle \Psi_0^{(\text{CCSD(T)})} | e^{T^{(\text{CCSD})}} | \Phi \rangle$ denominator in the CR-CCSD(T) energy formula is replaced by 1 and moments $\mathfrak{M}^{ijk}_{0,abc}(2)$ entering Eq. (57) through the $M_{0,3}(2)$ operators (cf. Eq. (42)) are replaced by $\langle \Phi^{abc}_{ijk} | (V_N T_2)_C | \Phi \rangle$ (one can easily show that $\langle \Phi^{abc}_{ijk} | (V_N T_2)_C | \Phi \rangle$ is the leading contribution to $\mathfrak{M}^{ijk}_{0,abc}(2)$).

The idea of renormalizing the CCSD(T) approach can also be extended to the CCSD(TQ) method. Two variants of the CR-CCSD(TQ) approach, which are labeled "a" and "b", are mentioned here. The CR-CCSD(TQ) energy formulas can be given in the following form [39–41]:

$$E_0^{(\text{CR-CCSD(TQ),x})} = E_0^{(\text{CCSD})} + \frac{\langle \Psi_0^{(\text{CCSD(TQ),x})} | [M_{0,3}(2) + T_1 M_{0,3}(2) + M_{0,4}(2)] | \Phi \rangle}{\langle \Psi_0^{(\text{CCSD(TQ),x})} | e^{T^{(\text{CCSD})}} | \Phi \rangle} \quad (\text{x} = \text{a}, \text{b}), \tag{59}$$

where

$$|\Psi_0^{(\mathrm{CCSD(TQ),a})}\rangle = |\Psi_0^{(\mathrm{CCSD(T)})}\rangle + \tfrac{1}{2}T_2T_2^{(1)}|\Phi\rangle \tag{60}$$

and

$$|\Psi_0^{(\mathrm{CCSD(TQ),b})}\rangle = |\Psi_0^{(\mathrm{CCSD(T)})}\rangle + \tfrac{1}{2}T_2^2|\Phi\rangle\,, \tag{61}$$

with $T_2^{(1)}$ representing the first-order MBPT estimate of T_2. The $M_{0,3}(2)$ operator is defined by Eq. (42) and $M_{0,4}(2)$ is defined by Eq. (43). As in the case of the CR-CCSD(T) method, one can obtain the conventional CCSD(TQ) approaches, including, among them, CCSD(TQ$_\mathrm{f}$) [68], by replacing the overlap denominator $\langle\Psi_0^{(\mathrm{CCSD(TQ),x})}|e^{T^{(\mathrm{CCSD})}}|\Phi\rangle$ in the CR-CCSD(TQ) energy expressions by 1, dropping the $T_1M_{0,3}(2)$ term in Eq. (59), and replacing the $\mathfrak{M}_{0,abc}^{ijk}(2)$ and $\mathfrak{M}_{0,abcd}^{ijkl}(2)$ moments that enter the definitions of $M_{0,3}(2)$ and $M_{0,4}(2)$, respectively, by their lowest-order estimates resulting from the MBPT analysis. We refer the reader to the original papers [39–41] for further details.

The standard CCSD(T) and CCSD(TQ) approaches, and their (C)R-CCSD(T) and (C)R-CCSD(TQ) counterparts, have nearly identical computer costs. For example, the costs of the conventional CCSD(T) calculations are $n_o^2n_u^4$ in the iterative CCSD steps and $n_o^3n_u^4$ in the non-iterative steps defining the triples correction while the CR-CCSD(T) approach scales as $n_o^2n_u^4$ in the iterative CCSD steps and $2n_o^3n_u^4$ in the non-iterative triples correction part. Similar remarks apply to other CR-CC methods. In particular, the CR-CCSD(TQ),x approaches have computational steps that scale as $n_o^2n_u^4$ in the CCSD part, $2n_o^3n_u^4$ in the triples correction parts, and $2n_o^2n_u^5$ in parts that deal with the quadruples corrections. This should be compared to the costs of conventional CCSD(TQ) calculations which are very similar, namely, $n_o^2n_u^4$ in the CCSD steps, $n_o^3n_u^4$ in the (T) part, and $n_o^2n_u^5$ in the (Q) parts. As already mentioned, the renormalized CC methods, such as CR-CCSD(T) and its recently formulated size extensive extension (not discussed here), termed CR-CC(2,3) [53–55, 57], are particularly useful in studies of reaction pathways involving single bond breaking and biradicals [39–42, 44–46, 48, 49, 51–55, 57–65, 133, 162, 163, 213, 214, 216, 217, 221, 223–225]. They remove or considerably reduce the failures of conventional CCSD(T), CCSD(TQ), and similar approximations without making the calculations more complex or considerably more expensive.

The idea of renormalizing conventional CC methods via the MMCC formalism can be extended to excited states. For example, in the CR-EOMCCSD(T) approach [61, 62, 98, 99] which is an example of the excited-state MMCC(2,3) scheme, the energies of ground and excited states E_μ are calculated as follows:

$$E_\mu^{(\mathrm{CR\text{-}EOMCCSD(T)})} = E_\mu^{(\mathrm{CCSD})} + \frac{\langle\Psi_\mu^{(\mathrm{CR\text{-}EOMCCSD(T)})}|M_{\mu,3}(2)|\Phi\rangle}{\langle\Psi_\mu^{(\mathrm{CR\text{-}EOMCCSD(T)})}|R_\mu^{(\mathrm{CCSD})}e^{T^{(\mathrm{CCSD})}}|\Phi\rangle}. \tag{62}$$

Depending on the specific form of the wavefunction $|\Psi_\mu^{(\text{CR-EOMCCSD(T)})}\rangle$ in Eq. (62), several variants of the CR-EOMCCSD(T) approach can be considered. Here, only one variant, called ID (the CR-EOMCCSD(T), ID method), which represents one of the most complete versions of the CR-EOMCCSD(T) approach and which usually provides the most accurate description of excited states compared to other variants, is presented. The $|\Psi_\mu^{(\text{CR-EOMCCSD(T)})}\rangle$ wavefunction entering Eq. (62) is defined in this case as

$$\begin{aligned}
|\Psi_\mu^{(\text{CR-EOMCCSD(T)})}\rangle &= \bar{P}(R_{\mu,0}+R_{\mu,1}+R_{\mu,2}+\tilde{R}_{\mu,3})e^{T^{(\text{CCSD})}}|\Phi\rangle \\
&= \{R_{\mu,0}+(R_{\mu,1}+R_{\mu,0}T_1) \\
&\quad +[R_{\mu,2}+R_{\mu,1}T_1+R_{\mu,0}(T_2+\tfrac{1}{2}T_1^2)] \\
&\quad +[\tilde{R}_{\mu,3}+R_{\mu,2}T_1+R_{\mu,1}(T_2+\tfrac{1}{2}T_1^2) \\
&\quad +R_{\mu,0}(T_1T_2+\tfrac{1}{6}T_1^3)]\}|\Phi\rangle, \qquad (63)
\end{aligned}$$

where $\bar{P}$ is a projection operator on the subspace spanned by the reference $|\Phi\rangle$ and all singly, doubly, and triply excited determinants. The triple excitation operator $\tilde{R}_{\mu,3}$, entering Eq. (63), is calculated as

$$\tilde{R}_{\mu,3} = \tfrac{1}{36}\,\tilde{r}_{abc}^{ijk}(\mu)\,a^a a^b a^c a_k a_j a_i, \qquad (64)$$

where

$$\tilde{r}_{abc}^{ijk}(\mu) = \frac{\mathfrak{M}_{\mu,abc}^{ijk}(2)}{D_{\mu,abc}^{ijk}} \qquad (65)$$

are the approximate values of the triple excitation amplitudes $r_{abc}^{ijk}(\mu)$ resulting from the analysis of the full EOMCCSDT eigenvalue problem [98]. As implied by Eq. (65), the approximate amplitudes $\tilde{r}_{abc}^{ijk}(\mu)$ are calculated using exactly the same set of triply excited moments $\mathfrak{M}_{\mu,abc}^{ijk}(2)$ of the CCSD/EOMCCSD equations that enters the MMCC(2,3) energy expression, Eq. (40). This greatly facilitates the computer coding effort, since one can reuse the moments $\mathfrak{M}_{\mu,abc}^{ijk}(2)$, which are needed to construct the triples correction of CR-EOMCCSD(T) anyway, to determine the $\tilde{r}_{abc}^{ijk}(\mu)$ amplitudes. The $D_{\mu,abc}^{ijk}$ quantities that enter Eq. (65) represent the perturbative denominators for triple excitations, which are defined (if we assume that there are no orbital degeneracies [57, 65]) as follows:

$$\begin{aligned}
D_{\mu,abc}^{ijk} &= E_\mu^{(\text{CCSD})} - \langle \Phi_{ijk}^{abc}|\bar{H}^{(\text{CCSD})}|\Phi_{ijk}^{abc}\rangle \\
&= \omega_\mu^{(\text{CCSD})} - \langle \Phi_{ijk}^{abc}|\bar{H}_1^{(\text{CCSD})}|\Phi_{ijk}^{abc}\rangle \\
&\quad - \langle \Phi_{ijk}^{abc}|\bar{H}_2^{(\text{CCSD})}|\Phi_{ijk}^{abc}\rangle \\
&\quad - \langle \Phi_{ijk}^{abc}|\bar{H}_3^{(\text{CCSD})}|\Phi_{ijk}^{abc}\rangle, \qquad (66)
\end{aligned}$$

where $\bar{H}_p^{(\mathrm{CCSD})}$, $p = 1-3$, are the one-, two-, and three-body components of the CCSD/EOMCCSD similarity-transformed Hamiltonian $\bar{H}^{(\mathrm{CCSD})}$, respectively, and $\omega_\mu^{(\mathrm{CCSD})}$ is the EOMCCSD vertical excitation energy.

One of the main advantages of all renormalized CC/EOMCC methods is the fact that these methods are as easy to use as the standard "black-box" approaches of the CCSD(T) type while considerably improving the description of the bond breaking region and excited states without the need to define active orbitals or other elements of multi-reference theory. We have already mentioned the benefits of using the CR-CC approaches in the ground-state applications. Similar benefits apply to the use of the CR-EOMCCSD(T) method in calculations for the electronically excited states [61, 62, 98, 99, 215, 218–222, 226]. However, as mentioned earlier, there are cases, where the degree of quasi-degeneracy is so big that one would be better off by using elements of multi-reference theory within the MMCC formalism (cf., e.g. [227, 228]). The CI-corrected MMCC methods are one possible way of incorporating multi-reference concepts into the MMCC considerations. The MRMBPT-corrected MMCC methods, which are the main focus on this work, represent another way. Brief information about the basic elements of MRMBPT is presented next.

3.4 The Basic Elements of Multi-Reference Many-Body Perturbation Theory (MRMBPT)

All genuine multi-reference theories involve two fundamental concepts, namely, that of the model or reference space $\mathscr{M}_0$ and that of the wave operator U. The model space $\mathscr{M}_0$,

$$\mathscr{M}_0 = \{|\Phi_p\rangle\}_{p=1}^{M}, \tag{67}$$

is spanned by M determinants or configuration state functions $|\Phi_p\rangle$ ($p = 1,\ldots,M$) that provide a reasonable zeroth-order description of the target space

$$\mathscr{M} = \{|\Psi_\mu\rangle\}_{\mu=0}^{M-1}, \tag{68}$$

spanned by M quasi-degenerate eigenstates $|\Psi_\mu\rangle$ ($\mu = 0,1,\ldots,M-1$) of the electronic Hamiltonian H,

$$H|\Psi_\mu\rangle = E_\mu|\Psi_\mu\rangle\,. \tag{69}$$

In order to define the reference configurations $|\Phi_p\rangle$, the employed molecular orbital basis set is partitioned into core, active, and virtual orbitals in a similar manner as in Fig. 1. The core orbitals are occupied and the virtual ones are unoccupied in all reference configurations. The references $|\Phi_p\rangle$ differ in the occupancies of active orbitals. All possible distributions of active electrons among the active orbitals result in a complete model or active space (CAS). The use of CAS is essential to obtain size extensive results in the MRMBPT calculations, if the "perturb then diagonalize" MRMBPT method, summarized below, is considered.

The wave operator U: $\mathscr{M}_0 \rightarrow \mathscr{M}$ is defined as a one-to-one mapping between $\mathscr{M}_0$ and $\mathscr{M}$ that satisfies the intermediate normalization condition,

$$PU = P, \tag{70}$$

and the relation determining its kernel, i.e.,

$$UQ = 0\,. \tag{71}$$

Here, P and Q are the projection operators onto the model space $\mathscr{M}_0$ and its orthogonal complement $\mathscr{M}_0^{\perp}$, respectively, in the N-electron Hilbert space,

$$P = \sum_{p=1}^{M} P^{(p)}, \qquad P^{(p)} = |\Phi_p\rangle\langle\Phi_p|, \tag{72}$$

$$Q = 1 - P. \tag{73}$$

Based on Eqs. (70) and (71), U is idempotent, $U^2 = U$, which is a property of projection operators, including P and Q. However, unlike the orthogonal projectors P and Q, the wave operator U is not Hermitian, $U \neq U^{\dagger}$.

The MRMBPT wavefunctions $|\Psi_\mu\rangle$ are calculated using the formula,

$$|\Psi_\mu\rangle = \sum_{p=1}^{M} c_{p\mu}|\Phi_p\rangle + \sum_{n=1}^{\infty}\left(\sum_{p=1}^{M} c_{p\mu}U^{(n)}|\Phi_p\rangle\right), \tag{74}$$

where $U^{(1)}$, $U^{(2)}$, etc., represent perturbative corrections to the wave operator U (expressed in terms of excited configurations from $\mathscr{M}_0^{\perp}$, i.e., configurations other than $|\Phi_p\rangle$, $p = 1, \ldots, \mathrm{M}$). These corrections describe dynamical correlation effects.

The coefficients $c_{p\mu}$, which describe the non-dynamical correlation effects, define the zeroth-order states belonging to $\mathscr{M}_0$,

$$|\Psi_\mu^{(0)}\rangle = \sum_{p=1}^{M} c_{p\mu}|\Phi_p\rangle\,. \tag{75}$$

In the "perturb then diagonalize" MRMBPT methods that follow the ideas laid down in [129], these coefficients and the corresponding energies E_μ of the ground and excited states $|\Psi_\mu\rangle$, $\mu = 0, 1, \ldots, M-1$, are obtained by diagonalizing the effective Hamiltonian,

$$H^{\mathrm{eff}} = PHUP = PHP + \sum_{n=1}^{\infty} PHU^{(n)}P\,, \tag{76}$$

in the model space $\mathscr{M}_0$,

$$H^{\mathrm{eff}}|\Psi_\mu^{(0)}\rangle = E_\mu|\Psi_\mu^{(0)}\rangle. \tag{77}$$

In the practical implementations of such MRMBPT theories, the wave operator U is truncated at some, preferably low, perturbation theory order n. When U is

truncated at the first-order term $U^{(1)}$, i.e., $U = P + U^{(1)}$, the second-order MRMBPT (MRMBPT(2)) wavefunction is obtained; second-order since the resulting energies E_μ are correct through second order.

One can considerably simplify the above considerations, which are based on the generalized Bloch formalism [262], in which the wave operator U is determined by solving the multi-root generalized Bloch equation $HU = UHU$ (in the case of MRMBPT, using perturbation theory), by formulating the "diagonalize then perturb" MRMBPT methods. In those methods, one continues to use Eq. (75) to determine the zeroth-order states, but the coefficients $c_{p\mu}$ of the zeroth-order states are obtained by diagonalizing the bare Hamiltonian H rather than the effective Hamiltonian $H^{\rm eff}$. Perturbative corrections to the zeroth-order energies $E^{(0)}$ are calculated *a posteriori* in a state-selective manner without using the multi-root generalized Bloch formalism. As mentioned in the Introduction, several methods, including the popular CASPT2 and MC-QDPT approaches, are in this category. The MRMBPT approach used to define the MRMBPT-corrected MMCC schemes discussed in detail in the next section belongs to the category of the "diagonalize then perturb" methods as well.

4 The MMCC Methods Employing Multi-Reference Many-Body Perturbation Theory (MMCC/PT)

In this section, an alternative variant of the MMCC theory, referred to as the MRMBPT-corrected MMCC approach or, for brevity, MMCC/PT, in which the wavefunctions $|\Psi_\mu\rangle$ in Eqs. (26) or (39) are approximated by the wavefunctions obtained from the low-order MRMBPT calculations, is described. The approximate MRMBPT wavefunctions used in the MMCC(m_A,m_B)/PT approaches implemented in this work are discussed. Moreover, the diagrammatic formulation of the resulting MMCC(2,3)/PT and MMCC(2,4)/PT schemes is presented. The details of the algorithm that enables one to achieve a high degree of code vectorization for the generalized moments of CC equations defining the MMCC methods are described as well.

4.1 The Multi-Reference Many-Body Perturbation Theory Wavefunctions Used in the MMCC/PT Approaches

As in all multi-reference considerations and in analogy to the CISDt and CISDtq methods discussed in Sect. 3.3.1, in order to define the computationally simple form of the low-order MRMBPT wavefunctions $|\Psi_\mu^{(\rm MRMBPT)}\rangle$ for the MRMBPT-corrected MMCC calculations, we begin by partitioning the molecular orbital basis set into four groups of (cf. Fig. 1) core spin-orbitals, active spin-orbitals occupied

in reference $|\Phi\rangle$, active spin-orbitals unoccupied in reference $|\Phi\rangle$, and virtual spin-orbitals. As in the CI-corrected MMCC schemes, reference $|\Phi\rangle$ is one of the many reference determinants that we choose as a Fermi vacuum for the CC/EOMCC and MMCC considerations. By distributing active electrons among active spin-orbitals in all possible ways, we generate a certain number (designated here by M) of reference determinants $|\Phi_p\rangle$, which include, among them, the Fermi vacuum state $|\Phi\rangle$ and which span the complete model space or P-space $\mathscr{M}_0$. Then, we define the zeroth-order wavefunctions of the ground and excited states of interest, $|\bar{\Psi}_\mu^{(P)}\rangle$, as linear combinations of the reference configurations $|\Phi_p\rangle$,

$$|\bar{\Psi}_\mu^{(P)}\rangle = \sum_{p=1}^{M} \overline{c}_{p\mu}|\Phi_p\rangle, \tag{78}$$

where the coefficients $\overline{c}_{p\mu}$ and the corresponding zeroth-order eigenvalues $\bar{E}_\mu$ are obtained by diagonalizing the Hamiltonian H in the model space $\mathscr{M}_0$.

Once the model space $\mathscr{M}_0$ is defined, we introduce the Q-space which in the MMCC/PT method pursued here is a subspace of the orthogonal complement $\mathscr{M}_0^\perp$ spanned by all singly and doubly excited determinants with respect to each reference $|\Phi_p\rangle$ ($p = 1,\ldots,M$), as is done, for example, in the MRCISD calculations. After eliminating the repetitions in the list of Q-space configurations, the resulting MRMBPT wavefunctions $|\Psi_\mu^{(\mathrm{MRMBPT})}\rangle$, which will eventually be used to design the MMCC/PT (e.g. MMCC(2,3)/PT and MMCC(2,4)/PT) energy corrections, are defined as linear combinations of the P-space and Q-space configurations,

$$|\Psi_\mu^{(\mathrm{MRMBPT})}\rangle = \sum_{p=1}^{M} c_{p\mu}|\Phi_p\rangle + \sum_{q=M+1}^{R} c_{q\mu}|\Phi_q\rangle, \tag{79}$$

where $|\Phi_p\rangle$ ($p = 1,\ldots,M$) are the reference determinants and $|\Phi_q\rangle$ ($q = M+1,\ldots,R$) are the Q-space determinants, as expressed above. In principle, we could use any of the existing low-order MRMBPT methods to determine the approximate values of the coefficients $c_{p\mu}$ and $c_{q\mu}$ that enter Eq. (79) and perform the corresponding MMCC(m_A,m_B)/PT calculations. In the simplified MRMBPT model used in the present implementation of the MMCC(2,3)/PT method [55, 56] and the MMCC(2,4)/PT scheme developed in this work, we evaluate the relevant coefficients $c_{p\mu}$ ($p = 1,\ldots,M$) and $c_{q\mu}$ ($q = M+1,\ldots,R$) in Eq. (79) by applying the Löwdin-style partitioning technique [263, 264] to the Hamiltonian matrix in the space spanned by the P-space and Q-space determinants, $|\Phi_p\rangle$ and $|\Phi_q\rangle$, respectively. Thus, if $\mathbf{C}_{P\mu}$ and $\mathbf{C}_{Q\mu}$ are the column vectors of coefficients $c_{p\mu}$ with $p = 1,\ldots,M$ and $c_{q\mu}$ with $q = M+1,\ldots,R$, respectively, and if $\mathbf{H}_{PP}$, $\mathbf{H}_{PQ}$, $\mathbf{H}_{QP}$, and $\mathbf{H}_{QQ}$ are the corresponding PP, PQ, QP, and QQ blocks of the Hamiltonian, we can write the Hamiltonian eigenvalue problem for the wavefunctions $|\Psi_\mu^{(\mathrm{MRMBPT})}\rangle$, Eq. (79), in the following manner:

$$\begin{pmatrix} \mathbf{H}_{PP} & \mathbf{H}_{PQ} \\ \mathbf{H}_{QP} & \mathbf{H}_{QQ} \end{pmatrix} \begin{pmatrix} \mathbf{C}_{P\mu} \\ \mathbf{C}_{Q\mu} \end{pmatrix} = E_\mu \begin{pmatrix} \mathbf{C}_{P\mu} \\ \mathbf{C}_{Q\mu} \end{pmatrix}. \tag{80}$$

In other words, we obtain

$$\mathbf{H}_{PP}\mathbf{C}_{P\mu} + \mathbf{H}_{PQ}\mathbf{C}_{Q\mu} = E_\mu \mathbf{C}_{P\mu}\,, \tag{81}$$

$$\mathbf{H}_{QP}\mathbf{C}_{P\mu} + \mathbf{H}_{QQ}\mathbf{C}_{Q\mu} = E_\mu \mathbf{C}_{Q\mu}\,. \tag{82}$$

If we approximate the QQ block of the Hamiltonian matrix entering Eq. (80), $\mathbf{H}_{QQ}$, by the diagonal matrix elements $\langle \Phi_q|H|\Phi_q\rangle$, we can write

$$\mathbf{C}_{Q\mu} \approx (E_\mu \mathbf{1} - \mathbf{D}_Q)^{-1}\, \mathbf{H}_{QP}\mathbf{C}_{P\mu}, \tag{83}$$

or, more explicitly,

$$c_{q\mu} \approx \sum_{p=1}^{M} (E_\mu - \langle \Phi_q|H|\Phi_q\rangle)^{-1}\, \langle \Phi_q|H|\Phi_p\rangle\, c_{p\mu}, \;\; (q = M+1,\ldots,R), \tag{84}$$

where $\mathbf{D}_Q$ in Eq. (83) is the diagonal part of $\mathbf{H}_{QQ}$. In practice, we obtain the working equation for the approximate values of the coefficients $c_{q\mu}$ $(q = M+1,\ldots,R)$ by replacing the energies E_μ and coefficients $c_{p\mu}$ $(p = 1,\ldots,M)$ in Eq. (84) by the zeroth-order energies $\bar{E}_\mu$ and coefficients $\overline{c}_{p\mu}$, respectively, resulting from the diagonalization of the Hamiltonian in the model space $\mathscr{M}_0$ (diagonalization of $\mathbf{H}_{PP}$; cf. Eq. (78)). We use the resulting approximate values of the coefficients $c_{q\mu}$,

$$\overline{c}_{q\mu} = \sum_{p=1}^{M} (\bar{E}_\mu - \langle \Phi_q|H|\Phi_q\rangle)^{-1}\, \langle \Phi_q|H|\Phi_p\rangle\, \overline{c}_{p\mu}, \;\; (q = M+1,\ldots,R), \tag{85}$$

along with the coefficients $\overline{c}_{p\mu}$ obtained by diagonalizing $\mathbf{H}_{PP}$, to define the perturbed states of the MRMBPT theory exploited in the present work, which are defined as

$$|\bar{\Psi}_\mu^{(\mathrm{MRMBPT})}\rangle = \sum_{p=1}^{M} \overline{c}_{p\mu}|\Phi_p\rangle + \sum_{q=M+1}^{R} \overline{c}_{q\mu}|\Phi_q\rangle. \tag{86}$$

The wavefunctions $|\bar{\Psi}_\mu^{(\mathrm{MRMBPT})}\rangle$, Eq. (86), are used instead of the exact $|\Psi_\mu\rangle$ states in the MMCC(m_A,m_B) energy expressions, Eqs. (38) and (39), to define the family of the MMCC(m_A, m_B)/PT approximations.

The above perturbative procedure based on the partitioning of the Hamiltonian into the P-space and Q-space contributions equivalent to the MRCISD problem has an advantage that we only have to consider the QP matrix elements of the Hamiltonian (the $\langle \Phi_q|H|\Phi_p\rangle$ matrix elements) and the diagonal $\langle \Phi_q|H|\Phi_q\rangle$ matrix elements in the process of defining $|\bar{\Psi}_\mu\rangle$. Another advantage of this procedure is the fact that the zeroth-order states are obtained by simply diagonalizing the Hamiltonian in $\mathscr{M}_0$ to obtain the relevant coefficients $\overline{c}_{p\mu}$.

We have developed computer codes for the MRMBPT model defined by Eqs. (78), (85), and (86). In the actual construction of the MRMBPT wavefunctions $|\bar{\Psi}_\mu\rangle$, we use a complete model space obtained by all possible distributions of active electrons among active orbitals allowed by the spin and spatial symmetries. As discussed earlier, we limit ourselves to the Q spaces corresponding to the MRCISD problem. Because of the fact that we are mainly interested in the MMCC(2,3) and MMCC(2,4) approximations and to further simplify our MRMBPT calculations, we decided to consider only those Q-space configurations that are at most quadruply excited with respect to the Fermi vacuum $|\Phi\rangle$ used in the CCSD/EOMCCSD and subsequent MMCC(2,3) and MMCC(2,4) calculations. Furthermore, the allowed singly excited Q-space configurations from $\mathscr{M}_0$ to $\mathscr{M}_0^\perp$ are

a. core $\longrightarrow$ active
b. core $\longrightarrow$ virtual
c. active $\longrightarrow$ virtual

and for all three cases the allowed excitations are of the $\alpha \rightarrow \alpha$ and $\beta \rightarrow \beta$ types (at this time, our codes are limited to the $S_z = 0$ states obtained out of the restricted Hartree-Fock (RHF) reference). Similarly, the doubly excited Q-space configurations from $\mathscr{M}_0$ to $\mathscr{M}_0^\perp$ can be divided into the following eight categories:

a. core, core $\longrightarrow$ active, active
b. core, core $\longrightarrow$ active, virtual
c. core, core $\longrightarrow$ virtual, virtual
d. core, active $\longrightarrow$ active, active
e. core, active $\longrightarrow$ active, virtual
f. core, active $\longrightarrow$ virtual, virtual
g. active, active $\longrightarrow$ active, virtual
h. active, active $\longrightarrow$ virtual, virtual

Again, due to the conservation of spin S_z, the allowed Q-space double excitations are $\alpha\alpha \rightarrow \alpha\alpha$, $\beta\beta \rightarrow \beta\beta$, $\alpha\beta \rightarrow \alpha\beta$, $\alpha\beta \rightarrow \beta\alpha$, $\beta\alpha \rightarrow \beta\alpha$, and $\beta\alpha \rightarrow \alpha\beta$, if the RHF determinant is used as reference $|\Phi\rangle$.

We have implemented the simplified MRMBPT scheme described above and tested its usefulness in the MMCC calculations by examining the performance of the resulting MMCC(2,3)/PT and MMCC(2,4)/PT approximations in a few benchmark calculations for ground and excited states discussed in Sect. 5. The MMCC(2,3)/PT and MMCC(2,4)/PT approaches are discussed next.

4.2 The MRMBPT-Corrected MMCC(2,3) and MMCC(2,4) Approaches: MMCC(2,3)/PT and MMCC(2,4)/PT

As already mentioned, in this paper we focus on the basic MMCC(2,3)/PT and MMCC(2,4)/PT approaches in which the CCSD/EOMCCSD energies are corrected for the leading triples or triples and quadruples effects via non-iterative corrections $\delta_\mu(2,3)$ and $\delta_\mu(2,4)$, respectively, calculated with the MRMBPT wavefunctions $|\bar{\Psi}_\mu^{(\mathrm{MRMBPT})}\rangle$ defined by Eq. (86). In order to use the multi-reference wavefunctions

$|\bar{\Psi}_\mu^{(\mathrm{MRMBPT})}\rangle$ in the single-reference MMCC formalism, first, we have to rewrite the $|\bar{\Psi}_\mu^{(\mathrm{MRMBPT})}\rangle$ states in the form of CI expansions relative to the reference determinant $|\Phi\rangle$ used in the CC/EOMCC and MMCC calculations, as shown below:

$$|\bar{\Psi}_\mu^{(\mathrm{MRMBPT})}\rangle = (\bar{C}_{\mu,0}+\bar{C}_{\mu,1}+\bar{C}_{\mu,2}+\bar{C}_{\mu,3}+\bar{C}_{\mu,4}+\cdots)|\Phi\rangle, \tag{87}$$

where

$$\bar{C}_{\mu,0} = \overline{c}_0(\mu)\,\mathbf{1}, \tag{88}$$

$$\bar{C}_{\mu,1} = \overline{c}_a^i(\mu)\,a^a a_i = \sum_{i,a} \overline{c}_a^i(\mu)\,a^a a_i, \tag{89}$$

$$\bar{C}_{\mu,2} = \tfrac{1}{4}\overline{c}_{ab}^{ij}(\mu)\,a^a a^b a_j a_i = \sum_{i<j,a<b} \overline{c}_{ab}^{ij}(\mu)\,a^a a^b a_j a_i, \tag{90}$$

$$\bar{C}_{\mu,3} = \tfrac{1}{36}\overline{c}_{abc}^{ijk}(\mu)\,a^a a^b a^c a_k a_j a_i = \sum_{i<j<k,a<b<c} \overline{c}_{abc}^{ijk}(\mu)\,a^a a^b a^c a_k a_j a_i, \tag{91}$$

and

$$\bar{C}_{\mu,4} = \tfrac{1}{576}\overline{c}_{abcd}^{ijkl}(\mu)\,a^a a^b a^c a^d a_l a_k a_j a_i = \sum_{i<j<k<l,a<b<c<d} \overline{c}_{abcd}^{ijkl}(\mu)\,a^a a^b a^c a^d a_l a_k a_j a_i \tag{92}$$

are the corresponding particle-hole excitation operators relative to $|\Phi\rangle$ defining the reference, singly, doubly, triply, and quadruply excited contributions to $|\bar{\Psi}_\mu^{(\mathrm{MRMBPT})}\rangle$, respectively. In the specific case of the MMCC(2,3)/PT and MMCC(2,4)/PT approximations explored in this work, we further simplify the wavefunctions $|\bar{\Psi}_\mu^{(\mathrm{MRMBPT})}\rangle$, Eq. (87), by truncating the CI expansions for $|\bar{\Psi}_\mu^{(\mathrm{MRMBPT})}\rangle$ at the triply excited determinants (the $\bar{C}_{\mu,3}|\Phi\rangle$ term) in the MMCC(2,3)/PT case and at the quadruply excited determinants (the $\bar{C}_{\mu,4}|\Phi\rangle$ term) in the MMCC(2,4)/PT case. The final energy expressions for the MMCC(2,3)/PT and MMCC(2,4)/PT energies, obtained by replacing $|\Psi_\mu\rangle$ in Eqs. (40) and (41) by $|\bar{\Psi}_\mu^{(\mathrm{MRMBPT})}\rangle$, Eq. (87), truncated at the triply (the MMCC(2,3) case) or triply and quadruply (the MMCC(2,4) case) excited determinants, respectively, relative to $|\Phi\rangle$, are

$$E_\mu^{(\mathrm{MMCC/PT})}(2,3) = E_\mu^{(\mathrm{CCSD})} + \sum_{i<j<k,a<b<c} \frac{[\overline{c}_{abc}^{ijk}(\mu)]^*\,\mathfrak{M}_{\mu,abc}^{ijk}(2)}{D_\mu} \tag{93}$$

and

$$E_\mu^{(\mathrm{MMCC/PT})}(2,4) = E_\mu^{(\mathrm{CCSD})} + \sum_{i<j<k,a<b<c} \frac{[\overline{c}_{abc}^{ijk}(\mu)]^*\,\mathfrak{M}_{\mu,abc}^{ijk}(2)}{D_\mu} + \sum_{i<j<k<l,a<b<c<d} \frac{[\overline{c}_{abcd}^{ijkl}(\mu)]^*\,(\mathfrak{M}_{\mu,abcd}^{ijkl}(2)+\mathscr{A}_{abc/d}\mathfrak{M}_{\mu,abc}^{ijk}(2)\,t_d^l)}{D_\mu}, \tag{94}$$

respectively, where the triply excited moments $\mathfrak{M}^{ijk}_{\mu,abc}(2)$ are defined by Eqs. (44) and (45) and the quadruply excited moments $\mathfrak{M}^{ijkl}_{\mu,abcd}(2)$ are defined by Eqs. (46) and (47). The $\mathscr{A}_{abc/d}$ partial antisymmetrizer is defined as

$$\mathscr{A}_{abc/d} = 1 - (ad) - (bd) - (cd), \tag{95}$$

where (pq) is a usual transposition of indices p and q, and

$$\begin{aligned} D_\mu &\equiv \langle \bar{\Psi}^{(\mathrm{MRMBPT})}_\mu | R^{(\mathrm{CCSD})}_\mu e^{T^{(\mathrm{CCSD})}} | \Phi \rangle \\ &= \bar{\Delta}_{\mu,0} + \bar{\Delta}_{\mu,1} + \bar{\Delta}_{\mu,2} + \bar{\Delta}_{\mu,3} + \bar{\Delta}_{\mu,4} + \ldots \end{aligned} \tag{96}$$

is the overlap denominator $\langle \Psi_\mu | R^{(\mathrm{CCSD})}_\mu e^{T^{(\mathrm{CCSD})}} | \Phi \rangle$ entering Eq. (40), written for the wavefunction $|\Psi_\mu\rangle = |\bar{\Psi}^{(\mathrm{MRMBPT})}_\mu\rangle$, Eq. (87), truncated at triples ($\bar{\Delta}_{\mu,3}$) for MMCC(2,3)/PT and at quadruples ($\bar{\Delta}_{\mu,4}$) for MMCC(2,4)/PT. The $\bar{\Delta}_{\mu,0}$, $\bar{\Delta}_{\mu,1}$, $\bar{\Delta}_{\mu,2}$, $\bar{\Delta}_{\mu,3}$, and $\bar{\Delta}_{\mu,4}$ contributions to the denominator D_μ, Eq. (96), are calculated as

$$\bar{\Delta}_{\mu,0} = [\overline{c}_0(\mu)]^* \, r_0(\mu), \tag{97}$$

$$\bar{\Delta}_{\mu,1} = \sum_{i,a} [\overline{c}^i_a(\mu)]^* \, \beta^i_a(\mu), \tag{98}$$

$$\bar{\Delta}_{\mu,2} = \sum_{i<j,a<b} [\overline{c}^{ij}_{ab}(\mu)]^* \, \beta^{ij}_{ab}(\mu), \tag{99}$$

$$\bar{\Delta}_{\mu,3} = \sum_{i<j<k,a<b<c} [\overline{c}^{ijk}_{abc}(\mu)]^* \, \beta^{ijk}_{abc}(\mu), \tag{100}$$

and

$$\bar{\Delta}_{\mu,4} = \sum_{i<j<k<l,a<b<c<d} [\overline{c}^{ijkl}_{abcd}(\mu)]^* \, \beta^{ijkl}_{abcd}(\mu), \tag{101}$$

where $\overline{c}_0(\mu)$, $\overline{c}^i_a(\mu)$, $\overline{c}^{ij}_{ab}(\mu)$, $\overline{c}^{ijk}_{abc}(\mu)$, and $\overline{c}^{ijkl}_{abcd}(\mu)$ are the CI coefficients obtained by rewriting the MRMBPT wavefunction $|\bar{\Psi}^{(\mathrm{MRMBPT})}_\mu\rangle$, Eq. (86), in the single-reference CI form of Eq. (87), and the coefficients $r_0(\mu)$,

$$\beta^i_a(\mu) = \langle \Phi^a_i | (R_{\mu,1} + R_{\mu,0} T_1) | \Phi \rangle, \tag{102}$$

$$\beta^{ij}_{ab}(\mu) = \langle \Phi^{ab}_{ij} | [R_{\mu,2} + R_{\mu,1} T_1 + R_{\mu,0}(T_2 + \tfrac{1}{2} T_1^2)] | \Phi \rangle, \tag{103}$$

$$\beta^{ijk}_{abc}(\mu) = \langle \Phi^{abc}_{ijk} | [R_{\mu,2} T_1 + R_{\mu,1}(T_2 + \tfrac{1}{2} T_1^2) + R_{\mu,0}(T_1 T_2 + \tfrac{1}{6} T_1^3)] | \Phi \rangle, \tag{104}$$

and

$$\begin{aligned} \beta^{ijkl}_{abcd}(\mu) = \langle \Phi^{abcd}_{ijkl} | [& R_{\mu,2}(T_2 + \tfrac{1}{2} T_1^2) + R_{\mu,1}(T_1 T_2 + \tfrac{1}{6} T_1^3) \\ & + R_{\mu,0}(\tfrac{1}{2} T_2^2 + \tfrac{1}{2} T_2 T_1^2 + \tfrac{1}{24} T_1^4)] | \Phi \rangle \end{aligned} \tag{105}$$

are the coefficients at the reference determinant $|\Phi\rangle$ and singly, doubly, triply, and quadruply excited determinants, $|\Phi_i^a\rangle$, $|\Phi_{ij}^{ab}\rangle$, $|\Phi_{ijk}^{abc}\rangle$, and $|\Phi_{ijkl}^{abcd}\rangle$, respectively, in the CI expansion of the CCSD/EOMCCSD wavefunction $R_\mu^{(\mathrm{CCSD})} e^{T^{(\mathrm{CCSD})}} |\Phi\rangle$, which can be easily determined using the CCSD/EOMCCSD cluster and excitation amplitudes t_a^i, t_{ab}^{ij}, $r_0(\mu)$, $r_a^i(\mu)$, and $r_{ab}^{ij}(\mu)$.

Although the summations over $i < j < k$, $a < b < c$ in Eqs. (93) and (100) and over $i < j < k < l$, $a < b < c < d$ in Eqs. (94) and (101) have the form of the complete summations over triples and quadruples, respectively, in reality the wavefunctions $|\bar{\Psi}_\mu^{(\mathrm{MRMBPT})}\rangle$, Eq. (86), contain only small subsets of all triples and quadruples, once we rewrite each $|\bar{\Psi}_\mu^{(\mathrm{MRMBPT})}\rangle$ in the form of the single-reference CI expansion, Eq. (87). This is a consequence of using active orbitals in designing the MRMBPT wavefunctions $|\bar{\Psi}_\mu^{(\mathrm{MRMBPT})}\rangle$, which limit the triple and quadruple excitations relative to the reference $|\Phi\rangle$ to a small class of triple and quadruple excitations that carry a certain number of active spin-orbital indices. Although the actual number of triples and quadruples in the $|\bar{\Psi}_\mu^{(\mathrm{MRMBPT})}\rangle$ wavefunctions depends on the dimension of the active space used in the MRMBPT calculations, one usually needs a small fraction of all triples and quadruples in the MMCC(2,3)/PT and MMCC(2,4)/PT considerations. As a result of using active orbitals in the MMCC(2,3)/PT and MMCC(2,4)/PT methods, we only need a small subset of all triexcited coefficients $\beta_{abc}^{ijk}(\mu)$, Eq. (104), and a similarly small subset of triply excited moments $\mathfrak{M}_{\mu,abc}^{ijk}(2)$, Eqs. (44) and (45), which match the nonzero coefficients $\overline{c}_{abc}^{ijk}(\mu)$, to calculate the MMCC(2,3)/PT energy, Eq. (93). Similarly, for the MMCC(2,4)/PT approach, one only needs a small subset of all quadruply excited coefficients $\beta_{abcd}^{ijkl}(\mu)$, Eq. (105), and a similarly small subset of all quadruply excited moments $\mathfrak{M}_{\mu,abcd}^{ijkl}(2)$, Eqs. (46) and (47), which match the nonzero coefficients $\overline{c}_{abcd}^{ijkl}(\mu)$, in the MMCC(2,4)/PT energy expression, Eq. (94).

One of the main advantages of the MRMBPT-corrected MMCC schemes, such as MMCC(2,3)/PT and MMCC(2,4)/PT, is their low computer cost, compared to the already relatively inexpensive CI-corrected MMCC methods described in Sect. 3.3.1. As in the case of the CI-corrected MMCC approaches, such as the MMCC(2,3)/CI and MMCC(2,4)/CI methods discussed in Sect. 3.3.1, in the MMCC(2,3)/PT and MMCC(2,4)/PT methods we have a good control of accuracy through active orbitals defining model space $\mathscr{M}_0$, which can always be adjusted to the excited states or the bond breaking problem of interest, but unlike in the MMCC/CI schemes, we do not have to solve the iterative CISDt and CISDtq equations to generate the wavefunctions $|\Psi_\mu^{(\mathrm{MRMBPT})}\rangle$ that enter the corrections $\delta_\mu(m_A, m_B)$ of the MRMBPT-corrected MMCC theories. We calculate the relevant CI-like coefficients, such as $\overline{c}_0(\mu)$, $\overline{c}_a^i(\mu)$, $\overline{c}_{ab}^{ij}(\mu)$, $\overline{c}_{abc}^{ijk}(\mu)$, and $\overline{c}_{abcd}^{ijkl}(\mu)$, by simply converting the expressions that define the MRMBPT wavefunctions $|\bar{\Psi}_\mu^{(\mathrm{MRMBPT})}\rangle$, Eq. (86), into the single-reference CI form defined by Eq. (87). Thus, the main computer effort of the MMCC(2,3)/PT approach goes into the calculations of a small subset of triexcited moments $\mathfrak{M}_{\mu,abc}^{ijk}(2)$, leading to the significant reduction of the

$n_o^3 n_u^4$ steps that are normally needed to calculate all moments $\mathfrak{M}^{ijk}_{\mu,abc}(2)$. Likewise, the main computer effort of the MMCC(2,4)/PT approach goes into the calculations of a small subset of quadruply excited moments $\mathfrak{M}^{ijkl}_{\mu,abcd}(2)$. In the efficient computer implementation, little effort is needed to determine the wavefunctions $|\bar{\Psi}^{(\mathrm{MRMBPT})}_{\mu}\rangle$ and the corresponding coefficients $\overline{c}_0(\mu)$, $\overline{c}^i_a(\mu)$, $\overline{c}^{ij}_{ab}(\mu)$, $\overline{c}^{ijk}_{abc}(\mu)$, and $\overline{c}^{ijkl}_{abcd}(\mu)$.

At this point, the remaining issue that we have to address before calculating the MMCC(2,3)/PT and MMCC(2,4)/PT energies is how to obtain the explicit algebraic expressions for the triply and quadruply excited moments $\mathfrak{M}^{ijk}_{\mu,abc}(2)$ and $\mathfrak{M}^{ijkl}_{\mu,abcd}(2)$. As in all CC/EOMCC considerations, the best way to handle these quantities is through the use of the diagrammatic methods of the many-body theory which are described in the subsequent section.

4.3 Diagrammatic Formulation and Factorization of the Triply and Quadruply Excited Moments of the CCSD and EOMCCSD Equations

In this section, the diagrammatic derivation of the explicit equations for the triply and quadruply excited moments of the CCSD/EOMCCSD equations, $\mathfrak{M}^{ijk}_{\mu,abc}(2)$ and $\mathfrak{M}^{ijkl}_{\mu,abcd}(2)$, respectively, is presented. The procedure of diagram factorization, which is deemed necessary to obtain highly efficient computer code, is discussed as well.

Historically, the use of diagrams originated in quantum field theory using the time-dependent formalism. However, as advocated by Čížek and Paldus already in the late 1960s and 1970s [11, 12, 261] (cf. [19, 23, 260] for additional remarks and further details), the time-independent formulation is sufficient in the development of quantum chemical and other many-body methods that rely on the time-independent Schrödinger equation. Diagrams are a graphical representation of Wick's theorem, which is a basic theorem for the algebraic manipulations involving operators in the second-quantized form. They carry information about interesting physics (e.g. connected vs. disconnected clusters), while providing powerful tool to derive and organize numerous algebraic expressions that almost any accurate many-body theory generates.

The entire discussion of diagrammatic methods used in this paper focuses on the time-independent formulation. It is important to note that the sequence in which the operators act (i.e., from right to left) is relevant; this is indicated in the diagram by means of a so-called formal time axis as shown below:

Thus, if we want to represent the operator product $V_N T_1$ diagrammatically, we begin with a diagrammatic representation of T_1 at the bottom, followed by a diagram representing the operator V_N drawn above the T_1 diagram. This bottom-top convention is the convention we will be using throughout this chapter (another common convention, which was pioneered by Čížek and Paldus, is to place the formal time axis for the operator ordering horizontally, from right to left, corresponding to the way we normally write a sequence of operators acting on a function; the only difference between the conventions used here and the convention introduced by Čížek and Paldus is the 90° rotation of the diagrams).

The general steps in deriving the explicit algebraic expressions for $\mathfrak{M}^{ijk}_{\mu,abc}(2)$ and $\mathfrak{M}^{ijkl}_{\mu,abcd}(2)$, Eqs. (44) and (46), in terms of the individual cluster and linear excitation amplitudes as well as one- and two-body integrals defining the Hamiltonian, include representing the formulas, as given by Eqs. (44) and (46), in a diagrammatic form, obtaining the so-called resulting diagrams by contractions of fermion lines representing the relevant creation and annihilation operators that enter the second-quantized forms of the operators, and applying the diagrammatic rules to convert the resulting diagrams back into algebraic language. Figure 2 shows the basic diagrams used to derive the equations for the generalized moments of the CCSD/EOMCCSD equations. A brief overview of the diagrammatic methods of many-body theory, describing the basic elements of the diagrammatic language used here, is presented in Appendix 1. The diagrammatic and algebraic structure of the one-, two-, three-, and four-body components of the CCSD similarity-transformed Hamiltonian $\bar{H}^{(\mathrm{CCSD})}$, which are the key elements for all CCSD-based methods, are shown in Appendix 2.

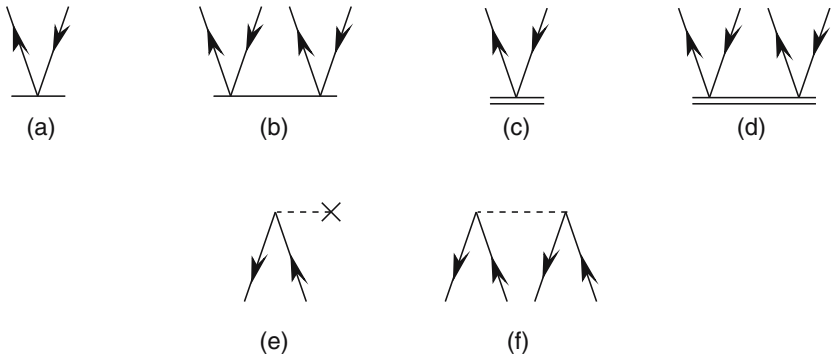

Fig. 2 Diagrammatic representation of (**a**) T_1 as defined by Eq. (6); (**b**) T_2 as defined by Eq. (7); (**c**) $R_{\mu,1}$ as defined by Eq. (20); (**d**) $R_{\mu,2}$ as defined by Eq. (21); (**e**) $F_N = f^p_q N[a^p a_q]$, and (**f**) $V_N = \frac{1}{4} v^{rs}_{pq} N[a^p a^q a_s a_r]$, where F_N and V_N are the one- and two-body components of the Hamiltonian in the normal-ordered form (H_N) and $N[\ldots]$ stands for the normal product of the operators. As shown in Appendix 1, the external fermion lines of F_N and V_N can point up or down. In (**e**) and (**f**), we show an example where they point down. The fermion lines in the cluster and excitation operators shown in (**a**)–(**d**) always point up

We use the Hugenholtz and the corresponding Brandow diagrams [260] to derive the explicit many-body expressions for all terms that correspond to the triply and quadruply excited moments of the CCSD/EOMCCSD equations, $\mathfrak{M}^{ijk}_{\mu,abc}(2)$ and $\mathfrak{M}^{ijk}_{\mu,abc}(2)$, respectively. Other representations, such as that of Goldstone, could be used as well, but Hugenholtz diagrams are best whenever we rely on the second-quantized operators using antisymmetrized matrix elements [260], as is the case here. There are several methods of obtaining all non-equivalent resulting diagrams. The usual approach, which is followed up here, is to first draw all of the elementary and then the resulting non-oriented Hugenholtz skeletons. The arrows are subsequently added to the resulting skeleton lines in all distinct ways to produce all of the distinct resulting diagrams. In the case of expressions for the generalized moments of CCSD equations, where we have to project $(H_N e^{T^{(\mathrm{CCSD})}})_C|\Phi\rangle$ on the excited determinants $|\Phi^{a_1\ldots a_n}_{i_1\ldots i_n}\rangle$, we do not draw the diagram representing the bra state $\langle\Phi^{a_1\ldots a_n}_{i_1\ldots i_n}|$. Instead, we draw all permissible resulting diagrams for $(H_N e^{T^{(\mathrm{CCSD})}})_C|\Phi\rangle$ with n incoming and n outgoing external fermion lines labeled by fixed indices $i_1,\ldots,i_n$ and $a_1,\ldots,a_n$, corresponding to the determinant $|\Phi^{a_1\ldots a_n}_{i_1\ldots i_n}\rangle$ on which we project [260]. Similar applies to moments of the EOMCCSD equations. This greatly facilitates the process of drawing the resulting diagrams and makes the resulting diagrams much less complicated [260].

The diagrams may be interpreted algebraically using the following rules [260, 261]:

a. Each upgoing external line is labeled with a "particle" (unoccupied) spin-orbital label *a, b, c, d, …* and each downgoing external line with a "hole" (i.e., occupied) spin-orbital label *i, j, k, l, …* . In the CC and EOMCC equations and diagrams representing the generalized moments of these equations, external lines should always be labeled in a canonical sequence defining the particle-hole excitations in the $|\Phi^{a_1\ldots a_n}_{i_1\ldots i_n}\rangle$ determinants on which we project, i.e., as *a,i* ; *b,j* ; *c,k* ; etc. The internal hole lines are labeled with *m, n, …*, whereas the internal particle lines are labeled with *e, f, …*.
b. The one-body vertex representing the one-body component $F_N = f^q_p N[a^p a_q]$ of H_N carries the numerical value of the Fock matrix element $\langle p|f|q\rangle = f^q_p$, where p is an outgoing line and q is an incoming line. For example,

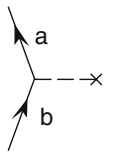

carries a value of matrix element f^b_a.
c. The two-body vertex representing the two-body component $V_N = \frac{1}{4} v^{rs}_{pq} N[a^p a^q a_s a_r]$ of H_N carries the numerical value of the antisymmetrized interaction matrix element $v^{rs}_{pq} = \langle pq|v|rs\rangle - \langle pq|v|sr\rangle$, where p and q are the outgoing lines and r and s are the incoming lines. For example,

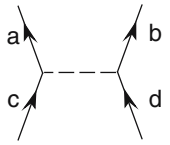

in a Brandow diagram carries a value of $v_{ab}^{cd} = \langle ab|v|cd\rangle - \langle ab|v|dc\rangle$. In general, $v_{pq}^{rs} = -v_{pq}^{sr} = -v_{qp}^{rs} = v_{qp}^{sr}$.

d. The one- and two-body vertices representing the T_1 and T_2 cluster operators and the linear excitation vertices representing $R_{\mu,1}$ and $R_{\mu,2}$, i.e.,

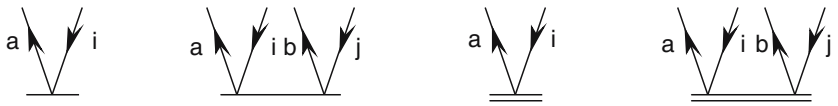

carry the numerical values of the t_a^i, t_{ab}^{ij}, $r_a^i(\mu)$, and $r_{ab}^{ij}(\mu)$ amplitudes, respectively. The two-body amplitudes are antisymmetric so that, for example, $t_{ab}^{ij} = -t_{ab}^{ji} = -t_{ba}^{ij} = t_{ba}^{ji}$ (similar applies to $r_{ab}^{ij}(\mu)$).

e. All the spin-orbital labels are summed over internal lines, which are obtained by contracting the external lines of F_N, V_N, T_1, T_2, $R_{\mu,1}$, and $R_{\mu,2}$.

f. The sign of the diagram is determined from $(-1)^{l+h}$, where l is the number of loops and h is the number of internal hole lines in a Brandow representation.

g. The combinatorial weight factor of the connected diagram is specified by $(\frac{1}{2})^m$, where m is the number of pairs of "equivalent" lines. A pair of equivalent lines is defined as being two lines beginning at the same vertex and ending at another, but also same vertex, and going in the same direction. This weight rule is specific to a Hugenholtz/Brandow representation used here, and lines that carry fixed labels (such as the external lines defining the $\langle \Phi_{i_1\ldots i_n}^{a_1\ldots a_n}|$ bra states on which we project in the CC/EOMCC equations and the generalized moments of these equations) are always regarded as non-equivalent.

h. The algebraic expression for each diagram should be preceded by a suitable complete or partial antisymmetrization operator, permuting the external lines in all distinct ways to keep the full antisymmetry of a final expression for a quantity, such as the moments $\mathfrak{M}_{\mu,a_1,\ldots,a_n}^{i_1,\ldots,i_n}(m_A)$, which are antisymmetric with respect to permutations of indices $i_1,\ldots,i_n$ and $a_1,\ldots,a_n$.

The procedure outlined above (cf., also, Appendix 1 for further details) can be greatly simplified if we realize that the generalized moments of CCSD/EOMCCSD equations, such as $\mathfrak{M}_{\mu,abc}^{ijk}(2)$ and $\mathfrak{M}_{\mu,abcd}^{ijkl}(2)$, are defined in terms of $\bar{H}^{(\mathrm{CCSD})}$. As shown in Appendix 2, various many-body components of $\bar{H}^{(\mathrm{CCSD})}$ contain several diagrams of the $(F_N e^{T_1+T_2})_C$ and $(V_N e^{T_1+T_2})_C$ types, which are part of more complex diagrams representing $\mathfrak{M}_{\mu,abc}^{ijk}(2)$ and $\mathfrak{M}_{\mu,abcd}^{ijkl}(2)$. By treating the many-body components of $\bar{H}^{(\mathrm{CCSD})}$ as more basic diagrams, which we represent by effective vertices with wavy lines, we can express moments $\mathfrak{M}_{\mu,abc}^{ijk}(2)$ and $\mathfrak{M}_{\mu,abcd}^{ijkl}(2)$ in terms of matrix elements $\bar{h}_p^q$, $\bar{h}_{pq}^{rs}$, $\bar{h}_{pqr}^{stu}$, etc. that define the one-body, two-body,

three-body, etc., components of $\bar{H}^{(\mathrm{CCSD})}$. In this way, instead of drawing large numbers of resulting diagrams corresponding to the original definitions of $\mathfrak{M}^{ijk}_{\mu,abc}(2)$ and $\mathfrak{M}^{ijkl}_{\mu,abcd}(2)$ in terms of F_N, V_N, T_1, T_2, $R_{\mu,1}$, and $R_{\mu,2}$, Eqs. (44)-(47), we can draw the relatively small number of diagrams in terms of the precomputed matrix elements of $\bar{H}^{(\mathrm{CCSD})}$, which serve as natural intermediates (cf. Appendix 2). All of the diagrams representing $\mathfrak{M}^{ijk}_{\mu,abc}(2)$, obtained in this way, are shown in Fig. 3. Note that all of the diagrams in Fig. 3 have six external lines corresponding to the projections of the triply excited determinant $|\Phi^{abc}_{ijk}\rangle$. The diagram

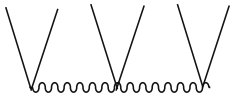

that shows up as the last term by Fig. 3 is the ground-state moment $\mathfrak{M}^{ijk}_{0,abc}(2)$ defined by Eq. (45). The fact that we can represent the entire ground-state moment $\mathfrak{M}^{ijk}_{0,abc}(2)$ in this compact way is a consequence of the fact that $\mathfrak{M}^{ijk}_{0,abc}(2)$ can be regarded as one of the three-body components of $\bar{H}^{(\mathrm{CCSD})}$; the complete set of diagrams corresponding to $\mathfrak{M}^{ijk}_{0,abc}(2)$ is shown in Fig. 24 in Appendix 2. The squared dot, $\boxdot$, at $\mathfrak{M}^{ijk}_{0,abc}(2)$ in Fig. 3 represents the constant $r_0(\mu)$.

For the quadruply excited moments $\mathfrak{M}^{ijkl}_{\mu,abcd}(2)$, Eq. (46), all of the resulting diagrams should have eight external lines extending to the top and corresponding to the projection onto the quadruply excited determinant $|\Phi^{abcd}_{ijkl}\rangle$. We can see this in Fig. 4, where all diagrams representing $\mathfrak{M}^{ijkl}_{\mu,abcd}(2)$ are presented. Again, in analogy to $\mathfrak{M}^{ijk}_{\mu,abc}(2)$, the diagram

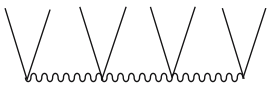

that shows up as the last term in Fig. 4 corresponds to the ground-state moment $\mathfrak{M}^{ijkl}_{0,abcd}(2)$ defined by Eq. (47), which can also be regarded as one of the four-body components of $\bar{H}^{(\mathrm{CCSD})}$; the complete set of diagrams corresponding to $\mathfrak{M}^{ijkl}_{0,abcd}(2)$ is shown in Fig. 25 in Appendix 2. Again, the squared dot, $\boxdot$, represents the coefficient $r_0(\mu)$. All of the diagrams that represent the two-, three-, and four-body components of $\bar{H}^{(\mathrm{CCSD})}$, which enter $\mathfrak{M}^{ijk}_{\mu,abc}(2)$ and $\mathfrak{M}^{ijkl}_{\mu,abcd}(2)$, including the ground-state triply and quadruply moments of the CCSD equations described above, are given in Appendix 2 (see Figs. 20–25). The diagrams representing the one-body components of $\bar{H}^{(\mathrm{CCSD})}$ do not show up in Figs. 3 and 4 directly, but do show up indirectly as intermediates when the diagram factorization discussed in Sect. 4.4, which leads to efficient computer codes, is fully carried out (see, also, Appendix 3).

Diagrams shown in Figs. 3 and 4, with two-, three-, and four-body components of $\bar{H}^{(\mathrm{CCSD})}$ represented diagrammatically in Figs. 20–25, provide correct algebraic expressions for moments $\mathfrak{M}^{ijk}_{\mu,abc}(2)$ and $\mathfrak{M}^{ijkl}_{\mu,abcd}(2)$, but these expressions, if coded

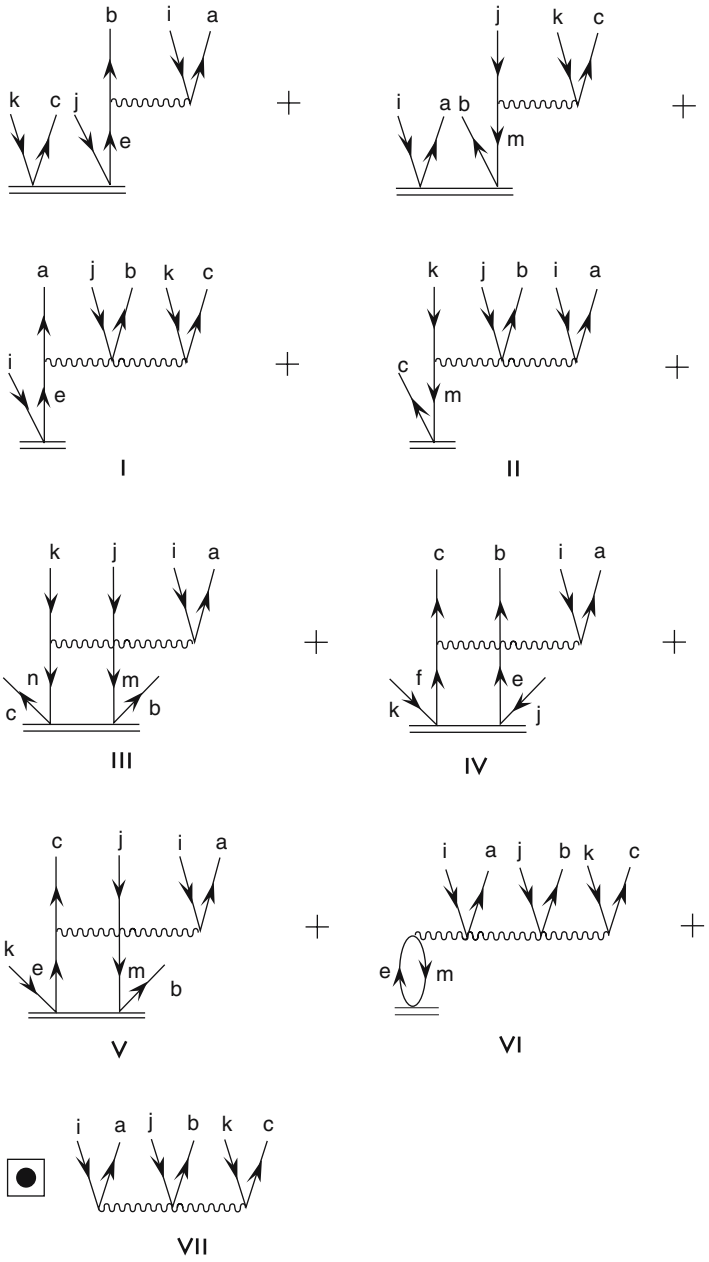

Fig. 3 Diagrammatic representation of $\mathfrak{M}^{ijk}_{\mu,abc}(2)$ using the Brandow forms of the relevant Hugenholtz diagrams. Vertices with wavy lines correspond to many-body components of $\bar{H}^{(\mathrm{CCSD})}$. $\boxdot$ in the last term represents $r_0(\mu)$

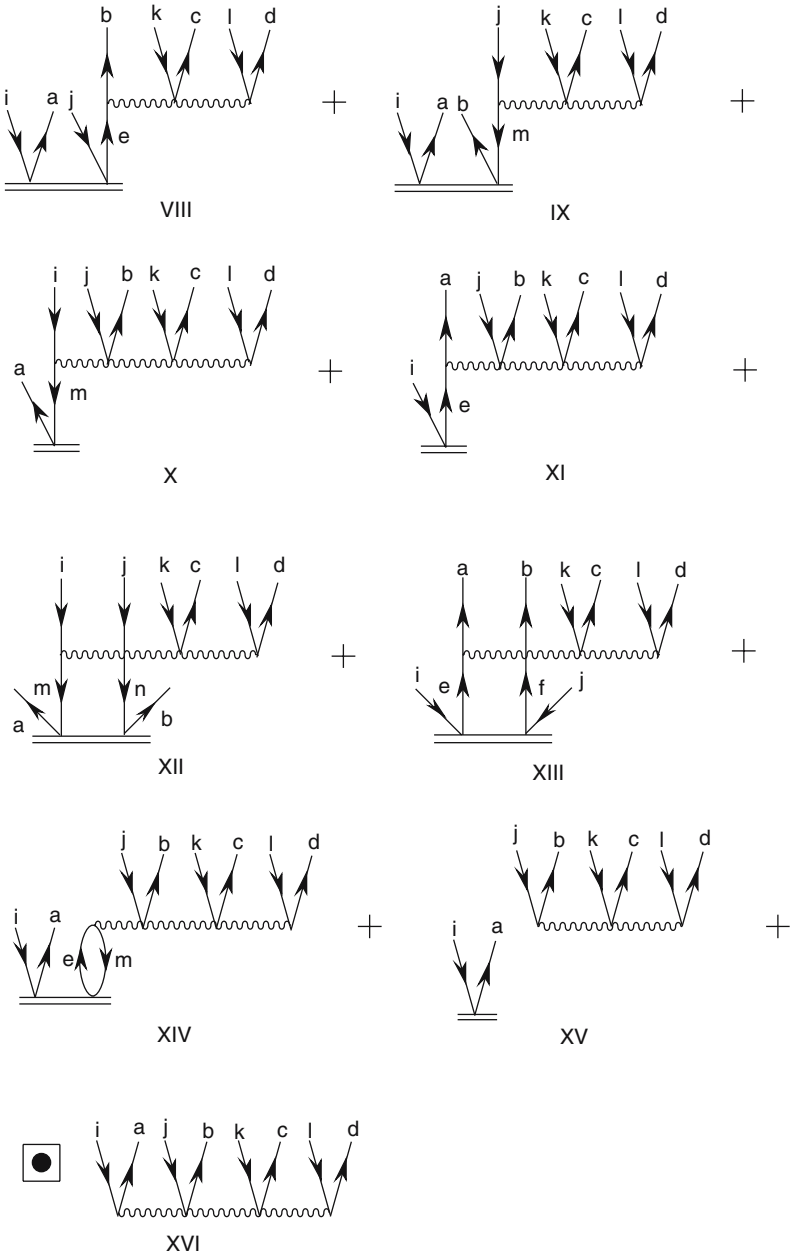

Fig. 4 Diagrammatic representation of $\mathfrak{M}^{ijkl}_{\mu,abcd}(2)$ using the Brandow forms of the relevant Hugenholtz diagrams. As in Fig. 3, vertices with wavy lines corresponds to many-body components of $\bar{H}^{(\mathrm{CCSD})}$ and $\boxdot$ represents $r_0(\mu)$

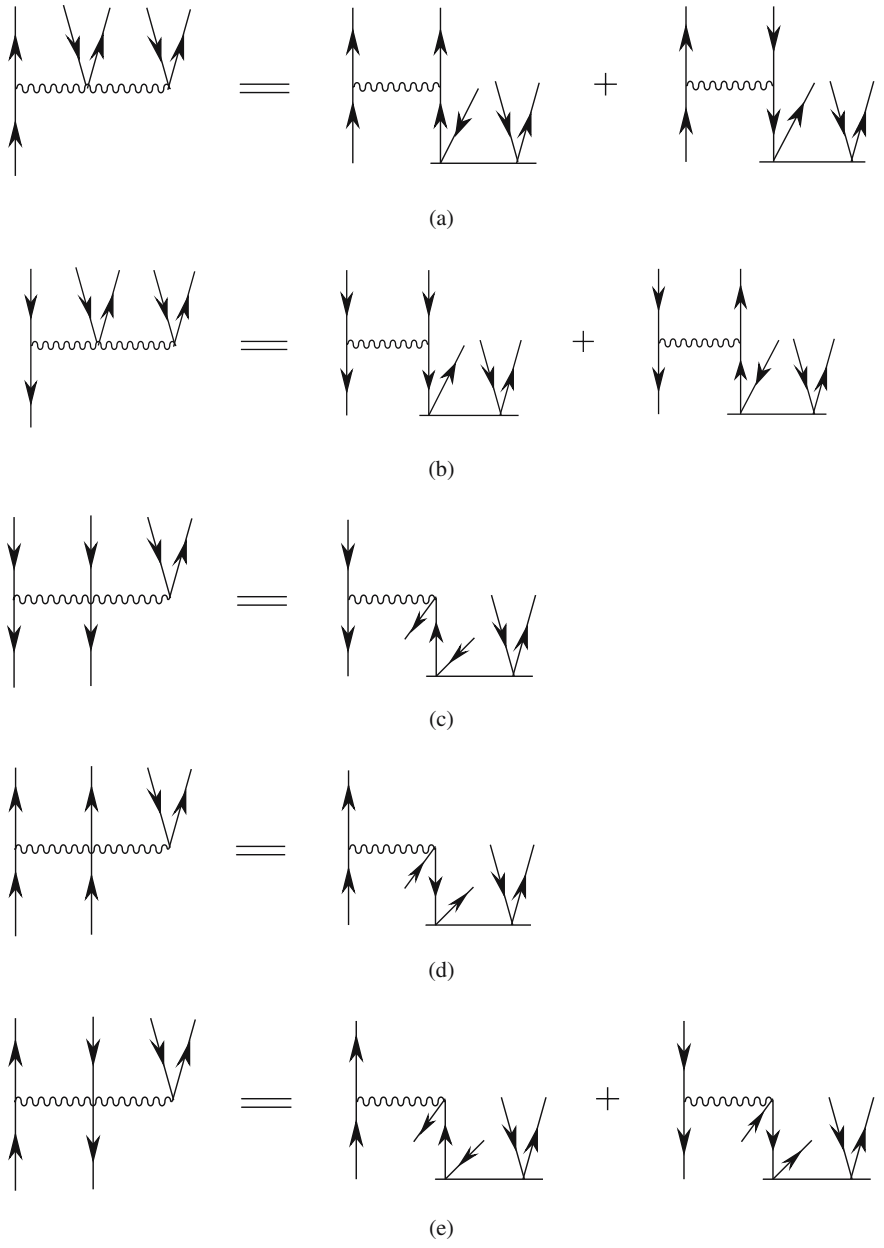

Fig. 5 Factorized forms of the three-body components of $\bar{H}^{(\mathrm{CCSD})}$ required in the derivation of $\mathfrak{M}^{ijk}_{\mu,abc}(2)$, expressed as products of two-body matrix elements of $\bar{H}^{(\mathrm{CCSD})}$ and T_2 cluster amplitudes

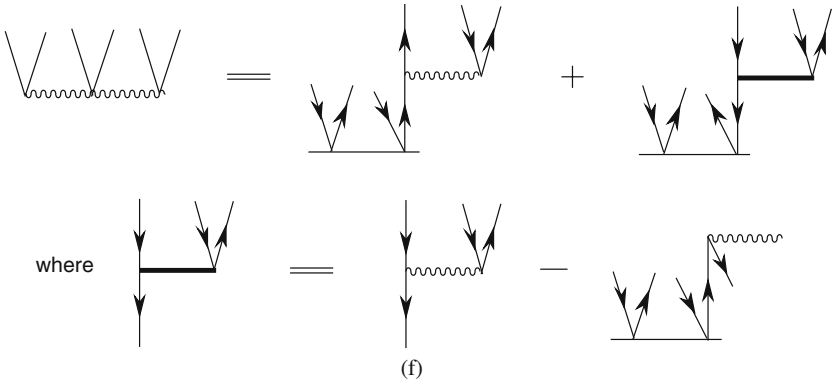

Fig. 5 (Continued)

term by term, do not yield efficient computer programs. In order to reduce the number of CPU operations that are required to calculate $\mathfrak{M}^{ijk}_{\mu,abc}(2)$ and $\mathfrak{M}^{ijkl}_{\mu,abcd}(2)$ in the most efficient manner, one has to factorize those $\mathfrak{M}^{ijk}_{\mu,abc}(2)$ and $\mathfrak{M}^{ijkl}_{\mu,abcd}(2)$ diagrams shown in Figs. 3 and 4 that relate $\mathfrak{M}^{ijk}_{\mu,abc}(2)$ and $\mathfrak{M}^{ijkl}_{\mu,abcd}(2)$ to the expensive three- and four-body components of $\bar{H}^{(\mathrm{CCSD})}$, shown in Figs. 20-25 in Appendix 2. The main ideas behind diagram factorization that lead to considerable reduction in the number of CPU operations characterizing the resulting many-body expressions are explained in Appendix 3. We illustrate the key steps that lead to the factorized, computationally efficient form of $\mathfrak{M}^{ijk}_{\mu,abc}(2)$ in Figs. 5–8.

In the initial step, shown in Fig. 5, we rewrite the expensive three-body matrix elements of $\bar{H}^{(\mathrm{CCSD})}$ that enter the $\mathfrak{M}^{ijk}_{\mu,abc}(2)$ diagrams shown in Fig. 3 (see diagrams I–V in Fig. 3) as tensor products of two-body matrix elements of $\bar{H}^{(\mathrm{CCSD})}$ and T_2 cluster amplitudes. We also rewrite diagram VI of Fig. 3, which uses a four-body component of $\bar{H}^{(\mathrm{CCSD})}$, in a more explicit form in terms of V_N, T_2, and $R_{\mu,1}$. As a result of these operations, the original diagrams shown in Fig. 3 acquire a new form shown in Fig. 6. The first two diagrams in Fig. 6 are in their final, computationally efficient, form. However, diagrams IA–VI are no longer linear in T or R_μ and represent multiple tensor products that need to be factorized further by bringing them to a linearized (vectorized) form and by reusing, as much as possible, the one- and two-body matrix elements of $\bar{H}^{(\mathrm{CCSD})}$, which are easy to generate. This is accomplished in Fig. 7 in three steps shown in Fig. 7 (a), (b), and (c), where we first factor out T_2 vertices (Fig. 7 (a) and (b)) and then group terms that have a similar overall structure to define the final set of intermediates linear in $R_{\mu,1}$ and $R_{\mu,2}$ and shown in Fig. 7 (c). As a result of all these operations, all of the diagrams in Figs. 3 or 6 acquire a compact, computationally, efficient form shown in Fig. 8.

A similar procedure can be performed for the original diagrams representing $\mathfrak{M}^{ijkl}_{\mu,abcd}(2)$ shown in Fig. 4. Again, by replacing the three-body matrix elements of $\bar{H}^{(\mathrm{CCSD})}$ that enter diagrams in Fig. 4 (diagrams VIII and IX) by their factorized

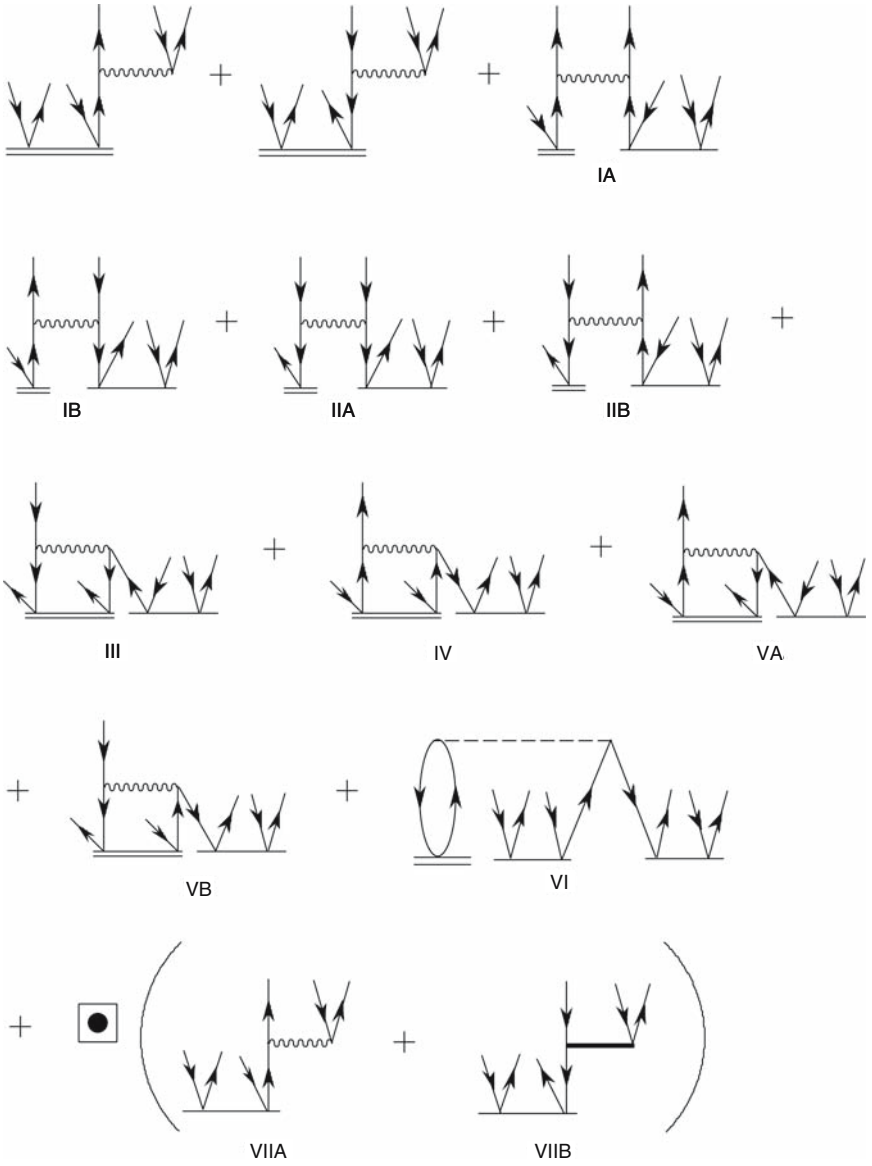

Fig. 6 Diagrammatic representation of $\mathfrak{M}^{ijk}_{\mu,abc}(2)$ obtained by substituting the three-body components of $\bar{H}^{(\mathrm{CCSD})}$ in Fig. 3 entering diagrams I–V by their factorized analogs shown in Fig. 5 and by expressing the four-body component of $\bar{H}^{(\mathrm{CCSD})}$ that defines diagram VI in terms of V_N, T_2, and $R_{\mu,1}$

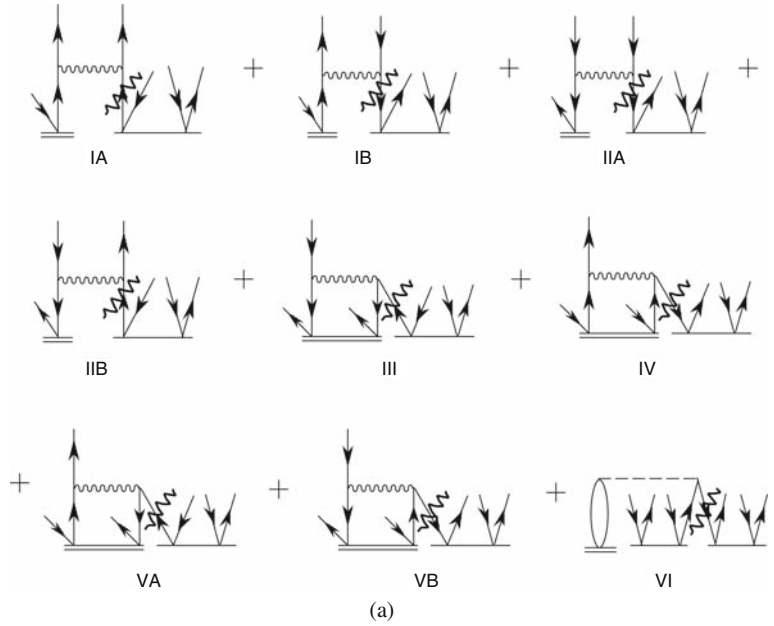

(a)

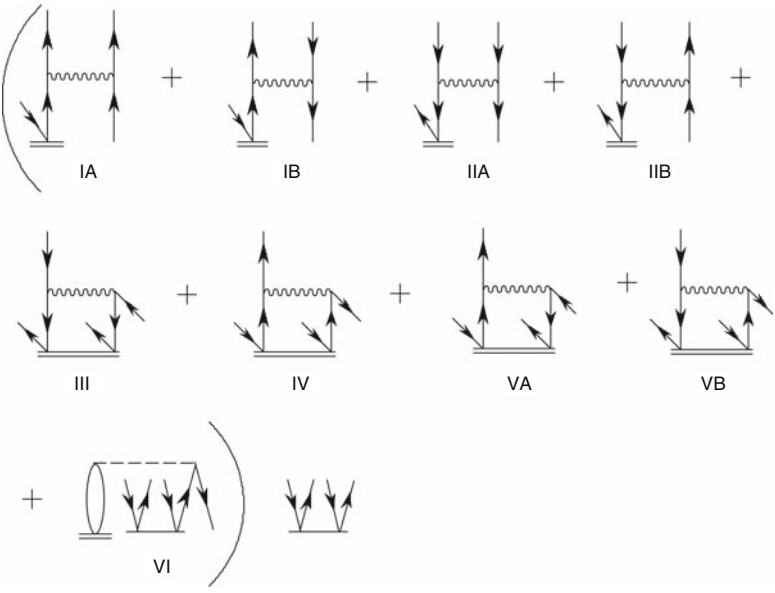

(b)

Fig. 7 Process of diagram factorization for the nonlinear terms in $\mathfrak{M}^{ijk}_{\mu,abc}(2)$ shown in Fig. 6 (diagrams IA–VI). (a) and (b) The T_2 vertex is factored out. (c) Diagrams in parentheses in (b) that have a similar structure are grouped together to define two intermediate vertices that are linear in $R_{\mu,1}$ and $R_{\mu,2}$

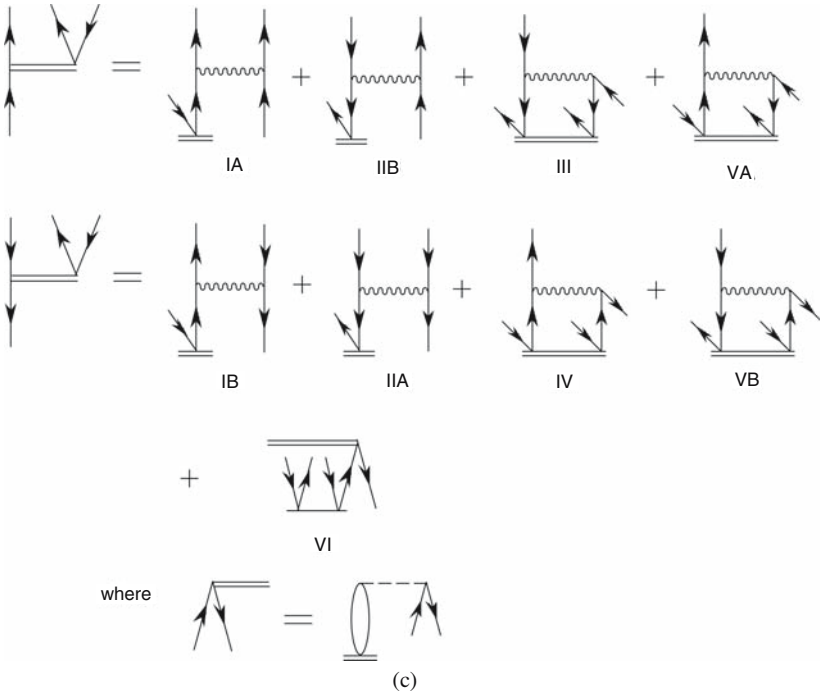

Fig. 7 (Continued)

analogs shown in Fig. 5 and by replacing the four-body $\bar{H}^{(\mathrm{CCSD})}$ vertices in the diagrams in Fig. 4 (diagrams X–XVI) by their factorized analogs shown in Fig. 9, we obtain the set of diagrams representing $\mathfrak{M}^{ijkl}_{\mu,abcd}(2)$ shown in Fig. 10. The factorization of diagrams that are non-linear in the T and R_μ components in Fig. 10 by factoring out common terms, grouping the diagrams that have a similar structure, and reusing recursively generated one- and two-body matrix elements of $\bar{H}^{(\mathrm{CCSD})}$ and other intermediates gives the final, computationally efficient and compact form of $\mathfrak{M}^{ijkl}_{\mu,abcd}(2)$ shown in Fig. 11.

Figures 8 and 11 show the most compact, fully factorized, diagrammatic forms of $\mathfrak{M}^{ijk}_{\mu,abc}(2)$ and $\mathfrak{M}^{ijkl}_{\mu,abcd}(2)$, that yield the highly efficient computer codes that are characterized by the $n_o^3 n_u^4$ steps in the $\mathfrak{M}^{ijk}_{\mu,abc}(2)$ case and $n_o^4 n_u^5$ steps in the $\mathfrak{M}^{ijkl}_{\mu,abcd}(2)$ case. Figures 12–14 show the diagrams representing all recursively generated intermediates that are needed to calculate $\mathfrak{M}^{ijk}_{\mu,abc}(2)$ and $\mathfrak{M}^{ijkl}_{\mu,abcd}(2)$ using diagrams shown in Figs. 8 and 11. The explicit algebraic expressions for the intermediates shown in Figs. 12–14 are given in Table 2. The final algebraic expressions for $\mathfrak{M}^{ijk}_{\mu,abc}(2)$ and $\mathfrak{M}^{ijkl}_{\mu,abcd}(2)$ used in this work and the remaining details of the computer implementation of the MMCC(2,3)/PT and MMCC(2,4)/PT methods are discussed next.

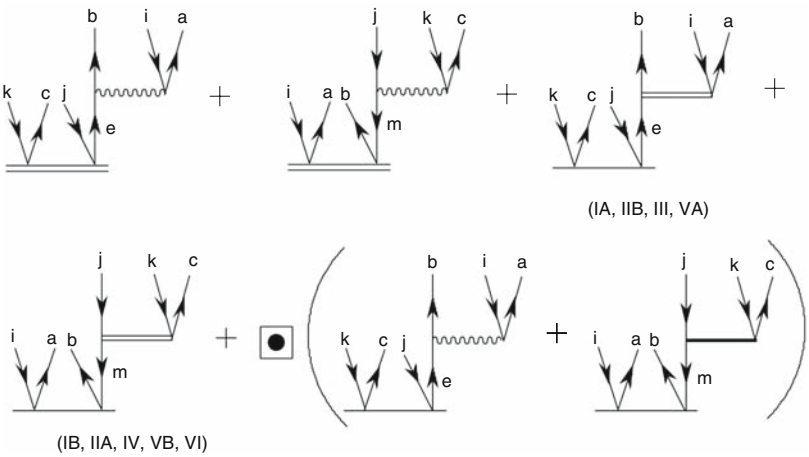

Fig. 8 Final factorized form of $\mathfrak{M}^{ijk}_{\mu,abc}(2)$. The two-body vertices marked with the thick single and thin double lines are defined in Figs. 5 (f) and 7 (c), respectively (cf., also, Fig. 13 (i), (j), and (k))

4.4 Final Equations for $\mathfrak{M}^{ijk}_{\mu,abc}(2)$ and $\mathfrak{M}^{ijkl}_{\mu,abcd}(2)$ and the Remaining Details of the Implementation of the MMCC(2,3)/PT and MMCC(2,4)/PT Approaches

The final, fully factorized expression for the triply excited moments of the CCSD/EOMCCSD equations $\mathfrak{M}^{ijk}_{\mu,abc}(2)$, in terms of the amplitudes defining the CCSD/EOMCCSD cluster and excitation operators, T_1, T_2, $R_{\mu,0}$, $R_{\mu,1}$, and $R_{\mu,2}$, and molecular integrals f^q_p and v^{rs}_{pq}, obtained from the diagrams shown in Fig. 8, which can be used in the highly efficient, vectorized, computer implementations of all MMCC(2,3) approximations, including the externally corrected MMCC(2,3) and MMCC(2,4) schemes, such as the MMCC(2,3)/PT and MMCC(2,4)/PT approaches pursued to this work, and their CI-corrected MMCC and renormalized CC/EOMCC analogs, can be given the following compact form:

$$\mathfrak{M}^{ijk}_{\mu,abc}(2) = \mathscr{A}_{abc}\,\mathfrak{T}^{ijk}_{\mu,abc}(2), \tag{106}$$

where

$$\begin{aligned}\mathfrak{T}^{ijk}_{\mu,abc}(2) = \mathscr{A}^{i/jk}\,[&(\tfrac{1}{2}\bar{h}^{ie}_{ab}r^{jk}_{ec} - \tfrac{1}{2}\bar{h}^{jk}_{mc}r^{im}_{ab} - \tfrac{1}{2}I^{jk}_{mc}t^{im}_{ab} + I^{ie}_{ab}t^{jk}_{ec}) \\ &+ \tfrac{1}{2}r_0(\mu)\,(\bar{h}^{ie}_{ab}t^{jk}_{ec} - I'^{jk}_{mc}t^{im}_{ab})\,].\end{aligned} \tag{107}$$

For simplicity, we dropped the symbol μ in the amplitudes $r^{jk}_{ec}(\mu)$, $r^{im}_{ab}(\mu)$, and $r_0(\mu)$ entering Eq. (107). The final, fully factorized and computationally highly efficient expression for the quadruply excited moments of the CCSD/EOMCCSD equations $\mathfrak{M}^{ijkl}_{\mu,abcd}(2)$, obtained from the diagrams shown in Fig. 11, can be written as

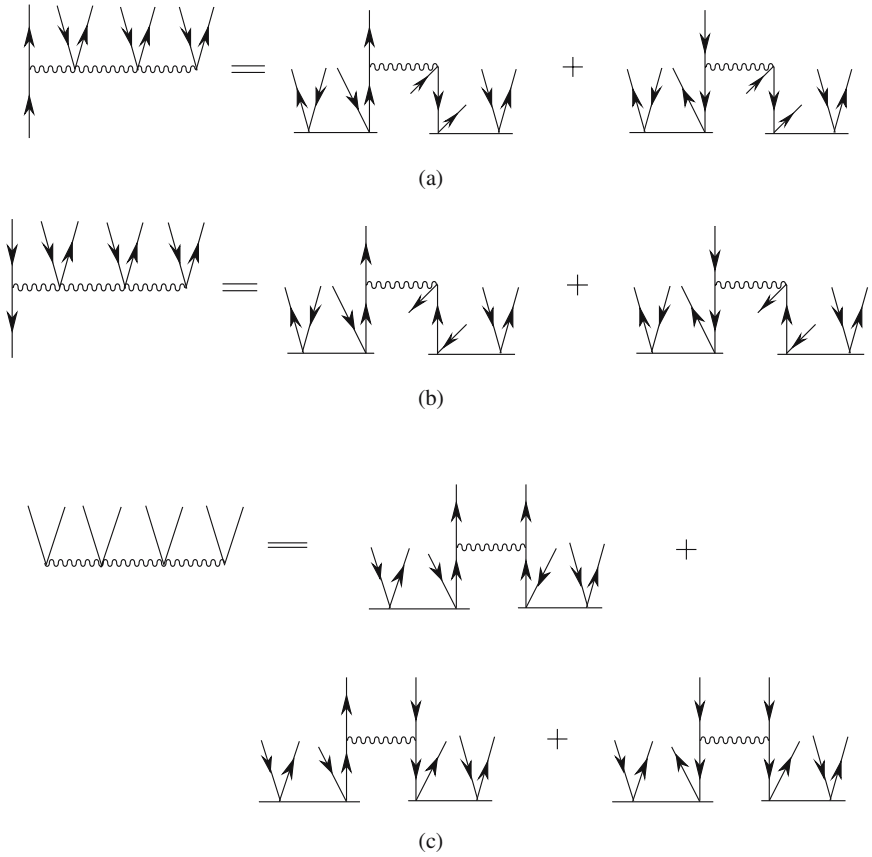

Fig. 9 Factorized forms of the four-body components of $\bar{H}^{(\mathrm{CCSD})}$ required in the derivation of $\mathfrak{M}^{ijkl}_{\mu,abcd}(2)$, expressed as products of two-body matrix elements of $\bar{H}^{(\mathrm{CCSD})}$ and T_2 cluster amplitudes

$$\mathfrak{M}^{ijkl}_{\mu,abcd}(2) = \mathscr{A}_{abcd}\,\mathfrak{T}^{ijkl}_{\mu,abcd}(2)\,, \tag{108}$$

where

$$\begin{aligned}\mathfrak{T}^{ijkl}_{\mu,abcd}(2) = {} & \mathscr{A}^{ij/kl}\,I'^{ijf}_{abc}\,t^{kl}_{fd} - \mathscr{A}^{ijk/l}\,I'^{ijk}_{abn}\,t^{nl}_{cd} + \tfrac{1}{6}\mathscr{A}^{ijk/l}\mathfrak{M}^{ijk}_{0,abc}(2)\,r^{l}_{d} \\ & + r_0(\mu)\,(\mathscr{A}^{ij/kl}\,I^{ijf}_{abc}\,t^{kl}_{fd} - \tfrac{1}{2}\mathscr{A}^{ijk/l}\,I^{ijk}_{abn}\,t^{nl}_{cd})\,,\end{aligned} \tag{109}$$

with $\mathfrak{M}^{ijk}_{0,abc}(2)$ representing the ground-state triexcited moments of the CCSD equations (see Table 2). The antisymmetrizers $\mathscr{A}_{pq}$, $\mathscr{A}_{pqr}$, $\mathscr{A}_{pq/r}$, $\mathscr{A}_{pqr/s}$, $\mathscr{A}_{pq/rs}$, $\mathscr{A}_{pq/r/s}$, and $\mathscr{A}_{pqrs}$, which enter Eqs. (106)–(109) directly or through the matrix elements of $\bar{H}^{(\mathrm{CCSD})}$, and other intermediates that are needed to construct Eqs. (107) and (109) and that are listed in Table 2, are defined in a usual way,

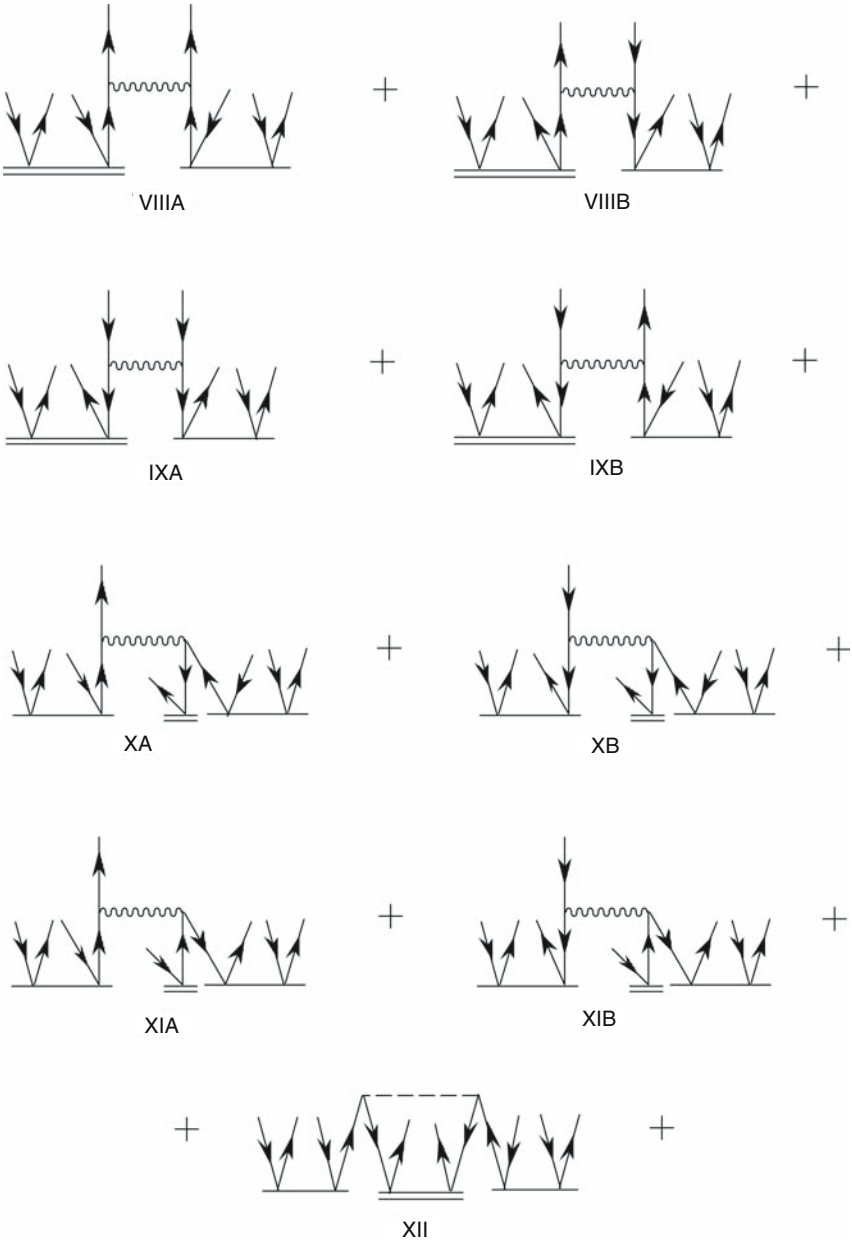

(a)

Fig. 10 Diagrammatic representation of $\mathfrak{M}^{ijkl}_{\mu,abcd}(2)$ obtained by substituting the three- and four-body components of $\bar{H}^{(\mathrm{CCSD})}$ in Fig. 4 by their factorized analogs shown in Figs. 5 and 9

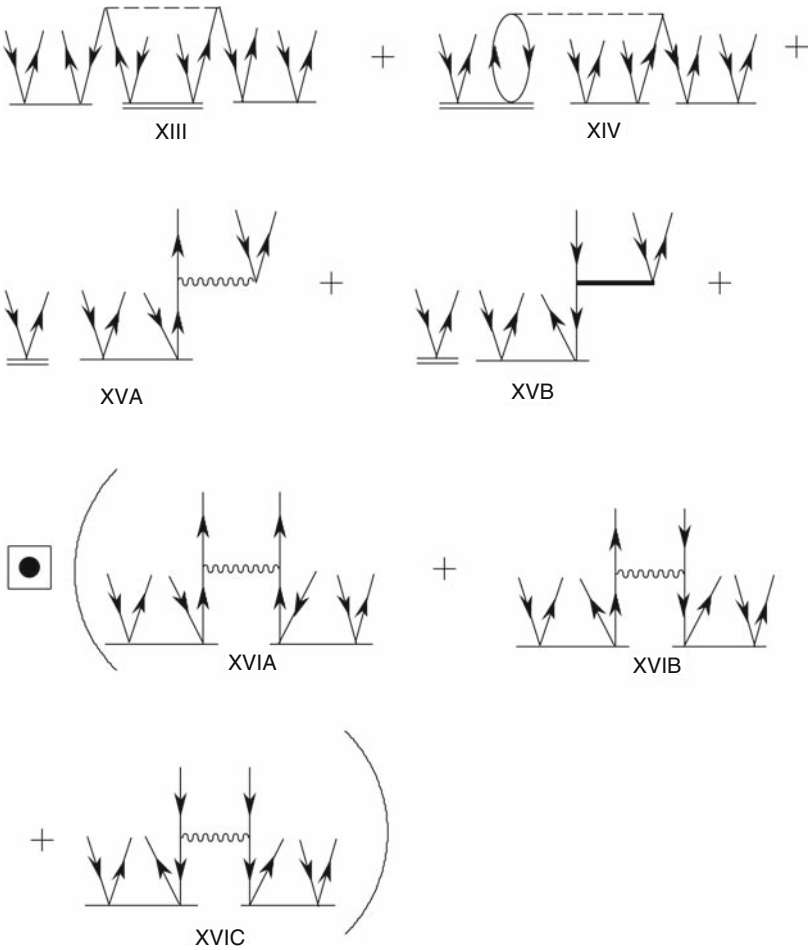

(b)

Fig. 10 (Continued)

$$\mathscr{A}_{pq} \equiv \mathscr{A}^{pq} = 1_{pq} - (pq), \tag{110}$$

$$\mathscr{A}_{pqr} \equiv \mathscr{A}^{pqr} = 1_{pqr} - (pq) - (pr) - (qr) + (pqr) + (prq), \tag{111}$$

$$\mathscr{A}_{p/qr} \equiv \mathscr{A}^{p/qr} \equiv \mathscr{A}_{qr/p} \equiv \mathscr{A}^{qr/p} = 1_{pqr} - (pq) - (pr), \tag{112}$$

$$\mathscr{A}_{pqr/s} \equiv \mathscr{A}^{pqr/s} \equiv \mathscr{A}_{s/pqr} \equiv \mathscr{A}^{s/pqr} = 1_{pqrs} - (ps) - (qs) - (rs), \tag{113}$$

$$\mathscr{A}_{pq/rs} \equiv \mathscr{A}^{pq/rs} = 1_{pqrs} - (pr) - (ps) - (qr) - (qs) + (pr)(qs), \tag{114}$$

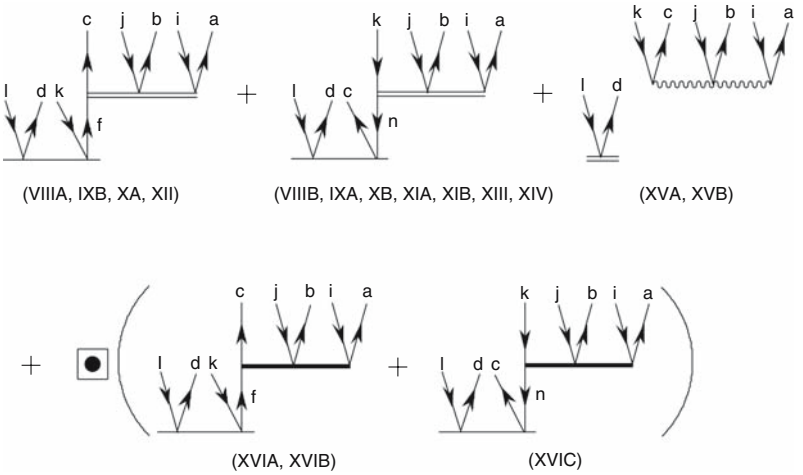

Fig. 11 Final factorized form of $\mathfrak{M}^{ijkl}_{\mu,abcd}(2)$. The three-body vertices marked with the thick single and thin double lines are defined in Fig. 14 (a), (b), (d), and (e). The thick line in the three-body intermediate entering diagram (XVIA,XVIB), which is shown in Fig. 14 (a), could be replaced by the wavy line, since the corresponding vertex represents the three-body matrix element of $\bar{H}^{(\mathrm{CCSD})}$, but since we do not use this intermediate in a conventional way and rearrange the associated numerical factors and antisymmetrizers in a non-traditional manner to obtain the computationally efficient Eqs. (108) and (109), we use the thick line and symbol I rather than $\bar{h}$ to represent this intermediate (cf. Eq. (109))

$$\begin{aligned}\mathscr{A}_{pq/r/s} &\equiv \mathscr{A}^{pq/r/s} \equiv \mathscr{A}_{r/pq/s} \equiv \mathscr{A}^{r/pq/s} \equiv \mathscr{A}_{r/s/pq} \equiv \mathscr{A}^{r/s/pq} \\ &= 1_{pqrs} - (pr) - (ps) - (qr) - (qs) + (pr)(qs) - (rs) \\ &\quad + (prs) + (psr) + (qrs) + (qsr) - (pqrs) \\ &= \mathscr{A}_{pq/rs}\mathscr{A}_{rs}, \end{aligned} \tag{115}$$

$$\begin{aligned}\mathscr{A}_{pqrs} \equiv \mathscr{A}^{pqrs} &= 1_{pqrs} - (pq) - (pr) - (ps) - (qr) - (qs) - (rs) + (qrs) \\ &\quad + (qsr) + (pqr) + (pqs) + (prq) + (prs) + (psq) \\ &\quad + (psr) + (pq)(rs) + (pr)(qs) + (ps)(qr) - (pqrs) \\ &\quad - (pqsr) - (prsq) - (prqs) - (psrq) - (psqr), \end{aligned} \tag{116}$$

with (pq), (pqr), and $(pqrs)$ representing the cyclic permutations of two, three, and four spin-orbital indices, respectively. As mentioned in the previous section, the explicit spin-orbital expressions for the one- and two-body matrix elements of $\bar{H}^{\mathrm{CCSD}}$, $\bar{h}^q_p$ and $\bar{h}^{rs}_{pq}$, respectively, and other recursively generated intermediates entering Eqs. (107) and (109), in terms of cluster amplitudes t^i_a and t^{ij}_{ab}, excitation amplitudes $r^i_a \equiv r^i_a(\mu)$ and $r^{ij}_{ab} \equiv r^{ij}_{ab}(\mu)$, and molecular integrals f^q_p and v^{rs}_{pq}, are given in Table 2.

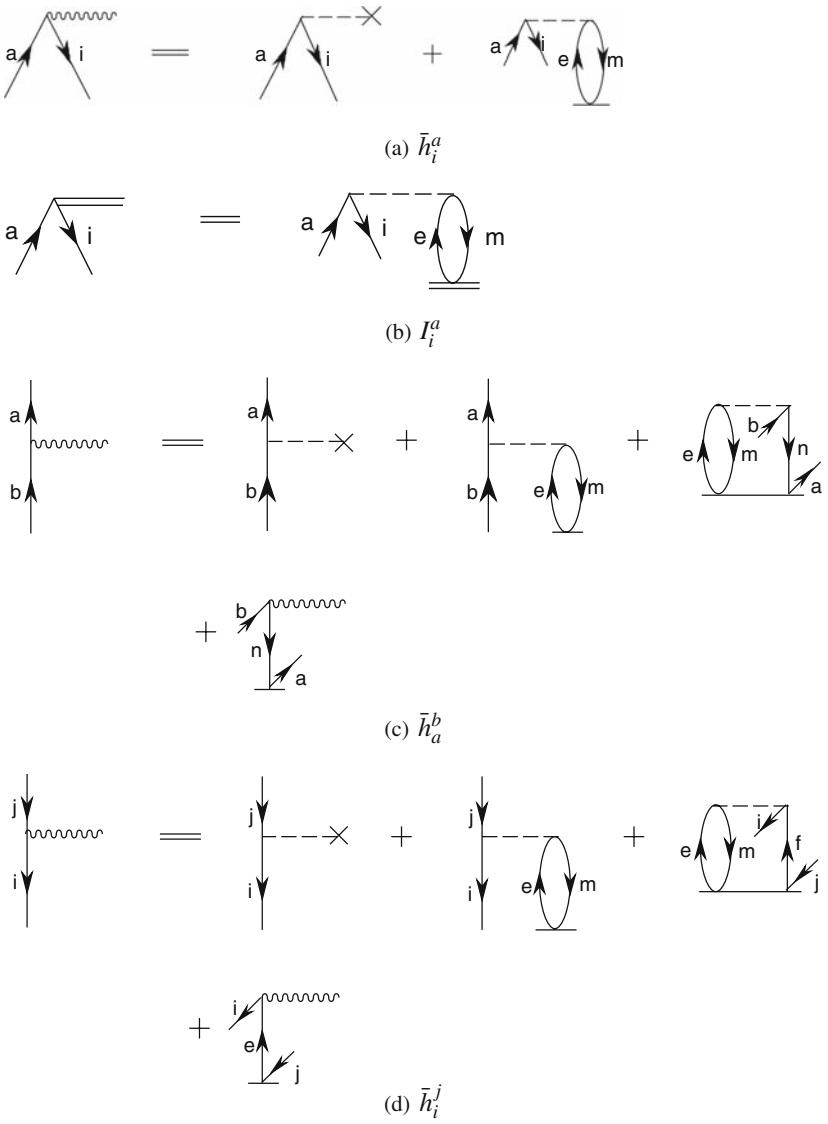

Fig. 12 One-body matrix elements of $\bar{H}^{(\mathrm{CCSD})}$ and other one-body intermediates needed to construct $\mathfrak{M}^{ijk}_{\mu,abc}(2)$ and $\mathfrak{M}^{ijkl}_{\mu,abcd}(2)$, Figs. 8 and 11, respectively

By using the idea of recursively generated intermediates and by reusing, as much as possible, the one and two-body matrix elements of $\bar{H}^{(\mathrm{CCSD})}$, which are generated in the CCSD/EOMCCSD calculations that precede the calculations of moments $\mathfrak{M}^{ijk}_{\mu,abc}(2)$ and $\mathfrak{M}^{ijkl}_{\mu,abcd}(2)$, we achieve a very high degree of code vectorization, while avoiding the explicit construction and storing of the most expensive three-

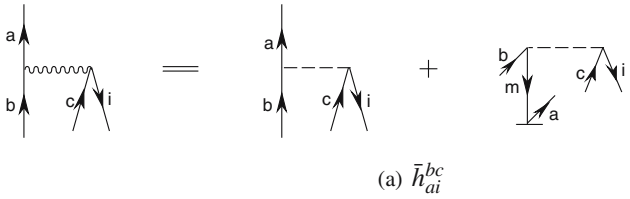

(a) $\bar{h}_{ai}^{bc}$

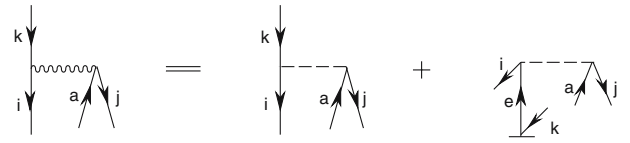

(b) $\bar{h}_{ij}^{ka}$

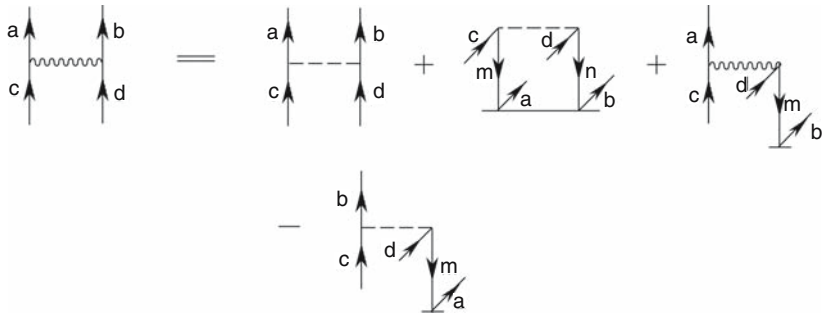

(c) $\bar{h}_{ab}^{cd}$

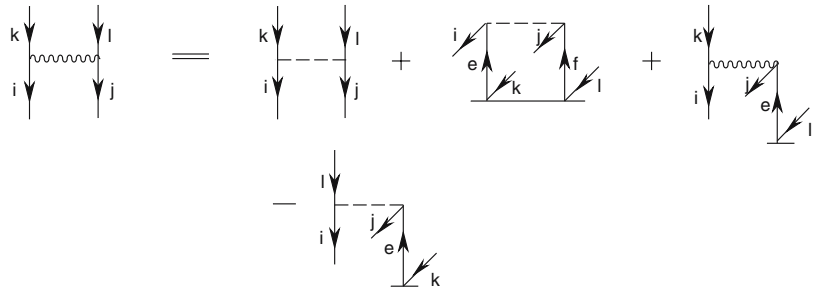

(d) $\bar{h}_{ij}^{kl}$

Fig. 13 Two-body matrix elements of $\bar{H}^{(\mathrm{CCSD})}$ and other two-body intermediates needed to construct $\mathfrak{M}^{ijk}_{\mu,abc}(2)$ and $\mathfrak{M}^{ijkl}_{\mu,abcd}(2)$, Figs. 8 and 11, respectively. The proper use of the intermediates other than two-body matrix elements of $\bar{H}^{(\mathrm{CCSD})}$, shown in (k)–(m), may require the incorporation of the additional numerical factors that cannot be read directly from diagrams (k)–(m). These additional numerical factors have been included in the algebraic expressions listed in Table 2

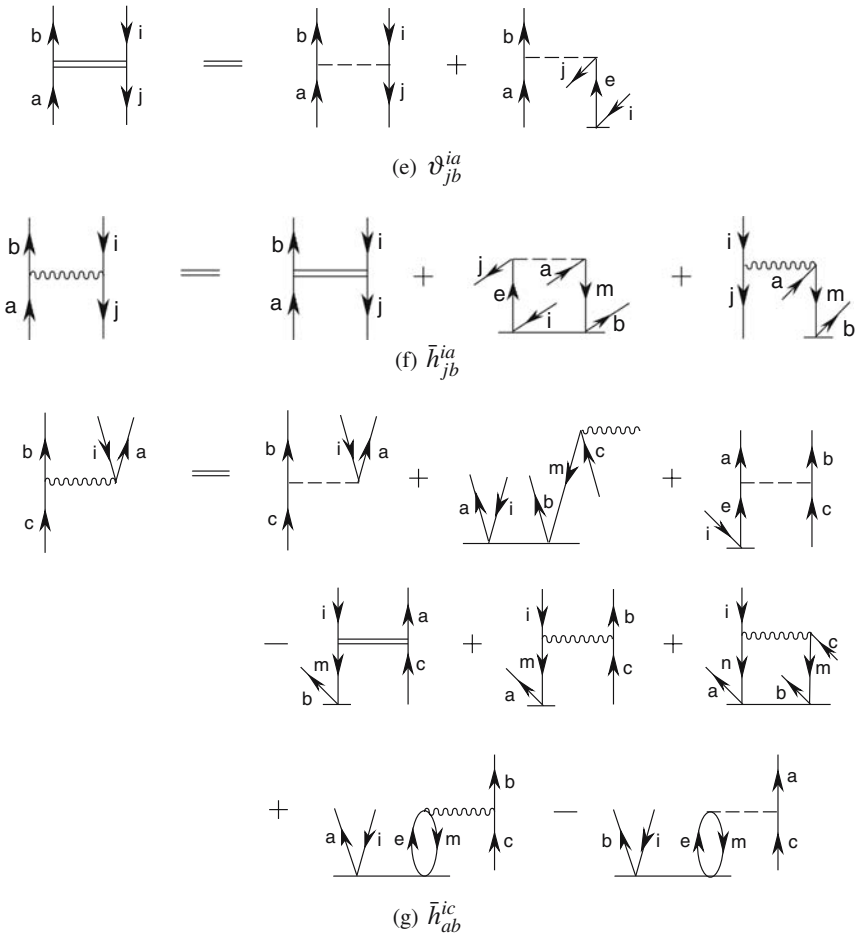

Fig. 13 (Continued)

and four-body matrix elements of $\bar{H}^{(\mathrm{CCSD})}$. Since the final factorized expressions defining $\mathfrak{M}^{ijk}_{\mu,abc}(2)$ and $\mathfrak{M}^{ijkl}_{\mu,abcd}(2)$, and the corresponding recursively generated intermediates are binary tensor (matrix) products, one can very effectively calculate $\mathfrak{M}^{ijk}_{\mu,abc}(2)$ and $\mathfrak{M}^{ijkl}_{\mu,abcd}(2)$ and the required intermediates with fast matrix multiplication routines available in the BLAS library.

Once the CCSD/EOMCCSD equations are solved for t^i_a, t^{ij}_{ab}, $r_0(\mu)$, $r^i_a(\mu)$ and $r^{ij}_{ab}(\mu)$, and the relevant moments $\mathfrak{M}^{ijk}_{\mu,abc}(2)$ and $\mathfrak{M}^{ijkl}_{\mu,abcd}(2)$ and the corresponding coefficients $\overline{c}^i_a(\mu)$, $\overline{c}^{ij}_{ab}(\mu)$, $\overline{c}^{ijk}_{abc}(\mu)$, $\overline{c}^{ijkl}_{abcd}(\mu)$, $\beta^i_a(\mu)$, $\beta^{ij}_{ab}(\mu)$, $\beta^{ijk}_{abc}(\mu)$, and $\beta^{ijkl}_{abcd}(\mu)$ are determined using Eqs. (106)-(109), the MRMBPT wavefunctions, $|\bar{\Psi}^{(\mathrm{MRMBPT})}_{\mu}\rangle$,

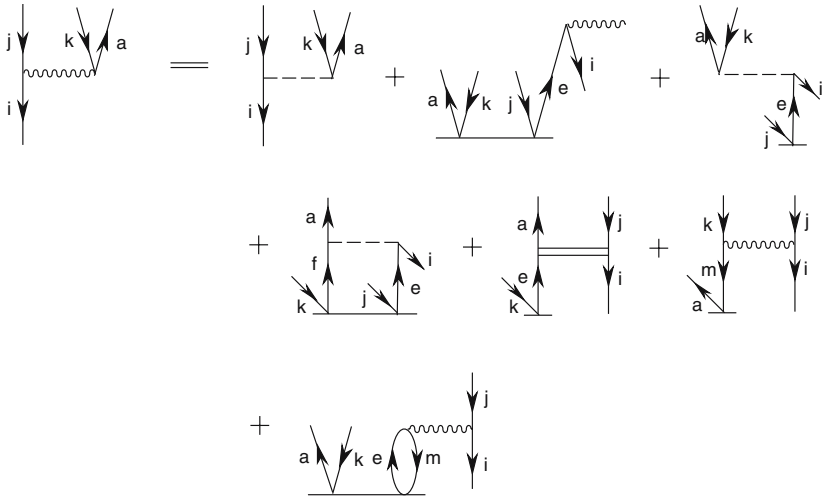

(h) $\bar{h}_{ia}^{jk}$

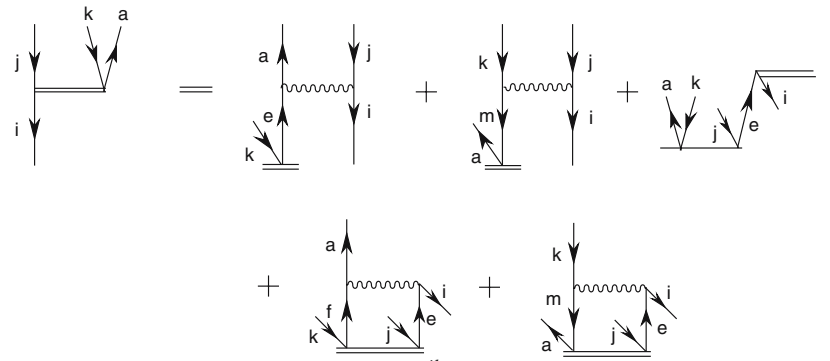

(i) I_{ia}^{jk}

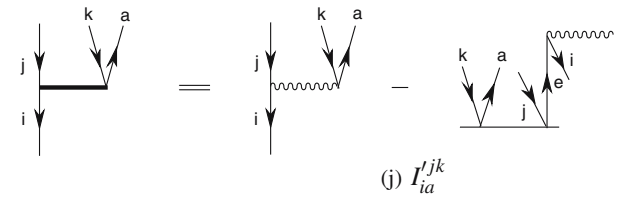

(j) I'^{jk}_{ia}

Fig. 13 (Continued)

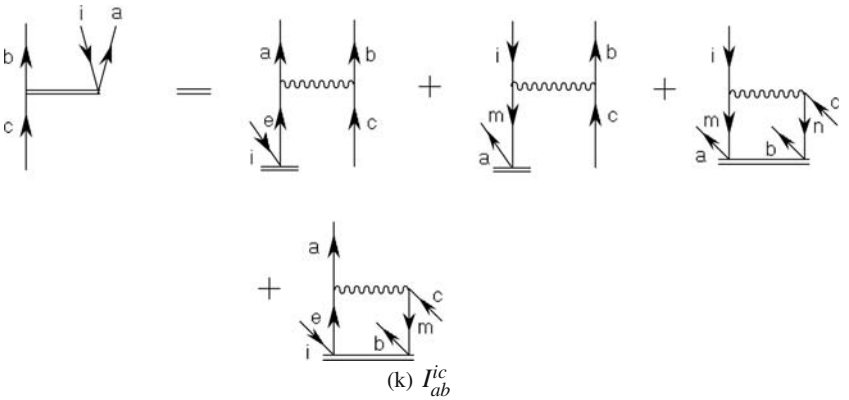

(k) I^{ic}_{ab}

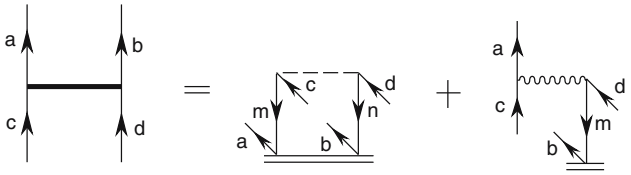

(l) I^{cd}_{ab}

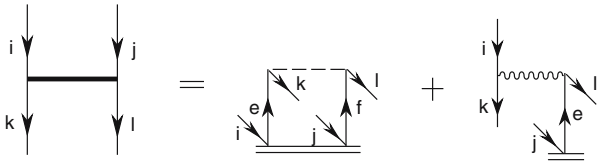

(m) I^{ij}_{kl}

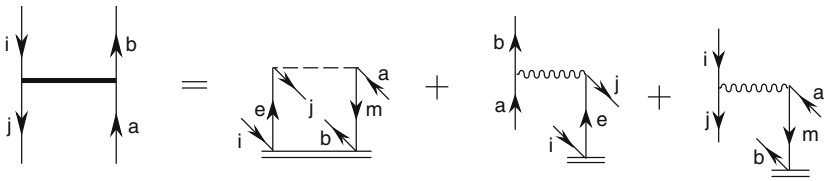

(n) I^{ia}_{jb}

Fig. 13 (Continued)

and Eqs. (102)-(105), we construct the overlap denominators D_μ, as in Eqs. (96)-(101), and, finally, the energy corrections due to triples or triples and quadruples defining the MMCC(2,3)/PT and MMCC(2,4)/PT methods, using Eqs. (93) and (94). Our MMCC(2,3)/PT and MMCC(2,4)/PT computer programs are interfaced with the RHF and integral transformation and sorting routines available in the GAMESS package [265].

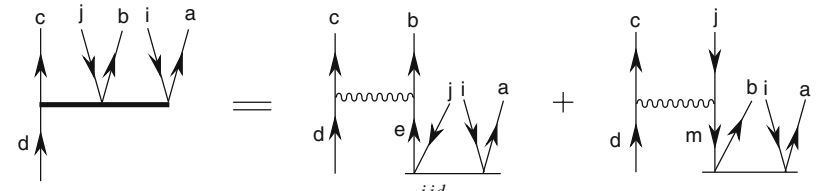

(a) I^{ijd}_{abc}

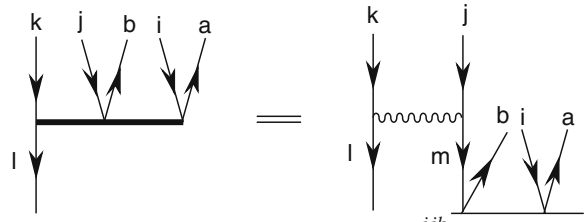

(b) I^{ijk}_{abl}

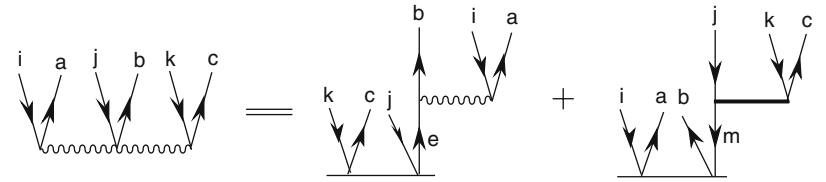

(c) $\mathfrak{M}^{ijk}_{0,abc}(2)$

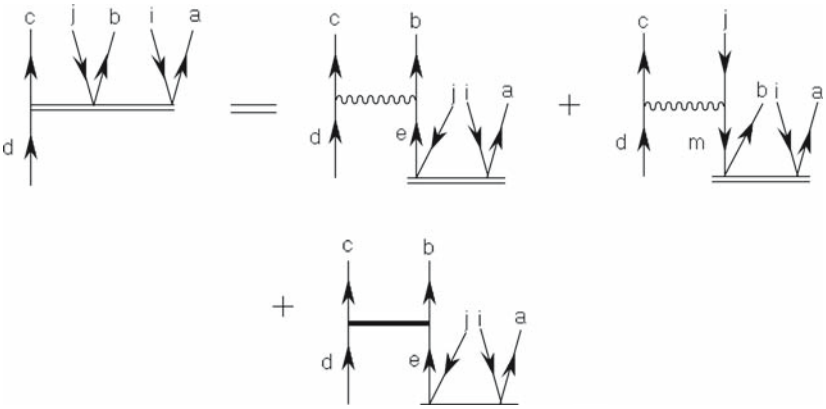

(d) I'^{ijd}_{abc}

Fig. 14 Three-body intermediates needed to construct $\mathfrak{M}^{ijkl}_{\mu,abcd}(2)$, Fig. 11. The three-body matrix element $\bar{h}^{ijk}_{abc} \equiv \mathfrak{M}^{ijk}_{0,abc}(2)$ shown in (c) also enters the definition of $\mathfrak{M}^{ijk}_{\mu,abc}(2)$, as in Eq. (44) (cf. the last two diagrams in Fig. 8). The proper use of these intermediates may require the incorporation of the additional numerical factors and/or a non-standard way of handling some antisymmetrizers to obtain the computationally efficient Eqs. (108) and (109), and expressions listed in Table 2

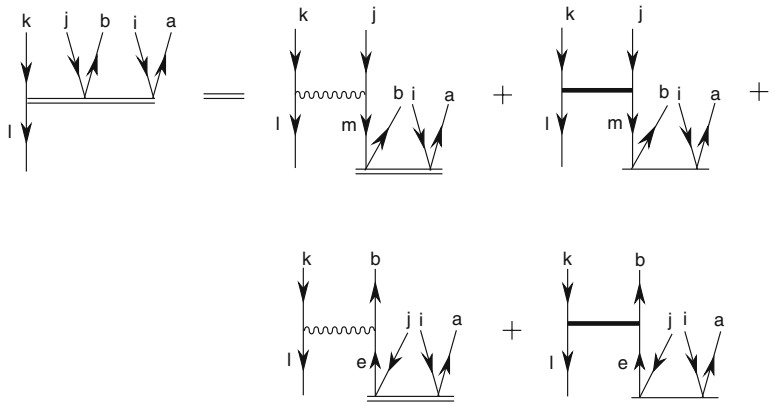

(e) I^{lijk}_{abl}

Fig. 14 (Continued)

5 Numerical Examples

We illustrate the performance of the MRMBPT-corrected MMCC approaches developed in this work by discussing the results of the benchmark MMCC(2,3)/PT and MMCC(2,4)/PT calculations for the single bond breaking in the HF and F_2 molecules, the simultaneous dissociation of both O–H bonds in the H_2O molecule, and the valence excited states of the CH^+ ion. We focus on a comparison of the MMCC(2,3)/PT and MMCC(2,4)/PT results with a few other ways of incorporating the triple and quadruple excitations in the CC and EOMCC formalisms, and the exact, full CI data, also obtained with GAMESS.

5.1 Bond Breaking in HF

In order to test the ability of the MRMBPT-corrected MMCC approaches to improve the poor description of bond breaking by the standard CCSD and CCSD(T) methods, we applied the MMCC(2,3)/PT approach to the potential energy curve of HF. We used a double zeta (DZ) basis set [266], for which the exact, full CI energies [36] and several other useful results, including, for example, the full CCSDT energies [36] and their standard and completely renormalized CCSD(T) analogs [40], are available. We also compare the MMCC(2,3)/PT results with the results of the CI-corrected MMCC(2,3) (MMCC(2,3)/CI) calculations [251], which provide yet another way of correcting the CCSD energies for the most essential effects due to triple excitations. We focus on the triples methods because generally the triply excited clusters along with the singly and doubly excited clusters are sufficient to obtain a virtually exact description of single bond breaking. In all calculations

Table 2 Explicit algebraic expressions for one- and two-body matrix elements of $\bar{H}^{\rm CCSD}$ (designated by $\bar{h}$) and other intermediates (designated by I or ϑ), shown in Figs. 12–14, used to construct the triply and quadruply excited moments of the CCSD/EOMCCSD equations, $\mathfrak{M}^{ijk}_{\mu,abc}(2)$ and $\mathfrak{M}^{ijkl}_{\mu,abcd}(2)$, respectively

	Expression[a]	*Figure*
$\bar{h}^a_i$	$f^a_i + t^m_e v^{ae}_{im}$	12 (a)
I^a_i	$r^m_e v^{ae}_{im}$	12 (b)
$\bar{h}^b_a$	$f^b_a + t^m_e v^{be}_{am} - \frac{1}{2} t^{mn}_{ea} v^{eb}_{mn} - t^n_a \bar{h}^b_n$	12 (c)
$\bar{h}^j_i$	$f^j_i + t^m_e v^{je}_{im} + \frac{1}{2} t^{mj}_{ef} v^{ef}_{mi} + t^j_e \bar{h}^e_i$	12 (d)
$\bar{h}^{bc}_{ai}$	$v^{bc}_{ai} - t^m_a v^{bc}_{mi}$	13 (a)
$\bar{h}^{ka}_{ij}$	$v^{ka}_{ij} + t^k_e v^{ea}_{ij}$	13 (b)
$\bar{h}^{cd}_{ab}$	$v^{cd}_{ab} + \frac{1}{2} t^{mn}_{ab} v^{cd}_{mn} - t^m_b \bar{h}^{cd}_{am} + t^m_a v^{cd}_{bm}$	13 (c)
$\bar{h}^{kl}_{ij}$	$v^{kl}_{ij} + \frac{1}{2} t^{kl}_{ef} v^{ef}_{ij} + t^l_e \bar{h}^{ke}_{ij} - t^k_e v^{le}_{ij}$	13 (d)
ϑ^{ia}_{jb}	$v^{ia}_{jb} + t^i_e v^{ea}_{jb}$	13 (e)
$\bar{h}^{ia}_{jb}$	$\vartheta^{ia}_{jb} - t^{im}_{eb} v^{ea}_{jm} - t^m_b \bar{h}^{ia}_{jm}$	13 (f)
$\bar{h}^{ic}_{ab}$	$v^{ic}_{ab} - t^{im}_{ab} \bar{h}^c_m + t^i_e v^{ec}_{ab} + t^m_b \vartheta^{ic}_{ma} - t^m_a \bar{h}^{ic}_{mb} + \frac{1}{2} t^{nm}_{ab} \bar{h}^{ic}_{nm} + t^{im}_{ae} \bar{h}^{ec}_{mb} - t^{mi}_{eb} v^{ce}_{am}$	13 (g)
$\bar{h}^{jk}_{ia}$	$v^{jk}_{ia} + t^{jk}_{ea} \bar{h}^e_i + t^j_e v^{ek}_{ia} + \frac{1}{2} t^{jk}_{ef} v^{ef}_{ia} + t^k_e \vartheta^{ej}_{ai} - t^m_a \bar{h}^{jk}_{im} + \mathscr{A}^{jk} t^{mk}_{ea} \bar{h}^{je}_{im}$	13 (h)
I^{jk}_{ia}	$\mathscr{A}^{jk} \bar{h}^{je}_{ia} r^k_e - \bar{h}^{jk}_{im} r^m_a + t^{jk}_{ea} I^e_i + \frac{1}{2} \bar{h}^{ef}_{ia} r^{jk}_{ef} - \mathscr{A}^{jk} \bar{h}^{ek}_{im} r^{jm}_{ea}$	13 (i)
I'^{jk}_{ia}	$\bar{h}^{jk}_{ia} - t^{jk}_{ea} \bar{h}^e_i$	13 (j)
I^{ic}_{ab}	$\frac{1}{2} \bar{h}^{ec}_{ab} r^i_e - \bar{h}^{ic}_{mb} r^m_a + \frac{1}{4} \bar{h}^{ic}_{mn} r^{mn}_{ab} - \bar{h}^{ec}_{am} r^{im}_{eb}$	13 (k)
I^{cd}_{ab}	$\frac{1}{4} v^{cd}_{mn} r^{mn}_{ab} - \bar{h}^{cd}_{am} r^m_b$	13 (l)
I^{ij}_{kl}	$\frac{1}{4} v^{ef}_{kl} r^{ij}_{ef} + \frac{1}{2} \mathscr{A}^{ij} \bar{h}^{ie}_{kl} r^j_e$	13 (m)
I^{ia}_{jb}	$-v^{ae}_{mj} r^{im}_{eb} + \bar{h}^{ae}_{bj} r^i_e - \bar{h}^{ia}_{jm} r^m_b$	13 (n)
I^{ijd}_{abc}	$\frac{1}{4} t^{ij}_{ae} \bar{h}^{ed}_{bc} - \frac{1}{2} \mathscr{A}^{ij} t^{im}_{ab} \bar{h}^{jd}_{mc}$	14 (a)
I^{ijk}_{abl}	$\frac{1}{2} \mathscr{A}^{i/jk} \bar{h}^{jk}_{ml} t^{im}_{ab}$	14 (b)
$\mathfrak{M}^{ijk}_{0,abc}(2)$	$\frac{1}{2} \mathscr{A}_{abc} \mathscr{A}^{i/jk} (\bar{h}^{ie}_{ab} t^{jk}_{ec} - I'^{jk}_{mc} t^{im}_{ab})$	14 (c)
I'^{ijd}_{abc}	$\frac{1}{2} \bar{h}^{ed}_{bc} r^{ij}_{ae} - \frac{1}{2} \mathscr{A}^{ij} \bar{h}^{jd}_{mc} r^{im}_{ab} + \frac{1}{2} t^{ij}_{ae} I^{ed}_{bc}$	14 (d)
I'^{ijk}_{abl}	$\mathscr{A}^{i/jk} (\frac{1}{2} \bar{h}^{jk}_{ml} r^{im}_{ab} - \frac{1}{2} I^{jk}_{ml} t^{im}_{ab}) + \mathscr{A}^{ij/k} (\bar{h}^{ek}_{bl} r^{ij}_{ae} + I^{ek}_{bl} t^{ij}_{ae})$	14 (e)

[a] Summation over repeated upper and lower indices is assumed; $f^q_p = \langle p|f|q\rangle$ and $v^{rs}_{pq} = \langle pq|v|rs\rangle - \langle pq|v|sr\rangle$ are the one- and two-electron integrals in a molecular spin-orbital basis $\{p\}$ corresponding to the Fock operator (f) and the two-body part of the Hamiltonian (v).

reported in this work, we used the ground-state RHF determinant as reference $|\Phi\rangle$. The active space employed in the CI- and MRMBPT-corrected MMCC calculations consisted of the three highest-energy occupied orbitals, 3σ, 1π, and 2π, and the lowest-energy unoccupied orbital 4σ that correlate with valence shells of the H and F atoms. This is a natural choice of active space for the description of bond breaking in HF, since for larger internuclear separations $R_{\text{H-F}}$ the ground-state full CI wavefunction of HF is dominated by the RHF configuration,

$$|\Phi\rangle = |(1\sigma)^2(2\sigma)^2(1\pi)^2(2\pi)^2(3\sigma)^2|, \tag{117}$$

the doubly excited configuration,

$$|\Phi'\rangle = |(1\sigma)^2(2\sigma)^2(1\pi)^2(2\pi)^2(4\sigma)^2|, \tag{118}$$

corresponding to the $(3\sigma)^2 \rightarrow (4\sigma)^2$ excitation, and the $(3\sigma) \rightarrow (4\sigma)$ singly excited configuration.

The results of our MMCC(2,3)/PT calculations for the potential energy curve of HF are shown in Table 3. In this particular case, there is a 1.634 millihartree difference between the CCSD and full CI energies at the equilibrium geometry, $R_{\text{H-F}} = R_e$, which increases to 12.291 millihartree at $R_{\text{H-F}} = 5R_e$ (for most practical purposes, $R_{\text{H-F}} = 5R_e$ can be regarded as a dissociation limit). As in other cases of single bond breaking, the large differences between the CCSD and full CI energies at larger values of $R_{\text{H-F}}$ are primarily caused by the absence of the connected T_3 clusters in the CCSD wavefunction. Indeed, the full CCSDT method, which includes T_3 clusters, reduces large errors in the CCSD results, relative to full CI, to as little as 0.173 millihartree at $R_{\text{H-F}} = R_e$ and 0.431 millihartree at $R_{\text{H-F}} = 5R_e$.

Table 3 A comparison of the CC and MMCC ground-state energies with the corresponding full CI results obtained for a few geometries of the HF molecule with a DZ basis set.The full CI total energies are given in hartree. The remaining energies are reported in millihartree relative to the corresponding full CI energy values. The non-parallelity errors (NPE), in millihartree, relative to the full CI results are given as well

Method	R_e [a]	$2R_e$	$3R_e$	$5R_e$	NPE
Full CI[b]	−100.160300	−100.021733	−99.985281	−99.983293	
CCSD	1.634	6.047	11.596	12.291	10.657
CCSDT[b]	0.173	0.855	0.957	0.431	0.784
CCSD(T)[c]	0.325	0.038	−24.480	−53.183	53.508
CR-CCSD(T)[c]	0.500	2.031	2.100	1.650	1.600
MMCC(2,3)/CI[d,e]	1.195	2.708	3.669	3.255	2.474
MMCC(2,3)/PT[e]	1.544	1.116	0.025	−0.889	2.433

[a] $R_e = 1.7328$ bohr is the equilibrium value of the internuclear H–F distance.
[b] From [36].
[c] From [40].
[d] From [251].
[e] The active space consisted of the 3σ, 1π, 2π, and 4σ orbitals.

The full CCSDT approach works, but, CCSDT is a rather impractical method. Unfortunately, the much more practical CCSD(T) approach completely fails at large internuclear separations $R_{\text{H-F}}$. Indeed, the small, 0.325 millihartree, error in the results of the CCSD(T) calculations at $R_{\text{H-F}} = R_e$ increases (in absolute value) to 24.480 millihartree at $R_{\text{H-F}} = 3R_e$ and 53.183 millihartree at $R_{\text{H-F}} = 5R_e$ (cf. Table 3). As shown, for example, in [36, 39, 40, 61, 62], the CCSD(T) potential energy curve lies significantly below the full CI curve at larger internuclear separations and is characterized by an unphysical hump in the region of intermediate $R_{\text{H-F}}$ values.

The CR-CCSD(T) approach, which is one of the "black-box" variants of the MMCC theory, considerably improves the results of the CCSD(T) calculations, eliminating the unphysical hump on the CCSD(T) curve and reducing the 53.183 millihartree error in the CCSD(T) results at $R_{\text{H-F}} = 5R_e$ to 1.650 millihartree [39, 40, 61, 62]. The errors in the CR-CCSD(T) energies, relative to full CI, do not exceed 2.1 millihartree over the entire range of $R_{\text{H-F}}$ values. The CI-corrected MMCC(2,3) approach, employing the 3σ, 1π, 2π, and 4σ orbitals as active orbitals, provides similar improvements [39, 61, 62, 251] (see Table 3).

As shown in Table 3, the MMCC(2,3)/PT calculations employing the same set of active orbitals, namely, the 3σ, 1π, 2π, and 4σ orbitals, used in the more expensive MMCC(2,3)/CI calculations reported, for example, in [251], provide the results which are better in the $R_{\text{H-F}} > R_e$ region than the already very good results of the CR-CCSD(T) and MMCC(2,3)/CI calculations. In particular, the MMCC(2,3)/PT approach reduces the large errors in the CCSD(T) results at $R_{\text{H-F}} = 3R_e$ and $R_{\text{H-F}} = 5R_e$ to small errors that do not exceed 1 millihartree. The signed errors in the MMCC(2,3)/PT results vary between 1.544 millihartree at $R_{\text{H-F}} = R_e$ and -0.889 millihartree at $R_{\text{H-F}} = 5R_e$. The overall qualities of the MMCC(2,3)/PT and MMCC(2,3)/CI results, as measured by the corresponding non-parallelity error (NPE) values, are quite similar (NPE is defined as the difference between the signed maximum and minimum errors along a potential energy curve). Indeed, the NPE values characterizing the MMCC(2,3)/PT and MMCC(2,3)/CI calculations are 2.433 and 2.474 millihartree, respectively. An obvious issue that may need further attention is the quality of the MMCC(2,3)/PT energy at $R_{\text{H-F}} = R_e$, which is only slightly better than that obtained with CCSD. This is related to the fact that we use the ground-state RHF orbitals and a small active space which is designed to describe the most essential non-dynamical correlation effects in the region of larger H–F distances. The suitable orbital optimization scheme would have to be developed to improve the results of the MMCC(2,3)/PT calculations at $R_{\text{H-F}} = R_e$. One possiblity could be to use CASSCF orbitals. Another possibility might be to utilize natural orbitals of CCSD. We plan to explore the issue of orbital optimization in the future work.

5.2 Bond Breaking in F_2

We now turn to the more challenging case of single bond breaking in F_2. The results for the F_2 molecule, as described by the cc-pVDZ basis set [267], are shown in

Table 4. Again, the ground-state RHF determinant was used as a reference. In the post-RHF calculations, the lowest two orbitals were kept frozen. The active space used in the MRMBPT-corrected MMCC calculation consisted of the five highest-energy occupied orbitals, $3\sigma_g, 1\pi_u, 2\pi_u, 1\pi_g$, and $2\pi_g$, as well as the lowest-energy unoccupied orbital, $3\sigma_u$. No CI-corrected MMCC and full CI calculations were performed for this system, so we rely on the full CCSDT energies, reported in [42], to assess the performance of the MMCC(2,3)/PT approach.

In this case, the CCSDT energies can serve as reference values, since it is well known that the full CCSDT approach provides an excellent description of a single σ-bond breaking (the previously discussed case of the HF molecule was an illustration of this statement). As one can see, the CCSD approach provides very poor results at all values of the F–F distance $R_{\text{F-F}}$, even at the equilibrium geometry R_e, where the difference between the CCSD and CCSDT energies is already 9.485 millihartree. The CCSD results become even worse for larger values of $R_{\text{F-F}}$. In fact, even the relatively small stretches of the F–F bond, such as $R_{\text{F-F}} = 1.5R_e$, lead to very large, $>$30 millihartree, errors in the CCSD energies relative to full CCSDT. The failure of the CCSD approach illustrates the important role played by the triply excited clusters in describing the F_2 molecule. The CCSD(T) method is very successful in describing the effects due to triply excited clusters at the equilibrium geometry, reducing the large error in the CCSD result relative to full CCSDT to 0.248 millihartree but, unfortunately, the CCSD(T) approach completely fails at larger F–F distances, where the unsigned errors in the CCSD(T) energies become as large as 39.348 millihartree at $R_{\text{F-F}} = 5R_e$.

The MRMBPT-corrected MMCC theory, explored in the present work, dramatically improves the CCSD and CCSD(T) results. As shown in Table 4, the MMCC(2,3)/PT method employing the small active space described above reduces the 9.485 millihartree error in the CCSD energy relative to CCSDT at $R_{\text{F-F}} = R_e$ to 3.725 millihartree. In contrast to CCSD(T), the MMCC(2,3)/PT method remains accurate in the bond breaking region. It is capable of producing the reasonably accurate results along the entire potential energy curve of F_2 from $R_{\text{F-F}} = 0.75R_e$ to $R_{\text{F-F}} = 5R_e$. The largest error relative to CCSDT characterizing the MMCC(2,3)/PT calculations along the whole curve is 5.618 millihartree. Errors on the order of 3–5 millihartree are, perhaps, not as small as one would like them to be, but the NPE value characterizing the MMCC(2,3)/PT energies (calculated relative to the full CCSDT results) is only 2.698 millihartree, demonstrating the ability of the relatively inexpensive MMCC(2,3)/PT approach to produce potential energy curves that accurately mimic the full CCSDT potential curve. The MMCC(2,3)/PT method seems to perform better in this regard than the CR-CCSD(T) approach, which works well at larger F-F separations but is characterized by a larger NPE value. Only the recently formulated size extensive version of CR-CCSD(T), termed CR-CC(2,3) (not discussed in this chapter), can lower the NPE value to less than 3 millihartree in calculations for F_2 [53–55].

Table 4 A comparison of various CC ground-state energies obtained for a few geometries of the F_2 molecule with a cc-pVDZ basis set. In all post-RHF calculations, the lowest two orbitals were kept frozen. The Cartesian components of d orbitals were used. The CCSDT total energies are given in hartree. The remaining energies are reported in millihartree relative to the corresponding CCSDT energies. The non-parallelity errors (NPE), in millihartree, relative to the full CCSDT results are given as well

Method	$0.75R_e$	R_e[a]	$1.25R_e$	$1.5R_e$	$1.75R_e$	$2R_e$	$3R_e$	$5R_e$	NPE
CCSDT [b]	−198.922138	−199.102796	−199.085272	−199.065882	−199.059433	−199.058201	−199.058511	−199.058586	
CCSD	4.504	9.485	19.917	32.424	41.184	45.638	49.425	49.816	45.312
CCSD(T)[b]	0.102	0.248	−0.503	−5.711	−15.133	−23.596	−35.700	−39.348	39.596
CR-CCSD(T)[b]	0.709	1.799	4.482	7.408	8.636	8.660	7.460	6.350	7.951
MMCC(2,3)/PT[c]	3.899	3.725	2.920	3.254	4.044	4.601	5.283	5.618	2.698

[a] $R_e = 2.66816$ bohr is the equilibrium value of the internuclear F–F distance.
[b] From [42].
[c] The active space included the $3\sigma_g$, $1\pi_u$, $2\pi_u$, $1\pi_g$, $2\pi_g$, and $3\sigma_u$ orbitals.

5.3 Double Dissociation in H_2O

5.3.1 The DZ Basis Set

Similar improvements in the relatively poor CCSD and CCSD(T) results are observed when the MMCC(2,3)/PT approach is applied to the simultaneous dissociation of both O–H bonds in H_2O. As explained in [37] (cf., also [251]), in this case a reasonable choice of active orbitals, which is needed to obtain a fairly uniform description of the equilibrium and bond breaking regions, is provided by the $1b_1$, $3a_1$, $1b_2$, $4a_1$, $2b_1$, and $2b_2$ orbitals. We used these orbitals to determine the MRMBPT-like wavefunctions that enter the MMCC/PT corrections to CCSD energies. Since double bond dissociations may be characterized by more significant quadruple effects, in addition to large effects due to triples, we also performed the MMCC(2,4)/PT calculations to explore the effects of quadruples. The simultaneous stretching or breaking of both O–H bonds in water provides us with an example of a situation where both T_3 and their T_4 counterparts are sizable and difficult to describe with the approximate CCSDT and CCSDTQ approaches.

As shown in Table 5, the MMCC(2,3)/PT method employing a small set of the $1b_1$, $3a_1$, $1b_2$, $4a_1$, $2b_1$, and $2b_2$ active orbitals reduces the 9.333 and 7.699 millihartree unsigned errors in the CCSD and CCSD(T) results at $R_{\text{O-H}} = 2R_e$ ($R_{\text{O-H}}$ is the O–H distance and R_e is the equilibrium value of $R_{\text{O-H}}$) to 0.335 millihartree. The overall description of the simultaneous stretching of both O–H bonds in H_2O by the MMCC(2,3)/PT approach, which produces the relatively small errors that do not exceed 2.2 millihartree in the entire $R_{\text{O-H}} = R_e - 2R_e$ region, is very good. The CR-CCSD(T) and MMCC(2,3)/CI methods (the active orbital space used in the MMCC(2,3)/CI calculations, which were originally reported in [251], was the same as that used in the present MMCC(2,3)/PT calculations) provide similar results. We also examined the effect of quadruples on the MMCC/PT results by considering higher-order MMCC corrections to CCSD energies employing the selected triples and quadruples contributions relative to the RHF determinant $|\Phi\rangle$ that originate from the low-order MRMBPT wavefunctions $|\bar{\Psi}_\mu^{(\text{MRMBPT})}\rangle$, Eq. (86). The MMCC(2,4)/PT method reduces the error in the MMCC(2,3)/PT result at $R_{\text{O-H}} = 1.5R_e$ further, from 2.174 to 0.380 millihartree. However, the MMCC(2,4)/PT overestimates the absolute value of the ground-state energy of the H_2O molecule at $R_{\text{O-H}} = 2R_e$ by 1.815 millihartree. We believe this is due to the simplified version of the MRMBPT theory used in this work. Clearly, it is encouraging to observe that the inexpensive MMCC calculations, in which the simple MRMBPT-like wavefunctions $|\bar{\Psi}_\mu^{(\text{MRMBPT})}\rangle$, Eq. (86), truncated at triple excitations relative to the RHF determinant $|\Phi\rangle$, are inserted into the MMCC(2,3) energy corrections, provide a much better overall description of the double bond breaking in H_2O than the standard CCSD and CCSD(T) approaches.

Table 5 A comparison of the CC and MMCC ground-state energies with the corresponding full CI results obtained for the equilibrium and two displaced geometries of the H_2O molecule with the DZ basis set. The full CI total energies are given in hartree. The remaining energies are reported in millihartree relative to the corresponding full CI energy values

Method	R_e [a]	$1.5R_e$ [b]	$2R_e$ [b]
Full CI	−76.157866[a]	−76.014521[b]	−75.905247[b]
CCSD	1.790	5.590	9.333
CCSDT[c]	0.434	1.473	−2.211
CCSD(T)[d]	0.574	1.465	−7.699
CR-CCSD(T)[d]	0.738	2.534	1.830
MMCC(2,3)/CI[e,f]	0.811	2.407	1.631
MMCC(2,3)/PT[f]	1.265	2.174	0.335
CCSDTQ[g]	0.015	0.141	0.108
CCSD(TQ_f)[d]	0.166	0.094	−5.914
CR-CCSD(TQ),a[d,h]	0.195	0.905	1.461
CR-CCSD(TQ),b[i]	0.195	0.836	2.853
MMCC(2,4)/CI[e,f]	0.501	0.942	2.416
MMCC(2,4)/PT[f]	1.069	0.380	−1.815

[a] The equilibrium geometry and full CI result from [268].
[b] The geometry and full CI result from [269].
[c] From [27].
[d] From [40].
[e] From [251].
[f] The active space consisted of the $1b_1$, $3a_1$, $1b_2$, $4a_1$, $2b_1$, and $2b_2$ orbitals.
[g] From [30].
[h] The "a" variant of the completely renormalized CCSD(TQ) method. The results are from [61].
[i] The "b" variant of the completely renormalized CCSD(TQ) method. The results are from [61].

5.3.2 The cc-pVDZ Basis Set

To explore the effect of a basis set and to examine the performance of the MRMBPT-corrected MMCC theory in a somewhat more complete scan of the potential energy surface of the doubly dissociating H_2O molecule, we tested our methods on the H_2O system as described by the cc-pVDZ basis set.

Though the CCSDT method provides an excellent description of the equilibrium region, producing an error relative to full CI of only 0.493 millihartree at $R_{O\text{-}H} = R_e$, it fails at larger O–H separations ($R_{O\text{-}H} > 2R_e$), where the errors in the CCSDT energies grow up to 40.126 millihartree at $R_{O\text{-}H} = 3R_e$. These results show that even the full inclusion of T_3 clusters is not sufficient to guarantee the proper description of the double dissociation of water if we go to very large stretches of both O–H bonds. As both O–H bonds in H_2O are simultaneously stretched, the effects of triples as well as quadruples (T_4 clusters) become very important due to a significant increase of a multi-reference character of the ground-state electronic

Table 6 A comparison of various CC ground-state energies obtained for the H_2O molecule, as described by the cc-pVDZ basis set, at the equilibrium geometry and several non-equilibrium geometries obtained by stretching both O–H bonds, while keeping the H–O–H angle fixed. The spherical components of the d orbitals were used. In all post-RHF calculations, all electrons were correlated. The full CI total energies are given in hartree. The remaining energies are reported in millihartree relative to the corresponding full CI energies

Method	R_e[a]	$1.5R_e$	$2R_e$	$2.5R_e$	$3R_e$
Full CI[b]	−76.241860	−76.072348	−75.951665	−75.917991	−75.911946
CCSD	3.744	10.043	22.032	20.307	10.849
CCSDT[b]	0.493	1.423	−1.405	−24.752	−40.126
CCSD(T)[b]	0.658	1.631	−3.820	−42.564	−90.512
CR-CCSD(T)[c]	1.025	3.355	7.252	−2.270	−15.040
MMCC(2,3)/PT[d]	2.780	3.329	4.251	−7.607	−21.456

[a] The equilibrium value of the O–H distance R_e equals 1.84345 bohr and the H-O-H bond angle is fixed at 110.6°. For further details of the equilibrium and non-equilibrium geometries used in this work, see [270].
[b] From [270].
[c] From [49].
[d] The active space consisted of the $1b_1$, $1b_2$, $3a_1$, $4a_1$, $2b_2$, $5a_1$, and $3b_2$ orbitals.

wavefunction. The MMCC(2,3)/PT approach provides a very good description of the double dissociation of H_2O up to $R_{\text{O-H}} = 2R_e$, reducing the 10.043 and 22.032 millihartree errors in the CCSD results at $R_{\text{O-H}} = 1.5R_e$ and $R_{\text{O-H}} = 2R_e$, respectively, to 3.329 and 4.251 millihartree. The errors in the MMCC(2,3)/PT results increase as we enter the $R_{\text{O-H}} > 2R_e$ region, where quadruples (neglected in the MMCC(2,3)/PT calculations) become important, but it is more interesting to compare the errors relative to full CI produced by the MMCC(2,3)/PT approach with the errors produced by the full CCSDT method. As one can see in Table 6, the use of the MRMBPT-like wavefunction in determining the ground-state triples correction $\delta_0(2,3)$ of the MMCC(2,3)/PT approach seems to reduce the degree of the failure of the CCSDT method in the $R_{\text{O-H}} > 2R_e$ region. We plan to perform the MMCC(2,4)/PT calculations in the future.

5.4 Excited States of $\mathbf{CH^+}$

One of the main advantages of the MMCC/PT formalism is that we can study ground and excited states. In principle, for a given M-dimensional model space $\mathscr{M}_0$, we can calculate up to M different MRMBPT wavefunctions $|\bar{\Psi}_\mu^{(\text{MRMBPT})}\rangle$, Eqs. (86) or (87), which represent the approximate forms of ground and excited states $|\Psi_\mu\rangle$ that enter the MMCC (e.g. MMCC(2,3) and MMCC(2,4)) corrections to CC and EOMCC (e.g. CCSD and EOMCCSD) energies. If we have an *a priori* knowledge about the dominant orbital excitations that define the excited states of interest (and the leading EOMCCSD amplitudes r_a^i and r_{ab}^{ij} may help us in this regard), we can use the corresponding orbitals as active orbitals for the

MRMBPT and subsequent MMCC/PT calculations. There is, however, an issue of matching the MRMBPT wavefunctions $|\bar{\Psi}_\mu^{(\mathrm{MRMBPT})}\rangle$, Eq. (86) or (87), with the corresponding EOMCC states $R_\mu^{(A)} e^{T^{(A)}} |\Phi\rangle$ (in the case of the MMCC(2,3)/PT and MMCC(2,4)/PT calculations, the EOMCCSD states $R_\mu^{(\mathrm{CCSD})} e^{T^{(\mathrm{CCSD})}} |\Phi\rangle$), so that we read the correct wavefunctions $|\bar{\Psi}_\mu^{(\mathrm{MRMBPT})}\rangle$ into the MMCC corrections $\delta_\mu^{(A)}$. This issue can be resolved by constructing, for example, the overlaps of all zeroth-order states $|\bar{\Psi}_\mu^{(P)}\rangle$, Eq. (78), obtained by diagonalizing the Hamiltonian in the model space $\mathscr{M}_0$, with all EOMCC states $R_\mu^{(A)} e^{T^{(A)}} |\Phi\rangle$ of interest. In most cases, only one specific zeroth-order state $|\bar{\Psi}_\mu^{(P)}\rangle$ gives a large overlap with a given EOMCC state $R_\mu^{(A)} e^{T^{(A)}} |\Phi\rangle$. If there are two or more states $|\bar{\Psi}_\mu^{(P)}\rangle$ that form similar overlaps with a given EOMCC state $R_\mu^{(A)} e^{T^{(A)}} |\Phi\rangle$, we can calculate the more complete MRMBPT wavefunctions $|\bar{\Psi}_\mu^{(\mathrm{MRMBPT})}\rangle$, Eq. (86) or (87), that correspond to these zeroth-order states $|\bar{\Psi}_\mu^{(P)}\rangle$ and search for the $|\bar{\Psi}_\mu^{(\mathrm{MRMBPT})}\rangle$ state that gives the maximum overlap with a given EOMCC state $R_\mu^{(A)} e^{T^{(A)}} |\Phi\rangle$. The resulting overlap enters the MMCC correction $\delta_\mu^{(A)}$ anyway (see, e.g. the overlap denominator $\langle \Psi_\mu^{(\mathrm{MRMBPT})} | R_\mu^{(A)} e^{T^{(A)}} |\Phi\rangle$ in Eq. (26)), and we can see now that the same denominator serves as a very important diagnostic for matching the EOMCC states $R_\mu^{(A)} e^{T^{(A)}} |\Phi\rangle$ and the MRMBPT wavefunctions $|\bar{\Psi}_\mu^{(\mathrm{MRMBPT})}\rangle$ for the purpose of determining the corresponding energy corrections $\delta_\mu^{(A)}$. In the specific case of the MMCC(2,3)/PT and MMCC(2,4)/PT approaches tested in this work, we matched the MRMBPT wavefunctions $|\bar{\Psi}_\mu^{(\mathrm{MRMBPT})}\rangle$ with the EOMCCSD states $R_\mu^{(\mathrm{CCSD})} e^{T^{(\mathrm{CCSD})}} |\Phi\rangle$ by analyzing first the overlaps of the zeroth-order states $|\bar{\Psi}_\mu^{(P)}\rangle$, Eq. (78), with the EOMCCSD wavefunctions of interest. If this was not sufficient for determining the matching pairs of the MRMBPT and EOMCCSD states, we calculated the complete overlap denominators $\langle \bar{\Psi}_\mu^{(\mathrm{MRMBPT})} | R_\mu^{(\mathrm{CCSD})} e^{T^{(\mathrm{CCSD})}} |\Phi\rangle$, which we need to determine the MMCC(2,3)/PT and MMCC(2,4)/PT corrections to the EOMCCSD energies anyway (see the denominators D_μ in Eqs. (93), (94), and (96)).

We illustrate the performance of the MRMBPT-corrected MMCC theory in excited-state calculations by analyzing the results of benchmark MMCC(2,3)/PT and MMCC(2,4)/PT calculations for the valence excited states of the CH^+ ion (see Table 7). We compare the MMCC(2,3)/PT and MMCC(2,4)/PT results for a few low-lying excited states of CH^+ of the $^1\Sigma^+$, $^1\Pi$, and $^1\Delta$ symmetries, obtained with the $[5s3p1d/3s1p]$ basis set described in [271] and the ground-state RHF orbitals, with the results of the corresponding full CI calculations reported in [271, 272]. Along with the MMCC/PT and full CI data, we show the EOMCCSD and full EOMCCSDT results (the latter ones obtained in [95]) and the results obtained with the perturbative triples response CC3 model [91]. In addition to the equilibrium geometry $R_{\mathrm{C\text{-}H}} = R_e$ ($R_{\mathrm{C\text{-}H}}$ is the C–H separation and R_e is the equilibrium value of $R_{\mathrm{C\text{-}H}}$), we consider two stretched geometries of CH^+, so that we can see how good the MMCC/PT theory can be in calculations of excited-state potential

Table 7 A comparison of various CC and MMCC vertical excitation energies of the CH^+ ion, as described by the [5s3p1d/3s1p] basis set, at the equilibrium geometry R_e and two stretched geometries, $1.5R_e$ and $2R_e$, with the corresponding full CI results. The full CI values are the excitation energies. All other values are the deviations from the full CI results. The $n\,^1Y$ energy is the vertical excitation energy from the ground state ($X\,^1\Sigma^+ \equiv 1\,^1\Sigma^+$) to the n-th singlet state of symmetry Y. All energies are in eV. The equilibrium bond length R_e in CH^+ is 2.13713 bohr

State	Full CI[a]	EOMCCSD	CC3[b]	EOMCCSDT[c]	CR-EOMCCSD(T)[d]	MMCC			
						(2,3)/CI[e,f]	(2,4)/CI[e,f]	(2,3)/PT[f]	(2,4)/PT[f]
				$R_{C\text{-}H} = R_e$					
$2\,^1\Sigma^+$	8.549	0.560	0.230	0.074	0.117	0.084	0.023	0.102	0.033
$3\,^1\Sigma^+$	13.525	0.055	0.016	0.001	0.011	0.000	−0.001	0.051	0.054
$1\,^1\Pi$	3.230	0.031	0.012	−0.003	0.007	0.007	0.010	0.015	0.017
$2\,^1\Pi$	14.127	0.327	0.219	0.060	0.113	0.105	0.037	−0.176	−0.211
$1\,^1\Delta$	6.964	0.924	0.318	0.040	0.027	0.051	0.031	0.090	0.050
				$R_{C\text{-}H} = 1.5R_e$					
$2\,^1\Sigma^+$	6.954	0.668		0.055	0.105	0.072	0.020	0.102	−0.008
$3\,^1\Sigma^+$	9.344	0.124		0.023	0.011	0.005	0.004	−0.053	−0.024
$1\,^1\Pi$	1.718	0.109		0.001	0.031	0.024	0.018	0.083	0.080
$2\,^1\Pi$	8.202	0.564		0.059	0.065	0.059	−0.006	−0.022	−0.053
$1\,^1\Delta$	5.847	1.114		0.069	0.004	0.065	0.025	0.085	0.004
				$R_{C\text{-}H} = 2R_e$					
$2\,^1\Sigma^+$	5.353	0.299		−0.032	0.093	0.074	0.013	−0.079	0.037
$3\,^1\Sigma^+$	6.681	0.532		0.126	0.084	0.048	0.016	−0.021	−0.045
$1\,^1\Pi$	0.566	0.234		0.002	0.061	0.045	0.021	0.133	0.115
$2\,^1\Pi$	5.363	0.467		0.026	0.018	−0.007	−0.004	−0.123	0.097
$1\,^1\Delta$	4.964	1.178		0.103	−0.009	0.079	0.029	0.005	−0.074

[a] The full CI results for R_e were taken from [271] and the full CI results for $1.5R_e$ and $2R_e$ were taken from [272].
[b] From [91].
[c] From [95].
[d] The ID variant of the CR-EOMCCSD(T) theory. From [98].
[e] From [97].
[f] The active space consisting of the 3σ, $1\pi_x \equiv 1\pi$, $1\pi_y \equiv 2\pi$, and 4σ orbitals.

energy curves along bond breaking coordinates. We also compare the MMCC/PT results with the results of the MMCC/CI calculations reported in [96, 97]. In calculating the MRMBPT wavefunctions $|\bar{\Psi}_\mu^{(\mathrm{MRMBPT})}\rangle$, Eq. (86), that enter the MMCC(2,3)/PT and MMCC(2,4)/PT energy formulas, Eqs. (93) and (94), we used the same set of active orbitals as used in the previously reported MMCC(2,3)/CI and MMCC(2,4)/CI calculations [96, 97]. Thus, the active space employed in the calculations for CH^+ consisted of the highest-energy occupied orbital, 3σ, and the three lowest-energy unoccupied orbitals, $1\pi_x \equiv 1\pi$, $1\pi_y \equiv 2\pi$, and 4σ. This choice of active space reflects the nature of orbital excitations defining the valence excited states of CH^+ shown in Table 7 and the nature of the bond breaking in this system (see [93, 94, 96, 97] for details). Finally, we compare the results of the MMCC(2,3)/PT and MMCC(2,4)/PT calculations with the CR-EOMCCSD(T) results reported in [98] as well as with the corresponding MMCC/CI results [96,97]. Let us recall that the CR-EOMCCSD(T) method is a "black-box" variant of the MMCC(2,3) approximation, in which we do not have to select active orbitals to determine the triples corrections to CCSD/EOMCCSD energies derived from the general MMCC formalism.

We begin our discussion with the vertical excitation energies at the equilibrium geometry. In this case, the doubly excited nature of the first-excited $^1\Sigma^+$ ($2\,^1\Sigma^+$) state and the lowest-energy $^1\Delta$ ($1\,^1\Delta$) state, and the partially biexcited character of the second $^1\Pi$ ($2\,^1\Pi$) state (cf., e.g. [79, 93, 94, 96, 97, 271]) cause significant problems for the EOMCCSD approach. The errors in the EOMCCSD excitation energies for these three states, relative to the corresponding full CI values, are 0.560, 0.924, and 0.327 eV, respectively. The conventional linear response CC approach to triple excitations via the CC3 method of Jørgensen and co-workers [86, 90–92] reduces these large errors to 0.219–0.318 eV [91], which is a significant improvement, but if we want to obtain errors which are less than 0.1 eV with the standard EOMCC methodology, we must use the full EOMCCSDT approach (or its active-space EOMCCSDt variant [94,95]). The full EOMCCSDT approach reduces the relatively large unsigned errors in the EOMCCSD results for the $2\,^1\Sigma^+$, $1\,^1\Delta$, and $2\,^1\Pi$ states to 0.074, 0.040, and 0.060 eV, respectively.

As shown in Table 7, the CR-EOMCCSD(T), MMCC(2,3)/CI, and MMCC (2,3)/PT methods, which represent three different flavors of the MMCC(2,3) theory and which are all much less expensive than the iterative CC3 and EOMCCSDT approaches, are capable of providing the results of near-EOMCCSDT quality. Indeed, the errors in the vertical excitation energies calculated at $R_{\mathrm{C\text{-}H}} = R_e$ for the $2\,^1\Sigma^+$, $1\,^1\Delta$, and $2\,^1\Pi$ states of CH^+, which have significant double excitation components, obtained with the non-iterative CR-EOMCCSD(T), MMCC(2,3)/CI, MMCC(2,3)/PT approximations, are 0.084–0.117 eV for the $2\,^1\Sigma^+$ state, 0.027–0.090 eV for the $1\,^1\Delta$ state, and 0.105–0.176 eV for the $2\,^1\Pi$ state. This should be compared to the 0.560, 0.924, and 0.327 eV errors, respectively, in the EOMCCSD results and the 0.230, 0.318, and 0.219 eV errors, respectively, obtained with the CC3 method. For the remaining two states shown in Table 7 (the third $^1\Sigma^+$ state and the lowest-energy $^1\Pi$ state), which at $R_{\mathrm{C\text{-}H}} = R_e$ are dominated by single excitations [79, 93, 94, 96, 97, 271], the errors in the CR-EOMCCSD(T), MMCC(2,3)/CI,

and MMCC(2,3)/PT results are 0.000–0.051 eV and 0.007–0.015 eV, respectively. In this case, the CR-EOMCCSD(T), MMCC(2,3)/CI, and MMCC(2,3)/PT methods provide the results of the CC3 or near-EOMCCSDT quality. The standard EOMCC methods, including the basic EOMCCSD approximation, have no troubles with describing excited states dominated by one-electron transitions, but it is encouraging to observe that even in this case all three MMCC(2,3) methods, including the MMCC(2,3)/PT approximation developed in this work, improve the EOMCCSD results. The MMCC(2,4)/PT approach provides small improvements in the MMCC(2,3)/PT results for the $2\,^1\Sigma^+$ and $1\,^1\Delta$ states, while keeping the high accuracy of the MMCC(2,3)/PT calculations for the remaining states.

The very good performance of the MMCC(2,3)/PT and other MMCC(2,3) methods is not limited to vertical excitation energies at the equilibrium geometry. As shown in Table 7, the CR-EOMCCSD(T), MMCC(2,3)/CI, and MMCC(2,3)/PT approaches are capable of providing an accurate description of excited-state potentials of CH^+ at larger values of $R_{C\text{-}H}$, where all excited states listed in Table 7 gain a considerable multi-reference character [93–97]. The very large (even ~ 1 eV) errors in the EOMCCSD results for the excited-state potential energy curves of CH^+, relative to the corresponding full CI potentials, are reduced in the CR-EOMCCSD(T), MMCC(2,3)/CI, and MMCC(2,3)/PT calculations to 0.1 eV or less. Indeed, the errors in the EOMCCSD excitation energies, relative to full CI, for the two lowest excited states of the $^1\Sigma^+$ symmetry, the two lowest $^1\Pi$ states, and the lowest $^1\Delta$ state are 0.668, 0.124, 0.109, 0.564, and 1.114, respectively, at $R_{C-H} = 1.5R_e$, and 0.299, 0.532, 0.234, 0.467, and 1.178 eV, respectively, at $R_{C-H} = 2R_e$. The MMCC(2,3)/PT method reduces these large unsigned errors to 0.102, 0.053, 0.083, 0.022, and 0.085 eV, respectively, at $R_{C-H} = 1.5R_e$, and 0.079, 0.021, 0.133, 0.123, and 0.005 eV, respectively, at $R_{C-H} = 2R_e$. As in the $R_{C-H} = R_e$ case, the only standard EOMCC approach that can provide the results of similar quality is the very expensive full EOMCCSDT method (cf. Table 7). The MMCC(2,4)/PT approach provides further improvements in a few cases or does not change the already very good MMCC(2,3)/PT energies.

The results in Table 7 show that all three MMCC(2,3) approximations, including CR-EOMCCSD(T), MMCC(2,3)/CI, and MMCC(2,3)/PT, provide similar improvements in the EOMCCSD energies. The improvements are particularly substantial for the excited states dominated by doubles and for the excited-state potentials at stretched internuclear geometries, where all excited states of CH^+ gain a significant multi-reference character. It is interesting to learn that the basic and relatively simple MMCC(2,3) approximation is capable of providing considerable improvements in the EOMCCSD results, independent of the form of the wavefunction $|\Psi_\mu\rangle$ used in the MMCC(2,3) correction formula. The CR-EOMCCSD(T) approach uses the perturbative, EOMCCSDT-like, wavefunctions $|\Psi_\mu\rangle$, the MMCC(2,3)/CI method uses the MRCI-like wave functions $|\Psi_\mu\rangle$, and the MMCC(2,3)/PT scheme described in detail in this work uses the MRMBPT-like wavefunctions $|\Psi_\mu\rangle$ defined by Eqs. (86) or (87), and yet the resulting MMCC(2,3) excitation energies for CH^+ are very similar. This demonstrates the robustness of the MMCC formalism, which is capable of improving the results of conventional CC and EOMCC calculations

independent of the specific form of $|\Psi_\mu\rangle$ used to calculate the energy corrections $\delta_\mu^{(A)}$ or $\delta_\mu^{(\mathrm{CCSD})}$. From the point of view of this work, it is encouraging to observe that we can considerably improve the CCSD and EOMCCSD results using the low-order MRMBPT-like wavefunctions $|\Psi_\mu\rangle$ defined by Eq. (86). As explained earlier, the MMCC(2,3)/PT is much less expensive than the MMCC(2,3)/CI approach, since we do not have to solve iterative MRCI-like equations to obtain the wavefunctions $|\Psi_\mu\rangle$ that enter the MMCC(2,3)/PT energy expression. Also, if the active space is small, the MMCC(2,3)/PT method is less expensive than the CR-EOMCCSD(T) approach, since the summation over $i < j < k$, $a < b < c$ in Eq. (93) includes only the selected types of triple excitations relative to $|\Phi\rangle$ that are included in the MRMBPT wavefunctions $|\bar{\Psi}_\mu^{(\mathrm{MRMBPT})}\rangle$, Eqs. (86) or (87). Finally, it is worth noticing that there is no apparent need to reoptimize orbitals to obtain an accurate description of excited states of CH^+ in the MMCC(2,3)/PT calculations (the ordinary RHF orbitals seem to suffice), although it would be interesting to examine the role of orbital optimization in MRMBPT calculations that precede the MMCC(2,3)/PT calculations. The MMCC(2,4)/PT method improves the description of the CH^+ system somewhat, but not to a degree that would favor this approach over the less expensive MMCC(2,3)/PT approximation.

6 Summary, Concluding Remarks, and Future Perspectives

In this chapter, a novel electronic structure theory, termed MMCC/PT, which combines the CC/EOMCC method with the low-order multi-reference perturbation theory, has been described. The MMCC/PT approaches have been formulated using diagrammatic methods. The key elements of the MMCC(2,3)/PT and MMCC(2,4)/PT methods, including the generalized moments of the CCSD and EOMCCSD equations that enter the MMCC(2,3)/PT and MMCC(2,4)/PT energy corrections, have been efficiently implemented using the idea of diagram factorization. This has given us an opportunity to discuss the most essential steps in diagrammatic considerations that lead to highly efficient implementations of all CC, EOMCC, and MMCC methods. The performance of the basic MMCC/PT approximations has been illustrated by the results of test calculations for the bond breaking in HF, F_2, and H_2O, and the excited states of CH^+. The test calculations show that the MMCC(2,3)/PT and MMCC(2,4)/PT approaches provide a good description of bond breaking and excited states dominated by doubles, eliminating failures of the conventional CC/EOMCC methods at larger internuclear distances and for excited states dominated by two-electron transitions without invoking expensive steps of high-order CC/EOMCC methods.

Clearly, several issues need further study. The role of different choices of active orbitals should be examined. The majority of multi-reference calculations are performed with the orbitals optimized at the CASSCF level. In this work, we have only used the ground-state RHF orbitals. It would be also interesting to examine different types of the MRMBPT wavefunctions that enter the MMCC/PT corrections. In this

work, we have tested a simplified, "home-grown", MRMBPT-like scheme based on the partitioning of the Hamiltonian into the model-space (P-space) and Q-space components (the latter component originates from single and double excitations from a multi-dimensional model space). The majority of contemporary MRMBPT calculations are performed with schemes, such as CASPT2, MC-QDPT, or MRMP2 mentioned in the Introduction. Several other low-order MRMBPT have been proposed in literature, as discussed in the Sect. 1. It would be useful to test how the conclusions of this work depend on the particular form of the MRMBPT theory used to provide wavefunctions $|\Psi_\mu\rangle$ for MMCC calculations.

Acknowledgements This work has been supported by the Chemical Sciences, Geosciences and Biosciences Division, Office of Basic Energy Sciences, Office of Science, U. S. Department of Energy (grant no. DE-FG02-01ER15228 awarded to P.P). Additional support has been provided by the James L. Dye Endowed Fellowship and the Michigan State University Dissertation Completion Fellowship (M.D.L.).

Appendix 1. An Introduction to the Diagrammatic Methods of Many-Body Theory

To introduce the diagrammatic methods of many-body theory, we begin our considerations with selecting a Fermi vacuum state $|\Phi\rangle$, which is a single-determinantal state that is typically chosen to provide a reasonable approximation to the ground electronic state of a given many-fermion system of interest. The Fermi vacuum state (reference state) is diagrammatically represented by an empty space. All other Slater determinants are represented with the help of *oriented lines*, pointing either *upward* for *particle states* (spin-orbitals unoccupied in the reference $|\Phi\rangle$) or *downward* for *hole states* (spin-orbitals occupied in the reference $|\Phi\rangle$), with labels associated with the corresponding spin-orbital excitations relative to $|\Phi\rangle$, and outgoing or incoming into a simple vertex.

We represent the second-quantized operators entering a given operator product with basic diagrams. In the design of these diagrams, we use vertices with *incoming lines* representing *annihilation operators* and *outgoing lines* representing the *creation operators*. Each basic *vertex* contains information about matrix elements in a spin-orbital basis defining the operator. For instance, the Slater determinant $|\Phi_i^a\rangle = a^a a_i|0\rangle$ is represented by

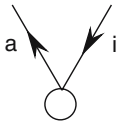

and $\langle \Phi_i^a | = \langle 0 | (a^a a_i)^\dagger = \langle 0 | a^i a_a$ is represented by

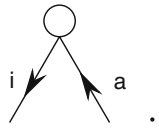

We assign different vertices to represent different operators. Since the one-body operator brings a pair of creation and annihilation operators, its diagrammatic representation contains only two oriented lines. Likewise, the diagram representing the two-body operator, which brings two pairs of creation and annihilation operators, contains four oriented lines, and so on and so forth.

There are several diagrammatic representations [260, 261]; the most popular are the Hugenholtz and Goldstone representations. The Hugenholtz representation employs the antisymmetrized matrix elements in the second-quantized definitions of operators (e.g. $v_{pq}^{rs} = \langle pq|v|rs\rangle - \langle pq|v|sr\rangle$ for the two-body operator V_N) while the Goldstone representation is based on the second-quantized form of operators that uses non-symmetric matrix elements (e.g. $\langle pq|v|rs\rangle$ in the case of V_N). In our analysis, we use the Hugenholtz representation, which produces fewer distinct resulting diagrams than the Goldstone representation. The Goldstone representation is useful in developing spin-adapted formalisms for spin-free Hamiltonians [260, 261].

The basic diagrams (in the Hugenholtz representation) for the one- and two-body parts of the electronic Hamiltonian in the normal-ordered form, F_N and V_N,

$$F_N = \sum_{p,q} f_p^q N[a^p a_q] \equiv f_p^q N[a^p a_q] \tag{119}$$

and

$$V_N = \tfrac{1}{4} \sum_{p,q,r,s} v_{pq}^{rs} N[a^p a^q a_s a_r] \equiv \tfrac{1}{4} v_{pq}^{rs} N[a^p a^q a_s a_r]\,, \tag{120}$$

respectively, and the cluster and excitation operators T_1, T_2, $R_{\mu,1}$, and $R_{\mu,2}$ are shown in Fig. 15.

The spin-orbitals that are attached to the oriented lines are referred to as *free* if they represent summation indices and as *fixed* otherwise. As shown in Fig. 15, the cluster operators and the linear excitation operators have the same diagrammatic form, the only difference is in the way we draw the corresponding vertices. In particular, T_1 and T_2 use unfilled oval vertices, while $R_{\mu,1}$ and $R_{\mu,2}$ use circled dots. A diagram stripped of the free labels is called a *skeleton* or, better, an oriented skeleton. The oriented skeleton determines the weight of a diagram (a combinatorial coefficient that enters the algebraic expression). The spin-orbital indices p, q, r, s can either be occupied or unoccupied in the Fermi vacuum. According to standard convention, the indices $i, j, \ldots$ label occupied spin-orbitals, while $a, b, \ldots$ refer to unoccupied spin-orbitals in the Fermi vacuum $|\Phi\rangle$. For example, the one-body component of the Hamiltonian in the normal-ordered form, H_N, can be expressed as

$$F_N = \sum_{a,b} f_a^b N[a^a a_b] + \sum_{i,j} f_i^j N[a^i a_j] + \sum_{i,a} f_i^a N[a^i a_a] + \sum_{i,a} f_a^i N[a^a a_i]. \tag{121}$$

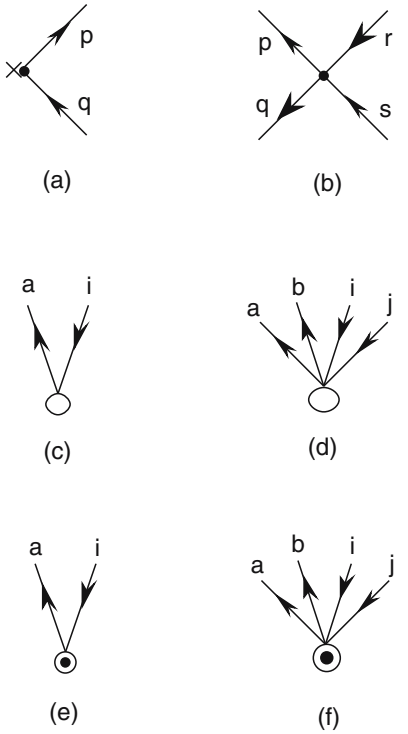

Fig. 15 The Hugenholtz representation of (**a**) F_N; (**b**) V_N; (**c**) T_1; (**d**) T_2; (**e**) $R_{\mu,1}$; and (**f**) $R_{\mu,2}$

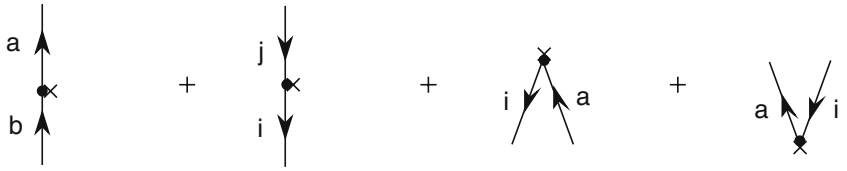

Fig. 16 The Hugenholtz representation of F_N

The corresponding diagrams are shown in Fig. 16. The two-body component of H_N, V_N, can be partitioned in a similar way, as shown in Fig. 17.

After assigning skeletons (or diagrams) to the basic operators, the diagrammatic calculation proceeds as follows:

1. Represent the operators by appropriate skeletons following the vertical time axis (as described in Sect. 4.3), that is, placing the operators from the bottom to the top corresponding to the right to left order of the operators in the algebraic expression when they act on the functions (vectors) in the Fock space. For instance, the operator $\frac{1}{2}(V_N T_1^2)$ is represented as

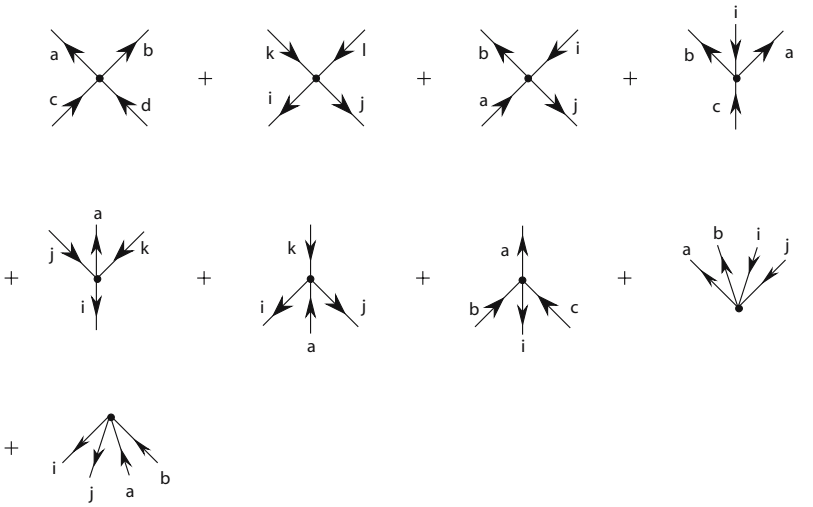

Fig. 17 The Hugenholtz representation of V_N

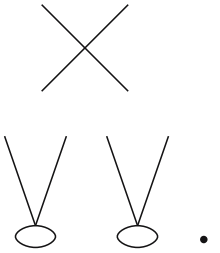

2. Form all permissible resulting skeletons by connecting the lines in all possible ways. Then, form all nonequivalent resulting diagrams, in which the oriented lines are labeled with their corresponding spin-orbital indices, representing only the non-vanishing contraction schemes that result when the Wick's theorem is applied, that is,

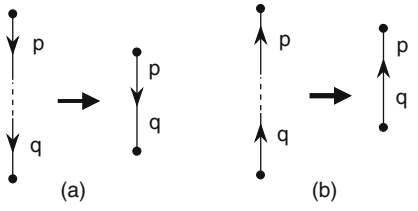

where (a) $\overbrace{a^p\ a_q} = \delta_{pq} H(q)$ and (b) $\overbrace{a_p\ a^q} = \delta_{pq}[1 - H(q)]$.

The $H(q)$ step function is equal to 1 for q being a hole and 0 for q representing a particle and δ_{pq} is the usual Kronecker delta.

3. Lastly, assign the algebraic expressions to all nonequivalent permissible resulting diagrams. The final expression for the operator product of interest is a sum of the algebraic expressions corresponding to all nonequivalent resulting diagrams allowed by a given many-body theory. In general, the algebraic expression corresponding to a given diagram is a product of (a) the weight factor, (b) the sign factor, (c) the scalar factor, and (for example, in the wavefunction expressions) (d) the operator part, accompanied by a summation over all relevant hole and particle indices, if such summations exist in the operators. For the connected Hugenholtz diagrams, the weight factor is specified by $(\frac{1}{2})^m$, where m is the number of pairs of "equivalent" lines. A pair of equivalent lines is defined as being two lines originating at the same vertex and ending at another, but same vertex, and going in the same direction. We must remember, however, that the identically oriented lines carrying fixed (i.e., not summed) spin-orbital indices can never be regarded as equivalent lines. The scalar factor is a product of matrix elements associated with the individual vertices entering the resulting diagram. The operator part (if it appears in the expression) is a product of the creation and annihilation operators associated with the uncontracted external lines.

The drawback of the Hugenholtz representation is that Hugenholtz diagrams do not specify the overall sign of the contribution of the diagram. This is due to the fact that the basic Hugenholtz diagrams, such as V_N or T_2, use antisymmetrized matrix elements v_{pq}^{rs}, t_{ab}^{ij}, etc. In order to determine the sign, it is necessary to draw one Goldstone representative, called the Brandow diagram, for each Hugenholtz diagram [260]. This can be done by "expanding" the Hugenholtz vertices. In other words, we replace all basic Hugenholtz vertices by Brandow vertices (the Brandow representations of F_N and V_N are shown in Figs. 18 and 19), while keeping the directions of the lines and the connectivity intact. Usually more than one possibility exists, since one can usually draw several Goldstone diagrams for each Hugenholtz diagram, but this is not a problem here: we can choose any Goldstone representative of a given Hugenholtz diagram as a Brandow diagram. The final results do not depend on that choice. Once the Brandow diagram is drawn, we determine the sign factor for it by counting the number of loops (l) and the number of internal hole lines (h), and by using the sign formula $(-1)^{l+h}$.

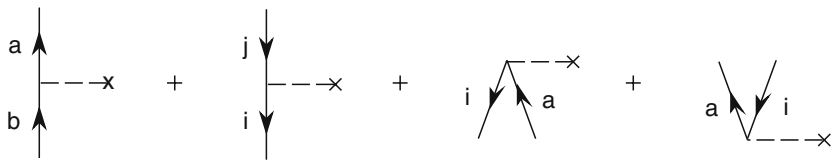

Fig. 18 The Brandow representation of F_N corresponding to Fig. 16

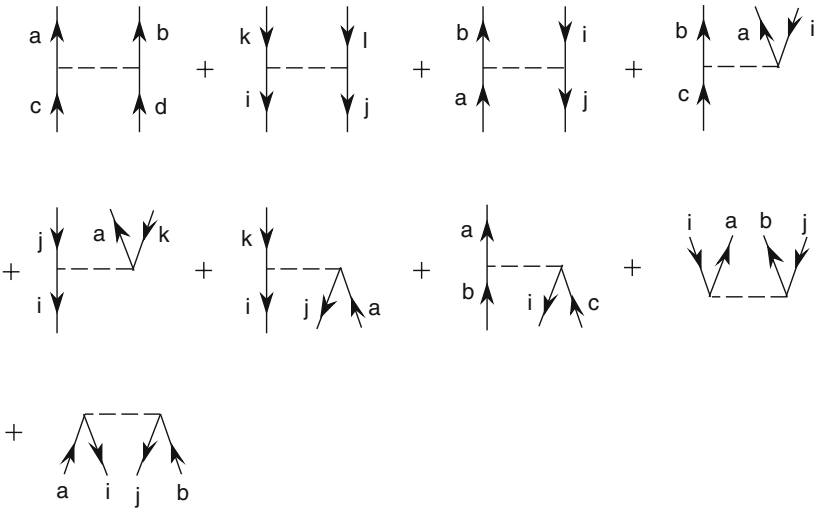

Fig. 19 The Brandow representation of V_N corresponding to Fig. 17

Appendix 2. The Structure of the Similarity-Transformed Hamiltonian of the CCSD Theory

By using the Campbell-Hausdorff-Baker formula, one can easily show that the $\bar{H} = e^{-T} H e^{T}$ operator can be written as a sum of the bare Hamiltonian H and commutators of H with one or more T operators (cf., e.g. [19, 21, 39, 260]. This is equivalent to the expansion of $\bar{H}$ in terms of the connected diagrams obtained by connecting zero, one, or more T vertices to H, as in Eqs. (9) and (12). This means that $\bar{H}$ is represented by a finite set of connected diagrams independent of the number of fermions in a system and truncation in T (cf. [19, 21, 39, 260]).

In order to construct the $\bar{H}^{(\mathrm{CCSD})}$ diagrams, we follow the diagrammatic rules discussed in Appendix 1. Thus, we contract the Hamiltonian in the normal ordered form, H_N, with a number (zero, one or more) of $T^{(\mathrm{CCSD})}$ operators appearing in the $e^{T^{(\mathrm{CCSD})}}$ expansion to obtain the connected the product of H_N and $e^{T^{(\mathrm{CCSD})}}$. Since the Hamiltonians used in chemistry contain at most two-body interactions, H_N can be contracted with at most four cluster operators $T^{(\mathrm{CCSD})}$ to produce the connected diagrams of $\bar{H}_N^{(\mathrm{CCSD})}$.

The one- and two-body components of $\bar{H}^{(\mathrm{CCSD})}$ have similar diagrammatic forms as the one- and two-body components of the Hamiltonian H_N. The only difference is in the manner we draw the interaction lines; the similarity transformed Hamiltonian $\bar{H}^{(\mathrm{CCSD})}$ uses the wavy interaction line, as in Figs. 20–23, while the bare Hamiltonian H_N uses the dashed line, as in Figs. 18 and 19.

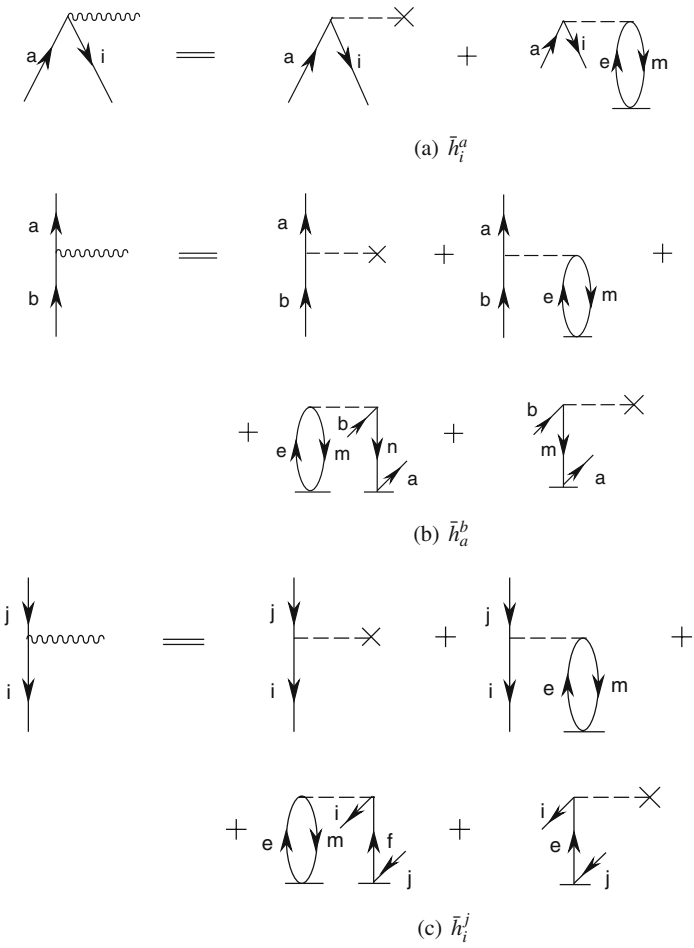

Fig. 20 One-body components of $\bar{H}^{(\mathrm{CCSD})}$ (the $\bar{h}_a^i$ component is not shown, since $\bar{h}_a^i$ represents the CCSD equations projected on a singly excited determinant $|\Phi_i^a\rangle$ and, as such, vanishes)

To illustrate how we use the diagrammatic methods in deriving the explicit algebraic expressions for $\bar{H}^{(\mathrm{CCSD})}$,

$$\bar{H}^{(\mathrm{CCSD})} = \langle \Phi | H | \Phi \rangle + (H_N e^{T_1+T_2})_C = \langle \Phi | H | \Phi \rangle + \bar{h}_p^q a^p a_q + \tfrac{1}{4} \bar{h}_{pq}^{rs} a^p a^q a_s a_r + \ldots , \tag{122}$$

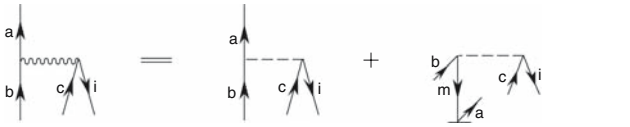

(a) $\bar{h}^{bc}_{ai}$

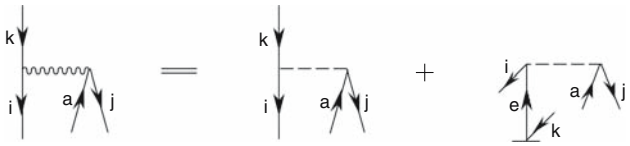

(b) $\bar{h}^{ka}_{ij}$

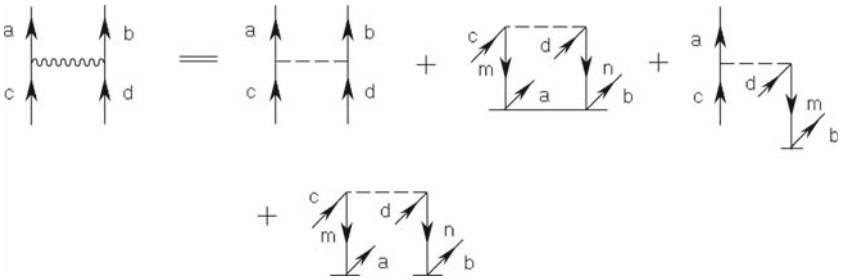

(c) $\bar{h}^{cd}_{ab}$

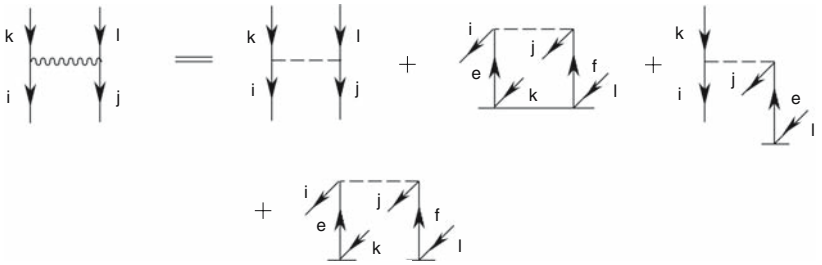

(d) $\bar{h}^{kl}_{ij}$

Fig. 21 Two-body components of $\bar{H}^{(\mathrm{CCSD})}$ (the $\bar{h}^{ij}_{ab}$ component is not shown, since $\bar{h}^{ij}_{ab}$ represents the CCSD equations projected on a doubly excited determinant $|\Phi^{ab}_{ij}\rangle$ and, as such, vanishes)

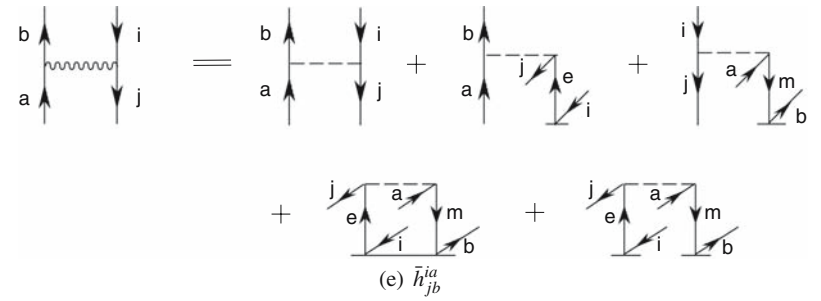

(e) $\bar{h}^{ia}_{jb}$

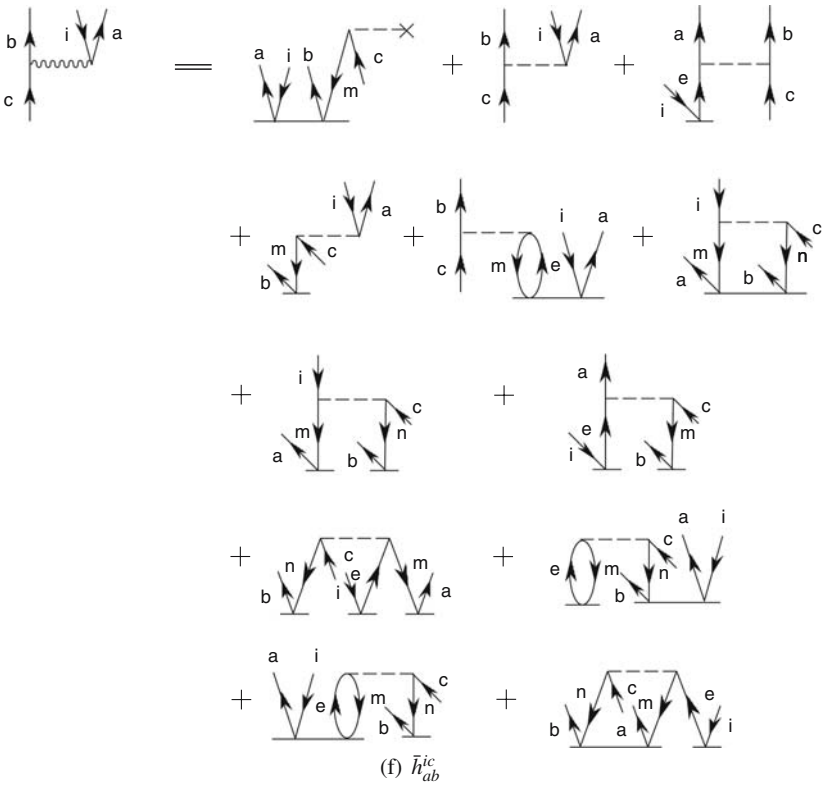

(f) $\bar{h}^{ic}_{ab}$

Fig. 21 (Continued)

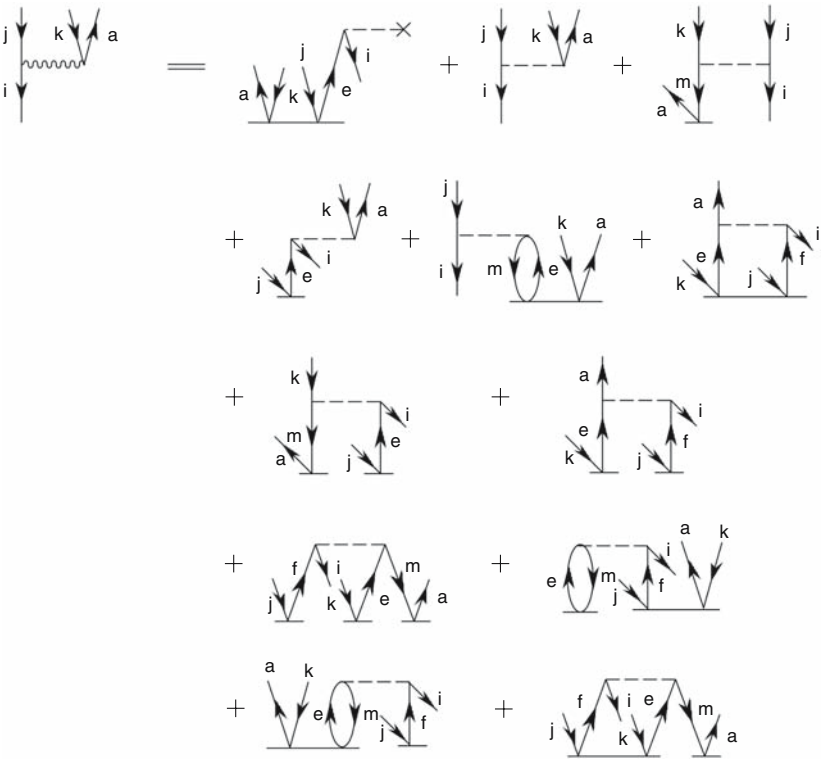

Fig. 21 (Continued)

we show an example on how one can obtain the diagrams contributing to the matrix elements $\bar{h}_a^b$,

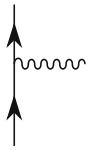

which define one specific (particle-particle) type of the one-body components of $\bar{H}^{(\mathrm{CCSD})}$. In this case, our goal is to generate diagrams of the above particle-particle form from the connected product of H_N and $e^{T^{(\mathrm{CCSD})}}$. The resulting diagrams must contain an oriented line above and below the vertex; both lines should be directed upward as particle lines a and b, as in the above graph. We can expand the $\bar{H}^{(\mathrm{CCSD})}$ operator in the following manner:

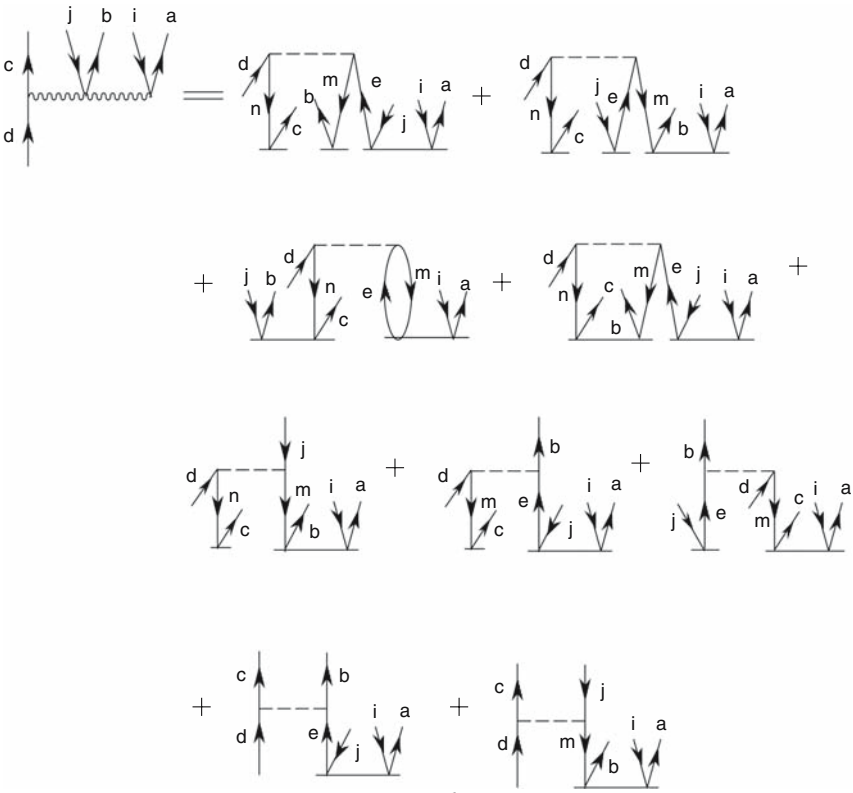

(a) $\bar{h}^{ijd}_{abc}$

Fig. 22 Three-body components of $\bar{H}^{(\mathrm{CCSD})}$ other than $\bar{h}^{ijk}_{abc} \equiv \mathfrak{M}^{ijk}_{0,abc}(2)$

$$\begin{aligned}\bar{H}^{(\mathrm{CCSD})} &= \langle \Phi|H|\Phi\rangle + (H_N e^{T^{(\mathrm{CCSD})}})_C \\ &= \langle \Phi|H|\Phi\rangle + [(F_N(1+T_1+T_2+\tfrac{1}{2}T_1^2+\ldots)+ \\ &\quad V_N(1+T_1+T_2+\tfrac{1}{2}T_1^2+\ldots)]_C. \end{aligned} \tag{123}$$

Let us identify which terms in Eq. (123) contribute to $\bar{h}^b_a$ by forming first the non-oriented Hugenholtz skeletons. We begin with the first term, F_N, which is represented diagrammatically in Fig. 16. As shown in Fig. 16, the leftmost diagram in that figure satisfies the above criteria and hence contributes to $\bar{h}^b_a$. Next, we consider the $(F_N T_1)_C$

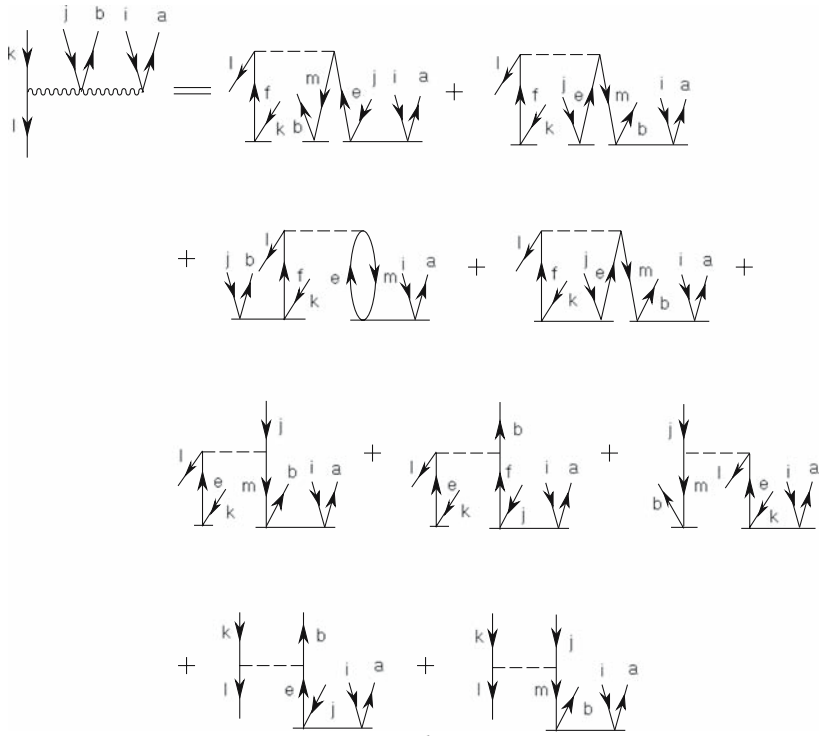

Fig. 22 (Continued)

term, which produces one resulting non-oriented Hugenholtz skeleton that contains one line above the vertex as well as one line below the vertex, as shown below:

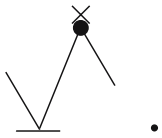

When we analyze other terms in Eq. (123) in the same fashion, we obtain all of the resulting non-oriented Hugenholtz skeletons of $\bar{h}^b_a$, which are

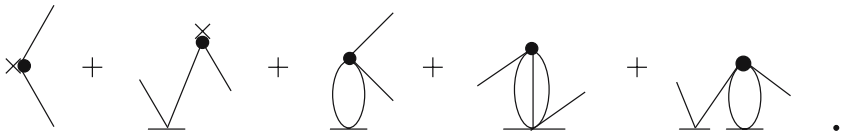

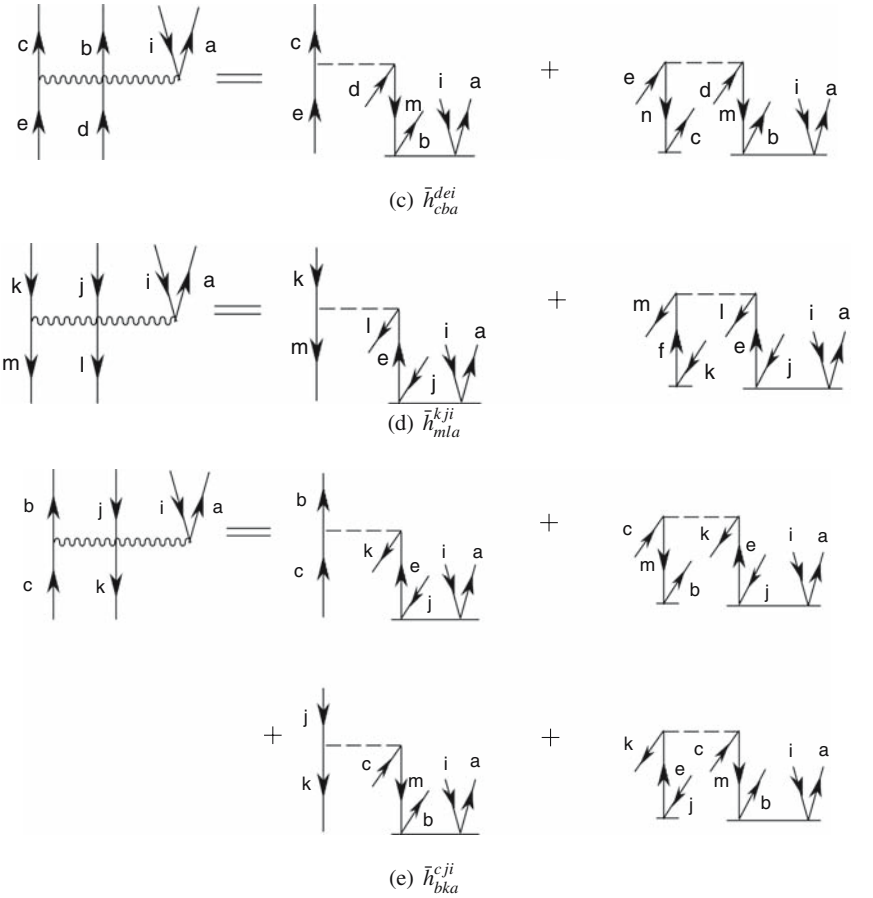

Fig. 22 (Continued)

The corresponding oriented Hugenholtz diagrams for $\bar{h}^b_a$ with their respective weights are as follows:

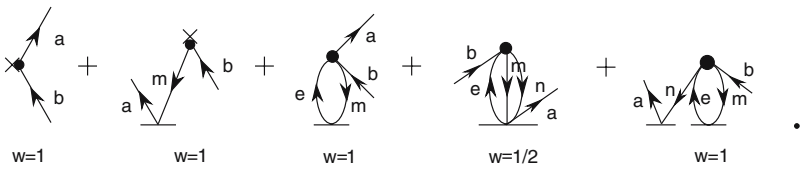

The corresponding Brandow diagrams for $\bar{h}^b_a$ with their corresponding sign factors are shown below

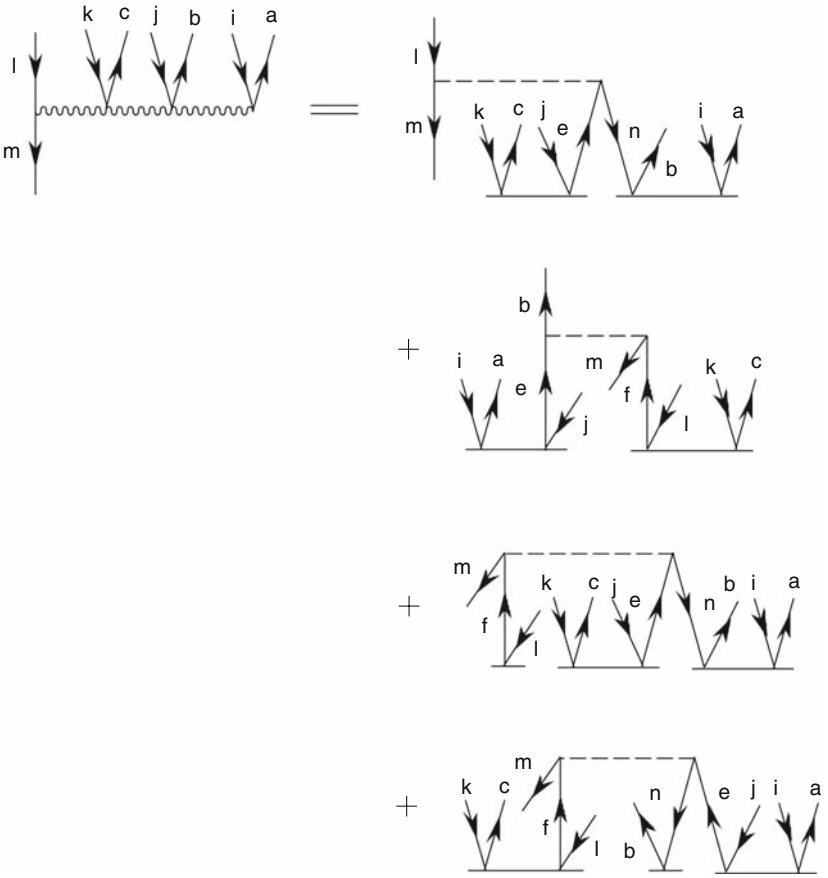

(a) $\bar{h}^{lkji}_{mcba}$

Fig. 23 Four-body components of $\bar{H}^{(\mathrm{CCSD})}$ other than $\bar{h}^{ijkl}_{abcd} \equiv \mathfrak{M}^{ijkl}_{0,abcd}(2)$

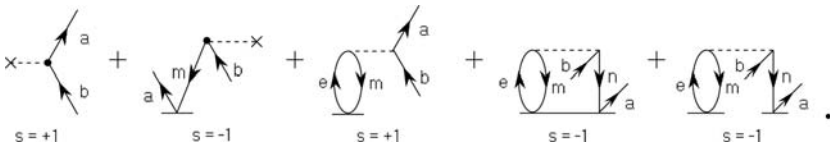

These diagrams yield the following algebraic expression for $\bar{h}^b_a$:

$$\bar{h}^b_a = f^b_a - f^b_m t^m_a + v^{eb}_{ma} t^m_e - \tfrac{1}{2} v^{eb}_{mn} t^{mn}_{ea} - v^{eb}_{mn} t^m_e t^n_a. \tag{124}$$

All of the resulting diagrams for one-, two-, three-, and four-body components of $\bar{H}^{(\mathrm{CCSD})}$ are obtained in a similar way. They are shown in Figs. 20–23. Figs. 24

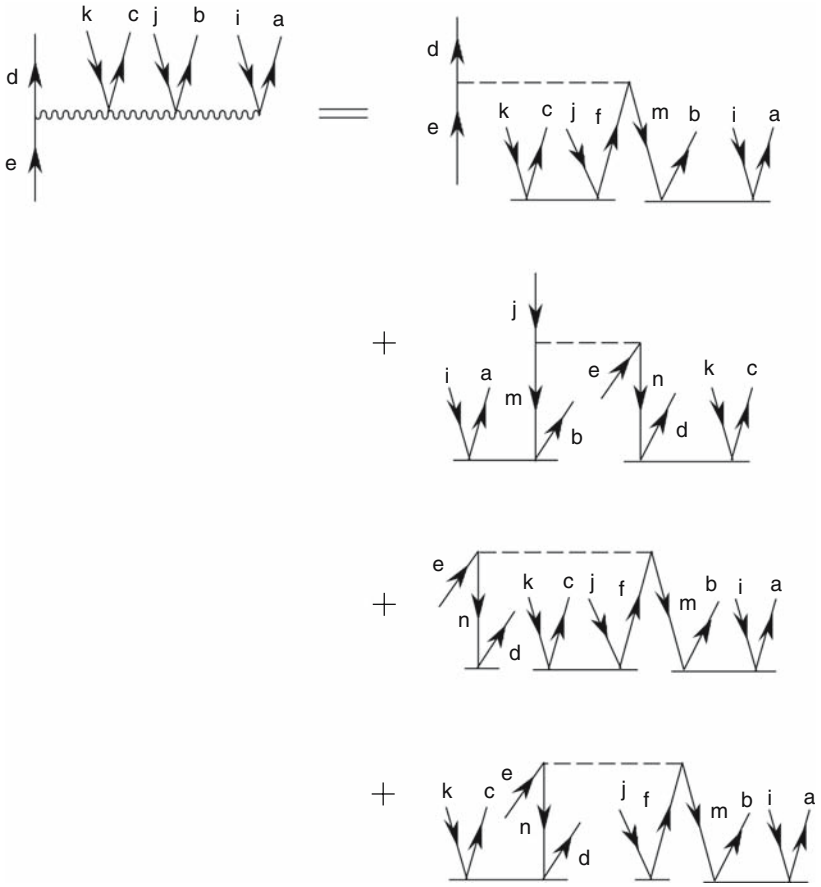

(b) $\bar{h}^{ekji}_{dcba}$

Fig. 23 (Continued)

and 25 show all of the resulting diagrams corresponding to the ground-state triply and quadruply excited moments of the CCSD equations, $\mathfrak{M}^{ijk}_{0,abc}(2)$ and $\mathfrak{M}^{ijkl}_{0,abcd}(2)$, respectively, which can also be regarded as the particular examples of the three- and four-body components of $\bar{H}^{(\mathrm{CCSD})}$. Tables 8–11 summarize all the algebraic expressions of the one-, two-, three-, and four-body components of $\bar{H}^{(\mathrm{CCSD})}$, including $\mathfrak{M}^{ijk}_{0,abc}(2)$ and $\mathfrak{M}^{ijkl}_{0,abcd}(2)$, which are obtained by reading the diagrams shown in Figs. 20–25.

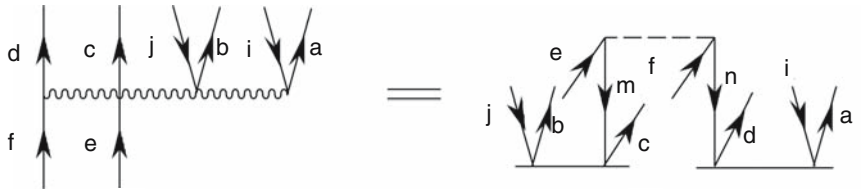

(c) $\bar{h}^{feji}_{dcba}$

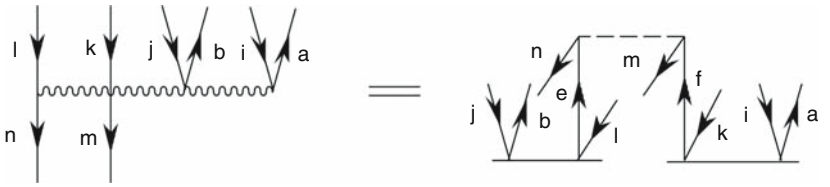

(d) $\bar{h}^{lkji}_{nmba}$

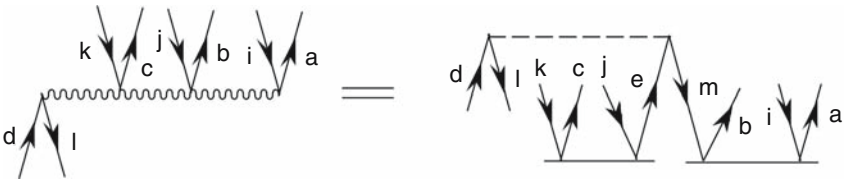

(e) $\bar{h}^{dkji}_{lcba}$

Fig. 23 (Continued)

Appendix 3. Factorization of Coupled-Cluster Diagrams

The diagrammatic technique is a very powerful tool. However, if we program the resulting diagrams in a naive manner, i.e., one by one and with the explicit loops that correspond to summations over spin-orbital indices that label internal lines, this will give an inefficient and hence impractical computer code. In this section, we rederive the expressions for the one- and two-body components of $\bar{H}^{(\mathrm{CCSD})}$, $\bar{H}^{(\mathrm{CCSD})}_1$ and $\bar{H}^{(\mathrm{CCSD})}_2$, respectively, in such a way that only linear terms (binary tensor products) with redefined vertices are retained. Ultimately, the factorized forms of $\bar{H}^{(\mathrm{CCSD})}_1$ and $\bar{H}^{(\mathrm{CCSD})}_2$ are used to define the higher-rank components of $\bar{H}^{(\mathrm{CCSD})}$, such as the three- and four-body components $\bar{H}^{(\mathrm{CCSD})}_3$ and $\bar{H}^{(\mathrm{CCSD})}_4$, as well as other intermediates entering the CC expressions of interest, such as $\mathfrak{M}^{ijk}_{\mu,abc}(2)$ and $\mathfrak{M}^{ijkl}_{\mu,abcd}(2)$, which are naturally expressed via $\bar{H}^{(\mathrm{CCSD})}_3$ and $\bar{H}^{(\mathrm{CCSD})}_4$.

To illustrate the diagrammatic factorization technique and the computational benefits that it offers, we analyze an example of $\bar{h}^b_a$, which is expressed in a diagram-

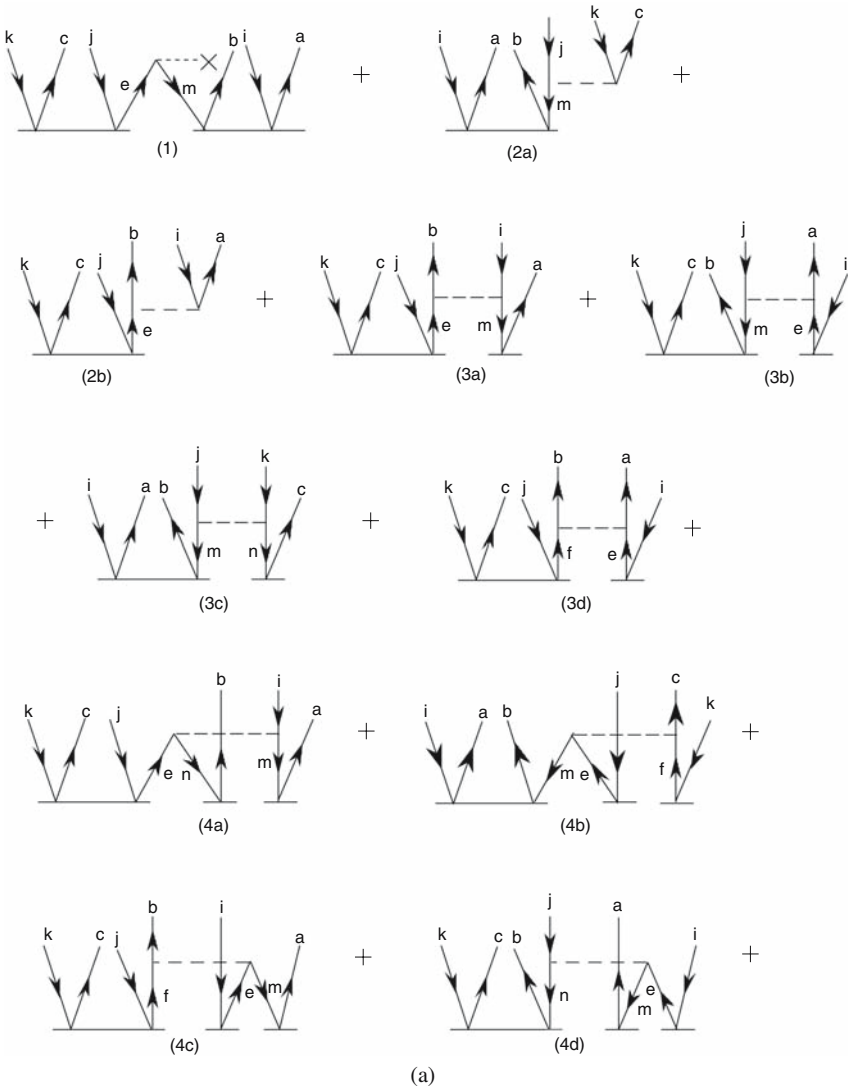

Fig. 24 Diagrammatic representation of $\mathfrak{M}^{ijk}_{0,abc}(2)$

matic form in Fig. 26. Clearly, the diagram A in Fig. 26 is a nonlinear contribution. Hence, diagram A is a good candidate for demonstrating the idea and the benefits of factorization. The cost of evaluating this diagram scales as $\mathcal{N}^5$ with the system size $\mathcal{N}$ or $n_o^2 n_u^3$.

Figure 27 presents the factorization of diagram A and its decomposition, for computational efficiency, into independently calculated parts. After factorization, the original computational cost associated with diagram A, $n_o^2 n_u^3$, is reduced to $n_o n_u^2$ (the

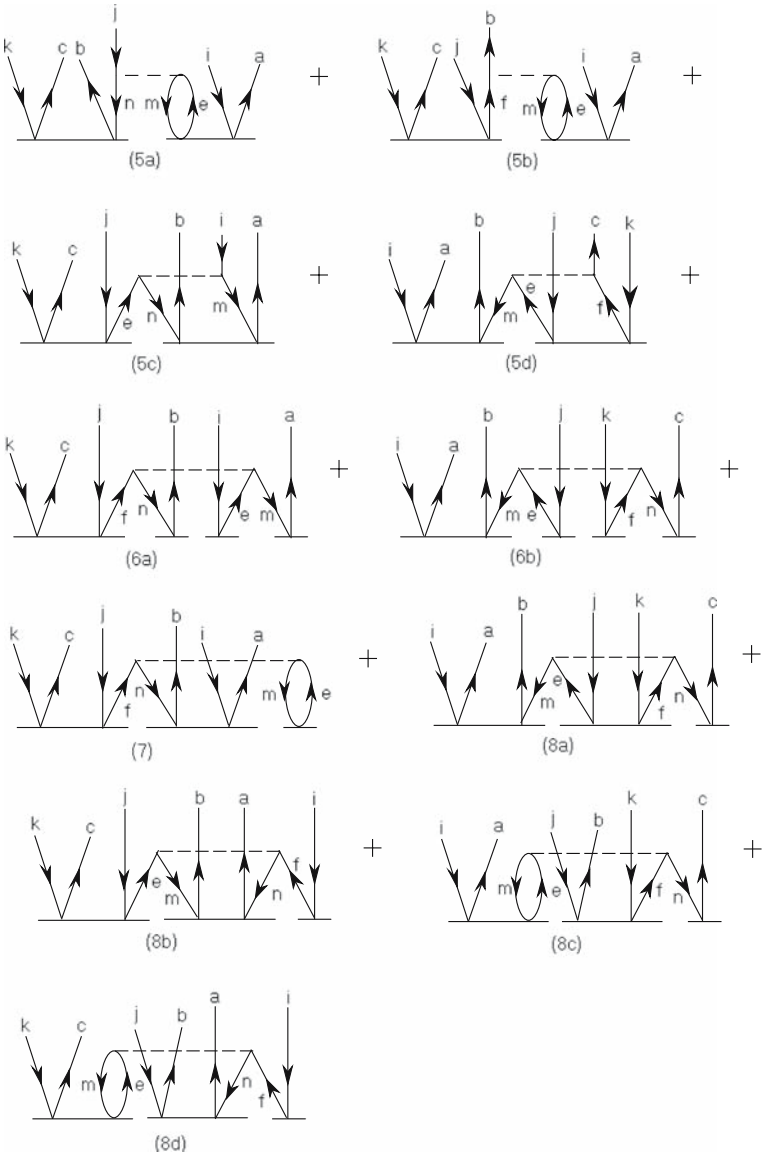

(b)

Fig. 24 (Continued)

cost associated with diagram D) plus $n_o^2 n_u^2$ (the cost associated with the intermediate C which is defined as diagram B). Furthermore, if we realize that the intermediate C actually takes one of the forms of $\bar{H}_1^{(\mathrm{CCSD})}$, which may have been calculated already, we can take advantage of this fact by extending the definition of the above

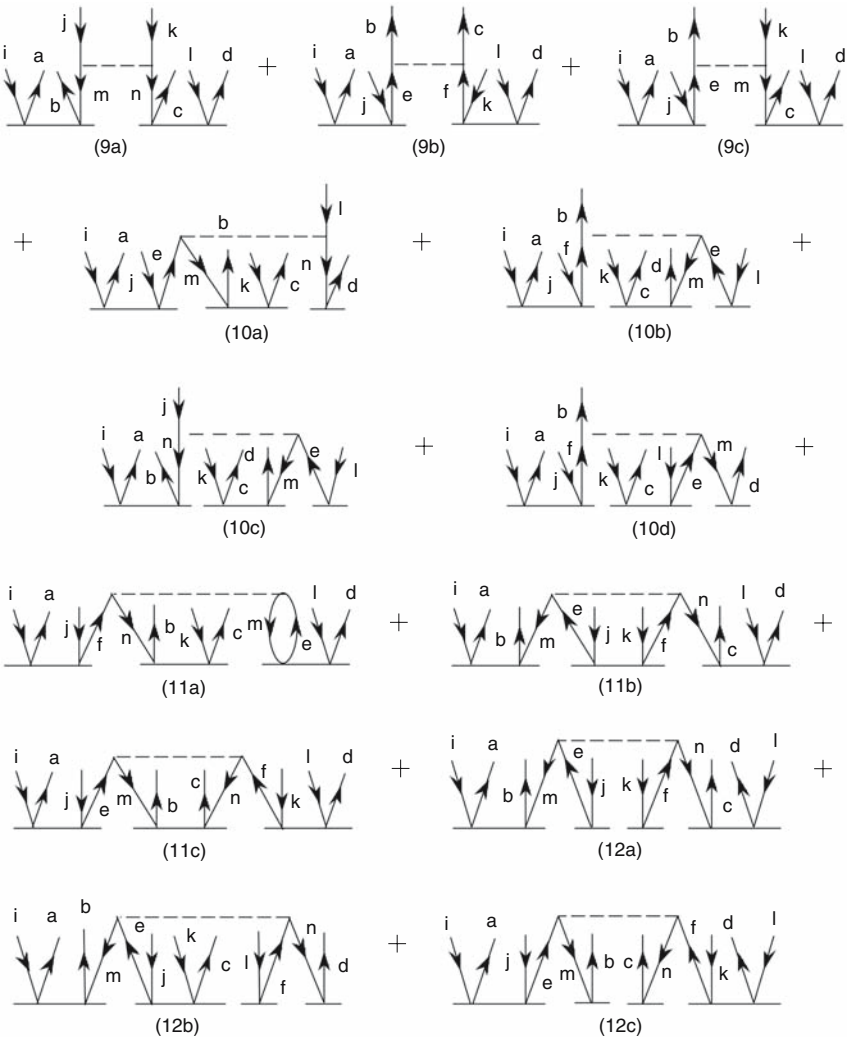

Fig. 25 Diagrammatic representation of $\mathfrak{M}^{ijkl}_{0,abcd}(2)$

intermediate C as one of the one-body components of $\bar{H}_1^{(\mathrm{CCSD})}$, in this case $\bar{h}^b_n$, which is defined in part (a) of Fig. 20. As a result, diagram D, which has initially represented a single diagram A in Fig. 27, becomes now equivalent to

Table 8 Explicit algebraic expressions for the one- and two-body body matrix elements of $\bar{H}^{(\mathrm{CCSD})}$ (designated by $\bar{h}$) shown in Figs. 20–21. The $\bar{h}_a^i$ and $\bar{h}_{ab}^{ij}$ matrix elements are not shown, since they represent the CCSD equations projected on singly and doubly excited determinants, $|\Phi_i^a\rangle$ and $|\Phi_{ij}^{ab}\rangle$, respectively, and, as such, vanish

	Expression[a]	*Figure*
$\bar{h}_i^a$	$f_i^a + v_{im}^{ae} t_e^m$	20 (a)
$\bar{h}_a^b$	$f_a^b + v_{am}^{be} t_e^m - \frac{1}{2} v_{mn}^{eb} t_{ea}^{mn} - v_{mn}^{eb} t_e^m t_a^n - f_m^b t_a^m$	20 (b)
$\bar{h}_i^j$	$f_i^j + v_{im}^{je} t_e^m + \frac{1}{2} v_{mi}^{ef} t_{ef}^{mj} + v_{mi}^{ef} t_e^m t_f^j + f_i^e t_e^j$	20 (c)
$\bar{h}_{ai}^{bc}$	$v_{ai}^{bc} - v_{mi}^{bc} t_a^m$	21 (a)
$\bar{h}_{ij}^{ka}$	$v_{ij}^{ka} + v_{ij}^{ea} t_e^k$	21 (b)
$\bar{h}_{ab}^{cd}$	$v_{ab}^{cd} + \frac{1}{2} v_{mn}^{cd} t_{ab}^{mn} - \mathscr{A}_{ab} v_{am}^{cd} t_b^m + v_{mn}^{cd} t_a^m t_b^n$	21 (c)
$\bar{h}_{ij}^{kl}$	$v_{ij}^{kl} + \frac{1}{2} v_{ij}^{ef} t_{ef}^{kl} + \mathscr{A}^{kl} v_{ij}^{ke} t_e^l + v_{ij}^{ef} t_e^k t_f^l$	21 (d)
$\bar{h}_{jb}^{ia}$	$v_{jb}^{ia} + v_{bj}^{ae} t_e^i - v_{jm}^{ia} t_b^m - v_{mj}^{ae} t_{be}^{mi} - v_{mj}^{ae} t_e^i t_b^m$	21 (e)
$\bar{h}_{ab}^{ic}$	$-f_m^c t_{ab}^{im} + v_{ab}^{ic} + v_{ab}^{ec} t_e^i - \mathscr{A}_{ab} v_{am}^{ic} t_b^m + \mathscr{A}_{ab} v_{mb}^{ec} t_{ae}^{im}$	21 (f)
	$+\frac{1}{2} v_{mn}^{ic} t_{ab}^{mn} + v_{mn}^{ic} t_a^m t_b^n - \mathscr{A}_{ab} v_{am}^{ec} t_e^i t_b^m + v_{mn}^{ec} t_a^m t_e^i t_b^n$	
	$-v_{mn}^{ec} t_e^m t_{ab}^{in} - \mathscr{A}_{ab} v_{mn}^{ec} t_{ae}^{im} t_b^n + \frac{1}{2} v_{mn}^{ec} t_{ab}^{mn} t_e^i$	
$\bar{h}_{ia}^{jk}$	$f_i^e t_{ea}^{jk} + v_{ia}^{jk} - v_{im}^{jk} t_a^m + \mathscr{A}^{jk} v_{ia}^{ek} t_e^j + \mathscr{A}^{jk} v_{im}^{je} t_{ea}^{mk}$	21 (g)
	$+\frac{1}{2} v_{ia}^{fe} t_{fe}^{jk} - \mathscr{A}^{jk} v_{im}^{ek} t_a^m t_e^j + v_{ia}^{fe} t_f^j t_e^k - v_{im}^{fe} t_a^m t_e^k t_f^j$	
	$+v_{im}^{fe} t_e^m t_{fa}^{jk} + \mathscr{A}^{jk} v_{im}^{fe} t_{ea}^{mk} t_f^j - \frac{1}{2} v_{im}^{fe} t_{fe}^{jk} t_a^m$	

[a] Summation over repeated upper and lower indices is assumed; $f_p^q = \langle p|f|q\rangle$ and $v_{pq}^{rs} = \langle pq|v|rs\rangle - \langle pq|v|sr\rangle$ are the one- and two-electron integrals in a molecular spin-orbital basis $\{p\}$ corresponding to the Fock operator (f) and the two-body part of the Hamiltonian (v).

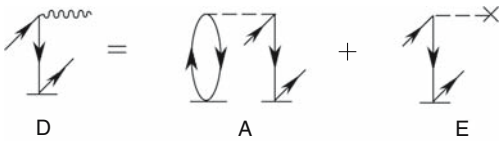

corresponding to diagrams A and E in the original, not factorized, diagrammatic formulation of $\bar{h}_a^b$, shown in Fig. 26. Thus, the fully factorized version of $\bar{h}_a^b$, shown in Fig. 28, uses four diagrams, which are considerably less expensive to calculate than the original five diagrams shown in Fig. 26.

Table 9 Explicit algebraic expressions for the three- and four-body body matrix elements elements of $\bar{H}^{(\mathrm{CCSD})}$ (designated by $\bar{h}$) shown in Figs. 22–23

	Expression[a]	*Figure*
$\bar{h}^{ijd}_{abc}$	$\mathscr{A}_{a/bc} v^{de}_{nm} t^n_c t^m_b t^{ji}_{ea} + \mathscr{A}_{ab/c} \mathscr{A}^{ij} v^{de}_{nm} t^n_c t^j_e t^{mi}_{ba}$	22 (a)
	$-\mathscr{A}_{a/bc} \mathscr{A}^{ij} v^{de}_{nm} t^{jn}_{bc} t^{mi}_{ea} + \frac{1}{2} \mathscr{A}_{a/bc} v^{de}_{nm} t^{nm}_{cb} t^{ji}_{ea}$	
	$+\mathscr{A}_{ab/c} \mathscr{A}^{ij} v^{dj}_{nm} t^n_c t^{mi}_{ba} - \mathscr{A}_{abc} v^{de}_{mb} t^m_c t^{ji}_{ea} - \mathscr{A}_{ac/b} \mathscr{A}^{ij} v^{ed}_{bm} t^j_e t^{mi}_{ca}$	
	$+\mathscr{A}_{a/bc} v^{de}_{cb} t^{ji}_{ea} - \mathscr{A}_{ab/c} \mathscr{A}^{ij} v^{dj}_{cm} t^{mi}_{ba}$	
$\bar{h}^{kji}_{lba}$	$-\mathscr{A}_{ab} \mathscr{A}^{ij/k} v^{fe}_{lm} t^k_f t^m_b t^{ji}_{ea} - \mathscr{A}^{i/jk} v^{fe}_{lm} t^k_f t^j_e t^{mi}_{ba}$	22 (b)
	$+\mathscr{A}_{ab} \mathscr{A}^{i/jk} v^{fe}_{lm} t^{jk}_{bf} t^{mi}_{ea} - \frac{1}{2} \mathscr{A}^{i/jk} v^{fe}_{lm} t^{kj}_{fe} t^{mi}_{ba}$	
	$-\mathscr{A}^{ijk} v^{ej}_{lm} t^k_e t^{mi}_{ba} + \mathscr{A}_{ab} \mathscr{A}^{ij/k} v^{ef}_{bl} t^k_e t^{ji}_{fa}$	
	$-\mathscr{A}_{ab} \mathscr{A}^{ik/j} v^{je}_{ml} t^m_b t^{ki}_{ea} + \mathscr{A}_{ab} \mathscr{A}^{ij/k} v^{ke}_{lb} t^{ji}_{ea} - \mathscr{A}^{i/jk} v^{kj}_{lm} t^{mi}_{ba}$	
$\bar{h}^{dei}_{cba}$	$-\mathscr{A}_{ab/c} v^{ed}_{cm} t^{mi}_{ba} + \mathscr{A}_{ab/c} v^{ed}_{nm} t^n_c t^{mi}_{ba}$	22 (c)
$\bar{h}^{kji}_{mla}$	$\mathscr{A}^{ij/k} v^{ke}_{ml} t^{ji}_{ea} + \mathscr{A}^{ij/k} v^{fe}_{ml} t^k_f t^{ji}_{ea}$	22 (d)
$\bar{h}^{cji}_{bka}$	$\mathscr{A}_{ab} v^{ce}_{bk} t^{ji}_{ea} - \mathscr{A}_{ab} v^{ce}_{mk} t^m_b t^{ji}_{ea}$	22 (e)
	$-\mathscr{A}^{ij} v^{jc}_{km} t^{mi}_{ba} - \mathscr{A}^{ij} v^{ec}_{km} t^j_e t^{mi}_{ba}$	
$\bar{h}^{lkji}_{mcba}$	$-\mathscr{A}_{ab/c} \mathscr{A}^{i/jk/l} v^{le}_{mn} t^{kj}_{ce} t^{ni}_{ba} + \mathscr{A}_{ac/b} \mathscr{A}^{ij/kl} v^{fe}_{mb} t^{ij}_{ae} t^{lk}_{fc}$	23 (a)
	$-\mathscr{A}_{ab/c} \mathscr{A}^{i/jk/l} v^{fe}_{mn} t^l_f t^{kj}_{ce} t^{ni}_{ba} - \mathscr{A}_{ac/b} \mathscr{A}^{ij/kl} v^{fe}_{mn} t^{kl}_{cf} t^n_b t^{ji}_{ea}$	
$\bar{h}^{ekji}_{dcba}$	$-\mathscr{A}_{ab/c/d} \mathscr{A}^{i/jk} v^{ef}_{dm} t^{kj}_{cf} t^{mi}_{ba} + \mathscr{A}_{ab/cd} \mathscr{A}^{ik/j} v^{je}_{mn} t^{im}_{ab} t^{nk}_{dc}$	23 (b)
	$+\mathscr{A}_{ab/c/d} \mathscr{A}^{i/jk} v^{ef}_{nm} t^n_d t^{kj}_{cf} t^{mi}_{ba} + \mathscr{A}_{ab/cd} \mathscr{A}^{ik/j} v^{ef}_{nm} t^{kn}_{cd} t^j_f t^{mi}_{ba}$	
$\bar{h}^{feji}_{dcba}$	$\mathscr{A}_{ad/bc} v^{ef}_{mn} t^{jm}_{bc} t^{ni}_{da}$	23 (c)
$\bar{h}^{lkji}_{nmba}$	$\mathscr{A}^{ik/jl} v^{ef}_{nm} t^{jl}_{be} t^{ki}_{fa}$	23 (d)
$\bar{h}^{dkji}_{lcba}$	$-\mathscr{A}_{ab/c} \mathscr{A}^{i/jk} v^{de}_{lm} t^{kj}_{ce} t^{mi}_{ba}$	23 (e)

[a] Summation over repeated upper and lower indices is assumed; $f^q_p = \langle p|f|q\rangle$ and $v^{rs}_{pq} = \langle pq|v|rs\rangle - \langle pq|v|sr\rangle$ are the one- and two-electron integrals in a molecular spin-orbital basis $\{p\}$ corresponding to the Fock operator (f) and the two-body part of the Hamiltonian (v).

The same factorization and cost reduction procedure can be applied to other components of $\bar{H}^{(\mathrm{CCSD})}$. The computational savings offered by the factorization procedure in the case of the two-body and other many-body components of $\bar{H}^{(\mathrm{CCSD})}$ are even more substantial than in the above example. Figures 29 and 30 show the factorized diagrams of the one- and two-body components of $\bar{H}^{(\mathrm{CCSD})}$, which can be generated in a recursive, fully vectorized (linearized) manner.

Table 10 Explicit algebraic expressions for $\mathfrak{M}^{ijk}_{0,abc}(2)$ obtained by reading the diagrams shown in Fig. 24

Term	*Expression*[a]
1	$-\mathscr{A}_{ab/c}\,\mathscr{A}^{i/jk}\, f^{e}_{m} t^{im}_{ab} t^{jk}_{ec}$
2a	$-\mathscr{A}_{ab/c}\,\mathscr{A}^{i/jk}\, v^{jk}_{mc} t^{im}_{ab}$
2b	$\mathscr{A}_{ab/c}\,\mathscr{A}^{i/jk}\, v^{ie}_{ab} t^{jk}_{ec}$
3a	$-\mathscr{A}_{abc}\,\mathscr{A}^{i/jk}\, v^{ie}_{mb} t^{m}_{a} t^{jk}_{ec}$
3b	$-\mathscr{A}_{a/bc}\,\mathscr{A}^{ijk}\, v^{ej}_{am} t^{i}_{e} t^{mk}_{bc}$
3c	$\mathscr{A}_{ab/c}\,\mathscr{A}^{i/jk}\, v^{jk}_{mn} t^{im}_{ab} t^{n}_{c}$
3d	$\mathscr{A}_{ab/c}\,\mathscr{A}^{i/jk}\, v^{ef}_{ab} t^{i}_{e} t^{jk}_{fc}$
4a	$\mathscr{A}_{ab/c}\,\mathscr{A}^{i/jk}\, v^{ie}_{mn} t^{m}_{a} t^{n}_{b} t^{jk}_{ec}$
4b	$-\mathscr{A}_{ab/c}\,\mathscr{A}^{i/jk}\, v^{ef}_{mc} t^{im}_{ab} t^{j}_{e} t^{k}_{f}$
4c	$-\mathscr{A}_{abc}\,\mathscr{A}^{i/jk}\, v^{fe}_{bm} t^{jk}_{fc} t^{i}_{e} t^{m}_{a}$
4d	$\mathscr{A}_{a/bc}\,\mathscr{A}^{ijk}\, v^{je}_{nm} t^{i}_{e} t^{m}_{a} t^{nk}_{bc}$
5a	$-\mathscr{A}_{a/bc}\,\mathscr{A}^{ijk}\, v^{ej}_{mn} t^{im}_{ae} t^{nk}_{bc}$
5b	$\mathscr{A}_{abc}\,\mathscr{A}^{i/jk}\, v^{ef}_{mb} t^{im}_{ae} t^{jk}_{fc}$
5c	$\frac{1}{2}\,\mathscr{A}_{ab/c}\,\mathscr{A}^{i/jk}\, v^{ie}_{mn} t^{mn}_{ab} t^{jk}_{ec}$
5d	$-\frac{1}{2}\,\mathscr{A}_{ab/c}\,\mathscr{A}^{i/jk}\, v^{ef}_{mc} t^{im}_{ab} t^{jk}_{ef}$
6a	$\mathscr{A}_{ab/c}\,\mathscr{A}^{i/jk}\, v^{ef}_{mn} t^{m}_{a} t^{i}_{e} t^{n}_{b} t^{jk}_{fc}$
6b	$\mathscr{A}_{ab/c}\,\mathscr{A}^{i/jk}\, v^{ef}_{mn} t^{im}_{ab} t^{j}_{e} t^{k}_{f} t^{n}_{c}$
7	$-\mathscr{A}_{ab/c}\,\mathscr{A}^{i/jk}\, v^{ef}_{mn} t^{jk}_{fc} t^{in}_{ab} t^{m}_{e}$
8a	$\frac{1}{2}\,\mathscr{A}_{ab/c}\,\mathscr{A}^{i/jk}\, v^{ef}_{mn} t^{im}_{ab} t^{jk}_{ef} t^{n}_{c}$
8b	$\frac{1}{2}\,\mathscr{A}_{ab/c}\,\mathscr{A}^{i/jk}\, v^{ef}_{mn} t^{jk}_{ec} t^{mn}_{ba} t^{i}_{f}$
8c	$-\mathscr{A}_{abc}\,\mathscr{A}^{i/jk}\, v^{ef}_{mn} t^{im}_{ae} t^{jk}_{bf} t^{n}_{c}$
8d	$-\mathscr{A}_{ab/c}\,\mathscr{A}^{ijk}\, v^{ef}_{mn} t^{i}_{f} t^{nj}_{ab} t^{mk}_{ec}$

[a] Summation over repeated upper and lower indices is assumed; $f^{q}_{p} = \langle p|f|q\rangle$ and $v^{rs}_{pq} = \langle pq|v|rs\rangle - \langle pq|v|sr\rangle$ are the one- and two-electron integrals in a molecular spin-orbital basis $\{p\}$ corresponding to the Fock operator (f) and the two-body part of the Hamiltonian (v).

Table 11 Explicit algebraic expressions for $\mathfrak{M}^{ijkl}_{0,abcd}(2)$ obtained by reading the diagrams shown in Fig. 25

Term	*Expression*[a]
9a	$\mathscr{A}_{ab/cd}\,\mathscr{A}^{jk/il}\,v^{jk}_{mn}\,t^{im}_{ab}\,t^{nl}_{cd}$
9b	$\mathscr{A}_{bc/ad}\,\mathscr{A}^{ij/kl}\,v^{ef}_{bc}\,t^{ij}_{ae}\,t^{kl}_{fd}$
9c	$-\mathscr{A}_{a/b/cd}\,\mathscr{A}^{ij/k/l}\,v^{ek}_{bm}\,t^{ij}_{ae}\,t^{ml}_{cd}$
10a	$\mathscr{A}_{a/bc/d}\,\mathscr{A}^{ij/k/l}\,v^{el}_{mn}\,t^{ij}_{ae}\,t^{mk}_{bc}\,t^{n}_{d}$
10b	$-\mathscr{A}_{a/b/cd}\,\mathscr{A}^{ij/k/l}\,v^{ef}_{mb}\,t^{ij}_{af}\,t^{km}_{cd}\,t^{l}_{e}$
10c	$\mathscr{A}_{ab/cd}\,\mathscr{A}^{ik/j/l}\,v^{ej}_{mn}\,t^{in}_{ab}\,t^{km}_{cd}\,t^{l}_{e}$
10d	$-\mathscr{A}_{ac/b/d}\,\mathscr{A}^{ij/kl}\,v^{ef}_{mb}\,t^{ij}_{af}\,t^{kl}_{ce}\,t^{m}_{d}$
11a	$-\mathscr{A}_{a/bc/d}\,\mathscr{A}^{ij/k/l}\,v^{ef}_{mn}\,t^{ij}_{af}\,t^{nk}_{bc}\,t^{ml}_{ed}$
11b	$\frac{1}{2}\,\mathscr{A}_{ab/cd}\,\mathscr{A}^{il/jk}\,v^{ef}_{mn}\,t^{im}_{ab}\,t^{jk}_{ef}\,t^{nl}_{cd}$
11c	$\frac{1}{2}\,\mathscr{A}_{ad/bc}\,\mathscr{A}^{ij/kl}\,v^{ef}_{mn}\,t^{ij}_{ae}\,t^{mn}_{bc}\,t^{kl}_{fd}$
12a	$\mathscr{A}_{ab/cd}\,\mathscr{A}^{il/jk}\,v^{ef}_{mn}\,t^{im}_{ab}\,t^{j}_{e}\,t^{k}_{f}\,t^{nl}_{cd}$
12b	$\mathscr{A}_{ab/c/d}\,\mathscr{A}^{i/jk/l}\,v^{ef}_{mn}\,t^{im}_{ab}\,t^{jk}_{ec}\,t^{l}_{f}\,t^{n}_{d}$
12c	$\mathscr{A}_{ad/bc}\,\mathscr{A}^{ij/kl}\,v^{ef}_{mn}\,t^{ij}_{am}\,t^{m}_{b}\,t^{n}_{c}\,t^{kl}_{fd}$

[a] Summation over repeated upper and lower indices is assumed; $f^q_p = \langle p|f|q\rangle$ and $v^{rs}_{pq} = \langle pq|v|rs\rangle - \langle pq|v|sr\rangle$ are the one- and two-electron integrals in a molecular spin-orbital basis $\{p\}$ corresponding to the Fock operator (f) and the two-body part of the Hamiltonian (v)

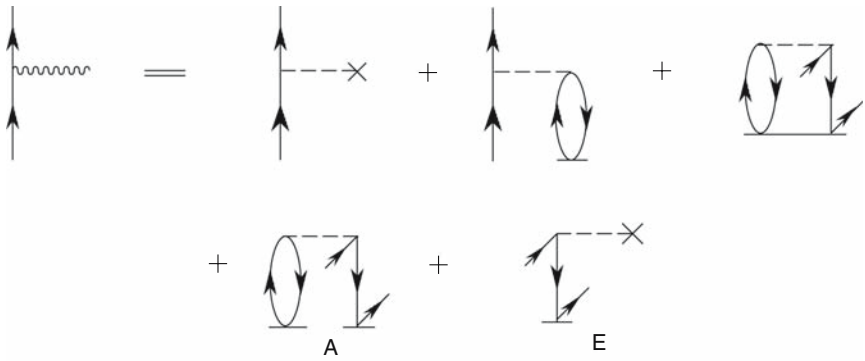

Fig. 26 Diagrammatic representation of $\bar{h}^b_a$

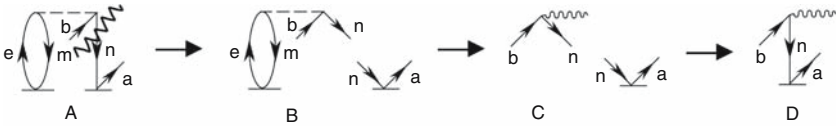

Fig. 27 Example of diagram factorization

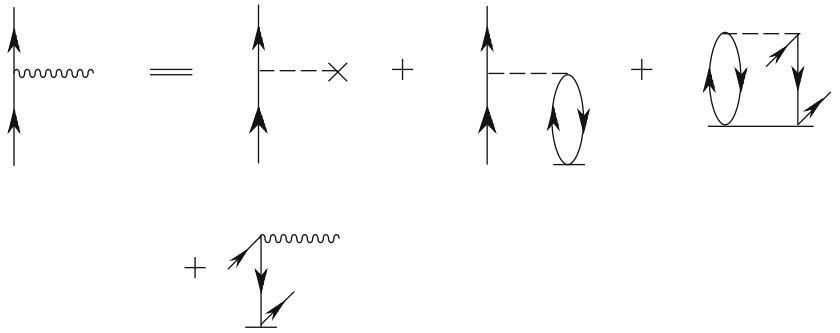

Fig. 28 Fully factorized diagrammatic formulation of $\bar{h}_a^b$

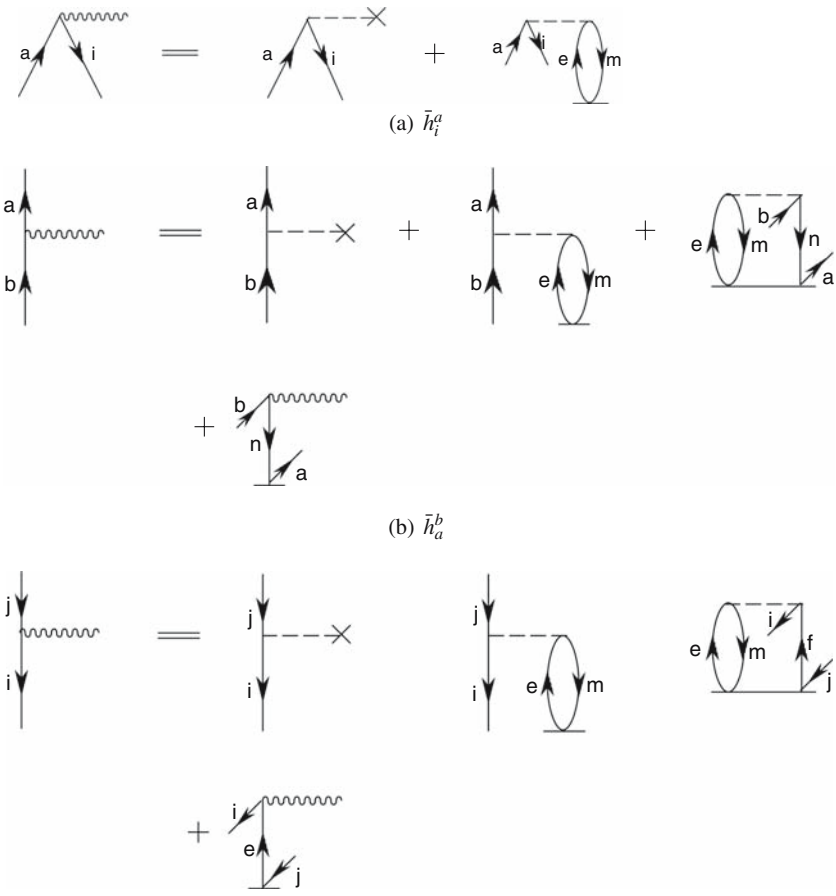

Fig. 29 Factorized one-body components of $\bar{H}^{(\mathrm{CCSD})}$

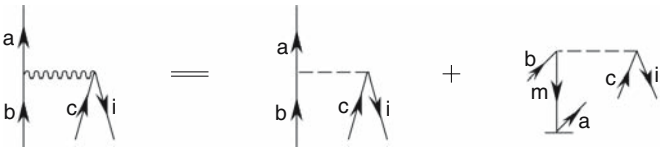

(a) $\bar{h}_{ai}^{bc}$

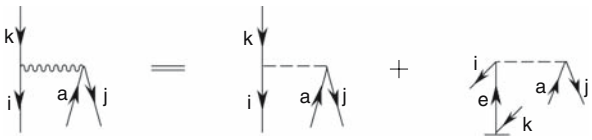

(b) $\bar{h}_{ij}^{ka}$

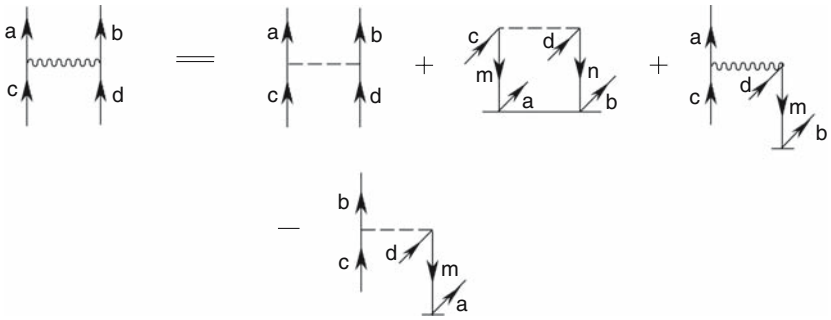

(c) $\bar{h}_{ab}^{cd}$

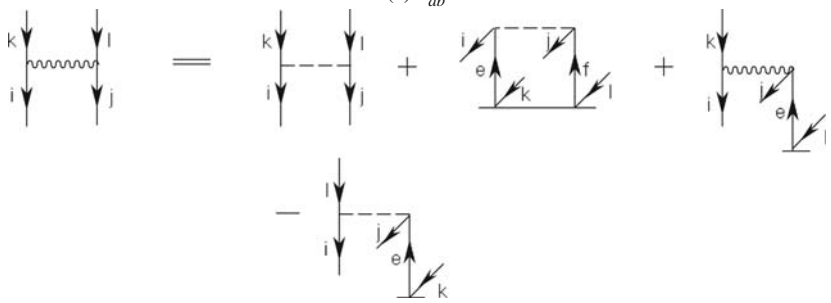

(d) $\bar{h}_{ij}^{kl}$

Fig. 30 Factorized two-body components of $\bar{H}^{(\mathrm{CCSD})}$

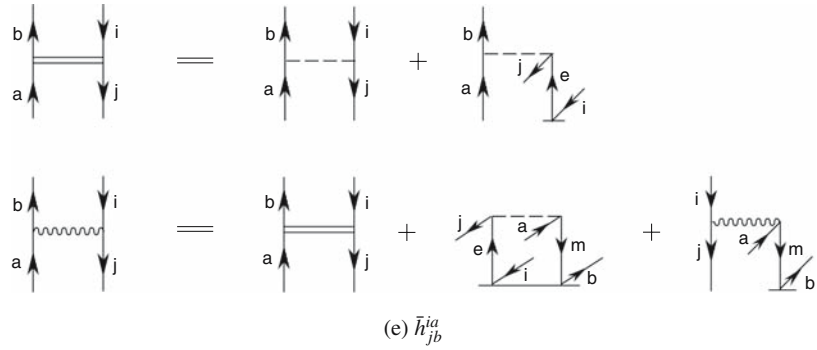

(e) $\bar{h}^{ia}_{jb}$

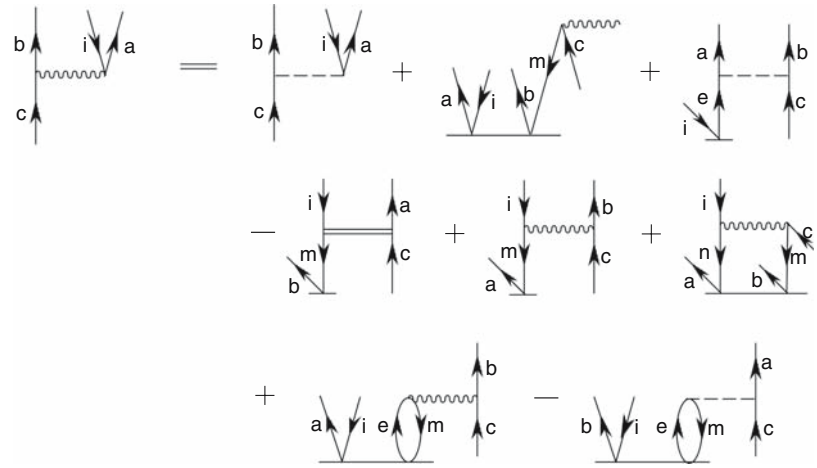

(f) $\bar{h}^{ic}_{ab}$

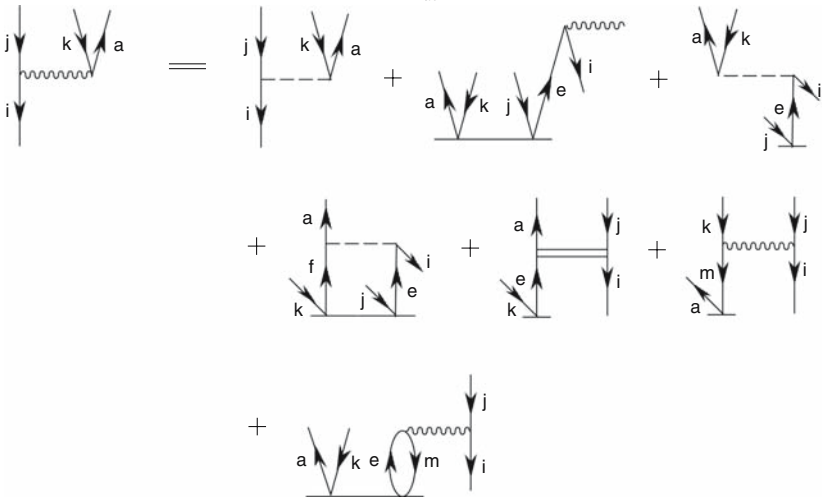

(g) $\bar{h}^{jk}_{ia}$

Fig. 30 (Continued)

References

1. E. Schrödinger, Ann. Phys. **384**, 361, 489, 734 (1926), *ibid.* **385**, 439 (1926)
2. P.A.M. Dirac, Proc. R. Soc. London, Ser. A **123**, 714 (1929)
3. P.O. Löwdin, Phys. Rev. **97**, 1474 (1955)
4. P.O. Löwdin, Phys. Rev. **97**, 1490 (1955)
5. P.O. Löwdin, Phys. Rev. **97**, 1509 (1955)
6. C. Møller, M.S. Plesset, Phys. Rev. **46**, 618 (1934)
7. K.A. Brueckner, Phys. Rev. **97**, 1353 (1955)
8. J. Goldstone, Proc. R. Soc. London, Ser. A **239**, 267 (1957)
9. J. Hubbard, Proc. R. Soc. London, Ser. A **240**, 539 (1957)
10. N.M. Hugenholtz, Physica **23**, 481 (1957)
11. J. Čížek, J. Chem. Phys. **45**, 4256 (1966)
12. J. Čížek, Adv. Chem. Phys. **14**, 35 (1969)
13. J. Čížek, J. Paldus, Int. J. Quantum Chem. **5**, 359 (1971)
14. F. Coester, Nucl. Phys. **7**, 421 (1958)
15. F. Coester, H. Kümmel, Nucl. Phys. **17**, 477 (1960)
16. R.J. Bartlett, J. Phys. Chem. **93**, 1697 (1989)
17. K. Raghavachari, Annu. Rev. Phys. Chem. **42**, 615 (1991)
18. K. Raghavachari, J.B. Anderson, J. Phys. Chem. **100**, 12960 (1996)
19. J. Paldus, in *Methods In Computational Molecular Physics*, *NATO Advanced Study Institute, Series B: Physics*, vol. 293, ed. by S. Wilson, G.H.F. Diercksen (Plenum, New York, 1992), p. 99
20. J. Gauss, in *Encyclopedia of Computational Chemistry*, vol. 1, ed. by P.V.R. Schleyer, N.L. Allinger, T. Clark, J. Gasteiger, P.A. Kollman, H.F. Schaefer III, P.R. Schreiner (Wiley, Chichester, 1998), p. 615
21. J. Paldus, X. Li, Adv. Chem. Phys. **110**, 1 (1999)
22. T.D. Crawford, H.F. Schaefer III, Rev. Comp. Chem. **14**, 33 (2000)
23. J. Paldus, in *Handbook of Molecular Physics and Quantum Chemistry*, vol. 2, ed. by S. Wilson (Wiley, Chichester, 2003), p. 272
24. G.D. Purvis III, R.J. Bartlett, J. Chem. Phys. **76**, 1910 (1982)
25. G.E. Scuseria, A.C. Scheiner, T.J. Lee, J.E. Rice, H.F. Schaefer III, J. Chem. Phys. **86**, 2881 (1987)
26. P. Piecuch, J. Paldus, Int. J. Quantum Chem. **36**, 429 (1989)
27. J. Noga, R.J. Bartlett, J. Chem. Phys. **86**, 7041 (1987), *ibid.* **89**, 3401 (1988) [Erratum]
28. G.E. Scuseria, H.F. Schaefer III, Chem. Phys. Lett. **152**, 382 (1988)
29. S.A. Kucharski, R.J. Bartlett, Theor. Chim. Acta **80**, 387 (1991)
30. S.A. Kucharski, R.J. Bartlett, J. Chem. Phys. **97**, 4282 (1992)
31. N. Oliphant, L. Adamowicz, J. Chem. Phys. **94**, 1229 (1991), *ibid.* **96**, 3739 (1992), *Int. Rev. Phys. Chem.* **12**, 339 (1993)
32. P. Piecuch, L. Adamowicz, J. Chem. Phys. **100**, 5792 (1994)
33. K. Raghavachari, G.W. Trucks, J.A. Pople, M. Head-Gordon, Chem. Phys. Lett. **157**, 479 (1989)
34. M. Urban, J. Noga, S.J. Cole, R.J. Bartlett, J. Chem. Phys. **83**, 4041 (1985)
35. P. Piecuch, J. Paldus, Theor. Chim. Acta **78**, 65 (1990)
36. K.B. Ghose, P. Piecuch, L. Adamowicz, J. Chem. Phys. **103**, 9331 (1995)
37. P. Piecuch, L. Adamowicz, J. Chem. Phys. **102**, 898 (1995)
38. P. Piecuch, A.E. Kondo, V. Špirko, J. Paldus, J. Chem. Phys. **104**, 4716 (1996)
39. P. Piecuch, K. Kowalski, in *Computational Chemistry: Reviews of Current Trends*, vol. 5, ed. by J. Leszczyński (World Scientific, Singapore, 2000), p. 1
40. K. Kowalski, P. Piecuch, J. Chem. Phys. **113**, 18 (2000)
41. K. Kowalski, P. Piecuch, J. Chem. Phys. **113**, 5644 (2000)
42. K. Kowalski, P. Piecuch, Chem. Phys. Lett. **344**, 165 (2001)
43. P. Piecuch, S.A. Kucharski, K. Kowalski, Chem. Phys. Lett. **344**, 176 (2001)

44. P. Piecuch, S.A. Kucharski, V. Špirko, K. Kowalski, J. Chem. Phys. **115**, 5796 (2001)
45. M.J. McGuire, K. Kowalski, P. Piecuch, J. Chem. Phys. **117**, 3617 (2002)
46. P. Piecuch, S.A. Kucharski, K. Kowalski, M. Musiał, Comp. Phys. Commun. **149**, 71 (2003)
47. I.S.O. Pimienta, K. Kowalski, P. Piecuch, J. Chem. Phys. **119**, 2951 (2003)
48. M.J. McGuire, P. Piecuch, K. Kowalski, S.A. Kucharski, M. Musiał, J. Phys. Chem. A **108**, 8878 (2004)
49. S. Hirata, P.D. Fan, A.A. Auer, M. Nooijen, P. Piecuch, J. Chem. Phys. **121**, 12197 (2004)
50. P.D. Fan, K. Kowalski, P. Piecuch, Mol. Phys. **103**, 2191 (2005)
51. K. Kowalski, P. Piecuch, J. Chem. Phys. **122**, 074107 (2005)
52. C.D. Sherrill, P. Piecuch, J. Chem. Phys. **122**, 124104 (2005)
53. P. Piecuch, M. Włoch, J. Chem. Phys. **123**, 224105 (2005)
54. P. Piecuch, M. Włoch, J.R. Gour, A. Kinal, Chem. Phys. Lett. **418**, 467 (2006)
55. M. Włoch, M.D. Lodriguito, P. Piecuch, J.R. Gour, Mol. Phys. **104**, 2149 (2006)
56. M.D. Lodriguito, K. Kowalski, M. Włoch, P. Piecuch, J. Mol. Struct.: THEOCHEM **771**, 89 (2006)
57. M. Włoch, J.R. Gour, P. Piecuch, J. Phys. Chem. A **111**, 11359 (2007)
58. Y. Ge, M.S. Gordon, P. Piecuch, J. Chem. Phys. **127**, 174106 (2007)
59. P. Piecuch, M. Włoch, A.J.C. Varandas, Theor. Chem. Acc. **120**, 59 (2008)
60. P. Piecuch, K. Kowalski, I.S.O. Pimienta, S.A. Kucharski, in *Low-Lying Potential Energy Surfaces*, vol. 828, ed. by M.R. Hoffmann, K.G. Dyall (American Chemical Society, Washington, DC, 2002), p. 31
61. P. Piecuch, K. Kowalski, I.S.O. Pimienta, M.J. McGuire, Int. Rev. Phys. Chem. **21**, 527 (2002)
62. P. Piecuch, K. Kowalski, I.S.O. Pimienta, P.D. Fan, M. Lodriguito, M.J. McGuire, S.A. Kucharski, T. Kuś, M. Musiał, Theor. Chem. Acc. **112**, 349 (2004)
63. P. Piecuch, K. Kowalski, P.D. Fan, I.S.O. Pimienta, in *Advanced Topics in Theoretical Chemical Physics*, *Progress in Theoretical Chemistry and Physics*, vol. 12, ed. by J. Maruani, R. Lefebvre, E. Brändas (Kluwer, Dordrecht, The Netherlands, 2003), p. 119
64. P. Piecuch, M. Włoch, M.D. Lodriguito, J.R. Gour, in *Recent Advances in the Theory of Chemical and Physical Sciences*, *Progress in Theoretical Chemistry and Physics*, vol. 15, ed. by J.P. Julien, J. Maruani, D. Mayou, S. Wilson, G. Delgado-Barrio (Springer, Berlin, 2006), p. 45
65. P. Piecuch, M. Włoch, A.J.C. Varandas, in *Topics in the Theory of Chemical and Physical Systems*, *Progress in Theoretical Chemistry and Physics*, vol. 16, ed. by S. Lahmar, J. Maruani, S. Wilson, G. Delgado-Barrio (Springer, Berlin, 2007), p. 65
66. P. Piecuch, S.A. Kucharski, R.J. Bartlett, J. Chem. Phys. **110**, 6103 (1999)
67. P. Piecuch, S.A. Kucharski, V. Špirko, J. Chem. Phys. **111**, 6679 (1999)
68. S.A. Kucharski, R.J. Bartlett, J. Chem. Phys. **108**, 9221 (1998)
69. H. Monkhorst, Int. J. Quantum Chem. Symp. **S11**, 421 (1977)
70. D. Mukherjee and P.K. Mukherjee, Chem. Phys. **39**, 325 (1979)
71. H. Sekino, R.J. Bartlett, Int. J. Quantum Chem. Symp. **S18**, 255 (1984)
72. E. Dalgaard, H.J. Monkhorst, Phys. Rev. A **28**, 1217 (1983)
73. M. Takahashi, J. Paldus, J. Chem. Phys. **85**, 1486 (1986)
74. H. Koch, H.J.A. Jensen, P. Jørgensen, T. Helgaker, J. Chem. Phys. **93**, 3345 (1990)
75. H. Koch, P. Jørgensen, J. Chem. Phys. **93**, 3333 (1990)
76. K. Emrich, Nucl. Phys. A **351**, 379 (1981)
77. J. Geertsen, C.M.L. Rittby, R.J. Bartlett, Chem. Phys. Lett. **164**, 57 (1989)
78. D.C. Comeau, R.J. Bartlett, Chem. Phys. Lett. **207**, 414 (1993)
79. J.F. Stanton, R.J. Bartlett, J. Chem. Phys. **98**, 7029 (1993)
80. P. Piecuch, R.J. Bartlett, Adv. Quantum Chem. **34**, 295 (1999)
81. H. Nakatsuji, K. Hirao, Chem. Phys. Lett. **47**, 569 (1977)
82. H. Nakatsuji, K. Hirao, J. Chem. Phys. **68**, 2053 (1978), *ibid.* **68**, 4279 (1978)
83. H. Nakatsuji, Chem. Phys. Lett. **59**, 362 (1978)
84. H. Nakatsuji, Chem. Phys. Lett. **67**, 329 (1979), *ibid.* **67**, 334 (1979)

85. H. Nakatsuji, in *Computational Chemistry: Reviews of Current Trends*, vol. 2, ed. by J. Leszczyński (World Scientific, Singapore, 1997), p. 62
86. O. Christiansen, H. Koch, P. Jørgensen, J. Olsen, Chem. Phys. Lett. **256**, 185 (1996)
87. J.D. Watts, R.J. Bartlett, Chem. Phys. Lett. **233**, 81 (1995)
88. J.D. Watts, R.J. Bartlett, Chem. Phys. Lett. **258**, 581 (1996)
89. J.D. Watts, R.J. Bartlett, J. Chem. Phys. **101**, 3073 (1994)
90. H. Koch, O. Christiansen, P. Jørgensen, J. Olsen, Chem. Phys. Lett. **244**, 75 (1995)
91. O. Christiansen, H. Koch, P. Jørgensen, J. Chem. Phys. **103**, 7429 (1995)
92. O. Christiansen, H. Koch, P. Jørgensen, J. Chem. Phys. **105**, 1451 (1996)
93. K. Kowalski, P. Piecuch, J. Chem. Phys. **113**, 8490 (2000)
94. K. Kowalski, P. Piecuch, J. Chem. Phys. **115**, 643 (2001)
95. K. Kowalski, P. Piecuch, Chem. Phys. Lett. **347**, 237 (2001)
96. K. Kowalski, P. Piecuch, J. Chem. Phys. **115**, 2966 (2001)
97. K. Kowalski, P. Piecuch, J. Chem. Phys. **116**, 7411 (2002)
98. K. Kowalski, P. Piecuch, J. Chem. Phys. **120**, 1715 (2004)
99. M. Włoch, J.R. Gour, K. Kowalski, P. Piecuch, J. Chem. Phys. **122**, 214107 (2005)
100. S. Hirata, J. Chem. Phys. **121**, 51 (2004)
101. S.A. Kucharski, M. Włoch, M. Musiał, R.J. Bartlett, J. Chem. Phys. **115**, 8263 (2001)
102. M. Kállay, J. Gauss, J. Chem. Phys. **121**, 9257 (2004)
103. H. Larsen, J. Olsen, P. Jørgensen, O. Christiansen, J. Chem. Phys. **113**, 6677 (2000), *ibid.* **114**, 10985 (2001) [Erratum]
104. I. Shavitt, in *Methods of Electronic Structure*, *Modern Theoretical Chemistry*, vol. 3, ed. by H.F. Schaefer III (Plenum, New York, 1977), p. 189
105. R. McWeeny, in *Molecular Quantum Mechanics*, 2nd edn. (Academic, New York, 1989)
106. R. Sheppard, I. Shavitt, R.M. Pitzer, D.C. Comeau, M. Pepper, H. Lischka, P.G. Szalay, R. Ahlrichs, R.B. Brown, J. Zhao, Int. J. Quantum Chem. Symp. **S22**, 149 (1988)
107. E.R. Davidson, in *The World of Quantum Chemistry*, ed. by R. Daudel, B. Pullman (Reidel, Dordrecht, Boston, 1974), p. 17
108. S.R. Langhoff, E.R. Davidson, Int. J. Quantum Chem. **8**, 61 (1974)
109. W. Butscher, S.K. Shih, R.J. Buenker, S.D. Peyerimhoff, Chem. Phys. Lett. **52**, 457 (1977)
110. K. Jankowski, L. Meissner, J. Wasilewski, Int. J. Quantum Chem. **28**, 931 (1985)
111. J. Paldus, in *New Horizons of Quantum Chemistry*, ed. by P.O. Löwdin, B. Pullman (Reidel, Dordrecht, 1983), p. 31
112. P.J. Bruna, S.D. Peyerimhoff, Adv. Chem. Phys. **67**, 1 (1987)
113. R.J. Gdanitz, R. Ahlrichs, Chem. Phys. Lett. **143**, 413 (1988)
114. P.G. Szalay, R.J. Bartlett, J. Chem. Phys. **103**, 3600 (1995)
115. P.G. Szalay, R.J. Bartlett, Chem. Phys. Lett. **214**, 481 (1993)
116. L. Füsti-Molnár, P.G. Szalay, Chem. Phys. Lett. **258**, 400 (1996)
117. J.P. Daudey, J.L. Heully, J.P. Malrieu, J. Chem. Phys. **99**, 1240 (1993)
118. J.P. Malrieu, J.P. Daudey, J. Chem. Phys. **101**, 8908 (1994)
119. P.J.A. Ruttink, J.H. van Lenthe, R. Zwaans, G. Groenenboom, J. Chem. Phys. **94**, 7212 (1991)
120. H.J. Werner, P.J. Knowles, J. Chem. Phys. **89**, 5803 (1988)
121. P.J. Knowles, H.J. Werner, Chem. Phys. Lett. **145**, 514 (1988)
122. A.J. Dobbyn, P.J. Knowles, R.J. Harrison, J. Comput. Chem. **19**, 1215 (1998)
123. P. Stampfuss, W. Wenzel, H. Keiter, J. Comput. Chem. **20**, 1559 (1999)
124. M. Schüler, T. Konvar, H. Lishka, R. Shepard, R.J. Harrison, Theor. Chim. Acta **84**, 489 (1993)
125. H. Dachsel, H. Lischka, R. Shepard, J. Nieplocha, R.J. Harrison, J. Comput. Chem. **18**, 430 (1997)
126. H. Dachsel, R.J. Harrison, D.A. Dixon, J. Phys. Chem. **103**, 152 (1999)
127. F. Stephan, W. Wenzel, J. Chem. Phys. **108**, 1015 (1998)
128. B. Suo, G. Zhai, Y. Wang, Z. Wen, X. Hu, L. Li, J. Comput. Chem. **26**, 88 (2004)
129. B.H. Brandow, Rev. Mod. Phys. **39**, 771 (1967)
130. I. Lindgren, J. Phys. B: Atom. Molec. Phys. **7**, 2441 (1974)

131. P. Durand, J.P. Malrieu, Adv. Chem. Phys. **67**, 321 (1987)
132. J.J.W. McDouall, K. Peasley, M.A. Robb, Chem. Phys. Lett. **148**, 183 (1988)
133. R.K. Chaudhuri, K.F. Freed, G. Hose, P. Piecuch, K. Kowalski, M. Włoch, S. Chattopadhyay, D. Mukherjee, Z. Rolik, Á. Szabados, G. Tóth, P.R. Surján, J. Chem. Phys. **122**, 134105 (2005)
134. P.M. Kozlowski, E.R. Davidson, J. Chem. Phys. **100**, 3672 (1994), *Chem. Phys. Lett.* **222**, 615 (1994)
135. J.P. Finley, J. Chem. Phys. **108**, 1081 (1998)
136. J.P. Finley, H.A. Witek, J. Chem. Phys. **112**, 3958 (2000)
137. K.F. Freed, in *Lecture Notes in Chemistry*, vol. 52 (Springer, Berlin, 1989), p. 1, and references therein
138. K. Andersson, P.A. Malmqvist, B.O. Roos, A.J. Sadlej, K. Wolinski, J. Phys. Chem. **94**, 5483 (1990)
139. K. Andersson, P.A. Malmqvist, B.O. Roos, J. Chem. Phys. **96**, 1218 (1992)
140. K. Hirao, Chem. Phys. Lett. **190**, 374 (1992), *ibid.* **196**, 397 (1992), *ibid.* **201**, 59 (1993)
141. P. Celani, H.J. Werner, J. Chem. Phys. **112**, 5546 (2000)
142. K. Hirao, Int. J. Quantum Chem. Symp. **S26**, 517 (1992), and references therein.
143. R.B. Murphy, R.P. Messmer, Chem. Phys. Lett. **183**, 443 (1991)
144. R.B. Murphy, R.P. Messmer, J. Chem. Phys. **97**, 4170 (1992)
145. M. Sejpal, R.P. Messmer, J. Chem. Phys. **114**, 4796 (2001)
146. K. Wolinski, P. Pulay, J. Chem. Phys. **90**, 3647 (1989)
147. R.B. Murphy, W.T. Pollard, R.A. Friesner, J. Chem. Phys. **106**, 5073 (1997)
148. M.R. Hoffmann, Chem. Phys. Lett. **195**, 127 (1992)
149. H. Nakano, J. Chem. Phys. **99**, 7983 (1993)
150. C. Angeli, R. Cimiraglia, S. Evangelisti, T. Leininger, J.P. Malrieu, J. Chem. Phys. **114**, 10252 (2001)
151. C. Angeli, R. Cimiraglia, J.P. Malrieu, J. Chem. Phys. **117**, 9138 (2002)
152. U.S. Mahapatra, B. Datta, D. Mukherjee, Chem. Phys. Lett. **299**, 42 (1999), J. Phys. Chem. A **103**, 1822 (1999)
153. P. Ghosh, S. Chattopadhyay, D. Jana, D. Mukherjee, Int. J. Mol. Sci. **3**, 733 (2002)
154. Z. Rolik, Á. Szabados, P.R. Surján, J. Chem. Phys. **119**, 1922 (2003)
155. P.R. Surján, Á. Szabados, in *Fundamental World of Quantum Chemistry, A Tribute to the Memory of Per-Olov Löwdin*, vol. III, ed. by E.J. Brändas, E.S. Kryachko (Kluwer, Dordrecht, 2004), p. 129
156. G. Hose, Theor. Chim. Acta **72**, 303 (1987)
157. J.P. Malrieu, P. Durand, J.P. Daudey, J. Phys. A: Math. Gen. **18**, 809 (1985)
158. H. Nakano, H. Hirao, Bull. Korean Chem. Soc. **24**, 812 (2003)
159. K. Wolinski, H.L. Sellers, P. Pulay, Chem. Phys. Lett. **140**, 225 (1987)
160. B.O. Roos, K. Andersson, M.P. Fülscher, P.A. Malmqvist, L. Serrano-Andrés, K. Pierloot, M. Merchán, Adv. Chem. Phys. **93**, 219 (1996), and references therein
161. C. Murray, E.R. Davidson, Chem. Phys. Lett. **187**, 451 (1991)
162. C.J. Cramer, M. Włoch, P. Piecuch, L. Gagliardi, J. Phys. Chem. A **110**, 1991 (2006)
163. C.J. Cramer, A. Kinal, M. Włoch, P. Piecuch, L. Gagliardi, J. Phys. Chem. A **110**, 11557 (2006)
164. M. Rode, H.J. Werner, Theor. Chem. Acc. **114**, 309 (2005)
165. J. Rintelman, I. Adamovic, S. Varganov, M.S. Gordon, J. Chem. Phys. **122**, 044105 (2005)
166. T.H. Schucan, H.A. Weidenmüller, Ann. Phys. **73**, 108 (1972)
167. G. Hose, U. Kaldor, J. Phys. B: Atom. Molec. Phys. **12**, 3827 (1979)
168. J.P. Finley, R.K. Chaudhuri, K. Freed, J. Chem. Phys. **103**, 4990 (1995)
169. I. Lindgren, Int. J. Quantum Chem. Symp. **12**, 33 (1978)
170. D. Mukherjee, R.K. Moitra, A. Mukhopadhyay, Mol. Phys. **30**, 1861 (1975), *ibid.* **33**, 955 (1977)
171. I. Lindgren, D. Mukherjee, Phys. Rep. **151**, 93 (1987)
172. D. Mukherjee, S. Pal, Adv. Quantum. Chem. **20**, 291 (1989)
173. B. Jeziorski, H.J. Monkhorst, Phys. Rev. A **24**, 1668 (1981)

174. B. Jeziorski, J. Paldus, J. Chem. Phys. **88**, 5673 (1988)
175. A. Balková, S.A. Kucharski, L. Meissner, R.J. Bartlett, Theor. Chim. Acta **80**, 335 (1991)
176. J. Paldus, L. Pylypow, B. Jeziorski, in *Many-Body Methods in Quantum Chemistry*, *Lecture Notes in Chemistry*, vol. 52, ed. by U. Kaldor (Springer, Berlin, 1989), p. 151
177. P. Piecuch, J. Paldus, Theor. Chim. Acta **83**, 69 (1992)
178. P. Piecuch, J. Paldus, J. Chem. Phys. **101**, 5875 (1994)
179. J. Paldus, B. Jeziorski, L. Pylypow, in *Recent Progress in Many-Body Theories*, vol. 3, ed. by T.L. Ainsworth, C.E. Campbell, B.E. Clemens, E. Krotschek (Plenum, New York, 1992), p. 287
180. J. Paldus, P. Piecuch, L. Pylypow, B. Jeziorski, Phys. Rev. A **47**, 2738 (1993)
181. P. Piecuch, J. Paldus, Phys. Rev. A **49**, 3479 (1993)
182. P. Piecuch, R. Toboła, J. Paldus, Chem. Phys. Lett. **210**, 243 (1993)
183. U.S. Mahapatra, B. Datta, B. Bandyopadhyay, D. Mukherjee, Adv. Quantum Chem. **30**, 169 (1998)
184. U.S. Mahapatra, B. Datta, D. Mukherjee, J. Chem. Phys. **110**, 6171 (1999)
185. P. Mach, J. Mášik, J. Urban, I. Hubač, Mol. Phys. **94**, 173 (1998)
186. J. Mášik, I. Hubač, Adv. Quantum Chem. **31**, 75 (1999)
187. J. Pittner, P. Nachtigall, P. Čársky, J. Mášik, I. Hubač, J. Chem. Phys. **110**, 10275 (1999)
188. I. Hubač, J. Pittner, P. Čársky, J. Chem. Phys. **112**, 8779 (2000)
189. I. Hubač, P. Mach, S. Wilson, Int. J. Quantum Chem. **104**, 387 (2005)
190. O. Demel, J. Pittner, J. Chem. Phys. **124**, 144112 (2006)
191. P. Piecuch, N. Oliphant, L. Adamowicz, J. Chem. Phys. **99**, 1875 (1993)
192. J.R. Gour, P. Piecuch, M. Włoch, J. Chem. Phys. **123**, 134113 (2005)
193. J.R. Gour, P. Piecuch, M. Włoch, Int. J. Quantum Chem. **106**, 2854 (2006)
194. J.R. Gour, P. Piecuch, J. Chem. Phys. **125**, 234107 (2006)
195. K. Kowalski, P. Piecuch, Phys. Rev. A **61**, 052506 (2000)
196. X. Li, J. Paldus, J. Chem. Phys. **119**, 5320 (2003)
197. X. Li, J. Paldus, J. Chem. Phys. **119**, 5334 (2003)
198. X. Li, J. Paldus, J. Chem. Phys. **119**, 5346 (2003)
199. X. Li, J. Paldus, J. Chem. Phys. **119**, 5890 (2003)
200. K. Kowalski, P. Piecuch, Chem. Phys. Lett. **334**, 89 (2001)
201. K. Kowalski, P. Piecuch, J. Mol. Struc.: THEOCHEM **547**, 191 (2001)
202. P. Piecuch, K. Kowalski, Int. J. Mol. Sci **3**, 676 (2002)
203. K. Kowalski, P. Piecuch, Mol. Phys. **104**, 2425 (2004)
204. F.A. Evangelista, W.D. Allen, H.F. Schaefer III, J. Chem. Phys. **127**, 024102 (2007)
205. S.R. Gwaltney, M. Head-Gordon, Chem. Phys. Lett. **323**, 21 (2000)
206. S.R. Gwaltney, C.D. Sherrill, M. Head-Gordon, A.I. Krylov, J. Chem. Phys. **113**, 3548 (2000)
207. S.R. Gwaltney, M. Head-Gordon, J. Chem. Phys. **115**, 2014 (2001)
208. S.R. Gwaltney, E.F.C. Byrd, T. Van Voorhis, M. Head-Gordon, Chem. Phys. Lett. **353**, 359 (2002)
209. M. Head-Gordon, T. Van Voorhis, S.R. Gwaltney, E.F.C. Byrd, in *Low-Lying Potential Energy Surfaces*, vol. 828, ed. by M.R. Hoffmann, K.G. Dyall (American Chemical Society, Washington, DC, 2002), p. 93
210. A.I. Krylov, Chem. Phys. Lett. **338**, 375 (2001)
211. A.I. Krylov, C.D. Sherrill, J. Chem. Phys. **116**, 3194 (2002)
212. L.V. Slipchenko, A.I. Krylov, J. Chem. Phys. **117**, 4694 (2002)
213. İ. Özkan, A. Kinal, M. Balci, J. Phys. Chem. A **108**, 507 (2004)
214. A. Kinal, P. Piecuch, J. Phys. Chem. A **110**, 367 (2006)
215. S. Coussan, Y. Ferro, A. Trivella, M. Rajzmann, P. Roubin, R. Wieczorek, C. Manca, P. Piecuch, K. Kowalski, M. Włoch, S.A. Kucharski, M. Musiał, J. Phys. Chem. A **110**, 3920 (2006)
216. M. McGuire, P. Piecuch, J. Am. Chem. Soc. **127**, 2608 (2005)
217. A. Kinal, P. Piecuch, J. Phys. Chem. A **111**, 734 (2007)
218. M.Z. Zgierski, S. Patchkovskii, E.C. Lim, Can. J. Chem. **85**, 124 (2007)
219. M.Z. Zgierski, S. Patchkovskii, E.C. Lim, J. Chem. Phys. **123**, 081101 (2005)

220. M.Z. Zgierski, S. Patchkovskii, T. Fujiwara, E.C. Lim, J. Phys. Chem. A **109**, 9384 (2005)
221. D.M. Chipman, J. Chem. Phys. **124**, 044305 (2006)
222. S. Tokura, K. Yagi, T. Tsuneda, K. Hirao, Chem. Phys. Lett. **436**, 30 (2007)
223. P.V. Avramov, I. Adamowic, K.M. Ho, C.Z. Wang, W.C. Lu, M.S. Gordon, J. Phys. Chem. A **109**, 6294 (2005)
224. M. Nooijen, R.J. LeRoy, J. Mol. Struct.: THEOCHEM **768**, 25 (2006)
225. M.I.M. Sarker, C.S. Kim, C.H. Choi, Chem. Phys. Lett. **411**, 297 (2005)
226. S. Nangia, D.G. Truhlar, M.J. McGuire, P. Piecuch, J. Phys. Chem. A **109**, 11643 (2005)
227. K. Kowalski, H. Hirata, M. Włoch, P. Piecuch, T.L. Windus, J. Chem. Phys. **123**, 074319 (2005)
228. P. Piecuch, S. Hirata, K. Kowalski, P.D. Fan, T.L. Windus, Int. J. Quantum Chem **106**, 79 (2006)
229. P. Piecuch, L. Adamowicz, Chem. Phys. Lett. **221**, 121 (1994)
230. K.B. Ghose, L. Adamowicz, J. Chem. Phys. **103**, 9324 (1995)
231. L. Adamowicz, P. Piecuch, K.B. Ghose, Mol. Phys. **94**, 225 (1998)
232. L. Adamowicz, J.-P. Malrieu, V.V. Ivanov, J. Chem. Phys. **112**, 10075 (2000)
233. V.V. Ivanov, L. Adamowicz, J. Chem. Phys. **112**, 9258 (2000)
234. D.I. Lyakh, V.V. Ivanov, L. Adamowicz, J. Chem. Phys. **122**, 024108 (2005)
235. J. Olsen, J. Chem. Phys. **113**, 7140 (2000)
236. J.W. Krogh, J. Olsen, Chem. Phys. Lett. **344**, 578 (2001)
237. A. Kohn, J. Olsen, J. Chem. Phys. **125**, 174110 (2006)
238. M. Kállay, P.G. Szalay, P. G. Surján, J. Chem. Phys. **117**, 980 (2002)
239. P.-D. Fan, S. Hirata, J. Chem. Phys. **124**, 104108 (2006)
240. P.-D. Fan, M. Kamiya, S. Hirata, J. Chem. Theory Comp. **3**, 1036 (2007)
241. L.V. Slipchenko, A.I. Krylov, J. Chem. Phys. **123**, 084107 (2005)
242. J. Paldus, J. Čížek, M. Takahashi, Phys. Rev. A **30**, 2193 (1984)
243. J. Paldus, J. Planelles, Theor. Chim. Acta **89**, 13 (1994)
244. J. Planelles, J. Paldus, X. Li, Theor. Chim. Acta **89**, 33 (1994), *ibid.* **89**, 59 (1994)
245. L.Z. Stolarczyk, Chem. Phys. Lett. **217**, 1 (1994)
246. X. Li, G. Peris, J. Planelles, F. Rajadall, J. Paldus, J. Chem. Phys. **107**, 90 (1997)
247. P. Piecuch, R. Toboła, J. Paldus, Phys. Rev. A **54**, 1210 (1996)
248. X. Li, I. Grabowski, K. Jankowski, J. Paldus, Adv. Quantum Chem. **36**, 231 (2000)
249. G. Peris, J. Planelles, J. Paldus, Int. J. Quantum Chem. **62**, 137 (1997)
250. X. Li, J. Paldus, J. Chem. Phys. **107**, 6257 (1997), *ibid.* **108**, 637 (1998), *ibid.* **110**, 2844 (1999), Chem. Phys. Lett. **286**, 145 (1998), Mol. Phys. **98**, 1185 (2000), J. Chem. Phys. **113**, 9966 (2000), *ibid.* **124**, 174101 (2006)
251. P. Piecuch, K. Kowalski, I.S.O. Pimienta, Int. J. Mol. Sci. **3**, 475 (2002)
252. X. Li, J. Paldus, J. Chem. Phys. **115**, 5759 (2001)
253. X. Li, J. Paldus, J. Chem. Phys. **115**, 5774 (2001)
254. X. Li, J. Paldus, J. Chem. Phys. **117**, 1941 (2002)
255. B.O. Roos, P. Linse, P.E.M. Siegbahn, M.R.A. Blomberg, Chem. Phys. **66**, 197 (1982)
256. P.M. Kozlowski, M. Dupuis, E.R. Davidson, J. Am. Chem. Soc. **117**, 774 (1995)
257. K. Wolinski, Theor. Chim. Acta **82**, 459 (1992)
258. M.W. Schmidt, M.S. Gordon, Annu. Rev. Phys. Chem. **49**, 233 (1998)
259. H. Nakano, Chem. Phys. Lett. **207**, 372 (1993)
260. J. Paldus, in *Diagrammatic Methods for Many-Fermion Systems* (University of Nijmegen, 1981), J. Paldus, J. Chem. Phys. **67**, 303 (1976), S.A. Kucharski, R.J. Bartlett, Adv. Quantum Chem. **18**, 281 (1986)
261. J. Paldus, J. Čížek, Adv. Quantum Chem. **9**, 105 (1975)
262. C. Bloch, Nucl. Phys. **6**, 329 (1958)
263. P.O. Löwdin, J. Math. Phys. **3**, 969 (1962)
264. P.O. Löwdin, in *Perturbation Theory and Its Applications in Quantum Mechanics*, ed. by C.H. Wilcox (Wiley, New York, 1966), p. 255

265. M.W. Schmidt, K.K. Baldridge, J.A. Boatz, S.T. Elbert, M.S. Gordon, J.H.A. Jensen, S. Koseki, N. Matsunaga, K.A. Nguyen, S.J. Su, T.L. Windus, M. Dupuis, J.A. Montgomery, J. Comput. Chem. **14**, 1347 (1993)
266. T.H. Dunning Jr., J. Chem. Phys. **53**, 2823 (1970)
267. T.H. Dunning Jr., J. Chem. Phys. **90**, 1007 (1989)
268. P. Saxe, H.F. Schaefer III, N.C. Handy, Chem. Phys. Lett. **79**, 202 (1981)
269. R.J. Harrison, N.C. Handy, Chem. Phys. Lett. **95**, 386 (1983)
270. J. Olsen, P. Jørgensen, H. Koch, A. Balková, R.J. Bartlett, J. Chem. Phys. **104**, 8007 (1996)
271. J. Olsen, A.M. Sánchez de Merás, H.J.A. Jensen, P. Jørgensen, Chem. Phys. Lett. **154**, 380 (1989)
272. A.I. Krylov, C.D. Sherrill, M. Head-Gordon, J. Chem. Phys. **113**, 6509 (2000)

Guidelines on the Contracted Schrödinger Equation Methodology

Carmela Valdemoro(✉), Diego Ricardo Alcoba, Luis Maria Tel, and Encarnación Pérez-Romero

Abstract In this article the aim is to provide a guide to the Contracted Schrödinger Equation (CSE) methodology for those readers who are not yet familiar with it. Therefore, the accent is put on giving a clear outlook of the two methods which are now being sucessfully applied: The iterative solution of the second-order CSE and the variational and also iterative solution of the second-order hypervirial equation which can be identified with the continuity equation, or contracted Liouville equation, and with the Antihermitian form of the 2-CSE (2-ACSE). This is not, therefore, a proper revision of the subject but an introduction to an accurate and competitive ab-initio methodology for the study of atoms, molecules and clusters. The results obtained when applying both these methods to the study of the BeH_2 and Li_2 molecules are also given here.

Keywords: Contracted Schrödinger equation, anti-Hermitian Contracted schrödinger equation, reduced density matrix, Correlation matrix, electronic correlation effects, N- and S- representability

1 Introductory Remarks and Plan of This Article

Several reviews on the theory of the second-order Contracted Schrödinger Equation (2-CSE) as well as on its methodology have recently been published in [1, 2]. In this article the aim is not, therefore, to carry out a proper revision of the research

C. Valdemoro
Instituto de Física Fundamental, Consejo Superior de Investigaciones Científicas, Serrano 123, 28006 Madrid, Spain, e-mail: c.valdemoro@imaff.cfmac.csic.es

D.R. Alcoba
Departamento de Física, Facultad de Ciencias Exactas y Naturales, Universidad de Buenos Aires, Ciudad Universitaria, 1428 Buenos Aires, Argentina

L.M. Tel and E.Pérez-Romero
Departamento de Química Física, Universidad de Salamanca, 37008 Salamanca, Spain

S. Wilson et al. (eds.) *Frontiers in Quantum Systems in Chemistry and Physics*.

on the 2-CSE but to provide a guide to a not yet well known, although competitive, ab-initio methodology to study the electronic structure of atoms and molecules. In order to attain this aim whenever possible the technical derivations will be avoided while emphasis will be placed on comunicating as clearly as possible the chain of arguments which constitute the essence of the method such as it is now used in our laboratory. Emphasis will also be placed in signalling the open questions where further research may still improve the performance of the method and extend the field of its applications.

A brief history of the development of the method for solving iteratively the second-order Contracted Schrödinger equation will be described in the following general Introduction. Then, the basic theoretical notions needed in order to understand the rest of the paper will be described in Sect. II. There are two main distinct parts in the method for solving the 2-CSE, such as it is applied in our group. The first part concerns the set of operations needed for performing a complete iteration of the 2-CSE. The second part of the method is formed by the sequence of necessary operations aimed at correcting the mathematical-physical defects of the second-order Reduced Density Matrix (2-RDM). These two parts will be described in Sects. III and IV, respectively. In Sect. V the method which consists in solving the second-order Hypervirial equation, which is closely related to the 2-CSE, will be described. In Sect. VI the results of various calculations which illustrate the previous theoretical developments will be reported. In the final Section a discussion of the questions which we still consider open will be given.

2 General Introduction

To look directly for the 2-RDM instead of searching first for N-electron wave-function from which it derives when studying the electronic structure of atoms and molecules is a theoretical line of research which started more than half a century ago with Husimi [3], Löwdin [4], Ayres [5] and Mayer [6]. The highlights of the contributions in this field ocurred with the paper by Coleman in 1963 [7] where he described the main 2-RDM properties and defined what was from then oncalled the N-representability problem. This problem consists in determining the set of conditions which would be sufficient to guarantee that a matrix, represented in a two-electron space and satisfying these conditions, derives by integration over the variables of N-2 electrons from an N-electron wave-function. Both Löwdin and Coleman's work, as well as Sanibel School and Symposiums, stimulated the search for a solution to the N-representability problem. There are several revisions and books where this rich litterature is analysed [1, 2, 8, 10–12, 23]. In particular, the important contribution by Garrod and Percus [13] about what they called the $\mathscr{G}$-matrix, directly related to the 2-RDM, followed by the penetrating analysis of the $\mathscr{G}$-matrix structure by Garrod, Mihailovich and Rosina [14, 15] are important milestones in RDM theory.

In 1976 a remarkable advance in the 2-RDM theory ocurred. Two important papers were published by Cohen and Frishberg [16] and by Nakatsuji [17]. These authors reported an integro-diferential equation which was obtained by integrating the Scrödinger equation, in its first quantization form, over the variables of $(N-2)$ electrons. The matrix representation of this equation in the two-electron space, can be schematically expressed as:

$$E\ {}^2\underline{\mathrm{D}} = function({}^0\underline{\mathrm{H}},\ {}^2\underline{\mathrm{D}},\ {}^3\underline{\mathrm{D}},\ {}^4\underline{\mathrm{D}})$$

where E is the system energy in the state considered, and ${}^p\underline{\mathrm{D}}$ represents the p-RDM. Although this equation is represented in the two-electron space it depends not only on the 2-RDM but also on the 3- and 4-RDMs which contribute in an averaged way to the equation. The matrix ${}^0\underline{\mathrm{H}}$ is formed by the usual one- and two-electron integrals expressed in an orthonormal finite basis set. This equation (called density equation by Nakatsuji and hierarchy equation by Cohen and Frishberg), which by itself is extremely attractive, becomes a fundamental one in view of Nakatsuji's theorem which states that when the RDMs involved in the equation are N-representable then there is a one to one correspondence between the solutions of Schrödinger's equation and those of this equation. Unfortunately, due to the dependence of the equation on the 3- and 4-RDMs, there are more unknowns (the RDM's elements) than equations. This caused this equation to be ignored for nearly ten years.

By applying a matrix contracting mapping reported in 1983 by Valdemoro [18, 19] to the Schrödinger and to the Liouville equations, both represented in the N-electron space, a second-order Contracted Schrödinger equation (2-CSE) and a Contracted Liouville Equation (CLE) were respectively obtained. When Valdemoro presented this result at Coleman's Symposium in 1985 [20], Löwdin pointed out that the 2-CSE reminded him of Nakatsuji's density equation and wondered whether they were related. Indeed, both equations, although derived within two different mathematical frameworks (integration in first-quantization and matrix contraction in second-quantization) can be shown to be equivalent.

In 1992, Valdemoro proposed [21] an approximated method for evaluating the 2-RDM in terms of the 1-RDM. This method was then extended for approximating the 3- and 4-RDMs in terms of the 1- and 2-RDMs [22]. These approximations permited to approach the problem of solving the 2-CSE in an iterative form [23]. The first account of the method for solving the 2-CSE in a spin-free representation was reported by Colmenero and Valdemoro in 1994 [24]. When applying this method to the study of the Berillium ground-state, the resulting 2-RDM satisfied the second-order hypervirial equation (or contracted Liouville equation for the state considered) with a reasonable accuracy; the values of the 1- and 2-RDM elements approximated quite closely the values of the corresponding FCI matrices except for three elements which showed non negligible errors. Finally, the energy error was of the order of 10^{-3} Hartrees.

This, and other similar calculations showed that the convergence pattern and rate of the iterative process had to be improved. Also, the fact that the energy obtained was lower than the FCI one indicated that the RDMS entering as data at each

iteration were not sufficiently N-representable. In spite of these shortcomings the results were very encouraging since there was a large margin for improving: the overall iterative process, the consistency among the approximated 2-, 3-, and 4-RDMS as well as their construction algorithms. It was also clear to us that the spin had to be explicitly taken into account.

The research in the following years in order to correct these defects was intense. Thus, since 1996 the contributions of the groups headed by Nakatsuji [25–27], Mazziotti [28–30], Harriman [31] and Valdemoro [32–38], have yielded several versions of the method which, although they may still be improved, can be now considered competitive. Recently Mazziotti [39], who noticed that the second-order hypervirial or Liouville equation is the anti-hermitian part of the 2-CSE, has proposed an effective method for solving this equation which he denotes 2-ACSE. Although we have not been able to show that Nakatsuji's theorem can be applied to this equation [40], the results which have been obtained with Mazziotti's method for the ground-state of several systems have been comparable with those obtained with the 2-CSE [41]. The advantage of the 2-ACSE over the 2-CSE is that it does not involve the 4-RDM, while the disadvantage is that the optimization included in Mazziotti's method favours the obtention of the exact solution but limits its use to the study of the system ground-state.

3 Notation, Definitions and Basic Theoretical Background

3.1 Notation and Definitions

The number N of electrons of the system is considered fixed as well as the finite number K of one-electron orthonormal orbitals which, jointly with the spin-functions α and β, form our spin-orbitals basis set. These orbitals are denoted by the letters $i, j, k, l..$ or $i_\sigma..$ according to whether or not the spin-function is made explicit. All developments are expressed in the Second-Quantization language in the occupation number representation. In order to render simpler the formulae appearance the creator/annihilator operators are schematically represented by the letters denoting the spin orbital with or without a dagger according to whether it is a creator or an annihilator.

The Hamiltonian

Let us define the reduced Hamiltonian matrix ${}^0\underline{\mathrm{H}}$ [42–45] whose elements groups the one-, $h_{i,j}$, and two electron integrals, $\langle ij|kl\rangle$, as follows:

$$ {}^0\mathrm{H}_{i,j;k,l} = \left[\frac{1}{N-1} \left(h_{i;k}\delta_{j,l} + h_{j;l}\delta_{i,k} \right) + \langle ij|kl\rangle \right] \tag{1} $$

then, the many-body Hamiltonian operator may be written as

$$\hat{H} = \sum_{r<s,k<l} {}^0\mathrm{H}^{\alpha\alpha}_{r,s;k,l}\, r^\dagger_\alpha, s^\dagger_\alpha l_\alpha k_\alpha + \sum_{u,v,m,n} {}^0\mathrm{H}^{\alpha\beta}_{u,v;m,n}\, u^\dagger_\alpha v^\dagger_\beta n_\beta m_\alpha + \sum_{r<s,k<l} {}^0\mathrm{H}^{\beta\beta}_{r,s;k,l}\, r^\dagger_\beta s^\dagger_\beta l_\beta k_\beta$$

where

$${}^0\mathrm{H}^{\alpha\alpha}_{r,s;k,l} = {}^0\mathrm{H}_{r,s;k,l} - {}^0\mathrm{H}_{r,s;l,k} \tag{2}$$

$${}^0\mathrm{H}^{\alpha\beta}_{u,v;m,n} = {}^0\mathrm{H}_{u,v;m,n} \tag{3}$$

$${}^0\mathrm{H}^{\beta\beta}_{r,s;k,l} = {}^0\mathrm{H}_{r,s;k,l} - {}^0\mathrm{H}_{r,s;l,k} \tag{4}$$

The Reduced Density Matrices

The general expression for an m-order Reduced Density Matrix (m-RDM) is defined as:

$${}^m\mathrm{D}^{\Phi\Phi'}_{i_1,i_2,\ldots,i_m;j_1,j_2,\ldots,j_m} = \frac{1}{m!}\,\langle\Phi|\, {i_1}^\dagger\, {i_2}^\dagger \ldots {i_m}^\dagger\, j_m \ldots j_2\, j_1\, |\Phi'\rangle \tag{5}$$

Where Φ and Φ', are N-electron states. This formula represents a Transition Reduced Density Matrix (m-TRDM) when $\Phi \neq \Phi'$ [4]. When there is no ambiguity about the state/states with respect to which one is taking the expectation value the upper indices referring to the N-electron states will be omitted. For instance, when we are referring in the text to a 2-RDM corresponding to state Φ we will simply denote it by the symbol ${}^2\mathrm{D}$.

The m-order Hole Reduced Density Matrix (m-HRDM) corresponding to state Φ is:

$${}^m\bar{\mathrm{D}}_{i_1,i_2,\ldots,i_m;j_1,j_2,\ldots,j_m} = \frac{1}{m!}\,\langle\Phi|\, j_m \ldots j_2\, j_1\, {i_1}^\dagger\, {i_2}^\dagger \ldots {i_m}^\dagger\, |\Phi\rangle \tag{6}$$

Here the creators destroy *holes* on state Φ, which is the ket state considered, i.e. the holes are referred to state Φ which, in general, is not the Fermi sea.

Both the RDM and the HRDM are by definition Hermitian, positive semidefinite matrices. Also due to the properties of the creators/annihilators they are antisymmetric under permutations of the row/column indices. These are basic RDM/HRDM necessary N-representability conditions.

The 2-RDM Contractions

The RDM's contractions are necessary N-representability conditions that any RDM must satisfy. Thus, any high-order RDM may be contracted into a lower-order one. For instance

$$\sum_k 2!\, {}^2\mathrm{D}_{i,k;j,k} \equiv \sum_k \langle\Phi|\, i^\dagger\, k^\dagger\, k\, j\, |\Phi\rangle = (N-1)\, {}^1\mathrm{D}_{i;j} \tag{7}$$

where definition of the number operator $\hat{N}$

$$\hat{N} = \sum_i i^\dagger\, i \tag{8}$$

has been applied. Clearly, a further contraction gives the 2-RDM trace $\binom{N}{2}$. This type of contraction, based on the properties of the number operator $\hat{N}$ or $\hat{N}_\sigma$, is the most usual one. It should however be noted that the $\hat{S}_{+/-}$ operators play also an important role when imposing spin-representability conditions upon the 2-RDM. Let us for instance consider:

$$\sum_k \langle \Phi | k_\beta^\dagger\, i_\alpha^\dagger\, k_\alpha\, j_\beta\, | \Phi \rangle \equiv {}^1\mathrm{D}_{i_\beta;j_\beta} - \langle \Phi |\, \hat{S}_-\, i_\alpha^\dagger\, j_\beta\, | \Phi \rangle \tag{9}$$

The second term of the *r.h.s.* of this expression will vanish whenever the spin-quantum numbers S and M_s of state Φ do not permit an increase of the M_s value: e.g. when Φ is a singlet state.

General Matrix Contracting Mapping

When one wishes to contract a general reduced matrix of order t into a space of v electrons, such that $v < t < N$, the operations to be carried out are given by the general Matrix Contracting Mapping reported by Valdemoro in 1983 [18–20, 44]. The form of this contracting algorithm is

$${}^v\mathscr{M}_{\lambda;\omega} \equiv C \sum_{\Pi,\Gamma} {}^v\mathrm{D}^{\Pi\,\Gamma}_{\lambda;\omega}\ {}^t\mathscr{M}_{\Pi;\Gamma} \tag{10}$$

where ${}^t\mathscr{M}$ is the t-order matrix to be contracted into its reduced form represented in the space of v-electrons. The Π and Γ letters represent t-electron configurations while λ and ω are v-electron configurations. The factor C depends on the particular choice for the normalization of the matrices; for the case of RDMs with the normalization expressed in Eq. (5) $C = \frac{\binom{N}{v}}{\binom{N}{t}\binom{t}{v}}$. As will be seen in the next Section, this mapping plays an important role in the derivation of the 2-CSE.

The Correlation and the $\mathscr{G}$ Matrices

Two other matrices which play an important role in the RDM methodology are the Correlation ($\mathscr{C}$) and the $\mathscr{G}$ matrices. The structure of the second-order $\mathscr{C}$-matrix is:

$$\begin{aligned} \mathscr{C}_{i,j;m,l} &= \sum_{\Phi' \neq \Phi} \langle \Phi |\, i^\dagger\, m\, | \Phi' \rangle \langle \Phi' |\, j^\dagger\, l\, | \Phi \rangle \\ &\equiv \langle \Phi |\, i^\dagger\, m\ \hat{P}\ j^\dagger\, l\, | \Phi \rangle \end{aligned} \tag{11}$$

where $\hat{P}$ is the operator which projects upon the complementary space to $|\Phi\rangle\langle\Phi|$.

The matrix $\mathscr{C}$ arises when decomposing the 2-RDM [13–15, 37, 38, 46, 47]

$$2!\,{}^2\mathrm{D}_{i_\sigma,j_{\sigma'};m_\sigma,l_{\sigma'}} = {}^1\mathrm{D}_{i_\sigma;m_\sigma}\,{}^1\mathrm{D}_{j_{\sigma'};l_{\sigma'}} - \delta_{\sigma,\sigma'}\,\delta_{j,m}\,{}^1\mathrm{D}_{i_\sigma;l_\sigma} + \mathscr{C}_{i_\sigma,j_{\sigma'};m_\sigma,l_{\sigma'}} \quad (12)$$

The elements of the correlation matrix –whose rows and columns labels are the same as those of the 2-RDM from which it is derived– form the well-known $\mathscr{G}$-matrix when rearranged. Thus,

$$\mathscr{C}_{i_\sigma,j_{\sigma'};m_\sigma,l_{\sigma'}} = \mathscr{G}_{i_\sigma,m_\sigma;l_{\sigma'},j_{\sigma'}} \quad (13)$$

The important property of the $\mathscr{G}$-matrix is that it is an hermitian positive semidefinite matrix. This is not the case of the $\mathscr{C}$-matrix. The positive semidefinite character of the $\mathscr{G}$-matrix is an important N-representability condition. Both the $\mathscr{C}$ and $\mathscr{G}$ matrices describe the virtual transitions ocurring in the system due to the electron correlation.

Let us consider the Kronecker δ appearing in equation (12). Due to the anti-commuting property of fermion operators, it can be written in terms of the 1-RDM and the 1-HRDM. Thus,

$$\delta_{\sigma,\sigma'}\,\delta_{j,m} = {}^1\mathrm{D}_{j_\sigma;m_\sigma} + {}^1\bar{\mathrm{D}}_{j_\sigma;m_\sigma} \quad (14)$$

It should be underlined that this important equation, together with the positive semidefinite character of the 1-RDM and 1-HRDM, establish the necessary and sufficient N-representability conditions for the 1-RDM [7].

The term involving this Kronecker δ in equation (12) can therefore be decomposed into the two following terms:

$$\delta_{\sigma,\sigma'}\,\delta_{j,m}\,{}^1\mathrm{D}_{i_\sigma;l_\sigma} = {}^1\mathrm{D}_{j_\sigma;m_\sigma}\,{}^1\mathrm{D}_{i_\sigma;l_\sigma} + {}^1\bar{\mathrm{D}}_{j_\sigma;m_\sigma}\,{}^1\mathrm{D}_{i_\sigma;l_\sigma} \quad (15)$$

These two terms describe respectively the exchange and a particle-hole product representing a second type of correlation mechanism.

3.2 Basic Relations Linking the 2-RDM, the 2-HRDM and the $\mathscr{G}$ Matrices

In the two-electron space the commuting relation of two creator operators with two annihilator operators jointly combined with relation (14), generates an equation linking a 2-RDM and the same 2-HRDM element with products of two 1-RDMs elements. Thus one has

$$\left.\begin{matrix} 2!\,{}^2\bar{\mathrm{D}}_{i,j;p,q} \\ - \\ 2!{}^2\mathrm{D}_{i,j;p,q} \end{matrix}\right\} = \left\{\begin{matrix} {}^1\bar{\mathrm{D}}_{i;p}\,{}^1\bar{\mathrm{D}}_{j;q} - {}^1\bar{\mathrm{D}}_{i;q}\,{}^1\bar{\mathrm{D}}_{j;p} \\ - \\ {}^1\mathrm{D}_{i;p}\,{}^1\mathrm{D}_{j;q} - {}^1\mathrm{D}_{i;q}\,{}^1\mathrm{D}_{j;p} \end{matrix}\right. \quad (16)$$

In 1992, Valdemoro [21] proposed to consider the duality holes-particles in order to approximate the 2-RDM by:

$$2!\,{}^2\mathrm{D}_{i_\sigma,j_{\sigma'};p_\sigma,q_{\sigma'}} = \sum_{\mathscr{P}} (-1)^{\mathscr{P}}\, \mathscr{P}\,(\,{}^1\mathrm{D}_{i_\sigma;p_\sigma}\,{}^1\mathrm{D}_{j_{\sigma'};q_{\sigma'}}\,) + 2!\,{}^2\Delta_{i_\sigma,j_{\sigma'};p_\sigma,q_{\sigma'}} \quad (17)$$

where $\sum_{\mathscr{P}} (-1)^{\mathscr{P}}\, \mathscr{P}$ antisymmetrizes the column labels of the 1-RDMs and where $2!\,{}^2\Delta_{i_\sigma,j_{\sigma'};p_\sigma,q_{\sigma'}}$ is a term to be approximated indirectly by rendering the 2-RDM positive semidefinite and normalized.

From equations (12) and (15) it follows that the ${}^2\Delta$ closed form is

$${}^2\Delta_{i_\sigma,j_{\sigma'};p_\sigma,q_{\sigma'}} = -\,\delta_{\sigma;\sigma'}\,{}^1\bar{\mathrm{D}}_{j_\sigma;p_\sigma}\,{}^1\mathrm{D}_{i_\sigma;q_\sigma} + \mathscr{C}_{i_\sigma,j_{\sigma'};p_\sigma,q_{\sigma'}} \quad (18)$$

That is, this matrix gathers the two terms describing electronic correlation. The first term is a product of an element of the 1-RDM times an element of the 1-HRDM and therefore its calculation does not imply any difficulty. The second term is a real two-electron term involving information about the whole spectrum of the system which in principle is not known.

Equation (17) can also be interpreted as describing the moment expansion of the 2-RDM where the 1-RDM is the moment and the ${}^2\Delta$ matrix is the cumulant [48–50].

It is easy to prove that the 2-HRDM correlation error is equal to the correlation error of the 2-RDM; which is why in the difference ${}^2\underline{\bar{\mathrm{D}}} - {}^2\underline{\mathrm{D}}$ (equation (16)) all correlation effects cancel out.

4 The Second-Order Contracted Schrödinger Equation and Our Updated Method for Its Iterative Solution

The theoretical tools given in the previous Section provide the basis for understanding the general lines of this method. Consequently, what will be emphasized here are those steps, approximations, etc which are critical in determining the success of the method and whose effectiveness can probably still be improved.

4.1 The Second-Order Contracted Schrödinger Equation

The matrix representation of the Schrödinger equation is:

$$\langle \Omega|\Phi\rangle\,\langle\Phi|\,\hat{H}\,|\Lambda\rangle = E_\Phi\,{}^N\mathrm{D}^{\Phi}_{\Lambda\Omega} \quad (19)$$

where $\Lambda,\Omega..$ are elements of an orthonormal N-electron basis set; i. e. N-electron Slater determinants. Let us now apply to both sides of the equation the matrix contracting mapping given in equation (10). The result of this contraction is:

$$\langle \Phi | \hat{H}\, i^{\dagger}_{\sigma}\, j^{\dagger}_{\sigma'}\, l_{\sigma'}\, k_{\sigma}\, | \Phi \rangle = E_{\Phi}\, {}^{2}\mathrm{D}_{i_{\sigma},j_{\sigma'};k_{\sigma},l_{\sigma'}} \tag{20}$$

This is the compact form of the 2-CSE. When the explicit form of $\hat{H}$ is replaced into this equation and the operators appearing in its *l.h.s.* are re-ordered so as to have terms involving normal products of creator and annihilator operators, one obtains an equation which has the functional form:

$$E_{\Phi}\, {}^{2}\underline{\mathrm{D}} \;=\; Function\left({}^{0}\underline{\mathrm{H}},\, {}^{2}\underline{\mathrm{D}},\, {}^{3}\underline{\mathrm{D}},\, {}^{4}\underline{\mathrm{D}} \right) \tag{21}$$

In what follows, in order to simplify the spin-notation, a bar above the letter indicates that the orbital involved represents a β spin. Thus, for instance,

$$2!\, {}^{2}\mathrm{D}_{i_{\alpha} j_{\beta};m_{\alpha} l_{\beta}} \;\equiv\; \langle \Phi | i^{\dagger}\; \bar{j}^{\dagger}\; \bar{l}\, m | \Phi \rangle \;\equiv\; 2!\, {}^{2}\mathrm{D}_{i,\bar{j};m,\bar{l}} \tag{22}$$

Using this simplified notation and assuming an implicit sum over repeated indices, the explicit form of the 2-CSE is:

$$E_{\Phi} \underset{(i<j,p<q)}{{}^{2}\mathrm{D}_{i,j;p,q}} = \begin{cases} {}^{2}\mathrm{D}_{i,j;r,s}\; {}^{0}\mathrm{H}^{\alpha\alpha}_{r,s;p,q} \\ -\,{}^{3}\mathrm{D}_{i,j,m;q,r,s}\; {}^{0}\mathrm{H}^{\alpha\alpha}_{r,s;p,m} \;+\; {}^{3}\mathrm{D}_{i,j,m;p,r,s}\; {}^{0}\mathrm{H}^{\alpha\alpha}_{r,s;q,m} \\ +\,{}^{3}\mathrm{D}_{i,j,\bar{m};p,u,\bar{v}}\; {}^{0}\mathrm{H}^{\alpha\beta}_{u,v;q,m} \;-\; {}^{3}\mathrm{D}_{i,j,\bar{m};q,u,\bar{v}}\; {}^{0}\mathrm{H}^{\alpha\beta}_{u,v;p,m} \\ +\,{}^{4}\mathrm{D}_{i,j,k,l;p,q,r,s}\; {}^{0}\mathrm{H}^{\alpha\alpha}_{r,s;k,l} \;+\; {}^{4}\mathrm{D}_{i,j,\bar{k},\bar{l};p,q,\bar{r},\bar{s}}\; {}^{0}\mathrm{H}^{\beta\beta}_{r,s;k,l} \\ +\,{}^{4}\mathrm{D}_{i,j,m,\bar{n};p,q,u,\bar{v}}\; {}^{0}\mathrm{H}^{\alpha\beta}_{u,v;m,n} \end{cases} \tag{23}$$

$$E_{\Phi}\;\; {}^{2}\mathrm{D}_{i,\bar{j};p,\bar{q}} = \begin{cases} {}^{2}\mathrm{D}_{i,\bar{j};u,\bar{v}}\; {}^{0}\mathrm{H}^{\alpha\beta}_{u,v;p,q} \\ -\,{}^{3}\mathrm{D}_{m,i,\bar{j};r,s,\bar{q}}\; {}^{0}\mathrm{H}^{\alpha\alpha}_{r,s;p,m} \;+\; {}^{3}\mathrm{D}_{i,j,\bar{m};p,r,\bar{s}}\; {}^{0}\mathrm{H}^{\beta\beta}_{r,s;q,m} \\ -\,{}^{3}\mathrm{D}_{m,i,\bar{j};p,u,\bar{v}}\; {}^{0}\mathrm{H}^{\alpha\beta}_{u,v;m,q} \;-\; {}^{3}\mathrm{D}_{i,\bar{j},\bar{n};u,\bar{v},\bar{q}}\; {}^{0}\mathrm{H}^{\alpha\beta}_{u,v;p,n} \\ +\,{}^{4}\mathrm{D}_{k,l,i,\bar{j};r,s,p,\bar{q}}\; {}^{0}\mathrm{H}^{\alpha\alpha}_{r,s;k,l} \;+\; {}^{4}\mathrm{D}_{i,\bar{j},\bar{k},\bar{l};p,\bar{q},\bar{r},\bar{s}}\; {}^{0}\mathrm{H}^{\beta\beta}_{r,s;k,l} \\ +\,{}^{4}\mathrm{D}_{i,m,\bar{j},\bar{n};p,u,\bar{q},\bar{v}}\; {}^{0}\mathrm{H}^{\alpha\beta}_{u,v;m,n} \end{cases} \tag{24}$$

$$E_{\Phi} \underset{(i<j,p<q)}{{}^{2}\mathrm{D}_{\bar{i},\bar{j};\bar{p},\bar{q}}} = \begin{cases} {}^{2}\mathrm{D}_{\bar{i},\bar{j};\bar{r},\bar{s}}\; {}^{0}\mathrm{H}^{\beta\beta}_{r,s;p,q} \\ -\,{}^{3}\mathrm{D}_{\bar{m},\bar{i},\bar{j};\bar{q},\bar{r},\bar{s}}\; {}^{0}\mathrm{H}^{\beta\beta}_{r,s;p,q} \\ -\,{}^{3}\mathrm{D}_{\bar{m},\bar{i},\bar{j};\bar{p},\bar{r},\bar{s}}\; {}^{0}\mathrm{H}^{\beta\beta}_{r,s;q,m} \\ -\,{}^{3}\mathrm{D}_{m,\bar{i},\bar{j};u,\bar{v},\bar{p}}\; {}^{0}\mathrm{H}^{\alpha\beta}_{u,v;m,q} \;+\; {}^{3}\mathrm{D}_{m,\bar{i},\bar{j};u,\bar{v},\bar{q}}\; {}^{0}\mathrm{H}^{\alpha\beta}_{u,v;m,p} \\ +\,{}^{4}\mathrm{D}_{\bar{i},\bar{j},\bar{k},\bar{l};\bar{p},\bar{q},\bar{r},\bar{s}}\; {}^{0}\mathrm{H}^{\beta\beta}_{r,s,k,l} \;+\; {}^{4}\mathrm{D}_{k,l,\bar{i},\bar{j};r,s,\bar{p},\bar{q}}\; {}^{0}\mathrm{H}^{\alpha\alpha}_{r,s;k,l} \\ +\,{}^{4}\mathrm{D}_{m,\bar{n},\bar{i},\bar{j};u,\bar{v},\bar{p},\bar{q}}\; {}^{0}\mathrm{H}^{\alpha\beta}_{u,v;m,n} \end{cases} \tag{25}$$

with the restriction that $r < s$ and $k < l$ when the orbitals have the same spin.

Note that the three spin-blocks of this equation are not independent since different spin-blocks involve the same p-RDM spin-block.

In his 1976s paper [17] Nakatsuji reported a powerful theorem; he proved that when the 2-, 3-,and 4-RDMs appearing in this equation are N-representable, the solutions of this equation coincide with those of the Scrödinger equation. Another proof of this theorem was also reported in 1998 by Mazziotti [28]. Unfortunately, the 2-CSE has more apparent unknowns, the elements of the 2-, 3- and 4-RDMs, than the number of equations, $\binom{K}{2}^2$. Consequently, the system only becomes determinate when all the corresponding N-representability conditions linking the unknown elements are taken into account. A way out of this problem consists in approximating the 3- and 4-RDM in terms of a trial 2-RDM and solving it iteratively until convergence. In 1994, Colmenero and Valdemoro [24] reported the first iterative solution of the 2-CSE. This was possible because Valdemoro's approximative method for the 2-RDM as a function of the 1-RDM, which has been sketched in the previous Section, was extended in order to approximate any high-order RDM as a function of the lower ones, jointly with some of the main N-representability conditions.

Main Lines of the Iterative Procedure

Let us represent symbolically the 2-CSE given in (21) as:

$$E_{\Phi}\ {}^2\underline{\mathrm{D}} \equiv \underline{\mathscr{M}} \tag{26}$$

In order to construct the second-order matrix $\underline{\mathscr{M}}$, the trial 2-RDM as well as the 3- and 4-RDMs which are approximated are replaced in the 2-CSE analytic form given above (23,24,25). In a following paragraph the approximating algorithms for the high-order matrices will be described. Therefore, we will focus our attention here on the main steps of the iterative solution.

- Once the $\underline{\mathscr{M}}$ has been evaluated, the trace of both sides of the equation is calculated in order to obtain a new value of the energy E'_{Φ}

$$E'_{\Phi} = \frac{Tr(\underline{\mathscr{M}})}{\binom{N}{2}} \tag{27}$$

- The new 2-RDM is obtained:

$${}^2\underline{\mathrm{D}}' = \frac{\underline{\mathscr{M}}}{E'_{\Phi}} \tag{28}$$

  Should the RDMs on the right of Eq. (21) exactly correspond to an eigenstate of the Hamiltonian, this new matrix would be identical to the previous 2-RDM. But for approximate matrices it may not even be symmetric and, hence, it is symmetrized. This new 2-RDM becomes in principle the new trial matrix for the new iteration.

These were the main operations which constituted the original iterative method proposed by Colmenero and Valdemoro. In order to render the process convergent they added fine spin constraints and several tests, such as the degree of fulfillment of the second-order hypervirial theorem. Since then, the following three very effective improvements have been incorporated to this iterative scheme.

- Originally the method was developed in a spin-free basis set. At present, the 2-CSE form used is a combination of that given in (21) and that of the second-order Spin Contracted equation [32]. This latter equation is obtained in a similar way to the 2-CSE one, the only difference being that the $\hat{S}^2$ operator replaces the Hamiltonian one.
- A regulating convergence device [35] consisting in a shift of the Energy origin has been introduced at each iteration. This device, which acts as either a damping or an accelerating agent, greatly fosters the convergence of the iterative process.
- One of the more critical points determining a good convergence and removal of final divergencies is the need for a 2-RDM as closely *N*- and *S*-representable as possible. Initially, only the positive semidefiniteness, the symmetry, and the trace of the trial 2-RDM as well as the ensemble *N*-representability of the 1-RDM were tested and corrected at each iteration. At present, at each iteration, we carry out an iterative 2-RDM purification procedure in order to ascertain that the 2-RDM entering as data in the next 2-CSE iteration is as closely *N*- and *S*-representable as possible [21, 24, 38, 51–55].

The next Section is dedicated to describe the main points concerning the purification procedure which we now consider an essential part of this methodology.

High-Order RDM's Constructing Algorithms

In this paragraph the approximating algorithms for the higher-order RDMs will be described. This is an important and also involved subject. It is not our aim here to consider in detail the more technical aspects which have been reported in detail in [37]. On the other hand, we will try to explain as clearly as possible the ideas which are at the base of these algorithms. Here, we will consider separately two different aspects of the algorithms. In the next sub-paragraph the general or zero-order approximation for the 3- and 4-RDMs will be described. The groups headed by Nakatsuji, Mazziotti, Harriman and Valdemoro have proposed different approaches in order to improve upon this zero-order approximation [25, 28, 29, 31, 36, 37, 41]. In what follows, only the improvements which are currently applied in our group and with which the different calculations reported in Section 5 have been carried out will be considered in detail.

Zero-Order Algorithms' Approximations

The arguments leading to the approximation of the 2-RDM according to equation (17) were extended in order to approximate the 3- and the 4-RDM. The spin-free

version of these zero-order approximations was initially reported [22–24]; and later on the zero-order algorithms in a spin-orbitals basis of representation was given. This last version of these algorithms was reported by Valdemoro, Tel and Pérez-Romero [32] and in what follows will be referred to as VTP. The VTP algorithm for the 3-RDM can be expressed as:

$$\begin{aligned} 3!\,{}^3\mathrm{D}_{i,j,k;p,q,r} = & -2\sum_{\mathscr{P}}(-1)^{\mathscr{P}}\,\mathscr{P}\,({}^1\mathrm{D}_{i;\,p}\,{}^1\mathrm{D}_{j;q}\,{}^1\mathrm{D}_{k;r}) \\ & +\sum_{\mathscr{P}'}(-1)^{\mathscr{P}'}\,\mathscr{P}'\,2!\,(\,{}^1\mathrm{D}_{i;p}\,{}^2\mathrm{D}_{j,k;q,r} \\ & \quad +{}^1\mathrm{D}_{j;q}\,{}^2\mathrm{D}_{i,k;p,r}+{}^1\mathrm{D}_{k;r}\,{}^2\mathrm{D}_{i,j;p,q}) \\ & +3!\,{}^3\Delta_{i,j,k;p,q,r} \end{aligned} \tag{29}$$

where the operations involving the permutation operator $\mathscr{P}$ antisymmetrize the column indices of the three 1-RDM elements and the operations involving the permutation operator $\mathscr{P}'$ antisymmetrize the column index of the 1-RDM with the column indices of the 2-RDM.

The VTP construction algorithm for the 4-RDM is [22, 32]:

$$\begin{aligned} 4!\,{}^4\mathrm{D}_{i,j,k,l;\,p,q,r,s} = & \sum_{\mathscr{P}}(-1)^{\mathscr{P}}\,\mathscr{P}\,3!\,({}^1\mathrm{D}_{i;p}\,{}^3\mathrm{D}_{j,k,l;q,r,s}+{}^1\mathrm{D}_{j;q}\,{}^3\mathrm{D}_{i,k,l;p,r,s} \\ & +{}^3\mathrm{D}_{i,j,l;p,q,s}\,{}^1\mathrm{D}_{k;r}+{}^3\mathrm{D}_{i,j,k;p,q,r}\,{}^1\mathrm{D}_{l;s}) \\ & +3\sum_{\mathscr{P}'}(-1)^{\mathscr{P}'}\,\mathscr{P}'\,({}^1\mathrm{D}_{i;p}\,{}^1\mathrm{D}_{j;q}\,{}^1\mathrm{D}_{k;r}\,{}^1\mathrm{D}_{l;s}) \\ & -\sum_{\mathscr{P}''}(-1)^{\mathscr{P}''}\,\mathscr{P}''\,2!\,({}^1\mathrm{D}_{i;p}\,{}^1\mathrm{D}_{j;q}\,{}^2\mathrm{D}_{k,l;r,s} \\ & +{}^1\mathrm{D}_{i;p}\,{}^2\mathrm{D}_{j,l;q,s}\,{}^1\mathrm{D}_{k;r}+{}^1\mathrm{D}_{i;p}\,{}^2\mathrm{D}_{j,k;q,r}\,{}^1\mathrm{D}_{l;s} \\ & +{}^2\mathrm{D}_{i,l;p,s}\,{}^1\mathrm{D}_{j;q}\,{}^1\mathrm{D}_{k;r}+{}^2\mathrm{D}_{i,k;p,r}\,{}^1\mathrm{D}_{j;q}\,{}^1\mathrm{D}_{l;s} \\ & +{}^2\mathrm{D}_{i,j;p,q}\,{}^1\mathrm{D}_{k;r}\,{}^1\mathrm{D}_{l;s}\,) \\ & +4!\,{}^4\Delta_{i,j,k,l;p,q,r,s} \end{aligned} \tag{30}$$

In these VTP algorithms the ${}^3\underline{\Delta}$ and ${}^4\underline{\Delta}$ matrices represent the unknown error of the approximation.

Approximating the $\underline{\Delta}$ Matrices

Nakatsuji approached the study of the 3- and 4-RDM's algorithms by analogy with the Green-function perturbation expansion [25]. On the other hand, Mazziotti [50] derived a generating functional from which he deduced a Taylor series whose coefficients were the different RDMs. By analogy with Kubo's cumulant expansion, Mazziotti identified the p-RDM with the p-order moment of this expansion and the connected part of this expansion with the ${}^p\underline{\Delta}$.

In both these approaches another term, ${}^4T$, was added to the 4-RDM VTP algorithm. In our notation, this extra term may be expressed as:

$$ {}^4T_{i,j,k,l;p,q,r,s} = \sum_{\mathscr{P}'''} (-1)^{\mathscr{P}'''} \, \mathscr{P}''' \, 2!\, 2! \begin{pmatrix} {}^2\Delta_{i,j;p,q} \, {}^2\Delta_{k,l;r,s} \\ + {}^2\Delta_{i,l;p,s} \, {}^2\Delta_{j,k;q,r} \\ + {}^2\Delta_{i,k;p,r} \, {}^2\Delta_{j,l;q,s} \end{pmatrix} \tag{31} $$

Although, when calculating excited states, the VTP algorithm performs better in many cases, adding this extra term generally lowers the value of the unknown ${}^4\underline{\Delta}$ error. In what follows the VTP algorithm to which this extra term, proposed both by Nakatsuji and Mazziotti, has been added will be called VTPNM.

In order to improve upon the VTPMN algorithm we replace by "0" any negative diagonal element of each of the resulting 4-RDM spin-blocks, and subsequently the corresponding diagonal is renormalized in order to ascertain that each 4-RDM spin-block has the correct trace [32, 33, 35].

It is important to note, before considering how to improve upon the VTP for approximating the 3-RDM, that this matrix plays a double role in this methodology. Thus, the 3-RDM is entered as data at two different stages which will be denoted respectively A and B. Thus, in stage A, it enters as data when approximating the 4-RDM; and in stage B, it enters as data when evaluating the $\underline{\mathscr{M}}$ part involving explicitly the 3-RDM. In our experience, it is extremely important that the three RDMs entering into the calculation of $\underline{\mathscr{M}}$ should be consistent. This implies that the lower-order ones should result from the contraction of the higher-order ones. In order to solve this consistency problem we employ two different approximating algorithms [32, 33, 37]. In stage B, when calculating the 3-RDM off-diagonal elements we use an algorithm resulting from the contraction of the 4-RDM algorithm; while the 3-RDM diagonal elements are obtained by contracting explicitly the positive and normalized 4-RDM diagonal which was previously evaluated and kept in the computer memory. In stage A, we use the VTP algorithm and approximate the ${}^3\underline{\Delta}$ with an algorithm [36] which has proved to be very efficient in the study of quite different states, provided there is no ambiguity when defining the occupied and empty spin-orbitals in the reference state.

The various approaches [25, 29, 31, 36] both for consistency among the different RDMs and for going beyond the VTP algorithm in the 3-RDM case differ significantly. In spite of what the results obtained in all the approximations compare reasonably well.

Before describing the algorithm that we use for approximating the ${}^3\underline{\Delta}$ elements in stage A, let us remark that in our experience the value of the ${}^3\Delta_{i_\sigma,j_\sigma,k_\sigma;p_\sigma,q_\sigma,r_\sigma}$ elements is very small and may be neglected. This may be due to the fact that, when all the spin-orbitals have the same spin-function, the exchange mechanism may be dominant, and the purely 3-body correlation effects are thus negligible.

On the other hand, some of the ${}^3\Delta_{i,j,\bar{k};p,q,\bar{r}}$ and ${}^3\Delta_{i,\bar{j},\bar{k};p,\bar{q},\bar{r}}$ elements had far from negligible values. When analysing which property characterized the elements whose error could not be ignored, we found that the elements involving frontier-orbitals in the zero-order reference configuration for each space symmetry had rather high

values. Let us consider, for instance, the minimal basis set, with seven orbitals, used in the calculation of the ground-state of the BeH_2. In this case, the symmetry of the orbitals is: 1,2,3 are σ_g; 4,5 are σ_u and 6,7 are degenerate π_u. Since the reference configuration in the ground-state is $|1\bar{1}2\bar{2}4\bar{4}\rangle$. The generalized frontier-orbitals are: 2, 4, 3, 5, 6, 7, where 2 and 4 are occupied (**o**) and 3, 5, 6, 7 are empty (**e**). Elements of the type ${}^3\Delta_{\mathbf{o},\mathbf{e},\mathbf{o};\mathbf{o},\mathbf{e},\mathbf{o}}$ and ${}^3\Delta_{\mathbf{e},\mathbf{o},\mathbf{e};\mathbf{e},\mathbf{o},\mathbf{e}}$ are those which have to be evaluated. Since ${}^3\Delta$ is antisymmetric one has:

$$ {}^3\Delta_{\mathbf{e},\mathbf{o},\mathbf{e};\mathbf{o},\mathbf{e},\mathbf{e}} = -{}^3\Delta_{\mathbf{e},\mathbf{o},\mathbf{e};\mathbf{e},\mathbf{o},\mathbf{e}} \tag{32} $$

The approximating algorithm, which we are about to describe, was obtained by analysing the different terms which were summed up in Nakatsuji's algorithm [36, 56, 57]. This analysis showed that only one of the terms entering the algorithm had non-negligible value, and this term was of the type just described. The two formulae resulting from this analysis are:

$$ 3!\,{}^3\Delta_{\mathbf{o_1},\mathbf{e_1},\bar{\mathbf{o}}_\mathbf{2};\mathbf{e_2},\mathbf{o_3},\bar{\mathbf{o}}_\mathbf{4}} = -2!\,{}^2\Delta_{\mathbf{o_1},\bar{\mathbf{o}}_\mathbf{2};\mathbf{e_2},\bar{\mathbf{x}}}\,2!\,{}^2\Delta_{\bar{e}_1,\bar{x};o_3,\bar{o}_4} \tag{33} $$

and

$$ 3!\,{}^3\Delta_{\mathbf{e_1},\mathbf{o_1},\bar{\mathbf{e}}_\mathbf{2};\mathbf{o_2},\mathbf{e_3},\bar{\mathbf{e}}_\mathbf{4}} = 2!\,{}^2\Delta_{\mathbf{e_1},\bar{\mathbf{e}}_\mathbf{2};\mathbf{o_2},\bar{\mathbf{y}}}\,2!\,{}^2\Delta_{\mathbf{o_1},\bar{\mathbf{y}};\mathbf{e_3},\bar{\mathbf{e}}_\mathbf{4}} \tag{34} $$

where *x*/*y* is an empty/occupied frontier orbital. When, due to symmetry reasons, the product is null, the index *x*/*y* to be selected should be the next empty/occupied frontier orbital.

5 The 2-RDM Purification Procedure

In 1956 McWeeny [58] proposed an algorithm in order to purify the 1-RDM. In this context, the term purification means correcting those *N*-representability defects that a RDM may present. In this sense, the corrections applied to the 2-RDM in [21, 24, 32] as well as those mentioned above can be considered as RDM's purification operations. In [53] Mazziotti proposed to apply a far more elaborated method for imposing that both the 2-RDM and the 2-HRDM be positive semidefinite (D and Q *N*-representability conditions) while keeping fixed a given initial 1-RDM. By applying his procedure to the 2-RDM obtained at each 2-CSE iteration, the accuracy of the results was significantly improved. Alcoba and Valdemoro [55] and later on Alcoba [38] proposed two purification procedures which, although different in their approach, they both succesfully succeded in imposing upon the 2-RDM not only the D and Q *N*-representability conditions but also the G-condition either in a direct or indirect manner. The requisite for the 2-RDM to be *S*-representable was manisfest in several ways; in particular, when calculating the expectation value of the $\hat{S}^2$, using the 2-RDM resulting from the 2-CSE iterative solution, the error was far from negligible. The idea was therefore to study how to impose simultaneously

the S-representability and the D-, Q- and G-conditions as well as the traces and different contractions of the 2-RDM and of the $\mathscr{G}$-matrix spin-components. In order to impose the spin-conditons, we focused on imposing the positive semidefiniteness to the $\mathscr{G}$-matrix by acting upon its spin-components.

At present, two different strategies may be followed in order to build up a 2-RDM purification procedure. In the singlet-state case both strategies led to a computationally very effective purification procedure. Here, we will only describe the basic and general ideas of both approaches and refer the interested reader to [55] and [38], where a detailed account of each of these procedures is respectively given. Although the 2-RDM purification procedure for a doublet-state is being completed [59] and that of the triplet-states has already been initiated, we will only specifically refer here to the two procedures for purifying a singlet 2-RDM.

The Basic Ideas underlying the Purification Procedures

The first requirement in the two purification approaches is that we have a good, ensemble N-representable 1-RDM which will be considered fixed during the the purification process of the approximate 2-RDM from which this 1-RDM is derived.

In view of equations (12) and (13), it is clear that, if the 2-RDM is not N-representable this must be due to the correlation matrix $\mathscr{G}$. The central role played by this matrix is also due to its spin properties determining the 2-RDM S-representability. Moreover, the $\mathscr{G}$-matrix is one of the matrices which must be rendered positive semidefinite in the 2-RDM purification process. Consequently, the strategy which is at the base of one of our purification procedures is to look directly for corrections on the 2-RDM, the 2-HRDM and the $\mathscr{G}$-matrix. These three matrices' corrections should be consistent among themselves. Moreover, these three matrices' contractions should generate the 1-RDM which is kept fixed. Also, the properties of the $\mathscr{G}$-matrix spin-components as well as their inter-relations must be those of a pure singlet state. The second 2-RDM purification strategy is based in the unitarily invariant decomposition of a second-order tensor. This 2-RDM decomposition, which was reported by Coleman [60], offers the possibility of correcting the two-body part of a tensor without modifying its 0- and 1-body parts. This decomposition is at the base of the 2-RDM purification procedure reported by Mazziotti [53]. This approach is effective when imposing the D- and Q-conditions, but it is not appropriate for imposing the $\mathscr{G}$- and S-conditions because two of the $\mathscr{G}$-matrix physically well defined contractions are not natural tensor contractions; while two of its tensor contractions involve two creators and two annihilators, which do not have any physical meaning. Alcoba [61] proposed a generalization of the Coleman's second-order invariant decomposition, which permitted its application not only to the $\mathscr{G}$-matrix but also to its spin-components.

The approaches just sketched led to very efficient purification codes in the singlet case but, since the results shown in Section 6 have been obtained with the procedure based on the the 2-RDM decomposition reported in (12,13), in what follows we will only describe the main features of this purification method.

Our purification procedure is subdivided into two closely inter-related parts: in one of these parts the 2-RDM and the 2-HRDM are simulataneously rendered positive semidefinite (D- and Q-conditions) and in the other part the $\mathscr{G}$-matrix spin-components are rendered positive or negative semidefinite according to each of the spin-component properties.

5.1 First Part of the 2-RDM Purification Procedure: Imposing the D- and Q-Representability Conditions

The 2-HRDM can be obtained by combining relations (6), (14) and (16). Let us start by diagonalizing both the 2-RDM and the 2-HRDM. Most of the eigenvalues of these matrices will be positive, but usually both these two matrices will initally have some negative eigenvalues. Let us denote the eigenvalues of the 2-RDM/2-HRDM by λ/γ, which correspond to eigenvectors **x/y** respectively. In the new matrices, the negative eigenvalues will be replaced by zero. Thus, the new matrices take the form

$$ {}^2\mathrm{D}^{(1)}_{i,j;k,l} = \sum_p \lambda_p \langle ij|x_p\rangle\langle x_p|kl\rangle \tag{35} $$

and

$$ {}^2\bar{\mathrm{D}}^{(1)}_{i,j;k,l} = \sum_q \gamma_q \langle ij|y_q\rangle\langle y_q|kl\rangle \tag{36} $$

where p/q label only positive eigenvalues.

Recalling now that the correlation matrix $\mathscr{G}$ is a common two-body part of both the 2-RDM and the 2-HRDM the new $\mathscr{G}^{(1)}$ may be approximated as

$$ \mathscr{G}^{(1)}_{i,k;l,j} = \mathscr{C}^{(0)}_{i,k;l,j} + \frac{1}{2}\left(\varepsilon_{i,j;k,l} + \bar{\varepsilon}_{i,j;k.l}\right) \tag{37} $$

where $\varepsilon, \bar{\varepsilon}$ are the 2-RDM and 2-HRDM errors respectively.

5.2 Second Part of the 2-RDM Purification Procedure: Imposing the S- and G-Representability Conditions

In 2005, Alcoba and Valdemoro [55] reported the general formulae describing the spin-structure and properties of the $\mathscr{G}$-matrix. These formulae, when applied to the singlet case, provide a set of relations linking the elements of the different spin-components. The derivation of these relations, which will be given now, will be omitted here, but the interested reader may find all the relevant details in [55] and in [38].

Basic Properties of the G Spin-Components

According to relations (11) and (13), when the state Φ is a singlet, the spin quantum numbers of the states Φ' can only be $S' = 0, M'_s = 0$ and $S' = 1$ with $M'_s = 0, 1, -1$. The $\mathscr{G}$-matrix may therefore be written in terms of its spin-components, which are denoted as ${}_{\{S',M'_s\}}\mathscr{G}$. Thus,

$$\begin{array}{l} \mathscr{G}_{i,l;k,j} = {}_{\{0,0\}}\mathscr{G}_{i,l;k,j} + {}_{\{1,0\}}\mathscr{G}_{i,l;k,j} \\ \mathscr{G}_{i,l;\bar{k},\bar{j}} = {}_{\{0,0\}}\mathscr{G}_{i,l;\bar{k},\bar{j}} + {}_{\{1,0\}}\mathscr{G}_{i,l;\bar{k},\bar{j}} \\ \mathscr{G}_{i,\bar{l};k,\bar{j}} = {}_{\{1,-1\}}\mathscr{G}_{i,\bar{l};k,\bar{j}} \end{array} \tag{38}$$

It can be shown [38, 55] that in the singlet case all the spin-components matrix elements can be determined as a function of the ${}_{\{1,-1\}}\mathscr{G}_{\alpha,\beta;\alpha,\beta}$ elements and, in some cases, as a function also of the 1-RDM.

The relations which permit to determine the spin-components in terms of the initial $\mathscr{G}$-matrix are:

$${}_{\{0,0\}}\mathscr{G}_{i,k;\bar{l},\bar{j}} = \mathscr{G}_{i,k;\bar{l},\bar{j}} + \frac{1}{2}\left({}^1\mathrm{D}_{i;l}\,{}^1\bar{\mathrm{D}}_{\bar{j};\bar{k}} - \mathscr{G}_{i,l;\bar{k},\bar{j}}\right) \tag{39}$$

and

$${}_{\{1,0\}}\mathscr{G}_{i,k;\bar{l},\bar{j}} = \frac{1}{2}\left(\mathscr{G}_{i,l;\bar{k},\bar{j}} - {}^1\mathrm{D}_{i;l}\,{}^1\bar{\mathrm{D}}_{\bar{j};\bar{k}}\right) \tag{40}$$

And, conversely, once the $\mathscr{G}$ spin-components have been corrected, the new $\mathscr{G}$-matrix may be obtained according to the relations

$$\mathscr{G}_{i,k;\bar{l},\bar{j}} = -\frac{2}{3}\left({}^1\mathrm{D}_{i;k}\,{}^1\bar{\mathrm{D}}_{\bar{j};\bar{l}} + {}^1\mathrm{D}_{i;l}\,{}^1\bar{\mathrm{D}}_{\bar{j};\bar{k}} - 2\,{}_{\{0,0\}}\mathscr{G}_{i,k;\bar{l},\bar{j}} - {}_{\{0,0\}}\mathscr{G}_{i,l;\bar{k},\bar{j}}\right) \tag{41}$$

and

$$\mathscr{G}_{i,k;\bar{l},\bar{j}} = \frac{1}{2}\left({}^1\mathrm{D}_{i;k}\,{}^1\bar{\mathrm{D}}_{\bar{j};\bar{l}} + {}^1\mathrm{D}_{j;l}\,{}^1\bar{\mathrm{D}}_{\bar{i};\bar{k}}\right) + {}_{\{1,0\}}\mathscr{G}_{i,l;\bar{k},\bar{j}} + {}_{\{1,0\}}\mathscr{G}_{j,k;\bar{l},\bar{i}} \tag{42}$$

These relations show that the 1-RDM is directly connected with the $\mathscr{G}$ spin-components. Indeed, the 1-RDM may be obtained by contracting different spin-components. Thus, it can be shown that:

$$\sum_j {}_{\{0,0\}}\mathscr{G}_{j,k;\bar{j},\bar{i}} = \frac{N}{4}\left(\delta_{i,k} - {}^1\mathrm{D}_{\bar{i};\bar{k}}\right) + \left({}^1\mathrm{D} - {}^1\mathrm{D}^2\right)_{\bar{i};\bar{k}} \tag{43}$$

$$\sum_j {}_{\{0,0\}}\mathscr{G}_{i,j;\bar{k},\bar{j}} = \frac{(2\,K - N)}{4}\,{}^1\mathrm{D}_{i;k} + \left({}^1\mathrm{D} - {}^1\mathrm{D}^2\right)_{i;k} \tag{44}$$

$$\sum_j {}_{\{1,0\}}\mathscr{G}_{i,j;\bar{k},\bar{j}} = -\frac{(2K - N)}{4}\,{}^1\mathrm{D}_{i;k} \tag{45}$$

$$\sum_j {}_{\{1,0\}}\mathscr{G}_{j,k;\bar{j},\bar{l}} = -\frac{N}{4}\left(\delta_{i,k} - {}^1\mathrm{D}_{\bar{i},\bar{k}}\right) \tag{46}$$

Consequently, the traces are:

$$\sum_{i,j} {}_{\{0,0\}}\mathscr{G}_{i,j;\bar{i},\bar{j}} = \frac{N}{8}\,(2K-N+4) - \sum_i \left({}^1\mathrm{D}^2\right)_{i,i} \tag{47}$$

$$\sum_{i,j} {}_{\{1,0\}}\mathscr{G}_{i,j;\bar{i},\bar{j}} = -\frac{N}{8}\,(2K-N) \tag{48}$$

In this procedure the different spin-components are corrected sequentially.

1. The ${}_{\{0,0\}}\mathscr{G}$ spin-component.
   The $\mathscr{G}^{(1)}_{\alpha,\alpha;\beta,\beta}$ is built up from the matrix $\mathscr{C}^{(1)}_{\alpha,\beta;\alpha,\beta}$ determined in part I.

$$\mathscr{G}^{(1)}_{i,k;\bar{l},\bar{j}} = \mathscr{C}^{(1)}_{i,\bar{j};k,\bar{l}} \tag{49}$$

   and then, the ${}_{\{0,0\}}\mathscr{G}^{(1)}_{\alpha,\alpha;\beta,\beta}$ is obtained through relation

$${}_{\{0,0\}}\mathscr{G}^{(1)}_{i,k;\bar{l},\bar{j}} = \mathscr{G}^{(1)}_{i,k;\bar{l},\bar{j}} + \frac{1}{2}\,({}^1\mathrm{D}_{i;l}\,{}^1\bar{\mathrm{D}}_{\bar{j};\bar{k}} - \mathscr{G}^{(1)}_{i,l;\bar{k},\bar{j}}) \tag{50}$$

   This matrix is rendered positive semidefinite by eliminating the negative eigenvalues and renormalizing the new resulting matrix. The renormalizing factor has to be such that the trace has the value:

$$\frac{N}{8}\,(2\,K - N + 4) - \sum_i \left({}^1\mathrm{D}^2\right)_{i;i} \tag{51}$$

   Let us mention here that the contractions of the spin-components into the one-electron space are functionals of the 1-RDM. At convergence of the procedure all these contractions yield the same 1-RDM which is fixed. However, they yield different matrices until convergence is attained. In view of this, we decided to use the different forms of the 1-RDM, in the intermediate steps in the following form: we denote ${}^1\underline{\mathrm{D}}^p$, ${}^1\underline{\mathrm{D}}^q$, ${}^1\underline{\mathrm{D}}^r$ and ${}^1\underline{\mathrm{D}}^s$ the 1-RDM derived from equations (43–46) respectively. Then one obtains a new $\mathscr{G}^{(2)}$ using equation (41) in the following way:

$$\mathscr{G}^{(2)}_{i,k;\bar{l},\bar{j}} = -\frac{2}{3}\,({}^1\mathrm{D}^p{}_{i;k}\,{}^1\bar{\mathrm{D}}^q_{\bar{j};\bar{l}} + {}^1\mathrm{D}^p{}_{i;l}\,{}^1\bar{\mathrm{D}}^q_{\bar{j};\bar{k}} - 2\;{}_{\{0,0\}}\mathscr{G}_{i,k;\bar{l},\bar{j}} - {}_{\{0,0\}}\mathscr{G}_{i,l;\bar{k},\bar{j}}) \tag{52}$$

   Clearly, at convergence ${}^1\underline{\mathrm{D}}^p = {}^1\underline{\mathrm{D}}^q = {}^1\underline{\mathrm{D}}$.
2. The ${}_{\{1,0\}}\mathscr{G}$ spin-component.
   Here, the arguments are similar to those applied for the $\{0,0\}$ spin-component, but the relations to be used are (40), (45) and (46).

In this case, however, the matrix ${}_{\{1,0\}}\mathscr{G} \leq 0$ and must be renormalized so as to have

$$\sum_{i,j} {}_{\{1,0\}}\mathscr{G}_{i,j;\bar{i},\bar{j}} = -\frac{N}{8}(2K-N) \tag{53}$$

also the form of equation (42) used at this point is

$$\mathscr{G}^{(3)}_{i,k;\bar{l},\bar{j}} = \frac{1}{2}\left({}^1\mathrm{D}^r_{i;k}\,{}^1\bar{\mathrm{D}}^s_{\bar{j};\bar{l}} + {}^1\mathrm{D}^r_{j;l}\,{}^1\bar{\mathrm{D}}^s_{\bar{i};\bar{k}}\right) + {}_{\{1,0\}}\mathscr{G}_{i,l;\bar{k},\bar{j}} + {}_{\{1,0\}}\mathscr{G}_{j,k;\bar{l},\bar{i}} \tag{54}$$

Clearly, at convergence ${}^1\underline{\mathrm{D}}^r = {}^1\underline{\mathrm{D}}^s = {}^1\underline{\mathrm{D}}$.

Once we have the new form of $\mathscr{G}^{(3)}$, it is transformed into the corresponding $\mathscr{C}^{(3)}$ which generates a new 2-RDM and 2-HRDM and a new iteration starts again.

In order to verify the degree of convergence attained, the following tests are carried out:

- The RMS deviation with respect to the ${}^1\underline{\mathrm{D}}$ of the ${}^1\underline{\mathrm{D}}^p$, ${}^1\underline{\mathrm{D}}^q$, ${}^1\underline{\mathrm{D}}^r$ and ${}^1\underline{\mathrm{D}}^s$ is calculated.
- The larger negative/positive eigenvalue of each of the matrices which had to be diagonalized and rendered positive/negative semidefinite is calculated at each iteration. The homogenous convergence of these values towards zero is verified.

In all the cases studied this procedure was very effective and only a few iterations were necessary for attaining convergence.

6 The Second-Order Antihermitian Contracted Schrödinger Equation

In the 2-CSE compact form reported in Sect. 3, equation (20), the Hamiltonian operator acts on the left of the density operator

$$\hat{\Gamma}_{i_\sigma\, j_{\sigma'}\, k_\sigma\, l_{\sigma'}} \equiv i^\dagger_\sigma\, j^\dagger_{\sigma'}\, l_{\sigma'}\, k_\sigma \tag{55}$$

but the Hamiltonian may also operate on the right of $\hat{\Gamma}$ and when considering the difference of these two forms of the 2-CSE one obtains the second-order hypervirial condition first deduced by Hirschfelder [62] in the early 1960s. This condition was extensively discussed in the context of variational methods by Epstein [63], Aslangul et al. [64, 65], Harriman [66], Kutzelnigg [67] and Fernández and Castro [68]. Although its usefulness is obvious, its sufficiency for ensuring its solution for being in one to one correspondence with those of the Schrödinger equation was not – to our knowledge – established. In second-quantization this equation is identical to the contracted Liouville equation reported by Valdemoro [20]. Very recently, Mazziotti has identified this equation with the Antihermitian form of the 2-CSE, which this author denoted 2-ACSE [39]. The interesting feature of this equation is that

the fourth-order terms appearing in equations (23–25) disappear, which renders the equation much simpler. Many authors realized the importance of this equation but no practical way for solving it while avoiding the explicit use of the N-electron wavefunctions was available until very recently, when Mazziotti proposed to introduce a variational parameter into the method. The iterative method for solving the 2-ACSE given by Mazziotti [39, 69] can be described in a compact form by the formula:

$$\langle \Phi | [\hat{S}, \hat{\Gamma}]_{-} | \Phi \rangle = 0 \tag{56}$$

where

$$\hat{S} = \sum_{i,j,k,l} \langle \Phi | \, [\, \hat{\Gamma}_{i,j;k,l}, \, \hat{H} \,]_{-} \, | \Phi \rangle \, \hat{\Gamma}_{i,j;k,l} \tag{57}$$

When this equation is not satisfied the error is a function of the 2-RDM error, which permits to correct the 2-RDM from which the 3-RDM is derived and both matrices enter as data in the new iteration for computing the operator $\hat{S}$.

Another advantage of this approach is that the 2-RDM is much closer, at each iteration, to be N-representable than the 2-RDM resulting from the 2-CSE. In practice, a purification procedure is not only unnecessary in this case but, in fact, it hampers the process. On the other hand, an important shortcoming of this method is that, due to its variational character it cannot be applied in the study of excited states of a given symmetry.

An important question which has not yet been settled is whether the variational optimization introduced by Mazziotti is sufficient to guarantee that the 2-ACSE's solution coincides with that of the Schrödinger equation. This question arises from the fact that Nakatsuji's theorem, enunciated in Section 3, has not been shown to be applicable to the 2-ACSE. Indeed, as will now be shown, to satisfy the hypervirial theorem does not imply, by itself, an exact solution.

Relations which Condition the 2-CSE and the 2-ACSE to be Satisfied

In an analysis recently carried out by Valdemoro et al. [40] it was shown that

$$\langle \Phi | [\hat{H}, \hat{\Gamma}]_{-} | \Phi \rangle \; = \; 0 = {}^{(4;2,2)}_{r}\Theta \; - \; {}^{(4;2,2)}_{l}\Theta \tag{58}$$

where

$${}^{(4;2,2)}_{r}\Theta = \sum_{\Phi' \neq \Phi} \langle \Phi | \, \hat{\Gamma} \, | \Phi' \rangle \, \langle \Phi' | \, \hat{H} \, | \Phi \rangle \tag{59}$$

and

$${}^{(4;2,2)}_{l}\Theta_{pq;rs} \equiv \sum_{\Phi' \neq \Phi} \langle \Phi | \, \hat{H} \, | \Phi' \rangle \, \langle \Phi' | \, \hat{\Gamma} \, | \Phi \rangle \tag{60}$$

Now, the terms ${}^{(4;2,2)}_{r}\Theta$ and ${}^{(4;2,2)}_{l}\Theta$ involve high-order correlation energy effects. Either of these terms cancel out *iff* the state Φ is an eigenstate of the Hamiltonian;

or, equivalently, *iff* the 2-CSE is satisfied [70]. The hypervirial being satisfied only implies that these two high-order correlation matrix energy terms are equal, which does not however imply that each of the Θ separately vanishes.

In spite of this reservation, the solution method proposed by Mazziotti, probably due to its variational nature, gives very satisfactory results, as will be reported in the following section.

7 Performance of the Iterative 2-CSE and 2-ACSE Methods

In order to show the performance of the iterative 2-CSE and 2-ACSE methods we report now a set of results obtained in the study of the ground-state of two molecules: the linear BeH_2 and the Li_2. For the sake of comparison, in all the cases the Hartree-Fock, (HF), and the FCI calculations are also shown.

1. The BeH_2 molecule.
   In this calculation we used a minimal basis set of HF orbitals. Figures 1 and 2 present the rate of convergence of the ground state energy with respect to the number of iterations at equilibrium geometry. In one case the energy has been calculated with the 2-CSE algorithm, whereas in the other case the 2-ACSE one has been used. As can be appreciated when comparing with the FCI value, the error is in the fourth decimal.

   In Fig. 3 the performance in the calculation of the potential energy curve describing the symmetric stretching of the Be-H bonds is shown, as well as the HF and FCI corresponding curves. Here, both the 2-CSE and the 2-ACSE

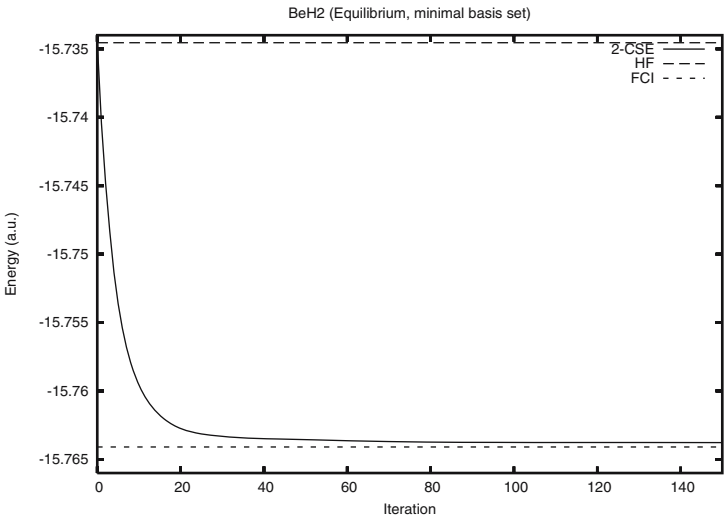

Fig. 1 Convergence of the 2-CSE iterative process for BeH_2

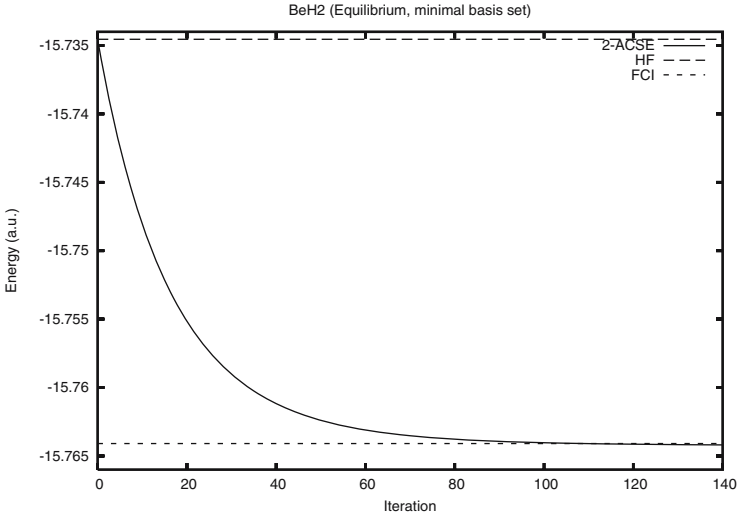

Fig. 2 Convergence of the 2-ACSE iterative process for BeH_2

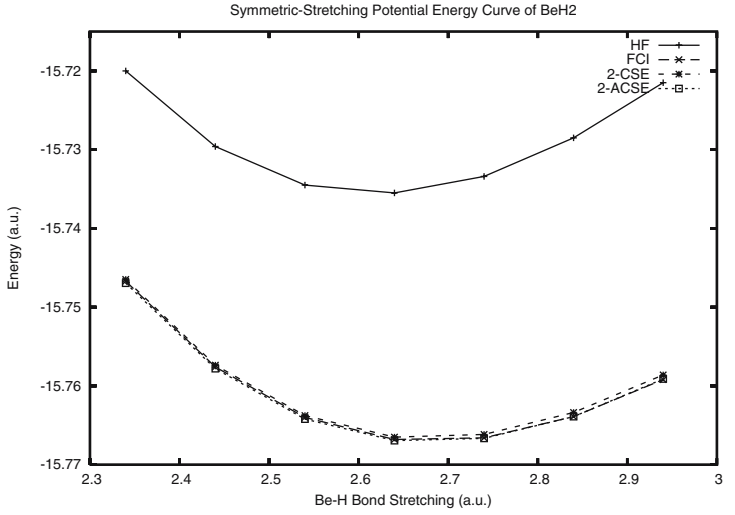

Fig. 3 Comparison of different approximations for the symmetric stretching of linear BeH_2

methods perform equally well. A slight separation from the FCI curve appears for bond distances larger than 2.7 a.u., and this error is more noticeable in the 2-CSE method.

2. The Li_2 molecule.
   Here also, we used a minimal basis set of HF orbitals. In Figures 4 and 5 the rate of convergence of the energy with respect to the number of iterations is shown for the ground state at equilibrium geometry with CSE and ACSE algorithms. In

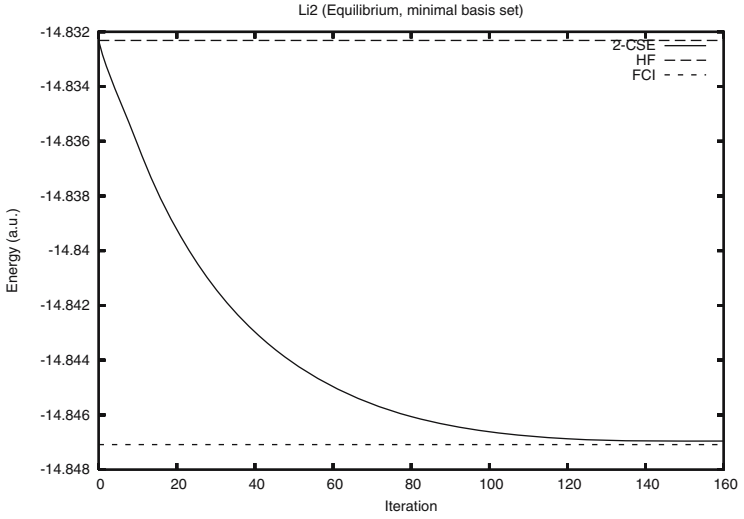

Fig. 4 Convergence of the 2-CSE iterative process for Li_2

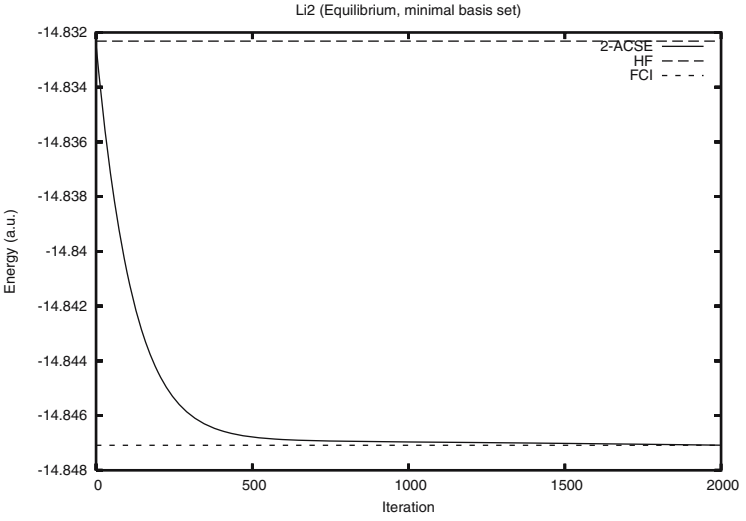

Fig. 5 Convergence of the 2-ACSE iterative process for Li_2

this case, the convergence is slower than in the calculation of the BeH_2 molecule; but the accuracy at convergence is also very high and of the same order as in the BeH_2 case.

In Figure 6 the results obtained in the calculation of the Li_2 dissociation energy curve are shown. The HF and FCI corresponding curves are also represented in this figure. In this case, although both methods perform well, the

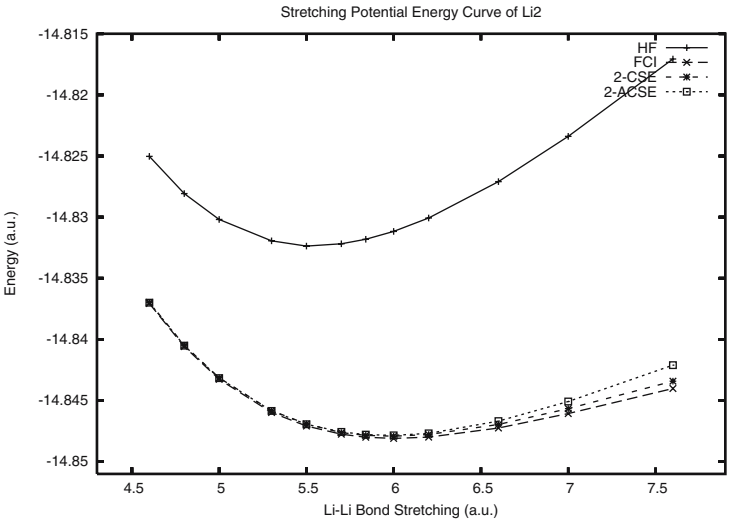

Fig. 6 Comparison of different approximations for the stretching of Li_2 bond

performance of the 2-CSE method at large internuclear distances is substantially better than that of the 2-ACSE.

The computational codes used are not optimized from an informatic point of view but, notwithstanding, they are very efficient. Thus, the results reported above have been rapidly obtained in a standard tabletop PC. From the theoretical point of view, these computational codes are continuously being updated. Indeed, there is still research going on in order to improve the 3-RDM approximation algorithm which has been described in Section 3. In our opinion, a highly accurate approximation of the 3-body correlation effects is necessary in order to be able to study with high accuracy all kind of excited and transition states.

Acknowledgements This report has been financially supported by the Spanish Ministerio de Educación y Ciencia under project BFM2003-05133. D. R. Alcoba acknowledges the financial support obtained from the *Universidad de Buenos Aires* under project X-024 and *Consejo Nacional de Investigaciones Científicas y Técnicas, República Argentina* under project PIP No 5098/05.

References

1. "*Many-electron Densities and Reduced Density Matrices.*", edited by J. Cioslowski, Kluwer, Dordrecht (2000).
2. "*Reduced-Density-matrix Mechanics with Applications to Many-electron Atoms and Molecules.*", *Adv. Chem. Phys.* **134**, edited by D. A. Mazziotti, Wiley, New York (2007).
3. K. Husimi, "Some formal properties of the density matrix.", *Proc. Soc. Japan* **22**, 264–314 (1940).

4. P. O. Löwdin, "Quantum Theory of Many Particle Systems. I. Physical Interpretation by Means of Density Matrices, Natural Spin Orbitals, and Convergence Problems in the Method of Configuration Interaction.", *Phys. Rev.* **97**, 1474–1489 (1955).
5. R. U. Ayres, "Variational approach to the Many-body problem.", *Phys. Rev.* **111**, 1453–1460 (1958).
6. J. E. Mayer, "Electron correlation.", *Phys. Rev.* **100**, 1579–1586 (1955).
7. A. J. Coleman, "Structure of fermion density matrices.", *Rev. Mod. Phys.* **35**, 668–689 (1963).
8. A. J. Coleman and V. I. Yukalov, "*Reduced Density Matrices: Coulson's Challenge.*", Springer, New York (2000).
9. E. R. Davidson, "*Reduced Density Matrices in Quantum Chemistry.*", Academic, New York (1976).
10. "*Reduced Density Matrices with Applications to Physical and Chemical Systems.*", Queen's Papers on Pure and Applied Mathematics - No. 11, edited by A. J. Coleman and R. M. Erdahl, Queen's University, Kingston, Ontario (1968).
11. "*Reduced Density Matrices with Applications to Physical and Chemical Systems II.*", Queen's Papers on Pure and Applied Mathematics - No. 40, edited by R. M. Erdahl, Queen's University, Kingston, Ontario (1974).
12. "*Density Matrices and Density Functionals.*", Proceedings of the A. J. Coleman Symposium, Kingston, Ontario, 1985, edited by R. M. Erdahl and V. Smith, Reidel, Dordrecht (1987).
13. C. Garrod and J. K. Percus, "Reduction of N-particle variational problem.", *J. Math. Phys.* **5**, 1756–1776 (1964).
14. C. Garrod and M. Rosina, "Particle-hole matrix - Its connection with symmetries and collective features of ground state.", *J. Math. Phys* **10**, 1855–1861 (1975).
15. M. V. Mihailovic and M. Rosina, "Excitations as ground state variational parameters.", *Nucl. Phys. A* **130**, 386–400 (1969).
16. L. Cohen and C. Frishberg, "Hierarchy equations for reduced density matrices.", *Phys. Rev. A.* **13**, 927–930 (1976).
17. H. Nakatsuji, "Equation for direct determination of density matrix.", *Phys. Rev. A.* **14**, 41–50 (1976).
18. C. Valdemoro, "An alternative approach to the calculation of the Hamiltonian matrix elements.", *Anales de Física A* **79**, 98–99 (1983).
19. C. Valdemoro, "A new method for the calculation of the electronic properties of atoms and molecules.", *Anales de Física A* **79**, 106–111 (1983).
20. C. Valdemoro, "*Density Matrices and Density Functionals*". Proceedings of the A. J. Coleman Symposium, Kingston, Ontario, 1985, edited by R. M. Erdahl and V. Smith, Reidel, Dordrecht (1987), pp. 275–288.
21. C. Valdemoro, "Approximating the second-order reduced density-matrix in terms of the first-order one.", *Phys. Rev. A* **45**, 4462–4467 (1992).
22. F. Colmenero, C. Pérez del Valle and C. Valdemoro, "Approximating q-order reduced density-matrices in terms of lower-order ones. I. General relations.", *Phys. Rev. A* **47**, 971–978 (1993).
23. F. Colmenero and C. Valdemoro, "Approximating q-order reduced density-matrices in terms of lower-order ones. II. Applications.", *Phys. Rev. A* **47**, 979–985 (1993).
24. F. Colmenero and C. Valdemoro, "Self-consistent approximate solution of the second-order Contracted Schrödinger equation.", *Int. J. Quantum Chem.* **51**, 369–388 (1994).
25. H. Nakatsuji and K. Yasuda, "Direct determination of the quantum-mechanical density matrix using the density equation.", *Phys. Rev. Letts.* **76**, 1039–1042 (1996).
26. K. Yasuda and H. Nakatsuji, "Direct determination of the quantum-mechanical density matrix using the density equation2.", *Phys. Rev. A* **56**, 2648–2657 (1997).
27. M. Nakata, M. Ehara, K. Yasuda and H. Nakatsuji, "Direct determination of second-order density matrix using density equation: Open-shell system and excited state.", *J. Chem. Phys.* **112**, 8772–8778 (2000).
28. D. A. Mazziotti, "Contracted Schrödinger equation: Determining quantum energies and two-particle density matrices without wave functions.", *Phys. Rev. A* **57**, 4219–4234 (1998).
29. D. A. Mazziotti, "Pursuit of N-representability for the contracted Schrödinger equation through density-matrix reconstruction.", *Phys. Rev. A* **60**, 3618–3626 (1999).

30. D. A. Mazziotti, "Variational method for solving the contracted Schrödinger equation through a projection of the N-particle power method onto the two-particle space.", *J. Chem. Phys.* **116**, 1239–1249 (2002).
31. J. M. Herbert and J. E. Harriman, "Contraction relations for Grassmann products of reduced density matrices and implications for density matrix reconstruction.", *Phys. Rev. A* **65**, 022511 (2002).
32. C. Valdemoro, L. M. Tel and E. Pérez-Romero, "The contracted Schrödinger equation: Some results.", *Adv. Quantum Chem.* **28**, 33–46 (1997).
33. C. Valdemoro, L. M. Tel, E. Pérez-Romero and A. Torre, "The iterative solution of the contracted Schrödinger equation: a new quantum chemical method.", *J. Mol. Struct. (Theochem)* **537**, 1–8 (2001).
34. D. R. Alcoba and C. Valdemoro, "Family of modified-contracted Schrödinger equations.", *Phys. Rev. A* **64**, 062105 (2001).
35. D. R. Alcoba, F. J. Casquero, L. M. Tel, E. Pérez-Romero and C. Valdemoro, "Convergence enhancement in the iterative solution of the second-order contracted Schrödinger equation.", *Int. J. Quantum Chem.* **102**, 620–628 (2005).
36. C. Valdemoro, L. M. Tel and E. Pérez-Romero, *"Many-electron Densities and Reduced Density Matrices*", edited by J. Cioslowski, Kluwer, Dordrecht (2000), pp. 117–137.
37. C. Valdemoro in "*Reduced-Density-matrix Mechanics with Applications to Many-electron Atoms and Molecules.*", *Adv. Chem. Phys.* **134**, edited by D.A. Mazziotti, Wiley, New York (2007), pp. 121–164.
38. D. R. Alcoba in "*Reduced-Density-matrix Mechanics with Applications to Many-electron Atoms and Molecules.*", *Adv. Chem. Phys.* **134**, edited by D.A. Mazziotti, Wiley, New York (2007), pp. 202–259.
39. D. A. Mazziotti, "Anti-Hermitian contracted Schrödinger equation: Direct determination of the two-electron reduced density matrices of many-electron molecules.", *Phys. Rev. Lett.* **97**, 143002 (2006).
40. C. Valdemoro, L. M. Tel, E. Pérez-Romero and D. R. Alcoba, "Four new forms of the Contracted Schrödinger equation and their connection with the second-order Hypervirial condition.", *Int. J. Quantum Chem.* **108**, 1090–1096 (2008).
41. C. Valdemoro, L. M. Tel, D. R. Alcoba and E. Pérez-Romero, "The contracted Schrödinger equation methodology: Study of the third-order correlation effects.", *Theor. Chem. Acc.* **118**, 503–509 (2007).
42. F. Bopp, "Ableitung der Bindungsenergie von Nteilchensystemen aus 2teilchendichtematrizen.", *Z. Phys.* **156**, 348–359 (1959).
43. A. J. Coleman and I. Absar, "Reduced Hamiltonian orbitals. III. Unitarily invariant decomposition of hermitian operators.", *Int. J. Quantum Chem.* **18**, 1279–1307 (1980).
44. C. Valdemoro, "Spin-adapted Reduced Hamiltonian. I: Elementary excitations.", *Phys. Rev. A* **31**, 2114–2122 (1985).
45. C. Valdemoro, "Spin-adapted Reduced Hamiltonian. II: Total energy and reduced density matrices.", *Phys. Rev. A* **31**, 2123–2128 (1985).
46. C. Valdemoro, M. P. de Lara-Castells, E. Pérez-Romero and L. M. Tel, "The first order contracted density equations: Correlation effects.", *Adv. Quantum Chem.* **31**, 37–52 (1999).
47. C. Valdemoro, L. M. Tel, D. R. Alcoba, E. Pérez-Romero and F. J. Casquero, "Some basic properties of the correlation matrices.", *Int. J. Quantum Chem.* **90**, 1555–1561 (2002).
48. R. Kubo, "Generalized cumulant expansion method.", *J. Phys. Soc. Jpn.* **17**, 1100–1120 (1962).
49. W. Kutzelnigg and D. Mukherjee, "Cumulant expansion of the reduced density matrices.", *J. Chem. Phys.* **110**, 2800–2809 (1999).
50. D. A. Mazziotti, "Approximate solution for electron correlation through the use of Schwinger probes.", *Chem. Phys. Lett.* **289**, 419–427 (1998).
51. E. Pérez-Romero, L. M. Tel and C. Valdemoro, "Traces of spin-adapted reduced density matrices.", *Int. J. Quantum Chem.* **61**, 55–61 (1997).
52. C. Valdemoro, L. M. Tel and E. Pérez-Romero, "N-representability problem within the framework of the contracted Schrödinger equation", *Phys. Rev. A* **61**, 032507 (2000).

53. D. A. Mazziotti, "Purification of correlated reduced density matrices.", *Phys. Rev. E* **65**, 026704 (2002).
54. C. Valdemoro, D. R. Alcoba, and L. M. Tel, "Recent developments in the contracted Schrödinger equation method: Controlling the N-representability of the second-order reduced density matrix.", *Int. J. Quantum Chem.* **93**, 212–222 (2003).
55. D. R. Alcoba and C. Valdemoro, "Spin structure and properties of the correlation matrices corresponding to pure spin states: Controlling the S-representability of these matrices.", *Int. J. Quantum Chem.* **102**, 629–644 (2005).
56. C. Valdemoro, *Topics in Current Chemistry: Correlation and Localization.*, edited by P. R. Surjan, Springer, (1999), pp. 187–200.
57. C. Valdemoro, L. M. Tel and E. Pérez-Romero, "*Quantum Systems in Chemistry and Physics I*", edited by A. Hernández-Laguna, J. Maruani, R. McWeeny and S. Wilson, Kluwer, Dordrecht, Netherlands (2000), pp. 3–16.
58. R. McWeeny, "The density matrix in self-consistent field theory. I. Iterative construction of the density matrix.", *Proc. Roy. Soc. A* **235**, 496–509 (1956).
59. D. R. Alcoba, C. Valdemoro, L. M. Tel and E. Pérez-Romero, "Controlling the *N*- and *S*-representability of the second-order Reduced Density Matrix: The Doublet-states case.", *submitted for publication*.
60. A. J. Coleman, "*Reduced Density Matrices with Applications to Physical and Chemical Systems II.*", Queen's Papers on Pure and Applied Mathematics - No. 40, edited by R. M. Erdahl, Queen's University, Kingston, Ontario (1974), pp. 2–8.
61. D. R. Alcoba, "Unitarily invariant decomposition of arbitrary hermitian matrices of physical interest.", *Int. J. Quantum Chem.* **97**, 776–783 (2004).
62. J. O. Hirschfelder, "Classical and quantum mechanical hypervirial theorems.", *J. Chem. Phys.* **33**, 1462–1466 (1960).
63. S. T. Epstein, "The Variational Method in Quantum Chemistry.", Academic, New York (1974).
64. C. Aslangul, R. Constanciel, R. Daudel, L. Esnault and E. V. Ludeña, "The loge theory as a starting point for variational calculations. I. General formalism.", *Int. J. Quantum Chem.* **8**, 499–522 (1974).
65. L. Esnault, "*Application du Formalisme des Opérateurs Densité Réduits à la Recherche des Fonctions d'Onde Atomiques et Moléculaires.*", These Univ. Paris IV (1974).
66. J. E. Harriman, "Geometry of density matrices. V. Eigenstates.", *Phys. Rev. A* **30**, 19–29 (1984).
67. W. Kutzelnigg, "Generalized k-particle Brillouin conditions and their use for the construction of correlated electronic wavefunctions.", *Chem. Phys. Lett.* **64**, 383–387 (1979).
68. F. M. Fernández, E. A. Castro, "Hypervirial theorems and restrictions on wavefunctions.", *Theoret. Chim. Acta (Berl.),* **59**, 87–89 (1981).
69. D. A. Mazziotti, "Anti-Hermitian part of the contracted Schrödinger equation for the direct calculation of two-electron reduced density matrices.", *Phys. Rev. A* **75**, 022505 (2007).
70. D. R. Alcoba, "Equivalence theorems between the solutions of the fourth-order modified contracted Schrödinger equation and those of the Schrödinger equation.", *Phys. Rev. A* **65**, 032519 (2002).

Molecular Energy Decompositions in the Hilbert-Space of Atomic Orbitals at Correlated Level

Diego R. Alcoba, Roberto C. Bochicchio(✉), Luis Lain, and Alicia Torre

Abstract This work describes a new model to partition the molecular energy into one- and two-center contributions in the Hilbert-space of atomic orbitals at correlated level. Our proposal makes explicit use of the pairing nature of chemical bonding phenomena to accommodate appropriately the correlation effects within these contributions. The model is based on the treatment of the kinetic energy as contributing to both one- and two-atom terms, according to the pairing or unpairing character of the electron cloud, and on the appropriate assignment of the density cumulant dependent contributions. Numerical results for selected systems are reported and compared with those arising from other models, showing the reliability of our predictions.

Keywords: molecular energy, partition, Hilbert space, paired density, unpaired density, cumulants

1 Introduction

The energy decomposition of a molecular system attempts to describe how the energy is distributed into its components [1, 2]. There are mainly two groups of methods to perform this task. Within a first group the atoms are defined by means

D.R. Alcoba
Departamento de Física, Facultad de Ciencias Exactas y Naturales, Universidad de Buenos Aires, Ciudad Universitaria, 1428, Buenos Aires, Argentina, e-mail: qfxaldad@ehu.es

R.C. Bochicchio
Departamento de Física, Facultad de Ciencias Exactas y Naturales, Universidad de Buenos Aires, Ciudad Universitaria, 1428, Buenos Aires, Argentina, e-mail: rboc@df.uba.ar

L. Lain, e-mail: qfplapel@ehu.es; A. Torre, e-mail: qfptogaa@ehu.es
Departamento de Química Física. Facultad de Ciencias. Universidad del País Vasco. Apdo. 644 E-48080 Bilbao, Spain

S. Wilson et al. (eds.) *Frontiers in Quantum Systems in Chemistry and Physics*.

of the one-electron basis functions centered at the nuclei; these methods constitute the techniques of partitioning in the Hilbert-space of atomic orbitals [3,4]. A second type of methodology is based on the partitioning of the three dimensional physical space (3D), where an atom is defined as a nucleus surrounded by a surface. This surface can also be defined in different ways, i.e., the "fuzzy" atom approach [5–8] uses atomic radii and "cutoff" parameters to partition the whole 3D physical space into atomic domains. Aternatively, the Bader's Atoms in Molecules (AIM) [9] and the Electron Localization Function (ELF) [10,11] models employ topological properties of the electron distribution to define these atomic domains.

Results of energy decompositions arising from both methodological schemes have been reported as at Hartree-Fock level [8,12,13] as at correlated one [2,14–16]. When we deal with correlated wave functions new terms associated with correlation effects appear. These terms must be appropriately examined and interpreted to obtain both numerically reliable and physically feasible results, as was reported in our previous population analysis studies [17–19]. In this work, we will use the quantum theory of chemical bonding as a guide for the treatment of the terms arising from the electronic correlation effects. The central idea we follow in this treatment is based on the universally admitted pairing nature of bonding phenomena, i.e., the electrons are paired in bonds and the non-pairing electrons are located only at atomic regions that are not involved in bondings. It indicates the energy decomposition must fulfill the same criteria as the chemical indicators for the bond orders [17], i.e., no energy terms arising from the non-pairing part of our tools may contribute to two-center terms related to bonding energies but only to one-center ones. This approach makes that this partitioning be adjusted to physical arguments.

In the present attempt to perform an energy partitioning scheme in the Hilbert-space of atomic orbitals with correlated wave functions, we split the kinetic energy term into one- and two-center contributions. Likewise, we also make explicit use of the cumulant of the second-order reduced density matrix (2-RDM), separating its contributions to the energy into appropriate terms. In previous works [2] the criterion to discriminate between atomic and bonding contributions has been to associate orbitals belonging to identical or different centers with one- or two-center contributions, respectively. However, in this work we follow physical criteria in the treatment of this problem, so that the model described here is based on two key ideas as follows. On the one side we decompose the first-order reduced density matrix [20] (1-RDM) into its *effectively paired* and *effectively unpaired* parts [21–23] and thus the kinetic energy becomes naturally splitted into one- and two-center contributions. The paired part of the 1-RDM provides kinetic energy contributions to one- and two-center terms while the unpaired part only contributes to the one-center energies because, as the chemical bonding theory states, this unpaired part is not involved in bond formation. On the other hand, the cumulant of the 2-RDM, that describes the statistically irreducible many-body effects, is of non-pairing nature [16, 17, 21, 24] and hence it cannot be involved in the formulation of the two-center or bonding terms. These considerations provide a physical foundation to previous heuristically proposed cumulant treatments [2]. Our modifications of the traditional partitioning schemes in the Hilbert-space of atomic orbitals have led us to accurate results

that fulfill all the properties usually required to consider the corresponding energy partitioning is applicable to chemical problems.

The article is organized as follows. Section 2 presents the details of the energy decomposition model into one- and two-center terms according to the above mentioned physical arguments for closed and open shell systems. Section 3 is devoted to the computational aspects of the calculations performed over a selected set of molecules; it also reports a comparison with other numerical results and the corresponding discussion. Section 4 is dedicated to the final remarks and conclusions.

2 Energy Decomposition Scheme for Correlated State Functions

The total energy for an N-electron molecular system, in the Born-Oppenheimer approximation, expressed in an atomic orbital (AO) basis set, $\{\mu,\nu,\lambda\ldots\}$, is given by

$$E_{total} = \sum_{A<B} \frac{Z_A Z_B}{R_{AB}} + \sum_{\mu\nu} {}^1P_{\mu\nu}(\nu|h|\mu) + \sum_{\mu\nu\lambda\sigma} {}^2P_{\mu\nu\lambda\sigma}(\mu\nu|\lambda\sigma) \tag{1}$$

where $(\nu|h|\mu)$ stands for the matrix elements of the one-electron operator $h = T - \sum_{A=1}^{M} {}^AV$ and M the number of nuclei in the system. T is the kinetic energy operator $(-\frac{1}{2}\nabla_i^2)$ and ${}^AV = \frac{Z_A}{r_{iA}}$ is the electron-nucleus interaction energy operator between the electron i and the nucleus A having a charge Z_A; r_{iA} is the electron-nucleus distance. $(\mu\nu|\lambda\sigma)$ are the standard matrix elements of the two-electron repulsion energy in the convection $(11|22)$ and $\frac{Z_A Z_B}{R_{AB}}$ is the nucleus-nucleus repulsion energy with R_{AB} the distance between the nucleus A and B [25]. ${}^1P$, ${}^2P$ stand for the spin-free *one-particle* and *two-particle reduced density matrices* respectively, which may be expressed by

$${}^1P_{\mu\nu} = \sum_{i=1}^{K} n_i c_{\mu i}^* c_{\nu i} \tag{2}$$

where $\{c_{\mu i} : \mu = 1,\ldots,K\}$ and $\{n_i : i = 1,\ldots,K\}$ are the sets of expansion coefficients and occupation numbers for the natural orbitals (NO) in the AO basis set, respectively [25]. K is the size of the basis set, and

$${}^2P_{\mu\nu\lambda\sigma} = \frac{1}{2}\,{}^1P_{\mu\nu}\,{}^1P_{\lambda\sigma} - \frac{1}{4}\,{}^1P_{\mu\sigma}\,{}^1P_{\nu\lambda} + \frac{1}{2}\,\Lambda_{\mu\nu\lambda\sigma} \tag{3}$$

where the symbol $\Lambda_{\mu\nu\lambda\sigma}$ stands for the matrix elements of the cumulant of the second-order reduced density matrix [26,27]. Therefore Eq. (1) can be formulated as

$$E_{total} = \sum_{A<B} \frac{Z_A Z_B}{R_{AB}} + \sum_{\mu\nu} {}^1P_{\mu\nu}(\nu|T|\mu) - \sum_{A}\sum_{\mu\nu} {}^1P_{\mu\nu}(\nu|{}^AV|\mu)$$

$$+ \frac{1}{2}\sum_{\mu\nu}\sum_{\lambda\sigma}\left[{}^1P_{\mu\nu}\,{}^1P_{\lambda\sigma} - \frac{1}{2}\,{}^1P_{\mu\sigma}\,{}^1P_{\nu\lambda}\right](\mu\nu|\lambda\sigma) + \frac{1}{2}\sum_{\mu\nu\lambda\sigma}\Lambda_{\mu\nu\lambda\sigma}(\mu\nu|\lambda\sigma) \tag{4}$$

where $(\nu|T|\mu)$ and $(\nu|^A V|\mu)$ stand for the matrix elements of the kinetic energy and the nucleus-electron interactions, respectively. Equation (4) expresses the non-relativistic total molecular energy arising from a general wave function.

Let us point out the foundations of our energy decomposition model, namely, the assignments of the correlation effects within a partitioning scheme into one- and two-center contributions. Two main proposals are introduced that follow the physical ideas arising from bonding theory and differ from previous heuristically proposed partitioning schemes. These proposals are strongly supported by previous results from the local partitioning of electronic density into *effectively paired* and *effectively unpaired* contributions and from the nature of the cumulant of the 2-RDM, which are consequences of the spin and correlation effects in the molecule.

2.1 Closed Shell Case

The first of our proposals is that the one-particle charge and bond order density matrix may be split into two terms of well-defined nature

$$ {}^1P_{\mu\nu} = {}^1P^{(p)}_{\mu\nu} + {}^1P^{(u)}_{\mu\nu} \tag{5} $$

with

$$ {}^1P^{(p)}_{\mu\nu} = \frac{1}{2}\sum_{\sigma\lambda} {}^1P_{\mu\sigma} S_{\sigma\lambda} {}^1P_{\lambda\nu} \tag{6} $$

and

$$ {}^1P^{(u)}_{\mu\nu} = {}^1P_{\mu\nu} - {}^1P^{(p)}_{\mu\nu} \tag{7} $$

where ${}^1P^{(p)}$ and ${}^1P^{(u)}$ mean the *effectively paired* and *effectively unpaired* parts of the density, respectively [21, 23] and $S_{\sigma\lambda}$ stand for overlap matrix elements in the AO basis. This structure will allow us to split the kinetic energy into one- and two-center contributions according to the physical nature of each density part. The paired electron cloud described by ${}^1P^{(p)}$ is delocalized over the whole system while the unpaired electron cloud described by ${}^1P^{(u)}$ is localized only on the atomic regions not involved in bondings. Hence, we may follow that the first one contributes to both atomic and bonding energies while the latter one only contributes to the atomic regions in which the unpaired electrons are localized [21].

The foundation of our second proposal is that, as it has been shown in previous works, the density cumulant does not contribute to bondings due to its unpaired electron nature [21]. Hence, we propose that its contributions will only be considered as part of the one-center energy terms. These two features define on physical grounds the considerations to take into account for the decomposition scheme into one- and two-center energy contributions. Let us now give the expressions of these ideas into the mathematical framework of Eq. (4).

The kinetic energy from the second r.h.s. term of Eq. (4) yields

$$\sum_{\mu\nu} {}^1P_{\mu\nu}(\nu|T|\mu) = \sum_{\mu\nu} {}^1P^{(p)}_{\mu\nu}(\nu|T|\mu) + \sum_{\mu\nu} {}^1P^{(u)}_{\mu\nu}(\nu|T|\mu) \tag{8}$$

and therefore each contribution of one-center or two-center type is given by

$$T_A = \sum_{\mu\in A}\sum_{\nu\in A} {}^1P^{(p)}_{\mu\nu}(\nu|T|\mu) + \sum_{\mu\in A}\sum_{\nu} {}^1P^{(u)}_{\mu\nu}(\nu|T|\mu) \tag{9}$$

or

$$T_{AB} = 2\sum_{\mu\in A}\sum_{\nu\in B} {}^1P^{(p)}_{\mu\nu}(\nu|T|\mu) \tag{10}$$

respectively.

The treatment of the density cumulant arising from the last r.h.s. term of Eq. (4) leads to one-center contributions as

$$\frac{1}{2}\sum_{\mu\in A}\sum_{\nu\lambda\sigma} \Lambda_{\mu\nu\lambda\sigma}(\mu\nu|\lambda\sigma) \tag{11}$$

because, as has been aforementioned, this term is not involved in bondings due to its non-pairing nature. It is important to note that the effectively unpaired part of the density arises from the contraction of the density cumulant into the one-electron space and consequently both quantities share this non-pairing character [24].

All these considerations lead us to write the energy decomposition in terms of one- and two-center contributions as

$$E_{total} = \sum_A E_A + \sum_{A<B} E_{AB} \tag{12}$$

with

$$E_A = \sum_{\mu\in A}\sum_{\nu\in A} {}^1P^{(p)}_{\mu\nu}(\nu|T|\mu) + \sum_{\mu\in A}\sum_{\nu} {}^1P^{(u)}_{\mu\nu}(\nu|T|\mu) - \sum_{\mu\in A}\sum_{\nu} {}^1P_{\mu\nu}(\nu|{}^AV|\mu)$$

$$+ \sum_{\mu\in A}\sum_{\lambda\in A}\sum_{\nu\sigma}\left(\frac{1}{2}{}^1P_{\mu\nu}{}^1P_{\lambda\sigma} - \frac{1}{4}{}^1P_{\mu\sigma}{}^1P_{\nu\lambda}\right)(\mu\nu|\lambda\sigma) + \frac{1}{2}\sum_{\mu\in A}\sum_{\nu\lambda\sigma}\Lambda_{\mu\nu\lambda\sigma}(\mu\nu|\lambda\sigma) \tag{13}$$

and

$$E_{AB} = \frac{Z_AZ_B}{R_{AB}} + 2\sum_{\mu\in A}\sum_{\nu\in B} {}^1P^{(p)}_{\mu\nu}(\nu|T|\mu) - \sum_{\mu\in A}\sum_{\nu} {}^1P_{\mu\nu}(\nu|{}^BV|\mu) - \sum_{\mu\in B}\sum_{\nu} {}^1P_{\mu\nu}(\nu|{}^AV|\mu)$$

$$+ 2\sum_{\mu\in A}\sum_{\lambda\in B}\sum_{\nu\sigma}\left(\frac{1}{2}{}^1P_{\mu\nu}{}^1P_{\lambda\sigma} - \frac{1}{4}{}^1P_{\mu\sigma}{}^1P_{\nu\lambda}\right)(\mu\nu|\lambda\sigma) \tag{14}$$

Eqs. (13) and (14) fulfill all the above discussed physical requirements and thus they represent a true energy partitioning scheme. Although in these equations the density cumulant contributions are assigned to one-center terms, correlation effects are also present in two-center ones through ${}^1P$, which arises from a correlated wave function. We must point out that the proposed partitioning has a general character, i.e. Eqs. (12)–(14) are applicable to any level of theory: correlated level [perturbative methods (MPn), couple-cluster (CC), self-consistent multiconfigurational (MCSCF) and configuration interaction (CI) among others] and uncorrelated restricted Hartree-Fock [self-consistent field (SCF)] one. In this latter case the terms $\sum_{\mu\in A}\sum_{\nu}{}^1P^{(u)}_{\mu\nu}(\nu|T|\mu)$ and $\frac{1}{2}\sum_{\mu\in A}\sum_{\nu\lambda\sigma}\Lambda_{\mu\nu\lambda\sigma}(\mu\nu|\lambda\sigma)$ in Eq. (13) vanish identically.

The above equations provide the molecular energy *exactly* as a sum of one- and two-center energy components through the appropriate management of the density cumulant for closed shell systems.

2.2 Open Shell Case

The above proposals need to be modified for open shell systems due to spin effects arising from the pairing and non-pairing terms of the one-particle charge and bond order density matrix as well as from the cumulant of the two-particle reduced density matrix. Therefore Eqs. (6) reads

$$ {}^1P^{(p)}_{\mu\nu} = \frac{1}{2}\sum_{\sigma\lambda}({}^1P_{\mu\sigma}S_{\sigma\lambda}{}^1P_{\lambda\nu} + {}^1P^{(s)}_{\mu\sigma}S_{\sigma\lambda}{}^1P^{(s)}_{\lambda\nu}) \tag{15} $$

where ${}^1P^{(s)}$ stands for the spin density matrix, ${}^1P^{(u)}$ remains defined by Eq. (7) and the cumulant may be expressed explicitely by its contributions as

$$ \Lambda_{\mu\nu\lambda\sigma} = \Delta_{\mu\nu\lambda\sigma} - \frac{1}{2}{}^1P^{(s)}_{\mu\sigma}{}^1P^{(s)}_{\nu\lambda} \tag{16} $$

where Δ is the many-body cumulant contribution and the last term in the r.h.s. of Eq. (16) stands for the spin density exchange term. It may be noted that the spin density appears as the new element in the theory as expected. Hence the energy contributions of Eq. (12) are

$$ \begin{aligned} E_A = &\sum_{\mu\in A}\sum_{\nu\in A}{}^1P^{(p)}_{\mu\nu}(\nu|T|\mu) + \sum_{\mu\in A}\sum_{\nu}{}^1P^{(u)}_{\mu\nu}(\nu|T|\mu) - \sum_{\mu\in A}\sum_{\nu}{}^1P_{\mu\nu}(\nu|{}^AV|\mu) \\ &+ \sum_{\mu\in A}\sum_{\lambda\in A}\sum_{\nu\sigma}(\frac{1}{2}{}^1P_{\mu\nu}{}^1P_{\lambda\sigma} - \frac{1}{4}{}^1P_{\mu\sigma}{}^1P_{\nu\lambda} - \frac{1}{4}{}^1P^{(s)}_{\mu\sigma}{}^1P^{(s)}_{\nu\lambda})(\mu\nu|\lambda\sigma) \\ &+ \frac{1}{2}\sum_{\mu\in A}\sum_{\nu\lambda\sigma}\Delta_{\mu\nu\lambda\sigma}(\mu\nu|\lambda\sigma) \end{aligned} \tag{17} $$

and

$$E_{AB} = \frac{Z_A Z_B}{R_{AB}} + 2\sum_{\mu\in A}\sum_{\nu\in B} {}^1P^{(p)}_{\mu\nu}(\nu|T|\mu) - \sum_{\mu\in A}\sum_{\nu} {}^1P_{\mu\nu}(\nu|{}^BV|\mu) - \sum_{\mu\in B}\sum_{\nu} {}^1P_{\mu\nu}(\nu|{}^AV|\mu)$$
$$+2\sum_{\mu\in A}\sum_{\lambda\in B}\sum_{\nu\sigma}\left(\frac{1}{2}{}^1P_{\mu\nu}{}^1P_{\lambda\sigma} - \frac{1}{4}{}^1P_{\mu\sigma}{}^1P_{\nu\lambda} - \frac{1}{4}{}^1P^{(s)}_{\mu\sigma}{}^1P^{(s)}_{\nu\lambda}\right)(\mu\nu|\lambda\sigma) \qquad (18)$$

In the present case we have considered the spin exchange term as contributing to both one-center and two-center terms because of its pairing nature. The remaining spin and correlation effects considered into the cumulant density only contribute to one-center terms.

In the next section we report numerical results derived from these equations. These results are compared with those arising from a previously reported model by Vyboishchikov and Salvador [2] (VS) of molecular energy partitioning in the Hilbert space in which the density cumulant is also explicitly used.

3 Computational Details, Numerical Results and Discussion

Our calculations have been carried out at restricted Hartree-Fock (RHF) and restricted open shell Hartree-Fock (ROHF) levels of SCF and at configuration interaction with single and double excitations (CISD) wave functions, using the 6-31G basis sets. The correlated 1-RDMs and 2-RDMs in the AO basis sets were calculated from the version 3.2 of the PSI package [28]. The computational implementation of our partitionings requires the calculation of the one-electron integrals $(\nu|T|\mu)$ and $(\nu|{}^AV|\mu)$ as well as the two-electron ones $(\mu\nu|\lambda\sigma)$. All these integrals have been computed using a modified version of GAMESS program [24]. For all systems experimental geometries have been used [30].

Table 1 gathers results obtained at RHF-SCF and CISD levels for simple systems (H_2), hydrocarbons with different bond multiplicities (CH_4, C_2H_6, C_2H_4, and C_2H_2) and some second-row hydrides (NH_3, H_2O and HF) all of them in the singlet ground state. This set has been chosen to show covalent bondings with different polarity. The results reported in the fourth column correspond to the RHF-SCF level while those reported in column five arise from the model for the energy decompositon by the authors of this work (ABLT) at CISD approximation. For the sake of comparison, we collect, in columns six and seven, the results at CISD level from the above mentioned energy partitioning models VS(M1) and VS(M2) of Ref. [2], which have been calculated with our own codes. At the RHF-SCF approach both VS(M1) and VS(M2) models and ABLT model are coincident for singlet states. Although it is not obvious to establish a simple correspondence between the dissociation energies and the two-center results derived from the energy partitionings proposed in this work and in other reported treatments [2,8,31], we have included in column eight the experimental values [30] in order to take into account a reference. As can be observed in the Table, the two-center energies for classical bonds show

Table 1 Energy partitioning in the Hilbert space of atomic orbitals for several molecular systems at RHF-SCF and CISD levels, using the 6-31G basis sets. All energies are expressed in atomic units

System	Fragment	Bond	E_{RHF}	E^{a}_{ABLT}	$E^{b}_{VS(M1)}$	$E^{b,c}_{VS(M2)}$	E^{d}_{exp}
H_2	H		−0.4706	−0.4908	−0.4922		
		HH	−0.1855	−0.1702	−0.1673	−0.1826	−0.1661
CH_4	C		−37.6504	−37.7449	−37.7377		
	H		−0.4558	−0.4737	−0.4765		
		CH	−0.2035	−0.1881	−0.1841	−0.1981	−0.1657
		$H...H$	0.0176	0.0162	0.0142	0.0161	
$C_2H_6(D_{3d})$	C		−37.6326	−37.7266	−37.7148		
	H		−0.4580	−0.4731	−0.4771		
		CC	−0.1809	−0.1777	−0.1778	−0.1980	−0.1402
		CH	−0.1964	−0.1831	−0.1761	−0.1927	−0.1562
		$C...H$	0.0036	−0.0044	0.0003	0.0042	
		$H...H$ (CH_3)	0.0184	0.0171	0.0145	0.0169	
		$H...H^{e}$	0.0066	0.0059	0.0061	0.0059	
		$H...H^{f}$	0.0012	0.0004	0.0005	0.0004	
C_2H_4	C		−37.5835	−37.6984	−37.6622		
	H		−0.4550	−0.4670	−0.4758		
		CC	−0.3030	−0.2782	−0.3099	−0.3292	−0.2741
		CH	−0.2011	−0.1858	−0.1814	−0.1950	−0.1721
		$C...H$	0.0081	0.0092	0.0042	0.0087	
		$H...H$ (CH_2)	0.0192	0.0183	0.0165	0.0182	
		$H...H^{g}$	0.0078	0.0072	0.0075	0.0072	
		$H...H^{h}$	0.0021	0.0003	0.0002	0.0003	
C_2H_2	C		−37.4163	−37.5784	−37.5087		
	H		−0.4113	−0.4151	−0.4510		
		CC	−0.7263	−0.6211	−0.7137	−0.7325	−0.3665
		CH	−0.1614	−0.1553	−0.1493	−0.1588	−0.1992
		$C...H$	−0.0506	−0.0337	−0.0272	−0.0350	
		$H...H$	0.01330	0.0085	0.0087	0.0085	
NH_3	N		−54.2866	−54.4123	−54.3993		
	H		−0.4162	−0.4346	−0.4396		
		NH	−0.2545	−0.2314	−0.2295	−0.2389	−0.1753
		$H...H$	0.0459	0.0416	0.0404	0.0413	
H_2O	O		−74.8071	−74.9403	−74.9304		
	H		−0.3824	−0.4002	−0.4061		
		OH	−0.2418	−0.2192	−0.2180	−0.2242	−0.1896
		$H...H$	0.0715	0.0651	0.0645	0.0648	
HF	F		−99.4590	−99.5842	−99.5802		
	H		−0.3444	−0.3624	−0.3683		
		HF	−0.1800	−0.1637	−0.1619	−0.1659	−0.2166

[a] Model reported in this work (ABLT) at CISD level.
[b] Models 1 and 2 of Vyboishchikov and Salvador (VS) (Ref. [2]) at CISD level.
[c] Atomic energy formulas are unavailable from the authors in Ref. [2].
[d] Experimental energies.
[e] Closer H atoms in different CH_3 groups.
[f] More distant H atoms in different CH_3 groups.
[g] Closer H atoms in different CH_2 groups.
[h] More distant H atoms in different CH_2 groups.

negative values while they are positive or slightly negative for non-bonded atoms in all reported treatments.

The differences between the ABLT model proposed in this work and the mentioned VS(M1) and VS(M2) models are two-fold. The first one is related with the decomposition of the kinetic energy terms. The ABLT and both VS models split this term into one- and two-center contributions. The VS models associate with one-center terms the contributions arising from kinetic energy with two AO indices centered at the same nucleus. Likewise, these models assign the contributions with two indices each centered at a different nucleus to two-center terms, so that [2]

$$\sum_{\mu\nu} {}^1P_{\mu\nu}(\nu|T|\mu) = \sum_A \sum_{\substack{\mu\in A \\ \nu\in A}} {}^1P_{\mu\nu}(\nu|T|\mu) + 2\sum_{A<B} \sum_{\substack{\mu\in A \\ \nu\in B}} {}^1P_{\mu\nu}(\nu|T|\mu) \tag{19}$$

However, the ABLT model splits the kinetic energy by means of Eqs. (9) and (10), according to the physical character of each part of the electronic density, i.e., the effectively paired density contributes to both one- and two-center terms, while the effectively unpaired part only causes atomic energies, as has been explained above.

The second difference is the treatment of the cumulant term. The VS(M1) model splits this term in the same manner as the kinetic energy one, i.e., into one- and two-center contributions according to the atomic localization of some orbitals, such as [2]

$$\frac{1}{2}\sum_{\mu\nu\lambda\sigma} \Lambda_{\mu\nu\lambda\sigma}(\mu\nu|\lambda\sigma) = \frac{1}{2}\sum_A \sum_{\substack{\mu\in A \\ \nu\in A}} \sum_{\lambda\sigma} \Lambda_{\mu\nu\lambda\sigma}(\mu\nu|\lambda\sigma) + \sum_{A<B} \sum_{\substack{\mu\in A \\ \nu\in B}} \sum_{\lambda\sigma} \Lambda_{\mu\nu\lambda\sigma}(\mu\nu|\lambda\sigma) \tag{20}$$

The VS(M2) model neglects the two-center cumulant contributions (cf. text just below Eq. (11) of Ref. [2]) proposed in the VS(M1) one and therefore it cannot provide neither a complete description of correlation effects nor the exact total energy. However, our model shifts the cumulant terms into only one-center contributions according to Eq. (11), in agreement to the fact that this term is the origin of the effectively unpaired density matrix [24] and does not contribute to form bondings as has been shown in Refs. [17, 21, 22].

Both ABLT and VS(M1) models predict similar results for all systems with single bonds but interesting differences appear in the C_2H_4 and C_2H_2 systems, which possess multiple bonds. These diferences lie between 0.03–0.09 a.u. for carbon atoms and *CC* bonds while they are even greater for VS(M2) model. These systems reflect the correlation effects throughout these strong bonds as expected, and this allows one to note the differences between the ABLT model and both VS models; the atomic energies are similar while the *CC* energies are notably different, i.e., the VS energies are close to RHF-SCF ones while those arising from the ABLT model are closer to experimental energies. In relation with the energies of the bonds $C-C$, all the approaches fulfill the tendency of the series C_2H_6, C_2H_4 and C_2H_2, according to the multiplicity of the bond.

Table 2 shows the results for systems in open-shell states, in order to discuss the capability of our partitioning model to describe such situations. To carry out this task

Table 2 Energy partitioning in the Hilbert space of atomic orbitals for several systems in open-shell states at levels ROHF-SCF and CISD, using the 6-31G basis sets. All energies are expressed in atomic units

System	Fragment	Bond	E_{ROHF}	E^{a}_{ABLT}	$E^{b}_{VS(M1)}$	$E^{b,c}_{VS(M2)}$	E^{d}_{exp}
O_2	O		−74.6018	−74.7613	−74.7350		
(triplet)		OO	−0.3243	−0.2517	−0.3043	−0.2987	−0.1898
CH_3	C		−37.6127	−37.7051	−37.6947		
(doublet)	H		−0.4563	−0.4738	−0.4761		
		CH	−0.2070	−0.1881	−0.1869	−0.2002	−0.1753
		HH	0.0197	0.0176	0.0151	0.0175	
CH_2	C		−37.6238	−37.6974	−37.6823		
(triplet)	H		−0.4485	−0.4655	−0.4697		
		CH	−0.2028	−0.1848	−0.1870	−0.1968	−0.1625
		$H...H$	0.0202	0.0190	0.0169	0.0189	

[a] Model reported in this work (ABLT) at CISD level.
[b] Models 1 and 2 of Vyboishchikov and Salvador (VS) (Ref. [2]) at CISD level.
[c] Atomic energy formulas are unavailable from the authors in Ref. [2].
[d] Experimental energies.

we must indicate that our model and both VS(M1) and VS(M2) models are coincident at ROHF-SCF level. At correlated level the cumulant splits into a many-body term (first term in the r.h.s. of Eq. (16)) describing the effectively unpaired electron effects due to the electron correlation and a term related with the spin contributions (second term in the r.h.s of Eq. (16)). Therefore our model differs from VS(M1) and VS(M2) in the same way as for the closed shell case, i.e., the many-body effects are collected only in atomic sites while in the present case spin effects from exchange terms (cf. Eq. (16)) are considered as contributing to both one-center and two-center terms due to its pairing nature. Numerical calculations have been performed for the O_2 and CH_2 systems in triplet states and for the CH_3 radical in doublet state within the ABLT, VS(M1) and VS(M2) models at ROHF and CISD levels of approximation. Both schemes lead to values which are different numerically and conceptually. To discuss these numerical results we will focus attention on the calculated bonding energies and the experimental ones. In the case of the O_2 molecule, the results for both schemes of partitioning (ABLT and both VS models) at ROHF and CISD levels are lower than the experimental value. Physically it may be interpreted as strongly bounded electrons as expected experimentally. The differences between the correlated values from both VS models and the ROHF value are small, while ABLT model shows a clear trend of its value towards the experimental one. This different behaviour is due to the management of the unpairing effects coming from the kinetic energy of the effectively unpaired electrons cloud and from the many-body cumulant density, confirming that the kinetic energy terms may be divided into both one-center and two-center contributions and the contributions from the many-body cumulant density may not be assigned to two-center terms. For both CH_2 and CH_3 radicals the correlated values are close to the experimental energies in both schemes indicating that the many-body effects are less important than in the O_2 molecule.

4 Concluding Remarks

In conclusion, this work presents a new model for the decomposition of the energy of molecular systems, at correlated level, in the Hilbert space of atomic orbitals for both closed and open shell systems. This decomposition produces chemically meaningful atomic and bonding energy terms. The partitioning scheme is based on the concepts of effectively paired and unpaired electron contributions to the first-order density matrix and on the non-bonding nature of the density cumulant. Although the results turn out to be comparable with those obtained in previously reported heuristic methods for simple systems, our method provides the incorporation of physical ideas for the assignment of contributions to atomic and bonding energies and leads to better results for systems in which the correlation and/or spin effects are important. It may be noted that the present work constitutes the first attempt – from a computational point of view – of partitioning the molecular energy for open shell systems.

Acknowledgements This report has been financially supported by Projects X-024 (Universidad de Buenos Aires), PIP No. 5098/05 (Consejo Nacional de Investigaciones Científicas y Ténicas, República Argentina), the Spanish Ministry of Education (Grant No. CTQ2006-01849) and the Universidad del Pais Vasco (Grant No. GIU06/03). We thank the Universidad del Pais Vasco for allocation of computational resources.

References

1. Mayer, I.: Energy partitioning schemes: A dilemma. Faraday Discuss. **135**, 439–450 (2007) and references therein
2. Vyboishchikov, S. F., Salvador, P.: Ab initio energy partitioning at the correlated level. Chem. Phys. Lett. **430**, 204–209 (2006) and references therein
3. Mulliken, R. S.: Electronic population analysis on LCAO MO molecular wave functions. I. J. Chem. Phys. **23**, 1833–1840 (1955)
4. Mulliken, R. S.: Criteria for the construction of good self-consistent-field molecular orbital wave functions, and the significance of LCAO-MO population analysis. J. Chem. Phys. **36**, 3428–3439 (1962)
5. Hirshfeld, F. L.: Bonded-atom fragments for describing molecular charge densities. Theor. Chim. Acta **44**, 129–138 (1977)
6. Davidson, E. R., Chakravorty, S.: A test of the Hirshfeld definition of atomic charges and moments. Theor. Chim. Acta **83**, 319–330 (1992)
7. Becke, A. D.: A multicenter numerical integration scheme for polyatomic molecules. J. Chem. Phys. **88**, 2547–2553 (1988)
8. Salvador, P., Mayer, I.: Energy partitioning for "fuzzy" atoms. J. Chem. Phys. **120**, 5046–5052 (2004)
9. Bader, R. F. W.: *Atoms in Molecules: A Quantum Theory* (Clarendon Press: Oxford, 1994) and references therein.
10. Becke, A. D., Edgecombe, K. E.: A simple measure of electron localization in atomic and molecular systems. J. Chem. Phys. **92**, 5397–5403 (1990)
11. Poater, J., Duran, M., Sola, M., Silvi, B.: Theoretical evaluation of electron delocalization in Aromatic Molecules by Means of Atoms in Molecules (AIM) and Electron Localization

Function (ELF) topological approaches. Chem. Rev. **105**, 3911–3947 (2005) and references therein
12. Alcoba, D. R., Lain, L., Torre, A., Bochicchio, R. C.: Energy decompositions according to physical space partitioning schemes. J. Chem. Phys. **122**, 074102-1-6 (2005) and references therein
13. Alcoba, D. R., Lain, L., Torre, A., Bochicchio, R. C.: Treatment of non-nuclear attractors within the theory of atoms in molecules II: energy decompositions. Chem. Phys. Lett. **426**, 426–430 (2006)
14. Imamura, Y., Takahashi, A., Nakai, H.: Grid-based energy density analysis: Implementation and assessment. J. Chem. Phys. **126**, 034103-1-10 (2007)
15. Salvador, P., Mayer, I.: One- and two-center physical space partitioning of the energy in the density functional theory. J. Chem. Phys. **126**, 234113-1-10 (2007)
16. Alcoba, D. R., Torre, A., Lain, L., Bochicchio, R. C.: Energy decompositions according to physical space partitioning schemes: treatments of the density cumulant. J. Chem. Phys. **426**, 104110-1-6 (2007)
17. Bochicchio, R. C., Lain, L., Torre, A.: On the definition of bond order at correlated level. Chem. Phys. Lett. **374**, 567–571 (2003)
18. Bochicchio, R. C., Lain, L., Torre, A.: Atomic valence in molecular systems. Chem. Phys. Lett. **375**, 45–53 (2003)
19. Torre, A., Alcoba, D. R., Lain, L., Bochicchio, R. C: Determination of three-center bond indices from population analyses: A fuzzy atom treatment. J. Phys. Chem. A **109**, 6587–6591 (2005)
20. Davidson, E. R.: *Reduced Density Matrices in Quantum Chemistry*, 1st. edn. Academic: New York, 1976) and references therein.
21. Lobayan, R. M., Bochicchio, R. C., Lain, L., Torre, A.: Electron density topology in molecular systems: paired and unpaired densities. J. Chem. Phys. **123**, 144116-1-9 (2005)
22. Lobayan, R. M., Bochicchio, R. C., Lain, L., Torre, A.: Laplacian field of the effectively unpaired electron density: Determination of many-body effects on electron distributions. J. Phys. Chem. A **111**, 3166–3172 (2007)
23. Alcoba, D. R., Bochicchio, R. C., Lain, L., Torre, A.: On the definition of the effectively unpaired electron density matrix: A similarity measure approach. Chem. Phys. Lett. **429**, 286–288 (2006)
24. Lain, L., Torre, A., Bochicchio, R. C., Ponec, R.: On the density matrix of effectively unpaired electrons. Chem. Phys. Lett. **346**, 283–287 (2001)
25. Szabo, A., Ostlund, N. S.: *Modern Quantum Chemistry*, 2nd. edn. (McGraw-Hill: New York, 1989)
26. Kutzelnigg, W., Mukherjee, D.: Irreducible Brillouin conditions and contracted Schrödinger equations for n-electron systems. II. Spin-free formulation. J. Chem. Phys. **116**, 4787–4801 (2002)
27. Lain, L., Torre, A., Bochicchio, R. C.: On the definition of spin-free cumulant of the second-order reduced density matrix. J. Chem. Phys. **117**, 5497–5498 (2002)
28. Crawford, T. D., Sherrill, C. D., Valeev, E. F., Fermann, J. T., King, R. A., Leininger, M. L., Brown, S. T., Janssen, C. L., Seidl, E. T., Kenny, J. P., Allen, W. D.: *PSI 3.2*, 2003.
29. Schmidt, M. W., Baldridge, K.K., Boate, J. A., Elbert, S. T., Gordon, M. S., Jensen, J. H., Koseki, S., Matsunaga, N., Nguyen, K. A., Su, S. S., Windus, T. L., Dupuis, M., Montgomery, J. A.: The general atomic and molecular electronic structure system. J. Comput. Chem. **14**, 1347–1363 (1993)
30. *Handbook of Chemistry and Physics*, 59th edn. (CRC: Cleveland, 1979)
31. Sierralta, A., Frenking, G.: Diatomic interaction energies in the topological theory of atoms in molecules. Theor. Chim. Acta **95**, 1–12 (1997)

Dirac-Coulomb Equation: Playing with Artifacts

Grzegorz Pestka, Mirosław Bylicki, and Jacek Karwowski(✉)

Abstract Recent developments based on the application of the Hylleraas-CI (Hy-CI) method to the variational solving the Dirac-Coulomb equation are reviewed. Three modes of the implementation of the Hy-CI method are discussed: a plain Hy-CI approach in which the effects related to the Brown-Ravenhall disease are treated by the appropriate selection of the model space, the Hy-CI approach combined with the complex coordinate rotation, in which these effects are controlled by the separation of the discrete and continuous spectra in the complex plane, and the positive-energy-space projected approach in which the influence of the effects of coupling with the continuum are removed by an appropriate restriction of the model space. Limits of applicability of these approaches as well as their advantages and disadvantages are discussed on the example of the ground states of helium isoelectronic series atoms.

Keywords: Dirac-Couloumb equation, complex coordinate rotation, variational methods, Hylleraas-CI method, continuum dissolution, Brown-Ravenhall disease, positive-energy-space projection

1 Introduction

The eigenvalue problem of the Dirac-Coulomb (DC) Hamiltonian has been a subject of many discussions and controversy, since Brown and Ravenhall noticed that the eigenvalues corresponding to the bound-state solutions are embedded in a continuum spreading from $-\infty$ to $+\infty$ and that the discrete and the continuum spectra are coupled by the electron-electron interaction [5]. For many years, different ways of dealing with this issue divided the community involved in solving

G. Pestka, M Bylicki, and J. Karwowski
Instytut Fizyki, Uniwersytet Mikołaja Kopernika, Grudziądzka 5, PL-87-100 Toruń, Poland, e-mail: gp@fizyka.umk.pl; mirekb@fizyka.umk.pl; jka@fizyka.umk.pl

S. Wilson et al. (eds.) *Frontiers in Quantum Systems in Chemistry and Physics*.

the problem to two groups. One of them claimed that the only legitimate approach has to be based on a projection of the DC Hamiltonian onto the positive-energy space (PES), i.e. the subspace composed of the positive-energy states [44–46]. According to the other group the projection is not necessary and securing the relations between the components of the wavefunction specific for the positive-energy bound states together with imposing the bound-state boundary conditions is sufficient [14–16, 19, 40]. Several years ago Grant and Quiney [15] wrote: *"It is commonly believed that variational methods cannot be used with Dirac-Coulomb operators (...). Computational problems experienced by many of those studying the matter between 1970 and 1980 were readily attributed to this fact (...) Sucher's warnings [45] were generally interpreted to mean that one should try to eliminate negative energy states by surrounding every operator by projection operators on to positive energy states. (...) Projection operators used in this way play no part in our formulation.*". Several years earlier Indelicato [20] reported: *"The necessity of using projection operators to avoid mixing of positive and negative energy Dirac eigenstates in multiconfiguration Dirac-Fock calculations is discussed. It is shown that convergence problems observed at high Z (...) are completely due to the absence of such projection operators in previous calculations*". From the formal point of view the bound states of a system described by a DC Hamiltonian are resonances. Thus, in the DC model the bound states are unstable and can autoionize. In a recent review Johnson, Cheng and Chen [21] wrote: *"The stability of atomic ground states is, of course, explained by the fact that the negative-energy sea is filled and that spontaneous pair production is prohibited by the Pauli exclusion principle. Here lies the real problem of the many-electron Dirac-Coulomb Hamiltonian: it has no provision to account for this fact (...) The standard cure is to use the no-pair Hamiltonian which excludes negative-energy states entirely*".

Johnson et al. in their review [21] state: *"It should be noted that errors in* E_{Dirac} *from incorrect treatments of electron-positron and positron-positron terms can be very subtle and* E_{Dirac} *may look perfectly normal (...) when negative-energy basis functions are also included. Nevertheless, it is very difficult, if not impossible, to identify and correct the intrinsic errors in* E_{Dirac} *and the use of many-electron Dirac Hamiltonian without the projection operators should be avoided (...)*". In order to record and to analyse these effects we used a very precise computational tool: the relativistic complex-coordinate rotated Hylleraas-CI (R-CCR-Hy-CI) method. Since in each of these two approaches the DC Hamiltonian is represented in a different model space, the results derived from them at the limit of a saturated variational basis, have to be different – the PES-projection removes all contributions from the virtual pairs. This difference has been estimated in a recent series of papers [6, 32, 33]. A similar analysis has also been performed by Watanabe et al. [48]. As one might expect [45], it is proportional to $(Z\alpha)^3$, i.e. it is of the same order as QED corrections.

The original idea of Sucher advocating the use of the free-particle projectors [17, 44], and other operator-based approaches, appeared to be either incorrect or infeasible [18, 19]. Therefore, in practical calculations the no-pair Hamiltonian is usually obtained by constraining the model space in which the DC Hamiltonian

is represented. To our knowledge, the trial functions of the variational methods based on the no-pair approximation were always constructed from one-electron spinors.[1] Thus, in these methods the no-pair model space is composed of antisymmetrized products of the Dirac spinors corresponding to the PES only. While the positive-energy spinors are relatively easy to identify, the procedure becomes less straightforward in the case of relativistic geminals. The construction of a no-pair approach within a non-orbital (R-CCR-Hy-CI) method has been presented in [6]. In this construction the complex coordinate rotation plays a crucial role: it makes the identification of the functions belonging to the positive energy space possible.

In the present paper the difficulties associated with the variational treatment of the DC eigenvalue problem within approaches utilizing geminal-containing trial functions are briefly reviewed. In particular, the recent developments on R-CCR-Hy-CI are summarised. In Sect. 2 some specific features of the one-electron Dirac variational problem essential for this discussion are presented. Then, in Sect. 2 the properties of the DC eigenvalue equation are discussed. In Sect. 3 the relativistic Hy-CI method is described. In Sect. 5 the idea of CCR is introduced and some illustrative examples are presented. The PES projected R-CCR-Hy-CI is described in Sect. 6. In a brief Sect. 7 the results derived from the non-projected methods are compared with the ones obtained using PES-projected approaches. The paper is concluded with final remarks. The Hartree atomic units are used and the energies are expressed in milihartree, unless otherwise stated. The fine structure constant has been taken as $\alpha = 1/137.0359895$.

2 Variational Approach to the Dirac Equation

The Dirac equation may be written as

$$\begin{bmatrix} (\mathsf{V}-E)\mathsf{I}_2, & c(\boldsymbol{\sigma}\cdot\mathbf{p}) \\ c(\boldsymbol{\sigma}\cdot\mathbf{p}), & (\mathsf{V}-E-2mc^2)\mathsf{I}_2 \end{bmatrix} \begin{bmatrix} \Psi^{\mathrm{l}} \\ \Psi^{\mathrm{s}} \end{bmatrix} = 0, \tag{1}$$

where Ψ^{l} and Ψ^{s} are two-component spinors, $\boldsymbol{\sigma}$ are 2×2 Pauli matrices, I_2 is a 2×2 unit matrix and the remaining symbols have their usual meaning. In the non-relativistic limit ($c\to\infty$) equation (1) transforms to the Lévy-Leblond equation:

$$\begin{bmatrix} (\mathsf{V}-E)\mathsf{I}_2, & (\boldsymbol{\sigma}\cdot\mathbf{p}) \\ (\boldsymbol{\sigma}\cdot\mathbf{p}), & -2m\mathsf{I}_2 \end{bmatrix} \begin{bmatrix} \Psi^{\mathrm{l}} \\ \Psi^{\mathrm{s}}_{\mathrm{L}} \end{bmatrix} = 0, \tag{2}$$

where

$$\Psi^{\mathrm{s}}_{\mathrm{L}} = \lim_{c\to\infty} c\Psi^{\mathrm{s}}. \tag{3}$$

From here one gets

$$\Psi^{\mathrm{s}}_{\mathrm{L}} = \frac{1}{2m}(\boldsymbol{\sigma}\cdot\mathbf{p})\,\Psi^{\mathrm{l}}. \tag{4}$$

[1] In the following, for briefness, the names *spinor* and *orbital* will be used for *one-electron Dirac spinor*. Similarly, by *orbital/non-orbital* method we understand a method in which the configuration state functions are constructed from orbitals/geminals.

The elimination of $\Psi_{\mathrm{L}}^{\mathrm{s}}$ from equation (2) results in the spin-dependent Schrödinger equation:

$$\left[\frac{(\sigma\cdot\mathbf{p})^2}{2m}+(\mathsf{V}-E)\mathsf{I}_2\right]\Psi^{\mathrm{l}}=0, \tag{5}$$

Since $(\sigma\cdot\mathbf{p})^2=\mathsf{p}^2\mathsf{I}_2$, we get two identical Schrödinger equations. Their solutions ψ correspond to two spinorbitals with spins α and β:

$$\Psi_\alpha^{\mathrm{l}}=\psi\begin{bmatrix}1\\0\end{bmatrix},\quad\text{and}\quad\Psi_\beta^{\mathrm{l}}=\psi\begin{bmatrix}0\\1\end{bmatrix}.$$

The spectrum of the one-electron Dirac Hamiltonian is composed of two continua: the upper (or the positive) one, Σ_{c}^{+}, spreading from 0 to $+\infty$ and the lower (or the negative) one, Σ_{c}^{-}, spreading from $-2mc^2$ to $-\infty$. The discrete (bound-state) energy levels are located in the energy gap below the lower threshold of Σ_{c}^{+}. A schematic diagram of this spectrum is shown in the left panel of Fig. 1.

The energy functional corresponding to the Dirac eigenvalue problem may be expressed as the appropriate Rayleigh quotient

$$K[\Phi]=\frac{\langle\Phi|\mathsf{H}|\Phi\rangle}{\langle\Phi|\Phi\rangle}, \tag{6}$$

where Φ is a trial function which may be expressed in the form:

$$\Phi=\begin{bmatrix}c_a\Phi^{\mathrm{l}}\\c_b\Phi^{\mathrm{s}}\end{bmatrix}.$$

After the elimination of c_a and c_b, the functional, expressed in terms of Φ_{l} and Φ_{s}, reads:

$$K_{\mathrm{D}}[\Phi]=W_{+}+\sqrt{W_{-}^2+2mc^2T}, \tag{7}$$

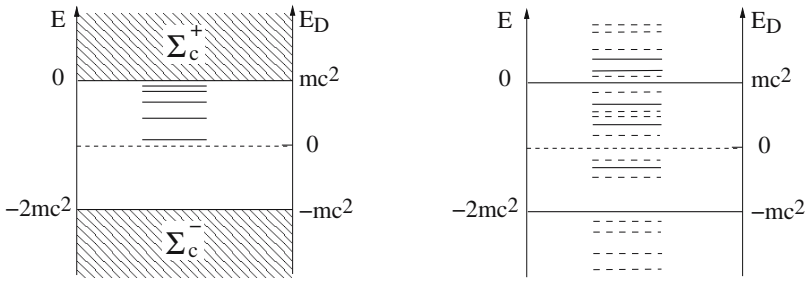

Fig. 1 The exact spectrum of a Dirac Hamiltonian (*left*). The same spectrum in the algebraic approximation is shown in the right panel. The solid lines correspond to the discrete energy levels and the broken ones represent the continua. In this example the algebraic representation does not reflect the structure of the real spectrum. The necessary conditions for a correct algebraic representation of the discrete part of the Dirac spectrum are described in the text

where

$$W_{\pm} = \frac{1}{2}\left(\frac{\langle \Phi^{\mathrm{l}}|\mathsf{V}|\Phi^{\mathrm{l}}\rangle}{\langle \Phi^{\mathrm{l}}|\Phi^{\mathrm{l}}\rangle} \pm \frac{\langle \Phi^{\mathrm{s}}|\mathsf{V}|\Phi^{\mathrm{s}}\rangle}{\langle \Phi^{\mathrm{s}}|\Phi^{\mathrm{s}}\rangle}\right) \mp mc^2, \tag{8}$$

and

$$T = \frac{1}{2m}\frac{\langle \Phi^{\mathrm{l}}|\sigma\cdot\mathbf{p}|\Phi^{\mathrm{s}}\rangle\langle \Phi^{\mathrm{s}}|\sigma\cdot\mathbf{p}|\Phi^{\mathrm{l}}\rangle}{\langle \Phi^{\mathrm{l}}|\Phi^{\mathrm{l}}\rangle\langle \Phi^{\mathrm{s}}|\Phi^{\mathrm{s}}\rangle}. \tag{9}$$

In the non-relativistic limit, as described by the Lévy-Leblond equation,

$$K_{\mathrm{L}}[\Phi] = T + \frac{\langle \Phi^{\mathrm{l}}|\mathsf{V}|\Phi^{\mathrm{l}}\rangle}{\langle \Phi^{\mathrm{l}}|\Phi^{\mathrm{l}}\rangle}. \tag{10}$$

The last equation should be equivalent to the one derived from the Schrödinger equation (5), i.e. to

$$K_{\mathrm{S}}[\Phi] = \frac{1}{2m}\frac{\langle \Phi^{\mathrm{l}}|(\sigma\cdot\mathbf{p})^2|\Phi^{\mathrm{l}}\rangle}{\langle \Phi^{\mathrm{l}}|\Phi^{\mathrm{l}}\rangle} + \frac{\langle \Phi^{\mathrm{l}}|\mathsf{V}|\Phi^{\mathrm{l}}\rangle}{\langle \Phi^{\mathrm{l}}|\Phi^{\mathrm{l}}\rangle}.$$

As one can easily see, this may be fulfilled only if

$$\Phi^{\mathrm{s}} \sim (\sigma\cdot\mathbf{p})\Phi^{\mathrm{l}}. \tag{11}$$

Condition (11) is known as the kinetic balance condition and its fulfillment is necessary for obtaining reliable variational results from both Dirac and Lévy-Leblond equations [40].

Usually, the variational approach to the Dirac equation is implemented within the algebraic approximation. In the algebraic approximation the trial functions are basis-set expanded:

$$\Phi^{\mathrm{l}} = \sum_{k=1}^{N_{\mathrm{l}}} C_k^{\mathrm{l}}\,\phi_k^{\mathrm{l}}, \quad \Phi^{\mathrm{s}} = \sum_{k=1}^{N_{\mathrm{s}}} C_k^{\mathrm{s}}\,\phi_k^{\mathrm{s}}, \tag{12}$$

where ϕ_k^{l} and ϕ_k^{s} are members of some predefined basis sets. The kinetic balance condition implies [11, 40]

$$\mathscr{H}\{\Phi^{\mathrm{s}}\} \supseteq \mathscr{H}\{(\sigma\cdot\mathbf{p})\Phi^{\mathrm{l}}\}, \tag{13}$$

where $\mathscr{H}\{\Phi\}$ is the model space in which Φ is expanded. In the algebraic approximation the Dirac and the Lévy-Leblond equations are represented as relations between finite-dimensional matrices. In the case of the Dirac equation it is a matrix representation of equation (1):

$$\begin{pmatrix} \mathbf{H}_{\mathrm{ll}} - E\mathbf{S}_{\mathrm{ll}} & c\,\mathbf{H}_{\mathrm{ls}} \\ c\,\mathbf{H}_{\mathrm{sl}} & \mathbf{H}_{\mathrm{ss}} - E\mathbf{S}_{\mathrm{ss}} \end{pmatrix} \begin{pmatrix} \mathbf{C}^{\mathrm{l}} \\ \mathbf{C}^{\mathrm{s}} \end{pmatrix} = 0, \tag{14}$$

where the labels l and s refer to the appropriate components of the trial function, matrices $\mathbf{H}_{\mathrm{ab}}$ stand for the representations of the appropriate operators in equation (1) and $\mathbf{S}_{\mathrm{ab}}$ are the overlap matrices, with $\mathrm{a},\mathrm{b} \in \{\mathrm{l},\mathrm{s}\}$. The Lévy-Leblond equation

is represented by an $N_\mathrm{l} \times N_\mathrm{l}$ eigenvalue problem:

$$(\mathbf{H} - E\mathbf{S}_\mathrm{ll})\,\mathbf{C}^\mathrm{l} = 0, \tag{15}$$

where

$$\mathbf{H} = \mathbf{H}_\mathrm{ll} + \frac{1}{2m}\mathbf{H}_\mathrm{ls}\mathbf{S}_\mathrm{ss}^{-1}\mathbf{H}_\mathrm{sl}. \tag{16}$$

Obviously, in the algebraic representation the entire spectrum is discrete. A part of it represents the Dirac continua and another part gives an approximation to the genuine discrete eigenvalues of the Dirac Hamiltonian. The exact Dirac spectrum is compared with its algebraic representation in Fig. 1.

Spectra of the algebraic representations of the Dirac Hamiltonian strongly depend on the choice of the basis set of the trial functions and may be essentially different from their exact counterparts. If $\mathscr{H}\{\boldsymbol{\Phi}^\mathrm{l}\} = \mathscr{H}\{\boldsymbol{\Phi}^\mathrm{s}\}$ then spurious roots, located below the roots describing the real states, may appear. In particular, spectra of the hydrogenic $s_{1/2}$ and $p_{1/2}$ manifolds are then the same and, consequently, a spurious root located below the $2p_{1/2}$ energy level appears [10, 12]. A detailed analysis of this problem shows that the spurious roots correspond to incorrectly represented states of the positive continuum and they enter the continuum for sufficiently large N_s [30]. A schematic behaviour of a spurious root in the case of a fixed $\mathscr{H}\{\boldsymbol{\Phi}^\mathrm{l}\}$ and systematically enlarging $\mathscr{H}\{\boldsymbol{\Phi}^\mathrm{s}\}$ is shown in Fig. 2.

Probably the first formally justified formulation of the relativistic variational principle is due to Grant et al. [13, 50]. It has been structured into a universal minimax principle by Talman [47] and by Datta and Deviah [8]. The minimax principle has been formulated as a recipe for reaching the appropriate stationary point in the energy hypersurface defined in the space of variational parameters:

$$E = \min_{\{\mathrm{l}\}} \left[\max_{\{\mathrm{s}\}} \frac{\langle \boldsymbol{\Psi} | \mathsf{H} | \boldsymbol{\Psi} \rangle}{\langle \boldsymbol{\Psi} | \boldsymbol{\Psi} \rangle} \right], \tag{17}$$

where $\boldsymbol{\Psi} = (\boldsymbol{\Psi}^\mathrm{l}, \boldsymbol{\Psi}^\mathrm{s})^\mathrm{T}$. A broad review of the subject has been given by Kutzelnigg [24].

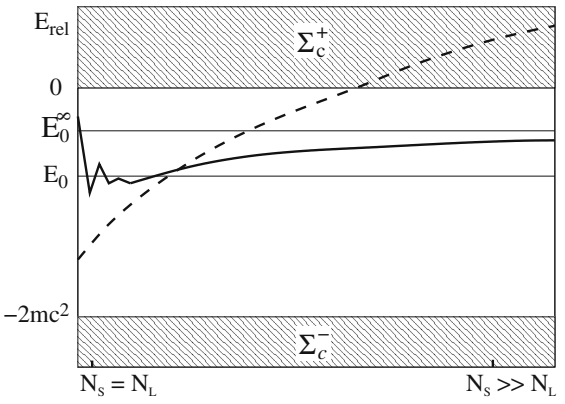

Fig. 2 The ground-state energy (*solid line*) and the position of the spurious root (*broken line*) as a function of the dimension of $\mathscr{H}\{\boldsymbol{\Phi}^\mathrm{s}\}$ when $\mathscr{H}\{\boldsymbol{\Phi}^\mathrm{l}\}$ is fixed; E_0 is the exact ground-state energy and E_0^∞ is the ground state energy obtained in the fixed $\mathscr{H}\{\boldsymbol{\Phi}^\mathrm{l}\}$ space when $\mathscr{H}\{\boldsymbol{\Phi}^\mathrm{s}\}$ is saturated

A theorem saying that the variational approximations are the upper bounds to the exact Dirac eigenvalues if the relations between the components of the wavefunction are the same as in the exact solution has been proved by Dolbeault et al. [9]. A proof that the eigenvalues of the algebraic approximation fulfil the Hylleraas-Undheim-McDonald bound conditions if

$$\bigcup_{\nu=1}^{N_{\mathrm{l}}} \mathscr{H}\{\left(E_\nu + 2mc^2 - \mathsf{V}\right)^{-1} (\boldsymbol{\sigma}\cdot\mathbf{p})\, \Phi^{\mathrm{l}}\} \subset \mathscr{H}\{\Phi^{\mathrm{s}}\}, \tag{18}$$

where E_ν are solutions of equation (14) corresponding to PES, and V is a negative-defined external potential, has been presented in [31]. Consequently, the minimax procedure may be effectively reduced to a minimalization with respect to the large component variational space. In practical calculations the exact fulfilment of condition (18) may be difficult. However, in the case of Coulomb-like potentials it may be approximated by the asymptotic balance condition

$$\mathscr{H}\{(\boldsymbol{\sigma}\cdot\mathbf{p})\, \Phi^{\mathrm{l}}\} \cup \mathscr{H}\{r\,(\boldsymbol{\sigma}\cdot\mathbf{p})\, \Phi^{\mathrm{l}}\} \subset \mathscr{H}\{\Phi^{\mathrm{s}}\}, \tag{19}$$

which in most cases is sufficient for securing the correct behaviour of the spectrum in the algebraic approximation [31].

3 Two-Electron Dirac-Coulomb Equation

The DC Hamiltonian

$$\mathsf{H}_{\mathrm{DC}}(\mathbf{1},\mathbf{2}) = \mathsf{H}_{\mathrm{D}}(\mathbf{1}) + \mathsf{H}_{\mathrm{D}}(\mathbf{2}) + \frac{1}{r_{12}}, \tag{20}$$

with $\mathsf{H}_{\mathrm{D}}(\mathbf{j})$, $\mathbf{j} = \mathbf{1},\mathbf{2}$ standing for the one-electron Dirac Hamiltonians is a rather strange hybrid composed of a relativistic one-electron part and a non relativistic two-electron term. Its eigenvalue equation

$$\mathsf{H}_{\mathrm{DC}}(\mathbf{1},\mathbf{2})\Psi(\mathbf{1},\mathbf{2}) = E_{\mathrm{DC}}\Psi(\mathbf{1},\mathbf{2}), \tag{21}$$

is referred to as the Dirac-Coulomb (DC) equation. The effects of coupling of the bound-states with the ones corresponding to continuum, known as the *Brown-Ravenhall disease*, results in numerous difficulties associated with solving this equation. Let us note that the essence of the difficulties is not due to the degeneracy of the discrete and continuous spectra. Such kind of degeneracy is common also in non-relativistic models. For example, it appears in the case of an electron moving in an axial external magnetic field and by no means obstructs finding the Landau levels. A special treatment is necessary when, in addition to this degeneracy, the Hamiltonian contains an interaction term coupling the bound states to the continuum ones.

A schematic diagram showing the structure of the spectrum of a two-electron DC Hamiltonian is shown in Fig. 3. Apart of the discrete energy levels and two continua

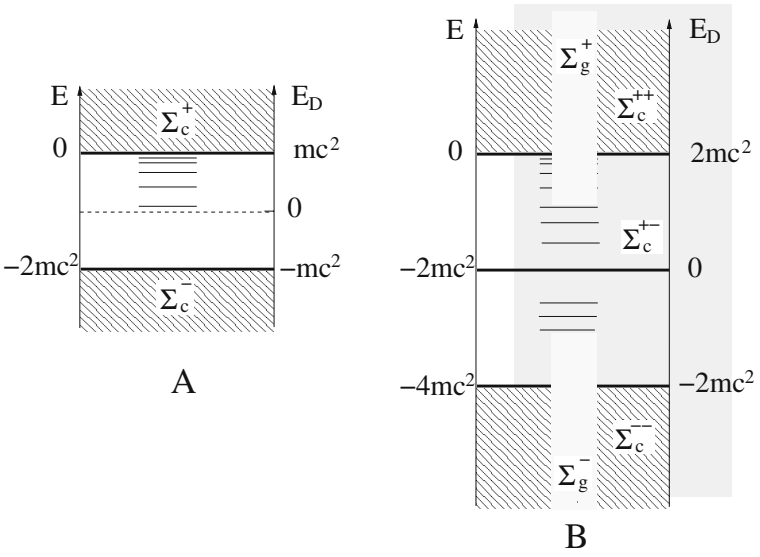

Fig. 3 Spectra of one-electron (A) and two-electron (B) DC Hamiltonian

denoted as Σ_c^{++} (both electrons in Σ_c^+) and Σ_c^{--} (both electrons in Σ_c^-), we have the Brown-Ravenhall (BR) continuum Σ_c^{+-} (one electron in Σ_c^+ and another one in Σ_c^-) and Σ_g^+/Σ_g^- (one electron in a bound state and another one in Σ_c^+/Σ_c^-). Let us note that Fig. 3 is not complete. For example, only two cases of one electron occupying a discrete level with another one in a continuum are shown.

As a consequence of the peculiar properties of the DC equation, its solutions, when compared to the physical reality, suffer from numerous artifacts. In particular:

- Since the electron-electron interaction term couples the bound and the continuum states, the eigenvalues of the DC Hamiltonian corresponding to the physically bound states (for example to the ground state of a helium-like atom) are autoionizing.
- The DC Hamiltonian does not have normalizable eigenfunctions.
- The presence of the unphysical BR continuum causes a shift of the bound state eigenvalues. On the other hand, removing the BR continuum by a projection results in an incomplete model space.

Nevertheless the most successful and commonly used relativistic models of atoms and molecules have been derived from variational methods applied to the DC equation. In fact, a large part of the relativistic quantum chemistry as well as of the atomic and molecular spectroscopy is based on the non-projected DC equation [14].

The two-electron DC Hamiltonian for a helium-like atom may be expressed as

$$\mathrm{H}(\mathbf{1},\mathbf{2}) = \begin{pmatrix} \mathrm{V}_0(\mathbf{1},\mathbf{2}) & \mathrm{t}_2 & \mathrm{t}_1 & 0 \\ \mathrm{t}_2 & \mathrm{V}_2(\mathbf{1},\mathbf{2}) & 0 & \mathrm{t}_1 \\ \mathrm{t}_1 & 0 & \mathrm{V}_2(\mathbf{1},\mathbf{2}) & \mathrm{t}_2 \\ 0 & \mathrm{t}_1 & \mathrm{t}_2 & \mathrm{V}_4(\mathbf{1},\mathbf{2}) \end{pmatrix}, \tag{22}$$

where $\mathsf{t}_1 = c(\sigma_1 \cdot \mathbf{p}_1)$, $\mathsf{t}_2 = c(\sigma_2 \cdot \mathbf{p}_2)$, $\sigma_1 = \sigma \otimes \mathsf{I}_2$, $\sigma_2 = \mathsf{I}_2 \otimes \sigma$,

$$\mathsf{V}_n(\mathbf{1},\mathbf{2}) = \left(-\frac{Z}{r_1} - \frac{Z}{r_2} + \frac{1}{r_{12}} - nmc^2 \right) \cdot \mathsf{I}_4, \tag{23}$$

and I_4 is a 4×4 unit matrix. The 16-component wavefunction is composed of four 4-component two-electron spinors

$$\Psi(\mathbf{1},\mathbf{2}) = \begin{pmatrix} \Psi^{\mathrm{ll}}(\mathbf{1},\mathbf{2}) \\ \Psi^{\mathrm{ls}}(\mathbf{1},\mathbf{2}) \\ \Psi^{\mathrm{sl}}(\mathbf{1},\mathbf{2}) \\ \Psi^{\mathrm{ss}}(\mathbf{1},\mathbf{2}) \end{pmatrix}, \tag{24}$$

with the antisymmetry condition $\Psi(\mathbf{1},\mathbf{2}) = -\Psi(\mathbf{2},\mathbf{1})$ implying that

$$\begin{aligned} \Psi^{\mathrm{ll}}(\mathbf{1},\mathbf{2}) &= -\Psi^{\mathrm{ll}}(\mathbf{2},\mathbf{1}), \\ \Psi^{\mathrm{ls}}(\mathbf{1},\mathbf{2}) &= -\Psi^{\mathrm{sl}}(\mathbf{2},\mathbf{1}), \\ \Psi^{\mathrm{ss}}(\mathbf{1},\mathbf{2}) &= -\Psi^{\mathrm{ss}}(\mathbf{2},\mathbf{1}). \end{aligned}$$

The non-relativistic approximation results in the two-electron Lévy-Leblond equation:

$$\begin{aligned} (\sigma_2 \cdot \mathbf{p}_2)\Psi_{\mathrm{L}}^{\mathrm{ls}} + (\sigma_1 \cdot \mathbf{p}_1)\Psi_{\mathrm{L}}^{\mathrm{sl}} &= (E_v^0 - \mathsf{V})\Psi^{\mathrm{ll}}, \\ (\sigma_2 \cdot \mathbf{p}_2)\Psi^{\mathrm{ll}} &= 2m\Psi_{\mathrm{L}}^{\mathrm{ls}}, \\ (\sigma_1 \cdot \mathbf{p}_1)\Psi^{\mathrm{ll}} &= 2m\Psi_{\mathrm{L}}^{\mathrm{sl}}, \end{aligned}$$

which transforms to the two-electron Schrödinger equation if

$$\Psi_{\mathrm{L}}^{\mathrm{ls}} = \frac{1}{2m}(\sigma_2 \cdot \mathbf{p}_2)\Psi^{\mathrm{ll}}, \quad \Psi_{\mathrm{L}}^{\mathrm{sl}} = \frac{1}{2m}(\sigma_1 \cdot \mathbf{p}_1)\Psi^{\mathrm{ll}}$$

[for the definition of Ψ_{L} see equation (3)].

In many-electron cases the DC Hamiltonian eigenvalue problem is usually replaced by an eigenvalue problem of its matrix representative in a properly constructed model space [34, 35, 40]. In a two-electron case it is convenient to split the model space to three subspaces. Each of these subspaces is spanned by a separate basis set of the variational functions:

1. The two-electron variational functions Φ^{ll} describe the cases when both electrons are in the PES:
$$\mathscr{H}^{\mathrm{ll}} = \mathsf{A}\mathscr{H}\{\Phi^{\mathrm{ll}}\}, \tag{25}$$
where A is the antisymmetrization operator. In the non-relativistic limit it is the model space of the spin-dependent Schrödinger equation.
2. In the variational functions one electron occupies PES and the other one the negative energy space:

$$\mathscr{H}^{[\mathrm{ls}]} = \mathsf{A}\left[\mathscr{H}\{\boldsymbol{\Phi}^{\mathrm{ls}}\} \oplus \mathscr{H}\{\boldsymbol{\Phi}^{\mathrm{sl}}\}\right]. \tag{26}$$

3. In the variational functions both electrons occupy the negative-energy space:

$$\mathscr{H}^{\mathrm{ss}} = \mathsf{A}\mathscr{H}\{\boldsymbol{\Phi}^{\mathrm{ss}}\}. \tag{27}$$

The basis sets have to be related by the two-electron kinetic balance conditions. These conditions may be derived in similar way as in the one-electron case. However, they have to establish relations between all three subspaces of the model space. As it was demonstrated in [33,36], the kinetic balance conditions may be expressed as

$$\begin{pmatrix} (\sigma_2 \cdot \mathbf{p}_2) \\ (\sigma_1 \cdot \mathbf{p}_1) \end{pmatrix} \mathscr{H}^{\mathrm{ll}} \cup \begin{pmatrix} (\sigma_1 \cdot \mathbf{p}_1) \\ (\sigma_2 \cdot \mathbf{p}_2) \end{pmatrix} \mathscr{H}^{\mathrm{ss}} \subset \mathscr{H}^{[\mathrm{ls}]}, \tag{28}$$

and

$$(\sigma_1 \cdot \mathbf{p}_1), (\sigma_2 \cdot \mathbf{p}_2)\, \mathscr{H}^{[\mathrm{ls}]} \subset \mathscr{H}^{\mathrm{ss}}. \tag{29}$$

The two-electron wavefunctions are obtained as a result of the diagonalisation of the Hamiltonian matrix. Each wavefunction contains contributions from all subspaces of the model space. The eigenvalues form a finite and discrete set. Some of them represent the bound states, but the majority correspond to the three continua of the DC Hamiltonian.

As it was already mentioned, the computational difficulties are related to the coupling between the bound states and the ones corresponding the BR continuum. There are several ways of stabilising the influence of the BR continuum on the energies of the bound states. Conceptually the simplest one is the PES projection which is intended to completely eliminate this influence. Another approach, free of many defects of the PES projection, is based on a very careful construction of the space of the trial functions so that it is relatively small, contains the solution we are looking for and remains invariant with respect to the action of the Hamiltonian. Of course, an exact fulfilment of these conditions is equivalent to an exact solving of the pertinent eigenvalue problem and, in general, is not feasible. However, these conditions may be fulfilled to a high degree of accuracy, as it has been done in an approach recently developed by Nakatsuji [27]. Then the trial space may be constructed in such a way that the spectrum is divided to three separated sections so that each of them may be linked to one of the subspaces of the model space. This kind of separation is possible under condition that the contribution from one of the spaces is dominant in each eigenvector. If the model space is constructed in such a way then the eigenvectors of the Hamiltonian matrix may be assigned to specific subspaces of the model space [18]. The sets of eigenvalues corresponding to $\mathscr{H}^{\mathrm{ll}}$, $\mathscr{H}^{[\mathrm{ls}]}$ and $\mathscr{H}^{\mathrm{ss}}$ are denoted, respectively as Σ^{++}, Σ^{+-} and Σ^{--}.

The structure of the algebraic spectrum of a two-electron DC Hamiltonian is shown in Fig. 4. The uppermost bundle is composed of Σ^{++} eigenvalues and its lower edge describes the ground state. The middle bundle, representing Σ^{+-}, describes the BR continuum which in the case of a complete space would spread from $-\infty$ to $+\infty$. The lowest bundle corresponds to the negative continuum. In the limit of a complete space it spreads from $-4mc^2$ to $-\infty$.

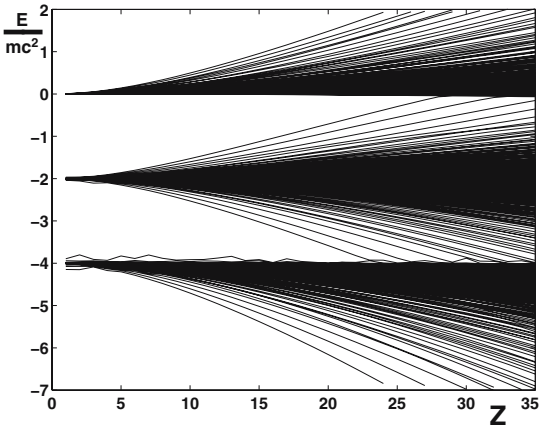

Fig. 4 Eigenvalues of the Dirac Hamiltonian matrix for helium-like atoms versus Z. The bundles of lines represent Σ^{++}, Σ^{+-} and Σ^{--} and correspond to the appropriate subspaces of a 1,131-dimensional Hy-CI model space. The number of the eigenvalues in each bundle is equal to the dimension of the corresponding subspace of the model space

If the energy gap between the discrete states and the highest eigenvalues representing the BR continuum is large enough then the influence of the continuum may be negligibly small. This can be seen in Fig. 4, where the gap is large for $Z < 25$, however for larger values of Z it disappears. The correct structure of the space of the trial functions[2] is crucial for retaining a large energy gap and, consequently, for a sufficiently high accuracy of variational solutions within an approach without PES-projection. The perturbation due to the BR continuum becomes essential in the case of near-degeneracy. This may be seen in figure 4. The penetration of the eigenvalues belonging to Σ^{+-} to the PES area is a numerical manifestation of the BR disease. The apparent degeneracies of the energy levels belonging to Σ^{+-} and the ones belonging to Σ^{++} are, in fact, very narrow avoided-crossings responsible for numerical instabilities in variational calculations.

In the following we shall analyse the issues related to the artifacts of the DC equation. They are connected with the genuine two-electron effects, i.e. with the effects beyond the Dirac-Fock model. The following terminology is used hereafter. The non-relativistic correlation energy is defined as the difference between the eigenvalue of the Schrödinger Hamiltonian and the corresponding Hartree-Fock energy:

$$E_{\mathrm{nr}}^{\mathrm{corr}} = E_{\mathrm{Schr}} - E_{\mathrm{HF}}.$$

Similarly, the relativistic correlation energy is the difference between the eigenvalue of the DC Hamiltonian and the corresponding Dirac-Fock (DF) energy:

$$E_{\mathrm{rel}}^{\mathrm{corr}} = E_{\mathrm{DC}} - E_{\mathrm{DF}}.$$

The difference between the relativistic and the non-relativistic correlation energies is referred to as the relativity-correlation cross correction:

$$E_{\mathrm{x}} = E_{\mathrm{rel}}^{\mathrm{corr}} - E_{\mathrm{nr}}^{\mathrm{corr}}.$$

[2] By the correct structure of the trial functions we understand the relations between their components, the behaviour at the singular points, the boundary conditions, etc., consistent with the structure of the DC equation.

Table 1 Relativistic and correlation corrections to the ground-state energies of helium-like atoms. ΔE_{BR} is the difference between the non-projected and PES-projected energies, i.e. the energy shift due to the interaction with the BR continuum (all-order contribution to the non-relativistic part of Coulomb interaction). For the explanation of the remaining symbols see text. All energies are in milihartree

Z	E_{HF}	$E_{\mathrm{DF}} - E_{\mathrm{HF}}$	$E_{\mathrm{nr}}^{\mathrm{corr}}$	E_{x}	ΔE_{BR}
2	−2,861.67999	−0.13331	−42.0444	0.0035	0.0001
20	−387,611.057	−2,055.707	−46.177	0.351	0.164
40	−1,575,111.03	−34,794.26	−46.42	1.36	1.57
60	−3,562611.02	−188,364.94	−46.50	2.70	4.70
80	−6,350,111.01	−656,335.85	−46.55	3.16	10.54
100	−9,937,611.00	−1,859,249.0	−46.6	0.0	21.6
118	−13,850,361.0	−4,494,444.1	−46.6	−18.4	36.4

Hartree-Fock energies as well as relativistic and correlation corrections for the ground states of several members of He isoelectronic series are collected in Table 1.

4 Relativistic Hylleraas-CI

Due to the singularity of the electron-electron interaction operator, the two-electron wavefunction has a cusp at $r_{12} = 0$, referred to as the electron correlation cusp [25]. If $r_{12} \to 0$ then

$$\Psi(\mathbf{r}_1, \mathbf{r}_2) \sim a\, r_{12}^{q} + b\, r_{12}^{q+1}, \tag{30}$$

where a, b are state-dependent constants and $q = \sqrt{1-\alpha^2/4} - 1 \approx -1.3 * 10^{-5}$. In the non-relativistic theory $q = 0$. Due to a poor representation of the cusp by expansions in the orbital space, a fast convergence of CI expansions may only be obtained if r_{12}-dependent terms are present in the trial function. Probably the most precise approach utilising explicitly correlated, i.e. r_{12}-dependent, trial functions is the Hy-CI method [43, 51]. A non-relativistic Hy-CI trial function may be expressed as

$$\Psi_{\mathrm{HyCI}} = \mathsf{A} \sum_k r_{12}^k \sum_i C_{ki} \Phi_i^k(\{\phi\}), \tag{31}$$

where C_{ki} are variational parameters, and $\Phi_i^k(\{\phi\})$ are products of spinorbitals (spinors in the relativistic formulation). The relativistic formulation of Hy-CI (R-Hy-CI) proved to be very promising [22,23] however, with the increasing lengths of the expansion, i.e. with the increasing accuracy, the results became unstable [36]. It has been shown that the main reason of this instability is the perturbation due to the BR continuum [32].

In order to construct a model space in which the BR continuum states are as much as possible separated from the ones describing the bound states, apart from the assurance of the correct behaviour of the trial functions in the singular points

of the Hamiltonian, the relations between the components of the wavefunction have to be fulfilled up to a high degree of accuracy. This implies, in particular, that the kinetic balance conditions have to be fulfilled. The most appropriate form of the basic correlation factor in R-Hy-CI is

$$f_s^{[0]}(r_{12}) = r_{12}^s, \tag{32}$$

where s is a real parameter chosen to satisfy the relativistic cusp condition. The kinetic balance conditions generate new correlation factors:

$$\begin{aligned} f_s^{[1]}(r_{12})_1 &= i\left[(\sigma_1\cdot\mathbf{p}_1)f_s^{[0]}(r_{12})\right](\sigma_1\cdot\hat{\mathbf{r}}_1),\\ f_s^{[1]}(r_{12})_2 &= i\left[(\sigma_2\cdot\mathbf{p}_2)f_s^{[0]}(r_{12})\right](\sigma_2\cdot\hat{\mathbf{r}}_2),\\ f_s^{[2]}(r_{12}) &= \left[(\sigma_1\cdot\mathbf{p}_1)(\sigma_2\cdot\mathbf{p}_2)f_s^{[0]}(r_{12})\right](\sigma_1\cdot\hat{\mathbf{r}}_1)(\sigma_2\cdot\hat{\mathbf{r}}_2). \end{aligned} \tag{33}$$

In fact, in this way an infinite chain of the correlation factors is generated and a cut-off of this sequence is necessary. In practical calculations retaining only the lowest-order correlation factors, as defined in (33), appears to be sufficient [36].

In the calculations for the ground states of helium-like atoms the trial functions have been taken as [32, 33, 36]

$$\Phi_{s,\Gamma;\lambda_1,\lambda_2}^{[r],JM\Pi}(\mathbf{x}_1,\mathbf{x}_2) = f_s^{[r]}(r_{12})r_1^{\gamma_1+n_1}r_2^{\gamma_2+n_2}e^{-(\beta_1 r_1+\beta_2 r_2)}\Omega_{\lambda_1,\lambda_2}^{JM\Pi}(\hat{\mathbf{r}}_1,\hat{\mathbf{r}}_2), \tag{34}$$

where $\Gamma = \{n_1, n_2, \gamma_1, \gamma_2, \beta_1, \beta_2\}$ is a collective index composed of the non-linear parameters and r is equal to the number of $(\sigma\cdot\mathbf{p})$ operators acting on $f_s^{[0]}(r_{12})$. The angular spinors have been defined as

$$\Omega_{\lambda_1\lambda_2}^{JM\Pi}(\hat{\mathbf{r}}_1,\hat{\mathbf{r}}_2) = \sum_{m_1,m_2}\begin{pmatrix} j_1 & j_2 & J\\ m_1 & m_2 & -M\end{pmatrix}\phi_{\lambda_1\lambda_2}(\hat{\mathbf{r}}_1,\hat{\mathbf{r}}_2), \tag{35}$$

where $\hat{\mathbf{r}} = \mathbf{r}/r$, $\lambda_j \equiv \{j_j, m_j, \pi_j\}$, J, M, Π are the angular momentum and parity quantum numbers, and

$$\phi_{\lambda_1\lambda_2}(\hat{\mathbf{r}}_1,\hat{\mathbf{r}}_2) = \varphi_{j_1 m_1\pi_1}(\hat{\mathbf{r}}_1)\otimes\varphi_{j_2 m_2\pi_2}(\hat{\mathbf{r}}_2), \tag{36}$$

with $\varphi_{jm\pi}(\hat{\mathbf{r}})$ standing for the spin-angular part of the one-electron Pauli spinor. The resulting matrix elements may be expressed in terms of the primitive two-electron integrals $\langle B|f(r_{12})\hat{\tau}|K\rangle$, where

$$\hat{\tau} = 1,\ (\sigma_1\cdot\sigma_2),\ (\sigma_\mathrm{a}\cdot\hat{\mathbf{r}}_\mathrm{a}),\ (\sigma_\mathrm{a}\cdot\hat{\mathbf{r}}_\mathrm{b}),\ [(\sigma_1\cdot\hat{\mathbf{r}}_1)(\sigma_2\cdot\hat{\mathbf{r}}_2)] \tag{37}$$

with $\mathrm{a},\mathrm{b}\in\{1,2\}$ and $f(r_{12}) = r_{12}^s$, where $s \geq -1$ may be either integer or real, or $f(r_{12}) = \ln(r_{12})$. Details of the algorithms for the evaluation of the integrals have been published in [29, 37].

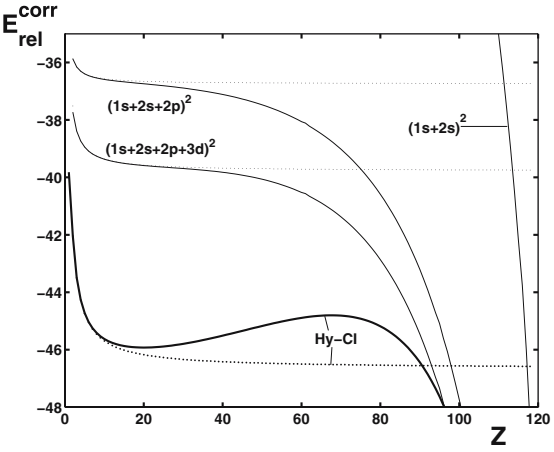

Fig. 5 The pattern of convergence of the MCDF correlation energies (in milihartree) of the ground states of helium-like atoms to the Hy-CI values. The thick solid line corresponds to the R-Hy-CI energy. The thin solid lines are the MCDF energies (the configuration basis is displayed as a label of each of these lines). The non-relativistic correlation energies (the exact and the MCDF ones) are shown by the dotted lines

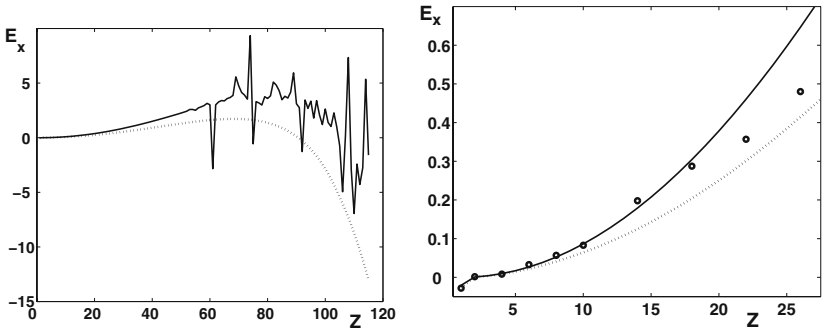

Fig. 6 R-Hy-CI relativity-correlation cross-term energies (milihartree) in He isoelectronic series. Dotted line: 502 functions. Solid line: 1,131 functions. The coupling of the ground-state with the BR continuum wavefunctions results in the instabilities. The right panel shows an enlargement of the small-Z part. The circles correspond to the extrapolated MCDF results [28]

The results of the R-Hy-CI calculations have been reported in [38]. In Fig. 5 one can see how the multiconfiguration Dirac-Fock (MCDF) energies approach the R-Hy-CI ones. The process of convergence of the MCDF results to the R-Hy-CI ones appears to be very slow. Besides, for large expansions the solutions of the MCDF equations were possible to obtain only for $Z \leq 26$ [28]. It seems that the problems with stability of the MCDF procedure may be related to the interference of the BR continuum (c.f. a discussion by Indelicato [20]).

The effects of an enlargement of the R-Hy-CI model space are presented in Fig. 6. As one can see, the extension of the dimension of the R-Hy-CI basis from 502 to 1,131 functions results in strong instability of the eigenvalues for medium and large values of Z. On the other hand, an inspection of the results obtained for small Z shows that the enlargement of the basis set results in a considerable improvement of the accuracy. We conclude that the requirement of very high accuracy implies using

very large R-Hy-CI basis. In the next section we present a simple way of solving this controversy.

5 Complex-Coordinate-Rotation

The approach known as the complex coordinate rotation (CCR) method has originally been developed to study the autoionizing states also referred to as resonances [1,2,41]. These are the states whose discrete energies are embedded in a continuum. The basic theorem of the method says that *the bound state energies of a Hamiltonian do not change under the complex rotation of the coordinates*,

$$\mathbf{r} \rightarrow \mathbf{r}e^{i\Theta}, \tag{38}$$

whereas the continua move to the complex plane. The CCR Hamiltonian matrix is non-Hermitian and its eigenvalues z are complex. The energies of the resonant states are equal to

$$E = \mathrm{Re}(z)$$

and the widths of the energy levels are

$$\Gamma = -2\,\mathrm{Im}(z).$$

From the formal point of view the bound-state eigenvalues of a many-electron DC Hamiltonian are resonances. To our knowledge, in the relativistic quantum mechanics the CCR method was used in studies on the one-electron Dirac eigenvalue equation only [42,49]. It is surprising that it has not been applied in studies on the artifacts of the DC equation until very recently [6,32,33]. The effects of the CCR on the spectra of a one-electron Dirac Hamiltonian and of a two-electron DC Hamiltonian with the electron-electron interaction neglected, are shown, respectively, in Figs. 7 and 8. Due to the CCR the one-electron continua are moved to the complex plane, while the discrete eigenvalues remain in the real axis. In the two-electron case the picture is slightly more complicated. In figure 8 one can see a separation of the three main continua: Σ_c^{++}, Σ_c^{+-} and Σ_c^{--}, where the subscript c is to identify the sets of energies of these states in which both electrons are unbound. Since the interaction term is neglected, the discrete states are not coupled to the continuum. Therefore also in this case the discrete eigenvalues remain in the real axis. If one electron occupies a bound state and the other one is in Σ_c^+ then the origin (the low energy threshold) of the continuum of the unbound electron is shifted to the position of the one-electron bound-state energy, forming a Σ_g^+ band (for simplicity only one Σ_g^+ and one Σ_g^- continuum is shown in Fig. 8). Thus, the CCR completely removes the degeneracy of the discrete states with the continuum and allows for a simple identification of the discrete eigenvalues in the algebraic spectrum.

Since the electron-electron interaction introduces a coupling between the discrete and the continuum states, also the eigenvalues of the CCR DC Hamiltonian

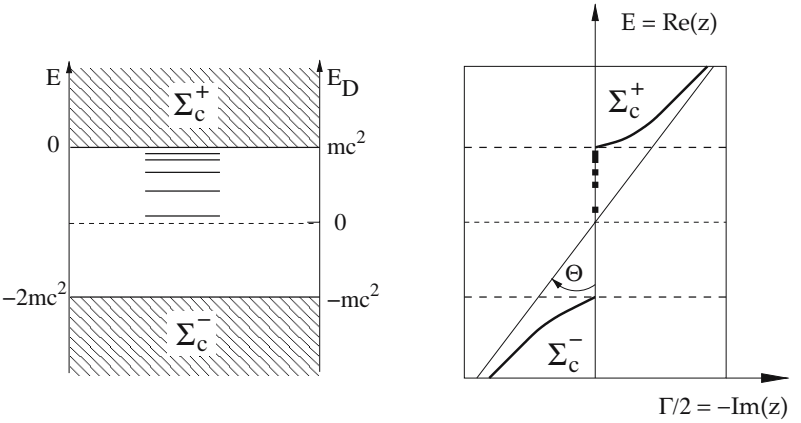

Fig. 7 Standard (left) and CCR (right) spectrum of a one-electron Dirac Hamiltonian. Solid lines represent the positive, Σ_c^+, and the negative, Σ_c^-, continua. The dots in the real axis represent the bound-state energies

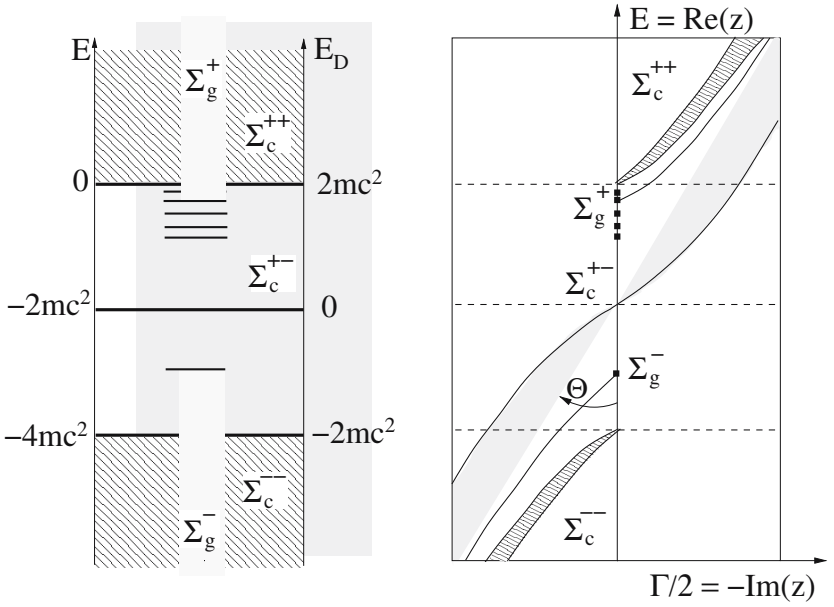

Fig. 8 The same as in Fig. 7 but for a two-electron system. For explanation see text and Fig. 3

corresponding to the bound states are complex. However, the behaviour of these eigenvalues, in terms of the rotation angle Θ, is different than the behaviour of the continua. The bound-state eigenvalues of the rotated Hamiltonian, when represented in the complex plane, are isolated from the continuum and, in a range of Θ, are Θ-independent. On the contrary, all components of the continuum depend on Θ in a regular way. Therefore the bound-state eigenvalues can easily be distinguished from

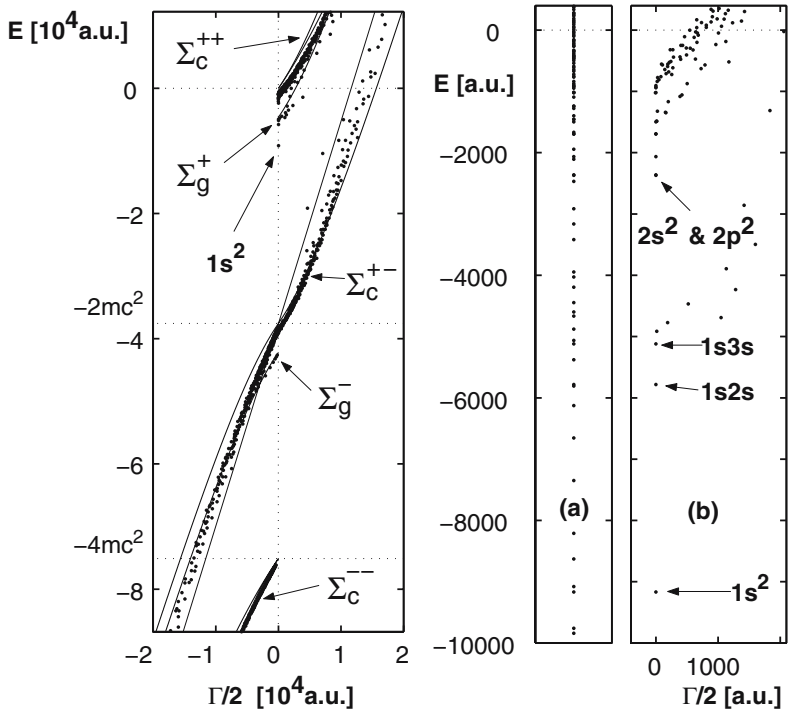

Fig. 9 R-CCR-Hy-CI spectrum of a $Z = 90$ helium-like atom in a basis of 1,826 explicitly correlated functions with $\Theta = 0.3$. The dots represent the computed eigenvalues. The lines mark the areas covered by the continua. The right panel shows an enlargement of the bound- and the resonance-state-energy region without CCR (part a) and with $\Theta = 0.3$ CCR (part b)

the continuum ones [32]. This behaviour may be seen in Fig. 9 where the results of a specific calculation are shown. All features of a CCR spectrum marked in Fig. 8 are also seen in Fig. 9. In particular, in the enlargements of the part of the spectrum containing the bound- and the resonance-state energies one can identify the dots located near the real axis and corresponding to the specific bound states.

CCR removes the degeneracy between the eigenvalues corresponding to the bound states and to the continuum [32, 33]. Therefore it stabilizes the bound-state eigenvalues. This can be seen in Fig. 10 – the application of CCR removed all spikes corresponding to the near-degeneracies and avoided crossings between the ground-state and the BR-continuum eigenvalues, being a nuisance to the plain R-Hy-CI calculations.

The appearance of the bound states as resonances is one of the artifacts of the DC model. The probability of their fictitious autodecay is finite and is represented by Γ. In order to estimate this effect we calculated Γ for the helium isoelectronic series as a function of Z and, additionally, we performed a series of calculations for $Z = 90$ with several values of the fine structure constant α. Plots of $\Gamma/2$ versus Z for the physical value of α and versus α for $Z = 90$ are shown in Fig. 11. The

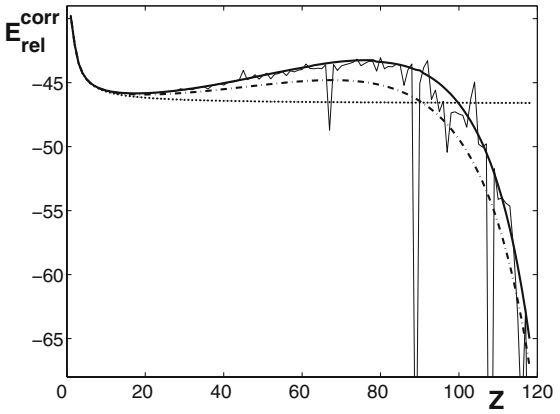

Fig. 10 Hy-CI correlation energies in the ground states of helium-like atoms. Dash-dotted line corresponds to R-Hy-CI results in a small (502 function) basis. Thin and thick solid lines correspond, respectively, to R-Hy-CI and R-CCR-Hy-CI in a large (1,826 function) basis. The non-relativistic correlation energy is represented by the dotted line

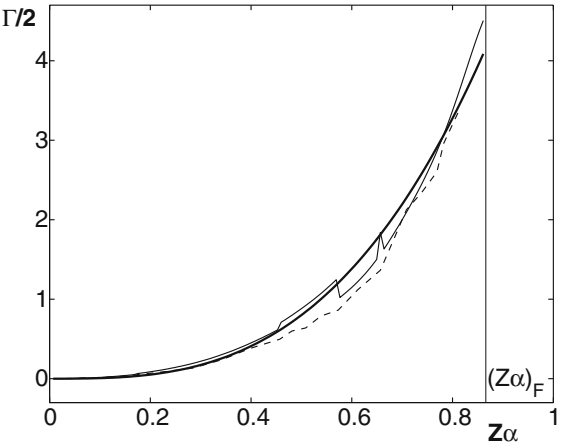

Fig. 11 The half-widths $\Gamma/2$ (in milihartree) of the R-CCR-Hy-CI eigenvalues as a functions of α (broken line) and Z (thin solid line). Thick solid line represents a fit: $6.4\,(Z\alpha)^3 \cdot 10^{-3}$. The vertical line marks $(Z\alpha)_{\mathrm{F}} = \sqrt{3}/2$, i.e. the limit of the applicability of the method

best monomial least-square fit has been obtained as $6.4 \cdot 10^{-3} \cdot (Z\alpha)^3$. In Fig. 11 it is represented by the smooth line. Except for some numerical instabilities of the computed values of Γ, the fit is very good and shows that Γ behaves as $(Z\alpha)^3$.

6 PES-Projected R-CCR-Hy-CI

The CCR-based approach facilitates a separation of the PES from the rest of the model space independently of the form of the trial function. Also if this function contains geminals. Figure 12 shows the CCR spectrum of a DC Hamiltonian with the electron-electron interaction neglected. Due to the rotation in the complex plane the PES eigenvalues are separated from the rest of the spectrum. In a complete basis set all eigenvalues with imaginary parts not larger than 0 and to the left of the border line shown in Fig. 12 correspond to PES. Then, by selecting a subspace of the entire

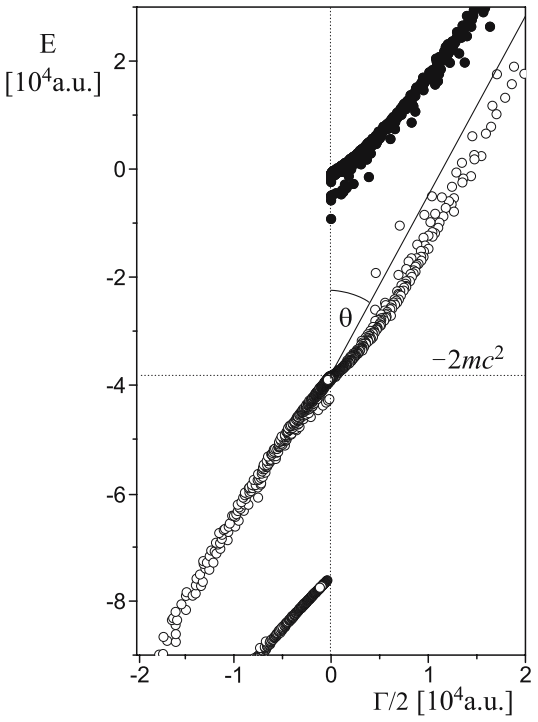

Fig. 12 The CCR spectrum of $Z = 90$ He-like atom with electron-electron interaction neglected, in a 1,826-function R-Hy-CI basis. Full circles – PES eigenvalues; Solid line – the theoretical border between the PES eigenvalues and the BR continuum

model space which is spanned by the PES eigenvectors, we effectively perform the PES projection. The representation of the DC Hamiltonian in the PES-projected basis gives a PES-projected DC Hamiltonian matrix. Its eigenvalues correspond to the PES-projected R-Hy-CI energies. A detailed description of this approach and the numerical results are given in [6].

7 Non-Projected Versus PES-Projected Results

Very recently by means of two different approaches (a large scale configuration interaction [48] and R-CCR-Hy-CI [6, 32, 33]) the difference between the ground state energies derived from the non-projected and from the PES-projected methods, ΔE_{BR}, has been evaluated (cf. Table 1). As one could expect, this difference, up to a high accuracy, is equal to the virtual pair contribution to the nonrelativistic electron-electron Coulomb repulsion energy. Thus, up to the first order, [3, 26]

$$\Delta E^0_{\mathrm{BR}} = \frac{(Z\alpha)^3}{6\pi}.$$

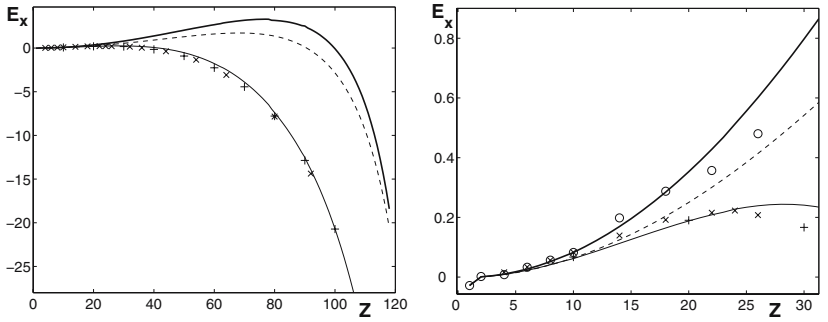

Fig. 13 Relativity-correlation cross-term energies: Thick solid line – R-CCR-Hy-CI energies in 1,826-function basis; broken line – R-Hy-CI in a 502-function basis; $+/\times$ – CI/MBPT PES-projected energies [7, 39]; $\circ$ – MCDF [28]; thin solid line – R-CCR-Hy-CI energy in a 1,826-function basis shifted by $(Z\alpha)^3/(6\pi)$

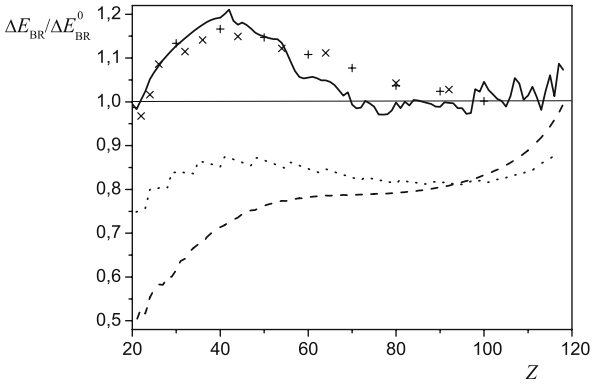

Fig. 14 Ratio $\Delta E_{\mathrm{BR}}/\Delta E^0_{\mathrm{BR}}$ versus Z. Solid line – R-CCR-Hy-CI in 1,826-function basis [6, 33]; dotted line – CI in a large Gaussian basis set [48]; broken line – R-Hy-CI in 502-function basis [32]; $+/\times$ – the difference between the non-projected 1826-function R-CCR-Hy-CI and PES projected CI/MBPT [7, 39]

The effect is shown in Figs. 13 and 14. As one can see, the increasing accuracy of the calculations results in a more precise fit of the difference between the two sets of results to ΔE^0_{BR}.

8 Final Remarks

If the quality of the basis set is sufficiently high relative to its dimension and to the value of Z, so that there is a sufficiently large energy gap between the ground state energy and the eigenvalues representing the BR continuum, then neither PES

projection nor CCR are necessary. However, for very high accuracy and, particularly, for large values of Z, when the disturbing influence of the BR states becomes noticeable, CCR offers an adequate way of removing this influence and, simultaneously, allowing for the asymptotic completeness of the model space. One should note that a vast majority of relativistic results for atoms containing more than two electrons and, probably, for nearly all molecules have been obtained at the level of accuracy which is manageable by the basis set selection using non-projected approaches.

The PES projected (no-pair) and the non-projected approaches converge to different limits. The difference is of the order $(Z\alpha)^3$. Thus, it is beyond the limits of validity of the DC model. The corresponding term can either be included or neglected while introducing QED corrections. This gives another confirmation of a twenty-year-old statemnt by Brown [4], that both approaches are correct if they are applied in a consistent way.

The truncation of the R-Hy-CI model space, facilitating a PES projection, is feasible but it is not necessary and has some disadvantages:

- The absence of the negative energy states in the PES-projected methods has to be corrected if we are interested in quantities other than energy.
- The PES projection is not unique even if the original space is complete. Therefore the results depend on the one-electron potential and the basis-set [19].

There are also some advantages of the PES projection:

- The PES-projected eigenvalue problem is bounded from below and for the same quality of the energy a smaller model space is necessary.
- Combining PES projection with CCR may be simpler than using CCR alone: In the non-projected CCR methods we need several diagonalisations of $\mathbf{H}$ (for several values of Θ) while in the PES-projected CCR approach a single diagonalisation, for one value of Θ, is sufficient in order to construct the basis for the PES-projected space.

In the DF calculations we have an effective one-electron problem and the relations between the components of the spinors consistent with the structure of the pertinent equation, combined with the bound-state boundary conditions, are always sufficient. Therefore, the results of correctly designed DF programs never suffered from any kind of the DC equation artifacts and no PES projection is necessary in this case. However, in MCDF calculations a PES projection (or CCR) may allow for a higher accuracy limit [20].

An implementation of CCR-based approaches to QED calculations for high-Z atoms seems to be the most attractive challenge.

Acknowledgements Supported by the Polish Ministry of Science and Higher Education, project No. N202 041 32/1045. Very useful remarks of a referee are gratefully acknowledged. JK is grateful to I. Lindgren for an illuminating discussion.

References

1. Aguilar, J., Combes, J. M.: A class of analytic perturbations for one-body Schrödinger Hamiltonians, Commun. Math. Phys. **22**, 269–279 (1971)
2. Balslev, E., Combes, J. M.: Spectral properties of many-body Schrödinger operators with dilation-analytic interactions, Commun. Math. Phys. **22**, 280–294 (1971)
3. Blundell, S. A., Mohr, P. J., Johnson, W. R., Sapirstein, J.: Evaluation of two-photon exchange graphs for highly charged helium-like ions. Phys. Rev. A **48**, 2615–2626 (1993)
4. Brown, G. E.: The relativistic atomic many-body problem. Phys. Scripta **36**, 71–76 (1987).
5. Brown, G. E., Ravenhall, D. G.: On the interaction of two electrons. Proc. R. Soc. A **208**, 552–559 (1951)
6. Bylicki, M., Pestka, G., Karwowski, J.: Relativistic Hylleraas configuration-interaction method projected into positive-energy space. Phys. Rev. A **77**, 044501 (2008)
7. Cheng, K. T., Chen, M. H., Johnson, W. R., Sapirstein, J.: Relativistic configuration-interaction calculations for the ground state and $n = 2$ singlet states of helium-like ions. Phys. Rev. A **50**, 247–255 (1994)
8. Datta, S. N., Deviah, G.: The minimax technique in relativistic Hartree-Fock calculations. Pramana, **30**, 387–405 (1988)
9. Dolbeault, J., Esteban, M. J., Séré, E., Vanbreugel, M.: Minimization methods for the one-particle Dirac equation. Phys. Rev. Letters **85**, 4020–4023 (2000)
10. Drake, G. W. F., Goldman, S. P.: Application of discrete-basis-set methods to the Dirac equation. Phys. Rev. A **23**, 2093–2098 (1982)
11. Dyall, K. G., Grant, I. P., Wilson, S.: Matrix representation of operator products. J. Phys. B: At. Mol. Opt. Phys. **17**, 493–504 (1984)
12. Goldman, S. P.: Variational representation of the Dirac-Coulomb Hamiltonian with no spurious roots. Phys. Rev. A **31**, 3541–3549 (1985)
13. Grant, I. P.: Conditions for convergence of variational solutions of Dirac's equation in a finite basis. Phys. Rev. A **25**, 1230–1232 (1982)
14. Grant, I. P.: Relativistic Quantum Theory of Atoms and Molecules: Theory and Computation. Springer Series on Atomic, Optical, & Plasma Physics. Springer, New York (2007)
15. Grant, I. P., Quiney, H. M.: Application of relativistic theories and quantum electrodynamics to chemical problems. Int. J. Quantum Chem. **80**, 283–297 (2000)
16. Grant, I. P., Quiney, H. M.: Rayleigh-Ritz approximation of the Dirac operator in atomic and molecular physics. Phys. Rev. A **62**, 022508-1-14 (2000)
17. Hardekopf, G., Sucher, J.: Relativistic wave equations in momentum space. Phys. Rev. A **30**, 703–711 (1984)
18. Heully, J.-L., Lindgren, I., Lindroth, E., Lundqvist, S., Mårtensson-Pendrill, A.-M.: Diagonalisation of the Dirac Hamiltonian as a basis for a relativistic many-body procedure. J. Phys. B: At. Mol. Phys. **19**, 2799–2815 (1986)
19. Heully, J.-L., Lindgren, I., Lindroth, E., Mårtensson-Pendrill, A.-M.: Comment on relativistic wave equation and negative-energy states. Phys. Rev. A **33**, 4426–4429 (1986)
20. Indelicato, P.: Projection operators in multiconfiguration Dirac-Fock calculations: Application to the ground state of helium like ions.. Phys. Rev. A **51**, 1132–1145 (1995)
21. Johnson, W. R., Cheng, K. T., Chen, M. H.: Accurate relativistic calculations including QED contributions for few-electron systems. In: Schwerdtfeger, P. (ed.) Relativistic Electronic Structure Theory: Part 2. Applications (Theoretical and Computational Chemistry, Vol. 14), Chap. 3, pp. 120–187, Elsevier, Amsterdam (2004).
22. Kolakowska, A.: Explicitly correlated trial functions in relativistic variational calculations. J. Phys. B: At. Mol. Opt. Phys. **30**, 2773–2779 (1997)
23. Kolakowska, A., Talman, J. D., Aashamar, K.: Minimax variational approach to the relativistic two-electron problem. Phys. Rev. A **53**, 168–177 (1996)
24. Kutzelnigg, W.: Relativistic one-electron Hamiltonians 'for electrons only' and the variational treatment of the Dirac equation. Chem. Phys. **225**, 203–222 (1997)

25. Kutzelnigg, W.: Theory of electron correlation. In: Rychlewski, J. (ed.) Explicitly Correlated Wave Functions in Chemistry and Physics: Theory and Application, pp. 3–90. Kluwer, Dordrecht (2003)
26. Lindgren, I., Persson, H., Salomonson, S., Labzowsky, L.: Full QED calculations of two-photon exchange for helium-like systems: Analysis in the Coulomb and Feynman gauges. Phys. Rev. A **51**, 1167–1195 (1995)
27. Nakatsuji, H., Nakashima, H.: Analytically solving the relativistic Dirac-Coulomb equation for atoms and molecules. Phys. Rev. Letters **95**, 050407-1-4 (2005), and references therein
28. Parpia, F. A., Grant, I. P.: Accurate Dirac-Coulomb energies for the ground states of helium-like ions. J. Phys. B: At. Mol. Phys. **23**, 211–217 (1990)
29. Pestka, G.: Variational solution of the Dirac-Coulomb equation using explicitly correlated wavefunctions. Matrix elements and radial integrals. J. Phys. A: Math. Gen. **31**, 6243–6252 (1998)
30. Pestka, G.: Spurious roots in the algebraic Dirac equation. Phys. Scripta **68**, 254–258 (2003)
31. Pestka, G.: Upper bounds to the eigenvalues of the Dirac Hamiltonian. Phys. Scripta **69**, 203–207 (2004)
32. Pestka, G., Bylicki, M., Karwowski, J.: Application of the complex coordinate rotation to the relativistic Hylleraas-CI method: A case study. J. Phys. B: At. Mol. Opt. Phys. **39**, 2979–2987 (2006)
33. Pestka, G., Bylicki, M., Karwowski, J.: Complex coordinate rotation and relativistic Hylleraas-CI: Helium isoelectronic series. J. Phys. B: At. Mol. Opt. Phys. **40**, 2249–2259 (2007)
34. Pestka, G., Karwowski, J.: Structure of Dirac-Coulomb-Breit Hamiltonian. In: Lulek, T., Lulek, B., Wal, A. (eds.) Symmetry and Structural Properties of Condensed Matter, pp. 111–115, World Scientific, Singapore (2001)
35. Pestka, G., Karwowski, J.: Dirac-Coulomb Hamiltonian in N-Electron Model Spaces. Collect. Czech. Chem. Commun. **68**, 275–294 (2003)
36. Pestka, G., Karwowski, J.: Hylleraas-CI approach to Dirac-Coulomb equation. In: Rychlewski, J. (ed.) Explicitly Correlated Wave Functions in Chemistry and Physics: Theory and Application, pp. 331–346. Kluwer, Dordrecht (2003)
37. Pestka, G., Karwowski, J.: Two-electron one-center integrals in relativistic Hy-CI method. In: Ozdogan, T., Ruiz, M. B. (eds.) Recent Advances in Computational Chemistry. Molecular Integrals over Slater orbitals, pp. 213–232. Transworld Research Network, Trivandrum (2008)
38. Pestka, G., Tatewaki, H., Karwowski, J.: Relativistic correlation energies of helium like atoms. Phys. Rev. A **70**, 024501-1-3 (2004)
39. Plante, D. R., Johnson, W. R., Sapirstein, J.: Relativistic all-order many-body calculations of the $n = 1$ and $n = 2$ states of heliumlike ions. Phys. Rev. A **49**, 3519–3530 (1994)
40. Quiney, H. M.: The Dirac equation in the algebraic approximation. In: Wilson, S. (ed.) Handbook of Molecular Physics and Quantum Chemistry, Vol. **2**, pp. 423–443. Wiley, Chichester (2003), and references therein
41. Reinhardt, W. P.: Complex coordinates in the theory of atomic and molecular structure and dynamics, Ann. Rev. Chem. **33**, 223–255 (1982)
42. Seba, P.: The complex scaling method for Dirac resonances. Lett. Math. Phys. **16**, 51–59 (1988)
43. Sims, J. S., Hagstrom, S. A.: Combined configuration-interaction Hylleraas-type wavefunction study of the ground state of the berylium atom. Phys. Rev. A **4**, 908–916 (1971)
44. Sucher, J.: Foundations of the relativistic theory of many-electron atoms. Phys. Rev. A **22**, 348–362 (1980)
45. Sucher, J.: Foundations of the relativistic theory of many-electron bound states. Int. J. Quantum Chem. **25**, 3–21 (1984)
46. Sucher, J.: Continuum dissolution and the relativistic many-body problem: A solvable model. Phys. Rev. Letters **55**, 1033–1035 (1985)
47. Talman, J. D.: Minimax principle for the Dirac equation. Phys. Rev. Letters **57**, 1091–1094 (1986)

48. Watanabe, Y., Nakano, H., Tatewaki, H.: Effect of removing the no-virtual-pair approximation on the correlation energy of the He isoelectronic sequence. J. Chem. Phys. **126**, 174105-1-8 (2007)
49. Weder, R. A.: Spectral Properties of the Dirac Hamiltonian. Ann. Soci. Scient. Bruxelles **T87** 341–355 (1973)
50. Wood, J., Grant, I. P., Wilson, S.: The Dirac equation in the algebraic approximation. IV. Application of the partitioning technique. J. Phys. B **18**, 3027–3042 (1985)
51. Woźnicki, W.: On the method of constructing the variational wave function for many-electron systems. In: Jucys, A. (ed.) Theory of Electronic Shell in Atoms and Molecules, pp. 103–106. Mintis, Vilnius (1971)

Are Einstein's Laws of Relativity a Quantum Effect?

Erkki J. Brändas

Abstract The problem of unifying quantum mechanics with special and general relativity is reconsidered from a relativistically invariant first principles theory. The ingredients are: (i) analytic extension of quantum mechanics into the complex plane via a complex symmetric *ansatz*, involving (ii) particle- antiparticle states interacting through a kinematical law including (iii) dynamical features such as time- and length-scale contractions and examining (iv) the likelihood of the so-called general Jordan block formations. The extended formulation has a wider set of solutions compared to standard mechanics, with general gauge invariance appropriately embedded. In the present development we establish connections with the Klein-Gordon-Dirac relativistic theories and confirm dynamical features like space and time contractions, Einstein's law of light deflection in a gravitational field, and the appearance of the Schwarzschild-gravitational radius associated with every mass-matter object.

Keywords: Klein-Gordon-, Dirac equation, particle-antiparticles, complex symmetry, non-positive metric, Jordan blocks, special- and general relativity, electromagnetic- and gravitational fields, Schwarzschild radius, supersymmetry

1 Introduction

In this study we reconsider the old problem of the purported inconsistency between quantum mechanics and the theory of relativity. To give further details on this subject, we emphasize that while the Dirac and Klein-Gordon equations [1–3], in spite of giving an almost perfect description of microscopic quantum effects, yet do not account for dynamical effects like the time- and length-scale contractions in the

E.J. Brändas
Department of Quantum Chemistry, Uppsala University, Box 518, SE-751 20 Uppsala, Sweden, e-mail: Erkki.Brandas@kvac.uu.se

S. Wilson et al. (eds.) *Frontiers in Quantum Systems in Chemistry and Physics*.

special theory of relativity or could be rigorously integrated with the general gravitational theory. Additional benefits from obtaining such a general unification with quantum mechanics would be to obtain the well-known Schwarzschild solution (or rather the correct Schwarzschild radius) along with a deduction of the Einstein law for the gravitational deviation of light.

A rigorous quantum many-body relativistically invariant theory is moreover lacking although excellent practical and valuable schemes exist today [4]. For a recent update on the study of molecules containing heavy elements demanding a relativistic formulation, see Ref. [5].

We will present here a description which is essentially of quantum mechanical origin. However, there is an important generalization built-in. This addition brings about the capability to analytically extend quantum mechanical quantities like, resolvents, Green's functions, S-matrices and general spectral properties, when appropriate, into the complex plane. Furthermore, there is an important quality provided, i.e., the means to include the dynamical characteristics such as time-, length- and temperature scales into the theory. The insertion of standard quantum mechanics into a complex symmetric arrangement with a wider set of broken symmetry solutions leads to the appearance of merged structures like Jordan blocks. The latter will turn out to be a "blessing in disguise". In general it is important to remember that proper invariance laws, like gauge invariance and covariance may be found appropriately embedded when necessary.

In the present article we will build upon such a quantum mechanical model using the flexibility of a complex symmetric *ansatz*. First we will briefly review the background, explanation and need to develop the representation under consideration. The relationship with the Klein-Gordon equation is identified displaying well-known formulas for the usual time and length contractions within the special theory of relativity. It will also be demonstrated how to incorporate gravitational interactions in the picture including dynamical features of the general theory of relativity. The model is finally extended to rigorously include fermions establishing the connection with the Dirac equation. With respect to the query given in the title we have represented the laws of relativity as a quantum effect based on the super-position principle.

2 The Complex Symmetric *Ansatz*

The feature to be discussed here emerges from the so-called complex scaling technique. Using well-known rigorous mathematical theorems on so-called dilatation analytic interactions Balslev and Combes proved important spectral properties of many-body Schrödinger operators [6]. The theorem led to a flurry of quantum theoretical applications in quantum chemistry and nuclear physics, for more details see e.g. [7]. The possibility to "move" the cut corresponding to the absolutely continuous spectrum of dilation analytic (or other appropriate classes) operators was successfully used both in accurate numerical applications based on Weyl's theory [8] and in analytic basis set expansions [9]. The complex scaling process in conjunction with a complex symmetric *ansatz* became a natural choice as a result of applying dilatation methods in e.g. quantum chemistry [10].

The permission to include complex symmetric interactions actually supports a transition from firmly quantum mechanical non-local behaviour to a decidedly classically local appearance. In this generalized picture a supposed class of resonance states can be defined, computed and analysed - compare for instance the illustrious Gamow waves – albeit standard quantum mechanical states remain embedded [6]. Although general Hamiltonians (or Liouvillians) may not every time subscribe to dilatation analyticity, complex symmetric perturbations, as the specific situation dictates, nevertheless have an additional appeal. In the forthcoming description, basic quantum mechanical physical law will rule, and at the same time localized features, cf. those of classical mechanics, take over when and where appropriate.

As an example we will take a simple 2×2 matrix problem in order to demonstrate the necessity, together with the associated consequences, of transforming the secular equation to complex symmetric form. In so doing we will also attach importance to the appearances of Jordan blocks off the real axis as an immediate result of the analytic extension. We will moreover refer to an analytic problem that has been considered in some detail in Ref. [13]. In addition to the attainment of complex eigenvalues one may here demonstrate the existence of crossing points on and/or off the real axis and investigate what type of degeneracy exhibited.

The Hamiltonian discussed in [13]

$$H = H_0 + aV = -\frac{1}{2}\frac{d^2}{dr^2} - \frac{1}{r} + a\frac{e^2}{4}r^2e^{-r} \tag{1}$$

describes the hydrogen atom perturbed by a barrier potential modelled by a barrier height parameter a displaying how the Coulomb spectrum varies with a.

Combined with the complex scaling method, see Ref. [6] and Eq. (2) below, complex eigenvalues are exposed as the scale factor η, defined by

$$r \rightarrow \eta r;\ \eta = e^{i\vartheta};\ |\ \vartheta\ | > \frac{1}{2}\ |\ \arg(E_{\text{res}})\ |, \tag{2}$$

has an angle ϑ sufficiently large to uncover the complex resonance energy E_{res}. In addition one might examine the spectrum for complex values of a. For a general discussion on resonances and their characterization in n-body systems with dilatation analytic potentials see Ref. [14].

As anticipated, the non-crossing rule is obeyed for real-valued barrier heights [13]. However, it was determined that for $a = a_0 = 0.5928 \pm 0.0166i$ two eigenvalues of the Hamiltonian (truncated to 13th dimensional problem) cross. In fact the full (non-truncated) problem leads to an infinity of branch points piling up at the threshold ($E = 0$). The perturbed ground state of the hydrogen atom will run through all unperturbed states and finally be expelled as a resonance state above the threshold. It is interesting to note that the resonance state, for all practical purposes, has the character of a ground state "moving through" all the bound states of the hydrogen atom; for more details see Ref. [13].

In order to understand the crossing situation a bit further we rewrite it as a two-state problem; employing standard multi-dimensional partitioning techniques, see

e.g. Ref. [15]. The 2×2 effective Hamiltonian matrix is hence a function of a (and the energy parameter, here evaluated at the crossing point). For simplicity the scaling parameter η is not explicitly indicated. The energy component $E(a)$ and the matrix elements $H_{ij}(a)$; $i,j = 1,2$ are basically given by (for details on crossing conditions, reference and complement manifolds, and related similarity transformations, see Ref. [16])

$$E(a) = \frac{\langle \Psi(a*) \mid H \mid \Psi(a) \rangle}{\langle \Psi(a*) \mid \Psi(a) \rangle}; \langle \Psi(a*) \mid \Psi(a) \rangle 0 \tag{3}$$

where $\Psi(a) = c_1\psi_1 + c_2\psi_2$ obtains from the secular equation associated with the matrix, see Eq. (4) below, via a complex symmetric similarity transformation producing the diagonal form

$$\begin{pmatrix} H_{11}(a) & H_{12}(a) \\ H_{21}(a) & H_{22}(a) \end{pmatrix} \rightarrow \begin{pmatrix} E_1(a) & 0 \\ 0 & E_2(a) \end{pmatrix} \tag{4}$$

with

$$H_{ij}(a) = \langle \psi_i(a*) \mid H \mid \psi_j(a) \rangle; \langle \psi_i(a*) \mid \psi_j(a) \rangle = \delta_{ij}. \tag{5}$$

Note that $a*$ (and $\eta*$ not explicitly displayed) must occur in the bra position in order to produce matrix elements of the Hamiltonian that are analytic in the parameter(s) a (and η). Equation (4), nevertheless, illustrates the expectation that the matrix at all times can be diagonalized and self-orthogonality amongst the solutions avoided, which is easily proven for Hermitean or self-adjoint problems. However, even if our secular equation derives from a so-called self-adjoint analytic family of operators [6], there is no guarantee that one will find simple eigenvalues, i.e. with Segrè characteristics equal to one. This complication can be demonstrated in the following way. First by noting that we have a general complex symmetric problem under study we consider a general complex symmetric non-Hermitean case with

$$H_{12} = H_{21} = \iota\nu; \iota = \pm i \tag{6}$$

where the indicator ι is introduced to express Schwarz' reflection principle.

To understand the manifestation of Jordan blocks in more detail, we will determine the condition for a degenerate eigenvalue of the matrix, see Eq. (4), As a result we find the anomalous but correct result that (4) can not always hold and instead

$$\begin{pmatrix} \mathrm{H}_{11} & -i\nu \\ -i\nu & H_{22} \end{pmatrix} \rightarrow \begin{pmatrix} E & 2\nu \\ 0 & E \end{pmatrix} \tag{7}$$

with the eigenvalue(s) given by

$$\lambda_{\pm} = \frac{1}{2}(H_{11} + H_{22}) \pm \sqrt{(H_{11} - H_{22})^2 - 4\nu^2} \tag{8}$$

exhibiting the degeneracy for

$$H_{22} = H_{11} \pm 2\nu; \lambda_+ = \lambda_- = E = \frac{1}{2}(H_{11} + H_{22}) = H_{11} \pm \nu. \tag{9}$$

Note that any given value of ν (or prescribed difference between the two diagonal elements) results in two different sets of degenerate solutions in Eq. (9), one of which should be unphysical/erroneous (for more on this see Ref. [17]). For appropriate values of a, such crossing conditions were examined in Ref. [13].

Moreover, if H_{11}, H_{22}, and $H_{12} = H_{21} = \iota\nu$; $\nu \in \Re$; $\iota = \pm i$ then the result is somewhat surprising in that the degenerate solution of the non-self-adjoint secular equation, sometimes referred to as "off the real axis", turns out to be real!

Thus we conclude the following from this analysis: (i) avoided crossings in e.g. standard molecular dynamics are accompanied by branch points in the complex plane corresponding to Jordan blocks in the classical canonical form of the associated matrix representation of the actual operator, (ii) the non-crossing rule is not observed when the picture is extended to unstable resonance states, (iii) the "complex resonance eigenvalues" may appear on the real axis and (iv) unphysical solutions may appear in the secular equation.

In the next section we will develop an analogous complex symmetric model for a suitable quantum mechanical formulation of the theory of relativity.

3 The Klein-Gordon Equation

Following the discussion of the previous section we will devise a simple, yet basic, complex symmetric *ansatz*. A Klein-Gordon-like equation will be obtained with precise restrictions and constraints. The starting point is, cf. example above, a 2×2 matrix that (without interaction) displays perfect symmetry between the states of the particle and of its antiparticle image [18]. To be more specific we write

$$\boldsymbol{H} = \begin{pmatrix} m & -i\nu \\ -i\nu & -m \end{pmatrix} \tag{10}$$

where, using mass units, the diagonal matrix elements are the energies associated with a particle being either in a particle- or its antiparticle state (they may be fermions although the Dirac equation would be required for a rigorous treatment, see more in a following section) respectively, and $-i\nu$ is the complex symmetric interaction, to be defined later; the minus sign is only by convention. Thus the matrix element H_{11} describes a quantum particle with mass m and state vector $\mid m\rangle$, and H_{22} the associated antiparticle with negative energy $-m$ corresponding to state vector $\mid \bar{m}\rangle$. For no interaction the diagonal elements are $\pm m_0$, i.e., the correspondent to the particle rest mass. The associated quantum vectors $|m_0\rangle$ and $|\bar{m}_0\rangle$ can be chosen orthonormal with no loss of generality. Note, however, that $|m\rangle$ and $|\bar{m}\rangle$ are generally biorthogonal. The *ansatz* Eq. (10) can also be derived using a non-positive definite metric [18].

Transforming the matrix, Eq. (10), to canonical form, yields, (note that the roots become $\lambda_{\pm} = \pm m_0$ according to the definition made above)

$$\lambda^2 = m^2 - \nu^2 \tag{11}$$

or

$$m_0^2 = m^2 - \nu^2. \tag{12}$$

By admitting the kinematical perturbation $\nu = p/c$, where c is the velocity of light, p the momentum of the particle, we find the well-known expression

$$m^2c^4 = m_0^2c^4 + p^2c^2. \tag{13}$$

Note that the quantities in Eq. (13) above are operators and further that we have not considered the character of the wave vectors and the structure of the associated spaces in any detail. For instance p is (normally) a self-adjoint operator, which in its extended form may not exhibit this property. Yet to link up with established representations it will be consistent with the relationship $p = m\upsilon$, (υ is the velocity relative a system in rest, wherever the rest mass of the particle is m_0) with appropriate modifications made for a particle in an electromagnetic or other field. As a result our general secular equation generates familiar relationships, which by usual operator substitutions leads to e.g. a Klein-Gordon type equation. Proceeding further one obtains in an obvious notation

$$\begin{aligned} &| m_0\rangle = c_1 \mid m\rangle + c_2 \mid \bar{m}\rangle;\ \lambda_+ = m_0 \\ &| \bar{m}_0\rangle = -c_2 \mid m\rangle + c_1 \mid \bar{m}\rangle;\ \lambda_- = -m_0 \end{aligned} \tag{14}$$

or

$$\begin{aligned} &| m\rangle = c_1 \mid m_0\rangle - c_2 \mid \bar{m}_0\rangle; \\ &| \bar{m}\rangle = c_2 \mid m_0\rangle + c_1 \mid \bar{m}_0\rangle \end{aligned} \tag{14'}$$

with

$$\begin{aligned} c_1 &= \sqrt{\frac{1+X}{2X}} \\ c_2 &= -i\sqrt{\frac{1-X}{2X}} \end{aligned} \qquad m = \frac{m_0}{X};\ c_1^2 + c_2^2 = 1. \tag{15}$$

In Eq. (15) $X = \sqrt{1-\beta^2}$; $\beta = p/mc =$ ("classical particles") $= \upsilon/c$. Since the matrix $\mathbf{H}$ is complex symmetric, the eigenvectors are biorthogonal and hence the absolute values squared of c_1 and c_2 do not sum up to unity. Note that $\upsilon/c \to 1$ implies

$$|c_1|^2 \,/\, |c_2|^2 \to 1. \tag{15'}$$

Before continuing we stress again that the secular equation contains operator quantities, which means that the order of non-commutative products should be respected in general, for more on this see later sections. It is also important to realize that m is the input quantity in the formulation from which m_0 is computed. To find m expressed in m_0 and vice versa is then trivial except when conflicting singularities occur. The latter case will be discussed in connection with the appearance of Jordan blocks.

As already made clear in the preceding section the current resonance model, might, under proper contiguous perturbations, allow fundamental complex

resonance energies commensurate with stringent mathematical boundary conditions and/or precise domain and range characteristics of appropriate families of operators [6–8, 14], i.e.

$$\begin{aligned} m_0c^2 &\to m_0c^2 - i\frac{\Gamma_0}{2};\ \tau_0 = \frac{\hbar}{\Gamma_0} \\ mc^2 &\to mc^2 - i\frac{\Gamma}{2};\quad \tau = \frac{\hbar}{\Gamma} \end{aligned} \tag{16}$$

where Γ, τ and Γ_0, τ_0 are respectively, the half width and lifetime of the state and $\hbar$ is Planck's constant divided by 2π. Inserting the definitions (16) into Eqs. (10–13) and separating the real and imaginary parts the following contractions obtains

$$\Gamma_0 = \Gamma\sqrt{1-\beta^2};\ \tau = \tau_0\sqrt{1-\beta^2} \tag{17}$$

By comparing times in the two scales we directly obtain

$$t = \frac{t_0}{\sqrt{1-\beta^2}}. \tag{18}$$

Enforcing Lorentz-invariance analogous relations for length scales hold. In summary we have derived the well-known relations of the special theory of relativity as a superposition of matter-antimatter quantum states within a general complex symmetric framework

$$l = \frac{l_0}{\sqrt{1-\beta^2}}; t = \frac{t_0}{\sqrt{1-\beta^2}}; m = \frac{m_0}{\sqrt{1-\beta^2}}. \tag{19}$$

In passing, we point out that one can easily incorporate appropriate electromagnetic fields [18] into the formulation, e.g.

$$(E_{op} - eA_0)^2 = m_0^2c^4 + (p - \frac{e}{c}\boldsymbol{A})^2c^2 \tag{20}$$

where in Eq. (20) $(A_0, \boldsymbol{A})$ are the usual vector and scalar potentials. The question of gauge invariance, in connection with analytic extensions of quantum mechanics, will not be considered explicitly here see Ref. [19] for some comments regarding dilatation analytic Hamiltonians. Here it is enough to say that solutions that meet appropriate invariance requirements are implicitly embedded.

Since the present model accepts a general complex symmetric interaction between particles and anti-particles, one may in principle also include the gravitational field. In the following sections we will merge the gravitational field to the Klein-Gordon type formalism [12] as well as to the Dirac equation.

4 The Gravitational Field

We will first extend the formulation of Sect. 3 to include gravitational interactions. Although there exists a plethora of scalar gravity theories, we will try to go beyond this constraint by a most straightforward approach. By augmenting the present

complex symmetric model, in the basis $\mid m,\bar{m}\rangle$, with the "scalar" interaction (the word scalar is placed in quotation marks since the potential is built into a 2×2 or a 4×4 matrix formalism, see next section):

$$m\kappa(r) = m\mu/r;\ \mu = \frac{f\cdot M}{c^2} \tag{21}$$

we end up with

$$H = \begin{pmatrix} m - m\kappa(r) & -i\nu \\ -i\nu & -(m - m\kappa(r)) \end{pmatrix} \tag{22}$$

with μ the gravitational radius, f the gravitational constant, M a "classical non-rotating mass" (which does not change sign when $m \to -m$) and $\nu = p/c$ as before. For more details on the fundamental nature of M and the emergence of black hole like objects within a strongly correlated framework exhibiting off-diagonal longe-range order, see Ref. [12]. Suffice it to say that our model concerns a quantum particle (for a discussion on spin see next section) in a gravitational field created by a black hole object M, containing a multidimensional quantum formulation. In analogy with the occurrence of the electromagnetic field, general invariance properties like covariance and general gauge invariance are not automatically fulfilled. Nevertheless solutions with various symmetry properties are by and large embedded. In this particular case we will see that our approach is not in conflict with the exterior geometry of Schwarzschild's gauge.

Note that $\kappa(r) \geq 0$ depends on the coordinate r of the particle m, with the origin at the center of mass of M. It is important to make the distinction between the coordinate r (and t) of a flat Euclidean space and the corresponding scales defining a curved space-time geometry obtained by the (operator)-secular problem Eq. (19), see also further discussions below. From Eq. (22) (and the associated characteristic equation) we get directly

$$\begin{aligned} \boldsymbol{H} &= \begin{pmatrix} m(1-\kappa(r)) & -i\nu \\ -i\nu & -m(1-\kappa(r)) \end{pmatrix}; \\ \lambda^2 &= m^2(1-\kappa(r))^2 - p^2/c^2 \\ \lambda &= m_0(1-\kappa(r)); \nu = p/c \end{aligned} \tag{23}$$

with the eigenvalues $\lambda_\pm$ (properly scaled for convenience), i.e.

$$\begin{aligned} & m_0^2 = m^2 - p^2/(1-\kappa(r))^2c^2 \\ & \lambda_\pm/(1-\kappa(r)) = \pm m_0 = \pm\sqrt{m^2 - p^2/(1-\kappa(r))^2c^2} \\ & m = m_0/\sqrt{1-\beta'^2};\ \beta' \leq 1;\ 1 > \kappa(r) \\ & \beta' = p/mc(1-\kappa(r)) = \upsilon/c(1-\kappa(r)). \end{aligned} \tag{24}$$

In passing we see that the equations above can be simply written in the dynamic representation

$$H = \begin{pmatrix} m & -ip'/c \\ -ip'/c & -m \end{pmatrix}; p' = p/(1-\kappa(r)). \tag{25}$$

So far nothing has been said about the restrictions incurred by complex symmetry, i.e. of the magnitude of kinematical interactions, of the discontinuous variation of eigenvalues as the mass increases with momentum and of the related manifestation of so-called Jordan blocks. In the following we will demonstrate how this feature emerges by the interaction with the gravitational field. Note that similar effects can also be generated by the electromagnetic field [12, 18].

To put this flexibility into practice we will implement a relationship obtained from standard quantum mechanics. Although the present model derives from a quasi stationary standpoint it is important to realize that many features of conventional quantum theory are still valid in the present generalized setting, i.e. constants of motion and commuting operators specifying the state of the system etc., albeit with an oblique yet unambiguous physical content. In Ref. [12] it was proven that the energy law, including the gravitational potential, is consistent with a given central force. The trick is to make a $\upsilon \to \upsilon' = \upsilon/(1-\kappa(r))$ replacement and use υ' and $\boldsymbol{r}$ as independent variables. Hence we find that the following "classical consistency" relations hold. For particles with a non-zero rest mass, the energy law gives

$$d\left(mc^2(1-\kappa(r))\right) = d\boldsymbol{r}\cdot\frac{d\mathbf{p}'}{dt} + mc^2\frac{\kappa(r)}{r^2}\mathbf{r}\cdot d\mathbf{r} = 0 \tag{26}$$
$$p' = m\upsilon';\ \upsilon' = \frac{\upsilon}{(1-\kappa(r))}$$

and since we employ central forces

$$\mathbf{f}' = \frac{d\boldsymbol{p}'}{dt} = \mathbf{n}\frac{\kappa(r)}{r}mc^2;\ \mathbf{n} = -\frac{\boldsymbol{r}}{r} \tag{27}$$

In deriving (26–27) we demand $r > \mu = r\kappa(r)$, which follows from the definition of p'. Quantum conditions, see below, will in addition request $r \geq 2\mu$. There is, in addition, an inconsistency between the force law, the momentum law and the energy, law defined by the theory of special theory of relativity, cf. Eqs. (27, 28) and Ref. [20]. Thus the law

$$\mathbf{f} = \frac{d\boldsymbol{p}}{dt} = \mathbf{n}\frac{\kappa(r)}{r}mc^2;\ \mathbf{n} = -\frac{\boldsymbol{r}}{r} \tag{28}$$

is not consistent with the energy law. For an interesting discussion and analysis on these aspects see Löwdin [20]. The pseudo problem defined by (27) is non-contradictory in this respect but on the other hand it is easy to see that υ' may exceed the velocity of light. Fortunately this paradox is eliminated by reference to our present quantum mechanical model. First we stress that the Hamiltonian behind Eq. (26) refers to an open system, where the degrees of freedom related to the mass object M are left out. Hence the variational principle becomes a stationary one without extremum properties.

Next, since our system is characterized by a central potential, we are justified in assuming that the velocity υ is a function(al) of r (certainly true for a stationnary situation when centrifugal and centripetal forces balance each other). For this reason the operators m, υ and r commute, and consequently the angular momentum $m\upsilon r$ can be chosen as a constant of motion. It also means that the order of the operators in the generalized secular equation is of no importance as convenient extensions to complex symmetry can be made at the most appropriate level of operator relations. Observing now that commuting operators have simultaneous eigenvalues we obtain equation (29) below, where the conserved angular momentum has been evaluated for the limiting velocity c assumed at the limiting distance μ, the gravitational radius ($m_0 \neq 0$),

$$m_0 \upsilon r = m_0 c \mu \tag{29}$$

This leads to the simple relation

$$\upsilon = \kappa(r) c = \mu c \big/ r \tag{30}$$

For a non-zero mass particle one finds directly that a degeneracy with a Segrè characteristic of 2 (Jordan block) occurs for $r = R_{LS}$ (provided the mass M is entirely localized inside the sphere with radius R_{LS})

$$\frac{m}{2} = m\upsilon/c = m\kappa(r);\ r = R_{LS} = 2\mu \tag{31}$$

where R_{LS} is the familiar Schwarzschild radius of the general theory of relativity. As we have seen, the equations of the special theory become generalized, cf. Eqs. (23, 24), replacing p by p', $\beta \rightarrow \beta'$; $\beta' = p'/mc$, and $\beta' \rightarrow 1$, as $r \rightarrow R_{LS} = 2\mu$ displaying a singularity in Eq. (24). It is also worth noting that p' appears to be generally r- dependent, which can be circumvented by using Eq. (30). Nevertheless, at $r = R_{LS}$, Eq. (22) may be directly written as

$$\begin{aligned} \boldsymbol{H}_{\text{deg}} = \frac{1}{2}\begin{pmatrix} m & -im \\ -im & -m \end{pmatrix} \rightarrow \boldsymbol{H}_{\text{deg}} = \begin{pmatrix} 0 & m \\ 0 & 0 \end{pmatrix} \\ |\,0\rangle = \frac{1}{\sqrt{2}}\,|\,m\rangle - i\frac{1}{\sqrt{2}}\,|\,\bar{m}\rangle \\ |\,\bar{0}\rangle = \frac{1}{\sqrt{2}}\,|\,m\rangle + i\frac{1}{\sqrt{2}}\,|\,\bar{m}\rangle \end{aligned} \tag{32}$$

explicitly displaying the Jordan block structure and associated similarity (also unitary !) transformation. From Eqs. (23, 24, 30) we find

$$m = \frac{m_0(1-\kappa(r))}{\sqrt{1-2\kappa(r)}} \tag{33}$$

with the singularity at the Schwarzschild radius. As stated earlier the singularity in Eq. (33) indicates that either $m \rightarrow \infty$ adiabatically (or nonadiabatically from

e.g. an electromagnetic fluctuation) with m_0 finite or $m_0 \to 0$ adiabatically or non-adiabatically with m finite.

The present approach is quite surprising yet simple. The *ansatz* Eq. (10) implies first of all that a fundamental quantum particle has the choice to occupy one of two possible quantum states. When the preference is made the associated antiparticle state will only be indirectly recognised through (a) the kinematical interaction ν, and (b) the appearance of length and time scale contractions. Mirror- (anti-) particles are observed provided such particles are bodily excited in its mirror state.

It can also be proven that "zero rest-mass particles" obey the gravitational law commensurate with the effect of light deflection in a gravitational field. This follows easily from Eq. (23)

$$\lambda^2 = m^2(1 - \kappa_0(r))^2 - p^2/c^2 = 0 \tag{34}$$

where $\kappa_0(r)$ is indexed to indicate that it concerns particles with zero rest mass, i.e. $\lambda_0 = m_0 = 0$. To be consistent with the degeneracy condition, see Eqs. (31, 32) , we demand the photon to be "bound" to the black hole object M. Taking the expectation values of both sides of Eq. (34), i.e. $\langle p \rangle = 0$ at $\langle r \rangle = R_{LS}$, one concludes that

$$\kappa_0(r) = 2\mu/r \tag{35}$$

Note that we have not employed any explicit coordinates for the analysis except making use of the assumption of an empty space outside a spherically symmetric black hole object. It is hence interesting to find out that Eq. (34) is commensurate with the Schwarzschild gauge in the minimal two component metric or

$$ds^2 = (1 - \kappa_0(r))c^2dt^2 - (1 - \kappa_0(r))^{-1}dr^2 - r^2d\Omega^2 \tag{35'}$$

where as usual Ω contains the co-latitude and longitude angles.

In the section below, we will generalize the discussion to fermions, particles with non-integral spin.

5 The Dirac Equation

We have in previous sections presented a generalized quantum description which transcends classical features like the contraction of scales, and also integrates some general dynamical features of general gravitational interactions. As pointed out, we need to address the problem of half-integral spin and hence to extend our model correspondingly, i.e. by including an *ansatz* that "transmits" the Dirac equation. In other words, we need to enlarge our formulation to a 4×4 complex symmetric matrix problem.

To begin let us first in analogy with Eq. (10) make an attempt to rewrite the Dirac equation based on the matrix

$$\boldsymbol{h}_D = \begin{pmatrix} mc^2 & c\boldsymbol{\sigma}\cdot\boldsymbol{p} \\ c\boldsymbol{\sigma}\cdot\boldsymbol{p} & -mc^2 \end{pmatrix} \tag{36}$$

or written out in more detail in the standard basis

$$\boldsymbol{h}_D = \begin{pmatrix} mc^2 & c\boldsymbol{\sigma}\cdot\boldsymbol{p} \\ c\boldsymbol{\sigma}\cdot\boldsymbol{p} & -mc^2 \end{pmatrix} = \begin{pmatrix} mc^2 & 0 & cp_z & c(p_x - ip_y) \\ 0 & mc^2 & c(p_x + ip_y) & -cp_z \\ cp_z & c(p_x - ip_y) & -mc^2 & 0 \\ c(p_x + ip_y) & -cp_z & 0 & -mc^2 \end{pmatrix} \tag{37}$$

where, as usual, the ingredients are the Pauli spin matrices

$$\sigma_x = \begin{pmatrix} 0 & 1 \\ 1 & 0 \end{pmatrix}; \sigma_y = \begin{pmatrix} 0 & -i \\ -i & 0 \end{pmatrix}; \sigma_z = \begin{pmatrix} 1 & 0 \\ 0 & -1 \end{pmatrix}. \tag{38}$$

In comparison with Sect. 3, we thus invoke the complex symmetric *ansatz*:

$$\boldsymbol{h}_{SD} = \begin{pmatrix} mc^2 & -ic\boldsymbol{\sigma}\cdot\boldsymbol{p} \\ -ic\boldsymbol{\sigma}\cdot\boldsymbol{p} & -mc^2 \end{pmatrix} \tag{39}$$

Suppose now that we want to describe a(n) (almost) free particle, subject to a weak gravitational field created by the mass object M. Before explicitly incorporating the gravitational interaction we will make some simplifying assumptions and conclusions. We will employ a local coordinate system on the (fermion) particle, with the y-axis pointing towards the (far away) center of mass and the x-axis perpendicular to it in the plane of the motion. Under the straightforward conditions of circular motion around the far away object M, the linear momentum will be $p = p_x$ and $p_y = p_z = 0$. Here it is of course clear that the particle spin must be pointing in the z-direction perpendicular to the $x-y$ plane, since the inclusion of a weak gravitational potential corresponds to a weak measurement (extracting information from a quantum system in the limit of vanishing disturbance to its state) of the spin direction. The matrix $\boldsymbol{h}_{SD}$ then reads

$$\boldsymbol{h}_{SD} = \begin{pmatrix} mc^2 & -ic\boldsymbol{\sigma}\cdot\boldsymbol{p} \\ -ic\boldsymbol{\sigma}\cdot\boldsymbol{p} & -mc^2 \end{pmatrix} = \begin{pmatrix} mc^2 & 0 & 0 & -ip_xc \\ 0 & mc^2 & -ip_xc & 0 \\ 0 & -ip_xc & -mc^2 & 0 \\ -ip_xc & 0 & 0 & -mc^2 \end{pmatrix} \tag{40}$$

If we permute the basis vectors appropriately we may write Eq. (40) or $\tilde{\boldsymbol{h}}_{SD}$ as

$$\tilde{\boldsymbol{h}}_{SD} = \begin{pmatrix} \boldsymbol{H} & \boldsymbol{0} \\ \boldsymbol{0} & \boldsymbol{H} \end{pmatrix} \tag{41}$$

The possibility to write the Dirac equation in the form (40–41) is obviously commensurate with the complex symmetric form seen in previous sections. Here we obtain two separate Klein-Gordon type problems, one for the large component and one for the small one. The secular equation and associated transformations factorize

accordingly. In a more general setting the full complex symmetric form corresponding to a 4×4 matrix problem containing Segrè characteristics larger than 2 needs further examination.

Following the formulation in Sect. 3, the inclusion of a gravitational potential follows analogously. The deductions regarding the emergence of the Jordan blocks and related consequences continue for the large and small components separately. In connection with the analysis of the break-down of the equations at $r = R_{LS}$, we note that for $\frac{1}{2}R_{LS} < r < R_{LS}$ the mass m becomes purely imaginary, see (24) or (33), since X in (15) becomes (for one of the branches)

$$X' = \sqrt{1-\beta'^2} = i\sqrt{\beta'^2-1};\ \beta' > 1 \tag{42}$$

and for $\frac{1}{2}R_{LS} > r$ the branches interchange. In order to reflect this behaviour we add the following block (*ad hoc* imposition) to the *ansatz* by defining the vector $|m\rangle = |m, \bar{m}, m_i, \bar{m}_i\rangle$ (here $m, \bar{m}$ and $m_i, \bar{m}_i$ corresponds to particle- antiparticle states and equivalent imaginary states respectively) in which the matrix $\boldsymbol{H}_S$ can be represented as

$$\boldsymbol{H}_S = \begin{pmatrix} \boldsymbol{H} & \boldsymbol{0} \\ \boldsymbol{0} & i\boldsymbol{H} \end{pmatrix} \tag{43}$$

cf. Eq. (41) above. This leads directly to the characteristic equation

$$(\lambda^2 - m^2 + \nu^2)(\lambda^2 + m^2 - \nu^2) = 0 \tag{44}$$

with the additional solutions:

$$\lambda^2 = -(m^2 - \nu^2) = (im_0)^2 \tag{45}$$

$$\begin{aligned} |m_{i0}\rangle &= c_1 |m_i\rangle + c_2 |\bar{m}_i\rangle;\ \lambda_+ = im_0 \\ |\bar{m}_{i0}\rangle &= -c_2 |m_i\rangle + c_1 |\bar{m}_i\rangle;\ \lambda_- = -im_0 \end{aligned} \tag{46}$$

$$\begin{aligned} |m_{i0}\rangle &= c_1 |m_{i0}\rangle - c_2 |\bar{m}_{i0}\rangle; \\ |\bar{m}_{i0}\rangle &= c_2 |m_{i0}\rangle + c_1 |\bar{m}_{i0}\rangle \end{aligned} \tag{47}$$

and

$$\begin{aligned} c_1 &= \sqrt{\tfrac{1+X'}{2X'}} \\ c_2 &= -i\sqrt{\tfrac{1-X'}{2X'}} \end{aligned} \qquad m = \frac{m_0}{X'}; \quad c_1^2 + c_2^2 = 1 \tag{48}$$

Hence we get inside the Swarzschild radius, i.e. when $\beta' > 1$ that

$$\begin{aligned} &m_0 \to m_{i0}; m \to m_i \\ &\bar{m}_0 \to \bar{m}_{i0}; \bar{m} \to \bar{m}_i \\ &m_{i0} \to \bar{m}_0; m_i \to \bar{m} \\ &\bar{m}_{i0} \to m_0; \bar{m}_i \to m \end{aligned} \tag{49}$$

Changing the basis again to $|\boldsymbol{H}_d\rangle = |m, m_i, \bar{m}_i, \bar{m}\rangle$ the matrix (43) in the gravitation free case becomes

$$\boldsymbol{H}_D = \begin{pmatrix} m & 0 & 0 & -i\nu \\ 0 & im & \nu & 0 \\ 0 & \nu & -im & 0 \\ -i\nu & 0 & 0 & -m \end{pmatrix} \tag{50}$$

with straightforward generalizations to the general situation including gravity.

In a certain sense we have introduced a representation that reminds of a so-called supersymmetric structure, although it is not what one usually means with supersymmetric order. The particle states described by the vectors indicated by $m_i, \bar{m}_i$ refer to particles with zero (real) mass and no charge. The symmetry is expected, since inside the Schwarzschild radius, i.e. for $\frac{1}{2}R_{LS} < r < R_{LS}$, real and imaginary masses interchange after "passing" the singularity at R_{LS}, cf. the formulation based on Eq. (43). Note also that we can make this extension both to the Klein-Gordon formalism Eqs. (22, 41) as well as the Dirac equivalent, i.e. in the latter case demanding an 8×8 construction

$$\tilde{\boldsymbol{H}}_{SD} = \begin{pmatrix} \tilde{\boldsymbol{h}}_{SD} & \boldsymbol{0} \\ \boldsymbol{0} & i\tilde{\boldsymbol{h}}_{SD} \end{pmatrix}. \tag{51}$$

One could also speculate whether the lower block in Eq. (43) might be a modification of the small component in the Dirac equation analytically continued by a 90-degree rotation. We will not dwell more on these aspects here except pointing out that the present development should be flexible enough to match the degrees of freedom of the nuclear structure inside the atomic nucleus. In the final section we will summarize our findings and inferences as well as consider potential scenarios.

6 Conclusion and Suggestion

As emphasized in this report, the present structure predicts, for the most part, the main physical laws of relativity theory. Yet, the remarkable feature is that, contrary to accepted classical beliefs, the physical laws derived are a direct consequence of the (extended) quantum mechanical superposition principle.

The present non-classical model is surprising in its simplicity, leading to well known equations, yet with a very different interpretation. The straightforward *ansatz*, Eq. (10), see also Eqs. (39–43, 50, 51), implies that every quantum particle, fermion or boson, will have the possibility to occupy several principal quantum states. Being excited in a (by definition) particle state, the interrelated anti-particle occupation will be recognised through the kinematical interaction ν and the appearance of length and time scale reductions. Mirror- (anti-) particles will not be experienced unless they are bodily physically excited. This description therefore projects a generalized quantum description transcending classical features, like the contraction of scales in the special relativity theory and the emergence of

the Schwarzschild radius and gravitational law of light deflection in the general relativity theory.

We have also incorporated, without contradiction, the electromagnetic field in the special theory. It has been observed that the extension of standard quantum mechanics to a complex symmetric description in general breaks gauge invariance. Howland [19] has discussed the question of gauge transformations in connection with dilatation analytic extensions (complex scaling) of Hamiltonians including an electromagnetic field. He proved that the essential spectrum of Floquet Hamiltonians rotate about a certain set of thresholds when subject to a suitable gauge. Nevertheless the present description is commensurate with embedded symmetry adapted solutions and appropriate invariance properties of the Klein-Gordon-Dirac fundamental formulation. Similar conclusions obtain for the shape of the Schwarzschild geometry in connection with the Jebsen-Birkoff theorem [22, 23].

The appearance of Jordan blocks, see Eq. (32), has been explicitly connected with the gravitational field, but an electromagnetic fluctuation could also be the cause. In particular the photon (or any zero rest-mass particle) trivially fulfils the conditions for a Jordan block. Hence the appearance of "triangular structures" might lead to important relations with the various properties of the vacuum as well as the mass generation puzzle. In fact the restriction $p/m \leq c$ (in the gravitational free case) obtains from the singular behaviour of the matrix eigenvalues. To briefly re-examine the situation we consider the matrix, Eq. (10), for $\nu = m$ (m finite), where e.g. the nonadiabatic interaction could be brought about by an electromagnetic fluctuation, see also the discussion in Sect. 3 following Eq. (3).

$$\boldsymbol{H}_{\text{deg}}^{\text{field}} = \begin{pmatrix} m & -im \\ -im & -m \end{pmatrix} \tag{52}$$

Comparing the description following Eq. (32) it follows directly that $\boldsymbol{H}_{\text{deg}}^{\text{field}}$ after the (unitary) transformation becomes

$$\bar{\boldsymbol{H}}_{\text{deg}}^{\text{field}} = \begin{pmatrix} 0 & 2m \\ 0 & 0 \end{pmatrix} \tag{53}$$

It is important to realize that that the vectors $|m_0\rangle$ and $|\bar{m}_0\rangle$ may be orthonormal, while $|m\rangle$ and $|\bar{m}\rangle$ in general are biorthogonal. Taking the complex conjugate of Eq. (52) (time reversal in this simple picture) yields under the same transformation

$$\bar{\boldsymbol{H}}_{\text{deg}}^{+\ \text{field}} = \begin{pmatrix} 0 & 0 \\ 2m & 0 \end{pmatrix} \tag{54}$$

Analogous formulas obtain for $m \to -m$.

It is tempting to consider the present Jordan form, cf. Eq. (32), as a description of the vacuum as a "particle antiparticle superposition", which may or may not lead to particle excitations. Obviously there appear no particle states corresponding to the diagonal of Eqs. (53, 54). The energy is concealed, i.e. appended to the transition between the states $|0\rangle$ and $|\bar{0}\rangle$, see also Eq. (32).

It has been demonstrated, see Ref. [12], that a strongly correlated manybody theory (including *ODLRO* [21]), based on particles (and anti-particles), will lead to enormous energy reductions, provided a *fundamental interaction* operates inside a principal radius (Schwarzschild radius). Whether these characteristics have anything to do with the puzzling dark-energy-matter enigma should be an inviting possibility. It has also been observed [12, 18] that the repeated addition of the Hamiltonians (53) and (54), followed by diagonalization and appropriate energy exchange, creating new Jordan blocks etc., and so on, yield processes reminiscent of e-doubling.

In summary the model, as described here, allows for basically three types of interactions between the mirror spaces: the kinematical perturbation, the electromagnetic interaction and the mass dependent gravitational potential including the adiabatic and sudden limits equivalent to Eq. (20) or Eqs. (23–32). We have further seen how the model based on the Klein-Gordon formalism could be extended to a Dirac 4×4 *ansatz*, including a modification of the small component, allowing particle structures inside the Schwarzschild radius. Further extensions to higher order nilpotencies should be examined incorporating all known forces outside R_{LS}.

The huge abundance of particles over antiparticles in the Universe is presently conjectured as an energy-particle balance, in our quantum mechanical picture, associated with the selection of the particular particle state occupied. Note also that the famous Minkowski metric of special relativity theory is compatible with a non-positive definite metric [12, 18], instigating a quantum model with a complex symmetric *ansatz*. Although this may result in broken symmetry solutions, it is nevertheless compatible with general gauge invariance embeddings as well as quite unexpectedly, the finding that unitary transformations relate canonical Jordan block representations with its corresponding complex symmetric forms, see e.g. Eq. (32).

A different question concerns whether the present picture would allow or predict gravitational waves. It is clearly obvious that the quantum model advocated here should not be in opposition to "action at a distance". Furthermore it also supports Birkoff's theorem [23] saying that a spherically symmetric mass object should not emit gravitational waves, Whether the graviton as a quantum particle in general possibly would produce such waves is not completely ruled out, since one might not exclude the possibility of diverse soliton-like mechanisms producing the latter.

Acknowledgements This work was supported in part by the Swedish Foundation for Strategic Research. The author is grateful to QSCP-XII organizers for generous hospitality.

References

1. W. Gordon, Z. Physik **40,** 117 (1926).
2. O. Klein, Z. Physik **41,** 407 (1927).
3. P. A. M. Dirac, Proc. Roy. Soc. (London) **A117,** 610 (1928); ibid. **A118,** 351 (1928); ibid. **A126,** 360 (1930).
4. I. P. Grant and H. M. Quiney, Int. J. Quant. Chem. **80,** 283 (2000).

5. S. Wilson and U. Kaldor, in *Theoretical Chemistry and Physics of Heavy and Superheavy Elements*, eds. U. Kaldor and S. Wilson, Kluwer, Dordrecht, 1 (2003).
6. E. Balslev and J. M. Combes, Commun. Math. Phys. **22,** 280–294 (1971).
7. E. J. Brändas and N. Elander, in *Resonances - The Unifying Route Towards the Formulation of Dynamical Processes - Foundations and Applications in Nuclear, Atomic and Molecular Physics.* E. Brändas and N. Elander (eds.), Springer, Berlin, Lecture Notes in Physics, Vol. **325** iii (1989).
8. E. Brändas, M. Rittby and N. Elander, J. Math. Phys. **26,** 2648–2658 (1985); E. Engdahl, E. Brändas, M. Rittby and N. Elander, Phys. Rev. **A37,** 3777–3789 (1988).
9. E. Brändas and P. Froelich, Phys. Rev. **A16,** 2207–2210 (1977); N. Moiseyev, P. R. Certain and F. Weinhold, Mol. Phys. **36,** 1613–1630 (1978).
10. N. Moiseyev, Phys. Rep. **302,** 211–293 (1998).
11. C. E Reid and E. Brändas, Lecture Notes in Physics, Vol. **325,** 476 (1989).
12. E. Brändas, Adv. Quant. Chem. **54**, 115–132 (2008).
13. A. R. Engelmann, M. A. Natiello, M. Höghede, E. Engdahl and E. Brändas, Int. J. Quant. Chem. **31,** 841–845 (1987); M. A. Natiello, E. Brändas and A. R. Engelmann, **S21,** 555–562 (1987).
14. B. Simon, Ann. Math. **97,** 247–274 (1973).
15. P.-O. Löwdin, J. Mol. Spectry. **10,** 12–33 (1963).
16. E. Brändas and P. Froelich, Int. J. Quant. Chem. **13,** 619–626 (1978).
17. E. Brändas, Advan. Quant. Chem. **41,** 121–138 (2002).
18. E. Brändas, Int. J. Quant. Chem. **106,** 2836–2839 (2006).
19. J. S. Howland, J. Math. Phys. **24,** 1240–1244 (1983).
20. P.-O. Löwdin, *Some Comments on the Foundations of Physics,* World Scientific, Singapore, (1998).
21. C. N. Yang, Rev. Mod. Phys. **34,** 694–704 (1962).
22. J. T. Jebsen, Ark. Mat. Ast. Fys. **15,** 1–9 (1921).
23. G. D. Birkoff, *Relativity and Modern Physics*, Cambridge University Press, Cambridge (1921).

Electron Correlation and Nuclear Motion Corrections to the Ground-State Energy of Helium Isoelectronic Ions from Li to Kr

Rossen L. Pavlov(✉), Jean Maruani, L.M. Mihailov, Ch.J. Velchev, and M. Dimitrova-Ivanovich

Abstract Nonrelativistic energies for the ground state of helium isoelectronic ions with $Z = 2-54$ are computed. Calculations are performed using explicitly correlated wavefunctions of a generalized Hylleraas type. The variational procedure used allows solving the two-electron Schrödinger equation with a practically unlimited number of parameters, for trial wavefunctions expanded in products of positive powers of the Hylleraas coordinates. A non-conventional optimization procedure, involving nonlinear programming, is applied. The contribution of the various terms is assessed, including nuclear finite mass and polarization corrections. Our results are compared to other theoretical results. Combined with noncorrelated relativistic energies, they yield good agreement with available experimental data.

Keywords: Helium isoelectronic ions, explicitly correlated wavefunctions, finite nucleus corrections, electron-electron and nucleus-electron correlations

1 Introduction

When investigating many-electron systems, one often applies *ab-initio* approaches while using a determinant class of trial wavefunctions. Hartree-Fock (HF) methods [1] have yielded reasonable values for the ground-state energy of atoms with

R.L. Pavlov, Ch.J. Velchev and M. Dimitrova-Ivanovich
Institute for Nuclear Research and Nuclear Energy, Bulgarian Academy of Sciences, 72 Tsarigradsko Chaussee, 1784 Sofia, Bulgaria, e-mail: ropavlov@inrne.acad.bg

R.L. Pavlov and J. Maruani
Laboratoire de Chimie Physique, CNRS and UPMC, 11 Rue Pierre et Marie Curie, 75005 Paris, France, e-mail: maruani@ccr.jussieu.fr

L.M. Mihailov
Institute of Solid State Physics, Bulgarian Academy of Sciences, 72 Tsarigradsko Chaussee, 1784 Sofia, Bulgaria, e-mail: lmm@issp.bas.bg

S. Wilson et al. (eds.) *Frontiers in Quantum Systems in Chemistry and Physics*.

atomic number $Z > 3$ [2]. For the helium atom, the Hartree-Fock scheme yields a ground-state energy of 2.86168 *au* [2], while the experimental value is 2.90357 *au* [3, 4]. The discrepancy between the HF and experimental values results from the neglect of various terms, mainly electron correlation for lighter atoms but more and more, for heavier atoms, various relativistic, quantum electrodynamics (*qed*) and nuclear size and motion (*nuc*) effects [3]. Hartree-Fock results can be improved by applying configuration interaction, coupled cluster or other schemes to account for electron correlation. But for atoms with few electrons, the best account of correlation is obtained using explicitly correlated wavefunctions [3, 5].

For He, the nuclear size effect was calculated to be 1.1095×10^{-10} *au* [3], but it increases steadily with increasing atomic number. However, for atoms with a small number of electrons, nuclear motion gives a more significant correction to the energy [3]. Taking this into account yields two specific contributions: the finite mass effect and nucleus-electron correlation. On one hand, both nucleus and electrons revolve around their common inertial center and, on the other hand, just as the behavior of each electron depends on the position of other electrons, it also depends on the exact location of the moving nucleus [3, 4].

Explicitly correlated wavefunctions (ECWF) provide precise numerical solutions for the few-particle Schrödinger equation [5]. The earliest ECWF were proposed by Hylleraas [6, 7], Pekeris [8–10], and their generalizations [11–28], but other ECWF were also used by various authors [29–34]. Even though these are not exact wavefunctions, results obtained for both ^{1}S and ^{3}S ground and excited states of He [6–15, 18, 19, 28], as well as of some He isoelectronic ions ($Z = 3-12$) [8, 13, 23–25], practically coincide with available experimental data. In some computations, nuclear size and motion effects were included [6–9, 12, 15, 16, 26].

In the present paper, an ECWF of a generalized Hylleraas type is used to study the non-relativistic ground-state energy of He isoelectronic ions, with $Z = 2-54$. The behavior of the correlated energy versus Z, including nuclear motion corrections, is investigated. The variational procedure devised allows solving the Schrödinger equation for a virtually unlimited number of coefficients, in the expansion series of a trial wavefunction with positive powers of the Hylleraas coordinates. A non-conventional optimization method is developed, making use of nonlinear programming. For each value of Z, a specific set of coefficients yields the minimal energy of the system, with no need to discuss the open question of the divergence of the variational procedure [3, 15, 35–37]. Our results are compared with other theoretical results, and with available experimental data.

2 Variational Procedure

The classical Hamiltonian operator of a two-electron system interacting with a fixed nucleus of charge Z can be written (in atomic units):

$$\hat{\mathbf{H}} = \hat{\mathbf{T}} + \hat{\mathbf{U}} = -\frac{1}{2}\nabla_1^2 - \frac{1}{2}\nabla_2^2 - \frac{Z}{r_1} - \frac{Z}{r_2} + \frac{1}{r_{12}} \tag{1}$$

where r_1 and r_2 are the distances of the two electrons to the nucleus center and r_{12} is their relative distance. The stationary wavefunction $\Psi(\mathbf{r}_1, \mathbf{r}_2)$ of the two electrons, in spinless 6D configuration space, can be derived from the variational equation:

$$\delta E = \delta \frac{\langle \Psi | \hat{\mathbf{H}} | \Psi \rangle}{\langle \Psi \mid \Psi \rangle} = 0 \tag{2}$$

As a trial wavefunction for the (singlet) ground state of the He isoelectronic ions, we use the (spinless) ECWF of generalized Hylleraas type [4, 13]:

$$\psi\left(s', t', u'\right) = e^{-\frac{s'}{2}} F\left(s', t', u'\right) \tag{3}$$

with the function F defined as:

$$F\left(s', t', u'\right) = \sum_{n,l,m=0}^{\infty} c_{n,l,m} s'^n t'^{2l} u'^m \tag{4}$$

where $s' = ks$, $t' = kt$, $u' = ku$; s, t, u are the generalized Hylleraas coordinates, $s = r_1 + r_2$, $t = r_1 - r_2$, $u = r_{12}$; k is a scaling factor, which depends on Z, and the c_{nlm} are the coefficients of the power series in s', t', u'. The problem of determining $\Psi(\mathbf{r}_1, \mathbf{r}_2)$ in 6D space is then reduced to that of deriving $\psi(s, t, u)$ in the 3D space of the internal variables s, t, u.

After switching from r_1, r_2, r_{12} to s, t, u in Eq. (1) and substituting ψ (s', t', u') given by Eqs. (3, 4) into Eq. (2), one deduces an explicit expression for the energy functional by using a procedure similar to those described in Refs. (4–7). The scaling factor k is obtained by solving the equation $\partial E/\partial k = 0$. After some tedious analytical manipulation, the following expression is obtained for the energy functional, in a form suitable for numerical computation:

$$E = -(E_P/2E_N)(E_P/2E_K) \tag{5}$$

where E_P and E_K are the potential and kinetic energy functionals built from the unnormalized wavefunction (3) with $k = 1$, and E_N is the overlap integral. These functionals take the form:

$$E_L = \sum_{r,p,q=0}^{\infty} c_{r,p,q}^2 R_{r,p,q}^L + A_L \sum_{\substack{n,l,m \\ r,p,q}} c_{n,l,m} c_{r,p,q} S_{n,l,m,\, r,p,q}^L, \quad L = P, K, N \tag{6}$$

where $A_L = 1$ for $L = K$ and $A_L = 2$ for $L = P$ or $L = N$, and the second summation sign (with l even) has the following, explicit form:

$$\sum_{\substack{n,l,m \\ r,p,q}} = \sum_{r,p,q=0}^{\infty} \left(\sum_{n=0}^{r-1} \sum_{l=0}^{\infty} \sum_{m=0}^{\infty} + \sum_{l=0}^{p-1} \sum_{\substack{m=0 \\ n=r}}^{\infty} + \sum_{\substack{m=0 \\ n=r \\ l=p}}^{q-1} \right).$$

In Eq. (6) the R^L and S^L (with $L = P, K, N$) have the following forms:

$$
\begin{aligned}
R^P_{r,p,q} &= 4Z\,\mathscr{I}\begin{Bmatrix} 2r+1 \\ 4p \\ 2q+1 \end{Bmatrix} - \mathscr{I}\begin{Bmatrix} 2r+2 \\ 4p \\ 2q \end{Bmatrix} + \mathscr{I}\begin{Bmatrix} 2r \\ 4p+2 \\ 2q \end{Bmatrix},\\
R^K_{r,p,q} &= (r^2 - 4p^2 + 2rq - 4pq)\mathscr{I}\begin{Bmatrix} 2r \\ 4p \\ 2q+1 \end{Bmatrix}\\
&\quad - r^2\mathscr{I}\begin{Bmatrix} 2r-2 \\ 4p+2 \\ 2q+1 \end{Bmatrix} + 0.25\mathscr{I}\begin{Bmatrix} 2r+2 \\ 4p \\ 2q+1 \end{Bmatrix}\\
&\quad - 0.25\mathscr{I}\begin{Bmatrix} 2r \\ 4p+2 \\ 2q+1 \end{Bmatrix} + 4p^2\mathscr{I}\begin{Bmatrix} 2r+2 \\ 4p-2 \\ 2q+1 \end{Bmatrix} + \left(q^2+4pq\right)\mathscr{I}\begin{Bmatrix} 2r+2 \\ 4p \\ 2q-1 \end{Bmatrix},\\
&\quad - \left(q^2+2rq\right)\mathscr{I}\begin{Bmatrix} 2r \\ 4p+2 \\ 2q-1 \end{Bmatrix} - (r+q)\mathscr{I}\begin{Bmatrix} 2r+1 \\ 4p \\ 2q+1 \end{Bmatrix}\\
&\quad + r\,\mathscr{I}\begin{Bmatrix} 2r-1 \\ 4p+2 \\ 2q+1 \end{Bmatrix} + q\,\mathscr{I}\begin{Bmatrix} 2r+1 \\ 4p+2 \\ 2q-1 \end{Bmatrix}\\
R^N_{r,p,q} &= \mathscr{I}\begin{Bmatrix} 2r+2 \\ 4p \\ 2q+1 \end{Bmatrix} - \mathscr{I}\begin{Bmatrix} 2r \\ 4p+2 \\ 2q+1 \end{Bmatrix};\\
S^P_{\substack{n,l,m\\r,p,q}} &= 4Z\,\mathscr{I}\begin{Bmatrix} n+r+1 \\ 2l+2p \\ m+q+1 \end{Bmatrix} - \mathscr{I}\begin{Bmatrix} n+r+2 \\ 2l+2p \\ m+q \end{Bmatrix} + \mathscr{I}\begin{Bmatrix} n+r \\ 2l+2p+2 \\ m+q \end{Bmatrix},\\
S^K_{\substack{n,l,m\\r,p,q}} &= 2\,(mr+nr-4lp-2mp+nq-2lp)\,\mathscr{I}\begin{Bmatrix} n+r \\ 2l+2p \\ m+q+1 \end{Bmatrix}\\
&\quad - 2nr\,\mathscr{I}\begin{Bmatrix} n+r-2 \\ 2l+2p+2 \\ m+q+1 \end{Bmatrix} - (n+m+r+q)\mathscr{I}\begin{Bmatrix} n+r+1 \\ 2l+2p \\ m+q+1 \end{Bmatrix}\\
&\quad + (n+r)\mathscr{I}\begin{Bmatrix} n+r-1 \\ 2l+2p+2 \\ m+q+1 \end{Bmatrix},\\
&\quad + 0.5\mathscr{I}\begin{Bmatrix} n+r+2 \\ 2l+2p \\ m+q+1 \end{Bmatrix} - 0.5\mathscr{I}\begin{Bmatrix} n+r \\ 2l+2p+2 \\ m+q+1 \end{Bmatrix} + 8lp\,\mathscr{I}\begin{Bmatrix} n+r+2 \\ 2l+2p-2 \\ m+q+1 \end{Bmatrix}\\
&\quad + 2(mq+2mp+2lq)\mathscr{I}\begin{Bmatrix} n+r+2 \\ 2l+2p \\ m+q-1 \end{Bmatrix}
\end{aligned}
$$

$$S^{N}_{\substack{n,l,m\\r,p,q}} = \mathscr{I}\begin{bmatrix} n+r+2 \\ 2l+2p \\ m+q+1 \end{bmatrix} - \mathscr{I}\begin{Bmatrix} n+r \\ 2l+2p+2 \\ m+q+1 \end{Bmatrix}, \tag{7}$$

where the integral $I\ \{U,V,W\}$ (U,V,W being arbitrary integers) takes the simple algebraic form:

$$\mathbf{I}\begin{Bmatrix} U \\ V \\ W \end{Bmatrix} = \int_0^{\infty} ds \int_0^{s} du \int_0^{u} e^{-s}\, s^U\, t^V\, u^W\, dt = \frac{(U+V+W+2)!}{(V+1)(V+W+2)}. \tag{8}$$

Applying the Ritz variational principle, the determination of the coefficients $c_{n,l,m}$ is reduced to solving the differential equations: $\partial E/\partial c_{n,l,m} = 0$. This procedure leads to a set of non-linear algebraic equations, yielding the generalized Hylleraas functions. No investigation was made on the convergence of this procedure relative to the number of coefficients, but we studied the variation of the speed of convergence with the number of coefficients when increasing Z [15]. Energy minimization was performed using a home-made algorithm for the numerical solution of systems of nonlinear algebraic equations involving an arbitrary number of coefficients. Frequently used methods are based on the determination of polynomial roots: each trial set of coefficients corresponds to a different polynomial; the number of coefficients used in the literature varies from 6 [15] to 308 [13]. However, according to Fock [37], results for the ground-state energy do not necessarily converge when increasing the number of coefficients in Hylleraas functions. Our program automatically omits those coefficients not improving the convergence. However, care must be taken to avoid local minima being taken as an absolute minimum in some particular cases.

3 Nuclear Motion Corrections

In a system described by a two-electron Schrödinger equation, taking into account nuclear motion entails two corrections:

(i) As in the one-electron case, a corrective term ε_1 appears because the expression of the kinetic energy involves reduced masses instead of electron masses, due to the shift of the inertial center.
(ii) An additional corrective term ε_2 appears, referred to as 'mass polarization'. This term is different for various atomic states, as it depends on the mutual disposition and space correlation of the electrons. For the ground state, the Pauli principle does not give any contribution to ε_2, and the 'mass polarization' correction is solely due to electrostatic repulsion.

Taking into account nuclear motion in the ground-state energy of a two-electron system, we thus add the perturbative corrections ε_1 and ε_2 to the unperturbed energy E_0 [3,4]:

$$\varepsilon_1 = -\frac{\varepsilon}{1+\varepsilon} E_0 \approx -\varepsilon E_0 \tag{9}$$

$$\varepsilon_2 = \varepsilon \int \nabla_1 \Psi^*(\mathbf{r}_1, \mathbf{r}_2)\, \nabla_2 \Psi(\mathbf{r}_1, \mathbf{r}_2)\, d\,\mathbf{r}_1\, d\,\mathbf{r}_2 \tag{10}$$

where $\varepsilon = m_e/M$, m_e being the electron mass and M the nucleus mass. The correction ε_1 increases the atomic energy by about $(m_e/M)|E_0|$, independently of the atomic state.

The 'mass polarization' effect requires accounting for the dependence of the wavefunction on the distance between the electrons, as is indeed the case with ECWFs. For the ground state, the electrons are located at relatively small distance from each other, and this effect may be significant. The term ε_2 can be derived by perturbation from the unperturbed Ψ_0. Following the procedure described in Sect. 2, we obtain:

$$\varepsilon_2 = \frac{\varepsilon k^2}{E_N} \left(\sum_{r,p,q=0}^{\infty} c_{r,p,q}^2 R_{r,p,q}^{Q} + \sum_{\substack{n,l,m \\ r,p,q}} c_{n,l,m}\, c_{r,p,q}\, S_{\substack{n,l,m \\ r,p,q}}^{Q} \right) \tag{11}$$

with k being introduced in Eq. (4), E_N being defined in Eq. (6), the second summation sign is expressed in Eq. (6), and R^Q, S^Q are given by the following expressions, the integral $I\{U,V,W\}$ being expressed as in Eq. (8):

$$\begin{aligned}
R_{rpq}^{Q} = {} & \left(r^2 - 4p^2 - 2rq + 4pq\right) \mathscr{I} \begin{Bmatrix} 2r \\ 4p \\ 2q+1 \end{Bmatrix} + r^2\, \mathscr{I} \begin{Bmatrix} 2r-2 \\ 4p+2 \\ 2q+1 \end{Bmatrix} \\
& + 0.25 \mathscr{I} \begin{Bmatrix} 2r+2 \\ 4p \\ 2q+1 \end{Bmatrix} + 0.25 \mathscr{I} \begin{Bmatrix} 2r \\ 4p+2 \\ 2q+1 \end{Bmatrix} - 4p^2 \mathscr{I} \begin{Bmatrix} 2r+2 \\ 4p-2 \\ 2q+1 \end{Bmatrix} \\
& + \left(q^2 + 4pq\right) \mathscr{I} \begin{Bmatrix} 2r+2 \\ 4p \\ 2q-1 \end{Bmatrix} + \left(q^2 + 2rq\right) \mathscr{I} \begin{Bmatrix} 2r \\ 4p+2 \\ 2q-1 \end{Bmatrix} \\
& + (q-r) \mathscr{I} \begin{Bmatrix} 2r+1 \\ 4p \\ 2q+1 \end{Bmatrix} - r \mathscr{I} \begin{Bmatrix} 2r-1 \\ 4p+2 \\ 2q+1 \end{Bmatrix} - q \mathscr{I} \begin{Bmatrix} 2r+1 \\ 4p+2 \\ 2q-1 \end{Bmatrix} \\
& - 2r^2 \mathscr{I} \begin{Bmatrix} 2r-2 \\ 4p \\ 2q+3 \end{Bmatrix} - 0.5 \mathscr{I} \begin{Bmatrix} 2r \\ 4p \\ 2q+3 \end{Bmatrix} \\
& + 2r \mathscr{I} \begin{Bmatrix} 2r-1 \\ 4p \\ 2q+3 \end{Bmatrix} + 8p^2 \mathscr{I} \begin{Bmatrix} 2r \\ 4p-2 \\ 2q+3 \end{Bmatrix} \\
S_{\substack{n,l,m \\ r,p,q}}^{Q} = {} & 2\left(nr - mr - 4lp + 2mp - nq + 2lq\right) \mathscr{I} \begin{Bmatrix} n+r \\ 2l+2p \\ m+q+1 \end{Bmatrix}
\end{aligned}$$

$$
\begin{aligned}
&+2nr\mathscr{I}\begin{Bmatrix} n+r-2 \\ 2l+2p+2 \\ m+q+1 \end{Bmatrix}+(m-n+q-r)\mathscr{I}\begin{Bmatrix} n+r+1 \\ 2l+2p \\ m+q+1 \end{Bmatrix} \\
&-(n+r)\mathscr{I}\begin{Bmatrix} n+r-1 \\ 2l+2p+2 \\ m+q+1 \end{Bmatrix}+0.5\mathscr{I}\begin{Bmatrix} n+r+2 \\ 2l+2p \\ m+q+1 \end{Bmatrix}+0.5\mathscr{I}\begin{Bmatrix} n+r \\ 2l+2p+2 \\ m+q+1 \end{Bmatrix} \\
&-8lp\mathscr{I}\begin{Bmatrix} n+r+2 \\ 2l+2p-2 \\ m+q+1 \end{Bmatrix}+16lp\mathscr{I}\begin{Bmatrix} n+r \\ 2l+2p-2 \\ m+q+3 \end{Bmatrix} \\
&-2(mq+2mp+2lq)\mathscr{I}\begin{Bmatrix} n+r+2 \\ 2l+2p \\ m+q-1 \end{Bmatrix} \\
&+2(mq+mr+qn)\mathscr{I}\begin{Bmatrix} n+r \\ 2l+2p+2 \\ m+q-1 \end{Bmatrix} \\
&-(m+q)\mathscr{I}\begin{Bmatrix} n+r+1 \\ 2l+2p+2 \\ m+q-1 \end{Bmatrix}-4nr\mathscr{I}\begin{Bmatrix} n+r-2 \\ 2l+2p \\ m+q+3 \end{Bmatrix} \\
&+2(n+r)\mathscr{I}\begin{Bmatrix} n+r-1 \\ 2l+2p \\ m+q+3 \end{Bmatrix}-\mathscr{I}\begin{Bmatrix} n+r \\ 2l+2p \\ m+q+3 \end{Bmatrix} \qquad (12)
\end{aligned}
$$

The nuclear masses used in our computations were derived from recent mass tables [38], choosing for each element the isotope most frequent (or most stable) in Nature. In order to obtain ε_2, we substitute in Eq. (11) the values of c_{nlm} yielded by the variational procedure. As $\varepsilon > 0$, and $E_0 < 0$ in Eq. (9) while the integral in Eq. (10) is positive, both ε_1 and ε_2 are positive and decrease the absolute value of E_0. Thus for a given element (with atomic number Z and uncorrected energy E_0), the absolute value of the corrected energy E_0' increases with increasing isotope mass M. It will be seen however that ε_2 is about two orders of magnitude smaller than ε_1.

4 Algorithm and Program

The ground-state energy of the He isoelectronic ions without mass corrections is derived by solving numerically the nonlinear system of integro-differential equations: $\partial E/\partial c_{nlm} = 0$. An algorithm and a program were developed on this purpose. The algorithm converts the variational procedure into a determination of ECWF coefficients. The optimization method employed is non-conventional, in that it involves nonlinear programming. The resulting optimization algorithm implies such methods as 1-D search, many-D random search (so-called Price method, using a heuristic algorithm with elements of cluster analysis), and gradient search (with

fixed or variable metric). Programs were written in C++, using object-oriented programming.

There are many deep minima with no physical meaning in the considered function. The minimization procedure was thus complicated in looking for the right local minimum. First we looked for minima by varying the parameters one by one. Then we switched to many-D optimization, varying the c_{nlm} in a small range around the best values. An important feature is that the energy may be quite sensitive to some coefficients. In those cases we perform a more careful search of the local minimum around the zero value of the corresponding coefficient.

5 Results and Discussion

Tables 1, 2 and 3 display the ground-state energies computed for He isoelectronic ions, using various approximations. In Table 1 there are gathered correlated ground-state energies, excluding nuclear motion corrections, for ions with $Z = 2-10$. Tables 2 and 3 provide some of the results obtained including nuclear motion corrections for the most abundant or stable isotopes, as well as some energy values, E'_{0SD}, derived by extrapolation from spectroscopic data [9, 39]. For comparison, there are also given noncorrelated, Hartree-Fock values, E_{0FF} (without nuclear motion corrections) and Dirac-Fock values, E'_{0BB} (including *qed* and *nuc* effects).

In order to figure out the relative importance of the various types of corrections to plain Hartree-Fock energies, we plotted in Fig. 1 the corrections computed by Christiane Bonnelle using Bruneau's MCDF code [40]. Upper left, relativistic corrections (including the Breit perturbative term). Upper right, quantum electrodynamics corrections (including vacuum polarization and self energy terms). Lower left: nuclear motion *and* size corrections in both the relativistic and nonrelativistic cases; lower right: correlation contribution, computed as the difference between

Table 1 Correlated ground-state energies E_0/au for helium isoelectronic ions with $Z = 2-10$, omitting nuclear motion corrections: E_{0BS} – computed using Bethe and Salpeter's semi-empirical formula [3]; E_{0TK} – yielded by Thakkar and Koga's optimized *ansatz* [13]; E_{0Pk} – Pekeris' results [9], and E_{0PM} – our results. For comparison, we also give the *Hartree-Fock* energies, E_{0FF}, yielded by Froese-Fischer's code [1]. For simplicity, the sign '$-$' in all energies is omitted

^{Z}Ion	E_{0BS}	E_{0TK}	E_{0Pk}	E_{0PM}	E_{0FF}
^{2}He	2.9037283	2.9037244	2.9037242	2.9037244	*2.8616800*
^{3}Li^{+}	7.2799088	7.2799088	7.2799132	7.2799134	*7.2364152*
^{4}Be^{2+}	13.655565	13.655566	13.655566	13.655566	*13.611299*
^{5}B^{3+}	22.030973	22.030972	22.030971	22.030972	*21.986235*
^{6}C^{4+}	32.406248	32.406247	32.406246	32.406247	*32.361193*
^{7}N^{5+}	44.781447	44.781445	44.781445	44.781445	*44.736164*
^{8}O^{6+}	59.156596	59.156595	59.156595	59.156595	*59.111143*
^{9}F^{7+}	75.531713	75.531712	75.531712	75.531712	*75.486126*
^{10}Ne^{8+}	93.906806	93.906807	93.906806	93.906807	*93.861114*

Table 2 Correlated ground-state energies E'_0/au for helium isoelectronic ions with $Z = 2-10$, including nuclear motion corrections: $E'_{0\mathrm{BS}}$ and $E'_{0\mathrm{TK}}$ – computed using Bethe and Salpeter's formula [3] and yielded by Thakkar and Koga's *ansatz* [13], including only the (largest) correction ε_1; $E'_{0\mathrm{Pk}}$ and $\mathbf{E}'_{0\mathrm{Pk}}$ – Pekeris' nonrelativistic *and* **relativistic** results, including both corrections ε_1 and ε_2 [9]; $E'_{0\mathrm{PM}}$ – our (nonrelativistic) results, including both corrections ε_1 and ε_2; $\mathbf{E}'_{\mathbf{0BB}}$ – for comparison, *noncorrelated* **relativistic** results, including all *qed* and *nuc* corrections, computed by C. Bonnelle using Bruneau's MCDF code [40]; $\mathbf{E}'_{\mathbf{0SD}}1$ [9] and $\mathbf{E}'_{\mathbf{0SD}}2$ [39] – some energy values derived by extrapolation from spectroscopic data. For simplicity, the sign '−' in all energies is omitted

^{Z}Ion	$E'_{0\mathrm{BS}}$	$E'_{0\mathrm{TK}}$	$E'_{0\mathrm{Pk}}$	$E'_{0\mathrm{Pk}}$	$E'_{0\mathrm{PM}}$	$E'_{0\mathrm{BB}}$	$E'_{0\mathrm{SD}}1$	$E'_{0\mathrm{SD}}2$
^{2}He	2.9033303	2.9033264	2.9035715	2.9035629	2.9033045	*2.8613417*	2.90356	2.90331
^{3}Li^{+}	7.2793395	7.2793441	2.7796516	7.2797057	7.2793215	*7.2362914*	7.27970	7.27963
^{4}Be^{2+}	13.654734	13.654735	13.655152	13.655550	13.654709	*13.612215*	13.6554	13.6562
^{5}B^{3+}	22.029875	22.029874	22.030395	22.031795	22.029846	*21.989981*	22.0316	22.034
^{6}C^{4+}	32.404766	32.404765	32.405444	32.409030	32.404733	*32.370641*	32.4091	32.4151
^{7}N^{5+}	44.779692	44.779690	44.780460	44.788101	44.779658	*44.755914*	44.7883	44.8007
^{8}O^{6+}	59.154567	59.154566	59.155419	59.169832	59.154533	*59.147504*	59.1692	59.1917
^{9}F^{7+}	75.529531	75.529531	75.530396	75.555307	75.529500	*75.547667*	75.5534	75.5907
^{10}Ne^{8+}	93.904229	93.904229	93.905225	93.945532	93.904196	*93.958495*	******	94.0106

the Froese-Fischer HF results and either Bethe-Salpeter results (dotted line) or our results (solid line) (see Table 4). It can be seen that for Krypton, for instance, relativistic corrections amount to about 600 eV, *qed* corrections to 22 eV, and nuclear corrections to 0.26 eV, while the correlation contribution approaches its maximum value of about 1.26 eV.

The correlation contribution has the effect of lowering the *relative* noncorrelated energy (increasing its *absolute* value). The relativistic corrections also have the effect of lowering the *relative* nonrelativistic energy, while both *qed* and *nuc* corrections tend to raise the level energy. The relativistic and *qed* corrections tend to increase as about Z^4, while the *nuc* corrections increase quasi-linearly and the correlation contribution first increases sharply and then reaches a plateau for larger values of Z.

The set of graphics displayed in Fig. 2 compares our results with those available from other authors. On the upper left side is shown the increase of our nuclear motion corrections with Z compared to that of isotope number A, showing how small irregularities in the increase of $\varepsilon_1 + \varepsilon_2$ relate to jumps in the number of nucleons, for the selected isotopes (see Fig. 1, lower left for the BB set of isotopes; where nuclear size effects were also included). The lower left diagram displays the quasi-linear dependence of the nuclear motion corrections on the isotope number A, which is similar to that appearing in the hydrogen isoelectronic series [3, 4]. This is because, in Eq. (9), the increase (grossly as Z^2) of E_0 is partly compensated by the decrease (grossly as $1/A \sim 1/Z$) of ε. The quadratic inflexion mainly stems from the nonlinear variation of ε_2 adding to the quasi-linear variation of ε_1 (Table 4 and Fig. 3).

Results given in Table 4 dispaly anomalies in the variation of the mass correction ε_1 for the element isotopes ^{18}Ar ($A = 40$), ^{21}Sc ($A = 45$), ^{29}Cu ($A = 63$), ^{31}Ga ($A = 69$), ^{32}Ge ($A = 74$), ^{34}Se ($A = 80$), and ^{36}Kr ($A = 84$) (Fig. 3, left diagram).

Table 3 Correlated ground-state energies E_0'/au for helium isoelectronic ions with $Z = 11-36$, including nuclear motion corrections: $E'_{0\mathrm{BS}}$ – computed using Bethe and Salpeter's formula [3], including only the (largest) correction ε_1; $E'_{0\mathrm{PM}}$ – our (nonrelativistic) results, including both corrections ε_1 and ε_2. For comparison, we also give the *Hartree-Fock* energies, $E_{0\mathrm{FF}}$, yielded by Froese-Fischer's code [1], and the *noncorrelated* **relativistic** energies, $\mathbf{E'_{0BB}}$, including all *qed* and *nuc* corrections, computed by C. Bonnelle using Bruneau's MCDF code [40]. For simplicity, the sign '−' in all energies is omitted

^{Z}Ion	$E'_{0\mathrm{BS}}$	$E'_{0\mathrm{PM}}$	$E_{0\mathrm{FF}}$	$\mathbf{E'_{0BB}}$
$^{11}Na^{9+}$	114.27916	114.27912	*114.23610*	*114.38326*
$^{12}Mg^{10+}$	136.65382	136.65379	*136.61109*	*136.82448*
$^{13}Al^{11+}$	161.02873	161.02870	*160.98609*	*161.28618*
$^{14}Si^{12+}$	187.40337	187.40334	*187.36108*	*187.77167*
$^{15}P^{13+}$	215.77827	215.77823	*215.73608*	*216.28558*
$^{16}S^{14+}$	246.15290	246.15287	*246.11107*	*246.83191*
$^{17}Cl^{15+}$	278.52778	278.52775	*278.48607*	*279.41598*
$^{18}Ar^{16+}$	312.90289	312.90286	*312.86106*	*314.04293*
$^{19}K^{17+}$	349.27729	349.27726	*349.23606*	*350.71744*
$^{20}Ca^{18+}$	387.65191	387.65188	*387.61106*	*389.44626*
$^{21}Sc^{19+}$	428.02703	428.02700	*427.98605*	*430.23589*
$^{22}Ti^{20+}$	470.40189	470.40186	*470.36105*	*473.09222*
$^{23}V^{21+}$	514.77674	514.77671	*514.73605*	*518.02244*
$^{24}Cr^{22+}$	561.15137	561.15134	*561.11105*	*565.03367*
$^{25}Mn^{23+}$	609.52623	609.52620	*609.48605*	*614.13395*
$^{26}Fe^{24+}$	659.90085	659.90083	*659.86104*	*665.33092*
$^{27}Co^{25+}$	712.27571	712.27568	*712.23604*	*718.63332*
$^{28}Ni^{26+}$	766.65009	766.65006	*766.61104*	*774.04937*
$^{29}Cu^{27+}$	823.02519	823.02516	*822.98604*	*831.58891*
$^{30}Zn^{28+}$	881.39981	881.39978	*881.36104*	*891.26065*
$^{31}Ga^{29+}$	941.77488	941.77486	*941.73604*	*953.07746*
$^{32}Ge^{30+}$	1004.1499	1004.1499	*1004.1110*	*1017.0500*
$^{33}As^{31+}$	1068.5246	1068.5245	*1068.4860*	*1083.1882*
$^{34}Se^{32+}$	1134.8996	1134.8996	*1134.8610*	*1151.5038*
$^{35}Br^{33+}$	1203.2740	1203.2740	*1203.2360*	*1222.0090*
$^{36}Kr^{34+}$	1273.6491	1273.6491	*1273.6110*	*1294.7160*

This is because, for these isotopes, A (which determines the decrease of ε in Eq. 9) gains 5 units while Z (which determines the increase of E_0) gains only 1 unit. These anomalies are likely to occur more frequently when Z increases, but their impact on mass corrections will become smaller.

The variation of ε_2 differs from that of ε_1 in two respects: (i) the anomalies are more frequent and take the form of a complex oscillatory behavior; (ii) the correction reaches a maximum about $Z = 20$ (Fig. 3, right diagram). This is because, while E (Eqs. 5, 6) – and then ε_1 in Eq. (9) – is a product of E_P/E_N and E_P/E_K, ε_2 (Eqs. 10, 11) is simply proportional to E_Q/E_N and then increases slower with Z. The correction ε_2 is therefore more sensitive to oscillations in the number of neutrons relative to that of protons, especially for $Z = 18$ ($A = 40$), and to the increase

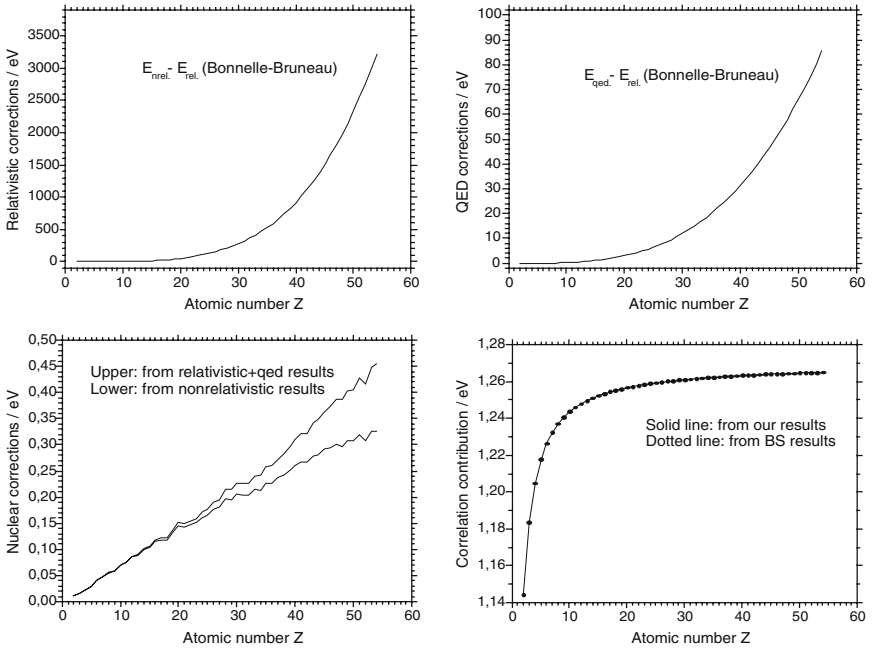

Fig. 1 Various corrections to the ground-state energy of He isoelectronic ions, from $Z = 2$ to 54. *Upper left*: absolute value of the relativistic corrections (these are negative and decrease the nonrelativistic value). *Upper right*: quantum electrodynamics corrections (they are positive and increase the ground-state energy). *Lower left*: nuclear size and motion corrections in the relativistic and nonrelativistic cases (they are also positive and increase the energy). *Lower right*: nonrelativistic correlation contributions computed from Bethe-Salpeter and from our results

of the ratio A/Z, which departs more and more from 2 after $Z = 20$ ($A = 40$): for $Z = 36$, $A - Z = 48$, and for $Z = 54$, $A - Z = 78$.

The upper right diagram of Fig. 2 compares our mass corrections (dotted line) with those computed by Pekeris (solid line), in the range $Z = 2-10$. Our values, more consistent with the BB values (Fig. 1, lower left), are clearly larger, due to a different choice of isotope masses. On the other hand, the correlation contributions computed from our results and from Pekeris' results for $Z = 2-10$ (Fig. 2, lower right) are in excellent agreement, as well as the agreement between our values and BS values outside this range (Fig. 1, lower right).

It may be tempting to use the *nonrelativistic correlated* energies of the present paper to extract correlation values by difference with the Froese-Fischer Hartree-Fock results, and then add these correlation energies to the Bonnelle-Bruneau Dirac-Fock *noncorrelated relativistic* energies to obtain accurate ground-state energies for He isoelectronic ions. For these ions, the correlation energy was shown to rise rapidly from about 1.114 eV to a limit of 1.265 eV. For the records, Table 5 gives the resulting 1s ionization energies for some He isoelectronic ions. However, just as nuclear motion corrections (Fig. 1, lower left), electron correlation contributions

Table 4 Correlation contributions and nuclear motion corrections (in eV) for helium isoelectronic ions with $Z = 2-36$

^{Z}Ion	BS correl. energy/-eV	Our correl. energy/-eV	A	ε_1/eV	ε_2/eV
^{2}He	1.144193	1.144086	4	0.010831	*0.000593*
^{3}Li^{+}	1.183522	1.183647	7	0.015492	*0.000615*
^{4}Be^{2+}	1.204539	1.204562	9	0.022623	*0.000697*
^{5}B^{3+}	1.217388	1.217359	11	0.029878	*0.000750*
^{6}C^{4+}	1.226016	1.225975	12	0.040322	*0.000853*
^{7}N^{5+}	1.232205	1.232165	14	0.047749	*0.000872*
^{8}O^{6+}	1.236852	1.236825	16	0.055223	*0.000888*
^{9}F^{7+}	1.240474	1.240459	19	0.059361	*0.000852*
^{10}Ne^{8+}	1.243372	1.243372	20	0.070134	*0.000909*
^{11}Na^{9+}	1.245744	1.245759	23	0.074223	*0.000877*
^{12}Mg^{10+}	1.247721	1.247751	24	0.085073	*0.000923*
^{13}Al^{11+}	1.249394	1.249438	27	0.089113	*0.000895*
^{14}Si^{12+}	1.250831	1.250885	28	0.100020	*0.000934*
^{15}P^{13+}	1.252074	1.252140	31	0.104021	*0.000908*
^{16}S^{14+}	1.253162	1.253239	32	0.114959	*0.000942*
^{17}Cl^{15+}	1.254123	1.254210	35	0.118931	*0.000918*
^{18}Ar^{16+}	1.254976	1.255073	**40**	**0.116911**	*0.000880*
^{19}K^{17+}	1.255743	1.255846	39	0.133850	*0.000926*
^{20}Ca^{18+}	1.256430	1.256541	40	0.144843	*0.000952*
^{21}Sc^{19+}	1.257052	1.257171	**45**	**0.142163**	*0.000891*
^{22}Ti^{20+}	1.257618	1.257744	48	0.146487	*0.000877*
^{23}V^{21+}	1.258135	1.258267	51	0.150878	*0.000864*
^{24}Cr^{22+}	1.258609	1.258747	52	0.161315	*0.000886*
^{25}Mn^{23+}	1.259046	1.259189	55	0.165660	*0.000874*
^{26}Fe^{24+}	1.259450	1.259597	56	0.176156	*0.000894*
^{27}Co^{25+}	1.259823	1.259975	59	0.180463	*0.000882*
^{28}Ni^{26+}	1.260171	1.260326	58	0.197588	*0.000932*
^{29}Cu^{27+}	1.260492	1.260653	**63**	**0.195280**	*0.000889*
^{30}Zn^{28+}	1.260794	1.260958	64	0.205862	*0.000907*
^{31}Ga^{29+}	1.261077	1.261244	**69**	**0.204016**	*0.000870*
^{32}Ge^{30+}	1.261340	1.261513	**74**	**0.202826**	*0.000838*
^{33}As^{31+}	1.261590	1.261765	75	0.212948	*0.000853*
^{34}Se^{32+}	1.261824	1.262002	**80**	**0.212038**	*0.000825*
^{35}Br^{33+}	1.262044	1.262226	79	0.227658	*0.000860*
^{36}Kr^{34+}	1.262254	1.262438	**84**	**0.226632**	*0.000833*

differ in the relativistic and nonrelativistic cases. Values computed using this *ansatz* start departing from experimental values when Z gets larger (Table 5).

To summarize our results, we display in Fig. 4 the relative magnitudes of the various corrections computed for ionization energies of He isoelectronic ions. It can be seen that up to $Z = 10$ (left diagram), the correlation contribution overcomes

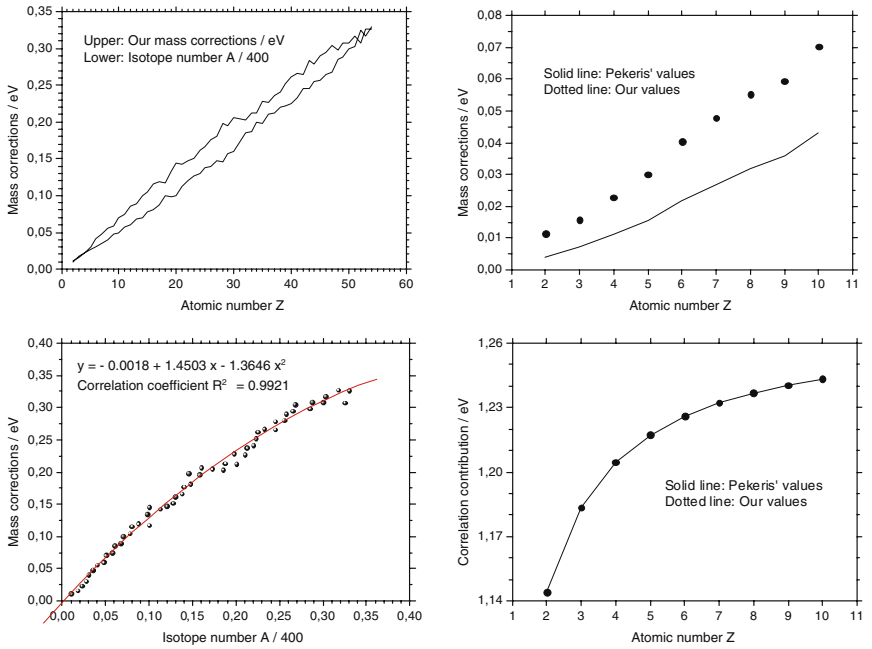

Fig. 2 Various correction to the ground-state energy of He isoelectronic ions, from $Z = 2$ to 54. *Upper left*: respective variations of our overall mass correction and isotope number A. *Lower left*: quadratic fit of our overall mass correction to isotope number A. *Upper right*: our overall mass correction compared to Pekeris' in the range $Z = 2-10$. *Lower right*: our correlation contribution compared to Pekeris' in the range $Z = 2 - 10$

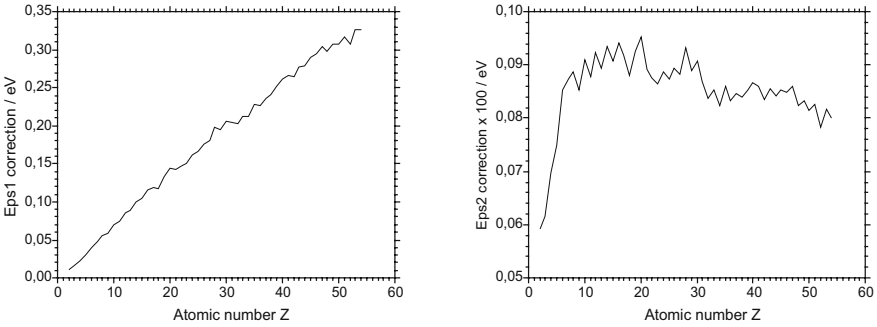

Fig. 3 Variations of nuclear motion corrections ε_1 (*left*) and ε_2 (*right*) in the range $Z = 2-54$

relativity corrections, while the quasi-exponential increase of *qed* corrections, an order of magnitude smaller than the relativity corrections, overcomes the quasi-linear increase of *nuc* corrections about $Z = 7$. For $Z > 10$ (right diagram), the correlation contribution, while remaining much larger than the *nuc* corrections,

Table 5 Calculated ionization potentials (in *au*) for some helium isoelectronic ions, using either corrected Dirac-Fock values [40] with correlation corrections from the present paper (Cal. 1) or Pekeris results [9] (Cal. 2). A few measured values, Exp. 1 [39] and Exp. 2 [9], are also given for comparison

IP/*au*	^{2}He	^{3}Li^{+}	^{4}Be^{2+}	^{5}B^{3+}	^{6}C^{4+}	^{7}N^{5+}	^{8}O^{6+}	^{9}F^{7+}
Cal. 1	0.90357	2.77968	5.65547	9.53165	14.4088	20.2877	27.1692	35.0545
Cal. 2	0.90356	2.77971	5.65555	9.53179	14.4090	20.2881	27.1698	35.0553
Exp. 1	0.90356	2.77964	5.65535	9.53130	14.4087	20.2878	27.1688	35.0530
Exp. 2	0.90356	2.77970	5.65539	9.53160	14.4091	20.2883	27.1692	35.0534
IP/*au*	^{10}Ne^{8+}	^{11}Na^{9+}	^{12}Mg^{10+}	^{13}Al^{11+}	^{14}Si^{12+}	^{15}P^{13+}	^{16}S^{14+}	^{17}Cl^{15+}
Cal. 1	43.9443	53.8404	64.7439	76.6568	89.5805	103.5174	118.4694	134.4391
Cal. 2	43.9455	******	******	******	******	******	******	******
Exp. 1	43.9522	54.0919	64.7401	76.7590	******	******	******	******
Exp. 2	******	******	******	******	******	******	******	******

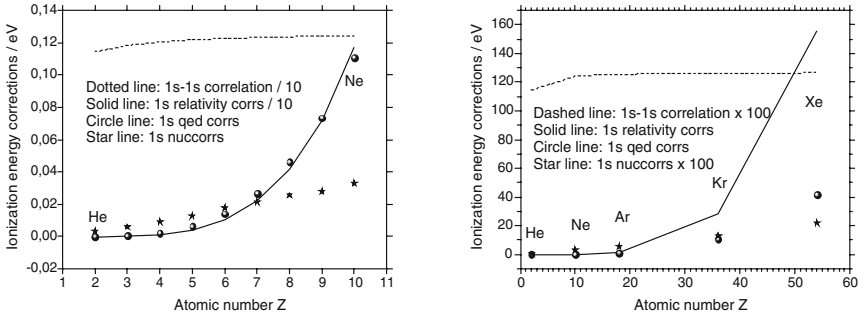

Fig. 4 Relative magnitudes of the various corrections to the ionization energies of He isoelectronic ions. *Left side*: all elements in the range $Z = 2-10$. *Right side*: all rare gases in the range $Z = 2-54$

becomes two orders of magnitude smaller than the relativity corrections close to $Z = 50$, the second main contribution being the *qed* corrections.

6 Conclusion

In this paper we have computed nonrelativistic energies for the ground state of helium isoelectronic ions, with $Z = 2-54$. Calculations were performed using a generalized Hylleraas type of explicitly correlated wavefunction. The variational procedure that was used allows solving the two-electron Schrödinger equation with a practically unlimited number of parameters for trial wavefunctions expanded in products of positive powers of the Hylleraas coordinates. A non-conventional optimization procedure, involving nonlinear programming, was applied. The contributions of the various terms, including nuclear finite mass and polarization corrections, were assessed. Our results were compared to other theoretical results.

It was shown that, except for nuclear motion corrections with Pekeris results (in the range $Z = 2-10$), our values are in excellent agreement with those computed by other authors (Pekeris and Bethe-Salpeter for electron correlation, Bethe-Salpeter and Bonnelle-Bruneau for nuclear corrections), while providing a more rigorous theoretical background for including the nonrelativistic correlation. Combined with noncorrelated relativistic energies, they yield a good agreement with available experimental data. However, as the 1s-1s term is the main correlation contribution to 1s-core ionization energies, it may be worth extending our treatment to the relativistic case, in order to allow more accurate reproduction of XPS or XAS experimental data for heavy atoms.

Acknowledgements The present work was supported by the Bulgarian National Science Foundation (project # 1501) and by the Saint-Kliment Ohridski University of Sofia. We wish to thank Dr. D. van Neck for his help in correcting results obtained using an earlier program. Professor Christiane Bonnelle is deeply acknowledged for providing relativistic results obtained using Bruneau's code. Dr. J. Bruneau, Professor J. Karwowski and Professor R. Lefebvre are acknowledged for a critical reading of the manuscript.

References

1. C. Froese-Fischer, *The Hartree-Fock Method for Atoms*, Wiley, New York (1977).
2. E. Clementi and C. Roetti, *Hartree-Fock-Roothaan Atomic Wavefunctions*, Atomic Data and Nuclear Data Tables **14**, pp. 177–478 (1974).
3. H. A. Bethe and E. E. Salpeter, *Quantum Mechanics of One- and Two-Electron Atoms*, Springer, Berlin (1967).
4. von P. Gombas, *Theorie und Losungsmethoden des Mehrteilchenproblems der Wellenmechanik*, Basel (1950).
5. J. Rychlewski (Ed.), *Explicitly Correlated Wavefunctions in Chemistry and Physics*, Progress in Theoretical Chemistry and Physics **13**, Kluwer, Dordrecht (2003).
6. E. A. Hylleraas, Z. Phys. **48**, 469 (1928); **54**, 347 (1929).
7. E. A. Hylleraas, Z. Phys. **60**, 624 (1930); **63**, 291 (1930); **65**, 209 (1930).
8. C. L. Pekeris, Phys. Rev. **112**, 1649 (1958).
9. C. L. Pekeris, Phys. Rev. **115**, 1216 (1959).
10. C. L. Pekeris, Phys. Rev. **126**, 1470 (1962).
11. H. M. Schwartz, Phys. Rev. **103**, 110 (1956).
12. H. M. Schwartz, Phys. Rev. **120**, 483 (1960).
13. A. J. Thakkar, T. Koga, Phys. Rev. A **50**, 854 (1994).
14. J. F. Hart and G. Herzberg, Phys. Rev. **106**, 79 (1957).
15. T. Kinoshita, Phys. Rev. **105**, 1490 (1957).
16. T. Kinoshita, Phys. Rev. **115**, 366 (1959).
17. A. S. Coolidge and H. M. James, Phys. Rev. **51**, 855 (1937).
18. P. Jolly, Int. J. Quant. Chem. **16**, 1149 (1979).
19. T. Koga, J. Chem. Phys. **93**, 3720 (1990); **96**, 1276 (1992).
20. T. Koga, Z. Phys. **D 34**, 71 (1995).
21. T. Koga, J. Chem. Phys. **104**, 6308 (1996).
22. J. H. Bartlett, Phys. Rev. **51**, 661 (1937).
23. D. E. Freund, B. D. Huxtable and J. D. Morgan III, Phys. Rev. A **29**, 980 (1984).
24. J. D. Baker, D. E. Freund, R. N. Hill and J. D. Morgan III, Phys. Rev. A **41**, 1247 (1990).
25. G. W. F. Drake, Nucl. Instr. Meth. Phys. Res. B **31**, 7 (1988).

26. L. Wilets and I. J. Cherry, Phys. Rev. **103**, 112 (1956).
27. P. S. C. Wang, J. Chem. Phys. **47**, 229 (1967).
28. K. Frankowski and C. L. Pekeris, Phys. Rev. **146**, 46 (1966).
29. H. M. James and A. S. Coolidge, Phys. Rev. **49**, 688 (1936).
30. E. A. Burke, Phys. Rev. **130**, 1871 (1963).
31. A. Luchow and H. Kleindienst, Int. J. Quant. Chem. **51**, 211 (1994).
32. F. W. King, J. Mol. Struct. (Theochem) **400**, 7 (1997).
33. Z.-C. Yan, M. Tambasco and G. W. F. Drake, Phys. Rev. A **57**, 1652 (1998).
34. A. J. Thakkar, T. Koga, T. Tanabe and H. Teruya, Chem. Phys. Lett. **366**, 95 (2002).
35. J. H. Bartlett, J. Gibbons and C. Dunn, Phys. Rev. **47**, 679 (1935).
36. T. Kato, Trans. Amer. Math. Soc. **70**, 212 (1951).
37. V. A. Fock, Proc. USSR Acad. Phys. **18**, 161 (1954).
38. J. K. Tuli, *Nuclear Wallet Cards*, National Nuclear Data Center, Upton, NY (2005).
39. (a) R. L. Kelly (ed.), *Atomic Emission Lines below 2000 Å: I. Hydrogen through Argon*, Naval Research Laboratory, Washington, DC (1968), Report # 6648. (b) A. A. Radctsig, B. M. Smirnov, *Parameters of Atoms and Atom Ions*, Atomizdat, Moscow (1986).
40. (a) J. Bruneau, J. Phys. B **16**, 4135 (1983). (b) J. Maruani and C. Bonnelle, Progr. Theor. Chem. & Phys. **16**, 217 (2007), references therein, and unpublished results.

Unusual Features in Optical Absorption and Photo-Ionisation of Quantum Dot Nano-Rings

Ioan Bâldea(✉) and Lorenz S. Cederbaum

Abstract We present theoretical results on nano-rings consisting of silver quantum dots (QD's) described within the extended Hubbard model. The parameter values, taken from literature, can be *tuned* in a controlled way in wide ranges, a fact that makes QD assemblies particularly interesting. As a result, such nano-systems can be smoothly driven from a weak correlation to a strong correlation regime. To reveal the cross-over between these two regimes, we present results on optical absorption and photo-ionisation. Astonishingly, although the picture based on molecular orbitals (MO's) completely breaks down in the strong correlation regime, both optical absorption and ionisation spectra are surprisingly simple, and can be rationalised within the MO picture. Therefore, the information obtained in this way is scarce, and we show that, by partially covering the nano-rings, is can be considerably enriched. In the nano-rings investigated here we observe the phenomenon called avoiding crossing by molecular physicists and anti-crossing by the solid state community. Unlike in all other cases of avoiding crossings of which we are aware, we often encounter situations where more than two states of identical symmetry are involved.

Keywords: quantum dots, nanostructures, optical absorption, ionisation, extended Hubbard model, electron correlations, avoided crossings, cyclic polyenes

I. Bâldea
Theoretische Chemie, Physikalisch-Chemisches Institut, Universität Heidelberg, Im Neuenheimer Feld 229, D-69120 Heidelberg, Germany. Also at ISS, NILPRP, RO-077125 Bucharest-Măgurele, Romania, e-mail: ioan@pci.uni-heidelberg.de

L.S. Cederbaum
Theoretische Chemie, Physikalisch-Chemisches Institut, Universität Heidelberg, Im Neuenheimer Feld 229, D-69120 Heidelberg, Germany, e-mail: lorenz.cederbaum@pci.uni-heidelberg.de

S. Wilson et al. (eds.) *Frontiers in Quantum Systems in Chemistry and Physics*.

1 Introduction

Modern nano-technologies succeeded to fabricate quantum dots (QD's) of semiconductors or metals, often considered as "artificial" atoms. Typical semiconducting QD's are nearly two dimensional, with a height of a few nanometers and a basal length of the order $\sim 10-100$ nm. Due to the large number of atoms ($\sim 10^5$) they contain, even the problem of a single dot is non-trivial, of interest of its own. Assemblies of semiconducting QD's were also investigated so far, but the most of the existing studies were devoted to two (or at most a few) dots that are vertically coupled.

By contrast, considerable smaller metallic QD's (nearly spherical, with diameter of a few nanometers) were prepared and, most important in the context of the present lecture, assembled in regular arrays, counterparts of ordinary molecules or solids. A few ("valence" or π) electrons can hop from one dot to another (lateral coupling) and become delocalised over the whole nano-structure. By means of a Langmuir technique, monolayers of silver QD's have been prepared and reversibly compressed [1–4], yielding electronic properties that can be varied almost continuous. The wide *tunability* makes these nano-structures showcase systems for studying effects of electron correlations at nano-scale.

In the present work, we present results on electron correlations obtained by extensive studies based on full CI (configuration interaction) exact numerical diagonalisation for N QD nano-rings (point group D_{Nh}) using parameters for QD's of silver taken from literature.

The remaining part of this lecture is organised as follows. In Sect. 2, we expose the model and the parameters used for QD nano-rings. To give further support to the model we employ, namely the extended Hubbard model, we next show (Sect. 3) a variety of results demonstrating that it provides a reasonable good description for cyclic polenes (annulenes). These molecules are counterparts of the nano-rings considered here. In Sect. 4, we present results demonstrating that the nano-rings can be smoothly driven from a regime of weak correlations to a regime of very strong correlations. As tools for possible experimental investigation, we show a variety of results for optical absorption (Sect. 5) and photo-ionisation spectra (Sect. 6). Surprisingly, both spectra are extremely scarce, and this seriously limits the information one can gather in such experiments. In Sect. 7 we present results on optical spectra for partially covered nano-rings, which demonstrate that much more information can be obtained when only a part of the nano-structure is irradiated. Finally, in Sect. 8 we summarise the results of this work.

2 Parameters for QD Nano-Rings

Assemblies of QD's are particularly interesting because their properties can be tuned by modifying parameters that can be easily controlled experimentally: dot size, interdot spacing, and electron number.

A "valence" electron in a spherical isolated QD of a few nanometers represents a textbook example of a particle in a box, possessing a discrete spectrum controlled by the dot diameter $2R$ ($\varepsilon_\alpha \sim -A_\alpha/R^2$). In addition, the dot diameter controls another important quantity, the charging energy (or Coulomb blockade) U, representing the energy to be paid for adding an electron to a QD where an excess electron already exists. It can be expressed in terms of the dot capacity C ($U = e^2/C$). Importantly, the dot capacity can and has been measured experimentally by means of scanning transmission microscopy. For QD's of silver with $2R = 2.6\,\mathrm{nm}$ a value $U = 0.34\,\mathrm{eV}$ has thus been determined [5]. By assuming a *spherical* dot (and the Ag-QD's appear spherical even when imaged in high resolution transmission electron microscopy [1]), one gets a theoretical estimate $U = 0.3\,\mathrm{eV}$ ($C = \kappa_r R$, κ_r being the dielectric constant of the medium) in good agreement with measurements.

By means of a Langmuir technique, films on which regular arrays of QD's are deposited can be compressed reversibly [1–4]. In this way, the interdot separation can be (almost) continuously varied within a broad range, $1.1 \lesssim d \lesssim 1.9$ ($d \equiv D/(2R)$, the interdot distance D being measured between adjacent dot centres). The parameter d is very important, especially because the hoping integral t_0 depends exponentially on it. This result was obtained [4] by fitting the second harmonic response measured experimentally [6]. In the range of experimental interest t_0 varies within about two order of magnitude. Besides electron hoping, QD's are coupled electrostatically, and the interdot Coulomb repulsion V, related to the mutual elastance (remember that elastance is the inverse of capacity), is also controlled by d.

Because the inter-level energy separation is larger than all the other energy scales discussed above, one can consider only the highest occupied level ε of electrons in isolated dots (single AO approximation).

Similar to other studies, e.g. Refs. [7–10], we shall describe nano-rings consisting of N QD's by means of an extended Hubbard Hamiltonian

$$H = -t_0 \sum_{l=1}^{N} \sum_{\sigma=\uparrow,\downarrow} \left(a^\dagger_{l,\sigma} a_{l+1,\sigma} + a^\dagger_{l+1,\sigma} a_{l,\sigma} \right) + \sum_{l=1}^{N} \left(\varepsilon_0 \hat{n}_l + U \hat{n}_{l,\uparrow} \hat{n}_{l,\downarrow} + V \hat{n}_l \hat{n}_{l+1} \right), \tag{1}$$

where, a ($a^\dagger$) denote creation (annihilation) operators for electrons, $\hat{n}_{l,\sigma} \equiv a^\dagger_{l,\sigma} a_{l,\sigma}$, $\hat{n}_l \equiv \hat{n}_{l,\uparrow} + \hat{n}_{l,\downarrow}$, For QD's, all the parameters ε, t_0, U, and V are tunable. In addition to these, the number of electrons N_e can also be varied within wide ranges, by changing the voltage of a gate electrode, which is placed on the top of the electron gas [11]. Therefore, it is also interesting to examine nano-rings with a given number of QD's and a variable number of electrons.

In the present considerations, we shall assume an ideal situation, where the parameters ε_0, t_0, U, and V are dot (l) independent. This can be considered a reasonable first-order approximation in view of the narrow size distributions ($\sim$2−5%) achieved in the arrays of Ag QD's assembled by Heath's group [1, 2, 5, 6, 12].

3 How Good Is the Extended Hubbard Model for Annulenes?

Equation (1) represents a version of what chemists call the Pariser-Parr-Pople (PPP) model [13–17], where the Coulomb repulsion $V_{l,m}$ between the sites l and m ($l < m$) is restricted to next neighbours, $V_{l,m} = V\delta_{m,\,l+1}$.

Before applying it to QD nano-rings, we shall show in this section that the extended Hubbard model is able to provide a reasonably good description of polyenes, the molecules for which the PPP model has been proposed. We shall consider the case of cyclic polyenes (annulenes) C_NH_N, the molecules that are the counterparts of the QD nano-rings investigated here. In these molecules, there are as many sites (CH-units) N as π electrons N_e, that is, half of the molecular orbitals (MO's) are occupied (half-filling case).

In the literature, most studies used t_0-values close to the "spectroscopic" value 2.5 eV [18–26] and that deduced from *ab initio* studies on small molecules [27] and experiments on polyacetylene [28] 3.0 eV, but significantly different values (e.g. 1.6 eV [29, 30]) also exist. The on-site Hubbard strength deduced from ionisation potential and electron affinity of carbon atoms is $U = 11.26$ eV [25] but considerably different values have been deduced from fitting various properties ($7-9$ [31], 5 eV [30] or even smaller than 4.5 eV [32]). Estimations for V derived by applying the extended Hubbard model (0.4 [24], 0.3 eV [33], and 1.75 eV [30]) are much smaller than the nearest-neighbor term ($V_{l,l+1}$) of the Pariser-Parr-Pople (PPP) model: one gets $V_{l,l+1} \approx 7.6$ eV and $V_{l,l+1} \approx 5.3$ eV by employing Ohno [34] and Mataga-Nishimoto's [35] parametrizations, respectively.

We shall use the benzene molecule (C_6H_6) to determine the model parameters. In view of the fact that all C–C bonds are equivalent in benzene, it is reasonably to assume that the electron-phonon coupling plays no significant role for the present considerations.

Below, we shall fix the hopping integral close to the "spectroscopic" value $t_0 = 2.5$ eV [18–26] used for polyacetylene and adjust the Hubbard strengths U and V to fit *all* the $\pi - \pi^*$ excitation energies measured experimentally in benzene. They are listed in Table 1. As seen in Table 1, by using *only two* adjustable parameters, $U = 4.5$ eV and $V = 1.27$ eV, it is possible to reproduce successfully both singlet and triplet $\pi - \pi^*$ excitation energies within an accuracy comparable to those of *ab initio* methods. Concerning the latter, we present in Table 1 CASSCF3- and CASPT2-results taken from literature along with those computed by us using the extended-ADC(2)-scheme [36, 37]. The latter successfully provides accurate results for many medium-size molecules (e.g. Refs. [38, 39]).

Let us now consider an open-shell molecule, double ionised benzene. In view of the fact that the pair of degenerate e_{1g} MO's is (half) occupied by two electrons, one expects a triplet ground state $^3A_{2g}$, in accordance with Hund's rule. *Ab initio* ADC(2) calculations [51] confirm this fact, and found the two lowest excitations as being the singlet states $^1E_{2g}$ and $^1A_{1g}$. Their excitation energies were predicted to be 0.62 and 0.79 eV, respectively. The extended Hubbard model yields the same ordering of these three states. With the parameter values for neutral benzene, the two excitation energies are 0.40 and 0.80 eV, respectively.

Table 1 Excitation energies in benzene: experiment, *ab initio* (CASSCF3, CASPT2, and ADC(2)) versus extended Hubbard model (EHM) with: $t_0 = 2.5\,\text{eV}$, $U = 4.5\,\text{eV}$, and $V = 1.27\,\text{eV}$ (point group D_{6h}; all energies in eV)

State	Exp.	CASSCF3[a]	CASPT2[b]	ADC(2)[l]	EHM
$^3B_{1u}$	3.94[c]; 3.9[d]	3.9	3.89	3.86	3.89
$^3E_{1u}$	4.7[c]	4.9	4.49	4.39	4.58
$^1B_{2u}$	4.90[e,f]; 5.0[c]	4.9	4.84	4.31	4.61
$^3B_{2u}$	5.60[c]	6.7	5.49	5.48	5.56
$^1B_{1u}$	6.20[c,g,h]; 6.3[f]	7.4	6.30	6.28	5.66
$^3E_{2g}$	6.55[i]; 7.5 ± 0.25[b]	7.2	7.12	6.85	6.42
$^1E_{1u}$	6.98[g]; 7.00[f]; 6.94[h,k]	7.8	7.03	6.92	6.43
$^1E_{2g}$	7.3[j]; 7.8 ± 0.2[b]	8.1	7.90	7.22	7.24

[a]Matos et al., Ref. [40]; [b]Lorentzon et al., Ref. [41]; [c]Doering, Ref. [42]; [d]King and Pinnington, Ref. [43]; [e]Callomon et al., Ref. [44]; [f]Lassettre et al., Ref. [45]; [g]Koch and Otto, Ref. [46]; [h]Hiraya and Shobatake, Ref. [47]; [i]Astier and Maier, Ref. [48]; [j]Bonneau et al., Ref. [49]; [k]Wilkinson, Ref. [50]; [l]Results obtained by means of the extended ADC(2) method using the Heidelberg ADC-package

Cyclo-octatetraene C_8H_8 (COT) is another open-shell molecule. It possesses a distorted ground state geometry, revealing the important role played by electron-phonon couplings in this state. Since $N(=8)$ is a multiple of four, COT is an anti-Hückel molecule unstable towards bond alternation [52–54]. This reduces the symmetry from D_{8h} to D_{4h}. In addition, COT is also unstable to ring inversion, which yields a further symmetry reduction from D_{4h} to D_{2d}, the actual symmetry of the ground state [55, 56]. But most interesting for the present purpose is the existence of a transition state of COT, in which the molecule is planar and all bonds are equivalent (D_{8h} symmetry) [55]. Electron-phonon couplings are less important for the transition state.

Planar COT has two electrons partially occupying the degenerate e_{2u} pair of (nonbonding) MO's [55], and according to Hund's rule, the ground state should be a triplet ($^3A_{2u}$) state. Confirming earlier *ab initio* calculations, transition state spectroscopy experiments found that the ground state is a singlet ($^1B_{1g}$) state, a fact which violates Hund's rule [55]. Experimentally, the lowest triplet state was found to be located $\sim 0.34-0.39\,\text{eV}$ ($8-9$ kcal/mol) above the singlet ground state [55]. With the above parameter set, the extended Hubbard model (1) correctly predicts a singlet ground state. Moreover, for the singlet-triplet splitting it yields a value of 0.31 eV (7.16 kcal/mol), much closer to the experimental value than that of 20.08 kcal/mol, as predicted by the MP2-CASSCF method [56]. The latter method represents the state-of-art of *ab initio* quantum chemical calculations for molecules like COT. To explain why the singlet lies below the triplet, a non-uniform distribution of electron spins in the ground state of D_{8h} COT was claimed previously [55]. Interestingly, this fact is also supported by the results obtained within the extended Hubbard model: in the phase diagram of anti-Hückel systems, the value of $U/V = 3.54 > 2$ is situated in the spin-density-wave region, characterised indeed by non-uniform spin distribution [57].

To conclude this section, the extended Hubbard model provides a surprisingly good descriptions of the ground state and $\pi - \pi^*$ excitations of annulenes. In the next sections we return to QD nano-rings, the systems of our present interest.

4 Cross-Over Between Weak and Strong Correlation Regimes

Intuitively, one expects that electrons are weakly correlated if the interaction strengths (U and V) are smaller than the bandwidth $4t_0$, and strongly correlated in the opposite case. By inspecting Fig. 1, one can see that these two situations correspond to QD's that are close enough of each other ($d \gtrsim 1$) and to sufficiently distant QD's, respectively. Results on the MO populations for 10 electrons over 10 QD's are shown in Fig. 2. (Notice that populations for degenerate e-MO's are summed up.) As one can see there, the MO picture holds for nearly touching QD's ($d \gtrsim 1$): the lower half of MO's is occupied, whereas the upper half is empty. The MO picture worsens gradually with increasing d. At large d, the lower and upper MO's tend to become democratically occupied (0.5 electrons per MO). This behaviour can be qualitatively understood, by noting that at small d electron hoping dominates

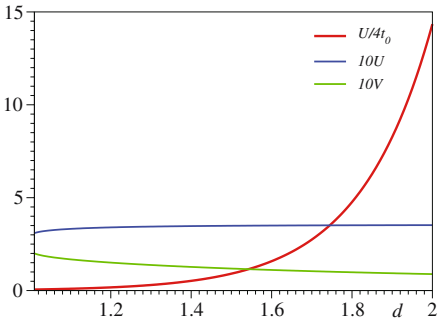

Fig. 1 Dependence on interdot spacing $d = D/(2R)$ of the parameters entering the extended Hubbard model (U and V are given in eV)

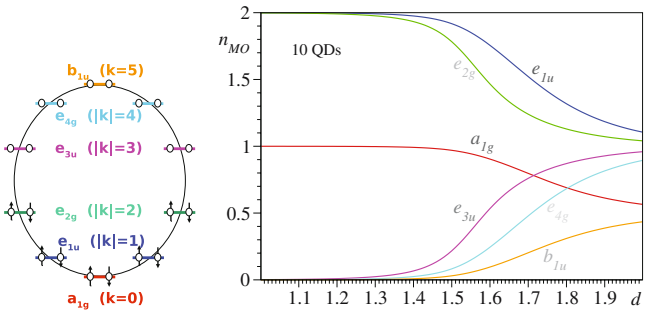

Fig. 2 MO scheme for the ground state of 10 electrons on 10 QD's (*left panel*) and MO populations as a function of interdot spacing (*right panel*). The populations of the two-fold degenerate e-MO's are added

over interaction ($4t_0 > U, V$), while at large d the situation is reversed: the height of the picture in the left panel of Fig. 2 (equal to $4t_0$) falls exponentially with d, and elementary interaction processes ($\sim U, V$) easily spread almost uniformly electrons over all MO's.

5 Optical Absorption

Let us now examine the effect of electron correlations on the optical absorption. The absorption coefficient in the ground state $|G\rangle$ of a nano-ring irradiated by light linearly polarized along j-direction ($j = x, y$) in the ring plane can be expressed as a sum of contributions of various excited states $\{|\Psi_\lambda\rangle\}$

$$\alpha_j(\omega) = \rho^{-2}\omega \sum_\lambda |\langle \Psi_\lambda | \mu_j | G\rangle|^2 \delta\left(\omega - \varepsilon_\lambda + \varepsilon_0\right), \tag{2}$$

where $\{\varepsilon_\lambda\}$ stand for excitation energies, and the operator of electric dipole momentum μ reads

$$\mu = -|e|\rho \sum_l \hat{n}_l \left[\hat{\mathbf{x}}\cos(2\pi l/N) + \hat{\mathbf{y}}\sin(2\pi l/N)\right]. \tag{3}$$

e and $\rho = D/2\sin(\pi/N)$ denote elementary charge and ring radius, respectively.

It is also helpful to express μ in terms of MO- (or Bloch-) operators $c_{p,\sigma} = 1/\sqrt{N}\sum_l a_{l,\sigma}\exp(-2\pi pli/N)$

$$\begin{aligned} \mu_x &= -|e|\rho/2 \sum_{p,\sigma} \left(c^\dagger_{p+1,\sigma} c_{p,\sigma} + c^\dagger_{p,\sigma} c_{p+1,\sigma}\right), \\ \mu_y &= i|e|\rho/2 \sum_{p,\sigma} \left(c^\dagger_{p+1,\sigma} c_{p,\sigma} - c^\dagger_{p,\sigma} c_{p+1,\sigma}\right), \end{aligned} \tag{4}$$

An important quantity characterising the optical absorption is the optical gap, i.e. the lowest frequency ε in the spectrum (2). The curves ε_6 and ε_{10} depicted in Fig. 3 are obtained for nano-rings consisting of 6 and 10 QD's at half filling ($N_e = N$), respectively. They clearly display a cross-over between two regimes. For small d, these curves exhibit an exponential decay (note the logarithmic scale on ordinate). This is the regime of weak correlations, where the optical gap scales as the hopping integral t_0. It is nothing but the HOMO-LUMO gap (or, in the solid state physics nomenclature, the band gap), the energy required to excite an electron from the highest occupied molecular orbital (HOMO) to the lowest unoccupied molecular orbital (LUMO). At large d, electron hoping is ineffective and electron correlations become strong. At half filling, all QD's are occupied by one electron in the ground state. The lowest optical process requires to create a double occupied dot, and for this one has to pay an energy U and one gains an energy amount V. As one can see in Fig. 3, the value $U - V$ obtained thereby (Hubbard-Mott gap) is approached asymptotically both for 6 and for 10 QD's. In this limit the hoping ceases to play a significant rôle. The only coupling is between adjacent dots via V, and therefore the excitation energy becomes independent of the number of QD's in the nano-ring.

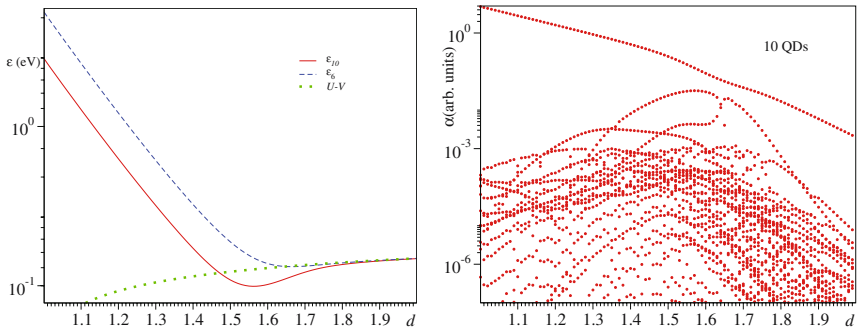

Fig. 3 Results on optical absorption of half-filled QD nano-rings as a function of interdot spacing d. *Left panel*: the optical gap for nano-rings with 6 (ε_6) and 10 (ε_{10}) QD's. The dotted line represents the asymptotic limit $U - V$ of vanishing hopping ($t_0 \to 0$). *Right panel*: spectral intensities for 10 QD nano-rings. Note the logarithmic scale on ordinate

The presence of indices p and $p+1$ in Eq. (4) indicates that only electronic transitions from adjacent MO's can contribute to optical absorption. Consequently, only a single optical transition is allowed within the MO picture for closed-shell systems, namely the HOMO-LUMO transition. But we have seen above that at larger d all MO's become partially occupied and the MO picture completely breaks down. Unless d is very close to unity, there is no dominant contribution to the ground state from a certain Slater determinant. For six electrons over 6 QD's, we checked by straightforward calculations that practically all Slater determinants with A_{1g}-symmetry contribute significantly to the A_{1g}-ground state. Therefore, one would expect a multitude of lines in the optical spectrum in the regime of strong correlation.

Strikingly is that, despite of strong correlations, out of the very numerous E_{1u}-excitations allowed by spatial symmetry, only a single state possesses significant spectral weight. Many other states give small but nonvanishing contributions (*cf.* the right panel of Fig. 3). This behaviour is a manifestation of a *hidden dynamical quasi-symmetry* in optical absorption of QD nano-rings, as we discussed recently [10] for the half-filling case.

Let us next examine another nano-ring, a closed-shell system, but not a half-filled one. This is the case, for instance, of six electrons on 10 QD's. The results for the significant optical transitions are collected in Fig. 4. Most interesting for this case is the region very close to $d \approx 1.87$, where a phenomenon called avoiding crossing by molecular physicists and anti-crossing by the solid-state community can be seen. This phenomenon corresponds to a situation where, by varying a certain parameter (d in our case) around a certain value (d_c), the energy difference $\delta E = E_2 - E_1$ of two eigenstates S_1 and S_2 of identical symmetry increases with increasing $|d - d_c|$. At $d = d_c$, δE possesses a nonvanishing minimum (repulsion effect due to symmetry). Concomitantly, these states smoothly interchange their physical properties around $d = d_c$. For instance, S_1 possesses significant spectral weight for $d \lesssim d_c$, which becomes practically vanishing for $d \gtrsim d_c$. For S_2, the situation is reversed: its

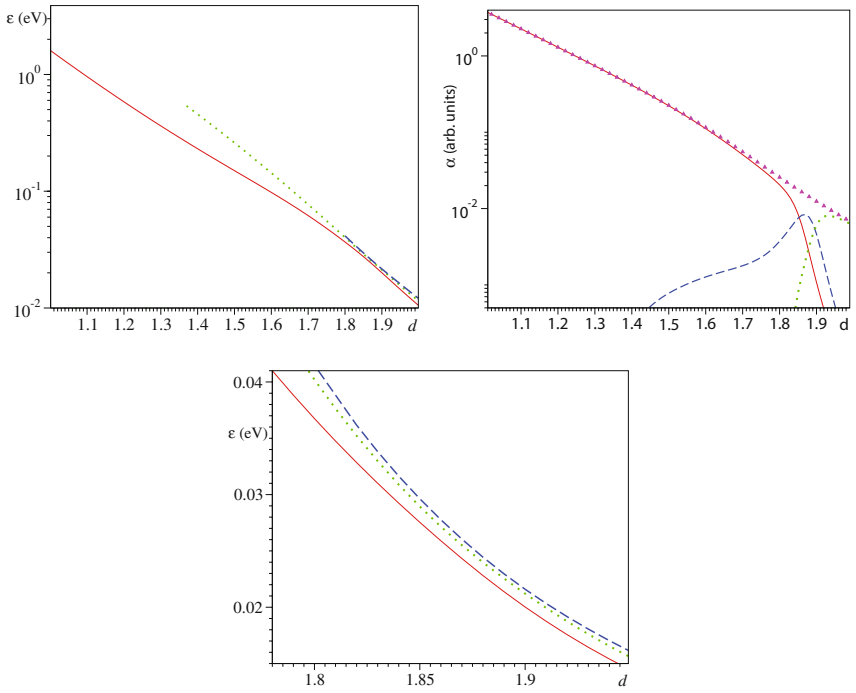

Fig. 4 Results for significant optical transitions for six electrons on 10 QD nano-rings as a function of interdot spacing d. *Left panel*: absorption frequencies of the optical transitions with significant spectral weights. *Right panel*: spectral intensities. Triangles in this panel, representing the sum of the other three curves, build a curve that varies smoothly with d

spectral weight is negligible for $d \lesssim d_c$, but becomes important for $d \gtrsim d_c$. Rather than this *adiabatic* description, a *diabatic* description, in terms of a bright diabatic state $\tilde{S}_1$ (approximating S_1 for $d < d_c$ and S_2 for $d > d_c$) and a dark diabatic state $\tilde{S}_2$ (approximating S_2 for $d < d_c$ and S_1 for $d > d_c$), is often more useful in practice [58].

What makes the difference between the situation presented in Fig. 4 from other cases of avoiding crossings discussed in the literature is that, in our case, *three* states are involved. Besides the spectral intensities of the relevant eigenstates, we added in Fig. 4 their individual intensities. The fact that the curve obtained in this way (represented by triangles) smoothly varies with d suggests that the diabatic description can be also useful for avoiding crossings involving more than two states. The occurrence of such complex avoiding crossings, with the participation of three or even more states of identical symmetry is not an exception, but rather the rule for assembled QD's like those investigated here. As a global characterisation, this behaviour is due to the fact that, for sufficiently distant QD's, electron hopping becomes less important, and numerous eigenstates (including those with identical symmetry) come energetically closer.

From a pragmatical point of view, one can conclude that a *hidden dynamical quasi-symmetry* in optical absorption also exists for closed-shell QD nano-rings

away from half filling. Because the states involved in an avoiding crossing like that depicted in Fig. 4 are energetically very close (∼meV), what one can measure in an experiment are not the individual intensities but their sum; that is, the optical is also practically monochromatic. This represents a generalisation of the result reported in Ref. [10].

6 Photo-Ionisation

In this section we shall consider effects of electron correlations on the photo-ionisation spectra of QD nanorings. For the analysis of ionisation spectra, the single-particle picture represents the common framework, successful or at least very helpful to describe electrons in many cases, e.g. in atoms, or in ordinary three-dimensional solids. Within the single-particle (MO) picture, there are as many ionisation signals as occupied (molecular) orbitals. This is normally the case for core and outer valence electrons in molecules.

As a particular case of the latter, the MO picture is very good for the so-called HOMO ionisation (i.e. process of lowest ionisation energy). In molecules, the single-particle (MO) picture breaks down only for the inner valence electrons, as amply documented in the literature [38, 59]. Therefore, our results of Ref. [60], demonstrating the failure of the orbital picture even for HOMO ionisation in QD nano-rings, represented a surprise. They pointed out that the assignment of assembled QD's as "artificial" molecules should be taken with caution.

A ionisation process is characterised by an ionisation energy ε_α and a spectroscopic factor (see e.g. Ref. [59])

$$w_{\alpha,k} \equiv \left| \left\langle \Psi^{\alpha}_{N_e-1} \left| c_{k,\uparrow} \right| \Psi^{0}_{N_e} \right\rangle \right|^2 . \tag{5}$$

The result of removing of an electron from a certain occupied MO (k) of an uncorrelated neutral system is a *unique* eigenstate of the ionised system. For that eigenstate, the spectroscopic factor is equal to unity ($w_{SCF} = 1$) and vanishes for all other eigenstates. For (strong) correlated systems, this is no more the case. The removal of an electron from an MO (k) of a given symmetry Γ will bring the neutral system from its ground state $\Psi^0_{N_e}$ into various eigenstates $\Psi^{\alpha}_{N_e-1}$ of the ionised system. The symmetries of the k-th MO and α are correlated for $w_{\alpha,k} \neq 0$. In the case of closed shells, $\Psi^0_{N_e}$ has A_{1g} symmetry, and the symmetry of $\Psi^{\alpha}_{N_e-1}$ coincides with Γ. For all these eigenstates, $0 \leq w_\alpha < 1$, and the following sum rule for spectroscopic factors, straightforwardly resulting from Eq. (5), holds

$$\sum_{\alpha} w_{\alpha,k} = \left\langle c^{\dagger}_{k,\uparrow} c_{k,\uparrow} \right\rangle \equiv n_k . \tag{6}$$

Above, n_k ($0 \leq n_k \leq 1$) represents the occupancy of the k-th MO. For a strongly correlated system one expects a rich ionisation spectra, corresponding to the large number of eigenstates with a certain symmetry.

However, similar to optical absorption, the ionisation spectrum is surprisingly scarce. To illustrate this, we show in Fig. 5 results on A_{1g}-ionisation for six valence electrons in 10-QD nano-rings. Out of all the 170 A_{1g}-processes allowed by symmetry, practically only a few processes possesses significant spectroscopic factors. In the upper left panel of Fig. 5 we depict the spectroscopic factors for all the significant A_{1g}-states. The careful inspection of these results reveals that there are contributions originating from states exhibiting the phenomenon of avoiding crossing; see the upper right panel of Fig. 5. Similar to optical absorption (*cf.* Sect. 5), of experimental interest in such cases is to sum up contributions of almost degenerate states (amounting to consider the bright diabatic state). The results for these diabatic bright states are presented in the lower panels of Fig. 5, revealing that, practically, there are only five significant contributions.

A more detailed analysis (which we defer to a separate publication) demonstrates that this is precisely the number of A_{1g}-processes possible in the configuration space that includes one hole and two-hole—one-particle processes. In this way, one can say that the ionisation spectra can also be rationalised by starting from the MO picture, in spite of strong electron correlations.

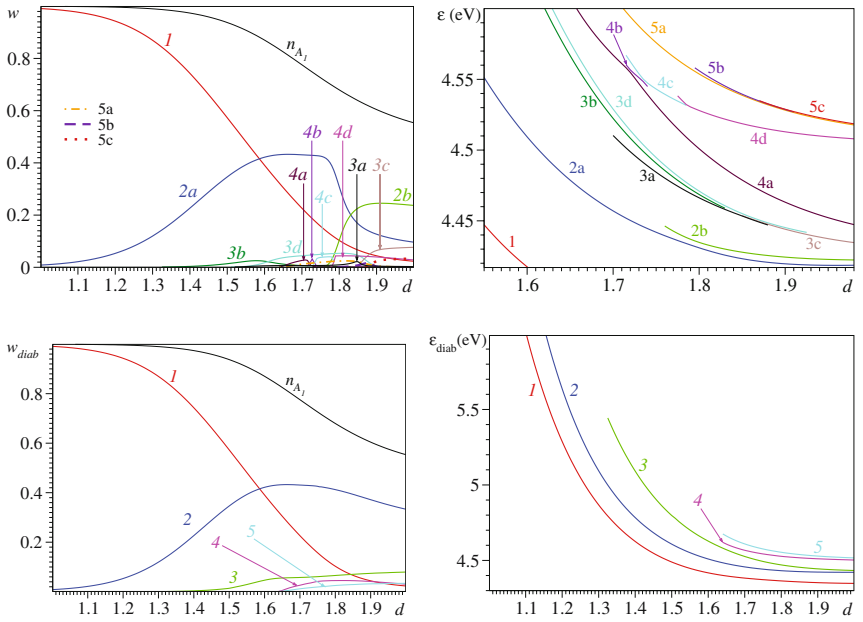

Fig. 5 Results on A_{1g}-ionisation for six electrons on 10 QD nano-rings as a function of interdot spacing d. In the upper panels, the spectroscopic factors w and ionization energies ε (by using $\varepsilon_0 = -4.504$ eV) of the significant A_{1g}-eigenstates are shown. For these, a series of avoiding crossings can be seen. In the lower panels, we present results for the same quantities for the bright diabatic states, i.e. those of experimental interest. See the main text for details

7 Method of Partial Covering

Recently, we proposed a new method enabling one to get valuable information on nano-systems, namely by partially covering them (for instance, by using a mask), and irradiate only a part thereof [10, 60]. By applying this method for

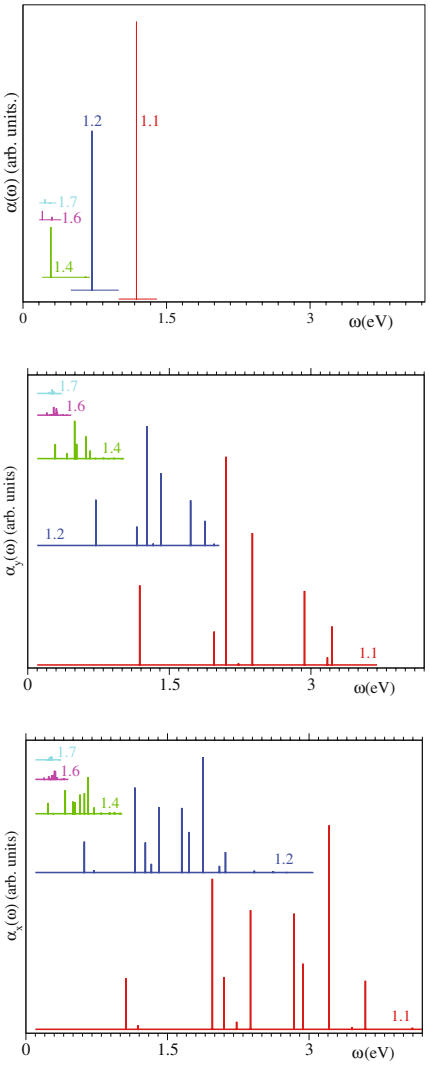

Fig. 6 Optical absorption spectra for 10-QD nano-rings at half filling by shining the whole ring (*upper panel*), and only two adjacent QD's. In the latter, the electric field is polarised perpendicular (*middle panel*) and parallel (*lower panel*) to the direction of the two QD's. The values of interdot spacing ($d = 1.1;\ 1.2;\ 1.4;\ 1.6;\ 1.7$) are inserted

photo-ionisation, interesting connections with the localisation-delocalisation transition observed in experiments have been established [60].

In view of the hidden quasi-symmetry discussed above, the information one can get on the excited states is rather scarce: only a single excited state can be studied by optical absorption. By applying the method of partial covering to optical absorption in systems with high symmetry (like the nano-rings examined here), more excited states can be targeted simply because the electromagnetic perturbation reduces the symmetry of the problem. To demonstrate this, we reported in Ref. [10] results in the limiting case where all but one QD are covered.

To give further support to the method of partial covering, we consider here the case where all but two adjacent QD's of the nano-ring are covered, and these two QD's and exposed to radiation. Results for nano-rings covered in this manner are depicted in Fig. 6 along with those for the case where the whole ring (upper panel in Fig. 6) is shone. As expected from the above reason, the absorption spectra of partially covered rings a richer than that of uncovered rings. For the same reason, the spectra for light polarised parallel to the segment joining the two uncovered QD's (lower panel) is richer than that where the polarisation is perpendicular to this segment (middle panel): in the former case, the symmetry is lower than in the latter.

8 Conclusion

Tunable QD nano-structures offer the fascinating opportunity of construction of materials with designer specified functional properties. Although the initial expectation of using QD's for quantum computing was not realised so far, they motivate physicists and chemists to further investigate basic quantum mechanical phenomena at nano-scale without limitations encountered in ordinary systems, e.g. instability against certain molecular distortions, or studies only at fixed (optimised) geometries. We hope that the results presented in this work will motivate experimentalists to prepare and investigate nano-rings consisting of quantum dots.

Acknowledgements Financial support for this work provided by the Deutsche Forschungsgemeinschaft is gratefully acknowledged.

References

1. J. Heath, C. Knobler, D. Leff, J. Phys. Chem. B **101**(2), 189 (1997). DOI 10.1021/jp9611582
2. J. Shiang, J. Heath, C. Collier, R. Saykally, J. Phys. Chem. B **102**(18), 3425 (1998). DOI 10.1021/jp981315s
3. K. Beverly, J. Sampaio, J. Heath, J. Phys. Chem. B **106**(9), 2131 (2002). DOI 10.1021/jp012261g
4. F. Remacle, C.P. Collier, J.R. Heath, R.D. Levine, Chem. Phys. Lett. **291**(3–4), 453 (1998). DOI 10.1016/S0009-2614(98)00612-5

5. G. Medeiros-Ribeiro, D.A.A. Ohlberg, R.S. Williams, J.R. Heath, Phys. Rev. B **59**(3), 1633 (1999). DOI 10.1103/PhysRevB.59.1633
6. C.P. Collier, R.J. Saykally, J.J. Shiang, S.E. Henrichs, J.R. Heath, Science **277**(5334), 1978 (1997). DOI 10.1126/science.277.5334.1978. URL http://www.sciencemag.org/cgi/content/abstract/277/5334/1978
7. F. Remacle, R. Levine, J. Amer. Chem. Soc. **122**(17), 4084 (2000). DOI 10.1021/ja9915448
8. I. Bâldea, A.K. Gupta, L.S. Cederbaum, N. Moiseyev, Phys. Rev. B **69**(24), 245311 (2004). DOI 10.1103/PhysRevB.69.245311. URL http://link.aps.org/abstract/PRB/v69/e245311
9. I. Bâldea, H. Köppel, L.S. Cederbaum, Phys. Rev. B **69**(7), 075307 (2004). DOI 10.1103/PhysRevB.69.075307. URL http://link.aps.org/abstract/PRB/v69/e075307
10. I. Bâldea, L.S. Cederbaum, Phys. Rev. B **75**(12), 125323 (2007). DOI 10.1103/PhysRevB.75.125323. URL http://link.aps.org/abstract/PRB/v75/e125323
11. A. Kawaharazuka, T. Saku, Y. Hirayama, Y. Horikoshi, J. Appl. Phys. **87**(2), 952 (2000). DOI 10.1063/1.371965
12. G. Markovich, C.P. Collier, J.R. Heath, Phys. Rev. Lett. **80**(17), 3807 (1998). DOI 10.1103/PhysRevLett.80.3807
13. R. Pariser, R.G. Parr, J. Chem. Phys. **21**(3), 466 (1953). DOI 10.1063/1.1698929. URL http://link.aip.org/link/?JCP/21/466/1
14. R. Pariser, R.G. Parr, J. Chem. Phys. **21**(5), 767 (1953). DOI 10.1063/1.1699030. URL http://link.aip.org/link/?JCP/21/767/1
15. R.G. Parr, *Quantum Theory of Molecular Electronic Structure* (W. A. Benjamin Inc., New York and Amsterdam, 1963)
16. J.A. Pople, Trans. Faraday Soc. **49**, 1375 (1953). DOI 10.1039/TF9534901375
17. J.A. Pople, Proc. Phys. Soc. A **68**, 81 (1955)
18. I. Ohmine, M. Karplus, K. Schulten, J. Chem. Phys. **68**(5), 2298 (1978). DOI 10.1063/1.436000. URL http://link.aip.org/link/?JCP/68/2298/1
19. W.P. Su, J.R. Schrieffer, A.J. Heeger, Phys. Rev. Lett. **42**(25), 1698 (1979). DOI 10.1103/PhysRevLett.42.1698
20. W.P. Su, J.R. Schrieffer, A.J. Heeger, Phys. Rev. B **22**(4), 2099 (1980). DOI 10.1103/PhysRevB.22.2099
21. J. Paldus, M.J. Boyle, Int. J. Quantum Chem. **22**(6), 1281 (1982). DOI 10.1002/qua.560220611. URL http://dx.doi.org/10.1002/qua.560220611
22. P.M. Grant, J. Batra, J. de physique C (Paris) **44**, C3 (1983)
23. J. Ashkenazi, E. Ehrenfreund, Z. Vardeny, O. Brafman, Molec. Cryst. & Liq. Cryst. **117**, 193 (1985)
24. E. Ehrenfreund, Z. Vardeny, O. Brafman, B. Horovitz, Phys. Rev. B **36**(3), 1535 (1987). DOI 10.1103/PhysRevB.36.1535
25. G.W. Hayden, Z.G. Soos, Phys. Rev. B **38**(9), 6075 (1988). DOI 10.1103/PhysRevB.38.6075
26. G.L. Bendazzoli, S. Evangelisti, L. Gagliardi, Int. J. Quantum Chem. **51**(1), 13 (1994). DOI 0.1002/qua.560510104
27. T. Kakitani, Progr. Theor. Phys. **51**, 656 (1974)
28. J. Fink, G. Leising, Phys. Rev. B **34**(8), 5320 (1986). DOI 10.1103/PhysRevB.34.5320
29. P. Horsch, Phys. Rev. B **24**(12), 7351 (1981). DOI 10.1103/PhysRevB.24.7351
30. M. Meneghetti, Phys. Rev. B **47**(20), 13151 (1993). DOI 10.1103/PhysRevB.47.13151
31. D. Baeriswyl, K. Maki, Phys. Rev. B **31**(10), 6633 (1985). DOI 10.1103/PhysRevB.31.6633
32. S. Kivelson, D.E. Heim, Phys. Rev. B **26**(8), 4278 (1982). DOI 10.1103/PhysRevB.26.4278
33. M. Springborn, K. Schmidt, K. Meider, L. de Maria, in *Organic Electronic Materials*, ed. by R. Furchioni, G. Grosso (Springer Verlag, Heidelberg, 2001), pp. 39–87
34. K. Ohno, Theor. Chem. Acta **2**, 219 (1964)
35. K. Nishimoto, N. Mataga, Z. Phys. Chem. **12**, 335 (1957)
36. J. Schirmer, Phys. Rev. A **26**(5), 2395 (1982). DOI 10.1103/PhysRevA.26.2395
37. J. Schirmer, J. Phys. B **28**, 2299 (1995)
38. M.S. Deleuze, A.B. Trofimov, L.S. Cederbaum, J. Chem. Phys. **115**(13), 5859 (2001). DOI 10.1063/1.1386414. URL http://link.aip.org/link/?JCP/115/5859/1

39. I. Bâldea, B. Schimmelpfennig, M. Plaschke, J. Rothe, J. Schirmer, A. Trofimov, T. Fanghanel, J. Electr. Spectr. Rel. Phenom. **154**(3), 109 (2007). DOI 10.1016/j.elspec.2006.12.024. URL http://dx.doi.org.ubproxy.ub.uni-heidelberg.de/10.1016/j.elspec.2006.12.024
40. J.M.O. Matos, B.O. Ross, P.Å. Malmqvist, J. Chem. Phys. **86**(3), 1458 (1987). DOI 10.1063/1.452235
41. J. Lorentzon, P. Malmqvist, M. Fülscher, B.O. Ross, Theoretica Chimica Acta **91**(1–2), 91 (1995)
42. J.P. Doering, J. Chem. Phys. **51**(7), 2866 (1969). DOI 10.1063/1.1672424
43. G.W. King, E.H. Pinnington, J. Mol. Spectroscopy **15**(3), 394 (1965). DOI 10.1016/0022-2852(65)90155-4
44. J.H. Callomon, T.M. Dunn, J.M. Mills, Phil. Trans. Roy. Soc. Lond., Ser. A: Math. Phys. Eng. Sci. **259**(1104), 499 (1966)
45. E.N. Lassettre, A. Skerbele, D.M. A., K.J. Ross, J. Chem. Phys. **48**(11), 5066 (1968). DOI 10.1063/1.1668178
46. E.E. Koch, A. Otto, Chem. Phys. Lett. **12**(3), 476 (1972). DOI 10.1016/0009-2614(72)90011-5
47. A. Hiraya, K. Shobatake, J. Chem. Phys. **94**(12), 7700 (1991). DOI 10.1063/1.460155
48. R. Astier, Y.H. Maier, Chem. Phys. Lett. **3**(6), 399 (1969). DOI 10.1016/0009-2614(69)80149-1
49. R. Bonneau, J. Joussot-Dubien, R. Bensasson, Chem. Phys. Lett. **3**(6), 353 (1969). DOI 10.1016/0009-2614(69)80134-X
50. P.G. Wilkinson, Can. J. Phys. **34**(7), 596 (1956)
51. F. Tarantelli, A. Sgamellotti, L.S. Cederbaum, J. Schirmer, J. Chem. Phys. **86**(4), 2201 (1987). DOI 10.1063/1.452118
52. L. Salem, *The Molecular Orbital Theory of Conjugated Systems* (Benjamin, New York, 1966)
53. I. Bâldea, H. Köppel, L.S. Cederbaum, Eur. Phys. J. B **3**(4), 507 (1998). DOI 10.1007/s100510050341
54. I. Bâldea, H. Köppel, L.S. Cederbaum, Phys. Rev. B **60**(9), 6646 (1999). DOI 10.1103/PhysRevB.60.6646
55. P.G. Wenthold, D.A. Hrovat, W.T. Borden, W.C. Lineberger, Science **272**(5267), 1456 (1996). DOI 10.1126/science.272.5267.1456
56. J.L. Andres, O. Castano, A. Morreale, R. Palmeiro, R. Gomperts, J. Chem. Phys. **108**(1), 203 (1998). DOI 10.1063/1.475388. URL http://link.aip.org/link/?JCP/108/203/1
57. I. Bâldea, H. Köppel, L.S. Cederbaum, Eur. Phys. J. B **20**(2), 289 (2001). DOI 10.1007/BF01352591
58. H. Köppel, W. Domcke, L.S. Cederbaum, Adv. Chem. Phys. **57**, 59 (1984). DOI 10.1002/9780470142813.ch2. URL http://dx.doi.org/10.1002/9780470142813.ch2
59. L.S. Cederbaum, W. Domcke, J. Schirmer, W. Von Niessen, Adv. Chem. Phys. **65**, 115 (1986). DOI 10.1002/9780470142899.ch3. URL http://dx.doi.org/10.1002/9780470142899.ch3
60. I. Bâldea, L.S. Cederbaum, Phys. Rev. Lett. **89**(13), 133003 (2002). DOI 10.1103/PhysRevLett.89.133003

Relative Energies of Proteins and Water Clusters Predicted with the Generalized Energy-Based Fragmentation Approach

Wei Li, Hao Dong, and Shuhua Li(✉)

Abstract A generalized energy-based fragmentation (GEBF) approach we developed recently [57] is applied to investigate the relative energies of many conformers of two proteins (PDB id: 2ETI and 1CMR) and one water cluster $(H_2O)_{20}$. The GEBF results are compared with those from conventional quantum chemistry methods, empirical molecular mechanics (MM), and semi-empirical quantum mechanical methods (AM1, PM3). Our computational results show that for all three systems, not only the total energies but also the relative stabilities of their different conformers predicted by the GEBF approach are fairly consistent with those from the corresponding conventional quantum chemistry method, while the widely used MM and semi-empirical QM methods give poor descriptions for the relative energies of different conformers.

Keywords: generalized energy-based fragmentation, protein conformers, water clusters

1 Introduction

For large systems such as biological molecules and molecular clusters, empirical molecular mechanics (MM) methods are still the most commonly used theoretical tools for studying their structures and properties. For example, MM methods have been employed for gradient-based structural optimizations, intermolecular forces, molecular dynamics (MD) and Monte Carlo (MC) simulations [1–4]. However, the accuracy of MM approaches is not good enough in many cases. It is also difficult for MM methods to describe the chemical reactions because electrons are not explicitly treated. On the other hand, conventional quantum chemistry methods can treat the

W. Li, H. Dong, and S. Li
School of Chemistry and Chemical Engineering, Institute of Theoretical and Computational Chemistry, Key Laboratory of Mesoscopic Chemistry of Ministry of Education, Nanjing University, 210093, P. R. China, e-mail: shuhua@nju.edu.cn

S. Wilson et al. (eds.) *Frontiers in Quantum Systems in Chemistry and Physics*.

chemical reactions with high precision, but are limited to medium-sized systems due to their high computational scaling with respect to the system size. In recent years, a variety of hybrid QM/MM methods, which combine a quantum mechanical (QM) method with a MM method, have been developed to investigate the chemistry of very large systems, especially the mechanism of enzymatic reactions in biological systems [5–8]. Nevertheless, there are still many cases in which the active region of the system is too large for conventional quantum chemistry treatments.

The extension of quantum chemistry calculations to large systems has been an active field for about two decades. Many linear scaling algorithms for carrying out Hartree-Fock (HF), density functional theory (DFT), and post-HF calculations have been proposed for computing the ground-state energies and molecular properties of large molecules [9–33]. However, although quantum chemistry methods implemented with these algorithms scale linearly with the molecular size in the large molecule asymptote, a large pre-factor for these algorithms has hindered their extensive applications to systems with a few hundreds of atoms. Instead, many fragment-based approaches, although less rigorous than standard linear scaling approaches, have been suggested as alternative approaches for performing ab initio quality calculations on large molecules in the recent years [34–58]. For example, fragment molecular orbital (FMO) method developed by Kitaura and his coworkers have been applied to obtain ground-state energies, optimized geometries, dynamic polarizability, solvation free energies, and interaction energies for a variety of large systems [44–47]. In comparison with the FMO method, an even simpler but still effective energy-based fragmentation approach was developed independently by us and Collins's group [39, 52]. Within this approach, the total energy of a large molecule can be approximately calculated from energy calculations on a series of small subsystems. This approach was found to give quite accurate ground-state energies and optimized geometries for neutral or less charged systems. Recently, we have suggested a generalized energy-based fragmentation (GEBF) approach for various large systems (for both neutral or charged) [57]. In GEBF approach, each subsystem is placed in the presence of background point charges so that long-range electrostatic interaction or polarization effects between remote fragments can be approximately taken into account. This approach has been shown to yield quite satisfactory results for ground-state energies, dipole moments, and static polarizabilities of a variety of large molecules [57]. In order to extend the GEBF approach to geometry optimizations, MD or MC simulations of large biological molecules or molecular clusters, we will investigate the performance of this approach on the estimate of relative energies for many different conformers of two protein molecules and a water cluster in the present work. The GEBF results will be compared with the results from full system calculations with conventional HF (or MP2 if available), semi-empirical AM1 or PM3, MM methods (AMBER99 [59] and CHARMM27 [60]).

This paper is organized as follows. In Sect. 2, the basic idea of the GEBF approach is described briefly. In Sect. 3, the GEBF approach is applied to compute relative energies of ten conformers of two proteins and a water cluster, and the results are compared with those from other theoretical methods. Finally, a brief summary is given in Sect. 4.

2 Methodology

The procedure of the GEBF approach [57] adopted in this work is basically the same as described before, but some steps are slightly modified. The present procedure includes: (1) Divide a target system into a series of fragments; (2) For each fragment, form a primitive subsystem by connecting its neighboring fragments (hydrogen atoms may be added if necessary). It should be mentioned that the neighboring fragment is successively added according to the distance between it and the central fragment. The coefficients of these primitive subsystems are all set to be unity. To save the computational time (without much loss of accuracy), we limit the maximum number of fragments in a subsystem to a given value (η), which is the only parameter to be set in the GEBF approach. Usually, a larger η value will lead to more accurate results. For convenience, a GEBF calculation with the parameter η is denoted as GEBF(η). (3) Construct derivative subsystems with m fragments ($m = \eta - 1$) and determine their coefficients according to the guiding rule that the net number of each specific m-fragment interaction term in the many-body energy expansion of all subsystems is unity. (4) Repeat the process described above to construct $m-$fragment ($m = \eta - 2, \cdots, 2, 1$) derivative subsystems. (5) For each subsystem, replace those remote atoms, which are not included in this subsystem, with point charges (in the positions of nuclei centers). Thus, each subsystem is electronically embedded in the presence of background point charges. By this way, the long-range electrostatic interaction and polarization effects between remote fragments are approximately treated. These point charges can be obtained from natural population analysis (NPA) [61, 62] for all primitive subsystems. The details of this step can be found in our previous work. Finally, from conventional quantum chemistry calculations on all "embedded" subsystems, the ground-state energy of the target system can be expressed as [57]

$$E_{Tot} = \sum_{m}^{M} C_m \tilde{E}_m - \left(\sum_{m}^{M} C_m - 1 \right) \sum_{A} \sum_{B>A} \frac{Q_A Q_B}{R_{AB}} \tag{1}$$

where $\tilde{E}_m$ is the total energy of the m-th subsystem including the self-energy of point charges, C_m is the coefficient of the m-th subsystem, and Q_A is the point charge on atom A.

3 Results and Discussion

In this section, we will apply the present GEBF approach to investigate the relative stabilities of some conformers for two proteins and one water cluster. Two proteins are trypsin inhibitor II (PDB id: 2ETI) [63] and charybdotoxin (PDB id:1CMR). For each protein, we first perform a MD simulation with the TINKER package [64] for 800 ps after 200 ps of equilibration (with a time step of 2 fs) at

298 K. The AMBER99 force field is employed for simulations. Along the trajectories ten conformers with the lowest energies are selected for our study. For a water cluster $(H_2O)_{20}$, its ten conformers with the lowest energies at the TIP4P level are from a systematic study by Kazimirski and Buch [65]. For these three systems and their subsystems, we perform conventional quantum chemistry calculations with the GAUSSIAN03 package [66]. The GEBF calculations are achieved by combining our LSQC package [[67] with the GAUSSIAN03 package [66]. The Cartesian coordinates of all studied structures are released in the web and available from authors on request [68].

Before doing GEBF calculations, we should specify how to fragment the studied systems. For water clusters, we take each water molecule as a fragment. For proteins, we cut the C–C bond between α–carbon and the carbonyl group in the central residues, the S–S bond between two residues, and the C–C bond between β– and γ–carbons in five residues with large side chains (Arg, Lys, Phe, Trp and Tyr).

First, the total energies of ten conformers calculated with the MM methods (AMBER99 and CHARMM27), semi-empirical QM methods (AM1 and PM3), GEBF-HF/6-31G(d) and conventional HF/6-31G(d) methods are listed in Table 1 for 2ETI and in Table 2 for 1CMR, respectively. For better comparison, the relative energies of ten conformers from different methods are displayed in Figs. 1 and 2, respectively. From Table 1 and Fig. 1, one can see that the AMBER99, CHARMM27, AM1 and PM3 methods predict the relative energies quite different from those obtained with the conventional HF method, whereas the GEBF-HF method can reproduce the relative energies with good accuracy. Among various theoretical methods, only the GEBF-HF method predicts the same lowest-energy conformer as the conventional HF method. In comparison with the total energies from the conventional HF/6-31G(d) method, the largest deviation of the GEBF-HF energies is 6.25 and 6.04 millihartrees (mH) for $\eta = 5$ and $\eta = 6$, respectively.

Table 1 The total energies for ten conformers of 2ETI calculated with the AMBER99, CHARMM27, AM1, PM3, GEBF-HF/6-31G(d), and conventional HF/6-31G(d) methods

No	AMBER99 (kcal/mol)	CHARMM27 (kcal/mol)	AM1 (au)	PM3 (au)	HF		
					Conventional (au)	GEBF(5) (mH)[a]	GEBF(6) (mH)[a]
1	−586.54	−528.75	−1.089 23	−1.208 34	−11993.203 06	−4.97	6.04
2	−579.35	−528.18	−1.162 41	−1.254 68	−11993.200 10	4.95	1.72
3	−577.75	−527.31	−1.142 30	−1.230 59	−11993.168 42	4.46	4.57
4	−577.54	−526.99	−1.073 64	−1.198 91	−11993.227 96	5.47	1.89
5	−577.31	−527.85	−1.089 53	−1.214 28	−11993.264 45	4.98	5.19
6	−577.06	−525.99	−1.067 63	−1.215 48	−11993.193 34	2.55	1.56
7	−576.78	−525.94	−1.121 80	−1.231 41	−11993.230 27	4.97	2.67
8	−576.70	−524.42	−1.153 06	−1.255 04	−11993.207 36	6.25	2.89
9	−576.61	−526.95	−1.076 23	−1.213 71	−11993.199 93	−0.66	4.20
10	−576.21	−528.83	−1.144 36	−1.202 16	−11993.162 65	−0.25	3.99

[a] The relative energies with respect to the conventional HF energies.

Table 2 The total energies for ten conformers of 1CMR calculated with the AMBER99, CHARMM27, AM1, PM3, GEBF-HF/6-31G(d), and conventional HF/6-31G(d) methods

No	AMBER99 (kcal/mol)	CHARMM27 (kcal/mol)	AM1 (au)	PM3 (au)	HF		
					Conventional (au)	GEBF(5) (mH)[a]	GEBF(6) (mH)[a]
1	−603.22	−420.59	−1.019 70	−1.202 51	−14044.532 75	−2.37	6.08
2	−597.38	−385.86	−1.042 14	−1.204 91	−14044.503 96	−2.74	3.47
3	−596.99	−382.28	−0.991 31	−1.179 24	−14044.492 99	−1.86	4.33
4	−596.75	−389.83	−0.996 86	−1.147 89	−14044.481 63	−7.51	1.76
5	−591.87	−397.25	−1.052 03	−1.210 05	−14044.480 96	−6.33	0.46
6	−591.59	−399.37	−1.033 20	−1.155 82	−14044.514 64	−3.99	0.99
7	−591.29	−379.36	−0.971 99	−1.128 56	−14044.510 43	−8.64	3.55
8	−591.00	−382.32	−0.988 61	−1.159 73	−14044.444 79	−13.53	1.61
9	−590.11	−366.55	−0.950 48	−1.116 33	−14044.469 76	−8.23	2.96
10	−589.98	−399.13	−0.997 91	−1.146 72	−14044.495 70	−12.42	1.83

[a] The relative energies with respect to the conventional HF energies.

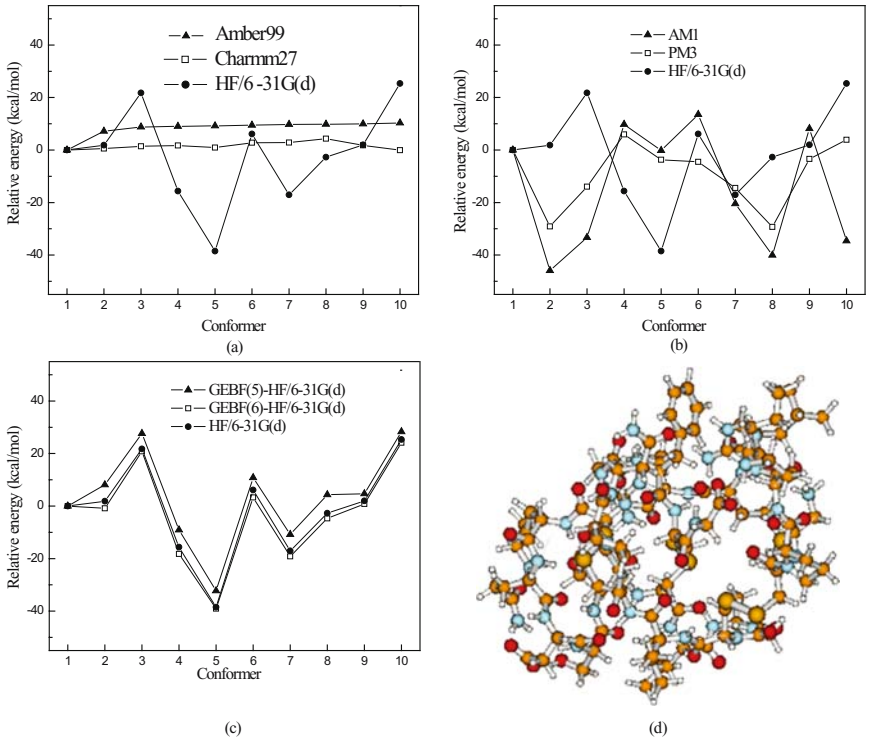

Fig. 1 The total energies of ten conformers of 2ETI, with the energy of conformer 1 being set to zero: (**a**) Comparison between AMBER99 (or CHARMM27) and conventional HF/6-31G(d) results. (**b**) Comparison between AM1 (or PM3) and conventional HF/6-31G(d) results. (**c**) Comparison between GEBF($\eta = 5, 6$) and conventional HF/6-31G(d) results. (**d**) The structure of the lowest-energy conformer predicted by the conventional HF/6-31G(d) calculation

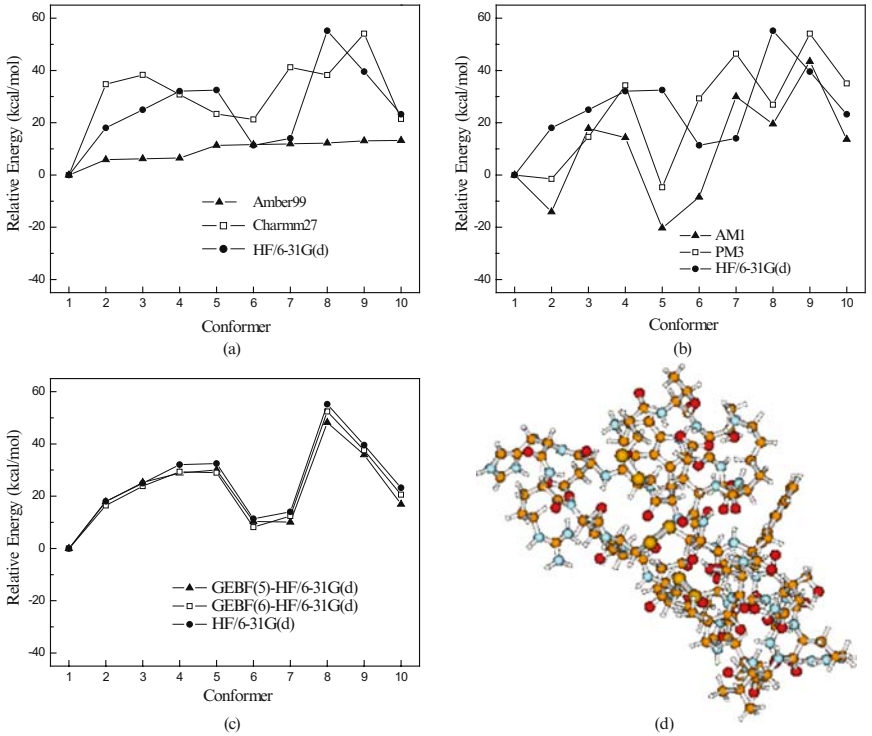

Fig. 2 The total energies of ten conformers of 1CMR, with the energy of conformer 1 being set to zero: (**a**) Comparison between AMBER99 (or CHARMM27) and conventional HF/6-31G(d) results. (**b**) Comparison between AM1 (or PM3) and conventional HF/6-31G(d) results. (**c**) Comparison between GEBF($\eta = 5, 6$) and conventional HF/6-31G(d) results. (**d**) The structure of the lowest-energy conformer predicted by the conventional HF/6-31G(d) calculation

Correspondingly, the mean deviation is 5.14 and 3.91 mH, respectively. For this molecule (2ETI), the GEBF-HF energies are almost convergent for $\eta = 6$, and in this case, the largest subsystem contains only 98 atoms, much less than the total number of atoms (382) in this system. For another protein molecule 1CMR, the performance of various theoretical methods is almost the same as observed in 2ETI (see Table 2 and Fig. 2). Thus, one can see that the MM (AMBER99 and CHARMM27) methods and semi-empirical QM methods (AM1 and PM3) give poor descriptions for the relative energies of large biological molecules (compared with the full *ab initio* HF results), while the GEBF-HF approach can be used to give fairly accurate predictions.

Second, for a water cluster $(H_2O)_{20}$, we collect the total energies of its ten lowest-energy conformers (see Fig. 3) calculated with TIP4P, HF or GEBF-HF, B3LYP or GEBF-B3LYP, MP2 or GEBF-MP2 methods in Table 3. The aug-cc-pVDZ basis set is employed for all quantum chemistry calculations. The relative energies of these conformers obtained from different methods are displayed in Fig. 4 for comparison. Because the relative energies of these structures are quite small, we set the

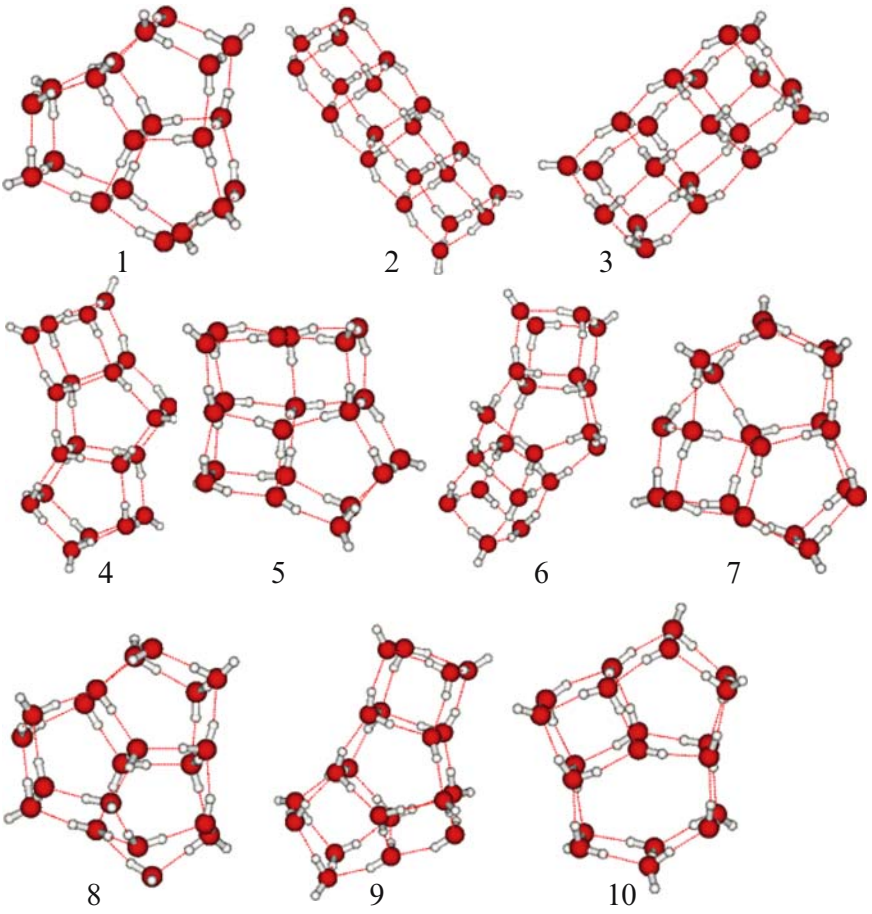

Fig. 3 Ten lowest-energy conformers of $(H_2O)_{20}$ calculated with the TIP4P force field method

parameter $\eta = 7$ for the corresponding GEBF calculations. Thus, the largest subsystem in GEBF calculations contains only seven water molecules with 287 basis functions. As seen from Table 3 and Fig. 4, the relative energies with the TIP4P force field method are quite different from those with the conventional HF, B3LYP and MP2 methods, while the relative energies from the GEBF approach are quite consistent with their corresponding conventional results. Within each method (HF, B3LYP, MP2), GEBF calculations give correct predictions for the lowest-energy and highest-energy conformers, consistent with those from the conventional calculations. But, one can see from Fig. 4 that for some conformers their relative order predicted by the GEBF approach is different from that obtained by the conventional calculations. This is because the energy difference between these conformers is smaller than the accuracy of the GEBF approach. With respect to the total energies from the conventional method, the largest deviation of the GEBF energies is

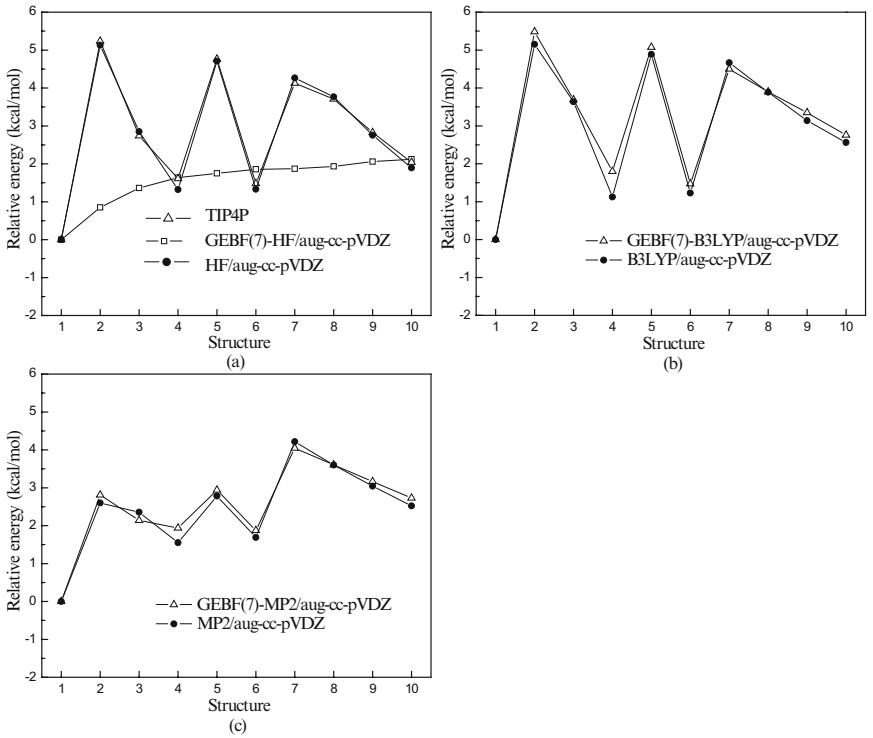

Fig. 4 The total energies of ten conformers of $(H_2O)_{20}$, with the energy of conformer 1 being set to zero: (**a**) Comparison between the TIP4P results, the GEBF-HF and conventional HF results. (**b**) Comparison between the GEBF-B3LYP and conventional B3LYP results. (**c**) Comparison between the GEBF-MP2 and conventional MP2 results

Table 3 The total energies for ten conformers of $(H_2O)_{20}$ calculated with the TIP4P method, conventional and GEBF methods at the HF, B3LYP, and MP2 levels (with the aug-cc-pVDZ basis set)

No	TIP4P (kcal/mol)	HF		B3LYP		MP2	
		Conventional (au)	GEBF(7) (mH)[a]	Conventional (au)	GEBF(7) (mH)[a]	Conventional (au)	GEBF(7) (mH)[a]
1	−208.73	−1521.042 04	−0.54	−1529.179 42	−0.80	−1525.550 03	0.03
2	−207.88	−1521.033 87	−0.37	−1529.171 21	−0.27	−1525.545 89	0.37
3	−207.37	−1521.037 49	−0.72	−1529.173 63	−0.71	−1525.546 28	−0.31
4	−207.10	−1521.039 93	−0.08	−1529.177 63	0.28	−1525.547 56	0.65
5	−206.99	−1521.034 54	−0.44	−1529.171 63	−0.49	−1525.545 59	0.28
6	−206.88	−1521.039 92	−0.30	−1529.177 46	−0.41	−1525.547 34	0.32
7	−206.87	−1521.035 24	−0.75	−1529.171 98	−1.06	−1525.543 31	−0.24
8	−206.80	−1521.036 03	−0.64	−1529.173 22	−0.78	−1525.544 29	0.04
9	−206.67	−1521.037 64	−0.42	−1529.174 42	−0.46	−1525.545 18	0.22
10	−206.61	−1521.039 02	−0.30	−1529.175 33	−0.49	−1525.546 01	0.36

[a] The relative energies with respect to the conventional energies.

0.46, 0.58 and 0.28 mH for HF, B3LYP and MP2, respectively. Within each quantum chemistry method, the GEBF approach can provide fairly reliable predictions for the relative stabilities of different conformers of water clusters, although the energies of these conformers are distributed in a narrow range. Regarding the computational cost (all the calculations are carried on a single workstation with dual dual-core Xeon 5150 CPU), the GEBF approach requires more computational time (by 2–3 times) than the conventional methods at the HF and B3LYP levels, whereas at the MP2 level the GEBF approach (with 0.6 GB memory) is about 2–3 times faster than the conventional MP2 method (with 1.6 GB memory). Of course, if the system under study becomes larger and larger, the GEBF approach should be eventually faster than the conventional method even at the HF or DFT level, because it computationally scales linearly with the system size.

4 Conclusions

In this work, we have applied the GEBF approach to investigate the relative energies for many conformers of two proteins (2ETI and 1CMR) and a water cluster $(H_2O)_{20}$. From our calculations, we found that for proteins the MM methods (AMBER99 and CHARMM27), and semi-empirical QM methods (AM1 and PM3) could not quantitatively reproduce the results from the conventional HF/6-31G(d) calculations, while for water clusters the TIP4P force field method is also not able to make quantitative predictions for the relative stabilities of many conformers. In contrast, for three systems, not only the total energies but also the relative stabilities of their different conformers predicted by the GEBF approach are fairly consistent with those from the corresponding conventional method. The GEBF approach exhibits similar performance at various theoretical levels (HF, DFT, MP2). Since GEBF calculations can be readily achieved with a parallel code (with a message-passing interface technique), the GEBF approach is expected to be applicable for the geometry optimizations, MC (or MD) simulations for general large molecules at the *ab initio* level, once a large number of compute nodes are available.

Acknowledgements This work was supported by the National Basic Research Program (Grant No. 2004CB719901), the National Natural Science Foundation of China (Grant Nos. 20625309 and 20433020), the Chinese Ministry of Education (Grant No. NCET-04-0450), and Fok Ying Tong Education Foundation (Grant No. 91014).

References

1. MacKerell, Jr., A. D.; Wiorkiewicz-Kuczera, J.; Karplus, M. *J. Am. Chem. Soc.* 1995, **117**, 11946.
2. MacKerell, A. D., Jr.; Bashford, D.; Bellott, R. L.; Dunbrack, R. L., Jr.; Evanseck, J. D.; Field, M. J.; Fischer, S.; Gao, J.; Guo, H.; Ha, S.; Joseph-McCarthy, D.; Kuchnir, L.; Kuczera, K.;

Lau, F. T. K.; Mattos, C.; Michnick, S.; Ngo, T.; Nguyen, D. T.; Prodhom, B.; Reiher, W. E., III.; Roux, B.; Schlenkrich, M.; Smith, J. C.; Stote, R.; Straub, J.; Watanabe, M.; Wiorkiewicz-Kuczera, J.; Yin, D.; Karplus, M. *J. Phys. Chem. B* 1998, **102**, 3586.
3. Cheatham, T. E.; Kollman, P. A. *Annu. Rev. Phys. Chem.* 2000, **51**, 435.
4. Wang, W.; Donini, O.; M., R. C.; Kollman, P. A. *Annu. Rev. Bioph. Biom.* 2001, **30**, 211.
5. Cui, Q.; Karplus, M. *J. Chem. Phys.* 2000, **112**, 1133.
6. Cui, Q.; Karplus, M. *J. Phys. Chem. B* 2000, **104**, 3721.
7. Gao, J. L.; Truhlar, D. G. *Annu. Rev. Phys. Chem.* 2002, **53**, 467.
8. Gao, J.; Ma, S.; Major, D. T.; Nam, K.; Pu, J.; Truhlar, D. G. *Chem. Rev.* 2006, **106**, 3188.
9. Strout, D. L.; Scuseria, G. E. *J. Chem. Phys.* 1995, **102**, 8448.
10. Strain, M. C.; Scuseria, G. E.; Frisch, M. J. *Science* 1996, **271**, 51.
11. White, C. A.; Head-Gordon, M. *J. Chem. Phys.* 1994, **101**, 6593.
12. Scuseria, G. E. *J. Phys. Chem. A* 1999, **103**, 4782.
13. Schwegler, E.; Challacombe, M. *J. Chem. Phys.* 1996, **105**, 2726.
14. Ochsenfeld, C.; White, C. A.; Head-Gordon, M. *J. Chem. Phys.* 1998, **109**, 1663.
15. Stratmann, R. E.; Scuseria, G. E.; Frisch, M. J. *Chem. Phys. Lett.* 1996, **257**, 213.
16. Millam, J. M.; Scuseria, G. E. *J. Chem. Phys.* 1997, **106**, 5569.
17. Li, X.; Millam, J. M.; Scuseria, G. E.; Frisch, M. J.; Schlegel, H. B. *J. Chem. Phys.* 2003, **119**, 7651.
18. Pulay, P. *Chem. Phys. Lett.* 1983, **100**, 151.
19. Saebo, S.; Pulay, P. *Annu. Rev. Phys. Chem.* 1993, **44**, 213.
20. Hampel, C.; Werner, H.-J. *J. Chem. Phys.* 1996, **104**, 6286.
21. Schutz, M.; Hetzer, G.; Werner, H.-J. *J. Chem. Phys.* 1999, **111**, 5691.
22. Schutz, M.; Werner, H.-J. *J. Chem. Phys.* 2001, **114**, 661.
23. Werner, H.-J.; Manby, F. R.; Knowles, P. J. *J. Chem. Phys.* 2003, **118**, 8149.
24. Ayala, P. Y.; Scuseria, G. E. *J. Chem. Phys.* 1999, **110**, 3660.
25. Scuseria, G. E.; Ayala, P. Y. *J. Chem. Phys.* 1999, **111**, 8330.
26. Ayala, P. Y.; Kudin, K. N.; Scuseria, G. E. *J. Chem. Phys.* 2001, **115**, 9698.
27. Almlof, J. *Chem. Phys. Lett.* 1991, **181**, 319.
28. Head-Gordon, M.; Maslen, P. E.; White, C. A. *J. Chem. Phys.* 1998, **108**, 616.
29. Nakao, Y.; Hirao, K. *J. Chem. Phys.* 2004, **120**, 6375.
30. Christiansen, O.; Manninen, P.; Jorgensen, P.; Olsen, J. *J. Chem. Phys.* 2006, **124**, 084103.
31. Forner, W.; Ladik, J.; Otto, P.; Cizek, J. *Chem. Phys.* 1985, **97**, 251.
32. Li, S.; Ma, J.; Jiang, Y. *J. Comput. Chem.* 2002, **23**, 237.
33. Li, S.; Shen, J.; Li, W.; Jiang, Y. *J. Chem. Phys.* 2006, **125**, 074109.
34. Yang, W. *Phys. Rev. Lett.* 1991, **66**, 1438.
35. Yang, W.; Lee, T.-S. *J. Chem. Phys.* 1995, **103**, 5674.
36. Exner, T. E.; Mezey, P. G. *J. Phys. Chem. A* 2004, **108**, 4301.
37. He, X.; Zhang, J. Z. H. *J. Chem. Phys.* 2005, **122**, 031103.
38. Chen, X.; Zhang, Y.; Zhang, J. Z. H. *J. Chem. Phys.* 2005, **122**, 184105.
39. Li, W.; Li, S. *J. Chem. Phys.* 2005, **122**, 194109.
40. Gu, F. L.; Aoki, Y.; Korchowiec, J.; Imamura, A.; Kirtman, B. *J. Chem. Phys.* 2004, **121**, 10385.
41. Kobayashi, M.; Akama, T.; Nakai, H. *J. Chem. Phys.* 2006, **125**, 204106.
42. Akama, T.; Kobayashi, M.; Nakai, H. *J. Comput. Chem.* 2007, **28**, 2003.
43. Kobayashi, M.; Imamura, Y.; Nakai, H. *J. Chem. Phys.* 2007, **127**, 074103.
44. Kitaura, K.; Ikeo, E.; Asada, T.; Nakano, T.; Uebayasi, M. *Chem. Phys. Lett.* 1999, **313**, 701.
45. Fedorov, D. G.; Kitaura, K. *J. Chem. Phys.* 2004, **120**, 6832.
46. Fedorov, D. G.; Kitaura, K. *J. Chem. Phys.* 2005, **122**, 134103.
47. Fedorov, D. G.; Kitaura, K. *J. Phys. Chem. A* 2007, **111**, 6409.
48. Hirata, S.; Valiev, M.; Dupuis, M.; Xantheas, S. S.; Sugiki, S.; Sekino, H. *Mol. Phys.* 2005, **103**, 2255.
49. Sakai, S.; Morita, S. *J. Phys. Chem. A* 2005, **109**, 8424.
50. Li, W.; Li, S. *J. Chem. Phys.* 2004, **121**, 6649.
51. Li, S.; Li, W.; Fang, T. *J. Am. Chem. Soc.* 2005, **127**, 7215.

52. Deev, V.; Collins, M. A. *J. Chem. Phys.* 2005, **122**, 154102.
53. Collins, M. A.; Deev, V. A. *J. Chem. Phys.* 2006, **125**, 104104.
54. Bettens, R. P. A.; Lee, A. M. *J. Phys. Chem. A* 2006, **110**, 8777.
55. Jiang, N.; Ma, J.; Jiang, Y. *J. Chem. Phys.* 2006, **124**, 114112.
56. Li, W.; Fang, T.; Li, S. *J. Chem. Phys.* 2006, **124**, 154102.
57. Li, W.; Li, S.; Jiang, Y. *J. Phys. Chem. A* 2007, **111**, 2193.
58. Ganesh, V.; Dongare, R. K.; Balanarayan, P.; Gadre, S. R. *J. Chem. Phys.* 2006, **125**, 104109.
59. Wang, J.; Cieplak, P.; Kollman, P. A. *J. Comput. Chem.* 2000, **21**, 1049.
60. Foloppe, N.; MacKerell, Jr., A. D. *J. Comput. Chem.* 2000, **21**, 86.
61. Foster, J. P.; Weinhold, F. *J. Am. Chem. Soc.* 1980, **102**, 7211.
62. Reed, A. E.; Weinstock, R. B.; Weinhold, F. *J. Chem. Phys.* 1985, **83**, 735.
63. Berman, H. M.; Westbrook, J.; Feng, Z.; Gilliland, G.; Bhat, T. N.; Weissig, H.; Shindyalov, I. N.; Bourne, P. E. *Nucleic Acids Res.* 2000, **28**, 235.
64. Ponder, J. W. Tinker Software Tools for Molecular Design; 4.2 ed.; (http://dasher.wustl.edu/tinker), 2004.
65. Kazimirski, J. K.; Buch, V. *J. Phys. Chem. A* 2003, **107**, 9762.
66. Frisch, M. J.; Trucks, G. W.; Schlegel, H. B.; Scuseria, G. E.; Robb, M. A.; Cheeseman, J. R.; Montgomery, Jr., J. A.; Vreven, T.; Kudin, K. N.; Burant, J. C.; Millam, J. M.; Iyengar, S. S.; Tomasi, J.; Barone, V.; Mennucci, B.; Cossi, M.; Scalmani, G.; Rega, N.; Petersson, G. A.; Nakatsuji, H.; Hada, M.; Ehara, M.; Toyota, K.; Fukuda, R.; Hasegawa, J.; Ishida, M.; Nakajima, T.; Honda, Y.; Kitao, O.; Nakai, H.; Klene, M.; Li, X.; Knox, J. E.; Hratchian, H. P.; Cross, J. B.; Adamo, C.; Jaramillo, J.; Gomperts, R.; Stratmann, R. E.; Yazyev, O.; Austin, A. J.; Cammi, R.; Pomelli, C.; Ochterski, J. W.; Ayala, P. Y.; Morokuma, K.; Voth, G. A.; Salvador, P.; Dannenberg, J. J.; Zakrzewski, V. G.; Dapprich, S.; Daniels, A. D.; Strain, M. C.; Farkas, O.; Malick, D. K.; Rabuck, A. D.; Raghavachari, K.; Foresman, J. B.; Ortiz, J. V.; Cui, Q.; Baboul, A. G.; Clifford, S.; Cioslowski, J.; Stefanov, B. B.; Liu, G.; Liashenko, A.; Piskorz, P.; Komaromi, I.; Martin, R. L.; Fox, D. J.; Keith, T.; Al-Laham, M. A.; Peng, C. Y.; Nanayakkara, A.; Challacombe, M.; Gill, P. M. W.; Johnson, B.; Chen, W.; Wong, M. W.; Gonzalez, C.; Pople, J. A. Gaussian 03; Revision B.04 ed.; Gaussian, Inc.: Wallingford CT, 2004.
67. Li, S.; Li, W.; Fang, T.; Ma, J.; Jiang, Y. LSQC; 1.1 ed.; Nanjing University: Nanjing, 2006.
68. Structures available from http://itcc.nju.edu.cn/itcc/shuhua/Mol/.

Generalised Spin Dynamics and Induced Bounds of Automorphic $[A]_n X$, $[AX]_n$ NMR Systems via Dual Tensorial Sets: An Invariant Cardinality Role for CFP

Francis P. Temme

Abstract For uniform spins and their *indistinguishable point sets* of tensorial bases defining automorphic group-based Liouvillian NMR spin dynamics, the role of recursively-derived coefficients of fractional parentage (CFP) bijections and Schur duality-defined $CFP(0)^{(n)} \equiv |GI|^{(n)}$ group invariant cardinality is central both to understanding the impact of *time-reversal invariance*(TRI) spin physics, and to analysis as density-matrix formalisms over democratic recoupled (DR) dual tensorial sets, $\{T^k_{\{\tilde{\nu}\}}(11.1)(SU2 \times \mathscr{S}_n)\}$. Over abstract spin space, these tensorial sets are $(\tilde{\nu})$ invariant-theoretic forms which lie beyond the Liouvillian graph recoupling and Racah-forms envisaged by Sanctuary [1]. This is a direct consequence of the dominance of the $\mathscr{S}_n$ group. It leads to new views on the value of *projective group actions as mappings* over specialised *Liouvillian carrier spaces*, and on the need for the replacement of Racah-Wigner (R-W) orthogonality for *distinct point sets*, by criteria based on explicit properties of invariants [J. Phys.: Math. & Theor. A **41**, 015210 (2008)] for multiple invariant systems. $\tilde{\mathbf{U}} \times \mathscr{P}$ group actions over disjoint (L) carrier subspaces, leading to *exclusively combinatorial views* of the nature of *quantal completeness for indistinguishable point-based tensorial sets*. Such generalised invariant-theoretic approaches lie beyond the range of Lévi-Civitá generator views, or of Lévy-Leblond and Lévy-Nahas [9] with its additional cyclic-commutators defining mono-invariant DR forms. Comparison of the latter with generalised multiple-invariant techniques provides an answer to the question of *precisely why* $[A]_{n\geq 4}(X)$ and $[AX]_{n\geq 4}$ NMR system spin dynamics are not ameniable to conventional R-W analysis of recoupled discrete-point tensorial systems. Our work augments earlier Hilbert space views, both of Louck and Biedenharn [21] on boson pattern projective mapping, and of Corio [19]. The roles of recent $\mathscr{S}_n$ group action and $(\lambda \vdash n)$-Schur combinatorial concepts, as well as of polyhedral-combinatorial modelling over invariance algebras, contribute significantly to our understanding of

F.P. Temme
Chemistry Department, Queen's University, Kingston-ON, Canada K7L 3N6,
e-mail: temmef@ibis.chem.queensu.ca

S. Wilson et al. (eds.) *Frontiers in Quantum Systems in Chemistry and Physics*.

invariant-based techniques of Liouville dual tensorial sets for automorphic NMR spin physics.[1]

Keywords: NMR spin dynamics, dual tensorial sets, automorphic spin symmetry, group invariants in Liouvillian projective mapping, CFP factors from bijective mapping

1 Introduction

The concepts of Schur duality, based on the unitary and permutation groups both being subgroups of the general linear group, $\mathscr{GL}_d$, is central to theoretical physics and thus to the theory of NMR spin dynamics. Additional ideas of simple reducibility (SR) (over a space) and of groups having invariants (GI) is equally important in the quantal spin physics from which the latter is derived. Conventional graph-theoretic views of recoupled bases in Liouvillian quantum physics [1] allow a role for Racah-Wigner(R-W) algebra [2] in density-matrix formalisms of NMR spin dynamics [3]. The adequacy of R-W methods in representing dual tensorial set formalisms has been questioned of late, as a consequence of Atiyah and Sutcliffe [4] pointing out that graphical recoupling methods are properly restricted to generalised tensors based on *distinct point sets*. In consequence, once an NMR system(s) is one based on generalised multiple invariants over uniform spin (inner k_i rank) tensorial sets, the classic R-W techniques are then regarded as simply no longer pertinent. This arises because such bases introduce the concept of *indistinguishable spin sets* [5–8] and also formalisms pertinent to *democratic recoupling*(DR) [9, 10]. A further important consequence of this realisation is that the generalised automorphic-group multispin NMR systems, such as those discussed by Whitman [5] – or more recently, Balasubramanian [6] – need to be treated by (multiple) group-invariant (G-invariant(GI)), and $|GI|^{(n)}$ cardinality based theoretic methods [9–12], in contrast to mono-invariant ones.

For the simplest of $[A]_n$ ($[A]_n(X)$) type NMR systems, it follows [7], that whilst it is the dominant intra-cluster spin (Liouvillian) interaction $J_{AA'}$ here, which generates the automorphic Liouvillian-based spin symmetry, this term itself does not appear in the $[\tilde{n}]$ principal subdomain. Its effect is constrained to the inaccessible $\widetilde{[n-1,1]},\ldots$ (non-symmetric) subdomain(s) which constitutes a spin-coherence inaccessible region – a result in agreement with a classic NMR theorem from the Hilbert space NMR era [13–15], as well as in accord with a recently revisited experimental result [16]. Conceptually it is the dominance of the permutation group in these n-fold automorphic spin systems which determines that the related NMR tensorial set bases constitute *indistinguishable point sets*. For tensorial structures

[1] Dedicated in memoriam to:
Profs. Johannes P. Colpa [1925–2005], of Queen's University, Kingston, Canada, and Paul L. Corio [1928–1998], of the University of Kentucky, Lexington, USA.

over *more than three identical spins* constituting a point set, or other examples of DR beyond explicit tridentate Lévi-Civitá operator forms of wider $\mathscr{GL}_n \supset \mathscr{G}$ tensorial structure [17], the DR basis problem of Liouvillian NMR now involves *multiple* group-invariants, within the criteria that $|GI|^{(n\geq 4)} \geq 3$. Clearly in handling automorphic NMR tensorial problems over their abstract spin-alone space(s), only invariant-theoretic (non-graphical) approaches are mathematically appropriate.

Beyond the maximal mono-invariant uniform three-fold $[A]_3^{(I_i)}$ spin case for generalised (identical) I_i spin magnitudes, first discussed by Lévy-Lebond and Lévy-Nahas [9] in terms of specialised additional auxiliary cyclic commutator formalisms that in the Hilbert formalism yield a Jacobian matrix form (from the retention of some elements of R-W algebra), all further identical n-fold NMR systems are no longer ameniable to any form of modified graphical recoupling R-W approach. Subsequent progress thereafter rests on deriving the group invariant set and its cardinality, where the latter draws on the role of time-reversal in spin physics and a well-established Weyl (TRI vs permutational pair) equivalency condition [18, 19]. In addition the presence of Schur duality ensures that $CFP(0)^{(n)}$, the zeroth-order coefficient of fractional parentage(CFP) for n-fold system, is identical to the $\mathscr{S}_n$ group -derived invariant cardinality [12, 20], despite the limitations of unitary recoupling and R-W methods noted above. Thereafter $\mathscr{S}_n$ combinatorical methods determine the NMR quantal basis sets and their completeness, boson (or superboson) pattern algebras and their related unit operators [21], (unit-superoperators [10, 22]) contributing to recent modelling applications involving automorphic NMR spin systems [11, 23–26]. The original work of Weyl [18], as applied to NMR (e.g.) by Corio [19] and others [11], highlights the fact that, in studying invariants by group theoretic techniques, one is essentially examining the role of time-reversal invariance(TRI) [27] in particle physics.[2] Finally, no overview of DR-based tensorial set structures would be complete without some brief mention of iso-scalar factors (ISF) based on group subduction chains and their role in particle physics, as reviewed by Chen et al. [28].

Beyond the early study of the uniform DR three-spin system as a theoretical problem [9] – or else its inter correlated work [33, 34], including our recent quasi-geometric approach to invariant cardinality [20] – one of the specific focii of this report is concerned with the nature of *group actions over carrier space* as a projective mapping and just how such established phenomena correlate with the invariant-theoretic aspects of NMR. By its nature this stands in marked contrast to the non-spin Hamiltonian structure-based group theoretic DR problem examined by Galbraith [35] in the 1970s. The idea of Liouvillian NMR quantal basis set completeness being defined by its invariant cardinality is central to these questions and to much of the subsequent discussion.[3]

[2] One should remark here that the single spin tensorial formalism of NMR spin dynamics has given rise to analogous approaches for both NQR [29, 30] and NAR [31, 32].

[3] E.g., for higher uniform individual spin I_i magnitudes involved in $[A]_n(X), [AX]_n$ automorphic system problems, the additional question of spin symmetry branching (implicit in group embedding) and its mathematical determinacy also becomes of some importance [24, 25].

It is clear that any formalism treating the role of multiple group invariants in automorphic NMR also introduces difficult questions concerning the limitations of the physical applicability of R-W algebra. This fact is clear in Galbraith's original 1971 group-theoretic work [35]; equally, it is central to the recent assertion establishing *indistinguishability criteria* for uniform point sets [4]. Since both views disallow the use of graphical recoupling R-W techniques, the alternative possibility of quasi-renormalisation of some automorphic spin systems to certain simpler partitioned subset-type problems (known from studies in the Hilbert space era for certain restricted automorphic group-defined NMR spin systems) is a welcome development in NMR spin dynamics. The early Whitman (composite particle) NMR technique [5] provides useful examples.

At its most fundamental level, the study of Weyl-type correlation between TRI and specific forms of permutational-exchange action defines the concept of group invariant cardinality. TRI thereby plays an analogous role to that of permutational cycle operations (over Weyl bracket algebra [18]) within the wider generality of group theory – including that of character tables, as cycle-based structures. It is the permutational role of TRI acting over the structure of Liouvillian tensorial sets which allows a unifying role for Schur duality. The unitary aspects allow for a ($\mathbf{Z}_{n0}$ type) recursive bijection processes for the CFPs, as $\{CFP(i)^{(n)}\}$ coefficient sets. They also provide an alternative $\mathbf{Z}_{22}$-like invariant cardinality enumeration-based on the smaller n-index $\{CFP(i)^{(n)}\}$ sets, which yield the 2n-th indexed single zeroth CFP, invariant cardinality term, on forming the sum of squares of the original series. The subsequent use of *even-pair polyhedral lattice-point modelling concepts* (itself derived from the lattice techniques of Erdös et al. [36]) in the context of Weyl TRI scalar-pair technique over a linear bracket-algebra provide a $\mathscr{S}_n$ group formulation of the tensorial set, invariant cardinality problem. Although originally reported [20] in terms of a geometric-based view, more generalised modelling is preferable in deriving the GI cardinality, such as that based on $\mathscr{S}_{2n}/\mathscr{S}_n$ abstract space lattices. The validity of the quasi-geometric model to a specific number of $(\hat{\mathbf{I}} \bullet \hat{\mathbf{I}})$ vertex pairs, corresponding to the (quasi-R_3-space) icosahedral limit of 12 pairs, in hindsight is seen as predictable. The Schur properties inherent in spin dynamics clearly arise because automorphic NMR is essentially a $SU2 \times \mathscr{S}_n$ group phenomena. It is its retention in these GI cardinality formulations, despite R-W techniques being inadmissible under tensorial k_i sub-rank indistinguishability, that is interesting.

The work set out here describes a generalised recursive bijection. As a type of mapping, it is used to generate the full n-index range of dual tensorial set structures $T^{k}_{\{\bar{v}\}}(111..11)$, as integer rank, $(k_i = 1)$ sub-rank Liouvillian tensors characterised by their invariants, alias GIs. Thereafter, Sect. 2 draws on the interrelationship between $CFP(i)^{(n)}$ set and $CFP(0)^{(2n)}$ result. This is a powerful n/2n-indexed map-like property that allows for the derivation of the $|GI|^{(2n)}$ cardinalities directly from the primary $i \leq n$ initial n-fold CFP sets. Whilst it is an important internal check on the recursive bijection process itself, it is particularly valuable in deriving the GI-cardinality of 'nano-structured' $n \geq 20$ systems with multiple invariants. Also, these results are useful in the context of a specific type of $\mathscr{S}_n$ group character sum-based result (as given in Appendix B, e.g.) for $|GI|^{(n)}$ – a technique demonstrated

in more detail elsewhere [12]. Sect. 3 subsequently treats the role of Liouvillian carrier projective mappings and quantal completeness (cf. to their less informative Hilbert analogues). The structured carrier subspaces and their mappings presented here are closely related to the role of $\mathscr{S}_n$ actions in combinatorics as an aspect of spin physics. Sect. 4 completes the discussion of specific details concerning Liouvillian projections, before moving on to outline the range of NMR systems to which quantal renormalisation (with recovery of applicable R-W algebraic properties) may be applied. In Sect. 5 (as the penultimate item), various examples of invariant cardinalities associated with more extensive (quasi-polyhedral 'nano-') related model NMR systems are given. Finally for brevity, whilst retaining some degree of completeness, various important but subsidiary matters are outlined in the appendices, Appendices A–D; in particular, Appendix B presents symmetric group character sum technique for GI cardinality and Appendix D sets out the notation adopted in the main text.

2 Group Actions over Hilbert and Liouville Spaces: $CFP(i)^{(n)}$ and $|GI|^{(n)}$ of $\{T^{k}_{\{\tilde{\nu}\}}(11.1)\}$ Liouville Sets

The well-established respective bi/tri-dentate schematic propagations over Hilbert and Liouville space of density-matrix formalisms derive from the inter-relationship between corresponding unitary group actions over these distinct spaces, as given by the expression:

$$\tilde{\mathbf{U}}|kqv>> \;\equiv\; \mathbf{U}|kqv>>\mathbf{U}^{\dagger}\,. \tag{1}$$

In describing the respective group actions as mappings over their respective Hilbert or Liouville carrier spaces, we denote these by $\mathbb{H}$ ($\tilde{\mathbb{H}}$), where for Hilbert space:

$$\mathbf{U}:\mathbb{H}\rightarrow\mathbb{H}\;\left\{D^{j}(\mathbf{U})|\;\mathbf{U}\in SU2\right\}, \tag{2a}$$

whereas for integer-rank Liouville space the corresponding simple mapping process is simply:

$$\tilde{\mathbf{U}}:\tilde{\mathbb{H}}\rightarrow\tilde{\mathbb{H}}\;\left\{D^{k}(\tilde{\mathbf{U}})|\;\tilde{\mathbf{U}}\in SU2\right\}. \tag{2b}$$

On recalling that SR is only retained over respective SU(2) product spaces,[4] this leads to the fundamental classic propagative schemata over their $j=(1/2)$, and subsequent $k=1$, (integer) Liouvillian, spaces being described by:

$$D^{(1/2)}\otimes D^{(1/2)}\;\equiv\;1D^{0}(\mathbf{U})+1D^{1}(\mathbf{U})\,, \tag{3}$$

$$D^{1}(\tilde{\mathbf{U}})\otimes D^{1}(\tilde{\mathbf{U}})\;\equiv 1D^{0}(\tilde{\mathbf{U}})+1D^{1}(\tilde{\mathbf{U}})+1D^{2}(\tilde{\mathbf{U}})\,; \tag{4}$$

[4] It should be noted here that Liouvillian $SU(2)\times\mathscr{S}_n$ symmetries span $p\leq 4$ partite irreps, cf. to the propagative formalisms of Hilbert space.

however, it is only for $\otimes D^{(k=1)}(\tilde{\mathbf{U}})$ Liouvillian density-matrix based sequence [17] (or subsequently on taking a sum of squares of RHS (lower n-index) $CFP(i)$s) that one obtains the multiplicities inclusive of the zeroth CFP terms, or scalar invariants, such that:

$$D^1(\tilde{\mathbf{U}}) \otimes D^1(\tilde{\mathbf{U}}) \otimes D^1(\tilde{\mathbf{U}}) \;\rightarrow\; (1:3:2:1) \begin{pmatrix} D^0(\tilde{\mathbf{U}}) \\ D^1(\tilde{\mathbf{U}}) \\ D^2(\tilde{\mathbf{U}}) \\ D^3(\tilde{\mathbf{U}}) \end{pmatrix}, \tag{5}$$

Over a full rank sequence this schemata behaves as a $\mathbf{Z}_{n0}$ type process and is a retained property, common to both distinct and indistinguishable point-set tensorial systems. The process of taking squares of both sides of the $(n = 2)$ Liouville space example, Eq. (4), yields the lone value of the zeroth CFP factor of the $n' = 2n$ $(= 4)$ fold problem, whose full rank $\mathbf{Z_{n0}}$-linear unitary mapping is simply the further bijective result:

$$(\otimes D^1(\tilde{\mathbf{U}}))^{(4)} \;\rightarrow\; (3:6:6:3:1) \begin{pmatrix} D^0(\tilde{\mathbf{U}}) \\ D^1(\tilde{\mathbf{U}}) \\ D^2(\tilde{\mathbf{U}}) \\ D^3(\tilde{\mathbf{U}}) \\ D^4(\tilde{\mathbf{U}}) \end{pmatrix}. \tag{6}$$

Clearly these additional enumerative $CFP(i)^{(n)} \rightarrow CFP(0)^{(n'=2n)}$ map-like process that arise from taking the sum of squares of all CFP(i) components for $0 \leq i \leq n$ may be likened to a $\mathbf{Z}_{22}$ recoupling. Likewise, an analogous treatment of the (initial) $i \leq n = 4$ full component CFP set in this $\mathbf{Z}_{22}$-like context directly yields the higher-index zeroth rank term, $CFP(0)^{(2n=8)} = |GI|^{(8)} = 91$ as a dual group invariant.

Further mathematical inspection of these contrasting schemata leads one to recognise, that in place of the tedious classic propagative tensorial schematic structure, a simple 1:1 bijection (with the column-vector of $(D^{k'}(\tilde{\mathbf{U}}))$ understood) should be utilised to automate the $\mathbf{Z}_{n0}$ process into an enumerative bijection mapping. Up to the index values $n = 20,\ (...),\ 24$, this is presented in Table 1, within an internal self-consistency in it, – i.e. on comparing the 2n index column $|GI|$ on the far right with values of the main bijective scheme. Naturally, the zeroth CFP-derived cardinalities for these even $\otimes D^k(\tilde{\mathbf{U}})$ operations are useful independent checks, based on the alternative $\mathbf{Z}_{22}$-like propagation from the lower n-fold complete $CFP(i)^{(n)}$ set. In addition to the $k = 0$ rank CFPs being derivable equally by either simple bijective mapping processes or summation of i-component squares of the n-fold set to sole zeroth CFP of 2n-fold set as unitary group processes, the corresponding (numerically identical)$\mathscr{S}_n$-invariant cardinality is a readily accessible quantity. This arises from a consideration of time-reversal invariance (TRI) over Weyl bracket algebras as $(\hat{\mathbf{I}} \bullet \hat{\mathbf{I}})...(\hat{\mathbf{I}} \bullet \hat{\mathbf{I}})$-based models that underlie automorphic spin physics of NMR. The above-reported $n \rightarrow 2n$ unitary group $\mathbf{Z}_{22}$ technique is particular valuable in allowing for the derivation of (e.g.) the higher $n \geq (20), 24, 40$-fold cases, via the various n-based sequences (e.g.) $\{3{:}6{:}12{:}24\}$, $\{\ 4{:}8{:}16\}$, or $\{5{:}10{:}20{:}40\}$, with these

being typical of (automorphic) $^{13}C_n, 20 \leq n \leq 60$, fullerene-based model, invariant cardinalities, or else its $[A]_{60-n}[X]_n$-systems, related to (e.g.) the boraza-substituted fullerenes as uniform quasi-polyhedral multispin models.

In the context of recursively obtained CFP sets of bijectional map results of Table 1, the sum of squares, for the full initial n-fold *i*-th component CFP set(s), by providing the 2n-indexed $CFP(0)^{(.)} \equiv |GI|^{(.)}$ values yield an invaluable running check on subsequent bijective hierarchy. The $n \rightarrow 2n$ mapping (progressively for 4, 5, 6, 8, 10, 12, and 20 index-sequence) GI-cardinalities provides the following sequence of inter-related sets of zeroth-CFP values:

$$|GI|^{(2n)} \equiv \{3, 6, 15, \ldots, 91, \ldots, 603, \ldots, 4213, \ldots, 13, 393689\}. \tag{7}$$

Conceptually however, there is a further independent confirmation of the above, beyond the $\mathbf{Z}_{n0}, \mathbf{Z}_{22}$ comparative mapping results noted here. This is in the form of the $\mathscr{S}_n$ group specialised 'even' character sum which directly draws on Weyl view of $|GI|^{(n)}$ enumeration [18] to give a direct route to the $|GI|^{(n)}$ invariant cardinalities. Of necessity, it utilises standard *generalised hooklength* methods for evaluating $\chi_{1^n}^{(\lambda)}(\mathscr{S}_n)$ group characters [37] – a viewpoint clearly beyond the classic $\mathscr{GL}_d$ form for a related fundamental tensorial property derived by Littlewood [38]. The distinctly similar forms of these separate properties of Schur-duality related groups is hardly coincidental. Three example calculations, deriving $GI^{(n)}$ values by the specific $\mathscr{S}_n$ character-sum method, are discussed briefly in Appendix B.

In the context of tensoral structure, these numerical values are simply the cardinality of the additional $\tilde{\nu}$ labels associated with generalised tensorial sets, so that for the first multi-invariant ($n = 4$) indexed set becomes:

$$(\otimes T^1(1))^{(4)} \equiv \left\{ T^k_{\{\tilde{\nu}\}}(1111) \right\} (SU2 \times \mathscr{S}_4), \tag{8}$$

where specific zeroth CFP value is now 3. Further, in accord with automorphic group view of NMR Liouvillian structures, these three unique invariants may be represented by subgroup chain structures established in iso-scalar factor particle physics discussions of Ref. [28], namely:

$$\begin{array}{l} \{[31] \supset [3] \supset [2]\} \\ \{[31] \supset [21] \supset [2]\}, \\ \{[2^2] \supset [21] \supset [2]\} \end{array} \tag{9}$$

which extends an earlier density matrix algebraic view [17].

In contrast to classic graph recoupling conventionally utilised to define (e.g.) $T^1 \otimes T^1 \equiv \{T^k(11)\}$ via the earlier (*distinct point set*) formalisms implicit in Sanctuary's 1976 work [1], the automorphic group $[A]_n(X)$ *or* $[AX]_n$ NMR problems here are specifically concerned with dual groups and with sets of *indistinguishable inner recoupled k_i components*. The latter point tensorial sets have their origins in specialised automorphic NMR spin symmetries that have specific properties, which are in contrast with those of the distinct k' sets under graph recoupling. However the

Table 1 Unitary bijective-derived $\{CFP^{(n)}(i)\}$ sets for $CFP(0)^{(n)} \equiv |GI|^{(n)}$ for $T^{k}_{\{\vec{v}\}}(11.1_n)$ sets to $n = 24$, based on $(\otimes D^1(\tilde{\mathbf{U}}))^n$ bijection. In addition, the $(\mathbf{Z}_{22})$-based $\sum_{i=0}^{n}|C(i)|^2 \rightarrow CFP(0)^{(2n)}$ $(\equiv |GI|^{(2n)})$ are shown in righthand $\mathbf{S}^{SQ}$ column – as an ongoing check on the initial process
{To compact the table, note use of: $aa = 13,393689; z = 834,086421$; $zz = 439742,222071; zzz = 17,047,255430,494497$.}

n	CFP(0)$^{(n)}$	CFP(i)s														**S^{SQ}**:2n
4:	3	6	6	3	1											
	6	15	15	10	4	1										
6:	15	36	40	29	15	5	1									**[4213**:12
	36	91	105	84	49	21	6	1								
8:	91	232	280	238	154	76	28	7	1							
	232	603	750	672	468	258	111	36	8	1						
10:	603	1585	2025	1890	1398	837	405	155	45	9	1					**[aa**:20
	1585	4213	5500	5313	4125	2640	1397	605	209	55	10	1				
12:	4213	11298	15026	14938	12078	8162	4642	2211	869	274	66	11	1			**[z**: 24
	11298	30537	41262	42042	35178	24882	15015	7722	3354	1209	351	78	12	1		
14:	30537	83097	113841	118482	102102	75075	47619	26091	12285	4914	1638	441	91	13	1	
	83097	227475	315420	334425	295659	224796	148785	85995	43290	18837	6993	2170	545	105	14	
															1	**[zz**:30
16:	227475	625992	877320	945504	854880	669240	459576	278070	148122	69120	28000	9708	2820	664	120	
														↪15	1	
	625992	1,730787	2,448816	2,677704	2,469624	1,983696	1,406886	885768	495312	245242	106828	40528	13192	3604	799	
													↪136	16	1	
18:	1,730787	4,805595	6,857307	7,596144	7,131024	5,860206	4,276350	2,787966	1,626322	847382	392598	160548	57324	17595	4539	
												↪951	153	17	1	
	4,805595	13,393689	19,259046	21,584475	20,587374	17,267580	12,924522	8,690638	5,261670	2,866302	1,400528	610470	235467	79458	↙	
										↪23085	5643	1121	171	18	1	
20:	13,393689	37,458330	54,237210	61,430895	59,439429	50,779476	38,882740	26,876830	16,818610	9,528500	4,877300	2,246465	925395	338010	↙	
									↪108186	29849	6935	1310	190	19	1	**[zzz**:40
	37,458330	105,089229	153,126435	175,107534	171,649800	149,101645	116,539046	82,578180	53,223940	31,224410	16,652265	8,049160	3,509870	↙		
							↪1,371591	476045	144970	38095	8435	1519	210	20	1	
22:	105,089229	295,673994	433,323198	499,883769	495,858979	437,290491	348,218871	252,341166	167,026530	101,100615	55,925835	↙				
				↪28,211295	12,930621	5,357506	1,992606	659109	191499	48048	10164	1749	231	21	1	
	295,673994	834,086421	1228,880961	1429,065946	1433,033239	1281,368341	1037,850528	767,586567	520,468311	324,052980	185,237745	↙				
			↪97,067751	46,499422	20,280733	8,009221	2843214	898656	249711	59961	12144	2001	253	22	1	
24:	834,086421	{..}														

latter are in general use in other types of spectroscopic applications.[5] The limitations of 6-j, 9-j, or 12-j or higher R-W algebras to distinct point-set graph modelling follows directly from recent mathematical remarks of Atiyah and Sutcliffe [4]. In consequence, the analytic properties of indistinguishable point sets (tensorial sets) which underlie democratic recoupling are problematic. Such arguments strongly imply that the automorphic NMR spin symmetries represent group-theoretic models that permit (or depend on) the direct use of $(\mathscr{S}_n)$-invariant theory in spin particle physics, as discussed in the following two sections that focus on the important property of *quantal completeness*.

3 Projective Mappings Properties and Hilbert Quantal Completeness

It is useful to compare Hilbert and Liouville space mapping properties under the dual group $SU2 \times \mathscr{S}_n$ and thereby draw on the distinct *combinatorial statements of quantal completeness* which apply in the two contrasting spin spaces. From the original boson pattern algebras of Louck and Biedenharn [21], the carrier space-based projective mapping associated with dual group actions takes the form:

$$\mathbf{U} \times \mathbf{P} : \mathbb{H} \rightarrow \mathbb{H} \ \left\{ D^j(\mathbf{U}) \Gamma(\mathbf{P}) |\ \mathbf{U} \in SU2; \mathbf{P} \in \mathscr{S}_n \right\}, \tag{10}$$

(i.e., as extension of Eq. (2a) above) which exhibits no explicit group invariant dependency in this Hilbert space format. Louck, in this original 1979 Bielefeld work [21] (with his co-author Biedenharn), draws on this formal carrier-space mapping to obtain the Hilbert space *quantal completeness condition*, namely,

$$\sum_{j}^{max\ j=n/2} D^j(\mathbf{U}) \Gamma^{[(n/2)+j,(n/2)-j]}\ ,\ j \geq (0), 1/2\ ; \tag{11}$$

this implies that Hilbert automorphic spin $[A]_n(X)$ problems (e.g.) span a (progressive) set of (non-Abelian) (bi)partite $\mathscr{S}_n$ irreps:

$$\{[n], [n-1,1], [n-2,2] ...\} \equiv \{<0>, <1>, <2>, ..\},$$

where the latter represents the form associated with the Wybourne reduced notation, in which the leading portion of the number partition is omitted – as given (e.g.) in Refs. [40, 41]).

The corresponding Liouvillian carrier space-based projective mapping given below has a quite specific structure, with its explicit dependence on the automorphic group invariants and their cardinality. It is these aspects of Liouvillian projective mapping structures that strongly stress many of the specific properties of *indistinguishable point sets* related to DR-based NMR problems.

[5] As discussed by Silver in his classic spectroscopic monograph [39] on role of applicable R-W algebra in graph theoretic viable problems.

4 Dual Mapping Over Explicit Liouville Carrier Spaces

Generalised tensorial structure of automorphic spin symmetry-based NMR problems are seen to arise within the context of dual group action, itself associated with superboson mapping over carrier spaces which derive from *indistinguishable point sets*. One stresses here the role of dual group actions and group invariants, in which the latter act as Schur duality-like properties (as between pairings of the U_n vs $\mathscr{S}_n$ groups, rather than related to the classic $\mathscr{GL}_d$ *vs* $\mathscr{S}_n$) groups. Hence the properties are equally derivable from either unitary or permutational group considerations. As a direct consequence of this, the set structure inherent in the Liouville abstract space furnishes a full description of *quantal basis set completeness*. Clearly, this is a primary requirement for fuller spin dynamics treatment of $[A]_n(X)$ or more extended NMR systems.

In contrast to Hilbert space mappings, here one find that the group invariant plays an explicit role in defining group actions over Liouvillian carrier spaces associated with dual tensorial sets, with the projective mappings now taking the form:

$$\tilde{\mathbf{U}} \times \mathscr{P} : \tilde{\mathbb{H}} \longrightarrow \tilde{\mathbb{H}} \left\{ D^k(\tilde{\mathbf{U}}) \tilde{\Gamma}^{[\lambda]}(\tilde{\nu})(\mathscr{P}) \mid \tilde{\mathbf{U}} \in SU2; \mathscr{P} \in \mathscr{S}_n; \tilde{\nu}, \text{ GI} \right\}, \tag{12}$$

within which the distinct $\tilde{\nu}$ GI terms define a disjoint set of carrier subspaces, as shown here by the specialised sum in the expression:

$$\tilde{\mathbb{H}} \equiv \bigoplus\nolimits_{\tilde{\nu}} \tilde{\mathbb{H}}_{\tilde{\nu}}, \tag{13}$$

where $\tilde{\nu}$ represents one of the $\{\tilde{\nu}\}$ complete set of invariants. The number of these disjoint subspaces naturally is identical to the cardinality associated with the GI set itself, as defined by $|GI|^{(n)} \equiv CFP(0)^{(n)}$. Clearly, these carrier subspaces are those of specific invariant-related superboson actions, with the superboson quasiparticles (QPs)s themselves being simply components of the Liouvillian *unit-tensor set* – conveniently represented by (augmented) double Gel'fand patterns. The actual (augmented) pattern basis components, $|(2k \underset{(k+q)}{\cdot} 0.) >>$, arise from the action of specific unit-tensors (superbosons) on the Liouvillian *null* basis (see discussion of Eqs. (19–21), Appendix A), a form of action directly analogous to that established for boson QPs acting on Hilbert null-spaces [21].

On taking Eqs. (11–13) together with the expression:

$$\sum_{\tilde{\nu}} T^k_{\tilde{\nu}}(11.1) \equiv \sum_{\tilde{\nu}} \left\{ D^k(\tilde{\mathbf{U}}) \tilde{\Gamma}^{[\lambda]}(\tilde{\nu})(\mathscr{P}) \right\}, \tag{14}$$

one has a useful combinatorial statement of Liouvillian *quantal completeness*, which is applicable quite generally over internally recoupled (DR) $\{T^k_{\{\tilde{\nu}\}}(111..1)\}$ basis sets, as representational set forms described by multiple GIs of the sets $\{\tilde{\nu}\}$ – more especially to those for which $|GI|^{(n)} \geq 3$ to which DR applies. These expressions signify that over each of the disjoint carrier subspaces $\tilde{\mathbb{H}}_{\tilde{\nu}}$, the property of SR over the individual $\{[\tilde{\lambda}]\}$ irreps is retained. From the point of view of (dual)

density-matrix algebraic theory [17], the mapping properties of Eqs. (12, 13) defining *quantal completeness* are more general than the earlier schematic formalisms, that involve DR properties typically based on a Lévi-Civitá-like operator. This is a consequence of the nature and restricted definition of the latter to the (identical) 3-fold case.

The questions on equivalence for analogous forms of 3-fold recoupling were noted [34] prior to the recognition and full realisation [9] of the specific properties of the Lévi-Civitá operator(s) in DR recoupling. The value of these operators to DR (Hilbert formulated) problems lies in their generating additional commutator relationships and a generalised-$\mathbf{I}_i$ spin Jacobian matrix formalism. The auxiliary commutators and the Hilbert space matrix forms permit the limited retention of applicable R-W algebra [9]. The augmented structure of the corresponding Liouville problem would seem to preclude the formation of the specialised matrix form from which the original mono-invariant-based Hilbert space solution was obtained. In the context of the wider multi-invariant problem, no further *multi*-dentate analogues to Lévi-Civitá (super) operator are known that would apply either to multi-invariant theory generally, or to the corresponding density-matrix formalism [17] – to the best of the author's knowledge. The authors of the latter 1965 schematic recoupling work related to Liouville density-matrix formalisms, stress that only a single usage of a tridentate Lévi-Civitá form is permissible; this clearly precludes (on the face of it) hierarchical use of these specialised operators in generalised invariant theory. Hence it only remains to stressed here that the 6-j, 9-j, 12-j or higher, applicable R-W functions are *exclusively concerned with distinct-point sets*, under their appropriate recoupling diagrams. These are excluded from the DR problems involving multi-invariant-based indistinguishable point sets and automorphic dual tensorial bases discussed here, by reason of Atiyah and Sutcliffe's mathematical assertion [4] that applications of graphical techniques are only valid for distinct point-set-based systems. In consequence such R-W graphical techniques are clearly excluded from generalised invariant theory, of recent years largely based on (polyhedral) combinatorics, or $\mathscr{GL}_d$, $\mathscr{S}_n$ Schur function techniques.

5 Disjoint Carrier Subspace Structure in Liouville Multi-Invariant NMR

Analytic treatment of the spin dynamics of the $[A]_2$ spin system, which underlies all $[A]_2(X)$, $[A]_n(X)$-type systems, has demonstrated the origins of the Hilbert era rule [7] concerned with the non-observation of (dominant) intra-cluster interactions in automorphic group-based spin systems. This asserts that the $[\tilde{n}](\mathscr{S}_n)$ forms in analytic dynamical terms are actually *null subspatial domains*, whereas the $[\widetilde{n-1},1]$ (etc.)-containing subspaces, though retaining the dominant $J_{intra-cluster}$ term(s), remain unobservable, for the reason that the corresponding *initial coherences* represent non-preparable forms. This was demonstrated in Ref. [7], – as an

extension to the Sanctuary analysis of the distinct spin AX case [42] – and some further details of the analysis are given in Appendix C, below.

In the context of renormalisation, retention of the disjoint structure of carrier subspaces allows for spin dynamics calculations here to be pursued for some *restrictive DR forms* of system, such as that for $[A]_n(X)$ within which only a single external cluster interaction is definable. This follows because the spin dynamics than becomes partitioned into a series of *possibly weighted* (say) $B^{(I \geq 1)}X$, .. spin systems, whose spin dynamical behaviour mirroring that of a AX system as given by Sanctuary [42], both in the latter work and as reviewed [3], in the wider context of general I spin dynamics and relaxation. Additional problems specifically involving higher I spins were analysed subsequently by Füro et al. [43]. Whilst it may well be convenient to regard the process that invokes a series of subsets of differing $I \geq 1/2$ spin angular momenta, (replacing a set of n-fold equivalent particles), as being a form of quasi-renormalisation to series of higher unitary groups. There is an important *caveat* to the use of this process; its applicability is limited to applications in which *multiple* $\{J_{AX}\}$ (etc.) couplings do not occur. It does not apply to generalised $[AX]_n$ DR NMR systems, in which the overall invariant cardinality is derived as $||GI|^{(n)}|^2$, This general result simply corresponds to taking all possible pair-product forms of $\tilde{v}\tilde{v}'$ subinvariant pairings.

6 Some Brief Conclusions: Limitations Induced by k_i Sub-Rank Indistinguishability

The invariant-theoretic approach utilised here explains the origins of certain well-known difficulties associated with generalised automorphic many-spin formalisms in NMR based on dual tensorial sets. Unlike earlier distinct point set Hilbert spaceproblems, as treated by Corio [19], or the single spin (or AX) Liouvillian formalisms, developed by Sanctuary and Halstead [3] and their coworkers, cited therein, the automorphic systems introduce *indistinguishability* so that the dual tensorial sets hence retain a dependency on multiple invariants. Whilst this gives rise to disjoint carrier subspaces under dual group actions by generating the (super)boson projective mapping in which the invariants provide for the completeness of the Liouvillian tensorial quantal bases, it also results in the *dominance* of the $\mathscr{S}_n$ group. In treatments based on density-matrix approaches utilising dual tensorial sets, these automorphic spin symmetric NMR problems are not Racah-Wigner algebra-compatible. This is attributed directly to R-W algebras being graph-theoretic-based, unitary group aspects of theoretical physics [2], despite their Gel'fand and Schur implied dependencies [21].

The specific results given in Table 1 show interrelationship between the direct recursive CFP bijection and the alternative $\mathbf{Z}_{22}$ analogue of squaring a set of lower-index based CFPs, which are especially useful in providing one with various higher-index invariant cardinalities, implicit in ^{13}C-fullerene, or $[A]_{60-n}[X]_n$ borazafullene cluster modelling of automorphic spin systems. The following additional $|GI^{(n)}|$

results (respectively) for $n = 24$, $n = 36$, $n = 40$:

$$|GI|^{(24)} = 834,086421\,, \tag{15}$$

$$|GI|^{(36)} = 245,613,376,802185\,, \tag{16}$$

$$|GI|^{(40)} = 17,047,255,430,494497\,, \tag{17}$$

demonstrate the value of the two form of bijective mapping. That all of these $|GI|$s may be derived equally by the use of *hooklength enumerative* methods [37] within a representational $\mathscr{S}_n$-character sum approach, as demonstrated elsewhere [11], [25], simply affirms the value of Schur duality and invariant-theoretic, polyhedral combinatorial methods.

In the physical science context of defining tensorial quantal bases, the above invariant-theoretic viewpoint lies beyond that given earlier [20] (or in Ref. [36] dealing with generalised lattice points approaches), or in material in the accessible discrete mathematics or theoretical physics (i.e. Hilbert space based) literature [40,41,44] is clearly a direct consequence of Atiyah and Sutcliffe's recent work [4] which strictly limits the use of graph theoretic recoupling in tensorial construction to (inner recoupled) distinct point set derived tensors. Various contrasting methods for determining the invariant cardinality of automorphic spin dynamics $[A]_n(X)$ problems have been presented including a recent $\mathscr{S}_n$ representational one [25] based on Weyl's original views of bracket pair-permutation and TRI being equivalent properties [18]. Questions about the limited applicability of R-W to monoinvariant (cf. multi-invariant indistinguishable) point sets (over dynamical abstract spin space) are consistent with the *maximal nature* of conventional Lévi-Civitá (super) operators [9], as well as with recent point set-based assertions [4] that graph-theoretic-based apparatus and modelling is restricted to distinct point sets. This view reinforces a much earlier assertion due to Galbraith [35] based on group theoretic considerations. The latter's 1971 work was concerned with a 4-body (non-spin) Hamiltonian-structured spectral problem. This was shown to depart from all R-W matrix-analytic applicable forms, essentially on the basis of group chain subduction-based reasoning; invariant theory and combinatorial approaches were considerably less-developed then, as compared to their status to-day.

The present work has stressed that the question of the role of invariants raised by considering the impact of DR in tensorial formalism of NMR spin dynamics in general remains a largely *open question* of considerable physical significance. This is quite apart from the use of mapping in fully defining the quantal tensorial basis completeness – via combinatorial forms in both Hilbert and Liouville space. The work has shown how invaluable and insightful are invariant theoretic and projective mapping techniques in deriving tensorial set structural overviews, especially in wider Schur function and duality contexts of Refs. [40,41]. It useful to recall that some of the earliest dynamical NMR studies (from 1960s) were based on wreath-product group structure (today cf. especially pertinent (e.g.) to the field of reaction dynamics). Of course, these generalised forms [44] and the methods advocated by Wybourne and King (cited above) are much more powerful than those of simple

permutation groups. Both the bijectional derivation of Table 1 and the specific representational character sum methods summarised in Appendix B deserve to be widely known for their conceptual simplicity, with the latter drawing on the *hooklength enumeration of* $\chi_{1^n}^{<\lambda>}$ *permutational group characters* [37, 45]. The value to physical science of elegant combinatorial methods due to (e.g.) Sagan [45] and Kerber et al. [46] deserves a wider recognition, since they provide direct access to invariant theory as well as to the automorphic NMR spin modelling discussed here.

Acknowledgements The author is indebted to a long-time coworker, Bryan Sanctuary, for his invaluable early discussions of the specifics of spin dynamics, and also to K. Balasubramanian, A. Kerber, A., Kohnert, J.D Louck, J.A Karwowski and R.C. King (amongst others) for their encouragement in pursuing various studies of the role of combinatorics in physical science. Finally, support from NSERC Council of Canada is gratefully acknowledged.

Appendix A: (Super)Boson QPs as Unit-Tensors

The Hilbert boson pattern QPs may be represented in following terms as a set of unit operators:

$$\{a_1;a_2;\bar{a}_1,(-)\bar{a}_2\} \equiv \left\{ \left\langle 1 \begin{smallmatrix} 1 \\ 1 \end{smallmatrix} 0 \right\rangle, \left\langle 1 \begin{smallmatrix} 1 \\ 0 \end{smallmatrix} 0 \right\rangle ; \left\langle 1 \begin{smallmatrix} 0 \\ 1 \end{smallmatrix} 0 \right\rangle, \left\langle 1 \begin{smallmatrix} 0 \\ 0 \end{smallmatrix} 0 \right\rangle \right\}, \tag{18}$$

from which, within properties of Eq. (1), the Liouvillian QP subset (and the corresponding conjugate subset) in their unit-tensor forms become (as given in detail in Eqs. (9–14) of Ref. [22]), where $\tilde{\Delta} \leq k$ is a Liouvillian shiftoperator:

$$\left\{ \left\langle \left\langle 2k \begin{smallmatrix} k+\tilde{\Delta} \\ k+q \end{smallmatrix} 0 \right\rangle \right\rangle \right\} ; \left\{ \left\langle \left\langle 2k \begin{smallmatrix} k-\tilde{\Delta} \\ k-q \end{smallmatrix} 0 \right\rangle \right\rangle \right\}, \tag{19}$$

or as equivalently realised for single spin-$(1/2)$ by:

$$\left\{ \left\langle \left\langle 2 \begin{smallmatrix} 2 \\ k+q \end{smallmatrix} 0 \right\rangle \right\rangle \right\} ; \left\{ \left\langle \left\langle 2 \begin{smallmatrix} 0 \\ k-q \end{smallmatrix} 0 \right\rangle \right\rangle \right\}, \tag{20}$$

where the action of each such unit tensor (superboson) on (Liouvillian) null space generates the pattern basis, now defined for the $k = 1$ (integer rank), $-k \leq q \leq k$ Liouvillian bases as:

$$\left| \left(2k \begin{smallmatrix} \cdot \\ (k+q) \end{smallmatrix} 0 \right) \right\rangle \rangle \equiv |kq>>, \tag{21}$$

where this is analogous to the corresponding Louck and Biedenharn, Hilbert space definitions, as given in Ref. [21].

Appendix B: $\sum_{even}\ \lambda\ \chi_{1^n}^{<\lambda>}\ (S_n)$-TRI $|GI|^{(n)}$ Invariant Cardinality

It has been shown elsewhere [12] how the recognised equivalence between $(\hat{\mathbf{I}}\bullet\hat{\mathbf{I}})...(\hat{\mathbf{I}}\bullet\hat{\mathbf{I}})$ permutational operations and time-reversal invariance (TRI) of Refs. [18, 19] governs GI cardinality, which has been derived here from unitary group considerations in Table 1. A more direct $\mathscr{S}_{2n}$ representational approach has been postulated in which a specific sum of even characters with analogous form to TRI equivalent permutational forms within *hooklength enumerations* [37] of $\mathscr{S}_n$ characters which yields a direct combinatorial route (see further proof in [12]) to $|GI|^{(n)}$ enumeration as:

$$|GI|^{(2n)} \equiv \chi_{1^{2n}}^{<0>} + \sum_{i=1}^{n-1} \chi_{1^{2n}}^{<2^i>}\,, \tag{22}$$

as in the following examples, whose realisations are based on standard hooklength combinatorial character enumerations – cited above:

$$|GI|^{2n=6} \equiv 1 + \chi_{1^6}^{<2>} + \chi_{1^6}^{<22>},\ \text{realised as},$$

$$(1+9+5) = 15\,, \tag{23}$$

$$|GI|^{2n=10} \equiv 1 + \chi_{1^{10}}^{<2>} + \chi_{1^{10}}^{<22>} + \chi_{1^{10}}^{<222>} + \chi_{1^{10}}^{<2^4>},\ \text{for which},$$

$$(1+35+225+300+42) = 603\,, \tag{24}$$

$$|GI|^{2n=12} \equiv 1 + \chi_{1^{12}}^{<2>} + \chi_{1^{12}}^{<22>} .... + \chi_{1^{12}}^{<2^5>},\ \text{for which},$$

$$(1+54+616+1925+1485+132) = 4213\,, \tag{25}$$

which by their equivalence to tabulated unitary results simply re-affirms the duality properties inherent in this map-based invariant cardinality. It is stressed that this TRI-based result is quite distinct from a more general tensorial polynomial product decompositional property – due to Littlewood [38], which also is derived over even characters of $\mathscr{GL}_n$, but without the restrictions implicit in Weyl's TRI condition.

Appendix C: Formal Analysis of $[A]_2$ Spin System

It is well-established that the relationships between $T^{kq}(k_1k_2)$ and the pair of individual $\mathscr{Y}^{k_1q_1}\mathscr{Y}^{k_2q_2}$ NMR multipoles is governed by a summation over $(-1)^{k-q}\begin{pmatrix} k & k_1 & k_2 \\ -q & q_1 & q_2 \end{pmatrix}$ where last bracket form is a 3-j coefficient, and that this relationship has strong similarities to the transformation between $\mathscr{Y}^{kq}$ individual multipole basis and the product basis $|IM><IM'|$. A comparative dynamical analysis of the $[A]_2$ automorphic spin cluster, cf AX spin system, in a rotating frame has been presented in earlier work, based on Liouvillan of the (symmetric) form, [7]:

$$\mathscr{L}/\hbar = [i\sqrt{2}\omega T^{10}([\tilde{2}]) + \sqrt{(3/2)}J_{AA'}T^0(11),\ ]_-\,. \tag{26}$$

The rotating-frame dynamical description of Eq. (4) of Ref. [42] shows that the eigenfrequencies, from some suitable initial condition span two subsets, take the forms:

$$\{\lambda_i\} = \{\emptyset\}_{[\tilde{2}]}^{k=\pm1,\pm2} \tag{27}$$

for symmetric sub-salient, and

$$\{\lambda_i'\} = \{\pm J/2\}_{[\widetilde{11}]}^{k=\pm1}, \tag{28}$$

over the corresponding anti-symmetric sub-salient, with the latter unobservable because of the absence of a physically-creatable initial coherence condition; the formal expression (i.e., Eq. (7) in the cited work above) depicts the $J_{AA'}$ only occurring associated with the development of the $\hat{\phi}_q^1([\widetilde{11}])[t]$ rotating frame coherence. The analysis suggests that the $[\tilde{n}]$ salients of the wider $[A]_n$ cluster problems represent *null subspaces*, in accord with earlier criteria, cf. to $A[B]_z$ spin system of Ref. [16].

It is stressed here that our presentation is one concerned with model conditions; actual molecular spin systems may deviate from automorphic symmetry condition and become AX or network-like systems, in which heteronuclear spin interactions are then dominant terms within the Liouvillian, as in $AA'A''XX'X''$ system discussed in Ref. [15] where only the CP/CPT fundamental symmetries are retained. It is important to be clear on these initial matters before drawing any conclusions from NMR observations and to note that the *only possible* involvement of 3-space symmetry considerations arises on account of P parity considerations.[6]

Appendix D: Summary of Notation Utilised:

SR: simply-reducible; DR: Democratic recoupling (cf graph recoupling);
GI, or G-Invariant: group invariant with specific cardinality;
R-W algebra: Racah - Wigner algebra, as in Ref. [2];
CFP: coefficient of fractional parentage; QP: quasiparticle in boson pattern mapping sense [21];
TRI: time-reversal invariance, one of the **CP/TCP** fundamental particle invariances;
$\chi_{1^n}^{<\lambda>}(\mathscr{S}_n)$: a group character in the Butler-Wybourne reduced irrep notation [40, 41];
$I, I_i, (\hat{\mathbf{I}} \bullet \hat{\mathbf{I}})$: respectively, spin angular momenta, cluster component spin, Weyl bracket algebra notation.
k, q, v : the Liouvillian tensor rank, z-projection and auxiliary labels;
$< (2j \;\; [.] \;\; 0.) >, << (2k \;\; [.] \;\; 0) >>$: denote unit-tensors in Hilbert and Liouville spaces, respectively.
Finally the $\tilde{v}$ notation here is reserved for components of the group invariant set.

[6] Unless the problem being examined is an actual rotomeric NMR (or quantum rotational tunnelling) example which would then draw on *wreath-product* group symmetry, as a mixed 'abstract – R_3 space' problem.

References

1. B.C. Sanctuary, J. Chem. Phys., **64**, 4352 (1976), *et loc. cit.*
2. J.D. Louck & L.C. Biedenharn, *Encyclopaedia of Mathematics.* Vols 8, 9, (Cambridge Univ. Press, Cambridge, 1985)- Esp. Vol. 9: Ch. 2–5.
3. B.C. Sanctuary, T.K. Halstead, Adv. in Opt. Magn. Reson., **15**, 97 (1991).
4. M. Atiyah, P.M. Sutcliffe, Proc R. Soc., Ldn., A **458**, 1089 (2002).
5. D.R. Whitman, J. Mol. Spectrosc., **10**, 1372 (1962).
6. K. Balasubramanian, J. Chem. Phys., **78**, 6358 (1983); 6369.
7. F.P. Temme, Czech Chem. Comm., **70**, 1177 (2005), et loc. cit.
8. F.P. Temme, J. Magn Reson., **167**, 119 (2004).
9. J.M. Lévy-Leblond, M Lévy-Nahas, J. Math. Phys., **6**, 1372 (1965) et loc. cit.
10. F.P. Temme, Physica A**198**, 245 (1993).
11. F.P. Temme, J. Phys.: Math & Theor. A **41**, 015210 (2008).
12. F.P. Temme, (unpublished MS; under review, Sept. 2007).
13. A. Abragam, *Nuclear Magnetism*, (OUP, Oxford, 1962) Ch. XI.
14. R.G. Jones, Princ. Progr. in NMR, **1** 97 (1967); R.G. Jones, S.M. Walker, Mol. Phys., **10** 349 (1966).
15. R.G. Jones, R.C. Hirst, H.J. Bernstein, Canad. J. Chem., **43**, 683 (1965).
16. A.G. Avent, J. Magn. Reson., **53**, 513 (1984).
17. J.A.R Coope, R.F. Snider, F.R. McCourt, J. Chem. Phys. **45**, 2264; F. Chen, H. Moraal, R.F. Snider, J. Chem. Phys., **57**, 542 (1972).
18. H. Weyl, *Representations & Invariants of Classic Groups*, (Princeton Univ Press, New Jersey, 1946).
19. P.L. Corio, J. Magn. Reson., **134**, 131 (1998).
20. F.P. Temme, Proc. Roy. Soc. Ldn., A **461**, 341 (2005).
21. J.D. Louck, L.C. Biedenharn, in: *Permutation Group in Physics & Chemistry.* [Edit.: J. Hinze],(Springer, Heidelberg, 1979) (pp. 121-, 148-).
22. F.P. Temme, Int. J. Quantum Chem., **89**, 429 (2002).
23. F.P. Temme & B.C. Sanctuary, J. Math. Chem., **43**, 1119 (2008). [publ'd online, Jul. 2007 as: 10910-007/9236-8].
24. F.P. Temme, B.C. Sanctuary, in: *Symmetry, Spectroscopy and SCHUR*, [Edit: M. Bylicki, J. Karwowski & R.C. King], (M.-K. Univ. Press, Toruń, 2006) (pp. 271.-).
25. F.P.Temme, *Proc. Quantum Systems & Chemical Physics, XII* (Springer, Berlin, 2008), pps 00990-009990, Chapt. 20.
26. F.P. Temme, Eurphys., J., B**11**, 177 (1999).
27. R.G. Sachs, *Physics of Time-reversal*, (Univ. of Chicago Press, 1987).
28. J.Q. Chen, J. Ping, F. Wang, *Group Representation Theory for Physicists*, [Sec'd. Edit.] (World Sci. Singapore, 2002).
29. G. Ramachandran, M.V. Murthy, Nucl. Phys., A**337**, 301 (1980).
30. S.M. Krishnan, F.P. Temme , B.C. Sanctuary, Mol. Phys., **78**, 1385 (1993).
31. P.A. Fedders, Phys. Rev., B**11**, 995 (1976).
32. D.I. Bolef, R.K. Sundfors, *Theory of Nuclear Acoustic Resonance*, (Academic Press, New York, 1993).
33. J. Listerud, S J. Glaser, G.P. Drobny, Mol. Phys, **78**, 629 (1993).
34. K. Chakrabarti, Ann. Inst. H. Poincaré, **1**, 303 (1964).
35. H.W. Galbraith, J. Math. Phys., **12**, 782 (1971).
36. P. Erdös, P.M. Grüber, J. Hammer, *Lattice Points*, (Longman-Sci., Harlow, 1998).
37. J.S. Frame, G. de Q Robinson, R.M. Thrall, Canad J. Math, **6**, 365 (1953).
38. D.E. Littlewood, *Theory of Group Characters & Matrix Representations*, [Sec'd Ed.], (Clarendon Press, Oxford, 1950).
39. B.L. Silver, *Irreducible Tensor Methods*, (Academic Press, New York, 1976).
40. B.G Wybourne, *Symmetry Principles in Atomic Spectroscopy*, (Wiley, New York, 1970).

41. R.C. King, in: *Symmetry, Spectroscopy and SCHUR*, [Edit: M. Bylicki, J. Karwowski & R.C. King] (M-K Univ. Press, Toruń, 2006), (pp. 163 -).
42. B.C. Sanctuary, Mol. Phys., **55**, 1017 (1985).
43. I. Füro, B. Halle, T. Wong, J. Chem. Phys., **89**, 5382 (1989).
44. K. Balasubramanian, J. Chem. Phys., **95**, 8273 (1991).
45. B.E. Sagan, *Symmetric Group: Its Representations, Combinatorial Algorithms, & Symmetric Functions*, [Sec'd Edit.], (Springer New York, 2001).
46. A. Kerber, A. Kohnert, A. Lascoux, J. Symbol Comput., **14**, 195 (1993) (for fuller details see the Kerber group manual: *Symmetrica*, a Discrete Maths. Package).

For additional Combinatorial Mathematics resource materials, see:

V. Krishnamurthy, *Combinatorics, Theory & Applications*, (Horwood & E-W Press, Chichester & Dehli, 1988).
D. Marcus, *Combinatorics, A Problem-Oriented Approach.*, (Amer. Maths. Assoc., Washington D.C, 1998).
R. Merris, *Combinatorics*, [Sec'd Edit.], (Wiley, New York, 2003).
D.J. Watts, *Small Worlds: The Dynamics of Networks Between Order & Randomness*, (Princeton Univ. Press, New Jersey, 1999).

The Macroscopic Quantum Behavior of Protons in the $KHCO_3$ Crystal: Theory and Experiments

François Fillaux(✉), Alain Cousson, and Matthias J. Gutmann

Abstract For hydrogen bonded crystals exhibiting proton transfer along hydrogen bonds, namely $O1-H\cdots O2 \longleftrightarrow O1\cdots H-O2$, there is a dichotomy of interpretation consisting in that while the crystal lattice is a quantum object with discrete vibrational states, protons are represented by a statistical distribution of classical particles with definite positions and momenta at any time. We propose an alternative theoretical framework for decoherence-free macroscopic proton states. The translational invariance of the crystal, the adiabatic separation of proton dynamics from that of heavy atoms, the nonlocal nature of proton states, and quantum interferences, are opposed to statistical distributions and semiclassical dynamics. We review neutron scattering studies of the crystal of potassium hydrogen carbonate ($KHCO_3$) supporting the existence of macroscopic quantum correlations, from cryogenic to room temperatures. In addition, quantum fluctuations calculated for superposition states in thermal equilibrium are consistent with measurements of the correlation time. There is no temperature induced transition from the quantum to the classical regime. The crystal can be therefore represented by a state vector and the dichotomy of interpretation must be abandoned.

Keywords: Quantum entanglement, Neutron diffraction, Hydrogen bonding, Proton tunneling, Quantum interferences

F. Fillaux
UPMC Univ Paris 06, UMR 7075, LADIR, F-75005, Paris, France
CNRS, UMR7075, LADIR, 2 rue H. Dunant, F-94320, Thiais, France, e-mail: fillaux@glvt-cnrs.fr

A. Cousson
Laboratoire L'eon Brillouin (CEA-CNRS), CE Saclay, 91191 Gif-sur-Yvette, cedex, France.
e-mail: alain-f.cousson@cea.fr

M.J. Gutmann
ISIS Facility, Rutherford Appleton Laboratory, Chilton, Didcot, OX11 0QX, UK.
e-mail: m.j.gutmann@rl.ac.uk

S. Wilson et al. (eds.) *Frontiers in Quantum Systems in Chemistry and Physics*.

1 Introduction

The linear formalism of quantum mechanics extrapolated from the level of electrons and atoms to that of everyday life leads to conclusions totally alien to commonsense, such as Schrödinger's Cat in a superposition of "alive-dead" states and nonlocal observables [12]. Such conflicts lead to a dichotomy of interpretation consisting in that, while at the microscopic level a quantum superposition indicates a lack of definiteness of outcome, at the macroscopic level a similar superposition can be interpreted as simply a measure of the probability of one outcome or the other, one of which is definitely realized for each measurement of the ensemble [6, 30–34]. For open systems, this can be legitimated by decoherence [50] stipulating that an initial superposition state should lose its ability to exhibit quantum interferences via interaction with the environment. However, since the quantum theory does not predict any definite dividing line between quantal and classical regimes, macroscopic quantum behavior is possible for systems decoupled from, or very weakly coupled to, the surroundings [7]. In principle, there is no upper limit in size, complexity, and temperature, beyond which such systems should be doomed to classicality.

For example, it is a matter of fact that defect-free crystals are macroscopic quantum systems with discrete phonon states at any temperature below melting or decomposition. This is an unavoidable consequence of the translational invariance of the lattice. However, the dichotomy of interpretation arises for the so-called "proton disorder" in crystals containing O–H$\cdots$O hydrogen bonds. The coexistence of two configurations at thermal equilibrium, say O1 $-$ H$\cdots$O2 and O1$\cdots$H $-$ O2, has been thoroughly investigated in many systems [40]. Although the light mass of protons suggests that dynamics should be quantum in nature, semiclassical approaches are widely used to rationalize correlation times measured with solid-state NMR and quasi-elastic neutron scattering (QENS). Semiclassical protons are thought of as dimensionless particles, with definite positions and momenta, moving in a double-wells coupled to an incoherent thermal bath. These protons undergo uncorrelated jumps over the barrier and "incoherent tunneling" through the barrier. In fact, these models describe a liquid-like surroundings, at variance with the spatial periodicity of the crystal, and strong interaction with the thermal bath is supposed to lead to fast decoherence. By contrast, vibrational spectra provide unquestionable evidences that the translational invariance and the quantum nature of lattice dynamics are not destroyed by proton transfer. Our purpose is therefore to elaborate a purely quantum rationale avoiding any mixture of quantum and classical regimes.

We shall concentrate on the crystal of potassium hydrogen carbonate ($KHCO_3$) composed of centrosymmetric dimers of hydrogen bonded carbonate ions $(HCO_3^-)_2$ separated by K^+ entities. At elevated temperatures, the coexistence of two configurations for dimers is commonly conceived of as a statistical distribution [5, 11, 45, 46]. By contrast, systematic neutron scattering experiments measuring a large range of the reciprocal space have revealed the macroscopic quantum behavior of protons, from cryogenic to room temperatures, and the theory suggests that this behavior is intrinsic to the crystal state [15,18,19,24]. The present contribution is a preliminary

attempt to elaborate a consistent presentation of experimental and theoretical works currently in progress.

In Sect. 2 we present the crystal structure and the thermally activated interconversion of dimers. We emphasize why this crystal is unique to observing macroscopic quantum effects. In Sect. 3, we show that the adiabatic separation of proton dynamics leads to decoherence-free states. Then, we introduce the theoretical framework for macroscopic proton states in Sect. 4 and the double-well for protons in Sect. 5. In Sect. 6, the calculated scattering cross-section allows us to interpret neutron scattering experiments in terms of quantum correlations. In Sect. 7, quantum beats arising from the superposition of macroscopic proton states in thermal equilibrium are compared with the correlation time determined with QENS. In the conclusion, we emphasize that the crystal is a macroscopic quantum object that can be represented by a state vector.

2 The Crystal Structure of $KHCO_3$

The crystal at 14 K is monoclinic, space group $P2_1/a$ (C_{2h}^5), with four equivalent $KHCO_3$ entities per unit cell (Fig. 1). Centrosymmetric dimers $(HCO_3^-)_2$ linked by moderately strong OH···O hydrogen bonds, with lengths $R_{O\cdots O} \approx 2.58$ Å, are well

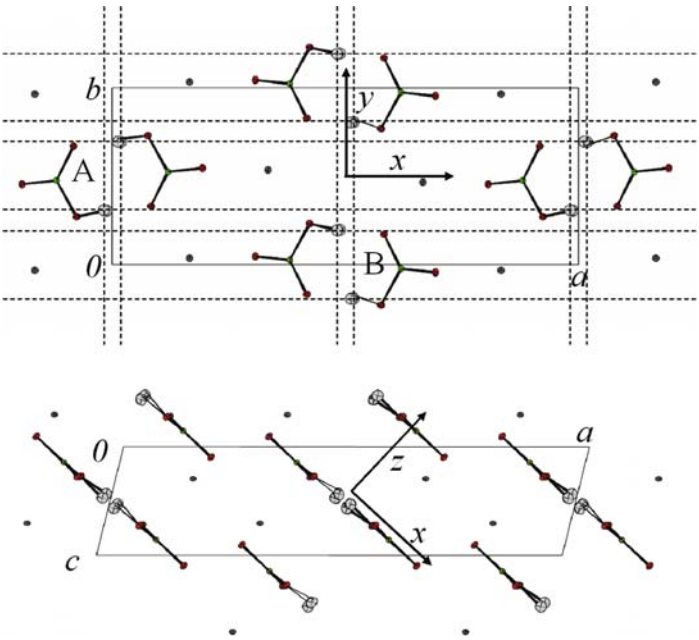

Fig. 1 Schematic view of the crystalline structure of $KHCO_3$ at 14 K. *Dashed lines* through protons are guides for the eyes. $a = 15.06(2)$ Å, $b = 5.570(15)$ Å, $c = 3.650(8)$ Å, $\beta = 103.97(15)^\circ$. The ellipsoids represent 50% of the probability density for nuclei

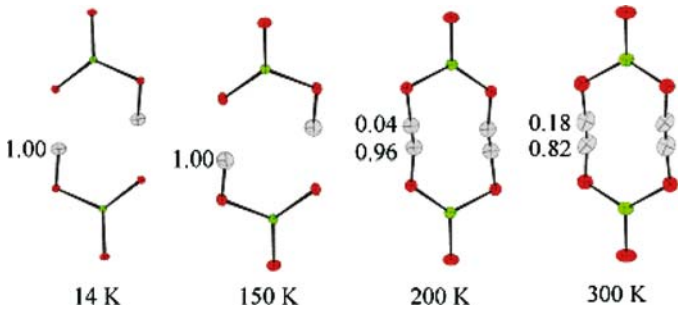

Fig. 2 Probability densities for protons in the $KHCO_3$ crystal at various temperatures, determined with single-crystal neutron diffraction. The ellipsoids represent 50% of the probability density for nuclei

separated by K^+ ions. All dimers lie practically in (103) planes, hydrogen bonds are virtually parallel to each other, and all protons are crystallographically equivalent (indistinguishable). This crystal is unique to probing proton dynamics along directions x, y, z, parallel to the stretching (νOH), the in-plane bending (δOH), and the out-of-plane bending (γOH) vibrational modes, respectively.

From 14 K to 300 K, there is no structural phase transition. The increase of the unit cell dimensions and of the hydrogen bond length are marginal, but the population of proton sites changes significantly (Fig. 2). Below $\approx$150 K, all dimers are in a unique configuration, say L. At elevated temperatures, protons are progressively transferred along the hydrogen bonds to the less favored sites (configuration R) at $\approx$0.6 Å from the main position. The center of symmetry is preserved and all proton sites remain indistinguishable. There is a general agreement that the population of the less favored site (or interconversion degree ρ) is determined by an asymmetric double-well potential along the hydrogen bonds [5, 11, 13, 22], but an in-depth examination of proton dynamics is necessary to distinguishing statistical disorder or quantum delocalization.

3 The Adiabatic Separation

Within the framework of the Born-Oppenheimer approximation, the vibrational Hamiltonian can be partitioned as

$$\mathscr{H}_{\mathrm{v}} = \mathscr{H}_{\mathrm{H}} + \mathscr{H}_{\mathrm{at}} + \mathscr{C}_{\mathrm{Hat}}, \tag{1}$$

where $\mathscr{H}_{\mathrm{H}}$ and $\mathscr{H}_{\mathrm{at}}$ represent the sublattices of protons (H^+) and heavy atoms, respectively, while $\mathscr{C}_{\mathrm{Hat}}$ couples the subsystems. For OH$\cdots$O hydrogen bonds, coupling terms between OH and O$\cdots$O degrees of freedom are rather large [38, 40], and beyond the framework of the perturbation theory. Two approaches, either semiclassical or quantum, are commonly envisaged.

In the semiclassical view, protons are thought of as dimensionless particles, with definite positions and momenta, moving across a potential hypersurface [3,4,23,42, 44]. Complex trajectories involving heavy atoms lead to mass renormalization, and to incoherent phonon-assisted tunnelling [5, 11, 41]. This approach is quite natural when the Born-Oppenheimer surface is calculated from first principles, but quantum effects can be severely underestimated.

Alternatively, if the classical concept of "trajectory", totally alien to quantum mechanics, is abandoned, adiabatic separation of the two subsystems, namely $\mathscr{H}_{\rm H}$ and $\mathscr{H}_{\rm at}$, may lead to tractable models [18,21,23,37,40,47]. Then, light protons in a definite eigen state should remain in the same state in the course of time, while heavy atoms oscillate slowly, in an adiabatic hyperpotential depending on the proton state, through the coupling term. This separation is relevant for $KHCO_3$ because adiabatic potentials for different protons states do not intersect each other. Then, protons are bare fermions and quantum correlations should occur [18].

In fact, the separation is rigorously exact in the ground state, since protons should remain in this state for ever, if there is no external perturbation. Furthermore, for asymmetric double-wells, with wave functions largely localized in each well (see below Sect. 5), the adiabatic separation should also hold for the lowest state of the upper minimum and long-lived superposition states should interfere.

4 Macroscopic Proton States

Consider a crystal composed of very large numbers $N_{\rm a}$, $N_{\rm b}$, $N_{\rm c}$ ($\mathscr{N} = N_{\rm a}N_{\rm b}N_{\rm c}$) of unit cells labelled j,k,l, along crystal axes (a), (b), (c), respectively. The two dimers per unit cell are indexed as j,k,l and j',k,l, respectively, with $j = j'$. For centrosymmetric dimers, there is no permanent dipolar interaction, so that inter-dimer coupling terms and phonon dispersion are negligible [22, 25, 26]. The eigen states of the sublattice of protons can be therefore represented in a rather simple way with the basis sets of eigen states for isolated dimers.

A H1–H2 dimer is modelled with coupled centrosymmetric collinear oscillators in three dimensions, along coordinates $\alpha_{1{\rm jkl}}$ and $\alpha_{2{\rm jkl}}$ ($\alpha = x,y,z$), with respect to the center at $\alpha_{0{\rm jkl}}$. The mass-conserving normal coordinates independent of j,k,l, and their conjugated momenta,

$$\begin{aligned} \alpha_{\rm s} &= \frac{1}{\sqrt{2}}(\alpha_1 - \alpha_2 + 2\alpha_0), & P_{\rm s\alpha} &= \frac{1}{\sqrt{2}}(P_{1\alpha} - P_{2\alpha}), \\ \alpha_{\rm a} &= \frac{1}{\sqrt{2}}(\alpha_1 + \alpha_2), & P_{\rm a\alpha} &= \frac{1}{\sqrt{2}}(P_{1\alpha} + P_{2\alpha}), \end{aligned} \tag{2}$$

lead to uncoupled oscillators at frequencies $\hbar\omega_{\rm s\alpha}$ and $\hbar\omega_{\rm a\alpha}$, respectively, each with $m = 1$ amu. The difference $(\hbar\omega_{\rm s\alpha} - \hbar\omega_{\rm a\alpha})$ depends on the coupling term (say λ_α). The wave functions, $\Psi^{\rm a}_{\rm njkl}(\alpha_{\rm a})$, $\Psi^{\rm s}_{\rm n'jkl}(\alpha_{\rm s} - \sqrt{2}\alpha_0)$, cannot be factored into wave functions for individual particles, so there is no local information available for these entangled oscillators. Consequently, the degenerate ground state of

indistinguishable fermions must be antisymmetrized. For this purpose, the wave function is rewritten as a linear combination of those for permuted oscillators as

$$\Theta_{0\mathrm{jkl}\pm} = \frac{1}{\sqrt{2}} \prod_{\alpha} \Psi^{\mathrm{a}}_{0\mathrm{jkl}}(\alpha_{\mathrm{a}}) \left[\Psi^{\mathrm{s}}_{0\mathrm{jkl}}(\alpha_{\mathrm{s}} - \sqrt{2}\alpha_0) \pm \Psi^{\mathrm{s}}_{0\mathrm{jkl}}(\alpha_{\mathrm{s}} + \sqrt{2}\alpha_0) \right], \tag{3}$$

and the antisymmetrized state vectors as:

$$\begin{aligned} |0jkl+\rangle \otimes |S\rangle &= \left|\Theta_{0\mathrm{jkl}+}\right\rangle \otimes \frac{1}{\sqrt{2}} [|\uparrow_1\downarrow_2\rangle - |\downarrow_1\uparrow_2\rangle]; \\ |0jkl-\rangle \otimes |T\rangle &= |\Theta_{0\mathrm{jkl}-}\rangle \otimes \frac{1}{\sqrt{3}} \left[|\uparrow_1\uparrow_2\rangle + |\downarrow_1\downarrow_2\rangle + \frac{1}{\sqrt{2}} [|\uparrow_1\downarrow_2\rangle + |\downarrow_1\uparrow_2\rangle] \right]. \end{aligned} \tag{4}$$

The oscillators are now entangled in position, momentum, and spin. In contrast to magnetic systems [9], there is no level splitting, so the symmetry-related entanglement is energy-free. It is also independent of λ_α. Furthermore, contrariwise to Keen and Lovesey [29], or Sugimoto et al. [43], we argue, as an experimental fact, that there is no significant exchange integral for protons separated by $\approx$2.2 Å [17]. Neutron diffraction and spectroscopy show that protons in $KHCO_3$ are neither delocalized nor itinerant particles and there is no sizable energy band structure.

In quantum mechanics, normal coordinates (2) define nonlocal pseudoprotons ($m = 1$ amu), say $\mathscr{P}_{\mathrm{sjkl}}$ and $\mathscr{P}_{\mathrm{ajkl}}$, with an internal degree of freedom corresponding to symmetric or antisymmetric displacements of two "half-protons", respectively. Each dimer site is a superposition of two such half-protons. Obviously, pseudoprotons are totally alien to the intuitive conception of particles, based on classical mechanics, but they are the actual observables, whereas individual particles are not.

Consider now the sublattice of protons. The spatial periodicity leads to collective dynamics and nonlocal observables in three dimensions. With the vibrational wave function for the unit cell j, k, l, namely $\Xi_{0\mathrm{jkl}\tau} = \Theta_{0\mathrm{jkl}\tau} \pm \Theta_{0\mathrm{j'kl}\tau}$, where $\tau =$ "+" or "−", usual phonon waves can be written as

$$\Xi_{0\tau}(\mathbf{k}) = \frac{1}{\sqrt{\mathscr{N}}} \sum_{\mathrm{l}=1}^{\mathrm{N_c}} \sum_{\mathrm{k}=1}^{\mathrm{N_b}} \sum_{\mathrm{j}=1}^{\mathrm{N_a}} \Xi_{0\mathrm{jkl}\tau} \exp(\mathrm{i}\mathbf{k}\cdot\mathbf{L}), \tag{5}$$

where $\mathbf{k}$ is the wave vector and $\mathbf{L} = j\mathbf{a} + k\mathbf{b} + l\mathbf{c}$, with the unit cell vectors $\mathbf{a}$, $\mathbf{b}$, $\mathbf{c}$. This equation represents collective dynamics of H–H dimers thought of as composed bosons. This would be correct if the crystal was composed of indistinguishable dimer entities $(KHCO_3)_2$. However, neutron diffraction shows that the crystal structure is composed of $KHCO_3$ entities related to each other through the appropriate symmetry operations. The probability density of each atom is equally distributed over all equivalent sites and, conversely, the probability density at each site includes contributions from all indistinguishable atoms of the same kind. Consequently, the sublattice of protons must be thought of as a sublattice of nonlocal indistinguishable fermions and antisymmetrization of the plane waves (5) leads to

$$\mathbf{k}\cdot\mathbf{L} \equiv 0 \text{ modulo } 2\pi. \tag{6}$$

Consequently, there is no phonon (no elastic distortion) in the ground state and this symmetry-related "super-rigidity" [18] is totally independent of proton–proton interaction. Then, the lattice state vectors in three dimensions can be written as:

$$\begin{array}{l} |\Xi_{0+}(\mathbf{k}=\mathbf{0})\rangle \otimes |S\rangle; \\ |\Xi_{0-}(\mathbf{k}=\mathbf{0})\rangle \otimes |T\rangle. \end{array} \tag{7}$$

Each macroscopic state of the sublattice represents a nonlocal pseudoparticle with a mass $m = 1$ amu, namely a pseudoproton, $\mathscr{P}_a$ or $\mathscr{P}_s$, with a definite spin-symmetry and an occupation number of $(4\mathscr{N})^{-1}$ per site. There is no local information available for these entangled states and the wave functions $\Xi_{0\tau}(\mathbf{k}=\mathbf{0})$ represent collective oscillations of the super-rigid lattice as a whole with respect to the center of mass of the crystal. Finally, the ground state of the sublattice is a superposition of the pseudoproton states as:

$$\begin{array}{l} \sqrt{\mathscr{N}}|\Xi_{0+}(\mathbf{k}=\mathbf{0})\rangle \otimes |S\rangle; \\ \sqrt{\mathscr{N}}|\Xi_{0-}(\mathbf{k}=\mathbf{0})\rangle \otimes |T\rangle. \end{array} \tag{8}$$

This ground state is intrinsically steady against decoherence. Irradiation by plane waves (photons or neutrons) may single out some excited pseudoprotons. Entanglement in position and momentum is preserved, while the spin-symmetry and super-rigidity are destroyed. However, the spin-symmetry is reset automatically after decay to the ground state, presumably on the time-scale of proton dynamics. Consequently, disentanglement reaches a steady regime such that the amount of transitory disentangled states is determined by the ratio of the density-of-states for the surrounding atmosphere and external radiations, on the one hand, and for the crystal, on the other. This ratio is so small that disentangled states are too few to be observed, but they allow the super-rigid sublattice to be at thermal equilibrium with the surroundings, despite the lack of internal dynamics. The main source of disentanglement is actually the thermal population of excited proton states. However, even at room temperature, the thermal population of the first excited state ($<1\%$ for γOH $\approx$1000 cm^{-1}) is of little impact to effective measurements.

For the sublattice of bosons in the isomorph crystal of $KDCO_3$, (3) and (6) are not relevant. There is neither spin-symmetry nor super-rigidity. Dynamics are represented with normal coordinates (2) and phonons (5). Needless to say, the H and D atoms have the same number of 12 degrees of freedom per unit cell, but the symmetrization postulate shrinks the size of the allowed Hilbert space from $\sim 12^{\mathscr{N}}$ for bosons to $\sim 12\mathscr{N}$ for fermions.

5 Proton Dynamics

The interconversion degree at thermal equilibrium (Fig. 2) is determined by the potential function for protons. On the one hand, the bending modes do not play any significant role, since they show rather modest anharmonicity and the population

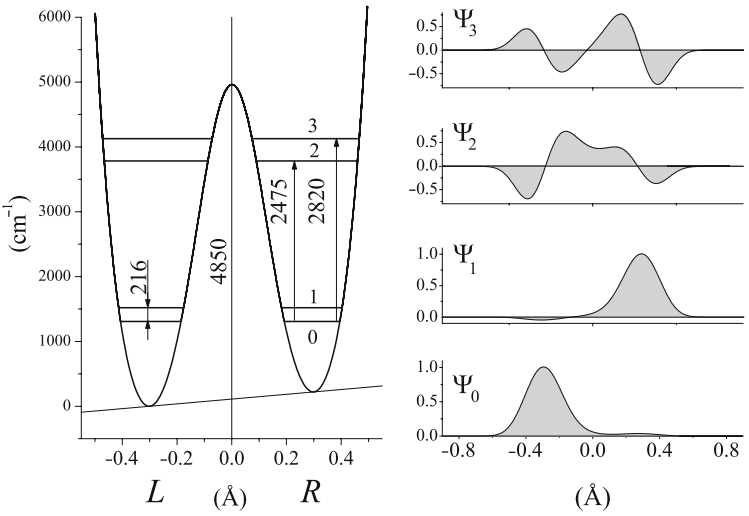

Fig. 3 Potential function and wave functions for the OH stretching mode along the hydrogen bond in the $KHCO_3$ crystal. $V(x) = 374x + 0.4389 \times 10^6 + 5516\ \exp(-30.8x^2)$. V and x are in cm^{-1} and Å units, respectively [13, 22]. The oscillator mass is 1 amu

of excited states is negligible. On the other hand, the double-wells for the OH stretching (Fig. 3) is known from experiments. The distance between minima ($2x_0 \approx 0.6$ Å) is given by the crystal structure. The upper states at $h\nu_{02}$ and $h\nu_{03}$ were determined from infrared and Raman band profiles [13,14], and the ground state splitting ($h\nu_{01}$) was observed with incoherent inelastic neutron scattering (IINS) [22, 26]. The potential obtained through best fitting exercises is over determined and largely model independent. In addition, the oscillator mass of 1 amu is not a free parameter. It is determined by $2x_0$ for a given set of energy levels.

For the $|0\rangle$ and $|1\rangle$ states, the potential asymmetry leads to substantial localization of the wave functions in the lower and upper wells, respectively. However, tunneling is possible through the tiny delocalized fraction ($\varepsilon \approx 0.05$) visible in Fig. 3.

This potential has been a puzzle ever since it was determined because the upper minimum was naively thought of as corresponding to the transfer of a proton. However, this is unlikely, for this would lead to unrealistic dimers composed of di-protonated (H_2CO_3) and non-protonated (CO_3^{2-}) entities [20]. Such entities are ruled out by the centrosymmetric character of proton dynamics established by the symmetry-related selection-rules observed in the infrared and Raman [36]. It is now clear that, if pseudoprotons are *the* observables, this nonlocal potential accounts for pseudoproton dynamics along x_a or x_s. The $|0\rangle \longleftrightarrow |1\rangle$ transition corresponds to the through-barrier transfer (tunneling) of a pseudoproton as a rigid entity, with no energy transfer to the internal degree of freedom. The IINS bandwidth, very close to the spectrometer resolution [22], shows that this transition is virtually dispersion-free and there is no visible splitting suggesting any difference for the

transfer of $\mathscr{P}_a$ or $\mathscr{P}_s$ [22, 26]. On the other hand, the upper states $|2\rangle$ and $|3\rangle$ correspond to excitations of internal stretching coordinates, ν_a (infrared) or ν_s (Raman). They are slightly different, but this is unimportant for interconversion since thermal populations are strictly negligible for these states.

The interconversion dynamics involving $\mathscr{P}_a$ and $\mathscr{P}_s$ can be rationalized with the potential surface along coordinates x_a and $x'_s = x_s \pm \sqrt{2}x_0$:

$$\mathscr{V}(x_a, x'_s) = V(x_a) + V(x'_s). \tag{9}$$

The energy level scheme comprises three states at 0, $h\nu_{01}$ (with twofold degeneracy) and $2h\nu_{01}$. The non-symmetrized local wave functions (Fig. 4) are simple product of the local wave functions in one dimension (Fig. 3). Proton configurations

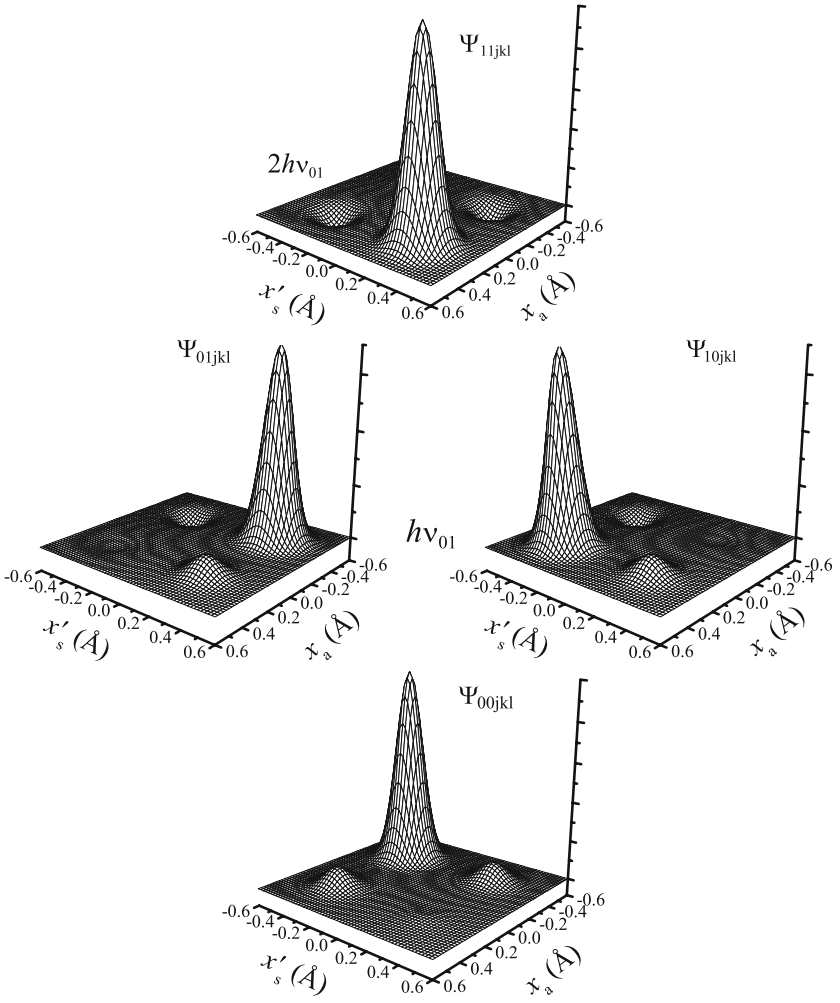

Fig. 4 Schematic view of the tunneling wave functions. For the sake of clarity, the weak component of the wave function in one dimension is multiplied by a factor of 2

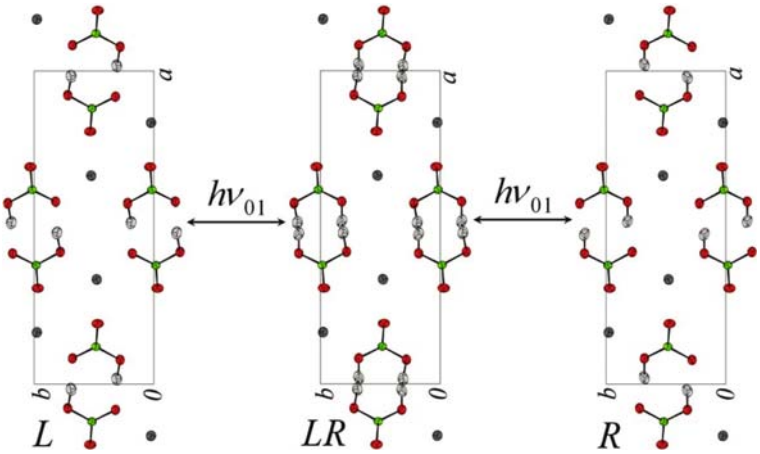

Fig. 5 Schematic view of proton configurations for the tunnelling states. In the ground state *LL* and in the upper state *RR* at $2h\nu_{01}$, protons are fully entangled. In the intermediate state *LR* (or *RL*) at $h\nu_{01}$ all proton sites are equally occupied. The spin symmetry and the super-rigidity are destroyed

for the three states are tentatively sketched in Fig. 5. The ground state corresponds to the structure observed at low temperature, with both $\mathscr{P}_a$ and $\mathscr{P}_s$ in the *L* configuration. The antisymmetrized macroscopic state analogous to (7), namely $|0+\rangle|S\rangle|0-\rangle|T\rangle$, can be obtained via (3) to (6). Similarly, the upper state vector at $2h\nu_{01}$ with both pseudoprotons in the *R* configuration is $|1+\rangle|S\rangle|1-\rangle|T\rangle$. In the intermediate state at $h\nu_{01}$, only one pseudoproton (either $\mathscr{P}_a$ or $\mathscr{P}_s$) is transferred to the *R* configuration, so the spin-symmetry and the super-rigidity are destroyed. Then, plane waves (5) lead to state vectors $|1+,0-,\mathbf{k}_{10}\rangle$ and $|0+,1-,\mathbf{k}_{01}\rangle$. Note that the $|0\rangle \longleftrightarrow |1\rangle$ transition is effectively observed with IINS, thanks to energy and momentum transfer, whereas the $|0\rangle \longleftrightarrow |2\rangle$ transition cannot be probed directly, according to the quantum theory of measurements.

The proton transfer degree calculated supposing the three levels at thermal equilibrium is

$$\rho(T) = [p_{01}(T) + 2p_{01}^2(T)][1 + p_{01}(T) + p_{01}(T)^2]^{-1}, \tag{10}$$

where $p_{01}(T) = \exp(-h\nu_{01}/kT)$ is the probability for the transfer of a pseudoproton. The dashed line in Fig. 6 clearly shows that this equation is at variance with observations.

In fact, owing to the adiabatic separation of proton dynamics, energy exchange with the surroundings occurs exclusively via photons, with the momentum conservation rule $\mathbf{k}_{10} + \mathbf{k}_{01} \equiv \mathbf{0}$. Consequently, re-entanglement occurs spontaneously in the intermediate state as

$$|1+,0-,\mathbf{k}_{10}\rangle + |0+,1-,\mathbf{k}_{01}\rangle = 2^{-1/2}[|0+\rangle|S\rangle|0-\rangle|T\rangle + |1+\rangle|S\rangle|1-\rangle|T\rangle] \tag{11}$$

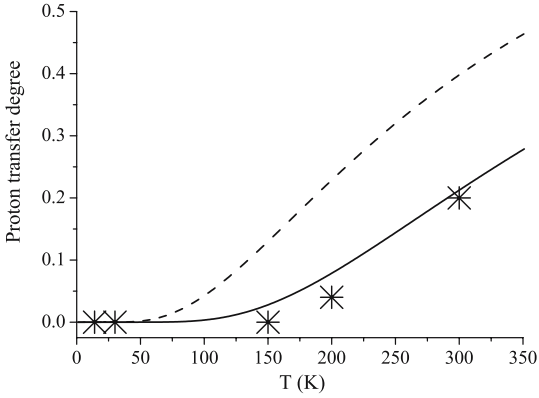

Fig. 6 Temperature effect on the proton transfer degree in the $KHCO_3$ crystal. *Stars*: experimental according to [18]. *Solid line*: Eq. (12) for two-levels. *Dashed line*: Eq. (10) for three-levels

and the transfer degree

$$\rho(T) = 2p_{01}^2(T)[1 + p_{01}^2(T)]^{-1}, \tag{12}$$

is in reasonably good agreement with measurements (see the solid line in Fig. 6). The energy difference of $2h\nu_{01}$ between *RR* and *LL* configurations is therefore confirmed and Fig. 6 is an indirect evidence that the degenerate intermediate state observed with IINS is not thermodynamically stable, thanks to the purely quantum re-entanglement mechanism (11).

However, the interpretation of Bragg diffraction is ambiguous because the *LL* and *RR* configurations of the proton sublattice are crystallographically equivalent, as they are related through a translation vector $(a/2, b/2, 0)$ (see Fig. 5). The reciprocal lattices are identical and it is unknown whether neutrons were diffracted by either sublattice, with probability $1-\rho$ and ρ, respectively, or by a superposition state, $(1-\rho)^{1/2}|0+\rangle|S\rangle|0-\rangle|T\rangle + \rho^{1/2}|1+\rangle|S\rangle|1-\rangle|T\rangle$. The former case is a mixture of *LL* and *RR* configurations analogous to disorder under consideration in many crystallographic [27, 45, 46], solid-state NMR [5, 39] and QENS [11] works. Alternatively, a superposition should give rise to quantum interferences corresponding to coherent fluctuations of the probability density at proton sites.

6 Probing Quantum Entanglement with Neutrons

Neutrons (spin $1/2$) are unique to observing the spin-symmetry of macroscopic states (7). However, quantum entanglement is extremely fragile, because it is not stabilized by any energy. Consequently, only "noninvasive" experiments, free of measurement-induced decoherence, are appropriate [34]. For neutron scattering, this means (i) no energy transfer (ii) no spin-flip and (iii) particular values of the neutron momentum transfer vector $\mathbf{Q}$ preserving the super-rigidity.

(By definition, $\mathbf{Q} = \mathbf{k}_i - \mathbf{k}_f$, where $\mathbf{k}_i$ and $\mathbf{k}_f$ are the initial and final wave vectors, respectively.)

The dotted lines in Fig. 1 enhance the network of double-lines of proton sites in dimer planes. We present below neutron scattering experiments for (i) double-lines of protons, (ii) arrays of double-lines in two dimensions, and (iii) the sublattice in three dimensions. For the sake of simplicity, it should be born in mind that elastic scattering events are identical for *LL* and *RR* configurations and, therefore, independent of the interconversion degree.

6.1 Double-Lines of Entangled Protons

Consider an incoherent elastic neutron scattering (IENS) experiment conducted with: (i) the best resolution in energy, in order to reject inelastic scattering events, (ii) a modest resolution in **Q**, so Bragg peaks merge into a continuum and long-range correlations are overlooked. For momentum transfer Q_α along α, the scattering function for an entangled pair (4) can be written as:

$$\begin{aligned} &S_{\tau_i\tau_f}(Q_\alpha,\omega_\alpha) = \sum_{\tau_f}\sum_{\tau_i} \\ &|\langle 0jkl\tau_i|\exp iQ_\alpha\left(\alpha_{2jkl}-\alpha_{0jkl}\right)+\tau_i\tau_f\exp iQ_\alpha\left(\alpha_{2jkl}+\alpha_{0jkl}\right)|0jkl\tau_f\rangle \\ &\times\langle 0jkl\tau_f|\exp iQ_\alpha\left(\alpha_{1jkl}-\alpha_{0jkl}\right)+\tau_f\tau_i\exp iQ_\alpha\left(\alpha_{1jkl}+\alpha_{0jkl}\right)|0jkl\tau_i\rangle|^2 \\ &\times\exp(-2W_{L\alpha})\delta(\omega_\alpha). \end{aligned} \tag{13}$$

Each bracket represents a scattering event by a pseudoproton located at both sites ($\pm\alpha_{0jkl}$). The product of two brackets means that each neutron is scattered simultaneously by the two pseudoprotons superposed at the same sites, either in-phase, $|\pm\rangle \longleftrightarrow |\pm\rangle$ ($\tau_f\tau_i = +1$), or anti-phase, $|\pm\rangle \longleftrightarrow |\mp\rangle$ ($\tau_f\tau_i = -1$). The spin-symmetry is probed along the neutron-spin direction with 100% probability and there is no spin-flip because the initial and final states are $|0jkl\tau_i\rangle$ and $|0jkl\tau_f\rangle$, respectively, for one scattering event and vice-versa for the other one. Thanks to adiabatic separation, the lattice Debye-Waller factor $\exp(-2W_{L\alpha})$ can be factored. The energy transfer is $\hbar\omega_\alpha$ and $\delta(\omega_\alpha)$ accounts for energy conservation. In the harmonic approximation, the scattering function is [15, 24]

$$\begin{aligned} &S_{\pm\pm}(Q_\alpha,\omega_\alpha) = \\ &\cos^4(Q_\alpha\alpha_0)\left[\exp-\frac{Q_\alpha^2u_{0\alpha}^2}{\sqrt{1+4\lambda_\alpha}}+\exp-Q_\alpha^2u_{0\alpha}^2\right]\exp(-2W_{L\alpha})\delta(\omega_\alpha), \\ &S_{\pm\mp}(Q_\alpha,\omega_\alpha) = \\ &\sin^4(Q_\alpha\alpha_0)\exp\left[-Q_\alpha^2\left(\frac{u_{0\alpha}^2}{2\sqrt{1+4\lambda_\alpha}}+\frac{u_{0\alpha}^2}{2}\right)\right]\exp(-2W_{L\alpha})\delta(\omega_\alpha). \end{aligned} \tag{14}$$

Here, $u_{0\alpha}^2 = \hbar/(2m\omega_{0\alpha})$ is the mean square amplitude for uncoupled harmonic oscillators in the ground state. The intensity is proportional to the incoherent nuclear

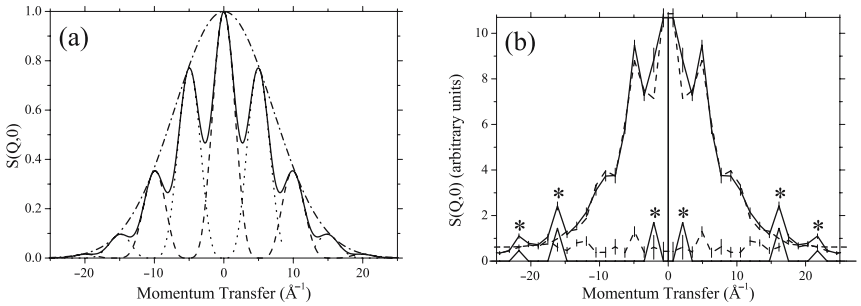

Fig. 7 (**a**): Comparison of the theoretical profiles $S(Q,0)$ for a non-entangled pair (*dot-dashed*), and for an entangled pair of fermions, according to (11) (*solid line*). The *doted* and *dashed* curves represent interference fringes for in-phase and out-of-phase scattering. (**b**): $S(Q_y,0)$ measured at 20 K for a single-crystal of $KHCO_3$ (*solid curve with error bars*). Comparison with the best fit (*dashed line*) obtained with (14) convoluted with a triangular resolution function. The *dashed line with error bars* is the difference spectrum. *: Triangular functions due to other scattering events

cross-section for protons, $\sigma_{\mathrm{Hi}} \approx 80.26$ b (1 barn $= 10^{-24}$ cm^2), and the gaussian-like profiles for uncorrelated scatterers are modulated by $\cos^4(Q_\alpha \alpha_0)$ and $\sin^4(Q_\alpha \alpha_0)$ (Fig. 7a).

Such interference fringes were effectively observed with the MARI spectrometer [1] at the ISIS pulsed-neutron source (Fig. 7b) [24]. Best fit exercises yield α_0-values in reasonable accordance with the crystal structure and the estimated oscillator mass is virtually equal to 1 amu. These experiments are positive evidences of pseudoproton states with spin-symmetry (4).

In fact, neutron plane waves are scattered coherently by double-lines of entangled pairs perpendicular to Q_α, which are reminiscent of Young's double-slits. However, the interference fringes (14) are clearly different from those anticipated for distinguishable (classical) double-slits, which should be proportional to $\cos^2(Q_\alpha \alpha_0)$ [10, 48, 49]. Equation (14) is also at variance with the scattering function for protons delocalized in a symmetric double-wells. In this case, there is no definite spin-symmetry for the tunneling states $|0+\rangle$ (ground state) and $|0-\rangle$ (at $\hbar\omega_{\mathrm{t}}$). The scattering functions for elastic scattering $|0\pm\rangle \longleftrightarrow |0\pm\rangle$ and inelastic scattering $|0\pm\rangle \longleftrightarrow |0\mp\rangle$ are

$$\begin{aligned} S_{\pm\pm}(Q_\alpha, \omega_\alpha) &= \cos^2(Q_\alpha \alpha_0) \exp\left(-Q_\alpha^2 u_{0\alpha}^2 - 2W_{\mathrm{L}\alpha}\right) \delta(\omega_\alpha), \\ S_{\pm\mp}(Q_\alpha, \omega_\alpha) &= \sin^2(Q_\alpha \alpha_0) \exp\left(-Q_\alpha^2 u_{0\alpha}^2 - 2W_{\mathrm{L}\alpha}\right) \delta(\omega_\alpha - \omega_{\mathrm{t}}). \end{aligned} \tag{15}$$

Then, interferences evidence that a single proton is located in two wells. They are visible if the instrument can effectively resolve the tunnel splitting. Otherwise, complementary fringes would merge into the gaussian profile anticipated for a single-well.

Clearly, scattering by a superposition of entangled double-lines with spin correlations cannot be confused with other double-slits experiments. The fringes are evidences of nonlocal pseudoprotons and there is no means whatever to probe the local particle behavior.

Since (13) and (14) hold in the same way for *LL* and *RR* configurations, interferences are independent of the interconversion degree. However, at elevated temperatures, the intensity at large Q_α-values is depressed by the lattice Debye-Waller factor and fringes are less visible.

Needless to say, interferences are neither expected, nor observed, for $KDCO_3$ [24].

6.2 Diffraction

A necessary condition for noninvasive neutron diffraction is that Q_x, Q_y, Q_z, should match a node of the reciprocal sublattice of protons, so neutrons probe super-rigid states without any induced distortion. The only information conveyed by such events is the perfect periodicity of the sublattice, so the Debye-Waller factor is equal to unity at any temperature. In addition, thanks to the spin-symmetry, the scattered intensity is proportional to the total cross-section $\sigma_H \approx 82.0$ b [18, 35]. Otherwise, the spin-symmetry is destroyed, so the intensity scattered by protons is proportional to the coherent cross-section $\sigma_{Hc} \approx 1.76$ b and to the Debye-Waller factor for non-rigid lattices. The enhancement factor $\sigma_H/\sigma_{Hc} \approx 45$ is quite favorable to observing quantum correlations. Furthermore, the intensity scattered by the sublattice of heavy atoms, proportional to $\sigma_{cKCO_3} \approx 27.7$ b, is depressed by the Debye-Waller factor $\exp -2W_{KCO_3}(\mathbf{Q})$. Therefore, the contribution of heavy atoms at large $\mathbf{Q}$-values is rather weak, compared to that of the entangled sublattice, especially at elevated temperatures.

The dashed lines in Fig. 1 show that proton sites are aligned along x and y, but not along z. Consequently, the noninvasive condition can be realized for Q_x and Q_y exclusively, whereas Q_z never coincides with a node of the reciprocal lattice of protons. Then, the diffraction pattern depends on whether we consider incoherent or coherent scattering along Q_z.

6.2.1 Super-Rigid Arrays in Two Dimensions

Consider diffraction by super-rigid arrays in (103) planes and incoherent scattering along Q_z. In the unit cell, there are two indistinguishable double-lines parallel to y, so the periodicity of the grating-like structure is $D_x/2$, with $D_x \approx a/\cos 42^\circ \approx 20.39$ Å. On the other hand, the spatial periodicity of double-lines parallel to x is $D_y = b$. The differential cross-section for a superposition of pseudoproton states (7) can be then written as

$$\frac{d\sigma_2}{d\Omega} \propto \sum_{l=1}^{N_c} \sum_{\tau_i} \sum_{\tau_f} \left| \sum_{j=1}^{N'_a} \sum_{k=1}^{N_b} \left\{ \left[\exp iQ_y \left(kD_y - y_0 \right) + \tau_i \tau_f \exp iQ_y \left(kD_y + y_0 \right) \right] \right. \right.$$
$$\left. \left. \times \left[\exp iQ_x \left(jD_x/2 - x_0 \right) + \tau_i \tau_f \exp iQ_x \left(jD_x/2 + x_0 \right) \right] \right\}^2 \right|^2 \exp -2W_z(Q_z), \tag{16}$$

with $N'_a = 2N_a$. Neutrons are scattered either in-phase ($\tau_f\tau_i = +1$) or anti-phase ($\tau_f\tau_i = -1$) by orthogonal pairs of lines separated by $2x_0 \approx 0.6$ Å and $2y_0 \approx 2.2$ Å, respectively. The phase matching condition, namely x_0 (y_0) commensurable with $D_x/2$ (D_y), is intrinsic to the crystal structure. $\{\cdots\}^2$ accounts for simultaneous scattering by the superposed pseudoproton states, without neutron-spin flip. The compound Debye-Waller factor $\exp -2W_z(Q_z)$, including contributions from all atoms, corresponds to incoherent scattering along Q_z. The permutation $x_0 \longleftrightarrow -x_0, y_0 \longleftrightarrow -y_0$ gives the same equation for *RR* and *LL* configurations.

The diffraction pattern is composed of rods of diffuse scattering parallel to Q_z, cigar-like shaped by the Debye-Waller factor, at Q_x, Q_y-values corresponding to divergences of (16). Such divergences occur at $Q_y = n_y\pi/y_0 \approx n_y \times 2.86$ Å^{-1} (Table 1), since $Q_yD_y/\pi \approx 5n_y$ is integer. Contrariwise, there is no divergence for anti-phase scattering at $Q_y = \pm(n_y + 1/2)\pi/y_0$, because $Q_yD_y/\pi \approx 5(n_y + 1/2)$ is not integer. For n_y even, Q_yD_y/π is also even, $\tau_i = \tau_f$, and ridges are anticipated at $Q_x = n_x\pi/x_0 \approx n_x \times 10$ Å^{-1}, since $Q_xD_x/\pi \approx 68n_x$ is even. Alternatively, for n_y odd, Q_yD_y/π is also odd, $\tau_i \neq \tau_f$, and ridges are anticipated at $Q_x = (n_x + 1/2)\pi/x_0$, since $Q_xD_x/\pi \approx 68(n_x + 1/2)$ is even.

The cigar-like shaped rods were effectively observed with the SXD [2,28] instrument at the ISIS pulsed neutron source (Figs. 8–10). For $k = 0$, they appear at $Q_x = 0$ and $\pm(10.00 \pm 0.25)$ Å^{-1}, in accordance with $2x_0 \approx 0.6$ Å. For $k = 1$, they are barely visible. For $k = 2$ or 3, we observe ridges at $Q_x = \pm(5 \pm 0.2)$ and $\pm(15 \pm 0.2)$ Å^{-1}, still along Q_z. These features are best visible in Fig. 9 for $k = 2.6$, in accordance with Table 1. There is no visible ridge at $k = 4$. Then, from $k = 5$ – 9, we observe in Fig. 8 the same sequence as for $k = 0$ – 4, and rods at $k = 7.7$ in Fig. 9.

Similar diffuse scattering was observed at low temperature in the $k = 0$ plane, at 14 K [19] and 30 K [18] (Fig. 10). As anticipated, the rods are unaffected by the interconversion degree. However, at low temperatures, they are partially hidden by the anisotropic diffuse intensity, centered at $\mathbf{Q} = \mathbf{0}$, due to elastic and inelastic incoherent scattering by protons. This continuum precludes observation of the ridges

Table 1 Orders n_y, n_x, and positions Q_y, Q_x, of rods of intensity arising from the entangled array of orthogonal doubles lines of protons in two dimensions. Obs. Q_x: positions in Å^{-1} of the observed rods of intensity along Q_z in Figs. 8 and 9. Q_yD_y/π is rounded to integers

n_y	Q_y (Å^{-1})	Q_yD_y/π	$\tau_i\tau_f$	$k = Q_y/b^*$	Q_x	Obs. Q_x (Å^{-1})
0	0	0	+1	0	$n_x\pi/x_0$	$0, \pm 10$
1	2.86	5	−1	2.57	$(n_x + 1/2)\pi/x_0$	$\pm 5, \pm 15$
2	5.71	10	+1	5.14	$n_x\pi/x_0$	$0, \pm 10$
3	8.57	15	−1	7.71	$(n_x + 1/2)\pi/x_0$	$\pm 5, \pm 15$

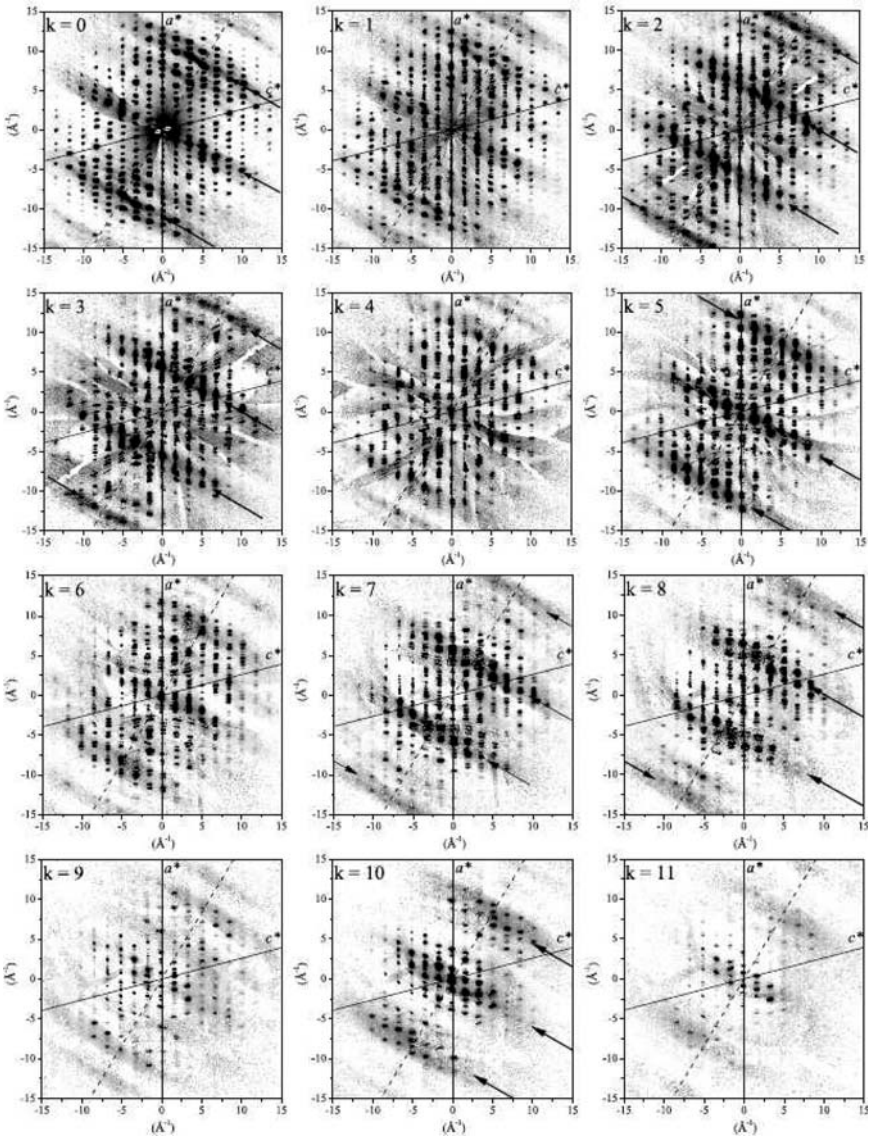

Fig. 8 Cuts of the diffraction pattern of $KHCO_3$ at 300 K in various (a^*, c^*) planes. The arrows emphasize ridges of intensity parallel to Q_z and perpendicular to dimer planes (dash lines along Q_x)

at ± 5 Å^{-1} for $2 \leq k \leq 3$. Quite paradoxically, quantum correlations are best visible at elevated temperatures.

As anticipated from Sect. 4, the same experiments performed with a crystal of $KDCO_3$ do not evidence any cigar-like shaped ridge of enhanced intensity, in addition to regular Bragg peaks, for the sublattice of bosons [19].

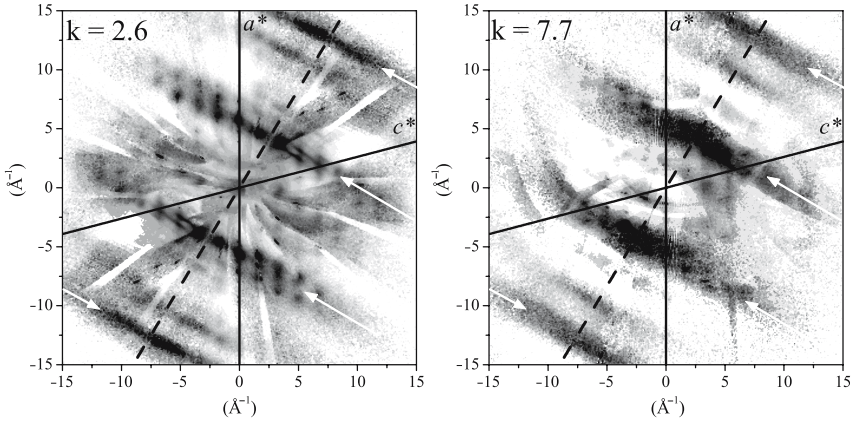

Fig. 9 Diffuse scattering of $KHCO_3$ at 300 K in between (a^*, c^*) reciprocal planes. The arrows emphasize ridges of intensity parallel to Q_z and perpendicular to dimer planes (dashed lines along Q_x)

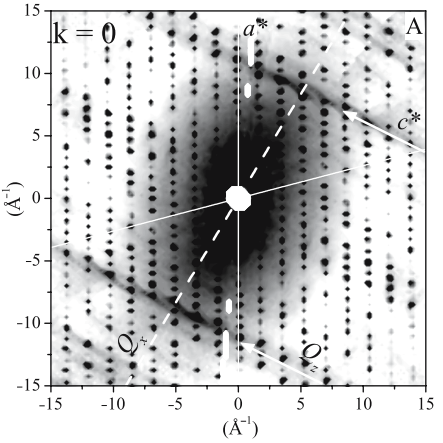

Fig. 10 Diffraction pattern of $KHCO_3$ at 30 K in the (a^*, c^*) reciprocal plane at $k = 0$. The arrows emphasize ridges of intensity parallel to Q_z and perpendicular to dimer planes (dash lines along Q_x)

6.2.2 Super-Rigid Arrays in Three Dimensions

From (16), the differential cross-section for the *LL* or *RR* pseudoproton states is written as

$$\frac{d\sigma_3}{d\Omega} \propto \sum_{\tau_i}\sum_{\tau_f}\left|\sum_{j=1}^{N'_a}\sum_{k=1}^{N_b}\sum_{l=1}^{N_c}\left\{\left[\exp iQ_y\left(kD_y - y_0\right) + \tau_i\tau_f \exp iQ_y\left(kD_y + y_0\right)\right]\right.\right.$$
$$\left.\left.\times\ \left[\exp iQ_x\left(jD_x/2 - x_0\right) + \tau_i\tau_f \exp iQ_x\left(jD_x/2 + x_0\right)\right]\exp iQ_z lD_z\right\}\right|^2 \quad (17)$$

This equation describes no spin-flip scattering events that do not destroy the spin-symmetry. Divergences occur along the previous rods of intensity at $Q_z = \pm n_z 2\pi/D_z$, with $D_z \approx c \times \cos 28^\circ \approx 3.28$ Å and $2\pi/D_z \approx 1.92$ Å^{-1}. These enhanced peaks are visible in Figs. 8–10, even at rather large Q_z-values, thanks to super-rigidity. At elevated temperatures, they clearly emerge from the rods of diffuse scattering (16) depressed by the Debye-Waller factor. These enhanced peaks were not observed for the deuterated crystal [19].

Experiments presented above, in this present section, are clearly consistent with pseudoprotons forming decoherence-free macroscopic single-particle states with spin-symmetry. The underlying theoretical framework presented in Sect. 4 is based on fundamental laws of quantum mechanics. There is no ad hoc hypothesis or parameter. The adiabatic separation, clearly validated by observations, can be regarded as an intrinsic property of hydrogen bonds in this crystal.

7 Quantum Interferences

Superposition of decoherence-free proton states must lead to quantum interferences, or quantum beats. The non-antisymmetrized wave functions for the states $|0\rangle$ and $|1\rangle$ (Fig. 3) can be written as [20]:

$$\begin{aligned} \Psi_{0\mathrm{jkl}} &= \quad \cos\phi\ \psi_0(x-x_\mathrm{m}) + \sin\phi\ \psi_0(x+x_\mathrm{m}); \\ \Psi_{1\mathrm{jkl}} &= -\sin\phi\ \psi_0(x-x_\mathrm{m}) + \cos\phi\ \psi_0(x+x_\mathrm{m}); \end{aligned} \tag{18}$$

where x stands for x_a or x'_s and $\psi_0(x \pm x_\mathrm{m})$ are harmonic eigen functions for the second-order expansion of the potential around the minima at $\pm x_\mathrm{m}$; $\tan 2\phi = \nu_{0\mathrm{t}}/(\nu_{01} - \nu_{0\mathrm{t}})$, where $h\nu_{0\mathrm{t}} \approx 18$ cm^{-1} is the tunnel splitting for the symmetric potential. Then, $\cos\phi \approx 1$ and $\sin\phi = \varepsilon \approx 5 \times 10^{-2}$. Superposition leads to harmonic oscillations of the probability density at the beating frequency $\nu_{0\mathrm{b}} = 8\varepsilon\nu_{01} \approx 4\nu_{0\mathrm{t}} \approx 2.5 \times 10^{12}$, in proton per second units (H s^{-1}) [8, 16, 20].

The $LL \longleftrightarrow RR$ fluctuation rate can be rationalized with two distinct mechanisms, either single-step or two-stepwise (Fig. 4). The single-step mechanism corresponds to superposition of the states at 0 and $2h\nu_{01}$, corresponding to *LL* and *RR* configurations (Fig. 5), respectively. The interconversion rate due to quantum beats is:

$$\nu_{1\mathrm{b}} = 2\varepsilon\nu_{0\mathrm{b}} \exp(-2h\nu_{01}/kT). \tag{19}$$

For the two-stepwise process, firstly, either $\mathscr{P}_\mathrm{a}$ or $\mathscr{P}_\mathrm{s}$ is transferred at $\mathbf{k} = \mathbf{0}$ to the *LR* configuration (Fig. 5) with probability $\exp(-h\nu_{01}/kT)$. Secondly, this state undergoes fast re-entanglement (11) leading to the upper state (configuration *RR*) with probability $\exp(-2h\nu_{01}/kT)$. The interconversion rate is then

$$\nu_{2\mathrm{b}} = 2\nu_{0\mathrm{b}} \exp(-3h\nu_{01}/kT). \tag{20}$$

These theoretical rates must be compared to QENS measurements of a $KHCO_3$ crystal, from 200 to 400 K [11]. The scattering geometry ($\mathbf{Q} \parallel x$) was selected in order to probe proton dynamics specifically along the hydrogen bonds. The inverse relaxation time (or attempt frequency), $\tau_0^{-1} = 2 \times 10^{12} \mathrm{s}^{-1}$, is sufficiently close to $\nu_{0\mathrm{b}}$ to suggest that (i) QENS and vibrational spectroscopy techniques probe the same dynamics and, (ii) the two-stepwise mechanism (20) is prevailing, in accordance with the larger pre-factor. In addition, the measured rate follows an Arrhenius law with an activation energy $E_\mathrm{a} = (336 \pm 32)\ \mathrm{cm}^{-1}$ significantly different from $3h\nu_{01} \approx 648\ \mathrm{cm}^{-1}$. In fact, (20) accounts for coherent fluctuations of two pseudoprotons, with probability $\exp(-3h\nu_{01}/kT)$, and pre-factor $2\nu_{0\mathrm{b}}$, while QENS probes the fluctuation rate of a pseudoproton with probability $\exp(-3h\nu_{01}/2kT)$, and pre-factor $\nu_{0\mathrm{b}}$. Hence, $3h\nu_{01}/2 = 324\ \mathrm{cm}^{-1}$ accords with E_a. It transpires that the QENS technique is an incoherent probe of coherent oscillations of the proton probability, because neutrons are plane waves, rather than a particle-like probe of incoherent stochastic jumps [11].

In fact, semiclassical models [5, 11, 41] are based on inappropriate premises. (i) The potential asymmetry supposedly due to static effects of neighbouring dimers should be temperature dependent. This is at variance with the interconversion degree (12) and Fig. 6. (ii) Coupling to phonons is posited to be necessary to mediate the through-barrier proton transfer at low temperatures. This is not relevant within the framework of the adiabatic separation. (iii) A smooth transition to the Arrhenius behaviour of classical jumps is supposed to occur at elevated temperatures. Contrariwise, neutron diffraction shows that there is no transition to the classical regime (Figs. 8–10). In addition, (19) and (20) show that an Arrhenius behavior is not necessarily an evidence of the semiclassical regime. Logically, these incorrect premises lead to confusing the activation energy E_a with the potential barrier [11].

8 Conclusion

It is often argued that a complex system in continuous interaction with its environment should be in a significantly mixed state that cannot be represented by a state vector. In marked contrast to this widespread opinion, we have accumulated consistent experimental evidences that the sublattice of protons can be represented by a state vector at any temperature up to 300 K. This macroscopic object exhibits all features of quantum mechanics: nonlocality, entanglement, superposition and quantum interferences. There is no transition to the classical regime because the plane waves of the thermal bath cannot destroy entanglement intrinsic to the lattice periodicity. The spin-symmetry of proton states can be transitorily destroyed but the decoherence degree is insignificant because the density-of-states of the surroundings is negligible compared to that of the crystal.

The cornerstones of the theoretical framework are: (i) adiabatic separation; (ii) the fermionic nature of protons; (iii) indistinguishability and degeneracy. There is no ad hoc hypothesis or parameter. Entanglement is intrinsic to the crystal

symmetry, irrespective of the strength of proton–proton interactions. Dynamics is rationalized with pseudoprotons forming macroscopic single-particle states with remarkable spin-symmetry and super-rigidity. These quantum correlations are effectively probed with neutrons and quantum interferences arising from entangled double-lines or long-range correlations in three dimensions emphasize that protons in the crystal field are not individual particles possessing properties on their own right. Collective dynamics suggest that the whole crystal should be conceived of as a matter field that is a superposition of macroscopic single-pseudoparticle states. In addition, super-rigidity adds a new item, along with superfluidity and superconductivity, to the list of quantum "super" properties in the condensed matter.

The interconversion degree at thermal equilibrium is consistent with the double-well potentials for pseudoprotons determined from vibrational spectra and quantum beats accord with QENS measurements of the fluctuation rate. The double-wells for protons is invariant over the whole range of timescales from νOH vibrations ($\sim 10^{-15}$ s) to diffraction, through QENS, and at any temperature.

This review emphasizes that the dichotomy of semiclassical protons in a quantum crystal lattice should be abandoned. There is every reasons to suppose that this conclusion holds for many hydrogen bonded crystals and macroscopic quantum behaviors open up new vistas for further investigations.

References

1. http://www.isis.rl.ac.uk/excitations/mari/
2. http://www.isis.rl.ac.uk/crystallography
3. Benderskii, V.A., Vetoshkin, E.V., Irgibaeva, I.S., Trommsdorff, H.P.: Tunneling splittings in vibrational spectra of non-rigid molecules: IX. malonaldehyde and its isotopomers as a test case for fully coupled multidimensional tunneling dynamics. Chem. Phys. **262**, 393–422 (2000)
4. Benderskii, V.A., Vetoshkin, E.V., Trommdorff, H.P.: Tunneling splittings in vibrational spectra of non-rigid molecules. X. Reaction path Hamiltonian as zero-order approximation. Chem. Phys. **271**, 165–182 (2001)
5. Benz, S., Haeberlen, U., Tegenfeldt, J.: Jump motion of deuterons along hydrogen bonds in $KDCO_3$. A deuteron relaxation study. J. Mag. Res. **66**, 125–134 (1986)
6. Bohr, N.: The quantum postulate and recent developments of quantum theory. Nature **121**, 580 (1928)
7. Caldeira, A.O., Leggett, A.J.: Quantum tunnelling in a dissipative system. Ann. Phys. **149**, 374–456 (1983)
8. Cohen-Tannoudji, C., Diu, B., Laloë, F.: Mécanique Quantique. Hermann, Paris, France (1977)
9. Cowley, R.A.: Quantum entanglement and neutron scattering experiments. J. Phys.: Condens. Matter **15**, 4143–4152 (2003)
10. Dürr, S., Nonn, T., Rempe, G.: Origin of quantum-mechanical complementarity probed by "which-way" experiment in an atom interferometer. Nature **395**, 33–37 (1998)
11. Eckold, G., Grimm, H., Stein-Arsic, M.: Proton disorder and phase transition in $KHCO_3$. Physica B **180–181**, 336–338 (1992)
12. Einstein, A., Podolsky, B., Rosen, N.: Can quantum-mechanical description of physical reality be considered complete? Phys. Rev. **47**, 777–780 (1935)

13. Fillaux, F.: Calculation of infrared and raman band profiles of strong hydrogen bonds. OH stretching band and proton dynamics in crystalline potassium hydrogen carbonate. Chem. Phys. **74**, 405–412 (1983)
14. Fillaux, F.: Theoretical model for calculation of infrared and raman band profiles of strong hydrogen bonds in ordered media. Chem. Phys. **74**, 395–404 (1983)
15. Fillaux, F.: The pauli principle and the vibrational dynamics of protons in solids: A new spin-related symmetry. Physica D **113**, 172 (1998)
16. Fillaux, F.: Proton transfer in the $KHCO_3$ and benzoic acid crystals: A quantum view. J. Mol. Struct. **844–845** (2007)
17. Fillaux, F., Cousson, A.: Comment on "quantum correlations between protons in potassium bicarbonate". J. Phys.: Cond. Matter **16**, 1007–1010 (2004)
18. Fillaux, F., Cousson, A., Gutmann, M.J.: Macroscopic quantum entanglement and "super-rigidity" of protons in the $KHCO_3$ crystal from 30 to 300 K. J. Phys.: Cond. Matter **18**, 3229–3249 (2006)
19. Fillaux, F., Cousson, A., Keen, D.: Observation of the dynamical structure arising from spatially extended quantum entanglement and long-lived quantum coherence in the $KHCO_3$ crystal. Phys. Rev. B **67**, 054301 and 189901(E) (2003)
20. Fillaux, F., Limage, M.H., Romain, F.: Quantum proton transfer and interconversion in the benzoic acid crystal: vibrational spectra, mechanism and theory. Chem. Phys. **276**, 181–210 (2002)
21. Fillaux, F., Romain, F., Limage, M.H., Leygue, N.: Extended tunnelling states in the benzoic acid crystal: Infrared and raman spectra of the OH and OD stretching modes. Phys. Chem. Chem. Phys. **8**, 4327–4336 (2006)
22. Fillaux, F., Tomkinson, J., Penfold, J.: Proton dynamics in the hydrogen bond. the inelastic neutron scattering spectrum of potassium hydrogen carbonate at 5 K. Chem. Phys. **124**(3), 425–437 (1988)
23. Giese, K., Petrović, M., Naundorf, H., Kühn, O.: Multidimensional quantum dynamics and infrared spectroscopy of hydrogen bonds. Phys. Rep. **430**, 211–276 (2006)
24. Ikeda, S., Fillaux, F.: Incoherent-elastic-neutron scattering study of the vibrational dynamics and spin-related symmetry of protons in the $KHCO_3$ crystal. Phys. Rev. B **59**, 4134–4145 (1999)
25. Ikeda, S., Kashida, S., Sugimoto, H., Yamada, Y., Bennington, S.M., Fillaux, F.: Inelastic neutron scattering study of the localized dynamics of protons in $KHCO_3$ single crystals. Phys. Rev. B **66**, 184302 (2002)
26. Kashida, S., Ikeda, S., Nakai, Y.: Inelastic neutron scattering study of $KHCO_3$. J. Phys. Soc. Jpn **63**(12), 4643–4647 (1994)
27. Kashida, S., Yamamoto, K.: Structural transition in $KHCO_3$. J. Solid State Chem. **86**(2), 180–187 (1990)
28. Keen, D.A., Gutmann, M.J., Wilson, C.C.: SXD – the single-crystal diffractometer at the isis spallation neutron source. J. Appl. Cryst. **39**, 714–722 (2006)
29. Keen, D.A., Lovesey, S.W.: Quantum correlation between protons in potassium bicarbonate. J. Phys.: Condens. Matter **15**, 4937–4946 (2003)
30. Laloë, F.: Quantum mechanics, strange correlations; paradoxes and theorems. Am. J. Phys. **69**, 655–701 (2001)
31. Leggett, A.J.: Macroscopic quantum systems and the quantum theory of measurement. Supplement of the progress of theoretical physics **69**, 80–100 (1980)
32. Leggett, A.J.: Testing the limits of quantum mechanics: motivation, state of play, prospects. J. Phys.: Condens. Matter **14**, R415–R451 (2002)
33. Leggett, A.J., Chakravarty, S., Dorsey, A.T., Fisher, M.P.A., Garg, A., Zwerger, W.: Dynamics of the dissipative two-state system. Rev. of Modern Phys. **59**(1), 1–85 (1987)
34. Leggett, A.J., Garg, A.: Quantum mechanics versus macroscopic realism: Is the flux there when nobody looks? Phys. Rev. Letters **54**(9), 857–860 (1985)
35. Lovesey, S.W.: Nuclear scattering, Theory of Neutron Scattered from Condensed Matter, vol. I. Clarendon Press, Oxford (1984)

36. Lucazeau, G., Novak, A.: Low temperature Raman spectra of $KHCO_3$ single crystal. J. Raman Spectroscopy **1**, 573–586 (1973)
37. Maréchal, Y., Witkowski, A.: Infrared spectra of H-bonded systems. J. Chem. Phys. **48**(8), 3697–3705 (1968)
38. Novak, A.: Hydrogen bonding in solids. Correlation of spectroscopic and crystallographic data. Struct. and Bonding (Berlin) **18**, 177–216 (1974)
39. Odin, C.: ^{13}C and ^{39}K high-resolution solid-state NMR study of the nonferroic phase transition of potassium hydrogen carbonate. Complementarity between NMR and incoherent neutron scattering. J. Phys. Chem. B **108**, 7402–7411 (2004)
40. Schuster, P., Zundel, G., Sandorfy, C.: The hydrogen bond. Recent developments in theory and experiments, vol. I, II and III. North-Holland Pub. Co., Amsterdam (1976)
41. Skinner, J.L., Trommsdorff, H.P.: Proton transfer in benzoic acid crystals: A chemical spin-boson problem. Theoretical analysis of nuclear magnetic resonance, neutron scattering, and optical experiments. J. Chem. Phys. **89**(2), 897–907 (1988)
42. Smedarchina, Z., Fernandez-Ramos, A., Siebrand, W.: Tunneling dynamics of double proton transfer in formic acid and benzoic acid dimers. J. Chem. Phys. **122**, 134, 309 (2005)
43. Sugimoto, H., Okumura, A., Yuuki, H.: Effects of entanglement on elastic and inelastic scattering functions for neutron scattering from a pair of nuclei in solids. Phys. Rev. B **73**, 014305 (2006)
44. Tautermann, C.S., Voegele, A.F., Liedl, K.R.: The ground-state tunneling splitting of various carboxylic acid dimers. J. Chem. Phys. **120**(2), 631–637 (2004)
45. Thomas, J.O., Tellgren, R., Olovsson, I.: Hydrogen-bond studies. LXXXIV. An X-ray diffraction study of the structures of $KHCO_3$ and $KDCO_3$ at 298, 219 and 95 K. Acta Cryst. B **30**, 1155–1166 (1974)
46. Thomas, J.O., Tellgren, R., Olovsson, I.: Hydrogen bond studies. XCII. Disorder in $(HCO_3)_2^{2-}$ and $(DCO_3)_2^{2-}$ dimers: A neutron diffraction study of $KHCO_3$ and $KDCO_3$. Acta Cryst. B **30**, 2540–2549 (1974)
47. Witkowski, A.: Infrared spectra of the hydrogen-bonded carboxylic acids. J. Chem. Phys. **47**(9), 3645–3648 (1967)
48. Zeilinger, A., Gähler, R., Shull, C.G., Treimer, W., Mampe, W.: Single and double-slit diffraction of neutrons. Rev. Modern Phys. **60**(4), 1067–1073 (1988)
49. Zeilinger, A.: Experiment and the foundations of quantum physics. Rev. Modern Phys. **71**(2), S288–S297 (1999)
50. Zurek, W.H.: Decoherence, einselection and the quantum origin of the classical. Rev. Modern Phys. **75**(3), 715–775 (2003)

A DFT Study of Adsorption of Gallium and Gallium Nitrides on Si(111)

Demeter Tzeli(✉), Giannoula Theodorakopoulos, and Ioannis D. Petsalakis

Abstract Adsorption of gallium (Ga, Ga^+) and gallium nitrides (GaN, GaN^+, GaN_2, GaN_2^+) on a model Si(111) surface was studied by density functional theory calculations. In total 30 structures were determined. The binding energies (corrected for basis set superposition error) of the lowest structures were found to be 2.13 for Ga, 2.39 for Ga^+, 4.23 for GaN, 6.13 for GaN^+, 1.90 for GaN_2, and 2.13 eV for GaN_2^+. Low-lying bridged structures, with the adsorbate bridging the Si rest atom and adatom were found for the diatomic and the triatomic neutral and cationic nitrides. Moreover, for the diatomics, structures with Ga-N vertical, attached to a Si adatom or a Si rest atom were also found. From electron charge distribution analysis it is confirmed that the Si cluster acts as a pool of electronic charge resulting in the adsorbed Ga and Ga^+ to have similar net charges.

Keywords: DFT calculations, gallium nitrides, Si(111), adsorption

1 Introduction

There is great interest in the study of chemisorption of group III metals and their nitrides at Si surfaces, especially in the geometric and electronic structure of the interface [1–3], in the change of the surface associated with metal diffusion on the surface and in the formation of metal-adsorbate atomic wires as well as the self-assembly of perfectly ordered nanocluster arrays [4, 5]. Moreover, the growth of GaN films on Si surfaces [6, 7] has great potential for application in optoelectronic devices and high-power, high-temperature electronic devices [6–8]. Although there are many experimental studies of gallium nitrides at Si(111) [4–8], as far as we know, there have not been as many theoretical studies, and most of them are on Ga at Si [1, 3].

D. Tzeli, G. Theodorakopoulos, and I.D. Petsalakis
Theoretical and Physical Chemistry Institute, National Hellenic Research Foundation, 48 Vassileos Constantinou Ave., Athens 116 35, Greece, e-mail: dtzeli@eie.gr

S. Wilson et al. (eds.) *Frontiers in Quantum Systems in Chemistry and Physics*.

The present work is a continuation of our previous study of chemisorbed structures of gallium (Ga, Ga^+) and gallium nitrides (GaN, GaN^+, GaN_2, GaN_2^+) on Si(111) using density functional theory (DFT) calculations and a $Si_{26}H_{22}$ model of the Si(111) surface [9]. In the present work more structures are presented and the distribution of the electron charges is analyzed confirming that the Si cluster acts as a pool of electronic charge resulting in the adsorbed Ga and Ga^+ to have similar net charges for all three neutral or charged adsorbates.

2 Computational Approach

Chemisorbed structures of Ga, Ga^+, GaN, GaN^+, GaN_2, and GaN_2^+, at Si (111) are calculated at a 5-layer one-rest one-adatom (1R-1A) cluster model of Si(111) (see Fig. 1) constructed as before [9, 10] using the dimer-adatom-stacking fault (DAS) structure [11] and the LEED data of Tong et al. [12] for the Si(111) reconstructed surface. Hydrogen atoms (white spheres in Fig. 1) have been added to terminate the 26-Si atom cluster (grey spheres $\equiv$ Si) at the sides as well as below the lowest Si level, while the adatom and rest atom are left with one dangling bond each, i.e., one unpaired electron.

Preliminary calculations were carried out on parts of the structures of interest in order to determine an adequate combination of functional and basis set. The diatomic GaN, GaN^+, SiGa, and SiN and triatomic GaNSi, GaN_2 and GaN_2^+ molecules were investigated using different kinds of basis sets such as LANL2DZ, 6-31+, 6-31(d), 6-311+G(2df), DGDZVP and functionals such as B3LYP, UB3PW91, UPBEPBE and LSDA. The results were compared with available experimental values and existing medium or high quality calculations in the literature. In the case of the GaSi and GaNSi molecules, where there is no theoretical or experimental work in the literature, calculations were carried out employing the second and fourth order perturbation theory (MP2, MP2(full), MP4) and the coupled cluster technique CCSD(T), combined with the augmented correlation-consistent basis aug-cc–pVTZ [9]. Calculations on the Si(111) cluster were done using the LANL2DZ, 6-31+, 6-31(d), and DGDZVP basis sets and the B3LYP functional.

Thus, we concluded that the best and computationally tolerable (since the systems studied have about 50 atoms) combination of functional and basis set for

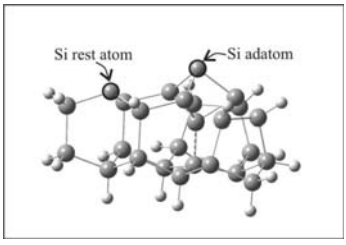

Fig. 1 5-layer one-rest one-adatom (1R-1A) cluster model of Si(111)

diatomics and triatomics and consequently for the chemisorbed gallium nitrides on Si(111) is the B3LYP/DGDZVP. B3LYP is a DFT functional using Becke's three parameter gradient corrected functional [13] with the gradient corrected correlation of Lee et al. [14]. The DGDZVP basis set is a double-zeta valence plus polarization, i.e., $[3s2p1d_N/4s3p1d_{Si}/5s4p2d_{Ga}]$ [15].

Employing the B3LYP/DGDZVP technique the electronic and geometric structures of chemisorbed gallium (Ga, Ga^+) and gallium nitrides (GaN, GaN^+, GaN_2, GaN_2^+) on the 5-layer 1R-1A cluster (cf. Fig. 1) were investigated. Three chemisorbed structures for each of Ga-Si(111); four for Ga^+-Si(111); eight for GaN-Si(111); six for GaN^+-Si(111); two for GaN_2-Si(111); and seven for GaN_2^+-Si(111) were determined by energy optimization with respect to the coordinates of the Si rest and Si adatom as well as those of the adsorbed species. The remaining cluster was kept fixed in order to retain the Si(111) surface structure.

For all stable geometries, binding energy (BE) and the corrected values with respect to the basis set superposition error (BE_{BSSE}) [16] of each species on the surface were calculated. All calculations were done using the Gaussian 03 program package [17].

3 Results and Discussion

The structures which were calculated for Ga- and Ga^+-Si(111) are given in Fig. 2, for GaN- and GaN^+-Si(111) in Fig. 3, and for GaN_2- and GaN_2^+-Si(111) in Fig. 4. The minima which have been determined are labeled by 2 characters followed by the name of the adsorbed species. The first character is refers to the spin multiplicity, and the second to the geometric structure. E.g., **2a-Ga**, means that the minimum

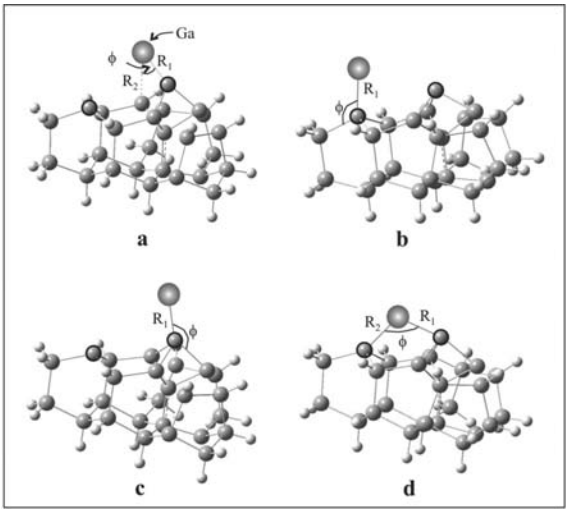

Fig. 2 Four structures of Ga-Si(111) and Ga^+-Si(111)

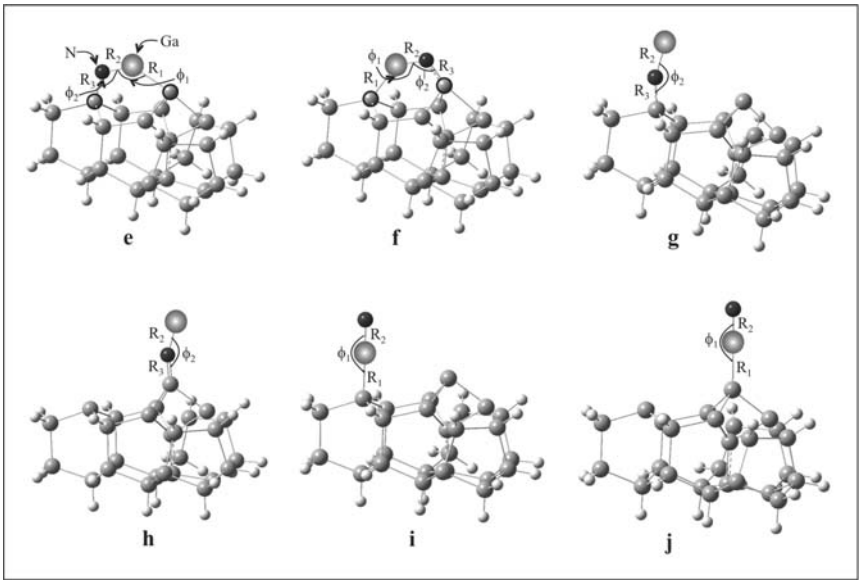

Fig. 3 Six structures of GaN-Si(111) and GaN^+-Si(111)

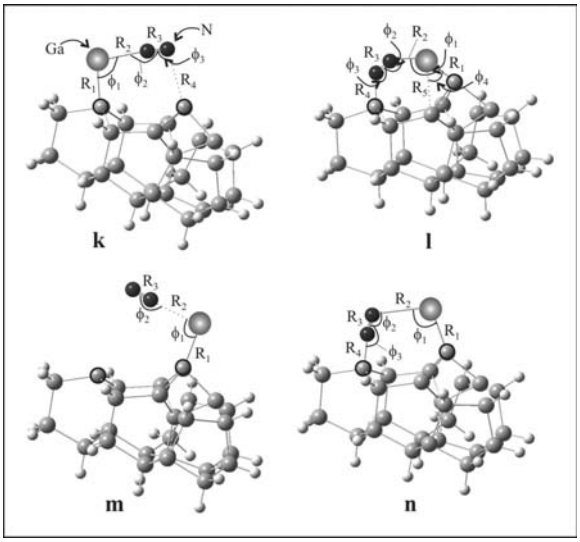

Fig. 4 Four structures of GaN_2-Si(111) and GaN_2^+-Si(111)

is a doublet corresponding to the **a** structure shown in Fig. 2 of the Ga-Si(111) cluster. The geometry, the binding energy and the natural population analysis of the structures determined are given in Table 1 for Ga- and Ga^+-Si(111), in Table 2 for GaN- and GaN^+-Si(111), and in Tables 3 and 4 for GaN_2- and GaN_2^+-Si(111).

Table 1 Geometry (bond distance R in Å, angle ϕ in degrees), binding energies BE and corrected values for BSSE BE_{BSSE} in eV and net charges of the Ga-Si(111) and Ga^+-Si(111) structures

Structures	R_1	R_2	ϕ	$BE(BE_{BSSE})$	Si-rest	Si-adat	Ga
Si(111)					+0.08	+0.22	
2a-Ga	2.55	2.91	56	2.16(2.13)	+0.06	−0.21	+0.59
2b-Ga	2.62		122	2.15(2.10)	−0.57	+0.20	+0.63
2c-Ga	2.58		141	1.72(1.69)	+0.06	−0.42	+0.65
3b-Ga^+	2.66		103	2.43(2.39)	−0.59	+0.30	+0.67
3d-Ga^+	2.79	2.73	107	2.35(2.27)	−0.33	−0.04	+0.79
3c-Ga^+	2.63		140	1.95(1.90)	+0.06	−0.35	+0.83
1d-Ga^+	2.65	1.69	111	1.88(1.81)	−0.27	−0.08	+0.84

Table 2 Geometry (bond distance R in Å, angle ϕ in degrees), binding energies BE and corrected values for BSSE BE_{BSSE} in eV and net charges of the GaN-Si(111) and GaN^+-Si(111) structures

Structures	R_1	R_2	R_3	ϕ_1	ϕ_2	$BE(BE_{BSSE})$	Si-rest	Si-adat	Ga	N
Si(111)							+0.08	+0.22		
GaN($X^3\Sigma^-$)		2.046							+0.66	−0.66
GaN($A^3\Pi$)		1.884							+0.75	−0.75
3e-GaN	2.50	1.78	1.73	133	119	4.32(4.23)	+0.75	−0.16	+1.14	−1.65
3f-GaN	2.47	1.77	1.73	143	106	4.10(3.95)	−0.30	+0.86	+1.27	−1.63
1e-GaN	2.48	1.78	1.74	137	117	3.98(3.89)	+0.74	−0.16	+1.18	−1.64
3g-GaN		1.89	1.70		161	3.93(3.84)	+0.73	+0.22	+0.77	−1.46
3h-GaN		1.85	1.63		159	3.79(3.70)	+0.09	+0.96	+0.78	−1.71
1f-GaN	2.47	1.77	1.73	143	107	3.78(3.64)	−0.30	+0.86	+1.27	−1.62
3i-GaN	2.40	1.78		179		1.72(1.62)	−0.39	+0.18	+1.10	−0.89
3j-GaN	2.41	1.78		179		1.50(1.41)	+0.09	−0.21	+0.97	−1.68
GaN^+($X^4\Sigma^-$)		2.740							+0.99	+0.01
GaN^+($^2\Pi$)		1.872							+1.39	−0.39
4g-GaN^+		1.90	1.70		161	6.19(6.13)	+0.69	+0.32	+0.84	−1.46
2f-GaN^+	2.45	1.78	1.71	138	112	6.12(6.00)	−0.29	+0.89	+1.31	−1.62
2e-GaN^+	2.51	1.78	1.74	133	119	5.96(5.81)	+0.73	−0.14	+1.24	−1.61
2h-GaN^+		1.95	1.66		164	5.73(5.66)	+0.10	+0.84	+0.85	−1.44
4i-GaN^+	metastable									
4j-GaN^+	metastable									

3.1 Ga-Si(111) and Ga^+-Si(111)

Four geometric structures, **a**, **b**, **c** and **d** (see Fig. 2), were examined with doublet and quartet spin symmetry for the Ga-Si(111) cluster and singlet and triplet spin symmetry for the Ga^+-Si(111) cluster. The geometry, the binding energy and the natural population analysis of only the lowest lying structures are given in Table 1.

The lowest minimum of Ga-Si(111), (**2a-Ga**), has the Ga atom connected to Si adatom. Moreover, Ga is directly above a 2nd layer Si atom, adjacent to the adatom. The BSSE corrected binding energy of adsorbed Ga is $BE_{BSSE} = 2.13$ (**2a-Ga**), 2.10 (**2b-Ga**) and 1.69 (**2c-Ga**) eV. The natural population analysis shows that the Si surface pulls electron charge from the Ga atom, leaving Ga with a positive partial

charge of +0.59 to +0.65 electrons, in the different structures. In all cases the Si atom connected to the Ga atom has a negative charge and the most negative charge, −0.57 electrons, is found on the Si rest atom of the **2b-Ga** structure.

The lowest **3b-Ga**$^+$ structure of Ga$^+$-Si(111) has Ga$^+$ connected to the Si rest atom. The BSSE corrected binding energy of adsorbed Ga$^+$ is $BE_{BSSE} = 2.39$ (**3b-Ga**$^+$), 2.27 (**3d-Ga**$^+$), 1.90 (**3c-Ga**$^+$) and 1.81 (**1d-Ga**$^+$) eV. Minima **3d-Ga**$^+$ and **1d-Ga**$^+$ have the same structure but different spin multiplicity with the triplet being lower by 0.5 eV, see Table 1. The natural population analysis shows that the Si surface transfers electron charge to Ga$^+$, and as a result the adsorbed Ga$^+$ has a positive partial charge of +0.67 to +0.84, rather than +1. In all cases the Si atom connected to Ga$^+$ cation has a negative charge and the most negative charge is found on the Si rest atom of the **3b-Ga**$^+$ structure, −0.59 as in the case of the **2b-Ga** of the Ga-Si(111). Hence, the partial charges on Ga and Ga$^+$ are very similar, with the surface withdrawing from Ga or providing to Ga$^+$ electron charge, while the Si rest and Si adatoms have negative charges −0.21 to −0.59.

3.2 GaN-Si(111) and GaN$^+$-Si(111)

Six geometric structures, **e**, **f**, **g**, **h**, **i**, and **j** (see Fig. 3), were calculated with singlet and triplet spin symmetry for GaN-Si(111) and doublet and quartet spin symmetry for GaN$^+$-Si(111). The geometry, the binding energy and the natural population analysis of the lowest lying structures are given in Table 2.

Eight local minima (**3e-GaN**, **3f-GaN**, **1e-GaN**, **3g-GaN**, **3h-GaN**, **1f-GaN**, **3i-GaN**, and **3j-GaN**) have been determined for adsorbed GaN. In the lowest minimum (**3e-GaN**) Ga is connected to Si adatom and N to the rest atom, and in **3f-GaN**, the GaN molecule is connected the opposite way. The BE_{BSSE} with respect to Si(111) + GaN($X^3\Sigma^-$) are calculated at 4.23 (**3e-GaN**) and 3.95 eV (**3f-GaN**). Structures **1e-GaN** and **1f-GaN** have a BE_{BSSE} about 0.3 eV smaller than the corresponding triplet structures. The geometries of **3e-GaN**, **3f-GaN**, **1e-GaN**, and **1f-GaN** minima are similar (cf. Table 2). In the remaining four structures GaN is nearly perpendicular to the surface with the N atom attached to either the Si-rest atom or to the Si adatom in **3g-GaN** and **3h-GaN**, respectively, while in **3i-GaN** and **3j-GaN** the Ga atom is attached to the Si-rest atom or to the Si adatom, respectively. The BE_{BSSE} of **3g-GaN** is 3.84 and of **3h-GaN** 3.70 eV larger about 2 eV than the BE_{BSSE} value of **3i-GaN** and **3j-GaN**.

The lowest minimum of the GaN$^+$-Si(111) cluster, **4g-GaN**$^+$, has the adsorbed GaN$^+$ with N attached to the Si rest atom with BE_{BSSE} = 6.13 eV with respect to Si(111) cluster + GaN$^+$($X^4\Sigma^-$); while in the second minimum **2f-GaN**$^+$, the GaN$^+$ forms a bridge between the Si rest and adatom with a BE_{BSSE} = 6.00 eV. These two minima lie very closely. The next two minima have a BE_{BSSE} value of 5.81 (**2e-GaN**$^+$) and 5.66 (**2h-GaN**$^+$) eV. The vertical structures with Ga atom connected to Si (**4i-GaN**$^+$ and **4j-GaN**$^+$) are higher in energy by ∼2.5 eV above **4g-GaN**$^+$ but they are not stable because they can easily changeover to a bridged structure.

In all 14 species calculated for adsorbed GaN and GaN^+, the Ga-N bond distance is significantly smaller than in the free diatomic GaN and GaN^+ systems. This is consistent with the transfer of electronic charge from the surface to GaN and GaN^+ with the result that adsorbed GaN and GaN^+ resemble free diatomic GaN^-, which was calculated to have a shorter bond than the neutral by 0.25 Å [18]. It appears that the same adsorbed GaN species is found in all the adsorbed structures calculated. This is consistent with the net charges on the Ga and N atoms in these structures, where N atom practically the same net charge obtains in all structures about -1.6 with the exception of **3i-GaN** while for Ga and Ga^+ the net charge ranges from $+0.8$ (when the Ga is not attached to Si(111)) to between $+1.0$ and $+1.3$ (when the Ga is attached to Si(111)). The above results show that the surface acts as a pool of electronic charge, (as in the case of adsorbed Ga and Ga^+ cf. Sect. 3.1 and Table 1) providing the required electronic charge to give nearly the same Ga-N adsorbed species in both cases, see Table 2. Furthermore, the significant shortening of the internuclear distance in adsorbed GaN and GaN^+ at Si(111), as compared to the free diatomic systems, makes this case a counter example to the general expectation that upon adsorption, the binding within the adsorbate is weakened, as, for example, is the case of adsorption of halobenzenes at Si(111) [10], where the C–X bond weakens and breaks.

3.3 GaN_2-Si(111) and GaN_2^+-Si(111)

Four geometric structures, **k**, **l**, **m** and **n** (see Fig. 4), were calculated with doublet and quartet spin symmetry for the GaN_2-Si(111) cluster and singlet and triplet spin symmetry for the GaN_2^+-Si(111) cluster. The geometry of the lowest energy structures is given in Table 3 while their binding energy and the natural population analysis are given in Table 4.

Two local minima of the chemisorbed GaN_2 molecule are found, with the adsorbate occupying bridging positions over the Si rest and Si adatom. Structure **2k-GaN$_2$**, has the outer N atom of GaN_2 just barely connected to the Si adatom, while structure **2l-GaN$_2$**, has the outer N atom tightly connected to the rest atom and its Ga interacts with a lower-layer Si atom, adjacent to the adatom (as in **2a-Ga**), see Tables 1 and 3. The BE_{BSSE} of **2k-GaN$_2$** and **2l-GaN$_2$** with respect to Ga+N_2+Si(111) are 1.98 and 1.62 eV, respectively. It should be noted that both structures are higher in energy than the lowest adsorbed Ga atom structure (**2a-Ga**), thus they are metastable structures (with respect to adsorbed Ga at Si plus free N_2) [9].

In all local minima (**3k-GaN$_2^+$**, **3l-GaN$_2^+$**, **3l′-GaN$_2^+$**, **3n-GaN$_2^+$**, **1l-GaN$_2^+$**, and **1n-GaN$_2^+$**) of chemisorbed GaN_2^+ with the exception of **3m-GaN$_2^+$** the cation bridges over the Si adatom and Si rest atom. In the lowest energy structure, **3k-GaN$_2^+$**, Ga^+ is connected to the rest atom, while in the other six structures Ga^+ is connected to the adatom. The BE_{BSSE} of **3k-GaN$_2^+$** is 2.13 eV with respect to the separated Si cluster and GaN_2^+ and 2.45 eV with respect to Si cluster + Ga^+ + N_2

Table 3 Geometry (bond distance R in Å, angle ϕ in degrees) of the GaN_2-Si(111) and GaN_2^+-Si(111) structures

Structures	R_1	R_2	R_3	R_4	R_5	ϕ_1	ϕ_2	ϕ_3	ϕ_4
$GaN_2(X^2\Pi)$		2.447							
2k-GaN_2	2.61	2.89	1.11	3.34		94	148	99	
2l-GaN_2	2.59	2.74	1.18	1.93	3.00	90	146	128	55
$GaN_2^+(X^4\Sigma^-)$		2.798							
3k-GaN_2^+	2.67	3.54	1.11	3.75		106	168	82	
3m-GaN_2^+	2.65	3.04	1.11			92	175		
3l-GaN_2^+	2.56	4.19	1.11	2.00	2.95	79	86	179	56
3l′-GaN_2^+	2.73	2.55	1.17	1.91	3.36	92	149	133	47
3n-GaN_2^+	2.56	3.32	1.12	1.95		102	111	172	
1l-GaN_2^+	2.56	4.74	1.11	2.00	3.19	102	107	174	52
1n-GaN_2^+	2.66	3.73	1.11	3.07		75	141	139	

Table 4 Binding energies BE and corrected values for BSSE BE_{BSSE} in eV [$BE(BE_{BSSE})$ with respect to GaN_2- or GaN_2^+-Si(111) and $BE1(BE1_{BSSE})$ with respect to Ga or $Ga^+ + N_2$-Si(111)] and net charges of the GaN_2-Si(111) and GaN_2^+-Si(111) structures

Structures	$BE(BE_{BSSE})$	$BE1(BE1_{BSSE})$	Si-rest	Si-adat	Ga	N	N
Si(111)			+0.08	+0.22			
$GaN_2(X^2\Pi)$					+0.18	−0.21	+0.03
2k-GaN_2	1.96(1.90)	2.10(1.98)	−0.56	+0.19	+0.60	−0.02	+0.05
2l-GaN_2	1.64(1.53)	1.78(1.62)	+0.42	−0.19	+0.58	−0.10	−0.37
$GaN_2^+(X^4\Sigma^-)$					+0.98	−0.14	+0.16
3k-GaN_2^+	2.19(2.13)	2.47(2.45)	−0.60	+0.27	+0.68	−0.01	+0.04
3m-GaN_2^+	1.94(1.91)	2.23(2.20)	+0.07	−0.37	+0.76	−0.06	+0.08
3l-GaN_2^+	1.69(1.52)	1.98(1.78)	+0.35	−0.22	+0.63	−0.10	+0.24
3l′- GaN_2^+	1.61(1.51)	1.90(1.74)	+0.40	−0.16	+0.72	−0.07	−0.26
3n- GaN_2^+	1.60(1.47)	1.89(1.71)	+0.36	−0.40	+0.66	+0.17	−0.13
1l- GaN_2^+	1.35(1.23)	1.64(1.50)	+0.36	−0.30	+0.69	+0.24	−0.09
1n- GaN_2^+	1.30(1.23)	1.58(1.55)	+0.28	−0.42	+0.73	+0.04	+0.01

species, which is larger than the binding energy of adsorbed Ga^+ (structure **3b-GaN_2^+**). Structures **3k-GaN_2^+** and **3l′-GaN_2^+** of GaN_2^+-Si(111) resemble **2k-GaN_2** and **2l-GaN_2** of GaN_2-Si(111), while the rest five minima are found only for the cation. In **3l′-GaN_2^+,** GaN_2^+ is more tightly connected to Si-rest and Si adatom, but it is more strained compared to the free GaN_2^+ cation, which favours a linear Ga^+-N-N geometry.

Structure **3m-GaN_2^+** is an open structure where a GaN_2^+ molecule is connected to the Si adatom with a BE_{BSSE} = 1.91 eV and a BE_{BSSE} = 2.20 eV with respect to $Ga^+ + N_2 + Si(111)$.

In some minima such as **3l-GaN_2^+** the $Ga^{+\cdots}N$ distances are long, thus, there is only a slight interaction between Ga^+ and N_2, but they are both stabilized through the Si surface. Moreover, in all **l-GaN_2^+** (**3l**, **3l′,** and **1l**) structures the Ga atom is connected to the Si adatom and it is directly above a 2nd layer Si atom.

As in the case of adsorbed Ga and Ga^+ (cf. Table 1) or GaN and GaN^+ (cf. Table 2), the Ga and Ga^+ of the triatomic adsorbed species have similar net charge (+0.58 to +0.76) showing that the surface acts as a pool of electron charge (see Table 4).

Finally, it should be noted that the Ga^+ of the adsorbed GaN_2^+, which forms a weak bond with the N_2, results in the stabilization of the N_2 molecule on the surface, which would not occur otherwise. This is consistent with our calculations on the adsorption of N_2 on Si(111) which yielded only unbound metastable structures with slight barriers to dissociation [9].

4 Remarks and Conclusions

The electronic and geometric structures of gallium (Ga, Ga^+) and gallium nitrides (GaN, GaN^+, GaN_2, GaN_2^+) adsorbed on Si(111) were studied by DFT calculations. A 5-layer 1R-1A Si cluster model of the Si(111) surface, terminated with H atoms was used. Three stable structures were determined for adsorbed Ga, four for Ga^+, eight for GaN, six for GaN^+, two for GaN_2 and seven for GaN_2^+. The binding energies to the Si surface (corrected for basis set superposition error) of the lowest structures were found to be 2.13 for Ga, 2.39 for Ga^+, 4.23 for GaN, 6.13 for GaN^+, 1.90 for GaN_2, and 2.13 eV for GaN_2^+. The diatomic neutral and cationic nitrides form low lying bridged structures, with the adsorbate bridging between the Si rest atom and Si adatom, as well as structures with only one bond with the surface and the molecular axis nearly perpendicular to the surface. The triatomic adsorbates form mostly bridged structures. The geometry as well as the electron population analysis of the adsorbed species and of the Si rest atom and Si adatom demonstrate the equivalence of bonding in the neutral and charged structures indicating that the charge can be drawn from or delivered to the surface as required to make the adsorbates studied have similar charges. Of course, there exist differences in the corresponding binding energies of the adsorbed neutral and cationic species, since the zero of the energy (i.e. the dissociation products) are quite different.

Acknowledgements Financial support has been provided by the Greek General Secretariat for Research and Technology through a Greece-Slovakia collaboration program (GGET-764).

References

1. T. Thundat, S. M. Mohapatra, B. N. Dev, W. M. Gibson, and T. P. Das, *J. Vac. Sci. Technol.* **6**, 681 (1998).
2. S. Tang, A. J. Freeman, Y. Qian, G. E. Franklin, and M. J. Bedzyk, *Phys. Rev. B* **51**, 1593 (1995).
3. S.-F. Tsay, M.-H. Tsai, M. Y. Lai, and Y. L. Wang, Phys. Rev. B **61**, 2699 (2000).
4. J. Cechal, M. Kolíbal, P. Kostelníc, and T. Šikola, *J. Phys.: Condens. Matter* **19**, 016011 (2007).

5. S. Xue, H. Zhuang, C. Xue, L. Hu, B. Li, and S. Zhang, *Appl. Phys. A- Mater. Science & Proc.* **87**, 645 (2007).
6. Y.-G. Yang, H.-L. Ma, C.-S. Xue, X.-T. Hao, H.-Z. Zhuang, and J. Min *Physica B* **325**, 230 (2003).
7. Y. Matsuo, Y. Kangawa, R. Togashi, K. Kakimoto, and A. Koukitu, *J. Cryst. Growth* **300** 66 (2007) and references therein.
8. Z. Hassan, Y. C. Lee, F. K. Yam, K. J. Abdullah, K. Ibrahim, and M. E. Kordesch, *Mater. Chem. Phys.* **84**, 369 (2004).
9. D. Tzeli, I. D. Petsalakis, and G. Theodorakopoulos, *Chem. Phys. Lett.* **448**, 88 (2007).
10. K. R. Harikumar, I. D. Petsalakis, J. C. Polanyi, and G. Theodorakopoulos, *Surface Science* **572**, 162 (2004).
11. K. Takayanagi, Y. Tanishiro, M. Takahashi, and S. Takahashi, *J. Vac. Sci. Technol. A* **3**, 1502 (1985).
12. S. Y. Tong, H. Huang, and C. M. Wei, *J. Vac. Sci. Technol. A*. **6**, 615 (1988).
13. D. Becke, *J. Chem. Phys.* **98**, 1372 (1993).
14. C. Lee, W. Yang, and R. G. Parr, *Phys. Rev. B* **37**, 785 (1988).
15. N. Godbout, D. R. Salahub, J. Andzelm, and E. Wimmer, *Can. J. Chem.* **70**, 560 (1992).
16. S.F. Boys and F. Bernardi, *Mol. Phys.* **19**, 553 (1970).
17. M. J. Frisch, et al. *Gaussian 03*, revision C.02; Gaussian, Inc.; Wallingford, CT, (2004).
18. P. A. Denis and K. Balasubramanian, *Chem. Phys. Lett.* **423**, 247 (2006).

Viscosity of Liquid Water via Equilibrium Molecular Dynamics Simulations

Gerardo Delgado-Barrio(✉), Rita Prosmiti, Pablo Villarreal, Gabriel Winter, Juan S. Medina, Begoña González, Jóse V. Alemán, Juan L. Gomez, Pablo Sangrá, Jóse J. Santana, and María E. Torres

Abstract Molecular dynamics simulations were carried out for liquid water in the NVE ensemble for calculating shear and bulk viscosities. We used two different intermolecular potential functions for the water dimer: the empirical SPCE model and the *ab initio* NCC one. The results obtained are compared with the available experimental values, and show that for a more accurate description of these macroscopic liquid properties a polarizable (rigid or flexible) interaction potentials should be employed. Such models, based on *ab initio* data, have been recently developed, and their incorporation for the viscosity calculations is discussed.

Keywords: molecular dynamics, theoretical simulations, electronic structure calculations, potential energy surfaces, liquid water

1 Introduction

Liquid water is perhaps the most popular system in computational chemistry in terms of the effort spend to model its chemical, transport, and solvation properties [1, 2]. Although, much attention has been devoted in the past to understand its microscopic properties, an accurate description of liquid water still remains a great challenge for both experiment and theory [3]. A number of experimental techniques have been developed, such as X-ray [4] and Neutron [5] diffractions,

G. Delgado-Barrio, R. Prosmiti, P. Villarreal
Instituto de Matemáticas y Física Fundamental (CSIC), Serrano 123, 28006 Madrid, Spain,
e-mail: rita@imaff.cfmac.csic.es

G. Winter, J.S. Medina, B. González
IUSIANI, ULPGC, Edif. Polivalente, 35017 Las Palmas de G. Canaria, Spain

J.V. Alemán, J.L. Gómez, P. Sangrá, J. Santana, M. Torres
Facultad de Ciencias del Mar, ULPGC, Campus Universitario de Tarifa, 35017 Las Palmas de G. Canaria, Spain

S. Wilson et al. (eds.) *Frontiers in Quantum Systems in Chemistry and Physics*.

as well as vibrational IR and Raman spectroscopy [6], NMR experiments [7], and ultrafast vibrational spectroscopy [8], to provide information about local structure in liquid water. More recently interpretation of X-ray absorption, X-ray Raman, and X-ray emission spectroscopy experiments has been quite controversial [9–14]. The general accepted picture for the local structure of water, with more o less tetrahedral arrangement with approximately 3.5 H bonds per molecule, has been questioned by the analysis of the X-ray absorption spectra, complemented with *ab initio* results. These investigations proposed a coordination number in liquid water close to 2 for each molecule, and a structural organization with H-bonded chains or rings of water molecules in a disordered H-bonded network.

The success of such investigations depends critically on the availability of intermolecular potential functions. Numerous force fields have been designed ranging from empirical models, with parameters fitted to experimental data [15, 16], to *ab initio* ones, which have been parameterized using the results of quantum chemistry calculations mainly of the water dimer and larger clusters [17–21]. Molecular dynamics (MD) simulation based on empirical force fields has been a usual method of choice to investigate the properties of liquid water. The quality and accuracy of such force fields have improved, leading to sophisticated descriptions of the interactions, and can reproduce with impressive accuracy the experimental radial distributions. However, results for dynamic properties obtained from classical calculations with empirical force field have been questioned [49]. At the same time, and in order to overcome the force field approach, simulations based on Car- Parrinello *ab initio* molecular dynamics (CPMD) methods have been applied to investigate the properties of liquid water [23]. In such type of simulations the atomic forces are computed on the fly from first principles electronic structure calculations, such as density functional theory (DFT), with no adjustable parameters. However, the reproducibility and accuracy of *ab initio* molecular dynamics methodology has been criticized in the literature. The discrepancies in structural and dynamic properties have been attributed to the different density functional models chosen to compute the molecular interactions, and to more technical factors, such as system size, duration of the run, convergence criterion for the electronic structure calculation, ensemble, time step or value of fictitious mass [24, 25]. Moreover, due to the computational cost a relative small number of molecules (32–64 molecules) has been employed to reproduce the properties of liquid water [23].

In this context, simulations based on so-called *ab initio* force fields [20, 21, 26–28], in which a many-body interaction potential is constructed from high quality *ab initio* potential surfaces of small water clusters, i.e. monomer, dimer, trimer, etc. provide an alternative for studying liquid water from first principles. Such force fields are exclusively fitted to *ab initio* data, thus their accuracy is limited by the level of theory, incompleteness of basis sets, and number of calculated grid points, as well as the form of the fitting function. *Ab initio*-based force fields have usually been employed in classical simulations, although more recently quantum calculations have been also reported with polarizable water models [29–33]. Such simulations are computationally less demanding than the *ab initio* CPMD ones, and thus a larger number of molecules can be involved for a more statistical description of liquid water.

As part of this study we aim to elucidate the importance of empirical and *ab initio* based force fields in determining transport properties, such as viscosities, performing MD simulations in pure liquid water. Shear viscosity is the one that can be easily determined by experiment [34], while experimental data on bulk viscosity of water are rather scarce [35]. Both shear and bulk viscosities are important transport properties [36], and their calculation can provide valuable information on intermolecular forces. Experimental observations on shear viscosity have proposed that the cause of the thermal anomalies in this property may be traced to structural transitions in ordered water structures near interfaces [37]. In the light of the new experimental data [9] on the structural configurations of liquid water, invites further investigation on this subject. Several methods are described in the literature for determining viscosities based on equilibrium (EMD) and non-equilibrium (NEMD) molecular dynamics simulations [38].

In this article, we first report in Sect. 2 on the potential models used to treat the intermolecular interactions of the liquid water. Then, in Sect. 3 we outline details on the molecular dynamics simulations, and on the computation of the stress autocorrelation functions. Results obtained for the shear and bulk viscosities are presented and discussed in Sect. 4, while conclusions are given in Sect. 5.

2 Model Potentials for Liquid Water

There is the broad classification of existing models for interaction potentials for water into pairwise additive (two-body) and polarizable (many-body) ones. Studies on static and dynamic properties of liquid water have confirmed, that many-body corrections are essential [39–42]. Additionally, the above mentioned categories of water models are subdivided to rigid or flexible depending on whether the model allows the individual monomers to interact with other molecules, and thus to deform geometrically. Combinations between these groups yield four types of interaction potentials, which by increasing the degree of complexity are: rigid/pairwise, rigid/polarizable, flexible/pairwise, and flexible/polarizable [43]. The majority of the existing potentials for water are within these categories, and are being constructed by parameterizing the model in order to reproduce properties/values of a specific environment, e.g. gas-phase or bulk, and for a limited thermodynamic range.

Based on the previous discussion, we are interested to investigate the reliability of such models in calculating viscosities of the liquid water in a range of temperatures. As there is a long way from properties of, for example, any water cluster in understanding the properties of liquid water, a systematic study of such property by employing different interaction models is a rational route to follow. Here, we chose to compare results on shear and bulk viscosities obtained from two rigid/pairwise additive potentials of the first group: the empirical SPCE [15], and an *ab initio* one, namely NCC [17]. The first has 3-site electrostatic interactions between point-charges on the O, H, and H atoms, and one van der Walls (vdW) interaction between O–O, given by a Lennard-Jones form. This model has been extensively used in equilibrium and non-equilibrium molecular dynamic simulations [44, 45],

so we chose it among several empirical model as a point of reference. The second one is a 3-site electrostatic model, with point-charges at M (fictitious massless site), and hydrogen atoms, and 4-site interactions between M, O, H, and H atoms represented by a MCY functional form [17]. The vdW two-body part has been fitted to MP4 *ab initio* data of water dimer [17], while for the electrostatic (two-body) and the polarization part of the NCC model, that includes the many-body corrections, the Hartree-Fock energies have been used. We should mentioned that for a direct comparison of the models the polarization term of the NCC model is omitted in our present study.

3 Equilibrium Molecular Dynamics Simulations

Classical molecular dynamics simulations are carried out using the program MOLDY [46]. All simulations are performed in the NVE ensemble for systems of 256 water molecules, in a cubic box with a density of 0.999 gr/cm^3, imposing periodic boundary conditions. For the long-range electrostatic interactions, the standard Ewald summation technique was employed, and the values of the Ewald parameters k and α are chosen as 3.0 Å^{-1} and 0.4 Å^{-1}, respectively. For the van der Waals interactions a cutoff of $r_c = 10.0$ Å is assumed, and shifted force potential is applied. First, an equilibration period of 8 ps in NVT ensemble at 303 K using the velocity-scaling procedure, and 5 ps in NVE is used. Second, the modified Beeman algorithm was used to propagate the trajectories for a total time of 200 ps, and a time step of 0.1 fs is chosen. The use of the NVE ensemble requires the conservation of the total energy of the system during the simulation. In the present calculations we adopted a tolerance of $\Delta E/E < 10^{-4}$, with ΔE the deviation in energy during the total time of a simulation. The value of the total energy, E, was estimated for each potential model, according to the temperature value in the NVT simulation.

From an equilibrium molecular dynamic simulation, the viscosity for a liquid can be obtained from pressure fluctuations using the Green-Kubo equation:

$$\eta_X = \lim_{t\to\infty} \frac{V}{k_B T} \int_0^t X_{ACF}(t')dt', \quad X = K, G, E \tag{1}$$

which is the relation between the transport coefficient (viscosity in our case), and the integral of the equilibrium time correlation function. V is the volume, T the temperature of the system, and k_B the Boltzmann constant. In Eq. (1) X_{ACF} are the autocorrelation functions of the stress tensor,

$$K_{ACF}(t) = \langle\langle \delta P(t)\delta P(0)\rangle\rangle \tag{2}$$

$$G_{ACF}(t) = \frac{1}{5}\sum_{\alpha,\beta} \langle\langle P_{\alpha\beta}(t)P_{\alpha\beta}(0)\rangle\rangle \tag{3}$$

$$E_{ACF}(t) = \frac{1}{3}\sum_{a=x,y,z} \langle\langle \delta P_{\alpha\alpha}(t)\delta P_{\alpha\alpha}(0)\rangle\rangle \tag{4}$$

with K, G, E for the bulk, shear, and longitudinal viscosities. In Eq. (2) $\delta P(t)$ represents the fluctuations of the pressure, $\delta P(t) = P(t) - P$, where $P(t)$ is the instantaneous pressure, computed as the average of the diagonal elements of the stress operator, i.e. $\langle \frac{1}{3} tr(P_{\alpha\beta}) \rangle$, and P the pressure of the system, i.e. the ensemble average of $P(t)$. In Eq. (3) $P_{\alpha\beta}$ are the off-diagonal elements of the stress tensor, with five independent components, $(P_{xx} - P_{yy})/2, (P_{yy} - P_{zz})/2, P_{xy}, P_{yz}, P_{zx}$, while in Eq. (4) $P_{\alpha\alpha}$ represents the diagonal elements of the stress tensor, which has three independent components, namely P_{xx}, P_{yy}, and P_{zz}.

An alternative way to estimate the viscosity values is by fitting the autocorrelation functions using a functional form. The stress autocorrelation functions for liquid water show an initially oscillatory fast decay followed by a long-time tail. Based on this behavior a 6-parameter function using the Kohlrausch law to describe both fast and slow relaxation processes has been proposed to fit the ACFs [44]. The analytical form is given by,

$$c_X(t) = (1 - C) \exp -(t/\tau_{K_f})^{\beta_f} \cos(\omega t) + C \exp -(t/\tau_{K_s})^{\beta_s} \tag{5}$$

where, the first and second term correspond to fast and slow timescale relaxations, respectively. C is the fraction of the slow relaxation, and $(1 - C)$ for the fast one. The circular frequency of the oscillation is ω, while β and τ_K are the Kohlrausch parameters [47]. The total relaxation time is given by $\tau_X = \tau_f + \tau_s$, where τ_f and τ_s are the average relaxation time for fast, and slow relaxations, respectively, and are calculated by numerical integration of the area under the adjusted c_X ACFs curves. The shear and bulk viscosities are then obtained by the expressions [48],

$$\eta_X = \frac{V}{k_B T} X_{ACF}(0) \tau_X \tag{6}$$

with $X = G$ and K, respectively.

4 Results and Discussion

As we mentioned above, we carried out simulations using two different types of model potential for liquid water. For each of them, we first evaluated the quality of the NVE simulations, and then the stress autocorrelation functions and the viscosities are calculated.

In Fig. 1 the normalized K'_{ACF}, G'_{ACF}, and E'_{ACF} stress autocorrelation functions, obtained from the simulations, are plotted up to 10 ps. For both SPCE (see Fig. 1a) and NCC (see Fig. 1b) models the X_{ACF} functions show a two-step relaxation, with different damped oscillations for the short-time part ($<$1 ps), and a monotonically slow decay for the long-time. We should mention that the corresponding X'_{ACF} functions obtained with the SPCE potential show a faster relaxation for short characteristic time, and a much more oscillating response with a significant long characteristic time in comparison with the ones calculated using the NCC model.

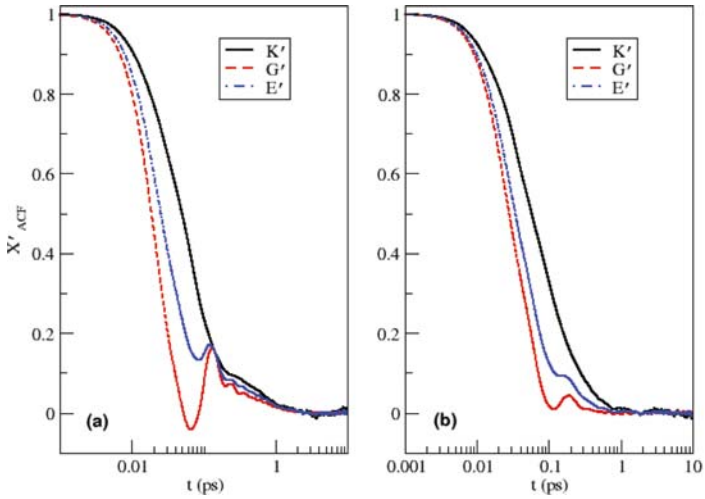

Fig. 1 Normalized autocorrelation functions, X'_{ACF}, for bulk (K), shear (G) and longitudinal (E) viscosities: (**a**) for SPCE model and (**b**) for NCC one

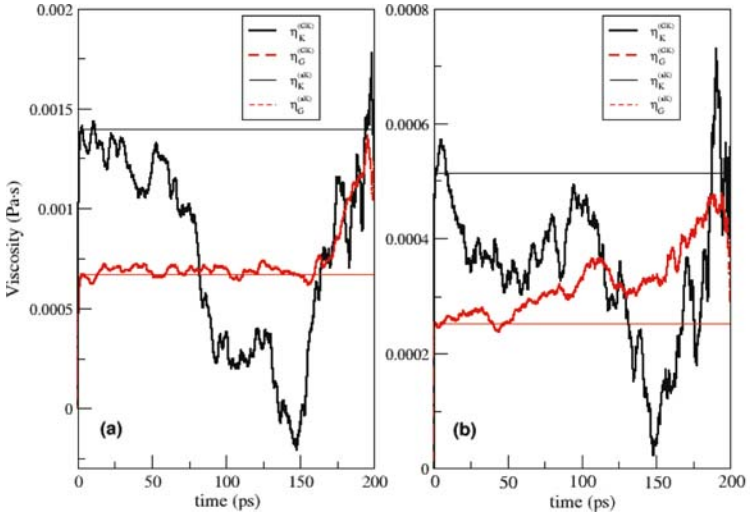

Fig. 2 Bulk (η_K), and shear (η_G) viscosities as a function of time. GK stands for viscosity values obtained from the original $X_{ACF}(t')$ functions using the Green-Kubo equation, while aK for values obtained using the Kohlrausch law. (**a**) for SPCE model and (**b**) for NCC one

The bulk (η_K) and shear (η_G) viscosities are then computed by the Eq. (1), and Eq. (6) by fitting the corresponding X_{ACF} functions to the Kohlrausch law expression of Eq. (5).

In Fig. 2 the integrals for the bulk and shear viscosity as a function of time are presented, and in Table 1 their plateau values (the three mean-values of the X_{ACF}

Table 1 Calculated viscosities and block average values of the EMD simulations

Property	SPCE[a]	NCC[a]	NCC	Expt.
N molecules/Ensemble	256/NVE	256/NVE	256/NVE	–
Density (ρ/Kg m^{-3})	999.00	999.00	999.00	995.64[b]
Temperature (T/K)	301.5 ± 0.2	302.89 ± 0.42	303.08 ± 0.11	300.2/302.2/303.2[c]
Energy (E/KJ mol^{-1})	-9833.362 ± 0.856	-12281.320 ± 0.006	-5697.992 ± 0.003	–
Pressure (P/MPa)	39.71 ± 2.11	-40.78 ± 5.22	376.27 ± 1.41	0.101
Dipole moment (μ/D)	2.35	2.35	1.85	–
Shear Visc. ($\eta_G/10^{-4}$ Pa·s)	6.73	9.78	2.52	8.51/8.15/7.98[c]
Bulk Visc. ($\eta_K/10^{-4}$ Pa·s)	14.11	24.99	5.21	≈24.0/21.5[d]

[a] Dipole moment as in SPCE model
[b] From Ref. [50]
[c] From Ref. [51]
[d] From Refs. [52, 53]

functions reach to zero at time e.g. 3.3 ± 0.2 ps for the SPCE), corresponding to the viscosity values with the smallest uncertainty, are given. The negative pressure value obtained by the MD simulations for the NCC^a implies that this model should predict a higher value for the liquid density than the experimental one at P = 0.101 MPa and T = 300 K.

Our results compare very well with previous theoretical studies using the SPCE model [44, 45] for both shear and bulk values. The shear viscosity value obtained here using the NCC model is very close to the one reported for the MCY form (∼0.3 mPa·s) [49]. Unfortunately, no more data on liquid water viscosities are available in the literature on such *ab initio* based potentials. As it can be seen the calculated values for both SPCE and NCC models are smaller than the experimental values, with the SPCE values to be closer to the experimental ones. Both models fail to reproduce the real liquid water viscosities, that demonstrate substantial deviation from a realistic description of the interaction potential. On one hand, the SPCE predicts quite accurately single-particle properties of water, only considers the O–O vdW interactions, and presents difficulty in predicting collective properties of water, such as viscosities. On the other hand, the NCC model reproduce well the structure of liquid water (e.g. radial distribution functions), includes polarizability, and a wide number of site vdW interactions, such as O–O, H–O, H–H, M–O, M–H ones. Thus, NCC can describe subtle changes in molecular orientations, as function of O–O distance, which account to the behavior of the stress tensor under fluctuations.

In order to evaluate the importance of such interactions on the viscosity, we assume the point hydrogen charge value as parameter in the NCC model, and simulations are carried out to calculate viscosities as a function of the total dipole moment of the system. The SPCE model predicts a dipole moment value of 2.35 D, while the NCC and NCC^a employed here, correspond to values of $\mu = 1.85$ and 2.35 D, respectively [54]. In Fig. 3 the results obtained for bulk (see Fig. 3a) and shear (see Fig. 3b) viscosities with the NCC potential form are plotted for three dipole moment values, μ, in the range of $1.85 - 2.35$ D at T = 303 K.

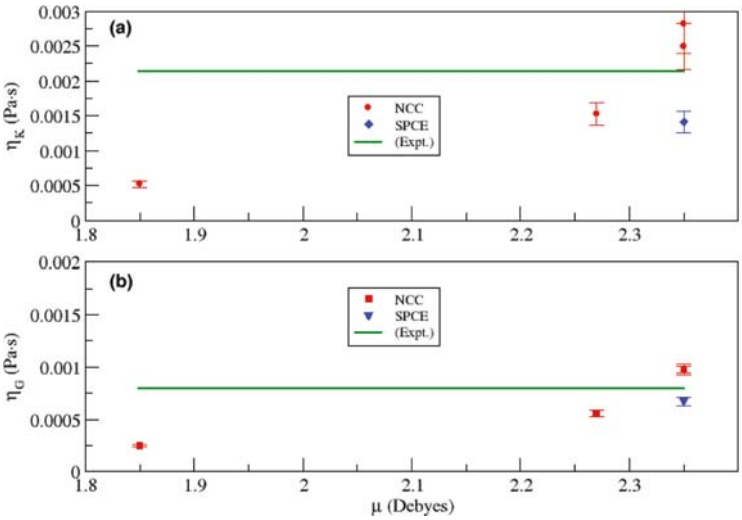

Fig. 3 (**a**) Bulk, η_K, and (**b**) shear, η_G, viscosities obtained with SPCE and NCC water model as a function of dipole moment. Solid lines are for the experimental values

We can see, that a wide range of viscosity values are obtained, and a direct comparison with the viscosity values for SPCE and NCC models is given in Table 1. For example shear viscosity values of 2.52×10^{-4}, 5.55×10^{-4} and 9.78×10^{-4} Pa·s are obtained for dipole moments of 1.85, 2.27 and 2.35 D, respectively. The accord with the experimental values seems to improved comparing the NCC^a with the original NCC model. As it was expected larger dipole moment has a significant contribution to the dynamic response of the X_{ACF} functions (specially to the shear one), and thus to the viscosity calculation. We found that, by increasing the dipole moment, the larger range interaction of the coulombic forces comparing with the short range interaction of vdW ones, implies the rise of the oscillatory part in the X_{ACF} functions. Also, we show that the frequency of the short time is increasing, and the long time response becomes more significant. As a consequence, the NCC^a model overestimates both shear and bulk viscosity values, and this can be attributed to the existence of multipole electrostatic moments, (e.g. quadrupole moment), in the coulombic interaction. In this point, we should note that the polarization (many-body) interactions are expected to reduce this effect. Further, viscosity values obtained of NCC^a and SPCE models shows different behavior in comparison with the experimental values. The SPCE underestimates both shear (by 21%) and bulk (by 34%) viscosities, while NCC^a overestimates them, by 20% the shear, and 16% the bulk viscosity values. In principal, the main difference of these two models is the representation of the vdW term, and this may indicates that such interactions are better described by the *ab initio*-based NCC model.

What is clear, however, is that these preliminary findings suggest that the complexity of the model potential should be increased, e.g. rigid/polarizable or flexible/polarizable types of interaction should be considered. There are at least two

more issues to be addressed: the effect of the polarization (many-body) terms, and the dependence of viscosity values with the temperature. Polarization effects are expected to play an important role in viscosity MD calculations, thus their contribution should be first evaluated, and then the dependence of the viscosity values, as a function of the temperature, should be investigated. Experimental values on shear viscosity are available down to -35°C at 1 bar [55] and up to 100°C [34], while on bulk viscosity only down to -27°C [56], for supercooled water [57]. Additionally, recent experimental data, from X-ray absorption spectroscopy and X-ray Raman scattering [9], have proposed different structural configurations, based on H bonds, of liquid water depending on temperature, e.g. tetrahedral structure for low values ($\approx 10-35$°C), and H-bonded chains arrangement for temperatures up to 90°C. In this vein, comparison of MD calculated viscosities using different types of water potential, (based on dimer – NCC model – or monomer – SPCE model – species), and for different temperature ranges, with the experimental values could serve to understand the intermolecular interactions in liquid water.

5 Conclusions

Molecular dynamics simulations, in the NVE ensemble and T = 303 K, were carried out using two different water model potentials of the rigid/pairwise additive category: the empirical SPCE, and the *ab initio* based NCC ones. The stress autocorrelation functions and viscosities (bulk and shear) for both models were calculated, and compared with previous theoretical studies, as well as with experimental data. Our results show that both SPCE and NCC models have faster structural relaxation than the real liquid water, and underestimate both shear and bulk viscosities. The importance of vdW interactions on the viscosity is evaluated using the modified NCC^a potential, which has the same total dipole moment as in the SPCE. The viscosities obtained with NCC^a water model are overestimated in comparison with the experimental ones. This behavior is mainly attributed to the existence of multipole moments in the electrostatic part, which is expected to be minimize by including the polarization terms, and to the representation of the vdw interaction.

In order to clarify the effect of such different contributions, further simulations with *ab initio*-based, rigid/flexible and polarizable water force fields [17, 20, 21, 58] are necessary, and over a wide range of temperatures. Analysis of the temperature dependence, and potential model on the calculated viscosities would be certainly useful to gain a better understanding in the dynamics of liquid water. Currently, work in this direction is in progress.

Acknowledgements The Centro de Cálculo (IMAFF), CTI (CSIC), CESGA and Red Española de Supercomputación (MareNostrum-BSC) are acknowledged for allocation of computer time. R. P. acknowledges support by Ramón y Cajal Programme Grant No. PDRYC-2006-001017. This work has been supported by DGICYT, Spain, Grant No. FIS2007-62002.

References

1. G.W. Robinson, S.-B. Zhu, S. Singh, M.W. Evans, *Water in Biology, Chemistry and Physics. Experimental Overviews and Computational Methodologies*, (World Scientific, Singapore, 1996).
2. F. Franks, *Water:A Matrix of Life*, 2nd ed. (Royal Society of Chemistry, Cambridge, 2000).
3. D. Kennedy, C. Norman, Science **309**, 75 (2005).
4. J.M. Sorenson, G. Hura, R.M. Glaeser, T. Head-Gordon, J. Chem. Phys. **113**, 9149 (2000).
5. A.K. Soper, Chem. Phys. **258**, 121 (2000).
6. J.D. Smith, C.D. Cappa, K.R. Wilson, R.C. Cohen, P.L. Geissler, R.J. Saykally, Proc. Natl. Acad. Sci. USA **102**, 14171 (2005).
7. K. Mofig, B.G. Pfrommer, B. Halle, Phys. Rev. Lett. **90**, 075502 (2003).
8. Y.L.A. Rezus, H.J. Bakker, J. Chem. Phys. **123**, 114502 (2005).
9. Ph. Wernet, D. Nordlund, U. Bergmann, M. Cavalleri, M. Odelius, H. Osawara, L.A. Naslund, T.K. Hirsch, L. Ojamae, P. Glatzel, L.G.M. Pettersson, A. Nilsson, Science **304**, 995 (2004).
10. J.D. Smith, C.D. Cappa, K.R. Wilson, B.M. Messer, R.C. Cohen, R.J. Saykally, Science **306**, 851 (2004).
11. A.K. Soper, J. Phys.:Condens. Matter, **17**, S3273 (2005).
12. D. Prendergast, G. Galli, Phys. Rev. Lett. **96**, 215502 (2006).
13. T. Head-Gordon, M.E. Johnson, Proc. Natl. Acad. Sci. USA **103**, 7973 (2006).
14. Y.A. Mantz, B. Chen, G.J. Martyna, J. Phys. Chem. B **110**, 3540 (2006).
15. H.J.C. Berendsen, J.R. Grigera, T.P. Straatsma, J. Phys. Chem. **91**, 6269 (1987).
16. W.L. Jorgensen, J. Chandrasekhar, J.D. Madura, R.W. Impey, M.L. Klein, J. Chem. Phys. **79**, 926 (1983).
17. U. Niesar, G. Corongiu, E. Clementi, G.R. Kneller, D.K. Bhattacharya, J. Phys. Chem. **94**, 7949 (1990).
18. L.X. Dang, T.-M. Chang, J. Chem. Phys. **106**, 8149 (1997).
19. H.A. Stern, B.J. Berne, J. Chem. Phys. **115**, 7622 (2001).
20. G.S. Fanourgankis, S.S. Xantheas, J. Phys. Chem. A **110**, 4100 (2006).
21. R. Bukowski, K. Szalewicz, G.C. Groenenboom, A. van der Avoird, Science **315**, 1249 (2007).
22. R. Ludwig, Chem. Phys. Chem. **8**, 44 (2007).
23. H.-S. Lee, M.E. Tuckerman, J. Chem. Phys. **126**, 164501 (2007).
24. J. VandeVondele, F. Mohamed, M. Krack, J. Hutter, M. Sprik, M. Parrinello, J. Chem. Phys. **122**, 014515 (2005).
25. J.C. Grossman, E. Schwegler, E.W. Draeger, F. Gygi, G. Galli, J. Chem. Phys. **120**, 300 (2004).
26. G. Corongiu, E. Clementi, J. Chem. Phys. **97**, 2030 (1992); **97**, 8818 (1992).
27. C.J. Burnham, S.S. Xantheas, J. Chem. Phys. **116**, 1500 (2002);**116**, 5115 (2002).
28. R. Bukowski, K. Szalewicz, G.C. Groenenboom, A. van der Avoird, J. Chem. Phys. **125**, 044301 (2006).
29. H.A. Stern, B.J. Berne, J. Chem. Phys. **115**, 7622 (2001).
30. A.G. Donchev, N.G. Galkin, A.A. Illarionov, O.V. Khoruzhii, M.A. Olevanov, V.D. Ozrin, M.V. Subbotin, V.I. Tarasov, Proc. Natl. Acad. Sci. USA **103**, 8613 (2006).
31. G.S. Fanourgakis, G.K. Schenter, S.S. Xantheas, J. Chem. Phys. **125**, 141102 (2006).
32. G.S. Fanourgakis, V. Tipparaju, J. Nieplocha, S.S. Xantheas, Theor. Chem. Acc. **117**, 73 (2007).
33. F. Paesani, S. Iuchi, G.A. Voth, J. Chem. Phys. **127**, 074506 (2007).
34. L. Korson, W. Drost-Hansen, F.J. Millero, J. Phys. Chem. **73**, 34 (1969).
35. C.M. Davis, J. Jarzynsji, *Water: A Comprehensive Treatise*, (Vol. 1, edited by F. Franks p. 443, 1972).
36. J.V. Alemán, J.L. Pelegrí, P. Sangrá, J. Non-Newt. Fluid Mech. **133**, 121 (2006).
37. W. Drost-Hansen, Ann. N.Y. Acad. Sci. **125**, 471 (1965).
38. M.P. Allen, D.J. Tildesley, *Computer Simulations of Liquids* (Clarendon Press, Oxford, 1987)
39. M. Wojcik, E. Clementi, J. Chem. Phys. **85**, 6085 (1986).
40. S.S. Xantheas, J. Chem. Phys. **100**, 7523 (1994).

41. J.K. Gregory, D.C. Clary, K. Liu, M.G. Brown, R.J. Saykally, Science **275**, 814 (1997).
42. S.S. Xantheas, Chem. Phys. **258**, 225 (2000).
43. C.J. Burnham, S.S. Xantheas, J. Chem. Phys. **116**, 1479 (2002).
44. G.-J. Guo, Y.-G. Zhang, K. Refson and Y.-J. Zhao, Mol. Phys. **100**, 2617 (2002).
45. B. Hess, J. Chem. Phys. **116**, 209 (2002).
46. K. Refson, Comp. Phys. Commun. **126**, 310 (2000).
47. J.C. Phillips, Rep. Prog. Phys. **59**, 1133 (1996).
48. D.M. Heyes, J. Phys.: Condens. Matter **6**, 6409 (1994).
49. G.C. Lie, E. Clementi, Phys. Rev. A **33**, 2679 (1986).
50. *Lange's Handbook of Chemistry*, 10th ed., (McGraw-Hill, New York, 1969).
51. R.C. Weast, in *CRC Handbook of Chemistry and Physics* (CRC Press, Boca Raton, 1986).
52. L.N. Lieberman, Phys. Rev. **75**, 1415 (1949).
53. T.A. Litovitz, E.H. Carnevale, J. App. Phys. **26**, 816 (1955).
54. J.C. Soeten, M.T.C. Martins-Costa, C. Millot, Mol. Phys. **94**, 577 (1998).
55. M.J. Assael, E. Bekou, D. Giakoumakis, D.G. Friend, M.A. Killeen, J. Millat, A. Nagashima, J. Phys. Chem. Ref. Data **29**, 141 (2000).
56. G. Maisano, P. Migliardo, F. Aliotta, C. Vasi, F. Wanderlingh, G. D'Arrigo, Phys. Rev. Lett. **52**, 1052 (1984).
57. P.G. Debenedetti, H.E. Stanley, Phys. Today **56**, 40 (2003).
58. G. Corongiu, Int. J. Quant. Chem. **42**, 1209 (1992).

Stochastic Description of Activated Surface Diffusion with Interacting Adsorbates

Ruth Martínez-Casado(✉), José Luis Vega, Ángel S. Sanz, and Salvador Miret-Artés

Abstract Activated surface diffusion on metal surfaces is receiving much attention both experimentally and theoretically. One of the main theoretical problems in this field is to explain the line-shape broadening observed when the surface coverage is increased. Recently, we have proposed a fully stochastic model, the *interacting single adsorbate* (ISA) *model*, aimed at explaining and understanding this type of experiments, which essentially consists of considering the classical Langevin formulation with two types of noise forces: (i) a Gaussian white noise accounting for the substrate friction, and (ii) a shot noise simulating the interacting adsorbates at different coverages. No interaction potential between adsorbates is included because any trace of microscopic interaction seems to be wiped out in a Markovian regime. This model describes in a good approximation, and at a very low computational cost, the line-shape broadening observed experimentally. Furthermore, its mathematical simplicity also allows to derive some analytical expressions which are of much help in the interpretation of the physics underlying surface diffusion processes.

Keywords: activated surface diffusion, interacting adsorbates, collision friction, Langevin dynamics

R. Martínez-Casado
Ruhr-Universität Bochum, Lehrstuhl für Physikalische Chemie I, D-44801 Bochum, Germany; and Instituto de Física Fundamental, Consejo Superior de Investigaciones Científicas, Serrano 123, 28006 Madrid, Spain, e-mail: ruth@imaff.cfmac.csic.es

J.L. Vega, A.S. Sanz, and S. Miret-Artés
Instituto de Física Fundamental, Consejo Superior de Investigaciones Científicas, Serrano 123, 28006 Madrid, Spain, e-mail: jlvega@imaff.cfmac.csic.es; asanz@imaff.cfmac.csic.es; smiret@imaff.cfmac.csic.es

S. Wilson et al. (eds.) *Frontiers in Quantum Systems in Chemistry and Physics*.

1 Introduction

The diffusion of atoms, molecules or small clusters on metal surfaces is a process of paramount importance in many technological and industrial applications. Molecular beam epitaxy, heterogeneous catalysis, crystal growth, chemical vapor deposition, associative desorption or the fabrication of nanostructures are just a few examples where the kinetics of diffusion plays a fundamental role. Different experimental techniques have been used to study activated surface diffusion [1–5], the quasi-elastic He atom scattering (QHAS) being a gentle and inert one commonly applied in this type of experimental research [6, 7]. This technique has been used to characterize different adsorbate/metal systems. Among them, the diffusion of Na atoms (at different coverages) on Cu(001) has been one of the most extensively studied systems [6, 7]. This is the reason why the Na/Cu(001) has become a paradigm system in theoretical studies on surface diffusion.

In general, adsorbate dynamics at low coverages can be described within the so-called *single adsorbate approximation* and analyzed in terms of the *motional narrowing effect* [8–10]. This effect governs the profile displayed by the line shapes as a function of different parameters, such as the substrate friction, the parallel momentum transfer, and/or the lattice structure (activation barrier, surface periodicity, etc.). In this type of studies, the adsorbates are always regarded as isolated and only the interaction with the substrate is taken into account. However, when the coverage is increased, adsorbate-adsorbate interactions can no longer be neglected. In such cases, pairwise interaction potentials are usually introduced into Langevin molecular dynamics (LMD) simulations [7], where the number of coupled equations to be solved is, in general, relatively large (it increases as $2N$, where N is the number of adparticles considered, typically of the order of 400–500). In most of systems, the Markovian–Langevin approximation is assumed because the Debye energy of the substrate excitations is greater than the lowest frequency mode of the adsorbate (or frustrated translational mode or T–mode) and therefore the damping can be considered as instantaneous (memory effects are negligible). The adsorbate–adsorbate interaction is given by a repulsive dipole–dipole potential. The so–called Topping's depolarization formula relates the dipole strength with the coverage [11]. This type of interaction is attributed to the electrostatic repulsion between the dipoles due to the charge transfer from the adatoms to the substrate. Numerical discrepancies between the experimental and molecular dynamic results for the broadening of the quasi–elastic peak as a function of the parallel wave vector transfer and the T–mode frequency are obtained. The discussion about the origin of such discrepancies is still an open problem [12]. In addition to the high computational demand, simple interpretations of the numerical results obtained from LMD simulations are also a hard task; analytical treatments are difficult to carry out and, in the end, additional statistical-like approaches have to be considered. To overcome this problem within the LMD perspective, it has been shown [13] that a good agreement with the experiment can be achieved using simple models where the adsorbate is allowed to also move perpendicularly to the surface.

In order to provide a theoretical and numerical alternative to the standard LMD procedure at intermediate coverages, we have proposed the so-called *interacting*

single adsorbate (ISA) *approximation* [14–17]. Within this approach, diffusion is described by means of the standard Langevin equation, where three contributions characterize the adsorbate dynamics:

1. The deterministic, adiabatic potential, V, which models the adsorbate-substrate interaction at $T = 0$
2. A Gaussian white noise accounting for the lattice vibrational effects that the surface temperature induces on the adsorbate
3. A white shot noise that stands for the adsorbate-adsorbate collisions and replaces the pairwise (dipole-dipole) interaction potential generally considered in LMD simulations

In this way, a typical LMD simulation where N adsorbates are involved at a time is substituted by the dynamics of a single adsorbate, with the action of the remaining $N-1$ adparticles being accounted for by a white shot noise. This is possible because any trace of the true interaction potential seems to be wiped out at very long times, which are the timescales relevant to the diffusion and low-frequency vibrations described by the line-shape peaks around or near zero energy transfers. Within the ISA approximation we have been able to obtain a good agreement (in comparison with that found with standard LMD calculations) with the experimental results for coverages up to $\sim$20%. Although further investigation at microscopic level and calculations from first principles are needed, at moderate coverages the ISA model is therefore able to provide a complementary view of both diffusion and low-frequency vibrational motions.

To present a broad perspective of the ISA model as well as its applicability and potentiality, we have organized this chapter as follows. In Sect. 2 we present the relevant magnitudes in surface diffusion. In Sect. 2 a brief overview of the two types of noise sources, Gaussian white noise and shot noise, is provided. Moreover, the simple model used in our calculations relating the coverage with the *collisional friction* of the shot noise is also introduced at the end of the section. The description of the adsorbate dynamics in terms of a Langevin equation and its relationship with the observable magnitude (the line shapes) are explained in Sect. 3. In particular, two corrugation models (representing low and high corrugation regimes) are examined analytically. Numerical results illustrating the dynamics within these two corrugation regimes are presented and discussed in Sect. 5. Finally, in Sect. 6 we summarize the main features of the ISA model and advance some of our future work.

2 Dynamic Structure Factor and Intermediate Scattering Function

In QHAS experiments one is usually interested in measuring the *differential reflection coefficient*, which can be expressed as

$$\frac{d^2\mathscr{R}(\Delta\mathbf{K},\omega)}{d\Omega d\omega} = n_d F S(\Delta\mathbf{K},\omega) \tag{1}$$

in analogy to neutron scattering by crystals and liquids [18]. This magnitude gives the probability that the probe He atoms scattered from the diffusing collective of adsorbates (spread out on the surface) reach a certain solid angle Ω with an energy exchange $\hbar\omega = E_f - E_i$ and a parallel (to the surface) momentum transfer $\Delta\mathbf{K} = \mathbf{K}_f - \mathbf{K}_i$. In (1), n_d is the (diffusing) surface concentration of adparticles; F is the *atomic form factor*, which depends on the interaction potential between the probe atoms in the beam and the adparticles on the surface; and $S(\Delta\mathbf{K},\omega)$ is the *dynamic structure factor* or *scattering law*, which consists of a series of peaks. Here, in particular, our interest focusses in the line shapes displayed by two types of these peaks: (i) the *quasi-elastic* (Q) peak ruling the diffusion process and (ii) the T-mode peaks related to the so-called *frustrated translational modes* or low frequency motions of the adsorbate. Other peaks also important (but that go beyond the scope of the work presented here) are the inelastic ones, associated with surface phonon excitations.

By studying the line shape of the dynamic structure factor, $S(\Delta\mathbf{K},\omega)$, one can obtain a valuable and complete information about the dynamics and structure of the adsorbates as well as their distribution on the surface. Experimental information about *long-distance* correlations is obtained from $S(\Delta\mathbf{K},\omega)$ when considering small values of $\Delta\mathbf{K}$, while information about *long-time* correlations is available at small energy transfers, $\hbar\omega$. Apart from this type of information, $S(\Delta\mathbf{K},\omega)$ can also be used to determine the adiabatic adsorption potential, $V(\mathbf{R})$, which describes the adsorbate-substrate interaction. The standard procedure employed consists in starting with a model potential that contains some adjustable parameters and that has to fit the experimental QHAS measurements [i.e., $S(\Delta\mathbf{K},\omega)$] after deconvolution with the apparatus response function [7].

From a theoretical-numerical viewpoint, $S(\Delta\mathbf{K},\omega)$ is studied through particle distribution functions, which takes advantage of the fact that surface diffusion is a problem that can be tackled by means of classical mechanics when dealing with heavy adsorbates. Let us consider an ensemble of interacting classical particles on a surface. Their distribution function is described by means of the so-called *van Hove* or *time-dependent pair correlation function* $G(\mathbf{R},t)$ [18], which is the Fourier transform in space and time of $S(\Delta\mathbf{K},\omega)$, i.e.,

$$S(\Delta\mathbf{K},\omega) = \iint G(\mathbf{R},t)e^{i(\Delta\mathbf{K}\cdot\mathbf{R}-\omega t)}\,d\mathbf{R}\,dt. \tag{2}$$

Given an adparticle at the origin at some arbitrary initial time, $G(\mathbf{R},t)$ represents the average probability for finding a particle (the same or another one) at the surface position $\mathbf{R} = (x,y)$ at a time t. This function is a generalization of the well-known (static) pair distribution function $g(\mathbf{R})$ from statistical mechanics [19, 20], since it provides information about the interacting particle dynamics.

In order to obtain some analytical results and therefore a guide for the interpretation of the numerical Langevin simulations, instead of computing $S(\Delta\mathbf{K},\omega)$ from $G(\mathbf{R},t)$, one can also express the dynamic structure factor [18] as

$$S(\Delta\mathbf{K},\omega) = \int e^{-i\omega t}\,I(\Delta\mathbf{K},t)\,dt, \tag{3}$$

where

$$I(\Delta\mathbf{K},t) \equiv \langle e^{-i\Delta\mathbf{K}\cdot[\mathbf{R}(t)-\mathbf{R}(0)]}\rangle = \langle e^{-i\Delta\mathbf{K}\cdot\int_0^t \mathbf{v}(t')\,dt'}\rangle \tag{4}$$

is the *intermediate scattering function* – which is the *space* Fourier transform of $G(\mathbf{R},t)$. In (4) the brackets denote an average over realizations and particles, and $\mathbf{v}$ is the adparticle velocity parallel to the surface. Now, we note that the intermediate scattering function can also be expressed as a second order cumulant expansion in $\Delta\mathbf{K}$,

$$I(\Delta\mathbf{K},t) \approx e^{-\Delta K^2\int_0^t (t-t')\mathscr{C}_{\Delta\mathbf{K}}(t')dt'}, \tag{5}$$

where

$$\mathscr{C}_{\Delta\mathbf{K}}(\tau) \equiv \langle v_{\Delta\mathbf{K}}(0)\, v_{\Delta\mathbf{K}}(\tau)\rangle \equiv \lim_{\mathscr{T}\to\infty}\frac{1}{\mathscr{T}}\int_0^{\mathscr{T}} v_{\Delta\mathbf{K}}(t)\, v_{\Delta\mathbf{K}}(t+\tau)\,dt \tag{6}$$

is the *autocorrelation function* of the velocity projected onto the direction of the parallel momentum transfer (whose length is $\Delta K \equiv \|\Delta\mathbf{K}\|$). Only differences τ between two times are considered because this function is assumed to be *stationary*. This is the so-called *Gaussian approximation* [19], which is exact when the velocity correlations at more than two different times are negligible, thus allowing to replace the average acting over exponential functions in the right hand side (r.h.s.) of the second equality in (4) by an average over their arguments. This approximation results of much help in the interpretation of the numerical results as well as in getting an insight into the underlying dynamics.

In general, calculating $S(\Delta\mathbf{K},\omega)$ through $G(\mathbf{R},t)$ implies using the standard LMD approach, the most standard technique to obtain the particle dynamics – the same happens if we want to obtain $I(\Delta\mathbf{K},t)$. This means to consider a Gaussian white noise simulating the effects (friction) due to the surface temperature and a dipole-like force depending on the coverage mediating the interaction among adsorbates. In reference [8] an analytical treatment based on a Markovian-Langevin approach with Gaussian white noise was derived within the single adsorbate approximation to study diffusion at low coverage, showing that the dynamical-statistical magnitudes given above could be well described analytically within the Gaussian approximation framework. When the coverage increases, adsorbate-adsorbate interactions can no longer be neglected and they have to be also taken into account to describe the diffusion process. We showed that the previous Markovian-Langevin treatment for single adsorbates could also be extended to the case of interacting adsorbates by including into the corresponding Langevin equation a new noise source accounting for the collisions among adsorbates: a white shot noise. That is, the dynamics of many interacting adsorbates is replaced by the dynamics of a single adsorbate subjected to a series of random pulses within a Markovian regime (i.e., pulses of relatively short duration in comparison with the system relaxation), a shot noise like force, which mimics the collisions with other surrounding adsorbates leading to the introduction of a collisional friction. This is what we have called the *interacting single adsorbate* (ISA) approximation [15, 16]. Note that, consequently, within this approach the averaging in (4) is carried out over realizations, but *not* over particles.

3 The Noise-Like Forces Acting on the Adsorbates

The ISA model is based on considering that, provided memory effects are not relevant, the adsorbate dynamics observed on a surface can be studied using the standard Langevin formalism. In this case, any interaction can be substituted by a noise-like force (except the adsorbate-substrate interaction): the action of surface thermal fluctuations (thermal phonons) by a Gaussian white noise and the dipole-dipole interactions among adsorbates by a shot noise. Here we present a brief overview of these two types of noise sources. Moreover, we also introduce a simple model that can be used to relate the coverage with the collisional friction of the shot noise in an easy manner when carrying out the corresponding simulations.

3.1 Gaussian White Noise and Surface Thermal Fluctuations

In 1930 Orstein and Uhlenbeck [21] formulated a stochastic model for Brownian motion based on considering the particle velocity as the (stochastic) variable of interest – this model contrasts with the Einstein-Wiener stochastic model, where the variable of interest is the particle position. The basic equation in the Orstein-Uhlenbeck model is the Langevin equation

$$m\dot{v} = -m\gamma v + mR_G(t). \tag{7}$$

This equation is the simplest expression to describe the Brownian motion of a particle of mass m in one dimension. As can be seen, the r.h.s. of this equation is constituted by two contributions: (i) a deterministic part, characterized by the friction force $-m\gamma v$, with γ being the friction coefficient depending on the *fluid viscosity*; and (ii) a stochastic part governed by the random force $mR_G(t)$, where $R_G(t)$ is a Gaussian white noise source. This type of noise satisfies two conditions:

1. Its mean value is zero: $\langle R_G(t)\rangle = 0$.
2. The associate force-force time correlation function has an infinitely short duration: $m^2\langle R_G(0)R_G(\tau)\rangle = K\delta(\tau)$.

Generally speaking, the particle is regarded as the system (of interest) while the stochastic force is the effect of a surrounding thermal bath, the constant K being related to the system-bath coupling strength. The validity of this model thus relies on the fact that the system-bath coupling is relatively weak, although the action of the bath over the system is *continuous* along time. In this way, although the perturbations caused by the bath over the system are negligible when considered individually, their combine effect affects dramatically the system dynamics. The random noise source is Gaussian because in the long-time limit the continuous action of the bath satisfies the *central limit theorem*. On the other hand, note that the detailed dynamical evolution of the bath degrees of freedom is not taken into account. Bath correlations, described by the second condition, decay in timescales shorter (fast decays) than the characteristic times involved in the system dynamics.

The first contribution in (7) describes the collective or overall effect observed in the system and is due to the second contribution, which refers to individual (random) events. In other words, there is a relationship between the macroscopic or average dynamical behavior of the system (the friction, in this context) and the "microscopic" cause that produces it (due to the bath fluctuations). The relationship between the friction and the fluctuations of the random force in (7) is given by *the fluctuation-dissipation theorem* [22], which reads as

$$\begin{aligned}\gamma(\omega) &= \frac{m}{k_B T}\int_0^\infty \langle \delta R_G(0)\,\delta R_G(\tau)\rangle\, e^{-i\omega\tau}\,d\tau \\ &= \frac{m}{2k_B T}\int_{-\infty}^\infty \langle \delta R_G(0)\,\delta R_G(\tau)\rangle\, e^{-i\omega\tau}\,d\tau \end{aligned} \tag{8}$$

where

$$\delta R_G(t) \equiv R_G(t) - \langle R_G(t)\rangle \tag{9}$$

is the fluctuation due to the random noise function $R_G(t)$. Making use of the aforementioned properties 1 and 2 above, the r.h.s. of (8) becomes

$$\gamma(\omega) = \frac{K}{2mk_B T}. \tag{10}$$

As seen from this expression, the frequency spectrum of the friction force is "flat" or frequency-independent. In analogy to white light, such an spectrum is also called *white* in the sense that all frequencies contribute equally. This allows to establish

$$\gamma(\omega) \equiv \gamma, \tag{11}$$

with the coupling strength thus being

$$K = 2m\gamma k_B T. \tag{12}$$

In general, the force-force time correlation function can be expressed in terms of the noise fluctuations (9) as

$$\mathscr{G}_G(\tau) \equiv \langle \delta R_G(0)\,\delta R_G(\tau)\rangle = \frac{2\gamma k_B T}{m}\,\delta(\tau). \tag{13}$$

Within the context of the adsorbate surface diffusion, the effects caused by the thermal fluctuations of the surface on the adsorbates can be treated as an overall random noise. This was shown by Ellis and Toennies [23] in 1994, who observed that molecular dynamics simulations taking into account the motion of both the surface atoms and the adsorbates at low coverages could be replaced by a Langevin equation for a single adsorbate characterized by a certain coupling strength or damping factor γ, whose value was obtained from dynamical arguments. Apart from this "semi-empirical" study, one could also reach the same conclusion by performing, for instance, a frequency analysis of adsorbate trajectories.

3.2 White Shot Noise and Adsorbate-Adsorbate Collisions

The concept of noise arises from the early days of radio, the so-called *shot noise* being one of the main sources of noise [24]. The study of this type of noise, first considered by Schottky [25] in 1918, was summarized and largely completed by Rice [26] in the mid 1940's. The paradigm of shot noise is a non steady electrical current generated by independent (i.e., no correlated) electrons arriving randomly at the anode of a vacuum tube. This random time-dependent electric current can be expressed as

$$I(t) = \sum_i b_i(t - t_i). \tag{14}$$

Here the pulse function $b_i(t - t_i)$ represents the contribution of the ith individual electron to the current and is assumed to be identical for each electron. Regarding the arrival times t_i, they are randomly distributed according to a Poisson distribution with a certain average number per unit time [21].

The same idea of electrons reaching randomly an anode can also be used to describe the problem of interacting adsorbates. This is done by identifying the anode receiving the electrons with a particular adsorbate (system) and the subsequent electrons reaching the anode with the different adsorbates (bath) that collide with the system-adsorbate. Within this picture the dipole-dipole interactions between two colliding adsorbates is then replaced by a shot-noise-like random force (accounting for the effects of all the bath-adsorbates) acting on a single adsorbate. The validity of this model is based on considering that: (i) the system-bath coupling is relatively weak and (ii) in the long time limit the microscopic effects of the dipole-dipole interaction forces are wiped out and only the effective number of impacts felt by the system-adsorbates expressed in terms of a collisional friction is relevant. Note that this idea is similar to that considered by Van Vleck and Weisskopf [27] to understand the line-shape broadening observed in the spectral lines of gases due to the increasing pressure.

The shot noise force undergone by the adsorbates can be expressed as $m\delta R_S(t)$, where

$$\delta R_S(t) \equiv R_S(t) - \langle\langle R_S \rangle\rangle \tag{15}$$

is defined as in (9), with

$$\langle\langle R_S \rangle\rangle \equiv \sum_K P_K(\mathscr{T}) \langle R_S(t') \rangle_{\mathscr{T}}. \tag{16}$$

The double average bracket in the last expression indicates averaging over the number of collisions (K) according to a certain distribution (P_K) and the total time considered ($\mathscr{T}$). In analogy to (14),

$$R_S(t) = \sum_{k=1}^{K} b_k(t - t_k), \tag{17}$$

with $b_k(t-t_k)$ providing information about the shape and effective duration of the kth adsorbate-adsorbate collision at t_k. The probability to observe K collisions after a time $\mathscr{T}$ follows a Poisson distribution

$$P_K(\mathscr{T}) = \frac{(\lambda\mathscr{T})^K}{K!}\, e^{-\lambda\mathscr{T}}, \tag{18}$$

where λ is the average number of collisions per unit time or *collisional friction*. Assuming sudden adsorbate-adsorbate collisions and that after-collision effects relax exponentially at a constant rate λ', the pulses in (17) can be modeled as

$$b_k(t-t_k) = c_k\lambda' \mathrm{e}^{-\lambda'(t-t_k)}, \tag{19}$$

with $t-t_k > 0$ and c_k giving the intensity of the collision impact. Within a realistic model, collisions take place randomly at different orientations and energies. Hence it is reasonable to assume that the c_k coefficients are distributed according to an exponential law,

$$g(c_k) = \frac{1}{\alpha}\, e^{-c_k/\alpha}, \qquad c_k \geq 0, \tag{20}$$

where $\alpha = \sqrt{m/k_BT}$ [15].

Notice that this stochastic description makes evident the following subtlety. In addition to the friction due to the surface thermal fluctuations, the collisions among adsorbates introduce a new type of friction, the collisional friction. As in Sect. 3.1, this friction can be related with its corresponding cause, the collisions, by means of the fluctuation-dissipation theorem. The time correlation function for the fluctuations of the shot noise is given by

$$\mathscr{G}_S(\tau) = \langle\langle \delta R_S(0)\, \delta R_S(\tau)\rangle\rangle, \tag{21}$$

where the double bracket is defined as in (16). A general expression for $\mathscr{G}_S(\tau)$ can be readily obtained after straightforward algebraic manipulations [15] to yield

$$\mathscr{G}_S(\tau) = \frac{\lambda\lambda'}{\alpha^2}\, \mathrm{e}^{-\lambda'|\tau|}. \tag{22}$$

Introducing (22) into the mathematical expression of the fluctuation-dissipation theorem,

$$\tilde{\xi}(\omega) = \frac{m}{k_BT}\int_0^\infty \mathscr{G}_S(\tau)\, e^{-i\omega\tau}\, d\tau, \tag{23}$$

we obtain

$$\tilde{\xi}(\omega) = \lambda\, \frac{\lambda'}{\lambda' + i\omega}, \tag{24}$$

whose real part is

$$\mathrm{Re}[\tilde{\xi}(\omega)] = \frac{1}{2}\,[\tilde{\xi}(\omega) + \tilde{\xi}^*(\omega)] = \lambda\, \frac{\lambda'^2}{\lambda'^2 + \omega^2}. \tag{25}$$

Two limits are interesting in this expression: $\lambda' \ll \omega$ and $\lambda' \gg \omega$. These limits are related to the two timescales associated with λ and λ'. Independently of their intensity, we consider that any pulse decays at the same rate λ' within this model for simplicity. This rate defines a decay timescale $\tau_c = 1/\lambda'$ for collision events. On the other hand, the collisional friction introduces another timescale $\tau_r = 1/\lambda$, which can be interpreted as the (average) time between two successive collisions; adsorbate diffusion is related to this timescale. Taking this into account, the first limit involves very short timescales (smaller than τ_c), where memory effects are important and the generalized Langevin equation should be applied. Note that in this case, (24) can be written as

$$\tilde{\xi}(\omega) \approx \lambda \frac{\lambda'^2}{\omega^2}. \tag{26}$$

This frequency-dependent friction does not allow to define an appropriate relaxation timescale τ_r. In this case, we refer to *colored shot noises* [28], which have been used to describe, for example, thermal ratchets [29], mean first passage times [30] or jump distributions in surface diffusion [31]. Conversely, in the second limit, the collision timescale rules the adsorbate dynamics, establishing a cutoff frequency. In this limit

$$\tilde{\xi}(\omega) \approx \lambda \left(1 - \frac{\omega^2}{\lambda'^2}\right), \tag{27}$$

which can be written as $\tilde{\xi}(\omega) \approx \lambda$ whenever $\lambda \ll \omega \ll \omega_c = \tau_c^{-1}$ (i.e., $\tau_r \ll \tau_c$). This limit holds for strong but localized (instantaneous) collisions as well as for weak but continuous kicks (Brownian motion). Moreover, since it is similar to the condition leading to (11), one can speak about a *Poissonian white shot noise* and make use of the standard Langevin equation.

3.3 Relationship Between the Coverage and the Collisional Friction

In principle, there is no a simple, straightforward relationship relating the coverage with the collisional friction which should be obtained either from microscopic observations, first principles or both. However, it is clear that such a relation is fundamental in order to carry out any calculation within this stochastic approach. Here we show how both parameters can be related in a simple manner. In the elementary kinetic theory of transport in gases [19] diffusion is proportional to the mean free path $\bar{l}$, which is proportionally inverse to both the density of gas particles and the effective area of collision when a hard-sphere model is assumed. For two-dimensional collisions the effective area is replaced by an effective length (twice the radius ρ of the adparticle) and the gas density by the surface density σ. Accordingly, the mean free path is given by

$$\bar{l} = \frac{1}{2\sqrt{2}\rho\sigma}. \tag{28}$$

Taking into account the Chapman-Enskog theory for hard spheres, the self-diffusion coefficient can be written as

$$D = \frac{1}{6\rho\sigma}\sqrt{\frac{k_B T}{m}}. \tag{29}$$

Now, from Einstein's relation (see below Sect. 3), and taking into account that $\theta = a^2\sigma$ for a square surface lattice of unit cell length a, we obtain

$$\lambda = \frac{6\rho}{a^2}\sqrt{\frac{k_B T}{m}}\,\theta. \tag{30}$$

This relationship allows to estimate λ readily once the surface coverage and temperature are known.

4 Langevin Description of Surface Diffusion

Except for the case of a free-potential problem, the analytical study of the particle motion in two dimensions results intractable in general due to the dynamical correlations at short times induced by the interaction potential. However, since we are interested in offering an analytical formulation that allows to better understand the process ruling surface diffusion and low-frequency vibrational motions, it is sufficient to proceed in one dimension and then try to adapt the resulting formulation to two dimensions.

The motion of an adsorbate subjected to the action of a bath consisting of another adsorbates on a static one-dimensional potential can be well described by the generalized Langevin equation

$$\ddot{x}(t) = -\int_0^t \xi(t-t')\,\dot{x}(t')\,dt' + F[x(t)] + \delta R_{GS}(t), \tag{31}$$

where x represents the adsorbate coordinate; $F = -\nabla V$ is the deterministic force per mass unit derived from the periodic surface interaction potential, $V(x) = V(x+a)$ (a is the period along the x-direction); and $\xi(t)$ is the bath memory function, which includes the effects arising from both the Gaussian white noise and the shot noise. Because of this, the stochastic noise source is expressed as the sum of both contributions:

$$\delta R_{GS}(t) = \delta R_G(t) + \delta R_S(t). \tag{32}$$

If τ_c is relatively small, the memory function will be local in time. This allows to reexpress it as $\xi(t-t') \simeq (\gamma+\lambda)\delta(t-t')$ and expand the upper time limit in the integral to infinity. Taking this approximation into account and defining $\eta \equiv \gamma+\lambda$,

(31) becomes

$$\ddot{x}(t) = -\eta \dot{x}(t) + F[x(t)] + \delta R_G(t) + \delta R_S(t). \tag{33}$$

This equation summarizes the essence of the ISA approximation.

The particle velocity and position can be straightforwardly obtained from (33) by formal integration to yield:

$$v(t) = v_0 e^{-\eta t} + \int_0^t e^{-\eta(t-t')} F[x(t')]\, dt' + \int_0^t e^{-\eta(t-t')} \delta R_{GS}(t')\, dt', \tag{34a}$$

$$x(t) = x_0 + \frac{v_0}{\eta}\left(1 - e^{-\eta t}\right) + \frac{1}{\eta}\int_0^t \left[1 - e^{-\eta(t-t')}\right] F[x(t')]\, dt' + \frac{1}{\eta}\int_0^t \left[1 - e^{-\eta(t-t')}\right] \delta R_{GS}(t')\, dt', \tag{34b}$$

where $v_0 = v(0)$ and $x_0 = x(0)$. It is clear that when $\delta R_{GS} = 0$, (34a) and (34b) become the formal solutions of purely deterministic equations of motion. If the system is initially thermalized (i.e., it follows a Maxwell-Boltzmann distribution in velocities) and has a uniform probability distribution in positions around $x = 0$, then $\bar{v}_0 = \langle v_0 \rangle = 0$, $\bar{v}_0^2 = \langle v_0^2 \rangle = k_B T/m$ and $\bar{x}_0 = \langle x_0 \rangle = 0$. For $\lambda' \gg \lambda$, i.e., in the Poissonian white noise limit, we obtain

$$\langle v \rangle(t) = 0, \tag{35a}$$

$$\langle v^2 \rangle(t) = \frac{k_B T}{m}, \tag{35b}$$

$$\langle x \rangle(t) = 0, \tag{35c}$$

$$\langle x^2 \rangle(t) = \bar{x}_0^2 + \frac{k_B T}{m\eta^2}\left[2\eta t + 1 - \left(2 - e^{-\eta t}\right)^2\right]. \tag{35d}$$

These equations constitute a limit and therefore for values of the parameters out of the range of validity of the approximation deviations are expected. However, they result very insightful in order to understand the system dynamics.

As happens with the Brownian motion ($V = 0$), two regimes are also clearly distinguishable from (35d). For $\eta t \ll 1$ collision events are rare and the adparticle shows an almost free motion with relatively long mean free paths. This is the *ballistic* or *free-diffusion regime*, characterized by

$$\langle x^2(t) \rangle \sim \frac{k_B T}{m} t^2. \tag{36}$$

On the other hand, for $\eta t \gg 1$ there is no free motion since the effects of the stochastic force (collisions) are dominant. This is the *diffusive regime*, where mean square displacements are linear with time:

$$\langle x^2(t) \rangle \sim \frac{2k_B T}{m\eta} t = 2Dt. \tag{37}$$

This is the so-called *Einstein's law*. Note from (37) that: (1) lowering the friction η acting on the adparticle leads to a faster diffusion (the diffusion coefficient D increases) and (2) the diffusion becomes more active as the surface temperature increases.

For $V \neq 0$ the average values given above are expected to show some deviations due to of the role played by the terms corresponding to the deterministic force. Because of the potential wells, adparticles may display an eventual bound motion together with the diffusion along the surface. This will lead to a decrease of the diffusion with respect to a case where the corrugation is negligible ($V \approx 0$). Moreover, the low-frequency vibrational motion observed when the particle remains bound within a potential well will give rise to the presence of T modes, which manifest as two symmetric peaks (with respect to the diffusive one) in the energy transfer spectrum (dynamic structure factor).

4.1 The Low Corrugation Regime. Quasi-free Adparticles

In the case of diffusion on low corrugated surfaces, where the role of the adiabatic adsorbate-substrate interaction potential is negligible, one can consider the approximation $V = 0$. The adparticle motion can then be regarded as quasi-free since it is only influenced by the two random forces. From (6), and again in the limit of Poissonian white noise ($\lambda' \gg \lambda$), one thus obtains

$$\mathscr{C}(t) = \bar{v}_0^2 e^{-\eta t}. \tag{38}$$

Introducing this relation into (5), we find

$$I(\Delta\mathbf{K},t) = \exp\left[-\chi^2\left(e^{-\eta t} + \eta t - 1\right)\right], \tag{39}$$

with $\chi^2 \equiv \langle v_0^2\rangle \Delta K^2/\eta^2$ being the *shape parameter*. With the coverage, η increases and the decay of $I(\Delta\mathbf{K},t)$ becomes slower. This leads to a narrowing in the line shape associated with the dynamic structure factor, which can be analytically obtained [16] from (3):

$$S(\Delta K,\omega) = \frac{e^{\chi^2}}{\pi}\sum_{n=0}^{\infty}\frac{(-1)^n\chi^{2n}}{n!}\frac{(\chi^2+n)\eta}{\omega^2+[(\chi^2+n)\eta]^2}. \tag{40}$$

In the high friction limit, this function has a Lorentzian shape and the full width at half maximum (FWHM) is $\Gamma = 2\eta\chi^2$, which approaches zero as η increases. On the other hand, in the low friction limit, the line shape is a Gaussian with $\Gamma = 2\sqrt{2\ln 2}\sqrt{k_BT/m}\,\Delta K$, which does not depend on η. This is the case for a two-dimensional free gas [32]. The gradual change of the line shape as a function of the magnitudes defining the shape parameter is known as the *motional narrowing effect* [8, 10].

4.2 The High Corrugation Regime. Bound Adparticles

When the surface corrugation is important, effects associated with the T modes are expected to manifest in the velocity autocorrelation function. An interesting example to examine which approximates this behavior is the anharmonic oscillator. The velocity autocorrelation function in this case takes the form [16]

$$\mathscr{C}(t) = \bar{v}_0^2 e^{-\tilde{\eta}\tau}\cos(\tilde{\omega}t + \tilde{\delta}), \tag{41}$$

where the values of the parameters $\tilde{\eta}$, $\tilde{\omega}$ and $\tilde{\delta}$ are free in principle and can be obtained by a fitting to the numerical results. Again, using (5), we can obtain an analytic expression for the intermediate scattering function,

$$I(\Delta K,t) = e^{-\chi_l^2\tilde{A}_1-\chi_l^2\tilde{A}_2 t}\sum_{m,n=0}^{\infty}\frac{(-1)^{m+n}}{m!\,n!}\chi_l^{2(m+n)}\tilde{A}_3^m\tilde{A}_4^n \times e^{i(m-n)\tilde{\delta}}e^{-(m+n)\tilde{\eta}t}e^{i(m-n)\tilde{\omega}t}, \tag{42}$$

with

$$\tilde{A}_1 = \frac{\tilde{\eta}^2[2\tilde{\eta}\tilde{\omega}\sin\tilde{\delta} + (\tilde{\omega}^2-\tilde{\eta}^2)\cos\tilde{\delta})}{(\tilde{\eta}^2+\tilde{\omega}^2)^2}, \tag{43a}$$

$$\tilde{A}_2 = \frac{\tilde{\eta}^2(\tilde{\eta}\cos\tilde{\delta} - \tilde{\omega}\sin\tilde{\delta})}{\tilde{\eta}^2+\tilde{\omega}^2}, \tag{43b}$$

$$\tilde{A}_3 = \frac{\tilde{\eta}^2}{2(\tilde{\eta}-i\tilde{\omega})^2}, \tag{43c}$$

$$\tilde{A}_4 = \frac{\tilde{\eta}^2}{2(\tilde{\eta}+i\tilde{\omega})^2}. \tag{43d}$$

As seen in (42), there is a linear dependence on time in the first exponential of $I(\Delta K,t)$ arising from the independence of $\tilde{\eta}$, $\tilde{\omega}$ and $\tilde{\delta}$ one another. This leads to an exponential decaying factor in (42), which accounts for the diffusion and the asymptotic vanishing of $I(\Delta K,t)$. In this sense, the intermediate scattering function describes both phenomena, diffusion and low-frequency vibrational motions.

As before, the information about the structure of the lattice can be found in the shape parameter, now expressed as χ_l. When large parallel momentum transfers are considered, both the periodicity and the structure of the surface have to be taken into account. Consequently, the shape parameter χ defined in the previous section will be different for different lattices. The simplest model including the periodicity of the surface is that developed by Chudley and Elliott [33], who proposed a master equation for the pair-distribution function in space and time assuming instantaneous discrete jumps on a two-dimensional Bravais lattice. However, very recently, a generalized shape parameter based on the Chudley-Elliott model has been

proposed [16, 34] within the context of the ISA approximation to be

$$\chi_l(\Delta\mathbf{K}) \equiv \sqrt{\frac{\Gamma_\nu(\Delta\mathbf{K})}{2\tilde{\eta}}}, \tag{44}$$

with

$$\Gamma_\nu(\Delta\mathbf{K}) = \nu \sum_{\mathbf{j}} P_{\mathbf{j}} \left[1 - \cos(\mathbf{j}\cdot\Delta\mathbf{K})\right] \tag{45}$$

represents the inverse of the correlation time, with ν being the total jump rate out of an adsorption site and $P_{\mathbf{j}}$ being the relative probability that a jump with a displacement vector $\mathbf{j}$ occurs.

It is straightforward to also derive an analytic expression for the dynamic scattering factor [16]:

$$S(\Delta K,\omega) = \frac{e^{-\chi_l^2\tilde{A}_1}}{\pi} \sum_{m,n=0}^{\infty} \frac{(-1)^{m+n}}{m!\,n!}\, \chi_l^{2(m+n)} \tilde{A}_3^m \tilde{A}_4^n e^{i(m-n)\delta} \times \frac{\chi_l^2\tilde{A}_2 + (m+n)\tilde{\eta}}{[\omega-(m-n)\tilde{\omega}]^2 + [\chi_l^2\tilde{A}_2 + (m+n)\tilde{\eta}]^2}. \tag{46}$$

From this expression we note that the Q peak consists of the contributions with $m = n$, each partial FWHM being $\Gamma = \chi_l^2\tilde{A}_2 + 2m\tilde{\eta}^2$. Analogously, the T-mode peaks come from the sums with $n \neq m$, with their partial FWHM being $\Gamma = \chi_l^2\tilde{A}_2 + (m+n)\tilde{\eta}$. If the Gaussian approximation is good enough, the value of $\tilde{\eta}$ will be not too different from the value of η and therefore the line shapes corresponding to the Q and T-mode peaks are predicted to display broadening as η increases. This is a very remarkable result since the ISA approximation, a relatively simple model, is able to explain the broadening as a function of the coverage experimentally observed: it arises from the temporary confinement of the adparticles inside potential wells during their dynamical evolution along the surface [14]. Moreover, within this approximation, the problem of the experimental deconvolution [34] can be handle in a simple manner: deconvolution could be carried out in a more appropriate way (i.e., with analytic functional forms) and the information about diffusion constants and jump mechanisms extracted would be more reliable. Finally, as mentioned above, the motional narrowing effect will again govern the gradual change of the whole line shape as a function of the coverage (via the collisional friction λ, which is contained in total friction η), the parallel momentum transfer and the jump mechanism.

4.3 Running and Bound Trajectories

When dealing with realistic adsorbate-substrate interaction potentials it is clear that trajectories are going to display temporary trapping and periods of time of unbound flights on the surface. Therefore, in order to better understand and interpret the

diffusion process, a model in which the adsorbate has to separate possibilities of motion, diffusion and vibration, can be invoked. In other words, two types of trajectories can be considered: running (R) and bound (B). Within this simple model, the velocity autocorrelation function reads [14] as

$$\mathscr{C}(t) = \alpha \mathscr{C}_R(t) + (1-\alpha)\mathscr{C}_B(t), \tag{47}$$

where $\mathscr{C}_R$ and $\mathscr{C}_B$ correspond to the velocity autocorrelation functions for a flat surface and an anharmonic oscillator given by (38) and (41), respectively. In (47), α represents the fraction of running trajectories. Accordingly, the intermediate scattering function can be written as

$$I(\Delta\mathbf{K},t) \approx [I_R(\Delta\mathbf{K},t)]^{\alpha}[I_B(\Delta\mathbf{K},t)]^{1-\alpha} \tag{48}$$

where $I_R(\Delta\mathbf{K},t)$ and $I_B(\Delta\mathbf{K},t)$ refer to the intermediate scattering functions for running and bound trajectories, given by (39) and (42), respectively. This expression allows to distinguish between the contributions arising from the unbound or diffusive motion and the bound or vibrational one. Physically, this distinction is very important: it participates directly in the broadening observed in the Q and T-mode peaks with the coverage. Although the percentage α of running trajectories is always larger than that one corresponding to the bound trajectories, depending on its value $I(\Delta\mathbf{K},t)$ will decay faster or slower. As the fraction of running trajectories increases, the correlation between particle oscillations will decay faster. This gives rise to a loss of phase among the complex exponentials involved in the r.h.s. of the first equality of (4), which translates into a faster decay of $I(\Delta\mathbf{K},t)$. On the contrary, the effect of the bound trajectories is to keep such correlations for longer times, giving place to delay the decay of $I(\Delta\mathbf{K},t)$. The line-shape broadening with η is thus a result of an increasing number of running trajectories.

5 Results

To better understand the concepts introduced above, here we present results for two different types of two-dimensional surfaces: flat and periodic. We will illustrate the applicability of the ISA approximation using the Na/Cu(001) system, for which a lot of experimental and theoretical work can be found in the literature [7]. The coverage $\theta_{\mathrm{Na}} = 1$ thus corresponds to one Na atom per Cu(001) surface atom or, equivalently, $\sigma = 1.53 \times 10^{19}$ atom/cm^2 [7]; $a = 2.557$ Å is the unit cell length; and $\rho = 2$ Å has been used for the atomic radius. The surface friction that we have considered in our simulations is taken from reference [6] to be $\gamma = 0.1\ \omega_0 = 2.2049 \times 10^{-5}$ (frictions and diffusion constants are given here in atomic units), where ω_0 is the harmonic frequency associated with the periodic adsorbate-substrate interaction potential. Frequencies and times are here given in atomic units. We are going to analyze four coverages for two surface temperatures of 200 K and 300 K: $\theta_{\mathrm{Na}} = 0.028$, 0.064, 0.106 and 0.18 (below, the first and forth values of θ_{Na} are referred to as θ_1 and θ_2,

respectively). Accordingly, using (30), we will have that at $T = 200$ K, for instance, the values of the collisional friction (total friction) for the smaller and larger values of the coverage are $\lambda = 3.34 \times 10^{-6}$ ($\eta = 2.53 \times 10^{-5}$) and $\lambda = 2.15 \times 10^{-5}$ ($\eta = 4.68 \times 10^{-5}$), respectively. Regarding the collision relaxation rate, we have chosen $\lambda' = 10^{-3}$ to satisfy the condition of Markovian dynamics.

5.1 Low Corrugation. The Flat Surface Model

In low corrugated surfaces the role of the activation barrier to pass from a cell to another one is negligible – this happens, for instance, with a two-dimensional gas [17,32]. Hence, one can use a flat surface model to study diffusion. According to the description given in Sect. 3, in this case $\langle x^2 \rangle(t)$ displays two well-defined dynamical regimes: ballistic ($t \ll 1/\eta$) and diffusive ($t \gg 1/\eta$). This can be seen in Fig. 1a, where $\langle x^2 \rangle(t)$ depends on t^2 at short times (of the order of $1/\eta$) and is proportional to t in the long-time regime. In the linear regime, $\langle x^2 \rangle(t)$ behaves in accordance with Einstein's law (37): diffusion decreases with the (total) friction. By fitting this linear part of the graphs to (37), we find $D = 6.045 \times 10^{-4}$ for θ_1 and $D = 3.510 \times 10^{-4}$ for θ_2. From these values, we obtain $\tilde{\eta} = 2.50 \times 10^{-5}$ and $\tilde{\eta} = 4.35 \times 10^{-5}$, which are in a good agreement with the nominal values introduced in the simulations. This agreement between simulation and analytical model confirms the validity of the ISA approximation in this case. These diffusion coefficients are not only related to the surface friction but also to the collisional one, as explained above. Notice that for a given surface friction, the diffusion is inhibited or enhanced depending on the number of collisions per time unit. This is a very remarkable result because in real experiments the surface friction is fixed and therefore diffusion can only be studied only taking into account the coverage of the surface.

Collisions also affect the velocity autocorrelation function: as seen in Fig. 1b, as θ increases $\mathscr{C}(t)$ decays faster. From the fitting of these results to (38) (normalized to unity), we have obtained $\tilde{\eta} \approx 2.52 \times 10^{-5}$ for θ_1 and $\tilde{\eta} \approx 4.32 \times 10^{-5}$ for θ_2, which again show a good agreement with the nominal values employed in the simulations. This agreement can also be interpreted as indicating that high order correlations (e.g., correlations at three or four times) will decay much faster, thus validating the use of the Gaussian approximation when passing from (4) to (5) – the effect of high order correlations on $I(t)$ will be meaningless. The comparison between the intermediate scattering function obtained from the calculations with its fitted homolog using (7) can be seen in Fig. 1c for $\Delta K = 1.23$ Å^{-1} (the fitting has been done considering the nominal values of η used in the simulation and assuming that χ as the fitting parameter). We observe that not only the correspondence between the simulations and the analytical formulas is excellent, but also from the fitted values of χ: $\chi_{fit} = 3.16$ vs $\chi_{sim} = 3.16$ for θ_1, and $\chi_{fit} = 1.81$ vs $\chi_{sim} = 1.83$ for θ_2. In agreement with (7), $I(t)$ presents an initial Gaussian falloff at short times, while for longer times its decay is exponential. Moreover, as also expected from (7), as the coverage increases a slower decay is observed, which will give rise to a *narrowing* in the line shapes of $S(\omega)$ (see below).

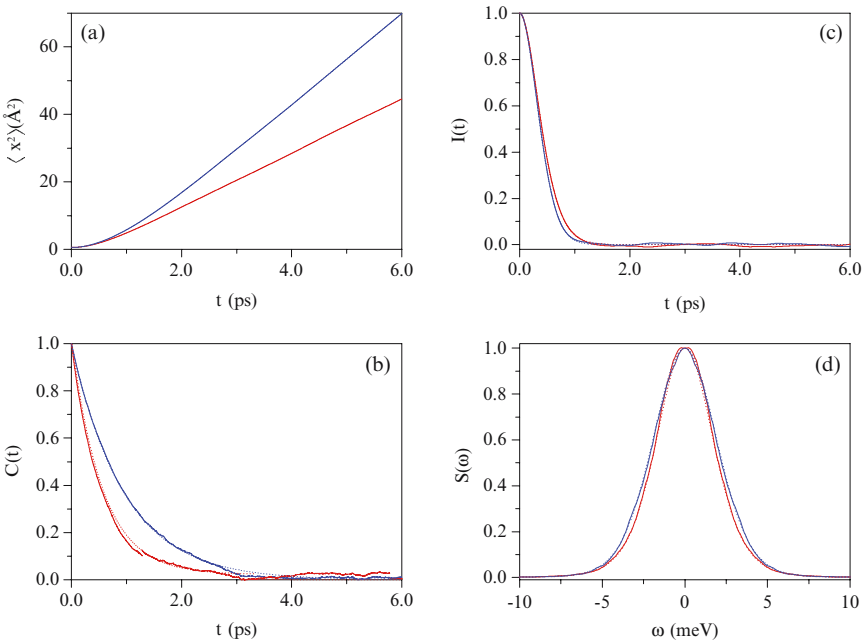

Fig. 1 Dynamical magnitudes for two different values of the coverage, θ_1 (*blue*) and θ_2 (*red*): (**a**) $\langle x^2 \rangle(t)$, (**b**) $\mathscr{C}(t)$, (**c**) $I(t)$ and (**d**) $S(\omega)$, with $\Delta K = 1.23$ Å^{-1}. Dotted lines are the numerical fittings to the corresponding analytical formulas given in Sect. 3. All magnitudes are given in atomic units

In Fig. 1d we have plotted the dynamic structure factor after time Fourier transforming the intermediate scattering function obtained from both the simulations and their corresponding analytical fittings. Since the agreement between the numerical and fitted intermediate scattering functions is fairly good, the same can also be observed here. However, note that increasing the coverage causes a narrowing of the Q peak, whose profile is a mixture of a Gaussian and a Lorentzian function. The Gaussian behavior is ruled by the short time limit of the intermediate scattering function, while the Lorentzian behavior arises from the long time exponential decay. The line shape associated with the Q peak thus depends on which regime is dominant. This is a consequence of the *motional narrowing effect* [8,10]. This analysis should be carried out when experimental results are deconvoluted [15] since it is very common to see fittings of the Q peak to a pure Lorentzian function.

5.2 *Periodic Surface Potential Models. The Relevance of Corrugation*

As an example of diffusion on a realistic potential, now we are going to consider the non-separable surface potential model proposed by Toennies and coworkers to

model the Na/Cu(001) interaction [6]:

$$V(x,y) = V_0(x,y) + V_1(x,y) + V_2(x,y). \tag{49}$$

The first term of this potential model is a separable cosine potential,

$$V_0(x,y) = V_0\,[2 - \cos(2\pi x/a) - \cos(2\pi y/a)]\,, \tag{50}$$

with a the lattice constant of the Cu(001) surface ($a = 2.557$ Å) and $V_0 = 41.4$ meV. The second term,

$$V_1(x,y) = -A \sum_{m,n} e^{-b\{[x/a-(m+1/2)]^2+[y/a-(n+1/2)]^2\}}, \tag{51}$$

with $A = 2V_0$ and $b = 11.8$, is added to produce a lowering of the potential barrier at on-top sites according to the experimental observations. The third term is an also nonseparable contribution,

$$\begin{aligned} V_2(x,y) = {} & \pi^2 C V_0 \sum_{m,n} [(x/a-m)^2 + (y/a-n)^2] \\ & \times \exp[-(x/a-m)^2 - (y/a-n)^2], \end{aligned} \tag{52}$$

with $C = -0.2$, which is introduced to modify the curvature near the minima and vary the difference between the potential at the minima and the bridge positions.

5.2.1 Line-Shape Broadening as a Function of the Coverage

The effect of the bound motion on diffusion (which is explained in more detail in next section) is apparent in Fig. 2, where $I(t)$ is plotted for $\Delta K = 1.23$ Å^{-1}, a surface temperature of 200 K and four different values of the coverage. When the coverage is increased, a higher number of particles escape from the potential wells. This contributes to having more particles displaying diffusive motion, and therefore leading to a faster decay of $I(t)$. Two different decay regimes are clearly

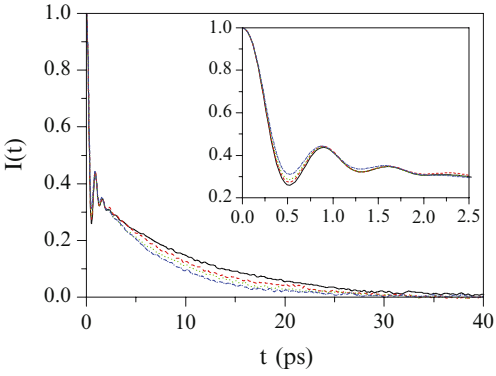

Fig. 2 $I(t)$ for coverages: $\theta = 0.028$ (*black solid line*), $\theta = 0.064$ (*red dashed line*), $\theta = 0.106$ (*green dotted line*) and $\theta = 0.18$ (*blue dashed-dotted line*) at $\Delta K = 1.23$ Å^{-1} and $T = 200K$. In the inset, the same graph for short times

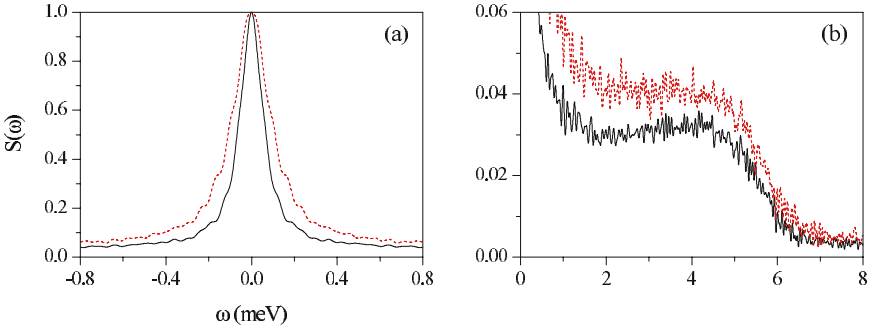

Fig. 3 $S(\omega)$ for two values of the coverage: θ_1 (*black solid line*) and θ_2 (*red dashed line*), at $\Delta K = 1.23$ Å^{-1} and $T = 200$ K. In each plot, details of the Q-peak region (**a**) and the (r.h.s.) T-mode peak region (**b**) are shown

seen: at long times $I(t)$ shows a damping exponential behavior, while at short times (see inset) the observed oscillations are due to the T-mode motion associated with vibrations inside the potential wells (bound trajectories).

The changes induced by the interaction potential (with respect to the flat case) are also apparent in the dynamic structure factor: the T mode manifest as two peaks placed around the frequency of oscillation (± 5 meV) on both sides of the Q peak. The Q and T-mode peaks are plotted separately in Figs. 3a and 3b for θ_1 and θ_2 at $T = 200$ K and $\Delta K = 1.23$ Å^{-1}. The broadening observed in both types of peaks is due to the fast decay displayed by the intermediate scattering function with the coverage. In particular, for the T-mode peak only a shift of the position is clearly seen, as also observed experimentally [6, 7].

The maximum value of the experimental peak widths is found to be increased by a factor of 3 as the coverage is increased from 0.028 to 0.18. LMD simulations have also been carried out but the corresponding results are just able to reproduce the general trend, predicting a smaller increase in the broadening of the Q peak [7]. As will be seen below, in next section, the line-shape broadening is a combined effect of both diffusive and vibrational motions. Moreover, notice that this broadening is related to the increment of the collisional friction since γ is constant (we assume that the surface friction does not depend on the coverage).

In Figs. 4a–d, the results of our model for the Q peak width have been plotted and compared with the experimental ones [6] for $\theta = 0.028$, 0.064, 0.106 and 0.18 at $T = 200$ K and $T = 300$ K along the diagonal direction. As can be seen the agreement is fairly good up to $\theta = 0.106$, where some discrepancies start appearing. This can be used as a limit for our model. This limit is reached with high coverages when the adsorbate-adsorbate interaction plays a more important role in the diffusion dynamics, giving rise to the formation of certain structures and collective phenomena. In such a case, the average motion of the adsorbates is slower and they feel the force exerted by its neighbors for longer times. The Markovian approximation then breaks down and not only memory effects but also the collective dynamics have to be taken into account.

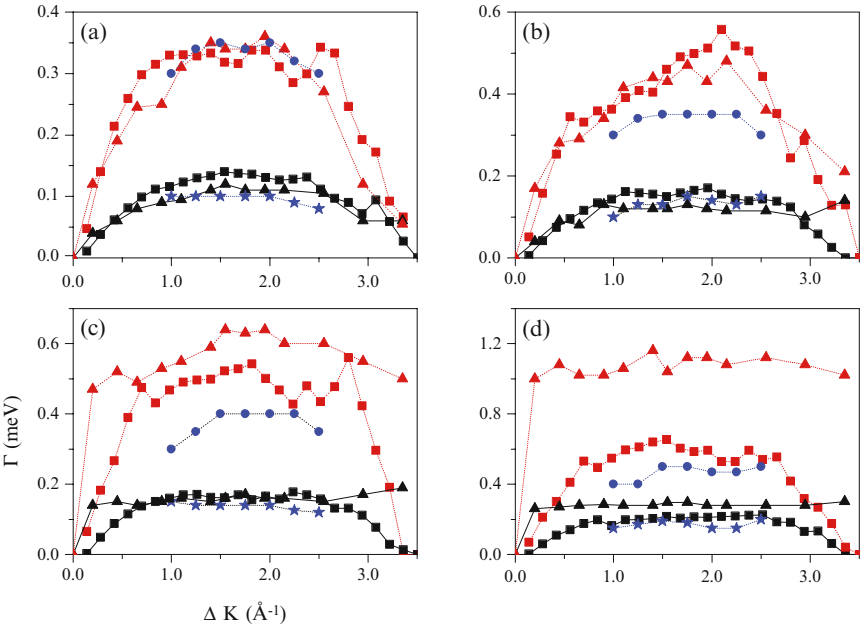

Fig. 4 Numerical (*squares*) and experimental (*triangles*) dependence of Γ on ΔK, at $T = 200$ K (*black/solid*) and $T = 300$ K (*red/dotted*), and different values of the coverage: (**a**) $\theta = 0.028$, (**b**) $\theta = 0.064$, (**c**) $\theta = 0.106$, and (**d**) $\theta = 0.18$. Blue symbols represent LMD simulations at $T = 200$ K (*stars*) and $T = 300$ K (*solid circles*)

Finally, it is also interesting to show the results for the Q peak width when diffusion is measured along the parallel direction, as displayed in Fig. 5. Experimental results have been carried out for low coverage and again the agreement with our model is fairly good, as can be seen in Fig. 5a.

5.2.2 Contribution of Running and Bound Trajectories

Equation (48), with free parameters, allows to distinguish the contributions arising from the unbound or diffusive motion and the bound or vibrational one. As seen in Fig. 6, (48) fits very well the numerical results obtained for the corrugated surface potential in both cases. Though fitted and nominal values are different, their order of magnitude and trend are correct. The fitted values of α are: $\alpha_1 = 2.94\%$ for θ_1 and $\alpha_2 = 4.10\%$ for θ_2. According to these values, it is clear that the contribution to $I(t)$ primarily arises from the bound trajectories – or, in terms of the real dynamics, from the long times spent by the trajectories inside the potential wells. Note from (4) that running trajectories lead to a relative much faster decay of $I(t)$ than the bound ones, which delays such a decay. As stated in Sect. 4.3, the bound motion keeps correlations for longer times than the diffusive one, since the latter provokes a fast loss of phase among the (correlation) oscillating terms that appear in the r.h.s.

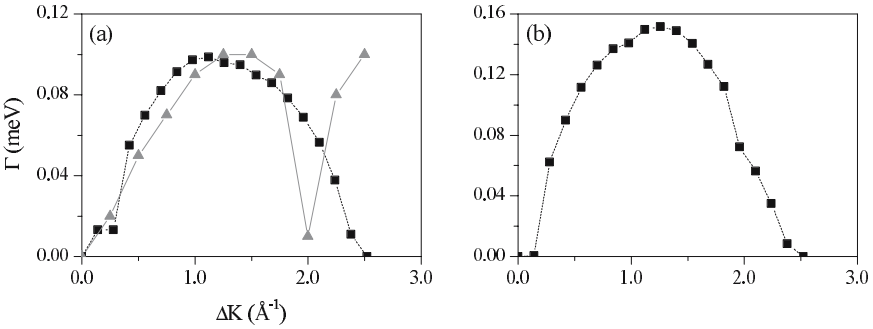

Fig. 5 Dependence of Γ on ΔK for the parallel direction (black/square) at $T = 200$ K and two values of the coverage: (**a**) θ_1 and (**b**) θ_2. Gray triangles in part (a) represent the experimental observations

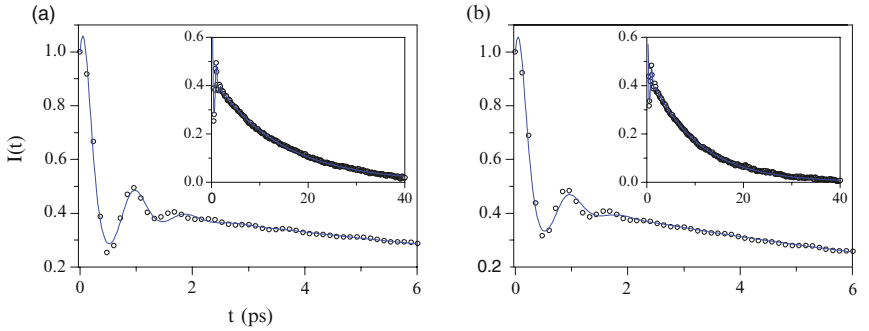

Fig. 6 $I(\Delta\mathbf{K},t)$ for Na on Cu(001) at $\Delta K = 1.23$ Å^{-1} and two different coverages: (**a**) $\theta_1 = 0.028$ and (**b**) $\theta_2 = 0.18$. Open circles indicate the numerical values obtained from the simulation and solid lines are the numerical fitting using (9)

of the first equality in (4). In this way, this explains, first, that $S(\omega)$ is about two orders of magnitude broader in the flat case than in the corrugated one (see Fig. 3). And, second, since $\alpha_2 > \alpha_1$ there is a slightly larger fraction of running trajectories for θ_2, which leads to an also slightly faster decay of $I(t)$, and therefore to observe broadening in $S(\omega)$ with increasing θ. It is worth stressing that a larger fraction of running trajectories does not mean more diffusion (which decreases with increasing θ), but only less particles inside the wells.

6 Conclusions

The good agreement between the experimental data and the results obtained from the ISA approximation including the adsorbate-substrate interaction gives an insight of how important this interaction is in surface dynamics. These simulations together with the theoretical analysis presented here not only provide a complete view of

what is happening along the surface, but it also explains the experimental line-shape broadening of the Q peak ruling the diffusion process as a function of the coverage. Moreover, for its simplicity and low computational cost is the best tool for experimentalists who want a simple, reliable method for explaining their observations. We think that our approach sheds some light on the physics involved in surface diffusion, and has helped us to find the main reason for the corresponding broadening which is the vibrational motion induced for the trapped adsorbates in the potential wells. Next step is to generalize Kramers' turnover theory to the diffusion of interacting adsorbates on a surface in order to infer more physical properties of the diffusing adparticles from the experiment [35]. Moreover, quantum corrections are under study which are thought to be important when the surface temperature is decreased below 50 K [36].

Acknowledgements This work was supported in part by DGCYT (Spain) under Project FIS2007-62006. R.M.-C. thanks the University of Bochum for support from the Deutsche Forschungsgemeinschaft, SFB 558. A.S. Sanz thanks the Ministerio de Educación y Ciencia (Spain) for a "Juan de la Cierva" Contract.

References

1. R. Gomer: Rep. Prog. Phys. **53**, 917 (1990)
2. G. Ehrlich: Surf. Sci. **300**, 628 (1994)
3. F. Hofmann, J.P. Toennies: Chem. Rev. **78**, 3900 (1996)
4. S. Miret-Artés, E. Pollak: J. Phys.: Condens. Matter **17**, S4133 (2005)
5. A.P. Jardine, S. Dworski, P. Fouquet, G. Alexandrowicz, D.J. Riley, G.Y.H. Lee, J. Ellis, W. Allison: Science **104**, 1790 (2004); P. Fouquet, A.P. Jardine, S. Dworski, G. Alexandrowicz, W. Allison, J. Ellis: Rev. Sci. Inst. **76**, 053109 (2005)
6. A.P. Graham, F. Hofmann, J.P. Toennies: J. Chem. Phys. **104**, 5311 (1996)
7. A.P. Graham, F. Hofmann, J.P. Toennies, L.Y. Chen, S.C. Ying: Phys. Rev. B **56**, 10567 (1997)
8. J.L. Vega, R. Guantes, S. Miret-Artés: J. Phys.: Condens. Matter **14**, 6193 (2002); J.L. Vega, R. Guantes, S. Miret-Artés: J. Phys.: Condens. Matter **16**, S2879 (2004)
9. R. Guantes, J.L. Vega, S. Miret-Artés, E. Pollak: J. Chem. Phys. **119**, 2780 (2003); R. Guantes, J.L. Vega, S. Miret-Artés, E. Pollak: J. Chem. Phys. **120**, 10768 (2004)
10. R. Martínez-Casado, J.L. Vega, A.S. Sanz, S. Miret-Artés: J. Phys.: Condens. Matter **19**, 176006 (2007)
11. J. Topping: Proc. R. Soc. A **A114**, 67 (1927)
12. J. Ellis, A.P. Graham, F. Hofmann, J.P. Toennies: Phys. Rev. B **63**, 195408 (2001)
13. G. Alexandrowicz, A.P. Jardine, H. Hedgeland, W. Allison, J. Ellis: Phys. Rev. Lett. **97**, 156103 (2006)
14. R. Martínez-Casado, J.L. Vega, A.S. Sanz, S. Miret-Artés: Phys. Rev. Lett. **98** 216102 (2007)
15. R. Martínez-Casado, J.L. Vega, A.S. Sanz, S.Miret-Artés: Phys. Rev. E **75**, 051128 (2007)
16. R. Martínez-Casado, J.L. Vega, A.S. Sanz, S. Miret-Artés: J. Phys.: Condens. Matter **19**, 305002 (2007)
17. R. Martínez-Casado, J.L. Vega, A.S. Sanz, S. Miret-Artés: Phys. Rev. B **77**, 115414 (2008); *ibid*, arXiv:0710.3266 (cond-mat.stat-mech)
18. L. Van Hove: Phys. Rev. **95**, 249 (1954)
19. D.A. McQuarrie: Statistical Mechanics. Harper and Row, New York (1976)
20. J.P. Hansen, I.R. McDonald: Theory of simple liquids. Academic Press, London (1986)

21. C.W. Gardiner: Handbook of Stochastic Methods. Springer-Verlag, Berlin (1983)
22. R. Kubo: Rep. Prog. Phys. **29**, 255 (1966)
23. J. Ellis, J.P. Toennies: Surf. Sci. **317**, 99 (1994)
24. C.V. Heer: Statistical Mechanics, Kinetic Theory, and Stochastic Processes. Academic Press, New York (1972)
25. W. Schottky: Ann. Phys. (Leipzig) **57**, 541 (1918)
26. S.O. Rice: Bell Syst. Tech. J. **23**, 282 (1944); S.O. Rice: Bell Syst. Tech. J. **24**, 46 (1945)
27. J.H. van Vleck, V.F. Weisskopf: Rev. Mod. Phys. **17**, 227 (1945)
28. P. Hänggi, P. Jung: Adv. Chem. Phys. **89**, 239 (1995)
29. T. Czernik, J. Kula, J. Luczka, P. Hänggi: Phys. Rev. E **55**, 4057 (1997); J. Luczka, T. Czernik, P. Hänggi: Phys. Rev. E **56**, 3968 (1997)
30. F. Laio, A. Porporato, L. Ridolfi, I. Rodriguez-Iturbe: Phys. Rev. E **63**, 036105 (2001)
31. R. Ferrando, M. Mazroui, R. Spadacini, G.E. Tommei: New J. Phys. **7**, 19 (2005)
32. J. Ellis, A.P. Graham, J.P. Toennies: Phys. Rev. Lett. **82**, 5072 (1999)
33. C.T. Chudley, R.J. Elliott: Proc. Phys. Soc. **77**, 353 (1960)
34. R. Martínez-Casado, J.L. Vega, A.S. Sanz, S. Miret-Artés: J. Chem. Phys. **126**, 194711 (2007).
35. R. Martínez-Casado, J.L. Vega, A.S. Sanz, S. Miret-Artés: (submitted, 2008)
36. R. Martínez-Casado, A.S. Sanz, S. Miret-Artés; *ibid*, arXiv: 0803.0535 (cond-mat.Stat-mech)

Interactions and Collision Dynamics in $O_2 + O_2$

José Campos-Martínez(✉), Marta I. Hernández, Massimiliano Bartolomei, Estela Carmona-Novillo, Ramón Hernández-Lamoneda, and Fabrice Dayou

Abstract We review the interaction between molecular oxygen molecules involving the $X\ ^3\Sigma_g^-$, $a\ ^1\Delta_g$ and $b\ ^1\Sigma_g^+$ states. The long radiative lifetimes of the excited electronic states imply that collision-induced energy transfer becomes a key mechanism to understand their role in a variety of physical and chemical processes ranging from photochemistry to nanocrystals. However, due to the open shell nature of these molecules and their weak intermolecular interactions, it is no easy to deal with problems involving these molecules both from the electronic structure calculation and from the dynamical or structural point of view. We will focus on several models recently developed in order to understand the outcome of recent experiments and observations for which the energy transfer between several electronic states play an important role as well as in the determination of accurate (rigid) full dimensional potentials of the dimer for the three lowest singlet, triplet and quintet states, where recent experiments and derived potential energy surface put *ab initio* theory on its edge.

Keywords: Oxygen dimer, spin-orbit coupling, non-adiabatic couplings, atmospheric chemistry, weakly bound complexes

J. Campos-Martinez, M. I. Hernández, M. Bartolomei, E. Carmona-Novillo
Instituto de Matemáticas y Física Fundamental, Consejo Superior de Investigaciones Científicas, Serrano 123, Madrid E-28006, Spain, e-mail: jcm@cfmac.csic.es

R. Hernández-Lamoneda
Centro de Investigaciones Químicas, Universidad Autónoma del Estado de Morelos, 62210 Cuernavaca, Mor. México

F. Dayou
Laboratoire d'Etude du Rayonnement et de la Matière en Astrophysique, UMR 8112 du CNRS, Observatoire de Paris-Meudon, 5 place Jules Janssen, 92195 Meudon Cedex, France

S. Wilson et al. (eds.) *Frontiers in Quantum Systems in Chemistry and Physics*.

1 Introduction

The dream of solving the Schrödinger Equation for complex systems is still quite ahead of us yet our progress in such direction today is impressive. This is particularly true when we refer to the calculation of molecular properties such as energy, among others. Thus computation of potential energy surfaces (PES) even for some big molecules can be now routinely carried out with close to chemical accuracy. However there still are systems of small size for which the computation of a potential energy surface is a challenge as in the case of weak intermolecular forces in open shell systems [1]. The main reasons for this lie on the fact that most accurate *ab initio* methodologies [1], such as SAPT and CCSD(T), cannot in general be applied since they are based on a single configuration description of the electronic structure, while in most cases this scheme is not suitable and multiconfigurational approaches are needed. Multireference *ab initio* methodologies are applicable in general but cannot be expected to approach high accuracy given their inherent limitations, such as size inconsistency. Bridging the gap between single and multireference methodologies is therefore an area of active research [2–4]. Additional complications arise due to the presence of low-lying electronic states that nearly always imply a breakdown of the Born-Oppenheimer approximation. In turn, these difficulties yield a rich variety of physical effects that can then appear in those systems: non-radiative processes such as internal conversion and intersystem crossings determining the associated energy transfer and reaction mechanisms.

In this report we will present some results that have been obtained over the last few years concerning the molecular oxygen dimer, its interactions and dynamics. Without being exhaustive, we list below several areas where the topics covered here could be of interest.

(a) The processes involved in the physics and chemistry of the atmosphere [5]. Molecular oxygen in its two lowest excited electronic states are easily generated in the upper atmosphere by three body recombination involving oxygen atoms. Besides, these molecular states posses relatively large radiative lifetimes which enable them to actively participate in the photochemistry of the atmosphere generating a rich dynamics for non-radiative decay processes and chemical reactions. In order to clarify these processes, many spectroscopical techniques have been applied in laboratory measurements [5]. Among many interesting findings, the group of Slanger has detected the formation of highly vibrationally excited states for several electronic states of O_2, including the ground $X^3\Sigma_g^-$ and lowest-lying, $a^1\Delta_g$ and $b^1\Sigma_g^+$, excited states. Although a significant amount of data has been produced, such as vibrational distributions [6] and state-selected removal rates [7–13], some peculiar features observed point out the need of uncovering the underlying energy transfer mechanisms. In this respect, theoretical studies of vibrational-to-electronic (V-E) energy transfer processes in $O_2(v)+O_2$ collisions are in demand, and one of our objectives is to present several models in this direction.

(b) The chemical oxygen-iodine laser (COIL), where the population inversion between the fine structure spin states of the atomic iodine is obtained through the

collisional energy transfer process $O_2(a^1\Delta_g) + I(^2P_{3/2}) \rightarrow O_2(X^3\Sigma_g^-) + I(^2P_{1/2})$. Clearly, the efficiency of the process depends on the rates of competing quenching mechanisms for the $a^1\Delta_g$ state, such as self-quenching with O_2 molecules in the $a^1\Delta_g$ and $X^3\Sigma_g^-$ states. Both theoretical and experimental characterization of such processes is still underway [14, 15].

(c) Properties and structure in solid oxygen. The peculiar properties of molecular oxygen carry on to the solid state [16, 17], where properties of a simple molecular solid and of a magnet are combined. Several solid phases exist at room temperature and high pressures which exhibit a dramatic change of color as the pressure is increased due to changes in the nature of the intermolecular forces, the detailed explanation still being an area of active research [18–20]. One of the most interesting open problems is the determination and explanation of the structural and optical properties of the epsilon(ε) phase which is stable in a broad range of temperatures and high pressures and which structure is still a matter of controversy, albeit very recent studies [20, 21] suggest a basic unit composed of four molecules, O_8 that might reconcile previous data and proposed basic building blocks.

(d) The accurate determination of intermolecular potentials plays an important role in the new and active field of cold and ultracold collision dynamics [22]. Moreover, paramagnetic molecules are thought to be good candidates for buffer gas cooling and trapping [23], which are basic steps needed in generating ultracold conditions. Preliminary studies on the O_2 + O_2 ultracold collision dynamics have been performed [24, 25] but no definitive answer concerning their practical use could be obtained. The decisive answer could depend on the accurate determination of the interaction potential and its spin-dependence. To this end, it will be critical a correct description of the dimer geometry as well as its spectral features [26–28].

The present review is concerned with collision-induced electronic energy transfer processes involving oxygen molecules, related to topics (a) and (b) above. The subject has been studied already for many years, yet there remain many unsolved questions. The aim will be to provide some theoretical insights and possible explanations for some recent experiments and observations. We also like to present some of our more accurate results concerning the intermolecular potential for the monomers in their ground electronic state, in connection with accurate hot beam experiments, of relevance for topics mentioned in (c) and (d). In the first case it is worthy to mention that not only the production of an accurate potential is problematic but also the computation of dynamical or structural properties. Indeed the oxygen molecule can be considered as a "heavy" one with the consequence that rotational levels are much closer than in systems consisting of "light" molecules as could be, for instance, hydrogen (where only recently full quantum mechanical calculations have been performed for rovibrational processes, see Ref. [29]). This feature made calculations extremely computationally demanding since convergency is reached after including many rotational channels. The presence of electronic manifolds further complicates calculations since extra channels have to be added, that in cases of spin degeneracy is even worse since new couplings, such as spin-rotation are to be included. It is therefore, necessary to resort to some kind of approximations. In our work we have used reduced dimensionality models for the dynamics with high level *ab initio* points for the potential.

The review will begin with a general description of the dimer. We will then present a model for collision induced spin-orbit coupling explaining some experiments due to Wodtke [7, 9]. In the following section we report calculations connected with laboratory experiments and field observations in the Slanger group [5]. Finally, progress in the development of accurate intermolecular potentials for the singlet, triplet and quintuplet multiplicities of $O_2(^3\Sigma_g^-) - O_2(^3\Sigma_g^-)$ is briefly presented in the last section.

2 The $O_2(v) + O_2$ System

What makes molecular oxygen such an interesting species is both the fact that it possesses very low-lying excited states, as it is shown in Fig. 1, and that it is a stable radical in its ground $X^3\Sigma_g^-$ electronic state. Furthermore, its two lowest excited states, $a^1\Delta_g$ and $b^1\Sigma_g^+$, have relatively large radiative lifetimes (tens of seconds for the first and more than one hour for the second [5]), which leads these states to play a significant role in a variety of processes.

We consider here the interaction between two oxygen molecules correlating asymptotically with the states $X^3\Sigma_g^- + X^3\Sigma_g^-$, $a^1\Delta_g + X^3\Sigma_g^-$, $b^1\Sigma_g^+ + X^3\Sigma_g^-$. In order to analyze and discuss the complexity and possible schemes to treat different processes within this system, it is useful to inspect which states arise when two diatomic fragments approach each other. To simplify we consider a given C_{2v} geometry of the dimer with the z axis along the intermolecular distance (which corresponds to an H geometry in the minimum of the van der Waals well [30, 31]). In this situation the three lowest electronic states of the oxygen molecule lead to nine possible states which are described in Table 1.

Note that when the two O_2 diatoms approach each other in different electronic states, either the one or the other can be in the higher state, which produces a doubling of the number of states [32] for the two excited dissociation limits. The states

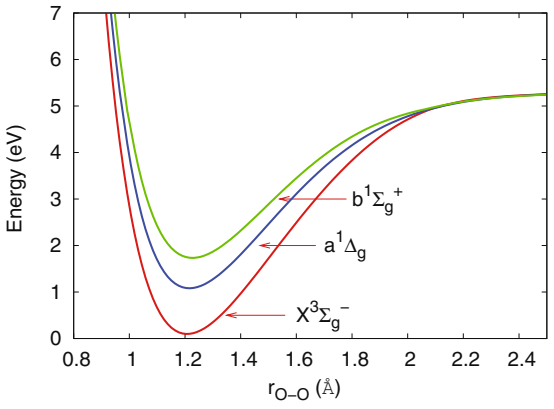

Fig. 1 Low-lying electronic states of O_2

Table 1 States in the oxygen dimer

Asymptotic states	Intermolecular states
$X^3\Sigma_g^- + X^3\Sigma_g^-$	$^1A_1, ^3A_1, ^5A_1$
$a^1\Delta_g + X^3\Sigma_g^-$	$^3A_1, ^3B_1, ^3A_1, ^3B_1$ [a]
$b^1\Sigma_g^+ + X^3\Sigma_g^-$	$^3B_1, ^3B_1$

[a] There is a doubling in the number of states.

appearing in Table 1 are degenerate in the asymptote but they can split as the two diatomic fragments approach each other. The problem is further complicated by the existence of avoided crossings leading to non-adiabatic coupling and also by spin-orbit coupling. In all cases, except for a spin-orbit coupling between the states $X\,^3\Sigma_{g0}^-$ and $b\,^1\Sigma_{g0}^+$ already existing in the diatomic, all coupling terms – nonadiabatic and spin-orbit – are strictly zero in the $O_2 + O_2$ asymptotic limit.

3 Effects of Spin-Orbit Coupling in $O_2(X^3\Sigma_g^-, v \gg 0) + O_2(X^3\Sigma_g^-, v = 0)$ Collisions

In a series of laboratory experiments carried out with the Stimulated Emission Pumping (SEP) technique, the Wodtke group [7, 9] found an unexpected sharp increase in total depletion rates of $O_2(X^3\Sigma_g^-, v \gg 0)$ by $O_2(X^3\Sigma_g^-, v = 0)$. These measurements together with previous studies due to the Slanger and Smith groups [33, 34], for the low vibrational excitation regime, gave a rather complete picture of the relaxation process for a whole range of initial vibrational states. The results showed a typical behavior of the total depletion rate (the rate constant for disappearance of the initially prepared v state) with a smooth negative slope, as the initial vibrational state increases, up to a given vibrational number, around $v = 18 - 19$, where the slope changes and the rate increases moderately with v. This trend was maintained up to vibrational states below $v = 25$, above which a sharp jump in the depletion rate was observed by Wodtke (at two different temperatures). The first change in the slope and, even, the quantitative values were well explained theoretically [35, 36]. Thus, the first change in the slope was attributed to the alternative energy transfer mechanism (see Ref. [36]) dominating at each vibrational regime (vibrational-to-vibrational, V-V for the low v, and vibrational-to-translational, V-T for the high v). Furthermore there had been also a good agreement regarding the final product states, with the channels $v - 1$, $v - 2$ being predominant. No theoretical treatment was, however, able to explain the sharp jump for the highest vibrational levels.

The deep disagreement between theory and experiment, the fact that in that v region, no $v-1$ channel was experimentally detected as a product and finally the circumstance that the initial $O_2(X, v=27)+O_2(X, v=0)$ state was already above the energy needed to form ozone, allowed the Wodtke group to propose that there was a "dark channel" (1) and that this was due to ozone formation through the reaction (2)

$$O_2(X, v \gg 0) + O_2(X, v = 0) \rightarrow ? \tag{1}$$

$$O_2(X, v \gg 0) + O_2(X, v = 0) \rightarrow O_3 + O. \tag{2}$$

The idea was tempting at that time since, besides the previous arguments, this reaction would provide an additional source of ozone that was needed to reconciliate the ozone measured in the stratosphere and the ozone appearing in the simulations (the so called "ozone deficit problem" [37]). With these premises we undertook the first quantum mechanical calculation [38] within a reduced dimensionality model on the Varandas and Pais [39] PES. Our results, later confirmed by new quantal calculations by Lauvergnat and Clary [40] within the same dynamical model but with a newly computed *ab initio* surface, showed that although there was reaction, the rates so obtained were too small to explain the sharp increase in depletion rates. In view of the previous results, efforts were directed toward other possibilities, and thus we also suggested that there was an enhancement of vibrational relaxation [41, 42] due to the presence of the reactive channel. The simulations using the same potential and dynamical model than that of the reactive calculations indicated that there was indeed an enhancement that was suppressed when the reactive channel was blocked – following the previous trend in relaxations rates computed so far using non-reactive PES – but unfortunately the populations analysis gave the $v-1$ channel as the most important one for relaxation in contrast with the experiment where monitoring of that channel gave no significant population after the collision. Next, it was also suggested the possibility of a four center reaction (the one in which two bonds are broken and formed during the reactive event). Electronic structure calculations [43,44] indicated, however, that large vibrational excitation was needed in both colliding partners given the geometry of the transition state. The problem of the "dark channel" remained then an open question.

More recently, spectroscopic studies of the diatomic O_2 by the same Wodtke group [45], found a spectral perturbation of $O_2(X^3\Sigma_g^-, v=28)$ and it was attributed to both the near resonance and spin-orbit coupling between that state and $O_2(b^1\Sigma_g^+, v=19)$. An analysis of the spin-orbit couplings as a function of the O_2 vibrational coordinate and the intermolecular separation in the $(O_2)_2$ dimer was then performed [46] , based in *ab initio* calculations. It was shown the persistence at short intermolecular distances of the spin-orbit couplings already existing in O_2, and the appearance of a significant collision-induced spin-orbit coupling, both features being relevant to the process (1).

In order to gain a further insight onto the energy transfer mechanisms, it is clear the need for more accurate treatments based on the *ab initio* calculation of potential energy surfaces, associated coupling terms and subsequent quantum scattering

calculations. We therefore considered the following processes as a possible outcome for (1)

$$O_2(X,v) + O_2(X,v=0) \rightarrow O_2(X,v') + O_2(X,v=0) \tag{3}$$

$$O_2(X,v) + O_2(X,v=0) \rightarrow O_2(a,v') + O_2(X,v=0) \tag{4}$$

$$O_2(X,v) + O_2(X,v=0) \rightarrow O_2(b,v') + O_2(X,v=0). \tag{5}$$

Due to the very specific nature of the dimer $(O_2)_2$, where two open-shell systems interact, there have been very few studies on this system suitable to characterize V-E energy transfer processes by means of *ab initio* quantum chemistry methods. In fact, the present study of processes (4) and (5) based on a full quantum treatment was, to our knowledge, the first one to be carried out [47–49]. Only very recently, Liu and Morokuma [15, 50] have undertaken a determination of the oxygen dimer potential energy surfaces up to the $a^1\Delta_g + a^1\Delta_g$ manifold by means of multiconfigurational *ab initio* methods, but the calculation of the associated spin-orbit coupling terms was restricted to the minima of the crossing seams. Similar calculations were performed by Vach et al. [51] but for a fixed intermolecular distance of the oxygen molecules for the states considered.

The potential energy and spin-orbit coupling surfaces suitable to characterize the latter two V-E mechanisms were computed [48] from multiconfigurational *ab initio* methods. In order to keep the problem tractable, we employed a reduced dimensionality model corresponding with the geometry described in Sect. 2, that included one active vibration (that of the vibrationally excited diatomic) and the intermolecular distance between the center of mass of the two oxygen, keeping at the equilibrium distance the bond length of the other oxygen molecule. We focused then on the determination of the ground singlet A_1 state and two excited triplet B_1 states which asymptotically correlate with the $X^3\Sigma_g^-$, $a^1\Delta_g$ and $b^1\Sigma_g^+$ states of O_2, respectively.

These three potential energy surfaces and their spin-orbit coupling terms were employed to treat the dynamical problem associated with the processes (4) and (5), by means of quantum scattering calculations based on the Close-Coupling method [47]. The effects of the first triplet and quintet A_1 states to processes (3, 4, 5) were also incorporated by considering their specific spin multiplicities to construct the associated spin-orbit coupling terms with the two excited triplet B_1 states. The results gave a positive answer on the possibility that process (1) were due to V-E energy transfer. However, with our *ab initio* PES the near degeneracy between vibrational states of electronic manifolds $O_2(X^3\Sigma_g^-)$ and $O_2(b^1\Sigma_g^+)$ was found between $v = 30$ and $v = 21$. This result reveals the difficulties of *ab initio* methods in leading results of spectroscopical accuracy for asymptotic fragments.

Therefore, we decided, in order to obtain a much closer agreement with experimental data, to include accurate RKR diatomic potentials [52] for the fragments but keeping the same *ab initio* interaction potential. By doing so, one can determine Boltzmann-averaged depletion probabilities, by means of

$$I^i(v,T) = \frac{1}{K_B T} \int_0^\infty P_v^i(E_k) e^{-\frac{E_k}{K_B T}}\, dE_k \tag{6}$$

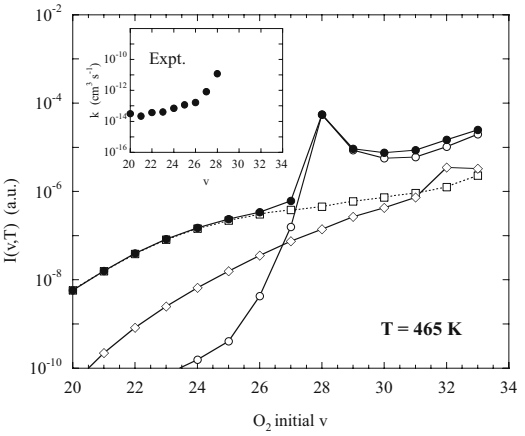

Fig. 2 Boltzmann-averaged depletion probabilities for $O_2(X^3\Sigma_g^-, v)$ colliding with O_2 at $T = 465$ K: (●) V-T+V-E; (□) V-T; (◊) V-E to $a^1\Delta_g$; (◯) V-E to $b^1\Sigma_g^+$. The inset shows the experimental values [7–9] of the total quenching rate coefficients $k_{v,T}$

for the vibrational levels of $O_2(X^3\Sigma_g^-, v)$ induced by collision with O_2, including the vibrational-to-translational (V-T) energy transfer as well as V-E energy transfer to the $a^1\Delta_g$ and $b^1\Sigma_g^+$ states. In Eq. (6), K_B, is the Boltzmann constant, T is the temperature, E_k the relative kinetic energy, whereas P^i, can be the total inelastic probability (that account for the total process (V-T + V-E), or in other words one minus the elastic probability), or total inelastic probabilities for going to states $X^3\Sigma_g^-$, $a^1\Delta_g$, $b^1\Sigma_g^+$. The values provided by this equation, for each energy transfer process, are displayed in Fig. 2 for a kinetic temperature of 465 K. It is readily seen that, up to $v = 26$, the main part of the depletion is due to a V-T mechanism, whereas for $v > 26$ the main contribution comes from V-E energy transfer. The sudden jump found at $v = 28$ relates to the very efficient V-E process:

$$O_2(X, v = 28) + O_2 \rightarrow O_2(b, v = 19) + O_2 \tag{7}$$

due to a near degeneracy between the $O_2(X^3\Sigma_g^-, v = 28)$ and $O_2(b^1\Sigma_g^+, v = 19)$ states of the diatom, which had been already pointed out experimentally. The close analogy between the theoretical results and the features displayed by the experimental depletion rates demonstrates that V-E processes are at the origin of the observed "dark channel". It is also very interesting to note that following level $v = 28$, the slope for higher vibrational states continues that of $v = 27$ and below, that is to say, what we really see is a large "peak" at the resonant level, overimposed to a relatively moderate slope. Unfortunately the experiments could not be carried on for levels higher than $v = 28$. Experimental measurement of just the next following level, $v = 29$, could confirm the conclusions of this work.

The model is, of course, incomplete, letting aside the fact that no rotation is included, we have to mention that some depletion processes are missing in our theoretical description. Among the limitations we cite the specificity of V-E energy transfer from the first triplet and quintet A_1 states of the dimer, which is only accounted for in an approximate manner in the present model. The possible presence

of non-adiabatic couplings to nearby states at these high levels and their influence cannot be completely ruled out.

Finally we would like to comment that besides the model presented above, there are much more approximate treatments that can guide us into gross features of these processes, for instance the Distorted Wave Approximation (see Ref. [49] for details.). Nevertheless, information about the intermolecular potentials and associated coupling terms are clearly needed to discriminate between the possible V-E processes and properly reproduce their relative strength.

4 Nonadiabatic Coupling Effects in $O_2(b^1\Sigma_g^+, v) + O_2$ Collisions

So far, we have concentrated in processes for which the presence of collision-induced spin-orbit coupling is important, and in the high vibrational level regime. There are however other observations and experiments that show interesting and puzzling features. In the year 2000, the Slanger group reported for the first time the vibrational distribution of the $b^1\Sigma_g^+$ state in the nightglow emission of the Atmospheric band system, for vibrational levels from $v = 0$ up to $v = 15$. Data collected for the upper Earth's atmosphere [6] display a vibrational distribution of $O_2(b^1\Sigma_g^+, v)$ with maxima at $v = 0$, $v = 3-4$ and $v = 12$, and a marked minimum at $v = 8$. The maximum peak at $v = 0$ is easily understood by the absence of efficient quenching mechanisms for the ground vibrational level, however an understanding of the other maxima and minima is more complicated and it requires the knowledge of the possible routes of removal and their corresponding rates. In order to clarify these observations, several laboratory measurements had been carried out to investigate the collisional removal of $O_2(b^1\Sigma_g^+, v)$ by different colliders [11–13]. Conclusions reached from theses experiments indicated that already for $v = 1$ the oxygen molecule is several orders of magnitude more efficient than others (i.e., N_2) as a quencher. The removal of $O_2(b^1\Sigma_g^+, v)$ by O_2 was found to impressively decrease its efficiency as v increases from $v = 1$ to $v = 3$. After analysis of the temperature dependence of the rates [13], which showed an Arrhenius behavior, Slanger and coworkers suggest that an electronic energy transfer mechanism was dominant

$$O_2(b, v_1) + O'_2(X, v = 0) \rightarrow O_2(X, v_2) + O'_2(b, v = 0), \tag{8}$$

(where primes are used to label the identity of the molecules). Propensity rules for the previous process where studied by Kirilov [53] using the Rosen-Zener model, achieving a qualitative agreement with the experiments, but the mechanisms causing this process has not been investigated yet.

We have decided to investigate the presence of electronic pathways by considering the effect of non-adiabatic radial couplings in the quenching of $O_2(b^1\Sigma_g^+, v)$ by oxygen. To this end, an almost complete map of collision-induced nonadiabatic couplings between the states given in Table 1 was determined from multiconfigurational *ab initio* calculations at the CASSCF level of theory. This was done with the aim of determining the range of nuclear geometries mapped by each nonadiabatic

coupling, and, by doing so, to check the validity of an electronic basis set truncation in dynamics calculations, since we want to deal with a particular avoided crossing region. The computation of nonadiabatic coupling matrix elements (NACMEs) between each pair of states relied on the analysis of configuration mixing coefficients [54, 55], using the $O_2 + O_2$ asymptotic limit as a reference geometry. The results were successfully checked along each degree of freedom by calculating the NACMEs through a three-point finite difference method. For the two excited triplet B_1 states of interest, those correlating with the $b^1\Sigma_g^+ + X^3\Sigma_g^-$ states, we found that the states mixing produced by exchange interactions between the oxygen molecules yields a large value for the NACME. The associated range of nuclear geometries along the r coordinate extends as the two molecules approach each other, but, up to relatively short intermolecular distances, the interaction region was found to be basically isolated from other avoided crossing regions. Consequently, a two state model is thought to be valid to treat the energy transfer which affect the low vibrational levels in process (8).

The dynamical problem was solved using a diabatic representation for the coupled electronic states. The diabatic representation was retained since it allows to circumvent the singularity of the NACME at the locus of the crossing in the adiabatic representation. An orthogonal adiabatic-to-diabatic transformation was thus performed, using the two-state mixing angle yielded by *ab initio* calculations. This led to diabatic intermolecular potentials and electronic coupling terms which are smooth functions of the internuclear distance. Using again the RKR diatomic potentials [52], we performed quantum scattering calculations [56] based on the Close-Coupling method to determine the Boltzmann-averaged depletion probabilities for the process (8). Note that in the present case the potential energy surfaces had to be corrected for the zero-point energies of the diatoms.

We report in Fig. 3 the computed Boltzmann-averaged depletion probabilities for the low vibrational levels $v = 1 - 3$ considered in experiments [13]. Clearly, the overall behavior displayed by the measured rate coefficient is not correctly reproduced by our theoretical calculations when only V-T energy transfer is accounted for. However, by including the energy transfer processes, one obtains a temperature

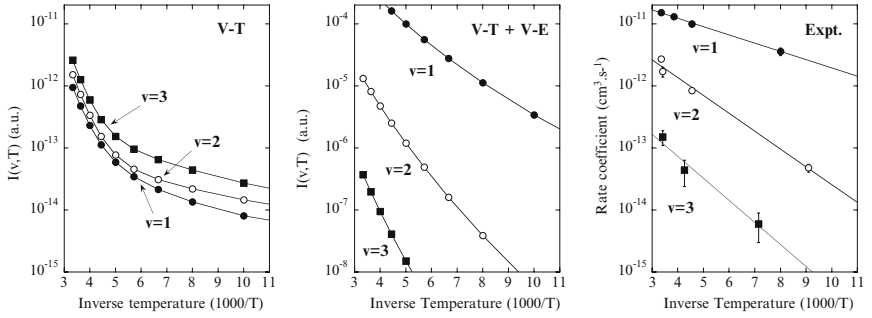

Fig. 3 Calculated Boltzmann-averaged probabilities (*left and middle panels*) and measured rate coefficients (*right panel*) for $O_2(b^1\Sigma_g^+, v)$ colliding with O_2, as a function of the inverse of temperature

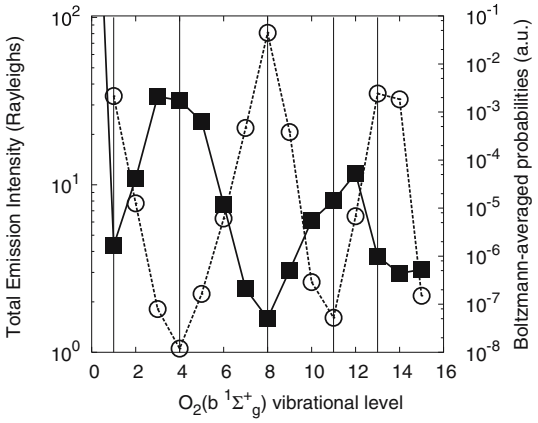

Fig. 4 Full squares, full lines, Total emission Intensity, taken from Ref. [57]. Open circles, dashed lines, Boltzmann-averaged probabilities for $O_2(b^1\Sigma_g^+, v)$ colliding with O_2 at $T = 200$ K. Vertical lines have been drawn at the minima of averaged probabilities as a guide to the eye

dependence for the depletion probabilities which is much closer to that followed by the measured rate coefficient, with a propensity rule for the depletion processes favoring low values of v in good agreement with the experimental observation. Furthermore, our theoretical model shows that the process (8) corresponding with $v_3 = v_1$ was by far the most efficient, which is understood in terms of a favorable energy mismatch.

We have also studied the depletion process (8) for higher vibrational levels of $O_2(b^1\Sigma_g^+, v)$, and the results are shown in Fig. 4 at a given temperature. As can be seen, dramatic changes are observed in the rate of process (8) according with the vibrational level selected. Such variations were found to agree with strong changes in energy mismatches associated with the vibrational levels of $O_2(b^1\Sigma_g^+, v_1)$ and $O_2(X^3\Sigma_g^-, v_2)$ involved in the V-E energy transfer, with $v_2 = v_1 - 1, v_1 - 2$ as a propensity rule for the higher vibrational levels. Interestingly, the vibrational distribution of $O_2(b^1\Sigma_g^+, v)$ molecules observed in the upper Earth's atmosphere [6] displays (full squares, full lines of Fig. 4) two maxima at $v = 3 - 4$ and $v = 12$, and a marked minimum at $v = 8$, which is just opposite of the trend obtained for the depletion probabilities shown in Fig. 4, with open circles. This strongly suggests that process (8) is at the origin of the sharp changes observed in the vibrational distribution of $O_2(b^1\Sigma_g^+, v)$ molecules, which would demonstrate that nonadiabatic couplings can have sizeable effects on the steady-state populations of oxygen molecules in the Earth's atmosphere.

5 Potential Energy Surfaces for the Three Lowest States in $(O_2)_2$ Dimer

As pointed out in the Introduction, even if the computation of PESs is nowadays easily carried out for molecules containing tens of atoms there still are small size systems that, due to their open shell character and to the weak van der Waals interaction involved, represent a true challenge for modern quantum chemistry especially

if a high accuracy for the determination of the intermediate and long range components of the intermolecular forces is required. This is the case of oxygen dimer in which both molecules are in their ground electronic and vibrational state. In fact the interaction potential in this dimer depends not only on the distance and relative orientation between molecules but also on the orientation of the molecular spin. This results in three different PESs corresponding to the singlet, triplet and quintet states of the dimer arising from different spin coupling of the monomers. Unfortunately the most accurate *ab initio* methods such as CCSD(T) (or SAPT) which properly include dynamical electronic correlation at high order (needed for an optimal determination of the weak intermolecular forces) rely on the validity of a single reference of the wave function and can be applied only for the quintet state of the oxygen dimer. For the remaining states it is mandatory to use multiconfigurational based methods such as Multireference Configuration Interaction (MRCI). Recently [58] accurate intermolecular potentials were obtained for the O_2-O_2 main four geometric configurations through the combination of results carried out with both CCSD(T) and MRCI methodologies. In order to test the reliability of the obtained results a stringent test was to compare with precise experimental measurements carried out by Aquilanti et al. [59] who also provided an empirical PESs (Perugia PES) determined through a multiproperty analysis. The main issue of these experimental data is that some of them (namely those obtained with effusive O_2 molecular beams) mainly probe the isotropic interaction acting within the dimer. In particular the glory effect interference measured for thermal collision energies permits to estimate with great accuracy both potential well area and long range tail of the interaction. After estimating an approximate isotropic interaction the cross sections were computed and compared, as shown in Fig. 5, with both experimental results and predictions carried out with previous semi-abinitio PESs obtained by Bussery and Wormer (BW) [30] by combining *ab initio* first order electrostatic and exchange interactions with semi-abinitio second order long range energies. It can be seen that BW results predict a glory pattern which is dephased with respect to the

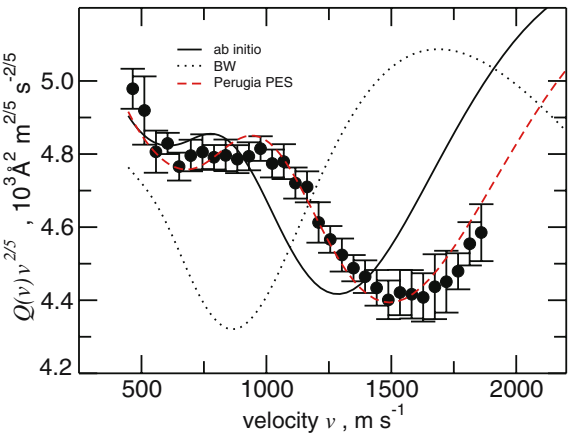

Fig. 5 Comparison of the total integral cross section measured from the rotationally "hot" molecular beam experiment and computed using full ab initio [58] (*solid line*), semi-abinitio [30] (*dotted line*) and Perugia [59] (*dashed line*) PESs

experimental one. This marked difference suggests that the isotropic potential well area needs to be much larger. An improvement can be observed for the full *ab initio* results which are much closer to the experimental findings indicating that the potential well is approaching that probed by the experiment. Nevertheless a certain gap still remains and can be attributed in the first instance to the approximated isotropic potential, which was carried out starting from only four limiting geometries, but probably also to the difficulties in achieving accurate PESs for the singlet and triplet states. Further investigations devoted to clarify these issues are in progress [60].

6 Conclusion

The open-shell nature of oxygen molecules leading to many interacting electronic manifolds, and the high symmetry of the $(O_2)_2$ dimer complex make collisions a complex subject to be treated theoretically. We hope we have shown that even in this case it should be possible to develop adequate models that, while being approximate, can reproduce the main specific features of a given process and to shed light on the microscopic underlying mechanisms supporting experimental data.

The purpose of the present contribution was to provide theoretical insight into the puzzling mechanisms associated with $O_2(v)+O_2$ collisions, when the ground state $X^3\Sigma_g^-$ and lowest excited states $a^1\Delta_g$ and $b^1\Sigma_g^+$ of the diatoms are involved. Among the rich variety of V-E energy mechanisms available, we focused on two particular processes, for which accurate theoretical treatments, based on *ab initio* calculations of potential energy surfaces, associated coupling terms and quantum scattering calculations, were employed within a reduced dimensionality model. Within this scheme, we studied V-E energy transfer mechanisms involved in the removal of both $O_2(X^3\Sigma_g^-, v)$ and $O_2(b^1\Sigma_g^+, v)$ by O_2, the two processes being mediated through spin-orbit and nonadiabatic radial couplings, respectively, between the states of the dimer.

In the two cases, it was found that state mixing within the molecular complex were at the origin of significant collision-induced coupling terms, and, subsequently, of significant V-E energy transfer. We hope to have shown that if a careful design of the theoretical model is made, we are able to mimic the sharp changes observed in the experimental removal rate coefficients, whose origin had been a matter of debate for over a decade. Our theoretical work has provided the most thorough and best supported analysis on the nature of the 'dark channel' to date. Furthermore, we have made predictions on the expected behavior of relevant dynamical properties of the system such as state-selected electronic relaxation rates which await experimental confirmation.

Finally we would like to stress that there is ample room for improvements in the models presented here. One way is to include more possible (electronic) mechanisms that can complete the picture exposed in Sect. 3 and that, also, they could explain the origin of another interesting finding, the one reported by Jongma and Wodtke [10] of a fast multiquantum vibrational relaxation of vibrationally excited

oxygen molecule, which has no complete explanation up to date. Clearly, other way is to add more degrees of freedom and in particular that of rotation or allow the system for V-V pathways. In this last case it is of crucial importance an accurate determination of PES with the difficulties mentioned in Sect. 5 to which it must be added the complications in dealing with high vibrational states and the corresponding couplings.

Acknowledgements We thank Profs. Slanger and Cosby for fruitful discussions and for providing us with their RKR potentials. This work has been partially supported by Ministerio de Educación y Ciencia (Spain), grants CTQ2007-62898 and CONACYT (Mexico) grant 44117 F. Financial support from binational CSIC-CONACYT programme, 2005MX0025, is also gratefully acknowledged. Thanks are also due to CESGA for allocation of computing time.

References

1. G. Chalasinski and M.M. Szczesniak, Chem. Rev. **100**, 4227 (2000)
2. P. Piecuch, M. Wloch, J.R. Gour and A. Kinal, Chem. Phys. Lett. **418**, 467 (2006)
3. X. Li and J. Paldus, J. Chem. Phys. **125**, 164107 (2006)
4. A. Dreuw and M. Head-Gordon, Chem. Rev. **105**, 4009 (2005)
5. T. G. Slanger and R. A. Copeland, Chem. Rev. **103**, 4731 (2003)
6. T. G. Slanger, P.C. Cosby, D.L. Huestis and D.E. Osterbrock, J. Geophys. Res. **105**, 557 (2000)
7. J. M. Price, J. A. Mack, C. A. Rogaski and A. M. Wodtke, Chem. Phys. **175**, 83 (1993)
8. X. Yang, J. M. Price, J. A. Mack, C. G. Morgan, C. A. Rogaski, D. McGuire, E. H. Kim and A. M. Wodtke, J. Phys. Chem. **97**, 3944 (1993)
9. C. A. Rogaski, J. A. Mack, and A. M. Wodtke, Faraday Discuss. Chem. Soc. **100**, 229 (1995)
10. R.T. Jongma and A.M. Wodtke, J. Chem. Phys. **111**, 10957 (1999)
11. H.I. Bloemink, R. A. Copeland and T. G. Slanger, J. Chem. Phys. **109**, 4237 (1998)
12. E.S. Hwang, A. Bergman, R.A. Copeland and T.G. Slanger, J. Chem. Phys. **110**, 8 (1999)
13. K.S. Kalogerakis, R.A. Copeland and T.G. Slanger, J. Chem. Phys. **116**, 4877 (2002)
14. I.O. Antonov, V.N. Azyazov and N.I. Ufimtsev, J. Chem. Phys. **119**, 10638 (2003)
15. J. Liu and K. Morokuma, J. Chem. Phys. **123**, 204319 (2005)
16. G. C. De Fotis, Phys. Rev. B **23**, 4714 (1981)
17. Y. A. Freiman and H. J. Jodl, Phys. Rep. **401**, 1 (2004)
18. F. A. Gorelli, L. Ulivi, M. Santoro and R. Bini, Phys. Rev. Lett. **83**, 4093 (1999)
19. J. B. Neaton and N. W. Ashcroft, Phys. Rev. Lett. **88**, 205503 (2002)
20. H. Fujihisa, Y. Akahama, H. Kawamura, Y. Ohishi, O. Shimomura, H.Yamawaki, M. Sakashita, Y. Gotoh, S. Takeya and K. Honda, Phys. Rev. Lett. **97**, 085503 (2006)
21. L. S. Lundegaard, G. Weck, M. I. McMahon, S. Desgreniers and P. Loubeyre, Nature **443**, 201 (2006)
22. R.V. Krems, Int. Rev. Phys. Chem. **24**, 99 (2005)
23. J. Weinstein, R. deCarvalho, T. Guillet, B. Friedrich and J.M. Doyle , Nature **395**, 148 (1998)
24. A. V. Avdeenkov and J. L. Bohn, Phys. Rev. A **64**, 52703 (2001)
25. K. Tilford, M. Hoster, P. M. Florian and R. C. Forrey, Phys. Rev. A **69**, 052705 (2004)
26. V. Aquilanti, E. Carmona-Novillo and F. Pirani, Phys. Chem. Chem. Phys. **4**, 4970 (2002)
27. E. Carmona-Novillo, F. Pirani and V. Aquilanti, Int. J. Quantum Chem. **99**, 616 (2004)
28. L. Biennier, D. Romanini, A. Kachanov, A. Campargue, B. Bussery-Honvault and R. Bacis, J. Chem. Phys. **112**, 6309 (2000)
29. A. N. Panda, F. Otto, F. Gatti and H.-D. Meyer , J. Chem. Phys. **127**, 114310 (2007)
30. B. Bussery and P.E.S. Wormer, J. Chem. Phys. **99**, 1230 (1993)

31. V. Aquilanti, D. Ascenzi, M. Bartolomei, D. Cappelletti, S. Cavalli, M. de Castro Vitores and F. Pirani, Phys. Rev. Lett. **82**, 69 (1999)
32. G. Herzberg, *Molecular Spectra and Molecular Structure III: Electronic Spectra of Polyatomic Molecules* (Van Nostran Reinhold Co., New York, 1966)
33. H. Park and T. G. Slanger, J. Chem. Phys. **100**, 287 (1994)
34. M. Klatt, I. W. M. Smith, R. P. Tuckett and G. N. Ward, Chem. Phys. Lett. **224**, 253 (1994)
35. G. D. Billing and R. E. Kolesnick, Chem. Phys. Letters **200**, 382 (1992)
36. R. Hernández , R. Toumi and D. C. Clary, J. Chem. Phys. **102**, 9544 (1995)
37. R. L. Miller, A. G. Suits, P. L. Houston, R. Toumi, J. A. Mack and A. M. Wodtke, Science **265**, 1831 (1994)
38. R. Hernández-Lamoneda, M. I. Hernández, E. Carmona-Novillo, J. Campos-Martínez, J. Echave and D. C. Clary, Chem. Phys. Letters **276**, 152 (1997)
39. A. Varandas and A. Pais, in *Theoretical and Computational Models for Organic Chemistry*, ed. by L.A. S.J. Formosinho, I.G. Czismadia (Nato ASI Series C (Kluver, Dordrecht),Vol.339, 1991)
40. D.M. Lauvergnat and D.C. Clary, J. Chem. Phys. **108**, 3566 (1998)
41. J. Campos-Martínez, E. Carmona-Novillo, J. Echave, M. I. Hernández, R. Hernández-Lamoneda and J. Palma, Chem. Phys. Letters **289**, 150 (1998)
42. J. Campos-Martínez, E. Carmona-Novillo, J. Echave, M. I. Hernández, R. Hernández-Lamoneda and J. Palma, Eur. Phys. J. D **4**, 159 (1998)
43. R. Hernández-Lamoneda and A. Ramírez-Solís, J. Chem. Phys. **113**, 4139 (2000)
44. R. Hernández-Lamoneda and A. Ramírez-Solís, J. Chem. Phys. **120**, 10084 (2004)
45. R.T. Jongma, S. Shi and A.M. Wodtke, J. Chem. Phys. **111**, 2588 (1999)
46. R. Hernández-Lamoneda and A. Ramírez-Solís, Chem. Phys. Letters **321**, 191 (2000)
47. F. Dayou, J. Campos-Martínez, M.I. Hernández and R. Hernández-Lamoneda, J. Chem. Phys. **120**, 10355 (2004)
48. F. Dayou, M.I. Hernández, J. Campos-Martínez and R. Hernández-Lamoneda, J. Chem. Phys. **123**, 74311 (2005)
49. F. Dayou, M.I. Hernández, J. Campos-Martínez and R. Hernández-Lamoneda, J. Chem. Phys. **126**, 194309 (2007)
50. Rui-Feng Lu, Pei-Yu Zhang, Tian-Shu Chu, Ting-Xian Xie and Ke-Li Han, J. Chem. Phys. **126**, 124304 (2007)
51. H. Vach, T-N.V. Nguyen, Q.K. Timerghazin and G.H. Peslherbe, Phys. Rev. Lett. **97**, 143402 (2006)
52. T.G. Slanger and P.C. Cosby, Private communication
53. A.S. Kirilov, Adv. Space Res. **33**, 998 (2004)
54. A. Dobbyn and P. Knowles, Mol. Phys. **91**, 1107 (1997)
55. D. Simah, B. Hartke and H.J. Werner, J. Chem. Phys. **111**, 4523 (1999)
56. F. Dayou, M.I. Hernández, J. Campos-Martínez and R. Hernández-Lamoneda, J. Chem. Phys. (submitted)
57. T. G. Slanger, Private Communication (2006)
58. R. Hernández-Lamoneda, M. Bartolomei, M. I. Hernández, J. Campos-Martínez and F. Dayou, J. Phys. Chem. A **109**, 11587 (2005)
59. V. Aquilanti, D. Ascenzi, M. Bartolomei, D. Cappelletti, S. Cavalli, M. de Castro Vitores and F. Pirani , J. Am. Chem. Soc. **121**, 10794 (1999)
60. M. Bartolomei, E. Carmona-Novillo, M. I. Hernández, José Campos-Martínez and R. Hernández-Lamoneda, J. Chem. Phys. **128**, 214304 (2008)

The Non-Adiabatic Molecular Hamiltonian: A Derivation Using Quasiparticle Canonical Transformations

Ivan Hubač(✉) and Stephen Wilson

Abstract The interaction between electrons and phonons in molecules is investigated using a formulation in which the total molecular Hamiltonian is subjected to two canonical transformations. The first of these transformations, which we term the normal coordinate transformation, passes from a crude representation, which we term the clamped nuclei representation, in terms of basis functions defined with respect to some fixed geometry of the nuclei, $\mathbf{R}_0$, to a representation in terms of basis functions depending on $\mathbf{R}$. This transformation mixes electronic and vibrational motions and leads to a simple formulae for adiabatic corrections. The second transformation, termed the momentum transformation, leads to a non-adiabatic (or diabatic) representation. Each representation supports a different partition of the total molecular Hamiltonian into a zero-order (or reference) Hamiltonian and a perturbation. For each representation, quasiparticles, i.e. renormalized electrons and phonons are defined will provide the theoretical apparatus required for the description of the electron-phonon interaction.

Keywords: non-adiabatic hamiltonian, quasi-particle canonical transformations, electron - phonon interaction

[1]For a review see Sutcliffe [1–5].

I. Hubač
Department of Chemical Physics, Faculty of Mathematics, Physics and Informatics, Comenius University, 84215 Bratislava, Slovakia;
Institute of Physics, Silesian University, 74601 Opava, Czech Republic, e-mail: hubac@tex.dbp.fmph.uniba.sk

S. Wilson
Physical & Theoretical Chemistry Laboratory, University of Oxford, South Parks Road, Oxford OX1 3QZ, England;
Department of Chemical Physics, Faculty of Mathematics, Physics and Informatics, Comenius University, 84215 Bratislava, Slovakia, e-mail: quantumsystems@gmail.com

S. Wilson et al. (eds.) *Frontiers in Quantum Systems in Chemistry and Physics*.

1 Introduction

Many-body quantum methods are most often applied to molecules after invoking the Born-Oppenheimer or adiabatic approximation thereby separating the electronic and nuclear motion problems.[1] The motion of the electrons is considered in the field of clamped nuclei. Then the motion of each of the nuclei takes place in an effective potential due to the electrons and the other nuclei in the system. The separation of electronic and nuclear motion underpins the concept of molecular structure, an idea which lies at the heart of much chemistry [6].

The many-electron problem can be successfully treated using 'many-body' methods[2] – many-body perturbation theory, cluster expansions, or hybrid methods, such as the method designated CCSD(T) which combines the use of a coupled cluster expansion with perturbative estimates of higher order (triple excitation) effects.

The Born-Oppenheimer approximation and adiabatic approximation break down when, for a given configuration of the nuclei, the electronic states are degenerate or quasi-degenerate. Recent years have witnessed a growing interest in the simultaneous description of electronic and nuclear motion. As early as 1969, Thomas published two papers [9, 10] in which a molecular structure theory was developed without invoking the Born-Oppenheimer approximation. In these publications and two further papers published in 1970 [11, 12], Thomas studied methane, ammonia, water and hydrogen fluoride adding the kinetic energy operators of the protons to the electronic hamiltonian and using Slater-type orbitals centred on the heavier nuclei for the protonic wave functions. Over the years, a number of authors [13–21] have attempted the development of a non-Born-Oppenheimer theory of molecular structure, but problems of accuracy and/or feasibility remain for applications to arbitrary molecular systems.

In 2002, Nakai [23] presented a non-Born-Oppenheimer theory of molecular structure in which molecular orbitals (MO) are used to describe the motion of individual electrons and nuclear orbitals (NO) are introduced each of which describes the motion of single nuclei. Nakai presents an *ab initio* Hartree-Fock theory, which is designated "NO+MO/HF theory", which builds on the earlier work of Tachikawa et al. [24]. In subsequent work published in 2003, Nakai and Sodeyama [25] apply many-body perturbation theory to the problem of simultaneously describing both the nuclear and electronic components of a molecular system. In more recent work, Nakai et al. [26] have presented a translation-free and rotation-free Hamiltonian for use in nuclear orbital plus molecular orbital theory. In a comment on this paper by Nakai et al., Sutcliffe [27] has suggested that their "chosen rotational term is not unique and is not valid over all regions of space". The approach of Nakai et al. [26] was considered in some detail by one of us [28] (for a review see also Wilson [29]) as a first step in the development of a literate quantum chemistry program for the simultaneous description of electronic and

[2] For a review of 'many-body' methods and their application in molecular studies see Paldus [7] and also Wilson [8].

nuclear motion. In order to develop a theory for the motion of both the nuclei and the electrons in a molecule, we write the total hamiltonian operator, $\mathscr{H}$, as a sum of an unperturbed or zero order hamiltonian, $\mathscr{H}_0$, and a perturbation, $\mathscr{H}_1$, that is $\mathscr{H} = \mathscr{H}_0 + \lambda\mathscr{H}_1$. Here λ is a perturbation parameter. We define a suitable independent particle model which can be used a reference for a diagrammatic many-body perturbation theory for the motion of both electrons and nuclei. The unperturbed hamiltonian operator is a sum of a kinetic energy term and an effective potential energy term $\mathscr{H}_0 = T + U$. The effective potential is a sum of a nuclear and an electron component $U = U_n + U_e$. It is a sum of one-particle terms. The total wave function for a system of nuclei and electrons can be written as a product of a nuclear component $\Phi_n = \|\varphi_P\varphi_Q...\|$ in which φ_P is a single nucleus state function, or nuclear orbital, and an electronic component $\Phi_e = \left\|\varphi_p\varphi_q...\right\|$ in which φ_p is a single electron state function or molecular orbital. The single nucleus state function or nuclear orbital is an eigenfunction of a Hartree-Fock eigenvalue equation for the nuclear motion $\mathscr{F}_n\varphi_P = \varepsilon_P\varphi_P$ in which the Fock operator has the form

$$\mathscr{F}_n = t_n + \sum_P^N (J_P \mp K_P) + \sum_p^n J_p = t_n + u_n \tag{1}$$

where the nuclear Fock potential is

$$u_n = \sum_P^N (J_P \mp K_P) + \sum_p^n J_p.$$

The Hartree-Fock equations for the electrons have the form $\mathscr{F}_e\varphi_p = \varepsilon_p\varphi_p$ where the Fock operator is given by

$$\mathscr{F}_e = t_e + \sum_p^n (J_p - K_p) + \sum_P^N J_P = t_e + u_e. \tag{2}$$

The effective potential for the electrons is

$$u_e = \sum_p^n (J_p - K_p) + \sum_P^N J_P$$

which includes a mean-field coupling between the electronic and the nuclear motion. Using the nuclear orbital–molecular orbital model as a reference, a practical diagrammatic many-body perturbation theory for the motion of electrons and nuclei can be developed. However, this approach makes no use of the clamped nuclei model and, therefore, the concept of an equilibrium structure does not arise neither does the idea of a potential energy curve or surface. The nuclear orbital–molecular orbital model does not appear to distinguish between different molecular structures.

The mixing of electronic states gives rise to vibrational-electronic states describing the coupled motion of electrons and nuclei. In solid state theory, the concept

of the phonon, that is, a quantized mode of vibration in a rigid crystal lattice, has been shown to be very useful [30]. The phonon can also be invoked in molecular theory. For molecular systems, the phonon should be interpreted as a *quantum of vibration*. The electron-phonon interaction arises in molecular theory when it is taken beyond the Born-Oppenheimer approximation. In this work, we shall be concerned with an approach to the non-adiabatic Hamiltonian, or the break-down of Born-Oppenheimer approximation, using quasiparticle canonical transformations to study the electron–phonon interaction.[3] The use of quasiparticle canonical transformations was first explored in this context a paper by Hubač and Svrček published in 1988 (see also the subsequent paper by Svrček and Hubač [35] and two review articles [36, 37]). This approach uses the methods of quantum field theory to describe systems of mixed quantum statistics [31]. Central to the approach described here is the assumption that there is some reference configuration of the nuclei (usually the equilibrium geometry). Furthermore, it is assumed that the potential function, V, associated with the nuclear motion can be written as a Taylor series in terms of the displacements from this reference geometry

$$V = V_0 + \tfrac{1}{2!}\sum_{i,j} W_{ij}\left(R_i - R_{0i}\right)\left(R_j - R_{0j}\right) + \tfrac{1}{3!}\sum_{i,j,k} W_{ijk}\left(R_i - R_{0i}\right)\left(R_j - R_{0j}\right)\left(R_k - R_{0k}\right)$$

$$+ \tfrac{1}{4!}\sum_{i,j,k,l} W_{ijkl}\left(R_i - R_{0i}\right)\left(R_j - R_{0j}\right)\left(R_k - R_{0k}\right)\left(R_l - R_{0l}\right) + \ldots . \tag{3}$$

In this expansion, $R_i - R_{0i}$, $R_j - R_{0j}$, … are the displacements and the force constants, $W_{ijk\ldots}$, are the derivatives of V for the reference geometry, i.e.

$$W_{ijk\ldots} = \left(\frac{\partial^n V}{\partial\left(R_i - R_{0i}\right)\partial\left(R_j - R_{0j}\right)\partial\left(R_k - R_{0k}\right)\ldots} \right)_0 . \tag{4}$$

For small displacements, (for example, of the order of vibrational amplitudes at room temperature) the terms in the above Taylor expansion are expected to converge fairly rapidly. Higher order terms are successively smaller. (For large amplitude vibrations, such as inversion or internal rotation, the above Taylor series is not appropriate and the force constants are defined in a different way. For example, a Fourier expansion is preferable for internal rotation. Such cases will not be considered here.) Quasiparticle canonical transformations are used to obtained dressed fermions and bosons suitable for the molecular vibrational-electronic problem. This approach has been used to develop a many-body perturbation theory for vibrational-electronic problem in molecules [6, 38]. In related work the method of quasiparticle canonical transformations has been used to investigate the effects of nonadiabaticity in the theory of superconductivity using the fermionic part of the vibrational-electronicHamiltonian [40].

[3] This work is based, in part, on research carried out by the former Ph.D. students of one of us (I.H.): M. Svrček [32–35], P. Babinec, J. Mášik.

The nonadiabatic coupling between the electronic and nuclear motion manifest itself in numerous and rather diverse phenomena. The theoretical study of many problems in nanoscience and nanotechnology, necessitate the use of the total vibrational-electronic Hamiltonian. Molecular wires or nanowires, of which DNA is the prototype organic example [41] and $Mo_6S_{9-x}I_x$ is a typical inorganic example [42], are nanostructures for which the underpinning theory mandates the use of the total vibrational-electronic Hamiltonian. In molecular electronics, one is usually concerned with open quantum systems in nonequilibrium (driven by voltage) [43, 44]. Because, in the theoretical description of such open systems, we are not dealing with a fixed number of particles, the use of the methods of second quantization is mandatory.

Chemical reactivity under extreme conditions – high pressure and/or temperature – can differ drastically from that observed at ambient conditions. This is largely a consequence of the substantial changes in the electronic structure induced by the high pressure and/or temperature. For example, many reactions involve electronic excited states and the energy gap between the ground and excited states may be greatly reduced under extreme conditions [45].

The coupling of electronic and nuclear motion is known to be important in the study of in scattering processes (see, for example, the work of Deumens et al.) [46].

We note that the development of the laboratory instruments, such as the scanning tunneling microscope (STM) and the atomic force microscope (AFM), have facilitated manipulation single molecules and thus the investigation of single-molecule electronics [47]. These and similar developments in experimental nanoscience must be complemented by theoretical studies of molecular electronics. The theoretical apparatus presented in this paper provides a firm foundation for the description of electron-phonon interactions in molecules and molecular systems.

This paper is organized as follows: In Sect. 2 we consider the total molecular Hamiltonian for an arbitrary molecular system. The Born-Oppenheimer approximation is introduced in Sect. 3. The vibrational-electronic Hamiltonian is considered in Sect. 4. Corrections to the adiabatic Hamiltonian are considered in Sect. 5. In Sect. 6, the generalization of the canonical transformations are introduced. Fermionic part of the vibrational-electronic Hamiltonian obtained by means of the canonical transformation is presented in Sect. 7. In Sect. 8, we make certain simplifications in order to gain a deeper understanding of the new Fermion vibrational-electronic Hamiltonian. Summary of the present work and a short discussion of future directions is given in Sect. 9.

The present paper provides an outline of our derivation of the non-adiabatic molecular Hamiltonian using quasiparticle canonical transformations and a brief discussion of the relation of our approach to other work on non-adiabatic effects in molecules. A more detailed account is in preparation and will be published elsewhere [48].

2 The Total Molecular Hamiltonian

Our derivation begins in the body-fixed coordinates in terms of which clamped nucleus Hamiltonian is defined.[4] Internal motion is described in terms of normal coordinates which are expressed as displacements from some suitably chosen reference equilibrium geometry. To first order, the internal motion of the molecule is described in terms of small amplitude harmonic vibrations with respect to the reference geometry.

The total molecular Hamiltonian operator in body-fixed coordinates may be written

$$\mathrm{H}(r, R) = \mathrm{H}(r) + \mathrm{V}(r, R) + \mathrm{T}(r) \tag{5}$$

where r denotes the spatial coordinates of the electrons and R the spatial coordinates of the nuclei. In Eq. (5), $\mathrm{H}(r)$ is the sum of the kinetic energy of electrons and the Coulomb interactions between the electrons. $\mathrm{V}(r, R)$ is the sum of attractive interactions between the electrons and the nuclei, and the repulsive interactions between the nuclei. The third term in Eq. (5), $\mathrm{T}(r)$, is the kinetic energy of the nuclei.

The problem to be solved is the time-independent molecular Schrödinger equation for the total molecular Hamiltonan operator (5). This equation may be written

$$\mathrm{H}(r, R)\Psi(r, R) = \mathscr{E}\Psi(r, R), \tag{6}$$

where $\Psi(r, R)$ is the total molecular wave function and $\mathscr{E}$ is the corresponding total molecular energy. As is well known, this molecular Schrödinger equation is **very** complicated and can only be solved for the very simplest of systems. The total molecular Hamiltonian in Eq. (6) depends on the spatial coordinates of all of the electrons and nuclei in the molecular system. The wave function $\Psi(r, R)$ depends on both space and spin coordinates of all electrons and all nuclei in the system, although the spin coordinates are not shown explicitly in Eq. (6).

3 The Born-Oppenheimer Approximation

Approximations to the solutions of the molecular Schrodinger equation, the eigenproblem (6), can be developed by separating the electronic motion from that of the nuclei. This is the essence of the Born-Oppenheimer approximation [49, 50].[5]

[4] In brief, the molecular Hamiltonian defined in a laboratory-fixed frame is invariant under uniform translations and can therefore be divided into two parts, one describing all translational motion and the other (the space-fixed part) being expressed in terms of translationally invariant coordinates. The molecular Hamiltonian is also invariant under orthogonal transformations in three dimensions, and thus the space-fixed Hamiltonian can be written as the sum of a component expressed in terms of rotation operators and a component depending on variables (internal coordinates) which are invariant to orthogonal transformations.

[5] For an English translations of the original paper by Born and Oppenheimer see Blinder [51].

To this end, the electronic Schrödinger equation can be introduced as

$$[\mathrm{H}(r) + \mathrm{V}(r, R)]\varphi_n(r, R) = E_n(R)\varphi_n(r, R) \tag{7}$$

in which the Hamiltonian operator consists of the first two terms in the total molecular Hamiltonian defined in Eq. (5). The eigenvalues, $E_n(R)$, and eigenfunctions, $\varphi_n(r, R)$, in Eq. (7) depend parametrically on the coordinates of the nuclei, R.

The exact total molecular wave function, $\Psi(r, R)$, in Eq. (6) can then be written in the form of the summation

$$\Psi(r, R) = \sum_n \chi_n(R)\varphi_n(r, R), \tag{8}$$

where $\varphi_n(r, R)$ is the electronic wave function, one of the eigenfunctions of Eq. (7), and $\chi_n(R)$ is identified as the nuclear wave function.

The equation describing the motion of the nuclei takes the form

$$\sum_n [\mathrm{T}_{mn}(R) + U_{mn}(R)]\chi_n(R) = \mathsf{E}\chi_m(R) \tag{9}$$

where

$$U_{mn}(R) = E_n(R)\delta_{mn}, \tag{10}$$

in which $E_n(R)$ is an eigenvalue of the electronic Schrodinger Eq. (7), δ_{mn} is the Kronecker δ function, and the matrix elements of the nuclear kinetic energy operator are given by

$$\mathrm{T}_{mn}(R) = \mathrm{T}(R)\delta_{mn} + \lambda_{mn}(R). \tag{11}$$

The second term on the right-hand side of Eq. (11) is given by

$$\lambda_{mn}(R) = -\hbar^2 \sum_i \frac{1}{M_i}\left[A^{(i)}_{mn}(R)\frac{\partial}{\partial R_i} + \frac{1}{2}B^{(i)}_{mn}(R)\right] \tag{12}$$

where the summation runs over all nuclei, M_i is the mass of the ith nucleus and the coefficients $A^{(i)}_{mn}$ and $B^{(i)}_{mn}$ are given by integrals

$$A^{(i)}_{mn} = \int \varphi^*_m \frac{\partial \varphi_n}{\partial R_i} dr, \quad B^{(i)}_{mn} = \int \varphi^*_m \frac{\partial^2 \varphi_n}{\partial {R_i}^2} dr \tag{13}$$

To make further progress, it will be assumed that the states do not display degeneracy, i.e. attention is restricted to the case in which the electronic state $\varphi_n(r, R)$ is taken to be non-degenerate. In this case, the Hamiltonian for the nuclei takes the form

$$\mathrm{H}_n(R) = \mathrm{T}(R) + \lambda_{nn}(R) + E_n(R) \tag{14}$$

and the molecular wave function has the form of a simple product of a nuclear function, $\chi_n(R)$, and an electronic function, $\varphi_n(r,R)$, i.e.

$$\Psi(r,R) = \chi_n(R)\varphi_n(r,R). \tag{15}$$

This is the essence of the Born-Oppenheimer approximation and also of the closely associated adiabatic approximation [50]. By neglecting the off-diagonal elements λ_{nm} for $n \neq m$, it has been possible to separate the system of electrons from that of the nuclei. The electrons are described by the function $\varphi_n(r,R)$, which depend parametrically on the nuclear coordinates R. There are no transitions between the different electronic states. The function $E_n(R)$ in Eq. (14) is the potential energy surface or adiabatic potential.

The second and third terms on the right-hand side of Eq. (14) can be replaced by the expansion

$$\lambda_{nn}(R) + E_n(R) \approx E_N^{(0)} + \frac{1}{2}\sum_{ij} W_{ij}(R_i - R_{0i})\left(R_j - R_{0j}\right) + \ldots \tag{16}$$

where $E_N^{(0)}$ is the energy associated with the reference geometry and the W_{ij} are the expansion coefficients in a Taylor expansion which in second order are the harmonic force constants.

Furthermore, the non-diagonal elements $\lambda_{nm}(R)$ can be treated as a perturbation which scales as $\left(\frac{m}{M}\right)^{\frac{1}{4}}$. The matrix elements $A_{nm}^{(i)}(R)$ and $B_{nm}^{(i)}(R)$, defined in Eq. (13), are calculated with respect to the equilibrium or reference point R_0.

The non-diagonal elements of $\lambda_{nm}(n \neq m)$ can be treated as a perturbation if

$$\frac{\hbar\omega}{|E_n^{(0)} - E_m^{(0)}|} \ll 1. \tag{17}$$

If this inequality is not satisfied then quasi-degeneracy effects are present and, under such circumstances, significant coupling of vibrational and electronic motion can arise.

4 The Vibrational-Electronic Hamiltonian

The total molecular Hamiltonian can be written in the form

$$\mathrm{H} = \mathrm{H}_{NN}(R) + \mathrm{H}_{EE}(r) + \mathrm{H}_{NE}(r,R) \tag{18}$$

where the first term on the right-hand side is the sum of the nuclear kinetic energy and a term describing the repulsive interactions between the nuclei:

$$\mathrm{H}_{NN}(R) = \mathrm{T}_N(R) + E_{NN}(R), \tag{19}$$

and the remaining terms are associated with the electronic motion and the attractive interactions between the electrons and the nuclei:

$$\mathrm{H}_{EE}(r) + \mathrm{H}_{EN}(r,R) = h + v. \tag{20}$$

Equation (20) defines the standard electronic Hamiltonian which is ubiquitous in quantum chemistry for describing the electronic structure of molecules. In Eq. (20), h is the one-electron operator, which is the sum a kinetic energy term and a nucleus-electron attraction term. v arises from the electron-electron repulsions.

Using the method of second quantization [52–54], the electronic Hamiltonian operator (20) can be written in the form

$$\mathrm{H}_{EN}+\mathrm{H}_{EE}=\sum_{PQ}\langle P|h|Q\rangle a_P^+ a_Q+\frac{1}{2}\sum_{PQRS}\langle PQ|v^0|RS\rangle a_P^+ a_Q^+ a_S a_R \tag{21}$$

where $\langle P|h|Q\rangle$ is a matrix element of the one-electron operator h and $\langle PQ|v^0|RS\rangle$ is an element of the matrix for the two-electron operator v^0 which now includes the superscript '0' to indicate that it is defined with respect to the equilibrium geometry R_0. These matrix elements are defined in terms of the spin-orbitals $P, Q, \ldots$. a_P^+ is the usual creation operator and a_Q is an annihilation operator.

By using Wick's theorem in its normal product (N-product) form [55–57], the Hamiltonian operator (21) can be written as

$$\begin{aligned}\mathrm{H}_{EN}+\mathrm{H}_{EE}=&\sum_I h_{II}+\frac{1}{2}\sum_{IJ}\left(v^0_{IJIJ}-v^0_{IJJI}\right)+\sum_{PQ}h_{PQ}N\left[a_P^+ a_Q\right]+\\&+\sum_{PQI}\left(v^0_{PIQI}-v^0_{PIIQ}\right)N\left[a_P^+ a_Q\right]+\frac{1}{2}\sum_{PQRS}v^0_{PQRS}N\left[a_P^+ a_Q^+ a_S a_R\right]\end{aligned} \tag{22}$$

In this equation, the indices $I, J, \ldots$ have been used to label spin-orbitals which are occupied whilst $P, Q, \ldots$ have been employed for unoccupied (or virtual) spin-orbitals. Here, and in the following, the indices $A, B, \ldots$ will be used to label spin-orbitals which can be either occupied or unoccupied. $N[\ldots]$ is a normal product of creation and annihilation operators. v^0_{ABAB} denotes a Coulomb integral and v^0_{ABBA} is an exchange integral. The first two terms on the right-hand side of Eq. (22) can be added to give the reference energy, usually the Hartree-Fock energy. The third and fourth terms can be combined to yield a Fock operator, f which can be written as the sum $h+u$ where u is some mean field potential. Equation (22) then becomes

$$\begin{aligned}\mathrm{H}_{EN}+\mathrm{H}_{EE}=&\langle\Phi_0|\,\mathrm{H}\,|\Phi_0\rangle+\sum_{PQ}\langle P|f|Q\rangle N\left[a_P^+ a_Q\right]+\\&+\frac{1}{2}\sum_{PQRS}\langle PQ|v^0|RS\rangle N\left[a_P^+ a_Q^+ a_S a_R\right]\end{aligned} \tag{23}$$

where $\langle\Phi_0|\,\mathrm{H}\,|\Phi_0\rangle$ is the reference energy.

By considering the nuclear coordinate R at some point reference point R_0 – usually taken to be the equilibrium geometry in the Hartree-Fock approximation, the terms in the Hamiltonian (23) can then be separated into two types:-

1. Terms which are determined at the reference point, R_0
2. Terms which correspond to a change in the geometry with respect to the reference point, R_0. (A prime is used to distinguish these terms in the following discussion.)

Rearranging the terms in Eq. (23) allows the electronic part of the vibrational-electronic Hamiltonian to be cast in the form

$$\mathrm{H}_{EN}+\mathrm{H}_{EE}=E^0_{SCF}+\Delta E'_{SCF}+\sum_P \varepsilon_P N\left[a_P{}^+ a_P\right]+\sum_{PQ}\Delta\varepsilon'_{PQ}N\left[a_P^+ a_Q\right]+$$
$$+\frac{1}{2}\sum_{PQRS} v^0_{PQRS}N\left[a_P^+ a_Q^+ a_S a_R\right] \tag{24}$$

where $\Delta E'_{SCF}$ is the change in the self-consistent field energy, E^0_{SCF}, resulting from a change in the geometry. $\Delta E'_{SCF}$ is given by

$$\Delta E'_{SCF}=u'_{SCF} \tag{25}$$

where

$$u_{SCF}=\sum_I u_{II} \tag{26}$$

In Eq. (24), $\Delta\varepsilon'_{PQ}$ is the change in the orbital energies, ε_P, following a change in the geometry and is given by

$$\Delta\varepsilon'_{PQ}=V^{\mathrm{n}\prime}_{PQ} \tag{27}$$

where

$$V^{\mathrm{n}}_{PQ}=\langle P|V^{\mathrm{n}}|Q\rangle \tag{28}$$

in which

$$V^{\mathrm{n}}=\sum_{ij}\frac{-z_j e^2}{|r_i-R_j|} \tag{29}$$

A Taylor expansion can be made in powers of the displacements (R_i-R_{0i}) from the reference point R_0 for the term E_{NN} describing the repulsion between the nuclei in Eq. (19):

$$E_{NN}=E^{(0)}_{NN}+E'_{NN}=\sum_{i=0}^{\infty}E^{(i)}_{NN} \tag{30}$$

where i labels the order of the expansion coefficient $E^{(i)}_{NN}$. A similar expansion for u_{SCF} can introduced

$$u_{SCF}=u^{(0)}_{SCF}+u'_{SCF}=\sum_{i=0}^{\infty}u^{(i)}_{SCF} \tag{31}$$

Using the expansions (30) and (31), the vibrational-electronic Hamiltonian can be expressed in the form

$$\mathrm{H}=E^{(0)}_{NN}+E^{(0)}_{SCF}+\mathrm{T}_N+E^{(2)}_{NN}+u^{(2)}_{SCF}+\sum_P\varepsilon_P N\left[a_P^+ a_P\right]$$
$$+\frac{1}{2}\sum_{PQRS}v^0_{PQRS}N\left[a_p^+ a_Q^+ a_S a_R\right]+E'_{NN}-E^{(2)}_{NN}$$
$$+u'_{SCF}-u^{(2)}_{SCF}+\sum_{PQ}u'_{PQ}N\left[a_p^+ a_Q\right]. \tag{32}$$

The Hamiltonian operator defined in Eq. (32) is the complete vibrational-electronic Hamiltonian and is entirely equivalent to (18).

It should be noted that in expression (32), the third, fourth and fifth terms on the right-hand side, $\mathrm{T}_N + E_{NN}^{(2)} + U_{SCF}^{(2)}$, are associated with harmonic nuclear motion. The boson (phonon) creation operator, b_r^+, and boson (phonon) annihilation operator, b_r, are define through the harmonic oscillator problem

$$T_N + E_{NN}^{(2)} + u_{SCF}^{(2)} = \sum_r \hbar\omega_r \left(b_r^+ b_r + \frac{1}{2} \right) \tag{33}$$

where ω_r is the frequency of harmonic oscillation.

Substituting Eq. (33) into Eq. (32) gives

$$\begin{aligned} \mathrm{H} = E_{NN}^{(0)} + E_{SCF}^{(0)} + \sum_r \hbar\omega_r \left(b_r^+ b_r + \frac{1}{2} \right) + \sum_P \varepsilon_P N \left[a_P^+ a_P \right] \\ + \frac{1}{2} \sum_{PQRS} v_{PQRS}^0 N \left[a_p^+ a_Q^+ a_S a_R \right] + E'_{NN} - E_{NN}^{(2)} \\ + u'_{SCF} - u_{SCF}^{(2)} + \sum_{PQ} u'_{PQ} N \left[a_p^+ a_Q \right]. \end{aligned} \tag{34}$$

All quantities in this equation are defined in cartesian coordinates. It is more useful if these terms are expressed in normal coordinates $\{B_r\}$. The normal coordinates in second quantized formalism are

$$B_R \sim \left(b_r + b_r^+ \right). \tag{35}$$

In normal coordinates, the Hamiltonian given in Eq. (34) becomes

$$\begin{aligned} \mathrm{H} = \mathrm{H}_0 + \mathrm{H}' = \\ E_{NN}^{(0)} + u_{scf}^{(0)} + \sum_P \varepsilon_P N \left[a_p^+ a_p \right] + \sum_r \hbar\omega_r \left(b_r^+ b_r + \frac{1}{2} \right) + \\ + \mathrm{H}'_E \left\{ \equiv \frac{1}{2} \sum_{PQRS} v_{PQRS}^0 N \left[a_p^+ a_Q^+ a_S a_R \right] \right\} + \\ + \mathrm{H}'_F \left\{ \equiv \sum_{\substack{n=1 \\ n \neq 2}}^{\infty} \sum_{k=0}^{(n/2)} \left(E_{NN}^{(k,n-2k)} + u_{SCF}^{(k,n-2k)} \right) . B^{(n-2k)} \right\} + \\ + \mathrm{H}'_I \left\{ \equiv \sum_{\substack{n=1 \\ n \neq 2}}^{\infty} \sum_{k=0}^{(n/2)} \sum_{PQ} u_{PQ}^{(k,n-2k)} . B^{(n-2k)} N \left[a_P^+ a_Q \right] \right\} \end{aligned} \tag{36}$$

where we have used Taylor expansions for E_{NN}, u_{SCF} and u_{PQ} expressed in normal coordinate space.[6] In Eq. (36), H'_E is the electron correlation operator, H'_F is the phonon-phonon interaction operator and H'_I is the operator describing the electron-phonon coupling. It should be noted that the term H'_I contains a *one*-electron–phonon interaction. We shall term (36) the "crude adiabatic Hamiltonian" since it is defined in terms of a spin orbital basis determined at the *fixed* reference geometry R_0. In this representation the electron-phonon coupling is expected to be unphysically large because the electrons do not experience the R dependence of the nuclear terms. A perturbation expansion based on this "crude adiabatic" representation cannot be expected to converge.

We are now in a position to carry out a series of canonical transformations by means of which the electronic and vibrational motions are coupled. This coupling will allow the electrons to experience the R-dependence of the nuclear terms. We wish to transform from a basis set defined with respect to a fixed geometry R_0: $\{|P\rangle\}$, to an R-dependent basis set: $\{|P(R)\rangle$:-

$$|P\rangle \rightarrow |P(R)\rangle = \sum_Q C_{QP}|Q\rangle \tag{37}$$

The required transformation uses the mixed set of second quantized operators. The new representation refers to fermions and bosons rather than electrons and phonons. We proceed by defining new fermion creation and annihilation operators: $\overline{a}_P$ and $\overline{a}_P^+$, and new boson operators: $\overline{b}_r$ and $\overline{b}_r^+$. Furthermore, we can require that the new fermion operators commute with the new boson operators. The quasi-particle transformation relating the representations may be written as follows:

$$\overline{a}_P = a_P + \sum_Q \sum_{k=1}^{\infty} \frac{1}{k!} \sum_{r_1 \ldots r_k} C_{PQ}^{r_1 \ldots r_k} B_{r_1} \ldots B_{r_k} a_Q \tag{38}$$

$$\overline{a}_P^+ = a_P^+ + \sum_Q \sum_{k=1}^{\infty} \frac{1}{k!} \sum_{r_1 \ldots r_k} C_{PQ}^{r_1 \ldots r_k} B_{r_1} \ldots B_{r_k} a_Q^+$$

$$\overline{b}_r = b_r + \sum_{PQ} \sum_{k=0}^{\infty} \frac{1}{k!} \sum_{s_1 \ldots s_k} D_{rPQ}^{s_1 \ldots s_k} B_{s_1} \ldots B_{s_k} a_P^+ a_Q \tag{39}$$

$$\overline{b}_r^+ = b_r^+ + \sum_{PQ} \sum_{k=0}^{\infty} \frac{1}{k!} \sum_{s_1 \ldots s_k} D_{rPQ}^{s_1 \ldots s_k *} B_{s_1} \ldots B_{s_k} a_Q^+ a_P .$$

In these equations, B_{r_i} are the normal coordinates. C_{PQ} and D_{rPQ} are the expansion coefficients.

Equation (38) can be cast in the more compact form

$$\overline{a}_P = \sum_Q \sum_{k=0}^{\infty} C_{PQ}^{(k)} a_Q = \sum_Q C_{PQ} a_Q . \tag{40}$$

[6] Explicit expressions for these expansions can be found in the work of Hubač and Svrček [33,36].

A similar form can be written for Eq. (39) in terms of the D_{rPQ} coefficients.

The operators for the fermions satisfy anticommutation relations whilst those for the bosons satisfy commutation relations. As stated above, we require that the operators for the fermions and bosons to commute and therefore

$$\Psi(r,R) = \psi_k(r,R)\chi_k(R) \tag{41}$$

We find that there are two invariants of transformation: the number of fermions is conserved, i.e.

$$\overline{N} = N \tag{42}$$

so that we are free to redefine the Fermi vacuum, and the normal coordinate is unchanged, i.e.

$$\overline{B} = B$$

The canonical transformation introduced above allows the total vibrational-electronic Hamiltonian operator to be written a sum of two parts:

$$\mathrm{H} = \mathrm{H}_A + \mathrm{H}_B\,. \tag{43}$$

The operator H_A can be written

$$\mathrm{H}_A = E_{NN}(B) - E^{(2)}_{NN}(B) - V^{(2)}_N(B) + E_{SCF} + \sum_{PQ} f_{PQ} N\left[a^+_P a_Q\right] + \tag{44}$$
$$+\frac{1}{2}\sum_{PQRS} v_{PQRS} N\left[a^+_P a^+_Q a_S a_R\right]$$

where the terms $E_{NN}(B)$ and $E^{(2)}_{NN}$ arise from the Taylor expansion (30) in normal coordinates and $V^{(2)}_N(B)$ is the new effective potential. The new quasi-particle Fermi vacuum allows us to define a new quasi-particle Hartree-Fock energy

$$E_{SCF} = \sum_{RSI} h_{RS} C_{RI} C_{SI} + \frac{1}{2}\sum_{RSTKIJ} (v^0_{RTSU} - v^0_{RSTU}) C_{RI} C_{SI} C_{TJ} C_{UJ}, \tag{45}$$

the new Hartree-Fock operator f with matrix elements

$$f_{PQ} = \sum_{RS} h_{RS} C_{RP} C_{SQ} + \sum_{RTSUI} (v^0_{RTSU} - v^0_{RSTU}) C_{RP} C_{SQ} C_{TI} C_{UI}, \tag{46}$$

and the new two-particle integral

$$v_{PQRS} = \sum_{TUVW} v^0_{TUVW} C_{TP} C_{UQ} C_{VR} C_{WS}. \tag{47}$$

The coefficients C_{PQ} can be determined by solving the *coupled perturbed Hartree-Fock* (*CPHF*) equations [58–64]. We can carry out the inverse transformation of

the transformations (38) and (39) and then substitute these into Eq. (36). Then, by applying Wick's theorem, we obtain the result:

$$\mathrm{H}_A = E^0_{NN} + E^0_{scf} + \sum_P N\left[a^+_P a_P\right] + \sum_{n=1}^{\infty}\sum_{k=0}^{[n/2]} E^{(k,n-2k)} B^{(n-2k)} + \tag{48}$$

$$+ \sum_{n=1}^{\infty}\sum_{k=0}^{[n/2]}\sum_{PQ} f^{(k,n-2k)}_{PQ} B^{(n-2k)} N\left[a^+_P a_Q\right] +$$

$$+ \frac{1}{2}\sum_{n=0}^{\infty}\sum_{k=0}^{[n/2]}\sum_{PQRS} v^{(k,n-2k)}_{PQRS} B^{(n-2k)} N\left[a^+_P a^+_Q a_S a_R\right].$$

The Hamiltonian H_B can be handled in a similar fashion. H_B is given by

$$\mathrm{H}_B = \sum_r \hbar\omega_r (b^+_r b_r + \frac{1}{2}) \tag{49}$$

and after carrying out the transformation this becomes

$$\mathrm{H}_B = \sum_r \hbar\omega_r (b^+_r b_r + \frac{1}{2}) + \sum_{Air} \hbar\omega_r (D_{rAi})^2 + \tag{50}$$

$$+ \sum_{PQr} \hbar\omega_r (b_r{}^+ D_{rPQ} + D_{rPQ} b_r) N\left[a^+_p a_Q\right] +$$

$$+ \sum_{PQAIr} \hbar\omega_r (D_{rPA} D_{rQA} - D_{rPI} D_{rQI}) N\left[a^+_p a_Q\right] +$$

$$+ \sum_{PQRSr} \hbar\omega_r D_{rPS} D_{rQR} N\left[a^+_p a^+_Q a_S a_R\right].$$

It should be noted that these Hamiltonians contain terms describing phonon–2-electron interactions. $\mathrm{H} = \mathrm{H}_A + \mathrm{H}_B$ is the adiabatic Hamiltonian.

5 Adiabatic Corrections

Corrections to the adiabatic Hamiltonian, i.e. non-adiabaticity, can usually be treated as a small perturbation. The method of canonical transformation can be extended to case where the Born-Oppenheimer approximation breaks down. Starting from the "crude adiabatic" representation in which the vibrational-electronic Hamiltonian is expressed in terms of second quantized electron and phonon operators, a canonical transformation can be used to obtain a vibrational-electronic Hamiltonian in which the new fermion operators correspond to electron which adiabatically follow the nuclear motion and the new boson operators correspond to renormalized phonons where the renormalization introduces non-adiabatic corrections. For details of the

non-adiabatic representation of the vibrational-electronic Hamiltonian, the reader is referred to the reviews published in 1992 by Hubač and Svrček [36, 37].

In their work on the vibronic interaction in one-dimensional polymer, Taschibana and his co-workers [65] obtain an expression for the adiabatic correction which is similar to that obtained in the present approach. Specifically, the correction reported by Taschibana and his co-workers may be written

$$\Delta_{ij} = \sum_{m,n} a^{mn} \langle \Psi_j | \partial \Psi_i / \partial g^m \rangle \langle \delta \Psi_i / \partial g^n | \Psi_j \rangle \tag{51}$$

where

$$|a^{mn}| \tag{52}$$

is Wilson's G matrix [66].

The adiabatic corrections resulting from the present approach take the form

$$\begin{aligned} \Delta\varepsilon = \sum_{AIr} \hbar\omega_r (\hat{c}^r_{AI} - \langle A(0)|\hat{I}^r\rangle|)^2 + \\ + \sum_{AIr} \hbar^2 \omega_r^2 (\hat{c}^r_{AI} - \langle A(0)|\hat{I}^r\rangle|)^2 \frac{1}{\varepsilon_I - \varepsilon_A - \hbar\omega_r} + \\ + \sum_{AIr} \hbar^2 \omega_r^2 (\hat{c}^r_{AI} - \langle A(0)|\hat{I}^r\rangle)^2 \frac{1}{\varepsilon_I - \varepsilon_A + \hbar\omega_r} \approx \\ \approx \left[2 \sum_{AIr} \hbar^2 \omega_r^2 (\hat{c}^r_{AI} - \langle A(0)|\hat{I}^r\rangle)^2 \frac{1}{\varepsilon_I - \varepsilon_A} + \sum_{AIr} \hbar\omega_r (\hat{c}^r_{AI} - \langle A(0)|\hat{I}^r\rangle)^2 \right] \end{aligned} \tag{53}$$

which is essentially the same as Eq. (51) since $A(0)$ corresponds to Ψ_j and $\hat{I}^r$ corresponds to $\delta\Psi_j/\delta g^n$. Taschibana and his co-workers explicitly diagonalize the Wilson G matrix. In the present work, we have employed harmonic frequencies instead of the Wilson G matrix.

6 Generalization of the Canonical Transformations

Up to this point in our discussion, we have based the quasi-particle transformation on the normal coordinates using the follow expressions:

$$\begin{aligned} \overline{a}_p &= \sum_Q C_{PQ}(B) a_Q \\ \overline{a}^+_p &= \sum_Q C_{PQ}(B)^+ a^+_Q \\ \overline{b}_r &= b_r \sum_{PQ} D_{rPQ}(B) a^+_P a_Q \\ \overline{b}^+_r &= b^+_r \sum_{PQ} D_{rPQ}(B)^+ a^+_Q a_Q \end{aligned} \tag{54}$$

where we have used the normal coordinate:

$$B = b + b^{+}. \tag{55}$$

For the non-adiabatic representation, we can generalize the transformations (54). By analogy with the normal coordinate operator B_r, we can introduce the momentum operator:

$$\tilde{B} = b - b^{+} \tag{56}$$

and then generalize the transformations (54) so as to define new fermion operators which represent the dependence of the motion of electrons on both the coordinates and the momenta of the nuclei. Because of their finite mass, the electrons do not follow to the motion of the nuclei adiabatically. The motion of the electrons is phase-shifted with respect to the motion of the nuclei.

The case of strong coupling has been consider in the recent work by Dahnovsky [67] on *"Ab Initio electron propagators in molecules with strong electron-phonon interaction"*. Dahnovsky uses the exponential transformation:

$$T = e^{S} \tag{57}$$

where

$$S = \sum_{i,g} c_i^{+} c_i \frac{N_g^i}{W_g} (b^{+} - b) \tag{58}$$

and

$$\overline{C}_i = e^{S} c_i e^{-S}. \tag{59}$$

In the present approach, the general canonical transformation from the old set of second quantized operators $\{a_P\}$, $\{a_P^{+}\}$, $\{b_r\}$ and $\{b_r^{+}\}$ to the new set of operators $\{\overline{a}_P\}$, $\{\overline{a}_P^{+}\}$, $\{\overline{b}_r\}$ and $\{\overline{b}_r^{+}\}$ should be [32]:

$$\begin{aligned}
\overline{a}_P &= \sum_Q C_{PQ}(B,\tilde{B}) a_Q \\
\overline{a}_P^{+} &= \sum_Q C_{PQ}(B,\tilde{B})^{+} a_Q^{+} \\
\overline{b}_r &= b_r + \sum_{PQ} D_{rPQ}(B,\tilde{B}) a_P^{+} a_Q \\
\overline{b}_r^{+} &= b_r^{+} + \sum_{PQ} D_{rPQ}(B,\tilde{B})^{+} a_P^{+} a_Q.
\end{aligned} \tag{60}$$

These general transformations are rather complicated. The general coefficients, $C_{PQ}(B,\tilde{B})$ and $D_{rPQ}(B,\tilde{B})$, satisfy complicated conditions. To make progress, we introduce a simple approximation in which the coefficients are written as products, i.e.

$$C_{PQ}(B,\tilde{B}) = C_{PQ}(B).\tilde{C}_{PQ}(\tilde{B}). \tag{61}$$

This is expected to be a good approximation since coordinates and momenta are independent variables. The coefficients $C_{PQ}(B)$ correspond to the adiabatic transformation describe above whilst coefficients $\tilde{C}_{PQ}(\tilde{B})$ correspond to the new transformation which we term the non-adiabatic transformation. The non-adiabatic representation results from the combination of both transformations. The canonical transformation from the old set of second quantized operators $\{a_P\}$, $\{a_P^+\}$, $\{b_r\}$ and $\{b_r^+\}$ to the new set of operators $\{\tilde{a}_P\}$, $\{\tilde{a}_P^+\}$, $\{\tilde{b}_r\}$ and $\{\tilde{b}_r^+\}$ is [32]:

$$\begin{aligned}
\tilde{a}_P &= \sum_Q \tilde{C}_{PQ}(\tilde{B}) a_Q \\
\tilde{a}_P^+ &= \sum_Q \tilde{C}_{PQ}(\tilde{B})^+ a_Q^+ \\
\tilde{b}_r &= b_r + \sum_{PQ} \tilde{D}_{rPQ}(\tilde{B}) a_P^+ a_Q \\
\tilde{b}_r^+ &= b_r^+ + \sum_{PQ} \tilde{D}_{rPQ}(\tilde{B})^+ a_P^+ a_Q .
\end{aligned} \tag{62}$$

The coefficients $\tilde{C}_{PQ}(\tilde{B})$ and $\tilde{d}_{rPQ}(\tilde{B})$ are given by the Taylor expansions

$$\tilde{C}_{PQ}(\tilde{B}) = \sum_{k=0}^{\infty} \frac{1}{k!} \sum_{r_1 \ldots r_k} \tilde{C}_{PQ}^{r_1 \ldots r_k} \tilde{B}_{r_1} \ldots \tilde{B}_{r_k} \tag{63}$$

$$\tilde{D}_{rPQ}(\tilde{B}) = \sum_{k=0}^{\infty} \frac{1}{k!} \sum_{s_1 \ldots s_k} \tilde{D}_{rPQ}^{s_1 \ldots s_k} \tilde{B}_{s_1} \ldots \tilde{B}_{s_k} . \tag{64}$$

We make the approximation that terms beyond first order can be neglected.

7 Fermionic Part of the Vibrational-Electronic Hamiltonian

By performing the generalized canonical transformation defined in Eq. (62), we can obtain an expression for the fermionic part of the non-adiabatic Hamiltonian in the non-adiabatic representation. To simplify the notation, we shall omit the tilde from the operators $\{\tilde{a}_P\}$, $\{\tilde{a}_P^+\}$, $\{\tilde{b}_r\}$ and $\{\tilde{b}_r^+\}$ in the following. Our expression for the fermionic part of the non-adiabatic Hamiltonian can then be written in the form

$$\begin{aligned}
H_F = \underline{E_{NN}^0 + E_{SCF}^0} + \sum_{AI} \hbar\omega_2 (|C_{AI}^r|^2 - |\tilde{C}_{AI}^r|^2) + \underline{\sum_P \varepsilon_P^0 N\left[a_P^+ a_P\right]} + \\
+ \sum_{PQr} \hbar\omega_2 \left[\sum_A (C_{PA}^r C_{QA}^{r*} - \tilde{C}_{PA}^r \tilde{C}_{QA}^{r*}) - \sum_I (C_{PI}^r C_{QI}^{r*} - \tilde{C}_{PI}^r \tilde{C}_{QI}^{r*}) \right] N\left[a_P^+ a_Q\right] - \\
-2 \sum_{PQr} E^{r*} \tilde{C}_{PQ}^r N\left[a_P^+ a_Q\right] +
\end{aligned}$$

$$+\sum_{PQr}\left[(h(P)-p(P))\varepsilon_P^{r*}+(h(Q)-p(Q))\varepsilon_Q^{r}\right]\tilde{C}_{PQ}^{\,r}N\left[a_P^+a_Q\right]-$$

$$-\sum_{PQAIr}\left[(v_{PIQA}^{r}-v_{PIAQ}^{r})\tilde{C}_{IA}^{\,r}+(v_{PAQI}^{r}-v_{PAIQ}^{r})\tilde{C}_{AI}^{\,r*}\right]N\left[a_P^+a_Q\right]+$$

$$+\underline{\frac{1}{2}\sum_{PQRS}v_{PQRS}^{0}N\left[a_P^+a_Q^+a_Sa_R\right]}+\sum_{PQRSr}\hbar\omega_2(C_{PR}^{r}C_{SQ}^{r*}-\tilde{C}_{PR}^{\,r}\tilde{C}_{SQ}^{\,r*})N\left[a_P^+a_Q^+a_Sa_R\right]-$$

$$-2\sum_{PQSr}\varepsilon_P^{r}\tilde{C}_{SQ}^{\,r*}N\left[a_P^+a_Q^+a_Sa_R\right]+ \tag{65}$$

$$+\sum_{PQRSTr}\{\sum_{I}\left[v_{PQTS}^{0}C_{TI}^{r}-v_{PQTI}^{0}C_{TS}^{r}+(v_{TQSI}^{0}-v_{TQIS}^{0})C_{PT}^{r}\right]\tilde{C}_{RI}^{\,r*}+$$

$$+\sum_{I}\left[v_{TIRS}^{0}C_{QT}^{r}-v_{TQRS}^{0}C_{IT}^{r}+(v_{IQTS}^{0}-v_{IQST}^{0})C_{TR}^{r}\right]\tilde{C}_{IP}^{\,r*}-$$

$$-\sum_{A}\left[v_{PQTS}^{0}C_{TA}^{r}-v_{PQTA}^{0}C_{TS}^{r}+(v_{TQSA}^{0}-v_{TQAS}^{0})C_{PT}^{r}\right]\tilde{C}_{RA}^{\,r*}-$$

$$-\sum_{A}\left[v_{TARS}^{0}C_{QT}^{r}-v_{TQRS}^{0}C_{AT}^{r}+(v_{AQTS}^{0}-v_{AQST}^{0})C_{TR}^{r}\right]\tilde{C}_{AP}^{\,r*}\}N\left[a_P^+a_Q^+a_Sa_R\right]$$

where we have underlined the terms which arise in the usual electronic Hamiltonian operator. We can see immediately that if we set the $\tilde{C}_{PQ}$ coefficients to zero then we obtain the adiabatic Hamiltonian. If we put both the $\tilde{C}_{PQ}$ coefficients and the C_{PQ} coefficients equal to zero, we get the electronic Hamiltonian, which is underlined in the above expression.

Let us now summarize, what we have achieved so far. We have derived a new kinetic energy term, as well as a new potential energy term, depending on the coefficients C_{PQ} and $\tilde{C}_{PQ}$.

$$H = H_A + H_B \tag{66}$$

$$H_B = E_{\text{kinetic}}(\tilde{B}) + E_{\text{potential}}(B) \tag{67}$$

$$E_{\text{potential}}(B) = E_{NN}^{(2)}(B) + V_N^{(2)}(B) \tag{68}$$

$$E_{\text{kinetic}}(\tilde{B}) = T_N(\tilde{B}) + W_N^{(2)}(\tilde{B}). \tag{69}$$

We have to specify the C_{PQ} and $\tilde{C}_{PQ}$ coefficients from our transformation. We shall require that our new fermions, which we call *'renormalized fermions'*, are such that when partitioning the Hamiltonian H_A into an unperturbed part and a perturbation, the first order corrections vanish.

The equations for the C_{PQ} and $\tilde{C}_{PQ}$ coefficients are

$$u_{PQ}^{r}+(\varepsilon_P^0-\varepsilon_Q^0)C_{PQ}^{\,r}+\sum_{AI}\left[(v_{PIQA}^{0}-v_{PIAQ}^{0})C_{AI}^{\,r}-(v_{PAQI}^{0}-v_{PAIQ}^{0})\right]-$$

$$-\hbar\omega_r\tilde{C}_{PQ}^{\,r}=\varepsilon_P^{r}\delta_{PQ} \tag{70}$$

and

$$(\varepsilon_P^0 - \varepsilon_Q^0)\tilde{C}_{PQ}^{\ r} + \sum_{AI}\left[(v_{PIQA}^0 - v_{PIAQ}^0)\tilde{C}_{AI}^{\ r} - (v_{PAQI}^0 - v_{PAIQ}^0)\tilde{C}_{IA}^{\ r}\right]$$
$$-\hbar\omega_r C_{PQ}^{\ r} = \varepsilon_P^r \delta_{PQ}. \tag{71}$$

The new vibrational potential energy V_N^{rs}, which originate from the interaction between the nuclei and electrons, is:

$$V_N^{rs} = \sum_I u_{II}^{rs} + \sum_{AI}\left[\left(u_{IA}^r + \hbar\omega_r \tilde{C}_{IA}^r\right) C_{AI}^s + \left(u_{IA}^s + \hbar\omega_s \tilde{C}_{IA}^s\right) C_{AI}^r\right]. \tag{72}$$

Let us compare this expression for the potential energy with that obtained in the representations considered previously in this paper. In the "crude adiabatic" approximation we have

$$V_N^{\ rs} = \sum_I u_{II}^{rs}. \tag{73}$$

In the "adiabatic" approximation, we have

$$V_N^{\ rs} = \sum_I u_{II}^{rs} + \sum_{AI}\left(u_{IA}^r C_{AI}^s + u_{IA}^s C_{AI}^r\right). \tag{74}$$

The kinetic energy term in the 'renormalized fermion' representation has the form

$$W_R^{rs} = 2\hbar\omega_r \sum_{AI} C_{AI}^{\ r} \tilde{C}_{IA}^{\ s}. \tag{75}$$

8 Simplifications and Connections with Solid State Theory

In this section, we shall introduce some simplifying approximations to the formalism developed above. In this way we shall establish connections with solid state theory.

In solid state theory, as in quantum chemistry, it is common to work with models or effective Hamiltonians. In general terms, a model is a conceptual representation of some physical phenomenon. Such models usually underpin computer programs which allow simulation and visualization of phenomena and/or processes. Examples of such approximations or models in solid state theory and quantum chemistry include the Hubbard model [68], the Hückel Hamiltonian [69], the Pariser-Parr-Pople (PPP) approximation [70] and the Anderson Hamiltonian [71].

In this section, we shall gain some understanding of the new terms which arise in the fermionic Hamiltonian given above in Eq. (65) by introducing some simplifying approximations, by considering model systems.

We have seen above that the $C_{PQ}^{\ r}$ and $\tilde{C}_{PQ}^{\ r}$ coefficients are solutions of the Eqs. (70) and (71).

Let us explore the simplifications obtained by putting

$$v_{PQRS}^0 \longrightarrow 0 \tag{76}$$

that is, by assuming that two-electron Coulomb interactions vanish. We then obtain from Eqs. (70) and (71) the following pair of equations:

$$u^r_{PQ} + (\varepsilon^0_P - \varepsilon^0_Q) C^r_{PQ} - \hbar\omega_r \tilde{C}^r_{PQ} = \varepsilon^r_P \delta_{PQ} \tag{77}$$

$$(\varepsilon^0_P - \varepsilon^0_Q) \tilde{C}^r_{PQ} - \hbar\omega_r C^r_{PQ} = \varepsilon^r_P \delta_{PQ}. \tag{78}$$

By solving these equations for C^r_{PQ} and $\tilde{C}^r_{PQ}$ we get:

$$C^r_{PQ} = u^r_{PQ} \frac{\varepsilon^0_P - \varepsilon^0_Q}{(\hbar\omega_r)^2 - (\varepsilon^0_P - \varepsilon^0_Q)^2} \tag{79}$$

and

$$\tilde{C}^r_{PQ} = \begin{cases} u^r_{PQ} \frac{\hbar\omega_r}{(\hbar\omega_r)^2 - (\varepsilon^0_P - \varepsilon^0_Q)^2}, & \text{for } P \neq Q, \\ 0, \quad \text{for} & P = Q \end{cases}. \tag{80}$$

Let us focus our attention on the term which corrects the ground state energy.

$$\Delta E_0 = \sum_{AIr} \hbar\omega_r (|C^r_{AI}|^2 - |\tilde{C}^r_{AI}|^2). \tag{81}$$

Substitute the expressions for C^r_{PQ} and $\tilde{C}^r_{PQ}$ given in Eqs. (79) and (80), respectively, we get:

$$\Delta E_0 = \sum_{AIr} |u^r_{AI}|^2 \frac{\hbar\omega_r}{(\varepsilon^0_A - \varepsilon^0_I)^2 - (\hbar\omega_r)^2}. \tag{82}$$

Now let us re-write Eq. (82) in a notation more familiar in solid state theory.[7] The boson vibrational modes will be denoted by the index of quasimomentum $\mathbf{q}$, and spin orbitals (fermion) by $(\mathbf{k}, \sigma)$, where $\mathbf{k}$ is the quasimomentum of the fermion and σ is the spin function. Then we can write:

$$\begin{aligned} r &\longrightarrow \mathbf{q}, \\ \tilde{r} &\longrightarrow -\mathbf{q}, \\ I &\longrightarrow (\mathbf{k}, \sigma), \quad \text{occupation factor: } f_{\mathbf{k}} \\ A &\longrightarrow (\mathbf{k}', \sigma'), \quad \text{occupation factor: } 1 - f_{\mathbf{k}'} \end{aligned} \tag{83}$$

together with

$$\varepsilon^0_I \longrightarrow \varepsilon_{\mathbf{k}}, \ \varepsilon^0_A \longrightarrow \varepsilon_{\mathbf{k}'} \tag{84}$$

and

$$u^r_{AI} \longrightarrow u^{\mathbf{q}}_{\mathbf{k}'\mathbf{k}} = u^{\mathbf{q}} = u^{\mathbf{k}'-\mathbf{k}}. \tag{85}$$

In the notation of solid state theory defined above, expression (82) for the energy correction becomes:

[7] See, for example, E.K.U. Gross, E. Runge and O. Heinonen [72].

$$\Delta E_0 = 2\sum_{\mathbf{k},\mathbf{k}'} |u^{\mathbf{k}'-\mathbf{k}}|^2 f_{\mathbf{k}}(1-f_{\mathbf{k}'}) \frac{\hbar\omega_{\mathbf{k}'-\mathbf{k}}}{(\overrightarrow{\varepsilon}_{k'} - \varepsilon_{\mathbf{k}})^2 - (\hbar\omega_{k'-k'})}. \tag{86}$$

This can be recognized as exactly the expression first given by Fröhlich [73].

In contrast to the derivation given by Fröhlich, the present approach makes no use of perturbation theory. Fröhlich assumed that due to electron-phonon interaction the ground state energy will be lowered and electronic state will be redistributed around the Fermi level.

Let us turn attention to one-fermion component of the fermionic Hamiltonian given in Eq. (65). We can write this component in the form:

$$H'_{ef} = \sum_{PQr} \hbar\omega_r \left[\sum_A \left(C^r_{PA} C^{r*}_{QA} - \tilde{C}^r_{PA} \tilde{C}^{r*}_{QA} \right) - \sum_I \left(C^r_{PI} C^{r*}_{QI} - \tilde{C}^r_{PI} \tilde{C}^{r*}_{QI} \right) \right] N\left[a^+_P a_Q\right] +$$

$$+ \sum_{PRr} \left[(\varepsilon^0_P - \varepsilon^0_R)(|C^r_{PR}|^2 + |\tilde{C}^r_{PR}|^2) - 2\hbar\omega_r R_e(\tilde{C}^r_{PR} C^{r*}_{PR}) \right] N\left[a^+_P a_P\right]. \tag{87}$$

Let us consider only the diagonal part of H'_{ef} (87)

$$H'_{ef}(diag) = \sum_{Pr} \hbar\omega_r \left[\sum_A (|C^r_{PA}|^2 - |\tilde{C}^r_{PA}|^2) - \sum_I (|C^r_{PI}|^2 - |\tilde{C}^r_{PI}|^2) \right] N\left[a^+_P a_P\right] +$$

$$+ \sum_{PRr} \left[(\varepsilon^0_P - \varepsilon^0_R)(|C^r_{PR}|^2 + |\tilde{C}^r_{PR}|^2) - 2\hbar\omega_r R_e(\tilde{C}^r_{PR} C^{r*}_{PR}) \right] N\left[a^+_P a_P\right]. \tag{88}$$

By using expressions (79) and (80), this can be written:

$$H'_{ef}(diag) = \sum_{Pr} \left(\sum_{A\neq P} \frac{|u^r_{PA}|^2}{\varepsilon^0_P - \varepsilon^0_A - \hbar\omega_r} + \sum_{I\neq P} \frac{|u^r_{PI}|^2}{\varepsilon^0_P - \varepsilon^0_I - \hbar\omega_r} \right) N\left[a^+_P a_P\right] \tag{89}$$

or:

$$H'_{ef}(diag) = \sum_{PRr_{P\neq R}} |u^r_{PQ}|^2 \frac{1}{\varepsilon^0_P - \varepsilon^0_I - \hbar\omega_r} N\left[a^+_P a_P\right] -$$

$$-2 \sum_{\substack{PIr \\ P\neq I}} |u^r_{PI}|^2 \frac{\hbar\omega_r}{(\varepsilon^0_P - \varepsilon^0_I) - (\hbar\omega_r)^2} N\left[a^+_P a_P\right]. \tag{90}$$

In solid state theory, we use the following notation:

$$r \longrightarrow \mathbf{q}$$
$$P \longrightarrow (\mathbf{k}, \sigma)$$
$$R \longrightarrow (\mathbf{k}-\mathbf{q}, \sigma)$$
$$I \longrightarrow (\mathbf{k}-\mathbf{q}, \sigma)$$
$$\text{occupation factor: } f_{\mathbf{k}-\mathbf{q}}$$

and the Hamiltonian (90) becomes

$$H'_{ef}(diag) = \sum_{\mathbf{kq}\sigma} |u^{\mathbf{q}}|^2 \frac{1}{\varepsilon_{\mathbf{k}} - \varepsilon_{\mathbf{k}-\mathbf{q}} - \hbar\omega_{\mathbf{q}}} N\left[a^+_{\mathbf{k},\sigma} a_{\mathbf{k},\sigma}\right] -$$

$$-2\sum_{\mathbf{kq}\sigma} |u^{\mathbf{q}}|^2 f_{\mathbf{k}-\mathbf{q}} \frac{\hbar\omega_{\mathbf{q}}}{(\varepsilon_{\mathbf{k}} - \varepsilon_{\mathbf{k}-\mathbf{q}})^2 - (\hbar\omega_{\mathbf{q}})^2} N\left[a^+_{\mathbf{k},\sigma} a_{\mathbf{k},\sigma}\right]. \tag{91}$$

The first term on the right-hand side of (91) describes polaron, i.e. composite particles each composed of an electron together with a phonon field. The second term in Eq. (91) represents a correction term which describes each polaron in the effective field of other polarons.

Now we turn our attention to the two particle terms in the fermionic Hamiltonian defined in Eq. (65). We can write the following expression for H''_{ef}:

$$H''_{ef} = \sum_{\substack{\mathbf{k},\mathbf{k}',\mathbf{q},\sigma,\sigma' \\ \mathbf{q}\neq 0}} |u^{\mathbf{q}}|^2 \frac{\hbar\omega_{\mathbf{q}}\left[(\varepsilon_{\mathbf{k}+\mathbf{q}} - \varepsilon_{\mathbf{k}})(\varepsilon_{\mathbf{k}'+\mathbf{q}} - \varepsilon_{\mathbf{k}'}) - (\hbar\omega_{\mathbf{q}})^2\right]}{\left[(\varepsilon_{\mathbf{k}+\mathbf{q}} - \varepsilon_{\mathbf{k}})^2 - (\hbar\omega_{\mathbf{q}})^2\right]\left[(\varepsilon_{\mathbf{k}'+\mathbf{q}} - \varepsilon_{\mathbf{k}'})^2 - (\hbar\omega_{\mathbf{q}})^2\right]}$$

$$.N\left[a^+_{\mathbf{k}+\mathbf{q},\sigma} a^+_{\mathbf{k}',\sigma} a_{\mathbf{k}'+\mathbf{q},\sigma'} a_{\mathbf{k},\sigma}\right]. \tag{92}$$

Let us consider the relation between the Fermi vacuum in crude adiabatic representation and that in the diabatic representation. Specifically, let us consider a situation in which the electronic states are quasidegenerate (or degenerate) in the crude adiabatic representation but this quasidegeneracy (or degeneracy) is removed in diabatic representation .

Let us consider two quasidegenerate electronic states with the energies ε^0_I (occupied) and ε^0_A (unoccupied). According to Eq. (89) we have:

$$\Delta\varepsilon_A = \varepsilon_A - \varepsilon_{A0} = \sum_r \frac{|u^r_{AI}|^2}{\varepsilon^0_A - \varepsilon^0_I + \hbar\omega_r} > 0 \tag{93}$$

and

$$\Delta\varepsilon_I = \varepsilon_I - \varepsilon_{I0} = -A\varepsilon_A < 0. \tag{94}$$

We observe that the occupied diabatic fermions have a lower energy with respect to crude electrons and the virtual diabatic fermions have tendency to have a raised energy with respect to the crude electrons. This lowering of the occupied levels and raising of the unoccupied levels for the diabatic fermions results in an energy gap.

In situations where there is a large number of quasidegenerate states, the Fermi vacuum for the diabatic fermions will differ significantly from that for the crude fermions. Indeed, the occupancies of the levels in the diabatic Fermi vacuum may be different from those in the crude adiabatic vacuum.

9 Summary and Future Directions

The theoretical study of many problems in nanoscience and nanotechnology, necessitate the use of the total vibrational-electronic Hamiltonian. In this work, we have been concerned with the break-down of Born-Oppenheimer approximation. We have developed a non-adiabatic molecular Hamiltonian. Building on previous work by Hubač and Svrček, we have used three distinct quasi-particle transformations to obtain different representations of the total vibrational-electronic Hamiltonian.

We began with the "crude adiabatic" representation, which is defined in terms of a spin orbital basis determined at the *fixed* reference geometry R_0. We observed that in this representation the electron-phonon coupling is expected to be unphysically large because the electrons do not experience the R dependence of the nuclear terms. A perturbation expansion based on this "crude adiabatic" representation cannot be expected to converge.

Next, we carried out a canonical transformation to couple the electronic and vibrational motions. This coupling will allowed the electrons to experience the R-dependence of the nuclear terms. We transformed from a basis set defined with respect to a fixed geometry to an R-dependent basis set.

Finally, we generalise the quasi-particle transformations defining new fermion operators which represent the dependence of the motion of electrons on both the coordinates and the momenta of the nuclei. We term this new transformation the non-adiabatic transformation. In the non-adiabatic representation, the electrons do not follow the motion of the nuclei adiabatically, but the motion of the electrons is phase-shifted with respect to the motion of the nuclei.

We present the fermionic part of the vibrational-electronic Hamiltonian in non-adiabatic representation. By introducing some simplifying approximations, we were able to explore the relation between the fermionic part of the vibrational-electronic Hamiltonian in non-adiabatic representation and other formulations used in solid state theory and quantum chemistry.

A more detailed account of the approach to the molecular vibrational-electronic problem described in this paper is in preparation [48]. Future work will be concerned with the development of a fully diagrammatic formulation of the method of quasi-particle canonical transformations described in the present work to describe the coupling of electronic and nuclear motion in arbitrary molecular systems. From the diagrammatic formalism practical algorithms, which can be exploited in a wide range of application areas, will be devised using literate programming methods.

Acknowledgements IH acknowledges support under grant MSM 4781305903 in the Czech Republic.

References

1. B.T. Sutcliffe, "Coordinate systems and transformations", in *Handbook of Molecular Physics and Quantum Chemistry, volume 1: Fundamentals*, edited by S. Wilson, P.F. Bernath and R. McWeeny, chapter 31, Wiley, Chichester, 2003.
2. B.T. Sutcliffe, "Molecular Hamiltonians", in *Handbook of Molecular Physics and Quantum Chemistry, volume 1: Fundamentals*, edited by S. Wilson, P.F. Bernath and R. McWeeny, chapter 32, Wiley, Chichester, 2003.
3. B.T. Sutcliffe, "Potential energy curves and surfaces", in *Handbook of Molecular Physics and Quantum Chemistry, volume 1: Fundamentals*, edited by S. Wilson, P.F. Bernath and R. McWeeny, chapter 34, Wiley, Chichester, 2003.
4. B.T. Sutcliffe, "Molecular structure and bonding", in *Handbook of Molecular Physics and Quantum Chemistry, volume 1: Fundamentals*, edited by S. Wilson, P.F. Bernath and R. McWeeny, chapter 35, Wiley, Chichester, 2003.
5. B.T. Sutcliffe, "Breakdown of the Born-Oppenheimer approximation", in *Handbook of Molecular Physics and Quantum Chemistry, volume 1: Fundamentals*, edited by S. Wilson, P.F. Bernath and R. McWeeny, chapter 36, Wiley, Chichester, 2003.
6. R.G. Woolley and B.T. Sutcliffe, in *Fundamental World of Quantum Chemistry*, edited by E.J. Brändas and E.S. Kryachko, Kluwer Academic Publishers (2003).
7. J. Paldus, "Coupled cluster theory", in *Handbook of Molecular Physics and Quantum Chemistry*, *volume 2: Molecular electronic structure*,edited by S. Wilson, P.F. Bernath and R. McWeeny, chapter 19, Wiley, Chichester, 2003.
8. S. Wilson, "Perturbation theory", in *Handbook of Molecular Physics and Quantum Chemistry*, *volume 2: Molecular electronic structure*, ed. S. Wilson, P.F. Bernath and R. McWeeny, chapter 8, Wiley, Chichester, 2003.
9. I.L. Thomas, Phys. Rev. **185**, 90, 1969.
10. I.L. Thomas, Chem. Phys. Lett. **1**, 705, 1969.
11. I.L. Thomas, Phys. Rev. A **2**, 1200, 1970.
12. I.L. Thomas, Phys. Rev. A **3**, 1200, 1970.
13. W. Kolos and L. Wolniewicz, Rev. Mod. Phys. 35, 473, 1963.
14. D.M. Bishop, Molec. Phys. **28**, 1397, 1974.
15. D.M. Bishop and L.M. Cheung, Phys. Rev. A **16**, 640, 1977.
16. B.A. Pettite, Chem. Phys. Lett. **130**, 399, 1986.
17. H.J. Monkhorst, Phys. Rev. A **36**, 1544, 1987.
18. H. Nagao, K. Kodama, Y. Shigeta, H. Kawabe, K. Nishikawa, M. Makano and K. Yamaguchi, Int. J. Quantum Chem. **60**, 45, 1996.
19. Y. Shigeta, Y. Ozaki, K. Kodama, H. Nagao, H. Kawabe and K. Nishikawa, Int. J. Quantum Chem. **69**, 629, 1998.
20. Y. Shigeta, H. Takahashi, S. Yamanaka, M. Mitani, H. Nagao, K. Yamaguchi, Int. J. Quantum Chem. **70**, 659, 1998.
21. Y. Shigeta, H. Nagao, K. Nishikawa and K. Yamaguchi, J. Chem. Phys. **111**, 6171, 1999.
22. H. Nakai, K. Sodeyama and M. Hoshino, Chem. Phys. Lett. **345**, 118, 2001.
23. H. Nakai, Int. J. Quantum Chem. **86**, 511, 2002.
24. M. Tachikawa, K. Mori, H. Nakai and K. Iguchi, Chem. Phys. Lett. **290**, 437, 1998.
25. H. Nakai and K. Sodeyama, J. Chem. Phys. **118**, 1119, 2003.
26. H. Nakai, M. Hoshino, K. Miyamato and S. Hyodo, J. Chem. Phys. **122**, 164101, 2005.
27. B.T. Sutcliffe, J. Chem. Phys. **123**, 237101, 2005.
28. S. Wilson, in *Topics in the Theory of Chemical and Physical Systems*, Proceedings of the 10th European Workshop on Quantum Systems in Chemistry and Physics, Carthage, Tunisia, September, 2005, edited by S. Lahmar, J. Maruani, S. Wilson and G. Delgado-Barrio, Spinger, Dordrecht, 2007.
29. S. Wilson, in *Specialist Periodical Reports: Chemical Modelling- Applications and Theory*, vol. 3, Senior Reporter: A. Hinchliffe, Royal Society of Chemistry, London, 2004.

30. J. Ziman, *Electrons and Phonons: The Theory of Transport Phenomena in Solids*, Clarendon Press, Oxford, 1960.
31. A.A. Abrikosov, L.P. Gorkov and I.E. Dzyaloshinski, *Methods of Quantum Field Theory in Statistical Physics*, (Prentice-Hall, New Jersey, 1963); (Dover Publications, New York, 1975).
32. M. Svrček, *Ph.D. thesis*, Faculty of Mathematics and Physics, Comenius University, Bratislava, 1986.
33. I. Hubač and M. Svrček, Int. J. Quantum Chem. **33**, 403, 1988.
34. I. Hubač, M. Svrček, E.A. Salter, C. Sosa and R.J. Bartlett, in *Many-body Methods in Quantum Chemistry*, edited by U. Kaldor, Lecture Notes in Chemistry **52** Springer-Verlag, Berlin, 1989.
35. M. Svrček and I. Hubač, *Separation of vibrational-electronic Hamiltonian in crude representation*, Czechoslovak Journal of Physics, **41** 556–568, 1991.
36. I. Hubač and M. Svrček , *Molecular Vibrations*, *Methods in Computational Chemistry 4*, 145, Plenum Press, New York, 1992.
37. I. Hubač and M. Svrček, in *Methods in Computational Molecular Physics*, edited by S. Wilson and G.H.F. Diercksen, NATO ASI Series B: Physics 293 Plenum Press, New York, 1992.
38. I. Hubač, P. Babinec, J. Urban, P. Mach, J. Mášik, M. Polášek and J. Leszczynski, *Canonical transformations method for calculation of molecular vibrational spectra*, Asian Journal of Spectroscopy **1** 181–188, 1997.
39. I. Hubač, P. Babinec, M. Polášek, J. Urban, P. Mach, J. Mášik and J. Leszczynski, *Non-adiabatic molecular Hamiltonian. Canonical transformation coupling electronic and vibrational motion*, in *Quantum Systems in Chemistry and Physics* Vol. 1, edited by A. Hernandez-Laguna, J. Maruani, R. McWeeny and S. Wilson, Progress in Theoretical Chemistry and Physics **2**, 383–400, 2000.
40. M. Svrček, P. Baňacký and A. Zajac, Int. J. Quantum Chem. **43**, 393, 1992; *ibid.* **43**, 415, 1992.
41. C. Dekker and M. Ratner, Physics World **14**, 29, 2001.
42. D. Vrbanić, M. Remškar, A. Jesih, A. Mrzel, P. Umek, M. Ponikvar, B. Jančar, A. Meden, B. Novosel1, S. Pejovniki, P. Venturini, J.C Coleman and D. Mihailović, Nanotechnology **15**, 635, 2004.
43. C. Joachim, J.K. Gimzewski and A. Aviram, Nature **408**, 541, 2000.
44. M.A. Reed and J. M. Tour, Sci. Am., 282 (6) 68, 2000.
45. V. Schettino and R. Bini, Phys. Chem. Chem. Phys., **5**, 1951, 2003.
46. E. Deumens, A. Diz, H. Taylor and Y. Öhrn, J. Chem. Phys. **96**, 6620, 1992.
47. E. Meyer, H.J. Hug and R. Bennewitz, *Scanning Probe Microscopy: The Lab on a Tip*, Springer, Dordrecht, 2004.
48. I. Hubač and S. Wilson, *(in preparation)*.
49. M. Born and J.R. Oppenheimer, Ann. Physik (Leipzig) **84**, 457, 1927.
50. M. Born and K. Huang, *Dynamical Theory of Crystal Lattices*, Oxford University Press, 1956.
51. S.M. Blinder, *English translation of "*M. Born and J.R. Oppenheimer, 1927, Ann. der Phys. 84, 457*"* (with emendations by B.T. Sutcliffe and W. Geppert) in *Handbook of Molecular Physics and Quantum Chemistry, volume 1: Fundamentals*, edited by S. Wilson, P.F. Bernath and R. McWeeny, Wiley, Chichester, 2003.
52. B.T. Pickup, "Classical field theory and second quantization", in *Handbook of Molecular Physics and Quantum Chemistry, volume 1: Fundamentals*, edited by S. Wilson, P.F. Bernath and R. McWeeny, chapter 26, Wiley, Chichester, 2003.
53. B.T. Pickup, "The occupation number representation and the many-body problem", in *Handbook of Molecular Physics and Quantum Chemistry, volume 1: Fundamentals*, edited by S. Wilson, P.F. Bernath and R. McWeeny, chapter 27, Wiley, Chichester, 2003.
54. B.T. Pickup, "Second quantization and Lie algebra", in *Handbook of Molecular Physics and Quantum Chemistry, volume 1: Fundamentals*, edited by S. Wilson, P.F. Bernath and R. McWeeny, chapter 28, Wiley, Chichester, 2003.
55. G.C. Wick, Phys. Rev. **80**, 268, 1950.
56. N.H. March, W.H. Young and S. Sampanthar, *The many-body problem in quantum mechanics*, Cambridge University Press, 1967.

57. J. Paldus and J. Cizek, Adv. Quantum Chem. **9**, 105, 1975.
58. R.M. Stevens, R.M. Pitzer and W.N. Lipscomb, J. Chem. Phys. **38**, 550, 1963.
59. J. Gerratt and I.M. Mills, J. Chem. Phys. **49**, 1719, 1968.
60. J. Gerratt and I.M. Mills, J. Chem. Phys. **49**, 1730, 1968.
61. J.A. Pople, K. Raghavachari, H.B. Schlegel and J.S. Binkley, Int. J. Quantum Chem. Symp. **13**, 225, 1979.
62. T. Takada, M. Dupuis and H.F. King, J. Comput. Chem. **4**, 234, 1983.
63. P. Pulay, in *Applications of Electronic Structure Theory*, Modern Theoretical Chemistry, Vol. 4, Plenum Press, New York, 1977.
64. J. Simons, P. J orgensen and T.U. Helgaker, Chem. Phys. **86**, 413, 1984.
65. A. Taschibana, T. Inoue, T. Yamabe and K. Hori, Int. J. Quantum Chem. **30**, 575, 1986.
66. E.B. Wilson, Jr., J.C. Decius and P.C. Cross, *Molecular Vibrations: The Theory of Infrared and Raman Vibrational Spectra*, Dover, New York, 1980; McGraw-Hill, New York, 1955.
67. Y. Dahnovsky, J. Chem. Phys. **126**, 234111, 2007.
68. J. Hubbard, Proc. Roy. Soc. A **276** 238, 1963.
69. E. Hückel, Z. f. Physik, **70**, 204, 1931; **72** 310, 1931; **76** 628 1932; **83** 632, 1933; A. Streitwieser, *Molecular Orbital Theory for Organic Chemists*, Wiley, New York, 1961; C.A. Coulson, B. O'Leary and R.B. Mallion, *Hückel Theory for Organic Chemists*, Academic Press, 1978.
70. R. Pariser and R.G. Parr, J. Chem. Phys. **21**, 466, 767, 1953; J.A. Pople, Trans. Faraday Soc. **49**, 1375, 1953; R. Pariser, Int. J. Quantum Chem. **37**, 319, 1990; R.G. Parr, Int. J. Quantum Chem. **37**, 327, 1990; J.A. Pople, Int. J. Quantum Chem. **37**, 349, 1990 and papers in the same issue.
71. P.W. Anderson, Phys. Rev. **124**, 41, 1961.
72. E.K.U. Gross, E. Runge and O. Heinonen, *Many-particle theory*, Adam Hilger, Bristol, 1991.
73. H. Fröhlich, Phys. Rev. **79**, 845 1950.
74. H. Frohlich, Proc. R. Soc. Lond. **A 215**, 291, 1952.
75. H.A. Jahn and E. Teller, Proc. R. Soc. Lond. **A 161**, 220, 1937.
76. E. Teller, J. Phys. Chem. **41**, 109, 1937.

Alternative Technique for the Constrained Variational Problem Based on an Asymptotic Projection Method: I. Basics

Vitaly N. Glushkov(✉), Nikitas I. Gidopoulos, and Stephen Wilson

Abstract An alternative approach to problems in quantum chemistry which can be written as an eigenvalue equation with orthogonality restrictions imposed on eigenvectors is reviewed. The basic tenets of a simply implemented asymptotic projection method for taking the necessary orthogonality constraints into account are presented. The eigenvalue equation for a modified operator is derived and the equivalence of the original and modified problem is rigorously demonstrated. The asymptotic projection method is compared with the conventional approach to constrained variational problems based on the elimination of off-diagonal Lagrange multipliers and with other methods. A general procedure for application of the method to excited state problems is demonstrated by means of calculations of excited state energies and excitation energies for the one-electron molecular systems, H_2^+ and H_3^{++}.

Keywords: eigenvalue problem, orthogonality constraints, excited state, basis set optimization

V.N. Glushkov
Department of Physics, National University, Dnepropetrovsk, 49050, per.Nauchny 13, Ukraine, e-mail: v_n_glushkov@yahoo.com

N.I. Gidopoulos
ISIS Facility, Rutherford Appleton Laboratory, Chilton, Didcot, Oxon, OX11 0QX, England, UK, e-mail: n.gidopoulos@rl.ac.uk

S. Wilson
Physical & Theoretical Chemistry Laboratory, University of Oxford, South Parks Road, Oxford OX1 3QZ, England;
Faculty of Mathematics, Physics and Informatics, Comenius University, 84215 Bratislava, Slovakia, e-mail: quantumsystems@gmail.com

S. Wilson et al. (eds.) *Frontiers in Quantum Systems in Chemistry and Physics*.

1 Introduction

It is well known that many problems in physics and, in particular, in quantum chemistry, can be formulated as an eigenvalue problem for a self-conjugate operator H with some orthogonality constraints imposed on its eigenfunctions.

In practice, one of the most important approximations inherent in essentially all standard *ab initio* calculations is to replace the exact solution of an eigenvalue problem in an infinite-dimensional Hilbert space of states X by a solution in a finite-dimensional subspace $M = PX$ with the corresponding orthoprojector P, i.e. we are concerned with the eigenproblem:

$$\begin{aligned} P(H - E_i)P|\Phi_i\rangle &= 0, \\ |\Phi_i\rangle &= P|\Phi_i\rangle, \ i = 0, 1, \ldots, n \end{aligned} \tag{1}$$

subject to the constraints

$$\langle u_s|\Phi_i\rangle = 0, \ s = 1, 2, \ldots, q < n. \tag{2}$$

It is should be noted that, in general, the constraint vectors $|u_s\rangle \in X$ are not completely contained in the subspace M and are *arbitrary* with respect to the operator PHP.

It is clear that such an approximation reduces the accuracy of calculations. Furthermore, a finite subspace which is optimal for the lowest eigenvalue, E_0, will not, in general, support an acceptable accuracy for the higher eigenvalues. It is, therefore, necessary to adjust the subspace to the eigenvalue(s) being studied, by, for example, rotating the subspace M in X in an optimal manner.

Variational methods, such as the Rayleigh-Ritz method, are well adapted to the approximate solution of eigenvalue problems. In this method the desired vectors are represented by a linear combination of a finite number of basis vectors $|\phi_k(\rho)\rangle$ which, in general, depend on variational parameters $\rho_a, (a = 1, 2, \ldots, r)$

$$|\Phi_i\rangle = \sum_{k=0}^{n} C_{ik}|\phi_k(\rho)\rangle = P|\Phi_i\rangle. \tag{3}$$

The eigenvalues are determined by finding minimum of the Rayleigh quotient, i.e. the functional

$$E(\Phi) = \langle\Phi|H|\Phi\rangle / \langle\Phi|\Phi\rangle, \quad \Phi \in M, \tag{4}$$

For example, the lowest eigenvalue, E_0, for the problem defined by Eqs. (1) and (2) is given by

$$E_0 = E(\Phi_0) = \langle\Phi_0|H|\Phi_0\rangle = \min_{\Phi \in M} E(\Phi), \ \ \langle\Phi_0|\Phi_0\rangle = 1 \tag{5}$$

$$\langle u_s|\Phi\rangle = 0, \ \ s = 1, 2, \ldots, q < n. \tag{6}$$

In other words, we are dealing with a constrained minimization problem. *Equations (5) and (6) define the constrained variational problem.* An example of this problem

arises in calculations for excited states in which a basis set specifically designed for the ground state is used to calculate the ground state energy and a different basis set is used in the description of an excited state. There has been a growing interest in quantum chemical problems of this type in recent years (see e.g. the work of Sadlej [1], of Assfeld and Rivail [2], and of Surjan [3]). Conventional methods of constrained optimization (see, e.g. the well-known texts by Himmelblau [4] and by Gill and Murray [5], and references therein) have not proved effective in solving the complicated problems of quantum chemistry, especially when for example, nonlinear basis set parameters are varied.

In this study, we shall show how the problem defined by Eqs. (5) and (6) can be solved in a way which is simpler than the traditional approaches employed in quantum chemical calculations. We review an easily implemented technique termed the *asymptotic projection method*. This work was proposed in earlier work by one of us (VNG) [6–8] and developed further in Refs. [9–15]. The asymptotic projection method was shown to be a useful tool for solving a wide class of problems in quantum chemistry which can be cast in the form of an eigenvalue equation with constraints.

This paper is arranged as follows: in Sect. 2, an overview of the asymptotic projection method is given. We compare asymptotic projection with other approaches to the constrained variational problem, in particular, the method of elimination of off-diagonal Lagrange multipliers method and the projection operators technique. A general approach to excited state problems using the asymptotic projection method method is described in Sect. 3. In Sect. 4, the potential of the method is demonstrated by means of calculations for the excited state energies and excitation energies for the one-electron molecular systems, H_2^+ and H_3^{++}. Some concluding remarks are given in Sect. 5.

2 Overview of the Asymptotic Projection Method

We shall demonstrate that the asymptotic projection method is based on the properties of self-conjugate operators. It is general and applicable to any problem that can be cast in the form of an eigenvalue equation with some orthogonality constraints imposed on the eigenvectors.

2.1 The Basic Theorem of the Asymptotic Projection Method

For the sake of simplicity, we limit ourselves initially to problems involving one constraint vector $|u\rangle$. In this case, the constrained variational problem is to minimize the Rayleigh quotient (4) subject to constraint

$$\langle u|\Phi\rangle = 0. \tag{7}$$

We can identify three possible situations for the constrainted vector $|u\rangle$ with respect to a subspace M spanned by the finite basis set:

(i) $P|u\rangle = 0$, this is a trivial case. The minimization can be performed by well-established unconstrained optimization methods.
(ii) $P|u\rangle = |u\rangle$, the constraint vector lies completely within the subspace M.
(iii) $P|u\rangle \neq 0,\ P|u\rangle \neq |u\rangle$, then the constraint vector can be divided into two parts

$$|u\rangle = P|u\rangle + (I-P)|u\rangle \tag{8}$$

where the first term on the right-hand side lies completely within M and the second term lies in $M^{\perp}$, the orthogonal complement of M.

Here and in the following I is the identity operator.

Thus, we are only required to consider the case (ii), i.e., the constraint vector is $P|u\rangle$. Without loss of generality, we can take this constraint vector to be normalized $|\widetilde{u}\rangle = P|u\rangle/(\langle u|P|u\rangle)^{\frac{1}{2}}$, i.e. $\langle\widetilde{u}|\widetilde{u}\rangle = 1$. Then the constraint (7) may be rewritten in a symmetrized form which is convenient when carrying out variations:

$$\langle\Phi|P_u|\Phi\rangle = 0, \quad P_u = |\widetilde{u}\rangle\langle\widetilde{u}|. \tag{9}$$

Multiplying Eq. (9) by an arbitrary real multiplier λ and adding this to the Rayleigh quotient (4), we get the functional

$$L(\Phi) = \langle\Phi|(H+\lambda P_u)|\Phi\rangle/\langle\Phi|\Phi\rangle, \ \ \Phi \in M. \tag{10}$$

We can immediately write the stationary condition for (10) as

$$\delta L(\Phi) = 0. \tag{11}$$

Using Eq. (3), the variations can be written in the form

$$|\delta\Phi\rangle = P|\delta\Phi\rangle + \sum_{a=1}^{r}(\partial_a P)|\Phi\rangle\delta\rho_a. \tag{12}$$

In this equation and in the following, we use the notation $\partial_a P \equiv \partial P/\partial\rho_a$ for simplicity.

The first term in Eq. (12) corresponds to variations within the finite-dimensional subspace M, whereas the second term allows this subspace to be rotated within Hilbert space X. Substituting Eq. (12) into the functional $L(\Phi)$, Eq. (10), and taking account of the independence and the arbitrariness of variations, we arrive at the equations

$$P(H+\lambda P_u - E)P\,|\Phi\rangle = 0, \tag{13}$$

and

$$\langle\Phi|(\partial_a P)(H+\lambda P_u)P\,|\Phi\rangle = 0. \tag{14}$$

Equation (13) is an eigenvalue problem on the subspace $M = PX$ for the modified operator

$$H_{\mathrm{mod}} = P(H + \lambda P_u)P. \tag{15}$$

Equation (14) allows the basis set parameters to be determined by means of the variational principle and thus the optimal position of M in X can be found. However, the Lagrangian multiplier λ is as yet undetermined and condition (7) is not satisfied.

We now introduce the key theorem of the asymptotic projection method [6, 8]:

> If it is assumed that the vector $|\widetilde{u}\rangle$ is not an eigenstate of the operator PHP, then the constraint vector $|\widetilde{u}\rangle$ tends to an eigenvector of the modified operator H_{mod}, *if and only if*
>
> $$\lambda \longrightarrow \pm\infty. \tag{16}$$

This theorem ensures that the constraint condition (7) will be automatically fulfilled because of the orthogonality of the eigenvectors corresponding to different eigenvalues of a self-conjugate operator.

To prove the theorem (16), we consider the action of H_{mod} on the vector $|\widetilde{u}\rangle$. Let $|e_k\rangle$, $k = 0, 1, \ldots, n$ be the basis set vectors in the subspace M. Without loss of generality, we may assume that $|e_1\rangle = |\widetilde{u}\rangle$ and $\langle e_i|e_j\rangle = \delta_{ij}$. The matrix corresponding to H_{mod} in the chosen basis is multiplied by the vector $|\widetilde{u}\rangle$, which is represented, in the same basis set, by a column vector $[1, 0, \ldots, 0]^T$. Then the action of H_{mod} on the vector $|\widetilde{u}\rangle$ can be written in the following matrix form [6]:

$$\begin{pmatrix} H_{11}+\widetilde{\lambda} & H_{12} & \ldots & H_{1n} \\ H_{21} & H_{22} & \ldots & H_{2n} \\ \cdot & \cdot & \cdot & \cdot \\ \cdot & \cdot & \cdot & \cdot \\ H_{n1} & H_{n2} & \ldots & H_{nn} \end{pmatrix} \begin{pmatrix} 1 \\ 0 \\ \cdot \\ \cdot \\ 0 \end{pmatrix} = \widetilde{\lambda} \begin{pmatrix} H_{11}/\widetilde{\lambda}+1 \\ H_{21}/\widetilde{\lambda} \\ \cdot \\ \cdot \\ H_{n1}/\widetilde{\lambda} \end{pmatrix}. \tag{17}$$

Here $H_{ik} = \langle e_i|H|e_k\rangle$, $\widetilde{\lambda} = \lambda\langle u|P|u\rangle$, and $\langle u|P|u\rangle > 0$. It is can be seen immediately that Eq. (17) becomes the eigenvalue problem for the modified operator H_{mod}, if and only if $\lambda \to \pm\infty$. Q.E.D.

As we can also see from Eq. (17), the constraint vector $|\widetilde{u}\rangle$ tends to an eigenvector of the operator H_{mod} as $1/\lambda$, therefore, $\langle u|\Phi\rangle \to 0$ as $1/\lambda$, so that the limit,

$$\lim_{\lambda\to\pm\infty} \lambda\,\langle u|\Phi\rangle\,,$$

exists. In practice, the choice of the value given to λ depends on the accuracy required. In Sects. 3 and 4, we will show that convergence behaviour is displayed for different properties. It is also clear that if $|\widetilde{u}\rangle$ is an eigenvector of PHP then it will be an eigenstate of H_{mod} for all values of λ.

The result obtained above for a single constraint vector can be easily extended to cases involving a number of constraints. In such cases, P_u in the above discussion is replaced by the orthoprojector on the subspace determined by all the constraint vectors.

We have called the technique described above the ***asymptotic projection method***.

Alternative Proof of Theorem (16)

We can require that the constraint vector $|\widetilde{u}\rangle$, which, in general, is not an eigenvector of the operator PHP, be an eigenvector of the modified operator, H_{mod}, so that

$$P(H+\lambda P_u - E_\lambda)P|\widetilde{u}\rangle = 0. \tag{18}$$

In this equation, E_λ is the, as yet unknown, eigenvalue corresponding to the vector $|\widetilde{u}\rangle$. The eigenvalue E_λ must not coincide with any eigenvalues of H_{mod}.

Let us find the value of λ for which Eq. (18) is satisfied. For this purpose Eq. (18) is rewritten, after some manipulation, in the form

$$\frac{1}{\lambda\langle u|P|u\rangle}PHP|\widetilde{u}\rangle + \left[1 - \frac{E_\lambda}{\lambda\langle u|P|u\rangle}\right]P|\widetilde{u}\rangle = 0 \tag{19}$$

where we repeat that it is assumed that the vector $|\widetilde{u}\rangle$ is not an eigenvector of the operator PHP. It is obvious that, when considered as a vector, the direction of the first term in (19) does not coincide with that of $P|\widetilde{u}\rangle$. Therefore, the fulfillment of (18) requires that each term in (1) tends to zero. This is possible if and only if $\lambda \to \pm\infty$ and $E_\lambda = \lambda\langle u|P|u\rangle$, which completes our alternative proof of theorem (16). Q.E.D.

It should be noted that, for an operator bounded from below, E_λ must be positive and $\lambda \to +\infty$. The eigenvalues are found by minimization. If we are dealing with an operator bounded from above then $\lambda \to -\infty$ and the eigenvalues are determined by maximization procedure.

2.2 Equivalence of the Original and Modified Problem

The problem defined in Eqs. (5) and (6), or in the corresponding constrained minimization problem defined in Eqs. (4) and (7), implies that the solutions are sought in the subspace $(P-P_u)X$. This is an eigenvalue problem for the effective operator $H_{\mathrm{eff}} = (P-P_u)H(P-P_u)$.

In order to clarify the validity of replacing the constrained minimization problem, Eqs. (4) and (7), by unconstrained problem, Eq. (10), we shall demonstrate that the spectra of the original operator PHP and the modified operator H_{mod} are identical

on the subspace $(P-P_u)X$ when $\lambda \to \pm\infty$. Indeed, since $|\widetilde{u}\rangle$ is an eigenvector of H_{mod}, the subspace M can be written as a direct sum of subspaces [16]

$$M = (P-P_u)X \oplus P_uX \tag{20}$$

which are invariant for the operator H_{mod}. Therefore, Eq. (13) is equivalent to the eigenvalue problem on the subspace P_uX, for which the solution is known (the eigenvector $|\widetilde{u}\rangle$ and the corresponding eigenvalue $E_\lambda \to \infty$), i.e.

$$P_u(H-E_\lambda)P_u\,|\Phi\rangle = 0,\ \ E_\lambda \to \infty \tag{21}$$

and equation on the subspace $(P-P_u)X$

$$(P-P_u)(H-E)(P-P_u)\,|\Phi\rangle = 0. \tag{22}$$

Here we used the fact that $\lambda\,(P-P_u)P_u(P-P_u) = 0$ for any value of λ.

Equation (22) implies that the spectra of the operators $(P-P_u)(H+\lambda P_u)(P-P_u)$ and $(P-P_u)H(P-P_u)$ are identical. However, from practical point of view, Eq. (13) is much simpler to solve than Eq. (22). Indeed, Eq. (22) requires additional calculations of $\langle\Phi|H|u\rangle$ and $\langle u|H|u\rangle$, whereas Eq. (13) requires only the overlap element $\langle\Phi|u\rangle$. (Further discussion of these practicalities is given in Sect. 2.3).

2.3 Comparison with Other Methods

There are several techniques for solving the problem defined in Eqs. (1) and (2) or their variational implementation, Eqs. (5) and (6). (See e.g. the texts by Himmelblau [4] and by Gill and Murray [5], and the papers by Feshbach [17], by Weeks and Rice [18] and by Huzinaga [19], and references therein). A natural solution of this problem is to derive the equations for the constrained function in such a manner that the orthogonality constraints are built into the variational procedure as an auxiliary condition. Traditionally, this can either be achieved by the method of Lagrangian multipliers or the projection operator technique. In the discussion below, we shall demonstrate the main features which distinguish our asymptotic projection method from other existing methods. The traditional methods of the elimination of Lagrangian multipliers and the projection operators will be described in more detail since many other approaches can be reduced to these techniques.

2.3.1 Elimination of Off-Diagonal Lagrangian Multipliers Method

We shall follow closely here the presentation given in Chapter 2 of Hurley's well-known book *Introduction to the electron theory of small molecules* [20].

The electronic Schrödinger equation for some molecular system may be written

$$H\Psi_i = E_i\Psi_i \tag{23}$$

where H is the electronic Hamiltonian and the eigenfunctions $\Psi_0, \Psi_1, \ldots$ may be chosen as a complete, orthonormal set, ordered in terms of the energy eigenvalues $E_0, E_1, \ldots$, so that

$$E_i \leqslant E_{i+1} \tag{24}$$

and

$$\langle \Psi_i | \Psi_j \rangle = \delta_{ij}. \tag{25}$$

Now the electronic Schrödinger Eq. (23) may be regarded as the condition that the energy expectation value

$$E = \langle \Psi | H | \Psi \rangle \tag{26}$$

should remain stationary for arbitrary variations $\delta\Psi$ of the many-electron wave function Ψ, which maintain the normalization condition

$$\langle \Psi | \Psi \rangle = 1. \tag{27}$$

In studies of excited states and in self-consistent field theory it is sometimes necessary to impose additional linear constraints on the wave function and the admissible variations. A linear constraint may be expressed as the orthogonality of Ψ to some fixed constraint function $u(\mathbf{r})$

$$\langle \Psi | u \rangle = \langle u | \Psi \rangle = 0, \tag{28}$$

which is taken to be normalized

$$\langle u | u \rangle = 1. \tag{29}$$

The constraints (27) and (28) can be incorporated by means of Lagrange multipliers E, ε and η, by considering the functional

$$L = \langle \Psi | H | \Psi \rangle - E \langle \Psi | \Psi \rangle - \varepsilon \langle \Psi | u \rangle - \eta \langle u | \Psi \rangle \tag{30}$$

and requiring that

$$\delta L = 0 \tag{31}$$

for arbitrary variations $\delta\Psi$ and suitably chosen values of E, ε and η. Exploiting the hermiticity of H, the condition (31) can be written in the form

$$\langle \delta\Psi | (H - E) | \Psi \rangle - \varepsilon \langle \delta\Psi | u \rangle + \langle \Psi | (H - E) | \delta\Psi \rangle - \eta \langle u | \delta\Psi \rangle = 0. \tag{32}$$

Since the variations $\langle \delta\Psi |$ and $| \delta\Psi \rangle$ are arbitrary, the condition (32) leads to two equations which can be written

$$H | \Psi \rangle = E | \Psi \rangle + \varepsilon | u \rangle \tag{33}$$

and

$$\langle \Psi | H = E \langle \Psi | + \eta \langle u |. \tag{34}$$

Comparing Eq. (33) with the complex conjugate of (34) leads to the conclusion that the off-diagonal Lagrange multipliers are related by

$$\eta = \varepsilon^*. \tag{35}$$

Imposing the condition (35) renders Eq. (34) equivalent to Eq. (33) so that the former may be dropped.

The values of the constants E and ε are found by multiplying Eq. (33) by $\langle\Psi|$ or by $\langle u|$, i.e.

$$E = \langle\Psi|H|\Psi\rangle \tag{36}$$

and

$$\varepsilon = \langle u|H|\Psi\rangle \tag{37}$$

Equation (33), together with the orthonormality conditions (27) and (28), provides the solution to our variational problem. Because of the second term on the right hand side the form of Eq. (33) is not that of an equation determining the eigenvalues and eigenfunctions of some Hermitian operator. However , it may be reduced to this standard form by introducing a suitable effective Hamiltonian. Indeed, taking the expression (37) into account, Eq. (33) can be rewritten in a form

$$H|\Psi\rangle - |u\rangle\langle u|H|\Psi\rangle = E|\Psi\rangle. \tag{38}$$

Using the definition of the orthoprojector

$$P_u = |u\rangle\langle u|, \tag{39}$$

$$P_u^2 = P_u \tag{40}$$

the Eq. (38) takes a form

$$H|\Psi\rangle - P_u H|\Psi\rangle = E|\Psi\rangle. \tag{41}$$

Generally speaking the operator $P_u H$ is not Hermitian, however the symmetrized product $P_u H + H P_u$ is necessarily Hermitian. Since $H P_u|\Psi\rangle = 0$ we arrive at the eigenvalue equation for the effective operator

$$H_{\text{eff}}^{[1]}|\Psi\rangle = E|\Psi\rangle \tag{42}$$

with

$$H_{\text{eff}}^{[1]} = H - (P_u H + H P_u). \tag{43}$$

It is easy to show that the vector $|u\rangle$ itself is an eigenvector of $H_{\text{eff}}^{[1]}$ with the eigenvalue $E_u = -\langle u|H|u\rangle$ and then the constraint (28) is automatically fulfilled due to orthogonality of eigenfunctions of $H_{\text{eff}}^{[1]}$.

2.3.2 Projection Operator Techniques and Other Methods

Following the work of Huzinaga and Cantu [21] and the more recent work of Surjan [3], we now consider the variational procedures based on the projected function

$$|\Psi\rangle = (I - P_u)|\Phi\rangle \tag{44}$$

which satisfies the constraint $\langle\Psi|u\rangle = 0$ for any $|\Phi\rangle$. Variation of the Rayleigh quotient

$$\delta E(\Psi) = \delta[\langle\Psi|H|\Psi\rangle/\langle\Psi|\Psi\rangle,] \tag{45}$$

leads to the Euler equation

$$[(I - P_u)H(I - P_u) - E(I - P_u)|\Phi\rangle = 0 \tag{46}$$

which can be interpreted as an eigenvalue problem for an effective Hermitian operator $H_{\text{eff}}^{[2]}$

$$H_{\text{eff}}^{[2]}|\Phi\rangle = E(I - P_u)]|\Phi\rangle \tag{47}$$

where

$$H_{\text{eff}}^{[2]} = H + E_u P_u - P_u H - H P_u \tag{48}$$

and $E_u = \langle u|H|u\rangle$.

It easy to verify that the projected excited functions $\Psi_i = (I - P_u)\Phi_i$ corresponding to different solutions of Eq. (47) will be orthogonal to each other. We may also observe that there is a close relation between the effective operator defined in Eq. (43) for the elimination of off-diagonal Lagrangian multipliers method and $H_{\text{eff}}^{[2]}$ defined in Eq. (21) for the projection operator technique.

Both the elimination of off-diagonal Lagrangian multipliers method and the projection operator technique require the evaluation of matrix elements of the form $\langle u|H|\Phi\rangle$ whereas the asymptotic projection method only involves overlap elements $\langle u|\Phi\rangle$, which are more easily computed. This difference in computational demands can be particularly significant when minimization is carried out with respect to nonlinear basis set parameters (i.e. exponents). For example, in self-consistent field calculations for excited state the elimination of off-diagonal Lagrangian multipliers method and the projection operator technique require the evaluation of $\sim m^4$ elements of the Fock operator whereas only $\sim m^2$ overlap elements are required for the asymptotic projection method, where m is dimension of one-particle basis set employed.

We comment briefly on a method for handling the orthogonality constraints in the self-consistent field theory developed by Colle, Fortunelli and Salvetti [22, 23]. The solution to the constrained variational problem presented by these authors is specific to the Hartree-Fock case. In contrast, the asymptotic projection method described in the present work is based on the properties of self-conjugate operators. It is a general method which can be applied to many systems and in many approximation schemes. In our accompanying paper [24], we shall demonstrate the

application of the asymptotic projection method to self-consistent field problems with orthogonality constraints.

The asymptotic projection method described in Sect. 2.1 may seem similar to the shift operator technique introduced by Huzinaga [19]. This technique was found to be useful for shifting the positions of eigenvalues in the spectrum of the Fock operator in the Hartree-Fock theory thereby accelerating the convergence of the iterative self-consistent field process. However, it is known [19] that this technique operates only on the exact eigenvectors of the operator PHP, whereas in the asymptotic projection method *arbitrary* constraint vectors are considered.

We also note the similarity of the asymptotic projection method to techniques for incorporating orthogonality constraints by means of an energy penalty term. However, we recognize that this penalty term method requires several calculations of a functional (e.g. the energy functional) in order to determine an optimal value of the multiplier λ. There have been some preliminary attempts to apply the penalty term method to excited state calculations. The reader is referred to the work of Dutta and Bhattacharya [25], where different penalty functions are considered.

In concluding this section, we note that, from practical point of view, the numerical solution of the eigenvalue equation for the operator H_{mod} is a stable process, although the condition number (i.e. ratio $E_{\max}/E_{\min}$) of the corresponding matrix can be quite large. The problem is that the sensitivity of the eigenvalue is measured by the condition number of diagonalizing matrix rather than the H_{mod} matrix [26].

3 Application to Excited State Problems

It is well known that the *ab initio* study of the excited electronic states of atoms and molecules contains elements which are not present in the treatment of ground states. In particular, excited state wave functions must be orthogonal to states of lower energy. For the lowest eigenstate in a given symmetry class, a trial wave function of that symmetry is automatically orthogonal to all lower eigenstates. For higher eigenstates, the imposition of the orthogonality constraints is often difficult and cumbersome.

The asymptotic projection method described above can be directly applied to the calculation of approximate wave functions and energies of excited states having the same spin and spatial symmetry as lower states. In this case, $u = \Phi_0$ and E_0 are an approximate ground state wave function and the corresponding ground state energy respectively. E_0 is defined as the lowest root of Eq. (13) at $\lambda = 0$. The operator H is the Hamiltonian of a system. The first excited state or the second eigenvalue is then defined by the relation

$$E_1 = E(\Phi_1) = \langle \Phi_1 | H | \Phi_1 \rangle = \min_{\Phi \in (\Phi_0)^{\perp}} E(\Phi), \quad \langle \Phi_1 | \Phi_1 \rangle = 1 \tag{49}$$

where the minimum is taken with respect to all vectors $|\Phi\rangle$ belonging to the orthogonal complement $(\Phi_0)^{\perp}$ of the vector $|\Phi_0\rangle$, i.e. the vectors $|\Phi\rangle \in (\Phi_0)^{\perp}$ satisfy the

condition $\langle \Phi | \Phi_0 \rangle = 0$. It should be stressed that, in general, $(\Phi_0)^{\perp} \not\subseteq M$, i.e., a subspace distinct from M can be used for E_1. Higher eigenvalues are determined in a similar fashion.

3.1 Bounds to Excited State Energies

Löwdin [27] has published a clear and detailed discussion of the general problem of variation in a restricted subspace. He has documented some of the technical difficulties that arise in using Eq. (49). In particular, we must require orthogonality of an excited state eigenfunction to the exact lower eigenfunctions of H if the minimum given by Eq. (49) is to be an upper bound to the exact eigenstate energy. A more practical formulation, which avoids the need for the exact lower eigenfunctions, has been given by Hylleraas and Undheim [28] and by MacDonald [29]. These authors have shown that convenient upper bounds are provided by the Rayleigh-Ritz method if the functions $|\Phi_i\rangle$ are determined in the *same* basis set $|\phi_k\rangle (k = 0, 1, \ldots, n)$ using the expansion given in Eq. (3).

If we use different basis sets for different states, then the imposition of the orthogonality constraint (7) with respect to an approximate wave function for a lower state does not, in general, yield an excited state energy which is an upper bound to the exact excited state energy. However such an approximation is often preferable since it can provide a more compact and accurate representation of the eigenvectors and eigenvalues. *"The desirability of using different basis sets for different states"* was pointed out by Shull and Löwdin [30] as long ago as 1958. Of course such a scheme requires significant computation, but, given the availability of an efficient method for solving the eigenvalue problem (1) with orthogonality constraints (2), it can be justified. In this case, the quality of the bounds to the excited state energies remains an open question.

Although the imposition of the orthogonality constraint (7) to an approximate lower state wave function does not, in general provide an upper bound to the excited state, there exists a so-called "weak bound" (introduced by Zener and coworkers [31]) with respect to the exact energies $\mathscr{E}_i$:

$$E_i \geq \mathscr{E}_i - \sum_{j}^{i-1} \delta_j (\mathscr{E}_i - \mathscr{E}_j). \tag{50}$$

In this equation,

$$\delta_j = 1 - |\langle \Phi_i | \Psi_j \rangle|^2 \tag{51}$$

and Ψ_j is the exact wave function for the j-th state. We can obtain an upper bound by imposing the additional constraint

$$\langle \Phi_i | H | \Phi_j \rangle = 0. \tag{52}$$

It should be noted that the asymptotic projection method can also be applied to the problem defined by Eq. (52).

In practical calculations, the excited state energies are expected to lie above the the exact energies if Φ_0 is a good approximation to the true ground state eigenfunction. Therefore, we shall now investigate the bounding properties when only the orthogonality constraint (7) is imposed on an excited function. In this case, it is our opinion that a min – max principle [16], which is not directly based on eigenvectors is useful. For example, for the first excited state we have

$$E_1 = \max_{\Phi_0} \quad \min_{\Phi \in (\Phi_0)^\perp} \quad E(\Phi). \tag{53}$$

In this equation, the maximum is attained when Φ_0 is equal to the exact wave function Ψ_0 of the ground state.

Equation (53) suggest that the value of E_1 is influenced by two effects. On the one hand, if a complete basis set is used for Φ_0 then a finite-dimensional approximation to the excited state leads to an upper bound for E_1, i.e. $E_1 \geq \mathscr{E}_1$. On the other hand, if the variation of Φ is carried out in the subspace $(I - |\Phi_0\rangle\langle\Phi_0|)X$ and a finite basis set approximation is made for Φ_0, then the min – max principle (53) gives $\mathscr{E}_1 \geq E_1$, that is E_1 is a lower bound to the true energy with the equality applying in the case $\Phi_0 = \Psi_0$.

The imposition of the orthogonality constraint $\langle \Phi_1 | \Phi_0 \rangle = 0$ alone does not guarantee that E_1 will be an upper bound to the exact energy. However, in contrast to the "weak bound" defined in Eq. (50), we are able to give a relation between E_1 and an upper bound E_1^{upper} [12, 13, 32] which proves useful from the point of view of practical calculations. Indeed, for the approximate wave functions Φ_0 and Φ_1, the secular determinant may be written

$$\det \begin{vmatrix} \langle \Phi_0 | H | \Phi_0 \rangle - \varepsilon & \langle \Phi_0 | H | \Phi_1 \rangle \\ \langle \Phi_1 | H | \Phi_0 \rangle & \langle \Phi_1 | H | \Phi_1 \rangle - \varepsilon \end{vmatrix} = 0. \tag{54}$$

This equation has two solutions which may be written

$$E_0^{\text{upper}} = \frac{1}{2}[E_0 + E_1] - \frac{1}{2}\left[(E_0 - E_1)^2 + 4|H_{01}|^2\right]^{\frac{1}{2}} \tag{55}$$

$$E_1^{\text{upper}} = \frac{1}{2}[E_0 + E_1] + \frac{1}{2}\left[(E_0 - E_1)^2 + 4|H_{01}|^2\right]^{\frac{1}{2}} \tag{56}$$

where the off-diagonal matrix element is $H_{01} = \langle \Phi_0 | H | \Phi_1 \rangle$. Using the Hylleras-Undheim-MacDonald theorem [29], we know that the solutions of the secular equations are upper bounds and, in particular,

$$E_1^{\text{upper}} \geqslant \mathscr{E}_1. \tag{57}$$

Furthermore, we note that

$$\left|E_0^{\text{upper}} - E_0\right| = \left|E_1^{\text{upper}} - E_1\right| \tag{58}$$

and so, if the ground state energy is determined to given accuracy then E_1 will have a comparable accuracy and the coupling matrix elements, H_{01}, may be neglected at this level of approximation.

3.2 Gradient of the Excited State Energy with Respect to Basis Set Parameters

There is, at present, no published analytical expression for the gradient of the energy of an excited state with respect to basis set parameters for excited states having the same symmetry as the ground state. The formalism developed in Sect. 2.1 allows us to derive a suitable expression. Indeed, the left-hand side of Eq. (14) represents the components of the gradient of the energy of the excited state $\partial_a E_1$ with respect to nonlinear basis set parameters ρ_a, i.e.

$$\partial_a E_1 = 2\langle \Phi_1 | (\partial_a P)(H + \lambda P_u) P | \Phi_1 \rangle \,, \tag{59}$$

In this equation, $P_u = |\Phi_0\rangle\langle\Phi_0|$. The factor of 2 arises from the complex conjugate which is equal to the real part.

Practical application of Eq. (59) requires knowledge of the limit

$$\lim_{\lambda \to \infty} \lambda \, \langle \Phi_0 | \Phi_1 \rangle \,. \tag{60}$$

This limit can be found from Eq. (13) which can be rewritten as

$$P(H - E_1)P | \Phi_1 \rangle = -\lambda | \Phi_0 \rangle \langle \Phi_0 | \Phi_1 \rangle. \tag{61}$$

Multiplying the left-hand side of Eq. (61) by $\langle \Phi_0 |$, we obtain a relation which is valid for any value of λ:

$$\lambda \langle \Phi_0 | \Phi_1 \rangle = -\langle \Phi_0 | P(H - E_1)P | \Phi_1 \rangle \,, \tag{62}$$

or

$$\lim_{\lambda \to \infty} \lambda \langle \Phi_0 | \Phi_1 \rangle = -\langle \Phi_0 | PHP | \Phi_1 \rangle \,. \tag{63}$$

Substituting Eq. (63) in Eq. (59), we arrive at the following expression

$$\partial_a E_1 = 2\langle \Phi_1 | (\partial_a P) H | \Phi_1 \rangle - 2\langle \Phi_1 | (\partial_a P) | \Phi_0 \rangle \langle \Phi_0 | PHP | \Phi_1 \rangle \,, \tag{64}$$

which is the gradient of the excited state energy with respect to non-linear basis set parameters.

It should be emphasised that when a common basis set is used in the description of both the ground state and the excited state with the corresponding projection operator P, then

$$\lim_{\lambda\to\infty} \lambda \langle \Phi_0 | \Phi_1 \rangle = 0, \tag{65}$$

because $PHP|\Phi_0\rangle = E_0|\Phi_0\rangle$ and

$$\lim_{\lambda\to\infty} \langle \Phi_0 | \Phi_1 \rangle = 0. \tag{66}$$

Furthermore, we can write

$$\langle \Phi_1 | (\partial_a P) | \Phi_0 \rangle = \langle \Phi_1 | P(\partial_a P) P | \Phi_0 \rangle = 0, \tag{67}$$

since $P(\partial_a P)P = 0$ because of the properties of the orthoprojectors. Thus, expression (59) for the gradient of the excited state energy with respect to nonlinear basis set parameters can be simplified and written as

$$\partial_a E_1 = 2\langle \Phi_1 | (\partial_a P) H | \Phi_1 \rangle . \tag{68}$$

This formulae is similar to that for the gradient of the ground state energy (see e.g. the paper by two of us [33])

For the purposes of practical calculations, the operators contained in Eqs. (64) and (68) can be expressed in terms of basis set functions ϕ_i if the derivatives of the projection operator are taken into account

$$\partial_a P = \sum_{k=0}^{n} [(I-P)|\partial_a \phi_k\rangle(\phi_k| + |\phi_k\rangle\langle\partial_a \phi_k|(I-P)] . \tag{69}$$

In this equation

$$|\phi_k) = \sum_{j=0}^{n} |\phi_j\rangle S^{-1}_{jk} \tag{70}$$

where S^{-1}_{jk} is an element of the inverse of the overlap matrix.

4 Illustrative Excited State Calculations of One-Electron Molecular Systems H_2^+ and H_3^{++}

The diatomic and triatomic molecular ions H_2^+ and H_3^{++} are the simplest molecular systems for which the exact numerical solutions of the Schrödinger's equation are known. For these systems numerical solutions are available to "machine accuracy" [34,35]. These numerical solutions provide excellent "benchmarks" for testing more approximate methods which have been developed for solving more complex problems.

For the H_2^+ ion, we studied both the ground state $1\sigma_g$ $(1s\,\sigma_g)$ and the first excited state of the same symmetry $2\sigma_g$ $(2s\,\sigma_g)$. The nuclear separation was set at 2.0 bohr.

For this geometry, the exact ground state electronic energy is $-0.602\,634\,214\,494\,9$ Hartree whereas the exact electronic energy of the $2\sigma_g\,(2s\,\sigma_g)$ excited state is $+0.139\,135\,124\,661\,7$ Hartree [34]. The difference between these two exact energies is $+0.741\,769\,339\,156\,6$ Hartree.

In the present study, we employed basis sets of *s*-type Gaussian functions centred on the internuclear axis with both exponents and positions determined by invoking the variational principle. Specifically, we used basis sets containing $2n+1$ functions distributed along the internuclear axis with $n = 3, 4, ..., 13$. For an odd number of basis function, symmetry considerations require that a single function is placed at the bond mid-point and the remaining functions are arranged in pairs symmetrically about this mid-point. We compared the energies supported by finite basis set expansions with the corresponding exact values. In particular, we carried out calculations using two schemes in the construction of basis sets: in the first, we used a common basis set for the different states, whilst in the second, different basis sets were employed for different states. We used basis sets consisting of $2 \times 13 + 1$ functions to compare the two approaches. In order to assess the effects of basis set truncation on the calculated energies and energy differences, we also used smaller basis sets, designated $2 \times 5 + 1$ and $2 \times 8 + 1$.

4.1 Common Basis Set for Different States

The parameters defining an optimized distributed basis set consisting of $(2 \times 13 + 1)$ *s*-type Gaussian functions for the ground state of the H_2^+ ion with a nuclear separation of 2.0 bohr can be found in Ref. [13]. The energies supported by this basis set for the $1\sigma_g\,(1s\,\sigma_g)$ and $2\sigma_g\,(2s\,\sigma_g)$ states of the hydrogen molecular ion are collected in Table 1. In this table, the column headed Δ displays the difference between

Table 1 Total energies (in Hartrees) for the H_2^+ molecular ion, with the nuclear separation of 2.0 bohr, calculated using the constrained variational method and a common basis set for different states

State	Basis set	E	Δ[a]
$2\sigma_g\,(2s\,\sigma_g)$	$(2\times13+1)$	$+0.151\,939\,303$	12804.178
	$(2\times8+1)$	$+0.157\,581\,881$	18446.756
$[+0.139\,135\,124\,661\,7]$	$(2\times5+1)$	$+0.199\,485\,926$	60350.801
$1\sigma_g\,(1s\,\sigma_g)$	$(2\times13+1)$	$-0.602\,633\,875$	0.339
	$(2\times8+1)$	$-0.602\,623\,992$	10.222
$[-0.602\,634\,214\,494\,9]$	$(2\times5+1)$	$-0.602\,512\,544$	121.670
$\Delta E_{1\sigma_g(1s\sigma_g),2\sigma_g(2s\sigma_g)}$	$(2\times13+1)$	$+0.754\,573\,178$	12803.839
	$(2\times8+1)$	$+0.760\,205\,873$	18436.534
$[+0.741\,769\,339\,156\,6]$	$(2\times5+1)$	$+0.801\,998\,470$	60229.131

[a] – Δ (in μ Hartrees) is the difference between the energy expectation value supported by the asymptotic projection method and the corresponding exact value.

the energy expectation value supported by the asymptotic projection method and the corresponding exact value.

For the constrained variational method with a common basis set for different states, the calculated ground and the excited state total energies become increasingly accurate with increasing size of basis set. Consequently, the accuracy of the calculated energy difference, ΔE also increases with the size of the basis set. However, the error in the calculated energy for the excited state is very much larger than that for the ground state. The error in the excited state energy is almost 500 times that in the ground state energy for the the $(2\times 5+1)$ basis set and roughly 4×10^4 times the corresponding energy for the $(2\times 13+1)$ basis set. This is not surprising since the basis sets are optimized for the ground state and therefore describe the ground state with increasing accuracy relative to the excited state as the basis set is extended. The error in the calculated total energy for the excited state dominates the error in the energy difference, ΔE.

4.2 Different Basis Sets for Different States

The parameters for the distributed basis set consisting of $(2\times 13+1)$ s-type Gaussian functions optimized for the excited state of the H_2^+ ion, with a nuclear separation of 2.0 bohr, can be found in Ref. [13]. Again, for basis sets containing an odd number of functions, there is one function centred on the bond mid-point with the remaining functions arranged symmetrically The pairs of exponents and z-coordinates are taken to be ordered according to their distance from the bond mid-point.

For calculations using the constrained variational method with different basis sets for different states, the orthogonality of the ground and excited state wavefunctions was imposed by solving the eigenproblem defined in Eq. (13) with

$$\lambda = 5\times 10^4 \text{a.u.} \tag{71}$$

This value of λ was determined so as to ensure that

$$\langle \Phi_0|\ \Phi_1\rangle = 0.000000000. \tag{72}$$

As we have already mentioned, the accuracy with which the orthogonality constraint is satistifed as a function of λ depends on specific features of the particular problem under consideration.

In the case of the hydrogen molecular ion, we show in Fig. 1 that the value λ $\sim$5–10 hartree ensures the overlap integral value $\langle \Phi_0|\Phi_1\rangle < 10^{-7}-10^{-8}$. As can be seen, the ground state-to-excited state transition occurs almost step-wise within the narrow range of $\lambda \sim 0.74-0.75$ hartree that corresponds to the excitation energy value (see ΔE from Table 1). In addition we observed that for a wide range $0.75 < \lambda < 10^4$, the value E_1 remains almost constant, indicating the stability of the solution achieved by the method.

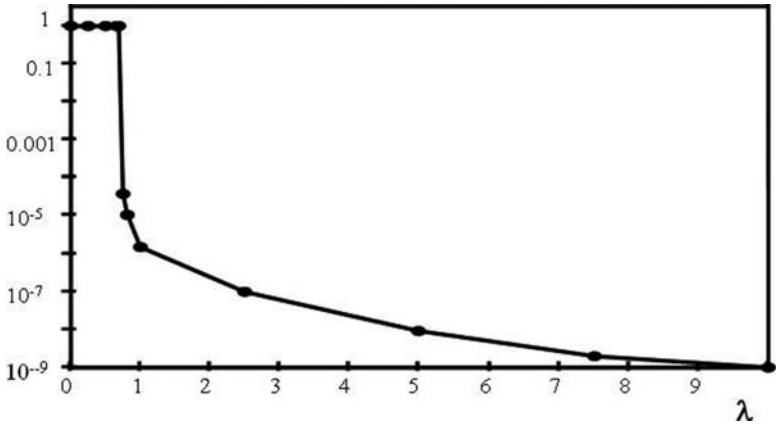

Fig. 1 The value of the overlap integral $\langle \Phi_0 | \Phi_1 \rangle$ as a function of the parameter λ for the ground state of the H_2^+ molecular ion with $R = 2.0$ bohr. Φ_0 and Φ_1 were calculated using a basis set optimized for the first excited state

Table 2 Total energies (in Hartrees) for the H_2^+ molecular ion, with the nuclear separation of 2.0 bohr, calculated using the constrained variational method and different basis sets for different states

State	Basis set	E	Δ[a]
$2\sigma_g\,(2s\,\sigma_g)$	$(2\times 13+1)$	$+0.139\,135\,657$	0.532
	$(2\times 8+1)$	$+0.139\,148\,302$	13.177
$[+0.139\,135\,124\,661\,7]$	$(2\times 5+1)$	$+0.139\,216\,795$	81.670
$1\sigma_g\,(1s\,\sigma_g)$	$(2\times 13+1)$	$-0.602\,633\,875$	0.339
	$(2\times 8+1)$	$-0.602\,623\,992$	10.222
$[-0.602\,634\,214\,494\,9]$	$(2\times 5+1)$	$-0.602\,512\,544$	121.670
$\Delta E_{1\sigma_g(1s\,\sigma_g),2\sigma_g(2s\,\sigma_g)}$	$(2\times 13+1)$	$+0.741\,769\,532$	0.193
	$(2\times 8+1)$	$+0.741\,772\,294$	2.955
$[+0.741\,769\,339\,156\,6]$	$(2\times 5+1)$	$+0.741\,729\,339$	-40.000

[a] – Δ (in μ Hartrees) is the difference between the value of the energy (or excitation energy) obtained with the asymptotic projection method and the corresponding exact value.

The energies supported by the $(2\times 5+1)$, $(2\times 6+1)$ and $(2\times 13+1)$ basis sets for the $1\sigma_g\,(1s\,\sigma_g)$ and $2\sigma_g\,(2s\,\sigma_g)$ states of the hydrogen molecular ion are collected in Table 2.

The accuracy of the excited state energies obtained by employing different basis sets for different states in the constrained variational method are much improved over those given in Table 1 for the common basis set case. For the $(2\times 5+1)$ basis set, the error in the calculated excited state energy displayed in Table 2 is 739 times smaller than the corresponding error in Table 1. This error is reduced by a factor of 24,000 for the $(2\times 13+1)$ basis set. This reduction in the error is not surprising because the basis sets are optimized for the respective states. The

Table 3 Electronic energies for the ground state, the first excited state and excitation energy (all in Hartrees) of linear H_3^{2+} for $R_{AB} = R_{BC} = 2$ bohr

Method	$E(GS)$	$E(ES)$	$E(ES) - E(GS)$
Presentwork	−1.524 159 62	−1.173 373 83	0.350 785 79
Exact	−1.524 159 90	−1.173 374 30	0.350 785 60
Δ[a]	0.28	0.47	0.19

[a] – Δ is the difference between the value of the energy obtained with the asymptotic projection method and the corresponding exact value.

constrained variational approach with different basis sets for different states yields the most accurate energies for a basis set of a given size. However, this approach also leads to the greatest computational demands. (Although these demands are small for the systems considered in the present work.) The calculated energy differences, ΔE, displayed in Table 2 using different basis sets for different states are also markedly improved over those given in Table 1. It should be noted that ΔE, is not an upper bound to its exact value as the results presented in Table 2 clearly demonstrate. The total energies and the energy differences converge with increasing size of basis set. In fact, the magnitude of ΔE decreases monotonically with the size of the basis set. For the excited state, the convergence pattern with increasing size of basis set size mirrors that observed for the ground state.

For our study of the linear H_3^{2+} molecular ion, the nuclei were positioned at $(0.0, 0.0, -2.0)$, $(0.0, 0.0, 0.0)$ and $(0.0, 0.0, +2.0)$ bohr. For this configuration, Hackel et al [35] reported a ground (1σ) state electronic energy of −1.524 159 9 hartree whilst for the first excited (2σ) state they determined an electronic energy of −1.173 374 3. These authors used the finite element method to perform their calculations. The present calculations were carried out by using an optimized basis set of *s*-type Gaussian functions constructed in a similar fashion to the sets employed for the H_2^+ ion. In Table 3, calculated electronic energies of the linear H_3^{2+} ion are displayed for the ground state and the excited state as well as the corresponding excitation energy. The energies presented in Table 3 were supported by the largest basis set employed in this study containing a total of 42s functions. This basis set is defined in Table 4.

The results presented above for the diatomic H_2^+ ion and the triatomic H_3^{++} ion demonstrate that the asymptotic projection method is capable of supporting an accuracy of $\sim$1 μHartree for excited state energies for one-electron systems when used in conjunction with optimized basis sets. Of course, the method described here can be applied to many-electron molecular systems where they can support a comparable accuracy.

Table 4 Optimal basis set parameters for the ground state (1σ) and excited state (2σ) of the linear H_3^{++} ion. The exponents, ζ_p, and positions, z_p, are variationally optimized for each state. The nuclei are located at the points (0, 0, -2), (0, 0, 0) and (0, 0, 2)[a]

1σ			2σ		
p	ζ_p	z_p	p	ζ_p	z_p
1,2	0.8418205(0)	±0.1910288(1)	1,2	0.7639302(0)	±0.1875791(1)
3,4	0.3476880(0)	±0.1650485(1)	3,4	0.3019611(0)	±0.1485761(1)
5,6	0.1517923(1)	±0.9561177(0)	5,6	0.1742844(1)	±0.4554557(0)
7,8	0.1339805(1)	±0.1838749(1)	7,8	0.8208070(0)	±0.1851638(1)
9,10	0.2381616(1)	±0.1917609(1)	9,10	0.1692262(1)	±0.1921101(1)
11,12	0.6478234(1)	±0.1975352(1)	11,12	0.4262420(1)	±0.1986405(1)
13,14	0.1627814(0)	±0.1641909(1)	13,14	0.1448846(0)	±0.1601241(1)
15,16	0.1929540(2)	±0.1995239(1)	15,16	0.1124180(2)	±0.1997629(1)
17,18	0.6749235(2)	±0.1997803(1)	17,18	0.3316262(2)	±0.1998046(1)
19,20	0.2959242(3)	±0.1999778(1)	19,20	0.4419684(3)	±0.1999778(1)
21,22	0.1973472(4)	±0.1999911(1)	21,22	0.2570299(4)	±0.1999911(1)
23,24	0.3684891(1)	±0.2103583(0)	23,24	0.1127609(3)	±0.1999975(1)
25,26	0.6332710(0)	±0.8738938(0)	25,26	0.5016808(1)	±0.5242137(−1)
27,28	0.2998761(1)	±0.2201661(1)	27,28	0.6567027(0)	±0.5547677(0)
29,30	0.7222268(0)	±0.3345823(1)	29,30	0.1944792(1)	±0.2210755(1)
31	0.4762336(4)	0	31,32	0.3748303(0)	±0.2355470(1)
32	0.7112966(3)	0	33,34	0.6357909(−1)	±0.1841511(1)
33	0.1618855(3)	0	35,36	0.2175831(2)	±0.1702267(−1)
34	0.4608506(2)	0	37,38	0.6985340(2)	±0.9988073(−2)
35	0.1508453(2)	0	39,40	0.4119900(1)	±0.1507338(0)
36	0.5479534(1)	0	41,42	0.2013408(5)	±0.2000000(1)
37	0.2022999(1)	0			
38	0.8570714(0)	0			
39	0.3584578(0)	0			
40	0.1779767(0)	0			
41	0.7531864(−1)	0			
42	0.3137232(−1)	0			

[a] Powers of ten are given in parentheses.

5 Concluding Remarks

We have described an alternative technique for solving a wide class of problems in quantum chemistry and in atomic and molecular physics, which can be reduced to an eigenvalue equation with some orthogonality constraints imposed on eigenvectors. This technique is based on an asymptotic projection method proposed, which was earlier and which can be simply implemented. The basic features of the asymptotic projection method have been presented and the method has been compared with conventional approaches to the constrained variational problem, namely, the elimination of off-diagonal Lagrangian multipliers method and the projection operators technique.

Some specific features of excited state calculations that implement the asymptotic projection method have been discussed. Unlike the major traditional methods where an improvement in accuracy is achieved by using extensive ways, for

instance, considerable extension of both atom-centered one-particle basis sets and increasing a number of many-particle configurations (sometimes up to several billions [36, 37]), we focused on the development alternative approaches capable of optimizing relatively small distributed basis sets.

Finally, it should be noted that the asymptotic projection method can also provide a suitable reference with respect to which a well-founded many-body expansion for correlation effects in open-shell states can be developed.

Acknowledgements V.N.G. thanks Prof. A. Theophilou for useful and stimulating discussions during the early stages of this work.

References

1. A.J. Sadlej, *Intern. J. Quantum. Chem.* **63**, 35 (1997).
2. X. Assfeld and J.-L. Rivail, *Chem. Phys. Lett.* **263**, 100 (1996).
3. P.R. Surjan, *Chem. Phys. Lett.* **325**, 120 (2000).
4. D.M. Himmelblau, *Applied Nonlinear Programming* McGraw-Hill, New York (1972).
5. P.E. Gill and W. Murray, *Numerical Methods of Constrained Optimization*, Academic Press, London, New York, San Francisco (1974).
6. V.N. Glushkov and A.Ya. Tsaune, *Zh. Vychisl. Mat. Mat. Fiz.* **25**, 298 (1985); *USSR Comp. Mathemat. Math. Phys.*, **25**, 196 (1986).
7. V.N. Glushkov, *J. Math. Chem.* **31**, 91 (2002).
8. V.N. Glushkov, *Opt. Spectrosc.* **93**, 11 (2002).
9. A.Ya. Tsaune, V.N. Glushkov and A.I. Aprashukhin, *J. Mol. Struct. (THEOCHEM)* **312**, 289 (1994).
10. V.N. Glushkov and A.Ya. Tsaune, *Chem. Phys. Lett.* **262**, 59 (1996).
11. V.N. Glushkov, *Chem. Phys. Lett.* **273**, 122 (1997).
12. V.N. Glushkov, *Chem. Phys. Lett.* **287**, 189 (1998).
13. N.I. Gidopoulos, V.N. Glushkov and S. Wilson, *Proc.R. Soc. Lond. A.* **457**, 1657 (2001).
14. V.N. Glushkov and S. Wilson, In: *Recent Advances in the Theory of Chemical and Physical Systems*, edited by J.-P. Julien et al., p.107, Springer, Dordrecht (2006).
15. V.N. Glushkov and A.Ya. Tsaune, *Opt. Spectrosc.* **87**, 267 (1999).
16. T. Kato, *Perturbation theory for linear operators*, Springer-Verlag, Berlin (1963).
17. H. Feshbach, *Ann. Phys. N.Y.* **19**, 287 (1962).
18. J.D. Weeks and S.A. Rice, *J. Chem. Phys.* **49**, 2741 (1968).
19. S. Huzinaga, *Method of molecular orbitals*, Tokyo, (1980), *Metod molekulyarnikh orbitaley* (in Russian), Mir, Moskva (1983) 461 p.
20. A.C. Hurley, *Introduction to the electron theory of small molecules*, p. 35, Academic Press, London, (1976).
21. S. Huzinaga and A.A. Cantu, *J. Chem. Phys.* **55**, 5543 (1971).
22. R. Colle, A. Fortunelli and O. Salvetti, *Theor. Chim. Acta* **71,** 467 (1987).
23. R. Colle, A. Fortunelli and O. Salvetti, *Theor. Chim. Acta* **75,** 323 (1989).
24. V.N. Glushkov, N.I. Gidopoulos and S. Wilson, *this volume*.
25. P. Dutta and S.P. Bhattacharya, *Chem. Phys. Lett.* **162,** 67 (1989).
26. G. Strang, *Linear algebra and its applications*, Academic Press, New York (1976).
27. P.-O. Löwdin, *Phys. Rev.* **139**, A357 (1965).
28. E.A. Hylleraas and B. Undheim, *Z. Phyzik* **65,** 759 (1930).
29. J.K.L. MacDonald, *Phys. Rev.* **43,** 830 (1933).
30. H. Shull and P.-O. Löwdin, *Phys. Rev.* **110**, 1466 (1958).

31. P. Corea De Mello, M. Hehenberger and M.C. Zerner, *Intern. J. Quant. Chem.* **21**, 251 (1982).
32. S. Wilson, *Intern. J. Quant. Chem.* **99**, 925 (2004).
33. V.N. Glushkov and S. Wilson, *Intern. J. Quant. Chem.* **99**, 903 (2004).
34. M.M. Madsen and J.M. Peek, *Atom Data* **2**, 171 (1971).
35. S. Hackel, D. Heinemann, D. Kolb and B. Fricke, *Chem. Phys. Lett.* **206**, 91 (1993).
36. A.O Mitrushenkov, *Chem. Phys. Lett.* **217**, 559 (1994).
37. A.O. Mitrushenkov and Y.Yu. Dmitriev, *Chem. Phys. Lett.* **235**, 410 (1995).

Alternative Technique for the Constrained Variational Problem Based on an Asymptotic Projection Method: II. Applications to Open-Shell Self-Consistent Field Theory

Vitaly N. Glushkov(✉), Nikitas I. Gidopoulos, and Stephen Wilson

Abstract The problem of the orthogonality of the closed- and open-shell orbitals in self-constistent field (SCF) theory are reviewed. An easily implemented asymptotic projection method for talking orthogonality constraints into account is used to develop an alternative open-shell SCF approach for ground and excited states. Variational derivation of the open-shell Hartree-Fock equations is described which does not involve off-diagonal Lagrangian multipliers. The possibilities of designing a well-defined, open-shell many-body perturbation theory using the orbitals of the asymptotic projection method is demonstrated by means of calculations of ground and excited state energies using the different levels of approximation. We also focus on the development of alternative computational strategies capable of optimizing relatively small distributed basis sets with respect to the positions and exponents of the basis functions.

Keywords: open-shell system, orthogonality constraints, self consistent field, excited state, many body perturbation theory

V.N. Glushkov
Department of Physics, National University, Dnepropetrovsk, 49050, per.Nauchny 13, Ukraine, e-mail: v_n_glushkov@yahoo.com

N.I. Gidopoulos
ISIS Facility, Rutherford Appleton Laboratory, Chilton, Didcot, Oxon, OX11 0QX, England, UK, e-mail: n.gidopoulos@rl.ac.uk

S. Wilson
Physical & Theoretical Chemistry Laboratory, University of Oxford, South Parks Road, Oxford OX1 3QZ, England;
Faculty of Mathematics, Physics and Informatics, Comenius University, 84215 Bratislava, Slovakia, e-mail: quantumsystems@gmail.com

S. Wilson et al. (eds.) *Frontiers in Quantum Systems in Chemistry and Physics*.

1 Introduction

Open-shell SCF theory is one of the most elegant techniques of contemporary quantum chemistry. Computational methods based on open-shell theory provide well-established tools which are applied routinely in modern molecular electronic structure studies (see, e.g. [1–14] and references therein). Today, open-shell methodology is available in many of the quantum chemical program packages, such as GAUSSIAN [23] and GAMESS [24], and is exploited in many practical applications.

In open-shell SCF theory, the optimal orbitals φ_i, $i = 1, 2, ..., N$ satisfy equations of the following form:

$$F_i|\varphi_i\rangle = \sum_j |\varphi_j\rangle\theta_{ji}$$

$$\theta_{ij} = \theta^*_{ji} \tag{1}$$

where the F_i are Fock operators and the θ_{ij} are Lagrangian multipliers, which arise from the orthogonality constraints

$$\langle\varphi_i|\varphi_j\rangle = \delta_{ij}.$$

The Fock operators are functionals of $\{\varphi_i\}$ and so the above equations are solved iteratively until self-consistency is attained. If a unitary transformation between the φ_i is possible without changing the total energy expectation, then some or all of conditions (1) can be fulfilled. This is a case, for example, in closed-shell SCF theory.

When describing open-shell systems, conventional approaches give rise to Hartree-Fock type equations which involve different Fock operators for the orbitals with the same spin. This results in off-diagonal Lagrange multipliers which couple the closed- and open-shells and which cannot be eliminated by a suitably chosen unitary transformation. Many studies have been devoted to the orthogonality problem for the closed- and open-shell orbitals [1–10]. In his seminal 1960 paper, Roothaan [1] proposed the elegant coupling operator formalism to overcome this difficulty. Considerable progress has been made in understanding the nature of the coupling operator method (see, e.g., [2–8], [11]) and useful computational experience has been accumulated in solving the restricted open-shell Hartree-Fock (ROHF) equations (see, e.g., [12–14]). Recent investigations have made it possible to find a canonical form of the open-shell Fock operator, which leads to useful relations between the open-shell orbital energies and the ionization potentials [17]. An excellent description of a history and evolution of the SCF theory for open-shell systems can be found in the review by Carbo and Riera [14] and references therein. At the present time, the coupling operator based methods, first proposed by Roothaan in 1960, form the basis of the most widely used computational procedure in studies of open-shell systems.

The choice of zero-order Hamiltonian is crucial to the success of perturbation approaches to the correlation problem and this choice is not as straightforward for open-shell systems as it is in the case of closed-shell species. A number of open-shell versions of many-body perturbation theory have been developed over

the years beginning with the work of Hubač and Čársky in 1980 [18], which was extended through fourth order by one of the present authors [19]. Much work on open-shell systems has concentrated on states of high spin. Of course, the description of arbitrary open-shell systems requires the use of a multireference perturbation expansion.

The Roothaan coupling operator formalism does not readily lend itself to a well-defined perturbation theory for describing the correlation effects in arbitrary open-shell systems [20–25]. In recent years, there has been renewed interest in the open-shell methods fuelled by the desire to define a cost-effective many-body perturbation theory based on restricted open-shell Hartree-Fock wave functions. For general open-shell systems, it can be difficult to devise a zero-order Hamiltonian $H^{(0)}$ for which the wave function has a simple form and is an eigenfunction of the total spin operator $\mathbf{S}^2$ [26]. Within the framework of the Roothaan coupling operator approach, there is no unique way of choosing a reference Hamiltonian, $H^{(0)}$, with respect to which a perturbation expansion for correlation effects can be developed. Several proposals have been made for open-shell many-body perturbation theory expansions (or open-shell Møller-Plesset-like perturbation theory (MPPT)) based on a reference from the ROHF formalism [22, 23] or the unrestricted Hartree-Fock (UHF) formalism [20, 21]. (It is well-known that the UHF formalism has a number of serious deficiencies, such as unphysical features in calculated potential energy curves.) These approaches to open-shell many-body perturbation theory differ primarily in the definition of the reference hamiltonian $H^{(0)}$. It is well established that the success or failure of a particular perturbation theory expansion is largely determined by the choice of the reference Hamiltonian, $H^{(0)}$. Ambiguities in the definition of the zero-order operator cannot be regarded as a desirable element of any perturbation theory.

In Sect. 2, we shall demonstrate that the method of asymptotic projection, which was reviewed in paper 1 [27], can be used to avoid ambiguities in the definition of zero-order operators for use in developing perturbation expansions for correlation effects. In previous work [28–38], the asymptotic projection method has been shown to be useful tool for solving quantum chemical problems which can be formulated in terms of an eigenvalue problem with orthogonality restrictions, i.e. the constrained variational problem reviewed in paper 1 [27].

Another aspect of SCF theory which deserves more detailed investigation is the study of electronically excited states, and especially excited states of the same spin and spatial symmetry as the ground or some lower-lying state. Indeed, Hartree-Fock calculations for electronically excited states cannot be considered routine. In particular, remembering that the ground and excited states are often of quite different character, it is desirable to use different basis sets for different states. *"The desirability of using different basis sets for different states"* was pointed out by Shull and Löwdin [39] as long ago as 1958. Such an approach provides a compact and accurate representation of excited state wave functions. Today, the most commonly used approaches to the study of excited states are based on multireference techniques, including configuration interaction, the multiconfigurational self-consistent field method and its "complete active space" variant designated CASSCF, multireference

perturbation theory and multireference coupled cluster expansions. These methods are indispensable in studies of systems for which single-configuration methods cannot be applied - for example, when the weight of the Hartree-Fock configuration in the wave function of the full configuration interaction expansion is less than $\sim$0.9 [40]. However, in cases where a multireference approach is necessary, *it is clear that the orbitals of a single-configuration, together with a basis set that has been specifically optimized for a given excited state, will prove more appropriate for the development of many-body correlation methods than orbitals expanded in a basis set constructed for the ground state.* Furthermore, progress in excited state SCF theory might be expected to aid the development of density functional theory for excited states.

In Sect. 3, we shall consider the use of the asymptotic projection method in excited state SCF calculations. The many-body Møller-Plesset-like perturbation theory based on optimal orbitals generated by the SCF-asymptotic projection method is the subject of Sect. 4. We shall demonstrate that, unlike existing open-shell perturbation theory formalisms, our alternative methodology can be easily extended to excited states and, thus, facilitate the computation of a large part of the correlation energy in a rather simple way. Our concluding remarks are given in Sect. 5.

2 Restricted Open-Shell Wave Functions and the Asymptotic Projection Method

In this section, we review an alternative to the Roothaan's open-shell method that does not involve off-diagonal Lagrange multipliers. We develop the asymptotic projection-SCF formalism to construct a single open-shell Slater determinant from which a well-defined, open-shell, many-body Møller-Plesset-like perturbation theory (MPPT) can be performed for both the ground and excited states.

2.1 Modified Open-Shell Hartree-Fock Equations for Ground States

2.1.1 Notation, Conventions and Restrictions

In this subsection, we shall consider systems for which the total SCF wave function can be written as a sum of several antisymmeterized products, each of which consists of a product of doubly occupied orbitals φ_k^c, the so-called core orbitals or closed-shell set, and singly occupied orbitals φ_m, the valence orbitals or open-shell set. To clarify our alternative technique, i.e. asymptotic projection, we shall restrict our attention to open-shell systems for which the expression for the energy expectation value can be partitioned as follows:

$$E = E^c + E^o + E^{co} \tag{2}$$

where the first term on the right-hand side is the closed-shell energy, the second term is the open-shell energy, and the last term arises from the interaction between the closed and open shells. This is a case considered in Roothaan's seminal article [1], for which the energy components have the form

$$E^c = 2\sum_k h_{kk} + \sum_{k,l}(2\langle\varphi_k|J_l|\varphi_k\rangle - \langle\varphi_k|K_l|\varphi_k\rangle)$$

$$E^o = f[2\sum_m h_{mm} + f\sum_{m,n}(2a\langle\varphi_m|J_n|\varphi_m\rangle - b\langle\varphi_m|K_n|\varphi_m\rangle)] \tag{3}$$

and

$$E^{co} = 2f\sum_{k,m}(2\langle\varphi_k|J_m|\varphi_k\rangle - \langle\varphi_k|K_m|\varphi_k\rangle).$$

In these expressions, *a, b,* and f are numerical constants depending on the particular state under consideration, $h_{kk} = \langle\varphi_k|h|\varphi_k\rangle$ where h is the one-electron operator describing the kinetic energy of an electron and its interactions with the nuclei, J_k and K_k are commonly called the Coulomb and exchange operators, which are defined as

$$\langle\varphi_i|J_j|\varphi_i\rangle = (\varphi_i\varphi_i|\varphi_j\varphi_j) = \int \varphi_i^*(1)\varphi_j^*(2)\frac{1}{r_{12}}\varphi_i(1)\varphi_j(2)dV_1dV_2$$

and

$$\langle\varphi_i|K_j|\varphi_i\rangle = (\varphi_i\varphi_j|\varphi_i\varphi_j) = \int \varphi_i^*(1)\varphi_i^*(2)\frac{1}{r_{12}}\varphi_j(1)\varphi_j(2)dV_1dV_2,$$

respectively. Following Roothaan [1], we reserve the indices *k, l* and *m, n* for the closed-shell and open-shall orbitals, respectively, and the indices *i, j* for orbitals of either set.

2.1.2 Orthogonality Constraints in the Restricted Open-Shell SCF Formalism

In the following discussion, we will be concerned with the orthogonality constraints which are to be imposed on the orbitals. Such constraints can be divided into two types. The first type of constraints are the orthogonality conditions within each of the orbital sets: $\{\varphi_k^c\}$, $\{\varphi_m\}$, i.e.

$$\langle\varphi_k^c|\varphi_l^c\rangle = \delta_{kl} \tag{4}$$

$$\langle\varphi_m|\varphi_n\rangle = \delta_{mn}. \tag{5}$$

These constraints are usually incorporated by introducing the Lagrange multipliers $\{\theta_{kl}^c\}$ and $\{\theta_{mn}^o\}$. The corresponding matrices can always be transformed to diagonal form by appropriate unitary transformations. The second type of constraints are the orthogonality conditions between the closed-shell and the and open-shell orbitals, i.e.

$$\langle\varphi_k^c|\varphi_m\rangle = 0. \tag{6}$$

It is from the condition (6) that the problem of off-diagonal Lagrange multipliers arises. In the present study, we shall use the asymptotic projection technique to handle these orthogonality constraints rather than the conventional coupling operator methods introduced by Roothaan. It is convenient when using the asymptotic projection method to rewrite Eq. (6) in two related symmetrical forms which are convenient for carrying out the variations; namely,

$$\sum_k \langle \varphi_k^c | P_o | \varphi_k^c \rangle = 0 \tag{7}$$

and

$$\sum_m \langle \varphi_m | P_c | \varphi_m \rangle = 0 \tag{8}$$

where

$$P_c = \sum_k |\varphi_k^c\rangle\langle\varphi_k^c| \tag{9}$$

and

$$P_o = \sum_m |\varphi_m\rangle\langle\varphi_m| \tag{10}$$

are the orthoprojectors on the subspaces spanned by the closed-shell and open-shell orbitals, respectively.

It should be noted that each term in the sum (7) [or (8)] is nonnegative, therefore, the requirement (7) [or (8)] is exactly equivalent to the orthogonality conditions (6). Thus, when implementing a variational principle, as we shall demonstrate in the next subsection, we may apply the constraint (7) [or (8)] instead of using (6).

2.1.3 Variational Derivation of the Open-Shell Hartree-Fock Equations

We start from the stationary condition for the total energy given in Eq. (2) subject to the constraints (4), (5) and (7).

Let us now define the functional

$$L = E - 2\sum_{k,l} \theta_{kl}^c \langle \varphi_k^c | \varphi_l^c \rangle - 2\sum_{m,n} \theta_{mn}^o \langle \varphi_m | \varphi_n \rangle + \lambda \sum_k \langle \varphi_k^c | P_o | \varphi_k^c \rangle \tag{11}$$

where $\theta_{mn}^c, \theta_{mn}^o$ and λ are Lagrange multipliers introduced to take account of the orthogonality constraints.

The stationary condition $\delta L = 0$ takes the form

$$\delta L = \delta\{E - 2\sum_{k,l} \theta_{kl}^c \langle \varphi_k^c | \varphi_l^c \rangle - 2\sum_{m,n} \theta_{mn}^o \langle \varphi_m | \varphi_n \rangle\} + \lambda\,\delta\{\sum_k \langle \varphi_k^c | P_o | \varphi_k^c \rangle\} = 0. \tag{12}$$

After some manipulation, the variations in the first bracket of Eq. (12) yield the standard result:

$$\sum_k \langle \delta\varphi_k^c | (F^c - \varepsilon_k^c) | \varphi_k^c \rangle + \sum_m \langle \delta\varphi_m | (F^o - \varepsilon_m^o) | \varphi_m \rangle + c.c. \tag{13}$$

where $c.c.$ denotes the complex conjugate and ε_k^c and ε_m^o are the diagonal elements of matrices θ_{kl}^c and θ_{mn}^o, respectively.

In Eq. (13) F^c and F^o are Fock operators (or Fockians), whose explicit form depends on the precise form of the energy expression of the state under consideration. For example, for the expression (2), we have [1]:

$$F^c = h + \sum_k (2J_k^c - K_k^c) + f \sum_m (2J_m - K_m)$$

$$F^o = h + \sum_k (2J_k^c - K_k^c) + f \sum_m (2aJ_m - bK_m)$$

where h is the one-electron operator describing the kinetic energy of an electron and its interaction with the nuclei. It can be shown [24] that the variations in the second bracket in Eq. (12) lead to the following expression

$$\delta\{\sum_k \langle\varphi_k^c|P_o|\varphi_k^c\rangle\} = \sum_k \langle\delta\varphi_k^c|P_o|\varphi_k^c\rangle + \sum_m \langle\delta\varphi_m|P_c|\varphi_m\rangle + c.c. \tag{14}$$

Combining Eqs. (13) and (14), the total variation in Eq. (12) can be written as follows:

$$\delta L = \sum_k \langle\delta\varphi_k^c|(F^c + \lambda P_o - \varepsilon_k^c)|\varphi_k^c\rangle + \sum_m \langle\delta\varphi_m|(F^o + \lambda P_c - \varepsilon_m^o)|\varphi_m\rangle + c.c. \tag{15}$$

In practice, the orbitals are approximated by means of some expansion in a finite one-particle basis set (the algebraic approximation is invoked), i.e.,

$$|\varphi_i\rangle = P|\varphi_i\rangle = \sum_{q=1}^{Q} C_{iq}|\chi_q\rangle$$

where P is an orthoprojector defined by a chosen basis set $\{\chi_q\}$. Using this expansion, the orbital variations can be written in the form

$$|\delta\varphi_i\rangle = P|\delta\varphi_i\rangle + \sum_a (\partial_a P)|\varphi_i\rangle\delta\mu_a, \tag{16}$$

where μ_a, a =1, 2,. . ., A, represents the basis set parameters (i.e. the exponents and the positions). The first term in Eq. (16) corresponds to variations within the finite-dimensional subspace spanned by the chosen basis set $\{\chi_q\}$, whereas the second term allows this subspace to be rotated within the Hilbert space of one-particle states to attain the deeper minimum with respect to the total energy.

Substituting Eq. (16) into Eq. (15) and taking into account the independence of the variations and their arbitrariness, we obtain the following equations:

$$P(F^c + \lambda P_o - \varepsilon_k^c)P|\varphi_k^c\rangle = 0 \tag{17}$$

and

$$P(F^o + \lambda P_c - \varepsilon_m^o)P|\varphi_m\rangle = 0. \tag{18}$$

According to the asymptotic projection methodology, the imposition of the condition $\lambda \to \infty$ in Eqs. (17) and (18) ensures the orthogonality between closed- and open-shell orbitals. The choice of λ, whose value determines the target accuracy for practical calculations, will be discussed below. Here it is worth noting that orbital energies will be shifted during the iterative solution of Eqs. (17) and (18). Therefore, after a solution has been obtained, these equations should be redefined as:

$$\varepsilon_k^c = \langle \varphi_k^c | F^c | \varphi_k^c \rangle \quad \text{and} \quad \varepsilon_m^o = \langle \varphi_m | F^o | \varphi_m \rangle.$$

The second term on the right-hand side of Eq. (16) leads to the equations for optimization of the basis set:

$$\sum_k \langle \varphi_k^c | (\partial_a P) F^c | \varphi_k^c \rangle + \sum_m \langle \varphi_m | (\partial_a P) F^o | \varphi_m \rangle = 0. \tag{19}$$

In Eq. (19) we took account of the fact that the term $\lambda P(\partial_a P)P$ vanishes for arbitrary λ. The left-hand side of Eq. (19) is the expression for the energy gradient with respect to the basis set parameters. This expression allows these parameters to be determined *variationally*.

2.1.4 Correct Variational Conditions and Orbitals Based on Asymptotic Projection

It is known that optimum set of orbitals must satisfy the correct variational conditions, which are equivalent to the generalized Brillouin's theorem [8]. There are two distinct types of variational conditions for optimal orbitals. The first type corresponds to the variational condition between virtual orbitals $\{\varphi_a\}$ and occupied $\{\varphi_i\}$ orbitals, i.e.

$$\langle \varphi_a | F^c | \varphi_k^c \rangle = 0 \tag{20}$$

and

$$\langle \varphi_a | F^o | \varphi_m \rangle = 0. \tag{21}$$

The second type of variational condition is that among occupied orbitals, i.e.

$$\langle \varphi_m | (F^c - F^o) | \varphi_k^c \rangle = 0 \tag{22}$$

From Eqs. (17) and (18) it is easy to show that the orbitals based on asymptotic projection obey these conditions. For example, multiplying Eq. (17) by $\langle \varphi_m |$ and Eq. (18) by $\langle \varphi_k^c |$ by taking into account the orthogonality of the limiting orbitals, we obtain

$$\langle \varphi_m | F^c | \varphi_k^c \rangle = -\lambda \langle \varphi_m | \varphi_k^c \rangle$$

and

$$\langle \varphi_k^c | F^o | \varphi_o \rangle = -\lambda \langle \varphi_k^c | \varphi_m \rangle.$$

Finally, by subtracting these equations and taking the Hermitian properties of operators F^c and F^o into account, we arrive at the second variational condition, Eq. (22). The relations (20) and (21) can be proved in a similar manner.

Thus, Eqs. (17) and (18) lead to an optimal set of orbitals. The energy expectation value supported by such orbitals is identical to that obtained by the Roothaan coupling operators formalism. However, when implemented in a finite basis set approach (the algebraic approximation), the coupling operator method deals with equations of fifth order with respect to the coefficients C_{iq} in the two operator formalism and seventh order in the unique coupling operator formalism because of the use of exchange coupling operators J_o and K_o (see Eq. (19) in Roothaan's paper [1]) whereas the self-consistent field equations in the asymptotic projection technique, Eqs. (17) and (18), are cubic equations.

2.2 *Unrestricted Hartree-Fock* (UHF) *Formalism for Obtaining High-Spin Restricted Open-Shell Hartree-Fock* (ROHF) *Functions*

It is well known that a large class of open-shell systems can be described by a single Slater determinant. The open-shell Slater determinant Φ is built from orbitals φ_k^α, $k = 1, 2, ..., n^\alpha$, associated with α spin and orbitals φ_k^β, $k = 1, 2, ..., n^\beta$, associated with β spin. In addition, $n^\alpha \geqslant n^\beta$ and $n = n^\alpha + n^\beta$ is the total number of electrons, and $S = S_z$. As we mentioned above, in the traditional open-shell method there is a degree of arbitrariness in the Fock operators that leads to different forms of perturbation expansion for the correlation energy. These ambiguities can be avoided by using the UHF formalism in which we allow the spatial part of the α spin orbitals to differ from that of the β spin orbitals. A spin purity constraint should be imposed on the spatial orbitals in order to eliminate spin contamination in the UHF function. This requirement is known [41] to be fulfilled if the occupied β orbitals are a linear combination of occupied α orbitals, i.e. the β set lies completely within the subspace defined by the α set. Below we shall see that this requirement leads to a restricted open-shell Hartree-Fock Slater determinant.

Now we have

$$P^\alpha P^\beta = P^\beta P^\alpha = P^\beta$$

with

$$P^\alpha = \sum_k^{n^\alpha} |\varphi_k^\alpha\rangle\langle\varphi_k^\alpha| \quad \textit{and} \quad P^\beta = \sum_k^{n^\beta} |\varphi_k^\beta\rangle\langle\varphi_k^\beta|.$$

This allows us to rewrite the spin-purity requirement as the orthogonality constraint

$$\sum_k^{n^\beta} \langle\varphi_k^\beta|Q^\alpha|\varphi_k^\beta\rangle = 0$$

where $Q^\alpha = I - P^\alpha$ is the orthoprojector on the subspace of the virtual α spin orbitals.

Following the asymptotic projection methodology, the Euler equations for orbitals can be then derived from the stationary condition

$$\delta L = \delta[E^{UHF} + \lambda \sum_{k}^{n^\beta} \langle \varphi_k^\beta | Q^\alpha | \varphi_k^\beta \rangle] = 0. \tag{23}$$

Similarly using Eq. (16), variations of the orbitals can be divided into independent parts. For example, for the α orbitals we have

$$|\delta\varphi_i^\alpha\rangle = P^\alpha|\delta\varphi_i^\alpha\rangle + (I - P^\alpha)|\delta\varphi_i^\alpha\rangle + \sum_a (\partial_a P)|\varphi_i^\alpha\rangle \delta\mu_a. \tag{24}$$

Energetically significant variations are described by the second and third terms in Eq. (24) because the first term does not lead to any change in the total energy since it is invariant to any orthogonal transformation of the orbitals associated with a given spin among themselves.

Substituting Eq. (24) into Eq. (23), after some manipulation, we arrive at the following set of equations, which determine the optimal orbitals (see Glushkov [24, 33] for more details):

$$\lim_{\lambda\to\infty} P(F^\alpha - \lambda P^\beta - \varepsilon_i^\alpha)P|\varphi_i^\alpha\rangle = 0, \quad i = 1,2,...,n^\alpha,...,M \tag{25}$$

$$\lim_{\lambda\to\infty} P(F^\beta + \lambda Q^\alpha - \varepsilon_i^\beta)P|\varphi_i^\beta\rangle = 0, \quad i = 1,2,...,n^\beta,...,M \tag{26}$$

and equations for basis set optimization

$$\sum_{k}^{n^\alpha} \langle \varphi_k^\alpha | (\partial_a P) F^\alpha | \varphi_k^\alpha \rangle + \sum_{k}^{n^\beta} \langle \varphi_k^\beta | (\partial_a P) F^\beta | \varphi_k^\beta \rangle = 0. \tag{27}$$

In Eqs. (25–27) F^α and F^β are the conventional UHF operators. It should be stressed that each of the additional term in (25) and (26) ensures spin purity, i.e.

$$\widehat{\mathbf{S}}_z|\Phi\rangle = S|\Phi\rangle, \quad \widehat{\mathbf{S}}^2|\Phi\rangle = S(S+1)|\Phi\rangle$$

but only both of the terms λP^β and λQ^α in combination with the limit $\lambda \to \infty$ lead to an optimum set of orbitals satisfying the generalized Brillouin's theorem (see next section for further discussion). Note, that together both additional terms also lead to spatial parts of the α set which are *identical* to those of the β set, but the corresponding orbital energies are different. The Slater determinant built from these orbitals gives a minimum of the total energy expectation value which is equivalent to that obtained by the Roothaan coupling operator method.

In concluding this section, we note that the Eq. (27) is the natural generalization of the equations for the optimization of the basis set for closed-shell systems. Indeed, Eq. (27) reduces to that for the optimization of the basis set for closed systems in the case $n^\alpha = n^\beta$ (see, [42–44]).

$$\partial_a E = 2\sum_i \langle \varphi_i | (\partial_a P) F | \varphi_i \rangle = 0 \tag{28}$$

2.2.1 Generalized Brillouin's Theorem in Terms of Unrestricted Hartree-Fock Orbitals Based on Asymptotic Projection

Below we shall show that the orbitals generated by Eqs. (25) and (26) in the limit $\lambda \to \infty$ satisfy the correct variational conditions i.e. the generalized Brillouin's theorem.

Without loss of generality, the full orbital space may be divided into a closed-shell part (c), an open-shell part (o) and a virtual part (v). According to the generalized Brillouin's theorem, we have [7, 8]

$$\langle \Phi | H | \Phi(i \to j) \rangle = 0 \tag{29}$$

$\Phi(i \to j)\rangle$ are configurations which are singly excited with respect to Φ. There are three types of well-defined singly excited configurations with the same multiplicity as Φ [7, 8], *viz.*:

$$\Phi(c \to o) = \det|c\alpha o\beta o\alpha|,$$

$$\Phi(o \to v) = \det|c\alpha c\beta v\alpha|,$$

$$\Phi(c \to v) = N(\det|c\alpha v\beta o\alpha| + \det|v\alpha c\beta o\alpha|),$$

in addition

$$\Phi = \det|c\alpha c\beta o\alpha|.$$

For the sake of simplicity, we denote only the spin-orbitals which take part in excitations in the determinants. N is a normalization multiplier. The indices c, o and v mean closed-shell (doubly occupied), open-shell (singly occupied) and the virtual parts of the full orbital space, respectively. In terms of the unrestricted Hartree-Fock operators F^α and F^β, Brillouin's theorem can be written:

$$\langle \Phi | H | \Phi(c \to o) \rangle = \langle \varphi_i^\beta | F^\beta | \varphi_m^\beta \rangle = 0, \quad (m \in o, i \in c) \tag{30}$$

$$\langle \Phi | H | \Phi(o \to v) \rangle = \langle \varphi_m^\alpha | F^\alpha | \varphi_a^\alpha \rangle = 0, \quad (m \in o, a \in v) \tag{31}$$

$$\langle \Phi | H | \Phi(c \to v) \rangle = \langle \varphi_a^\alpha | F^\alpha | \varphi_i^\alpha \rangle + \langle \varphi_a^\beta | F^\beta | \varphi_i^\beta \rangle = 0, \quad (i \in c, a \in v). \tag{32}$$

Brillouin's theorem is obeyed for the set of orbitals satisfying Eqs. (25) and (26) in the limit $\lambda \to \infty$ as well as the 'traditional' orbitals obtained by the Roothaan approach. Indeed, multiplying Eq. (25) by $\langle \varphi_a^\alpha |$ and Eq. (26) by $\langle \varphi_a^\beta |$, we obtain

$$\langle \varphi_a^\alpha | F^\alpha | \varphi_i^\alpha \rangle = \lambda \langle \varphi_a^\alpha | \varphi_i^\beta \rangle, \quad \textit{and} \quad \langle \varphi_a^\beta | F^\beta | \varphi_i^\beta \rangle = -\lambda \langle \varphi_a^\alpha | \varphi_i^\beta \rangle. \tag{33}$$

A constraint vector has been shown to tend to an eigenvector of the modified operator as $1/\alpha$ (see Part I of this work [27]). Therefore, the limit $\lambda \langle \varphi_a^\alpha | \varphi_i^\beta \rangle$, $\lambda \to \infty$, exists and from Eq. (33) we can confirm that the condition (32) is satisfied. In the same manner, we can show that conditions (30) and (31) are also satisfied for the orbitals in the limit $\lambda \to \infty$.

Thus, the unrestricted Hartree-Fock orbitals based on asymptotic projection lead to wave function and energy expressions which are equivalent to those obtained by the Roothaan method. However, the asymptotic projection approach has some advantages:

- The method avoids introducing the off-diagonal Lagrange multipliers coupling the closed-shell and open-shell orbitals and, therefore, arbitrariness in the definition of the Fock operators does not arise. Equations (25) and (26) are cubic equations with respect to orbital expansion coefficients (lcao) and can be easily implemented in established unrestricted Hartree-Fock codes. The 'traditional' open-shell Roothaan-based methods give rise to equations of fifth and seventh degree with respect to these coefficients.
- The scheme defined in Eqs. (25) and (26) provides a well-defined zero-order approximation for open-shell many-body perturbation theory that ensures that single excitations do not contribute to the second-order energy. This should be contrasted with the method of Knowles et al. [21], the restricted Møller-Plesset approach, and the method of Amos et al. [20], here designated AAHK, which employ different orbitals for different spins and for which the generalized Brillouin's theorem is not satisfied and consequently single replacement contributions enter the second-order energy expression.

The structure of the Fock matrices occurring in the asymptotic projection–self-consistent field method is displayed in Fig. 1. The structure of the Fock matrices arising in the RMP and the AAHK methods is shown in Figs. 2 and 3, respectively.

The asymptotic projection–self-consistent field equations are similar to those reported for the RMP and AAHK methods. However, it should be emphasized that Eqs. (25) and (26) give rise to spatial parts of the α set which are identical to those of β set. In contrast, for the RMP and AAHK methods the α orbitals are not coincident with the β orbitals [21] since these orbitals are rotated with respect to the orbitals given by the Roothaan procedure and Brillouin's theorem is not obeyed. The differences between the methods is evident when we compare the Fock matrices F^{α} and F^{β}. It can be seen in Fig. (1) that $s+v$ block of the asymptotic projection–self-consistent field F^{α} matrix has diagonal form and, therefore, the condition (31) is satisfied. Furthermore, the diagonal form of $d+s$ block of the F^{β} matrix confirms that condition (30) is also satisfied. However, it is clear by inspection of Figs. (2) and (3) for the RMP and AAHK approaches that these do not satisfy Brillouin's theorem.

2.2.2 Matrix Hartree-Fock Energies for Ground States

In this subsection, some features of the alternative self-consistent field procedure based on the asymptotic projection technique are demonstrated by means of Hartree-Fock calculations of the ground state energies for the HeH and BeH molecules. The Hartree-Fock ground state for the three-electron HeH molecule with electronic configuration $1\sigma^2 2\sigma$ is unbound. In this study, we used a He−H distance of 1.500 bohr,

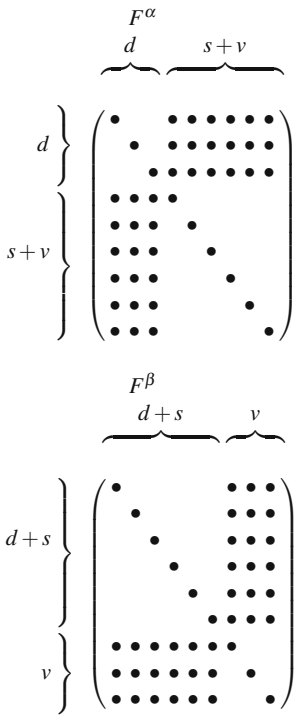

Fig. 1 Structure of the Fock matrices in the asymptotic projection method. d denotes the doubly occupied component of the orbital space, s denotes the singly occupied component and v the virtual (or unoccupied) part. • denotes a non-zero element of the matrix

which corresponds to the minimum in the potential energy curve for the first excited Σ state. To assess the potential of the approach based on asymptotic projection, we compare the matrix Hartree-Fock energies with the finite difference ROHF energy obtained on a grid designated [217×349; 65] (J. Kobus, 2004, personal communication): $E_{\mathrm{fdHF}} = -3.220\,315\,124\,616$ hartree which provides an exact Hartree-Fock result to near-machine accuracy.

The ground state of the five-electron BeH molecule with the electronic configuration $1\sigma^2 2\sigma^2 3\sigma$ was studied for a nuclear separation of 2.500 bohr. The finite difference ROHF energy of this molecule at this geometry is $E_{\mathrm{fdHF}} = -15.153\,182\,339\,96$ hartree (J. Kobus, 2004, personal communication).

Self-consistent field energy calculations were carried out using a single reference wave function. For all calculations, basis sets of s-type Gaussian functions were used with exponents and positions determined by minimizing the Hartree-Fock energy. Equation (27) were used to construct numerical procedures for basis set optimizations. It has been found recently that such basis sets are capable of supporting an accuracy at the sub-μhartree level for simple molecules [42, 44]. The expectation value of the energy given by the alternative SCF method depends on a parameter λ, where $\lambda = 0$ corresponds to the UHF energy and tends asymptotically to the ROHF energy given by Roothaan's method as $\lambda \to \infty$. Table 1 presents the calculated energies for HeH as a function of λ together with the expectation value $\langle S^2 \rangle$ for the case of 14s basis functions. We can see that setting $\lambda = 100000$ yields practically

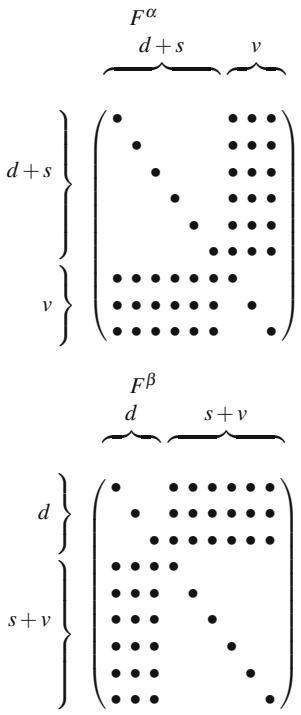

Fig. 2 Structure of the Fock matrices in the restricted Møller-Plesset method. d denotes the doubly occupied component of the orbital space, s denotes the singly occupied component and v the virtual (or unoccupied) part. • denotes a non-zero element of the matrix

the energy obtained by Roothaan's method ($E_{\text{Roothaan}} = -3.219\ 198\ 91$ hartree). For $\lambda \sim 5{,}000-10{,}000$, we achieve a sub-$\mu$hartree level of agreement between our method and the Roothaan method. The expectation value $\langle S^2 \rangle$ is given to our target accuracy for values $\lambda > \sim 100-500$. In Table 2, we record the total restricted open-shell matrix Hartree-Fock energies for Gaussian s-type basis sets of increasing size. In this table, N denotes the *total* number of basis functions in a given basis set. Δ is the difference, in μhartree, between successive entries in Table 2. Δ_n is the value of Δ divided by the number of basis functions added between successive rows of Table 2. δ is the difference, again in μhartree, between the matrix Hartree-Fock energy supported by a given basis set and corresponding value obtained by the finite difference method. It can be seen that the largest basis set considered in Table 2, which contains 48 s-type Gaussian functions, supports an accuracy at the sub-μhartree level. The energy reported for this basis set corresponds to $\lambda = 6{,}000$.

Table 3 illustrates the dependence of the open-shell matrix Hartree-Fock energy and $\langle S^2 \rangle$ for the BeH molecule on the parameter λ. The basis set of 30 s-type Gaussian functions was used in this case. Values of λ in the range $\sim 5{,}000-10{,}000$ provided the required accuracy in the energy when compared with the traditional Roothaan method. We can see that the study of the BeH molecule is similar to that of HeH molecule, in particular, it can be seen that when λ increases the expectation value of the square of the spin operator $\langle S^2 \rangle$ decreases much more rapidly than the total energy increases. The total restricted open-shell Hartree-Fock energies are

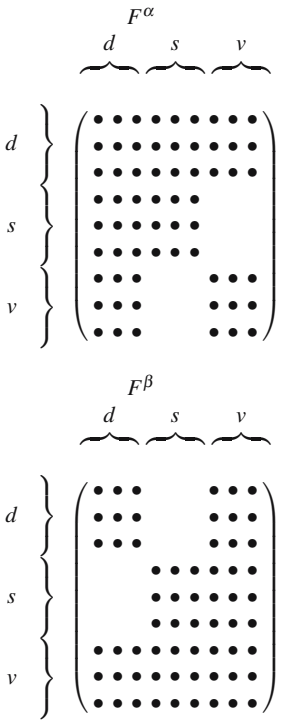

Fig. 3 Structure of the Fock matrices in the method of Amos, Andrews, Handy and Knowles (AAHK). *d* denotes the doubly occupied component of the orbital space, *s* denotes the singly occupied component and *v* the virtual (or unoccupied) part. • denotes a non-zero element of the matrix

Table 1 Dependence of the open-shell matrix Hartree-Fock energy based on asymptotic projection on the parameter λ for the ground state of the HeH molecule at $R = 1.5$ bohr with the basis set of 14*s* functions. Atomic units are used

λ [a]	$\langle S^2 \rangle$	*Energy*
0	0.750 428 93	−3.219 765 61
50	0.750 000 31	−3.219 308 32
100	0.750 000 08	−3.219 215 27
500	0.750 000 00	−3.219 202 25
5,000	0.750 000 00	−3.219 199 24
10,000	0.750 000 00	−3.219 199 07
100,000	0.750 000 00	−3.219 198 92

[a] The value $\lambda = 0$ corresponds to the unrestricted Hartree-Fock energy, whereas $\lambda = 100{,}000$ yields practically the energy obtained by the Roothaan method ($E_{Roothaan} = -3.219\ 198\ 91$ hartree).

given in Table 4 for basis sets of increasing size. The largest basis set considered in this table contains 62 functions and supports an accuracy at the sub-μhartree level. A total energy of −15.153 181 43 hartree was obtained with $\lambda = 10{,}000$ a.u. which lies 0.91 μhartree above the finite difference Hartree-Fock energy.

In concluding this section, we point out that optimal basis set parameters for the largest basis sets for the HeH and BeH molecules can be found in Ref. [44].

Table 2 Convergence of the open-shell matrix Hartree-Fock-asymptotic projection energy for the ground state of the HeH molecule, at $R = 1.5$ bohr, as a function of the basis set size. Atomic units are used

N	*Energy*[a]	Δ	Δ_n	δ
14	−3.219 199 07	–	–	1116.05
24	−3.219 201 72	1002.65	100.27	113.40
30	−3.219 294 93	93.214	15.54	20.19
43	−3.219 313 19	18.26	1.40	1.93
48	−3.219 314 34	1.15	0.23	0.78

[a] The value $\lambda = 10{,}000$ was used. The energy differences, Δ, Δ_n and δ, which are defined in the text, are given in μhartree.

Table 3 Dependence of the open-shell matrix Hartree-Fock-asymptotic projection energy on the parameter λ for the ground state of the BeH molecule at $R = 2.5$ bohr with the basis set of 30 s-type Gaussian functions. Atomic units are used

λ[a]	$\langle S^2 \rangle$	*Energy*
0	0.751 788 28	−15.153 428 93
100	0.750 000 12	−15.153 091 16
1,000	0.750 000 00	−15.153 089 13
5,000	0.750 000 00	−15.153 089 13
6,000	0.750 000 00	−15.153 088 92
10,000	0.750 000 00	−15.153 088 90

[a] Values of $\lambda =$ in the range $\sim$5,000−10,000 provide the required accuracy when compared with the traditional Roothaan method.

Table 4 Convergence of the open-shell matrix Hartree-Fock-asymptotic projection energy for the ground state of the BeH molecule at $R = 2.5$ bohr, as a function of the basis set size. Atomic units are used

N	*Energy*[a]	Δ	Δ_n	δ
24	−15.152 457 00	–	–	725.34
30	−15.153 088 92	631.92	105.35	93.42
36	−15.153 140 32	51.40	8.57	42.02
43	−15.153 164 08	23.76	3.39	18.26
60	−15.153 179 41	15.33	0.90	2.93
62	−15.153 181 43	2.02	0.01	0.91

[a] The value $\lambda = 10{,}000$ was used. The energy differences, Δ, Δ_n and δ, which are defined in the text, are given in μhartree.

3 Excited State SCF Theory Based on the Asymptotic Projection Method

3.1 Specific Features of Excited State SCF Calculations

Existing open-shell self-consistent field methods for ground states cannot be applied directly to excited states of the same symmetry as a lower state without ‘variational

collapse'; that is, the approximation to the excited state wave function is contaminated by components of a lower state. Several useful methods have been proposed to overcome the 'variational collapse' problem and a number of different schemes have been proposed for obtaining Hartree-Fock wave functions for excited states [45–50], [34, 36]. Some of these approaches [45–47], [34, 36, 50] explicitly introduce orthogonality constraints to lower states. Other methods [48], [49] introduce this restriction implicitly. In both types of scheme, the excited state self-consistent field wave function of interest is orthogonal to the wave function for a lower state or states of the same symmetry, but this lower state or states are not necessarily the best self-consistent field functions for these states [50]. An interesting ensemble Hartree-Fock approach [51] based on the extended Raleigh-Ritz variational principle [52] have been also proposed. This is a good compromise in applications to the excited state problem within the framework of density functional theory and has found application in wave function based formulation as well [35]. In particular, calculations for *atoms* have showed that the ensemble Kohn-Sham theory, with the exact ensemble-exchange potential, can be as accurate as the ground state calculations [53, 54]. However, partly due to the lack so far of an accurate correlation energy functional, there exist very few reported applications for *molecules*, where a finite basis set choice is important to achieve reasonable results. Some preliminary calculations concerning the choice of an optimal basis set for an ensemble of states can be found in the work of Glushkov and Theophilou [55, 56].

3.2 Orthogonality Constraints for Single Determinantal Wave Functions

Before deriving the Hartree-Fock equations for the excited state orbitals, we shall consider the orthogonality constraints imposed on these orbitals.

The *exact* many-electron wave function for an excited state, Ψ_i, $i \neq 0$, satisfies orthogonality conditions with respect to other many-electron states including the ground state, Ψ_0. For example, for the first excited state with many-electron wave function Ψ_1 we have

$$\langle \Psi_0 | \Psi_1 \rangle = 0. \tag{34}$$

The exact ground state wave function, Ψ_0, can be written

$$\Psi_0 = \Phi_0 + \chi_0 \tag{35}$$

where Φ_0 is the many-electron ground state Hartree-Fock wave function and χ_0 is the correlation correction. Without loss of generality, we can require

$$\langle \Phi_0 | \chi_0 \rangle = 0. \tag{36}$$

Similarly, the exact excited state wave function, Ψ_1, can be written

$$\Psi_1 = \Phi_1 + \chi_1 \tag{37}$$

where Φ_1 is the many-electron excited state Hartree-Fock wave function and χ_1 is the corresponding correlation correction. Again, without loss of generality, we can require

$$\langle \Phi_1 | \chi_1 \rangle = 0. \tag{38}$$

Substituting Eq. (37) into Eq. (34) we get

$$\begin{aligned} \langle \Psi_0 | \Psi_1 \rangle &= \langle \Psi_0 | \Phi_1 \rangle + \langle \Psi_0 | \chi_1 \rangle \\ &= 0. \end{aligned} \tag{39}$$

If we require that

$$\langle \Psi_0 | \Phi_1 \rangle = 0 \tag{40}$$

which implies that

$$\langle \Psi_0 | \chi_1 \rangle = 0 \tag{41}$$

then it is easily shown that

$$\frac{\langle \Phi_1 | H | \Phi_1 \rangle}{\langle \Phi_1 | \Phi_1 \rangle} \geqslant \mathscr{E}_1, \tag{42}$$

where $\mathscr{E}_1$ is the exact energy of the excited state and H is the total electronic hamiltonian operator. However, Eqs. (40) and (41) cannot be used directly because the exact wave function for the ground state, Ψ_0, is unknown.

Substituting Eqs. (35) and (37) into Eq. (34) we have

$$\begin{aligned} \langle \Psi_0 | \Psi_1 \rangle &= \langle \Phi_0 | \Phi_1 \rangle + \langle \Phi_0 | \chi_1 \rangle + \langle \chi_0 | \Phi_1 \rangle + \langle \chi_0 | \chi_1 \rangle \\ &= 0 \end{aligned} \tag{43}$$

or

$$\langle \Phi_0 | \Phi_1 \rangle = - \left[\langle \Phi_0 | \chi_1 \rangle + \langle \chi_0 | \Phi_1 \rangle + \langle \chi_0 | \chi_1 \rangle \right]. \tag{44}$$

We see that the Hartree-Fock wave functions, do not, in general, satisfy orthogonality constraints analogous to those obeyed by the exact wave functions. However, we may impose constraints upon the Hartree-Fock function so that, for example,

$$\langle \Phi_0 | \Phi_1 \rangle = 0. \tag{45}$$

From (44) we see that this constraint requires that

$$\langle \Phi_0 | \chi_1 \rangle + \langle \chi_0 | \Phi_1 \rangle = - \langle \chi_0 | \chi_1 \rangle .$$

The imposition of the constraint (45) on an approximate lower state wave function, such as the Hartree-Fock function, does not, in general, yield an excited state energy which is an upper bound to the exact excited state energy. An upper bound to the excited state energy is obtained if we impose the additional constraint

$$\langle \Phi_0 | H | \Phi_1 \rangle = 0.$$

In practice, if the lower state energy and the corresponding wave function are known accurately then the coupling matrix element $\langle \Phi_0 | H | \Phi_1 \rangle$ is small (see Part I of this

work for more detailed discussion [27]). Experience shows that, because the finite basis set approximation is usually more restrictive for Φ_1 than it is for Φ_0, the calculated excited state energy lies above the corresponding exact value.

The imposition of the constraint (45) is important since

(i) any lack of orthogonality of the Hartree-Fock wave functions may lead to excited state energies lying below the corresponding exact energies. (For example, Cohen and Kelly [57] found for the He atom the first singlet excited state energy $E_1 = -2.16984$ hartree, whereas the observed energy $E_{1,exact} = -2.14598$ hartree. (see also the work of Tatewaki et al. [58]).);
(ii) it facilitates the development of a simple perturbation theory expansion for correlation effects in excited states [37];
(iii) it facilitates the study of properties which depend on the wave functions of different states, for example the evaluation of transition properties (see also the work of Colle et al. [50]).

We shall be concerned with ground and excited electronic states which can be adequately described by a single determinantal wave function, i.e. doublet states, triplet states, etc. with spin $S \neq 0$).

Let Φ_0 be the ground state Slater determinant constructed from a set of spin-orbitals consisting of spatial part $\left|\varphi_{0i}^{\alpha}\right\rangle$, $(i^{\alpha} = 1, 2, ..., n^{\alpha})$ associated with α spin functions and orbitals $\left|\varphi_{0i}^{\beta}\right\rangle$, $(i^{\beta} = 1, 2, ..., n^{\beta})$ associated with β spin functions, i.e.

$$\Phi_0 = (N!)^{-\frac{1}{2}} \det\left|\varphi_{01}^{\alpha}\alpha, ..., \varphi_{0n}^{\alpha}\alpha; \varphi_{01}^{\beta}\beta, ..., \varphi_{0n}^{\beta}\beta\right|. \tag{46}$$

Without loss of generality, we define $n^{\alpha} > n^{\beta}$, $n^{\alpha} + n^{\beta} = N$, where N is a number of electrons and $S = S_z = (n^{\alpha} - n^{\beta})/2$ is the total spin. Similarly, Φ_1 is a single determinant wave function for the first excited state:

$$\Phi_1 = (N!)^{-\frac{1}{2}} \det\left|\varphi_{11}^{\alpha}\alpha, ..., \varphi_{1n}^{\alpha}\alpha; \varphi_{11}^{\beta}\beta, ..., \varphi_{1n}^{\beta}\beta\right|. \tag{47}$$

It is well known that the orthogonality constraint for functions (46) and (47)

$$\langle\Phi_0|\Phi_1\rangle = 0 \tag{48}$$

can be written in terms of the spatial orbitals in the form

$$\begin{aligned}\langle\Phi_0|\Phi_1\rangle &= \det|\langle\varphi_{01}^{\alpha}|\varphi_{11}^{\alpha}\rangle ... \langle\varphi_{0n}^{\alpha}|\varphi_{1n}^{\alpha}\rangle| \times \\ &\quad \det\left|\left\langle\varphi_{01}^{\beta}|\varphi_{1n}^{\alpha}\right\rangle ... \left\langle\varphi_{0n}^{\beta}|\varphi_{1n}^{\beta}\right\rangle\right| \\ &= 0.\end{aligned} \tag{49}$$

The annihilation of either one of the two determinants in (49) leads to fulfillment of the orthogonality condition (48). From energy considerations and previous computational experience, we impose the orthogonality restrictions only via the first

determinant which is associated with the α set and involves the occupied orbital highest in energy.

As is well known, the condition

$$\det|\langle\varphi_{01}^{\alpha}|\varphi_{11}^{\alpha}\rangle\ldots\langle\varphi_{0n}^{\alpha}|\varphi_{1n}^{\alpha}\rangle|=0$$

is fulfilled if either the rows or columns in the first overlap determinant are linearly dependent. Therefore, two *physically* different schemes are possible to satisfy (49): either

$$\sum_{j}^{n^{\alpha}} b_j^1\left\langle\varphi_{0i}^{\alpha}|\varphi_{1j}^{\alpha}\right\rangle=0,\quad i=1,2,\ldots,n^{\alpha} \tag{50}$$

or

$$\sum_{i}^{n^{\alpha}} b_i^0\left\langle\varphi_{0i}^{\alpha}|\varphi_{1j}^{\alpha}\right\rangle=0,\quad j=1,2,\ldots,n^{\alpha}. \tag{51}$$

Equation (50) requires that all occupied ground state orbitals be orthogonal to a linear combination of the excited state orbitals $\sum_j^{n^{\alpha}} b_j^1\left|\varphi_{1j^{\alpha}}\right\rangle$, which describes an excited electronic state. Equation (51) requires the orthogonality of all occupied excited state orbital associated with α spin functions to the arbitrary vector $\sum_i^{n^{\alpha}} b_i^0\left|\varphi_{0i}^{\alpha}\right\rangle$ from the subspace of the occupied ground state orbitals associated with α spin functions. In general, the coefficients b_i^0 can be determined by minimizing the excited state Hartree-Fock energy. However, calculations show that the choice

$$\sum_{i}^{n^{\alpha}} b_i^0|\varphi_{0i}^{\alpha}\rangle=|\varphi_{0n}^{\alpha}\rangle, \tag{52}$$

where φ_{0n}^{α} is the orbital from the ground state Slater determinant with the highest energy, leads to a minimum energy for the excited state. In the limit of a complete basis set or a common basis set for the ground and excited state the schemes defined by (50) and (51), yield the same energy values.

In this work, we use the second scheme to impose the orthogonality constraint (48), i.e. that defined by Eq. (51), which upon using (52) becomes

$$\left\langle\varphi_{0n}^{\alpha}|\varphi_{1j}^{\alpha}\right\rangle=0,\ j=1,2,\ldots,n^{\alpha}. \tag{53}$$

Equation (53) can be rewritten in symmetrical form, which is useful when deriving the Hartree-Fock equations, as follows:

$$\left\langle\varphi_{1j}^{\alpha}|\varphi_{0n}^{\alpha}\right\rangle\left\langle\varphi_{0n}^{\alpha}|\varphi_{1j}^{\alpha}\right\rangle=0,\ j=1,2,\ldots,n^{\alpha} \tag{54}$$

or, since the left-hand side of Eq. (54) is not negative

$$\sum_{j}^{n^{\alpha}}\left\langle\varphi_{1j}^{\alpha}|P_n^{\alpha}|\varphi_{1j}^{\alpha}\right\rangle=0, \tag{55}$$

where P_n^{α} is the projection operator

$$P_n^{\alpha}=|\varphi_{0n}^{\alpha}\rangle\langle\varphi_{0n}^{\alpha}|. \tag{56}$$

3.3 Variational Derivation of Hartree-Fock Equations for Excited States

We shall follow the unrestricted Hartree-Fock formalism for obtaining the ROHF functions developed in Sect. 2.2 to derive the Hartree-Fock equations for excited states. For the sake of simplicity, we restrict our attention to the first excited state. This means that we start with the minimization of the total energy expressed in terms of the UHF orbitals:

$$\begin{aligned} E_1^{UHF} &= \sum_i^{n^\alpha} \langle \varphi_{1i}^\alpha | h | \varphi_{1i}^\alpha \rangle + \frac{1}{2} \sum_{i,j}^{n^\alpha} [(\varphi_{1i}^\alpha \varphi_{1i}^\alpha | \varphi_{1j}^\alpha \varphi_{1j}^\alpha) - (\varphi_{1i}^\alpha \varphi_{1j}^\alpha | \varphi_{1i}^\alpha \varphi_{1j}^\alpha)] \\ &+ \sum_i^{n^\beta} \langle \varphi_{1i}^\beta | h | \varphi_{1i}^\beta \rangle + \frac{1}{2} \sum_{i,j}^{n^\beta} [(\varphi_{1i}^\beta \varphi_{1i}^\beta | \varphi_{1j}^\beta \varphi_{1j}^\beta) - (\varphi_{1i}^\beta \varphi_{1j}^\beta | \varphi_{1i}^\beta \varphi_{1j}^\beta)] \\ &+ \sum_i^{n^\alpha} \sum_i^{n^\beta} (\varphi_{1i}^\alpha \varphi_{1i}^\alpha | \varphi_{1j}^\beta \varphi_{1j}^\beta) \end{aligned}$$

subject to the following constraints:

(i) orbitals must satisfy the restrictions (55) which ensure the orthogonality of Slater determinants for the ground state and the first excited state;

(ii) the excited Slater determinant must be an eigenfunction of the $\mathbf{S}^2$ operator, i.e. we impose the spin purity condition in the form

$$\sum_k^{n^\beta} \langle \varphi_{1k}^\beta | Q^\alpha | \varphi_{1k}^\beta \rangle = 0 \tag{57}$$

where $Q^\alpha = I - P^\alpha$ is the orthoprojector on the subspace of the virtual α spin orbitals. It is useful to remember that Eq. (57) implies that the set of orbitals associated with the β spin functions lies completely within the space defined by the set associated with the α spin functions.

The Hartree-Fock equations for the excited state orbitals can now be obtained by constructing a functional consisting of the UHF energy expression together with terms imposing the orthogonality constraints (55) and (57) by the method of Lagrange undetermined multipliers. In particular, the constraints (55) and (57) multiplied by Lagrange multipliers λ_1 and λ_2, respectively, are added to the UHF energy $E_1^{UHF} = \langle \Phi_1 | H | | \Phi_1 \rangle$, so as to give the following functional

$$L = E_1^{UHF} + \lambda_1 \sum_i^{n^\beta} \left\langle \varphi_{1i}^\beta | Q^\alpha | \varphi_{1i}^\beta \right\rangle + \lambda_2 \sum_i^{n^\alpha} \langle \varphi_{1j}^\alpha | P_n^\alpha | \varphi_{1j}^\alpha \rangle . \tag{58}$$

The stationary condition has the form

$$\delta L = \delta \left[E_1^{UHF} + \lambda_1 \sum_i^{n^\beta} \left\langle \varphi_{1i}^\beta | Q^\alpha | \varphi_{1i}^\beta \right\rangle + \lambda_2 \sum_i^{n^\alpha} \left\langle \varphi_{1j}^\alpha | P_n^\alpha | \varphi_{1j}^\alpha \right\rangle \right] = 0. \qquad (59)$$

It should be emphasised that, although this condition is based on the UHF energy expression, it leads to a result corresponding to ROHF theory.

In practical applications, we invariably invoke the algebraic approximation by parameterizing the orbitals in a finite basis set. This approximation may be written

$$|\varphi_1\rangle = P|\varphi_1\rangle$$

where P is an orthoprojector defined by a chosen basis set with dimension M_1, i.e.

$$P = \sum_{p,q}^{M_1} \left|\chi_p^1\right\rangle (\mathbf{S}^{-1})_{pq} \left\langle \chi_q^1 \right|$$

where $\mathbf{S}$ is the overlap matrix and $\mathbf{S}^{-1}$ is its inverse.

It should be stressed that, in general, the basis set for the excited state,

$$\left\{\chi_p^1; p = 1, 2, ..., M_1\right\},$$

is distinct from that for the ground state,

$$\left\{\chi_p^0; p = 1, 2, ..., M_0\right\}.$$

The stationary condition (59) leads, after some manipulation, to the following equations

$$\begin{aligned} &lim_{\lambda_1,\lambda_2\to\infty} P(\mathbf{F}^\alpha - \lambda_1 P^\beta + \lambda_2 P_n^\alpha - \varepsilon_i^a) P \left|\varphi_{1i}^\alpha\right\rangle = 0,\ i^\alpha = 1, 2, ..., n^\alpha, ..., M_1 \\ &lim_{\lambda_1\to\infty} P(\mathbf{F}^\beta + \lambda_1 Q^\alpha - \varepsilon_i^\beta) P \left|\varphi_{1i}^\beta\right\rangle = 0, \qquad\qquad i^\beta = 1, 2, ..., n^\beta, ..., M_1 \end{aligned} \qquad (60)$$

Here $\mathbf{F}^\alpha$ and $\mathbf{F}^\beta$ are the standard UHF operators constructed from the excited state orbitals φ_{1i}. According to the asymptotic projection technique the terms $\lambda_1 P^\beta$ and $\lambda_1 Q^\alpha$, $\lambda_1 \to \infty$, ensure spin purity (see the work of Glushkov and Tsaune [34] and also Glushkov [24] for more details) whereas the term $\lambda_2 P_n^\alpha$, $\lambda_2 \to \infty$, provides the orthogonality of states.

This result can be easily extended to the higher energy levels. For example, for the second excited state the operator P_n^α should be substituted by the orthoprojector

$$P_n^\alpha = |\varphi_{0n}^\alpha\rangle \langle\varphi_{0n}^\alpha| + |\varphi_{1n}^\alpha\rangle \langle\varphi_{1n}^\alpha|$$

etc., i.e. the problem of choosing a determinantal wave function for the higher excitations does not arise. The only additional computation beyond that required for the UHF scheme is the evaluation of the overlap matrix element $\left\langle \varphi_{0n}^\alpha | \varphi_{1j}^\alpha \right\rangle$. It should

be noted that for practical calculations, the value $\lambda_1 \sim 100-500$ a.u. ensures spin purity [24], whereas $\lambda_2 \sim 1{,}000$ a.u. ensures that $\langle \Phi_0 | \Phi_1 \rangle < 10^{-6}-10^{-7}$ [36].

It is worth also noting that because of the asymptotic projection method, all excited configurations based on the excited Slater determinant Φ_1, viz., Φ_{1i}^{a}, Φ_{1ij}^{ab}, etc., are orthogonal both to Φ_0 and among themselves. Therefore, these functions form the orthonormal basis set in the many-body space and can be used, unlike other SCF methods which do not satisfy the orthogonality of states in the explicit form, to develop many-body methods incorporating the correlation effects, in particular, a many-body Møller-Plesset-like perturbation theory (see Sect. 5).

3.4 Numerical Results and Discussion

At present, there are only very few published finite basis set calculations for excited states having the same symmetry as the ground state which are based on existing Hartree-Fock methods. For some atoms, numerical Hartree-Fock (NHF) results are available [59]. They can be used to examine the performance of the excited state SCF theory presented above.

3.4.1 Even-Tempered Basis Set Implementation for Excited States of Atoms

In this section, we describe three different schemes for developing systematic sequences of even-tempered basis sets for excited states. We define each scheme, which we label (a), (b) and (c) in turn.

In each scheme, we generate a sequence of even-tempered basis sets, with exponents given by

$$\zeta_p = \alpha\beta^p,\ p = 1, 2, ..., M. \tag{61}$$

Following Schmidt and Rudenberg(61), in the following we shall use α and β for the parameters that generate a sequence of even-tempered basis sets and *not* for spin function as we did above. The parameters α and β must be taken to be functions of M, the number of basis functions, i.e. $\alpha = \alpha(M)$ and $\beta = \beta(M)$, if the Gaussian sets defined by (61) are to become complete in the appropriate subspace as $M \to \infty$.

In the scheme which we label (a), the same basis set is employed for *both* the ground and excited state. Therefore, the same integrals over basis functions are used for both states. The values of the even-tempered parameters α and β are those which were optimized for the ground state of the atom as reported by Schmidt and Ruedenberg [60]. These values are given in Table 1 of Schimdt and Ruedenberg's paper [60].

In scheme (b) the basis set is optimized by invoking the variation principle for each state considered. For the ground state the optimized values of the even-tempered parameters α and β given by Schmidt and Ruedenberg [60] are used whereas for the excited state optimal values for a sequence of M values are determined by minimizing the corresponding excited state energy.

In our third scheme, which we label (c), we optimized the parameter α and β for the smallest basis set considered, i.e. $M = 6$ and then determine values of these parameters for the basis sets of larger size by using the recursions [61]:

$$\alpha[M] = \left[\frac{\beta[M]-1}{\beta[M-1]-1}\right]^{a} \alpha[M-1]$$

and

$$\ln(\beta[M]) = \left[\frac{M}{M-1}\right]^{b} \ln\beta[M-1]$$

with the values of a and b taken from the work of Schmidt and Ruedenberg [60]. These values are given in Table 3 of reference [60].

We performed prototype calculations on some simple atoms in order to study the rate of convergence of the excited state energies and the accuracy which could be supported before problems associated with the precision of our calculations arising from computational linear dependence became significant. In particular, we studied the ^3S states of the He atom corresponding to the configurations $1s2s$, $1s3s$ and $1s4s$, and the ^3S states of the Be atom corresponding to the configurations $(\mathrm{He})\,2s3s$ and $(\mathrm{He})\,2s4s$.

Using scheme (b) we also computed excitation energies for the Be isoelectronic series in a comparison with the numerical Hartree-Fock values.

3.4.2 Matrix Hartree-Fock Energies and Excitation Energies of Atoms

The ground and excited state matrix Hartree-Fock energies for the He and Be atoms are presented in Tables 5 and 6, respectively. All energies are given in atomic units, (Hartree). In each of these tables, we label the columns according to the three schemes, *(a)*, *(b)* and *(c)*, described above. We consider each system in turn.

For the excited states of the He atom considered in Table 8 the numerical Hartree-Fock energies are known from the work of Froese-Fischer [59] to be – $E(1s2s) = -2.174\,26$ Hartree, $E(1s3s) = -2.068\,49$ Hartree, $E(1s4s) = -2.036\,44$ Hartree. For none of the three states considered does the sequence of basis sets constructed according to scheme (a) achieve satisfactory accuracy. For the $1s2s$ state, the energy supported by the largest basis set, i.e. $M = 72$, is in error by $\sim$0.8 *m*Hartree. For the $1s3s$ state this error is $\sim$0.056 Hartree, whilst for the $1s4s$ state the calculation with the largest basis set failed to converge and for the next largest set the error is $\sim$0.348 Hartree. Not surprisingly, a basis set designed for the ground state supports an increasingly poor description of excited states as the level of excitation increases. Equally, it is not surprising that if the sequence of even-tempered basis sets for each excited state is optimized independently then the matrix Hartree-Fock energies converge to values in good agreement with the corresponding numerical Hartree-Fock energies. What is more this level of agreement is achieved for basis sets of only 42 functions in the case of the He states considered here. Scheme (c) leads to sequences of energies which begin, of course, with values equal to those for scheme

Table 5 Self-Consistent Field energies (in hartree) of the He atom for some ^{3}S excited states as a function of the size, M, of the even-tempered basis set used to parameterize the orbitals. In the column headed *(a)*: the same even-tempered basis set – optimized for the ground state, is used for all states; *(b)*: the even-tempered basis set is optimized for each state; *(c)*: the even-tempered parameters α and β are optimized for each basis set for the smallest basis set ($M = 6$) and larger basis sets are generated using the recursions

M	^{3}S $1s2s$		
	(a)	*(b)*	*(c)*
6	−1.83461514	−2.16969148	−2.16969148
12	−2.09589565	−2.17420691	−2.17416233
18	−2.14125461	−2.17424990	−2.17424758
24	−2.15704132	−2.17425075	−2.17425059
30	−2.16421386	−2.17425077	−2.17425076
42	−2.17012977	−2.17425078	−2.17425078
54	−2.17228698	–	–
60	−2.17284371	–	–
72	−2.17348174	–	–
M	^{3}S $1s3s$		
	(a)	*(b)*	*(c)*
6	1.73706970	−2.05902284	−2.05902285
12	−1.10978995	−2.06833906	−2.06768910
18	−1.58429285	−2.06847975	−2.06845041
24	−1.76064449	−2.06848472	−2.06847385
30	−1.84981446	−2.06848493	−2.06848386
42	−1.93754688	−2.06848496	−2.06848488
54	−1.97977236	–	–
60	−1.99338333	–	–
72	−2.01255580	–	–
M	^{3}S $1s4s$		
	(a)	*(b)*	*(c)*
6	17.38262804	−2.00192936	−2.00192936
12	2.01602912	−2.03624788	−2.03501230
18	−0.09897153	−2.03641613	−2.03601202
24	−0.81661258	−2.03643495	−2.03641298
30	−1.16049508	−2.03643584	−2.03641853
42	−1.48612549	−2.03643641	−2.03643607
54	−1.64005315	–	–
60	−1.68986935	–	–
72	–	–	–

(b) when $M = 6$ and converge almost as rapidly towards the numerical Hartree-Fock values. For the $1s2s$ state schemes (b) and (c) lead to energies which agree to all figures quoted, i.e. 0.01 μHartree when $M = 42$. For the $1s3s$ state there is a difference of $\sim$0.08 μHartree between the energies supported by the two schemes when $M = 42$. The corresponding difference for the $1s4s$ state is $\sim$0.34 μHartree.

For the two excited states of the Be atom considered in Table 6 the numerical Hartree-Fock energies are known [59] to be as follows: $E([\text{He}]2s3s) = -14.377\,54$

Table 6 Self-Consistent Field energies (in hartree) of the Be atom for some ^{3}S excited states as a function of the size, M, of the even-tempered basis set used to parameterize the orbitals. In the column headed *(a)*: the same even-tempered basis set – optimized for the ground state, is used for all states; *(b)*: the even-tempered basis set is optimized for each state; *(c)*: the even-tempered parameters α and β are optimized for each basis set for the smallest basis set ($M = 6$) and larger basis sets are generated using the recursions

M	$(He)2s3s$		
	(a)	*(b)*	*(c)*
6	−13.68597324	−14.28743398	−14.28743398
12	−14.30875164	−14.37655131	−14.37615739
18	−14.35583967	−14.37747784	−14.37745253
24	−14.36814873	−14.37749790	−14.37749650
30	−14.37282326	−14.37749869	−14.37749856
42	−14.37602885	−14.37749874	−14.37749874
54	−14.37694934	–	–
60	−14.37714828	–	–
72	−14.37735193	–	–
M	$(He)2s4s$		
	(a)	*(b)*	*(c)*
6	−5.20614793	−14.10328399	−14.10328399
12	−13.45962762	−14.32284981	−14.32018366
18	−14.01343862	−14.32455109	−14.32446205
24	−14.15980890	−14.32460713	−14.32458356
30	−14.22107884	−14.32461093	−14.32460787
42	−14.27239938	−14.32461121	−14.32461113
54	−14.29355025	–	–
60	−14.29978829	–	–
72	−14.30798338	–	–

Table 7 Optimized even-tempered parameters α and β for ^{3}S excited states of He as a function of size of basis set

M	$1s2s$		$1s3s$		$1s4s$	
	α	β	α	β	α	β
6	0.009 397	4.210 973	0.001 684	4.979 103	0.000 376	5.420 623
12	0.009 088	2.641 628	0.002 742	2.758 438	0.000 924	3.033 467
18	0.008 243	2.211 957	0.002 785	2.202 424	0.001 226	2.212 713
24	0.007 443	1.999 366	0.001 967	1.999 755	0.001 232	1.932 314
30	0.006 989	1.897 299	0.002 043	1.845 165	0.001 176	1.794 637
42	0.005 045	1.702 089	0.002 176	1.661 148	0.001 068	1.666 500

Hartree, $E([\mathrm{He}]2s4s) = -14.324\,66$ Hartree. For scheme (a) the iterative process failed to converge for basis sets containing more than 72 functions. For the $[\mathrm{He}]2s3s$ state, the largest basis set supports an energy expectation value which is within $\sim$0.2 mHartree of the numerical Hartree-Fock value, whilst for the $[\mathrm{He}]2s4s$ state, the corresponding difference is $\sim$16.7 mHartree. Again, a basis set designed for the ground state supports an increasingly poor description of excited states as the

Table 8 Optimized even-tempered parameters α and β for ^{3}S excited states of Be as a function of size of basis set

M	[He] $2s3s$		[He] $2s4s$	
	α	β	α	β
6	0.004 884	5.142 401	0.001 057	5.809 367
12	0.004 799	2.947 601	0.001 459	3.191 957
18	0.004 552	2.370 166	0.001 709	2.424 045
24	0.004 237	2.083 730	0.001 736	2.080 558
30	0.003 912	1.921 824	0.001 663	1.899 549
42	0.003 667	1.745 016	0.001 537	1.719 092

Table 9 Total energies (hartree) and excitation energies (eV) for the Be isoelectronic series

System	State	Hartree-Fock–asymptotic projection	NHF
Be	$1s^2 2s3s$	−14.377 48	−14.377 54
	$1s^2 2s4s$	−14.324 55	−14.324 66
	$\Delta E(3s \to 4s)$	1.440	1.439
B^+	$1s^2 2s3s$	−23.700 12	−23.700 18
	$1s^2 2s4s$	−23.539 19	−23.539 30
	$\Delta E(3s \to 4s)$	4.379	4.378
C^{2+}	$1s^2 2s3s$	−35.388 09	−35.388 26
	$1s^2 2s4s$	−35.069 25	−35.069 43
	$\Delta E(3s \to 4s)$	8.676	8.676
O^{4+}	$1s^2 2s3s$	−65.852 21	−65.852 58
	$1s^2 2s4s$	−65.070 35	−65.070 69
	$\Delta E(3s \to 4s)$	21.276	21.277

level of excitation increases. When the sequence of even-tempered basis sets are individually optimized for a particular state (scheme (b)) an accuracy of ∼0.04 mHartree is supported for the [He]$2s3s$ state and ∼0.05 mHartree for the [He]$2s4s$ state. A comparable accuracy is observed for the excited state energies of the Be atom corresponding to scheme (c) in which only the basis set for $M = 6$ is optimized.

The even-tempered basis set parameters obtained by optimization of α and β with respect to the energy for each size of a basis set, that is scheme (b) can be found in Table 7 for the He atom and in Table 8 for the beryllium atom.

Table 9 lists excitation energies (in eV) for Be, B^+, C^{2+} and O^{4+} computed with the even-tempered basis set of 18 s-type functions (scheme (b)). In Tables 9, 10 and 11 we label our implementation of SCF method the "HF – asymptotic projection" technique. The numerical Hartree-Fock energies are given in the column headed "NHF". The results of the Table 9 show that the HF – asymptotic projection method for excited states is capable of supporting high accuracy both for excited state energies and for excitation energies of the atoms and ions.

Table 10 Total ground and some excited state energies of HeH at $R = 1.5$ bohr. Atomic units are used

State	Hartree-Fock - asymptotic projection[b]	CI[a]	$\frac{E^{HF}-E^{CI}}{E^{CI}}\%$
$X^2\Sigma^+$	−3.219 851	−3.263 164	1.3
$A^2\Sigma^+$	−3.066 606	−3.112 706	1.5
$C^2\Sigma^+$	−3.014 785	−3.055 797	1.3
$D^2\Sigma^+$	−2.988 232	−3.030 025	1.4

[a] – Hartree-Fock energies based on the asymptotic projection method.
[b] – configuration interaction method.

Table 11 Vertical excitation energies (eV) from $A^2\Sigma^+$ of HeH at $R = 1.5$ bohr

State	Hartree-Fock– asymptotic projection[b]	CI[a] [62]	Expt [62]
$A^2\Sigma^+$	0	0	0
$C^2\Sigma^+$	1.41	1.53	1.55
$D^2\Sigma^+$	2.13	2.25	2.26

[a] – Hartree-Fock energies based on the asymptotic projection method.
[b] – configuration interaction method.

3.4.3 Matrix Hartree-Fock Energies and Excitation Energies of the HeH Molecule

The HeH molecule is of experimental interest and has been studied using accurate *ab initio* calculations (see, e.g. the work of Petsalakis et al. [62]), which provide excellent reference data. These data were obtained with the configuration interaction (CI) method. The CI space consisted of 4,732 configurations. Certainly, a comparison of absolute values computed by the present Hartree-Fock method with those given by the CI method would not be useful. However, the comparison of relative errors for different states is of value and permits an assessment of the performance of the method. Basis sets consisting of 18s Gaussian functions were used for all states under consideration ($X^2\Sigma^+$, $A^2\Sigma^+$,$C^2\Sigma^+$ and $D^2\Sigma^+$). All basis functions were centred on points lying on the line passing through the nuclei (the z-axis). The He nucleus was placed at the origin $(0, 0, 0)$ and the H nucleus at the point $(0, 0, 1.500)$.

The total energy of each excited state was minimized to determine non-linear basis set parameters (orbital exponents and positions) for a given state i.e. *basis sets were individually optimized for each state*. By exploiting the asymptotic projection method, this procedure takes practically the same computational time for excited states as it does for the ground state. (Some details of basis set optimization for the ground state can be found in the work of Glushkov and Wilson [42–44] and

references therein). The values $\lambda_1 = 100$ a.u. and $\lambda_2 = 10{,}000$ a.u. were used to solve Eq. (60).

In Tables 10 and 11, the performance of the SCF-asymptotic projection method for excited states can be observed. In these Tables, the total energies and excitation energies are given respectively make it possible to observe (see the column Hartree-Fock-AP).

The degree of agreement between computed and experimental values of excitation energies can be improved by taking account of electron correlation effects. It is to this problem that we turn our attention in the next section.

4 Many-body Møller-Plesset-*Like* Perturbation Theory Based on Open-Shell Asymptotic Projection Orbitals

It is well known that the choice of the zero-order Hamiltonian, $H^{(0)}$, is crucial to the success of any perturbation theory. As we have already mentioned, this choice is known to be particularly problematic for open-shell systems. On the one hand, although the theory for the construction of the ROHF wave function, which is an eigenfunction of $\mathbf{S}^2$, was developed by Roothaan [1] long ago, this approach does not readily lend itself to a perturbational treatment [20,21,23,25]. On the other hand, the UHF theory facilitates the construction of a suitable $H^{(0)}$, but the UHF Slater determinant is not, of course, an eigenfunction of $\mathbf{S}^2$. At present, the open-shell perturbation theory based on the so-called RMP method [21] is widely used. It is, for example, incorporated in computational quantum chemistry software packages such as GAMESS [24]. However, as we have pointed out, this method employs different orbitals for different spins for which the generalized Brillouin's theorem is not satisfied. Consequently, singly excited configurations enter the expansion for the energy at second-order. This also complicates higher-order perturbation theory calculations. In contrast, by employing an optimum set of asymptotic projection orbitals, we can develop a well-defined open-shell perturbative treatment which is a natural extension of the widely used closed-shell many-body Møller-Plesset perturbation theory. This new open-shell formalism leads to algorithms which exhibit computational costs comparable with the closed-shell algorithms. Moreover, we will show that, unlike existing open-shell perturbation theories, the new methodology can be easily extended to excited states having the same symmetry as the ground state.

4.1 Open-Shell Perturbation Theory for the Ground State

4.1.1 Basic Theory

The spin-unrestricted formalism for the ROHF functions developed in Sect. 2.2 facilitates the development of a well-defined open-shell many-body Møller-Plesset-like

perturbation theory. Indeed, the zero-order Hamiltonian can be written as a sum of Fock operators for each electron:

$$H_0^{(0)} = \sum_k^{n^\alpha} F_0^\alpha(k) + \sum_k^{n^\beta} F_0^\beta(k) \tag{62}$$

with Fock operators

$$F_0^\alpha = \sum_i^M |\varphi_{0i}^\alpha\rangle \varepsilon_{0i}^\alpha \langle\varphi_{0i}^\alpha|, \quad F_0^\beta = \sum_i^M |\varphi_{0i}^\beta\rangle \varepsilon_{0i}^\beta \langle\varphi_{0i}^\beta| \tag{63}$$

and the perturbation operator $V = H - H_0^{(0)}$. Here the subscript indicates the ground state, i.e. the orbitals and orbital energies are determined from Eqs. (25) and (26).

It is clear that the Slater determinant $\Phi_0^{(0)}$ constructed from orbitals (25), (26) and the determinants Φ_{0i}^a, Φ_{0ij}^{ab}, etc. corresponding to single, double, etc. excitations, obtained by replacing the occupied spin-orbitals by virtual spin-orbitals, form the orthonormal basis set in the many-particle space of states and are eigenfunctions of $H_0^{(0)}$, i.e.

$$\begin{aligned}
&H_0^{(0)}|\Phi_0^{(0)}\rangle = E_0^{(0)}|\Phi_0^{(0)}\rangle, \quad E_0^{(0)} = \langle\Phi_0^{(0)}|H_0^{(0)}|\Phi_0^{(0)}\rangle = \sum_i^{n^\alpha} \varepsilon_{0i}^\alpha + \sum_i^{n^\beta} \varepsilon_{0i}^\beta \\
&H_0^{(0)}|\Phi_{0i}^a\rangle = E_{0i}^a|\Phi_{0i}^a\rangle, \quad E_{0i}^a = E_0^{(0)} - \varepsilon_{0i}^\gamma + \varepsilon_{0a}^\gamma, \quad \gamma = \alpha, \beta \\
&H_0^{(0)}|\Phi_{0ij}^{ab}\rangle = E_{0ij}^{ab}|\Phi_{0ij}^{ab}\rangle, \quad E_{0ij}^{ab} = E_0^{(0)} - \varepsilon_{0i}^\gamma - \varepsilon_{0j}^\gamma + \varepsilon_{0a}^\gamma + \varepsilon_{0b}^\gamma.
\end{aligned} \tag{64}$$

Applying Rayleigh-Schrödinger perturbation theory to the problem (62),(63), it is then easy to show that the sum of the zero-order and first-order energy $E_0 = E_0^{(0)} + E_0^{(1)}$ yields the energy expectation value evaluated with respect to the reference function $\Phi_0^{(0)}$. Indeed

$$E_0^{(0)} + E_0^{(1)} = \langle\Phi_0^{(0)}|H_0^{(0)}|\Phi_0^{(0)}\rangle + \langle\Phi_0^{(0)}|V|\Phi_0^{(0)}\rangle = \langle\Phi_0^{(0)}|H|\Phi_0^{(0)}\rangle.$$

Note that the reduced resolvent operator

$$R_0^{(0)} = Q_0^{(0)}(E_0^{(0)} - H_0^{(0)})^{-1} Q_0^{(0)}, \quad Q_0^{(0)} = I - |\Phi_0^{(0)}\rangle\langle\Phi_0^{(0)}|$$

has a diagonal form in the basis set of excited configurations. Therefore, this can be expressed in the form

$$R_0^{(0)} = \sum_i^{occ} \sum_a^{virt} \frac{|\Phi_{0i}^a\rangle\langle\Phi_{0i}^a|}{E_0^{(0)} - E_{0i}^a} + \sum_{i<j}^{occ} \sum_{a<b}^{virt} \frac{|\Phi_{0ij}^{ab}\rangle\langle\Phi_{0ij}^{ab}|}{E_0^{(0)} - E_{0ij}^{ab}} + \ldots$$

The summations in this expression are over spin orbitals. We omitted the summations corresponding to the higher order excitations.

Because of the Brillouin theorem, the first-order corrections to the wave functions have the form:

$$|\Phi_0^{(1)}\rangle = R_0^{(0)} V |\Phi_0^{(0)}\rangle = \sum_{i<j}^{occ} \sum_{a<b}^{virt} |\Phi_{oij}^{ab}\rangle \langle \Phi_{0ij}^{ab} | H | \Phi_{oij}^{ab}\rangle (\varepsilon_{0i} + \varepsilon_{0j} - \varepsilon_{0a} - \varepsilon_{0b})^{-1}.$$

The second-order correction to the ground state energy $E_0^{(2)}$ is expressed in terms of spin-orbitals and orbital energies:

$$E_0^{(2)} = \sum_{i>j}^{occ} \sum_{a>b}^{virt} \frac{|(\varphi_{0a}\varphi_{0i}|\varphi_{0b}\varphi_{0j}) - (\varphi_{0a}\varphi_{0j}|\varphi_{0b}\varphi_{0i})|^2}{\varepsilon_{0i} + \varepsilon_{0j} - \varepsilon_a - \varepsilon_{0b}}. \tag{65}$$

We emphasise that the summations are over spin-orbitals. a and b are virtual orbitals while i and j are occupied orbitals. The above expression is suitable for practical calculations.

Thus, the orbitals based on asymptotic projection lead to a many-body perturbation theory similar in form to the original to the original Møller-Plesset perturbation theory. In terms of computational cost, this new open-shell perturbation theory, like the OPT1 and OPT2 theories of Murray and Davidson [23] and the ZAPT theory of Lee and Jayatilaka [25], has an obvious advantage over the RMP [21]. The new theory is based on only one set of spatial molecular orbitals whereas the RMP has two sets.

4.1.2 Application to the Singlet-Triplet Separation in the CH_2 Molecule

There have been a large number of experiments and theoretical studies of the singlet-triplet $^1A_1 - {}^3B_1$ separation in the CH_2 molecule (see, e.g. the work of Sherrill, van Huis, Yamaguchi and Schaefer [63] and also that of Bauschlicher and Taylor [64]) which provide excellent data for assessing new methods. The different spin and spatial symmetry of the states imposes stringent requirements on the methods employed at both the SCF level and in the perturbation theory calculations. We carried out calculations with three basis sets containing 24s, 28s, and 42s Gaussians, respectively. The orbital exponents and positions were determined by minimizing the energy for each individual state. The parameters for our largest basis set of 42s functions can be found in the work of Glushkov [24]. The nuclear coordinates are as follows: the $^1A_1$ state: C$(0, 0, 0)$; H1$(-1.64403, -1.32213, 0)$; H2$(1.64403, -1.32213, 0)$ and the $^3B_1$ state: C$(0, 0, 0)$; H1$(-1.871093, -0.82525, 0)$; H2$(1.871093, -0.82525, 0)$.

The energies of the $^1A_1$ and $^3B_1$ states at the SCF and second order perturbation theory levels are given in Table 12 together with the corresponding energy splittings. The $^1A_1$ state is described by a closed-shell determinant and, therefore, the standard restricted Hartree-Fock and the second-order many-body Møller-Plesset perturbation expansion were used.

Table 12 SCF and second order perturbation theory energies (hartrees) of methelene in the $^1A_1$ and $^3B_1$ states and the $^1A_1 - {}^3B_1$ separation energy (in kcal/mol)

Energy	Basis set	$^3B_1$	$^1A_1$	$\Delta E(^1A_1 - {}^3B_1)$
E_{SCF}	24*s*	−38.897 795	−38.858 109	24.90
	28*s*	−38.909 868	−38.872 370	23.53
	42*s*	−38.929 603	−38.889 249	25.33
	DZP [63]	−38.927 640	−38.885 590	26.39
E_{PT2}[a]	24*s*	−38.984 048	−38.957 602	16.59
	28*s*	−39.008 662	−38.984 938	14.88
	42*s*	−39.045 811	−39.023 562	13.96
CASPT2[b]	*DZP*	−39.037 660	−39.013 080	15.43
RMP[c]	*TZ2P*	–	–	18.05
OPT2[c]	*TZ2P*	–	–	17.99
ZAPT[c]	*TZ2P*	–	–	17.07
FCI[d]	*DZP*	−39.046 260	−39.027 183	11.97

[a] – $E_{PT2} = E_{SCF} + E^{(2)}$.
[b] – CASPT2, second-order of multireference perturbation theory based on a CAS wave function [40].
[c] – Values were taken from Ref. [25].
[d] – Full configuration interaction method (FCI) [64].

One can see that our basis set of 42*s* functions yields SCF energies that are close to those obtained with the DZP basis set. We observe that the value of the energy splitting computed by using our scheme is improved when the size of the basis set increases. A comparison of our asymptotic projection based technique in its second-order implementation with other open-shell perturbation theories (CASPT2, OPT2, RMP and ZAPT) shows the new method yields values of the singlet-triplet splitting closest to the FCI reference value.

In concluding this section, we note that the present results could be improved by using multireference perturbation theory since the singlet state $^1A_1$ is known to have two important configurations [64]. An alternative asymptotic projection-based multireference perturbation theory [65] can be used for this.

4.2 Open-Shell Perturbation Theory for the Excited States

To our knowledge, there is, at present, no analogue of many-body Møller-Plesset perturbation theory for excited states having the same symmetry as the ground state or some lower lying excited state. The study of such systems often involves the use of a multireference formalism. Such methods are indispensable in studies of systems where single-configuration methods cannot be applied. Nevertheless, it would be very useful to have a perturbation theory formalism the description of excited states

which can be adequately described by a single Slater determinant. Such an approach shares the computational advantages of the widely used many-body Møller-Plesset perturbation theory. It would be especially useful for calculations of energy differences. In addition, it is important to calculate the ground-state and excited-state energies in a balanced manner, i.e.:

(i) Reference configurations are constructed by employing the same computational scheme. For example, the ground and excited SCF functions are constructed using the Hartree-Fock equations, whose solutions are approximated in one-particle basis sets adjusted specifically to the state under consideration.
(ii) Correlation effects are taken into account using comparable schemes for the ground- and excited-states, for example, using many-body Møller-Plesset-like perturbation theory.

4.2.1 Second-Order Correlation Energy for Excited States

For simplicity, we shall consider the first excited state energy. In this case, the zero-order Hamiltonian is similar to that for the ground state, but the Fock operators are based on the excited state orbitals and orbital energies from Eqs. (60), i.e.

$$H^{(0)} = \sum_{k}^{n^\alpha} F^\alpha(k) + \sum_{k}^{n^\beta} F^\beta(k) \tag{66}$$

with Fock operators

$$F^\alpha = \sum_{i}^{M-1} |\varphi_i^\alpha\rangle \varepsilon_i^\alpha \langle\varphi_i^\alpha|, \qquad F^\beta = \sum_{i}^{M-1} |\varphi_i^\beta\rangle \varepsilon_i^\beta \langle\varphi_i^\beta|. \tag{67}$$

In the following, we shall omit the lower subscript for the excited states. The the upper limit of the summations is $M-1$ because the vector $|\varphi_{0n}^\alpha\rangle$ is excluded from the subspace of virtual molecular orbitals. *It is important* that singly, Φ_i^a, doubly, Φ_{ij}^{ab}, etc. excited configurations with respect to an excited state Slater determinant $\Phi^{(0)}$ are eigenfunctions of the Hamiltonian $H^{(0)}$ (66) and they are orthogonal to the ground state Slater determinant $\Phi_0^{(0)}$ because $\langle\varphi_{0n}^\alpha|\varphi_i^\alpha\rangle = 0$, $i = 1, 2, ..., M-1$.

In contrast to the ground state case, for the excited state it is necessary to take into consideration the orthogonality constraints. For the first-order correction to the excited state reference function, $\Phi^{(1)}$, these constraints have the form

$$\left\langle \Phi^{(0)} | \Phi^{(1)} \right\rangle = 0. \tag{68}$$

The first-order correction can be written in the following form

$$|\Phi^{(1)}\rangle = (I - P_0^{(0)})|\Phi^{(1)}\rangle + P_0^{(0)}|\Phi^{(1)}\rangle$$

where I is the identity operator and $P_0^{(0)} = |\Phi_0^{(0)}\rangle\langle\Phi_0^{(0)}|$.

It should be stressed that $|\Phi^{(1)}\rangle$ is constructed in the basis of singly, doubly, etc. excited configurations of $|\Phi^{(0)}\rangle$, which, due to the asymptotic projection method, are orthogonal both to $|\Phi^{(0)}\rangle$ and $|\Phi_0^{(0)}\rangle$. Therefore, the solution of the first-order equation

$$(H^{(0)} - E^{(0)})|\Phi^{(1)}\rangle = -(V - E^{(1)})|\Phi^{(0)}\rangle, \quad V = H - H^{(0)}$$

determines only part of the correction, the projection $(I - P_0^{(0)})|\Phi^{(1)}\rangle$ satisfying the condition (68), but does not determine the other part, $P_0^{(0)}|\Phi^{(1)}\rangle$. This projection should be determined by the orthogonality condition for the states in the first-order perturbation theory, i.e.

$$P_0^{(0)}|\Phi^{(1)}\rangle = -P_0^{(1)}|\Phi^{(0)}\rangle, \tag{69}$$

where

$$P_0^{(1)} = |\Phi_0^{(0)}\rangle\langle\Phi_0^{(1)}| + |\Phi_0^{(1)}\rangle\langle\Phi_0^{(0)}|.$$

Such a scheme of the construction for $\Phi^{(1)}$ is compatible with both the perturbation theory equations and the orthogonality restrictions (68) and (69).

The final expression for the first-order correction to the excited state reference function takes the form

$$|\Phi^{(1)}\rangle = R^{(0)}V|\Phi^{(0)}\rangle - |\Phi_0^{(0)}\rangle\langle\Phi_0^{(1)}|\Phi^{(0)}\rangle \tag{70}$$

where $R^{(0)} = Q^{(0)}(E^{(0)} - H^{(0)})^{-1}Q^{(0)}$ is the reduced resolvent operator, and $Q^{(0)}$ is the orthoprojector onto the complementary space, i.e. $Q^{(0)} = I - |\Phi^{(0)}\rangle\langle\Phi^{(0)}|$.

It is well-known that the Rayleigh-Schrödinger perturbation theory leads to the following expression for the second order correction to the energy

$$E^{(2)} = \langle\Phi^{(0)}|H|\Phi^{(1)}\rangle$$

or, taking (70) into account, we have the expression

$$E^{(2)} = \sum_{i>j}^{occ}\sum_{a>b}^{virt} \frac{|(\varphi_a\varphi_i|\varphi_b\varphi_j) - (\varphi_a\varphi_j|\varphi_b\varphi_i)|^2}{\varepsilon_i + \varepsilon_j - \varepsilon_a - \varepsilon_b} - \langle\Phi^{(0)}|H|\Phi_0^{(0)}\rangle\langle\Phi_0^{(1)}|\Phi^{(0)}\rangle. \tag{71}$$

The first term in Eq. (71) is immediately recognized as the second-order perturbation theory expression for the ground state energy (*cf.* with (65)). Single excitations do not contribute because the excited state orbitals, like the ground state orbitals, satisfy the generalized Brillouin theorem. The second term in Eq. (71) appears because the Hartree-Fock ground and excited state functions are not eigenfunctions of the Hamiltonian H. In practice, if the ground state and excited state energies and the corresponding wave functions are known accurately then the coupling matrix element $\langle\Phi_0|H|\Phi_1\rangle$ is expected to be small (see also paper I [27], Sect. 3.1). Furthermore, as the overlap element $\langle\Phi_0^{(1)}|\Phi^{(0)}\rangle < 1$, then during the first stage of calculations the last term in Eq. (71) may be neglected.

Thus, we obtain comparable perturbation schemes for the ground and excited state energies. Use of the asymptotic projection technique ensures that calculations for excited states require practically the same computational time as those for the ground state.

4.2.2 Numerical Examples

Below we demonstrate some possibilities of the single reference-based perturbation theory based on orbitals obtained by asymptotic projection for calculations of the total energies and excitation energies of the HeH and BeF molecules. We studied the $X^2\Sigma^+$, $A^2\Sigma^+$, $C^2\Sigma^+$, and $D^2\Sigma^+$ states of HeH and the $X^2\Sigma^+$, $B^2\Sigma^+$ and $C^2\Sigma^+$ states of the BeF molecule.

For HeH, the basis set of 18s Gaussians employed in Sect. 2.2.2 was extended to a 18s3p set, i.e. 18s functions were distributed along the molecular axis (z-axis) with the basis set parameters determined by minimizing the total SCF energy for each individual state. It should be noted that such basis set extension does not modify the subspace of occupied orbitals nor, therefore, the SCF energy, but it facilitates and improved description of correlation effects. The orbital exponents and positions of the p-functions (p_x and p_y) were determined by using Hylleraas' variational principle [66]. This allowed us to minimize the error associated with truncation of one-particle basis sets and, thus, to assess more precisely the errors of the method itself. In addition, each p function (p_x, p_y) was represented by a linear combination of two s-functions, i.e. the so-called Gaussian lobe representation [67] was used.

The results of our calculations of the total energies and excitation energies are presented in Table 13 where they are compared to those obtained by the CI method [62] and experimental data.

The BeF molecule was studied in detail in [68] where its various properties were determined using the CI method. Experimental data are also available for this molecule [69]. The best results in [68] were obtained with the mixed one-particle basis set consisting of the Slater and two-center functions. We carried out calculations with the basis sets consisting of 24s Gaussian functions for the $X^2\Sigma^+$, $B^2\Sigma^+$

Table 13 Excited state energies (hartrees) and excitation energies (ΔE, eV) from the $A^2\Sigma^+$ state of HeH at the different levels of approximation at $R = 1.5$ bohr

Method	$A^2\Sigma^+$	$B^2\Sigma^+$	$D^2\Sigma^+$
Hartree-Fock–asymptotic projection	−3.066 606	−3.014 785	−2.988 232
$E^{(2)}$	−0.033 363	−0.029 915	−0.030 027
E_{MP2}	−3.099 969	−3.044 700	−3.018 259
E_{CI}[62]	−3.112 706	−3.055 797	−3.030 025
ΔE_{HF}	0	1.41	2.13
ΔE_{MP2}	0	1.50	2.22
ΔE_{CI} [62]	0	1.53	2.25
ΔE_{exp} [62]	0	1.55	2.26

states and 26*s* functions for the $C^2\Sigma^+$ state and 4*p*-functions ($4p_x$ and $4p_y$), which, in turn, were represented by the lobe approximated using lobes functions as we did for HeH. These *p*-functions simulated the behavior of $1\pi_x$ and $1\pi_y$ orbitals in the $1\sigma_2 1\sigma_2 1\sigma_2 1\sigma_2 1\pi_4\phi$ configurations, where $\phi = 5\sigma, 6\sigma$ and 7σ correspond to the $X^2\Sigma^+$, $B^2\Sigma^+$ and $C^2\Sigma^+$ states, respectively. The calculations were performed at internuclear distance $R = 2.5$ bohr, which is close to the equilibrium separation for all the states under consideration. In this case, the basis set parameters both of *s*-functions and *p*-functions were determined for each individual state by minimizing the corresponding energy in the single determinant approximation. Such an optimization of the restricted basis sets is very important for the excited states, and *its contribution to the total energy is comparable with the second-order correlation correction* as can be seen in Table 14, where the zero-, first- and second-order energies are given. The energies in the column headed A were computed with basis sets optimized for the state under study whereas the energies presented in column B were obtained with the basis set adjusted to the ground state ($X^2\Sigma^+$). In addition, a comparison of columns A and B also shows that the correlation energy (the row $E^{(2)}$) depends slightly on the basis set optimization.

Of course, the basis sets employed are not of sufficient size to approach the complete basis limit and thus the comparison of absolute values with more precise ones is not meaningful. However, if basis set optimization has been carried out for each individual state and the similar scheme for accounting the correlation effects has been used (Møller-Plesset like perturbation theory in our case), then energy contributions from incompleteness of basis set may be assumed to be similar for adjacent excited states and, therefore, comparisons of relative positions of energy levels computed against more precise or experimental ones are instructive to estimate the performance of the method. We can see from Table 15 that the method introduced in this paper yield reasonable excitation energies which are closer to experimental results [69] than the CI values obtained in Ref. [68].

Table 14 The total energies (hartrees) of the BeF molecule calculated in different orders of perturbation theory at $R = 2.5$ bohr

Order of perturbation	$A\,(X^2\Sigma^+)$	$A\,(B^2\Sigma^+)$	$B\,(B^2\Sigma^+)$	$A\,(C^2\Sigma^+)$	$B\,(C^2\Sigma^+)$
$E^{(0)}$	−69.221 2	−70.864 9	−68.980 0	−70.209 8	−68.667 4
$E^{(0)} + E^{(1)}$	−114.103 6	−113.882 3	−113.790 9	−113.875 1	−113.595 3
$E^{(2)}$	−0.174 3	−0.172 5	−0.173 0	−0.169 0	−0.168 4
E_{MP2}	−114.277 9	−114.054 8	−113.964 7	−114.044 1	−113.763 7

Table 15 Excitation energies (ΔE, eV) from the $X^2\Sigma^+$ state of BeF at the different levels of approximation at R = 2.5 bohr

State	Hartree-Fock–asymptotic projection	MP2	CI [68]	Experiment [69]
$B^2\Sigma^+$	6.02	6.07	6.25	6.12
$B^2\Sigma^+$	6.22	6.36	6.69	6.24

5 Conclusions

We have presented a detailed description of open-shell SCF theory for the ground and excited states based on an easily implemented asymptotic projection method for taking the orthogonality constraints into account in eigenvalue problems which was proposed earlier. The effectiveness of such a SCF-asymptotic projection theory and its performance have been demonstrated:

(i) By solving the long-standing problem of off-diagonal Lagrange multipliers in open-shell self-consistent theory. We have considered an alternative to the Roothaan's open-shell technique that does not involve off-diagonal Lagrange multipliers. We have constructed a well-defined perturbation theory based on this technique which can be used to account for correlation effects.

(ii) We have given an example of the variational determination of excited electronic states having the same spatial and spin symmetry as the ground state. The results given above in *(i)* have thus been extended to excited state self-consistent theory and an analogue of the many-body Møller-Plesset perturbation theory for excited states has been developed.

Finally, it is worth pointing out the similarity between the SCF-asymptotic projection formalism developed here and the Optimized Effective Potential method for practical excited state calculations within density functional theory. Preliminary results can be found in the work of Glushkov, of Glushkov and Levy and of Glushkov and Gidopoulos [70–72].

Acknowledgment V.N.G. thanks Prof. A. Theophilou for useful and stimulating discussions during the early stages of this work.

References

1. C.C.J. Roothaan, *Rev. Mod. Phys.* **32**, 179, 1960.
2. S. Huzinaga, *Phys. Rev.* **120**, 866, 1960.
3. F.W. Birss and S. Fraga, *J. Chem. Phys.* **38**, 2552, 1963.
4. E.R. Davidson, *Chem. Phys. Lett.* **21**, 565, 1963.
5. J.P. Dahl, H. Johanson, D.R. Truax and T. Zeiger, *Chem. Phys. Lett.* **6**, 64, 1970.
6. V.A. Kuprievich and O.V. Shramko, *Int. J. Quantum. Chem.* **6**, 327, 1972.
7. K. Hirao and H. Nakatsuji, *J. Chem. Phys.* **59**, 1457, 1973.
8. K. Hirao, *J. Chem. Phys.* **60**, 3215, 1974.
9. D. Peters, *J. Chem. Phys.* **57**, 4351, 1972.
10. R. Albat and N. Gruen, *Chem. Phys. Lett.* **18**, 572, 1973.
11. R. McWeeny, *Chem. Phys. Lett.* **35**, 13, 1975.
12. R. McWeeny and B.T. Sutcliffe, *Methods of Molecular Quantum Mechanics*, Academic Press, New York, 1976.
13. R. McWeeny and G.H.F. Diercksen, *J. Chem. Phys.* **49**, 4852, 1968.
14. R. Carbo and J.M. Riera, in *Lecture Notes in Chemistry* v.5, G. Berthier, ed., Springer-Verlag, Berlin, 1978.

15. M.J. Frisch, G.W. Trucks, H.B. Schlegel, G.E. Scuseria, M.A. Robb, J.R. Cheeseman, J.A. Montgomery, Jr., T. Vreven, K.N. Kudin, J.C. Burant, J.M. Millam, S.S. Iyengar, J. Tomasi, V. Barone, B. Mennucci, M. Cossi, G. Scalmani, N. Rega, G.A. Petersson, H. Nakatsuji, M. Hada, M. Ehara, K. Toyota, R. Fukuda, J. Hasegawa, M. Ishida, T. Nakajima, Y. Honda, O. Kitao, H. Nakai, M. Klene, X. Li, J.E. Knox, H.P. Hratchian, J.B. Cross, V. Bakken, C. Adamo, J. Jaramillo, R. Gomperts, R.E. Stratmann, O. Yazyev, A.J. Austin, R. Cammi, C. Pomelli, J.W. Ochterski, P.Y. Ayala, K. Morokuma, G.A. Voth, P. Salvador, J.J. Dannenberg, V.G. Zakrzewski, S. Dapprich, A.D. Daniels, M.C. Strain, O. Farkas, D.K. Malick, A.D. Rabuck, K. Raghavachari, J.B. Foresman, J.V. Ortiz, Q. Cui, A.G. Baboul, S. Clifford, J. Cioslowski, B.B. Stefanov, G. Liu, A. Liashenko, P. Piskorz, I. Komaromi, R.L. Martin, D.J. Fox, T. Keith, M.A. Al-Laham, C.Y. Peng, A. Nanayakkara, M. Challacombe, P.M.W. Gill, B. Johnson, W. Chen, M.W. Wong, C. Gonzalez and J. A. Pople, Gaussian 03, Revision C.02, Gaussian, Inc., Wallingford CT, 2004.
16. M.W. Schmidt, K.K. Baldridge, J.A. Boatz, S.T. Elbert, M.S. Gordon, J.H. Jensen, S. Koseki, N. Matsunaga, K.A. Nguyen, S. Su, T.L. Windus, M. Dupuis and J.A. Montgomery J. Comput. Chem., 14, 1347–1363(1993); M.S. Gordon and M.W. Schmidt, in *Theory and Applications of Computational Chemistry: the first forty years*, edited by C.E. Dykstra, G. Frenking, K.S. Kim, G.E. Scuseria, Elsevier, Amsterdam, pp. 1167–1189, 2005.
17. B.N. Plakhutin and E.V. Gorelik, Breslavskaya, *J. Chem. Phys.* **125**, 204110, 2006.
18. I. Hubač and P. Čársky, Phys. Rev. **A22**, 2392, 1980.
19. S. Wilson, Theoret. chim. Acta. **61**, 343, 1984.
20. J.S. Andrews, D. Jayatilaka, R.G.A. Bone, N.C. Handy, and R.D. Amos, *Chem. Phys. Lett.* **183**, 423, 1991.
21. P.J. Knowles, J.S. Andrews, R.D. Amos, N.C. Handy and J.A. Pople, *Chem. Phys. Lett.* **186**, 130, 1991.
22. W.J. Lauderdale, J.F. Stanton, J. Gauss, J.D. Watts and R.J. Bartlett, *Chem. Phys. Lett.* **187**, 21, 1991.
23. C. Murray and E.R. Davidson, *Chem. Phys. Lett.* **187**, 451, 1991.
24. V.N. Glushkov, *Int. J. Quantum. Chem.* **99**, 236, 2004.
25. T.J. Lee and D. Jayatilaka, *Chem. Phys. Lett.* **201**, 1, 1993.
26. P.J. Knowles and N.C. Handy, *J. Phys. Chem.* **92**, 3097, 1988.
27. V.N. Glushkov, N.I. Gidopoulos and S. Wilson, *this volume*.
28. V.N. Glushkov and A.Ya. Tsaune, *Zh. Vychisl. Mat. Mat. Fiz.* **25**, 298, 1985; USSR Comp. Mathemat. Math. Physics, **25**, 196, 1986.
29. V.N. Glushkov, *J. Math. Chem.* **31**, 91, 2002.
30. V.N. Glushkov, *Opt. Spectrosc.* **93**, 11, 2002.
31. A.Ya. Tsaune, V.N. Glushkov and A.I. Aprashukhin, *J. Mol. Struct. (THEOCHEM)* **312**, 289, 1994.
32. V.N. Glushkov and A.Ya. Tsaune, *Chem. Phys. Lett.* **262**, 59, 1996.
33. V.N. Glushkov, *Chem. Phys. Lett.* **273**, 122, 1997.
34. V.N. Glushkov, *Chem. Phys. Lett.* **287**, 189, 1998.
35. N.I. Gidopoulos, V.N. Glushkov and S. Wilson, *Proc. R. Soc. Lond. A.* **457**, 1657, 2002.
36. V.N.Glushkov and S. Wilson, in: *Recent Advances in the Theory of Chemical and Physical Systems*, edited by J.-P. Julien et al., p. 107, Springer, Dordrecht, 2006.
37. V.N. Glushkov and A.Ya. Tsaune, *Opt. Spectrosc.* **87**, 267, 1999.
38. V.N. Glushkov and A.Ya. Tsaune, *Opt. Spectrosc.* **101**, 516, 2006.
39. H. Shull and P.-O. Löwdin, *Phys. Rev.* 1958, **110**, 1466, 1958.
40. K. Andersson and B.O. Roos, in: *Modern Electronic Structure Theory*, Part II, edited by D. Yarkony, pp. 55–109, World Scientific, Singapore, 1995.
41. V.A. Fock, *Z. Exsp. Teor. Fiz.* **10**, 961, 1940.
42. V.N. Glushkov and S. Wilson, *Int. J. Quantum. Chem.* **89**, 237, 2002.
43. V.N. Glushkov, *Opt. Spectrosc.* **100**, 807, 2006.
44. V.N. Glushkov and S. Wilson, *Int. J. Quantum. Chem.* **99**, 903, 2004.
45. K. Morokuma and S. Iwata, *Chem. Phys. Lett.* **16**, 195, 1972.

46. R. McWeeny, *Molec. Phys.* **28**, 1273, 1974.
47. J. Mrozek and A, Golebiewski, *Int. J. Quant. Chem.* **12**, 207, 1977.
48. E.R. Davidson and L.Z. Stenkamp, *Int. J. Quant. Chem. (Symp).* **10**, 21, 1976.
49. E.R. Davidson and E.L. McMurchie. in *Excited States* 1 **5**, 1, 1985.
50. R. Colle, A. Fortunelli and O. Salvetti, *Theor. Chim. Acta* **71**, 467, 1987.
51. N.I. Gidopoulos and A. Theophilou, *Phil. Mag.* **69**, 1067, 1994.
52. A. Theophilou, *J. Phys. C* **12**, 5419, 1979.
53. N.I. Gidopoulos, P.G. Papaconstantinou and E.K.U. Gross, *Phys. Rev. Lett.* **88**, 33003, 2002.
54. N.I. Gidopoulos, P.G. Papaconstantinou and E.K.U. Gross, *Physica B:* **318**, 328, 2002.
55. V.N. Glushkov and A. Theophilou, *Phys. Rev. A* **64**, 064501, 2001.
56. V.N. Glushkov and A. Theophilou, *J. Phys. B: At. Mol. Opt. Phys.* **35**, 2313, 2002.
57. M. Cohen and P.S. Kelly, *Can. J. Phys.* **43**, 1867, 1965.
58. H. Tatewaki, T. Koga, Y. Sakai and A.J. Thakkar, *J. Chem. Phys.* **101**, 4945, 1994.
59. Ch. Froese, *J. Chem. Phys.* **47**, 4010, 1967.
60. M.W. Schmidt and K. Ruedenberg, *J. Chem. Phys.* **71**, 3951, 1979.
61. E.S. Kryachko and S. Wilson, *Int. J. Quant. Chem.* **93**, 112, 2003.
62. I.D.Petsalakis , G.Theodorakopoulos , C.A. Nicolaides and R.J.Buenker, *J. Phys. B: At. Mol. Phys.* **20**, 2339, 1987; **20**, 5959, 1987.
63. C.D. Sherrill, T.J. van Huis, Y. Yamaguchi and H.F. Schaefer III, *J. Mol. Struct. (THEOCHEM)* **400**, 139, 1997.
64. C.W. Bauschlicher, Jr. and P.R. Taylor, *J. Chem. Phys.* **85**, 6510, 1986.
65. V.N. Glushkov, *Chem. Phys. Lett.* **244**, 1, 1995.
66. E.A. Hylleraas, *Z. Phys.* **65**, 209, 1930.
67. J. Harisson, *J. Chem. Phys.* **46**, 1115, 1967.
68. Stepanov N.F., Nemukhin A.V., Khrustov V.F. and Safonov A.A. in: *Stroenie molekul*, Moscow State Univ., p. 229–245, 1986.
69. K.P. Huber and G. Herzberg, *Molecular Spectra and Molecular Structure: IV Constants of Diatomic Molecules*, Van Nostrand Reinhold, New York, 1979.
70. V.N. Glushkov, *Opt. Spectrosc.* **99**, 684, 2005.
71. V.N. Glushkov and M. Levy, *J. Chem. Phys.* **126**, 174106, 2007.
72. V.N. Glushkov and N.I. Gidopoulos, *Int. J. Quant. Chem.* **107**, 2604, 2007.

$SU(m(\leq 4)) \times \mathscr{S}_{20} \downarrow A_5$ Group Branching Rules Revisited: Inverse Polyhedral Combinatorial Modelling via (λ) to $\{<\lambda'>\} \trianglerighteq \lambda_{SA}$ *SST* Maps

Francis P. Temme

Abstract Various mathematical physics concepts based on recent $\mathscr{S}_n$ group actions and combinatorical techniques associated with $\lambda \vdash n$ -based (λ) Schur functions, as well as their polyhedral-combinatorial models of (subgroup) invariance algebras, have been drawn on in this work to treat $m \leq 4$ partite dual G-branching, as an inherent aspect of spin algebras. In clarifying the detailed nature of projective mapping of augmented quasiparticles (superbosons) on Liouvillian carrier space (as outlined in [15, 22]), the role of group invariants in Liouville space generalised dual tensorial sets (derived from automorphic NMR spin physics) is discussed beyond techniques outlined in [11]; this is included here in the appendix material for completeness. In particular the potentially determinate $SU(m \leq 4) \times \mathscr{S}_{20} \downarrow A_5$ NMR spin subduction, together with its $SU(2) \times \mathscr{S}_{20}$ group invariants (or their cardinalities), are derived as branching rules (as analogues to the $[^{11}\mathrm{B}]_{20}[\mathrm{C}]_{40}$ borazafullerenes, or as in *encago* $[^{11}\mathrm{B}]_{20}$ cluster-based $(A)[X]_{20}$ NMR systems) i.e., via appropriate $(\lambda) = (\bar{r}_2\bar{r}_3)$, $(\bar{r}_2\bar{r}_3\bar{r}_4)$ Schur maps both in terms of model invariance sets and (λ) Schur function semi-standard tableaux (*SST*) decompositions onto (Kosktaweighted) $\{<\lambda>\}, \lambda \trianglerighteq \lambda_{SA}$ irrep sets.The results extend an earlier modelling of $SU(3) \times \mathscr{S}_{20} \downarrow A_5$ subduction [5], cf. with earlier *cycle-index studies* of [6]. For smaller n-fold systems, a proof (by exhaustion) of such types of subduction being *universal determinate* has been demonstrated in respect of the $[\mathrm{BH}]_{12}^{2-}$ NMR system [8], within the wider Cayley rule determinacy contexts of [7]. To demonstrate such a property here may not be so practical, on account of the much larger (λ) partite branching set.

Keywords: NMR spin dynamics, dual tensorial sets, automorphic spin symmetry, Schur-based G-subductional modelling

F.P. Temme
Department of Chemistry, Queen's University, Kingston-ON, K7L 3N6, Canada,
e-mail: temmef@ibis.chem.queensu.ca

S. Wilson et al. (eds.) *Frontiers in Quantum Systems in Chemistry and Physics*.

1 Introduction

The use, in the context of invariance algebra, of $(\lambda)(\mathbf{GL}_n)$ Schur modelling [1, 2] and its combinatorial algorithmic decompositions [3, 4] has proved invaluable in establishing certain branching rules [5] for natural subduction [6,7] of $SU(m) \times \mathscr{S}_n \downarrow \mathscr{G}$, for $m \leq n$ automorphic multispin NMR symmetries [6] and in the search for the universal determinacy [8] of many of these subduction-based symmetries, as exemplified (e.g.) by $SU(m) \times \mathscr{S}_{12} \downarrow A_5$. The study of such forms implies that the subduction -based invariance algebra is associated with unique numeric $\{\chi_i\}(\mathscr{S}_n \downarrow \mathscr{G})$ invariance sets [3,5,8]. For the indistinguishable multispin NMR problems under democratic recoupling, a knowledge of the system the scalar invariants, or of their group invariant cardinalities [9, 12] $|GI|^{(2n)}$, of the individual spin ensembles and of their spin systems (beyond Corio's Hilbert space views [13]) is of particular importance. This arises because of specific role of invariants in Liouvillian discussions of *tensorial set completeness* [9, 11]. It is in this context that Weyl's original views of the *role of time-reversal invariance (TRI) in physics* (via the properties of classic groups in group theory) [12] yields an interesting re-interpretation of a *specialised* $(\chi^{<\lambda>}(\mathscr{S}_n))$ (even) character-sum [9–11],for numeric $\mathscr{S}_n$ characters (of $< \lambda >$ group irreps given here in the Wybourne notation [1, 2]) themselves being derived from *standard combinatorial hooklength* considerations [4, 14]. The role of TRI and group invariants in NMR spin physics arise from their significance as invariant labels of Liouville superboson carrier subspaces leading to their role in defining tensorial set completeness. These ideas which date from 1993 [15] represent a *substantive augmentation of the (unlabelled) Hilbert dual projective mapping*, (e.g.) as discussed by Biedenharn and Louck [16] in the context of (Gel'fand shape-related) Hilbert space formalisms.

Because of the role of indistinguishability in point sets that describe $[A]_n X$, $[AX]_n$ identical NMR multispin ensembles naturally introduces the concept of democratic recoupling (DR) into tensorial sets and their associated *projective carrier space formalisms* [9–11, 17], it is now important to distinguish between the two types of point sets, with valid uses of graph recoupling and of its related Racah-Wigner algebraic(RWA) properties only pertinent to the earlier conventional point *distinct spin* sets. The specific properties [10,17] of indistinguishable point set -based specialised (Liouvillian) DR tensorial sets represent the principal focus of this work, because they necessarily underlies the NMR spin dynamics of systems under dual automorphic spin symmetries [18]. Such generalised systems also may be contrasted with the earlier restricted Hilbert treatment of DR quantum physics problems, such as those formulated via Lévi-Civitá projection operator techniques set out by Lévy-Leblond and Lévy-Nahas [19]. Here we shall be concerned with those that respond to the more general *semi-standard-tableaux* (sst) combinatorial techniques [4], or equivalent symbolic computational techniques of applied discrete mathematics [14]. Such techniques (in their Schur function -based format here, referred to as *polyhedral combinatorial modelling*) are pertinent to various post-1990 NMR studies, including that concerned with (e.g.) (dual) $SU(m) \times \mathscr{S}_{2n} \downarrow \mathscr{G}(A_5)$ natural subduction modelling of multispin ensemble NMR problems [3,5,8–11]. Naturally, these apply

in particular to various the $m \leq (2n) = 12, (20)$ ensemble systems under $\mathscr{S}_n \downarrow A_5$ *automorphic-group subduction*.

The role of TRI and $\mathscr{S}_n$ group invariants is more explicit in Liouville space NMR formalisms. This follows because both the projective mapping and DR tensorial sets of these formalisms directly utilise the invariants as sub-spatial mapping and group-action labels in projective formalisms and in arriving at the *tensorial completeness condition*. Insight into the specific subduction aspects of NMR automorphic spin symmetries and their branching rules [4, 14] draws on comparative studies of their $(\lambda)(\mathscr{G}\mathscr{L}_d)$ Schur decompositions and the corresponding (λ) invariance modelling onto the subduction group, i.e., as a quasi-geometric symmetry [3, 8].

Much of the conceptual background to this topic has been covered in treating the earlier $[^{\mu}\mathrm{B}H]^{2-}_{12}(SU(m) \times \mathscr{S}_{12}),\ \mu = 10, 11\ (m \leq 7, 4)$ borohydride anionic systems [8], or else in more recent work on $\{< \lambda > \longrightarrow \Gamma\}(SU(3) \times \mathscr{S}_{20} \downarrow A_5)$, i.e. for both $\lambda \trianglerighteq \lambda_{SA}$ - see Ref. [5], noting the use here of $< \hat{r}_2\hat{r}_3.. >$ reduced notation (omitting the leading partitional element of the conventional $[\lambda]$ irrep forms). Various aspects of invariant cardinality given here may be derived in terms of (recursive) unitary bijections. These actually yield the full range of $CFP(i)^{(n)}$ multiplicities, rather than simply the zeroth $CFP(0)^{(n)} = |GI|^n$ terms. Here these are specifically in the context of *Liouvillian descriptions* of the group invariants(GIs) as unitary bijective maps [9]; in the latter space, these results are no longer constrained to 'even' indexed GIs.

Recent mathematical physics work [20] has stressed the inherent limitations that attend the application of graph recoupling techniques to point-recoupled tensorial structures, i.e., strictly to simple point sets – rather than (multi-invariant) indistinguishable point sets and their dual tensorial sets of dual multispin NMR problems. Whilst this realisation is important, it does not highlight the severity of such restrictions, that comes from RWA algebra of quantum physics [21] also being graph-based in its origins; the Lévi-Civitá operator leads to additional cyclic commutation quantal properties [19] which are specific to the simple three-fold point multispin case. In consequence the study of indistinguishable (multi)spin tensorial structures in the context of superboson projective mapping [22] has a rather wider quantum physics significance. This places the $\mathscr{S}_n$ group, and its TRI-based invariants [23] in a more central focal position with respect to the formal quantal physics of reduced matrix algebra for *indistinguishable multi-point/multiparticle problems* to be analytic, i.e., within the completeness of the democratically recoupled tensorial set, $\{T^k_{\{\tilde{\nu}\}}(11.1)\}$, as specified by the set of $\{\tilde{\nu}\}((\mathscr{G}\mathscr{L}_n \supset .. \supset)\mathscr{S}_n)$-invariants and their associated cardinalities [9–11].

2 (λ) Schur SST Decomposition Onto $\{< \lambda' >\}$ Set for $\lambda, \lambda' \trianglerighteq \lambda_{SA}$

Earlier studies concerning $\mathscr{S}_n$ group properties, especially for $n = 12,\ 20$ algebras have shown [5, 7, 8] that only the pre λ_{SA} irreps are needed, and these for $\mathscr{S}_{20}$ case are defined by the various multipartite (sub)sets preceding:

$$\{[\lambda]\} \trianglerighteq \{[\lambda_{SA}]\} \,\big|\, (initial)\ (5)5442 \sim \lambda_{SA} \ > \ (A)21^8 \ \}\ , \tag{1}$$

the self-associate (alias self-conjugate) Schur subset $\{\lambda_{SA}\}$. Clearly the multipartite forms for these $\{\lambda_{SA}\}$ subsets all have a more extensive p-partite structure than the $p \leq 4$ partite Schur (or Schur model on $SU(4) \times \mathscr{S}_{20} \downarrow A_5$) forms, for the $[^{11}\mathrm{B}]_{20}$ spin ensemble discussed in detail in the text below, and/or summarised in the various tables. The approach adopted here, in the spirit of various earlier works cited above, develops a recursive series of correlations, essentially as a consequence of invoking semi-standard (tableaux (sst)) algorithmic decomposition(s) of pure $(\lambda)\mathscr{GL}_n$ Schur forms (of $\mathscr{GL}_n \supset .. \supset \mathscr{S}_n$ subgroup chain) on the first-hand, whilst on the other seeking their multicolour $(\lambda),\ \trianglerighteq \{\lambda_{SA}\},\ \equiv\ (\bar{r}_2\bar{r}_3(..\bar{r}_4))$ modelling as invariance properties, on the space of the natural automorphic subuction group $\mathscr{S}_{20} \downarrow A_5$.

Because the question of the existence of a unique set of invariance (sub)set(s) is central to retaining a viable bijection over the $SU(m)$ universal determinacy of the overall problem – as demonstrated in earlier work on the corresponding $[^{\mu}\mathrm{B}]_{12}, \mu = 10, 11$ spin-ensemble -based $SU(m) \times \mathscr{S}_{12} \downarrow A_5$ automorphic natural subduction symmetry-, it is natural to focus on the *multicolour invariance* problem, in part since the Schur-decompositional techniques themselves involve conventional semi-standard tableaux methods to enumeratively derive the $< \lambda' >$-based Koskta coefficient sets. These represents a well-established aspect of modern algorithmic combinatorics [1,2,4] which have been absorbed (along with other aspects of Schur λ-based discrete mathematics [2]) into a number of symbolic computational packages, including *SYMMETRICA* due to Kerber et al. [14] and the package *SCHUR* (due to Wybourne coworkers cited in Ref. [2]) in recent years. They are invaluable in handling higher multipartite Schur function sst-decompositions. There remains one further structural question in the presentation of the resultant branching rules given here. This arises because we have pursued a recursive approach in deriving the associated bijective mappings relating $(\lambda)\ to\ \Gamma(\mathscr{S}_{20} \downarrow A_5)$. By their nature, such recursive approaches preclude the use of traditional full matrix formulations for the branching rules, a point mentioned in our earlier work [5].

3 G-Subduction via Multicolour PC Schur Models from $\{(\lambda) \equiv \{\chi_i\}(\mathscr{S}_{20} \downarrow A_5)\}$ Invariance Sets

The invariance properties of such automorphic subduction symmetries are directly realisable as quasi-geometric multicolour polyhedral combinatorial models of the various $(\lambda = (\bar{r}_2\bar{r}_3)$, else $(\bar{r}_2\bar{r}_3\bar{r}_4))(\mathscr{S}_n)$ for $p = 3,4$ partite Schur functions, in the compact reduced (i.e., suppressed leading part) notation, (λ) cf. with similarly notated irreps denoted $< \lambda' >$. In the context of combinatorial decompositional considerations [4, 14], (e.g.) as illustrated in earlier initial conference report [5] for $(\bar{r}_2\bar{r}_3)$ Schur forms related to the $SU(3) \times \mathscr{S}_{20}(. \downarrow A_5)$ (automorphic) NMR spin symmetries. In constructing the requisite identity and class algebras, it is noted that the identity property has specific generalised forms for each of the $p = 2,3,4$ partite algebra, whereas the class algebras reduce to simple or modified combinatorial

Table 1 Illustrative (λ) reduced-Schur quasi-geometric projective modelling given here as $SU(3) \times \mathscr{S}_{20} \downarrow A_5$ characters, after the authors' earlier studies [5]. Since the Identity E is a simple monomial, its value has been suppressed here for brevity. The subsequent $\{\chi_i\}(C_i)$ derive directly (or in modified form in the C_{123} case) from combinatorial choices that is governed by the PC lattice point equivalent sets, being ten, six or four -fold sets. Such tabulations are illustrative of the primary data utilised in the models given. The subsequently derived complete set of irreps involving $p \leq 3$ branching rules [5], based on these observations, is summarised in Table 5 below, for completeness

$(\lambda), RSF$	$E, omitted$	$\chi(C_{()()})$	$\chi(C_{123})$	$\chi(C_{-5})$	$\chi(C'_{-5})$
(31)	.	0	12	0	0
(22)	.	90	0	0	0
..					
(6)	.	120	12	0	0
(42)	.	360	0	0	0
(33)	.	0	30	0	0
(61)	.	0	30	0	0
..					
(53)	.	0	30	0	0
(44)	.	1260	0	0	0
..					
(63)	.	0	60	0	0
..					
(A)	.	252	40	6	6
..					
(64)	.	2520	120	0	0
(55)	.	0	0	12	12
..					
(66)	.	4200	90	0	0
(76)	.	0	180	0	0

products, based on there being multipart sets on maximal ten (pair-), six (modified) (three-part-), and four (five-fold) sets associated with the various respective automorphic spin symmetry class operators. Tables 1 and 2 gives summaries of the derivation of the numeric invariance sets for these automorphic subductional algebra, $\mathscr{S}_{20} \downarrow A_5$; these results utilise the Schur sst- decompositional maps of Tables 3 and 4 for the respective $p = 3,4$ partite forms, with only $p = 3$ examples considered in the earlier report [5]. Such mapping[1] gives rise to a useful initial overview concerned with the question of the uniqueness of such invariance sets. Here the universal determinacy arises over the range of different $SU(m)$..-branched subuctional automorphic forms. The careful reader of the literature will have noted the similarities and distinctions from the three-space work of Harter and Reimer [26], based on $\mathscr{O}_n \supset .. \supset \mathscr{O}_3 \supset \mathscr{G}$ subduction processes as applied to fullerene – the analogous ^{13}C-fullerene cf[2] NMR spin structure, which has been discussed elsewhere [27, 28].

[1] Originally studied in the context of $[^2HC]_{20}$ dodecahedrane work Ref. [24] with pertinence also to the (*encageo*) $[^{14}N]_{20}$ azadodecahedrane structure of Bliznyuk et al. work [25].

[2] The inelastic neutron scattering cross-section can used to the study (as in [28]) the full subductional $SO(3) \downarrow G$ finite group (FG) including the symmetry-disallowed vibrations associated with conventional SO3-based spectroscopies.

Table 2 Illustrative $(r_2 r_3 r_4)(\mathscr{S}_{20})$ reduced-Schur -based quasi-geometric projective modelling over: $\{\chi_i\}$ $(E, C_{(12)(34)}, C_{123}, C_{1-5}, C'_{1-5})$ $(SU(4) \times \mathscr{S}_{20} \downarrow A_5)$ automorphic group characters. [Here the identity has the general analytic forms: $E = \binom{20}{s}\binom{s}{s'=r_3+r_4}\binom{s'}{r_4}$; the remaining $C_{(12)(34)}$s terms are enumerated by taking suitable (product) combinatorials derived from the maximal implicit sets, based on the respective ten, six and four-fold sets underlying the $C_{(12)(34)}$, *or* C_{123}, *or* C_{12345}, C'_{12345} operations.]

(λ)	E	$C_{(12)(34)}$	$C_{(123)}$	C_{-5}	C'_{-5}
(311)		.0	$2\binom{6}{1} = 12$	0	0
(222)		$2\binom{10}{3}\binom{3}{2} = 720$	0	0	0
(511)					
(421)					
(331)		0	$2\binom{6}{2}\binom{2}{1} = 60$	0	0
(322)					
(611)	.	0	$2\binom{6}{2} = 30$	0	0
(521)					
(431)	.	0	$= 60$	0	0
(422)	.	$2\binom{10}{4}\binom{4}{2} = 2520$	0	0	0
(332)	.	0	$\binom{6}{2}\binom{2}{1} = 30$		
(531)					
(441)					
(432)					
(333)	.	0	$\binom{6}{3}\binom{3}{2}\binom{2}{1} = 120$	0	0
(442)	.	$\binom{10}{5}\binom{5}{2}\binom{3}{1} = 7560$	0	0	0
(433)		0	$.2\binom{6}{3}\binom{3}{2}\binom{2}{1} = 240$	0	0
((9)911)	.	0	$2\binom{6}{3} = 90$	0	0
....					
(533)	.	0	$\binom{6}{3}\binom{3}{2}\binom{2}{1} = 120$	0	0
(443)	.	0	$2\binom{6}{3}\binom{3}{2}\binom{2}{1} = 240$	0	0
...					
((8)633)	.	0	$.\binom{6}{4}\binom{4}{2}\binom{2}{1} = 180$	0	0
...					
(444)	.	18900	.	.	.
((5)555)	.	0	0	$\binom{4}{3}\binom{3}{2}\binom{2}{1} = 24$	$.= 24$

4 $SU(4) \times \mathscr{S}_{20} \downarrow A_5$ Branching-rules & $SU(m)$ Determinacy Aspects

The use of quasi-geometric polyhedral combinatorial -modelled invariance, with the constraints mentioned above, is central to both total overall matrix solutions and the recursive form of calculation utilised here for higher-indexed symmetric group properties. In either formalism, there are three matrix quantities involved, where $\underline{K}^{-1}$, $\underline{X}^{-1}$ are the inverse-Kostka and inverse-character table matrices (with suitable $\mathscr{K}_{\lambda,\lambda'}$, and $\chi_{i,j}(\mathscr{S}_n)$ elements), respectively, whereas $\mathscr{T}_{\lambda,i}$ of $\underline{T}$ are the physical automorphic group invariances over (unit) class algebra, $\{\mathbf{1}(C_i)\}$ – corresponding here to the A_5 group irrep set $\{\mathscr{A}, \mathscr{G}, \mathscr{H}, \mathscr{T}_1, \mathscr{T}_3\}$. Hence individual subductional

Table 3 The (r_2), $(r_2 r_3)$, or $((r_2 r_3 r_4)) \rightarrow \{1\ldots\ldots;\ldots.1\}\mathscr{L}(\mathscr{S}_{20})$ semi-standard tableaux (*SST*)-derived mappings involving (unique) $\{K_{\lambda\lambda'}\}$ Kostka coefficient sets, with each derived from a specific (λ) (Reduced) Schur function

$(A) \longrightarrow \{1110100;10000\ 10000:\ 10000\ 10000;10000\ 10000;1\}\mathscr{L}$
..
(22) $\{1231220;1110\}$
(33) $\{1231420;3310\ \ 22200;\ 11101\ \}$
(44) $\{1231420;5310\ \ 4420;\ 33301\ \ 222020;\ 1110101\}\mathscr{L}$
(55) $\{1231420;5310\ \ 6420;\ 553010\ \ 444020;\ 33303010\ \ 22202020;\ 1110101010;\}\mathscr{L}$
(65) $\{1231420;5310\ \ 6420;\ 653010\ \ 554020;\ 55402000\ \ 44403010;\ 3330302000;$
$122020201;\ (--)1010101\ \}$
..
(75) $\longrightarrow$
$\{1231420;5310\ \ 6420;\ 653010\ \ 654020;\ 5540301\ \ 34403020;\ 1230302010;$
$(--)102010;\ (----)1010.\}\mathscr{L}$
(66) $\{1231420{:}5310\ \ 6420;\ 753010\ \ 664020;\ 5550301\ \ 34404020;\ 1230303010;$
$(--)102022;\ (----)1011\}$
(76) $\{1231420;5310\ \ 6420;\ 753010\ \ 764020;\ 5650301\ \ 34504020;\ 1230403010;$
$(--)102032;\ (----)1021;(..)1\}\mathscr{L}$

mapping in the recursive calculation become:

$$< \lambda > \longrightarrow \sum_{\lambda,i} \mathscr{K}^{-1}_{\lambda,\lambda'}\ \mathscr{T}_{\lambda,i}\ (\chi_i^{(0)}), \tag{2}$$

which, with retention of 1:1 bijective map uniqueness property, yields the requisite mapping defining the individual $[\lambda]$ recursive mapping approach used here as:

$$< \lambda > \longrightarrow \sum_{\lambda,i,j} \mathscr{K}^{-1}_{\lambda',\lambda}\ \mathscr{T}_{\lambda,i}\ \mathscr{X}^{-1}_{i,j}\ \Gamma'_j; \tag{3}$$

this shows that the origin of any (subsequent) indeterminacy would arise as the result of lack of independence in the automorphic subgroup invariance sets. Fortunately to the $p \leq 4$ branching level investigated here, the A_5 group algebra $(C_i)(\mathscr{S}_{20} \downarrow A_5)$ appears free of any random degeneracy(ies).

For completeness in the description of the concepts underlying such irrep branching rules, it is useful to outline the nature of the formal matrix approach associated with smaller index-based $\mathscr{S}_n$ group order cases. This takes the form:

$$(< \lambda >) \equiv \underline{K}^{-1}\ \underline{T}\ \left(\chi^{(0)}\right)^{\dagger} \tag{4}$$

for $(< \lambda >)$, $\left(\chi^{(0)}\right)^{\dagger}$ being respectively the unit $\mathscr{S}_n$ (reduced) irrep set $(= \mathscr{L})$ and the subgroup algebra (over unit $\{C_i\}^{\dagger}$ column vectors). Hence finally the full matrix approach, now in a suitable form for use with say $n \leq 10$ indexed symmetric group mappings, is defined by the expression:

$$(< \lambda >) = \underline{K}^{-1}\ \underline{T}\ \underline{X}^{-1}\ \ \left(\Gamma'\right)^{\dagger}, \tag{5}$$

Table 4 The $SU(4) \times \mathscr{S}_{20}$-based reduced-Schur decompositions yielding the $\{K_{\lambda,\lambda'}\}$ sets of Kostka coefficients, over $\{<\lambda>\} \equiv \mathscr{L}$ for $(\lambda) = (r_2 r_3 r_4) \longrightarrow \{..\}\mathscr{L}$, where $\mathscr{L}$ is column listing of is a reduced $\mathscr{S}_n$ (descending order) listing: $\{<0> .. \; to \; .. <\lambda_{SA}>\}$, generally in single hexadecimal notation

$(111) \longrightarrow$
{1333121; }$\mathscr{L}$
(211) {1343341;12110 00 }
(311) {1343441;34110 121100;}
(221) {1353561;35320 122110;}
(411) {1343441;44110 341100; 121100}$\mathscr{L}$
(321) {1353661;57320 354210; 1221110}
(222) {1363781;69630 366330; 12311201}

(511) {1343441;44110 441100; 3411000 1211000;}$\mathscr{L}$
(421) {1353661;67320 574210; 35421100 1221110;}
(331) {1353761;79320 586310; 35523200 122121010;}
(322) {1363881;8B630 6A9430; 36733401 1231220110;
(611) {1343441;44110 441100; 44110000 3411000000; 1211000}$\mathscr{L}$
(521) {1353661;67320 674210; 57421100 3542110000; 12211100}
(431) {1353761;89320 7A6310; 587332000 3552420100; 1221210110;}
(422) {1363881;9B630 8C9430; 6AA434010 3673440110; 12312201110;}
$(332) \longrightarrow$
{1363981;AD630 9EC530; 6BC566010 3683650320; 12313201210010;}
$(711) \longrightarrow$
{1343441;44110 441100; 441100000 4411000000; 3411000000; 121100;}
(621) {1353661;67320 674210; 674211000 5742110000; 3542110000; 12211100;}
(531) {1353761;89320 8A6310; 7A7332000 5873420100; 3552420110; 12212101100;}$\mathscr{L}$
(522) {1363881;9B630 9C9430; 8CA434010 6AA4440110; 36734401110; 12312201110;}
(441) {1353761;99320 9C6310; 7B9432000 5883630100; 35525203200; 12212102100010;}
(432) {1363981;BD630 B$\widehat{11}$C530; 9FF6660100 6BD5970320; 36837503420010;
1231320221001100;}
$(333) \longrightarrow$
{1363A81;CF630 C$\widehat{13}$F630; A$\widehat{1212}$A8010 6CF6C90630;
36939603630030; 12314202310012000 01;}$\mathscr{L}$

The first self-associate Schur function occurs at $\lambda_{SA} \equiv (5)(5442)$, $for\ p = 5$ part form, with the final SA-form (in hexadecimal notation) being denoted $\lambda_{SA} \equiv (A)21^8$. The ordering of the $\mathscr{S}_n$ group irreps (each in hexadec. or two-digit hatted hexadec.) on which the $K_{\lambda\lambda'}$ act denoted here by $\mathscr{L}$, is (in reduced irrep notation) taken in lexical order as: $<0>, <1>, <2>, <11>, ...$ Beyond n-3 suppressed elements, the '; ' symbol indicates a break in an 'even' sequence, whereas odd sequences starts with a space

and its inverse relationship. Here the unit $(\Gamma'(A_5))$ irrep forms has been retained, as given above in the earlier context.

5 Contextual Discussion

By utilising a recursive formulation for branching rules involving $\mathscr{S}_{20} \downarrow A_5$ natural subduction (onto the automorphic finite group $A_5 \equiv I$), it has been shown above that the quasi-geometric projective view furnishes one with further determinable

1:1 bijection sets, beyond those reported earlier [5]. Such mappings, to the $p \leq 4$ branching level investigated here, are found to be free of random accidental degeneracies in this λ model-based invariance algebra. For simple Hilbert spin space, it is clear that these PC combinatorial techniques represent extended generalisations of either empirical multispin- $(1/2)$ views from an earlier NMR era [29], or to other approaches such as those discussed in the works of Flurry and Siddall [30], or that of Siddall [31]. The involvement of *particle indistinguishability* over $\mathscr{S}_{n\geq 4}$ algebras, introduces the question of the DR structure and completeness of multi-invariant dual tensorial sets, based on:

$$GL_n \supset .. \supset \mathscr{S}_n \supset \mathscr{S}_{n-1} \supset .. \supset \mathscr{S}_2\,, \tag{6}$$

chain-based DR properties - in contrast to the analogous unitary group chains, or orthogonal group chains.

For the dominant $J_{intracluster}$ models discussed here, clearly the dual tensorial sets and their Liouvillian $\{T^k_{\{\tilde{\nu}\}}(1..11)\}$ set completeness, based on the $\{\tilde{\nu}\}(GL_n..\mathscr{S}_n)$ invariant sets, as strictly symmetric group chain-based properties – incompatible cf. with either $\mathscr{O}_n$ chains, or with the restricted SO(3) view of tensorial sets, as proven by Galbraith in his classic 1971 work [32] on the existence of non-analytic forms inherent in $n \geq 4$ *identical body (multi-invariant)* vibrational analyses. The discussion given in a recent mathematical work [20] stresses that *indistinguishable point/spin sets* are not consistent with either the traditional unitary chain, or graphical recoupling properties. Since these were utilised in RWA approaches in various earlier Liouvillian NMR spin dynamics studies [33], the general use of tensorial methods in spin dynamics needs to be re-examined, essentially because known applicable RWA mathematics is restricted to discrete point/spin sets and bases describing simple mono-invariant tensorial sets.

Underlying the actual problem of higher $SU(m) \times \mathscr{S}_{20}$ algebras discussed here, there remains still the question of dual tensorial set roles in analytic descriptions of Liouvillian NMR, including the completeness question for $SU(2) \times \mathscr{S}_{n=20}$ covering group. Whilst use of the correct group subduction chain holds one key to obtaining analytic solutions to handling spin problems, the necessary use of the scalar invariant(s) within the quantum labelling, as in Ref. [19] – initially to generate additional commutator relationships that then utilise a slightly modified RWA algebra-, as yet appears limited in scope to mono-invariant $\mathscr{S}_3$ spin systems.

6 Some Concluding Comments

No satisfactory general treatment of extensive *multi-invariant* problems involving *indistinguishable point/spin sets* and their Liouvillian tensorial sets has appeared to date. This is essentially because no further general analogues exist for a augmented equivalent n-fold operator forms to the long-established $\mathscr{S}_3$-specificaction

[19] Lévi-Civitá operator. These comments stress the importance of the point made by Atiyah and Sutcliffe [20] i.e., that graph-recoupling (and in consequence direct simple RWA analytic methods) are strictly limited to distinguishable point sets and thus (from the above and Ref. [17]) their corresponding (Liouvillian) tensorial sets are governed by a *single invariant*, rather than more general DR tensors, based on wider dual projective (carrier subspace) techniques [9].

From earlier discussions of (Liouvillian) disjoint carrier subspace (superboson) mapping [15,17], but note cf.[3], the use of permutation group chain(s) and a further δ condition are necessary conditions to the quantal physics of indistinguishable point sets. Beyond systems governed by the Lévi-Civitá operator-induced commutations (of Ref. [19]), a further *sufficiency* condition is needed to treat multi-invariant -based problems as implied by the views expressed in Ref. [20]. This would seem to imply the need for a new permutational group equivalent formalisms to the RWA algebras of graph theory, in order to eventually treat *indistinguishable point set, multi-invariant* -based spin problems. This is a deep open theoretic question which arises as consequence of the Atiyah and Sutcliffe [20] assertion concerning the limitations of graph recoupling, i.e., that such formalism are only applicable to distinct points-sets and their related non-DR tensorial forms (e.g. those set out in Ref. [33]- based on the 1976 Sanctuary distinct point set-based work cited therein).

The main focus of this article has been on mappings under specific branching rules for $\mathscr{S}_{20} \downarrow A_5$, down to $p = 4$ multipartite level set out in Tables 3–6. The question of universal determinacy over m-partite-branched forms of the full weight set (beyond the highest specific mappings discussed here, e.g., Table 6) has not been resolved as yet for practical reasons; this is mainly on account of the depth of branching which generates too numerous intervening m-partite forms prior to last of the $\lambda_{SA}(= (A)(21^8))$ form. To highlight both the contributions arising from studying Liouville space projective properties and to appreciate the nature of the open theoretical questions arising in studying indistinguishable point-sets and multi-invariant tensorial sets, some brief reference to $SU(2) \times \mathscr{S}_n$ carrier space properties discussed in Refs. [9, 17, 22] has been included here. Recent progress in applicable $(\lambda)(\mathscr{GL}_n(\supset .. \supset \mathscr{S}_n))$ -based combinatorial mathematics within suitable subchain context would seem to offer some hope for future insight into the *indistinguishable point set/ multiple invariant tensorial* formulation of eigenvalue-problems in dynamical spin physics. The original development of disjoint carrier subspace projective views [15, 17, 22], as being only realisable in Liouville space formalisms, arose from a comparative simple reducibility(SR) study of unitary and symmetric group algebras. This arose in the context of combinatorially-defined Liouvillian $T^k_{\{\tilde{\nu}\}}(11.1)(SU(2) \times \mathscr{S}_n)$ tensorial set completeness [9, 22], cf. to the simpler combinatorial forms of Hilbert space basis completeness – as originally

[3] One notes here that explicit invariant labelling of carrier subspaces only occurs in *Liouville space formalisms* [15, 15, 22]; however such labelling is not a feature of the original Hilbert space boson projection techniques of Biedenharn and Louck [16].

Table 5 Group Branching Rule Mappings (from independent sets of automorphic subduction group invariance, see Ref. [5]) for $< \bar{r}_2 \bar{r}_3 >$ (reduced λ-notated) onto $SU(\leq 3) \times \mathscr{S}_{20}$ irreps and subsequently onto $\Gamma(\mathscr{S}_{20} \downarrow A_5)$ $(\equiv \{A, G, H, T_1, T_3\})$ automorphic group representations mappings, for labels as used in Harter and Weekes' work [26]

$< \lambda >$, RSF;	χ_E:	A	G	H	T_1	T_3
$< 5 >$	10659	166	707	879	545	545
$< 41 >$	43776	728	2920	3648	2188	2188
$< 32 >$	55575	915	3705	4620	2790	2790
$< 6 >$	23256	419	1555	1965	1132	1132
$< 51 >$	121125	1995	8070	10080	6075	6075
$< 42 >$	223839	3811	13921	18732	11114	11114
$< 33 >$	125970	2040	8406	10422	6366	6366
$< 7 >$	38760	621	2589	3195	1968	1968
$< 61 >$	248064	4138	16538	20670	12404	12404
$< 52 >$	604656	10013	40309	50331	30292	30292
$< 43 >$	620160	10344	41352	51672	31008	31008
$< 8 >$	48450	855	3225	4095	2370	2370
$< 71 >$	377910	6276	25194	31470	18918	18918
$< 62 >$	1,162800	19560	77520	97080	57960	57960
$< 53 >$	1,705440	28319	113711	141985	85392	85392
$< 44 >$	872100	14760	58140	72900	43380	43380
$< 9 >$	41990	649	2801	3445	2152	2152
$< 81 >$	413440	6884	27556	34460	20672	20672
$< 72 >$	1,598850	26490	106590	133080	80100	80100
$< 63 >$	3,100800	51690	206730	258390	155040	155040
$< 54 >$	2,848860	47686	189904	237650	142218	142218
$< A >$	16796	352	1124	1456	778	778
$< 91 >$	277134	4611	18483	23079	13866	13866
$< 82 >$	1,469650	24755	97975	122735	73220	73220
$< 73 >$	3,779100	62895	251955	314805	189060	189060
$< 64 >$	5,038800	84405	335925	420315	251520	251520
$< 55 >$	2,469012	40485	164571	205131	124098	124098
$< 92 >$	604656	9828	40308	50136	30486	30486
$< 83 >$	2,687360	44776	179133	223960	134368	134368
$< 74 >$	5,290740	87519	352701	440265	265182	265182
$< 65 >$	4,837248	80576	322448	403144	241860	241860
$< 84 >$	2,309450	28950	153950	192940	115000	115000
$< 75 >$	4,157010	69471	277149	346575	207678	207678
$< 66 >$	2,217072	37426	147850	185126	110435	110435
$< 76 >$	1,385670	22842	92388	115200	69546	69546

reported by Biedenharn and Louck in their classic boson-pattern algebraic mapping work [16].

The essence of the $SU(3)..$, $SU(4) \times \mathscr{S}_{20} \downarrow A_5$ present modelling results are set out in Table 2, and in Tables 4–6; here the present work amplifies our earlier brief report [5]. For a wider view of the value of applicable combinatorial mathematics in physics the report of King [2] on the properties of Schur functions and extensive views expressed by other contributors to the Wybourne commemorative physics meeting should be consulted, e.g., [2, 5, 9, 11] *et loc. cit.*.

Table 6 The final overall mappings central to this work. Here, the $p = 4$ partite reduced Schur fn. Maps onto both the Invariance Set $\{.,.,.,.,.\}(\chi^{(0)})^{\dagger}$ and then maps (with coefficients shown) onto the $A_5 \equiv \mathscr{I}$ Automorphic NMR Spin Group Irrep set, where $\Gamma'^{\dagger}$ is the irrep unit column vector

$< \bar{r}_2\bar{r}_3\bar{r}_4 >$	$\{E$	$C_{()()}$	C_{123}	C_5	$C'_5\}$	$(A,$	$G,$	$H,$	$T_1,$	$T_3)$ $(\Gamma')^{\dagger}$
$< 111 >$	969	9	6	−1	−1	20	67	81	46	46
$< 211 >$	11475	−45	0	0	0	180	765	945	585	585
$< 311 >$	67184	80	−1	4	4	1141	4477	5619	3340	3340
$< 221 >$	56525	−35	5	0	0	935	3770	4700	2835	2835
$< 411 >$	250800	−240	15	0	0	4125	16,725	20,835	12,600	12,600
$< 321 >$	408576	0	−24	−4	−4	6800	27,232	34,056	20,428	20,428
$< 222 >$	129675	315	18	0	0	2246	8651	10,879	6405	6405
..										
$< 511 >$	654,075	315	0	0	0	43,605	10,980	54,585	32,625	32,625
$< 421 >$	1574,625	−75	−15	0	0	26,220	104,970	131,205	78,750	78,750
$< 331 >$	959,310	270	0	0	0	16,056	63,954	80,010	47,898	47,898
$< 322 >$	969969	1125	−6	4	4	16,447	64,661	81,114	48,218	48,218
..										
$< 611 >$	1,234506	−630	−6	−4	−4	20,414	82,300	102,720	61,882	61,882
$< 521 >$	3,969024	0	−36	4	4	66,140	264,588	330,764	198,452	198,452
$< 431 >$	4,476780	−420	−69	0	0	74,485	298,429	372,983	223,944	223,944
$< 422 >$	3,627936	1440	60	−4	−4	60,844	241,884	302,668	181,036	181,036
$< 332 >$	2,771340	−2340	6	0	0	45,606	184,758	230,358	139,152	139,152
..										
$< 711 >$	1,679600	720	20	0	0	28,180	111,980	140,140	83,800	83,800
$< 621 >$	6,928350	−90	−30	0	0	115,440	461,880	577350	346,440	346,440
$< 531 >$	11,337300	−420	−45	0	0	188,835	755,805	944,670	566,970	566,970
$< 522 >$	8,527200	−1440	120	0	0	142,160	568,520	710,290	426,720	426,720
$< 441 >$	6,046560	−1800	60	0	0	100,346	403,124	50,3410	302,778	302,778
$< 432 >$	12,403200	−480	3	0	0	206,601	826,881	1033,479	620,280	620,280
$< 333 >$	3,197700	4140	117	0	0	54,369	213,219	267,471	158,850	158,850

Acknowledgements Members of the Kerber-Kohnert-Lascoux combinatorial mathematics group of Bayreuth Mathematiks Inst. II are warmly thanked for the provision of a copy of their SYMMETRICA package and Dr Axel Kohnert for his kind assistance with its platform implementation on various additional UNIX/LINUX -based machines. Support for this combinatorics-in-physics research from NSERC of Canada is acknowledged.

7 Appendix

Whilst the full $\{< \lambda >\}$ sets of the $[^{10}\mathrm{B}]_{20}$ (sub)ensemble with their $SU(m \leq 7)$ -based group symmetries and extensive subset of $\{\lambda_{SA}\}$ terms lies beyond what is considered here, some initial Schur decompositions for the SU(5) branching level are given in Table A.1 to indicate the practical problems involved in handling such problems. An initial calculation of a single example based on reduced notation yields the expression:

$$< 1^4 > \equiv \{15,521,-179,5,1,1\}(\chi^{(0)})^{\dagger}, \tag{7}$$

Table A.1 Some initial $\lambda = (r_2 r_3 r_4 r_5)$ RSF Decompositional Mappings onto the $[\lambda'](SU(5) \times \mathscr{S}_{20})$ -based sets (showing sets of actual Koskta weights), the initial λs being a modest set from the extensive $\hat{\mathbf{f}}_{\mathbf{i}} = 3$, $[^{10}B]_{20}$ ensemble properties, with only non-trivial weights for extensive sets of λ' (RH) terms shown. Each of the λ RSFs is associated with a specific high-weight set of expanding Kostkas. The numeric letters generally refer to single-symbol hexadecimal notation, with the exception of the $\hat{}$ hatted entries, which are double-symbol (hexadecimal) weight forms. Naturally, these sst-tableaux -based maps are greatly facilitated by the combinatorial methods referred to in the text

$(1^4) \longrightarrow$	1466 484; 13231;		
(21^3)	1476 7*B*4; 49561;	1333210;	
(31^3)	1476 8*B*4; 7*C*561;	4966210; 1333121;	
(221^2)	1486 *AE*4; $8\widehat{20}991$;	4*AA*8620; 134324111;	
(41^3)	1476 8*B*4; 8*C*561;	7*C*66210; 4966121000;	1333121;
(321^2)	1486 *BE*4; $B\widehat{23}991$;	$8\widehat{21}EB620$; 4*AB*8582110;	1343341211;
(2^31)	1496 $D\widehat{21}4$; $D\widehat{28}EC1$;	$9\widehat{25}\widehat{25}FC30$; 4*BFA*7*E*34300;	135346133201;
(51^3)	1476 8*B*4; 8*C*561;	8*C*66210; 7*C*661210;	49661210000; 1333121;
(421^2)	1486 *BE*4; $C\widehat{23}991$;	$B\widehat{24}EB620$; $8\widehat{21}FB582110$;	4*AB*86822110; 13433411211;
(3311)	1486 *CE*4; $D\widehat{26}991$;	$C\widehat{28}\widehat{22}E620$; $8\widehat{22}\widehat{23}D9C311$;	4*AC*8*AA*26220; ↙ ↪ 13434412411011

a result which maps onto the unit (subductional) automorphic irrep set. This gives the first of the $SU(5) \times \mathscr{S}_{20} \downarrow A_5$ set of mappings, e.g.:

$$< 1^4 > \longrightarrow \{216, 1036, 1247, 821, 821\}(\Gamma)^{\dagger}. \tag{8}$$

The extensiveness of the higher $SU(4 < m \leq 7)$ partitional set precludes any immediate derivation of the (exhaustive) proof of universal determinacy question, comparable to that derived for the earlier $[^{10}\mathrm{B}]_{12}$ spin subensemble problem [8].

8 Glossary of Notation

The notation adopted here retains earlier usage (essentially defined in the text), with RS(F), RWA, DR, and TRI referring respectively to: reduced-notation Schur functions: Racah-Wigner algebra: democratic recoupling: and, time-reversal Invariance, or **T** of **CP/CPT**. In addition, the SA labels refer to the self-associate (else self-conjugate) Schur function of irrep forms, 'sst' refers to the 'semi-standard tableaux' methods of enumeration, and CFP to weightings (from recoupling theory) known as 'coefficients of fractional parentage'. The term *automorphic group* [18] refers to the spin symmetries which are induced by the internal structure of the (mobile media) NMR Hamiltonian (Liouvillian) – i.e., as distinct from SO(3)/ three-space -related physical FG symmetry(ies) of other (non-NMR-spin) spectroscopic problems. In

the former NMR symmetry context, it is stressed that three-space FG-like effects in NMR are strictly limited to **P** parity (of **CP/CPT**), as a *residual particle symmetry*.[4]

References

1. B.G. Wybourne, *Symmetry Principles in Atomic Spectroscopy*, (Wiley, New York, 1970).
2. R.C. King, in: *Symmetry, Spectroscopy, & SCHUR*, (M-K Press, Torun, 2006) pp 163–70.
3. F.P. Temme, J. Math. Chem., **24**, 133 (1998).
4. B.E. Sagan, *Symmetric Group: Its Representations, Algorithmic Combinatorics & Symmetric Functions*, (Springer. Berlin, 2001).
5. F.P. Temme, B.C. Sanctuary, in: *Symmetry, Spectroscopy & SCHUR*, (M-K Press, Torun, 2006) pp 271–280.
6. K. Balasubramanian, Chem. Phys. Lett., **391**, 64; **391**, 69 (2002).
7. F.P. Temme, Molec. Struct. (Theochem.), **548**, 145 (2002); *Idem*, Int. J. Quantum Chem., **78**, 71 (2002).
8. *Idem.*, Eurphys. J., **B11**, 177 (1999).
9. *Idem*, Theo. Phys. Chem. **XII** (this publ.) (Springer, 2008), chap. 11
10. *Idem.*, Unpubl'd MS. (2008/9; to be publ'd.)
11. F.P. Temme, J. Phys.: Math & Theo., **A 41**, 015210 (2008).
12. H. Weyl, *Representation & Invariants of Classic Groups*, (Univ. Press, Princeton, 1946).
13. P.L. Corio, J. Magn. Reson., **134** 131 (1998).
14. A. Kerber, A. Kohnert, A. Lascoux, J. Symbol. Comput., **14**, 195 (1993).
15. F.P. Temme, Physica **A198**, 245 (1993).
16. J.D. Louck, L.C. Biedenharn, in: *Permutation Group in Physics & Chemistry*, (Springer, Heidelberg, 1979) pp 121–148.
17. F.P. Temme, Proc. R. Soc., Lond., **A461**, 341 (2005).
18. K. Balasubramanian, J. Chem. Phys., **78**, 6358 (1983).
19. J.M. Lévy-Leblond, M. Lévy-Nahas, J. Math. Phys., **6**, 1372 (1965).
20. M.F. Atiyah, P.M. Sutcliffe, Proc. R. Soc., Lond., **A458**, 1089, (2002), *et loc. cit.*
21. L.C. Biedenharn, J.D. Louck, *Angular Momentum Theory; Racah-Wigner Algebras*, [Vols. 8, 9 Encyclopaedia of Mathematics], (Cambridge University Press, Cambridge, 1985).
22. F.P. Temme, Int. J. Quantum Chem., **89**, 429 (2002).
23. R.G. Sachs, *Time-reversal in Physics*, (Univ. Press, Chicago, 1987).
24. F.P. Temme, Chem. Phys. Lett., **200**, 534 (1997).
25. A. Bliznyuk, M. Shen, H.F. Schaefer, Chem. Phys. Lett., **198**, 249 (1992).
26. W.G. Harter, J. Reimer, *ibid.*, **198**, 429 (1992).
27. F.P. Temme, C.E. Mitchell, M.S. Krishnan, Mol. Phys., **79**, 953 (1993); (also see:) F.P. Temme, Physica A**227**, 314; A **230**, 313 (1996), *et loc. cit.*.
28. J.D. Axe, S.C. Moss, D.A. Neuman, Sol. State Phys., **48**, 149 (1994).
29. D. Whitman, J. Mol. Spectrosc., **10**, 1372 (1962).
30. R.J. Flurry, T.H. Siddall-III., Phys. Rev. B**31**, 4513 (1985); *Idem.*, in: *Adv. in Group Theory* (Ed. J.C. Donini), (Plenum, New York, 1979).
31. T.H. Siddall-III. J. Phys. Chem., **86**, 91 (1982).
32. H.W. Galbraith, J. Math. Phys., **12**, 782; 2380 (1971).
33. B.C. Sanctuary, T.K. Halstead, Adv. Opt. Magn. Reson., **15**, 97 (1991). *et loc. cit.*.

[4] This point is all too frequently overlooked in the NMR lit.. It has lead to some totally false assertions, such as the one, that bis-quadrupolar relaxation can cause symmetry-breaking, it *cannot*! Those of us familiar with earlier texts and lit. on NMR [34–36] deeply regret all of these recent inconsistencies, i.e., that arise from totally disregarding the true nature of $\hat{\mathbf{L}}$-based *automorphic NMR spin-alone symmetry*, that it is *not* an actual R_3 space phenomena.

34. J.W. Emsley, J. Feeney, L.H. Sutcliffe, *Nuclear Magnetic Resonance*, (Pergamon, Oxford, 1967)
35. A. Abragam, *Nuclear Magnetism*, (OUP, Oxford, 1962).
36. R.G Jones, R.C. Hirst, H.J. Bernstein, Canad. J.Chem., **43**, 683 (1965).

Gauge-Invariant QED Perturbation Theory Approach to Calculating Nuclear Electric Quadrupole Moments, Hyperfine Structure Constants for Heavy Atoms and Ions

Alexander V. Glushkov(✉), Olga Yu. Khetselius, Elena P. Gurnitskaya, Andrey V. Loboda, Tat'yana A. Florko, Denis E. Sukharev, and Ludmila Lovett

Abstract Relativistic calculation of the spectrum hyperfine structure parameters for heavy atoms and multicharged ions with an account of the relativistic, correlation, nuclear, quantum electrodynamics (QED) effects is carried out. Our calculation method is based on the gauge-invariant QED perturbation theory (PT) with using the optimized one-quasiparticle representation firstly in the theory of the hyperfine structure for relativistic systems. The energies and constants of the hyperfine structure, derivatives of the one-electron characteristics on nuclear radius, nuclear electric quadrupole, magnetic dipole moments Q for atom of the hydrogen ^{1}H (test calculation), superheavy H-like ion with nuclear charge $Z = 170$, Li-like multicharged ions with $Z = 20 \div 100$, neutral atoms of ^{235}U, ^{201}Hg and ^{227}Ra are calculated.

Keywords: atom, quantum electrodynamics, perturbation theory, hyperfine structure

1 Introduction

Traditionally an investigation of spectra of the heavy and superheavy elements atoms and ions is of a great interest for further development atomic and nuclear theories and different applications in the plasma chemistry, astrophysics, laser physics,

A.V. Glushkov
Inst. of Spectroscopy (ISAN), Russian Acad. Sci., Troitsk-Moscow, 142090, Russia;
Odessa University, P.O. Box 24a, Odessa-9, 65009, Ukraine, e-mail: glushkov@paco.net

O.Yu. Khetselius
Odessa University, P.O. Box 24a, Odessa-9, 65009, Ukraine;
Abdus Salam International Centre for Theoretical Physics Strada Costiera, 11 - 34014 Trieste, Italy

E.P. Gurnitskaya, A.V. Loboda, T.A. Florko and D.E. Sukharev
Odessa University, P.O. Box 24a, Odessa-9, 65009, Ukraine and L. Lovett
UK National Academy of Sciences and Bookdata Co., London SW1Y 5AG, UK

S. Wilson et al. (eds.) *Frontiers in Quantum Systems in Chemistry and Physics*.

etc. (cf. [1–73]). Theoretical methods of calculation of the spectroscopic characteristics for heavy and superheavy atoms and ions may be divided into a few main groups [1–25], [43–67]. First, the well known, classical multi-configuration Hartree-Fock method (as a rule, the relativistic effects are taken into account in the Pauli approximation or Breit hamiltonian etc.) allowed to get a great number of the useful spectral information about light and not heavy atomic systems, but in fact it provides only qualitative description of spectra of the heavy and superheavy ions. Second, the multi-configuration Dirac-Fock (MCDF) method (cf. [3–10, 16–20, 50]) is the most reliable version of calculation for multielectron systems with a large nuclear charge. In these calculations the one- and two-particle relativistic effects are taken into account practically precisely. The calculation program of Desclaux (the Desclaux program, Dirac package) is compiled with proper account of the finiteness of the nucleus size. However, a detailed description of the role of the different nuclear effects (finite nuclear size etc.) is lacking. Though, in last years there is a great progress in this topic. Naturally, the well known relativistic density functional Dirac-Kohn-Sham approach [48] (cf. also [49, 72]) should be mentioned.

In a region of the small Z (Z is a charge of the nucleus) the calculation error in the MCDF approximation is connected mainly with incomplete inclusion of the correlation and exchange effects which are weakly dependent on Z. In studying the lower states for ions with $Z \leq 40$, an expansion into the PT double series on the parameters $1/Z$, αZ (α is the fine structure constant) is often used. It permits an evaluation of the relative contributions of the different expansion terms: non-relativistic, relativistic, QED contributions as the functions of Z. Nevertheless, the serious problems in calculation of the heavy element spectra leads to a necessity of developing new, high exact methods of account for the QED effects, in particular, the Lamb shift (LS), self-energy (SE) part of the Lamb shift, vacuum polarization (VP) contribution, correction on the nuclear finite size for superheavy elements and its account for different spectral properties of these systems (the energies and constants of the hyperfine structure, derivatives of the one-electron characteristics on nuclear radius, nuclear electric quadrupole, magnetic dipole moments etc. (cf. [1–38, 54–73])). In this essence it should be given special attention to two very general and important computer systems for relativistic and QED calculations of atomic and molecular properties developed in the Oxford group and known as GRASP (“GRASP”, “Dirac”; “BERTHA”, “QED”, “Dirac”) (cf. [68–73] and references there). In particular, the BERTHA program embodies a new formulation of relativistic molecular structure theory within the framework of relativistic QED. This leads to a simple and transparent formulation of Dirac-Hartree-Fock-Breit (DHFB) self-consistent field equations along with algorithms for molecular properties, electron correlation, and higher order QED effects. The DHFB equations are solved by a direct method based on a relativistic generalization of the McMurchie-Davidson algorithm for molecular integrals that economizes memory requirements and is not significantly more expensive computationally than comparable nonrelativistic calculations (cf. [69, 70]).

The useful overview of relativistic electronic structure theory is presented in Ref. [72] from the point of view of QED. The participation of the negative-energy states in practical calculations is described from complementary points of view, in

order to illustrate how they enter into the operation of relativistic mean-field theories. Examples of the implementation of relativistic electronic structure theory are drawn from studies of gauge invariance, many-body PT theory, inner-shell processes, electron momentum spectroscopy, and relativistic density functional theory. Let us note here that these principal moments are accurately taken into account in our theory, presented below. Naturally, a great interest attracts the use of many-body PT and QED in molecular electronic structure theory (cf. [73])

In the present paper a new, highly exact, ab initio approach to relativistic calculation of the spectra for multi-electron heavy and superheavy ions with an accurate account of the relativistic, correlation, nuclear, radiative effects is presented. The method is based on the gauge-invariant QED PT. Relativistic calculation of the spectra hyperfine structure parameters for heavy atoms and multicharged ions with account of relativistic, correlation, nuclear, QED effects is carried out (the Superatom [19–21, 23–40, 43] and Dirac packages (DP) [22] are used; the DP using in a progress; the Superatom package is the PC complex of Fortran programs, which numerically realize the presented method). Our calculation method is based on the gauge-invariant QED PT formalism and generalized relativistic dynamical effective field nuclear model with using the optimized one-quasiparticle representation firstly in the theory of the hyperfine structure for relativistic systems [23–26,31–35]. The wave function zeroth basis is found from the Dirac equation with a potential, which includes the core ab initio potential, the electric and polarization potentials of a nucleus (the gaussian form of charge distribution in a nucleus is used) [28, 30, 35, 40, 51, 67]. The correlation corrections of the PT high orders are taken into account within the Green functions method (with the use of the Feynman diagram's technique). All correlation corrections of the second order and dominated classes of the higher orders diagrams (electrons screening, particle-hole interaction, mass operator iterations) [19–23,27–29,36–38,67] are taken into account. The magnetic inter-electron interaction is accounted for in the lowest (on α^2 parameter), the LS polarization part – in the Uehling-Serber approximation. The self-energy part of the LS is accounted for effectively within the Ivanov-Ivanova non-perturbative procedure [19,27,28]. A generalized relativistic dynamical effective field nuclear model is presented in [40, 51] (see also Refs. [11–13, 15, 30, 35]). The energies and constants of the hyperfine structure, derivatives of the one-electron characteristics on nuclear radius, nuclear electric quadrupole, magnetic dipole moments Q for atom of hydrogen ^{1}H (test calculation), superheavy H-like ion with nuclear charge $Z = 170$, Li-like multicharged ions with $Z = 20 \div 100$, neutral atoms of ^{235}U, ^{201}Hg and ^{227}Ra are calculated.

2 QED Perturbation Theory Method for Calculation of Heavy and Superheavy Ions

Let us describe the key moments of our approach to relativistic calculation of the spectra for multi-electron superheavy ions with an account of relativistic, correlation, nuclear, radiative effects (more details can be found in ref. [19–21, 23–43, 67]).

2.1 Definition of the Basis of Relativistic Orbitals

One-particle wave functions are found from solution of the relativistic Dirac equation, which can be written in the central field in a two-component form:

$$\begin{aligned} \frac{\partial F}{\partial r} + (1+\chi)\frac{F}{r} - (\varepsilon + m - v)G = 0, \\ \frac{\partial G}{\partial r} + (1-\chi)\frac{G}{r} - (\varepsilon - m - v)F = 0. \end{aligned} \tag{1}$$

Here we put the fine structure constant $\alpha = 1$. The moment number

$$\chi = \begin{cases} -(1+1), & j > 1 \\ 1, & J < 1 \end{cases}. \tag{2}$$

At large χ the radial functions F and G vary rapidly at the origin of co-ordinates:

$$\begin{aligned} F(r), G(r) \approx r^{\gamma - 1}, \\ \gamma = \sqrt{\chi^2 - \alpha^2 Z^2}. \end{aligned} \tag{3}$$

This involves difficulties in numerical integration of the equations in the region $r \to 0$. To prevent the integration step becoming too small it is convenient to go to new functions with isolating the main power dependence: $f = Fr^{1-|\chi|}$, $g = Gr^{1-|\chi|}$. The Dirac equation for F and G components are transformed as follows:

$$\begin{aligned} f' = -(\chi + |\chi|)\frac{f}{r} - \alpha Z V g - \left(\alpha Z E_{n\chi} + \frac{2}{\alpha Z}\right) g, \\ g' = (\chi - |\chi|)\frac{g}{r} - \alpha Z V f + \alpha Z E_{n\chi} f. \end{aligned} \tag{4}$$

Here the Coulomb units (C.u.) are used; 1 C.u. of length = 1 a.u. Z; 1 C.u. of energy = 1 a.u. Z^2. In Coulomb units the atomic characteristics vary weakly with Z. $E_{n\chi}$ is one-electron energy without the rest energy, the system of Eq. (4) has two fundamental solutions. We are interested in the solution regular at $r \to 0$. The boundary values of the correct solution are defined by the first terms of the expansion into the Taylor series:

$$\begin{aligned} g = \frac{(V(0) - E_{n\chi}) r \alpha Z}{2\chi + 1}; \qquad f = 1 \quad \text{at} \quad \chi < 0, \\ f = \left(V(0) - E_{n\chi} - \frac{2}{\alpha^2 Z^2}\right) \alpha Z; \qquad g = 1 \quad \text{at} \quad \chi > 0. \end{aligned} \tag{5}$$

The conditions $f, g \to 0$ at $r \to \infty$ determine the quantified energies of the state $E_{n\chi}$. At correctly determined energy $E_{n\chi}$ the asymptotic f and g at $r \to \infty$ is as follows:

$$f, g \sim \exp\left(-r/n^*\right), \tag{6}$$

where $n^* = \sqrt{\frac{1}{2|E_{n=\chi}|}}$ is the effective quantum number. The Eq. (4) is solved by the Runge-Kutt method. The initial integration point is $r = R/10^6$, where R is the nucleus radius. The end of the integration interval is determined as $r_k \approx 30n^*$.

2.2 Nuclear Potential

Earlier we have calculated some characteristics of the hydrogen-like ions with the nucleus in the form of a uniformly charged sphere. Analogous calculation by means of an improved model was carried out too. Here the smooth Gaussian function of the charge distribution in a nucleus is used. Using the smooth distribution function (instead of the discontinuous one) simplifies the calculation procedure and permits flexible simulation of the real distribution of the charge in a nucleus. As in Refs. [27, 28] we set the charge distribution in a nucleus $\rho(r)$ by the Gaussian function. With regard to normalization we have:

$$\begin{aligned} \rho(r|R) &= \frac{4\gamma^{3/2}}{\sqrt{\pi}} \exp(-\gamma r^2); \\ \int_0^\infty dr r^2 \rho(r|R) &= 1; \\ \int_0^\infty dr r^3 \rho(r|R) &= R, \end{aligned} \tag{7}$$

where $\gamma = frac4\pi R^2$, R is the effective nucleus radius. The following simple dependence of R on Z assumed:

$$R = 1.60 \cdot 10^{-13} Z^{1/3} \quad \text{(cm)}. \tag{8}$$

Such definition of R is rather conventional. We assume it as some zeroth approximation. Further the derivatives of various characteristics on R are calculated. They describe the interaction of the nucleus with outer electron; this permits recalculation of results, when R varies within the reasonable limits. The Coulomb potential for the spherically symmetric density $\rho(r|R)$ is as follows:

$$V_{\text{nucl}}(r|R) = -\frac{1}{r}\int_0^r dr' r'^2 \rho(r'|R) + \int_r^\infty dr' r'^2 \rho(r'|R). \tag{9}$$

It is determined by the following system of the differential equations:

$$\begin{aligned} V_{\text{nucl}}(r,R) &= \frac{1}{r^2}\int_0^r dr' r'^2 \rho(r',R) \equiv \frac{1}{r^2} y(r,R); \\ y'(r,R) &= r^2 \rho(r,R); \\ \rho'(r,R) &= -8\gamma^{5/2}\frac{r}{\sqrt{\pi}} \exp(-\gamma r^2) = -2\gamma r \rho(r,R) = -\frac{8r}{\pi r^2}\rho(r,R) \end{aligned} \tag{10}$$

with the boundary conditions:

$$\begin{aligned} V_{\rm nucl}(r,0) &= -\frac{4}{\pi r}; \\ y(0,R) &= 0; \\ \rho(0,R) &= \frac{4\gamma^{3/2}}{\sqrt{\pi}} = \frac{32}{R^3}. \end{aligned} \tag{11}$$

2.3 General Scheme of Calculation for a Three-Electron System

Consider the Dirac-Fock type equations for a three-electron system $1s^2$nlj. Formally they fall into one-electron Dirac equations for the orbitals 1s1s and nlj with the potential:

$$V(r) = 2V(r|1s) + V(r|1nlj) + V_{ex}(r) + V(r|R). \tag{12}$$

$V(r|R)$ includes the electrical and the polarization potentials of a nucleus; the components of the Hartree potential:

$$V(r|i) = \frac{1}{Z}\int d\vec{r}\,' \frac{\rho(r|i)}{|\vec{r} - \vec{r}\,'|}, \tag{13}$$

where $\rho(r|i)$ is the distribution of the electron density in the state $|i\rangle$, V_{ex} is the exchange inter-electron interaction. The main exchange effect is taken into account if we assume in the equation for the 1s orbital

$$V(r) = V(r|1s) + V(r|nlj) \tag{14}$$

and in the equation for the nlj orbital

$$V(r) = 2V(r|1s). \tag{15}$$

The rest of the exchange and correlation effects is taken into account in the first two orders of the PT by the total inter-electron interaction [23, 25, 27–32, 36–38, 43].

The used expression for $\rho(r|1s)$ coincides with the precise one for a one-electron relativistic atom with a point nucleus. The finiteness of the nucleus and the presence of the second 1s electron are included effectively into the energy E_{1s}. Actually, for determination of the properties of the outer nlj electron one iteration is sufficient. The refinement resulting from second iteration (by evaluations) does not exceed correlation corrections of the higher orders omitted in the present calculation. The relativistic potential of core (the 'screening' potential) $2V^{(1)}(r|1s) = V_{scr}$ has the correct asymptotic at zero and in the infinity; at $\alpha \to 0$ it coincides with the appropriate potential constructed on the basis of the nonrelativistic hydrogen-like functions. General gauge-invariant QED procedure for construction of the optimized basis's of relativistic orbitals is proposed and described in Refs. [23, 67].

2.4 Calculation of the Self-Energy Part of Lamb Shift and Vacuum Polarization Correction

The procedure for account for the radiative QED corrections is in details given in the Refs. [23,25,27,28,35,40,41]. Regarding the vacuum polarization effect let us note that this effect is usually taken into account in the first PT theory order by means of the Uehling potential. This potential is usually written as follows (cf. [1,9,19,28]):

$$U(r) = -\frac{2\alpha}{3\pi r}\int_1^\infty dt \exp\left(-\frac{2rt}{\alpha Z}\right)\left(1+\frac{1}{2t^2}\right)\frac{\sqrt{t^2-1}}{t^2} \equiv -\frac{2\alpha}{3\pi r}C(g), \qquad (16)$$

where $g = \frac{r}{\alpha Z}$. In our calculation we use more exact approach. The Uehling potential, determined as a quadrature 16, may be approximated by a simple analytical function with high precision. The use of new approximation for the Uehling potential permits one to decrease the calculation error for this term down to $0.5 \div 1\%$. Besides, the use of such a simple analytical function form for approximating the Uehling potential allows to make quite easy inclusion into the general system of differential equations. This system includes the Dirac equations and the equations for matrix elements too. A method for calculation of the self-energy part of the Lamb shift is based on idea by Ivanov-Ivanova (cf. [10,11,15,23]). The radiative shift and the relativistic part of the energy in an atomic system are in principle determined by the same physical field. It may be supposed that there exists some universal function that connects the self-energy correction and the relativistic energy. The self-energy correction for states of the hydrogen-like ion is presented by Mohr [1,2] as follows:

$$E_{SE}(H|Z,\mathrm{nlj}) = 0.027148\frac{Z^4}{n^3}F(H|Z,\mathrm{nlj}). \qquad (17)$$

The values of F are given at $Z = 10 \div 100$, $\mathrm{nlj} = 1\mathrm{s}, 2\mathrm{s}, 2\mathrm{p}_{1/2}, 2\mathrm{p}_{3/2}$. These results are modified here for the states $1\mathrm{s}^2$ nlj of the Li-like ions. It is supposed that for any ion with nlj electron over the core of closed shells the sought value may be presented in the form:

$$E_{SE}(Z,\mathrm{nlj}) = 0.027148\frac{\xi^4}{n^3}f(\xi,\mathrm{nlj}) \quad (\mathrm{cm}^{-1}). \qquad (18)$$

The parameter $\xi = (Er)^{1/4}$, E_R is the relativistic part of the bond energy for outer electron. The universal function $f(\xi,\mathrm{nlj})$ is not dependent on composition of the closed shells and the actual potential of a nucleus. The procedure of generalization for a case of Li-like ions with the finite nucleus consists of the following steps [15,23]:

- Calculation of the values E_R and ξ for the states nlj of H-like ions with the point nucleus (in accordance with the Zommerfeld expression)
- Construction of the approximating function $f(\xi,\mathrm{nlj})$ for the corresponding Z and the appropriate $F(H|Z,\mathrm{nlj})$ [19,23,28,35]
- Calculation of E_R and ξ for the states nlj of Li-like ions with a finite nucleus
- Calculation of E_{SE} for the sought states by the Eq. 18

The energies of the states for Li-like ions are calculated twice: with a conventional constant of the fine structure $\alpha = 1/137$ and with $\tilde{\alpha} = \alpha/1000$. The results of latter calculations are considered as non-relativistic. It permits an isolation of E_R and ξ. A detailed evaluation of their accuracy may be fulfilled only after a complete calculation of $E^n_{SE}(\mathrm{Li}Z, \mathrm{nlj})$. It may be stated that the above extrapolation method is more justified than the using widely spread expansions by the parameter αZ.

2.5 Definition of the Hyperfine Structure Parameters

Energies of the quadruple (W_q) and magnetic dipole (W_μ) interactions, which define a hyperfine structure, are calculated as follows [44]:

$$\begin{aligned} W_q &= [\Delta + c(C+1)]B; \\ W_\mu &= 0.5AC; \\ \Delta &= -\frac{4}{3}\frac{(4\chi-1)(I+1)}{I-(I-1)(2I-1)}; \\ C &= F(F+1) - J(J+1) - (I+1). \end{aligned} \tag{19}$$

Here I is a spin of nucleus, F is a full momentum of system, J is a full electron momentum. The constants of the hyperfine splitting are expressed through the standard radial integrals:

$$\begin{aligned} A &= \frac{4.32587 \cdot 10^{-4} Z^2 \chi g_I}{4\chi^2 - 1}(RA)_{-2}; \\ B &= \frac{7.2878 \cdot 10^{-7} Z^3 Q}{(4\chi^2-1)I(I-1)}(RA)_{-3}. \end{aligned} \tag{20}$$

Here g_I is the Lande factor, Q is a quadruple momentum of a nucleus (in Barn); the radial integrals are defined as follows:

$$\begin{aligned} (RA)_{-2} &= \int_0^\infty dr r^2 F(r) G(r) U(1/r^2, R); \\ (RA)_{-3} &= \int_0^\infty dr r^2 [F^2(r) + G(r) U(1/r^2, R)] \end{aligned} \tag{21}$$

and calculated in the Coulomb units ($= 3.57 \cdot 10^{20} Z^2$ m^{-2}; $= 6.174 \cdot 10^{30} Z^3$ m^{-3} for variables of the corresponding dimension). The radial parts F and G of two components of the Dirac function for electron, which moves in the potential $V(r,R) + U(r,R)$, are determined by solution of the Dirac equations (see above; system (1)). For definition of the potentials of the hyperfine interaction $U(1/r^n, R)$, we solve the following differential equations:

$$U(1/r^n, R) = -\frac{ny(r,R)}{r^{n+1}}$$

Table 1 Experimental [45] and theoretical (our test calculation) results for the hyperfine splitting energies of 1s, 2s levels for the hydrogen atom

Electron term Quantum numbers of full moment	Experiment $\Delta\nu(F,F')$, MHz $\Delta E(F,F'), 10^{-3}$ cm^{-1}	Our calculations $\Delta\nu(F,F')$, MHz $\Delta E(F,F'), 10^{-3}$ cm^{-1}
$1s^2S_{1/2}$ (1.0)	1420.406	1419.685
	47.379	47.355
$2s^2S_{1/2}$ (1.0)	177.557	177.480
	5.923	5.920

They are analogous to the Eqs. (9) and (10). The functions $dU(1/r^n,R)/dR$ are calculated within the analogous procedure. The electric quadrupole spectroscopic HFS constant B of an atomic state related to the electric field gradient q and to electric quadrupole moment eQ of the nucleus as: $B = eqQ/h$. So, to obtain the corresponding value of Q one must combine the HFS constants data with the electric field gradient obtained in our approach from the QED PT calculation. The details of calculation are presented in [27, 28, 32, 34, 43, 51].

3 Results of Calculation and Conclusion

3.1 Atom of Hydrogen and Superheavy H-Like Ion with Z = 170

We have carried out the test calculation of the hyperfine structure parameters (plus derivatives of the energy contribution on nuclear radius) for atom of hydrogen ^{1}H and superheavy H-like ion with the nuclear charge $Z = 170$. For hydrogen atom there are available sufficiently exact data for hyperfine splitting energies of 1s, 2s levels. For superheavy ion $Z = 170$ there is no experiment and we can compare only the theoretical results (with the Fermi function as function for charge distribution in a nucleus) with data of analogous calculation with the gauss function for charge distribution. The electron moves in the nuclear potential V plus vacuum-polarization potential (the core potential is naturally absent). In Table 1 we present the experimental [45] and theoretical (our test calculation) results for the hyperfine splitting energies of 1s, 2s levels for the hydrogen atom. There is sufficiently good agreement between theory and experiment.

In Table 2 we present the results of our calculation for the hyperfine structure parameters (plus derivatives of the energy contribution on nuclear radius) for the superheavy H-like ion with nuclear charge $Z = 170$. We have used the denotations as follows:

$$A = \frac{10^8 A}{Z^3 g_I}, \quad \text{(eV)};$$

$$DA = \frac{10^{-2}}{Z^4 g_I}\frac{\partial A}{\partial R}, \quad \text{(eV/cm)};$$

Table 2 Characteristics of one-electron states for H-like ion with the nuclear charge $Z = 170$ (our calculation)

	$1s_{1/2}$	$2s_{1/2}$	$2p_{1/2}$	$2p_{3/2}$	$3s_{1/2}$	$3sp_{1/2}$	$3p_{3/2}$
A	4337	837	3867	1.59	207	322	0.615
DA	1039	228	941	0.0001	56.8	84.0	0.0001
B	9091	1897	8067	0.007	475	707	0.04
DB	7245	1557	6405	0.0008	394	574	0.0003
DV	1255	273	1108	0.0011	67.7	98.3	0.0005
U	1453	282	1301	1.31	69.3	109	0.62
DU	2343	503	2071	0.0015	127	185	0.0007

$$B = \frac{10^7 BI(2I-1)}{Z^3 Q}, \quad (\mathrm{eV/Barn});$$

$$DB = \frac{10^{-3} I(2I-1)}{Z^4 Q}\frac{\partial B}{\partial R}, \quad (\mathrm{eV/(Barn\ cm)});$$

$$U = -\frac{10^4}{Z^4}\langle U(r,R)\rangle, \quad (\mathrm{eV});$$

$$DU = \frac{10^{-1}}{Z^4}\frac{\partial \langle U(r,R)\rangle}{\partial R}, \quad (\mathrm{eV/cm});$$

$$DV = \frac{10^{-8}}{Z^3}\frac{\partial \langle V\rangle}{\partial R}, \quad (\mathrm{eV/cm}).$$

3.2 Li-Like Multicharged Ions

The results of calculation of the different energy contributions (eV) into energy of the $2s_{1/2}$-$2p_{1/2}$ transition in spectrum of the U^{89+}, received within different theoretical schemes (our approach (column F), MCDF (Cheng et al.;); model PT with the Dirac-Fock "0" approximation (Ivanov et al.; B); relativistic multibody PT with the zeroth Hartree-Fock-Slater potential (Persson et al.; C); multibody PT with Dirac-Fock "0" approximation (Blundell; D)) are presented in Refs. [3,5,8–10,19,28,67]. Though an agreement between all theoretical and experimental data is quite acceptable it should be noted that more exact results are obtained on the calculations by the methods (C) and (F). The results of our calculation for contributions to an energy due to the self-energy (SE) part of the Lamb shift and vacuum polarization correction (VP) of the Lamb shift for Li-like ions (account from core $1s^2$ energy) are also presented in Ref. [35, 51, 67]. The detailed analysis of the VP and SE energy contributions shows that for ions with small Z the QED effect contribution is not significant, but with growth of Z ($Z > 40$) a contribution of the QED corrections became very important. Moreover for heavy and superheavy ions an account of the QED effects is principally important. Regarding the role of the nuclear finite size

Table 3 Results calculation of the nuclear finite size correction into energy (cm^1) of the low transitions for Li-like ions and values of the effective radius of nucleus (10^{13} cm)

Z	$2s_{1/2}$-$2p_{1/2}$	$2s_{1/2}$-$2p_{3/2}$	R
20	−15.1	−15.5	3.26
30	−117.5	−118.0	3.73
41	−659.0	−670.0	4.14
59	−6610.0	−6845.0	4.68
69	−20690.0	−21712.0	4.93
79	−62315.0	−66931.0	5.15
92	−267325.0	−288312.0	5.42

effect, let us underline that its contribution is very small for multicharged ions with $Z < 20$, but it can approximately be equal to the vacuum polarization contribution on absolute value for ions with $Z > 70$. In Table 3 the results of calculation of the nuclear correction into energy of the low transitions for Li-like ions are presented. Our calculation showed also that a variation of the nuclear radius on several percents could lead to changing the transition energies on dozens of thousands 10^3 cm^{-1}.

We have carried out the calculation of constants of the hyperfine interaction: the electric quadruple constant B, the magnetic dipole constant A with an account of the nuclear finite size effect and the Uehling potential for Li-like ions. Analogous calculations of the constant A for ns states of the hydrogen-, lithium- and sodium-like ions have been are carried out. The corresponding results are presented in Refs. [3, 7–9, 13, 19]. In these papers other basis's of the relativistic orbitals are used. Besides, another model for the charge distribution in a nucleus is accepted and another method of numerical calculation of the Uehling potential is used. In Table 4 the calculation results for constants of the hyperfine splitting of the lowest excited states of the Li-like ions are presented. Analogous data for other states have been presented earlier (see Ref. [27, 28]).

In Tables 5 and 6 we present the calculated values of derivatives of the one-electron characteristics on nuclear radius (in cm^{-1}/cm) for 2l, 3l, 4l (l = 0, 1) states of the Li-like ions with minimally possible values of j:

$$\frac{\partial\langle|V|\rangle}{\partial R} = Z^3 DV, \quad (\mathrm{cm}^{-1}/\mathrm{cm});$$

$$\frac{\partial\langle|U|\rangle}{\partial R} = Z^5 DU, \quad (\mathrm{cm}^{-1}/\mathrm{cm});$$

$$\frac{\partial A}{\partial R} = Z^4 g_I DA, \quad (\mathrm{cm}^{-1}/\mathrm{cm}).$$

Here 1 cm^{-1} is an energy unit and 1 cm is a length unit. Let us remember that here V is a potential of the electron-nuclear interaction and U is the Uehling vacuum-polarization potential. Considered value of full momentum is $j = 3/2$ for derivative of the constant B on nuclear radius $\partial B/\partial R$ and value $j = 3/2$ for other operators. It should be noted that the corresponding characteristics are less sensitive

Table 4 Constants of the hyperfine electron-nuclear interaction: $A = Z^3 g_I \bar{A}$ cm^{-1}, $B = \frac{Z^3 Q}{I(2I-1)} \bar{B}$ cm^{-1}

nlj	Z	20	69	79	92
2s	$\bar{A}$	93 −03	176 −02	215 −02	314 −02
3s	$\bar{A}$	26 −03	51 −03	63 −03	90 −03
3s	$\bar{A}$	15 −03	19 −03	24 −03	36 −03
$2p_{1/2}$	$\bar{A}$	25 −03	56 −03	71 −03	105 −02
$3p_{1/2}$	$\bar{A}$	81 −04	16 −03	20 −03	31 −03
$4p_{1/2}$	$\bar{A}$	32 −04	72 −04	91 −04	11 −03
$2p_{3/2}$	$\bar{A}$	50 −04	67 −04	71 −04	72 −04
	$\bar{B}$	9 −04	13 −04	15 −04	17 −04
$3p_{3/2}$	$\bar{A}$	13 −04	19 −04	21 −04	22 −04
	$\bar{B}$	31 −05	51 −05	55 −05	65 −05
$3d_{3/2}$	$\bar{A}$	88 −05	10 −04	11 −04	12 −04
	$\bar{B}$	51 −06	9 −05	10 −05	11 −05
$4d_{3/2}$	$\bar{A}$	35 −05	51 −05	55 −05	58 −05
	$\bar{B}$	12 −06	44 −06	50 −06	56 −06
$3d_{5/2}$	$\bar{A}$	36 −05	48 −05	50 −05	52 −05
	$\bar{B}$	21 −06	38 −06	39 −06	40 −06
$4d_{5/2}$	$\bar{A}$	15 −05	19 −05	20 −05	21 −05
	$\bar{B}$	59 −07	15 −06	16 −06	17 −06

Table 5 Derivatives of the one-electron characteristics on nuclear radius (in cm^{-1}/cm) for 2s, 3s, 4s states of the Li-like ions

nlj	Z	20	30	41	59	69	79	92
$2s_{1/2}$	DV	10 +11	20 +11	41 +11	121 +12	223 +12	415 +12	967 +12
	DU	15 +06	14 +06	16 +06	20 +06	25 +06	36 +06	64 +06
	DA	15 +06	19 +06	24 +06	44 +06	63 +06	101 +07	197 +07
$3s_{1/2}$	DV	28 +10	60 +10	12 +11	35 +11	65 +11	122 +12	293 +12
	DU	45 +05	42 +05	44 +05	60 +05	81 +05	10 +06	18 +06
	DA	44 +05	56 +05	74 +05	12 +06	18 +06	29 +06	57 +06
$4s_{1/2}$	DV	11 +10	24 +10	51 +10	13 +11	26 +11	50 +11	121 +12
	DU	18 +05	17 +05	18 +05	24 +05	32 +05	47 +05	80 +05
	DA	18 +05	23 +05	30 +05	55 +05	81 +05	11 +05	23 +05

Table 6 Derivatives of the one-electron characteristics on nuclear radius (in cm^{-1}/cm) for 2p, 3p, 4p states of the Li-like ions

nlj/Z		20	30	41	59	69	79	92
$2p_{1/2}$	DV	31 +08	15 +09	66 +09	43 +10	10 +11	29 +11	108 +12
	DU	50 +03	11 +04	21 +04	72 +04	12 +05	25 +05	72 +05
	DA	55 +03	16 +04	42 +04	15 +05	34 +05	78 +05	20 +06
$3p_{1/2}$	DV	10 +08	57 +09	22 +09	14 +10	41 +10	11 +11	38 +11
	DU	18 +03	39 +03	84 +03	25 +04	49 +04	10 +05	25 +05
	DA	19 +03	56 +03	13 +04	60 +04	12 +05	27 +05	81 +05
$4p_{1/2}$	DV	49 +07	25 +08	10 +09	69 +09	17 +10	46 +10	16 +11
	DU	87 +02	17 +03	37 +03	11 +04	21 +04	42 +04	10 +05
	DA	86 +02	24 +03	67 +03	26 +04	58 +04	11 +05	34 +05

Table 7 Derivatives of the HFS constant B on nuclear radius (in cm^{-1}/cm)

nlj/Z		20	30	41	59	69	79	92
$2p_{3/2}$	DB	02 +02	05 +02	11 +02	17 +02	27 +02	40 +02	71 +02
$3p_{3/2}$	DB	19 +01	26 +01	37 +01	57 +01	95 +01	15 +01	27 +02
$4p_{3/2}$	DB	03 +01	06 +01	11 +01	21 +01	38 +01	06 +02	12 +02

Table 8 The HFS constants (cm^{-1}) for the ^{201}Hg ($^1S_0$) (nuclear spin 3/2)

HFS constants	Electron term	Recommended [17]	Present
A	$6\,^3P_2$	0.3024	0.2902
A	$6\,^3D_2$	−0.0817	−0.0795
B	$6\,^3D_2$	–	0.0019

to the nuclear size for states with the large values of momentum j. In any case the cited effects are not observed in the modern experiment.

In Table 7 we present the calculated values of derivatives of the HFS constant B on nuclear radius (in cm^{-1}/cm); $\frac{dB}{dR} = -\frac{Z^4 QDB}{I(2I-1)}$. Let us note that the main member of degree dependence upon a charge Z is separated for derivatives in Tables 5–7. The remained Z-dependence is directly connected with the relativistic and nuclear (the nuclear finite size effect) effects in the one-electron functions.

3.3 Atoms of ^{235}U, ^{201}Hg, and ^{227}Ra

We carried out calculation of the hyperfine structure parameters, magnetic and electric moments of a nucleus for ^{235}U and ^{201}Hg. In Table 8 we present the values of the HFS constants for ^{201}Hg together with available experimental results (cf. Refs. [18, 27, 45]).

Further we consider the induced electric transitions in the spectrum of ^{201}Hg. As it indicated above, the changing nuclear spin under changing the neutrons number in a nucleus can influence on the selection rules. As result, the atoms of some isotopes can have the spectral lines, which are forbidden for other isotopes. If nuclear spin makes possible the non-zeroth angle momentum of atom then the electron-nuclear interaction can induce electrically dipole transitions for a case $J = 0 \to J' = 0$. The forbidden line 2270 A ($6^3P_2 \to 6^1S_0$) and 2656 A ($6^3P_0 \to 6^1S_0$) in the even isotope ^{201}Hg are the classical examples of manifestations of this effect. Let us note that Zel'dovich and Sobelman (cf. [19]) proposed to use this effect for selective excitation of the odd and even isotopes of Hg, Sr, Ba, Zn, Cd.

Another object of our studying is the HFS of the spectral line 5915.3 A for transition $f^3ds^2\ ^5L_6 \to f^3dsp\ ^7M_7$ in the spectrum of the uranium ^{235}U. This line is corresponding to permitted transition from the ground state into one of the many excited states. The indicated transition is often used for isotopically selected excitation of the uranium atoms in the task of the industrial isotopes and nuclear

Table 9 The HFS constants, magnetic dipole moment μ and electric quadrupole moment Q for the ^{235}U nucleus

HFS constants (cm^{-1}), moments	Experiment	Theory MCDF	Present QED PT
$J = 6, -A_6$	0.00125	0.001	0.00118
$J = 6, -B_6$	0.1185	–	0.1138
$J = 7, A_7$	0.00464	0.0038	0.00437
$J = 7, B_7$	0.05588	–	0.05370
$-\mu/\mu_n$	0.315	0.289	0.305
Q (10^{-24} cm^2)	6.398	–	6.201

Table 10 Experimental and theoretical data on magnetic dipole constant of the hyperfine structure A (in MHz) for the states: 7s7p $^1P_1$, $^3P_1$, and $^3P_2$ of radium (calculation by different methods: DF, MCDF with accounting for the Breit and QED corrections, relativistic method of configuration interaction with accounting for correlation corrections within the random phase approximation (RCI-RPA) and QED PT method) [17, 18, 45, 51]

Method / State	$^1P_1$	$^3P_1$	$^3P_2$
DF	−226.59	803.97	567.22
MCDF (Breiht+QED)	−330.3	1251.9	737.1
RCI-RPA	−242.4	–	–
QEDPT	−339.1	1209	704.5
Experiment	−344.5 (0.9)	1201.1 (0.6)	699.6 (3.3)

isomers separation. In Table 9 we present the values of the HFS constants, magnetic dipole moment μ and electric quadrupole moment Q for ^{235}U nucleus, obtained experimentally and theoretically (including the MCDF method) [45].

The key quantitative factor of agreement between theory and experiment is connected with the correct accounting for the inter-electron correlations, nuclear, Breit and QED radiative corrections [1–32, 40–51]. The well-known MCDF method is not gauge-invariant one and an accounting of multi-electron correlations is not fully fulfilled, though, for example, in Ref. [52] it has been used the gauge-invariant local DF version in calculating the N-like ion of Bi. A contribution of the nuclear core-polarization effects and the high order QED corrections can correspond to the difference between theory and experiment for the nuclear moments.

Further we present the experimental data and our theoretical results (QED PT with the gauss model of charge distribution in a nucleus) of calculating the energies and constants of the hyperfine structure, nuclear moments Q for atom of radium $^{223}_{88}$Ra. It has the external valent shell $7s^2$ and can be treated as the two-quasiparticle system. In Table 10 we present the experimental and theoretical data for magnetic dipole constant of the hyperfine structure A (in MHz) for the states: 7s7p $^1P_1$, $^3P_1$, and $^3P_2$ of radium $^{223}_{88}$Ra. In Table 10 we present the results of calculation by other methods, namely: standard uncorrelated Dirac-Fock (DF) method, multi-configuration DF method (MCDF) with accounting for the Breit and QED corrections, relativistic method of configuration interaction with accounting for correlation corrections within the random phase approximation (RCI-RPA) [17, 18, 45, 67].

Table 11 Values of electric quadrupole moment Q (in Barn) for the isotope of $^{223}_{88}$Ra [17, 18, 45, 51, 67]

Method	Q (Barn)
MCDF (Breiht+QED)	1.21 (0.03)
ISOLDE Collaboration fs RaII	1.254 (0.003){0.066}
Wendt et al., fs RaI	1.19 (0.12)
RMBPT	1.28
ISOLDE Collaboration fs RaI	1.190 (0.007){0.126}
ISOLDE Collaboration B(E2)	1.2
QEDPT	1.22 (0.03)

In Table 11 we present the values for an electric quadrupole moment Q (in Barn) of the isotope of $^{223}_{88}$Ra [17, 18, 45, 51, 67], which are experimentally obtained by the ISOLDE Collaboration (CERN) within different methodologies. The corresponding theoretical results of calculation within the MCDF method (with an account of the QED and Breit corrections), relativistic multi-body perturbation theory (RMBPT) and our QED perturbation theory (QEDPT) are presented too.

The key reason of the agreement between theory and experiment is connected with the correct accounting for the interelectron correlation effects, corrections due to the finite size of a nucleus, the Breit and radiative QED corrections. The analysis shows that the interelectron correlations contribution to the hyperfine structure constants is $\sim 100 \div 500$ MHz for different states. This fact explains the low correlation between presented theoretical data on accuracy. The key difference between calculation results by the MCDF, RMBT, QEDPT methods is connected with the using different schemes of accounting for interelectron correlations. The contribution of the high orders QED PT corrections and nuclear contribution may reach the dozens of MHz and must be correctly accounted for. It is necessary to take into account more correctly the spatial distribution of the magnetic moment inside a nucleus (the Bohr-Weisskopf effect), the nuclear-polarization corrections etc. too. It can be done within solving the corresponding nuclear task, for example, with the using the shell model with the Woods-Saxon and spin-orbit potentials (cf. Refs. [11, 12, 15, 27, 30, 40, 41, 51]).

Acknowledgements One of the author (A.G.) is very much thankful to Professor S. Wilson for invitation to make oral contributions on the XII European workshop on Quantum Systems in Chemistry and Physics (London, UK). The useful discussion and comments by Professors L. Ivanov, E. Ivanova, W. Kohn, C. Rothaan, E. Brandas, S. Wilson, C. Maruani, I. Kaplan, A. Theophilou, M. Bonitz, J. Karwowski, C. Rothaan are very much acknowledged. The authors would like to thank the referees for helpful comments too. The support of the Institute for Spectroscopy ISAN (Russian Academy of Sciences, Moscow-Troitsk, Russia), the Max-Plank Institute for Physics of Complex Systems of Dresden (Germany), University of Dresden (Germany), Christian-Albrechts University of Kiel (Germany), University of Frieburg (Germany), Universities of Geneva and Zurich (Switzerland), the Abdus Salam ICTP Centre (Trieste, Italy) and NATO ESF-"Research Integrity" (Lisbon-Portugal) is very much acknowledged.

References

1. P. Mohr, Atom. Data Nucl. Data Tabl. **24**, 453–474 (1993)
2. P. Mohr, Phys. Scripta **46**, 44–52 (1993)
3. K. Cheng, Y. Kim, J. Desclaux, Atom. Data Nucl. Data Tabl. **24**, 11–88 (1979)
4. G. Drake, Phys. Scripta **46**, 116–124 (1993); H.M. Quiney, I.P. Grant, Phys. Scripta **46**, 132–138 (1993)
5. J.F. Seely, J.O. Ekberg, C.M. Brown et al., Phys. Rev. Lett. **57**, 2924–2928 (1996)
6. G. Gould, Phys. Scripta **46**, 61–68 (1993); S. Blundell, Phys. Scripta **46**, 144–149 (1993)
7. V. Dzuba, V. Flambaum, P. Silvestrov, O. Sushkov, Phys. Rev. A **44**, 2828–2832 (1991)
8. H. Persson, I. Lindgren, S. Salomonson, Phys. Rev. Lett. **76**, 204–208 (1996)
9. W. Johnson, J. Sapirstein, S. Blundell, Phys. Scripta **46**, 184–200 (1993)
10. J.P. Desclaux, Phys. Scripta **46**, 110–114 (1993)
11. L.N. Labzowsky, W.R. Johnson, G. Soff, S.M. Schneider, Phys. Rev. A **51**, 4597–4608 (1995)
12. M. Tomaselli, S.M. Schneider, E. Kankeleit, T. Kuhl, Phys. Rev. C **51**, 2989–2998 (1995)
13. V.M. Shabaev, M. Tomaselli, T. Kuhl, V.A. Yerokhin, A.N. Artemyev, Phys. Rev. A **56**, 252–260 (1997)
14. V.A. Yerokhin, A.N. Artemyev, V.M. Shabaev, Phys. Rev. A **75**, 062501-1–062501-8 (2007)
15. T. Nagasawa, A. Naga, M. Nakano, Phys. Rev. C **69**, 034322-1–034322-8 (2004)
16. P. Pyykkö, L.B. Zhao, J. Phys. B **36**, 1469–1476 (2003)
17. J. Bieron, P. Pyykkö, Phys. Rev. A **71**, 032502-1–032502-6 (2005)
18. J. Bieron, P. Pyykkö, P. Jonsson, Phys. Rev. A **71**, 012502-1–012502-12 (2005)
19. E.P. Ivanova, L.N. Ivanov, E.V. Aglitsky, Phys. Rep. **164**, 315–386 (1988)
20. L.N. Ivanov, E.P. Ivanova, L. Knight, Phys. Rev. A **48**, 4365–4380 (1993)
21. L.N. Ivanov, V.S. Letokhov, JETP **68**, 748–756 (1975)
22. H.J.A. Jensen, T. Saue, L. Visscher with contributions from V. Bakken, E. Eliav, T. Enevoldsen, T. Fleig, O. Fossgaard, T. Helgaker, J. Laerdahl, C. V. Larsen, P. Norman, J. Olsen, M. Pernpointner, J. K. Pedersen, K. Ruud, P. Salek, J. N. P. van Stralen, J. Thyssen, O. Visser, and T. Winther in *Dirac, a relativistic ab initio electronic structure program, Release DIRAC 04.0*, (http://dirac.chem.sdu.dk). Cited 10 Jan 2007
23. A.V. Glushkov, L.N. Ivanov, Phys. Lett. A **170**, 33–38 (1992)
24. A.V. Glushkov, L.N. Ivanov, J. Phys. B: At. Mol. Opt. Phys. **24**, L379–386 (1993)
25. A.V. Glushkov, JETP Lett. **55**, 95–98 (1992)
26. A.V. Glushkov, S. Ambrosov, V. Ignatenko, D. Korchevsky, Int. J. Quant. Chem. **99**, 936–939 (2004)
27. A.V. Glushkov, S.V. Ambrosov, A.V. Loboda, Yu. G. Chernyakova, O.Yu. Khetselius, A.V. Svinarenko, Nucl. Phys. A **734**, 21–28 (2004)
28. A.V. Glushkov, S.V. Ambrosov, A.V. Loboda, E.P. Gurnitskaya, O.Yu. Khetselius, in *Recent Advances in Theoretical Physics and Chemistry Systems*, ed. by J.-P. Julien, J. Maruani, D. Mayou, S. Wilson, G. Delgado-Barrio, series: Progress in Theoretical Chemistry and Physics, vol 15, (2006) 285–300
29. A.V. Glushkov, S.V. Ambrosov, A.V. Loboda, E.P. Gurnitskaya, G.P. Prepelitsa, Int. J. Quant. Chem. **104**, 562–569 (2005)
30. A.V. Glushkov, S.V. Malinovskaya, in *New Projects and New Lines of Research in Nuclear Physics*, ed. by G. Fazio, F. Hanappe (World Scientific, Singapore, 2003) pp. 242–264
31. A.V. Glushkov, S.V. Malinovskaya, Yu.G. Chernyakova, A.A. Svinarenko, Int. J. Quant. Chem. **99**, 889–896 (2004)
32. A.V. Glushkov, S.V. Malinovskaya, A.V. Loboda, E.P. Gurnitskaya, D.A. Korchevsky, J. Phys. CS **11**, 188–198 (2004)
33. A.V. Glushkov, S. Ambrosov, V. Ignatenko, D. Korchevsky, Int. J. Quant. Chem. **99**, 936–940 (2004)
34. A.V. Glushkov, S.V. Malinovskaya, G.P. Prepelitsa, V. Ignatenko, J. Phys. CS **11**, 199–208 (2004)

35. A.V. Glushkov, E.P. Gurnitskaya, A.V. Loboda, in *Low Energy Antiproton Physics*, ed. by D. Grzonka, R. Czyzykiewicz, W. Oelert, T. Rozek, P. Winter, vol 796, (2005) pp. 217–226
36. A.V. Glushkov, L.N. Ivanov, E.P Ivanova, *Autoionization Phenomena in Atoms*, (Moscow University Press, Moscow, 1986)
37. A.V. Glushkov, E.P. Ivanova, J. Quant. Spectr. Rad. Transfer. **36**, 127–145 (1986)
38. E.P. Ivanova, L.N. Ivanov, A.V. Glushkov, A.E. Kramida, Phys. Scr. **32**, 512–534 (1985)
39. A.V. Glushkov, V.D. Rusov, S.V. Ambrosov, A.V. Loboda, in *New Projects and New Lines of Research in Nuclear Physics*, ed. by G. Fazio, F. Hanappe (World Scientific, Singapore, 2003) pp. 126–136
40. A.V. Glushkov, In: in *Low Energy Antiproton Physics*, ed. by D. Grzonka, R. Czyzykiewicz, W. Oelert, T. Rozek, P. Winter, vol 796, (2005) pp. 206–210
41. A.V. Glushkov, S.V. Malinovskaya, Yu.V. Dubrovskaya, L.A. Vitavetskaya, in *Recent Advances in Theoretical Physics and Chemistry Systems*, ed. by J.-P. Julien, J. Maruani, D. Mayou, S. Wilson, G. Delgado-Barrio, series: Progress in Theoretical Chemistry and Physics, vol 15, (2006) pp. 301–308
42. O. Bohr, B. Motelsson, *Structure of Atomic Nucleus*, (Plenum, New York, 1971)
43. A. Glushkov, *Atom in a electromagnetic field. Numerical Models*, (Nauka-KNT, Moscow-Kiev, 2005), 400p.
44. I. Sobel'man, *Introduction into Theory of Atomic Spectra*, (Nauka, Moscow, 1977)
45. A.A. Radtsig, B.M. Smirnov, *Parameters of Atoms and Ions*, (Nauka, Moscow, 1986)
46. S. Wilson, in *Recent Advances in Theoretical Physics and Chemistry Systems*, ed. by J. Maruani, S. Lahmar, S. Wilson, G. Delgado-Barrio, Series: Progress in Theoretical Chemistry and Physics, vol 16, (2007) p. 11
47. S. Wilson, Ed., in *Handbook on Molecular Physics and Quantum Chemistry*, (Wiley, Chichester, 2003)
48. P. Hohenberg, W. Kohn, Phys. Rev. **B136**, 864–878 (1964);W. Kohn, L.J. Sham, Phys. Rev. **A140**, 1133–1142 (1964)
49. R.M. Dreizler, Phys. Scripta **46**, 167–173 (1993)
50. P. Indelicato, J.P. Desclaux, Phys. Scripta **46**, 110–115 (1993)
51. A.V. Glushkov, O.Yu. Khetselius, Proc. NPA III, Dresden(Germany), (2007), p. 95; J. Phys. G., to be publ.
52. K.N. Koshelev, L.N. Labzowsky, I.I. Tupitsyn, J. Phys. B **37**, 843–851 (2004)
53. P. Pyykkö, in *Relativistic Theory of Atoms and Molecules II – A Bibliography 1986–1992*, Lecture Notes in Chemistry, (Springer, Berlin), vol 60 (1993)
54. S.N. Tiwary, Rivista del Nuovo Cimento. **18**, 1–24 (1995)
55. K.N. Koshelev, L.N. Ivanov, Phys. Rev A. **42**, 5784–5790 (1990)
56. L.N. Ivanov, E.P. Ivanova, JETP. **110**, 483–496 (1996)
57. J. Bieron, C. Froese-Fisher, S. Fritzsche, K. Pachucki, J. Phys. B: At. Mol. Opt. Phys. **37**, L305–311 (2004)
58. U.I. Safranova, T.E. Cowan, M.S. Safranova, J. Phys. B: At. Mol. Opt. Phys. **38**, 2741–2763 (2005)
59. V. Dzuba, V. Flambaum, M.S. Safranova, Phys. Rev A **73**, 022112-1–022112-10 (2006)
60. U.I. Safranova, M.S. Safranova, W.R. Johnson, Phys. Rev A **71**, 052506-1–052506-8 (2005)
61. B.K. Sahoo, G. Gopakumar, R. Chaudhuri, B.P. Das, H. Merlitz, U. Mahapatra, D. Mukherjee, Phys. Rev A **68**, 040501-1–040501-8 (2003)
62. J.P. Santos, F. Parenre, S. Boucard, P. Indelicato, J.P. Desclaux, Phys. Rev A **71**, 032501-1–032501-10 (2005)
63. A. Derevianko, S.G. Porsev, Phys. Rev. A **71**, 032509-1–032509-10 (2005)
64. V.I. Zagrebaev, Yu.Ts. Oganessian, M.G. Itkis, W. Greiner, Phys. Rev. C **73**, 031602-1–031602-6 (2006)
65. V.A. Yerokhin, A.N. Artemyev, V.M. Shabaev, Phys. Rev. A. **75**, 062501-1–062501-12 (2007)
66. I. Theophilou, S. Thanos, A. Theophilou, J. Chem. Phys. **127**, 234103-1–234103-8 (2007)
67. A. Glushkov, *Relativistic and Correlation Effects in Spectra of Atomic Systems*, (Nauka, Moscow-Odessa, 2006), 700 p.

68. I.P. Grant, in *Relativistic Quantum Theory of Atoms and Molecules Theory and Computation*, Springer Series on Atomic, Optical, and Plasma Physics, vol 40, (2007) pp. 587–626
69. I.P. Grant, H.M. Quiney, Int. J. Quant. Chem. **80**, 283–297 (2000)
70. K.L. Bell, K.A. Berrington, D.S.F. Crothers, A. Hibbert, K.T. Taylor, Bertha: 4-Component Relativistic Molecular Quantum Mechanics, in *Supercomputing, Collision Processes, and Application*, Series: Physics of Atoms and Molecules, Springer, (2002) pp. 213–224
71. M. Reiher, B. Hess, in *Modern Methods and Algorithms of Quantum Chemistry*, ed. by J. Grotendorst, John von Neumann Institute for Computing, Julich, NIC Series, vol 3, (2000) pp. 479–505
72. H.M. Quiney, in *Relativistic Quantum Mechanics of Atoms and Molecules. New Trends in Quantum Systems in Chemistry and Physics*, Series: Progress in Theoretical Chemistry and Physics, vol 6,(2002) pp. 135–173
73. S. Wilson, Journ. of Mol. Str.: Theochem. **547**, 279–291 (2001)

New Laser-Electron Nuclear Effects in the Nuclear γ Transition Spectra in Atomic and Molecular Systems

Svetlana V. Malinovskaya, Alexander V. Glushkov(✉), and Olga Yu. Khetselius

Abstract A consistent QED perturbation theory approach is applied to calculation of the electron-nuclear γ-transition spectra of nucleus in the multicharged ion. The intensities of satellites are defined in the relativistic version of the energy approach (S-matrix formalism). As example, the nuclear transition in the isotope $^{57}_{26}Fe$ with energy 14.41 keV is considered. The results of the relativistic calculation for the electron-nuclear γ-transition spectra (set of electron satellites) of the nucleus in a multicharged atomic ion FeXIX are presented. The possible experiments for observation of the new effect in the thermalized plasma of O- like ions are discussed. Consistent, quantum approach to calculation of the electron-nuclear γ transition spectra (set of vibration-rotational satellites in molecule) of nucleus in molecule, which generalizes the well known Letokhov-Minogin model, is presented and based on the Dunham model potential approximation for potential curves of the diatomic molecules. Estimates are made for vibration-rotation-nuclear transition probabilities in a case of the emission and absorption spectrum of nucleus ^{127}I ($E_\gamma^{(0)} = 203$ keV) in the molecule of H^{127}I. Estimates of the vibration-nuclear transition probabilities in a case of the emission and absorption spectrum of nucleus ^{191}Ir ($E_\gamma^{(0)} = 82$ keV) in the molecule of IrO_4 and nucleus ^{188}Os ($E_\gamma^{(0)} = 155$ keV) in the molecule of OsO_4 are presented too.

Keywords: atoms, molecules, spectra, laser-electron nuclear effects

A.V. Glushkov
Institute for Spectroscopy (ISAN), Russian Acad. Sci., Troitsk-Moscow, 142090, Russia;
Odessa University, P.O. Box 24a, Odessa-9, 65009, Ukraine, e-mail: glushkov@paco.net

S.V. Malinovskaya
Odessa University, P.O. Box 24a, Odessa-9, 65009, Ukraine

O.Yu. Khetselius
Odessa University, P.O. Box 24a, Odessa-9, 65009, Ukraine;
Abdus Salam International Centre for Theoretical Physics Strada Costiera, 11 - 34014 Trieste, Italy

S. Wilson et al. (eds.) *Frontiers in Quantum Systems in Chemistry and Physics*.

1 Introduction

The field of laser-matter interactions is usually dealing with the atomic and molecular response to an external light wave. However, due to a large technological progress, it is possible today to produce by lasers keV photons, MeV ions and GeV electrons, which lies far beyond the typical energy scale of atomic optics. The direct interaction of atoms and laser fields allows in many cases for a controlled preparation, manipulation and measurement of the internal and external degrees of freedom of the atoms giving rise to a multitude of applications (cf. [1–9]). The question arises whether light-matter interaction, reminiscent of quantum optics, is also possible in quantum systems characterized by high energy scales as recently it was shown that the super-intense laser fields make the direct interaction of laser and nuclei (cf. [1–3]). It is of a great interest for understanding the key physical processes in the multi-charged ion plasma in a thermonuclear reactor, laser plasma etc. A development of methods of the laser spectroscopy [1,8–10] allowed observing and further using the little changes in a structure of the atomic and molecular spectra because of the corresponding alteration of the internal state of a nucleus (co-operative laser-electron-nuclear effects) [11–42]. Speech is about such effects as the isomer shift in the vibrational spectrum of a molecule because of the equivalent increasing of the excited nucleus mass. It should be also mentioned an effect of the selective photoionization of atoms with the isomer nucleus and possibility of the quick physical separation of the isomer nuclei. This effect is of a great importance for the γ-laser problem (cf. [1, 32–41]). It is of a great importance to observe new co-operative laser-electron-nuclear effects in multicharged ions in the corresponding plasma and use them as new basis for the plasma parameters diagnostics [32–34].

Any alteration of the atomic, ionic or molecular state must be manifested in the quantum transitions, for example, in a spectrum of the γ-radiation of a nucleus. It is well known that it is possible to transfer a part of the nuclear energy to an atom or molecule under radiating (absorption) γ quanta by a nucleus (cf. [11–28, 32–36]). The first references to the neutral recoil are due to Migdal (1941) and Levinger (1953), who evaluated approximately the ionization of an atom undergoing sudden recoil in due to neutron impact and in a radioactive disintegration respectively. The neutral recoil situation differs radically from processes involving a charged particle for which the sudden recoil approximation is often invalid (cf. [20,21]). Simple, as a rule, non-relativistic quantum-mechanical models (cf. [11–15,17–19,22–29,32–36]) have been developed to evaluate an excitation or ionization of an atom, the electronic redistribution of an ion or an atom induced a sudden recoil of its nucleus occurring when a neutral particle is either emitted (γ-radioactivity) or captured (neutron capture for instance).

The most consistent approach to considered problems must be based on the quantum electrodynamics (QED)(cf. [43–50]). The nuclear emission or absorption spectrum of an atom possesses a set of electron satellites, which are due to an alteration of the state of the electron shell [3,4,32–37,39,41]. The mechanism of formation of the satellites in the neutral atoms and highly charged ion is different. In the first case (loose electron shell) a shaking of the shell resulting from the interaction

between the nucleus and γ-quantum is predominant. In the second case (rigid electron shell) the mechanism involves a direct interaction between γ-quantum and electrons. The traditional selection rules and familiar intensity hierarchy with respect to electron transition multiplicity do not pertain to the second mechanism. Consequently, the satellite spectrum is much enriched and transitions between the fine and hyper fine structure components, 0-0 transitions and transitions, which do not involve a change in the electron configuration, can be considered.

The intensive vibrational satellites can appear in a spectrum of the γ-radiation in a molecule under radiating (absorption) the γ quanta by a nucleus. An appearance of these molecular nuclear lines is interesting as it opens a possibility of the changing the γ-radiation spectrum by means of the changing vibrational state of a molecule by coherent laser light [32, 34]. Probability of the vibrational or rotational state changing (in difference from the atomic electrons state changing) is not small and must be taken into account even in the zeroth approximation. In any case there is a great number of different channels for the electron-nuclear processes in atoms, ions and molecules. A possibility of their interference makes the analysis more complicated. A consistent analysis of cited processes in the multielectron atoms and multicharged ions must be, as a rule, based on the QED. Naturally, in a case of the diatomic and multiatomic molecules (without heavy atoms in a molecule) one can use the standard methods of quantum chemistry [51–53].

This paper is going on our studying the co-operative dynamical phenomena (cf. [4, 7, 32–36]) due the interaction between atoms, ions, molecule electron shells and nuclei nucleons. Earlier a consistent QED perturbation theory approach is developed and applied to calculation of the electron-nuclear γ-transition spectra of nucleus in the different atomic systems. In this paper the new laser-electron nuclear effects in the molecular systems will be studied within consistent quantum approach. But, at the beginning we consider a consistent QED perturbation theory approach, applied to calculation of the electron-nuclear γ-transition spectra of nucleus in the multicharged ion. The intensities of satellites are defined in the relativistic version of the energy approach (S-matrix formalism) [32,36]. Decay and excitation probabilities are linked with imaginary part of the energy of the 'nuclei nucleons-electron shells-field' system. For radiative decays it is manifested as an effect of the retarding in interaction and self-action and calculated within QED perturbation theory. As example, the nuclear transition in the isotope $^{57}_{26}Fe$ with energy 14.41 keV is considered. The results of the relativistic calculation for the electron-nuclear γ-transition spectra (set of electron satellites) of the nucleus in a multicharged atomic ion FeXIX are presented and compared with the corresponding non-relativistic estimates [7, 32, 34]. The possible experiments for observation of the new effect in the thermalized plasma are discussed. It is considered a situation when electron satellites are not overlapped by the Doppler contour of the γ-line (plasma source). We will present a consistent approach to description of a new class of the dynamical laser-electron-nuclear effects in molecular systems, in particular, the nuclear emission or absorption spectrum of the diatomic molecule too. In the molecule a spectrum is naturally more complicated in comparison with an atom. Under nuclear γ-quantum emission or absorption there is a change of the

electron (vibration-rotation) states. A consistent, quantum- mechanical approach to calculation of the electron-nuclear γ transition spectra (set of vibration-rotational satellites in molecule) of a nucleus in the diatomic molecule is presented. It is based on the using the Durham model potential approximation for potential curves of the diatomic molecules [7, 32, 34, 54–58]. It generalizes the well known Letokhov-Minogin model [9, 41]. Estimates are made for vibration-rotation-nuclear transition probabilities in a case of the emission and absorption spectrum of nucleus ^{127}I ($E_\gamma^{(0)} = 203$ keV) in the molecule of H^{127}I. At last, a consistent, quantum approach to calculation of the electron-nuclear γ transition spectra (set of vibration-rotational satellites in molecule) of a nucleus in the multiatomic molecules is described too. Estimates of the vibration-nuclear transition probabilities in a case of the emission and absorption spectrum of nucleus ^{191}Ir ($E_\gamma^{(0)} = 82$ keV) in the molecule of IrO_4 and nucleus ^{188}Os ($E_\gamma^{(0)} = 155$ keV) in the molecule of OsO_4 are presented.

2 QED Theory of Co-operative Laser-Electron-Nuclear Processes in Atomic Systems

Following to Refs. [32–36, 40], we consider the following model of the atomic system: rigid nuclear core (c), above core proton (p) and electron (e). The masses of three particles are equal correspondingly: $\mu_c M$, $\mu_p M$, $\mu_e M$, where M mass of all atom; $\mu_c + \mu_p + \mu_e = 1$; the space co-ordinates of the particles are denoted as r_c, r_p, r_e. The charge of nuclear core is z. Besides, the value of z^* denotes an effective charge for Coulomb field of the optically active electron in ion. Naturally, the majority of the excited states of nuclei have the multi-particle character [9, 16, 45]. As exclusion, one may consider the first excited states with one or two quasi-nucleons or quasi-vacancies above the 'even-even' core. These states are more suitable for theoretical consideration as the one-particle model could be used. It is very important to underline that a generalization on the multi-particle case does not lead to qualitatively new results as the dynamical (radial) parts of the nuclear matrix elements do not enter into expressions for relative intensities of the electron satellites and ground line of the nuclear transition. QED is needed here as for obtaining the correct formula as carrying out the precise calculations.

Within the QED energy approach the main our purpose is calculating the imaginary part of energy of the excited state for atomic system. Detailed description of an approach was given earlier (cf. [4, 31–34, 36]). Here we consider only the key elements of the calculation procedure. Following the quasi-potential method, we introduce the bare interaction as follows:

$$V(r_c, r_p, r_c) = v(r_{pc}) - Ze^2/r_{ec} - e^2/r_{pe}. \tag{1}$$

Here $v(r_{pc})$ imitates the interaction of the proton with the core (nuclear and Coulomb); other interactions are obvious. Then imaginary part of the energy of the excited state for three-quasi-particle system Ψ_I in the lowest QED perturbation

theory order can be written as follows:

$$\begin{aligned} \mathrm{Im}E = e^2 \mathrm{Im} i \lim_{\gamma\to 0} \iint d^4x_1 d^4x_2 e^{\gamma(t_1+t_2)} \left(D(r_{c_1t_1}, r_{c_2t_2}) \times \right. \\ \times \langle \Psi_I | (j_c(x_1) j_c(x_2)) | \Psi_I \rangle + D(r_{p_1t_1}, r_{p_2t_2}) \left\langle \Psi_I | (j_p(x_1) j_p(x_2)) | \Psi_I \right\rangle + \\ \left. + D(r_{e_1t_1}, r_{e_2t_2}) \langle \Psi_I | (j_e(x_1) j_e(x_2)) | \Psi_I \rangle \right). \end{aligned} \tag{2}$$

Here $D(r_1t_1,\ r_2t_2)$ is the photon propagator; j_c, j_p, j_e are the four-dimensional components for the current operator for particles: core, protons, electrons; $x = (r_c,\ r_p,\ r_e,\ t)$ includes the space co-ordinates of three particles and time (equal for all particles); γ is the adiabatic parameter. For the photon propagator the exact electrodynamical expression is used:

$$D(12) = -\frac{i}{8\pi^2} \frac{1}{r_{12}} \int\limits_{-\infty}^{\infty} d\omega e^{i\omega t_{12} + i|\omega| r_{12}}. \tag{3}$$

In expressions (2), (3) the summation on directions of the photon polarization is fulfilled. Below we are limited by the lowest order of the QED perturbation theory, i.e. the next QED corrections to ImE will not be considered. Note also that the expression (2) describes the one-photon processes. We need further relativistic solutions of the Dirac equation whose radial part is represented by

$$\begin{aligned} F' = -(\text{œ} + |\text{œ}|)F/r - \alpha(E + 2M\alpha^{-2})G - \alpha V G, \\ G' = (\text{œ} - |\text{œ}|)G/r + \alpha(E - V)F. \end{aligned} \tag{4}$$

Here α is the fine structure constant; œ is the Dirac angular quantum number; E is the state energy, F, G being the large and small radial components correspondingly. In the non-relativistic limit the large radial component converts into the only component-solution of the non-relativistic radial Schrödinger equation. Substituting all expressions into Eq. (2), one may get the following general expression for imaginary part of the excited state energy of the three-quasi-particle system as a sum of the core, proton and electron contributions:

$$\mathrm{Im}E = \mathrm{Im}E_c + \mathrm{Im}E_p + \mathrm{Im}E_e,$$

$$\mathrm{Im}E_a = -\frac{Z_a^2}{4\pi} \sum_F \iint dr_{c_1} dr_{c_2} \iint dr_{p_1} dr_{p_2} \iint dr_{e_1} dr_{e_2} \Psi_I^*(1) \Psi_F^*(2) T_a(1,2) \Psi_F(1) \Psi_I(2), \tag{5}$$

$$T_a(1,2) = (\sin(w_{IF} r_{a_{12}})/r_{a_{12}}) \left(1/M\mu_a(\nabla_{r_{a_1}}, \nabla_{r_{a_2}}) + 1\right).$$

Here $r_{a_{12}} = |r_{a_1} - r_{a_2}|$; w_{IF} is the transition full energy, which includes changing the kinetic energy of an ion, i.e. the recoil energy; Ψ_c, Ψ_p, Ψ_e are the second quantized field operators of the core particles, protons and electrons respectively. The sum according to F gives the summation of the final states of the system. In the second order of QED perturbation theory, the full width of a level is divided into the sum of the partial contributions, connected with the radiation decay into concrete

final states of a system. These contributions are proportional to the probabilities of the corresponding transitions. The system of red (blue) satellites corresponds to the transitions with excitation (de-excitation) of the electron shell. The important quantity is a contribution of ImE_e to the relative intensity of satellite $k = P(pe)/P(p)$ (here $P(pe)$ is the satellite intensity; $P(p)$ is the intensity of nuclear transition). An intensity of the line is linked with ImE Eq. (5) as:

$$P = 2\mathrm{Im}E/h. \tag{6}$$

A frequency of the γ-transition for a nucleus with changing the electron state is defined by the following expression:

$$\hbar\omega_{\gamma}^{if} = \hbar\omega_{\gamma 0} \pm (\hbar\Delta_{\gamma} + E_i - E_f). \tag{7}$$

Here $\omega_{\gamma 0}$ is the frequency of the γ-transition without recoil; $\hbar\Delta_{\gamma}$ is the recoil energy; E_i and E_f are the initial and final energies of electron (sign '+' is corresponding to absorption of the γ-quantum; sign '$-$' is corresponding to emission of the γ-quantum). In Fig. 1 we present a schematic spectrum of the electron-nuclear lines of emission (lines, directed up) and absorption (lines, directed down) of the γ-radiation for a nucleus in the non-excited (a) and excited (b) neutral atom (left part of the figure). In the right part of the figure the corresponding quantum transitions in a system are presented.

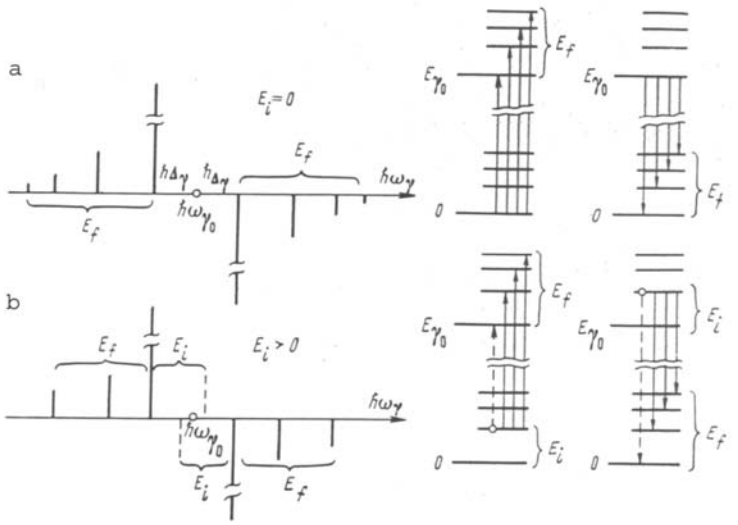

Fig. 1 Spectrum of the electron-nuclear lines of emission (lines, directed up) and absorption (lines, indicated down) of the γ-radiation for nucleus in non-excited (**a**) and excited (**b**) neutral atom (left part of the figure); in right part of the figure there are presented the corresponding quantum transitions in the system (E_i and E_f are the initial and final energies of electron, $E_{\gamma 0}$ is an energy of nuclear level)

Further it is convenient to separate a motion of the center of mass of the system, introducing the new variables:

$$R = \mu_c r_c + \mu_p r_p + \mu_e r_e, \qquad R_p = r_p - r_c, \qquad R_e = r_e - r_c.$$

In the zeroth order of the perturbation theory a dependence of Ψ_I, Ψ_F from the variables R, R_p, R_e is factorized:

$$\Psi_A(R, R_p, R_e) = \Psi_A(R)\Psi_{Ap}(R_p)\Psi_{Ae}(R_e). \tag{8}$$

Here Ψ_A is the plane wave, Ψ_{Ap} is a function of the state of proton in the potential $V(R_p)$, Ψ_{Ae} is the Coulomb relativistic function.

One should note that there are the combined electron-proton one-photon transitions already in the zeroth approximation. A contribution of the proton-electron interaction into the satellite intensity is manifested only in the second order of the perturbation theory on this interaction. It has an additional order of smallness $\sim 1/z^{*2}$ (for the Coulomb part) and μ^2 (for the recoil interaction) in comparison with the main contribution. So, the main effect of causing the electron satellites for nuclear transitions has kinematics nature, which is in shifting a center of mass of the system under emission of γ-quanta relatively of the proton or electron orbital. In the concrete calculation one can use the standard expansion for operator **T** on the spherical functions, which generates the multiple expansion for the decay probability. The details of the calculation procedure, the definition of all contributions and the corresponding matrix elements are described in Refs. [3, 30–36, 43–45, 49, 50].

3 Results for Atomic Systems and Discussion

It is very important to discuss the possible experimental observation of satellite effect. As indicated in ref. [3, 5, 7, 32], in neutral atoms under standard experimental conditions the intensive satellites are overlapping by the Doppler contour of line of the γ-radiation. For their observation one should use the methods of inside Doppler spectroscopy [8–10]. In principle it is possible an observation of the satellites in the spectrum of emission or absorption without overlapping by the Doppler contour of the γ-line. Such a situation could be realized in plasma of multicharged ions [7, 32]. The energy intervals between lowest electron levels may significantly exceed the Doppler shift of the γ radiation line. Let us suppose that the K shell is significantly destroyed. According to [4, 31, 32, 40], an average kinetic energy for ions in such plasma: $\sim E_i/10 \sim 1/20$ c.u. (the Coulomb units are used), where E_i is the '1s' electron bond energy. The Doppler shift is as follows: $\delta\hbar\omega_D \approx \alpha\omega/(10M)^{1/2}$. The value $\alpha\omega$ is connected with the energy of γ quantum by the following formulae: $E_\gamma[keV] \approx 4Z(\alpha\omega)$. If, say, $\alpha\omega = 1$, then $\delta\hbar\omega_D \approx 1/200(Z)^{1/2}$ c.u. $\approx 0.15(Z)^{1/2}$ eV. For comparison let us give the values of the 1s,2s,2p-2p electron transitions for one-electron ions with $Z = 10{-}50$: $E(1s - 2p_{3/2}) = 1.3 \cdot 10^3 - 2.3 \cdot 10^4$ eV,

Table 1 Energies of the L-levels for ion of *Fe*XIX, counted from the ground level $2s^2 2p^2\ ^3P_2$

Configuration	$2s^2 2p^4$				$2s^2 2p^5$				$2p^6$
State	$^3P_0$	$^3P_1$	$^1D_2$	$^1S_0$	$^3P_2$	$^3P_1$	$^3P_0$	$^1P_1$	$^1S_0$
E, eV	9.4	11.1	20.9	40.3	114.4	122.0	127.7	157.1	264.6

$E(2s - 2p_{3/2}) = 0.1{-}3.3 \cdot 10^2$ eV. One can see that the transition energies have an order of the Doppler shift value. A little value of the splitting in the one-electron ions is entirely provided by the relativistic corrections. In the multielectron system situation is more favourable. Let us consider a case of the O-like and F-like multicharged ions. An additional splitting is defined by the inter electron interaction. In Table 1 we present the energies of levels for L shell of the oxygen-like ion *Fe*XIX ($Z = 26$), counted from the ground level $2s^2 2p^2\ ^3P_2$ [35, 40, 50].

The lines of big number of the electron satellites, connected with 2–2 transitions, are sufficiently far from the Doppler contour. We consider the nuclear transition in the isotope $^{57}_{26}Fe$ with the quantum energy 14.41 keV. The period of the half decay of state $T(1/2) = 9.77 \cdot 10^{-8}$ sec., the recoil energy $1.96 \cdot 10^{-6}$ keV. The parameter $\alpha\omega = 0.27$. We consider the following transitions: 1s–2s (monopole), 1s–$2p_{1/2}$, 2s–$2p_{3/2}$ (dipole), $2p_{1/2}$–$2p_{3/2}$ (quadruple). The detailed results of calculation for some of these transitions have been presented in Ref. [33, 35, 36], where are also indicated the corresponding non-relativistic data [4, 9, 39, 40]. An account of the relativistic effects resulted in the shift of the curves to the region of the more large energies. The numerical difference of values for intensities of different satellites is connected with different values of the electron radial integrals, which are defined by the overlapping the wave functions. The intensity of satellite for transition to the $2p_{1/2}$ state is twice less than to the $2p_{3/2}$ state. The strongest satellites are ones, which are corresponding to the transitions 2s–2p. In Fig. 2a scheme of disposition for some electron satellites in relation to the nuclear transition line is considered. The Doppler widths are shown qualitatively ($\delta\hbar\omega_d \approx 5$ eV).

The relative intensities for these satellites are equal $\approx 7 \cdot 10^{-5}$. Satellites connected with the 1-2 transitions are separated from $\omega_{0\gamma}$ on value $\approx$6 keV, but their intensity is less. It is easy to understand that naturally the relative electron satellite intensity values are sufficiently little because of the weak link between an electron motion and motion of a nucleus under recoil. In Fig. 2 there are presented the lines which are accompanied by electron transitions: 1–$2s^2 2p^4\,^1S_0$–$2s2p^5\,^3P_1$; 2–$2s^2 2p^4\,^3P_1$–$2s2p^5\,^3P_2$; 3–$2s^2 2p^4\,^3P_2$–$2s2p^5\,^3P_1$; 2–$2s2p^5\,^3P_1$–$2p^6\,^1S_0$.

The relative intensities for these satellites are $P(pe)/P(p) \approx 7 \cdot 10^{-5}$, the Doppler broadening is $\delta\hbar\omega_D \approx 5$ eV (shown on Fig. 2 qualitatively). Thus, it is obvious that the electron-nuclear lines in the spectra of emission or absorption can be experimentally observed in plasma of the O-and F-like multicharged ions and they are not overlapping by the Doppler broadening [4, 7, 33, 34].

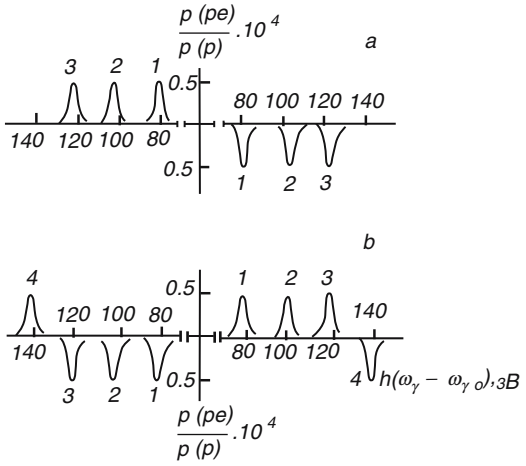

Fig. 2 The positions of emission and absorption lines electron satellites (in a positive and negative direction of abscissa axe correspondingly) for ions *Fe*XIX, *Fe*XVIII in lowest states of the ground configurations $2s^2 2^4$, $2s^2 2^5$ (**a**) and states of the excited configuration $2s2^5$, $2s^2 2^5 nl$ (**b**) relatively the nuclear γ-transition in isotope of $^{57}_{26}Fe$ with energy $\hbar\omega_{0\gamma} = 14.41$ keV; $P(pe)/P(p)$ is relation of the satellite intensity to the nuclear transition line intensity

4 Quantum Approach to Calculation of the Electron-Nuclear γ Transition Spectra in Diatomics

Our purpose is calculation of a structure of the gamma transitions (probability of transition) or spectrum of the gamma satellites because of the changing the electron-vibration-rotational states for the diatomic molecules under gamma quantum radiation (absorption). In the adiabatic approximation a wave function of a molecule is multiplying the electronic wave function and wave function of nuclei: $\psi(r_e)\psi(R_1, R_2)$. Hamiltonian of interaction of the gamma radiation with system of nucleons for the first nucleus can be expressed through the co-ordinates of nucleons r'_n in a system of the mass centre of the first nucleus [9, 33, 34, 41]:

$$H(r_n) = H(r_n)\exp(-ik_\gamma R_1), \tag{9}$$

where k_γ is a wave vector of the gamma quantum. The matrix element for transition from the initial state 'a' to the final state 'b' is presented as usually:

$$\langle \Psi_b^*(r_n)|H(r_n)|\Psi_a(r_n)\rangle\langle \Psi_b^*(r_e)Psi_b^*(R_1,R_2)|e^{-ik_\gamma R_1}|\Psi_a(r_e)Psi_a(R_1,R_2)\rangle. \tag{10}$$

The first multiplier in Eq. (10) is defined by the gamma transition of a nucleus and is not dependent upon an internal structure of the molecule in a good approximation. The second multiplier is a matrix element of transition of the molecule from the initial state 'a' to the final state 'b':

$$M_{ba} = \langle \Psi_b^*(r_e)|\Psi_a(r_e)\rangle\langle \Psi_b^*(R_1,R_2)|e^{-ik_\gamma R_1}|\Psi_a(R_1,R_2)\rangle. \tag{11}$$

The expression (11) gives a general formula for calculation of the probability of changing the internal state of a molecule under absorption or emitting gamma quantum by a nucleus of the molecule. In fact it defines an amplitude of the

corresponding gamma satellites. Their positions are fully determined by the energy and pulse conserving laws as follows [33, 34, 41]:

$$\pm E_\gamma + E_a + (1/2)Mv_0^2 = \pm E_\gamma^{(0)} + E_b + (1/2)Mv^2, \tag{12}$$

$$Mv_0 \pm \hbar k_\gamma = Mv. \tag{13}$$

Here M is the molecule mass, v_0 and v are velocities of a molecule before and after interaction of a nucleus with γ quantum, E_a and E_b are the energies of a molecule before and after interaction, E_γ is an energy of the nuclear transition. Then an energy of the γ satellite is as follows from Eq. (12):

$$E_\gamma = E_\gamma^{(0)} + \hbar k_\gamma v_0 \pm R_{om} \pm (E_b - E_a). \tag{14}$$

Here R_{om} is an energy of recoil: $R_{om} = [(E_\gamma^{(0)}]^2/2Mc^2$. It is well known (cf. [8, 34]) that only the transitions between vibration-rotational levels of the ground electron state, including transitions into continuum with further molecular dissociation, are of a great practical interest. The matrix element for these transitions is as follows:

$$M_{ba} = \langle \Psi_b^*(R_1, R_2) | e^{ik_\gamma R_1} | \Psi_a(R_1, R_2). \tag{15}$$

The values of energy, accepted by the vibrational and rotational degrees of the freedom of a molecule are as follows:

$$\begin{aligned} \varepsilon_{vib} &\approx v\hbar\omega = R_{om}(m_2/m_1), \\ \varepsilon_{rot} &\approx BJ^2 = R_{om}(m_2/m_1). \end{aligned} \tag{16}$$

The simple adequate model for definition of the rotational motion is the rigid rotator approximation. In this approximation the wave functions with definite values of quantum numbers J, K are the eigen functions of the angle momentum operator, i.e.:

$$\psi(R_1, R_2) = Y_{J,K}(\theta, \varphi). \tag{17}$$

In a case of the vibration motion the wave functions with definite value of the vibration quantum number are numerically found by solving the corresponding Schrödinger equation with potential, which is chosen in the Dunham-like form (cf. [51, 56–58]:

$$E(R) = B_0[(R - R_e)/R]^2 \left\{ 1 + \sum_{n=1}^{\infty} b_n [(R - R_e)/R]^2 \right\}. \tag{18}$$

Such an approximation is surely more consistent than the harmonic oscillator one. The harmonic oscillator wave functions were used for estimating matrix elements of the vibration-nuclear transitions in Ref. [41]. In general the matrix element of the vibration-rotation-nuclear transition can be written as follows:

$$M^{v_b,v_a}_{J_b,K_b;J_a,K_a} = (4\pi)^{1/2}[(2J_a+1)(2J_b+1)]^{1/2}(-1)^{K_b}\times$$
$$\times \sum_{l=|J_b-J_a|}^{J_a+J_b} i^l (2l+1)^{1/2}\langle\Psi_{v_b}|(\pi/2a)^{1/2}J_{l+1/2}(a)|\Psi_{v_a}\rangle \begin{pmatrix} J_a & J_b & l \\ 0 & 0 & 0 \end{pmatrix}$$
$$\sum_{m=-l}^{+l} Y^*_{lm}\begin{pmatrix} J_a & J_b & l \\ k_a & -k_b & m \end{pmatrix},$$
$$a = \frac{E^{(0)}_\gamma}{\hbar c}\frac{m_2}{M}R^*\left(1+\frac{Q}{\sqrt{m}R^*}\right). \tag{19}$$

Here $Q = (R-R_0)m^{1/2}$, $m = m_1m_2/M$ is the reduced mass of the molecule, m_1 and m_2 are the masses of nuclei. The co-ordinate of mass centre of the first nucleus relatively the molecule mass centre is defined by expression:

$$R_1 = -\frac{m_2}{M}R = -\frac{m_2}{M}\left(R_0+\frac{Q}{\sqrt{m}}\right) = -\frac{m_2}{M}R_0 - \sqrt{\frac{m_2}{m_1M}}Q.$$

The corresponding probability can be written in the following form:

$$P^{v_bv_a}_{J_bJ_a} = (2J_b+1)\sum_{l=|J_a-J_b|}^{J_a+J_b}(2l+1)\langle\Psi_{v_b}|\sqrt{(\pi/2a)}J_{l+1/2}(a)|\Psi_{v_a}|^2\begin{pmatrix} J_a & J_b & l \\ 0 & 0 & 0 \end{pmatrix}^2. \tag{20}$$

5 Numerical Results for Diatomic Molecules and Discussion

As example we present the results of calculation of the probabilities for vibration-rotation-nuclear transitions from the state with $v_a = 0$, $J_a = 0$ and the state $v_a = 1$, $J_a = 0$ in a case of the emission and absorption spectrum of nucleus ^{127}I ($E^{(0)}_\gamma = 203$ keV) in the molecule of H^{127}I in the ground electron state $X^1\Sigma$ (molecular parameters: $R_0 = 1.61$Å, $\nu_e = 2309$ cm^{-1}, B $= 6.55$ cm^{-1}) (cf. [34,61]). The recoil energy for this molecule is 0.172 eV. Parameters which define an excitation of the vibrations and rotations for this molecule because of the recoil, are as follows: $a_0 = 1.30$ and $\varepsilon_0 = 5.29\cdot 10^{-2}$. It should be noted also that a width of the gamma lines are corresponding to temperature $T = 300$ K. In Fig. 3 we present the calculated spectrum of emission and adsorption of the nucleus ^{127}I in the molecule of H^{127}I (Fig. 3a is corresponding to the initial state of molecule: $v_a = 0, J_a = 0$; Fig. 3b $\sim v_a = 1, J_a = 0$). It should be noted that the values for probabilities, calculated within the Dunham model potential approximation for potential curve [33, 34, 61], differ from the corresponding ones, calculated within the harmonic oscillator approximation [9, 41], in average on 5–20%. It is obvious that a direct experimental observation of the laser-electron-nuclear effect is of a great interest.

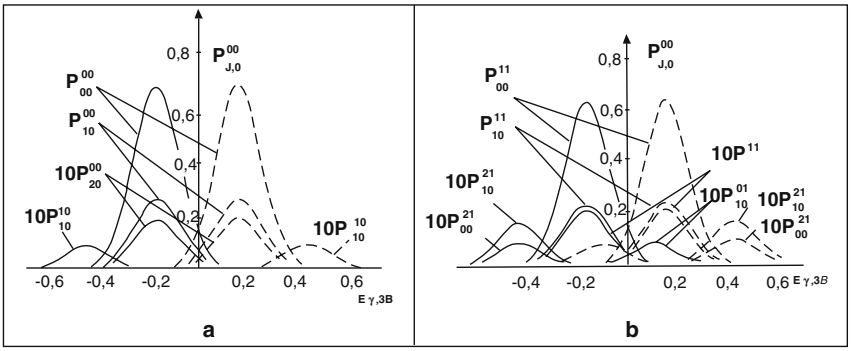

Fig. 3 Calculated emission (*solid curve*) and absorption spectrum of nucleus ^{127}I ($E_\gamma^{(0)} = 203$ keV) linked with molecule H^{127}I. Initial state of molecule: (**a**) above $\nu_a = 0$, $J_a = 0$ and (**b**) below $\nu_a = 1$, $J_a = 0$.

6 Quantum Approach to Calculation of the Electron-Nuclear γ Transition Spectra of Nucleus in Multiatomic Molecules

In this section we present consistent, quantum approach to calculation of the electron-nuclear γ transition spectra (a set of the vibration-rotational satellites in a molecule) of a nucleus in the multiatomic molecules. Estimates of the vibration-nuclear transition probabilities in a case of the emission and absorption spectrum of nucleus ^{191}Ir ($E_\gamma^{(0)} = 82$ keV) in the molecule of IrO_4 and nucleus ^{188}Os ($E_\gamma^{(0)} = 155$ keV) in the molecule of OsO_4 [62] are presented.

Let us consider the key moments of theory. The main purpose is calculation of a structure of the gamma transitions (probability of transition) or spectrum of the gamma satellites because of the changing the electron-vibration-rotational states for the multiatomic molecules under the gamma quantum radiation (absorption). Further we are limited by a case of the five-atomic molecules (of the XY_4 type; T_d). Hamiltonian of interaction of the gamma radiation with a system of nucleons for the first nucleus can be expressed through the co-ordinates of nucleons r'_n in a system of the mass centre of the one nucleus [41, 56, 58, 59]

$$H(r_n) = H(r'_n)\exp(-ik_\gamma u), \tag{21}$$

where k_γ is a wave vector of the gamma quantum, u is the shift vector from equality state (coinciding with molecule mass centre) in the system of co-ordinates in the space. The matrix element for transition from the initial state 'a' to the final state 'b' is represented as usually

$$\langle \Psi_b^* | H | \Psi_a \rangle \langle \Psi_b^* | \exp(-ik_\gamma u) | \Psi_a \rangle, \tag{22}$$

where a and b is a set of quantum numbers, defining the vibrational and rotational states before and after interaction (with gamma- quantum). The first multiplier in

Eq. (22) is defined by the gamma transition of a nucleus and is not dependent upon an internal structure of a molecule in a good approximation. The second multiplier is the matrix element of transition of the molecule from the initial state 'a' to the final state 'b'

$$M_{ba} = \langle \Psi_b^*(r_e)|\Psi_a(r_e)\rangle \langle \Psi_b^*(R_1,R_2)|\exp(-ik_\gamma u)|\Psi_a(R_1,R_2)\rangle. \tag{23}$$

The expression 23 gives a general formula for calculation of the probability of changing the internal state of a molecule under absorption or emitting gamma quantum by a nucleus of the molecule. In fact it defines an amplitude of the corresponding gamma satellites. Their positions are fully determined by the energy and pulse conserving laws as follows [41, 56, 58, 62]:

$$E_\gamma = E_\gamma^0 \pm R + \hbar k_\gamma v \pm (E_b - E_a). \tag{24}$$

Here R is an energy of recoil: $R = [(E_\gamma^{(0)}]^2/(2Mc^2)$, M is the molecule mass, v is a velocity of molecule before interaction of a nucleus with γ quantum, E_a and E_b are the energies of molecule before and after interaction, E_γ is an energy of nuclear transition. The averaged energies for excitation of the rotations and vibrations under absorption or emitting gamma quantum by nucleus of the molecule can be easily evaluated as follows [41, 58, 62]. One can suppose that only single non-generated normal vibration (vibration quantum $\hbar\omega$) is excited and initially a molecule is on the vibrational level $v_a = 0$. If we denote a probability of the corresponding excitation as $P(v_b, v_a)$ and use expression for shift u of the γ-active nucleus through the normal co-ordinates, then an averaged energy for excitation of single normal vibration is as follows:

$$\bar{E}_{\rm vib} = \sum_{v=0}^{\infty} \hbar\omega \left(v + \frac{1}{2}\right) \bar{P}(v,0) - \frac{\hbar\infty}{2} = \sum_{v=0}^{\infty} \hbar\omega \left(v + \frac{1}{2}\right) P(v,0) - \frac{\hbar\omega}{2} = \tag{25}$$

$$= \sum_{v=0} \hbar\omega \left(v + \frac{1}{2}\right) \frac{z^v}{v!} - \frac{\hbar\omega}{2} = \frac{1}{2} R \left(\frac{M-m}{m}\right),$$

where $z = \dfrac{R}{\hbar\omega}\dfrac{M-m}{m}\cos^2\vartheta$, m is the mass of γ-active nucleus, ϑ is the angle between nucleus shift vector and wave vector of γ-quantum and line in $\bar{E}_{\rm vib}$ means averaging on orientations of molecule (or on angles ϑ).

To estimate an averaged energy for excitation of the molecule rotation one must not miss the molecule vibrations as they provide non-zeroth momentum $L = k_\gamma u \sin\vartheta$, which is transferred to a molecule by γ-quantum . In supposing that a nucleus participates only in the single non-generated normal vibration and vibrational state of the molecule is not changed $v_a = v_b = 0$, one could evaluate an averaged energy for excitation of the molecule rotation as follows:

$$\bar{E}_{\rm rot} = \langle \overline{BL^2} \rangle = Bk_\gamma^2 \langle u^2 \rangle \overline{\sin^2\vartheta} = \frac{1}{2} R \frac{B}{\hbar\omega} \frac{M-m}{m}. \tag{26}$$

So, it is correct the following relation $\bar{E}_{\text{rot}}/\bar{E}_{\text{vib}} \sim B/(\hbar\omega)$, i.e. under absorption or emitting gamma quantum by nucleus of the molecule a relationship between averaged energies for excitation of the molecule rotations and vibrations coincides on order of value with relationship between the energies of rotational and vibrational quanta. As for multiatomic molecules it is typical $B/(\hbar\omega) \sim 10^{-4} \div 10^{-2}$, so one could miss the molecule rotations and consider γ-spectrum of a nucleus in the molecule mass centre as a spectrum of the vibration-nuclear transitions.

Further a shift u of the γ-active nucleus can be expressed through the normal co-ordinates $Q_{s\sigma}$ of a molecule:

$$u = \frac{1}{\sqrt{m}} \sum_{s\sigma} b_{s\sigma} Q_{s\sigma}, \tag{27}$$

where m is a mass of the γ-active nucleus; components of vector $b_{s\Phi}$ of the nucleus shift due to the Φ-component of 's' normal vibration of a molecule are the elements of matrix **b** [9]; it realizes the orthogonal transformation of the normal co-ordinates matrix **Q** to the matrix of masses of the weighted Cartesian components of the molecule nuclei shifts q. According to Eq. (21) the matrix element can be written as multiplying the matrix elements on molecule normal vibration, which takes contribution to a shift of the γ-active nucleus:

$$M(b,a) = \prod_s \left\langle v_s^b \left| \prod_\sigma \exp\left(\frac{ik\gamma b_{s\sigma} Q_{s\sigma}}{\sqrt{m}} \right) v_s^a \right| \right\rangle. \tag{28}$$

It is obvious that missing molecular rotations means missing rotations, connected with the degenerated vibrations. Usually wave functions of molecule can be written for non-degenerated vibration as:

$$|v_s\rangle = \Phi_{vs}(Q_s), \tag{29}$$

for double degenerated vibration in the form:

$$|v_s\rangle = \frac{1}{\sqrt{v_s+1}} \sum_{v_{s\sigma_1}, v_{s\sigma_2}, v_{s\sigma_3}} \Phi_{v_{s\sigma_1}}(Q_{s\sigma_1}) \Phi_{v_{s\sigma_2}}(Q_{s\sigma_2}) \tag{30}$$

(where $v_{s\sigma_1} + v_{s\sigma_2} = v_s$) and for triple degenerated vibration as follows:

$$|v_s\rangle = \sqrt{\frac{2}{(v_s+1)(v_s+2)}} \sum_{v_{s\sigma_1}, v_{s\sigma_2}, v_{s\sigma_3}} \Phi_{v_{s\sigma_1}}(Q_{s\sigma_1}) \Phi_{v_{s\sigma_2}}(Q_{s\sigma_2}) \Phi_{v_{s\sigma_3}}(Q_{s\sigma_3}) \tag{31}$$

(where $v_{s\sigma_1} + v_{s\sigma_2} + v_{s\sigma_3} = v_s$).

In the simple approximation function $\Phi_{v_{s\sigma}}(Q_{s\sigma})$ can be chosen in a form of the linear harmonic oscillator one. More exact calculating requires the numerical determination of these functions. Giving directly wave functions $|v_s^a\rangle$ and $\langle v_s^a|$, calculating the matrix element (28) is reduced to a definition of the matrix elements on each component Φ of the normal vibration.

7 Numerical Results for Multiatomic Molecules and Discussion

Below we present the results of calculation for the vibration-nuclear transition probabilities in a case of the emission and absorption spectrum of nucleus ^{191}Ir ($E_\gamma^{(0)} = 82$ keV) in the molecule of IrO_4 and nucleus ^{188}Os ($E_\gamma^{(0)} = 155$ keV) in the molecule of OsO_4. Note that the main difficulty of calculating (28) is connected with definition of values $b_{s\sigma}$ of the normalized shifts of the γ-active decay. It is known that if a molecule has the only normal vibration of the given symmetry type, then the corresponding values of $b_{s\sigma}$ can be found from the well known Eckart conditions, normalization one and data about molecule symmetry. For several normal vibrations of the one symmetry type, a definition of $b_{s\sigma}$ requires solution of the secular equation for molecule $|GF - \lambda E| = 0$ [58–63]. We have used the results of theoretical calculating electron structure of studied system within relativistic scheme of the $X_\forall$-scattered waves method (version [63]; see details also in Refs. [54–58, 62]).

In Table 2 we present the results of calculating probabilities of the first several vibration-nuclear transitions for the molecule of IrO_4. In Table 3 we present the results of calculating probabilities of the first several vibrational-nuclear transitions for molecule OsO_4 in this paper and from refs. [9, 41], where the linear harmonic oscillator approximation has been used. Analysis shows that a more sophisticated calculation gives the higher values for probabilities. These values, calculated within our approach, differ from the corresponding ones, calculated in Ref. [41], in average on 5–20%. In conclusion let us note that obviously the direct experimental observation of the considered gamma-electron-nuclear phenomena in multiatomic molecules is of a great interest for laser chemistry, photo- and biochemistry etc.

Table 2 Probabilities of vibrational-nuclear transitions for molecule IrO_4

Vibrational transitions $v_3^a, v_4^a – v_3^b, v_4^b$	$\bar{P}(v_3^a, v_4^a – v_3^b, v_4^b)$ present paper
0,0–0,0	0.863
1,0–0,0	0.025
0,1–0,0	0.097
1,0–1,0	0.812
0,1–0,1	0.731

Table 3 Probabilities of the vibration-nuclear transitions for molecule OsO_4

Vibrational transitions $v_3^a, v_4^a – v_3^b, v_4^b$	$\bar{P}(v_3^a, v_4^a – v_3^b, v_4^b)$ [9, 41]	$\bar{P}(v_3^a, v_4^a – v_3^b, v_4^b)$ present paper
0.0–0.0	0.731	0.795
1.0–0.0	0.013	0.018
0.1–0.0	0.063	0.074
1.0–1.0	0.704	0.750
0.1–0.1	0.614	0.673

Acknowledgements The authors are very much thankful to Professor S. Wilson for invitation to make contributions on the XII European workshop on Quantum Systems in Chemistry and Physics (London, UK). Authors would like to thank Professors L. Ivanov, E. Ivanova, V. Letokhov for invaluable advises and Professors W. Kohn, C. Rothaan, E. Brandas, S. Wilson, C. Maruani,I. Kaplan, A. Theophilou, M. Bonitz, A. Becker for useful discussion and comments. Authors would like to thank anonymous referees for useful comments too. The support of the Max-Plank Institute for Physics of Complex Systems of Dresden (Germany), Christian-Albrechts-University of Kiel and University of Dresden (Germany), Universities of Geneva and Zurich (Switzerland), ISAN (Russian Acad.Sci., Troitsk, Moscow region, Russia) and the Abdus Salam ICTP Centre (Trieste, Italy) is very much acknowledged.

References

1. M. Scully, M. Zubairy, *Quantum Optics*, (Cambridge, 1997); F. Aumar, H. Winter (eds.), *Photonic, Electronic and Atomic Collisions*, (World Scientific, Singapore, 1997)
2. T.J. Burnevich, J. Evers, C.H. Keitel, Phys. Rev. C **74** 044601-1–044601-10 (2006); K.N. Koshelev, Y.V Sidelnikov, V.V. Vikhrov, V.I. Ivanov, in *Spectroscopy of Multicharged Ions*, ed. by U.I. Safronova, (Nauka, Moscow, 1991), p. 163.
3. L.N. Ivanov, E.P. Ivanova, L. Knight, Phys. Rev. A **48** 4365–4380 (1993)
4. A.V. Glushkov, L.N. Ivanov, E.P Ivanova, *Autoionization Phenomena in Atoms*, (Moscow University Press, Moscow, 1986)
5. A.V. Glushkov, S.V. Malinovskaya, A.V. Loboda, E.P. Gurnitskaya, D.A. Korchevsky, J. Phys. CS **11**, 188–198 (2004)
6. A.V. Glushkov, S.V. Ambrosov, A.V. Loboda, E.P. Gurnitskaya, G.P. Prepelitsa, Int. J. Quant. Chem. **104**, 562–569 (2005)
7. A.V. Glushkov, S.V. Malinovskaya, G.P. Prepelitsa, V. Ignatenko, J. Phys. CS **11**, 199–208 (2004)
8. V.S. Letokhov, *Laser Spectroscopy*, (Academic Press, New York, 1977)
9. V.S. Letokhov, in *Apllication of Lasers in Atomic, Nolecular and Nuclear Physics*, ed. by A.M. Prokhorov, V.S. Letokhov, (Nauka, Moscow, 1979), pp. 412–445
10. A. Glushkov, *Atom in Electromagnetic Field. Numerical Models*, (KNT, Kiev, 2005)
11. A.B. Migdal, J. Phys. USSR **4**, 449–454 (1941)
12. J.S. Levinger, Phys. Rev. **90**, 11–22 (1953)
13. J.S. Levinger, J. Phys. Radium **16**, 556–568 (1955)
14. P.A. Amudsen, P.H. Barker, Phys. Rev. C **50**, 2466–2474 (1994)
15. R. Anholt, P.A. Amundsen, Phys. Rev. A **25**, 169–178 (1982)
16. O. Bohr, B. Motelsson, *Structure of Atomic Nucleus*, (Plenum, New York, 1971)
17. Th. Carlson, C.W. Nestor, T.C. Tucker, F.B. Malik, Phys. Rev. **169**, 27–36 (1968)
18. G. Ciocchetti, A. Molinari, Nuovo Cim. **40**, 69–82 (1965)
19. T. Mukoyama, Sh. Ito, Phys. Lett. A **131** 182–186 (1988)
20. L. Wauters, N. Vaeck, Phys. Rev. C **53**, 497–500 (1996)
21. L. Wauters, N. Vaeck, M. Godefroid, H. var der Hart, M. Demeur, J. Phys. B **30**, 4569–4580 (1997)
22. I.G. Kaplan, A.P. Markin, JETP **64**, 424–432 (1973)
23. I.G. Kaplan, A.P. Markin, Reports of the USSR Acad.Sci. **223**, 1172–1176 (1973)
24. I.G. Kaplan, G.L. Yudin, JETP **69**, 9–16 (1975)
25. I.G. Kaplan, G.L. Yudin, Reports of the USSR Acad.Sci. **232**, 319–324 (1977)
26. J.S. Hansen, Phys. Rev. A **9**, 40–50 (1974)
27. J. Law, Nucl. Phys. A **286**, 339–352 (1977)
28. J. Law, Can. J. Phys. **58**, 504–512 (1980)
29. J. Law, J.L. Campbell, Phys. Rev. C **25**, 514–524 (1982)

30. A.V. Glushkov, S.V. Malinovskaya, Russian J. Phys. Chem. **62**, 100–108 (1988)
31. A.V. Glushkov, S.V. Malinovskaya, Russian J. Phys. Chem. **65**, 2970–2978 (1988)
32. A.V. Glushkov, S.V. Malinovskaya, in *New Projects and New Lines of Research in Nuclear Physics*, ed. by G. Fazio, F. Hanappe (World Scientific, Singapore, 2003) p. 242
33. A.V. Glushkov, L.N. Ivanov, S.V. Malinovskaya, Preprint of Institute for Spectroscopy, Russian Academy off Sciences, N 1AS, (1992)
34. A.V. Glushkov, S.V. Malinovskaya, A.V. Loboda, G.P. Prepelitsa, J. Phys. CS **35**, 420–424 (2004);
35. A.V. Glushkov, S.V. Malinovskaya, Yu.G. Chernyakova, A.A. Svinarenko, Int. J. Quant. Chem. **99**, 889–898 (2004)
36. S.V. Malinovskaya, Int. J. Quant. Chem. **104**, 496–500 (2005)
37. V.S. Letokhov, Phys. Lett. A **46**, 257–260 (1974)
38. V.I. Goldansky, V.S. Letokhov, JETP **67**, 513–520 (1974)
39. L.N. Ivanov, V.S. Letokhov, JETP **68**, 748–756 (1975)
40. L.N. Ivanov, V.S. Letokhov, JETP **71**, 19–28 (1976)
41. V.S. Letokhov, V.G. Minogin, JETP **69**, 1568–1578 (1985)
42. E.P. Ivanova, L.N. Ivanov, JETP **83**, 258–270 (1996)
43. A.V. Glushkov, L.N. Ivanov, Phys. Lett. A **170**, 33–38 (1992)
44. A.V. Glushkov, JETP Lett. **55**, 95–98 (1992)
45. A.V. Glushkov, in *Low Energy Antiproton Physics*, ed. by D. Grzonka, R. Czyzykiewicz, W. Oelert, T. Rozek, P. Winter, vol 796,(2005)p. 206–210.
46. A.V. Glushkov, S. Ambrosov, V. Ignatenko, D. Korchevsky, Int. J. Quant. Chem. **99**, 936–940 (2004)
47. A.V. Glushkov, S.V. Ambrosov, A.V. Loboda, Yu.G. Chernyakova, O.Yu. Khetselius, A.V. Svinarenko, Nucl. Phys. A **734**, 21–28 (2004)
48. A.V. Glushkov, S.V. Ambrosov, A.V. Loboda, E.P. Gurnitskaya, O.Yu. Khetselius, in *Recent Advances in Theoretical Physics and Chemistry Systems*, ed. by J.-P. Julien, J. Maruani, D. Mayou, S. Wilson, G. Delgado-Barrio, G., series: Progress in Theoretical Chemistry and Physics, vol 15, (2006) p. 285
49. A.V. Glushkov, E.P. Ivanova, J. Quant. Spectr. Rad. Transfer. **36**, 127–145 (1986)
50. E.P. Ivanova, L.N. Ivanov, A.V. Glushkov, A.E. Kramida, Phys. Scr. **32**, 512–534 (1985)
51. G. Simons, R.G. Parr, *Quantum Chemistry*, (Academic Press, New York, 2002)
52. J.C. Slater, *The Consistent Field Method for Molecules and Solids: Quantum Theory of Molecules and Solids*, vol 4 (McGraw-Hill, New York, 1974)
53. S. Wilson, in *Recent Advances in Theoretical Physics and Chemistry Systems*, ed. by J. Maruani, S. Lahmar, S. Wilson, G. Delgado-Barrio, Series: Progress in Theoretical Chemistry and Physics, vol 16, (2007) p. 11
54. A.V. Glushkov, J. Struct. Chem. **31**, 9–15 (1990)
55. A.V. Glushkov, J. Struct. Chem. **32**, 11–16 (1992)
56. A.V. Glushkov, J. Struct. Chem. **34**, 3–10 (1993)
57. A.V. Glushkov, Rus. J. Phys. Chem. **66**, 589–596 (1992)
58. A.V. Glushkov, Rus. J. Phys. Chem. **66**, 1259–1276 (1992)
59. A.V. Glushkov, S.V. Malinovskaya, Yu.V. Dubrovskaya, L.A. Vitavetskaya, in *Recent Advances in Theoretical Physics and Chemistry Systems*, ed. by J.-P. Julien, J. Maruani, D. Mayou, S. Wilson, G. Delgado-Barrio, Series: Progress in Theoretical Chemistry and Physics, vol 15, (2006) pp. 301–308.
60. A.V. Glushkov, S.V. Malinovskaya, I.M. Shpinareva, V.P. Kozlovskaya, V.I. Gura, Int. J. Quant. Chem. **104**, 512–519 (2005)
61. A.V. Glushkov, S.V. Malinovskaya, O.Yu. Khetselius, Europ. Phys. Journ. *to be printed*, (2008)
62. A.V. Glushkov, S.V. Malinovskaya, O.Yu. Khetselius, Molec. Phys. *to be submitted*, (2008)
63. V.N. Gedasimov, A.G. Zelenkov, V.M. Kulakov, V.A. Pchelin, M.V. Sokolovskaya, A.A. Soldatov, L.V. Chistyakov, JETP **94**, 1169–1178 (1984)

QED Approach to Atoms in a Laser Field: Multi-Photon Resonances and Above Threshold Ionization

Alexander V. Glushkov(✉), Olga Yu. Khetselius, Andrey V. Loboda, and Andrey A. Svinarenko

Abstract A new consistent method for studying the interaction of atom with a realistic laser field, based on the quantum electrodynamics (QED) and S-matrix adiabatic formalism Gell-Mann and Low, is presented. In relativistic case the Gell-Mann and Low formula expressed an energy shift δE through QED scattering matrix including the interaction with as the laser field as the photon vacuum field. It is natural to describe the laser field-atom interaction by means of the radiation emission and absorption lines. Their position and shape fully determine the spectroscopy of atom in a field. The radiation atomic lines can be described by moments of different orders μ_n. The main contribution into μ_n is given by the resonant range. The values μ_n can be expanded into perturbation theory (PT) series. As example, the method is used for numerical calculation of the three-photon resonant, four-photon ionization profile of atomic hydrogen (1s-2p transition; wavelength = 365 nm) and multi-photon resonance width and shift for transition 6S-6F in the atom of Cs (wavelength 1,059 nm) in a laser pulses with the Gaussian and soliton-like shapes. The results of calculation the above threshold ionization (ATI) characteristics for atom of magnesium field are presented too.

Keywords: atoms, quantum electrodynamics, laser field, multi-photo resonances

A.V. Glushkov
Inst. of Spectroscopy (ISAN), Russian Acad. Sci., Troitsk-Moscow, 142090, Russia;
Odessa University, P.O. Box 24a, Odessa-9, 65009, Ukraine, e-mail: glushkov@paco.net

O.Yu. Khetselius
Odessa University, P.O. Box 24a, Odessa-9, 65009, Ukraine;
Abdus Salam International Centre for Theoretical Physics Strada Costiera, 11 - 34014 Trieste, Italy

A.V. Loboda and A.A. Svinarenko
Odessa University, P.O. Box 24a, Odessa-9, 65009, Ukraine

S. Wilson et al. (eds.) *Frontiers in Quantum Systems in Chemistry and Physics*.

1 Introduction

The interaction of atomic systems with the external alternating fields, in particular, laser fields has been the subject of intensive experimental and theoretical investigation (cf. [1–79]). The appearance of the powerful laser sources allowing to obtain the radiation field amplitude of the order of atomic field in the wide range of wavelengths results to the systematic investigation of the nonlinear interaction of radiation with atoms and molecules. Calculation of the deformation and shifts of the atomic emission and absorption lines in a strong laser field, definition of the k-photon emission and absorption probabilities and atomic levels shifts, study of laser emission quality effect on characteristics of atomic line, dynamical stabilization and field ionization etc. are the most actual problems to be solved. Naturally, it is of the great interest to study a phenomenon of the multiphoton ionization. At present time, a great progress is achieved in the description of the processes of interaction atoms with the harmonic emission field [1–9, 74, 76]. But in the realistic laser field the corresponding processes are in significant degree differ from the similar processes in the harmonic field. The latest theoretical works claim a qualitative study of the phenomenon though in some simple cases it is possible to get quite acceptable quantitative description. Among existed approaches it should be mentioned such methods as the Green function method (the imaginary part of the Green function pole for atomic quasienergy state), the density–matrix formalism (the stochastic equation of motion for density–matrix operator and its correlation functions), a time-dependent density functional formalism, direct numerical solution of the Schrödinger (Dirac) equation, multi-body multi-photon approach etc. [1–36, 66–79]. Decay probabilities of the hydrogen atom states in a super-strong laser field are calculated by the Green function method (see [1, 2, 36]) in a case when the electron- proton interaction is very small regarding the atom-field interaction. Note that this approach can not be easily generalized for multielectron atoms. In Ref. [4] the double-time Gell-Mann and Low formalism is used for studying the line shape of a multi-ionized atom in a strong field of the electromagnetic wave. Effects of the different laser line shape on the intensity and spectrum of resonance fluorescence from a two-level atom are studied in Refs. [11–14]. The laser model considered is that of an ideal single-mode laser operating high above threshold, with constant field amplitude and undergoing phase-frequency fluctuations analogous to Brownian motion. As a correlation time of the frequency fluctuations increases from zero to infinity, the laser line shape changes from Lorentzian to Gaussian in a continuous way. For the intermediate and strong fields, an averaged intensity of fluorescence in a case of the resonant broadband Lorentzian line shape is higher than in a case of the Gaussian line shape with the same bandwidth and total power. This is in contrast to the weak-field case where the higher peak power of the Gaussian line shape makes it more effective than the Lorentzian line shape. In a case of a nonzero frequency correlation time (the non-Lorentzian line shape) an intensity of fluorescence undergoes the non-Markovian fluctuations. In relation to the spectrum of resonance fluorescence it is shown that as the line shape is varied from Lorentzian to Gaussian the following changes take place: in a case of the off-resonance excitation, an asymmetry of the

spectrum decreases. In a case of the resonant excitation, the center peak to side-peak height ratio for the triplet structure increases. The predicted center-line dip in the spectrum for a case of broadband excitation becomes deeper, when the Rabi frequency and bandwidth are almost equal. In the modern experiment it has been found an anomalously strong nonlinear coupling of radiation with atom which can not be fully explained by the modern theoretical models. In any case the problem requires a consistent QED consideration.

Another important topic is connected with the governing and control of non-linear processes in a stochastic, multi-mode laser field [1–8, 36–40, 73–76]. The principal aim of quantum coherent control is to steer a quantum system towards a desired final state through interaction with light while simultaneously inhibiting paths leading to undesirable outcomes. This type of quantum interference is inherent to the non-linear multiphoton processes. The controlling mechanisms have been proposed for atomic, molecular and solid-state systems [1–32, 67–88]. The experimental work by Dudovich et al. tests an effect of the pulse-shaping on transient populations for the excited Rb atoms (cf. [1–4]). The detailed calculations have been carried out for three-level systems within 1D model of a two-electron molecule [5–7,73–77]. Transitions to the excited state occur via a 12-photon interaction for an 800 nm intense pulse of length 244 au, or just over two cycles. Theoretical study of the laser-atom non-linear interaction is often based on solving the time-dependent Schrödinger equation or using the time-independent Floquet formalism. In [6, 69] authors extended the non-Hermitian multi-state Floquet dynamics approach of Day et al. to treat one-electron atomic system for a case of the multi-electron atoms. The result is a generalization of the R-matrix Floquet theory, developed by Burke et al. that allows for pulse shape effects whilst retaining the ab initio treatment of detailed electron correlation. The approach based on the eigenchannel R-matrix method and multichannel quantum-defect theory, introduced by Robicheaux and Gao to calculate two-photon processes in light alkaline-earth atoms has been implemented by Luc-Koenig et al. [15] in j-j coupling introducing explicitly spin-orbit effects and employing both the length and velocity forms of the electric dipole transition operator. In Ref. [15] the two-photon processes including above-threshold ionization in magnesium have been in details studied. Nevertheless in many theories there is a serious problem of the gauge invariance, connected with using non-optimized one-electron representation (in fact provided by not entire account for the multi-body inter electron correlations). The known example is non-coincidence of values for the length and velocity forms of the electric dipole transition operator [15, 36, 40]. In whole one can note that a problem of correct description of the non-linear atomic dynamics in a stochastic, multi-mode laser field is quite far from the final solution. It requires developing the consistent, advanced approaches to description of multi-photon dynamics and new schemes for sensing the stochasticity and photon-correlation effects.

In this paper we present a new consistent method for studying the interaction of atom with a realistic laser field, based on QED and S-matrix adiabatic formalism Gell-Mann and Low [32–50]. In relativistic case the Gell-Mann and Low formula expressed an energy shift δE through the QED scattering matrix including

the interaction with as the laser field as the photon vacuum field. It is more natural to describe the interaction of atom with the realistic laser field by means of the radiation emission and absorption lines [36–40]. Their position and shape fully determine the spectroscopy of atom in a laser field. The radiation atomic lines can be described by moments of different orders μ_n. The first order moment is directly connected with the field shift and width of the corresponding resonances. The main contribution into μ_n is given by the resonant range. The values μ_n can be expanded into perturbation theory (PT) series, though in resonant range the PT can't be used for the transition probabilities. The effective Ivanov-Ivanova approach [34–36] is used for calculating the corresponding QED PT second order sums. As examples we present the results of numerical calculating the three-photon resonant, four-photon ionization profile of atomic hydrogen (1s-2p transition; wavelength = 365 nm) and the multi-photon resonance shift and width for transition 6S-6F in the atom of Cs (wavelength 1,059 nm) in a laser pulse of the Gaussian and soliton-like shapes. The results of calculation the above threshold ionization (ATI) characteristics for atom of magnesium in a intense laser field are presented too.

2 Structure of the Multi-Mode Laser Pulse

As it is well known, for a laser with more than one longitudinal mode, mode beating gives rise to intensity fluctuations within the laser pulse [1, 2, 11–14]. The beat frequencies for n modes range up to $nc/2L = B$, where L is the optical length of the laser oscillator. A detailed analysis of the mode structure of the typical dye laser [11] shows that it has about 15 modes, separated by 1 GHz with a Gaussian amplitude distribution. Classically, the field can be written as follows:

$$\begin{aligned} &E(t) = \varepsilon(t)\mathrm{e}^{-i\omega t} + c.c., \\ &\textit{where} \\ &\varepsilon(t) = \sum_i 0.5 a_i(t)\mathrm{e}^{-i(\Delta\omega_i t + \phi_i)}. \end{aligned} \tag{1}$$

Each mode has amplitude a_i containing a gaussian time envelope, a frequency detuning $\Delta\omega_i$ from the central laser frequency and phase ϕ_i. As experimental study [11, 13] of described laser pulse shows that there is no evidence of the phase coherence in the temporal behavior of laser pulse. Thus, it is usually assumed that the modes have the random phases. Figure 1 shows the temporal variation of intensity for the multi-mode pulse of stochastic laser radiation with the emission line width $b = 0$, 1 cm^{-1}, the coherence time -3×10^{-10}s [11].

Further to make sensing a stochastic structure of the multi-mode laser pulse one should consider the interaction: 'atomic system – stochastic multi-mode laser pulse'. Below it will be shown that this interaction is influenced by the specific chaotic, photon-correlation effects. New theoretical scheme for sensing stochasticity and photon-correlation effects is based on the S-matrix energy approach [36–50] to calculating the multi-photon resonance characteristics for atomic systems in a stochastic laser field.

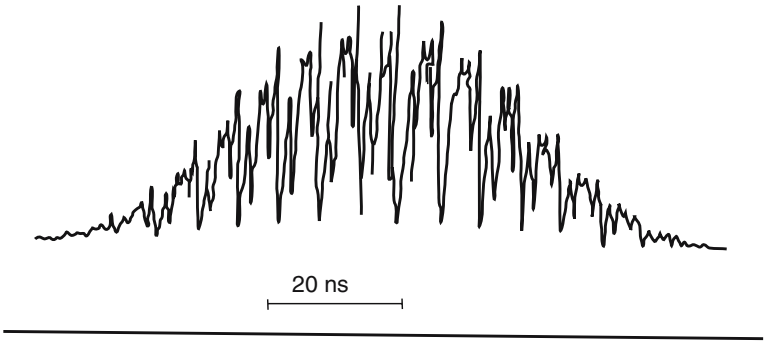

Fig. 1 The temporal variation of intensity for the multi-mode pulse of stochastic laser radiation with the emission line width $b = 0,1\ cm^{-1}$, the coherence time -3×10^{-10} s.

3 S-Matrix Energy Approach to Atoms in a Multi-Mode Laser Field

Following to Refs. [37–40], we describe the interaction of an atom with the realistic laser field by a set of characteristics, which are directly observed in the experiment. We are studying the radiation emission and absorption lines. Their position and shape fully determine the spectroscopy of atom in a field. It is natural to describe these lines by their moments of the different orders μ_n. The moments μ_n are strongly dependent upon the laser pulse quality: intensity and the mode constitution. In particular, the k-photon absorption line center shift in the transition $\alpha \to p$ can not be obtained from the corresponding expression for the "one"-photon absorption by changing $\omega_0 \to \omega_0/k$ and introduction of the multiplier 1/k (ω_0 – the central laser emission frequency). The difference arises already in the first non-appearing perturbation theory (PT) order. It is connected with the unusual behavior of the dynamic polarizability of an atom in the resonant range [36–38].

Let us describe the interaction of atom with laser radiation by means the Ivanov potential:

$$V(r,t) = V(r) \int d\omega f(\omega - \omega_0) \sum_{n=-\infty}^{\infty} \cos[\omega_0 t + \omega_0 n\tau], \tag{2}$$

where n is the whole number. The potential V represents the infinite duration of laser pulses with known frequency τ. Here we consider the effects of interaction of an atom with the single pulse. The representation $V(rt)$ as the infinite sequence of pulses is a formal moment connected with the application of the stationary PT formalism. The function $f(\omega)$ is a Fourier component of the laser pulse. The condition $\int d\omega f^2(\omega) = 1$ normalizes potential $V(rt)$ on the definite energy in a laser pulse. Let us consider the pulse with Lorentzian shape (coherent 1-mode pulse): $f(\omega) = N/(\omega^2 + \Delta^2)$, Gaussian shape (multi-mode chaotic laser pulse): $f(\omega) = N\exp[\ln 2(\omega^2/\Delta^2)]$, and soliton-like pulse of the following shape: $f(t) = N$

$ch^{-1}[t/D]$. Further we will be interested by a cases of the Gaussian and soliton-like pulses. A case of the Lorentzian shape has been considered by us earlier [34–38].

The further program results in the calculating an imaginary part of the energy shift Im $E_\alpha(\omega_0)$ for any atomic level as a function of the laser pulse central frequency. The corresponding function has the shape of resonant curve. Each resonance is connected with the transition $\alpha - p$, in which the definite number of photons is absorbed or radiated. Let us consider following situation: $\alpha - p$ transition with the absorption of k photons (α, p-discrete levels). For the resonance which corresponds to this transition, we calculate the following values:

$$\delta\omega(p\alpha|k) = \int \imath \mathrm{d}\omega Im E_\alpha(\omega)(\omega - \omega_{p\alpha}/k)/N, \tag{3}$$

$$\mu_\mathrm{m} = \int \imath \mathrm{d}\omega Im E_\alpha(\omega)(\omega - \omega_{p\alpha}/k)^\mathrm{m}/N, \tag{4}$$

where $\int \imath d\omega$ Im E_α is the normalizing multiplier; $\omega_{p\alpha}$ is a position of the non-shifted line for atomic transition $\alpha - p, \delta\omega(pa|k)$ is the line shift under k-photon absorption and $\omega_{p\alpha} = \omega_{p\alpha} + k \times \delta\omega(p\alpha|k)$. The first moments μ_1, μ_2 and μ_3 determine the atomic line center shift, its dispersion and coefficient of the asymmetry. To calculate μ_m, we need to get an expansion of E_α to PT series: $E_\alpha = \sum E_\alpha^{(2k)}$ (ω_0). To get this expansion, we use method, based on the Gell-Mann and Low adiabatic formula for δE_α [33–38]. The representation of the S-matrix in the form of PT series induces the expansion for δE_α:

$$\delta E_\alpha(\omega_0) = \lim_{\gamma\to 0}\gamma \sum_{k_1 k_2 \ldots k_n} a(k_1, k_2, \ldots, k_n), \tag{5}$$

$$I_\gamma(k_1, k_2, \ldots, k_n) = \prod_{j=1} S_\gamma^{(kj)}, \tag{6}$$

$$S_\gamma^{(m)} = (-1)^m \int_{-\infty}^{0} \mathrm{d}t_1 \ldots \int_{-\infty}^{t_m - 1} \mathrm{d}t_m \langle \Phi_\alpha | V_1 V_2 \ldots V_m | \Phi_\alpha \rangle, \tag{7}$$

$$V_j = exp(1H_0 t_j) V(rt_j) exp(-1H_0 t_j) exp(\gamma t_j). \tag{8}$$

Here H is the atomic hamiltonian, a (k_1, $k_2, \ldots, k_n$) are the numerical coefficients. The structure of the matrix elements $S_\gamma^{(m)}$ is in details described in [37,38]. After sufficiently complicated calculation one can get the expressions for the line moments as follows. For a case of the Gaussian laser pulse we have:

$$\begin{aligned} &\delta\omega(p\alpha|k) = \{\pi\Delta/(k+1)k\}[E(p, \omega_{p\alpha}/k) - E(\alpha, \omega_{p\alpha}/k)], \\ &\mu_2 = \Delta^2/k \\ &\mu_3 = \{4\pi\Delta^3/[k(k+1)]\}[E(p, \omega_{p\alpha}/k) - E(\alpha, \omega_{p\alpha}/k)], \end{aligned} \tag{9}$$

where

$$E(j, \omega_{p\alpha}/k) = 0{,}5 \sum_{p_i} V_{jpi} V_{pij} \left[\frac{1}{\omega_{jp_i} + \omega_{p\alpha}/k} + \frac{1}{\omega_{jp_i} - \omega_{p\alpha}/k}\right]. \tag{10}$$

The summation in (10) is fulfilled on all states of atomic system. For a case of the Lorentzian pulse the corresponding expressions are given in Refs. [37, 38]. In a case of the laser pulse with shape $ch^{-1}[t/D]$ it is necessary to carry out a direct numerical calculation (we did it) or use different approximations to simplify the final expressions. Indeed, the last procedure may result in a great mistake. Each term in Eq. (9) for $\delta\omega$ is formally similar to the known expression for the off-resonant shift of atomic level (p or α) in the monochromatic radiation field with frequency $\omega_{p\alpha}/k$. However, here these values have other physical essence. When $k \to \infty$ (an infinite little laser pulse central frequency) the formula for δE gives the correct expression for energy level shift in the stationary field. The expressions (9), (10) for $\delta\omega$ and μ_n describe the main characteristics of the absorption line near resonant frequency $\omega_{p\alpha}/k$. One can see that these characteristics are determined not only by the radiation frequency, but also by the quantiness of the process. For example, the line shift is proportional $1/(k+I)$, but no – to value of $1/k$, as one can wait for. Under $k = 1$ there is an additional non-standard term. It will be shown below that this approach allows to obtain the theoretical results in an excellent agreement with experiment. The details of the numerical procedure are given below and presented in Refs. [33–50] too.

4 Ivanova-Ivanov Approach to Calculating the Perturbation Theory Second Order Sums

In this chapter we present the Ivanova-Ivanov approach to calculating sums of the second order of the QED perturbation theory [33–36]. It will be used in calculation of the expressions (9), (10). In fact, speech is about determination of the matrix elements for operator of the interelectron interaction over an infinitive set of virtual states, including the states of the negative continuum. A sum on the principal quantum number is defined in quadratures of the Dirac function and auxiliary functions x, x (look below). All computational procedure results in solution of simple system of the ordinary differential equations with known boundary conditions under $r = 0$. Exchange of the interelectron interaction operator $1/r_{12}$ on one-electron operator $V(r)$ decreases a brevity of summation on the virtual states. In a one-particle representation the cited sums are expressed through sums of the one-electron matrix elements:

$$\sum_{n_1} \langle n\chi m|V|n_1\chi_1 m_1\rangle \langle n_1\chi_1 m_1|V|n\chi m\rangle / \left(\varepsilon_{n_1\chi_1 m_1} - \varepsilon\right), \tag{11}$$

where $\varepsilon = \varepsilon_{n\chi m} + \omega_{p\alpha}/k$ is the energy parameter. One-electron energies $\varepsilon_{n\chi m}$ include the rest energy $(\alpha Z)^{-2}$. Let us note that here we use the Coulomb units (an energy in the Coulomb units [q.u.]: 1 q.u. $= Z^2$ a.u.e. [Z – –a charge of a nucleus; a.u.e. = 1 atomic unit of energy).

Consider a scheme of calculating the sum (11). Fundamental solutions of one-electron Dirac equations with potential $V_C = U(r)$ have the same asymptotic as the

Dirac equation with Coulomb potential under $r \to 0$ and $r \to \infty$. Let us consider a bi-spinor of the following form:

$$\Phi_{\chi_1 \overline{m_1}} = \sum_{n_1} \varphi_{n_1 \chi_1 m_1} \langle n_1 \chi_1 m_1 | V | n \chi m \rangle / \left(\varepsilon_{n_1 \chi_1 m_1} - \varepsilon \right). \tag{12}$$

The radial parts $F, G$of bi-spinor Φ satisfy to system of the differential equations:

$$\begin{array}{l} -F' / \alpha Z + (1 + \chi_1) F / \alpha Z r + A_2 G = \Lambda_2, \\ G' / \alpha Z + (1 - \chi_1) G / \alpha Z r + A_1 F = \Lambda_1. \end{array} \tag{13}$$

$$\begin{array}{l} A_1(r) = U(r) + 1 / (\alpha Z)^2 - \varepsilon, \\ A_2(r) = U(r) - 1 / (\alpha Z)^2 - \varepsilon. \end{array} \tag{14}$$

The radial functions Λ_1, Λ_2 in a case of the dipole interaction are presented below. Solution of the system (13) can be represented as follows:

$$\begin{array}{l} F(r) = \alpha Z \left[x(r) \tilde{f}(r) - \tilde{x}(r) f(r) \right] / 2\gamma, \\ G(r) = \alpha Z [x(r) \tilde{g}(r) - \tilde{x}(r) g(r)] / 2\gamma, \ \gamma = \left[\chi^2 - \alpha^2 Z^2 \right]^{1/2}. \end{array} \tag{15}$$

A pair of functions f, g and $\tilde{f}$, $\tilde{g}$ are two fundamental solutions of the equations (13) without right parts. These functions satisfy to conditions: $f \sim r^{\gamma - 1}$, f, $g \sim r^{-\gamma - 1}$ under $r \to 0$. Here we introduce the following functions:

$$\begin{array}{l} x = \alpha Z \int\limits_0^r dr' r'^2 [\Lambda_1(r') f(r') + \Lambda_2(r') g(r')], \\ \tilde{x} = \alpha Z \int\limits_0^r dr' r'^2 \left[\Lambda_1(r') \tilde{f}(r') + \Lambda_2(r') \tilde{g}(r') \right] + D. \end{array} \tag{16}$$

Further let us define constant D in the expressions (16). Let us suppose that $\varepsilon < (\alpha Z)^{-2}$ (i.e. an energy lies below the boundary of ionization), but an energy does not coincide with any discrete eigen value of the Dirac equation. Then

$$D = -\alpha Z \int\limits_0^\infty dr r^2 \left(\Lambda_1 \tilde{f} + \Lambda_2 \tilde{g} \right). \tag{17}$$

Let an energy ε coincides with energy of some discrete level $n_0 \chi_1 m_1$. It is supposed that this state is excluded from (11) and (13). Then the constant D can be found from condition:

$$\int\limits_0^\infty dr\, r^2 \left(F f_{n_0 \chi_1 m_1} + G g_{n_0 \chi_1 m_1} \right) = 0. \tag{18}$$

Now let $\varepsilon > (\alpha Z)^{-2}$ (i.e. an energy lies above the boundary of ionization). Then a constant D can be found from the following condition:

$$\lim_{r\to\infty} r^2 \int_r^{T+r} dr'\, r'^{/2} \left(F f_{\varepsilon\chi_1 m_1} + G g_{\varepsilon\chi_1 m_1}\right) = 0. \tag{19}$$

Here $\varepsilon\chi_1 m_1$ is one-electron state of scattering with energy ε; T is a period of asymptotic oscillations of the functions f, g:

$$T = 2\pi\left[\varepsilon^2 - (\alpha Z)^{-2}\right]^{1/2}.$$

Let us give the corresponding expressions for functions Λ_1, Λ_2 in the most typical case of the dipole interaction of atom with a laser field. The corresponding potential is as follows:

$$V(r) = (a, \alpha). \tag{20}$$

Here a is a vector of polarization of radiation; α is a vector of the Dirac matrices.

Let us remember that usually the vectors $a_1 = (1,0)$, $a_2 = (1,-0)$ are corresponding to the circular polarization and the vector $a_3 = (1,00)$ is corresponding to linear one. Under definition of the multi-photon resonance energies and widths there is a task of calculating the sums (11), where an index n_1 runs the whole spectrum of states or some state n_0 is excluded from the sum. In the first case the functions Λ_1 and Λ_2 are defined by the expressions:

$$\begin{aligned} \Lambda_1 &= B\left(a|j_1 l_1 m_1,\ j\tilde{l}m\right) g_{n\chi}/\alpha Z, \\ \Lambda_2 &= B\left(a|j_1 \tilde{l}_1 m_1,\ jlm\right) f_{n\chi}/\alpha Z. \end{aligned} \tag{21}$$

In the second case one can substitute the following functions to the right parts of (13):

$$\begin{aligned} &\bar{\Lambda}_1 = \Lambda_1 - f_{n_0\chi_1 m_1} Y/\alpha Z; \\ &\bar{\Lambda}_2 = \Lambda_2 - g_{n_0\chi_1 m_1} Y/\alpha Z; \\ &Y = \int dr\, r^2 \left[f_{n_0\chi_1 m_1} g_{n\chi m} B\left(a|j_1 l_1 m_1, j\tilde{l}m\right) - g_{n_0\chi_1 m_1} f_{n\chi m} B\left(a|j_1 \tilde{l}_1 m_1, jlm\right)\right]. \end{aligned} \tag{22}$$

Here the functions $\Lambda_1$and Λ_2 are defined by the expressions (21).

The angle functions are dependent upon the polarization vector and defined by the following formula:

$$\begin{aligned} &B(a_1|jlm,\ j'l'm') = (-1)^{j'+l'-1/2}\, \delta_{u'}\delta_{m',m-1} b(-m,\, m'), \\ &B(a_2|jlm,\ j'l'm') = (-1)^{j+l-1/2}\, \delta_{u'}\delta_{m',m+1} b(-m,\, m'), \\ &B(a_3|jlm,\ j'l'm') = \delta_{u'}\delta_{m,m'}\left[b(-m,\, -m) + (-1)^{j+j'} b(m,\, m')\right], \\ &b(m,\, m') = \left[2\frac{\chi+1/2+m}{2\chi+1} - \frac{\chi'+1/2+m'}{2\chi'+1}\right]^{1/2}. \end{aligned} \tag{23}$$

The final expression for the sum (11) can be written as follows:

$$\int \mathrm{d}r^2 \left[f_{n\chi_1} G B\left(a|jlm, j_1\tilde{l}_1 m_1\right) + g_{n\chi} F \times B\left(a|j\tilde{l}m_1, j_1 l_1 m_1\right)\right]. \tag{24}$$

Finally the computational procedure results in a solution of sufficiently simple system of the ordinary differential equations for above described functions and integral (24).

5 Energy QED Approach to Multiphoton Resonances and Above Threshold Ionization

In this section we apply an approach based on the QED perturbation theory [7, 11–13, 16, 19, 22, 26, 28] to calculating the characteristics of multi-photon ionization in different atomic systems. We calculate numerically the above threshold ionization (ATI) cross-sections for atom of magnesium in a intense laser field. The two-photon excitation process will be described in the lowest QED PT order. This approach is valid away from any one-photon intermediate-sate resonance. We start from the two-photon amplitude for the transition from an initial state Ψ_0 with energy E_0 to a final state $|Psi_f$ with energy $E_f = E_0 + 2\omega$ is:

$$T_{f0}^{(2)} = \lim_{n\to 0_+} \int d\varepsilon \langle \Psi_f | D \times e | \varepsilon \rangle (E_0 + \omega - \varepsilon + in)^{-1} \langle \varepsilon | d \times e | \Psi_0 \rangle. \qquad (25)$$

Here D is the electric dipole transition operator (in the length r form), e is the electric field polarization and ω is a laser frequency. It is self-understood that the integration in Eq. (25) is meant to include a discrete summation over bound states plus an integration over continuum states. Usually explicit summation is avoided by using the approach of Dalgarno-Lewis, setting [15]:

$$T_{f0}^{(2)} = C_f \langle \| D \times e \| \Lambda_p \rangle, \qquad (26)$$

where $\langle \| ... \| \rangle$ is a reduced matrix element and C_f is an angular factor depending on the symmetry of the Ψ_f, Λ_p, Ψ_0 states. Λ_p can be found from solution of the following inhomogeneous equation [15, 36]

$$(E_0 + \omega \times H | \Lambda_p \rangle = (D \times e) | \Psi_0 \rangle \qquad (27)$$

at energy $E_0 + \omega$, satisfying outgoing-wave boundary conditions in the open channels and decreasing exponentially in the closed channels. The total cross section (in $\mathrm{cm}^4\ \mathrm{W}^{-1}$) is expressed as

$$\sigma / I = \sum_J \sigma_J / I = 5.7466 \times 10^{-35} \omega_{\mathrm{au}} \sum_J |T_{J,0}^{(2)}|^2, \qquad (28)$$

where I (in $\mathrm{W/cm}^2$) is the laser intensity. Different quantities can be used to describe two-photon processes [34]: the generalized cross section $\sigma^{(2)}$, given in units of $\mathrm{cm}^4\mathrm{s}$, by

$$\sigma_{\mathrm{cm}^4\mathrm{s}}^{(2)} = 4.3598 \times 10^{-18} \omega_{\mathrm{au}} \sigma / I_{\mathrm{cm}^4\mathrm{W}^{-1}} \qquad (29)$$

and the generalized ionization rate $\Gamma^{(2)}/I^2$, (and probability of two-photon detachment) given in atomic units, by the following expression

$$\sigma/I_{\mathrm{cm^4W^{-1}}} = 9.1462 \times 10^{-36}\omega_{\mathrm{au}}\Gamma^{(2)}_{\mathrm{au}}/I^2_{\mathrm{au}}. \tag{30}$$

Described approach is realized as computer program block in our atomic numeric code "Superatom" (complex of programs, which numerically realize the methods [33–60]), which includes the numerical solution of the Dirac equation and calculation of the matrix elements of the Eqs. 17–18 type. The original moment is connected with using the consistent QED gauge invariant procedure for generating the atomic functions basis's (optimized basis's) [40]. This approach allows getting results in an excellent agreement with experiment and they are more precise in comparison with similar data, obtained with using the non-optimized basis's.

6 Results and Discussion

6.1 The Multi-Photon Resonance Spectra and Above Threshold Ionization

Let us present the results of calculating the multi-photon resonances spectra characteristics for atom of magnesium in a laser field. Note that in order to calculate spectral properties of atomic systems, different methods are used: relativistic R-matrix method (R-method; Robicheaux-Gao, 1993; Luc-Koenig E. et al. 1997), added by multi channel quantum defect method, K-matrix method (K-method; Mengali-Moccia,1996), different versions of the finite L^2 method (L^2 method) with account of polarization and screening effects (SE) (Moccia-Spizzo, 1989; Karapanagioti et al. 1996), Hartree-Fock configuration interaction method (CIHF), operator QED PT (Glushkov-Ivanov, 1992; Glushkov et al. 2004) etc. (cf. [15, 36, 40]. In Table 1 we present results of calculating characteristics for $3p^2{}^1S_0$ resonance of Mg; *E*- energy, counted from ground state (cm^{-1}), Γ-autoionization width (cm^{-1}), σ/I- maximum value of the generalized cross-section ($\mathrm{cm}^4\mathrm{W}^{-1}$). R-matrix calculation with using the length and velocity formula led to results, which differ on 5–15%, that is an evidence of non-optimality of the atomic basis's. This problem is absent in our approach and agreement between theory and experiment is very good. Further let us consider process of the multi-photon ATI from the ground state of Mg. The laser radiation photons energies ω in the range of 0.28–0.30 a.u. are considered, so that the final autoionization state (AS) is lying in the interval between 123350 cm^{-1} and 131477 cm^{-1}. First photon provides the AS ionization, second photon can populate the Rydberg resonance's, owning to series *4snl, 3dnl, 4pnp* where J = 0 and J = 2 [15]. In Table 2 we present energies (cm^{-1} ; counted from the ground level of Mg $3s^2$) and widths (cm^{-1}) of the AS (resonance's) $4snl, 3dnl, 4p^2\ {}^1D_2$, calculated by the K-, R-matrix and our methods. In a case of $^1S_0$ resonance's one can get an excellent identification of these resonance's. Let us note that calculated spectrum of

Table 1 Characteristics for $3p^2\,{}^1S_0$ resonance of atom of the magnesium: E- energy, counted from ground state (cm^{-1}), Γ- autoionization width (cm^{-1}), σ/I- maximum value of generalized cross-section (cm^4W^{-1})

Methods	E	Γ	σ/I
Luc-Koenig E. et al. 1997	Without	Account	SE
Length form	68,492	374	$1.96\ 10^{-27}$
Velocity form	68,492	376	$2.10\ 10^{-27}$
Luc-Koenig E. et al. 1997	With	Account	SE
Length form	68,455	414	$1.88\ 10^{-27}$
Velocity form	68,456	412	$1.98\ 10^{-27}$
Moccia and Spizzo (1989)	68,320	377	$2.8\ 10^{-27}$
Robicheaux and Gao (1993)	68,600	376	$2.4\ 10^{-27}$
Mengali and Moccia (1996)	68,130	362	$2.2\ 10^{-27}$
Karapanagioti et al. (1996)	68,470	375	$2.2\ 10^{-27}$
Our calculation	68,281	323	$2.0\ 10^{-27}$

Table 2 Energies and widths (cm^{-1}) of the AS (resonance's) $4snl, 3dnl, 4p^2\,{}^1D_2$ for Mg (see text)

${}^1D_2$	$R-$method $E\ \Gamma$	${}^1D_2$	Our approach $E\ \Gamma$		$K-$ method $E\ \Gamma$
4s3d	109900 2630	4s3d	109913 2645		110450 2600
$3d^2$	115350 2660	$3d^2$	115361 2672		115870 2100
4s4d	120494 251	4s4d	120503 259	(ds)	120700 170
3d5s	123150 1223	3d5s	123159 1235	(ds)	123400 2000
$4p^2$	124290 446	$4p^2$	124301 458		124430 500
3d4d	125232 400	3d4d	125245 430		125550 590
4s5d	126285 101	4s5d	126290 113	(ds)	126250 120
3d6s	127172 381	3d6s	127198 385	(ds)	127240 350
4s6d	127914 183	4s6d	127921 215		127870 1900
3d5d	128327 208	3d5d	128344 215		
4s7d	128862 18	4s7d	128874 24	(ds)	128800 30
3d5g	128768 4,5	3d5g	128773 5,2	3d5g	128900 2,2
3d7s	129248 222	3d7s	129257 235		129300 160
4s8d	129543 114	4s8d	129552 125	(ds)	129500 140
		3d6d	129844 115		
		4s9d	129975 64		
		4s10d	130244 5		
		3d8s	130407 114		
		4s11d	130488 118		
		4s12d	130655 28		
		3d7d	130763 52		
		4s13d	130778 36		
		4s14d	130894 14		
		4s15d	130965 7		

to-photon ATI is in a good agreement with the R-matrix data and experiment. In a whole other resonances and ATI cross-sections demonstrate non-regular behavior.

The studied system is corresponding to a status of quantum chaotic system with very interesting stochastization mechanism. It realizes through laser field induction of the overlapping (due to random interference and fluctuations) resonances in spectrum, their non-linear interaction, which lead to a global stochasticity in the system and quantum chaos phenomenon. The quantum chaos is well known in physics of the hierarchy, atomic and molecular physics, in particular, in theory of atomic systems in an external electromagnetic field. Earlier this effect has been found in simple atomic systems H, He, and also Ca (cf. Refs. in [3, 47, 60]). Analysis indicates on its existence in the Mg spectrum. Spectrum of resonance's can be divided on three intervals: (1) An interval, where states and resonances are clearly identified and not strongly perturbed; (2) quantum-chaotic one, where there is a complex of the overlapping and strongly interacting resonances; (3). Shifted interval on energy, where behavior of the energy levels and resonances is similar to the first interval. The quantitative estimate shows that the resonance distribution in the second quantum-chaotic interval is satisfied to the Wigner distribution as follows:

$$W(x) = xexp(-\pi x^2/4).$$

At the same time, in the first interval the Poisson distribution is valid.

6.2 The Three-Photon Resonant, Four-Photon Ionization Profile of Atomic Hydrogen

Below we present the results of calculating the multi-photon resonances for atomic systems in a stochastic laser field and show the possibilities for sensing a structure of the stochastic, multi-mode laser pulse and photon-correlation effects for atomic (and nano-optical) systems in this field. We start from results of the numerical calculation for the three-photon resonant, four-photon ionization profile of atomic hydrogen (1s-2p transition; wavelength = 365 nm). In Fig. 2 we present the shift S ($= \delta\omega$) and width W of the resonance profile as the function of the mean laser intensity at the temporal and spatial center of the UV pulse: experimental data 3s, 3w (Kelleher, Ligare and Brewer [11]; multi-mode Gaussian laser pulse with bandwidth 0.25 cm^{-1}; full width at half of one), theoretical calculation results on the basis of the stochastic differential equations method 1s and 1w by Zoller [12]) and results of our calculation: 2s, 2w.

At first, one can see the excellent agreement between the theory and experiment. At second, a comparison of these results with analogous data for a Lorentzian laser pulse [37,49] shows that the corresponding resonance shift in a case of the Gaussian shape pulse is larger than the shift in a case of the Lorentzian pulse at $\sim$3 times. This fact is connected with the photon-correlation effects and stochasticity of the laser pulse.

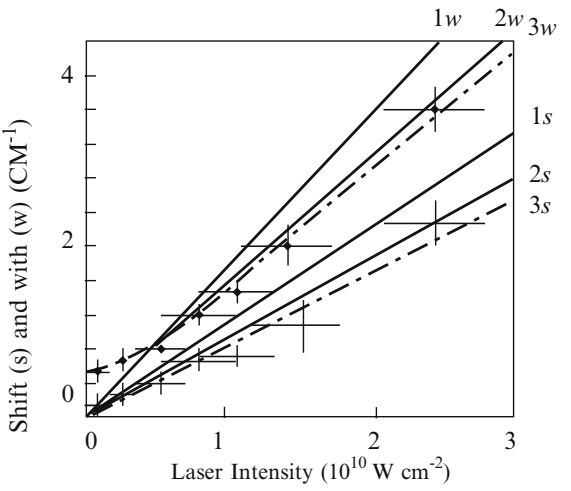

Fig. 2 Shift (S) and width (W) of resonant profile as laser intensity function: experiment – S_3, W_3 (Kelleher, Ligare, Brewer); theory of Zoller – S_1, W_1 and our results – S_2, W_2

6.3 Calculation Results of the Multi-Photon Resonance Width and Shift for Transition 6S-6F in the Atom of Cs

Further let us consider the numerical calculation results for three-photon transition 6S-6F in the Cs atom (wavelength 1,059 μm). The detailed experimental study of the multi-photon processes in the Cs atom has been carried out in Ref. [13]. In this paper it is experimentally studied a statistics of the laser radiation and characteristics of the multi-photon ionization are measured.

According to Ref. [13], the line shift is linear function of the laser intensity (laser intensity is increased from 1.4 to 5.7 $10(7)W/cm^2$) and is equal (a case of the Gaussian multi-mode laser pulse): $\delta\omega(p\alpha|k) = bI$ with $b = (5.6 + -0.3)$ cm$^{-1}/GW \times cm^{-2}$ (b is expressed in terms of energy of the three-photon transition 6S-6F).

The corresponding shift obtained with coherent (one-mode) laser pulse is defined as follows: $\delta\omega 0(p\alpha|k) = aI, a = 2$ cm$^{-1}/GW \times$ cm^{-2}. Theoretical values, obtained with using no-optimized atomic basis's, are as follows: (i). for soliton-like laser pulse: $\delta\omega(p\alpha|k) = bI, b = 6.7$ cm$^{-1}/GW \times$ cm^{-2}; (ii). for the gaussian multi-mode pulse (chaotic light): $\delta\omega(p\alpha|k) = bI$ with $b = 5.8$ cm$^{-1}/GW \times$ cm^{-2}; (iii). for the coherent one-mode pulse: $\delta\omega 0(p\alpha|k) = aI, a = 2,1$ cm$^{-1}/GW \times$ cm^{-2}.

The analogous theoretical values, obtained in our calculation within described above S-matrix formalism, are as follows:

1. The gaussian multi-mode pulse (chaotic light) $\delta\omega(p\alpha|k) = bI, b = 5.63$ cm$^{-1}/GW \times$ cm^{-2};
2. The coherent one-mode pulse: $\delta\omega 0(p\alpha|k) = aI$, $a = 2.02$ cm$^{-1}/GW \times$ cm^{-2};
3. The soliton-like laser pulse: $\delta\omega(p\alpha|k) = bI, b = 6.5$ cm$^{-1}/GW \times$ cm^{-2}.

One can see that for the multi-mode pulse the radiation line shift is significantly larger (in $\sim$3 times), than the corresponding shift in a case of the single-mode pulse. In fact the radiation line shift is enhanced by the photon-correlation effects. In Fig. 3

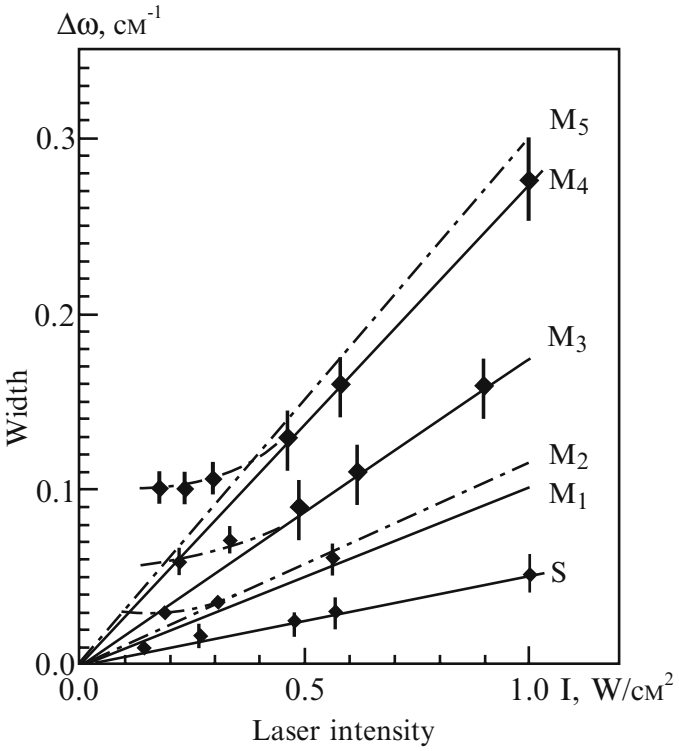

Fig. 3 The multi-photon resonance width for transition 6S-6F in the atom of Cs (wavelength 1059 nm) in dependence upon the laser intensity I: S – for single-mode Lorentz laser pulse; M_1, M_3, M_4 – for multi-mode Gauss laser pulse respectively with line band 0.03, 0.08 and 0.15 cm^{-1}; M_2, M_5 – for multi-mode soliton-type with line band 0.03 cm^{-1} and 0.15 cm^{-1}; marker – experiment [13].

we present the results of calculation for the multi-photon resonance width for transition 6S-6F in the atom of Cs (wavelength 1059 nm) in dependence upon the laser intensity.

We use the following denotations: S – for single-mode Lorentz laser pulse; M_1, M_3, M_4 – for multi-mode Gauss laser pulse respectively with line band 0.03 cm^{-1}, 0.08 cm^{-1} and 0.15 cm^{-1}; M_2, M_5 – for multi-mode soliton-type with line band 0.03 cm^{-1} and 0.15 cm^{-1}; marker – experimental data [13]. In Ref. [13] the experimental data for laser pulse of the Gaussian shape with line band respectively 0.03 cm^{-1}, 0.08 cm^{-1}, 0.15 cm^{-1} are presented. In general there is a physically reasonable agreement between theory and high-qualitative experiment. Analysis shows that the shift and width of the multi-photon resonance line in a case of interaction of an atom with the multimode laser pulse is greater than the corresponding resonance shift and width in a case of interaction of an atom with the single-mode laser pulse. It is corresponding to the experimental data [13]. From physical point of

view it is provided by action of the photon-correlation effects and influence of the multimodity of the laser pulse (cf. [13–15, 36–40, 49]).

Acknowledgements The authors are very much thankful to Professor S. Wilson for invitation to make contributions on the XII European workshop on Quantum Systems in Chemistry and Physics (London, UK). One of the authors (A.G.) thank Professors L. Ivanov, E. Ivanova, W. Kohn, E. Brandas, S. Wilson, I. Kaplan, J. Maruani, A. Theophilou for helpful discussion and comments. The useful comments of referees are very much acknowledged. One of the authors (A.G.) acknowledges support of Russian Academy of Sciences (Moscow, Russia), a NATO ESF-'Research Integrity' (Lisbon-Portugal), the Christian-Albrechts-University of Kiel (Germany), Max-Plank Institute for Physics of Complex systems of Dresden and Universities of Dresden and Frieburg (Germany), Universities of Geneva and Zurich (Switzerland) grants. Two authors (A.G. and O.K.) would like also to thank Dr. A. Messina and CEWQO (Palermo, Italy) and the Abdus Salam International Centre for Theoretical Physics (Trieste, Italy) for support.

References

1. D. Batani, C.J. Joachain (eds.), *Matter in super-intense laser fields*, (AIP Serie, N.-Y., 2006)
2. C.A. Ullrich., S. Erhard., E.K. Gross (eds.), *Superintense Laser Atoms Physics*, (Kluwer, N.-Y., 2005)
3. F. Aumar, H. Winter (eds.), *Photonic, Electronic and Atomic Collisions*, (World Scientific, Singapore, 1997)
4. K.N. Koshelev, Y.V. Sidelnikov, V.V. Vikhrov, V.I. Ivanov, in *Spectroscopy of Multicharged Ions*, ed. by U.I. Safronova, (Nauka, Moscow, 1991), p. 163
5. A. Staudt, C.H. Keitel, J. Phys. B: At. Mol. Opt. Phys. **36** L203–209(2003)
6. M. Plummer, C.J. Noble, J. Phys. B: At. Mol. Opt. Phys. **36** L219–L226(2003)
7. R. Hasbani, E. Cormier, H. Bachau, J. Phys. B: At. Mol. Opt. Phys. **33** 2101–2116 (2000)
8. T. Mercouris, C.A. Nikolaides, Phys. Rev. A **67** 063403-1–063403-12 (2003)
9. E. Brandas, P. Floelich, Phys. Rev. A **16** 2207–2216 (1977)
10. A.V. Glushkov, JETP Lett. **55**, 97–100 (1992)
11. D.E. Kelleher, M. Ligare, L.R. Brewer, Phys. Rev. A **31** 2747–2762 (1985)
12. P. Zoller, J. Phys. B: At. Mol. Opt. Phys. **15** 2911–2926 (1982)
13. L.-A. Lompre, G. Mainfrau, C. Manus, J.P. Marinier, J. Phys. B: At. Mol. Opt. Phys. **14** 4307–4322 (1981)
14. M. Grance, J. Phys. B: At. Mol. Opt. Phys. **11** 1931–1939 (1978)
15. E. Luc-Koenig, A. Lyras, J.-M. Lecomte, M. Aymar, J. Phys. B: At. Mol. Opt. Phys. **30** 5213–5232 (1997)
16. V.D. Rodriguez, E. Cormier, R. Gayet, Phys. Rev. A **69** 053402-1–053402-8 (2004)
17. M.V. Fedorov, Physics-Uspekhi **169** 66–71 (1999)
18. N.B. Delone, V.P. Kraynov, Physics-Uspekhi **168** 531–549 (1998)
19. V.S. Popov, Physics-Uspekhi **174** 921–946 (2004)
20. I.A. Ivanov, Y.K. Ho, Phys. Rev. A **69** 023407-1–023407-6 (2004)
21. J. Caillat, J. Zanghellini, M. Kitzler, O. Koch, W. Kreuzer, A. Scrinzi, Phys. Rev. A **71** 012712-1–012712-12 (2005)
22. V.S. Letokhov, *Laser Spectroscopy*, (Academic Press, New York, 1977)
23. V.S. Letokhov, in *Apllication of Lasers in Atomic, Nolecular and Nuclear Physics*, ed. by A.M. Prokhorov, V.S. Letokhov, (Nauka, Moscow, 1979), p. 412–445
24. I.G. Kaplan, A.P. Markin, JETP **64**, 424–432 (1973)
25. I.G. Kaplan, G.L. Yudin, JETP **69**, 9–16 (1975)
26. I.G. Kaplan, G.L. Yudin, Reports of the USSR Acad.Sci. **232**, 319–324 (1977)

27. V.S. Letokhov, Phys. Lett. A **46**, 257–260 (1974)
28. V.I. Goldansky, V.S. Letokhov, JETP **67**, 513–520 (1974)
29. L.N. Ivanov, V.S. Letokhov, JETP **68**, 748–756 (1975)
30. L.N. Ivanov, V.S. Letokhov, JETP **71**, 19–28 (1976)
31. V.S. Letokhov, V.G. Minogin, JETP **69**, 1568–1578 (1985)
32. E.P. Ivanova, L.N. Ivanov, E.V. Aglitsky, Phys. Reports **164**, 315–395 (1988)
33. E.P. Ivanova, L.N. Ivanov, JETP **83**, 258–270 (1996)
34. E.P. Ivanova, L.N. Ivanov, Theor. Math, Phys. **12**, 251–268 (1974)
35. L.N. Ivanov, E.P. Ivanova, L. Knight, Phys. Rev. A **48**, 4365–4380 (1993)
36. A.V. Glushkov, L.N. Ivanov, E.P. Ivanova, *Autoionization Phenomena in Atoms*, (Moscow University Press, Moscow, 1986)
37. A.V. Glushkov, L.N. Ivanov, Preprint of Institute for Spectroscopy, Russian Academy off Sciences, N 3AS, (1992)
38. A.V. Glushkov, L.N. Ivanov, in *Atomic Spectroscopy*, ed. by U.I. Safronova, (Nauka, Chernogolovka, 1992)
39. A.V. Glushkov, Soviet Physics (Izv. Vuzov. Ser. Phys.) **41**, 29–38 (1991)
40. A.V. Glushkov, L.N. Ivanov, Phys. Lett. A **170**, 33–38 (1992)
41. A.V. Glushkov, L.N. Ivanov, J. Phys. B: At. Mol. Opt. Phys. **26**, L379–L386 (1993)
42. A.V. Glushkov, S.V. Ambrosov, S.V. Malinovskaya, Bound Volume of Paris-Meudon Observatory **1**, 148–152 (1996)
43. A.V. Glushkov, S.V. Ambrosov, G.P. Prepelitsa, V.P. Polischuk, J. Techn. Phys. **38**, 219–224 (1997)
44. A.V. Glushkov, Sensor Electr. and Micros.Techn. **1**, 16–22 (2004)
45. A.V. Glushkov, Sensor Electr. and Micros.Techn. **3**, 29–35 (2006)
46. A.V. Glushkov, A.V. Loboda, J. Appl. Spectr. **74**, 271–278 (2007)
47. A. Glushkov, *Atom in Electromagnetic Field. Numerical Models*, (KNT, Nauka, Moscow-Kiev, 2005)
48. A.V. Glushkov, S.V. Malinovskaya, in *New Projects and New Lines of Research in Nuclear Physics*, ed. by G. Fazio, F. Hanappe (World Scientific, Singapore, 2003) p. 242
49. A.V. Glushkov, in *Low Energy Antiproton Physics*, ed. by D. Grzonka, R. Czyzykiewicz, W. Oelert, T. Rozek, P. Winter, vol 796, (2005) pp. 206–210.
50. A.V. Glushkov, S.V. Malinovskaya, Yu.G. Chernyakova, A.A. Svinarenko, Int. J. Quant. Chem. **99**, 889–898 (2004)
51. A.V. Glushkov, S. Ambrosov, V. Ignatenko, D. Korchevsky, Int. J. Quant. Chem. **99**, 936–940 (2004)
52. S.V. Malinovskaya, Int. J. Quant. Chem. **104**, 496–500 (2005)
53. A.V. Glushkov, S.V. Malinovskaya, A.V. Loboda, E.P. Gurnitskaya, D.A. Korchevsky, J. Phys. CS **11**, 188–198 (2004)
54. A.V. Glushkov, S.V. Ambrosov, A.V. Loboda, E.P. Gurnitskaya, G.P. Prepelitsa, Int. J. Quant. Chem. **104**, 562–569 (2005)
55. A.V. Glushkov, S.V. Malinovskaya, G.P. Prepelitsa, V. Ignatenko, J. Phys. CS **11**, 199–208 (2004)
56. A.V. Glushkov, S.V. Ambrosov, A.V. Loboda, Yu.G. Chernyakova, O.Yu. Khetselius, A.V. Svinarenko, Nucl. Phys. A **734**, 21–28 (2004)
57. A.V. Glushkov, S.V. Ambrosov, A.V. Loboda, E.P. Gurnitskaya, O.Yu. Khetselius, in *Recent Advances in Theoretical Physics and Chemistry Systems*, ed. by J.-P. Julien, J. Maruani, D. Mayou, S. Wilson, G. Delgado-Barrio, Series: Progress in Theoretical Chemistry and Physics, vol 15, (2006) p. 285
58. A.V. Glushkov, S.V. Malinovskaya, A.V. Loboda, G.P. Prepelitsa, J. Phys. CS **35**, 420–424 (2006)
59. A.V. Glushkov, S.V. Malinovskaya, Yu.V. Dubrovskaya, L.A. Vitavetskaya, in *Recent Advances in Theoretical Physics and Chemistry Systems*, ed. by J.-P. Julien, J. Maruani, D. Mayou, S. Wilson, G. Delgado-Barrio, Series: Progress in Theoretical Chemistry and Physics, vol 15, (2006) pp. 301–308.

60. A.V. Glushkov, S.V. Malinovskaya, I.M. Shpinareva, V.P. Kozlovskaya, V.I. Gura, Int. J. Quant. Chem. **104**, 512–519 (2005)
61. A.V. Glushkov, S.V. Malinovskaya, E.P. Gurnitskaya, O.Yu. Khetselius, Yu.V. Dubrovskaya, J. Phys. CS **35**, 425–430 (2006)
62. A.V. Glushkov, S.V. Malinovskaya, Russian J. Phys. Chem. **62**, 100–108 (1988)
63. A.V. Glushkov, S.V. Malinovskaya, Russian J. Phys. Chem. **65**, 2970–2978 (1988)
64. A.V. Glushkov, E.P. Ivanova, J. Quant. Spectr. Rad. Transfer. **36**, 127–145 (1986)
65. E.P. Ivanova, L.N. Ivanov, A.V. Glushkov, A.E. Kramida, Phys. Scr. **32**, 512–534 (1985)
66. D. Dundas, J.M. Rost, Phys. Rev. A **71**, 013421-1–013421-8 (2005)
67. A. Jaron-Becker, A. Becker, F.H.M. Faisal, Phys. Rev. A **69**, 023410-1–023410-10 (2004)
68. A. Becker, R. Dorner, R. Moshammer, J. Phys. B: At. Mol. Opt. Phys. **38**, 5753–5772 (2005)
69. D.A. Telnov, Shih-I. Chu, Phys. Rev. A **71**, 013408-1–013408-10 (2005)
70. U.W. Rathe, C.-H. Keitel, M. Protopapas, P.L. Knight, J. Phys. B: At. Mol. Opt. Phys. **30**, L531–L539 (1997)
71. S.V. Fomichev, D.F. Zaretsky, D. Bauer, W. Becker, Phys. Rev. A **71**, 013201-1–013201-24 (2005)
72. L.P. Pitaevsky, Physics-Uspekhi **176**, 345–365 (2006)
73. M.Yu. Emelin, M.Yu. Ryabikin, A.M. Sergeev, M. Chernobrovtseva, T. Pfayfer, D. Valter, G. Gerber, JETP Lett. **77**, 254–259 (2003)
74. A.V. Kim, M.Yu. Ryabikin, A.M. Sergeev, Physics-Uspekhi **169**, 58–65 (1999)
75. N.H. March, J. Mol. Str. **300**, 479–500 (1993)
76. V.P. Kraynov, B.M. Smirnov, Physics-Uspekhi **170**, 969–992 (2000)
77. S.X. Hu, Z.Z. Xu, Appl. Phys. Lett. **71**, 2605–2610 (1997)
78. V. Veniard, R. Taieb, A. Maquet, Phys. Rev. A **60**, 3952–3964 (1999)
79. J. Zweiback, T. Ditmire, M.D. Perry, Phys. Rev. A **59**, R3166–3198 (1999)
80. G. Simons, R.G. Parr, *Quantum Chemistry*, (Academic Press, New York, 2002)
81. J.C. Slater, *The Consistent Field Method for Molecules and Solids: Quantum Theory of Molecules and Solids*, vol 4 (McGraw-Hill, New York, 1974)
82. S. Wilson, in *Recent Advances in Theoretical Physics and Chemistry Systems*, ed. by J. Maruani, S. Lahmar, S. Wilson, G. Delgado-Barrio, Series: Progress in Theoretical Chemistry and Physics, vol 16, (2007) p. 11
83. A.V. Glushkov, J. Struct. Chem. **31**, 9–15 (1990)
84. A.V. Glushkov, J. Struct. Chem. **32**, 11–16 (1992)
85. A.V. Glushkov, J. Struct. Chem. **34**, 3–10 (1993)
86. A.V. Glushkov, Rus. J. Phys. Chem. **66**, 589–596 (1992)
87. A.V. Glushkov, Rus. J. Phys. Chem. **66**, 1259–1276 (1992)
88. V.N. Gedasimov, A.G. Zelenkov, V.M. Kulakov, V.A. Pchelin, M.V. Sokolovskaya, A.A. Soldatov, L.V. Chistyakov, JETP **94**, 1169–1178 (1984)

A Collaborative Virtual Environment for Molecular Electronic Structure Theory: A Prototype for the Study of Many-Body Methods

Stephen Wilson(✉) and Ivan Hubač

Abstract A prototype collaborative virtual environment is described which has been specifically designed for the development of theory, the associated algorithms and computer code in the study of the molecular electronic structure problem. The environment was constructed as part of a project aimed at the further development of Brillouin-Wigner many-body methods for the handling of the electron correlation problem for systems where the use of a multireference formalism is required; a formalism which can often be plagued by the 'intruder state' problem in practical applications. The collaborative virtual environment is web-based and contains three main elements:- *(i)* details of the participants, *(ii)* a knowledge base, *(iii)* tools for collaboration. By developing the prototype virtual environment whilst carrying out collaborative research on a specific problem, these three elements have been carefully tailored for the needs of the molecular physics/quantum chemistry researcher. The further development of a collaborative virtual environment for molecular electronic structure theory is briefly considered.

Keywords: e-science, collaborative virtual environment, molecular electronic structure, many-body methods

S. Wilson
Physical & Theoretical Chemistry Laboratory, University of Oxford, South Parks Road, Oxford OX1 3QZ, England; Department of Chemical Physics, Faculty of Mathematics, Physics and Informatics, Comenius University, 84215 Bratislava, Slovakia, e-mail: quantumsystems@gmail.com

I. Hubač
Department of Chemical Physics, Faculty of Mathematics, Physics and Informatics, Comenius University, 84215 Bratislava, Slovakia. e-mail: hubac@tex.dbp.fmph.uniba.sk

S. Wilson et al. (eds.) *Frontiers in Quantum Systems in Chemistry and Physics*.

Introduction

The internet offers new ways for communication between scientists especially when they are situated in geographically distributed locations. As Ziman [1] has pointed out:

> the communication system is *[...]* vital to science; it lies at the very heart of the 'scientific method'.

Most learned journals are today available both in print and on line. Some new journals are only available on line. On line versions of journals can offer significant advantages:- fast, economical distribution, hypertext links to cited literature, easy incorporation of colour figures and illustrations, in-text movies, and so on.

But, as well as changing the way in which scientists formally present their completed work to their peers, the internet is also changing the way that researchers collaborate whilst carrying out their projects. This paper describes some of our recent work aimed at the development of methods for collaborative research in molecular physics and quantum chemistry via the internet.

A collaborative virtual environment has been developed for quantum chemistry whilst actually carrying out a significant, 'real life' project so that those features which were found to be useful in facilitating the collaboration could be evaluated and incorporated in the emerging environment. A collaborative virtual environment actively supports human-human communication in addition to human-machine communication and uses a virtual environment as the interface. The specific quantum chemical project considered involved the development of Brillouin-Wigner methods for handling the many-body problem which arises in molecular electronic structure theory especially when a multireference formulation is required. This project is concerned with the development of robust methods which can be applied routinely in situations where a multireference formalism is required. It involves the development of theory and associated algorithms as well as computation.

This project was carried out under the auspices of the EU COST programme - Action D23 - METACHEM (*Metalaboratories for Complex Computational Applications in Chemistry*).[1] The establishment of a European Metalaboratory[2] for *ab initio* multireference quantum chemical methods had two main objectives:

1. The development of a comprehensive suite of capabilities for remote scientific collaboration between geographically distributed sites, creating a prototypical environment tailored to the needs of the quantum chemistry community. This

[1] Project number: D23/0001/01: European Metalaboratory for multireference quantum chemical methods (01/02/2001 - 18/07/2005). Participants: P. Čársky, J. Pittner *(J. Heyrovsky Institute, Prague, Czech Republic)*, I. Hubač *(Comenius University, Slovakia)*, S. Wilson *(Rutherford Appleton Laboratory, UK)*, W. Wenzel *(Universität Dortmund, Germany)*, L. Meissner *(Nicholas Copernicus University, Poland)*, V. Staemmler *(Ruhr Universität Bochum Germany)*, C. Tsipis *(Aristotle University of Thessaloniki, Greece)*, A. Mavridis *(National and Kapodistrian University of Athens, Greece)*.

[2] Loosely speaking, a *metalaboratory* may be defined as a cluster of geographically distributed resources.

environment is supposed to provide a cross-platform suite of tools for data exchange and sharing and sharing of computer resources. The tools should help to easily build and share our common knowledge base and allow the exchange of draft manuscripts, documents, preprints and reprints, data preparation and analysis, program execution, training, etc. The use of a web-based communication for the Metalaboratory should ensure that all of the data, notes, sketches, molecular structures under consideration, etc., are always available from any desktop to all participants.

2. The Metalaboratory focuses on a specific problem at the cutting-edge of modern *ab initio* quantum chemical methodology – the development of multireference quantum chemical methods together with the associated algorithms. Such methods are essential for the description of the breaking of bonds, a process which might be regarded as the very essence of chemistry. By establishing a European Metalaboratory directed towards the solution of a specific and challenging scientific problem, a rapid evaluation of facilities for remote collaboration will be achieved as well as a coordinated problem-solving programme directed towards the development of robust, reliable and cost-effective *ab initio* multireference quantum chemical methods. Such methods are still far from being routine since their widespread use in practical applications is frequently hampered by their complexity and by the problem of intruder states.

The need to establish more effective mechanisms for collaboration has become evident in our previous work under EU COST Action D9.[3] Therefore, in parallel with further development of accurate multireference quantum chemical methods, we decided to investigate the use of web-based and internet tools for remote scientific collaboration. In the past, some of the participants have exchanged data, draft manuscripts and the like by *e*-mail, supplemented by occasional correspondence by post and face-to-face meetings. By exploring alternative mechanisms, in particular, real-time collaboration procedures, we aim to establish a more productive environment. This includes remote execution of computer programs, the use of web-based interfaces for remote collaboration. The intention has been to use only a publicly accessible and user-friendly software for making the expertise accumulated in this project profitable for national and international collaborations in other domains of chemistry and physics.

The development of collaborative virtual environments is a key element of what is becoming known as "*e*-science".[4] In 2000, Sir John Taylor, Director General of Research Councils, Office of Science and Technology, UK, wrote

> *e*-Science is about global collaboration in key areas of science, and the next generation of infrastructure that will enable it.

[3] EU COST Action D9 "Advanced computational chemistry of increasingly complex systems".

[4] For some details see, for example the Wikipedia entry on *e*-science at

http://en.wikipedia.org/wiki/E-Science

Currently the largest focus in *e*-science is in the United Kingdom. In the United States similar initiatives are termed cyberinfrastructure projects.

He predicted that

> *e*-Science will change the dynamic of the way science is undertaken.

We submit that key elements of *e*-science such as collaborative virtual environments will evolve most rapidly and deliver a functionality required by practicing scientists if they are developed as part of a research project in the target discipline. This is the approach that we have followed in this work. We have developed a collaborative virtual environment for molecular electronic structure theory whilst undertaking research into aspects of the Brillouin-Wigner theory for many-body systems.

In the following section, we give a brief overview of molecular electronic structure theory using Brillouin-Wigner expansions. This is only intended to provide the necessary background for the description of our collaborative virtual environment which is given in Sect. 2. Section 3 contains a summary and our conclusions.

1 Molecular Electronic Structure Theory Using Brillouin-Wigner Expansions

A fundamental understanding of the structure and properties of molecular entities lies in the solution of the appropriate quantum mechanical equations which govern the behaviour of the component particles, electrons and nuclei. The large disparity of the masses of the electrons and the nuclei allows the separation of the equations describing their respective motion to a good approximation in most case. This is the Born-Oppenheimer approximation.[5] The motion of the electrons is then described in the field of fixed or clamped nuclei by the electronic Schrödinger equation. Solution of this equation for different configurations of the nuclei provides an effective potential in which the nuclear motion takes place.

The solution of the electronic Schrödinger equation is frequently approximated by decoupling the motion of each electron by invoking an independent electron model (or independent particle model). Each electron is taken to move in the mean field arising from the nuclei and the other electrons in the system. The resulting equations are solved self-consistently.[6] The approximation provided by the independent electron model is then refined by taking account of the instantaneous interactions of the electrons, that is, by accounting for electron correlation effects.[7] Such effects may be described by the method of configuration interaction, by the coupled cluster expansion or by many-body perturbation theory. These techniques

[5] For a recent discussion of the separation of electronic and nuclear motion in molecules see the chapters by B.T. Sutcliffe in the *Handbook of Molecular Physics and Quantum Chemistry*, volume 1 [2].

[6] For a recent discussion of the separation of the electronic Schrödinger equation for molecules see the chapter by R. McWeeny in the *Handbook of Molecular Physics and Quantum Chemistry*, volume 2 [3].

[7] For a recent discussion of the electron correlation problem for molecules see the chapter by R. McWeeny in the *Handbook of Molecular Physics and Quantum Chemistry*, volume 2 [4].

are well understood and form the basis of robust computational procedures in cases where the correlation treatment is developed with respect to a single reference function. In many cases, however, a multireference formulation is required. For example, the description of bond breaking processes invariable demands the use of a multireference formalism.

Multireference configuration interaction is robust and thus, for example, Meissner et al. recently wrote [5]

> The multi-reference configuration interaction (*MRCI*) method with singles and doubles (*MR-CISD*) is one of very few quantum chemical methods which are used in routine calculations for systems requiring a multi-reference description. The main reason for that is its formal and computational simplicity and resistance to the intruder-state problem which frequently occurs in other multi-reference-type calculations.

However, these authors also caution

> "An important drawback of the *MR-CISD* scheme is, however, a relatively poor description of the dynamic electron correlation provided by the linear expansion."

This fundamental difficulty with the *MR-CISD* formalism has fostered the development of "many-body" techniques over the past 50 years including perturbation theory and cluster expansions. In their multireference formulations, these techniques are plagued by the intruder state problem which can degrade or even destroy the convergence of the expansion.

In recent years, Brillouin-Wigner methods have been applied to the "many-body" problem in molecules in a "state specific" formulation. Although the Brillouin-Wigner expansion is not itself a "many-body" theory, it can be subjected to *a posteriori* correction which removes unphysical terms, which in the diagrammatic formalism correspond to unlinked diagrams [6].

It is not our purpose here to describe the details of the application of Brillouin-Wigner methods to many-body systems in molecular physics and quantum chemistry. Such details can be found elsewhere [6–8].

2 Elements of a Collaborative Virtual Environment for Molecular Electronic Structure Theory

A collaborative virtual environment for molecular electronic structure theory evolved during research into the use of Brillouin-Wigner methodology in handling the electron correlation problem in molecules. We describe all of the elements of a collaborative virtual environment that we have considered and give a brief assessment of how useful each element turned out to be in practice. Others may find different elements to be more or less useful in their own collaborative work. Others may find elements that we have not listed here to be useful. We believe that collaborative virtual environments will become increasing important in the years ahead. They will undoubtedly be at their most useful when tailored to participants' research projects.

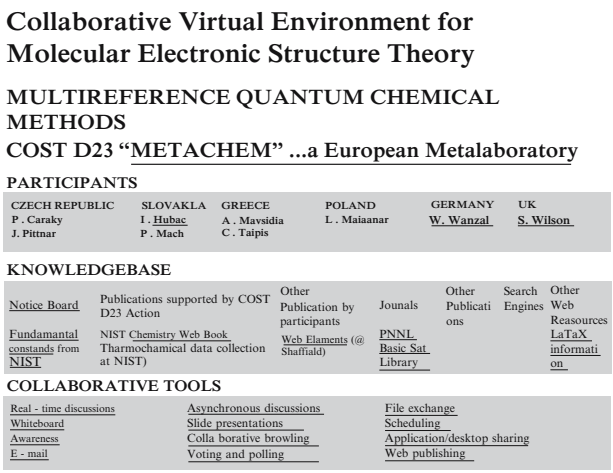

Fig. 1 Prototype collaborative virtual environment for molecular electronic structure theory

We are not aware of any previous work which has examined the use of collaborative virtual environments in molecular electronic structure theory or quantum chemistry.

The environment is web-based. This has the advantage that it can be accessed from any machine with an internet connection from home or office or mobile computer. Also the web-pages associated with the environment can be distributed, that is different pages can be hosted by different machines in different locations.

Our collaborative virtual environment consists of three main elements:-

(i) Details of the participating scientists, i.e. the human resources for the collaboration

(ii) A knowledge base of key information of use to scientists involved in the project, i.e. the intellectual foundations upon which the research is built and the intellectual products of the collaborative research

(iii) A set of tools for collaboration, i.e. mechanisms for exchanging ideas and for criticising proposals, sharing information and pooling resources

The prototype environment home page is shown in Fig. 1. The three main regions of this page correspond to the three elements listed above. We shall describe each of these key components in the following sections.

2.1 Participants Details

Obviously, it is important for effective collaboration to take place that the details of the participating scientists be available to all participants. The details must be current. We found the following items to be useful:

- Postal address. Each participants affiliation is required in writing reports, proposals and manuscript. Since there is almost no physical exchange of material between participating scientists, the postal address are not used frequently.

- Telephone number. Both calls to office land line and mobile telephones are useful, but more recently internet telephony has become practical and more economic. SMS[8] is a useful feature.
- Internet telephone identity: This has become practical recently. We have used the service provided by Skype[9] which is free-of-charge and also allows conference calls.
- Fax number. Fax is seldom used in recent years since it is easier and more economic to scan a document and dispatch it as an attachment to an *e*-mail message.
- *E*-mail address. *e*-mail is vital for effective collaboration. It is accurate, fast and reliable. Unlike telephone calls (including those via the internet) is not intrusive, not requiring immediate response. *e*-mail messages can include a variety of attachments, including LaTeX files, which facilities the exchange of typeset mathematical equations, or scanned images as pdf files, which allows the exchange of hand written notes and diagrams.
- World Wide Web home page
- Calendar. Essential for scheduling meetings whether virtual or real.
- Curriculum Vitae. Often required for the preparation of new proposals and reports on work completed.
- Publications. A database organized by author, title, journal, date of publication, and keywords.

2.2 Knowledge Base

The second element of a collaborative virtual environment is a 'knowledge base' – a set of items that are required or found useful in carrying out the research project.

- *E*-notice board, including details of upcoming conferences, workshops, meetings and summer schools
- *E*-note book. A database organized by date of entry, author and keywords
- Draft manuscripts. A database organized by date of entry, author, title and keywords
- The NIST Reference on Constants, Units and Uncertainty:-

http://physics.nist.gov/cuu/Constants/

[8] Short message service (SMS), available on most digital mobile phones, for sending of short messages between mobile phones, other handheld devices and even landline telephones.

[9] Details can be found at

http://www.skype.com

Skype provides free global telephony allowing unlimited voice calls using peer-to-peer software. The authors' skype identifiers are dr_stephen_wilson and dr_ivan_hubac

- NIST Chemistry Web-book:-

  http://webbook.nist.gov/chemistry/

- Web elements:-

  http://www.webelements.com/

- Basis set library, e.g. the EMSL Gaussian Basis Set Order Form:-

  http://www.emsl.pnl.gov/forms/basisform.html

- LaTeX, e.g. the official LaTeX project home page

  http://www.latex-project.org/

  the Comprehensive TeX Archive Network (CTAN)

  http://www.ctan.org/

  LaTeX[10] is the well known documentation preparation systems which can be used to typeset a wide variety of documents. LaTeX focuses on the logical structure of the document rather than the format of the individual pages. It is particularly suitable for the typesetting of mathematical formulae and yet a LaTeX input file contains only standard (ASCII) text characters and can therefore be created and edited by any text editor and easily exchanged by *e*-mail. In remote collaborations LaTeX is particularly important for the fast and accurate exchange of mathematical formulae. For example, the recursion

$$\Omega_\alpha = 1 + \mathscr{B}_\alpha \mathscr{H}_1 \Omega_\alpha, \tag{1}$$

  which arises in the quantum chemical research project briefly described in the previous section and which represents the Bloch equation [16] in Brillouin-Wigner form, takes the following form in LaTeX:

```
\begin{equation}
\Omega_{\alpha}=1+\mathcal{B}_{\alpha}\mathcal{H}_1
\Omega_{\alpha},
\label{1}
\end{equation}
```

  There are many books providing information about and help with the use of LaTeX. We mention Kopka and Daly *A Guide to LaTeX2e: Tools and Techniques for Computer Typesetting* [13], Diller *LaTeX Line by Line* [14], and Mittelbach et al. *The LaTeX Companion* [15], as well as the original publications by Knuth [9, 10] and by Lamport [11, 12]. A set of help pages in hypertext markup language by Sheldon Green were also found useful.

[10] The TeX computer program and programming language was created by D.E. Knuth [9, 10]. It consists of about 300 *primitive* commands which, together with a further 600 commands, constitute what is known as *plain* TeX [10]. LaTeX is a collection of TeXmacros which was designed by L. Lamport for use as a markup language. The version designated LaTeX2e, defined by Lamport in 1994, was used in the present work.

- feynmf: A combined LaTeX/Metafont package for easy drawing of professional quality Feynman diagrams. feynmf lays out most diagrams satisfactorily from the structure of the graph without any need for manual intervention. Nevertheless all the power of Metafont is available for more obscure cases. Ohl's feynmf is designed for use with current LaTeX, and works in combination with Metafont. The feynmf package reads a description of the diagram written in TeX , and writes out code. Metafont can then produce a font for use in a subsequent LaTeX run.

  http://www.ctan.org/tex-archive/macros/latex/contrib/feynmf/

- COST, European Cooperation in the field of Scientific and Technical Research:

  http://cost.cordis.lu/src/home.cfm

- COST Action D23 "European Metalaboratory for multireference quantum chemical methods":-

  http://cost.cordis.lu/src/extranet/publish/D23WGP/d23-0001-01.htm

- Publications produced under the present COST action. A database organized by author, title, journal, date of publication, and keywords.
- Other publications by participants. A database organized by author, title, journal, date of publication, and keywords.
- Other publications of interest to the project. A database organized by author, title, journal, date of publication, and keywords.
- Journals: see Table 1 for a partial list of journals included in the 'knowledge base'. Access to each journal was governed by the licensing arrangements in place at each participants host institution.

Table 1 Some typical journals included in the 'knowledge base' component of our prototype environment together with their current web addresses

Journal	Web address
Chem. Phys. Lett.	www.sciencedirect.com/science/journal/00092614
Int. J. Quantum Chem.	www3.interscience.wiley.com/cgi-bin/jhome/29830
J. Am. Chem. Soc.	pubs.acs.org/journals/jacsat/
J. Chem. Phys.	scitation.aip.org/jcpo/
J. Comput. Chem.	www3.interscience.wiley.com/cgi-bin/jhome/33822
J. Phys. B: At. Mol. Opt. Phys.	www.iop.org/EJ/journal/JPhysB
J. Phys. Chem. A	pubs.acs.org/journals/jpcafh/index.html
J. Phys. Chem. B	pubs.acs.org/journals/jpcbfk/index.html
J. Molec. Struct. (THEOCHEM)	www.elsevier.com/locate/theochem
Molec. Phys.	www.tandf.co.uk/journals/titles/00268976.asp
Prog. Theor. Chem. & Phys.	www.springeronline.com/sgw/cda/frontpage/ 0,11855,4-135-69-33109911-0,00.html
Phys. Rev. Lett.	prl.aps.org/
Phys. Rev. A	pra.aps.org/
Phy. Chem. Chem. Phys.	www.rsc.org/Publishing/Journals/CP/index.asp

- Search engines, e.g. Google:-

  http://www.google.com

- Programming tools, including literate programming methods. We have describe the use of literate programming methods in quantum chemistry elsewhere [18]. Literate programming provides a mechanism for introducing higher standards of code documentation and thus greater levels of collaboration in quantum chemistry code development and distribution. Literate programming combines the theoretical development of a particular model with the associated computer code. In 1984, D.E. Knuth published his seminal paper [19] entitled *"Literate programming"* in The Computer Journal. Knuth proposed a system of programming, which he termed the WEB,[11] for the generation of structured and documented programs. The philosophy of the WEB system is described by Knuth as follows:-

  > I believe that the time is ripe for significantly better documentation of programs, and that we can best achieve this by considering programs to be works of literature. Hence, my title: *"Literate Programming*.

  Knuth advocates a radical shift of emphasis in the writing of computer programs. He makes this point as follows:-

  > Let us change our traditional attitude to the construction of programs: Instead of imagining that our main task is to instruct a computer what to do, let us concentrate rather on explaining to human beings what we want a computer to do.

  Although Knuth made these observations 20 years ago, to date they have had surprising little impact in computational quantum chemistry or, indeed, computational chemistry in general. For example, there is no mention of literate programming methods in, for example, the *Encyclopedia of Computational Chemistry* [20], a major reference work in the field published in 1998. Indeed, to the authors knowledge, literate programming techniques have not been widely adopted in any of the computational sciences.
  Knuth recognizes that the task facing a literate programmer extends beyond that of a computer programmer. The literate programmer strives not only to create correct and efficient computer code but also a description of the theoretical concepts that lie behind the code. Knuth [21] explains the literate programmers task as follows:-

  > The practitioner of literate programming can be regarded as an essayist, whose main concern is with exposition and excellence of style. Such an author, with thesaurus in hand, chooses the names of variables carefully and explains what each variable means. He or she strives for a program that is comprehensible because its concepts have been introduced in an order that is best for human understanding, using a mixture of formal and informal methods that reinforce each other.

[11] This is **not** to be confused with the World Wide Web which had not been proposed at the time Knuth first published his idea.

The literate programming approach offers significant benefits including: *(i)* structured code, *(ii)* collaborative development, *(iii)* code integrity, *(iv)* economy/efficiency, *(v)* education. For more details see, for example, Ref. [18].

- Numerical libraries, e.g. Numerical Algorithms Group

  http://www.nag.co.uk/

  and *Numerical Recipes in C* [22]

  http://www.nr.com/

- *Ab initio* quantum chemistry program suites, e.g. GAUSSIAN [23]

  http://www.gaussian.com/

  which is the most widely used quantum chemical software suite, and GAMESS [24]

  http://www.msg.ameslab.gov/GAMESS/GAMESS.html

  for which the source code is freely available.
- Other web resources, e.g. wikipedia:-

  http://en.wikipedia.org/wiki/Main_Page

  and wiktionary:-

  http://en.wiktionary.org/wiki/Main_Page

2.3 Collaborative Tools

The third element of a collaborative virtual environment is a set of 'collaborative tools', including

- *E*-mail: This is vital for effective collaboration. It is accurate, fast, reliable and economic. Unlike telephone calls (including those made via the internet) is not intrusive, not requiring immediate response. *e*-mail messages can include a variety of attachments, including LaTeX files, which facilities the exchange of typeset mathematical equations, or scanned images as pdf[12] files, which allows the exchange of hand written notes and diagrams.

[12] Adobe's Portable Document Format (pdf) [17] guarentees page fidelity down to the smallest glyph or piece of white space. pdf files can be viewed and printed on many different computer platforms by means of Adobe's Acrobat Reader

http://www.adobe.com/products/acrobat/readermain.html

or ghostscript

http://www.cs.wisc.edu/~ghost/

The latter can also convert Postscript into pdf format.

- Slide presentations, workshop and conference presentations for discussion before they are delivered and for reference afterwards. These are usually created as pdf files and stored in a database.
- Real-time discussions using internet telephone (skype www.skype.com). Conference calls are also facilitated. Accurate scheduling is vital for their effective exploitation.
- Video conferencing. Not useful given the currently available bandwidths, but this may change in the future.
- Whiteboard.
- Collaborative browsing. Easier to exchange web addresses by *e*-mail.
- Voting and polling.
- File exchange.
- Application/desktop sharing.
- Web publishing.

3 Summary and Conclusions

We have developed a prototype collaborative virtual environment, which actively supports human-human communication in addition to human-machine communication, for molecular electronic structure theory. We submit that key elements of *e*-science, such as collaborative virtual environments, will evolve most rapidly and deliver a functionality required by practicing scientists if they are developed as part of a research project in the target discipline. This is the approach that we have followed in this work. We have developed a collaborative virtual environment for molecular electronic structure theory whilst undertaking research into aspects of the Brillouin-Wigner theory for many-body systems. Others working in molecular physics and quantum chemistry may find this a useful starting point for the development of improved environments. Such environments will undoubtedly evolve with time as higher bandwidths and new tools become available.

Postscript

Advances in information and communications technology are facilitating widespread cooperation between groups and individuals, who may be physically located at geographically distributed sites (– sites in different laboratories, perhaps in different countries or even different continents), in a way that may disrupt and challenge the traditional structures and institutions of science (as well bringing change to society as a whole). Collaborative virtual environments, such as the one described here, have the potential to transform the 'scientific method' itself by fuelling the genesis, dissemination and accumulation of new ideas and concepts, and the exchange of alternative perspectives on current problems and strategies for their solution. Because of their openness and their global reach, as well as their emergent and

thus agile nature, such environments may transform the practice of science over the next decades.

"[T]he communication system is *[...]* vital to science; it lies at the very heart of the 'scientific method"' [1]. But, at the same time as technology is facilitating radical improvements in communications which can only serve to fuel scientific progress, there are factors in the contemporary structures and institutions governing science which have to potential to seriously inhibit scientific communication and thereby scientific progress. These factors are potentially as limiting as the 'iron curtain'. The science policies of governments and universities increasingly link funding for science with economic return. This can foster practices, such as the proprietary capture of genetic databases, which inhibit the free and open exchange of information. With scientific results cloaked in a veil of commercial confidentiality and/or vested interests, the communication which is the engine of progress in science is curtailed. Even in those areas of science which are of no direct economic benefit there is the outdated 'copyright economy' which forces scientists to assign all rights to a major commercial journal publisher for no remuneration and then buy back their work through monopolistic subscriptions.

Acknowledgment This work was carried under the auspices of EU COST programme – Action D23, Project number D23/0001/01: *European Metalaboratory for multireference quantum chemical methods*.

References

1. J. Ziman, *The Force of Knowledge. The Scientific Dimension of Society*, pp. 90–91, Cambridge University Press, Cambridge (1976)
2. B.T. Sutcliffe, in *Handbook of Molecular Physics and Quantum Chemistry*, volume 1, ed. S. Wilson, P.F. Bernath and R. McWeeny, chapters 31, 32, 34, 35, Wiley, Chichester (2003)
3. R. McWeeny, in *Handbook of Molecular Physics and Quantum Chemistry*, volume 2, ed. S. Wilson, P.F. Bernath and R. McWeeny, chapter 1, Wiley, Chichester (2003)
4. R. McWeeny, in *Handbook of Molecular Physics and Quantum Chemistry*, volume 2, ed. S. Wilson, P.F. Bernath and R. McWeeny, chapter 15, Wiley, Chichester (2003)
5. L. Meissner, J. Gryniaków, I. Hubač, Chem. Phys. Letts. **397**, 34 (2004)
6. I. Hubač and S. Wilson, J. Phys. B: At. Mol. Opt. Phys. **33**, 365 (2000)
7. I. Hubač and S. Wilson, in *Encyclopedia of Computational Chemistry*, electronic edition, ed. P. von Ragué Schleyer, N.L. Allinger, H.F. Schaefer III, T.Clark, J. Gasteiger, P. Kollman and P. Schreiner, Wiley, Chichester (2003)
8. S. Wilson, I. Hubač, P. Mach, J. Pittner and P. Čársky, Prog. Theor. Chem. & Phys. **12**, 71 (2003)
9. D.E. Knuth, *The TEX book*, Addison-Wesley, Boston, MA, (1986)
10. D.E. Knuth, *TEX: The Program*, Addison-Wesley, Boston, MA, (1986)
11. L. Lamport, *LATEX: A Document Preparation System*, Addison-Wesley, Boston, MA, (1986)
12. L. Lamport, *LATEX: A Document Preparation System – User's Guide and Reference Manual*, Addison-Wesley, Boston, MA, (1994)
13. H. Kopka and P.W. Daly, *A Guide to LATEX2e: Tools and Techniques for Computer Typesetting*, 4th edition, Addison-Wesley, Boston, MA, (2004)
14. A. Diller, *LATEX Line by Line*, Wiley, Chichester (1998)

15. F. Mittelbach and M. Goossens, with J. Braams, D. Carlisle and C. Rowley, *The LaTeX Companion*, 2nd edition, Addison-Wesley, Boston, MA, (2004)
16. C. Bloch, Nucl. Phys. **6**, 329 (1958)
17. Adobe Systems Incorportated, PDF Reference, version 1.4, 3rd edition, Addison-Wesley, Boston, MA, (2002)
18. H.M. Quiney and S. Wilson, Molec. Phys. **103**, 387 (2005)
19. D.E. Knuth, The Computer J. **27:2**, 97 (1984)
20. P. von Ragué Schleyer (Editor-in-Chief), N.L. Allinger, H.F. Schaefer III, T. Clark, J. Gasteiger, P. Kollman and P. Schreiner, *Encyclopedia of Computational Chemistry*, Wiley, Chichester (1998)
21. D.E. Knuth, "Literate Programming (1984)" in Literate Programming, Center for the Study of Language and Information, p. 99. (1992)
22. W.H. Press, S.A. Teukolsky, W.T. Vetterling and B.P. Flannery, *Numerical Recipes in C*, Cambridge University Press (1992)
23. M. J. Frisch, G. W. Trucks, H. B. Schlegel, G. E. Scuseria, M. A. Robb, J. R. Cheeseman, J. A. Montgomery, Jr., T. Vreven, K. N. Kudin, J. C. Burant, J. M. Millam, S. S. Iyengar, J. Tomasi, V. Barone, B. Mennucci, M. Cossi, G. Scalmani, N. Rega, G. A. Petersson, H. Nakatsuji, M. Hada, M. Ehara, K. Toyota, R. Fukuda, J. Hasegawa, M. Ishida, T. Nakajima, Y. Honda, O. Kitao, H. Nakai, M. Klene, X. Li, J. E. Knox, H. P. Hratchian, J. B. Cross, V. Bakken, C. Adamo, J. Jaramillo, R. Gomperts, R. E. Stratmann, O. Yazyev, A. J. Austin, R. Cammi, C. Pomelli, J. W. Ochterski, P. Y. Ayala, K. Morokuma, G. A. Voth, P. Salvador, J. J. Dannenberg, V. G. Zakrzewski, S. Dapprich, A. D. Daniels, M. C. Strain, O. Farkas, D. K. Malick, A. D. Rabuck, K. Raghavachari, J. B. Foresman, J. V. Ortiz, Q. Cui, A. G. Baboul, S. Clifford, J. Cioslowski, B. B. Stefanov, G. Liu, A. Liashenko, P. Piskorz, I. Komaromi, R. L. Martin, D. J. Fox, T. Keith, M. A. Al-Laham, C. Y. Peng, A. Nanayakkara, M. Challacombe, P. M. W. Gill, B. Johnson, W. Chen, M. W. Wong, C. Gonzalez, and J. A. Pople, Gaussian 03, Revision C.02, Gaussian, Inc., Wallingford CT, 2004.
24. *General Atomic and Molecular Electronic Structure System*, M.W.Schmidt, K.K.Baldridge, J.A.Boatz, S.T.Elbert, M.S.Gordon, J.H.Jensen, S.Koseki, N.Matsunaga, K.A.Nguyen, S.Su, T.L.Windus, M.Dupuis, J.A.Montgomery J. Comput. Chem., **14**, 1347–1363(1993).

Index